

Государственное образовательное учреждение
высшего профессионального образования
**«Томский государственный университет
систем управления и радиоэлектроники»**



**ТЕМАТИЧЕСКИЙ
РЕФЕРАТИВНЫЙ СБОРНИК № 44-1/2**

**“Light Emitting Diode”
(«Светодиоды»)
Журнальные публикации**

Источник: *Digital Library IEEEExplore*
Язык: *английский*
Глубина поиска: *2006 – 2008 гг.*
Дата формирования: *март 2011 г.*
Составитель: *В.И. Карнышев*

Томск – 2011

ТЕМАТИЧЕСКИЙ РЕФЕРАТИВНЫЙ СБОРНИК № 44-1/2

"Light Emitting Diode"

(«Светодиоды»)

Журнальные публикации

"Luminescent properties in the strain adjusted phosphor-free GaN based white light-emitting diode"

A kind of phosphor-free GaN based white light-emitting diode was fabricated with a strain adjusting InGaN interlayer. The origin of the strain adjusted white luminescent properties was studied with cathodoluminescence, asymmetrically reciprocal space mapping with high resolution x-ray diffraction, and scanning electron microscopy. The yellow and blue components of the electroluminescence spectrum were attributed to the high indium core and the adjacent indium depleted region in the inverted pyramidal pits on the device surface, respectively. These pits existed at the end of the dislocations induced by the strain relaxation process of the InGaN interlayer. [J1106]

"Comment on "Surface plasmon coupled electroluminescent emission" [JAppl. Phys. Lett. 92, 103304 (2008)]"

First Page of the Article [J1107]

"Response to "Comment on 'Surface plasmon coupled electroluminescent emission'" [JAppl. Phys. Lett. 93, 266101 (2008)]"

First Page of the Article [J1108]

"Lithium salt doped conjugated polymers as electron transporting materials for highly efficient blue polymer light-emitting diodes"

Highly efficient blue polymer light-emitting diodes (PLEDs) are fabricated using a conjugated polymer, poly[9,9-bis(2-(2-(2-diethanol-amino-ethoxy) ethoxy) ethyl) fluorene-alt-4, 4'-phenylether] as an electron transporting layer (ETL). It was found that the performance of these blue-emitting devices could be greatly improved if the ETL was doped with LiF or Li₂CO₃ salts. A bis[(4,6-di-fluorophenyl)-pyridinato-N, C2] (picolinate) Ir(III) (FIrpic) complex based blue phosphorescent PLED exhibited a maximum luminance efficiency of 20.3 cd/A with a luminance of 1600 cd/m² at the current density of 7.9 mA/cm² and drive voltage of 8.0 V. [J1109]

"Design of an efficient light-emitting diode with 10 GHz modulation bandwidth"

We present a high-speed light-emitting-diode (LED) design for efficient modulation at speeds higher than 10 GHz. It relies on a tensile-strain GaAsP quantum well coupled with surface plasmon polaritons on a silver surface. We present optical pumping experiments showing a tenfold reduction in carrier lifetime when the quantum well is located 40 nm above the silver surface. We believe this represents the first step toward an efficient LED compatible with 10 GHz modulation speed for use in short distance optical communication systems. [J1110]

"A p-n homojunction ZnO nanorod light-emitting diode formed by As ion implantation"

We report stable and repeatable UV and red electroluminescence (EL) from ZnO nanorod (NR) array light-emitting diodes (LEDs), where the p-type ZnO was formed by As⁺ ion implantation into the as-grown ZnO NRs. Both doped and undoped single ZnO NRs were probed using nanomanipulator, where the former ones showed good rectification characteristics, confirming the formation of p-n homojunctions by ion implantation. Distinct EL emissions in UV and red regions were observed at room temperature under forward bias, where the emission intensity shows amplified spontaneous emission characteristics, suggesting high efficiency of these LEDs. [J1111]

"Highly stable amorphous-silicon thin-film transistors on clear plastic"

Hydrogenated amorphous-silicon (a-Si:H) thin-film transistors (TFTs) have been fabricated on clear plastic with

highly stable threshold voltages. When operated at a gate field of $2.54 \times 10^5 \text{ V/cm}$, the threshold voltage shift extrapolated to only 1.2V after ten years. This stability is achieved by a high deposition temperature for the gate silicon nitride insulator which reduces charge trapping and high hydrogen dilution during a-Si:H growth to reduce defect creation in a-Si:H. This gate field of $2.54 \times 10^5 \text{ V/cm}$ is sufficient to drive phosphorescent organic light emitting diodes (OLEDs) at a brightness of 1000 Cd/m^2 . The half-life of the TFT current is over ten years, slightly longer than the luminescence half-life of high quality green OLEDs. [J1112]

"A pure 1.5 μm electroluminescence from metal-oxide-silicon tunneling diode using dislocation network"

This letter has demonstrated a light emitting diode (LED) with a pure 1.5 μm emission using a metal-oxide-silicon (MOS) tunneling structure based on dislocation network in direct silicon bond wafer. It is found that under negative gate bias, the electrons in the metal gate electrode tunnel through the thin oxide to silicon and then recombine radiatively with holes at the dislocation related states to emit the D1-line with a wavelength of 1.5 μm . The calculation of energy band diagram indicates that a potential well for electrons forms at the charged bonding interface under negative bias, therefore, the electrons tunneled from the gate can rapidly be attracted by the electric field and then confined at the interface, which essentially increases the efficiency of D1 luminescence from MOS tunneling LED. These results are of interest for the development of silicon based photonics with 1.5 μm light emission. [J1113]

"Low voltage organic light-emitting devices with triphenylphosphine oxide layer"

We have developed low voltage driving organic light-emitting devices using triphenylphosphine oxide (Ph3PO) layers. The devices with a Ph3PO layer show high current density at a low voltage. For example, the current density of 20 mA/cm^2 is achieved at a low voltage of 2.9V for the device consisted of 4,4',4''-tris[N-(2-naphthyl)-N-phenyl-amino]-triphenylamine (2-TNATA), 4,4'-bis(2,2'-diphenylvinyl)-1,1'-biphenyl (DPVBi), and Ph3PO layers. Due to the good electron conduction property of Ph3PO, a luminance of 1017 cd/m^2 is achieved at a low voltage of 3.0V in a device with a structure of ITO/2-TNATA/DPVBi:rubrene (1%, 10nm)/DPVBi(30nm)/Ph3PO(60nm)/LiF/Al. [J1114]

"High-efficiency monochrome organic light emitting diodes employing enhanced microcavities"

We demonstrate enhanced light outcoupling from bottom emitting monochrome high-efficiency red, green, and blue organic light emitting diodes by adding silver layers on the indium tin oxide (ITO) anode. The devices contain the phosphorescent emitting dyes tris(2-phenylpyridine)iridium and iridium(III)bis[2-methyl-2,2'-biquinoline](acetylacetonate), and the blue singlet emitter 2,2',7,7'-tetrakis 2,2'-(diphenylvinyl)spiro-9,9'-bifluorene. We follow the p-i-n doping concept to increase the power efficiencies. We reach 81 lm/W for red, 101 lm/W for green, and 4.0 lm/W for blue color. These efficiencies are improved by up to a factor of 2.3 compared to standard ITO devices, which we attribute to microcavity amplification between the cathode and the Ag layer. [J1115]

"Current-injected 1.54 μm light emitting diodes based on erbium-doped GaN"

Current-injected 1.54 μm emitters have been fabricated by heterogeneously integrating metal organic chemical vapor deposition grown Er-doped GaN epilayers and 365nm nitride light emitting diodes. It was found that the 1.54 μm emission intensity increases almost linearly with input forward current. The results represent a step toward demonstrating the feasibility for achieving electrically pumped optical amplifiers for optical communication that possess advantages of both semiconductor optical amplifiers and Er-doped fiber amplifiers. [J1116]

"Polarization-matched Ga In N /Al Ga In N multi-quantum-well light-emitting diodes with reduced efficiency droop"

Blue multi-quantum-well light-emitting diodes (LEDs) with GaInN quantum wells and polarization-matched AlGaInN barriers are grown by metal-organic chemical vapor deposition. The use of quaternary alloys enables an independent control over interface polarization charges and bandgap and has been suggested as a method to reduce electron leakage from the active region, a carrier loss mechanism that can reduce efficiency at high injection currents—an effect known as the efficiency droop. The GaInN/AlGaInN LEDs show reduced forward voltage, reduced efficiency droop, and improved light-output power at large currents compared to conventional GaInN/GaN LEDs. [J1117]

"Enhanced light extraction efficiency from AlGaInP thin-film light-emitting diodes with photonic crystals"

We investigate the use of photonic crystals for light extraction from high-brightness thin-film AlGaInP light-emitting diodes with different etch depths, lattice constants, and two types of lattices (hexagonal and Archimedean). Both simulations and experimental results show that the extraction of high order modes with a low effective index neff is most efficient. The highest external quantum efficiency without encapsulation is 19% with an Archimedean A7 lattice with reciprocal lattice constant $G=1.5k_0$, which is 47% better than an unstructured reference device. [J1118]

"A revised Kubelka-Munk theory for spectral simulation of phosphor-based white light-emitting diodes"

We developed a simulation method for designing the luminescence profiles of white light-emitting diodes (LEDs) with multicolor phosphor blend. By taking into account the effect of the light scattering by phosphor particles as well as the reabsorption effect by phosphor species, we found a model of white LEDs to calculate the light output as a function of various parameters such as the thickness of the resins, the concentration of phosphors, and the spatial distribution of phosphor particles. This method is widely applicable to phosphor-based white LEDs with either blue or UV excitation. [J1119]

"Optical nanolithography using a scanning near-field probe with an integrated light source"

An ultracompact near-field optical probe is described that is based on a single, integrated assembly consisting of a gallium nitride (GaN) light-emitting diode (LED), a microlens, and a cantilever assembly containing a hollow pyramidal probe with a subwavelength aperture at its apex. The LED emits ultraviolet light and may be used as a light source for near-field photolithographic exposure. Using this simple device compatible with many commercial atomic force microscope systems, it is possible to form nanostructures in photoresist with a resolution of 35 nm, corresponding to $\lambda/10$. [J1120]

"Metal patterning using maskless vacuum evaporation process based on selective deposition of photochromic diarylethene"

We developed an electrode/wiring patterning method that does not employ evaporation shadow masks; this method is based on selective metal deposition of photochromic diarylethene (DAE). In the selective Mg deposition based on the photoisomerization of DAE, Mg vapor atoms are deposited only on colored DAE film obtained upon UV irradiation, but not on uncolored film. We demonstrated fine metal Mg patterning with a minimum width of 3 μm and the preparation of a patterned cathode. The selective metal deposition method has significant potential for preparing fine electrodes/wiring for various organic electronic devices. [J1121]

"Elimination of total internal reflection in GaInN light-emitting diodes by graded-refractive-index micropillars"

A method for enhancing the light-extraction efficiency of GaInN light-emitting diodes (LEDs) by complete elimination of total internal reflection is reported. Analytical calculations show that GaInN LEDs with multilayer graded-refractive-index pillars, in which the thickness and refractive index of each layer are optimized, have no total internal reflection. This results in a remarkable improvement in light-extraction efficiency. GaInN LEDs with five-layer graded-refractive-index pillars, fabricated by cosputtering TiO_2 and SiO_2 , show a light-output power enhanced by 73% and a strong side emission, consistent with analytical calculations and ray-tracing simulations. [J1122]

"Diffusion of atmospheric gases into barrier-layer sealed organic light emitting diodes"

Organic light emitting diodes (OLEDs) are protected from the atmosphere with a barrier layer. Even when this permeation barrier is hermetic, dark spots still may grow and dark sheets may extend into the OLED. These grow by diffusion from the atmosphere along the interfaces between the barrier layer with embedded particles or with the substrate. Observed growth rates of dark spots and sheets are modeled by a single diffusion mechanism. Similar normalized flux densities along the two pathways and a diffusion coefficient of $10^{-8} \text{ cm}^2/\text{s}$ suggest a similar polymeric structure of the barrier/particle and barrier/substrate interfaces. [J1123]

"Narrow-band deep-ultraviolet light emitting device using $\text{Al}_{1-x}\text{Gd}_x\text{N}$ "

We demonstrated mercury-free narrow-band deep-ultraviolet luminescence from field-emission devices with $\text{Al}_{1-x}\text{Gd}_x\text{N}$ thin films. The $\text{Al}_{1-x}\text{Gd}_x\text{N}$ thin films were grown on fused silica substrates by a radio frequency reactive magnetron sputtering method. The deposited film shows a strong c-axis preferential orientation. A resolution limited, narrow intra-4f luminescence line from Gd^{3+} ions has been observed at 315 nm. The luminescence

spectrum depends on the growth temperature of the thin film, and the intensity varies as a function of the GdN mole fraction. [J1124]

"Synthesis and photoluminescence characteristics of color-tunable BaY₂ZnO₅:Eu³⁺ phosphors"

Color-tunable phosphors of BaY₂-xEu_xZnO₅(x=0.001-0.9) were synthesized using a vibrating milled solid state reaction. The results indicate that the emission spectra of BaY₂-xEu_xZnO₅ samples excited at 395 nm exhibit a series of shaped peaks assigned to the 5D₀→7F_J(J=0,1,2,3,4) transitions. Luminescence from the higher excited states, such as 5D₁, 5D₂, and 5D₃, were also observed even though the Eu³⁺ concentration was up to x=0.2. The chromaticity coordinate of BaY₂-xEu_xZnO₅ phosphors varies with the Eu³⁺-doped concentrations from blue, white, to red, and which may be potentially applicable as a white light emitting phosphor for ultraviolet light emitting diodes. [J1125]

"Efficient energy transfer for Ce to Nd in Nd³⁺/Ce³⁺ codoped yttrium aluminum garnet"

A two order of enhancement in near-infrared emission from Nd³⁺ in Ce³⁺/Nd³⁺ codoped yttrium aluminum garnet (YAG) matrix is obtained. This is due to efficient absorption by the allowed 4f-5d transition of Ce³⁺ ions then transfer to Nd³⁺ ions via a well matched energy level. This is among the most efficient near-infrared emission from Nd³⁺ ions strongly sensitized by exciting with an allowed transition in an inorganic matrix. This means that a new class of material, YAG:Ce,Nd, was produced and it potentially can be an efficient near-infrared phosphor that could be easily excited by a GaN light emitting diode, producing a new type of near-infrared emitter. [J1126]

"Directional light extraction from thin-film resonant cavity light-emitting diodes with a photonic crystal"

We report directional light extraction from AlGaInP thin-film resonant cavity light emitting diodes (RCLEDs) with shallow photonic crystals (PhCs). Diffraction of guided modes into the light extraction cone enhances the light extraction by a factor of 2.6 compared to unstructured RCLEDs, where the farfields still show higher directionality than Lambertian emitters. The external quantum efficiency is 15.5% to air and 26% with encapsulation, respectively. The PhC-RCLEDs are also more stable to a temperature induced wavelength shift than unstructured RCLEDs. [J1127]

"Enhanced and partially polarized output of a light-emitting diode with its InGaN/GaN quantum well coupled with surface plasmons on a metal grating"

The enhanced and partially polarized output of a green light-emitting diode (LED), in which its InGaN/GaN quantum well (QW) couples with surface plasmons (SPs) on a surface Ag grating structure, is demonstrated. Compared with a LED sample without (flat) Ag coating, the total output intensity of an LED of SP-QW coupling can be enhanced by 59% (200%) when the grating period and groove depth are 500 and 30 nm, respectively. Also, a bottom-emission polarization ratio of 1.7 can be obtained under the condition of 15 nm in groove depth. [J1128]

"InGaN/GaN multiple quantum wells grown on microfacets for white-light generation"

We report the white color electroluminescence (EL) emission from InGaN/GaN multiple quantum wells (MQWs) grown on GaN microfacets. The white color was realized by combining EL emission from InGaN/GaN MQWs on c-plane (0001), semipolar {11-22}, and {1-101} microfacets of trapezoidal n-GaN arrays. The color of EL emission was changed from reddish to bluish color with injection current and showed a white color in the current range of 180-230 mA. The variation in the color of EL emission was attributed to differences in current injection and quantum efficiency of MQWs grown on c-plane (0001) and semipolar GaN microfacets. [J1129]

"Light-emitting polymer space-charge-limited transistor"

Polymer light-emitting transistor is realized by vertically stacking a top-emitting polymer light-emitting diode on a polymer space-charge-limited transistor. The transistor modulates the current flow of the light-emitting diode by the metal-grid base voltage. The active semiconductor of the transistor is poly(3-hexylthiophene). Yellow poly(para-phenylene vinylene) derivative is used as the yellow emitting material. As the cathode is fixed at -12 V and the grid base voltage varies from 0.9 to -0.9 V, the light emission is turned on and off with on luminance up to 1208 cd/m². The current efficiency of the light-emitting transistor is 10 cd/A. [J1130]

"Erratum: "Degradation studies on high-voltage-driven organic light-emitting device using in situ on-

operation method with scanning photoelectron microscopy" [JAppl. Phys. Lett. 93, 133310 (2008)]"

First Page of the Article [J1131]

"Erratum: "Very low turn-on voltage and high brightness tris-(8-hydroxyquinoline)aluminum-based organic light-emitting diodes with a MoO_x p-doping layer" [JAppl. Phys. Lett. 92, 093305 (2008)]"

First Page of the Article [J1132]

"Enhancement of surface plasmon-mediated radiative energy transfer through a corrugated metal cathode in organic light-emitting devices"

We report enhanced top emission from organic light-emitting devices by surface plasmon-mediated radiative energy transfer. A dye-doped dielectric acceptor layer was deposited onto the surface of a one-dimensionally corrugated silver cathode and was excited by the electroluminescence of a donor layer, which is located at the other side of the cathode. Ten times enhancement in emission intensity from the acceptor was observed compared to flat devices; this is due to the enhanced radiative energy transfer from the donor to the acceptor by the coupled surface plasmons on the opposite interfaces of the silver cathode. [J1133]

"Indium tin oxide modified transparent nanotube thin films as effective anodes for flexible organic light-emitting diodes"

Sn-doped In₂O₃(ITO) modified single-walled carbon nanotube (SW-CNT) transparent electrodes are fabricated on flexible polyethyleneterephthalate (PET) substrates by stamp printing SW-CNT films, followed by room temperature ion-assisted deposition of ITO. Polymer light-emitting diodes (PLEDs) using such film as anodes exhibit superior performance versus CNT-only controls. Flexible PLEDs with the following structure: PET/CNT(30 nm)-ITO(45 nm)/poly (3,4-ethylenedioxythiophene) poly (styrenesulfonate)/[poly(9,9-dioctyl-fluorene-co-N-(4-butylphenyl)diphenylamine)]+[4,4'-bis[(p-trichlorosilyl propylphenyl)-phenylamino]biphenyl]/[poly(9,9-dioctylfluorene-co-benzothiadiazole)]/CsF/Al, achieve a maximum light output of 8900cd/m² with a current efficiency of 4.5cd/A. Bending test comparisons with ITO/PET show the ITO modified CNT/PET electrodes to be far more mechanically flexible. [J1134]

"A comparison of CuO and Cu₂O hole-injection layers for low voltage organic devices"

Cu₂O and CuO have been grown with an aim to reduce junction electrical resistance when interfaced with N,N'-bis(1-naphthyl)-N,N'-diphenyl-1,1'-biphenyl 4,4'-diamine (NPB). Organic light-emitting diodes employing Cu/CuO anodes have equivalent driving voltages as devices made with indium tin oxide. Hole-injection barriers are calculated from current-voltage characteristics of CuO/NPB/Cu and Cu₂O/NPB/Cu devices via theoretical simulation. Photoelectron spectroscopies are used to measure oxide valence band spectra, interfacial dipole formation, and band bending during in situ sequential deposition of NPB on each oxide. Calculated hole-injection barriers and those derived from photoemission results accord well, explaining the superior hole injection at the CuO-NPB interface. [J1135]

"A combined experimental and simulation study on thickness dependence of the emission characteristics in multicolor single layer organic light-emitting diodes"

The impact of the active layer thickness on the emission characteristics of multicolor single layer organic light-emitting diodes based on poly(9-vinylcarbazole) is examined by combining experimental results with model simulations. We compare experimental electroluminescence spectra with simulations using photon-emitting point dipoles and find a very good agreement. We also simulate the location of the recombination zone, considering that the emission probability distribution has a peak located 25 nm from the cathode, which decays exponentially above and below that point. Simulated radiation patterns show that microcavity effects dominate the thickness dependent emitting properties of these devices. [J1136]

"Influence of annealing temperature on optical properties of InGaN quantum dot based light emitting diodes"

Electron-luminescence (EL) and high-resolution transmission electron microscopy (TEM) measurements have been carried out on the InGaN quantum dot (QD) based light emitting diodes (LEDs) annealed at different temperatures for p-type GaN activation. The annealing temperatures are chosen based on the growth temperature for our InGaN QDs as a reference point. A significant improvement with a factor of up to 3.5 in EL intensity has been achieved when the annealing temperature is increased from 720 to 800°C. However, the EL intensity dramatically decreases if the annealing temperature further increases to 830°C. In addition, a clear

blueshift in EL emission energy has been observed as a result of increasing annealing temperature. In combination with our TEM study, the change in optical properties of the QD based LEDs due to the thermal annealing can be attributed to the shrinkage of the QDs and then eventual mergence into the wetting layer if the annealing temperature is further increased. The data based on detailed driving-current dependent EL measurements also support the conclusion. [J1137]

"Lifetime of organic light emitting diodes on polymer anodes"

We report on the use of a thin layer of poly(3,4-ethylenedioxythiophene) poly(styrenesulfonate) (PEDOT:PSS) as anode for bottom emission organic light emitting diodes (OLEDs). The combination of polymer anodes with OLEDs having either electrically doped or undoped hole transport layers in direct contact with the polymer is shown. We discuss the impact of the annealing conditions of the polymer on the OLED lifetime in comparison to indium tin oxide anodes. Supported by a differential thermal analysis of PEDOT:PSS, a strong influence of residual water in the polymer on the device lifetime is found. Additional heating of the polymer anode in a dry ambient prior to OLED deposition is necessary to achieve high device lifetimes. At a luminance of 260cd/m², pin-OLEDs on a PEDOT:PSS anode show no measurable device degradation during 5200 h of operation. [J1138]

"Mechanism of charge generation in p -type doped layer in the connection unit of tandem-type organic light-emitting devices"

A p-type doped organic layer combined with a hole-blocking layer has been experimentally demonstrated to serve as the charge generation unit in tandem-type organic light-emitting devices. The p-type layer functions as the source of both holes and electrons. Charge separation is explained by the tunneling model that the hole-blocking layer reduces the energy barrier for the electrons generated in the p-type layer to tunnel through into one light-emitting unit, while the holes generated in the p-type layer can transport to the other light-emitting unit easily under operation voltage. [J1139]

"Contact formation at the C 60 /alkali-metal fluoride/Al interface"

Efficient contact formation is critical in organic electroluminescence and photovoltaic devices that utilize fullerene (C60). Unlike traditional electron transport molecules, such as tris-(8-hydroxy-quinolino)aluminum (Alq3), C60 is found to be highly selective of injection layers. Charge injection properties of alkali-metal fluoride injection layers at the C60/Alcathode interface of organic light emitting diodes were studied. LiF is found to be unique amongst the alkali-metal fluorides in producing an Ohmic contact. The device performance is strongly linked to the size of the vapor phase fluoride molecules. The observed phenomena are explained by an intercalation region at the metal/organic interface. [J1140]

"Exciton dissociation in tris(2-phenylpyridine) iridium (III) probed by electric field-assisted time-resolved photoluminescence"

We have investigated the mechanism of exciton dissociation in organometallic phosphorescent emitters by measuring the electric field-dependent time-resolved photoluminescence for thin vacuum-evaporated films of a model compound-tris(2-phenylpyridine) iridium (III) [Ir(ppy)₃]. We have shown that the dissociation occurs from higher lying spin-mixed states before their relaxation to the lowest emissive levels, the lifetime of the latter not being significantly affected by external electric field. Knowledge about the mechanism of exciton dissociation in this class of materials is relevant for theoretical simulations of exciton kinetics in phosphorescent diodes as well as for optimization of the performances of these devices. [J1141]

"Solution processable ionic p-i-n phosphorescent organic light-emitting diodes"

We report efficient light-emission from solution-processed single-layered phosphorescent organic light-emitting diodes (PHOLEDs) that were doped with ionic salt and treated with simultaneous electrical and thermal annealing. Because the simultaneous annealing causes the adsorption of salt ions at the electrode surfaces, the energy levels of the organic molecules are bent by the electric fields due to the adsorbed ions; i.e., the annealing can induce the proper formation of an ionic p-i-n structure. As a result, an ionic p-i-n PHOLED with a peak luminescence of over 35000cd/m² and a power efficiency of 42lm/W was achieved through increased and balanced carrier injections. [J1142]

"Current efficiency in organic light-emitting diodes with a hole-injection layer"

We have systematically investigated the effect of layer structures on the current efficiency of prototypical hole-injection layer (HIL)/hole-transport layer (HTL)/electron-transport layer (ETL) organic light-emitting diodes based

on 4,4',4"-tris[N-(3-methylphenyl)-N-phenylamino]triphenylamine (MTDATA) as the HIL, 4,4'-bis[N-(1-naphthyl)-N-phenylamino]biphenyl (NPB) as the HTL, and tris(8-quinolinolato)aluminum (Alq) as the ETL. With bilayer devices, the current efficiency is limited by exciplex emissions in the case of MTDATA/Alq and quenching of Alq emissions by NPB+radical cations in NPB/Alq. The improved current efficiency in trilayer MTDATA/NPB/Alq devices can be attributed to a reduction in NPB+radical cations at the NPB/Alq interface and a strong electric field in the NPB layer. [J1143]

"Electrical characterization of organic light-emitting diodes using dipotassium phthalate as n -type dopant"

An efficient n-doped electron transport layer composed of 4,7-diphenyl-1,10-phenanthroline (BPhen) and dipotassium phthalate (PAK2) has been developed. By temperature-dependent admittance spectroscopy, the incorporation of PAK2 into BPhen is found to raise the Fermi level from 1.7eV to only around 0.5eV below BPhen's lowest unoccupied molecular orbital, which further enhances the efficiency of electron injection from an Al cathode. When this n-doped layer is adopted in an organic light-emitting diode device, the green fluorescent 10-(2-benzothiazolyl)-1,1,7,7-tetramethyl-2,3,6,7-tetrahydro-1H,5H,11H-benzo[*l*]-pyrano[6,7,8-*ij*]quinolizin-11-one doped device can achieve a current efficiency of 16cd/A and a power efficiency of 10.9lm/W at 1000cd/m². [J1144]

"Room temperature midinfrared electroluminescence from InSb/InAs quantum dot light emitting diodes"

Self-assembled InSb submonolayer quantum dots (QDs) in an InAs matrix have been grown by molecular beam epitaxy using Sb₂ and As₂ fluxes. The structures exhibit bright midinfrared photoluminescence up to room temperature. Intense room temperature electroluminescence with a peak at wavelength near 3.8μm was observed from p-i-n light emitting diode structures containing ten InSb submonolayer QD sheets inserted within the InAs active region. [J1145]

"A yellow-emitting Ce 3+ phosphor, La 1-x Ce x Sr 2 Al O 5, for white light-emitting diodes"

A yellow-emitting phosphor, La_{1-x}Ce_xSr₂AlO₅, is reported that displays a peak in the excitation at 450nm and a peak in the emission at 556nm. When this phosphor is pumped by a blue InGaN light-emitting diode (λ_{max}=450nm) we obtain white light with color rendering index (Ra) between 81 and 85 and color temperatures between 4200 and 5500K, suggesting that this material is competitive as a blue-pumped yellow phosphors. [J1146]

"High output power GaN-based light-emitting diodes using an electrically reverse-connected p - Schottky diode and p-InGaN -GaN superlattice"

We demonstrate the high-performance and excellent reliability characteristics of InGaN-GaN light-emitting diodes (LEDs) using an electrically reverse-connected p-Schottky diode and p-InGaN-GaN superlattice (SL). Measurements show that the LED with the Schottky diode and SL yields lower series resistance and higher output power compared to normal LEDs. In addition, the device degradation rate of the proposed LED is 33 times as low as that of the normal LED at high electrical stress of 410A/cm², indicating excellent reliability behavior. These results mean that the use of p-Schottky diode and p-SL is very promising for the realization of high-performance GaN-based LEDs. [J1147]

"Solution-processed small molecule-based blue light-emitting diodes using conjugated polyelectrolytes as electron injection layers"

Organic blue light-emitting diodes were studied using the solution processable small molecule 2,7-dipyrenyl-9,9'-dioctyl-fluorene (DPF) as the light-emitting material. The devices were fabricated in two simple structures: indium tin oxide (ITO)/poly(3,4-ethylenedioxythiophene)-poly(styrenesulfonate) (PEDOT:PSS)/DPF/LiF/Al and ITO/PEDOT:PSS/DPF/PFN-BIm4/Al, where PFN-BIm4 is poly[9,9'-bis[6"-(N,N,N-trimethylammonium)hexyl]fluorene-alt-co-phenylene] with tetrakis(imidazolyl)borate counterions. The LiF or PFN-BIm4 act as electron injection layers. The ITO/PEDOT:PSS/DPF/PFN-BIm4/Al device, in which all organic layers are cast from solution, has a turn-on voltage of 3.8V, a luminance of 2000cd/m², and an efficiency of 0.6cd/A. Using the PFN-BIm4 layer shows a significant improvement of the device performance when compared to the LiF layer. [J1148]

"Polymer infrared proximity sensor"

A proximity sensor that combines a polymer light-emitting diode and a polymer photodiode is presented. The operation wavelength is in the near infrared from 700 to 850 nm. The infrared emission is obtained by adding a color conversion film of polyvinylpyrrolidone polymer matrix blended with infrared dye 1,1-diethyl-2,2-dicarbocyanine iodide to a red polymer light-emitting diode. The photodetector relies on the direct charge-transfer exciton generation in a donor-acceptor polymer blend of poly(3-hexylthiophene) and (6,6)-phenyl-C61-butyric acid methyl ester. The detection distance is up to 19 cm for objects with various colors and roughness under ambient indoor lighting. [J1149]

"100% internal quantum efficiency and stable efficiency roll-off in phosphorescent light-emitting diodes using a high triplet energy hole transport material"

Highly efficient green phosphorescent organic light-emitting diodes were developed by using high triplet energy hole transport materials. The quantum efficiency of green devices could be improved from 12% to 20% at 1000 cd/m² by using a phenylcarbazole based hole transport material. In addition, the high quantum efficiency could be stably maintained up to a high luminance of 10000 cd/m². [J1150]

"Migration enhanced lateral epitaxial overgrowth of AlN and AlGaN for high reliability deep ultraviolet light emitting diodes"

We report on the growth of low-defect thick films of AlN and AlGaN on trench AlGaN/sapphire templates using migration enhanced lateral epitaxial overgrowth. Incoherent coalescence-related defects were alleviated by controlling the tilt angle of growth fronts and by allowing Al adatoms sufficient residence time to incorporate at the most energetically favorable lattice sites. Deep ultraviolet light emitting diode structures (310 nm) deposited over fully coalesced thick AlN films exhibited cw output power of 1.6 mW at 50 mA current with extrapolated lifetime in excess of 5000 hours. The results demonstrate substantial improvement in the device lifetime, primarily due to the reduced density of growth defects. [J1151]

"Spectral optimization of phosphor-conversion light-emitting diodes for ultimate color rendering"

We apply an optimization scheme based on rendering of all colors of the enhanced Munsell palette to phosphor-conversion (PC) light-emitting diodes (LEDs). This approach yields combinations of peak wavelengths and bandwidths for white PC LEDs with partial and complete conversion that enable lighting with better quality than that obtained using designs based on the standard color-rendering assessment procedure. [J1152]

"Organic light emitting bistable memory device with high on/off ratio and low driving voltage"

Organic light emitting bistable memory devices (OLEBDs) with a dual function of organic light emitting diodes and organic memory devices were developed by using 0.5 nm thick MoO₃ as an interlayer between hole injection layer and hole transport layer. The hole transport unit with MoO₃ interlayer played a role of a memory unit as well as a hole transport unit. High on/off ratio over 1000 was obtained at a reading voltage of 1 V and driving voltage was lowered by MoO₃. In addition, two different luminances were obtained at the same driving voltage by changing writing voltage of OLEBDs. [J1153]

"High efficiency, color stability, and stable efficiency roll off in three color hybrid white organic light emitting diodes"

High efficiency, good color stability, and stable efficiency roll off were achieved in three color white organic light emitting diodes by developing a device architecture with red and green phosphorescent materials codoped in a mixed host emitting structure. A fluorescent blue material was used in a blue emitting layer and a mixed interlayer structure was applied. A high quantum efficiency of 9.7% was obtained and color coordinate of (0.40, 0.40) was kept constant up to luminance of 10000 cd/m². In addition, efficiency decrease at 10000 cd/m² was only 2% of the maximum quantum efficiency. [J1154]

"Nanoscale epitaxial lateral overgrowth of GaN-based light-emitting diodes on a SiO₂ nanorod-array patterned sapphire template"

High efficiency GaN-based light-emitting diodes (LEDs) are demonstrated by a nanoscale epitaxial lateral overgrowth (NELO) method on a SiO₂ nanorod-array patterned sapphire substrate (NAPSS). The transmission electron microscopy images suggest that the voids between SiO₂ nanorods and the stacking faults introduced during the NELO of GaN can effectively suppress the threading dislocation density. The output power and external quantum efficiency of the fabricated LED were enhanced by 52% and 56%, respectively, compared to those of a conventional LED. The improvements originated from both the enhanced light extraction assisted by

the NAPSS and the reduced dislocation densities using the NELO method. [J1155]

"A hybrid green light-emitting diode comprised of n-ZnO/(InGaN/GaN) multi-quantum-wells/p-GaN"

Hybrid green light-emitting diodes (LEDs) comprised of n-ZnO/(InGaN/GaN) multi-quantum-wells/p-GaN were grown on semi-insulating AlN/sapphire using pulsed laser deposition for the n-ZnO and metal organic chemical vapor deposition for the other layers. X-ray diffraction revealed that high crystallographic quality was preserved after the n-ZnO growth. LEDs showed a turn-on voltage of 2.5 V and a room temperature electroluminescence (EL) centered at 510 nm. A blueshift and narrowing of the EL peak with increasing current was attributed to bandgap renormalization. The results indicate that hybrid LED structures could hold the prospect for the development of green LEDs with superior performance. [J1156]

"Electrical spin injection and optical detection in InAs based light emitting diodes"

Results of low temperature circularly polarized electroluminescence (EL) studies of InAs-based spin-light emitting diodes in magnetic fields up to 10 T are presented. Spin polarized electrons injected from cubic n-(CdMn)Se recombine with unpolarized holes resulting in emission with a positive degree of optical polarization over this entire magnetic field range. Detailed rate equation modeling of the optical polarization degree (OPD) confirms a high spin injection efficiency (74%-95%) and a spin lifetime τ_s longer than the optical recombination time τ_r . Estimates of the temperature dependence of the ratio τ_s/τ_r from the OPD are compared with the Elliot-Yafet and Dyakonov-Perel models. [J1157]

"Balanced ambipolar charge carrier mobility in mixed layers for application in hybrid white organic light-emitting diodes"

We investigate the electron and hole mobility in mixed layers of N,N'-di(naphthalen-1-yl)-N,N'-diphenyl-benzidine and bis(2-methyl-8-quinolinato)-4-phenylphenolate aluminum with different mix ratios, using both space-charge limited currents of single-carrier devices with electrically doped charge transport layers and time-of-flight measurements. Both experimental methods yield consistent results. The 1:1 blend shows balanced ambipolar charge carrier transport, which is advantageous for the application as exciton blocking interlayer in hybrid white organic light-emitting diodes. The electroluminescence spectrum is rather stable against changes in interlayer thickness and driving current. Moreover, the external quantum efficiency is enhanced by a factor of 2.5 as compared to a device without interlayer. [J1158]

"Indium-free transparent organic light emitting diodes with Al doped ZnO electrodes grown by atomic layer and pulsed laser deposition"

We present highly efficient transparent organic light emitting diodes (OLEDs) with Al doped ZnO (AZO) electrodes prepared by atomic layer deposition and pulsed laser deposition (PLD). The power and current efficiencies exceed 27 lm/W and 44 cd/A at a brightness level of 100 cd/m², respectively. At the same time, the transmissivity of the devices is above 73% in the visible part of the spectrum. Owing to an efficient WO₃ buffer layer and an optimized PLD process for the deposition of the top AZO electrode, the OLEDs show leakage current densities as low as 3.4 × 10⁻⁵ mA/cm² at a reverse bias of 6 V. Therefore, our study paves the way for indium-free, see-through OLED displays. [J1159]

"GaSb based light emitting diodes with strained InGaAsSb type I quantum well active regions"

Mid-IR ($\lambda \approx 3\text{--}3.5\text{ }\mu\text{m}$) light emitting diodes with quaternary AlInGaAsSb barriers and InGaAsSb strained quantum wells grown on GaSb substrates have been demonstrated. The devices produced a quasi-cw emission power of 0.7 mW at room temperature and 2.5 mW at T=80 K. [J1160]

"The magnetic field effect on the transport and efficiency of group III tris(8-hydroxyquinoline) organic light emitting diodes"

Magnetoresistance and efficiency measurements of organic light emitting diode structures based on the group III hydroxyquinolates (Mq₃) have been made as a function of magnetic field and Mq₃ thickness, where M=Al, Ga, and In. For all quinolates, independent of thickness, we observed very similar behavior for the efficiency of the devices, with large increases in efficiency occurring at low values of applied field, which rapidly saturate as the field is increased. The current through these devices is found to be a strong function of both the device thickness and the metal ion. For Alq₃ based devices, the current changes appear to correlate strongly with the triplet population in the devices. For Gaq₃ and Inq₃ devices, the magnetoresistance is found not to correlate with

the triplet concentration and this may be evidence that there is little energetic barrier for carrier trapping in these materials. For all materials, a further dependence of the magnetoresistance on applied field was observed, which needs closer investigation. [J1161]

"Polarization-tunable electroluminescence using phase retardation based on photonic bandgap liquid crystal"

We have demonstrated polarization-tunable electroluminescence (EL) from organic light-emitting diodes (OLEDs) using a combination of polymeric cholesteric liquid crystal (PCLC) and nematic liquid crystal (NLC). By electrically controlling NLC alignment, the proposed EL device shows a continuous polarization tunability including two circular (right and left) and two linear polarizations without loss of light. This simple polarization-tunable EL device is based on photonic-device concept using spin-coatable PCLC. Hence, there is no limitation for choosing emissive materials with high internal efficiency. Also, its polarization tunability will be available in various optical devices and can extend OLED application to photonic technologies. [J1162]

"Hole transport in blue and white emitting polymers"

Hole transport in a blue emitting polyspirobifluorene polymer and in a white emitting polymer consisting of a polyspirobifluorene backbone and two dyes (green and red) was studied. The hole mobility was measured using the time-of-flight method as a function of the electric field and temperature in the range 105-106V/cm and 285-335K, respectively. The observed temperature and electric field dependence of the hole mobility was analyzed in the framework of the Bassler disorder model. Also, steady-state current-voltage characteristics were measured over a wide range of electric fields and temperatures and the hole mobility was determined. Our measurements have shown that the hole mobility in the white emitting polymer is the same as in the blue emitting polymer. The performed disorder model analysis gives the same values for the effective energetic disorder (115 meV) and for the positional disorder (1.85) for both polymers. Therefore, we have concluded that the added green and red dyes do not act as hole traps as they have no influence on the hole mobility. It can therefore be concluded that their highest occupied molecular orbital (HOMO) levels are aligned with the HOMO level of the polyspirobifluorene backbone. [J1163]

"Defects and transport in complex oxide thin films"

Epitaxial oxide thin films are at the heart of new "oxide electronic" applications, such as excitonic ultraviolet light-emitting diodes and resistive switching memories. Complex oxide films are often grown by pulsed laser deposition (PLD) because the technique is believed to be material agnostic. Here, we show that one of the fundamental premises used to justify the use of PLD, that material is transferred from an ablation target to the film without stoichiometry deviations, is incorrect even when no volatile elements are involved. Even more importantly, the commonly used solution of increasing the laser energy density above a material-specific threshold value to obtain stoichiometric films cannot be used in the case of low carrier density systems such as SrTiO₃, where even minute 10⁻³ order cation nonstoichiometry can have a dramatic effect on transport. Lattice parameter deviations in oxide films, which are often incorrectly ascribed to oxygen loss, correlate very well with cation nonstoichiometry. We show that proper simultaneous choice of ablation laser fluence and ablation area is essential and often more important than the growth temperature and oxygen pressure for obtaining bulklike properties in oxide heterostructures. [J1164]

"Digital communication using Ge metal-insulator-semiconductor light-emitting diodes and photodetectors"

Both Ge light-emitting diodes and photodetectors are demonstrated by using the same metal-insulator-semiconductor (MIS) tunneling structure. A Ge MIS tunneling diode biased at the accumulation region is used as a light-emitting device and a Ge MIS tunneling diode biased at the inversion region is used as a photodetector. The ultrathin gate oxide film used in the MIS tunneling diode was grown by liquid phase deposition at 50 °C to lower the thermal budget. A Ge light-emitting diode has a higher quantum efficiency than a similar Si device (at least one order of magnitude stronger) due to the higher radiative recombination coefficient. With the detection of the Ge MIS photodetector, the data communication in free space is reported and demonstrated for the first time. [J1165]

"Enhanced efficiency in near-infrared inorganic/organic hybrid optical upconverter with an embedded mirror"

We report a hybrid organic-inorganic optical upconverter with an embedded mirror, which converts 1.5 μm infrared light to visible light. The device was fabricated through direct tandem integration of an organic

light-emitting diode with an inorganic InGaAs/InP photodetector. It was found that the device with an embedded mirror exhibited a low turn-on voltage (~ 3.2 V) and an enhanced efficiency. The ratio of photocurrent-induced light with an input power density of 0.67 mW/mm^2 versus dark-current-induced visible light was over 500 at a device bias of 6 V at room temperature. The results show that the embedded mirror at the inorganic-organic interface plays a vital role in the performance enhancement of a hybrid upconverter. [J1166]

"The persistent photoconductivity effect in AlGaIn/GaN heterostructures grown on sapphire and SiC substrates"

In the present study, we reported the results of the investigation of electrical and optical measurements in $\text{Al}_x\text{Ga}_{1-x}\text{N}/\text{GaN}$ heterostructures ($x=0.20$) that were grown by way of metal-organic chemical vapor deposition on sapphire and SiC substrates with the same buffer structures and similar conditions. We investigated the substrate material effects on the electrical and optical properties of $\text{Al}_{0.20}\text{Ga}_{0.80}\text{N}/\text{GaN}$ heterostructures. The related electrical and optical properties of $\text{Al}_x\text{Ga}_{1-x}\text{N}/\text{GaN}$ heterostructures were investigated by variable-temperature Hall effect measurements, photoluminescence (PL), photocurrent, and persistent photoconductivity (PPC) that in turn illuminated the samples with a blue ($\lambda = 470 \text{ nm}$) light-emitting diode (LED) and thereby induced a persistent increase in the carrier density and two-dimensional electron gas (2DEG) electron mobility. In sample A ($\text{Al}_{0.20}\text{Ga}_{0.80}\text{N}/\text{GaN}/\text{sapphire}$), the carrier density increased from 7.59×10^{12} to $9.94 \times 10^{12} \text{ cm}^{-2}$ via illumination at 30 K. On the other hand, in sample B ($\text{Al}_{0.20}\text{Ga}_{0.80}\text{N}/\text{GaN}/\text{SiC}$), the increments in the carrier density were larger than those in sample A, in which it increased from 7.62×10^{12} to $1.23 \times 10^{13} \text{ cm}^{-2}$ at the same temperature. The 2DEG mobility increased from 1.22×10^4 to $1.37 \times 10^4 \text{ cm}^2/\text{V s}$ for samples A and B, in which 2DEG mobility increments occurred from 3.83×10^3 to $5.47 \times 10^3 \text{ cm}^2/\text{V s}$ at 30 K. The PL results show that the samples possessed a strong near-band-edge exciton luminescence line at around 3.44 and 3.43 eV for samples A and B, respectively. The samples showed a broad yellow band spreading from 1.80 to 2.60 eV with a peak maximum at 2.25 eV with a ratio of a near-band-edge excitation peak intensity up to a deep-level emission peak intensity ratio that were equal to 3 and 1.8 for samples A and B, respectively. Both of the samples that were illuminated with three different energy photon PPC decay behaviors can be well described by a stretched-exponential function and relaxation time constant τ as well as a decay exponent β that changes with the substrate type. The energy barrier for the capture of electrons in the 2DEG channel via the deep-level impurities (DX-like centers) in AlGaIn for the $\text{Al}_{0.20}\text{Ga}_{0.80}\text{N}/\text{GaN}/\text{sapphire}$ and $\text{Al}_{0.20}\text{Ga}_{0.80}\text{N}/\text{GaN}/\text{SiC}$ heterojunction samples are 343 and 228 meV, respectively. The activation energy for the thermal capture of an electron by the defects ΔE changed with the substrate materials. Our results show that the substrate material strongly affects the electrical and optical properties of $\text{Al}_{0.20}\text{Ga}_{0.80}$ [J1167]

"Degradation of GaN-based quantum well light-emitting diodes"

Electrical and optical properties of AlGaIn/InGaIn-based near-ultraviolet (UV) multiquantum well light-emitting diodes have been studied during operation at high junction temperatures. Light output decreased exponentially by 40% in the first 30 h after which there was no obvious change. The current-voltage characteristics were almost ideal before degradation, with an ideality factor of approximately 2. During degradation, an additional contribution to the current becomes apparent at voltages of below 2.5 V, with a temperature-independent logarithmic slope of the current-voltage characteristic, suggesting an additional transport mechanism by tunneling through defects created during degradation. The evolution of the additional current component corresponded to the two different stages observed in the reduction of the light emission with stress time. Generation of defects with similar effects on forward and reverse bias currents could be correlated with the rapid degradation during the first 30 h, but for the second stage, the change in the I-V characteristics did not correlate with the change in light emission. Electroluminescence spectra showed that the emission peaks shifted to slightly lower energies during degradation. [J1168]

"Implications of changes in the injection mechanisms on the low temperature electroluminescence in InGaIn/GaN light emitting diodes"

The presence of traps is sometimes favorable, and sometimes detrimental to the electrical transport and optical efficiency in III-nitride quantum heterostructures. This work presents the results of a joint analysis of electrical features and electroluminescence in InGaIn/GaN-based blue light emitting diodes; a detailed and exhaustive reading of the carrier injection mechanisms highlights the central role of trap centers near the active region. Some suggestions will be eventually advanced as to the design of devices with better emission performances. [J1169]

"Enhanced hole injection and transport in molybdenum-dioxide-doped organic hole-transporting layers"

We have found that molybdenum dioxide (MoO₂) is an excellent dopant for enhancing electrical conductivities in organic hole-transporting layers. We fabricated hole-only devices with an alpha-sexithiophene (alpha-6T) layer doped with MoO₂ at various concentrations to investigate how doping MoO₂ into the alpha-6T layers influences the hole-injection and hole-transport characteristics of these layers. We observed a marked increase in electrical conductivity as a result of the MoO₂ doping. The 30-mol % MoO₂-doped alpha-6T layer had a high electrical conductivity of $8.9 \pm 1.3 \times 10^{-6} \text{ S/cm}$. From the results of our visible/near-infrared absorption spectra study of these doped layers, we confirmed that this increase in electrical conductivity is caused by a charge transfer between MoO₂ and alpha-6T, which leads to an increase in free hole concentration in the doped layers and the formation of an ohmic contact at an electrode/alpha-6T interface. In the latter part of this paper, we discuss current flow and electroluminescence (EL) characteristics of organic light-emitting diodes (OLEDs) with a 30-mol % MoO₂-doped alpha-6T hole-transporting layer and a 30-mol % Cs-doped phenyldipyrenylphosphine oxide (POPy₂) electron-transporting layer. We achieved an extremely low driving voltage of 3.1 V required for a current density of 100 mA/cm² in the doped OLEDs owing to the use of the alpha-6T and POPy₂ layers with high carrier mobilities and the excellent p-type MoO₂ and n-type Cs dopants. We demonstrated the enhancement of power efficiencies by ≈ 2 times in the doped OLEDs compared with undoped OLEDs and observed bright EL at low driving voltages in the doped OLEDs, for example, 100 cd/m² at 2.3 V, 1000 cd/m² at 2.7 V, and 10 000 cd/m² at 3.3 V. [J1170]

"Simple white organic light emitting diodes with improved color stability and efficiency using phosphorescent and fluorescent emitters"

White organic light emitting diodes (WOLEDs) with both phosphorescent and fluorescent emitting layers (EML) usually adopt an interlayer between them to achieve high efficiency by preventing mutual quenching, but insertion of the interlayer causes a higher operating voltage as well as additional fabrication steps. Here, we demonstrate that simple-structure WOLEDs without an interlayer could be achieved using the combination of phosphor-sensitized-fluorescent red and phosphorescent blue EMLs. In addition, the main cause of the color shift with increasing current density was identified, and the color shift of the WOLED was successfully suppressed by properly balancing emission from the red and blue EMLs. Consequently, a maximum external quantum efficiency of 6.2% (a current efficiency of 14.3 cd/A) and very stable color coordinates of $(0.32 \pm 0.01, 0.42 \pm 0.002)$ were achieved. However, the elimination of an interlayer for the combination with a fluorescent blue EML causes about 50% decrease in the efficiency and a large change in the color coordinates with the driving current density. [J1171]

"Increase in indium diffusion by tetrafluoromethane plasma treatment and its effects on the device performance of polymer light-emitting diodes"

The effects of tetrafluoromethane (CF₄) plasma treatment of indium-tin-oxide (ITO) anode on indium diffusion into a poly(3,4-ethylene dioxythiophene):poly(styrene sulphonate) (PEDOT:PSS) layer were studied. Auger electron spectroscopy (AES) depth profile showed that 0.2 at.% indium was present in the PEDOT:PSS layer when ITO was not plasma treated. The plasma treatment of ITO increased the indium concentration to 6 at.%. The increase in indium can be explained by an oxygen deficiency in the CF₄ plasma treated ITO. The presence of indium in the PEDOT:PSS layer showed a correlation with performance degradation of polymer light-emitting diodes. [J1172]

"Theoretical investigation of the influence of nozzle diameter variation on the fabrication of thin film transistor liquid crystal display color filters"

Printing technologies have gained widespread attention from industry as an alternative to expensive photolithographic processes. Among the various kinds of printing technologies, piezoelectric drop-on-demand (piezo-DOD) inkjet printing is regarded as a promising patterning method because of its inherent simplicity and very low levels of material waste generation, especially for display industries such as thin film transistor liquid crystal displays and polymer light emitting diode displays. However, its key engineering difficulty is the variation of droplet volume across the nozzles in a piezo-DOD inkjet printhead, which causes visible swathe marks on a printed display screen. In this paper, it is suggested that the occurrence of these swathe marks could result from the influence of the mechanical nozzle tolerance, i.e., the variation in nozzle diameter of the piezo-DOD printhead. The effect of the mechanical nozzle tolerance on droplet velocity and volume is investigated using mathematical models. Finally, the future research and development direction of piezo-DOD inkjet printing technology for the large area flat panel display industry are discussed. [J1173]

"Spectrally narrow emissions at cutoff wavelength from edges of optically and electrically pumped anisotropic organic films"

The authors investigated the characteristics of spectrally narrow emissions at the cutoff wavelength from the edges of optically and electrically pumped organic semiconductor films. They estimated the optical properties of 4,4'-bis[(N-carbazole)styryl]biphenyl (BSB-Cz) films using variable angle spectroscopic ellipsometry, revealing that the BSB-Cz films have uniaxial anisotropy and that BSB-Cz molecules lie nearly parallel to substrate surfaces. The authors discuss here the spectral changes in the edge emissions from neat BSB-Cz and tris(8-hydroxyquinoline)aluminum (Alq3) films of 15 different thicknesses under continuous-wave (cw) optical excitation. The spectrally narrow emissions of transverse electric (TE) and transverse magnetic (TM) modes were observed. The authors showed that the peak wavelengths of these emissions varied according to the cutoff wavelengths of asymmetric slab waveguides and that their spectral widths changed depending on the angular dispersion of the Fabry-Perot interferometer composed of the organic film and its interfaces. The edge emissions from the BSB-Cz films had narrower bands than those from the Alq3 films and increased with a superlinear dependence on the stripe length of the excitation area, indicating the occurrence of light amplification under cw optical excitation. Finally, the authors demonstrate spectrally narrow emissions from the edges of electrically pumped organic light-emitting diodes (OLEDs) having a fine line-shaped waveguide structure with a silver metal cladding layer. Narrow emissions of TE mode were observed, and the peak wavelengths of the emission spectra corresponded well to the cutoff wavelength of the waveguide with the silver cladding layer. In addition to the narrow emissions, the authors observed some intriguing phenomenon - a suggestive of the occurrence of light amplification in OLEDs under electrical pumping. [J1174]

"Patterned backgating using single-sided mask aligners: Application to density-matched electron-hole bilayers"

We report our work on fabricating lithographically aligned patterned backgates on thin (50-60nm) III-V semiconductor samples using single sided mask aligners only. Along with this we also present a way to photograph both sides of a thin patterned chip using inexpensive infrared light emitting diodes and an inexpensive (consumer) digital camera. A robust method of contacting both sides of a sample using an ultrasonic bonder is described. In addition we present a mathematical model to analyze the variation in the electrochemical potential through the doped layers and heterojunctions that are normally present in most GaAs based devices. We utilize the technique and the estimates from our model to fabricate an electron-hole bilayer device in which each layer is separately contacted and has tunable densities. The electron and hole layers are separated by barriers either 25 or 15 nm wide. In both cases, the densities can be matched by using appropriate bias voltages. [J1175]

"Characterization of copper selenide thin film hole-injection layers deposited at room temperature for use with p -type organic semiconductors"

Copper selenide, $\text{Cu}_x\text{Se}_{(x-2)}$, was examined as a hole-injection layer for low-temperature organic devices. Crystalline Cu_xSe films grown at room temperature with atomically flat surfaces exhibited metallic conduction with a high electrical conductivity of $4.54 \times 10^3 \text{ S/cm}$, a hole concentration of $1.44 \times 10^{22} \text{ cm}^{-3}$, and a mobility of $2.0 \text{ cm}^2/(\text{Vs})$. Analysis of the free carrier absorption using the Drude model estimated the effective mass of a hole as $1.0 m_e$. Photoemission spectroscopy measurements of the interfaces between Cu_xSe and organic hole transport layers, N,N'-bis(naphthalen-1-yl)-N,N'-bis(phenyl) benzidine (NPB) and copper phthalocyanine (CuPc), verified that the hole-injection barriers of these interfaces (0.4 eV for NPB and 0.3 eV for CuPc) are smaller than that of a conventional indium tin oxide (ITO) hole-injection electrode/NPB interface (0.6 eV) but are comparable to that of an ITO electrode/CuPc interface (0.3 eV). Hole-only devices using the Cu_xSe layer as a hole-injection anode exhibited very low threshold voltages (0.4-0.5 V) and nearly Ohmic characteristics. The NPB layer on the Cu_xSe layer was found to be highly doped at 10^{17} - 10^{19} cm^{-3} , probably due to copper diffusion, while the CuPc layer is nearly intrinsic with a doping concentration lower than 10^{15} cm^{-3} . These results indicated that a Cu_xSe film combined with CuPc is a promising candidate for a low-voltage hole-injection anode or a buffer layer in low-temperature devices such as organic light-emitting diodes and thin film transistors. [J1176]

"Nanoscale surface electrical properties of aluminum zinc oxide thin films investigated by scanning probe microscopy"

Conducting atomic force microscopy and scanning surface potential microscopy were adopted to study the nanoscale surface electrical properties of aluminum zinc oxide (AZO) films that were prepared by pulsed laser deposition (PLD) at various substrate temperatures for use as anode materials in polymer light-emitting diodes (PLEDs). Experimental results indicate that when substrate temperatures exceed 100°C , the local conductivity and work function are positively correlated with the concentrations of Al dopant and O_2 on AZO surface. When the substrate temperature is approximately 150°C , the percentage coverage of conducting regions of the AZO surface and the mean work function are 90.20% and 4.85 eV, respectively. Additionally, both microcosmic uniformities meet the standard applied to PLEDs. This low-temperature condition for PLD significantly reduces

the yield rate of impurities when AZO vacuum evaporation is performed on a plastic substrate, supporting various applications of AZO films. [J1177]

"The roles of thermally evaporated cesium carbonate to enhance the electron injection in organic light emitting devices"

The properties of thermally evaporated cesium carbonate (Cs_2CO_3) and its role as electron injection layers in organic light emitting diodes were investigated. According to the ultraviolet photoemission spectra (UPS), the Fermi level of tris-(8-hydroxyquinoline)-aluminum (Alq_3) after being doped with Cs_2CO_3 shifts toward or into the lowest unoccupied molecular orbital as a result of chemical reaction and charge transfer between Cs_2CO_3 and Alq_3 , which lowers the electron injection barrier and improves the current efficiency. As for whether Cs_2CO_3 being decomposed during the evaporation, we found that Cs_2CO_3 molecules were deposited on the substrates without decomposition, regardless of the evaporation rates, based on the signature features of carbonate groups and ionization energies measured in UPS spectra and the binding energy shifts of core level electrons. The reaction mechanisms between Cs_2CO_3 and Alq_3 are also proposed. Since Cs_2CO_3 is not only used in the electron injection layer but also in converting high work function materials to cathodes, we further quantitatively investigated the work function modification of indium tin oxide (ITO) with deposition of Cs_2CO_3 at the surfaces. We found that while 0.5 eV thick Cs_2CO_3 is sufficient to reduce the electron injection barrier of Alq_3 , the thickness needed to convert ITO surface to low work function cathode is about 10 eV. [J1178]

"Electronic and optical properties of 530 nm strain-compensated hybrid InGaN/InGaN/ZnO quantum well light-emitting diodes"

Electronic and optical properties of 530 nm strain-compensated hybrid InGaN/InGaN/ZnO quantum well (QW) light-emitting diodes (LEDs) using a ZnO substrate are investigated using the multiband effective mass theory. These results are compared to those of conventional InGaN/GaN QW LEDs using a GaN substrate. A strain-compensated QW structure is found to have much larger spontaneous emission than an InGaN/GaN QW structure. This can be explained by the fact that a strain-compensated QW structure has much larger matrix element than an InGaN/GaN QW structure due to the reduction in the internal field. [J1179]

"On the c-Si surface passivation mechanism by the negative-charge-dielectric Al_2O_3 "

Al_2O_3 is a versatile high- κ dielectric that has excellent surface passivation properties on crystalline Si (c-Si), which are of vital importance for devices such as light emitting diodes and high-efficiency solar cells. We demonstrate both experimentally and by simulations that the surface passivation can be related to a satisfactory low interface defect density in combination with a strong field-effect passivation induced by a negative fixed charge density Q_f of up to 10^{13} cm^{-2} present in the Al_2O_3 film at the interface with the underlying Si substrate. The negative polarity of Q_f in Al_2O_3 is especially beneficial for the passivation of p-type c-Si as the bulk minority carriers are shielded from the c-Si surface. As the level of field-effect passivation is shown to scale with Q_f^2 , the high Q_f in Al_2O_3 tolerates a higher interface defect density on c-Si compared to alternative surface passivation schemes. [J1180]

"Study of trap states in polyspirobifluorene based devices: Influence of chromophore addition"

The defect states in spiro copolymer based light emitting diodes were investigated by charge based deep level transient spectroscopy (Q-DLTS). Two types of polymers have been studied: blue emitting spiro copolymer and white emitting spiro blend polymer. The white emitting spiro polymer was obtained by adding green and red chromophores into the host blue copolymer. The devices are composed of indium-tin oxide-polyethylene dioxythiophene:polystyrene sulfonate-spiro copolymer-Ba-Al. Q-DLTS measurements were performed on these diodes with various conditions of charging time, charging voltage, and temperature aiming at determining the role of chromophores in the defect formation process. Analysis of the Q-DLTS spectra obtained in both devices revealed at least five trap levels. The mean activation energies of traps are distributed in the range 0.17-0.85 eV within the band gap of the copolymers with capture cross sections of the order of 10^{-16} - 10^{-20} cm^2 . The trap densities are in the range of 10^{15} - 10^{16} cm^{-3} . The results show that incorporation of dyes into the copolymer resulted in creation of an additional electron trap level and an increase in the density of the existing trap levels, indicating a more disordered state of the emitting material containing chromophores [J1181]

"Enhancement of the light output power of InGaN/GaN light-emitting diodes grown on pyramidal patterned sapphire substrates in the micro- and nanoscale"

Sapphire substrates were patterned by a chemical wet etching technique in the micro- and nanoscale to enhance the light output power of InGaN/GaN light-emitting diodes (LEDs). InGaN/GaN LEDs on a pyramidal

patterned sapphire substrate in the microscale (MPSS) and pyramidal patterned sapphire substrate in the nanoscale (NPSS) were grown by metalorganic chemical vapor deposition. The characteristics of the LEDs fabricated on the MPSS and NPSS prepared by wet etching were studied and the light output powers of the LEDs fabricated on the MPSS and NPSS increased compared with that of the conventional LEDs fabricated on planar sapphire substrates. In comparison with the planar sapphire substrate, an enhancement in output power of about 29% and 48% is achieved with the MPSS and NPSS at an injection current of 20 mA, respectively. This significant enhancement is attributable to the improvement of the epitaxial quality of GaN-based epilayers and the improvement of the light extraction efficiency by patterned sapphire substrates. Additionally, the NPSS is more effective to enhance the light output power than the MPSS. [J1182]

"Electron mobility of 4,7-diphenyl-1,10-phenanthroline estimated by using space-charge-limited currents"

The electron mobility of 4,7-diphenyl-1,10-phenanthroline (BPhen) at various thicknesses (50-300nm) has been estimated by using space-charge-limited current measurements. The measured bulk mobility is in excellent agreement with results from time-of-flight method. It has been observed that the electron mobility of BPhen approaches its true value when the thickness is more than 150nm. The estimated electron mobility of BPhen at 300nm is found to be $3.4 \times 10^{-4} \text{ cm}^2/\text{Vs}$ (at 0.3MV/cm) with weak dependence on electric field. For thickness typical of organic light-emitting devices, the electron mobility of BPhen is also investigated. [J1183]

"Analysis of mass transport mechanism in InGaN epitaxy on ridge shaped selective area growth GaN by metal organic chemical vapor deposition"

In this work, the evolution of the InGaN layer growth on the ridge shaped GaN was studied. A mass transport model was presented to simulate the epitaxy process of the InGaN layer. The model consisted of two consecutive components, gas-phase diffusion process and surface diffusion process. The mean lifetime of adatoms on epitaxial surface was associated with their reaction rate in this model. An InGaN layer on ridge shaped GaN, including (0002) and {1122} facets, was grown by metal organic chemical vapor deposition to confirm the mass transport model. Gradient indium content distribution and inhomogeneous thickness of the InGaN layer were observed. Simulation of the InGaN layer growth process was performed by finite difference method with the mass transport model. By analyzing the results from calculations and experiments, the origins of the InGaN layer characteristics were attributed to the two diffusion components in the growth process. Surface diffusion resulted in the inhomogeneous thickness and gas-phase diffusion chiefly led to the gradient indium content. In addition, the adatoms reaction rate on epitaxial surface determined their mean lifetime as speculated by the analysis. The demonstration of the growth process of InGaN layer offers valuable insight in obtaining high efficiency white light emitting diodes by selective area growth technology. [J1184]

"High doping level in Mg-doped GaN layers grown at low temperature"

We have studied the properties of Mg-doped GaN epilayers grown by molecular beam epitaxy (MBE) with ammonia as nitrogen source. GaN p-n homojunctions have been developed to determine the optoelectronic characteristics of the junctions as a function of the p-type GaN growth conditions. It is shown that the electrical characteristics strongly depend on the Mg flux and the growth temperature. As a result, the junction characteristics have been drastically improved and state of the art MBE-grown p-type layers have been obtained: the hole concentration, the mobility, and the resistivity are $1.4 \times 10^{18} \text{ cm}^{-3}$, $9 \text{ cm}^2/\text{Vs}$, and $0.75 \Omega \text{ cm}$, respectively. These characteristics lead to an increase of the homojunction light emitting diode (LED) optical output power by two orders of magnitude. To further assess the quality of these MBE-grown p-type layers, we have prepared a hybrid LED which consists of an InGaN/GaN quantum well active structure grown by metal organic vapor phase epitaxy followed by a p-type region grown by MBE. An optical power in the milliwatt range at 20mA is demonstrated confirming thereby the quality of low temperature MBE-grown p-type layers. [J1185]

"Effects of bias on cathodoluminescence in ZnCdSe quantum well light emitting diodes"

Bias voltages applied to $\text{Zn}_{0.24}\text{Cd}_{0.76}\text{Se}$ quantum well light emitting diodes (QW-LEDs) affect both the intensity and wavelength of room temperature cathodoluminescence (CL). These effects have been studied experimentally and theoretically to advance understanding of the CL and optoelectronic behavior of these devices. QW CL intensity and photon energy are increased by forward bias, and they are decreased by reverse bias, with an exponential dependence of CL intensity on bias voltage from -1 to +1V and little dependence from 1.5 to 2.5 V. The p-n junction current and electroluminescence increase rapidly for forward bias greater than 2.34 V, the calculated built-in potential. The bias dependence of QW CL intensity is little affected when electron beam currents change by 300 times, from 0.1 to 29 nA with 10 kV beam voltage and 1 cm^2 irradiated area. The QW CL intensity increases sublinearly with beam current. Small hysteresis effects are seen in bias-dependent

CL intensity for low beam currents. The effects of bias voltage on CL intensity and photon energy have been modeled, including bias dependence of carrier transport, QW energy levels, wave functions, overlap integrals, internal electric fields, exciton ionization, and rates of carrier capture in and escape from the QW. For the QW-LED and experimental conditions used in this study, the bias dependence of CL intensity at room temperature results mainly from electric field dependence of exciton ionization and of electron and hole captures in the QW, and the bias dependence of CL photon energy results from field-dependent shifts in QW energy levels of electrons and holes. [J1186]

"Top-emitting organic light-emitting diodes with Ba /Ag /indium tin oxide cathode and built-in potential analyses in these devices"

Top-emitting organic light-emitting diodes (TEOLEDs) with a thin semitransparent conducting cathode (STCC) of Ba/Ag/indium tin oxide (ITO) were fabricated and their electric/optical characteristics were investigated. At the wavelength of 520nm, optical properties of STCC of the Ba(3nm)/Ag(15nm)/ITO (100nm) structure showed the transmittance of 63% and the reflectance of 37%. The light out-coupling properties of the TEOLED, which is composed of glass/Ag(150nm)/ITO (130nm)/4,4',4''-tris[2-naphthylphenyl-1-phenylamino]triphenylamine (2-TNATA, 30nm)/4,4'-bis[N-(1-naphthyl)-N-phenyl-amino]-biphenyl (18nm)/tris(8-quinolinolato)aluminum (III) (62nm)/Ba(xnm, x=3,2, and 1nm)/Ag(15nm)/ITO (100nm), was increased as the deposition thickness of Ba is increased. This driving performance of the devices could be interpreted on the base of carrier injection barrier by measuring built-in voltage as well as both the optical properties and electric properties of the cathode. The optical properties (e.g., transmittance and reflectance) and electric properties of all STCCs (Ba/Ag/ITO) used in this study were nearly equal. However, built-in voltage studied using modulated photocurrent technique was increased as the thickness of barium composing of STCC was increased. This rising of a built-in voltage means a lowering of barrier height for electron injection in the devices. [J1187]

"2.0 mcm electroluminescence from Si /Si 0.2 Ge 0.8 type II heterojunctions"

A metal-oxide-semiconductor tunneling diode is used to emit electroluminescence from a Si/Si_{0.2}Ge_{0.8} heterojunction. Besides the 1.1mcm and 1.6mcm infrared emission from the band edges of Si and SiGe, respectively, 2mcm infrared emission is also observed due to the radiative recombination between the electrons in the Si conduction band and the holes in the SiGe valence band. This type II recombination can emit photons whose energy is below the SiGe band gap to extend the emission range of Si/Ge-based light-emitting devices. The emission line shape can be fitted by the electron-hole-plasma recombination model. [J1188]

"Undercut structure fabricated by complementary-structure micropatterning technique for the passive-matrix display of organic light-emitting diodes"

This paper reports a new patterning method, the complementary-structure micropatterning (CSMP) technique, to fabricate the undercut structures for the passive-matrix display of organic light-emitting diodes (OLEDs). First, the polyvinylpyrrolidone (PVP) stripe patterns with a trapeziform cross-section were formed by micromolding in capillaries. Then the photoresist was spin coated on the substrate with the patterned PVP stripes and developed in water. The PVP was dissolved and lifted off from the substrate with the photoresist deposited on it, resulting in the undercut structures of the remaining photoresist. The undercut structures with different configurations were obtained by adjusting the photoresist thickness. The undercut structures were further used as separators in the patterning of the passive-matrix display of OLEDs. No visible performance difference was observed compared with OLEDs patterned by the traditional method. [J1189]

"Insights in junction photovoltage based sheet resistance measurements for advanced complementary metal-oxide semiconductor"

Earlier work has clearly shown that only a very few tools are able to measure reliably sheet resistances on advanced complementary metal-oxide semiconductor (CMOS) structures. One of these promising techniques is the junction photovoltage based technique, which uses a modulated light emitting diode to generate, in a millimeter size area of a single junction isolated structure, excess carriers which are separated by the underlying electrical field, and subsequently outdiffuse laterally. From the lateral variation in junction photovoltage, one can extract in a noncontact way the sheet resistance (R_s) of the top layer and the junction leakage (L) of the junction. First, a simplified theoretical solution of the underlying diffusion equations will be presented. Next, a recently developed simulation framework will be discussed, combining the SCILAB environment with SYNOPSIS/MEDICI device simulations, allowing for the detailed study of both ideal (in agreement with the theoretical solution) and less ideal advanced CMOS structures. Using this simulation framework, new insights will be proposed relating to the capability of R_sL to characterize the impact of the presence of oxide charges on the accuracy of the measurements, and the relevance of the R_sL leakage value for the actual diode (device) reverse bias

characteristics in the presence of an underlying halo/well implant. [J1190]

"Fully sealed carbon nanotube flat-panel light source and its application as thin film transistor-liquid-crystal display backlight"

The authors investigated a full sealed flat-panel light source, which is based on a triode structure with a metal mesh gate electrode and uses a carbon nanotube cold cathode. It has a flat surface luminance distribution with good uniformity, a stable luminance of 12000cd/m², and a luminous efficiency that was measured to be 14.5lm/W. It also shows a high color rendering index of 88 and a wide optical emission spectrum. Further, its application as thin film transistor-liquid-crystal display (TFT-LCD) backlight was demonstrated and the resulted performance of the TFT-LCD display was studied and compared to the commercial TFT-LCD products, which use the cold-cathode fluorescent lamp backlight and light emitting diode backlight. It is shown that the light transmission ratio in the TFT-LCD module using our light source is 8%, as compared to 4% of the commercial products. With this and the very high luminance, our light source is very useful to the situation, in which the TFT-LCD screen is employed to work under outdoor sunshine conditions. [J1191]

"Interfacial reactions between indium tin oxide and triphenylamine tetramer layers induced by photoirradiation"

The effects of photoirradiation on the interfacial chemical reactions between indium tin oxide (ITO) films and layers of triphenylamine tetramer (TPTE) were investigated by using in situ x-ray photoelectron spectroscopy (XPS). Thin TPTE layers deposited onto sputter-deposited ITO films were irradiated with violet light-emitting diodes (peak wavelength: 380 nm). Shifts in the peak positions of spectral components that originated in the organic layer toward the higher binding-energy side were observed in the XPS profiles during the early stages of irradiation. No further peak shifts were observed after additional irradiation. An increase in the ratio of the organic component in the O 1s spectra was also observed during the photoirradiation. The ratio of the organic component increased in proportion to the cube root of the irradiation time. These results suggest that photoirradiation induces an increase in the height of the carrier injection barrier at the interface between TPTE and ITO in the early stages of the irradiation, possibly due to the rapid diffusion controlled formation and growth of an oxidized TPTE layer, which is considered to act as a high resistance layer. [J1192]

"Measurement of the junction temperature in high-power light-emitting diodes from the high-energy wing of the electroluminescence band"

By using pulsed driving currents with a small duty cycle, the high-energy wing of the electroluminescence band in AlGaInP and InGaN high-power light-emitting diodes (LEDs) was calibrated to measure the junction temperature in the range of 223-358K. In a red AlGaInP LED with a thick active layer, an accuracy of 2% was achieved for the junction temperature derived from the high-energy slope in the spectral range free from parasitic absorption by taking into account the three-dimensional density of band states. Meanwhile, the far high-energy region of the slope distorted by parasitic absorption can be used for the extraction of the junction temperature by using only an appropriate linear correction procedure (7% accuracy). In a blue InGaN LED with multiple-quantum-well active layers, the junction temperature can be determined with an accuracy of 2% from the inverse derivative of the spectra in a narrow spectral region 150meV above the peak energy by using a linear correction. [J1193]

"Conductor grid optimization for luminance loss reduction in organic light emitting diodes"

The recently increased efficiency of organic light emitting devices (OLED) brings lighting applications within reach. If the area of the OLED is of the order a cm², voltage and brightness losses related to the square resistance of the transparent electrode become important. The homogeneity of the voltage and brightness can be improved by contacting the transparent electrode from all edges and by adding a metallic grid to the transparent electrode. This grid should have narrow lines to minimize transmission losses and improve the total light emission from the OLED. The voltage losses in grids with different shapes (triangular, square, and hexagonal) are evaluated and the grid parameters are optimized to maximize the total light emission. It turns out that a hexagonal grid has lower loss than a square grid with the same line width. [J1194]

"Field dependence of the carrier injection mechanisms in InGaN Quantum wells: Its effect on the luminescence properties of blue light emitting diodes"

Carrier injection and radiative recombination processes in InGaN/GaN blue light emitting diodes are investigated by bias-dependent cathodoluminescence. The samples are designed with a single-quantum-well (SQW) light emitter and an adjacent multi-quantum-well (MQW) carrier injector of lower In content. In unbiased samples, the

MQW emission dominates over the SQW at high temperatures ($T = 160\text{K}$) or low beam currents ($I_B = 5\text{nA}$). This is ascribed to changes in the device energy band diagram, dependent on the field in the p-n junction and on the level of electron beam induced excitation of excess carriers. A field screening, resulting in a forward biasing of the devices, is highlighted. A maximum value of $+2.65\text{V}$ is reached at $T=100\text{K}$ for a carrier generation rate $G_0 = 5.44 \times 10^{13}\text{s}^{-1}$. At a fixed electron beam power, the effects of an external applied field on the emitter efficiency are considered. The SQW emission is promoted in the forward-current regime, while in the reverse-current regime ($-1 \leq V < 2.65$ at $T=100\text{K}$) it undergoes a quenching of at least one order of magnitude and a blueshift (60meV at $T=100\text{K}$) due to a partial compensation between the junction field and the internal piezoelectric field (minimum residual field of about 1.9MV/cm at $T=100\text{K}$). The observed blueshift is in a fairly good agreement with the voltage dependence predicted by calculating the energy band profiles and SQW confined states with a self-consistent Schrodinger-Poisson solver. [J1195]

"A switched supply tunable red-green-blue light emitting diode driver"

This paper presents a new switched supply tunable red-green-blue (RGB) light emitting diode (LED) driver. The RGB LEDs act not only as light emitting devices but also as rectifying diodes in the presented driver circuit. The RGB LED color control is realized by controlling the switched supply voltage amplitude, frequency, and duty cycle. The driver efficiency is high since the only loss in the driver circuit is the switch and can be further reduced by direct alternate current supply. [J1196]

"A whole-field polariscope using a liquid crystal polarization rotator"

A novel polariscope using a liquid crystal (LC) polarization rotator is proposed for full-field subfringe photoelastic stress analysis. The system uses a light-emitting diode-based modified Senarmont polariscope with an added liquid crystal polarization rotator to generate phase shifts by applying suitable voltages to the LC element. Four phase shift polariscope images are captured and analyzed to get the stress distribution. A comparative study with the gray-field polariscope method which uses a rotating analyzer shows good agreement. [J1197]

"Improvement of a dynamic scanning force microscope for highest resolution imaging in ultrahigh vacuum"

We report on a modification of a commercial scanning force microscope (Omicron UHV AFM/STM) operated in noncontact mode (NC-AFM) at room temperature in ultrahigh vacuum yielding a decrease in the spectral noise density from 2757 to $272\text{fm}/\sqrt{\text{Hz}}$. The major part of the noise reduction is achieved by an exchange of the originally installed light emitting diode by a laser diode placed outside the vacuum, where the light is coupled into the ultrahigh vacuum chamber via an optical fiber. The setup is further improved by the use of preamplifiers having a bandpass characteristics tailored to the cantilever resonance frequency. The enhanced signal to noise ratio is demonstrated by a comparison of atomic resolution images on $\text{CeO}_2(111)$ obtained before and after the modification. [J1198]

"Development of a compact optical system for microarray scanning using a DVD pickup head"

We present a compact optical system using a commercially available DVD pickup head for microarray scanning. Our instrument successfully provides a low-cost, compact, and simple microarray scanning optical system in comparison to conventional ones due to the use of small-sized optical components and the implementation of a simple autofocus system using an embedded voice coil motor. The performance of this system was validated by using a microarray slide with spots of fluorescent dyes. It was confirmed that our optical head performed satisfactorily and was suitable for practical use in microarray scanners. This result provides evidence of the superiority of our microarray scanning optical system over conventional ones because of its space-saving properties and cost effectiveness. [J1199]

"Flexible organic light-emitting diodes with improved performance by insertion of an UV-sensitive layer"

A flexible organic light-emitting diode (FOLED) was fabricated on an indium tin oxide (ITO) plastic substrate by inserting an UV-curable epoxy resin as a buffer layer between the plastic substrate and ITO film. The structure of the FOLED devices was ITO/NPB (50nm)/Alq(50nm)/Mg:Ag(100nm). The surface morphology of three kinds of substrates was characterized by atomic force microscopy. The results show that with a spin-coated buffer layer, the surface roughness of ITO films on PET substrate decreased from 1.08 to 0.34nm . With the assistance of UV-sensitive resin, the adhesive force between the plastic substrate and ITO anode was significantly increased. The maximum luminance of FOLEDs was enhanced from 2720 to 4860cd/m^2 at 12V . [J1200]

"Portable light-emitting diode-based photometer with one-shot optochemical sensors for measurement in the field"

This report describes the electronics of a portable, low-cost, light-emitting diode (LED)-based photometer dedicated to one-shot optochemical sensors. Optical detection is made through a monolithic photodiode with an on-chip single-supply transimpedance amplifier that reduces some drawbacks such as leakage currents, interferences, and parasitic capacitances. The main instrument characteristics are its high light source stability and thermal correction. The former is obtained by means of the optical feedback from the LED polarization circuit, implementing a pseudo-two light beam scheme from a unique light source with a built-in beam splitter. The feedback loop has also been used to adjust the LED power in several ranges. Moreover, the low-thermal coefficient achieved ($-90\text{ppm}/^\circ\text{C}$) is compensated by thermal monitoring and calibration function compensation in the digital processing. The hand-held instrument directly gives the absorbance ratio used as the analytical parameter and the analyte concentration after programming the calibration function in the microcontroller. The application of this photometer for the determination of potassium and nitrate, using one-shot sensors with ionophore-based chemistries is also demonstrated, with a simple analytical methodology that shortens the analysis time, eliminating some calibrating solutions (HCl, NaOH, and buffer). Therefore, this compact instrument is suitable for real-time analyte determination and operation in the field. [J1201]

"Hyperthermal neutral beam sources for material processing (invited)"

Hyperthermal neutral beams have a great potential for material processes, especially for etching and thin film deposition for semiconductor and display fabrication as well as deposition for various thin film applications. Plasma-induced damage during plasma etching is a serious problem for manufacturing deep submicron semiconductor devices and is expected to be a problem for future nanoscale devices. Thermal and plasma-induced damage is also problematic for thin film depositions such as transparent conductive oxide films on organic light emitting diodes or flexible displays due to high temperature processes in plasma environments. These problems can be overcome by damage-free and low-temperature processes with hyperthermal neutral beams. We will present the status of the hyperthermal neutral beam development and the applications, especially, in semiconductor and display fabrication and introduce potential applications of thin film growing for optoelectronic devices such as light emitting diodes. [J1202]

"Enhanced light absorption in GaN/AlGaNMIR midinfrared detectors and application for pixel-less upconversion imaging"

Based on the experimental responsivity of single-period GaN/AlGaNMIR midinfrared (MIR) heterojunction interfacial work-function internal photoemission (HEIWIP) detectors, we have optimized in detail the single- and multiperiod GaN/AlGaNMIR HEIWIPs to enhance the light absorption in the detectors. The yielded parameters of emitter, intrinsic, and bottom contact layers could achieve large improvement of the MIR peak absorption efficiency in the multiperiod GaN/AlGaNMIR HEIWIPs. Employing the concept of photon frequency upconversion, we have further investigated the realization of MIR pixel-less upconversion imaging through the integration of GaN/AlGaNMIR HEIWIP with a GaN/AlGaNViolet light-emitting diode (LED). Under the optimized device structures, good imaging characteristics and high upconversion efficiency could be expected in the GaN/AlGaNHEIWIP-LED MIR upconverter. [J1203]

"Effects of high pressure annealing on the characteristics of solid phase crystallization poly-Si thin-film transistors"

Integrating circuits into organic light emitting diode displays require fabrication of polycrystalline silicon (poly-Si) based thin-film transistors (TFTs) on glass substrates. In this work we evaluated the use of high pressure annealing (HPA) process of poly-Si films in H_2O atmosphere to improve TFT characteristics via reducing defect density in poly-Si films. We attempted to develop a HPA process at temperatures below 600°C without causing any glass distortion and reducing the throughput. The HPA-treated poly-Si film was analyzed using various spectroscopic methods such as Raman, x-ray photoelectron spectroscopy, and transmission electron microscope, and the evaluation of the characteristics of TFTs fabricated by such poly-Si films was made. The heating at 550°C with 1MPa H_2O vapor increased the carrier mobility from 8.5 to $20\text{cm}^2/\text{Vs}$ and reduced the absolute value of the threshold voltage from 9.6 to 6.5V , as compared with the conventional solid phase crystallization (SPC) process. The sub-threshold swings also decreased from 1.2 to $0.8\text{V}/\text{decade}$. Since the realization of good performance in poly-Si depends on the defect density, the poly-Si formed by a combined process of SPC and HPA may be well suited for fabrication of poly-Si TFTs for flat panel displays such as liquid crystal display and active matrix organic light emitting diode that require circuit integration on panels. [J1204]

"Intrinsic luminance loss in phosphorescent small-molecule organic light emitting devices due to

bimolecular annihilation reactions"

Operational degradation of blue electrophosphorescent organic light emitting devices (OLEDs) is studied by examining the luminance loss, voltage rise, and emissive layer photoluminescence quenching that occur in electrically aged devices. Using a model where defect sites act as deep charge traps, nonradiative recombination centers, and luminescence quenchers, we show that the luminance loss and voltage rise dependence on time and current density are consistent with defect formation due primarily to exciton-polaron annihilation reactions. Defect densities 10^{18}cm^{-3} result in 50% luminance loss. Implications for the design of electrophosphorescent OLEDs with improved lifetime are discussed. [J1205]

"Characteristics of organic light-emitting diodes with conducting polymer anodes on plastic substrates"

The fabrication of conducting polymer films by a screen-printing method and characterization of an organic light-emitting diode (OLED) implemented using these films as an anode on plastic substrates are reported. Organic transparent electrode materials containing poly(3,4-ethylenedioxythiophene) (PEDOT) doped with poly(styrenesulfonic acid) (PSS) (PEDOT:PSS) were used after the modification by a unique nanoparticle binder design. The electro-optical properties as well as mechanical stabilities of these films were measured. The OLED performances when employing these films were comparable to that of OLEDs using indium tin oxide (ITO) despite their relatively poor conductivity. An external quantum efficiency of the OLED using this anode is 3.5%, which is about twice as that of OLEDs using ITO. These results show that the organic transparent electrode of a conducting polymer film patterned by the screen-printing method is a potential candidate for an electrode of the flexible OLED. [J1206]

"Blue organic light-emitting diodes based on Mes 2 B [Jp-4,4' -biphenyl-NPh(1-naphthyl)]"

Here, we report highly efficient blue organic light-emitting diodes (OLEDs) with Mes2B[p-4,4'-biphenyl-NPh(1-naphthyl)] (BNPB) as a blue emitter. It is found that both efficiencies and electroluminescent color are very sensitive to the selection of electron transport materials in the devices. For an optimized structure [indium tin oxide/2,3,5,6-tetrafluoro-7,7,8,8-tetracyanoquinodimethane (1nm)/N,N'-di(naphthalen-1-yl)-N,N'-diphenylbenzidine (45nm)/BNPB (20nm)/1,3,5-tris(2-N-phenylbenzimidazolyl) benzene (30nm)/LiF (1nm)/Al] with BNPB as an undoped blue emitter, a maximum current efficiency can reach 3.5cd/A. It is found that BNPB emits two distinct peaks, one of around 450nm and the other of 485nm, and their respective emission intensities depend on the nature of majority charge carrier in the emission layer. [J1207]

"Near-infrared organic light emitting diodes based on heavy metal phthalocyanines"

We demonstrate near-infrared (NIR) organic light-emitting diodes containing the phthalocyanines of copper (CuPc), palladium (PdPc), and platinum (PtPc) as emitting material. The devices show NIR emission from the triplet excitonic states of those phthalocyanines at 1095, 1025, and 966nm, respectively. A yellow singlet emitter serves as host for the emitter materials, reducing triplet exciton quenching and improving energy transfer to the emitter. Using the emitter PtPc as guest and the yellow singlet emitter as host, an external quantum efficiency of 0.3% is achieved for infrared light emission at 966nm. Due to the use of electrically doped charge transport layers, operation at voltages significantly below 3V is possible. Light output reaches 80 $\mu\text{W}/\text{cm}^2$ at a current density of 140 mA/cm^2 . [J1208]

"Magnetoresistance in triphenyl-diamine derivative blue organic light emitting devices"

Magnetoresistance measurements have been performed on thin layers of the triphenyl-diamine derivative, N,N'-diphenyl-N,N'-bis(3-methylphenyl)-(1,1'-biphenyl)-4,4'-diamine (TPD). At low drive voltages, where the current transport is solely hole mediated, no magnetoresistance is observed. At higher drive voltages, where electron injection into the TPD is occurring, magnetoresistance is seen and the sign of the magnetoresistance depends on the current density in the device. [J1209]

"High-refractive-index TiO₂-nanoparticle-loaded encapsulants for light-emitting diodes"

A high-refractive-index (high-n) encapsulant is highly desirable because it can result in enhancement of light-extraction efficiency from high-n semiconductor light-emitting diode (LED) chips. A uniform dispersion of TiO₂ nanoparticles in epoxy for LED encapsulation is demonstrated for surfactant-coated TiO₂ nanoparticles by drying, mixing with a solvent, refluxing, centrifuging, and mixing with epoxy. The refractive index of surfactant-coated TiO₂-nanoparticle-loaded epoxy is 1.67 at 500nm, significantly higher than that of conventional epoxy (n=1.53). Theoretical analysis of optical scattering in nanoparticle-loaded encapsulants reveals that the diameter of nanoparticles and the volume loading fraction of nanoparticles are of critical importance for optical scattering.

Quasispecular transparency of the encapsulant film can be achieved if the thickness of the film is kept below the optical scattering length. A graded-refractive-index multilayer encapsulation structure with the thickness of each layer being less than the mean optical scattering length is proposed in order to reduce optical losses from scattering and Fresnel reflection. Furthermore, three-dimensional optical ray-tracing simulations demonstrate that encapsulants with an optimized scattering coefficient, k_s , benefit from optical scattering by extracting deterministic trapped modes. Theoretical light-extraction enhancements larger than 50% are found when comparing scattering-free to scattering encapsulation materials. [J1210]

"Spin cast thin polymer interlayers in polymer light-emitting diodes: Thickness control through use of cross-linkable polymers"

The effect of very thin polymer interlayers made of either acid-initiated cross-linkable polyfluorenes or the parent non-cross-linkable polyfluorenes, on top of poly(3,4-ethylenedioxythiophene) doped with polystyrene sulfonic acid, on the efficiency of light-emitting diodes based on three different electroluminescent (EL) polymers is studied. We find that the use of non-cross-linkable polymers leads to the formation of interlayers with a thickness not exceeding 1 nm and their effect on the light-emitting diode characteristics is not directly correlated with the energetic position of the frontier levels, indicating that other effects, such as interfacial morphology and contact area, which may depend on the specific interlayer/EL polymer combination, play a significant role. When cross-linkable polymers are used, thicker interlayers are formed (up to about 7 nm), and their effect is better related to their frontier level energy. In particular, we found that with these interlayers, a quite significant EL efficiency increase can be obtained. [J1211]

"Tunneling entity in different injection regimes of InGaN light emitting diodes"

The forward I-V characteristics of InGaN-based light emitting diodes heteroepitaxially grown have previously been shown to be dominated by tunneling over a wide range of bias, as indicated by unrealistic values for the ideality factor. Comparison of the electrical characteristics in different bias regimes for InGaN light emitting diodes (LEDs) to expressions for the tunneling current enables one to achieve an understanding of the tunneling entities involved. At low bias for LEDs grown on sapphire, data are consistent with electron tunneling to deep levels in the vicinity of mixed/screw dislocations and are characterized by an energy near 200 meV. This component is absent for those devices homoepitaxially grown. In the intermediate bias regime, LEDs both heteroepitaxially and homoepitaxially grown exhibit a tunneling component that is proposed to be associated with the heavy hole tunneling via intermediate states and to have a characteristic energy near 80 meV. [J1212]

"Quantum efficiency of ambipolar light-emitting polymer field-effect transistors"

The emission characteristics and external quantum efficiencies of ambipolar polymer light-emitting field-effect transistors are investigated as a function of applied voltage, current density, and ratio of hole to electron mobility. Green-emitting poly(9,9-di-n-octylfluorene-alt-benzothiadiazole) (F8BT) with balanced electron and hole mobilities and red-emitting poly((9,9-dioctylfluorene)-2,7-diyl-alt-[4,7-bis(3-hexylthien-5-yl)-2,1,3-benzothiadiazole]-2',2''-diyl) (F8TBT) with strongly unbalanced hole and electron mobilities as semiconducting and emissive polymers are compared. The current-voltage and light output characteristics of the two types of light-emitting transistors were found to be fundamentally alike independent of mobility ratio. Device modeling allowing for a single (Langevin-type) charge recombination mechanism was able to reproduce the device characteristics for both cases but could not replicate the experimentally observed dependence of external quantum efficiency on current density. The increase of quantum efficiency with current density up to a saturation value could be indicative of a trap-assisted nonradiative decay mechanism at the semiconductor-dielectric interface. Optical output modeling confirmed that the maximum external quantum efficiency of F8BT light-emitting transistors of 0.8% is consistent with complete recombination of all charges and a singlet exciton fraction of 25%. [J1213]

"Triplet host engineering for triplet exciton management in phosphorescent organic light-emitting diodes"

The device performances of green phosphorescent organic light-emitting diodes with a triplet mixed host emitting layer were correlated with the energy levels and composition of the host materials. Two hole-transport-type host materials, (4,4'-N,N'-dicarbazole)biphenyl (CBP) and 4,4',4''-tris(N-carbazolyl)triphenylamine (TCTA), were combined with two electron-transport-type host materials, 1,3,5-tris(N-phenylbenzimidazole-2-yl)benzene (TPBI) and PH1. The maximum quantum efficiency was obtained in the 5:5 mixed host in the case of TCTA:TPBI and TCTA:PH1, while CBP:PH1 showed the best performances in the 9:1 mixed host. The quantum efficiency of the green mixed host devices was improved by more than 50% compared with that of the corresponding single host devices. [J1214]

"Electroluminescence characteristics of n -type matrix materials doped with iridium-based green and red phosphorescent emitters"

The electroluminescence characteristics of various n-type matrix materials with various orders of electron mobility doped with the phosphorescent green emitter fac-tris(2-phenylpyridine) iridium(III) [Ir(ppy)₃] and the phosphorescent red emitter bis(2-(2'-benzo [4,5-a] thienyl)pyridinato-N,C3')iridium(acetyl-acetonate) [btp2Ir(acac)] were evaluated and compared to those of the p-type 4,4''-N,N'-dicarbazole-biphenyl (CBP) reference matrix. For Ir(ppy)₃, the device with the n-type matrix 1,3,5-tris(N-phenylbenzimidazol-2-yl)benzene was found to have the highest efficiency and operational lifetime, whereas for btp2Ir(acac) the device with the p-type matrix CBP was found to have the highest efficiency. Our study of hole- and electron-dominant devices and analyses of electroluminescence spectra show that the main recombination zone position and the electron-hole balance change as the matrix material changes, resulting in changes in the characteristics of the organic light emitting diodes. [J1215]

"A model for the thermal degradation of metal/(p-Ga N) interface in GaN-based light emitting diodes"

This paper analyzes the thermal degradation of GaN-based light emitting diodes with hydrogen-rich passivation layer by combined capacitance and current measurements. The decrease of optical power arising during thermal treatment at T=250°C is well related to a decrease in the high-frequency capacitance and to the generation of a further peak in the conductance/frequency curves. Deep level transient spectroscopy measurements excluded the role of further deep levels introduced/generated in the p-n junction region. Transmission line method analysis showed that stress induces nonlinearity of the characteristics of the contacts, related to the increase of Ohmic contact resistivity. All these modifications are explained using a small-signal model in which a parasitic impedance arises as a consequence of stress in the portion of metal/(p-GaN) interface exposed to diffusion of hydrogen from the passivation layer. Therefore, degradation is shown to be related to the worsening of the properties of the metal/semiconductor interface at the p-side of the diode, due to the interaction between the hydrogen-rich passivation layer and the acceptor dopant. This interaction is well confined to the immediate proximity of the interface, leaving the activated acceptor concentration in the bulk almost unaffected. [J1216]

"Influence of exposure to 980 nm laser radiation on the luminescence of Si:Er/O light-emitting diodes"

Erbium (Er) codoping with oxygen (O) in Si is a well-known method for producing electroluminescent material radiating at 1.54 μm through a 4f shell transition of Er³⁺ ions. In this work the influence of exposure to 980 nm radiation on the electroluminescence (EL) of reverse biased Si:Er/O light-emitting diodes (LEDs), which give a strong room temperature 1.54 μm intensity, is presented and discussed. All the device layers, including Er/O doped Si sandwiched between two Si_{0.82}Ge_{0.18} layers, have been grown on silicon on insulator substrates using molecular beam epitaxy and processed to fabricate edge emitting Si:Er/O waveguide LEDs. Electromagnetic mode confinement simulations have been performed to optimize the layer parameters for waveguiding. The temperature dependence of the 1.54 μm EL intensity exhibits an abnormal temperature quenching with a peak near -30 °C, and at -160 °C it has decreased by a factor of 5. However, irradiating the devices with a 980 nm laser gives an enhancement of the 1.54 μm EL intensity, which is more dramatic at low temperatures (e.g., -200 °C) where the quenched EL signal is increased up to almost the same level as at room temperature. The enhancement of the EL intensity is attributed to the photocurrent generated by the 980 nm laser, reducing the detrimental avalanche current. [J1217]

"p -type doping in organic light emitting diodes based on fluorinated C60"

We report on hybrid organic light emitting diodes based on spin coated PVK (poly(vinylcarbazole))/poly-TPD (poly(triphenylamine)) formulation electron blocking and conjugated peptide emitter layers while the hole blocking, BCP (2,9-dimethyl-4,7-diphenyl-1,10-phenanthroline), layer is vacuum sublimed. The device structure is realized through the use of fluorinated C60 as a p-dopant in a cross-linked hole transporting formulation. The lowering of the turn-on voltage is demonstrated using a conjugated peptide as the emitter layer. We suggest that fluorinated C60s could play a major role as tunable dopants in organic electronics. [J1218]

"Fabrication of Ag-tetracyanoquinodimethane nanostructures using ink-jet printing/vapor-solid chemical reaction process"

In this study, microscale patterns of the charge-transfer organic compound silver-tetracyanoquinodimethane (Ag-TCNQ) were prepared using a novel two-step ink-jet printing/vapor-solid chemical reaction process. First, silver nanoparticles were patterned on silicon using a piezoelectric ink-jet printer. Ag-TCNQ nanostructures were then

processed on these patterned surfaces using a vapor-solid chemical reaction growth process. Scanning electron microscopy revealed that 50-100nmwide, 2mcmlong Ag-TCNQ nanocones, crystallites, and ribbons were fabricated using this two-step process. Patterns with a higher number density of silver nanoparticles demonstrated a greater number of nanocone structures. Micro-Raman spectroscopy results confirmed charge transfer between silver and TCNQ in the Ag-TCNQ nanostructure. Patterned Ag-TCNQ nanostructures fabricated using this novel two-step ink-jet printing/vapor-solid chemical reaction process could find use in high density, high-speed optical memory devices, magnetic devices, field effect transistors, organic light emitting diodes, metal/insulator/metal photoswitches, biosensors, and other advanced devices. [J1219]

"Light extraction and optical loss mechanisms in organic light-emitting diodes: Influence of the emitter quantum efficiency"

The internal quantum efficiency of organic light-emitting diodes (OLEDs) can reach values close to 100% if phosphorescent emitters to harvest triplet excitons are used; however, the fraction of light that is actually leaving the device is considerably less. Loss mechanisms are, for example, waveguiding in the organic layers and the substrate as well as the excitation of surface plasmon polaritons at metallic electrodes. Additionally, absorption in the organic layers and the electrodes can play a role. In this work we use numerical simulations to identify and quantify different loss mechanisms. Changing simulation parameters, for example, the distance of the emitter material to the cathode or thicknesses of the various layers, enables us to study their influence on the fraction of light leaving the OLED. An important parameter in these simulations and for the actual device is the radiative quantum efficiency q , which is defined as the efficiency of radiative exciton decay in an unbounded space filled by the emitting dye and its matrix. The simulations show that due to microcavity effects the radiative decay channel can be considerably changed in an OLED as compared to free space emission of a dipole. Thus the knowledge of the radiative quantum efficiency is crucial for the optimization of OLEDs. As an example, we present simulations of bottom-emitting OLEDs based on the well-known green emitter tris-(8-hydroxyquinoline) aluminum with transparent indium tin oxide anode and a calcium/aluminum cathode. [J1220]

"Reduced efficiency roll-off in phosphorescent organic light emitting diodes at ultrahigh current densities by suppression of triplet-polaron quenching"

High-performance phosphorescent organic light emitting devices with reduced efficiency roll-off at ultrahigh current densities were realized. The devices were Ir(ppy)₃-based phosphorescent organic light emitting diodes that employed 1,3-bis[2-(2,2'-bipyridine-6-yl)-1,3,4-oxadiazole-5-yl]benzene as a high mobility electron transfer layer. The device's brightness was enhanced while the efficiency roll-off was reduced. The device exhibits high current efficiency (21cd/A) at high brightness (80000cd/m²), with a maximum luminescence of 136000cd/m² at over 1A/m² (with an efficiency of 13cd/A). This reduction in efficiency roll-off is attributed to the suppression of the triplet-polaron quenching rate through balancing the charge carrier ratio in the device. [J1221]

"A broadband absorption spectrometer using light emitting diodes for ultrasensitive, in situ trace gas detection"

A broadband absorption spectrometer has been developed for highly sensitive and target-selective in situ trace gas measurements. The instrument employs two distinct modes of operation: (i) broadband cavity enhanced absorption spectroscopy (BBCEAS) is used to quantify the concentration of gases in sample mixtures from their characteristic absorption features, and (ii) periodic measurements of the cavity mirrors' reflectivity are made using step-scan phase shift cavity ringdown spectroscopy (PSCRDS). The latter PSCRDS method provides a stand-alone alternative to the more usual method of determining mirror reflectivities by measuring BBCEAS absorption spectra for calibration samples of known composition. Moreover, the instrument's two modes of operation use light from the same light emitting diode transmitted through the cavity in the same optical alignment, hence minimizing the potential for systematic errors between mirror reflectivity determinations and concentration measurements. The ability of the instrument to quantify absorber concentrations is tested in instrument intercomparison exercises for NO₂ (versus a laser broadband cavity ringdown spectrometer) and for H₂O (versus a commercial hygrometer). A method is also proposed for calculating effective absorption cross sections for fitting the differential structure in BBCEAS spectra due to strong, narrow absorption lines that are under-resolved and hence exhibit non-Beer-Lambert law behavior at the resolution of the BBCEAS measurements. This approach is tested on BBCEAS spectra of water vapor's 4v+delta absorption bands around 650 nm. The most immediate analytical application of the present instrument is in quantifying the concentration of reactive trace gases in the ambient atmosphere. The instrument's detection limits for NO₃ as a function of integration time are considered in detail using an Allan variance analysis. Experiments under laboratory conditions produce a 1sigma detection limit of 0.25 pptv for a 10 s acquisition time, which improves with further signal averaging to 0.09 pptv in 400 s. Finally, an example of the instrument's performance under field work conditions is presented, in this case of measurements of the sum of NO₃+N₂O₅ concentrations in the marine boundary layer acquired during the

Reactive Halogens in the Marine Boundary Layer field campaign. [J1222]

"Enhanced efficiency and reduced spectral shift of green light-emitting-diode epitaxial structure with prestrained growth"

The enhanced emission efficiency and reduced spectral shifts of a green InGaN/GaN quantum-well (QW) light-emitting-diode epitaxial structure by using the prestrained growth technique when compared with a control sample of the same emission spectrum with conventional growth are demonstrated. By adding an 7%-indium InGaN/GaN QW to the structure before the growth of designated emitting high-indium QWs, the growth temperature of the emitting QWs can be raised by 30 °C while keeping about the same emission wavelength around 544 nm in photoluminescence (PL) and 525 nm in electroluminescence (EL). The internal quantum efficiency, room-temperature PL intensity, and EL intensity at the injection current of 20 mA are increased by 167%, 140%, and 182%, respectively. Also, the spectral blueshift range in increasing injection current in the range of 50 mA is decreased by 46%. Based on the pump-power dependent PL measurement, it is found that the quantum-confined Stark effect (QCSE) becomes weaker in the prestrained growth sample. Also, from the calibration of the Arrhenius plots, the carrier localization effect is observed to become weaker under prestrained growth. Therefore, the enhanced emission efficiency is mainly attributed to the decreased defect density and the reduced QCSE in the prestrained sample. [J1223]

"Light extraction enhancement of GaN-based light emitting diodes using MgF₂/Al omnidirectional reflectors"

We report on the enhancement of the light extraction of GaN-based light emitting diodes (LEDs) by using MgF₂/Al omnidirectional reflectors (ODRs). The ODRs consisting of a quarter-wavelength-thick MgF₂ having a refractive index of 1.39 and Al metal produce a high-angle-integrated reflectivity of 96.6%. To optimize the electrical injection and light reflection, the MgF₂/Al ODRs are combined with Pd/Ag metallic reflectors using mesh configuration. Compared to reference LEDs, LEDs fabricated with the MgF₂/Al ODRs show an enhanced output power by 23% and a slight increase in the forward voltage by 0.18 V, leading to the improvement in power efficiency by 17%. [J1224]

"Surface modification of ZnO film by hydrogen peroxide solution"

The effect of hydrogen peroxide (H₂O₂) treatment on the microstructure and luminescent properties of ZnO thin films has been investigated. Governed by high-resolution transmission electron microscopy and selected-area electron diffraction patterns, the oxygen radicals dissociated from H₂O₂ solution at room temperature and substantially changed the polycrystalline ZnO film into an insulator. In addition, the photoluminescence spectra showed that H₂O₂ solution had nearly no effect on the intensity of ultraviolet emission, whereas it significantly enhanced the intensity of deep-level emission. These observations strongly reveal the fact that the oxygen radicals penetrating into a ZnO film are reasonably speculated to occupy the interstitial sites to form oxygen interstitials or fill the Zn vacancies to form antisite oxygen O_{Zn} defects. Because of these extra defects involved, an enhancement of the green light luminescence is significantly promoted in our ZnO samples after handling with H₂O₂ solution. Based on the characteristics mentioned above, our hydrogen peroxide solution treated ZnO film has the potential for applying to the light-emitting diode with metal-insulator-semiconductor structure. [J1225]

"Electroluminescent characteristics of scandium and yttrium 8-quinolinolates"

Efficient electroluminescence (EL) was obtained in organic light-emitting devices using 8-quinolinolate complexes of scandium (Scq₃) and yttrium (Yq₃) as emitters. Compared to the device based on the analogous Alq₃ complex, no notable difference in the EL performances of the Yq₃ device can be found; however, the EL characteristics of device with Scq₃ were significantly enhanced. The device with the configuration of indium tin oxide/ N,N'-bis(3-methylphenyl)-N,N'-diphenylbenzidine/Scq₃/Yb exhibits a maximum current efficiency of 4.6 cd/A and a maximum power efficiency of 2.6 lm/W at a luminance of 300 cd/m². The improvement of the performance of this device should be attributed to the higher hole mobility of the Scq₃ as compared to Alq₃ or a smaller barrier for hole injection into Scq₃ compared to Alq₃. [J1226]

"GaN-based microdisk light emitting diodes on (111)-oriented nanosilicon-on-insulator templates"

InGaN/GaN microdisk light emitting diodes (LEDs) on (111)-oriented nanosilicon-on-insulator (nano-SOI) substrates are demonstrated. The (111)-oriented thin SOI substrates are prepared by separation by implantation of oxygen (SIMOX) method. The InGaN/GaN LED structures are grown on these SIMOX templates by metal-organic chemical vapor deposition. The circular mesa patterns are created by standard LED processing steps

including photolithography, inductively coupled plasma etching, and contact metallization. Due to the reflectivity changes at the bottom Si/SiO₂ interfaces beneath AlN buffer, an improved light extraction from these LEDs has been observed. The room-temperature electroluminescence (EL) spectrum of the microdisk LEDs on SOI shows multiple interference peaks due to the reflections at the Fabry-Perot boundaries and such effect resulted in an increased integrated EL intensity. For a comparative analysis of light extraction with respect to similar LED structures grown on bulk Si(111), a detailed reflectivity analysis has been carried out to verify the LED structures and to model the EL lineshapes. [J1227]

"Patterning of polyfluorene based polymer light emitting diodes by reversal imprint lithography"

The authors demonstrated the fabrication of patterned arrays of polymer light emitting diodes (PLEDs) with a polyfluorene based emissive layer using reversal imprint lithography. A stack of patterned metal and polymer films is transferred to a glass substrate in a single reversal imprint step. Two different techniques for coating the patterned Si mold are shown, one involving the spin coating of polymer layers directly onto the mold and one involving inking of the polymers onto the mold from a spin-coated PDMS inkpad. Using these techniques, PLED devices with a minimum feature sizes as small as 1 μm and luminescence starting at 3.5 V have been demonstrated. [J1228]

"Dependence of spectral behavior in an InGaN/GaN quantum-well light-emitting diode on the prestrained barrier thickness"

The dependencies of output spectral overall redshift and current-density-induced spectral blueshift on the prestrained barrier thickness in the InGaN/GaN quantum-well light-emitting diodes (LEDs) of prestrained growth are demonstrated. Due to the stronger prestrain effect in a sample of a thinner prestrained barrier, the overall spectral redshift range increases and the current-density-induced blueshift range decreases with decreasing prestrained barrier thickness. Also, in terms of device resistance and saturation current, the LED performances of prestrained samples are superior to that of a conventional LED. With a thinner prestrained barrier, the device performance becomes better. The results are attributed to the higher average-indium content and stronger indium-rich clustering behavior in a sample of stronger prestrain. Such attributions are supported by the observations of strain state analysis in transmission electron microscopy measurements. [J1229]

"Moisture exposure to different layers in organic light-emitting diodes and the effect on electroluminescence characteristics"

Moisture effect on electroluminescence characteristics, including current density versus voltage, luminance versus voltage, luminous efficiency versus current density, dark spot formation, and operational stability of organic light-emitting diodes, has been systematically investigated by exposing each layer of the devices to moisture at room temperature. Moisture has a different effect on each of the interfaces or surfaces, and the influence increases as exposure time increases. There is a slight effect on the electroluminescence characteristics after the anode surface has been exposed to moisture. However, severe luminance decrease, dark spot formation, and operational stability degradation take place after the light-emitting layer or the electron-transporting layer is exposed to moisture. It is also demonstrated that the effect of moisture can be substantially reduced if the exposure to moisture is in a dark environment. [J1230]

"High-efficiency endothermic energy transfer in polymeric light-emitting devices based on cyclometalated Ir complexes"

We report polymeric light-emitting diodes (PLEDs) made from pinene-substituted iridium(III) phosphorescent dopants: tris(5-(4-difluoro phenyl)-10,10-dimethyl-4-aza-tricycloundeca-2,4,6-triene) iridium (III) [Ir(F-pppy)₃] and tris(5-(2,4-difluorophenyl)-10,10-dimethyl-4-aza-tricycloundeca-2,4,6-triene) iridium (III) [Ir(F2-pppy)₃]. The pinene substitution introduces steric hindrance to molecular structure of the dopant that reduces triplet-triplet annihilation between dopants and consequently enhances device performance. Via endothermic energy transfer from poly(vinylcarbazole) to Ir(F-pppy)₃ and Ir(F2-pppy)₃, a peak electroluminescent efficiency of 32.8 cd/A or 12.3 cd/A at 12 wt% Ir(F-pppy)₃ or 15 wt% Ir(F2-pppy)₃ doped and solution-processed PLEDs have been obtained. These values represent significant improvement in performance over previously reported endothermic energy-transfer based electrophosphorescent devices. [J1231]

"Transparent organic light-emitting diodes consisting of a metal oxide multilayer cathode"

The authors have developed a semitransparent, multilayered cathode of indium tin oxide (ITO)/Ag/tungsten oxide (WO₃) for transparent organic light-emitting diodes. The device showed a weak negative differential resistance (NDR), until the operating voltage of 8 V was reached. NDR was due to the resonant tunneling by both the

quantum barrier and quantum well. The silver oxide (Ag₂O) on the Ag metal was confirmed by x-ray photoelectron spectroscopy, and the energy levels of Ag₂O were quantized due to the quantum size effect and this produced the resonant tunneling channels. The device using ITO/Ag/WO₃ with a LiF/Al bilayer was superior to those devices which only used ITO or WO₃, mainly because the out coupling was enhanced by employing a WO₃ material, which is much more transparent than ITO. [J1232]

"Stable efficiency roll-off in phosphorescent organic light-emitting diodes"

Origin of efficiency roll-off in phosphorescent organic light-emitting diodes was investigated with triplet mixed host devices and stable devices with little efficiency roll-off was developed. Efficiency roll-off was significant in the device with narrow recombination zone (RZ) and charge leakage out of emitting layer at high luminance was critical to efficiency roll-off. Efficiency roll-off could be reduced in triplet mixed host device with broad RZ and little charge leakage at high driving voltage. Triplet mixed host devices with an exciton blocking layer showed a quantum efficiency over 90% of maximum quantum efficiency at a luminance of 20000 cd/m². [J1233]

"Mist fabrication of light emitting diodes with colloidal nanocrystal quantum dots"

In this letter, we report a mist-deposition process for the assembly and patterning of nanocrystal quantum dots (NQDs) during the fabrication of quantum dot light emitting diodes (QD-LEDs), which allows for tight controls over the thickness, surface morphology, composition, and resolution of NQD emissive layers. A defect-free featuring uniform brightness QD-LED containing a mist-deposited emissive CdSe(ZnS) NQD layer was demonstrated. Additionally, the technique of successive mist deposition of multicolor NQDs through a set of registered shallow masks was employed to create a 646 matrix of alternating pixels composed of 5 nm diameter CdSe(ZnS) NQDs (green) and 8 nm diameter CdSe(ZnS) NQDs (red) on the same substrate. The results obtained demonstrate the potential of mist-deposition technology in the future development of full-color QD-LED displays. [J1234]

"Physical properties and efficiency of GaNP light emitting diodes"

GaNP/GaP is promising for yellow-amber-red light emitting diodes (LEDs). In this study, pressure and temperature dependent electroluminescence and photocurrent measurements on bulk GaP/GaN_{0.006}P_{0.994}/GaP LED structures are presented. Below 110 K, emission is observed from several localized nitrogen states. At room temperature, the band-edge energy increases weakly with pressure at a rate of +1.6 meV/kbar, substantially lower than the Gamma band gap of GaP (+9.5 meV/kbar). Thus, despite the multiplicity of nitrogen levels, the band anticrossing model reasonably describes this system based on an average of the nitrogen states. Furthermore, carrier leakage into the X minima of GaP reduces the efficiency in GaNP-LEDs with increasing pressure. [J1235]

"A Sn-based metal substrate technology for the fabrication of vertical-structured GaN-based light-emitting diodes"

Through the use of tin (Sn) based solder balls and patterned laser lift-off technique, a metal substrate technology was proposed for the fabrication of vertical-structured metal substrate GaN-based light-emitting diodes (VM-LEDs). Advantages including reserving the merits of metallic substrate and simplifying the fabrication processes of vertical-structured GaN-based LEDs were demonstrated. As compared to conventional sapphire substrate GaN-based LEDs, the fabricated VM-LEDs with an emission area of 6204620 μm² show an increase in light output power about 145.36% at 350 mA with a significant decrease in forward voltage from 4.51 to 3.46 V. [J1236]

"Phosphor-conversion white light using InGaN ultraviolet laser diode"

We fabricated a phosphor-conversion white light using an InGaN laser diode that emits 405 nm near-ultraviolet (n-UV) light and phosphors that emit in the blue and yellow regions when excited by the n-UV and blue light, respectively. The relationship of the luminous flux and the luminous efficacy of the white light with injection current was discussed. The luminous flux increased linearly with increasing current above the threshold of the laser diode, and at 80 mA injection current, the luminous flux and luminous efficacy were estimated to be 5.7 lm and 13 lm/w, respectively. The shift of the Commission International de l'Eclairage coordinates, color temperature, and color rendering index with current are very slight and negligible, which indicates that the blue and the yellow phosphors have an excellent stability and a highly stable white light can be obtained by this way. [J1237]

"Light extraction enhancement of InGaN light-emitting diode by roughening both undoped micropillar-structure GaN and p-GaN as well as employing an omnidirectional reflector"

Light extraction enhancement of InGaN-GaN light-emitting diode (LED) is demonstrated with double-side roughening both on the p-GaN surface and the micropillar undoped GaN as well as an omnidirectional reflector via patterning sapphire substrate, wafer-bonding, laser lift-off, and chemical wet etching technologies. This device design enhances the light output power up to 77% compared to the conventional LED with a single roughened p-GaN on patterned sapphire substrate at an injection current of 350mA. Due to the employment of Si carrier, the junction temperature measurement at 350mA yields a 46.6°C lower than that of the conventional LEDs. [J1238]

"Emission color tunable light-emitting diodes composed of InGaN multifacet quantum wells"

We demonstrate that the apparent emission colors of InGaN-based light-emitting diodes using microstructured multifacet quantum wells as active layers can externally be controlled over a wide spectral range that encompasses green to blue or white at a color temperature of 4000K to blue along the Planckian locus. The controllability relies on facet-dependent polychromatic emissions. The pulsed current operation with the appropriate duties varied their relative intensities and the consequent apparent colors without seriously affecting the total number of emitted photons, particularly for the blue to green variation. [J1239]

"Highly efficient polarized polymer light-emitting diodes utilizing oriented films of beta -phase poly(9,9-dioctylfluorene)"

Uniaxially oriented films of beta -phase poly(9,9-dioctylfluorene) (PFO) were realized by a friction-transfer technique followed by thermal annealing and vapor treatments. Absorption and photoluminescence (PL) spectra show the characteristics of beta -phase: an additional absorption peak at 433nm and redshifted PL peaks compared with those of the usual nematic (N) phase. We fabricated polarized polymer light-emitting diodes utilizing oriented films of beta -phase PFO. Highly polarized beta -phase emission with an integrated polarization ratio of 51 was observed from the devices. The efficiency of the devices based on beta -phase reached 2.0cd/A, which is two times higher than that based on N-phase. [J1240]

"Enhanced light extraction efficiency in flip-chip GaN light-emitting diodes with diffuse Ag reflector on nanotextured indium-tin oxide"

We investigated a flip-chip light emitting diode (FCLED) with a diffuse reflector fabricated by depositing a Ag film on a nanotextured indium-tin oxide (ITO) layer. The FCLED with a diffuse Ag reflector showed remarkably good adhesion and high reflectance than that with a specular Ag reflector deposited on the planar ITO layer. The optical output power of FCLED with the diffuse Ag reflector was enhanced by 161.3% at 300mA compared to that with the specular Ag reflector. [J1241]

"Barrier effect on hole transport and carrier distribution in In Ga N /Ga N multiple quantum well visible light-emitting diodes"

Carrier distributions governed by hole transport in InGaN/GaN multiple quantum well (MQW) visible light-emitting diodes (LEDs) were investigated using conventional blue LEDs and dual-wavelength blue-green LEDs. It was found that holes were dominantly distributed in the QW close to the p-GaN layer in LEDs with conventional MQW active regions at a current of 20mA. A decrease in the thickness or the height of the quantum-well potential barrier enhanced hole injection into the MQWs located near the n-GaN layer. Reducing the thickness of a GaN quantum-well barrier between the blue QW and green QW did not degrade the electroluminescence (EL) intensity of the LED. In contrast, reducing the potential height of the barrier with material of possibly compromised quality resulted in a degradation of the EL intensity of the LED. [J1242]

"Rendering a color palette by light-emitting diodes"

We present a new approach to the optimization of sources of white light based on colored light-emitting diodes (LEDs) and show that a pentachromatic source composed of LEDs with the equidistant peak wavelengths at about 450, 500, 550, 600, and 650nm renders all 1269 colors of the Munsell palette almost indistinguishably from daylight. [J1243]

"Room temperature electrical spin injection in remanence"

We demonstrate electrical spin injection from ferromagnetic Fe/Tb multilayer structures with remanent perpendicular magnetization into GaAs-based light-emitting diodes at room temperature. Using a reverse-biased Schottky contact and a MgO tunnel contact, respectively, we achieve spin injection at remanence. The maximum degree of circular polarization of the emitted light is 3% at room temperature. [J1244]

"Energy transfer in hybrid quantum dot light-emitting diodes"

Energy transfer in a host-guest system consisting of a blue-emitting poly(2,7-spirofluorene) (PSF) donor and red-emitting CdSe/ZnS core-shell quantum dots (QDs) as acceptor is investigated in solid films, using time-resolved optical spectroscopy, and in electroluminescent diodes. In the QD:PSF composite films, the Forster radius for energy transfer is found to be 4-6nm. In electroluminescent devices lacking an electron transport layer, the electroluminescence (EL) spectrum of the QD:PSF polymer composite is similar to the photoluminescence (PL), giving evidence for energy transfer from PSF to the QDs. The addition of an electron transport layer between the emitting layer and the cathode results in a significant change in the EL spectrum and a considerable improved device performance, providing almost pure monochromatic emission at 630nm with a luminance efficiency of 0.32cd/A. The change in spectrum signifies that the electron transport layer changes the dominant pathway for QD emission from energy transfer from the polymer host to direct electron-hole recombination on the QDs. [J1245]

"Long-lifetime thin-film encapsulated organic light-emitting diodes"

Multiple fluorocarbon (CF_x) and silicon nitride (Si₃N₄) bilayers were applied as encapsulation cap on glass-based organic light-emitting diodes (OLEDs). When CF_x/Si₃N₄ bilayers were deposited onto the OLED structure, the devices showed performance worse than one without any encapsulation. The adverse effects were attributed to the damage caused by reaction species during the thin-film deposition processes. To solve this problem, a CuPc interlayer was found to provide effective protection to the OLED structure. With a structure of CuPc/(CF_x/Si₃N₄)₄₅, the encapsulated device showed an operation lifetime over 8000 h (higher than 80% of that achieved with a conventional metal encapsulation). [J1246]

"Influence of charge balance and exciton distribution on efficiency and lifetime of phosphorescent organic light-emitting devices"

We discuss the importance of appropriate charge carrier confinement and exciton management for the realization of highly efficient and stable organic light-emitting diodes (OLEDs). As an example, we choose red p-i-n-type OLEDs based on the iridium-based electrophosphorescent emitter Ir(MDQ)₂(acac) doped in α-NPD as host material. We show how an appropriate choice of the hole blocking layer material allows external quantum efficiencies as high as 20% for this emitter. At the same time, the display-relevant brightness of 100cd/m² is reached at an operation voltage of only 2.4 V, which is close to the thermodynamic limit. As a result, a high total power efficiency of 37.5lm/W at 100cd/m² is reached. In a further step, we study the influence of the blocker materials on device lifetime. We investigate the chemical reactions causing the degradation process by use of matrix assisted laser desorption time-of-flight mass spectrometry. It can be shown that discovered degradation reactions can be suppressed by an appropriate choice of the hole blocking material. [J1247]

"Comparison of Alq₃/alkali-metal fluoride/Al cathodes for organic electroluminescent devices"

The tris-(8-hydroxy-quinolinato) aluminum (Alq₃)/LiF/Al cathode is one of the most studied interfaces in organic electronics. Charge injection properties of the other alkali-metal fluorides (i.e., NaF, KF, RbF and CsF) at the Alq₃/electron injection layer/Al cathode interface of organic light emitting diodes were studied. It is found, in contrast to most literature, that the alkali-metal fluorides all yield equivalent device performance, despite the significant difference in the physicochemical properties of these metal fluorides. The observed phenomena are explained by the comparable strong intrinsic molecular dipole moment of these fluorides, which result in strong interfacial dipoles at the Alq₃/Al interface. This is consistent with ultraviolet photoelectron spectroscopy results and recent theory in literature. Difference in thickness dependence was also observed. LiF is found to be unique amongst the alkali-metal fluorides in terms of the thickness dependence of the device performance. This trend is found to strongly correlate with the growth mode of the metal fluoride on the Alq₃ surface; LiF quickly transitions to layer-by-layer growth after the initial island nucleation, while the other alkali-metal fluorides tend to grow as clustered islands on top of a surface wetting layer. [J1248]

"Luminescence quenching in low doped polymer light-emitting diodes"

Transient luminescent dynamics in low doped porphyrin side-chain polymer film, poly(porphyrin acrylate-styrene) (P[(por)A-S]), were measured by using time-resolved photoluminescence spectroscopic technology. At relative higher intrachain porphyrin comonomer concentration (0.27%), the transient luminescence relaxation becomes more rapid with the increase in the interchain polymer concentration, resulting in low luminescence efficiency. The origin has been analyzed according to the Forster-type bimolecular annihilation theory. However, at the porphyrin comonomer concentration (0.1%), the luminescence relaxation of the P[(por)A-S] film becomes faster with the decrease in the interchain polymer concentration, inducing lower luminescence efficiency. The

luminescence quenching has been analyzed according to the theory of MM+force field and exciton rotational diffusion. The theoretical analyses are in good agreement with the experimental results. [J1249]

"High-efficiency, low-voltage phosphorescent organic light-emitting diode devices with mixed host"

We report high-efficiency, low-voltage phosphorescent green and blue organic light-emitting diode (PHOLED) devices using mixed-host materials in the light-emitting layer (LEL) and various combinations of electron-injecting and electron-transporting layers. The low voltage does not rely on doping of the charge-transport layers. The mixed LEL architecture offers significantly improved efficiency and voltage compared to conventional PHOLEDs with neat hosts, in part by loosening the connection between the electrical band gap and the triplet energy. Bulk recombination in the LEL occurs within 10 nm of the interface with an electron-blocking layer. A "hole-blocking layer" need not have hole- or triplet-exciton-blocking properties. Optical microcavity effects on the spectrum and efficiency were used to locate the recombination zone. The effect of layer thickness on drive voltage was used to determine the voltage budget of a typical device. The behavior of undoped devices was investigated, and the electroluminescence is attributed to an exciplex of the two host materials. Electrically detected electron paramagnetic resonance was used to study the behavior of doped and undoped PHOLED devices from 20 to 200 K, which largely mimics the behavior of the same devices at room temperature. [J1250]

"Carrier recombination mechanisms in nitride single quantum well light-emitting diodes revealed by photo- and electroluminescence"

Light emission of nitride single quantum well light-emitting diodes operating in the range from 395 to 440 nm, grown by metal-organic vapor phase epitaxy, was investigated by means of photoluminescence (PL) and electroluminescence (EL) spectroscopies as functions of temperature and current injection level. The indium content of the active layers was varied via the growth temperature, which ranged from 770 to 810 °C. It was found that samples with higher indium contents (grown at lower temperatures) exhibit larger luminescence full widths at half maximum (FWHMs) and higher EL intensities. The larger FWHM points to a larger amplitude of the potential profile fluctuations, which suggests that these fluctuations may be useful for the increase in the device output power. In agreement with this result, the performed examination by PL measurements shows large thermal stability of the luminescence intensity for the lowest growth temperature sample. On the other hand, a nontrivial dependence of thermal stability on growth temperature suggests the additional involvement of different nonradiative recombination center concentrations in the individual samples, for example, because of dissimilar substrate qualities. [J1251]

"The effect of current crowding on the heat and light pattern in high-power AlGaAs light emitting diodes"

The results of the light and temperature micromapping in AlGaAs light emitting diodes grown by liquid phase epitaxy as double heterostructures and emitting at $\lambda = 0.87 \mu\text{m}$ are presented. At a driving current well above the safe operating limit (300 mA), the nonuniform light pattern and local self-heating (with temperature gradient of about 950 °C/cm) followed by catastrophic degradation of a device were detected with the charge coupled device and infrared microscopes operating in a pulsed mode. These were shown to result from the current crowding effect in the active and contact areas of a device. Good agreement between the theory and experiment was found. [J1252]

"Enhancing power conversion efficiencies and operational stability of organic light-emitting diodes by increasing carrier injection efficiencies at anode/organic and organic/organic heterojunction interfaces"

We fabricated long-lived multilayer organic light-emitting diodes (OLEDs), in which a 0.75 nm thick hole-injection layer of molybdenum oxide (MoO₃) and a 5 nm thick mixed layer at an organic/organic heterojunction interface were embedded. The use of the MoO₃ layer and of the mixed layer enhanced carrier injection at anode/organic and organic/organic heterojunction interfaces, resulting in a marked decrease in driving voltage and an increase in power conversion efficiency in the OLEDs. We observed about a factor of 9 improvement in the operational lifetime of the OLEDs by using the MoO₃ layer and the mixed layer as well. We assume that the lifetime improvement originates from the suppression of a thermally induced electrochemical degradation process of organic emitting molecules due to the reduction in the probability of the generation of Joule heat. [J1253]

"Charge generation layer in stacked organic light-emitting devices"

Three types of organic-based connection units were examined for use in stacked or tandem organic light-emitting devices, which include (i) Mg-doped tris(8-hydroxyquinoline) aluminum(III) (Alq₃)/4,4',4''-tris{N,-(3-

methylphenyl)-N-phenylamino}-triphenylamine (m-MTDATA), (ii) Alq3/tetrafluorotetracyanoquinodimethane (F4-TCNQ)-doped m-MTDATA, and (iii) Mg-doped Alq3/F4-TCNQ-doped m-MTDATA. Device (iii) shows the highest current efficiency and the differences in device performance can be correlated with the electronic structure of the connection unit and its interface with the neighboring active layers. The working mechanisms of the connection-unit works are discussed in terms of band bending and charge carrier density. The electronic structures of the interface between layers in a connection unit are of particular importance to the device performance. Dopings of Mg in Alq3 and F4-TCNQ in m-MTDATA led to bipolar heterojunction. Removal of either the n-type or the p-type dopants suppresses the band bending and the formation of space charge regions. The charge density accumulated at this interface estimated from Poisson's equation is $10^{18}/\text{cm}^3$, which is respectively 12 and 6 orders of magnitude higher than that in the Mg:Alq3/m-MTDATA and Alq3/F4-TCNQ:m-MTDATA connection units. Based on these results, the critical roles of dopants in an efficient connecting unit for stacked organic light-emitting diodes are elucidated. [J1254]

"Correlation of photoluminescent quantum efficiency and device characteristics for the soluble electrophosphorescent light emitter with interfacial layers"

We have investigated the effects of interfacial layers on the properties of soluble phosphorescent organic light emitting devices. Two kinds of polyfluorene-based interfacial layer materials have been studied; both were spin coated on top of PEDOT:PSS to form the insoluble layers by thermal annealing. The molecular-doped, phosphorescent light emitting layer comprising a polymeric host, small molecular host, and guest molecule was fabricated onto the thin interfacial layer. The photoluminescence quantum yield (PLQY) of these layers was measured with an integrating sphere. We have calculated the PLQY values of the single phosphorescent light emitting layer and various organic multilayers incorporating the interfacial layers, showing that a reduction in PLQY due to the interfacial quenching is more significant in the thicker interfacial layer structures. In spite of the decrease in PLQY induced by the triplet energy mismatch, polyfluorene-based interfacial layers improved the charge injection from PEDOT:PSS to the emitting layer, which results in the enhanced brightness and current. The triplet quenching by the interfacial layer could explain the reduction in luminous efficiency of the devices compared to the reference. This was also investigated by studying the charge carrier trapping, change in the spectral characteristics induced by the shift in the emission zone, and the analysis on the carrier balance of devices. [J1255]

"Ferromagnetic Cu doped ZnO as an electron injector in heterojunction light emitting diodes"

Ferromagnetic and highly conductive copper doped ZnO (ZnO:Cu) films were prepared by filtered cathodic vacuum arc technique. By employing a biasing technique during growth, the electron concentration and resistivity of the ZnO:Cu films can be as high as $10^{20}/\text{cm}^3$ and $5.2 \times 10^{-3} \Omega \text{cm}$, respectively. The ferromagnetic behavior is observed in all the conductive films, but its magnetization is quenched with an increment in carrier concentration, suggesting that carrier induced exchange is not directly responsible for the ferromagnetism. Heterojunction light emitting diodes have been fabricated using the conductive ZnO:Cu layer as an electron injector and a p-type GaN as hole injector. Electroluminescence can be detected from the devices. [J1256]

"Self-doping and partial oxidation of metal-on-organic interfaces for organic semiconductor devices studied by chemical analysis techniques"

The performance of organic electronic devices, such as organic light emitting diodes, transistors, or organic solar cells, depends critically on the chemical composition of the metal/organic and organic/metal interfaces which inject or extract charges into or from the device. By combining a number of techniques, such as x-ray photoemission spectroscopy (XPS) sputter depth profiling, XPS itself, secondary ion mass spectrometry, and laser desorption/ionization time-of-flight mass spectrometry, we investigate the reasons for differences in charge injection from metallic bottom and top contacts into either preferentially hole or preferentially electron transporting materials. We find that the deposition of metal onto organic semiconductors creates an organic-inorganic mixed interlayer in between the organic bulk material and the metal. In the case of electron injection, this interlayer acts as highly doped injection layer, while for hole injection, no significant improvement is visible. In addition to the self-doping, some cathode materials form partially oxidized metal-on-organic interfaces caused by oxygen in the residual gas. Depending on the evaporation conditions, the oxygen content varies. The effect of the oxygen incorporation, the origin, and the binding behavior in between the metal-on-organic interlayer is investigated and discussed. In contrast, organic materials evaporated on top of metals create an abrupt interface, where no self-doping effect is observed. [J1257]

"The role of poly(3,4-ethylenedioxythiophene):poly(styrenesulphonate) as a hole injection layer in a"

blue-emitting polymer light-emitting diode"

The authors study the role of the conducting polymer poly(3,4-ethylenedioxythiophene): poly(styrenesulphonate) (PEDOT:PSS) in determining the transient and steady-state operation of a blue-emitting polymer light-emitting diode. Combining the results from photoemission spectroscopy, time-of-flight photocurrent measurements, and studies on hole-only devices reveals a significant barrier for the injection of holes into the polymer. Simulations with a numerical drift-diffusion model, however, show that the injection currents determined from single-carrier devices cannot account for the rapid transient luminance onset and the efficient steady-state luminance output of the corresponding bipolar light-emitting devices. It is shown that the transient electroluminescence traces measured at different external bias can be well reproduced when assuming the presence of a weak barrier for electron extraction at this interface, which is attributed to electron accumulation at a thin phase-segregated PSS-rich layer at the surface of PEDOT:PSS. In addition, interface conditioning, presumably due to electron trapping near PEDOT:PSS, renders the anode-polymer interface nearly Ohmic. This conditioning, however, occurs on intermediate time scales normally not addressed by either transient or steady-state measurements. [J1258]

"The modification of self-assembled monolayer on indium tin oxide as cathode in inverted bottom-emitting organic light-emitting diodes"

Self-assembled monolayers (SAMs) of a series of p-substituted benzoyl chlorides were formed on indium tin oxide as the cathode for the fabrication of inverted bottom-emitting organic light-emitting diodes (IBOLEDs). The studies on the efficiency of electron injection and device performances showed that the direct tunneling of electron and the formation of dipole associated with the monolayer-forming molecule lead to significant enhancement in electron injection. Consequently, the device efficiency is greatly improved. The maximum current efficiency and power efficiency, respectively, reach 4.60 cd/A and 2.40 lm/W, which are over 1.2 times that of the conventional IBOLED without SAM modification. [J1259]

"Improvement of light extraction from high-power flip-chip light-emitting diodes by femtosecond laser direct structuring of the sapphire backside surface"

We report on the structuring of the backside surface of sapphire substrates in high-power flip-chip light-emitting diodes (LEDs) by femtosecond laser direct writing. Varying the laser powers has been found to affect the sizes of the inscribed patterns on a submicron scale which facilitates the control of the structure sizes with high precision. Accordingly, since on the one hand the light extraction efficiency reveals a strong dependence on pattern sizes, and on the other hand, femtosecond laser structuring provides a simple opportunity to inscribe diverse structures along the LED surfaces, LEDs with laterally controlled light extraction efficiencies can be fabricated. [J1260]

"Operating lifetime recovery in organic light-emitting diodes having an azaaromatic hole-blocking/electron-transporting layer"

Azaaromatic compounds (AACs) are widely used in organic light-emitting diodes (OLEDs), especially as efficient electron transporters. Yet, the operating lifetime of OLEDs is always compromised when AACs are involved in anything more than electron transport (e.g., hole blocking). We show (i) the operating lifetime of OLEDs incorporating AACs as a hole-blocking/electron-transporting layer (HBETL) depends strongly on the charge-conducting ability and excited state energy of the light-emitting layer (LEL) materials and (ii) shifting the charge recombination zone away from the LEL|HBETL interface deeper into the LEL can recover the lost lifetime. Thus, a pure red fluorescent OLED is demonstrated having 5.3 V drive voltage, 6.5% external quantum efficiency, 6.6 cd/A electroluminescent yield, and 125 000 h half-life, all at 20 mA/cm². This device utilizes an AAC as HBETL followed by an aluminum triquinolate (Alq) ETL doped with Li metal. Alternatively, the lifetime recovery might be assigned to the presence of the n-dopant (Li) at the LEL|HBETL interface (e.g., effected by diffusion of Li) because such presence stabilizes a wide range of OLEDs, e.g., those based on Alq mixed with polycyclic aromatic hydrocarbons and those based on 9,10-diarylanthracenes. Yet, this rationale is discarded in view of a strong deleterious interaction between the triazine-based AAC used in this work and n-dopants. [J1261]

"High efficient two color white phosphorescent organic light emitting diode"

We report on high efficient white organic light emitting diodes comprising the two phosphorescent emitter materials platinum(II)[2-(4',6'-difluorophenyl)pyridinato-N,C2']](2,4-pentanedionato) (FPt1) and iridium(III)bis[4,6-difluorophenyl-pyridinato N, C2']picolinate (Flrpic). Investigating the influence of the dopants in the emission layers on the device performance, a series of devices with different Flrpic and FPt1 concentrations have been processed. After optimizing the device with respect to efficiency and white color coordinates the influence of a thickness variation of the emission layers was investigated. The experiments revealed that the device performance is more sensitive to the parameters of the emission layer containing FPt1. Additional optical

simulations showed that interference effects play a crucial role in this device setup. The optimized device resulted in an external quantum efficiency of 10%, a power efficiency of 16 lm/W, near warm white color coordinates of 0.39/0.41, and a color rendering index of 81 at 1000cd/m². [J1262]

"Marked improvement in electroluminescence characteristics of organic light-emitting diodes using an ultrathin hole-injection layer of molybdenum oxide"

We show that the performance of organic light-emitting diodes (OLEDs) is markedly improved by optimizing the thickness of a hole-injection layer (HIL) of molybdenum oxide (MoO₃) inserted between indium tin oxide and N,N'-diphenyl-N,N'-bis(1-naphthyl)-1,1'-biphenyl-4,4'-diamine (α -NPD). From results of the electroluminescence (EL) characteristics of OLEDs with various thicknesses of a MoO₃HIL, we found that the OLED with a 0.75-nm-thick MoO₃HIL had the lowest driving voltage and the highest power conversion efficiency among the OLEDs. Moreover, the operational lifetime of the OLED was improved by about a factor of 6 by using the 0.75-nm-thick MoO₃HIL. These enhanced EL characteristics are attributable to the formation of an Ohmic contact at the interfaces composed of ITO/MoO₃/ α -NPD. [J1263]

"Effects of the GaN and AlN nucleation layers on the crack-free AlGaIn templates"

This paper reports the effects of GaN and AlN nucleation layers (NLs) on the characteristics of the subsequently grown AlGaIn templates, which were grown by a two-step growth method on sapphire substrates using metal-organic chemical vapor deposition. The in situ monitored reflectance spectra reveal that the thickness variation in AlGaIn templates grown on the GaN NL is much smaller than that on the AlN NL. X-ray diffraction patterns show that the AlGaIn template with a GaN NL exhibits a better crystalline quality as compared to that with an AlN NL. Observed from the transmission electron microscopy, it is also shown that the dislocation density of the AlGaIn template with a GaN NL can be substantially reduced. In addition, the fabricated light-emitting diodes from the AlGaIn template with a GaN NL exhibit a lower forward voltage, a lower series resistance, a lower leakage current, and a narrower linewidth of electroluminescence peak than those with the AlN NL. [J1264]

"Recombination processes in midinfrared Al_xIn_{1-x}Sb light-emitting diodes"

Emission characteristics, spectral properties, and quantum efficiencies of Al_xIn_{1-x}Sb light-emitting diodes, with aluminum compositions between 0% and 8.75%, have been investigated as a function of temperature from 25 to 300 K, and a function of current from 1 to 100 mA. As both current and temperature are varied a change in the dominant recombination mechanism is observed as indicated by changes in the measured emission. An analysis of the light-current characteristics shows that Auger processes become important in all devices at temperatures above 100 K, implying an activation energy of approximately 7-13 meV depending on the aluminum composition. [J1265]

"Hybrid CdZnO/GaN quantum-well light emitting diodes"

We report on the demonstration of light emission from hybrid CdZnO quantum-well light emitting diodes. A one-dimensional drift-diffusion method was used to model the expected band structure and carrier injection in the device, demonstrating the potential for 90% internal quantum efficiency when a CdZnO quantum well is used. Fabricated devices produced visible electroluminescence that was found to redshift from 3.32 to 3.15 eV as the forward current was increased from 20 to 40 mA. A further increase in the forward current to 50 mA resulted in a saturation of the redshift. [J1266]

"On the origin of efficiency roll-off in InGaIn-based light-emitting diodes"

The external quantum efficiency (EQE) of AlInGaIn-based light-emitting diodes (LEDs) on sapphire and bulk GaIn substrates was measured over a wide range of pulsed currents with small duty cycles. The current dependence of the EQE appeared to be a strong function of the In content but nearly independent of the dislocation density in the active region. The EQE of the InGaIn LEDs peaked at very low currents and decreased dramatically at high currents, whereas the AlGaIn UV LED attained a saturated EQE as current increases. In contrast to minimal peak shift in the UV LED, a monotonic current-induced blueshift of the peak energy was seen up to 1 kA/cm² for the InGaIn blue and green LEDs. These results suggest that the capture of delocalized carriers by nonradiative recombination centers such as misfit defects is the major nonthermal mechanism of efficiency roll-off in InGaIn LEDs. [J1267]

"Large-scale patterning of indium tin oxide electrodes for guided mode extraction from organic light-emitting diodes"

We describe a cost-efficient and large area scalable production process of organic light-emitting diodes (OLEDs)

with photonic crystals (PCs) as extraction elements for guided modes. Using laser interference lithography and physical plasma etching, we texture the indium tin oxide (ITO) electrode layer of an OLED with one- and two-dimensional PC gratings. By optical transmission measurements, the resonant mode of the grating is shown to have a drift of only 0.4% over the 5mm length of the ITO grating. By changing the lattice constant between 300 and 600nm, the OLED emission angle of enhanced light outcoupling is tailored from -24.25° to 37°. At these angles, the TE emission is enhanced up to a factor of 2.14. [J1268]

"High power light-emitting diode junction temperature determination from current-voltage characteristics"

Optical and electrical characteristics of power light-emitting diodes (LEDs) are strongly dependent on the diode junction temperature. However, direct junction temperature determination is not possible and alternative methods must be developed. Current-voltage characteristics of commercial high power LEDs have been measured at six different temperatures ranging between 295 and 400 K. Modeling these characteristics, including variation in the bandgap with temperature, revealed a linear temperature dependence of the forward voltage if the drive current is chosen within a rather limited current range. Theoretically, the voltage intercept can be deduced from the bulk semiconductor bandgap. However, accurate junction temperature determination is only possible if at least two calibration measurements at a particular drive current are performed. The method described in this paper can be applied to calculate the thermal resistance from the junction to any other reference point for any particular LED configuration. [J1269]

"Color control of white photoluminescence from carbon-incorporated silicon oxide"

Color control of the white photoluminescence (PL) from carbon-incorporated silicon oxide is demonstrated. The carbon-incorporated silicon oxide was fabricated by carbonization of porous silicon in acetylene flow (at 650 and 850 °C) followed by wet oxidation (at 650 and 800 °C). It was shown that PL color can be controlled in the range of blue-white and yellow-white by selecting the porosity of starting porous silicon as well as the carbonization and oxidation temperatures. Low-temperature oxidation resulted in bluish light emission in lower porosity series, while high-temperature oxidation promoted yellow-white light emission. The maximal integral intensity of PL was observed after oxidation at 800 °C. It was shown that white PL from carbon-incorporated silicon oxide has blue and yellow-white PL bands originating from different light-emitting centers. The origin of blue PL is attributed to defects in silicon dioxide. Some trap levels at the interface of the carbon clusters and silicon oxide are suggested to be the origin of the yellow-white light emission. [J1270]

"Separating the roles of electrons and holes in the organic magnetoresistance of aluminum tris(8-hydroxyquinoline) organic light emitting diodes"

Measurements of the effect of a magnetic field on the photocurrent in an aluminum tris(8-hydroxyquinolate) based organic light emitting diode have shown that it is possible to identify the contribution to the organic magnetoresistance of both electrons and holes. For holes the effect of a magnetic field is to decrease the mobility, whereas for electrons the magnetic field appears to increase the mobility. These changes are suggested to be brought about through the magnetic field dependence of the scattering of electrons and holes with excited states within the device. [J1271]

"Role of chemical reactions of arylamine hole transport materials in operational degradation of organic light-emitting diodes"

We report that the representative arylamine hole transport materials undergo chemical transformations in operating organic light-emitting diode (OLED) devices. Although the underlying chemical mechanisms are too complex to be completely elucidated, structures of several identified degradation products point at dissociations of relatively weak carbon-nitrogen and carbon-carbon bonds in arylamine molecules as the initiating step. Considering the photochemical reactivities, the bond dissociation reactions of arylamines occur by the homolysis of the lowest singlet excited states formed by recombining charge carriers in the operating OLED device. The subsequent chemical reactions are likely to yield long-lived, stabilized free radicals capable of acting as deep traps-nonradiative recombination centers and fluorescence quenchers. Their presence in the hole transport layer results in irreversible hole trapping and manifests as a positive fixed charge. The extent and localization of chemical transformations in several exemplary devices suggest that the free radical reactions of hole transporting materials, arylamines, can be sufficient to account for the observed luminance efficiency loss and voltage rise in operating OLEDs. The relative bond strengths and excited state energies of OLED materials appear to have a determining effect on the operational stability of OLED devices. [J1272]

"Microchip Self-Assembly on a Substrate Using Plasma Treatment"

This paper demonstrates a flux/2-ethyl-1-hexanol mixture capable of performing a self-assembly process. An /Ar plasma treatment controls the surface free energy of Si, leading to better self-assembly driven by capillary force. Hydrophobic bonding pads resulting from ODT (1-octadecanethiol) SAMs (self-assembled monolayers) on a microchip can be self-assembled on hydrophobic bonding sites caused by a flux/2-ethyl-1-hexanol mixture on a substrate within 0.4 s. Microchips with 400200-rectangle bonding pads exhibited higher alignment precision (displacement error ; rotation error) than 400400 -squares. The Owens-Wendt method was used to calculate the contact angle of 2-ethyl-1-hexanol to different bonding surfaces in water. Plasma treatment enabled the smallest contact angle of 2-ethyl-1-hexanol to ODT-modified Au surface (4.4), and the largest contact angle of 2-ethyl-1-hexanol to plasma-modified Si surface (153.5) in water. It explained why the plasma treatment exhibited benefit of self-assembly. This self-assembly technique could be used to assemble light emitting diodes, RFID tags, biosensors, or other types of microchips. [J1273]

"High-Efficiency GaN-Based Light-Emitting Diodes Fabricated With Metallic Hybrid Reflectors"

We report on high-efficiency GaN-based light-emitting diodes (LEDs) fabricated with metallic hybrid reflectors (MHRs). It is shown that the MHRs consisting of an injection part (with low p-contact resistance and intermediate reflectance) and a spreading part (with high p-contact resistance and good reflectance) can enhance current injection and overall light reflectivity. Compared with reference LEDs with single reflectors, LEDs fabricated with Ag-based MHRs give higher output power by 8.9% and a reduction in forward voltage by 0.02 V (at 20 mA), resulting in the improvement of the power efficiency by 10%. [J1274]

"Tailoring of the Color Conversion Elements in Phosphor-Converted High-Power LEDs by Optical Simulations"

Ray-tracing simulations are used to identify the demands for angular homogeneity of the white light emitted from phosphor-converted white light-emitting diodes having color conversion elements (CCEs) of constant thickness. The simulations reveal that a constant thickness of the CCE by itself is not sufficient for a homogeneous white light emission. Rather the height and the broadness of the CCE as well as the phosphor concentration have to be precisely adjusted in order to assure a homogeneous white light emission. [J1275]

"A Current-Mode Comparator for Digital Calibration of Amorphous Silicon AMOLED Displays"

We present a digital calibration driving scheme for stabilizing the uniformity of large area amorphous silicon active-matrix organic light emitting diode displays. A current-mode analog-to-digital converter (ADC) is used to extract the differential aging of the individual pixels. For the ADC, a configurable current comparator is designed that employs the output buffer of the source driver to reduce the die area. The comparator and pixel circuit were fabricated in 0.8- μ m high-voltage CMOS and amorphous silicon technologies, respectively. Analysis and measurement results show a calibration refresh time of 2 s for a high-definition display (1920 times RGB times 1080). Moreover, the pixel current is highly stable despite a 5-V shift in the threshold voltage of the thin-film transistor driver. [J1276]

"Ultraviolet Communications: Potential and State-Of-The-Art"

Motivated by the recent and rapid developments in deep ultraviolet LEDs, solar blind ultraviolet filters, and detectors, this article reviews wireless UV technology used for communications and sensing in either line-of-sight or non-line-of-sight channel conditions. We present the state-of-the-art of associated systems and their components and discuss related issues including communication link characterization, channel modeling, and link capacity study, as well as transceiver design, link duplexing, multiple access, and networking. We also envision applications in the commercial and military sectors. [J1277]

"Gamesman problems"

{no data available} [J1278]

"Corrections to "Use of Elastic Conductive Adhesive as the Bonding Agent for the Fabrication of Vertical Structure GaN-Based LEDs on Flexible Metal Substrate" [J1 Apr 08 523-525]"

In the above titled paper (ibid., vol. 20, no. 7, pp. 523-525, 1 Apr 08), there were errors in Table I. The correct table is presented here. [J1279]

"The Hybridization of CdSe/ZnS Quantum Dot on InGaN Light-Emitting Diodes for Color Conversion"

We have demonstrated the fabrication and characterization of hybrid CdSe/ZnS quantum dot (QD)-InGaN blue LEDs. The chemically synthesized red light ($\lambda = 623$ nm) QD solutions with different concentrations were dropped onto the blue InGaN LEDs with an emission peak of 453 nm and the turn-on voltage of 2.6 V. In this configuration, the CdSe/ZnS core/shell QDs played the role of a color-conversion center. It was clearly observed that the emission intensity from QDs was increased with increasing QD concentration. With a QD concentration of 10 mg/ml in toluene was incorporated, the ratio of emission intensity of QDs to that of InGaN quantum wells reached 0.17, whereas the Commission Internationale de l'Eclairage (CIE) chromaticity coordinates greatly shifted to (0.29, 0.14). From the spatial mapping of electroluminescence spectra, the decrease of the intensity of EQW seems to be faster than that of EQD, which suggests that the QD film thickness may be thicker in the edge of the surface of InGaN chip. There will, therefore, convert higher proportion of blue light to red light. Also, the resin-encapsulated hybrid LEDs have a divergence angle (the full angle at 1/e² intensity) of about 20 deg as the device is operated at 10 mA. Furthermore, under the injection current of 20 mA and room temperature, this device can be operated for more than 1000 h without any obvious degradation. From our results, it can be proven that the synthesized QDs are promising nanophosphors for color-conversion applications of solid-state LEDs. However, to more efficiently convert the blue light to red light, a denser QD solution with higher quantum yield must be utilized. [J1280]

"White Light Emission From DBPPV and CdSe/ZnS Quantum Dots Dually Hybridized on InGaN Light-Emitting Diodes"

We have demonstrated the white light emission from the novel hybrid light-emitting diodes. With a polymer/QD composite film thickness of 0.61, the Commission Internationale de l'Eclairage chromaticity coordinates of the emitting light from the device attain (0.33, 0.36). The coordinates are shifted to (0.43, 0.46) as the thickness is further increased. Meanwhile, the luminescence spectrum shows that more than 90% of the blue light is effectively energy transferred to green and red lights. For a long-term operation, the luminescence intensity from the polymer is decreased by 62% within 5 h due to the photooxidation effect. [J1281]

"One-Component, Low-Temperature, and Fast Cure Epoxy Encapsulant With High Refractive Index for LED Applications"

The cationic polymerization of diglycidyl ether of bisphenol-A (DGEBA) using a latent cationic thermal initiator, ammonium antimony hexafluoride, and the effect of addition of cycloaliphatic epoxy resin on the polymerization were studied with DSC, TGA, and hardness measurement. It was found that the cationically polymerized DGEBA at 0.5 phr initiator level gives the best compromise of chemical reactivity and optical properties, and therefore is suitable for light emitting diodes (LED) applications as an optically transparent encapsulant. This encapsulant, on one hand, is room temperature stable for at least six months, yet cures fast at low temperature, on the other hand. Moreover, the encapsulant has a high refractive index of 1.6 resulting from the high density of aromatic structure in the cross-linked network. Packaged with this encapsulant, the LED device is shown to exhibit an increased light output as demonstrated by both simulation and experimental measurement. The introduced system provides a new one-component encapsulant that is optically transparent, cures fast at low temperature with no sacrifice of room temperature stability, and has high refractive index at the same time. [J1282]

"Improved Light Output of Nitride-Based Light-Emitting Diodes by Lattice-Matched AlInN Cladding Structure"

We report the growth of AlInN nearly lattice-matched to GaN using metal-organic vapor phase epitaxy. The full-width at half-maximum of the AlInN peak measured by double crystal X-ray diffraction was 219.8 arcsec for the indium content of 20.8%. The effects of AlInN cladding layers on InGaN-GaN multiple-quantum-well light-emitting diodes (LEDs) were also investigated. From the room-temperature photoluminescence spectra, the shorter emission wavelength and the higher intensity were observed after employing AlInN cladding layers. Compared to the conventional LED, the light output intensity of the LED with AlInN cladding layers was increased due to the enhanced carrier confinement. Besides, we found the light output intensity could be saturated at higher injection current. Although the electrical property of the LED with AlInN cladding layers was slightly degraded, the experimental results in this study could explain the potential applicability of AlInN to the fabrication of cladding layers. [J1283]

"News brief: I See You"

{no data available} [J1284]

"Optical Injection-Induced Polarization Switching Dynamics in 1.5- μ m Wavelength Single-Mode Vertical-Cavity Surface-Emitting Lasers"

We report the first experimental investigation of the polarization-mode switching dynamics and injection-wavelength-dependent polarization-mode bistability of a 1.5- μ m wavelength single-mode vertical-cavity surface-emitting lasers (VCSELs) under external laser beam injection. An injection beam with polarization orthogonal to that of the stand-alone VCSEL caused polarization-mode instability and switching of the VCSEL output. By varying the optical injection detuning for fixed injection power observation was made of a novel form of polarization bistability which will have applications in a new type of all-optical flip-flop and signal processing scheme. [J1285]

"High-Power Quantum-Dot Superluminescent LED With Broadband Drive Current Insensitive Emission Spectra Using a Tapered Active Region"

High-power and broadband quantum-dot (QD) superluminescent light-emitting diodes are realized by using a combination of self-assembled QDs with a high density, large inhomogeneous broadening, a tapered angled pump region, and etched V groove structure. This broad-area device exhibits greater than 70-nm 3-dB bandwidth and drive current insensitive emission spectra with 100-mW output power under continuous-wave operation. For pulsed operation, greater than 200-mW output power is obtained. [J1286]

"Using Integrated Optical Feedback to Counter Pixel Aging and Stabilize Light Output of Organic LED Display Technology"

We define a metric of useful operating lifetime of an organic light-emitting device (OLED) display and relate it to the commonly measured half-life of constituent OLED pixels. We enumerate sources of OLED operational instability and propose an optical feedback solution in a novel integrated configuration to counter pixel aging and maintain stable light output across all of the pixels of an OLED display. Such optical feedback can correct pixel imperfections in both active matrix and passive matrix OLED displays. As an example, we analyze lifetime data previously published by Kwong et al., in 2002, and demonstrate that our optical feedback technique could maintain 100 cd/m² display light output within a 2% brightness accuracy for more than 25 000 hours of continuous use for this specific OLED system. From this example we draw conclusions generally applicable to extending stable operating lifetime of other OLED structures. [J1287]

"A Method for Current Spreading Analysis and Electrode Pattern Design in Light-Emitting Diodes"

We successfully developed a 3D electrical circuit model consisting of resistances and intrinsic diodes to analyze the current spreading effect in an InGaN/GaN multiple-quantum-well light-emitting diode. Each circuit element was formulated by physical parameters such as structural dimensions or material properties. We obtained a good agreement between the measured 2D light intensity distribution emitted from the surface of a fabricated device and that calculated with our model. With our design tool and each epitaxial layer parameter, we investigated the correlation of the geometrical pattern of the electrode with the light intensity distribution, saturation of output power, and reliability. Our analysis method also shows that defect locations due to electrostatic discharge stress are closely related to the area of current crowding. [J1288]

"Optical Data Link Employing Organic Light-Emitting Diodes and Organic Photodiodes as Optoelectronic Components"

An optical interconnect solely using organic optoelectronic components is presented. The data link is based on an organic light-emitting diode as the transmitter and an organic photodiode as the receiver. Light is transmitted via a polymer optical fiber coupled to the active components. A digitized audio signal based on the Sony/Philips Digital Interface Format standard at a signal bit rate of 2.8224 Mbit/s (44.1-kHz sampling frequency) is successfully transmitted. [J1289]

"Thermal Stability Improvement of Vertical Conducting Green Resonant-Cavity Light-Emitting Diodes on Copper Substrates"

Green light vertical-conducting resonant-cavity light-emitting diodes (RCLEDs) have been fabricated on a Cu substrate by the combination of laser lift-off and plating techniques. The structure of the RCLED/Cu is consisted of the InGaN-GaN multiple-quantum-well active layer between three layers of the dielectric TiO₂-SiO₂ distributed Bragg reflector as a top mirror and an Al metal layer as a bottom mirror. It was found that the RCLED with Cu substrate presents superior thermal dissipation and a stable electroluminescence emission peak wavelength (507 nm) under a high injection current. It is attributed to the Cu substrate providing a good heat sink and effectively reducing the junction temperature. [J1290]

"Degradation Study of Organic Semiconductor Devices Under Electrical and Optical Stresses"

Degradation due to electrical and optical stresses on organic semiconductor devices fabricated with imidazolin-5-one as an active layer is studied in this letter. It is found that while both electrical and optical stresses degrade device performance, the former leads to much faster degradation as compared with the latter. It is found that in electrical-stress degradation, the drop in current is a strong function of the charge flowing through the device during stress (charge fluence). For optical-stress degradation, it is strongly dependent on the duration of stress. It is also found that the input electrical and light energy during the stress may be annealing out some of the defects in the device and, hence, mitigating the degradation due to the applied stress. [J1291]

"Improved ESD voltage by inserting floating metal ring in GaN-based light emitting diodes"

Improvement of the electrostatic discharge (ESD) voltage in an InGaN/GaN blue light emitting diode (LED) grown on sapphire substrate is presented by inserting floating metal near the n-electrode. ESD voltages about four times larger than previously observed are experimentally obtained for LEDs with floating metal compared to those without. [J1292]

"Enhanced Vertical Extraction Efficiency From a Thin-Film InGaN-GaN Light-Emitting Diode Using a 2-D Photonic Crystal and an Omnidirectional Reflector"

An InGaN-GaN thin-film vertical-type light-emitting diode with a two-dimensional photonic crystal (PC) on the emitting surface and a TiO-SiO omnidirectional reflector on the bottom was fabricated. The device was investigated by performing a series of experiments and numerical computations. Electroluminescence measurement revealed a strong extraction enhancement in the vertical direction at 433-nm wavelength. The emission spectrum of the light was found to be strongly modified by the PC to have a significantly narrow linewidth of 5 nm. Our experimental results were in accord with those obtained from our numerical findings. [J1293]

"Further Enhancement of Nitride-Based Near-Ultraviolet Vertical-Injection Light-Emitting Diodes by Adopting a Roughened Mesh-Surface"

In this letter, the nitride-based near-ultraviolet (NUV) vertical-injection light-emitting diodes (VLEDs) with roughened mesh-surface are proposed and demonstrated by a combination of pattern sapphire substrate, wafer bonding, laser lift-off, and chemical wet etching processes. With the help of adopting a roughened mesh-surface, the light-output power (at 350 mA) of the NUV-VLEDs could be further enhanced about 20% as compared with that of the conventional NUV-VLED. [J1294]

"Diamond Heat Spreader Layer for High-Power Thin-GaN Light-Emitting Diodes"

A diamond-coating layer is studied as a heat spreading layer for a thin-GaN light-emitting diode (LED) chip. Our results show that this diamond layer can effectively spread the heat and improve the temperature uniformity of a thin-GaN LED chip, which enhances the heat dissipation efficiency down to the heat sink. With the diamond heat spreading layer, the junction temperature of the thin-GaN LED was reduced by 20 C at 1-A current input and the uniformity of the temperature distribution is also greatly improved. [J1295]

"Enhanced Output Power of GaN-Based LEDs With Nano-Patterned Sapphire Substrates"

GaN-based light-emitting diodes (LEDs) with an emitting wavelength of 450 nm were grown on nano-patterned sapphire substrates (NPSS) fabricated by nanosphere lithography. The crystalline quality of the epitaxial film could be improved by using the NPSS technique. The output power of LED grown on NPSS was 1.3 and 1.11 times higher than those of LEDs grown on conventional and patterned sapphire substrates at the injection current of 20 mA, respectively. The enhancement in output power could be contributed to the efficiently scattering by NPSS. But some voids formed at the GaN/NPSS interface cause a thermal dissipation problem of NPSS LED operated at high injection current. [J1296]

"Improved Emission Efficiency in InGaN Light-Emitting Diodes Using Reverse Bias in Pulsed Voltage Operation"

Improved emission efficiency in InGaN near-ultraviolet light-emitting diodes (LEDs) was demonstrated using reverse bias in pulsed voltage operation. Pulsed voltage operation of the LEDs from 3 to 3.2 V with a duty cycle of 50% at Hz produced a radiant flux of 4.0 mW, while pulsed operation from 0 to 3.2 V showed a radiant flux of 3.2 mW. The radiant flux further increased as the reverse voltage increased, at the same forward voltage. The

improved radiant flux was attributed to uniform carrier redistribution at the multiquantum wells, due to a periodically applied voltage from reverse voltage to forward voltage with a frequency ranged from to Hz, resulting in improved emission efficiency in InGaN LEDs. [J1297]

"Study of GaN-Based Light-Emitting Diodes Grown on Chemical Wet-Etching-Patterned Sapphire Substrate With V-Shaped Pits Roughening Surfaces"

We investigate the mechanism responding for performance enhancement of gallium nitride (GaN)-based light-emitting diode (LED) grown on chemical wet-etching-patterned sapphire substrate (CWE-PSS) with V-Shaped pit features on the top surface. According to temperature-dependent photoluminescence (PL) measurement and the measured external quantum efficiency, the structure can simultaneously enhance both internal quantum efficiency and light extraction efficiency. Comparing to devices grown on planar sapphire substrate, the threading dislocation defects of LED grown on CWE-PSS are reduced from 1.28 times $10^9/\text{cm}^2$ to 3.62 times $10^8/\text{cm}^2$, leading to a 12.5% enhancement in internal quantum efficiency. In terms of the theoretical computing of radiation patterns, the V-Shaped pits roughening surface can be thought of as a strong diffuser with paraboloidal autocorrelation function, increasing the escape probability of trapped photons and achieving a 20% enhancement in light extraction efficiency. Moreover, according to the measurement of optical diffraction power, CWE-PSS demonstrated superior guided light extraction efficiency than that of planar sapphire substrate, thus an extra 7.8% enhancement in light extraction efficiency was obtained. Therefore, comparing to the conventional LED, an overall 45% enhancement in integrated output power was achieved. [J1298]

"Nano-Processing Techniques Applied in GaN-Based Light-Emitting Devices With Self-Assembly Ni Nano-Masks"

We have developed a simple method to fabricate nanoscale masks by using self-assembly Ni clusters formed through a rapid thermal annealing (RTA) process. The density and dimensions of the Ni nano-masks could be precisely controlled. The nano-masks were successfully applied to GaN-based light-emitting diodes (LEDs) with nano-roughened surface, GaN nanorods, and GaN-based nanorod LEDs to enhance light output power or change structure properties. The GaN-based LED with nano-roughened surface by Ni nano-masks and excimer laser etching has increased 55% light output at 20 mA when compared to that without the nano-roughened process. The GaN nanorods fabricated by the Ni nano-masks and ICP-RIE dry etching showed 3.5 times over the as-grown sample in photoluminescence (PL) intensity. The GaN-based nanorod LEDs assisted by photo-enhanced chemical (PEC) wet oxidation process were also demonstrated. The electroluminescence (EL) intensity of the GaN-based nanorod LED with PEC was about 1.76 times that of the as-grown LED. The fabrication, structure properties, physical features, and the optical and electrical properties of the fabricated devices will be discussed. [J1299]

"Microwatt MOSLED Using With Buried Si Nanocrystals on Si Nano-Pillar Array"

Microwatt light emission from a metal-oxide-semiconductor light-emitting diode (MOSLED) made by using SiOx film with buried Si nanocrystals on Si nano-pillar array is demonstrated. The Si nano-pillar array obtained by drying the rapidly self-aggregated Ni nano-dot-masked Si substrate exhibit size, aspect ratio, and density of 30 nm, 10, and $2.8 \times 10^{10}/\text{cm}^2$, respectively. These high-aspect-ratio Si nano-pillar array helps to enhance the Fowler-Nordheim tunneling-based carrier injection and to facilitate the complete relaxation on total internal reflection, thus increasing the quantum efficiency by one order of magnitude and improving the light extraction from the nano-roughened device surface by three times at least. The light-emission intensity, turn-on current and power-current slope of the MOSLED are 0.2 mW/cm², 20-30 μA , and 3×10^{-5} mW/A, respectively. At a biased current of 400 μA , the highest external quantum efficiency is over 0.2% to obtain the maximum EL power of > 1 μW . Compared with the same device made on smooth Si substrate under a power conversion ratio of 1×10^{-4} , such an output power performance is enhanced by at least one order of magnitude. [J1300]

"SSPM Readout of LSO, (Lu-Y)AP:Ce and PWO-II Pixels for PET Detector Modules"

We have studied the performance of recently developed solid state photomultipliers (SSPMs) with 2.1×2.1 mm² sensitive area as a readout for small LSO, (Lu-Y)AP:Ce and PWO-II scintillator crystals. The SSPM is based on the p+-p-n+ structure which was optimized for blue/UV light detection. It operates at a gain of >105 and shows >25% photon detection efficiency in the 380-600 nm spectral range. Energy and timing spectra were measured using a ²²Na gamma source. Energy resolutions of 13%, 25% and 50% FWHM were measured for 511 keV gammas with the LSO, (Lu-Y)AP:Ce and PWO-II scintillator crystals respectively. A coincidence timing resolution of 710 ps (FWHM) was measured between two identical LSO+SSPM modules. [J1301]

"Organic light-emitting device with surface-modified tungsten-doped indium oxide anode"

The work function of tungsten-doped indium oxide (IWO) thin films could be enhanced to 5.5 eV by forming platinum and tungsten codoped indium oxide ($\text{In}_2\text{O}_3\text{:Pt,W}$) thin layers on them. With the IWO/ $\text{In}_2\text{O}_3\text{:Pt,W}$ double-layer as the anode, an OLED device with the structure of IWO/ $\text{In}_2\text{O}_3\text{:Pt,W}$ /NPB/Alq3/LiF/Al was fabricated. When the voltage is 14 V, the current density and the brightness of the device reach 1600 mA/cm^2 and $2.5 \times 10^4 \text{ cd}/\text{m}^2$, respectively. [J1302]

"Highly Polarized Single-Chip ELED Sources Using Oppositely Strained MQW Emitters and Absorbers"

Integrated polarizer components with polarization extinctions 40 dB are desirable for state-of-the-art photonic integrated circuits. We demonstrate 60-dB polarization extinction from a single-chip InGaAsP-InP broadband source by combining an edge light-emitting diode consisting of compressively strained quantum wells (QWs) with an absorber consisting of tensile strained QWs. A 600-m polarizer exhibits only 5 dB of insertion loss. [J1303]

"A Numerical Scheme to Model Current and Voltage Excitation of Organic Light-Emitting Diodes"

We present a method to model organic light-emitting devices driven by a current source in the context of drift-diffusion models. The method is extended to the case of voltage excitation, and calculations with current and voltage excitation are compared. An advantage over the application of Poisson's equation is that standard numerical solvers can be used for the ordinary differential equations that result from the spatial discretization of the model equations. We employ the model to calculate I- V characteristics and to examine the transient response of an organic light-emitting diode under pulsed current operation. The approach is generalized to the case of an arbitrary number of layers. [J1304]

"High-Speed Visible Light Communications Using Multiple-Resonant Equalization"

White light-emitting diodes (LEDs) are becoming widespread in commercial lighting applications, and there are predictions that they will be in common use in domestic applications in the future. There is also growing interest in using these devices for both illumination and communications. One of the major challenges in visible light communications is the low modulation bandwidth (BW) available from devices, which is typically several megahertz. In this letter, we describe a link that uses 16 LEDs which are modulated using a resonant driving technique, creating an overall BW of 25 MHz. This is used to implement a 40-Mb/s nonreturn-to-zero on-off keying link which operates at low error rates, and also provides illumination at levels sufficient for a standard office environment. [J1305]

"Investigation of Extracting Photonic Crystal Lattices for Guided Modes of GaAs-Based Heterostructures"

The issue of extracting guided modes from a standard light-emitting heterostructure similar to those of visible or near-infrared light-emitting diodes is considered with respect to the role of lattices and of the amount of omnidirectionality in the extraction performances. Triangular lattices are first-order natural candidates. We examine first whether they can be made omnidirectional thanks to a grating + coupler combination initially proposed by Fehrembach et al (2001), whereby the short periodicity concentrates emission in few in-plane modes, and the double periodicity extracts it. We then examine lattices that directly extract, for a Ga(Al)As system on a GaAs substrate, with a specific 3-D mode decay calculation. We compare triangular and Archimedean lattices experimentally and point out the role of photonic strength also through a spectrally and angularly resolved experiment. [J1306]

"High-Capacity Optical Transmission Systems"

The 25 years since the founding of the Journal of Lightwave Technology have seen more than three orders of magnitude increase in the capacity of optical transmission systems. This dramatic increase was brought about by the deployment of WDM and advances in high-speed transmission technologies. [J1307]

"Effect of Thickness of the p-AlGaIn Electron Blocking Layer on the Improvement of ESD Characteristics in GaN-Based LEDs"

The following letter presents a study regarding GaN-based light-emitting diodes (LEDs) with p-type AlGaIn electron blocking layers (EBLs) of different thicknesses. The study revealed that the LEDs could endure higher electrostatic discharge (ESD) levels as the thickness of the AlGaIn EBL increased. The observed improvement in the ESD endurance ability could be attributed to the fact that the thickened p-AlGaIn EBL may partly fill the

dislocation-related pits that occur on the surface of the InGaN-GaN multiple-quantum well (MQW) and that are due to the strain and the low-temperature-growth process. If these dislocation-related pits are not partly suppressed, they will eventually result in numerous surface pits associated with threading dislocations that intersect the InGaN-GaN (MQW), thereby reducing the ESD endurance ability. The results of the experiment show that the ESD endurance voltages could increase from 1500 to 6000 V when the thickness of the p-AlGaN EBL in the GaN LEDs is increased from 32.5 to 130 nm, while the forward voltages and light output powers remained almost the same. [J1308]

"Automotive Safety and Convenience Electronics [JAutomotive Electronics]"

First Page of the Article [J1309]

"Phosphor-Free White Light From InGaN Blue and Green Light-Emitting Diode Chips Covered With Semiconductor-Conversion AlGaInP Epilayer"

A phosphor-free white lamp was fabricated using the InGaN-based blue and green light-emitting diode (LED) chips covered with semiconductor-conversion layer AlGaInP. The lamp can provide three bands: a 460-nm blue emission coming from the blue LED, a 555-nm green emission coming from the green LED, and 630-nm red emission coming from the excited AlGaInP epilayer. As 50 mA was injected into the white lamp at room temperature, the chromaticity coordinates and correlated color temperature (TC) are (0.338,0.335) and 5348 K, respectively. By separating injection current into blue and green LED chips, TC of lamp can be tuned from about 4000 K to 5400 K. [J1310]

"Creating a chemical"

First Page of the Article [J1311]

"Investigation of the Nonthermal Mechanism of Efficiency Rolloff in InGaN Light-Emitting Diodes"

We present a comparative study on the optical characteristics of InGaN-based multiple quantum well light-emitting diodes (LEDs) with peak emission ranging from green to ultraviolet (UV) over a wide injection range. It is found that by pulsing the LEDs with a duty cycle that is below 1%, thermally induced peak red shift and efficiency reduction are largely eliminated. The current dependence of both the quantum efficiency and peak shift appears to be a strong function of the indium content in the active region. The quantum efficiencies of the blue and green LEDs peak at very low currents and dramatically decrease at high currents, whereas the UV LED has a nearly constant quantum efficiency under high injection conditions. In contrast to the minimal current-induced energy shift in the UV LED, a monotonic blue shift of the peak energy, which has a total amount of ~110 meV-1 kA/cm², is seen for the green LED. These results offer a strong support for the argument that the current overflow from localized states is the major nonthermal mechanism underlying the efficiency rolloff in InGaN-based visible LEDs. [J1312]

"From crystallography to visible light [JHistory]"

Silicon-carbon crystallites (carborundum), formed when silicon (Si) and carbon (C) are combined at electric furnace temperatures of 2,000-2,600degC, were applied in the earliest recorded experiments of electromagnetic wave crystal detectors. [J1313]

"Real-Time Color-Tunable Electroluminescence From Stacked Organic LEDs Using Independently Addressable Middle Electrode"

Independently controllable stacked organic light emitting devices (OLEDs) are fabricated by using interconnecting electrode of Al (2 nm)/WO₃(3 nm)/Au (16 nm) for connecting two primary color OLED units of blue and red. The middle electrode simultaneously functions as the cathode and anode for the bottom and top units respectively with a feature of over 60% optical transmission in a wide wavelength range from 500 to 700 nm such that the color can be tuned in real time from red to blue by changing the bias voltage to the two units. The undistorted primary colors and high efficiency have been obtained through optimizing structure and properly arranging the ordering of the blue and red subpixels. [J1314]

"History, Development, and Applications of High-Brightness Visible Light-Emitting Diodes"

In a practical sense, the development of high-performance visible-spectrum light-emitting diodes (LEDs) has occurred over a period of over 60 years, beginning with the discovery of the first semiconductor p-n junction in 1940, the development of solid-state electronic band theory in the 1940s, the invention of the first bipolar

transistor in 1947, and the demonstration of efficient light generation from III-V alloys in the 1950s and 1960s. This paper reviews some of the major scientific and technological developments and observations that have created the materials and device technologies currently used in the commercial mass production of high-brightness visible-spectrum LEDs and that have culminated in white-light sources exhibiting luminous efficacies of over 150 lm/W, far beyond what has been achieved with conventional lighting technologies. [J1315]

"A Review on the Reliability of GaN-Based LEDs"

We review the degradation mechanisms that limit the reliability of GaN-based light-emitting diodes (LEDs). We propose a set of specific experiments, which is aimed at separately analyzing the degradation of the properties of the active layer, of the ohmic contacts and of the package/phosphor system. In particular, we show the following: 1) low-current density stress can determine the degradation of the active layer of the devices, implying modifications of the charge/deep level distribution with subsequent increase of the nonradiative recombination components; 2) high-temperature storage can significantly affect the properties of the ohmic contacts and semiconductor layer at the p-side of the devices, thus determining emission crowding and subsequent optical power decrease; and 3) high-temperature stress can significantly limit the optical properties of the package of high-power LEDs for lighting applications. [J1316]

"A look on the bright side"

This paper shows that the external quantum efficiency, as well as the luminous efficiency of WOLEDs, is increasing continuously. This is mainly owing to the development of phosphorescent dopants and the optimization of device structure. Presently, the luminous efficiency of WOLEDs exceeds that of incandescent lamps (typically 5-18 lm/W). Therefore, they could soon offer new possibilities of lighting sources (e.g., flexible lighting panels) and applications. Large investments have been made for WOLED development in Europe and the United States. Despite the high values of efficiency measured on prototypes, the future commercialization of WOLEDs requires sufficient lifetimes, good color stability, and uniformity over large surfaces, together with relatively low elaboration costs. [J1317]

"Qualify with flying colors"

In this paper, the authors have developed a wide color gamut WXGA LCD monitor with a color calibrator. We have successfully developed a six-primary-color liquid crystal display (LCD) using six-color light-emitting diodes (LEDs). More specifically, a prototype of a six-primary-color LCD having a color gamut of 170% or wider than that of conventional techniques has been constructed. Furthermore, this monitor has our original color conversion circuit and a newly developed calibration system using an integrated color sensor, so that it can reproduce appropriate colors and keep its white point chromaticity stable. [J1318]

"Quasi-Active Power Factor Correction Circuit for HB LED Driver"

High brightness light emitting diodes (HB LEDs) are likely to be used for general lighting applications due to their high efficiency and longer life. The paper presents a quasi-active power factor corrector (PFC) for driving a string of HB LEDs. The single-stage PFC circuit has a high efficiency, and it does not increase the voltage/current stress on the active switch used in the switching converter due to PFC. The circuit has two operating modes based on the input voltage level and its features, like power factor correction and power balance, are explained. The experimental results obtained on a prototype converter along with waveforms are presented. [J1319]

"Ash Nehro-Everything is Illuminated [Jdream jobs 2008]"

First Page of the Article [J1320]

"Demonstration of semipolar (11-22) InGaN/ GaN blue-green light emitting diode"

A semipolar (11-22) (Ga, In)N/GaN blue-green light emitting diode directly grown on a 2 inch (11-22) GaN template on (10-10) m-plane sapphire by metal organic vapour phase epitaxy is demonstrated. The processed devices show uniform output power and an emission wavelength at ~490 nm across the entire wafer. No blue shifting of the peak emission could be observed by electroluminescence measurements, when the drive current was increased. On-wafer measurements yielded an average power output of 7 and 23 mW for drive currents of 20 and 80 mA, respectively. [J1321]

"Ney Robinson Salvi dos Reis-Into the Wild [Jdream jobs 2008]"

First Page of the Article [J1322]

"A Testing Method on Poly-Si Thin-Film Transistor Array for Active-Matrix Organic Emitting Display"

A novel method is introduced using to evaluate the quality of thin-film transistor (TFT) array for driving active-matrix display (OLED). By the means of this method, the operation states of the TFT or the defects of TFT can be judged. It is a current testing method with the advantages of fast response, excellent precision, no effect to aperture and no damage to the display array. [J1323]

"Karaoke-bot [Jtools & toys]"

The paper discusses the patent rights for engineers. [J1324]

"Nanostructured polymer microcomposites: A distinct class of insulating materials"

Experimental evidence was produced and gathered to demonstrate the distinct nature of nanostructured polymer microcomposites. The case of a polymer composite consisting of a high-content of micrometric quartz with a small adjunct of nanoclay is discussed. Emphasis is put on dielectric behavior studies while some results on thermal characteristics are presented. Overall results strongly support the potential of this class of insulating material for electrotechnical applications. [J1325]

"InAsSb based mid-infrared optical upconversion devices operable at thermoelectric temperatures"

A mid-infrared optical upconverter fabricated by using wafer fusion technology is reported. The device integrates an InAsSb/GaSb photodetector with a GaAs/AlGaAs light emitting diode. Mid-infrared to near infrared optical upconversion was demonstrated with an external upconversion efficiency of 0.06 W/W at 200 K-a temperature attainable with a thermoelectric cooler. [J1326]

"Flat-panel autostereoscopic 3D display"

Three-dimensional (3D) autostereoscopic images can be synthesised by scanning the illumination of a sequence of views on a liquid crystal display but few liquid crystal displays have adequate frame rate while simple scanning optics are bulky. A high-framerate ferroelectric microdisplay is combined with a slim front-illuminator comprising a line of light emitting diodes (LEDs) coupled into a slab light-guide embossed with a grating. One view at a time of a 3D object is displayed on the microdisplay while one LED at a time is switched on. The light-guide collimates the emission from the LED across the screen so that each view is made visible to a distinct direction. The result has high resolution and wide field of view, and has the potential to be small and slim enough for use on a mobile phone. [J1327]

"Combining Multicore Imaging Fiber With Matrix Addressable Blue/Green LED Arrays for Spatiotemporal Photonic Excitation at Cellular Level"

We have developed a microscale flexible optical image projection device, integrating a matrix addressable blue/green 2-D LED array to a multicore imaging fiber. The scalable matrix addressing LED design was to enable electrical access to individual elements in the densely packed 2-D LED array. A prototype 10times10 element array was fabricated by specific device process sequence, using deep reactive ion etching and polyimide etch-back processes for device isolation and planarization. Individual elements of the array have been operated under continuous-wave current injection up to a few kiloamperes per square centimeter suggesting uncompromised performance and robustness of the planarized device structure. The device was butt-coupled to a 30 000 pixel multicore image fiber to generate a spatiotemporal pattern of light at the output end of the fiber. As application demonstrations, selected spatiotemporal patterns of illumination have been projected either to the eye of *Xenopus laevis* tadpoles in studies of their developing visual system, or directly to excitable neural cells in the brain. [J1328]

"Enhancement of InGaN-Based Vertical LED With Concavely Patterned Surface Using Patterned Sapphire Substrate"

To improve the external quantum efficiency, we have proposed a new method utilizing surface roughening of vertical-type light-emitting diodes (VT-LEDs) fabricated on hemispherical patterned sapphire substrate by using a laser lift-off technique. The advantages of this method are simple and reproducible in transferring the well-defined patterns on sapphire into GaN layer. The VT-LED with concavely patterned surface showed a nearly twofold increase in the output power compared to the normal planar surface. This improvement in the VT-LED

performances is attributed to the increase in the escaping probability of photons from the LED surface. [J1329]

"Enhancing the Light Extraction of $(\text{Al}_x\text{Ga}_{1-x})_{0.5}\text{In}_{0.5}\text{P}$ -Based Light-Emitting Diode Fabricated via Geometric Sapphire Shaping"

AlGaInP-based light-emitting diodes (LEDs) with a transparent sapphire substrate were fabricated by the glue-bonding (GB) method. This transparent sapphire substrate is a geometric shaping structure by wet etching processes. Furthermore, the n-side-up surface has a nano-roughened texture by natural mask and chemical wet etching processes. The light output of this novel LED structure could be enhanced about 26.7% (at 350 mA) due to the higher light extraction as compared with the conventional GB-LEDs. [J1330]

"Improved Light Output of Photonic Crystal Light-Emitting Diode Fabricated by Anodized Aluminum Oxide Nano-Patterns"

A photonic crystal (PC) light-emitting diode (LED) was fabricated using an anodized aluminum oxide (AAO) nano-pattern technique, which has potential applications to mass production. The AAO nano-pattern, which was anodized in 0.3-M oxalic acid at 70 V, was transferred to the n-GaN bottom cladding through reactive ion etching and covered during the regrowth of GaN to form periodic air holes. The PC was embedded into the bottom cladding, which resulted in a low operating voltage. For the PC LED, the light output was enhanced by more than 20%, while the operating voltage increased only slightly. The radiation pattern of the PC LED showed two lobes at approximately $\pm 30^\circ$, which originated from the diffraction by PC. [J1331]

"Failure Mechanisms Associated With Lens Shape of High-Power LED Modules in Aging Test"

High-power light-emitting diode (LED) modules encapsulated with different lens shapes after a thermal-aging test were studied experimentally and numerically. Samples from different manufacturers were aged at 80degC, 100degC, and 120degC under a constant driving voltage of 3.2 V. The results showed that the LED modules encapsulated with a hemispherical-shaped plastic lens exhibited a better lifetime due to better thermal dissipation than those with cylindrical-or elliptical-shaped plastic lenses. Results also showed that the optical power of the LED modules increased after removing the plastic lens because degradation of the lens material decreased the amount of light. The key module package-related failure modes under thermal-aging were identified as the degradation of the plastic lens and lens material. A finite-element method (FEM) simulation showed that thermal and major principle stress distributions of the high-power LED modules were dependent on aging temperature. Both experimental and FEM simulated results clearly indicated that a uniformly thermal dissipation to minimize the thermal effect along the thermal path from the LED chip to the plastic lens is essential to extend the operating life of high-power LED modules. [J1332]

"Design of Highly Transparent Organic Photodiodes"

In this brief, various approaches for the realization of transparent photodiodes based on bulk heterojunction blends of poly-3-hexylthiophene and [6,6]-phenyl C61-butyric acid methyl ester are studied. The choice of the constituents of the device is discussed concerning transmittance and light-detecting properties as dark current and external quantum efficiency (EQE). Blending several light-absorbing materials makes tailoring of the transmittance spectrum possible. Transmittance of 36% of the incident light together with 46% EQE at a wavelength of 530 nm are promising results and show the potential for highly transparent photodiodes based on organic layers. [J1333]

"Analytical Evaluation of the Ratio Between Injection and Space-Charge Limited Currents in Single Carrier Organic Diodes"

An analytical, complete framework to describe the current-voltage (I-V) characteristics of organic diodes without the use of previous approaches, such as injection or bulk-limited conduction is proposed. Analytical expressions to quantify the ratio between injection and space-charge-limited current from experimental I-V characteristics in organic diodes have been derived. These are used to propose a numerical model in which both bulk transport and injection mechanisms are considered simultaneously. This procedure leads to a significant reduction in computing time with respect to previous rigorous numerical models. In order to test the model, different diode structures based on two different polymers: poly(2-methoxy-5-{3',7'-dimethyloctyloxy}-p-phenylenevinylene) (MDMO-PPV) and a derivative of the poly(2,7-fluorene phenylidene) [PFP:(CN)2], have been fabricated. The present model is excellently fitted to experimental curves and yields the microscopic parameters that characterize the active layer. [J1334]

"Light Extraction Efficiency Enhancement of GaN Blue LED by Liquid-Phase-Deposited ZnO Rods"

We investigate the light extraction efficiency of a GaN light-emitting diode (LED) by using liquid-phase-deposited ZnO rods at near-room temperature. Zinc nitrate and hexamethylenetetramine were used as the deposition precursors. Compared with the conventional GaN LED, the optical power output of the GaN LED with crystalline ZnO rods on its surface has about 1.6 times enhancement. [J1335]

"High-Speed GaN-Based Green Light-Emitting Diodes With Partially n-Doped Active Layers and Current-Confined Apertures"

We demonstrate a high-speed GaN-based green light-emitting diode for plastic optical fiber (POF) communication applications. By using a combination of n-type doping and undoped $\text{In}_x\text{Ga}_{1-x}\text{N}/\text{GaN}$ based multiple quantum wells (MQWs), and a 76- μm -diameter current-confined aperture structure, we can obtain an extremely high electrical-to-optical (E-O) 3 dB bandwidth (~ 330 MHz), which is limited by the spontaneous recombination lifetime of the MQWs. A reasonable coupled power (~ 264 μW) can be simultaneously achieved for a 2 mm in diameter POF with a 0.5 numerical aperture (NA). [J1336]

"Comparison of Pentacene and Amorphous Silicon AMOLED Display Driver Circuits"

Organic light-emitting diode (OLED) displays offer distinct advantages over liquid crystal displays for portable electronics applications, including light weight, high brightness, low power consumption, wide viewing angle, and low processing costs. They also are attractive candidates for highly flexible substrates. In active-matrix OLED (AMOLED) displays, a small transistor circuit is used to drive each OLED device. This paper compares the simulated performance of two state-of-the-art AMOLED drivers with a proposed 5 thin-film-transistor (TFT) voltage programmed driver circuit which combines the advantages of the first two configurations. A competitive evaluation is also done between amorphous silicon ($\alpha\text{-Si}$) and organic TFTs (OTFTs,) using comparable empirical device models for $\alpha\text{-Si}$ and pentacene OTFTs. The 5-TFT circuit is found to match the speed of the 2-TFT while achieving a stability closer to the 4-TFT circuits and demonstrating a better speed-stability tradeoff. [J1337]

"Single-Layered Hybrid DBPPV-CdSe-ZnS Quantum-Dot Light-Emitting Diodes"

We have demonstrated the fabrication and characterization of single-layered hybrid polymer-quantum-dot light-emitting diodes (PQD-LEDs) with the emissive composite film of 2,3-dibutoxy-1,4-poly(phenylene vinylene) (DBPPV) and inorganic CdSe-ZnS core/shell quantum dots (QDs). It is observed that both the electrical and optical characteristics are significantly improved by adjusting the thickness of the emissive layer. For the device with composite film thickness of 103 nm, the turn-on voltage is 4.1 V, and the maximum luminance of 4100 cd/m^2 as well as maximum luminous efficiency of 1.35 cd/A are achieved at 9.6 and 7.6 V, respectively. The optimum emission contribution of luminescence from QDs to the whole luminance is 38%. However, the QD luminescence is mainly limited by the Fomrster energy transfer mechanism and no obvious QD-related injected carrier trapping is observed. To our knowledge, this is the first demonstration of PQD-LEDs that consist of DBPPV and CdSe-ZnS QDs. [J1338]

"Improved External Quantum Efficiency of GaN p-i-n Photodiodes With a TiO_2 Roughened Surface"

Gallium nitride p-i-n ultraviolet photodiodes (PDs) with a titanium dioxide (TiO_2) nano-particles roughened surface have been fabricated. It was found that the responsivity and external quantum efficiency can be improved 60% on the surface roughened PDs. It was also found that light absorption can be enhanced from various incident angles by the TiO_2 roughened surface. Furthermore, the high detectivity of 9.2 times $10^{13} \text{ cm}^2/\text{Hz}^{1/2}$ can be achieved from the PD with a rough surface. [J1339]

"Performance Degradation of High-Brightness Light Emitting Diodes Under DC and Pulsed Bias"

This paper presents the results of an experimental investigation of the performance of commercially available high-brightness light emitting diodes (HBLEDs). Three different families of white HBLEDs from three different manufacturers are considered. The main issues taken into account and reported in detail are the following: quality of the emitted light, impact of the driving strategy on the expected device lifetime, thermal management and related aging effects. The execution of a large number of accelerated stress tests reveals the weaknesses of the technology with respect to thermal degradation and the sensitivity of the device performance degradation to the adopted driving strategy. Furthermore, square-wave driving has been compared to conventional dc driving in terms of device performance and reliability. Comparison has been carried out for the same average current value of the driving waveforms. It has been found that square-wave driving can be an effective alternative to dc driving in terms of device efficiency only for high duty cycles. For low duty cycles, worse performance was detected due

to the saturation of efficiency at high peak current levels. Reliability tests did not univocally indicate whether the use of pulsed bias can be more convenient than dc driving in terms of lumen maintenance. The three families of devices submitted to dc and pulsed stresses showed different behaviors, indicating that stress kinetics strongly depends on the LED technological structure and package thermal design. [J1340]

"GaN/AlGaN nanocolumn ultraviolet light-emitting diodes grown on n-(111) Si by RF-plasma-assisted molecular beam epitaxy"

GaN nanocolumns have excellent optical characteristics owing to their dislocation-free nature. GaN/AlGaN nanocolumn ultraviolet light-emitting diodes were demonstrated on n-(111) silicon by RF-plasma-assisted molecular beam epitaxy for the first time. Clear diode characteristics and ultraviolet emission with a peak wavelength of 354 nm were observed under continuous current injection at room temperature. [J1341]

"Robust Optical Time-of-Flight Range Imaging Based on Smart Pixel Structures"

The reliable detection of the three-dimensional position of arbitrary objects in a scene is a key capability of most animals and one of the most important tasks in machine vision. Today's preferred technical solution is optical time-of-flight (TOF) range imaging, due to its simplicity, its distance resolution, its large and adaptable measurement range, as well as the absence of shadowing problems. In order significantly to extend the application areas of TOF 3-D cameras, in particular for outdoor use, we show how their performance can be improved in all relevant respects: background light suppression is improved by an order of magnitude by the minimum charge transfer method. Multicamera operation is achieved by a binary pseudo-noise modulation/demodulation technique. This method also avoids all practical ambiguity problems typically encountered with harmonic modulation. Higher temporal demodulation resolution becomes possible with a pixel structure employing lateral electric fields. We have realized such pixels with a commercially available CCD/CMOS process, and our measurement results confirm that gigahertz demodulation imaging is possible. The practicality of all theoretical concepts is demonstrated with a miniaturized TOF 3-D camera platform whose LED array light source is modulated at a typical rate of 20 MHz. Our work contributes, therefore, to opening up new application domains of the soaring optical TOF range imaging techniques. [J1342]

"Multistring LED Backlight Driving System for LCD Panels With Color Sequential Display and Area Control"

In this paper, a multistring light-emitting diode (LED) backlight driving system for liquid crystal display (LCD) panels with color sequential display (CSD) and area control is proposed. In large-scale LCD panels, multistring LED backlights are required to provide sufficient back lighting. The most popular structure to achieve multistring current regulation is a current mirror. However, it cannot be applied to high-power LED (>100 mA) driving, and the number of LEDs in each string is highly limited. In the driving system, a multioutput flyback converter associated with a novel control IC is proposed to tightly regulate LED driving currents and to readily achieve CSD and area control. The proposed driving system for a 32-in LCD panel has been built, from which experimental measurements have verified that the proposed driving system has the following features: low power consumption, high power conversion efficiency, stable driving currents, and high reliability. [J1343]

"Tandem Light-Guides With Micro-Line-Prism Arrays for Field-Sequential-Color Scanning Backlight Module"

An optically partitioned backlight system consisting of tandem wedge-shaped light-guides (LGs) with micro-line-prism arrays was developed for scanning field-sequential-color (FSC) liquid crystal display (LCD) in large size. The unit of wedge-shaped LG combined with a light-emitting diode (LED) light-bar was designed and fabricated to collimate the extraction light within a narrow angular extent. Based on the edge lighting approach, the volume of backlight system can be reduced down to 25 mm without sacrifice of the optical behavior. As a result, 2750 nits average luminance subject to 50% duty cycle and 83% uniformity can be achieved. The leakages into the consecutive adjacent blocks were well suppressed to 11.86%. [J1344]

"Efficiency Enhancement of Light Extraction in LED With a Nano-Porous GaP Surface"

Electrodeless photoelectrochemical etching is developed to produce a nano-porous n-GaP surface. Pores of diameter 300-700 nm are distributed on the surface with a density 1.2 times 10^8 cm^{-2} . Such a porous surface structure exhibits a short mean free path for the transport of visible light and enhances photon scattering in a red AlInGaP-based light-emitting device. The efficiency of extraction of light emitted from the active layer becomes about 30%-50% greater than that without an etching treatment at a current of 20-40 mA. [J1345]

"Accelerated Life Test of High Brightness Light Emitting Diodes"

Short-term accelerated life test activity on high brightness light emitting diodes is reported. Two families of 1-W light-emitting diodes (LEDs) from different manufacturers were submitted to distinct stress conditions: high temperature storage without bias and high dc current test. During aging, degradation mechanisms like light output decay and electrical property worsening were detected. In particular, the degradation in light efficiency induced by thermal storage was found to follow an exponential law, and the activation energy of the process was extrapolated. Aged devices exhibited a modification of the package epoxy color from white to brown. The instability of the package contributes to the overall degradation in terms of optical and spectral properties. In addition, an increase in thermal resistance was detected on one family of LEDs. This increase induces higher junction temperature levels during operative conditions. In order to correlate the degradation mechanisms and kinetics found during thermal stress, a high dc current stress was performed. Results from this comparative analysis showed similar behavior, implying that the degradation process of dc current aged devices is thermal activated due to high temperatures reached by the junction during stress. Finally, the different effects of the stress on two families of LEDs were taken into account in order to identify the impact of aging on device structure. [J1346]

"InGaN/GaN multi-quantum-well planar metal-semiconductor-metal light-emitting diodes"

Planar metal-semiconductor-metal light-emitting diodes with InGaN/GaN multi-quantum-wells (MQWs) as the active layer have been demonstrated for the first time. The diodes with interdigitated Schottky electrodes fabricated on p-GaN contact layer exhibit symmetrical current-voltage characteristic with a turn-on voltage of ~ 13 V at 20 mA. The violet light emission centred at 408 nm is generated by radiative recombination taking place in the MQWs. The evolution of light output power against injection current reveals an enhanced carrier collecting efficiency of the active MQWs at higher injection current level, which follows a $P \propto I^{2.8}$ trend below 30 mA. [J1347]

"High-Brightness InGaN-GaN Flip-Chip Light-Emitting Diodes With Triple-Light Scattering Layers"

The flip-chip light-emitting diodes (FC-LEDs) with triple-light scattering layers were investigated comprising a top surface sapphire textured layer, an interface patterned sapphire layer, and a bottom naturally textured p-GaN layer. Such triple-textured layers are useful for light extraction efficiency enhancement. The light output power of FC-LEDs was increased 60% (at 350-mA current injection) compared to that of conventional FC-LEDs by implementing the triple-light scattering layers. [J1348]

"Multidimensional Electro-Opto-Thermal Modeling of Broad-Band Optical Devices"

This paper investigates the self-consistent modeling of broad-band optical devices such as super-luminescent light-emitting diodes (SLEDs) and semiconductor optical amplifiers. A multidimensional electro-opto-thermal approach using many-body gain theory, and temperature-dependent microscopic transport equations is presented. In addition, a Green's function based model for amplified spontaneous emission is derived from Maxwell's equations in a consistent way. To illustrate the model's validity it is implemented into an existing simulation tool and benchmarked with two InP-based edge-emitting SLEDs operating around 1310 nm, featuring nonidentical quantum wells as active region. A comparison between simulated and measured characteristics (both electro-thermal and spectral) proves the applicability of the novel model. [J1349]

"Effects of Impact Inertia and Surface Characteristics on Deposited Polymer Droplets in Microcavities"

Microflow visualization and computational fluid dynamics (CFD) are complementarily performed to study the evolution of a single poly(ethylenedioxythiophene) (PEDOT) droplet ejected from a piezoelectric ink-jet printhead and the equilibrium film characteristic of the droplet deposition in a microfabricated cavity. The verified CFD code is further applied to investigate the influences of contact angles θ_{ass} of the PEDOT droplet/air interface and the PEDOT droplet/cavity sidewall interface as well as droplet impact velocity V_d on the transient deposition process in the micro cavity. Impact inertia was studied by varying the droplet Weber number from 30.3 to 42.6. The surface characteristics are explored by choosing θ_{ass} of 10deg, 30deg, 50deg, 70deg, 90deg, and 110deg. The influences of impact inertia are also examined by increasing V_d from 2.0 to 12.0 m/s at 2.0 m/s interval. The computed results are found in good agreement with the experimental ones. For the first time, critical Weber numbers have been found relating to the ability of the droplet to wet the side walls and fill a microcavity with a uniform film. The results are also new in terms of the identifications of the critical contact angle ($\theta_{\text{ass}})_c$ and critical impact velocity ($V_d)_c$. At ($\theta_{\text{ass}})_c$ and at and beyond ($V_d)_c$, the formation of an intact flat film in the cavity is fulfilled. [J1350]

"Spontaneous Emission and Characteristics of Staggered InGaN Quantum-Well Light-Emitting Diodes"

A novel gain media based on staggered InGaN quantum wells (QWs) grown by metal-organic chemical vapor deposition was demonstrated as improved active region for visible light emitters. Fermi's golden rule indicates that InGaN QW with step-function like In content in the well leads to significantly improved radiative recombination rate and optical gain due to increased electron-hole wavefunction overlap, in comparison to that of conventional InGaN QW. Spontaneous emission spectra of both conventional and staggered InGaN QW were calculated based on energy dispersion and transition matrix element obtained by 6-band k midpoint formalism for wurtzite semiconductor, taking into account valence-band-states mixing, strain effects, and polarization-induced electric fields. The calculated spectra for the staggered InGaN QW showed enhancement of radiative recombination rate, which is in good agreement with photoluminescence and cathodoluminescence measurements at emission wavelength regime of 425 and 500 nm. Experimental results of light-emitting diode (LED) structures utilizing staggered InGaN QW also show significant improvement in output power. Staggered InGaN QW allows polarization engineering leading to improved luminescence intensity and LED output power as a result of enhanced radiative recombination rate. [J1351]

"Improved performance of 264 nm emission AlGaIn-based deep ultraviolet light-emitting diodes"

AlGaIn-based multiple-quantum-well light-emitting diodes (LEDs) with peak emission at UV-C region of 264 nm were successfully grown on AlN template using metal organic chemical vapour deposition. It was found that a subband emission around 320 nm can be drastically reduced by inserting a thin 1 nm-thick AlN interlayer between the active region and p-type layers. This is presumably a result of the suppression of electron overflow or Mg diffusion. It was also observed that the output power in LEDs was increased up to more than 20 times by changing the layer construction. [J1352]

"Current Spreading and Blocking Designs for Improving Light Output Power from the Vertical-Structured GaN-Based Light-Emitting Diodes"

In this work, use of localized Ti deposition associated with a transparent indium-zinc-oxide (IZO) layer is proposed to serve as Schottky current blocking and current spreading layer, respectively. In addition, an inductively coupled plasma (ICP) mesa etching on the surface layer (n-GaN) of regular vertical-conducting metal-substrate GaN-based light-emitting diodes (VM-LEDs) is also proposed to further enhance current spreading of the device. Through a two-dimensional device simulator, the calculated results indicate that significant avoidance of the current-crowding effect under cathode contact pad could be obtained once the n-GaN layer etching depth and width, IZO thickness, and Schottky current blocking width have been optimized. In experiments, 1000 m 1000 m GaN-based blue LEDs with an ICP mesa etching of 250 m in width and 2 m in depth on the surface n-GaN layer, 200 m in Schottky current blocking width, and a 300-nm-thick IZO layer have been successfully fabricated. As compared to the regular VM-LEDs without the use of the present technology, typical improvement in light emission uniformity and light output power by about 6% and 38% at an injection current of 350 mA have been obtained. [J1353]

"Thermal and Mechanical Analysis of High-Power LEDs With Ceramic Packages"

In this paper, we present the thermal and mechanical analysis of high-power light-emitting diodes (LEDs) with ceramic packages. Transient thermal measurements and thermomechanical simulations were performed to study the thermal and mechanical characteristics of ceramic packages. Thermal resistances from the junction to the ambient were decreased from 79.6 to 46.7degC/W by replacing the plastic mold with a ceramic mold for LED packages. Thermomechanical stress induced in the heat-block test was simulated using a finite-element method. Higher level of thermomechanical stress in the chip was found for LEDs with ceramic packages, despite less mismatching coefficients of thermal expansion, compared with that with plastic packages. The thermomechanical-stress components in the direction of the thickness were found to be larger than that in other two directions. The results suggest that the thermal performance of LEDs can be improved by using ceramic packages, but the mounting process of the high-power LEDs with ceramic packages is critically important and should be the reason for causing delaminating interface layers in the packages. [J1354]

"News Brief [JEYE-PODS]"

Silicon circuits that bend and stretch recently took an important step away from the world of science-fiction novels and Hollywood movies toward the real world of medical devices and media players. A team of researchers at the University of Illinois at Urbana-Champaign (UIUC) says it has printed silicon circuits onto plastic in the form of the same CMOS circuits that dominate digital logic today. The breakthrough brings

researchers closer to printing circuits on plastic that approach the performance and reliability of silicon chips. The team had earlier shown that they could form circuits by transferring thin ribbons of silicon onto glue-coated plastic using a patterned rubber stamp. But the resulting devices used only n-type silicon, whereas CMOS logic has both n-type and p-type. CMOS circuits are generally more power-efficient, because current should flow through them only when their bits are flipping. In any portable electronic device, that means longer battery life. But in the case of plastic electronics, CMOS is even more important, because it reduces the amount of heat produced-which, left unchecked, could melt the plastic. [J1355]

"Laser Noise Cancellation in Single-Cell CPT Clocks"

We demonstrate a new technique for the suppression of noise associated with the laser source in atomic clocks based on coherent population trapping (CPT). The technique uses differential detection of the transmission of linearly and circularly polarized beams that propagate through different parts of a single rubidium vapor cell filled with a buffer gas mixture. The common-mode noise associated with the laser frequency and amplitude noise is suppressed by the differential detection of the two laser beams. The CPT signal, which is present only in the circularly polarized laser beam, is unaffected. The implementation of the technique requires only a change of the polarization of part of the laser beam and an additional photodiode. The technique is simple and applicable to CPT frequency references where a major source of noise is the laser, such as compact and chip-scale devices. [J1356]

"Silicon Slivers for Flexible Circuits"

{no data available} [J1357]

"Improved Extraction Efficiency of Light-Emitting Diodes by Modifying Surface Roughness With Anodic Aluminum Oxide Film"

An anodic alumina oxide (AAO) film with nano-roughening is added on the top window layer of AlGaInP light-emitting diodes (LEDs) to improve the light extraction of the device. The AAO film has a natural porosity to provide light scattering centers at the surface, allowing an increase of light emission intensity with no loss of or damage to the semiconductor material. Further, the fabricated AAO film with a refractive index is about which is intermediate between those of air and the window layer of GaP. By inserting this layer between the ambient and GaP, it broadens the critical angle for light emission and reduces internal reflection. Experiments with laboratory-fabricated AlGaInP devices of conventional design demonstrated a 32% improvement in the luminous intensity at 20 mA for the device with the AAO layer. This letter shows by theory and experiment that AAO films can be used as a low-cost, easily implemented surface nano-roughening for improving extraction efficiency of AlGaInP LEDs. [J1358]

"Phosphor-Free GaN-Based Transverse Junction White-Light Light-Emitting Diodes With Regrown n-Type Regions"

In this study, we demonstrate a GaN-based phosphor-free white-light light-emitting diode (LED), which is composed of GaN-based dual-wavelength (blue and yellow-green) multiple-quantum-wells (MQWs) and a transverse p-n junction. The device was realized by the regrowth of n-type GaN layers on the sidewall of p-type GaN and undoped MQWs. The problems related to the bias-dependent shape of the electroluminescence spectra that occur in traditional phosphor-free white-light LEDs (with vertical p-n junctions) are greatly minimized. The current-voltage performance of our device is comparable to that of the commercially available phosphor white-light LEDs. In addition, the dynamic measurement results indicate that we can attain a much higher modulation bandwidth (22 versus 3 MHz) with this device than with the currently available commercial ones. [J1359]

"Optoelectronic Characteristics of Direct-Current and Alternating-Current White Thin-Film Light-Emitting Diodes Based on Hydrogenated Amorphous Silicon Nitride Film"

Direct-current and alternating-current white thin-film light-emitting diodes (DCW and ACW TFLEDs) have been fabricated and demonstrated with the intrinsic hydrogenated amorphous silicon nitride (i-a-SiN:H) film as the luminescent layer. The achievable brightness of the representative DCW and ACW TFLEDs were 200 and 170 cd/m² at an injection-current density of 600 and 100 mA/cm², respectively. The electroluminescence (EL) threshold voltage of the DCW TFLED was 10.9 V, and its peak wavelength and full-width at half-maximum (FWHM) of the EL spectrum were about 455 and 230 nm, respectively. For the ACW TFLED, the EL threshold voltage was 8.4 V, and its peak wavelength and FWHM of the EL spectrum were about 535 and 260 nm, respectively. In addition, their current-conduction mechanism was also investigated. Within the lower applied-

voltage region, they showed an ohmic current, while for the higher applied-voltage region, the Frenkel-Poole emission was the main mechanism. It was also found that the H₂-plasma treatment of luminescent i-a-SiN:H layer of an ACW TFLED played an important role in improving device performances, such as decreased EL threshold voltage, increased brightness, and broadened and blue-shifted EL spectrum. The EL spectra of an ACW TFLED under either DC forward or reverse bias or the sinusoidal AC voltage were qualitatively very similar, with a peak wavelength at about 535 nm and a broad FWHM about 260 nm. Moreover, the EL intensity of an ACW TFLED increased with an AC frequency of up to 180 kHz and, then, decreased rapidly and became very weak as the frequency was up to about 500 kHz. [J1360]

"5.6-W Broad-Area Lasers With a Vertical Far-Field Angle of 31° Emitting at 670 nm"

Highly efficient 670-nm high-power broad-area laser diodes with a single InGaP quantum-well embedded in AlGaInP waveguide layers and n-AlInP and p-AlGaAs cladding layers are presented. The developed vertical layer structure leads to a vertical far-field angle of 31°. At 15°C, 100- μ m-wide broad-area lasers reach an output power of 5.6 W limited by thermal rollover. The conversion efficiency was 41% at 1.5 W. A 7600-h reliable operation at 1.5 W and a mean time to failure of about 37550 h will be reported. [J1361]

"Reliability of Deep-UV Light-Emitting Diodes"

This paper analyzes the performance and reliability of deep-ultraviolet light-emitting diodes (LEDs) on AlGaIn emitting at 280 and 295 nm. By means of detailed electroluminescence characterization, we show that the optical properties of the LEDs are strongly influenced by the presence of deep-level-related radiative transitions, and we separately evaluate the contribution of each of these recombination mechanisms on the overall light emission. The reliability analysis presented in this paper shows that stress determines the gradual decrease of the output power of the LEDs, which is more prominent at low measuring current levels. Degradation is attributed to the increase of the nonradiative recombination rate. By means of C-V analysis, we give evidence of modifications of the charge distribution in the active layer, taking place as a consequence of stress: this mechanism is considered to be related to the generation of new defect states near/within the active region. [J1362]

"Use of Elastic Conductive Adhesive as the Bonding Agent for the Fabrication of Vertical Structure GaN-Based LEDs on Flexible Metal Substrate"

Through the use of elastic conductive adhesive (ECA) as the bonding agent and patterned laser lift-off technology, a flexible metal substrate technology for the fabrication of vertical structured GaN-based light-emitting diodes (flex-LEDs) was proposed and demonstrated. It showed that the flex-LEDs have negligible changes in dominant wavelength-current and light output intensity-current-voltage characteristics when subjected to an external bending stress, indicating that the ECA used in the present technology performed well as a buffer to external stresses. As compared with conventional sapphire substrate GaN-based LEDs, Flex-LEDs with a chip size of 600 x 600 μ m² showed an increase in light output intensity (power) about 216% (80%) at 120 mA with an essential decrease in forward voltage from 3.51 to 3.3 V. [J1363]

"Low-Power Low-Cost Voltage-Programmed a-Si:H AMOLED Display for Portable Devices"

This paper presents a driving scheme to achieve highly stable low-power amorphous silicon (a-Si:H) active-matrix organic light-emitting diode (AMOLED) displays. Although the conventional 2-thin-film transistor (TFT) a-Si:H AMOLED display has demonstrated interesting features, including simplicity, it is prone to growing nonuniformity due to the temporal instability of the a-Si:H material. Several compensating techniques have been proposed to control the nonuniformity, but they tend to compromise the key attributes of the simple 2-TFT display such as low power consumption, high yield, high aperture ratio, low implementation cost, and fast programming. For mobile applications which have tight constraints on power consumption, cost, and escalating resolution requirements, we propose a new driving and addressing scheme that not only improves the backplane stability, but also compensates for the OLED luminance degradation while maintaining the attractive features of the simple 2-TFT pixel circuit. The overhead in power consumption and implementation cost is reduced by over 90% compared to existing compensation driving schemes. [J1364]

"InGaN-GaN Nanorod Light Emitting Arrays Fabricated by Silica Nanomasks"

We present a practical process to fabricate InGaN-GaN multiple quantum well nanorod structures. By using silica nanoparticles as the etch mask and followed by dry etching, nanorods with diameter 100 nm can be uniformly fabricated over the entire 2-in wafer. The photoluminescence spectra of the InGaN-GaN p-i-n nanorod structure are extracted at room and low temperatures. Also, discrete density of states can be observed at the temperature below 60 K. We further fabricate nanorod light emitting devices using a planarization approach to deposit p-type electrode on the tips of nanorods. Current-voltage curves and electroluminescent results of nanorod light emitting

diode arrays are demonstrated. [J1365]

"Hybrid CdSe-ZnS Quantum Dot-InGaN-GaN Quantum Well Red Light-Emitting Diodes"

We have demonstrated the fabrication and characterization of hybrid CdSe-ZnS quantum dot (QD)-InGaN-GaN quantum well (QW) red light-emitting diodes (LED). The red-emitting QD-resin blend was dropped on the InGaN blue LED to complete the device fabrication. With proper blend ratio, the blue light from the InGaN QWs can be effectively down converted to the red light. In our case, when the QD concentration is as high as 40 mg/1 ml of resin, the luminous flux from the hybrid LED biased at 20 mA is 0.65 lm, from which the luminous efficiency of 9.3 lm/W can be obtained. Also, the corresponding electroluminescence spectrum exhibits the contribution of red light emission to the total light intensity is 98%, while the Commission Internationale de l'Eclairage chromaticity coordinates of the red light are (0.635, 0.275). However, the coordinates would be gradually shifted with current increasing from 10 to 60 mA due to the fluctuation of red/blue light ratio and thermal effect. [J1366]

"Thermal Study of High-Power Nitride-Based Flip-Chip Light-Emitting Diodes"

This paper presents a chip-level thermal study of high-power nitride-based flip-chip (FC) light-emitting diodes (LEDs). In order to understand the thermal performance of the high-power FC LEDs thoroughly, a quantitative parametric analysis of the thermal dependence on the chip contact area, bump configuration, and bump defects was performed by finite-element model (FEM) numerical simulation and thermal infrared (IR) microscopy testing, respectively. FEM numerical simulation results proved that the optimized bump configuration design was essential to get a uniform temperature distribution in the active layer and improve the thermal performance of the FC LED. IR microscopy testing results recognized that bump defects formed in the LED chip solder processing would lead to surface hot spots around the vicinity of these bump defects, particularly under high-current working conditions. In addition, a light-emitting dark zone was also observed in the optical field for FC LEDs with bump defects. In summary, optimized LED FC bump configuration design and good bonding quality in the chip bonding process are proved to be critical for improving the thermal performance and extending the operating longevity of high-power FC LEDs. [J1367]

"Enhanced Luminance Efficiency of Wafer-Bonded InGaN-GaN LEDs With Double-Side Textured Surfaces and Omnidirectional Reflectors"

A p-side-up GaN-based light-emitting diode (LED) on a silicon substrate was designed and fabricated using a combination of omnidirectional reflector (ODR) and double-side textured surface (both p-GaN and undoped-GaN) structures via surface-roughening, laser lift-off (LLO) and wafer-bonding technologies. The reflectivity of the designed ODR can reach 99.1% at a wavelength of 460 nm. The textured surface of top p-GaN was achieved under low temperature (LT) conditions using metalorganic chemical vapor deposition. It was found that the GaN LED with an extra 200-nm-thick LT p-GaN layer exhibits a 50% enhancement in luminance intensity. The luminance efficiency of double-side roughened silicon-ODR-GaN LED with a small chip size of 250 μm times 500 μm can be improved from 23.2% to 28.2% at an injection current of 20 mA. For the case of 1 mm times 1 mm in chip size, the saturation behavior of the light output power is not observed when an injection current increased from 20 to 350 mA, where the luminance efficiency at 20 mA can reach 28.9%, demonstrating an enhancement by 46%, as compared with that of the conventional GaN-sapphire LEDs. These enhanced results can be attributed to higher reflectivity from the ODR and multiple chances of light emitted from the active region to escape, as well as a centralizing effect of light along the vertical direction. [J1368]

"Blue Electroluminescence From Metal/Oxide/6H-SiC Tunneling Diodes"

The tunneling current of Pt/oxide/n-6H-SiC tunneling diodes was used for electroluminescence (EL). The negative gate bias can inject electrons from Pt to n-SiC and leads to a radiative donor-acceptor pair (DAP) transition. The blue EL at room temperature is observed at negative gate bias, and the intensity increases with increasing drive current. The DAP transition is enhanced by the electric field due to carrier tunneling. Thus, strong luminescence is observed at negative (inversion) bias, while no luminescence is observed at positive (accumulation) bias. [J1369]

"A Low-Power CMOS Front-End for Photoplethysmographic Signal Acquisition With Robust DC Photocurrent Rejection"

A micro-power CMOS front-end, consisting of a transimpedance amplifier (TIA) and an ultralow cutoff frequency lowpass filter for the acquisition of photoplethysmographic signal (PPG) is presented. Robust DC photocurrent rejection for the pulsed signal source is achieved through a sample-and-hold stage in the feed-forward signal path and an error amplifier in the feedback path. Ultra-low cutoff frequency of the filter is achieved with a

proposed technique that incorporates a pair of current-steering transistors that increases the effective filter capacitance. The design was realized in a 0.35- μm CMOS technology. It consumes 600 μW at 2.5 V, rejects DC photocurrent ranged from 100 nA to 53.6 μA , and achieves lower-band and upper-band-3-dB cutoff frequencies of 0.46 and 2.8 Hz, respectively. [J1370]

"Bottom-Gate Gallium Indium Zinc Oxide Thin-Film Transistor Array for High-Resolution AMOLED Display"

The fabrication process and the characteristics of bottom-gate $\text{Ga}_2\text{O}_3\text{-In}_2\text{O}_3\text{-ZnO}$ (GIZO) thin-film transistors (TFTs) are reported in detail. Experimental results show that oxygen supply during the deposition of GIZO active layer and silicon oxide passivation layer controls the threshold voltage of the TFT. The field-effect mobility and the threshold voltage of the GIZO TFT fabricated under the optimum process conditions are 2.6 $\text{cm}^2/\text{V s}$ and 3.8 V, respectively. A 4-in QVGA active-matrix organic light-emitting diode display driven by the GIZO TFTs without any compensation circuit in the pixel is successfully demonstrated. [J1371]

"Active Region Cascading for Improved Performance in InAs-GaSb Superlattice LEDs"

Cascading of active regions in InAs-GaSb superlattice light-emitting diodes (LEDs) grown by molecular beam epitaxy is demonstrated as an effective means of increasing optical emission. Devices were fabricated into 120 x 120 μm^2 mesas to demonstrate suitability for high resolution projection systems. Devices with 1, 4, 8, and 16 stages were designed for midwave infrared emission at 3.8 μm operating at 77 K, and quasi-continuous-wave output powers in excess of 900 μW from a 16-stage LED have been demonstrated. External quantum efficiency is shown to improve substantially with cascading, approaching 10% for a 16-stage device. [J1372]

"5 GHz 200 Mbit/s radio over polymer fibre link with envelope detection at 650 nm wavelength"

All-optical envelope detection of a 5 GHz 200 Mbit/s modulated radio frequency signal is achieved using a 650 nm resonant cavity light emitting diode. Error-free transmission is achieved over a 50 m-long link of 1 mm diameter graded index polymer optical fibre (POF). The presented system has potential applications in low cost and low complexity short range wireless and wireline POF-based transmission links. [J1373]

"Electrically driven ZnO nanoparticle light emitting device"

A light emitting device with commercially available ZnO nanoparticles as an active layer was realised without the help of organic support layers. A tight ZnO nanoparticle layer with thickness of 500 nm was spin coated on the top of an indium tin oxide fused silica substrate. After evaporation of a top aluminium electrode, diode-like I-V characteristics and a pronounced electroluminescence in the visible spectral range were obtained. [J1374]

"The Effect of Electrode Layout on Nitride-Based Light-Emitting Diodes"

Nitride-based light-emitting diodes (LEDs) with different electrode layouts were fabricated and analyzed. The turn-on voltage (V_f) was proved to be highly related to the layout design of N-extending electrode. In addition, the electroluminescence intensity was almost proportional to the area of transparent contact layer (ATCL) subtracting the area of P-extending electrode (AP). Moreover, the current spreading was highly sensitive to the location and route of P- and N-extending electrodes. Good location and route can avoid thermal effect and damage. Finally, this paper proposed an easy and direct concept to estimate and predict the performance of nitride-based LEDs in turn-on voltage, electroluminescence intensity, and current spreading. It was highly potential to improve and change the currently mask design of nitride-based LEDs. [J1375]

"Ga-Doped ZnO Transparent Conductive Oxide Films Applied to GaN-Based Light-Emitting Diodes for Improving Light Extraction Efficiency"

In this study, Ga-doped ZnO (GZO) thin films were deposited on a sapphire substrate utilizing a magnetron sputtering approach. ZnO and Ga_2O_3 targets were employed as the sputtering sources during a cosputtering deposition. After thermal annealing in nitrogen ambient conditions, the electrical resistivity and optical transparency of the GZO films were analyzed in detail. The GZO films exhibited high transparency ($\sim 90\%$) in visible light and low resistivity ($\sim 5.3 \times 10^{-4} \Omega\text{-cm}$) when they were annealed at a temperature of 600-800 deg C. Although the utilization of indium tin oxide (ITO) serving as the transparent contact layer (TCL) in conventional GaN-based light-emitting diodes (LEDs) is a well accepted technology, ZnO-based TCLs with a high refractive index of around 2.0 would render another advantage when a roughening process is performed on the surface. In other words, since packaged LEDs are generally encapsulated using epoxy with a refractive index of around 1.5, surface roughening performed on ITO TCL would thus result in only a minor improvement in light extraction because the typical refractive index of an ITO film prepared by our e-beam evaporator is around

1.7. In this study, GaN-based LEDs that utilized ITO/GZO composite oxide films as a TCL were also demonstrated. The light output power of an LED (LED-C) with a textured ITO/GZO composite TCL is markedly improved by 42 % and 48 % of magnitude as compared to LEDs with a planar GZO TCL (LED-A) and a ITO/GZO composite TCL (LED-B), respectively. This enhancement is due to the fact that a ZnO-based TCL with a higher refractive index ($n \sim 2.0$) allows further enhancement of light extraction through the creation of a textured structure on the TCL that is deposited on the top surface of LEDs. [J1376]

"Solid State Headlights [JAutomotive Electronics]"

Following years of technology demonstrations, concept cars, and promises for the future, light-emitting diode (LED) headlights finally achieved the reality of that promise with the introduction of the 2008 Cadillac Escalade Platinum, the world's first production vehicle with high- and low-beam LED headlights (Carney, 2008). While the Lexus LS 600h achieved the distinction of being the first production car with LED headlights of any kind, it employs conventional halogen high beams. And Audi has announced that it will offer full LED lighting on its R8 sports car. [J1377]

"Zinc Oxide Nanostructures and High Electron Mobility Nanocomposite Thin Film Transistors"

This paper reports on the synthesis of zinc oxide (ZnO) nanostructures and examines the performance of nanocomposite thin-film transistors (TFTs) fabricated using ZnO dispersed in both n- and p-type polymer host matrices. The ZnO nanostructures considered here comprise nanowires and tetrapods and were synthesized using vapor phase deposition techniques involving the carbothermal reduction of solid-phase zinc-containing compounds. Measurement results of nanocomposite TFTs based on dispersion of ZnO nanorods in an n-type organic semiconductor ([6, 6]-phenyl-C61-butyric acid methyl ester) show electron field-effect mobilities in the range $0.3\text{--}0.6\text{ cm}^2\text{V}^{-1}\text{s}^{-1}$, representing an approximate enhancement by as much as a factor of 40 from the pristine state. The on/off current ratio of the nanocomposite TFTs approach 10^6 at saturation with off-currents on the order of 10 pA. The results presented here, although preliminary, show a highly promising enhancement for realization of high-performance solution-processable n-type organic TFTs. [J1378]

"A New AlGaInP Multiple-Quantum-Well Light-Emitting Diode With a Thin Carbon-Doped GaP Contact Layer Structure"

A new AlGaInP multiple quantum-well light-emitting diode (LED) with a thin carbon-doped GaP contact layer and a transparent conducting indium tin oxide film is fabricated and studied. For comparison, the LEDs with different contact layer structures are also included in this work. Experimental results indicate that the LED with a carbon-doped GaP contact layer exhibits a higher output power of 31.4 mW and a higher external quantum efficiency of 9%. The light-output power, under dc 20-mA operation, of this LED is increased by a factor of 18% as compared with that of conventional LEDs. These results are mainly attributed to the significantly lower series resistance and lower optical absorption effect. Moreover, the new device shows the reduced wavelength shift with 1.7-nm variation between 10 and 200 mA in electroluminescence spectrum. [J1379]

"Enhanced Light Output Power of GaN-Based Vertical Light-Emitting Diodes by Using Highly Reflective ITO-Ag-Pt Reflectors"

Highly reflective and thermally stable indium-tin-oxide (ITO)-Ag-Pt p-type reflectors for use in high-performance GaN-based light-emitting diodes (LEDs) have been investigated. The specific contact resistance of the ITO-Ag-Pt contacts was found to be $7.2 \times 10^{-5} \Omega \text{cm}^2$. The ITO-Ag-Pt contacts showed a higher reflectance after thermal annealing (82% at 460 nm), while the reflectance of the ITO-Ag contacts was reduced from 81% to 65%. In addition, surface agglomeration was drastically decreased, indicating that the Pt layer efficiently prevents the surface agglomeration of the Ag layer. The vertical LEDs (VLEDs) fabricated with the ITO-Ag-Pt contacts had a 17% higher output power (at 20 mA) than the VLEDs fabricated with the ITO-Ag contacts. [J1380]

"GaN-Based MSM Photodetectors Prepared on Patterned Sapphire Substrates"

GaN-based metal-semiconductor-metal ultraviolet photodetectors (PDs) prepared on a patterned sapphire substrate (PSS) and a conventional flat sapphire substrate were both fabricated and characterized. It was found that we can reduce dark leakage current and enhance by about two orders of magnitude by using a PSS. The internal gain of the PDs prepared on a PSS was also much smaller. [J1381]

"Displays 2.0 [JCOMMS display technology]"

Just as a nation of TV watchers finishes bolting their first flat panels to the living-room wall, a new set of display technologies is emerging to offer better image quality, bigger screens and thinner panels. [J1382]

"Polarization-Insensitive All-Optical Flip-Flop Using Tensile-Strained Multiple Quantum Wells"

We demonstrate a polarization-insensitive all-optical flip-flop based on a multimode-interference bistable laser diode. Polarization-insensitive flip-flop operation is demonstrated with the set power as low as -3 dBm, by applying 0.3% tensile strain to the multiple quantum wells gain medium. The output state of polarization is stabilized to the transverse-magnetic mode irrespective of input polarization, indicating that our device also offers a polarization-stabilizing function. Dynamic switching is achieved without waveform distortion even when the input polarization state is scrambled. [J1383]

"High-Performance (Al Ga) In P-Based Flip-Chip Light-Emitting Diode With a Geometric Sapphire Shaping Structure"

AlGaInP-based flip-chip light-emitting diodes (LEDs) with geometric sapphire shaping structures were fabricated by sapphire chemical etching and glue-bonded techniques. Furthermore, a nanoscale rough texture was applied on the epiwafer surface. This novel structure improved the output light power, wall-plug efficiency, and reliability. The output power of this structure was enhanced 31.2% under 350-mA current injection as compared with the conventional AlGaInP flip-chip LEDs. [J1384]

"Laser Liftoff GaN Thin-Film Photonic Crystal GaN-Based Light-Emitting Diodes"

We fabricated a thin-film vertical-injection light-emitting diode (LED), which uses a highly efficient coherent external scattering of trapped light by photonic crystal (PhC). The PhC patterns ($a = 1200$ nm) were formed on top of the n-GaN surface after laser liftoff of the sapphire substrate. This light extraction structure just above micron scale was prepared by a conventional photolithography ($\lambda_{\text{dca}} = 405$ nm). The Si-gel-encapsulated thin-film LED with PhC patterns ($a = 1200$ nm), which had a depth of 500 nm, demonstrated up to 76% improvement in light output power at a forward current of 60 mA, compared with the nonpatterned thin film LED. [J1385]

"Very Long Operational Lifetime at High Initial Luminance of Deep Red Phosphorescent Organic Light-Emitting Diodes With Double Emission Layers"

We report a double emission layer structure, incorporating a double phosphorescent Ir^{III} complex/host system of tris (1-Phenylisoquinoline) iridium (III) (Ir(piq)₃) 15wt% doped into two different host molecules, 4,4'-bis[N-(1-naphthyl)-N-phenyl-amino] biphenyl (NPB) and bis-(2-methyl-8-quinolinolato)-4-(phenyl-phenolato) aluminum-(III) (BAIq). The proposed configuration reduces the efficiency rolloff, providing high stability at high operating luminance. A maximum current efficiency of 9.5 cd/A, at a driving voltage of 3 V, and a remarkably long device lifetime of more than 2500 h at a starting luminance of 6000 cd/m² have been measured. [J1386]

"Stable Binary Complementary White Light-Emitting Diodes Based on Quantum-Dot/Polymer-Bilayer Structures"

A binary complementary white light-emitting diode (LED) was designed and fabricated by employing a colloidal quantum-dot (QD)/polymer-bilayer configuration in the device active region. Stable white electroluminescence is observed from the cumulative emission of the yellow-emitting CdSe-ZnS core-shell QDs and blue-emitting poly(N,N'-bis (4-butylphenyl)-N,N'-bis(phenyl)benzidine) (Poly-TPD) molecules. The white chromaticity of the LED output can be tailored by varying the respective thicknesses of the constituent emissive layers; whereas the emission color exhibits little dependence on the applied bias over a wide voltage range. The maximum luminance of the device reaches 2600 cd/m² under a bias of 9.4 V. [J1387]

"Light Extraction Improvement From GaN-Based Light-Emitting Diodes With Nano-Patterned Surface Using Anodic Aluminum Oxide Template"

An improvement of light extraction from GaN-based light-emitting diodes (LEDs) was demonstrated by forming surface nano-structures using an anodic aluminum oxide (AAO) template as a dry etching mask. Nano-pores were simultaneously formed on indium tin oxide and GaN surfaces of LED with different pore depths by the same procedural steps, with a pore density and pore diameter of $1.14 \times 10^9/\text{cm}^2$ and 163 nm, respectively. The nano-patterned LEDs achieved a top-face light output power enhancement of 72% compared to the conventional LEDs at 20 mA. The light extraction effects of the nano-structures on the trapped optical modes in LED were revealed by scanning electron microscopy and microscopic electroluminescence. [J1388]

"Optical Analysis of Color Distribution in White LEDs With Various Packaging Methods"

Uniform color distribution is essential for the packaging of light emitting diodes (LEDs). The Monte Carlo ray tracing method is applied to analyze the color distribution of white LEDs. Five packaging methods are investigated and the location of phosphor layer is varied. Results reveal that the packaging method is the primary factor affecting the color distribution and a nonreflector packaging method presents better color uniformity. The location of phosphor has a small impact on the color uniformity but remote location, if too far, can reduce the uniformity significantly. The reduction of color uniformity may exceed 88%. [J1389]

"Design Methodology for High Brightness Projectors"

The low luminance levels of light-emitting diodes (LEDs) compared to arc lamps make it difficult to design high-brightness LED-based projectors. Besides, the specificities of LEDs do not always allow using the same design schemes as with arc lamp-based projection displays. This paper performs a taxonomy of the techniques that can be used to increase the brightness of LED-based projection displays. We show that, in etendue-limited systems, the perceived brightness depends on the system etendue limit, the efficiency of the light engine, and the source luminance. The ability to improve each of these parameters depends on the design constraints. The system etendue limit can be increased at the expense of bulkier, more complex, and more expensive designs. The light engine efficiency can be increased by using free-form shape components adapted to the shapes and the emission patterns of the considered LEDs. The apparent source luminance can be increased at the expense of the flux by either recycling light or restricting the light collection to a smaller etendue with higher average luminance. Luminance can also be increased by using multiple color primaries (spatial multiplexing) or pulsed LEDs (temporal multiplexing). Finally, we review how light recycling can be implemented to convert polarization without increasing etendue. [J1390]

"Fabrication of Efficient Light-Emitting Diodes With a Self-Assembled Photonic Crystal Array of Polystyrene Nanoparticles"

A low-cost method of fabricating large photonic crystal arrays of hexagonal posts without the use of lithography is described, along with an application of enhancing light extraction efficiency in semiconductor light-emitting diodes (LEDs). Polystyrene spheres are deposited onto a wafer surface and then processed to achieve control over photonic crystal lattice properties in a method suitable for fast and repeatable patterning. The spheres serve as an etch mask to extend the photonic crystal formed into the semiconductor surface. This technique is applied to LEDs to increase the top surface light extraction, and 51% wall plug enhancement is demonstrated in deep junction liquid phase epitaxially grown LEDs with absorbing substrates, though is adaptable to any substrate and photonic crystal dimensions. [J1391]

"Dual Partial Dye Doping for Chromaticity Tuning and Performance Enhancement of White OLEDs"

In general, a guest dopant is doped into a single host matrix for white-light emission with two complementary colors. In this work, however, we have fabricated a white organic light-emitting diode (WOLED) based on dual partial dye doping in which a guest dopant is partially doped into two different host emitters; namely, orange-red emitting 4-(dicyanomethylene)-2-methyl-6-(p-dimethylaminos-tyrly)-4H-pyran (DCM) is partially doped into both blue-emitting 4, 4'-bis(2,2'-diphenylvinyl)-1,1'-biphenyl (DPVBi) and green-emitting Tris-(8-hydroxyquinoline) aluminum (Alq3). We demonstrate that dual partial dye doping allows us to finely tune the Commission Internationale d'Eclairage (CIE) chromaticity coordinates to the equienergy white point ($x = 0.33$, $y = 0.33$). In addition, it enhances device performance further, compared to WOLEDs based on DCM partially doped into a single host matrix (either DPVBi or Alq3). Moreover, the dual partial doping scheme is shown to provide a way of suppressing the self-quenching effect (singlet-singlet annihilation). For a systematic study, we have implemented a comprehensive numerical model and performed simulations of the OLED structure, providing a clear understanding with regard to the underlying physics of OLEDs. We also carry out an investigation of the effects of key design parameters such as the doped layer position and thickness and dye. [J1392]

"Reliability of Active-Matrix Organic Light-Emitting-Diode Arrays With Amorphous Silicon Thin-Film Transistor Backplanes on Clear Plastic"

We have fabricated active-matrix organic light emitting diode (AMOLED) test arrays on an optically clear high-temperature flexible plastic substrate at process temperatures as high as 285 degC using amorphous silicon thin-film transistors (a-Si TFTs). The substrate transparency allows for the operation of AMOLED pixels as bottom-emission devices, and the improved stability of the a-Si TFTs processed at higher temperatures significantly improves the reliability of the light emission over time. [J1393]

"Direct Fabrication of Nanoscale Light Emitting Diode on Silicon Probe Tip for Scanning Microscopy"

We have fabricated a silicon microprobe integrated with a nanometer-sized light emitting diode (Nano-LED) on the tip. This paper describes the fabrication procedure and preliminary topographic testing results. The silicon probe with electrode pattern was made by wet-etching a silicon-on-insulator wafer using oxide as the mask. Subsequently, the probe tip was cut using a focused ion beam (FIB) to form a 150 nm-wide gap. Semiconductor nanoparticles (CdSe/ZnS core-shell nanoparticles) were electrostatically trapped and excited within the electrode gap made on the probe tip. The LED-tip is approximately 150 nm 150 nm. The nano-LED light intensity and current were measured as a function of the driving voltage up to 25 V. In addition to the electroluminescence peaks from the CdSe particles, possible emission from silicon dioxide doped in the FIB milling process was also observed in the measured spectra. Basic mechanical characteristics of the silicon probe were measured by mounting the probe on a tuning fork in a standard near-field scanning optical microscopy (NSOM) set up. It was observed that the drag force reduces the probe oscillation as the vibrating tip approached the near-field of the sample surface. The topographic images of a chromium test pattern on a glass substrate were successfully acquired by keeping the probe tip within roughly 5 nm from the sample surface. Although the probe tip shape and the location of the Nano-LED are yet to be further optimized before realizing near-field optical scanning experiment, the result showed its great promise as a new type of NSOM tip with the light-source. [J1394]

"A Plastic Optical Fiber Sensor for the Dual Sensing of Temperature and Oxygen"

This study presents a low-cost plastic optical fiber sensor for the dual sensing of temperature and oxygen. The sensor features commercially available epoxy glue coated on the side-polished fiber surface for temperature sensing and a fluorinated xerogel doped with platinum tetrakis pentafluorophenyl porphyrin coated on the fiber end for oxygen sensing. The temperature and oxygen indicators are both excited using an ultraviolet light-emitting diode light source with a wavelength of 380 nm. The luminescence emission spectra of the two indicators are well resolved and exhibit no crosstalk effects. Our studies show that the temperature response of the sensor is independent of the oxygen concentration. Overall, the results indicate that the dual sensor presented in this study provides an ideal solution for the noncontact, simultaneous sensing of temperature and oxygen in general biological and medical applications. [J1395]

"A Novel Voltage-Feedback Pixel Circuit for AMOLED Displays"

This study presents a novel voltage-modulated pixel circuit for active-matrix organic light-emitting diode (AMOLED) consisting of five n-type thin-film transistors (TFTs), one additional control signal, and one storage capacitor. The proposed circuit, which can be implemented in all-n-type and all-p-type low temperature polysilicon (LTPS) TFT technologies, successfully compensates for threshold voltage deviation of TFTs and facilitates correction of OLED degradation using a voltage feedback method. Simulation and experimental results for all-n-type TFTs indicate that the proposed pixel circuit reduced the nonuniformity brightness problem effectively by compensating for threshold voltage variation in TFTs and reduced the degradation of emission efficiency in OLEDs. [J1396]

"Power Consumption and Temperature Increase in Large Area Active-Matrix OLED Displays"

We model and analyze the power consumption and resulting temperature rise in active-matrix organic-light-emitting device (AMOLED) displays as a function of the OLED efficiency, display resolution and display size. Power consumption is a critical issue for mobile display applications as it directly impacts battery requirements, and it is also very important for large area applications where it affects the display temperature rise, which directly impacts the panel lifetime. Phosphorescent OLEDs (PHOLEDs) are shown to offer significant advantage as compared to conventional fluorescent OLEDs due to high luminous efficiency resulting in lower pixel currents, reducing both the power consumed in the OLED devices and the series connected driving thin-film transistor (TFT). The power consumption and temperature rise of OLED displays are calculated as a function of the device efficiency, display size, display luminance and the type of backplane technology employed. The impact of using top-emission OLEDs is also discussed. [J1397]

"Effects of Saccade Length and Target Luminance on the Refresh Frequency Threshold for the Visibility of Color Break-Up"

Field-sequential color displays are susceptible to a visual artefact called color break-up, which is an image-quality problem and may also cause visual discomfort. However, the effect can be greatly reduced by increasing the refresh frequency of the display. In this study, we measured refresh frequency thresholds for color break-up visibility by using a two-alternative forced choice staircase method. Subjects made controlled horizontal saccades

so that the gaze followed a white target which abruptly changed position. The white target was a red, green, and blue (RGB) light-emitting diode (LED), in which the red, green, and blue colors were shown sequentially. Saccade length (2, 4, 8, and 14 deg) and target luminance level (2, 31.5, and 500 cd/m) were varied. The contrast between stimulus and background and the size of the stimulus were held constant. The results showed that a refresh frequency as high as 1200 Hz would be needed to completely eliminate the phenomenon. Further, the threshold value increased with saccade length and target luminance. However, the effect of luminance saturated relatively early. [J1398]

"Development of an Implantable Pulse Oximeter"

A long-term implantable photoplethysmographic sensor system is proposed. The system employs an elastic cuff which is directly wrapped around an arterial blood vessel. The optically transparent cuff is equipped with light emitting diodes and a photo transistor including the technology of pulse oximetry. The sensor will permit real-time, continuous monitoring of important vital parameters such as arterial blood oxygen saturation and pulse rate over a long-term period in vivo. We emphasize on the specific requirements for design and instrumentation of the implantable sensor and discuss first in vitro data acquired with that new photonics-based sensor. [J1399]

"Representations of Relative Display Gamut Size"

Gamut size of a wide gamut display is usually represented with the ratio of its chromaticity triangle area and the chromaticity triangle area of a standard display in CIE xy color coordinates. Such a chromaticity area ratio (CAR) is a rough relative gamut size, because CIE xy is a nonuniform color coordinate system and display gamut is a volume in color space. The representation of relative gamut size with the ratio of the discernible color numbers in a display gamut and NTSC TV gamut is studied. This ratio is called the discernible color number ratio (DCNR). Discernible color number is counted with CIE94 color difference formula in CIELAB color space. It is found that CAR is larger than DCNR for the display with primary purity higher than NTSC primary purity. For example, the CAR of a practical light-emitting diode (LED) display with respect to NTSC TV is 7.8% overestimated, in which red, green, and blue LED primary wavelengths are 625, 520, and 470 nm, respectively; red, green, and blue LED bandwidths are 20, 40, and 30 nm, respectively. In addition, the DCNRs of wide gamut displays with respect to the object color of the same white illuminant are investigated. It is shown that the gamut size improvement for laser display compared with LED display is not significant. [J1400]

"Correlation of Current Noise Behavior and Dark Spot Formation in Organic Light-Emitting Diodes"

A correlation between current 1/f noise and dark spot formation is reported. Our results show that the dark spot is primarily correlated to current 1/f noise slope; the higher the slope, the poorer the interface, and the more abnormal dark spot growth rate and the shorter lifetime. Besides, there is a correlation between current 1/f noise magnitude and the dark spot initial size. A higher 1/f noise magnitude generally indicates a larger dark spot initial size. A seemingly identical current-voltage curve does not render the same characteristics of dark spot formation, which can be clearly distinguished from the subtle difference in 1/f noise behavior. The noise measurement can be used to predicate device lifetime and degradation behavior. [J1401]

"Radiation Effects on InGaN Quantum Wells and GaN Simultaneously Probed by Ion Beam-Induced Luminescence"

InGaN quantum well structures on GaN epilayers were exposed to 500 keV alpha particles to fluences above 1014cm² to probe the relative radiation tolerance of the epilayer and wells. Performance was estimated by the intensity of ion-beam induced luminescence. Two separate types of quantum well structures emitted at 470 and 510 nm prior to irradiation, and only small wavelength shifts were observed even with the highest alpha fluences. Complementary cathodoluminescence experiments showed that luminescence in the quantum wells is strongly influenced by charges injected deep into the GaN epilayer. The 500 keV alpha penetration depth was ~ 1 μm, so that defects were created at a faster rate in GaN compared to InGaN as alpha particles slowed and stopped within a minority carrier diffusion length of the quantum wells. However, the rate of luminescent decay was similar for both materials. Taken together with the cathodoluminescence data, this ion-beam induced luminescence comparison indicates that the quantum well luminescence decay rate is dominated by radiation-induced defects in the GaN epilayer. InGaN quantum wells are then demonstrated to be not more than a factor of ten more radiation sensitive than GaN, and may be substantially less sensitive than this upper bound. [J1402]

"Nitride-Based LEDs With a Hybrid Al Mirror DBR Backside Reflector"

Nitride-based light-emitting diodes (LEDs) with a hybrid backside reflector combining a TiO₂/SiO₂ distributed Bragg reflector (DBR) and an Al mirror were proposed and realized. It was found that we can significantly enhance the 35% reflectivity of the 2-pair TiO₂/SiO₂ DBR to 94% by combining with Al mirror (hybrid reflector).

Furthermore, reflectivity of the proposed reflector depends only slightly on incident light wavelength and the incident angle. With 350-mA current injection, it was found that the output powers were 145.7, 178.2, and 201.9 mW for the LEDs with 2-pair DBR, with an Al mirror and with a hybrid reflector, respectively, when packaged in TO-cups. It was also found that reliability for the LED with the hybrid reflector is good. [J1403]

"Hybrid Spintronic Structures With Magnetic Oxides and Heusler Alloys"

Hybrid spintronic structures, integrating half-metallic magnetic oxides and Heusler alloys with their predicted high spin polarization, are important for the development of second-generation spintronics with high-efficient spin injection. We have synthesized epitaxial magnetic oxide Fe₃O₄ on GaAs(100) and the unit cell of the Fe₃O₄ was found to be rotated by 45° to match the gallium arsenide GaAs. The films were found to have a bulk-like moment down to 3-4 nm and a low coercivity indicating a high-quality magnetic interface. The magnetization hysteresis loops of the ultrathin films are controlled by uniaxial magnetic anisotropy. The dynamic response of the sample shows a heavily damped precessional response to the applied field pulses. In the Heusler alloy system of Co₂MnGa on GaAs, we found that the magnetic moment was reduced for thicknesses down to 10 nm, which may account for the lower than expected spin-injection efficiency from the spin-light-emitting diode structures. Using the element-specific technique of X-ray magnetic circular dichroism (XMCD), the reduced spin moments were found to originate from the Mn rather than the Co atoms, and the improvement of the interface is thus needed to increase the spin injection efficiency in this system. Further studies of the I-V characteristics of Fe₃O₄/GaAs(100) and Fe₃O₄/MgO/GaAs(100) show that the Fe₃O₄-based spintronic structures have a well-defined Schottky or tunneling barrier of moderate barrier height, which is encouraging for high-efficient spin injection. [J1404]

"Design, Fabrication, and Characterization of Near-Field Apertures for 1 Tbit/in Areal Density"

Today, conventional magnetic recording schemes are coming to an end because of the superparamagnetic limit. Heat-assisted magnetic recording (HAMR) may ultimately extend data densities beyond 1 TB/in². HAMR systems utilize the phenomenon during which the magnetic properties of the recording media could be locally modified via heating (optionally, by an optical source in the near field) to temperature in the vicinity of the Curie value of the media material. As a result, heat induced by the optical source can temporarily reduce the magnetic coercivity of high anisotropy material to a level attainable by the magnetic writing head, thus making it feasible to record on relatively small ultra-high anisotropy (and thermally stable) grains, consequently enhancing the areal density dramatically. The key challenge is to develop a near-field transducer capable of delivering over 50 nW into a spot diameter of 30 nm. Traditional fiber schemes are barely capable of 0.1 nW. To resolve the issue, a laser diode could be placed with the emitting edge only a few nanometers away from the recording media. The light can propagate through a nanoaperture on the surface of an aluminum-coated emitting edge. This paper will present an experimental study of recording characteristics of various near-field transducers fabricated via focused ion beam (FIB). To count the number of photons emitted in the near field, a scanning near-field optical microscopy system has been implemented. The experiments indicate that the FIB-fabricated transducers could deliver power of over a few microwatt into a 30-nm spot (Fig. 7). [J1405]

"Observation of Phonon Replica Emission in an In-Situ Fe/GaAs Spin LED"

GaAs-based spin LEDs were used to study spin injection through a Schottky barrier from a ferromagnetic contact formed by an in-situ technique. Optical measurements were performed in both oblique Hanle and Faraday geometry. In addition to direct recombination at the Gamma-point in the quantum well, emission peaks were seen due to phonon-assisted recombination from the X and L valleys in the semiconductor. The presence of the phonon replica peaks indicates that strong tunneling occurs from the Fe into the X and L minima at the interface. As measured in the oblique Hanle geometry, the satellite peaks display optical polarization, which indicates spin polarized injection into these minima. It is argued that enhanced tunneling into the X and L minima leads to a lower spin polarization in the device due to the transport properties of these valleys. This mechanism then limits the maximum effective spin polarization that can be achieved at a coherent interface. [J1406]

"Studies of Phosphor Concentration and Thickness for Phosphor-Based White Light-Emitting-Diodes"

The dependence of luminous efficacy on phosphor concentration and thickness for high-power white light-emitting-diode (WLED) lamps is investigated by employing three-dimensional ray-tracing simulations. The simulations show that the brightness or luminous efficacy of WLED lamps highly depends on the combination of phosphor concentration and phosphor thickness (or phosphor-matrix composite volume). The package with lower concentration and higher phosphor thickness has higher luminous efficacy because the light trapping efficiency is lower with the low phosphor concentration. At the correlated color temperature (CCT) value of

around 4000 K, ray-tracing simulation and experimental results show 20% and 23% improvement in lumen, respectively, with a 1.8-mm-phosphor package over a 0.8-mm-phosphor package. A package with convex lens can improve the lumen output over flat lens, but this improvement is small, and it requires higher amount of phosphor, up to 25%, to achieve same CCT value. [J1407]

"Aluminium-based packaging platform for led using selectively anodising method"

An aluminium-based packaging platform with microreflector and electrical via for an interconnection electrode is first proposed for a package component of a light-emitting diode (LED). The electrode-guided interconnection with 180 μm thickness has been successfully fabricated by using the selectively anodising process, and not by either the plating or the solder paste technique. The reflector was formed during the isotropic etching process. By mainly a two-step chemical process, the LED packaging platform integrated microreflector and electrical via in one body was developed in a low-cost process. [J1408]

"Aging and Stability of GaN High Electron Mobility Transistors and Light-Emitting Diodes With-and Ir-Based Contacts"

There is interest in developing more stable contacts to a variety of GaN-based devices. In this paper, we give two examples of devices that show improved thermal stability when boride or Ir diffusion barriers are employed in ohmic-contact stacks. AlGaIn/GaN high electron mobility transistors (HEMTs) were fabricated with Ti/Al/X/Ti/Au source-drain ohmic (where X is Ir) contacts and were subjected to long-term annealing at 350 °C. By comparison with companion devices with conventional Ti/Al/Ni/Au ohmic contacts, the HEMTs with boride-based ohmic metal showed superior stability of both source-drain current and transconductance after 25 days of aging at 350 °C. The gate current for standard HEMTs increases during aging, and the standard ohmic contacts eventually fail by shorting to the gate contact. Similarly, InGaIn/GaN multiple quantum well light-emitting diodes (MQW-LEDs) were fabricated with either Ni/Au//Ti/Au or Ni/Au/Ir/Au p-ohmic contacts. Both of these contacts showed superior long-term thermal stability compared to LEDs with conventional Ni/Au contacts. [J1409]

"Active Packaging Method for Light-Emitting Diode Lamps With Photosensitive Epoxy Resins"

A novel active light-emitting diode (LED) packaging method is presented. Our method utilizes the emission from the LED chip itself to package the LED with photosensitive epoxy. Such a photon-induced polymerization method, leading to the formation of specific lamp shapes and characteristics, eliminates the utilization of the mold. By controlling the packaging parameters, for example, the polymerization current and the polymerization time, the emission properties of the LED lamps can be controlled. It is found that the self-focusing effect plays an important role in the active packaging process. [J1410]

"Broadband Information Broadcasting Using LED-Based Interior Lighting"

Emergence of white-light LEDs allows the combination of lighting and information broadcast functionality in one optical source. We investigate analytically and by Monte Carlo simulations feasible data transmission rates in a moderate-size office room, where we assume illumination conforming to standards and the use of commercially available LEDs and photodiodes. The performances of systems relying on baseband [i.e., pulse-amplitude modulation (PAM)] and discrete multitone (DMT) transmission show that data rates of more than 100 Mbit/s can be expected despite the rather low bandwidth of the system. [J1411]

"Analysis of Gain and Luminescence in Violet and Blue GaInN-GaN Quantum Wells"

In this paper, gain in GaInN quantum wells with 8% and 19% indium is analyzed using a comparison of a microscopic model to experimental data. It is shown that localized valence states can explain the characteristics of the gain spectra, in particular the broadening features at the red side of the spectrum. From an analysis of experimental and simulation data, the nonradiative current component is extracted, and is shown to dominate the total current density at laser threshold operation. The increase of nonradiative current with density explains the drop in internal quantum efficiency in GaInN light-emitting diodes. [J1412]

"Thermal Analysis of GaN-Based Light Emitting Diodes With Different Chip Sizes"

In this paper, we present the thermal, electrical, and optical analyses of light emitting diode (LED) packages with different chip sizes. The LED packages under investigation employed the same configuration of package components, except for the chip sizes. The forward current was found to increase with the chip size at the same forward voltage due to the area increase of current spreading. The luminous flux and optical power were found to increase with the chip size at the same current density. The thermal analysis was made by the transient thermal measurement and thermal simulation using the finite volume method. It was demonstrated that the

thermal resistance decreased with the chip size under the same package conditions both by simulation and experiment. The bulk thermal resistance and spreading thermal resistance were combined together to give out a quantitative investigation of the partial thermal resistance variation. Moreover, the spreading thermal resistance was found to have a great effect on the total thermal resistance of LED packages. [J1413]

"Materials and Process Development for ZnMgO/ZnO Light-Emitting Diodes"

We report on the fabrication of UV LEDs based on a p-n junction p-ZnMgO/n-ZnO/n-ZnMgO double heterostructure. Pulsed-laser deposition was used to grow the complete heterostructure on c-plane sapphire templates. The LEDs were patterned by simple wet etching. Band-edge electroluminescence emission most likely associated with ZnO excitonic transitions was observed at room temperature. However, the devices show sensitivity to the presence of hydrogen in the measurement ambient due to formation of a surface conduction layer. The results show the potential of ZnO-based materials for UV emitters of potentially lower cost and with comparable or higher emission intensity than AlGaIn/GaN devices provided adequate surface passivation techniques are developed. [J1414]

"Design of the Radiation Pattern of Infrared Short-Range Communication Systems for Electronic-Toll-Collection Applications"

This paper proposes a very simple method for enhancing the performance of infrared electronic-toll-collection systems. Using two typical low-cost commercial LEDs with different half-intensity angles $\Phi_{1/2} = 22^\circ$ and 10° , the radiation pattern of the emitting module of an infrared short-range communication system for electronic-toll-collection applications is designed. This enables us to construct a system that has an extended communication region and can withstand high signal attenuation. When the module is fabricated with a proper combination of the numbers of these two different LEDs, together with a suitable mounting angle of each LED, an effective radiation pattern is obtained. The mounting angle of each LED is found with the aid of an optimization algorithm. The performances of three different designs are compared in terms of signal strength, communication length, and 2-D communication region. The results show that a module consisting of ten LEDs divided into three groups, with each group having a proper mounting angle and containing an appropriate number of LEDs, can have much better performance than conventional single-group unidirectional designs. The influence of the defect of the radiation pattern, which may happen on many LEDs, on system performance is also discussed. The results of the analysis are confirmed by experimental measurements. [J1415]

"Solution-Processed Infrared Optoelectronics: Photovoltaics, Sensors, and Sources"

The fabrication of optoelectronic devices via spin-coating onto an arbitrary substrate offers ease of integration, low cost, and physical flexibility. Reports of active optoelectronic devices operating in the IR, and made via solution-processing, emerged in the early 2000s. Here, we review progress in IR solar cells, image sensors, and optical sources based on solution-processed materials. The latest solution-processed photovoltaics (PV) now provide 4.2% power conversion efficiencies in the IR, placing them a factor of 3 away from enabling a doubling in overall solar power conversion efficiency of today's best visible-wavelength solution-processed PV. The best solution-processed photodetectors now provide sensitivities in the 10¹³ Jones D* range, exceeding the sensitivity of the best epitaxially grown short-wavelength infrared photodetectors. Infrared optical sources, both broadband light-emitting diodes and, more recently, lasers, have now also been reported at 1.5 μm . We review the progress and future prospects of this rapidly advancing field. [J1416]

"Light Emission From Silicon in Photonic Crystal Nanocavity"

We have introduced a photonic crystal into a single-crystal silicon slab in order to manipulate the light emission. When the lattice constant of a defect-free photonic crystal matches the wavelength of light in the medium, the light emitted from the silicon is resonantly extracted at the photonic band edge within the escape light cone. When the lattice constant is larger than the wavelength, Brillouin zone folding of the photonic band also allows the light to be extracted; we achieved an intensity that was enhanced by a factor of ~ 20 due to the diffraction of internal light into the light cone. We have also created a point defect in photonic crystals with smaller lattice constants that functions as a nanocavity and strongly interacts with the silicon emitter. Four cavity modes were observed, with different Q-factors and emission patterns. The mode orders were assigned using the resonant wavelengths and polarizations. The observed emission at room temperature was enhanced by a factor of ~ 30 in comparison to that of an unprocessed area of silicon-on-insulator. Our study demonstrates that employing a photonic crystal nanocavity in silicon can greatly improve the light extraction efficiency, the characteristics of the radiation pattern, and the internal quantum efficiency. [J1417]

"Tabletop Resonant Infrared Matrix-Assisted Pulsed Laser Evaporation of Light-Emitting Organic"

Thin Films"

Structural optimization of light-emitting polymer, or organic semiconductor, thin films deposited by tabletop 2.9 μm resonant infrared matrix-assisted pulsed evaporation (RIR-MAPLE) is investigated. Surface morphology of poly[2-methoxy-5-(2'-ethylhexyloxy)-1,4-(1-cyanovinylene) phenylene] (MEH-CN-PPV) and poly[2-methoxy-5-(2'-ethylhexyloxy)-1,4-phenylene vinylene] (MEH-PPV) films are analyzed using optical and atomic force microscopy. These films are deposited using different target-to-substrate distances, ambient base pressures, laser fluences, and substrate temperatures, and with different target compositions comprising tetrahydrofuran (THF), chlorobenzene, toluene, o-xylene, chloroform, phenol:THF, and phenol:water. The corresponding optical behavior and chemical structure of the deposited films is investigated with photoluminescence spectroscopy and Fourier transform infrared spectroscopy. The use of a novel RIR-MAPLE emulsion target recipe enables the successful incorporation of MEH-CN-PPV and MEH-PPV polymers into ice matrices, and an MEH-PPV thin film with near-featureless surface morphology and an unprecedented rms surface roughness of 0.292 nm is demonstrated. [J1418]

"Indium Tin Oxide Modified by Au and Vanadium Pentoxide as an Efficient Anode for Organic Light-Emitting Devices"

Au/Vanadium pentoxide (V₂O₅) films on indium tin oxide (ITO) as composite anodes for hole injection in organic light-emitting devices (OLEDs) have been investigated. The device with ITO/Au(6 nm)/V₂O₅(6 nm) anode shows improved current density-voltage characteristics as compared with the device with ITO/Au as anode. Hole injection is significantly reduced when Au was added on ITO as an anode. However, while a thin V₂O₅ film is deposited on a Au anode, the barrier height is substantially reduced. The hole injection is facilitated, and the driving voltage of the device decreased by 10 V. In addition, the maximum current efficiency for the ITO/Au/V₂O₅OLED is ~3.5 cd/A, which is higher than that of the ITO/Au anode device (~1.1 cd/A) and ITO/V₂O₅OLED of ~2.8 cd/A. [J1419]

"Corrections to "Low-Forward-Voltage-Drop 4H-SiC BJTs Without Base Contact Implantation""

{no data available} [J1420]

"Dynamic Response of Normal and Corbino a-Si:H TFTs for AM-OLEDs"

The dynamic characteristics of normal and Corbino hydrogenated amorphous silicon (a-Si:H) thin-film transistors (TFTs) have been investigated. Top- and bottom-gate normal a-Si:H TFTs and bottom-gate Corbino a-Si:H TFTs were fabricated with a five-photomask process used in the processing of the active-matrix liquid crystal displays. The charging time and feedthrough voltage ΔV_P measurement indicates that the normal a-Si:H TFT shows a similar behavior regardless of its TFT geometrical structure. Using a simple gate-to-source capacitance CGS model, the dependence of ΔV_P on gate-to-source overlap and storage capacitor has closely been estimated using analytical calculation. Due to a unique electrode geometry, the Corbino a-Si:H TFT shows a small deviation from an analytical model used for the normal a-Si:H TFT, and consequently, a modified analytical model was developed. We also developed concepts of its possible application as a switching device to active-matrix organic light-emitting displays. [J1421]

"Stress Reduction and Enhanced Extraction Efficiency of GaN-Based LED Grown on Cone-Shape-Patterned Sapphire"

High-quality InGaN-GaN film was grown on a cone-shape-patterned sapphire substrate (CSPSS) by using metal-organic chemical vapor deposition. The growth mode of GaN on CSPSS was similar to that of the epitaxial lateral overgrowth (ELOG), because the growth, in the initial stage, proceeds only on flat basal sapphire substrate and there is no preferential growth plane on the cone region. An analysis of X-ray diffraction showed a shorter lattice constant of 5.1877 Å along the c-axis for the GaN thin films grown on CSPSS, compared to 5.1913 Å for the samples grown on a conventional sapphire substrate (CSS). This is because the ELOG-like mode of the GaN layer over the cone-shaped region results in less lattice mismatch and incoherency between the GaN layer and the sapphire substrate. The output power of a sideview light-emitting diode (LED) grown on CSPSS was estimated to be 7.3 mW at a forward current of 20 mA, which is improved by 34% compared to that of an LED grown on CSS. The significant enhancement in output power is attributed to both the increase of the extraction efficiency, resulted from the increase in photon escaping probability due to enhanced light scattering at the CSPSS, and the improvement of the crystal quality due to the reduction of dislocation. [J1422]

"Lattice Constant Effect of Photonic Crystals on the Light Output of Blue Light-Emitting Diodes"

Photonic crystal (PC) slabs with triangular lattice constants of 230, 345, 460, and 690 nm have been fabricated

onto InGaN-GaN multiquantum-well light-emitting diodes with a wavelength of 461 nm. For the shallow nanoholes in the depth range of 10-38.5 nm, the current-voltage characteristics were not changed but the electroluminescence intensities were enhanced by a factor of 3.5. The light output was most enhanced with the lattice constant corresponding to the wavelength due to the PC diffraction with constructive interference but was suppressed with the lattice constant of the half wavelength by forming a photonic bandgap. [J1423]

"Design of a color sensing system to aid the color blind"

A color sensing device is implemented using two different color sensors, a microcontroller, and a display. Nine different colors of tissue paper were measured with the color sensors. The performance of the sensors was evaluated by converting the red, green, blue (RGB) values they produced back into colors on a computer and then comparing these colors with the colored tissue paper. An inexpensive commercial color sensor produced very accurate color for all nine color samples while the homemade sensor produced recognizable but washed-out looking color for most of the colors. The performance of the homemade sensor is strongly dependent on the positioning of the color sample relative to the light emitting diodes (LEDs). [J1424]

"Fabrication and Characterization of GaSb-Based Monolithic Resonant-Cavity Light-Emitting Diodes Emitting Around 2.3 μm and Including a Tunnel Junction"

In this paper, the process of fabrication of GaSb-based electrically injected resonant-cavity LEDs near 2.3 μm is detailed. The electrical and optical properties of these diodes operating in continuous wave at room temperature are also presented. The different tested monolithic structures have similar designs with two doped AlAsSb/GaSb Bragg mirrors and an active region with eight GaInAsSb quantum wells. Performances of devices containing or not an n⁺⁺-InAsSb/p⁺⁺-GaSb tunnel junction (TJ) can be compared. The large improvements of electrical resistance as well as output power, observed when a TJ is included, demonstrate all the advantages to use such a technology for the realization of electrically injected vertical cavity structures emitting in the mid-IR on GaSb substrate. [J1425]

"A Novel Gaze Estimation System With One Calibration Point"

The design of robust and high-performance gaze-tracking systems is one of the most important objectives of the eye-tracking community. In general, a subject calibration procedure is needed to learn system parameters and be able to estimate the gaze direction accurately. In this paper, we attempt to determine if subject calibration can be eliminated. A geometric analysis of a gaze-tracking system is conducted to determine user calibration requirements. The eye model used considers the offset between optical and visual axes, the refraction of the cornea, and Donder's law. This paper demonstrates the minimal number of cameras, light sources, and user calibration points needed to solve for gaze estimation. The underlying geometric model is based on glint positions and pupil ellipse in the image, and the minimal hardware needed for this model is one camera and multiple light-emitting diodes. This paper proves that subject calibration is compulsory for correct gaze estimation and proposes a model based on a single point for subject calibration. The experiments carried out show that, although two glints and one calibration point are sufficient to perform gaze estimation (error $\sim 1^\circ$), using more light sources and calibration points can result in lower average errors. [J1426]

"Reliable Organic Nonvolatile Memory Device Using a Polyfluorene-Derivative Single-Layer Film"

This letter describes the reversible switching performance of metal-organic-semiconductor (MOS) memory devices containing a polyfluorene-derivative single-layer film. The space-charge-limited current contributes to the switching behavior of WPF-oxy-F memory devices. The polyfluorene derivative reported here provides a significant advance to the field of organic semiconductors because it provides a type of organic memory material for nonvolatile memory devices. The following properties are responsible for its memory capabilities: its use of a single-layer film, a large on/off ratio ($I_{\text{on}}/I_{\text{off}} \sim 10^4$), a long retention time (more than 10 000 s), acceptable thermal stability up to 120 degC, and an excellent device-to-device switching uniformity. [J1427]

"Enhancement of Light Extraction Efficiency of Gallium Nitride Flip-Chip Light-Emitting Diode With Silicon Oxide Hemispherical Microlens on its Back"

Silicon oxide (SiO_2) hemispherical microlens with the density of 8.2 times 10^8 cm^{-2} has been formed on a sapphire substrate of gallium nitride (GaN) light-emitting diode (LED) by liquid phase deposition to enhance the light extraction efficiency. For flip-chip LED, the SiO_2 microlens exhibits 1.25 times enhancement of optical output power. In comparison of the conventional LED, there is 61% enhancement for flip-chip LED with a SiO_2 microlens. [J1428]

"Improvement of External Extraction Efficiency in GaN-Based LEDs by Nanosphere Lithography"

A practical approach to fabricate textured GaN-based light-emitting diodes (LEDs) by nanosphere lithography is presented. By spin coating a monolayer of SiO₂ nanoparticles as the mask, textured LEDs can be fabricated. Both textured p-GaN and textured indium tin oxide LEDs show significant improvement over conventional LEDs without damaging the electrical characteristics. The results show that the method is promising for manufacturing low-cost high-efficient GaN-based LEDs. [J1429]

"Improved GaN-Based LED Light Extraction Efficiencies via Selective MOCVD Using Peripheral Microhole Arrays"

GaN-based light-emitting diodes with peripheral microhole arrays (PMA-LEDs) have been grown, and fabricated, on SiO₂ hexagonal pattern masks using selective metal-organic chemical vapor deposition. The PMA-LED structure promises to enhance the light extraction efficiency via simple fabrication processes, as compared to conventional LED structures. The geometrical shape of the peripheral microhole structure serves to enhance the light extraction efficiency due to the effect of the PMA in facilitating multiple chances for photons to escape. Thus, the light output intensity of PMA-LED was 30% higher than that of conventional LEDs. [J1430]

"Dynamic Thermal Analysis of High-Power LEDs at Pulse Conditions"

In this letter, the thermal evaluation of high-power LED packages at pulse conditions was reported. A theoretical calculation model was proposed based on the analogy between the thermal and electrical RC circuits. The thermal performance of LED packages driven by pulse input was calculated using the RC network extracted from transient thermal measurement. The junction temperature fluctuation band decreases with the frequency at certain duty cycles. The saturated average junction temperature rise linearly increases with the duty cycle at certain frequencies. These predictions were verified by the real-time junction temperature measurement using the peak shift method at pulse conditions. The theoretical model was found to be effective and applicable to the evaluation of the thermal performance of LEDs working at pulse conditions. [J1431]

"Numerical Study on Quantum Efficiency Enhancement of a Light-Emitting Diode Based on Surface Plasmon Coupling With a Quantum Well"

We demonstrate the numerical study results of the enhancements of internal quantum efficiency (IQE) and external quantum efficiency (EQE) of a semiconductor quantum well when it is coupled with surface plasmons (SPs) induced on a grating interface between Ag and semiconductor. The IQE and EQE enhancements depend on the emission dipole position and the assigned intrinsic IQE. The SP dissipation in metal and the grazing-angle SP radiation lead to a significant difference between IQE and EQE. The enhancement of EQE is less significant when the intrinsic IQE becomes larger. In applying the SP coupling phenomenon to an InGa_{0.5}N-GaN quantum-well light-emitting diode, the efficiency enhancement is more significant in the green-red range, in which the intrinsic IQE is normally quite low. [J1432]

"Energy Loss Mechanism in Organic and Inorganic Light-Emitting Diodes"

We report that there exists a similar energy loss mechanism in fluorescent/phosphorescent organic light-emitting diodes (F/P OLEDs) and inorganic semiconductor optoelectronic devices [1310-nm InGaAsP-InP superluminescent diodes (SLDs)]. The loss of energy in inorganic SLDs based on thickness-altered asymmetric multiple quantum-well (QW) structures occurs depending sensitively on the sequence of QWs, an analogous behavior also observed in F/P OLEDs depending on the sequence of phosphorescent dopants for different colors. It is shown that such an energy (power) loss is evitable by placing long-wavelength QWs near the p-side in inorganic SLDs and similarly long-wavelength phosphors near the hole-transporting layer in F/P OLEDs. [J1433]

"Software Prediction of Threshold Voltage Shift for Amorphous Silicon TFT-Based Displays"

This paper deals with software compensation of threshold voltage shift (VT shift) in amorphous silicon based active matrix OLED displays by use of an external microcontroller. The use of compensating circuits can result in lower aperture ratios, increased power consumption and complex driving methods and is hence unsuitable. The algorithm for software control makes use of quick parameter extraction of device physical parameters, thereby enabling prediction of VT shift corresponding to a data stream seen by a pixel. [J1434]

"Behaviors of Emission Wavelength Shift in AlInGa_{0.5}N-Based Green Laser Diodes"

InGa_{0.5}N quantum-well (QW) green laser diodes (LDs) with an emission wavelength of 483.7 nm were

characterized by controlling the injection pulsewidth. The emission wavelength of LDs showed a large blueshift (> 20 nm) of spontaneous emission peak with increasing injection current below the threshold current. The huge blueshift was ascribed to the deep In localization states and the strong piezoelectric field in the green InGaN QW structure with higher In contents than conventional violet/blue InGaN QWs. However, the lasing wavelength of LDs was slightly redshifted by increasing the injection pulsewidth due to the thermal heating effects. [J1435]

"Source/Drain Series-Resistance Effects in Amorphous Gallium-Indium Zinc-Oxide Thin Film Transistors"

In this letter, we investigated the effects of source/drain series resistance on amorphous gallium-indium-doped zinc-oxide (a-GIZO) thin film transistors (TFTs). A linear least square fit of a plot of the reciprocal of channel resistance versus gate voltage yields a threshold voltage of 3.5 V and a field-effect mobility of about 13.5 cm²/V·s. Furthermore, in a-GIZO TFTs, most of the current flows in the distance range of 0-0.5 μm from the channel edge and shorter than that in a-Si:H TFTs. Moreover, unlike a-Si:H TFTs, a-GIZO TFTs did not show an intersection point, because they did not contain a highly doped ohmic (n+) layer below the source/drain electrodes. [J1436]

"Fabrication and Thermal Analysis of Wafer-Level Light-Emitting Diode Packages"

Wafer-level packaged light-emitting diodes (LEDs) are useful for the high-power applications such as back light unit and general solid-state lighting due to the compactness and integrated fabrication process. In this letter, wafer-level packaged LEDs with red, green, and blue multichips were fabricated, and the thermal characteristics of wafer-level packaged LEDs with multichips such as thermal resistance and junction temperature are investigated using both serial and matrix measurement methods. [J1437]

"GaN Metal-Semiconductor-Metal Photodetectors With SiN/GaN Nucleation Layer"

In this paper, GaN metal-semiconductor-metal (MSM) photodetectors with SiN/GaN nucleation layer were proposed and fabricated. Compared with the GaN MSM photodetector with conventional single low-temperature GaN nucleation layer, it was found that we achieved much smaller dark current and much lower bias-dependent photocurrent. We also achieved much lower bias-dependent spectral response and larger ratio of photoresponse at 360-450 nm from the photodetector with SiN/GaN nucleation layer. Furthermore, it was found that we can significantly reduce noise-equivalent power (NEP) and enhance normalized detectivity by using the SiN/GaN nucleation layer. [J1438]

"Modeling of Short-Channel Effects in Organic Thin-Film Transistors"

We propose a model for short-channel organic thin-film transistors, which accounts for Poole-Frenkel field-dependent mobility and space-charge-limited current effects. The model is developed for devices operating in the linear regime, as well as in depletion and saturation regimes. Super linear output curves for low drain voltages, as well as nonsaturating currents, can be adequately described. Experimental results for short-channel P3HT devices have been fitted, showing good agreement with the proposed model. [J1439]

"Model for Studies of Lateral Photovoltaic Effect in Polymeric Semiconductors"

We present here a discrete circuit spreading impedance network model for highly disordered semiconducting polymeric Schottky devices. Qualitative arguments are presented to correlate the parameters of the spreading function, which represents the network connectivity in the model, to the underlying morphology of the polymer. A detailed theoretical study of the lateral charge transport in organic Schottky devices is carried out using the model. We observe and analyze the dependence of the lateral photovoltage (LPV) on the polymer morphology, incident power, material specific Schottky junction parameters and the modulation frequency. The model is shown to account for a variety of experimental observations on poly-(3-hexylthiophene) and poly-[2-{methoxy}-5-(2-ethylhexoxy)-1,4-phenylene-vinylene]-based position sensitive devices, while being physically transparent and computationally efficient. Using the model, we highlight those parameter regimes that would be optimal for position sensing applications. [J1440]

"Mechanism of Resistive Switching in 3, 4, 9, 10 Perylenetetracarboxylic Dianhydride (PTCDA) Sandwiched Between Metal Electrodes"

Electrical-field-induced resistive transitions in thin films of perylenetetracarboxylic dianhydride sandwiched between two metal electrodes, from an insulating state to a conducting state with a high ON-OFF ratio, have been studied. Temperature dependence of resistivity and scanning tunneling spectroscopic studies show insulating behavior in OFF state and metallic behavior in ON state. Devices with a thin intermediate layer of LiF

between metal electrode and organic layer, or devices fabricated in planar configuration, do not show switching behavior. All these suggest that conducting pathways are responsible for the electric- field-induced conductance transition. [J1441]

"Integration of Photonic Crystals on GaN-Based Blue LEDs Using Silicon Mold Substrates"

In this paper, we demonstrate a novel method to integrate photonic crystals (PhCs) on GaN-based blue light-emitting diodes (LEDs) using a silicon substrate as a mold for forming the PhCs. This method starts with fabricating a 2D grooved Si substrate as that mold. Subsequently, GaN-based epitaxial layers are grown on the Si mold-substrate, which effectively reduces the dislocation density in GaN by enhanced lateral epitaxial growth. After the epitaxial layers are bonded onto a highly reflective substrate, the Si mold-substrate is removed. This substrate-transfer technique replicates PhC from the mold-substrate on the LED surface free from processing damages. The resultant LEDs with PhC have outperformed the LEDs without PhC in the optical output power by 80%, taking advantage of the enhanced light extraction by PhC. [J1442]

"Organic-Inorganic Hybrid Materials for Photonic Applications"

Organic-inorganic hybrid materials are derived from the chemical reaction of silane coupling reagents and metal alkoxides, involving O-Si-C bonds in the matrix. They offer superior characters of combined organic groups and inorganic linkages for various optical applications. This paper reviews preparation and characterization of optical devices and materials derived from these hybrid materials. We mainly describe three topics for micrometer-nanometer scale optical components in our laboratories using organic-inorganic hybrid materials: 1) film formation; 2) patterning by the photolithography techniques; and 3) laser emission from dye-doped hybrid spheres and coated glass spheres. [J1443]

"Thermal Analysis of LED Arrays for Automotive Headlamp With a Novel Cooling System"

In this paper, we report the thermal performance of a light-emitting diode (LED) headlamp module with a novel cooling system. An air-circulating cooling system was design for the LED headlamp module. The precise fluid field modeling and heat transfer analysis using computational fluid dynamics were performed according to the practical working conditions for the headlamp. The junction temperatures of LEDs were found to decrease by using the air-cooling system and, thus, improved the heat dissipating capability of the LED array. The junction temperature of the LED array was decreased from 70.6degC to 30.25degC when the circulating speed of the air increased from 0 to 120 km/h. Also, the temperature decrease of 2degC ~ 4degC was obtained by using fins. By thermal analysis, the cooling system of LED arrays for the headlamps was found to be feasible. Also, the reliability of the headlamp with LED arrays can be improved with a good cooling system. [J1444]

"Luminescence Characteristics of YAG Glass-Ceramic Phosphor for White LED"

Luminescence characteristics of Ce:Y3Al5O12(YAG) glass-ceramic (GC) phosphor for a white LED were investigated. The GC phosphor was obtained by a heat treatment of a Ce-doped SiO2-Al2O3-Y2O3mother glass between 1300degC and 1500degC for the prescribed time period. The quantum efficiency (QE) of Ce3+fluorescence in the GC materials, the color coordinate, and the luminous flux of electroluminescence of LED composite were evaluated with a blue LED (465 nm) set in an integrating sphere. The QE increased with increasing ceramming temperature of the as-made glass. The color coordinates (x, y) of the composite were increased with increasing thickness of the GC mounted on a blue LED chip. The effect of Gd2O3substitution on the optical properties of the GC materials was also investigated. The excitation and emission wavelengths shifted to longer side up to Gd/(Y + Gd) = 0.40 in molar composition. As a result, the color coordinate of the LED with GdYAG-GC of various thickness shifted to closer to the Planckian locus for the blackbody radiation. These results were explained by partial substitution of Gd3+ions in the precipitated YAG microcrystals, leading to the increase of lattice constant of unit cell, which was confirmed by XRD. [J1445]

"GaN-Based Schottky Barrier Photodetectors With a 12-Pair Mg N -GaN Buffer Layer"

GaN-based ultraviolet (UV) photodetectors (PDs) separately prepared with a conventional single low-temperature (LT) GaN buffer layer and a 12-pair Mg_xNy-GaN buffer layer were both fabricated. It was found that we could reduce threading dislocation (TD) density and thus improve crystal quality of the GaN-based UV PDs by using the 12-pair Mg_xNy-GaN buffer layer. With a -2-V applied bias, it was found that the reverse leakage currents measured from PDs with a single LT GaN buffer layer and that with a 12-pair Mg_xNy-GaN buffer layer were 4.57 times 10⁻⁶and 1.44 times 10⁻¹²A, respectively. It was also found that we could use the 12-pair Mg_xNy-GaN buffer layer to suppress photoconductive gain, enhance UV-to-visible rejection ratio, reduce noise level, and enhance the detectivity. [J1446]

"Improved Light Extraction Efficiency in AlGaInP Light-Emitting Diodes by Applying a Periodic Texture on the Surface"

In this letter, AlGaInP-GaP-based light-emitting diodes (LEDs) were fabricated with an Si substrate and an SiO₂-ITO-Ag omni-directional reflector using a metal-to-metal bonding technique. To enhance light extraction efficiency, a periodic texture was applied to the (Al_{0.5}Ga_{0.5})_{0.5}In_{0.5}P surface layer of AlGaInP-Si LEDs by photolithography and a wet etching process. The exterior of the etched texture consists of a series of bowl-shaped recesses. With a 350-mA current injection, the typical output power of the AlGaInP-Si LEDs with and without the textured surface (LED-I and LED-II, respectively) were measured at approximately 118 and 81 mW, respectively, when the LED chips were bonded on the TO 46 without resin encapsulation. The enhancement of output power in LED-I can be attributed to a multitude of bowl-shaped notches on the surface, which resulted in a reduction of the reabsorption probability of the photons due to the fact that the photon path length in LED-I is shorter than in LED-II before the photons escape into the free space. [J1447]

"Wavelength-Stabilized Compact Diode Laser System on a Microoptical Bench With 1.5-W Optical Output Power at 671 nm"

A wavelength-stabilized compact diode laser system emitting at 671 nm mounted on a microoptical bench with the dimensions of 13 mm×4 mm is presented. A reflecting Bragg grating was aligned on the rear side of a broad-area gain medium for wavelength stabilization at 671 nm. A maximum output power of 1.5 W was obtained together with a spectral width of 40 pm (full-width at half-maximum). At 1.0 W, a center wavelength stability below 20 pm over 5 h was determined. With these features, the devices are well-suited for spectroscopic applications. [J1448]

"Ultraviolet Electroluminescence From n-ZnO-SiO₂-ZnO Nanocomposite/p-GaN Heterojunction Light-Emitting Diodes at Forward and Reverse Bias"

Ultraviolet (UV) light-emitting diodes composed of n-ZnO:Al-SiO₂-ZnO nanocomposite/p-GaN:Mg heterojunction were fabricated on the (0002) Al₂O₃ substrate. A SiO₂ layer embedded with ZnO nanodots was prepared on the p-type GaN using spin-on coating of SiO₂ nanoparticles together with atomic layer deposition (ALD). An n-type Al-doped ZnO layer was deposited also by ALD. The SiO₂-ZnO nanocomposite layer accomplishes a role of the current blocking layer and also causes, by its low refractive index, the increase in the light extraction efficiency from n-ZnO. Significant UV electroluminescence from n-ZnO was achieved at a low forward-bias current of 1.8 mA. Strong UV emission arising from impact ionization in GaN, ZnO, and GaN:Mg states was also observed at reverse breakdown bias. [J1449]

"Flexible Organic Light-Emitting Diodes Using a Metal Peel-Off Method"

Organic light-emitting diodes were fabricated on a glass-MgOx-Ag layered substrate and separated between Ag and MgOx interface, showing the bending properties. Adhesive force decreased from 18 to 1.4 gf/cm after insertion of the MgOx layer between the Ag and glass. The Ag-O component in Ag 3d_{5/2} spectra and O-Ag (ionic bond) component in O 1s spectra increased as the MgOx layer was thickened. This supports that Ag oxidized to AgOx while the thickness of MgOx increased, resulting in a reduction of the adhesive forces of Ag layer. Therefore, it is concluded that a metal at the interface with a metal oxide is easily oxidized, reducing the adhesive forces and enabling the peel-off process. [J1450]

"Effect of Silicon Doping in the Quantum-Well Barriers on the Electrical and Optical Properties of Visible Green Light-Emitting Diodes"

The effect of Si doping in the GaN quantum-well (QW) barriers of the InGaN-GaN multiple QW active region in visible green light-emitting diodes (LEDs) was studied. As the doping level of Si increases, the intensity of electroluminescence (EL) decreases, while the forward voltage of the diodes is improved. Degradation of EL is believed to be mainly due to the hole transport blocking effect caused by Si doping in the QW barriers resulting in increased potential barriers. This effect is believed to be more significant in green LEDs than in violet and blue LEDs. [J1451]

"A Color Stable Blue Light-Emitting Device Using a Pyrazolo[3,4-b]Quinoline Derivative as an Emitter"

A color stable and pure blue multilayered light-emitting device is obtained via suppressing voltage-dependent color change. Photophysical properties of a blue fluorescent organic compound 1-phenyl-3,4-dimethyl-1H-pyrazolo[3,4-b]quinoline (PAQ5) are investigated; its highest occupied and lowest unoccupied molecular orbital

levels are also measured. A multilayer electroluminescent device is fabricated using PAQ5 as an emitter dopant in a polymer matrix. The dopant has several functions in balancing injection and transport as well as bright blue light emission. The multilayered device using PAQ5 dopant substantially reduces voltage-dependent color changes, enhances the brightness of the device, and stabilizes general performance of the device. A color stable and pure blue electroluminescence with Commission Internationale de L'Eclairage (CIE) color coordinates of (x,y)=(0.168,0.100) is achieved. [J1452]

"Effect of the Phase Shift in a Periodic Anode on the Emission Spectra of Top-Emitting Organic Light-Emitting Diodes"

Top-emitting organic light-emitting diodes with an Al-Ag cathode and Al +(Ni-Au)nanode were proposed and fabricated. The multiple layered anode results in a phase shift at the metal interfaces. It was also found that theoretically calculated peak wavelengths of the intensity spectra agree well with those experimentally measured from the fabricated devices. These results also indicate that the phase shift effect in periodic anode is important for microcavity devices. [J1453]

"Optical and Structural Properties of InGaN-AlGaIn Ultraviolet Light-Emitting Diodes"

We fabricated and investigated the performances of InGaN-AlGaIn ultraviolet (UV) light-emitting diodes (LEDs) emitting at 380 nm. The output power of a conventional LED, a patterned sapphire substrate LED (PSS LED), and a PSS flip-chip LED (PSS FCLED) were about 0.94, 1.86, and 5.18 mW, respectively, at a forward injection current of 20 mA. These results indicate that the light output-powers of the PSS LED and PSS FCLED were enhanced as much as 97% and 451% compared to the conventional LED. Subsequent optical simulations confirm the remarkable enhancements in optical power of the PSS FCLED at UV wavelengths. [J1454]

"Linear Cascade GaN-Based Green Light-Emitting Diodes With Invariant High-Speed/Power Performance Under High-Temperature Operation"

We demonstrate the performance of linear cascade green light-emitting diode (LED) arrays suited for use in plastic optical fiber (POF) communications in automobiles or harsh environments. With this three-LED array, driven by the constant voltage bias of an in-car battery output (12 V) we obtain high-speed (~ 100-Mb/s eye-opening), high-coupling power (0.9 mW), and a very small variation of coupled power versus temperature [-0.12%/degC-1at room temperature (RT)] for the whole measured temperature range (i.e., RT to 120degC). Even under high bias current (100 mA) operation, our device can sustain a clear 150-Mb/s eye-opening from RT to 120degC. The static and dynamic measurement results indicate that the speed and power performance of this device are less sensitive to variations in ambient temperature than are those of the red resonant-cavity LEDs utilized for POF communication. [J1455]

"Light Output Enhancement of InGaIn Light-Emitting Diodes Grown on Masklessly Etched Sapphire Substrates"

A maskless wet-etching method is used to prepare patterned sapphire substrates for enhancing the output power of InGaIn light-emitting diodes (LEDs). Blue LEDs grown on the patterned sapphire substrates exhibit an output power of 24.9 mW, which is 19.4% higher than that of the devices grown on flat substrates. The uniformity of the optical and electrical properties of LEDs across a 2-in wafer is slightly improved as well. [J1456]

"Fabrication and Characterization of Temperature Insensitive 660-nm Resonant-Cavity LEDs"

InGaP/AlGaInP 660-nm resonant-cavity light-emitting diodes (RCLEDs) with stable temperature characteristics have been achieved by extending the resonant cavity length from one optical wavelength (1 lambda) to three optical wavelengths (3 lambda) and tripling the number of quantum wells. When the operation temperature increases from 25degC to 95degC, the degree of power variation at 20 mA is reduced from -2.1 dB to -0.6 dB for the conventional 1- lambda cavity RCLEDs and 3- lambda cavity RCLEDs, respectively. In order to interpret the temperature-dependent experimental results, advanced device simulation is applied to model the RCLEDs with different cavity designs. According to the numerical simulation results, we deduce that the stable temperature-dependent output performance should originate from the reduction of electron leakage current and thermally enhanced hole transport for the 3- lambda cavity AlGaInP RCLEDs. [J1457]

"Metal-Core Printed Circuit Board With Alumina Layer by Aerosol Deposition Process"

Heat dissipation properties of metal-core printed circuit boards (MCPCBs) having a ceramic dielectric layer are presented for high-power light-emitting diodes (LEDs). The proposed MCPCB is composed of a dense alumina thin film on an aluminum plate, instead of the conventional MCPCB with ceramic polymer composite, which

shows low thermal conductivity. Dense alumina thin films, deposited by an aerosol deposition process, showed low leakage current and good dielectric breakdown for high-power applications. Thermal transient measurements of LEDs with the proposed MCPCB were compared to that of LEDs with conventional MCPCB. The MCPCBs proposed here showed better heat dissipation performance and lower thermal resistance. [J1458]

"Real-time corrosion mapping of steel surfaces using an optoelectronic instrument based on lightwave scattering"

The application of an optoelectronic-sensor-based virtual instrument designed by the authors, for visualising and estimating the degree of corrosion of steel surfaces exposed to different concentrations of sulphuric acid, is reported. The optoelectronic sensor consisting of a light-emitting diode (LED) and a pair of photo detectors was fixed very close to the sample placed on a stepper motor-driven moving platform so that the sample surface may be scanned by a thin light beam from the LED. The reflected and scattered light signals from each point in the scanned area were acquired separately by the two detectors in the sensor module. A parameter incorporating the relative value of these signals proved to be a fairly reliable measure of the degree of corrosion. The corrosion factor values were computed by a personal computer and presented in the form of a three-dimensional graph. The average values of the corrosion factor for different steel samples were plotted against the concentration levels of the corroding agent. The variation of the corrosion factor was found to obey a bilogarithmic law, which was in conformity with the previous results. [J1459]

"Optical polarization characteristics of In Ga N /Ga N light-emitting diodes fabricated on GaN substrates oriented between (101 0) and (101 1) planes"

Optical polarization characteristics of InGaN/GaN light-emitting diodes (LEDs) were studied. Light-emitting diode samples were fabricated on four types of GaN substrates near (1010) orientation with intentional off-axis cuts of 0°, 5°, 10°, and 27° towards [0001]. A confocal microscope was used to characterize the optical polarization of electroluminescence at various currents. The highest polarization ratio of 0.91 was measured on samples fabricated on a 5° off-cut substrate. First moments were calculated on emission spectra to assess emission peak shifts of two polarization components. We drew a conclusion that substrate off-axis cut is a technique to improve optical polarization characteristics of nonpolar-oriented InGaN/GaN LEDs. [J1460]

"Electron and hole transport in a wide bandgap organic phosphine oxide for blue electrophosphorescence"

We report blue phosphorescent organic light-emitting devices (OLEDs) using an ambipolar host, N-(4-diphenylphosphoryl phenyl) carbazole (MPO12), doped with iridium (III) bis[(4,6-difluorophenyl)-pyridinato-N,C2']picolinate (FIrpic). The external quantum efficiency and operating voltage is 9.1(±0.1)% and 4.8V, respectively, measured at a brightness of 800cd/m² with no outcoupling enhancement. By varying the layer structure of the OLEDs, we show that MPO12 is capable of transporting both electrons and holes, in contrast to previous demonstrations using diphosphine oxides, which only transported electrons. The improved hole transport results in improved device efficiency. [J1461]

"Phosphor-free white light-emitting diode with laterally distributed multiple quantum wells"

A phosphor-free white light-emitting diode (LED) was fabricated with laterally distributed blue and green InGaN/GaN multiple quantum wells (MQWs) grown by a selective area growth method. Photoluminescence and electroluminescence (EL) spectra of the LED showed emission peaks corresponding to the individual blue and green MQWs. The integrated EL intensity ratio of green to blue emission varied from 2.5 to 6.5 with the injection current below 300mA, but remained constant at high injection currents above 300mA. The stability of the emission color at high currents is attributed to parallel carrier injection into both MQWs. [J1462]

"Upconversion electroluminescence in InAs quantum dot light-emitting diodes"

We investigate the low-temperature upconversion electroluminescence (UCEL) in GaAs p-i-n diodes with a layer of self-assembled InAs quantum dots (QDs) in the intrinsic region (i). Injection of carriers into the QD states at an applied bias well below the flatband condition results in near-band-edge GaAs electroluminescence, i.e., emission of photons with energies much larger than that supplied by the applied voltage and the thermal energy. We attribute the UCEL to an Auger-like recombination process and discuss its influence on carrier thermalization processes and the effect of an applied magnetic field. [J1463]

"White-light light-emitting device based on surface plasmon-enhanced Cd Se /Zn S nanocrystal wavelength conversion on a blue/green two-color light-emitting diode"

The authors demonstrate the implementation of a white-light device by spin-coating CdSe/ZnSnanocrystals (NCs) on the top of a blue/green two-color InGaN/GaNquantum-well light-emitting diode for converting blue and green emissions into red light through the absorption/reemission process. Meanwhile, Au nanoparticles are mixed with CdSe/ZnSNCs for generating localized surface plasmon (LSP) modes to couple with the CdSe/ZnSNCs. The LSP modes can absorb green emission and effectively transfer the energy into the CdSe/ZnSNCs through the coupling process for enhancing red emission. With the LSP coupling process, the conversion efficiency from the blue/green range into red light can be increased by around 30%. The conversion quantum efficiency can reach 52.8%. [J1464]

"Enhancement of normally directed light outcoupling from organic light-emitting diodes using nanoimprinted low-refractive-index layer"

The authors have demonstrated increased light outcoupling from organic light-emitting diodes (OLEDs) based on nanoimprinted amorphous fluoropolymer, poly[perfluoro(4-vinyloxy-1-butene)] (PPFVB). Because PPFVB has a low refractive index and a high transmittance over wide wavelength range, the first-order Bragg diffracted light shows high directionality and decreased waveguide absorption. These characteristics provide an advantage for small- or medium-sized OLEDs, which are mainly viewed from the normal direction. [J1465]

"Eu 2+ -Mn 2+ phosphor saturation in 5 mm light emitting diode lamps"

This letter reports on phosphor quenching by saturation, a sublinear phosphor response with excitation intensity, in light emitting diode (LED) packages using 405nmLEDs and Ca₅(PO₄)₃Cl:Eu²⁺,Mn²⁺phosphors. This saturation is due to the high light flux incident on the phosphors in these LED packages and the slow radiative relaxation rate of Mn²⁺. Apart from known saturation processes of Mn²⁺ground state depletion and energy transfer between excited Mn²⁺ions, an additional quenching pathway, Eu²⁺→Mn²⁺(excited) energy transfer, is taken into account to quantitatively fit both the efficiency under pulsed operation and the time-resolved luminescence of Ca₅(PO₄)₃Cl:Eu²⁺,Mn²⁺. [J1466]

"Star-configured carbazole as an efficient near-ultraviolet emitter and hole-transporting material for organic light-emitting devices"

A novel organic material, 9-methyl-1,3,6,8-tetraphenyl-carbazole (MTPC-Me), for use in organic electroluminescent devices has been developed. This star-configured carbazole gives a strong near-ultraviolet (n-UV) emission (lambda max=389nm)with a high emission quantum efficiency of 47% and a narrow full width half maximum of 40nm. Two types of high-performance organic light-emitting devices were obtained using MTPC-Me as a n-UV emitter and hole-transporting material with maximum external quantum efficiency, brightness, and turn-on voltage of 1.2%, 1040cd/m², and 3.5Vfor the former and 1.1%, 1800cd/m², and 2.4Vfor the latter, respectively. [J1467]

"Monolithic InGaN-based white light-emitting diodes with blue, green, and amber emissions"

We demonstrated a monolithic white light-emitting diodes (LEDs) epitaxial structure with blue, green, and amber emissions by introducing the blue InGaN/GaNfive quantum wells (QWs) and InGaN/GaNsingle quantum well (SQW) with In-phase separated green/amber emissions as an active layer. Three wavelength emissions were developed by increasing the thickness of InGaN SQW grown on blue InGaN five QWs. From high resolution transmission electron microscope, In-phase separation was clearly observed in a 3.5-nm-thick InGaN SQW. In-phase separation would be generated by the spinodal decomposition which was promoted by the composition pulling effect related to the increment of well thickness. Therefore, white lighting LEDs with three wavelengths for blue emission from InGaN/GaNfive QWs and green/amber emissions were achieved by the In-phase separation in InGaN SQW. [J1468]

"Very high-efficiency organic light-emitting diodes based on cyclometallated rhenium (I) complex"

A phosphorescent (Ph) cyclometallated rhenium (I) (ReI)complex was synthesized by reacting 2,9-dimethyl-4,7-diphenyl-1,10-phenanthroline with pentacarbonylbromorhenium in refluxing toluene solutions. The precipitates were easily sublimed to obtain a pure electrically neutral carbonyl diamine ReIcomplex, (2,9-dimethyl-4,7-diphenyl-1,10-phenanthroline)Re(CO)₃Br. The Re complex was used as an orange emitting dopant in 4,4'-N,N'-dicarbazole-biphenyl host to fabricate Ph organic light-emitting diodes (PhOLEDs). The maximum electroluminescence (EL) efficiency and luminance of 21.8cd/Aand 8315cd/cm²were harvested, respectively, which were the highest EL results among the PhOLEDs based on ReIcomplexes. The improvements of the EL performances could be ascribed to the synergistic effects of together incorporation of two reciprocally repulsive phenyl and methyl groups on the backbone of 1,10-phenanthroline molecule of the ligand. [J1469]

"High-efficiency and color-stable white organic light-emitting devices based on sky blue electrofluorescence and orange electrophosphorescence"

Highly efficient and color-stable two-wavelength white organic light-emitting devices (WOLEDs) combining an orange phosphor [Ir(Cz-CF₃)] and a sky blue fluorescent dye BUBD-1 are fabricated where the host singlet is resonant with the fluorophore singlet state and the host triplet is resonant with the phosphor triplet level. A thin layer of 1,3,5-tris[N-(phenyl)benzimidazole]benzene between the phosphorescent and the fluorescent regions confines both singlet and triplet excitons efficiently and suppress Dexter transfer of the phosphor excitons to the nonradiative triplet state of BUBD-1. The best device reaches peak efficiencies of 19.3cd/A and 11.1lm/W which are superior to common two-color all-fluorescent or all-phosphor WOLEDs. [J1470]

"Leakage current origins and passivation effect of GaN-based light emitting diodes fabricated with Ag p-contacts"

The origins of leakage currents and passivation effects of GaN-based light emitting diodes fabricated with Ag p-contacts have been investigated by electrical measurements. A significant increase in reverse leakage current is attributed to the surface migration of Ag. A passivation of mesa sidewalls by SiO₂ is found to be effective in suppressing the reverse leakage. However, the passivation results in a somewhat increase in the forward leakage at moderate voltages. Such forward leakage is explained in terms of the presence of local deep-level states in p-GaN generated during SiO₂ deposition, acting as a parasitic diode with a lower barrier height. [J1471]

"Monolithic white light emitting diodes using a (Ga,In)N/GaN multiple quantum well light converter"

A monolithic white light emitting diode using a (Ga,In)N/GaN multiple quantum well (MQW) light converter is demonstrated. Blue photons emitted under electrical injection by (Ga,In)N/GaN QWs located inside a GaN p-n junction are partly absorbed by another (Ga,In)N/GaN MQW situated outside the junction which emits yellow-green light. The combination of the blue and yellow-green components results in white light emission. [J1472]

"The effect of the last quantum barrier on the internal quantum efficiency of InGaN-light emitting diode"

The effect of the last quantum barrier (LQB) on the internal quantum efficiency of GaN-light emitting diode (LED) was systematically investigated using a dual-wavelength GaN-LED design. Compared with a conventional GaN-LQB, a high indium contained In_{0.03}Ga_{0.97}N-LQB efficiently reduced the unintentional Mg impurity in the last quantum well and improved its photoluminescence and electroluminescence intensity up to 72% and 15%, respectively. [J1473]

"Enhanced electroluminescence intensity of InGaN/GaN multi-quantum-wells based on Mg-doped GaN annealed in O₂"

InGaN/GaN multi-quantum-well blue (461±4nm) light emitting diodes with higher electroluminescence intensity are obtained by postgrowth thermal annealing at 720°C in O₂-ambient. Based on our first-principle total-energy calculations, we conclude that besides dissociating the Mg-H complex by forming H₂O, annealing in O₂ has another positive effect on the activation of acceptor Mg in GaN. Mg can be further activated by the formation of an impurity band above the valence band maximum of host GaN from the passivated MgGa-ON complex. Our calculated ionization energy for acceptor Mg in the passivated system is about 30meV shallower than that in pure GaN, in good agreement with previous experimental measurement. Our model can explain that the enhanced electroluminescence intensity of InGaN/GaN MQWs based on Mg-doped p-type GaN is due to a decrease in the ionization energy of Mg acceptor with the presence of oxygen. [J1474]

"Enhancement of electron injection into a light-emitting polymer from an aluminum oxide cathode modified by a self-assembled monolayer"

A self-assembled monolayer (SAM) of octylphosphonate was deposited on an AlOx electrode using the tethering by aggregation and growth (T-BAG) procedure. Ultraviolet photoemission spectroscopy (UPS) measurements showed a decrease in the substrate work function from 3.8 to 3.3eV. Poly[9,9'-dioctylfluorene-co-bis-N,N'-(4-butylphenyl)-diphenylamine] (TFB) films spin coated on the bare and the SAM-modified oxide surfaces were investigated by UPS. A shift in molecular levels, corresponding to a reduction in the electron injection barrier, was observed for the SAM-modified electrode. This barrier lowering was confirmed by current-voltage measurements showing a corresponding increase in electron current through the TFB/SAM/AlOx device. [J1475]

"Highly efficient tandem p-i-n organic light-emitting diodes adopting a low temperature evaporated rhenium oxide interconnecting layer"

High quality interconnection units (ICUs) with a high transparency and superior charge generating capability for tandem organic light-emitting diodes (OLEDs) are developed. The ICUs of rubidium carbonate-doped 4,7-diphenyl-1,10-phenanthroline/rhenium oxide (ReO₃)-doped N,N'-diphenyl-N,N'-bis(1,1'-biphenyl)-4,4'-diamine layers with or without an additional ReO₃ interlayer produce high transmittance (88%-92% at 420-700nm) and spontaneous internal charge generation properties. A very high efficiency of 129cd/A has been demonstrated from only two stacked green p-i-n OLEDs by employing the developed ICUs. The relationship between the device efficiency and internal charge generation within the ICUs is further described by means of the capacitance measurements. [J1476]

"Single-photon-emitting diode at liquid nitrogen temperature"

We report on the study of a single-photon-emitting diode at 77K. The device is composed of InAs/GaAs quantum dots embedded in the i-region of a p-i-n diode structure. The high signal to noise ratio of the electroluminescence, as well as the small second order correlation function at zero-delay $g(2)(0)$, implies that the device has a low multiphoton emission probability. By comparing the device performances under different excitation conditions, we have, in detail, discussed the basic parameters, such as signal to noise ratio and $g(2)(0)$, and provided some useful information for the future application. [J1477]

"Solution-based formation of multilayers of small molecules for organic light emitting diodes"

We developed an approach for fabricating small molecule organic light emitting diodes by solution-based processing. The approach involves dissolving a small molecule organic in a solvent, spin coating it on a mold, and then transferring the layer onto the existing organic layer on a substrate. This ability to form multilayers of small molecule organics allows one to take advantage of both the efficiency offered by the multilayer structures and the low cost fabrication made possible by the solution processing. [J1478]

"Very low turn-on voltage and high brightness tris-(8-hydroxyquinoline) aluminum-based organic light-emitting diodes with a Mo O x p -doping layer"

We have demonstrated an organic light-emitting diode based on molybdenum oxide (MoO_x) doped 4,4',4"-tris(3-methylphenylphenylamino)triphenylamine (m-MTDATA) as a p-type doping hole injection layer. The tris-(8-hydroxyquinoline) aluminum (Alq₃)-based organic light-emitting diodes show high brightness at very low operating voltage, 100cd/m² at 3.2V and 1000cd/m² at 4.4V, corresponding to a low turn-on voltage of 2.4V. Such improved properties are attributed to the formation of the charge transfer complex produced by doping MoO_x into m-MTDATA, which provides much more free hole carriers, and the introduction of an efficient electron-injecting layer to improve the performance. [J1479]

"Polymer hot-carrier transistor with low bandgap emitter"

Vertical polymer hot-carrier transistor using the low bandgap material poly(3-hexylthiophene) as both the emitter and the collector are studied. The common emitter current gain is shown to depend on the LiF thickness and the emitter thickness, with maximal value at 31. Current density as high as 31mA/cm² is achieved when collector voltage is -10V. For the device using blend of poly(3-hexylthiophene) and high bandgap polymer poly(9-vinylcarbazole) as the emitter, the current density rises sharply to 428mA/cm². The brightness of 3000cd/m² is obtained as a polymer light-emitting diode is driven by the transistor with the same area. The transistor can be operated at 100kHz. [J1480]

"Ultraviolet and visible electroluminescence from n-Zn O /Si O x /(n,p)-Si heterostructured light-emitting diodes"

n-ZnO/SiO_x/n-Si and n-ZnO/SiO_x/p-Si heterostructured light-emitting diodes have been fabricated using metal-organic chemical-vapor deposition for a comparison study. n-ZnO/SiO_x/p-Si heterostructures show diode-like rectifying current-voltage characteristic with low breakdown voltage, while n-ZnO/SiO_x/n-Si heterostructures show symmetric nonlinear current-voltage behavior due to the double Schottky barriers at the interface. Both types of diodes emit light when a positive bias is applied at Si side. Ultraviolet emission at 390nm with an orange-emission centered at 600nm were observed in electroluminescence spectra of n-ZnO/SiO_x/n-Si diodes, while whitish emission centered at 520nm was observed for n-ZnO/SiO_x/p-Si diodes. The emission mechanisms were discussed. [J1481]

"Transparent organic light emitting diodes using a multilayer oxide as a low resistance transparent cathode"

Transparent organic light emitting diodes were developed by using a thermally evaporable WO₃/Ag/WO₃(WAW) as a transparent cathode. A thin Ag layer was introduced as an interlayer between the Li doped electron transport layer and the WAW electrode. A high transparency over 80% was obtained and electron injection was greatly improved by using the thin Ag interlayer between the Li doped layer and the WAW electrode. The driving voltage at 1000cd/m² was only 4.5V and the sheet resistance of the WAW electrode was as low as 12Ω/sq. [J1482]

"Electroluminescence imaging and microstructure of organic light-emitting field-effect transistors"

The effect of morphology and microstructure on the emission characteristics of ambipolar light-emitting field-effect transistors is studied using the polyfluorene copolymer F8BT [poly(9,9-di-n-octylfluorene-alt-benzothiadiazole)] as a model system. Different intensity distributions of the emission zones of amorphous, polycrystalline, and aligned F8BT films are demonstrated. Electroluminescence maps of the channel region are produced by overlaying a series of images recorded during gate voltage sweeps. They show a correlation to the microcrystalline structure of the F8BT and are assumed to visualize the current density distribution within the transistor channel. [J1483]

"High-efficiency stacked white organic light-emitting diodes"

We report efficient tandem white organic light-emitting diodes (WOLEDs) by using bathocuproine:Cs₂CO₃/MoO₃ as an effective interconnecting layer. We utilized two primary colors of sky blue and orange fluorescent emitters to obtain efficient white electroluminescence. Although single WOLEDs using two adjacent emitting layers showed a maximum current efficiency of 7.96cd/A with Commission Internationale d'Eclairage (CIE) coordinates of (0.28, 0.34), the tandem WOLED device made by stacking two single color OLEDs in series demonstrated doubled maximum current efficiency of 17.14cd/A with CIE coordinates of (0.28, 0.41). The stacking of different single color OLEDs in series instead of double stacking of WOLEDs can be useful to achieve highly efficient WOLEDs because it can reduce the number of layers of the devices. [J1484]

"Studies of oxide/ZnO near-interfacial defects by photoluminescence and deep level transient spectroscopy"

The evolution of near-interfacial defects from Al₂O₃/ZnO and MgO/ZnO upon thermal annealing has been studied by photoluminescence, deep level transient spectroscopy, and secondary ion mass spectroscopy. We find that all the results are strongly connected and that they point to the direction that Zn outdiffuses from ZnO to the oxide layer during annealing and creates deep level defects near the interfacial region. These defects reduce the band-edge emission and increase the deep level emission at 2.37eV. Our study shows that the oxide/ZnO interface is relatively fragile and caution must be taken for making metal-oxide-ZnO based transistors and light emitting diodes. [J1485]

"Efficient, visible organic light-emitting diodes utilizing a single polymer layer doped with quantum dots"

We demonstrate organic light-emitting diodes (OLEDs) using a single active layer consisting of CdSe/ZnS quantum dots (QDs) dispersed in poly(9,9-dioctylfluorene) (PFO). The diodes have an external quantum efficiency of 0.5% and reach 0.1A/cm² at 6.5V. These results are comparable to complex, multilayer QD OLEDs. Built-in potential measurements show that the QD valence levels are shifted to lower binding energy when compared to quantum confinement based estimates, and are close to PFO valence levels. Devices using red and green QDs emit predominantly from the QDs but the spectrum of blue QDs is perturbed by interactions with PFO. [J1486]

"Effects of ultraviolet light irradiation on poly(vinylcarbazole)"

In this paper, we present a study of the photophysical and photochemical effects that influence phosphor-doped polymer light-emitting diodes based on poly(vinylcarbazole). With ultraviolet (UV) light irradiation, the relative concentration of partially overlapping carbazole groups [poly(vinylcarbazole), (p-PVK)] to the fully overlapping conformation (f-PVK) is decreased via photoisomerization, which affects both the energies and the probability of forming singlet versus triplet excitons. As a result, phosphor-doped polymer light-emitting diodes fabricated using UV irradiated PVK exhibited higher efficiencies as compared with control devices (doped PVK without UV light irradiation). These data demonstrate a new route for the production of more efficient electrophosphorescent light-emitting diodes. [J1487]

"Direct vapor jet printing of three color segment organic light emitting devices for white light illumination"

Organic-vapor jet printing (OVJP) is used to directly pattern small molecular weight electrophosphorescent white organic light-emitting devices (WOLEDs) consisting of parallel stripes of separate red, green, and blue OLEDs. The spatial patterning of the WOLEDs with peak forward viewing external quantum and luminous efficiencies of $7.1 \pm 0.3\%$ and $7.0 \pm 0.4 \text{ lm/W}$, respectively, is accomplished by transporting the vapors of organic semiconductors through a nozzle to a translating sample substrate. Using multiple color segments to generate white light allows for the individual optimization of each color, is continuously color tunable, and can be used to compensate for differential aging of the constituent dopants. The theory and experimental results of WOLED printing via OVJP are discussed. [J1488]

"Compositional inhomogeneity of a high-efficiency $\text{In}_x\text{Ga}_{1-x}\text{N}$ based multiple quantum well ultraviolet emitter studied by three dimensional atom probe"

An $\text{In}_x\text{Ga}_{1-x}\text{N}$ based multiple quantum well structure emitting in the ultraviolet, which has the highest reported efficiency (67%) at its wavelength (380nm), was analyzed with the three-dimensional atom probe. The results reveal gross discontinuities and compositional variations within the quantum well layers on a 20-100nm length scale. In addition, the analysis shows the presence of indium in the $\text{Al}_y\text{Ga}_{1-y}\text{N}$ barrier layers, albeit at a very low level. By comparing with analogous epilayer samples, we suggest that the quantum well discontinuities we observe may play an important role in improving the efficiency of these structures. [J1489]

"Color-converting combinations of nanocrystal emitters for warm-white light generation with high color rendering index"

Warm-white light emitting diodes with high color rendering indices are required for the widespread use of solid state lighting especially indoors. To meet these requirements, we propose and demonstrate warm-white hybrid light sources that incorporate the right color-converting combinations of CdSe/ZnS core-shell nanocrystals hybridized on InGaN/GaN LEDs for high color rendering index. Three sets of proof-of-concept devices are developed to generate high-quality warm-white light with (1) tristimulus coordinates $(x,y)=(0.37,0.30)$, luminous efficacy (LE)=307lm/W, color rendering index (CRI)=82.4, and correlated color temperature (CCT)=3228K; (2) $(x,y)=(0.38,0.31)$, LE=323lm/W, CRI=81.0, and CCT=3190K; and (3) $(x,y)=(0.37,0.30)$, LE=303lm/W, CRI=79.6, and CCT=1982K. [J1490]

"Cesium hydroxide doped tris-(8-hydroxyquinoline) aluminum as an effective electron injection layer in inverted bottom-emission organic light emitting diodes"

We demonstrate highly efficient inverted bottom-emission organic light-emitting diodes (IBOLEDs) by using cesium hydroxide (CsOH) doped tris-(8-hydroxyquinoline) aluminum (Alq_3) as the electron injection layer on indium tin oxide cathode, which could significantly enhance the electron injection, resulting in a large increase in luminance and efficiency. The maximum luminance, current efficiency, and power efficiency reach 21000 cd/cm^2 , 6.5 cd/A , and 3.5 lm/W , respectively, which are 40%-50% higher in efficiency than that of IBOLEDs with cesium carbonate (Cs_2CO_3) doped Alq_3 as the electron injection layer, where the efficiencies are only 4.5 cd/A and 2.2 lm/W . Our results indicate that CsOH doped Alq_3 should be an effective electron injection layer on a wide range of electrodes to fabricate high performance OLEDs. [J1491]

"Integrated organic electronic based optochemical sensors using polarization filters"

A compact, integrated photoluminescence based oxygen and pH sensor, utilizing an organic light emitting device (OLED) as the light source and an organic photodiode (OPD) as the detection unit, is described. The main challenge in such an integrated sensor is the suppression of the excitation light at the detector, which is typically by many orders of magnitude higher in intensity than the emitted fluorescence. In our approach, we refrain from utilizing edge filters which require narrow band excitation sources and dyes with an adequate large Stokes shift. We rather developed an integrated sensor concept relying on two polarizers to separate the emission and excitation light. One polarizer is located right after the OLED, while the other one, oriented at 90° to the first, is placed in front of the OPD. The main advantage of this solution is that any combination of excitation and emission light is acceptable, even if the two signals overlap spectrally. This is especially important for the use of OLEDs as the excitation sources, as these devices typically exhibit a broad spectral emission. [J1492]

"Simultaneous color and luminance control of organic light-emitting diodes for mood-lighting applications"

Organic light-emitting diodes (OLEDs) using polymer blends as a single emissive layer often suffer from large color shifts with changing operational voltage. Until now, such devices cannot stand the critical demands of lighting industry. In this contribution, we introduce a pulse-width-modulation-based driver concept, enabling the user to simultaneously and independently adjust color and luminance of a single device with two contacts. This concept makes color-shifting OLEDs highly interesting for "mood-light" applications. [J1493]

"Cavity effects on light extraction in organic light emitting devices"

We have demonstrated that the light extraction efficiency of an organic light emitting device is a strong function of device geometry. Specifically, we have found that the ratio of the extracted mode to the substrate-guided mode varies from 22% to 55% depending on the location of the recombination zone. Our simulation results also indicate that more light is trapped in the substrate as the optical length of device increases. We further show that the light intensity profile varies from a Lambertian shape to a non-Lambertian shape depending on the device geometry due to the cavity effect. [J1494]

"Highly efficient green organic light-emitting diodes from single exciplex emission"

Spectral single and stable green exciplex emission was demonstrated from organic light-emitting diodes (OLEDs) with 4,4',4"-tris[3-methylphenyl(phenyl)amino] triphenylamine and 4,7-diphenyl-1,10-phenanthroline that function as electron donor (D) and acceptor (A), respectively. As 8-hydroxyquinoline aluminum (Alq3) was attached to the acceptor layer, electroluminescent (EL) properties of the two exciplex-type OLEDs with D/A-bilayer and D:A mixture layer configurations were markedly improved, i.e., a peak current efficiency of 7.6cd/A at 2.38mA/cm² in three-layer device and a maximum luminance of 6620cd/m² at 8.7V in blend layer device were obtained, respectively, without changing the peak position (535nm) and the shape of EL spectrum. Discussion is given on the harvest of the pure green exciplex emission and enhancement of luminance which is obtained by inserting Alq3 layer. [J1495]

"Laminated active matrix organic light-emitting devices"

Laminated active matrix organic light-emitting device (AMOLED) realizing top emission by using bottom-emitting organic light-emitting diode (OLED) structure was proposed. The multilayer structure of OLED deposited in the conventional sequence is not on the thin film transistor (TFT) backplane but on the OLED plane. The contact between the indium tin oxide (ITO) electrode of TFT backplane and metal cathode of OLED plane is implemented by using transfer electrode. The stringent pixel design for aperture ratio of the bottom-emitting AMOLED, as well as special technology for the top ITO electrode of top-emitting AMOLED, is unnecessary in the laminated AMOLED. [J1496]

"High-efficiency and solution processible multilayer white polymer light-emitting diodes using neutral conjugated surfactant as an electron injection layer"

High-efficiency white polymer light-emitting diodes were fabricated by using an yellow-emitting osmium complex Os(fptz)₂(dppe)[fptz=3-trifluoromethyl-5-(2-pyridyl)-1,2,4-triazole, dppe=cis-1,2-bis-(diphenyl-phosphino) ethylene] doped into blue fluorescent copolymer based on an ultraviolet-blue light emitting host poly[2,7-(9,9-dioctylfluorene)-co-1,3-(5-carbazolophenylene)] and a blue light emitting component 4-N,N-diphenylaminostilbene (PFCz-DPS1-OXD5) as the emissive layer and a neutral conjugated surfactant, poly[9,9-bis(6'(diethanolamino)hexyl)-fluorene] (PFN-OH), as the electron injection layer sandwiched between the emissive layer and Al cathode. The device with the configuration of indium tin oxide/poly(3,4-ethylenedioxythiophene):poly(styrenesulfonic acid)/poly(N-vinylcarbazole)/Os(fptz)₂(dppe)(1wt%):PFCz-DPS1-OXD5/PFN-OH/Al exhibited efficient white light emission at the Commission Internationale de l'Eclairage coordinates of (0.33, 0.34) and a maximum luminance efficiency of 16.9cd/A and brightness of 22100cd/m². [J1497]

"Suppression of exciton annihilation at high current densities in organic light-emitting diode resulting from energy-level alignments of carrier transport layers"

We manufactured an organic light-emitting diode (OLED) in which the hole and electron transport layers are chemically doped with p- and n-type dopants and energy levels in between neighboring carrier transport layers and emitting molecules are aligned. From the results of the electroluminescence (EL) characteristics of the OLED, we found that (1) the OLED has an extremely low driving voltage of 2.65±0.05V at a current density of 100mA/cm²; (2) the onset voltage of EL (≈2.4V) corresponds to the photon energy of emitting molecules (≈2.5eV), while the onset voltage of currents is ≈1.8V; and (3) a decrease in EL efficiency at high current densities can be suppressed by matching the energy levels. [J1498]

"Passivated p -type silicon: Hole injection tunable anode material for organic light emission"

We find that hole injection can be enhanced simply by selecting a lower-resistivity p-Sianode to match an electron injection enhancement for organic light emitting diodes with ultrathin-SiO₂-layer-passivated p-Sianode (Si-OLED). For a Si-OLED with ordinary AlQ electron transport layer, the optimized resistivity of the p-Sianode is 40Ω cm; for that with n-doped Bphen electron transport layer, it decreases to 5Ω cm. Correspondingly, the maximum power efficiency increases from 0.3 to 1.9 lm/W, even higher than that of an indium tin oxide control device (1.4 lm/W). This passivated p-type silicon is a hole injection tunable anode material for OLED. [J1499]

"Lithium cobalt oxide as electron injection material for high performance organic light-emitting diodes"

Lithium cobalt oxide was introduced into organic light-emitting diodes as the electron injection layer. The device with tris(8-hydroxyquinolato) aluminum doped with 10-(2-benzothiazolyl)-1,1,7,7-tetramethyl-2,3,6,7-tetrahydro-1H,5H,11H-[1]benzopyrano[6,7,8-ij]quinolizin-11-one as the light-emitting layer and LiCoO₂ as the electron injection layer showed promising efficiency (10.74 cd/A at 11 V) and longer lifetime (2.8 times as much as LiF/Al control device). Lithium cobalt oxide proved to be thermally decomposed in vacuum to form lithium oxide, which was responsible for the enhanced electron injection. [J1500]

"Electroless nickel/gold Ohmic contacts to p -type GaN"

A solution based approach to forming Ohmic contacts to p-type GaN is described. Electroless plated Ni/Au contacts are shown to compare favorably with traditional evaporated contacts, with contact resistivities ρ_c in the region of 10-20 Ω cm². These values are readily achieved after a rapid thermal annealing in an O₂ atmosphere. The tunneling nature of the contact is confirmed via temperature dependant measurements. X-ray diffraction measurements confirm the similarity between evaporated and plated contacts. Current-photocurrent (I-L) and current-voltage (I-V) measurements from light emitting diodes formed using an electroless p-type contact are shown. Electroless deposition of the contact metals allows for a reduction in processing time and cost. [J1501]

"Carrier distribution in (0001)In Ga N /Ga N multiple quantum well light-emitting diodes"

We study the carrier distribution in multi quantum well (multi-QW) InGaN light-emitting diodes. Conventional wisdom would assume that a large number of QWs lead to a smaller carrier density per QW, enabling efficient carrier recombination at high currents. We use angle-resolved far-field measurements to determine the location of spontaneous emission in a series of multi-QW samples. They reveal that, no matter how many QWs are grown, only the QW nearest the p-layer emits light under electrical pumping, which can limit the performances of high-power devices. [J1502]

"Reduced efficiency roll-off in high-efficiency hybrid white organic light-emitting diodes"

White organic light emitting diodes harvesting triplet excitons from the fluorescent blue emitter N,N'-di-1-naphthalenyl-N,N'-diphenyl-[1,1':4',1'':4'',1''':4''',1''''-quaterphenyl]-4,4'-diamine (4P-NPD) are presented. Direct doping of the phosphorescent orange iridium(III)bis(2-methyldibenzo-[f,h]quinoxaline)(acetylacetonate) into 4P-NPD results in a strongly reduced efficiency roll-off as compared to separate emission layers, and yields 49.3 lmW-1 total external power efficiency (24.1% quantum efficiency) at a luminance of 1000 cd m⁻² [CIE 1931 chromaticity coordinates (0.49,0.41)], measured in an integrating sphere. Introduction of an exciton balancing interlayer improves the chromaticity (0.43,0.43) toward the CIE illuminant A warm white point and keeps a high efficiency of 40.7 lmW-1, 20.3%. [J1503]

"High light extraction efficiency of gallium nitride light emitting diode with silicon oxide hemispherical microlens"

Silicon oxide hemispherical microlens with the density of 9.54 × 10⁸ cm⁻² was formed on gallium nitride light emitting diode to enhance the light extraction efficiency by liquid phase deposition. The light output power exhibits 1.29 times enhancement compared to that without microlens. After the thermal annealing with nitrous oxide, the output power is further improved to 1.44 times due to higher silicon oxide quality and gallium nitride surface passivation. [J1504]

"Optically induced ultrafast quenching of the semiconductor quantum well luminescence"

We present an experimental configuration that enables the ultrafast, transient quenching of the excitonic

photoluminescence in quantum wells. Our scheme is based on two, delayed, short pulses experiment. A first pulse excites carriers in the system, while a second pulse induces an ultrafast redistribution of excitons that results in abrupt dips in the photoluminescence. We present a model that quantitatively accounts for the measured dip depth. The magnitude of the dip, determined by the temperature change of the carriers, can be controlled by varying the power and delay of the second pulse. [J1505]

"Spatial distribution of crown shaped light emission from a periodic inverted polygonal deflector embedded in an In Ga N /Ga N light emitting diode"

We investigated spatial light emission from a periodic inverted polygonal deflector, which included six {10-1-1} facets and six {11-2-2} facets embedded in an InGaN/GaN light emitting diode by using confocal scanning electroluminescence microscopy. We found a noticeable crown shape with the contrast of luminescence intensity and wavelength observed on these facets mainly due to the variation of growth rate for the InGaN quantum wells. In addition, a very low intensity and blueshifted emission wavelength on the {11-2-2} facets indicated the deficiency of indium incorporation and/or much thinner well thickness as compared to that of the {10-1-1} facets. [J1506]

"Highly polarized white-light emission from a single copolymer based on fluorene"

Polarized white-light emission was realized from a single copolymer with green and red-light-emitting chromophores incorporated into the blue-light-emitting poly(9,9-dioctylfluorene) backbone through intrachain energy transfer. Based on the good thermal stability and nematic liquid crystalline state of the copolymer, the emissive layer spin coated on a rubbed poly(3,4-ethylene dioxythiophene):poly(styrenesulfonate) layer was aligned under thermal treatment at a temperature of 180 °C for 5 min. The polarized white-light emission was stable with a Commission Internationale de L'Eclairage coordinates of (0.33, 0.35). A high polarization ratio of up to 24 with a luminance of 419 cd/m² at voltage of 15 V was achieved. [J1507]

"Stabilization of the work function of indium tin oxide using organic surface modifiers in organic light-emitting diodes"

We herein report on the performance and improved stability of organic light-emitting diodes (OLEDs) in which the transparent indium tin oxide (ITO) electrode is modified using organic surface modifiers based on phosphonic acid anchoring groups. In contrast to air plasma treatment, a commonly used technique to increase the work function of ITO, treatment of the ITO surface with a partially fluorinated phosphonic acid results in a comparable change in work function but with a higher stability over time. The resultant lifetime of OLEDs also increased when this phosphonic acid modified ITO was used. [J1508]

"Reduction of efficiency droop in InGaN light emitting diodes by coupled quantum wells"

Light emitting diodes (LEDs) based on InGaN suffer from efficiency droop at current injection levels as low as 50 A cm⁻². We investigated multiple quantum well InGaN LEDs with varying InGaN barrier thicknesses (3-12 nm) emitting at 400-410 nm to investigate the effect of hole mass and also to find out possible solutions to prevent the efficiency droop. In LEDs with electron blocking layers, when we reduced the InGaN barriers from 12 to 3 nm, the current density for the peak or saturation of external quantum efficiency increased from 200 to 1100 A cm⁻² under pulsed injection conditions, which eliminates the heating effects to a large extent. Our calculations show that such reduction in the barrier thickness makes the hole distribution more uniform among the wells. These results suggest that the inferior low hole transport through the barriers exacerbated by large hole effective mass and low hole injection due to relatively low hole concentration and the consequent electron leakage are responsible for the efficiency droop at high current injection levels. [J1509]

"The effect of electrode heat sink in organic-electronic devices"

Most of organic devices showed poor thermal stability and short lifetime due to Joule heating by current injection during operation. To increase the lifetime of the devices, thermal management must be considered. We demonstrated the polymer light-emitting diodes with thermally conductive substrate and Al/Cu double cathode to enhance the thermal stability of the device. Also, we proposed the correlation between lifetime (Δt) and device heat sink (ΔT). The heat sink of all organic devices is required to enhance device durability. [J1510]

"Electrically driven single quantum dot emitter operating at room temperature"

We present a green emitting single quantum dot light emitter integrated into a resonant-cavity diode design. Most important, electroluminescence stemming from one individual quantum dot is obtained at room temperature with a surprisingly low operation voltage of 2.6 V. This demonstrates that our single quantum dot device is ideally

suited for electrically driven nonclassical light generation under ambient conditions. [J1511]

"High-purity white light from a simple single dopant host-guest white organic light-emitting diode architecture"

White light with good color properties (color rendering index=82-87) is generated in a simple organic light-emitting diode comprising an emissive layer, composed of an undoped tris(4-methyl-8-quinolinato)aluminum (Almq3) sublayer and region doped with an orange-red phosphorescent dopant, bis(2-phenyl-1-quinoline)iridium acetylacetonate (Ir(pq)2acac). Electron-hole recombination in a thin spacing Almq3 layer results in blue-green fluorescence, while the formed triplet excitons diffuse to the doped region and are harvested by the dopant to emit orange-red phosphorescence. The combination of blue-green and orange lights results in warm white light. This approach takes advantage of efficient migration of triplet excitons while being less demanding in terms of fabrication and color matching. [J1512]

"Nanomaterial enabled laser transfer for organic light emitting material direct writing"

Organic light emitting material direct writing is demonstrated based on nanomaterial enabled laser transfer. Through utilization of proper nanoparticle size and type and the laser wavelength choice, a single laser pulse could transfer well-defined and arbitrarily shaped tris-(8-hydroxyquinoline)Al patterns ranging from several microns to millimeter size. The unique properties of nanomaterials allow laser induced forward transfer at low laser energy (0.05J/cm²) while maintaining good fluorescence. The technique may be well suited for the mass production of temperature sensitive organic light emitting devices. [J1513]

"Investigation of Eu-Mn energy transfer in A₃ Mg Si₂ O₈ :Eu²⁺, Mn²⁺ (A=Ca, Sr, Ba) for light-emitting diodes for plant cultivation"

We report a plant growth lamp utilizing near-ultraviolet light-emitting diode and A₃MgSi₂O₈:Eu²⁺, Mn²⁺ (A=Ca, Sr, Ba) phosphors with emission spectra consisting of blue and red bands, which conform well to the action spectra of plants and absorption spectra of chlorophylls. Either peak positions of the two bands or intensity ratio of red to blue band can be tailored by tuning the compositions of the cations. Eu-Mn energy transfer in the phosphors was investigated on the bases of photoluminescence, life decay time, and microstructure. This functional solid-state lighting provides a simple, compact, and efficient solution to illuminator for plant cultivation. [J1514]

"MgO thickness dependence of spin injection efficiency in spin-light emitting diodes"

We have studied the electron spin injection efficiency from a CoFeB/MgO spin injector into AlGaAs/GaAs semiconductor light emitting diodes. The circular polarization of the electroluminescence signal reaches a value as large as 32% at 100K under a 0.8T magnetic field. We show that the spin injection efficiency increases with the increase in the MgO barrier thickness from 1.4 to 4.3 nm. Moreover, a higher spin injection efficiency is obtained for MgO barriers grown at 300°C compared to the ones grown at room temperature. This effect is attributed to the MgO texturing occurring at high temperatures. [J1515]

"Color-stable and efficient stacked white organic light-emitting devices comprising blue fluorescent and orange phosphorescent emissive units"

We have demonstrated two kinds of stacked white organic light-emitting diodes (WOLEDs) employing tri(8-hydroxyquinoline) aluminum:20 wt % Mg/MoO₃ as charge generation layer. White light emission can be obtained by mixing blue fluorescence and orange phosphorescence. Stacked WOLED with individual blue fluorescent and orange phosphorescent emissive units has better color stability and higher efficiency than that with double white emissive units, which is attributed to the avoidance of the movement of charges recombination zone and elimination of the Dexter energy transfer between blue and orange emission layers occurring in the latter. The efficiency of the stacked WOLED is 35.9 cd/A at 1000 cd/m². [J1516]

"Multilayer polymer light-emitting diodes by blade coating method"

Multilayer polymer light-emitting diodes fabricated by blade coating are presented. Multilayer of polymers can be easily deposited by blade coating on a hot plate. The multilayer structure is confirmed by the total thickness and the cross section view in the scanning electron microscope. The film thickness variation is only 3.3% in 10 cm scale and the film roughness is about 0.3 nm in the micron scale. The efficiency of single layer poly(para-phenylene vinylene) copolymer Super Yellow and poly(9,9-dioctylfluorene) (PFO, deep blue) devices are 9 and 1.7 cd/A, respectively, by blade coating. The efficiency of the PFO device is raised to 2.9 cd/A with a 2-(4-tert-butylphenyl)-5-(4-biphenyl)-1,3,4-oxadiazole (PBD) hole-blocking layer and to 2.3 cd/A with a poly[(9,9-

dioctylfluorenyl-2,7-diyl)-co-(4,4'-(N-(4-sec-butylphenyl))diphenylamine)] elec-tron-blocking layer added by blade coating. [J1517]

"Organic cesium salt as an efficient electron injection material for organic light-emitting diodes"

Cesium quinoline-8-oxide (Csq), as an organic salt, was synthesized and applied as an electron injection material for organic light-emitting diodes. A typical bilayer structure of N,N'-bis-(1-naphthyl)-N,N'-diphenyl-1,1'-biphenyl-4,4'-diamine/tris-(8-hydroxy-quinolinolato) aluminum (III) (Alq3) was used to evaluate the electron injection of Cs. The results showed Csq/Al had better electron injection than LiF/Al cathode, and a maximum current efficiency of 4.13 cd/A (3.33 cd/A for LiF/Al) was obtained when the Csq layer is 2.0 nm. It is proposed that the enhanced electron injection by Csq is related to the interfacial chemical reaction between Csq and Al and the self-doping of Csq by liberated Cs. [J1518]

"Highly efficient excimer-based white phosphorescent devices with improved power efficiency and color rendering index"

Power efficiency, Commission Internationale d'Éclairage (CIE) coordinates, and color rendering index (CRI) of white phosphorescent excimer devices were improved by utilizing two platinum complexes as emissive dopants and exploring different device structures. Compared with devices containing two emissive layers each having a different dopant, devices having two dopants incorporated in a single host layer showed better color stability with the change in operating voltage. White phosphorescent excimer devices having the double-doped emissive layer showed an external quantum efficiency and a power efficiency of 14.5% and 17 lm/W, respectively, at 500 cd/m². The CIE coordinates and CRI of the devices were (0.382, 0.401) and 81, which were almost independent of the drive voltage. [J1519]

"Encapsulation of organic light-emitting devices using a perfluorinated polymer"

Films of Cytop™, a perfluorinated polymer, are spin cast as a single barrier layer for evaluation of barrier properties on organic light-emitting devices and on Ca thin films. Cytop™ is water repellent, resulting in encapsulated organic light-emitting field effect transistors and organic light-emitting diodes (OLEDs), which remain active even after immersion into water or exposure to water droplets on the Cytop™ surface. OLEDs encapsulated with Cytop™ exhibit up to five times longer continuous operation under identical environmental and driving conditions compared with devices that are not encapsulated with Cytop™. [J1520]

"Stacked white organic light emitting devices consisting of separate red, green, and blue elements"

We demonstrate a white organic light-emitting device where individual red, green, and blue (R, G, and B) phosphorescent organic light-emitting devices are vertically stacked and electrically interconnected by a compound MoO₃/Li-doped charge generation layer. For the order of B, G, and R cells positioned relative to the indium tin oxide anode, the device yields a peak total external quantum efficiency (EQE) and power efficiency (PE) of $\eta_{\text{ext}} = (36 \pm 2)\%$ at a current density of $J = 82 \text{ mA/cm}^2$ and $\eta_p = 21 \pm 1 \text{ lm/W}$ at $J = 17 \text{ mA/cm}^2$, respectively. The EQE and PE of the device roll off to $(32 \pm 2)\%$ and $13 \pm 1 \text{ lm/W}$ at 1000 cd/m², corresponding to $J = 2 \text{ mA/cm}^2$. At this luminance, the device shows Commission Internationale de L'Éclairage chromaticity coordinates of (0.45, 0.36) and a color rendering index of 63. [J1521]

"Improving light output power of InGaN-based light emitting diodes with pattern-nanoporous p-type GaN:Mg surfaces"

InGaN-based light emitting diodes (LEDs) with a top pattern-nanoporous p-type GaN:Mg surface were fabricated by using a photoelectrochemical (PEC) process. The peak wavelengths of electroluminescence (EL) and operating voltages were measured as 461.2 nm (3.1 V), 459.6 nm (9.2 V), and 460.1 nm (3.3 V) for conventional, nanoporous, and pattern-nanoporous LEDs using 20 mA operation current. The EL spectrum of the nanoporous LED had a larger blueshift phenomenon as a result of a partial compression strain release in the InGaN active layer through the formation of a top nanoporous surface. The light output power had 12.1% and 26.4% enhancements for the nanoporous and the pattern-nanoporous LEDs compared with conventional LEDs. The larger operating voltage of the nanoporous LED was due to the non-ohmic contact on the PEC treated p-type GaN:Mg surface. By using a pattern-nanoporous p-type GaN:Mg structure, the operating voltage of the pattern-nanoporous LED was reduced to 3.3 V. A lower compression strain in the InGaN active layer and a higher light extraction efficiency at the top nanoporous surface were observed in pattern-nanoporous LEDs for higher efficiency nitride-based LED applications. [J1522]

"A monolithically integrated magneto-optoelectronic circuit"

The monolithic integration of a spin valve, an amplifier, and a light emitting diode to form a magneto-optoelectronic integrated circuit on GaAs is demonstrated. The circuit converts the spin polarization information in the channel of the spin valve to an amplified change in light intensity with a gain of 20. The monolithic circuit therefore operates as a magnetoelectronic switch which modulates the light intensity of the light emitting diode.

[J1523]

"Analysis of efficiency characteristics of green phosphorescent organic light-emitting devices"

Efficiency characteristics of green phosphorescent organic light-emitting devices (PHOLEDs) with different host materials and device structures were investigated by examining the luminance efficiency-current density curves and electroluminescence spectra. The efficiency of PHOLEDs at low current density as well as at high current density was greatly affected by energy levels and carrier transport properties of the host and hole/electron transporting materials. The devices exhibited high initial luminance efficiency when hole-electron recombination was well confined in the emitting layer (EML). Efficiency roll off with increasing current density was observed as hole-electron recombination and charge balance in EML deteriorated with current density. [J1524]

"Electroluminescence and magnetoresistance of the organic light-emitting diode with a La 0.7 Sr 0.3 Mn O 3 anode"

Electroluminescence (EL) with brightness up to 300cd/m² is observed from organic light-emitting diodes fabricated on oxygen-treated La_{0.7}Sr_{0.3}MnO₃ anodes. An external magnetic field of 150mT applied parallel to the device surface can enhance the EL intensity by 10%, accompanied by a raised current efficiency. In-plane magnetization of the ferromagnetic anode is found to be the main origin of increase in the current contributable to EL, though magnetoresistance of the organic functional materials also plays a role in the EL enhancement observed in the magnetic field. [J1525]

"Simultaneous light emissions from two different types of fluorophores in diblock copolymer micellar films"

We report a simple strategy to realize simultaneous light emissions from a single layer of poly(styrene-block-2-vinyl pyridine) (PS-*b*-P2VP) copolymer micelles incorporated with a fluorescent dye in the P2VP core and a conjugated polymer in the PS corona. The fluorescence resonance energy transfer between the dye and the conjugated polymer is effectively inhibited due to the isolation of micelles. This study may offer an effective way to facilitate the ongoing exploration of white light emission in optics and optoelectronics. [J1526]

"Multiwalled carbon nanotube sheets as transparent electrodes in high brightness organic light-emitting diodes"

We have fabricated efficient organic light emitting diodes using strong, transparent carbon nanotube (CNT) sheets as the hole-injecting anode. These devices show a brightness of 4500cd/m² and current efficiency near 2.5 cd/A, which is close to the efficiency we achieve with a similar device, which uses indium tin oxide (ITO) as the anode. We demonstrate that proper planarization of the electrode using the water-soluble polymer poly(3,4-ethylenedioxythiophene) poly(styrenesulfonate) is necessary for achieving high efficiency and can be accomplished by spin casting multiple layers. We believe that increased conductivity of the sheets could lead to CNT-based devices with efficiencies exceeding those on ITO. [J1527]

"Quantum-dot light-emitting diodes utilizing Cd Se /Zn S nanocrystals embedded in Ti O 2 thin film"

Quantum-dot (QD) light-emitting diodes (LEDs) are demonstrated on Si wafers by embedding core-shell CdSe/ZnS nanocrystals in TiO₂ thin films via plasma-enhanced metallorganic chemical vapor deposition. The n-TiO₂/QDs/p-Si LED devices show typical p-n diode current-voltage and efficient electroluminescence characteristics, which are critically affected by the removal of QD surface ligands. The TiO₂/QDs/Si system we presented can offer promising Si-based optoelectronic and electronic device applications utilizing numerous nanocrystals synthesized by colloidal solution chemistry. [J1528]

"Air-voids embedded high efficiency InGaN-light emitting diode"

To improve the light extraction efficiency of InGaN-light emitting diode (LED), inverted hexagonal cone shaped air voids with {10-11} GaN crystal planes were formed between a patterned sapphire substrate and GaN epitaxial layer using a H₃PO₄-based hot chemical etching method. The air-voids embedded LED showed 12% and 210% higher optical power than a patterned substrate LED and a flat substrate LED, respectively. A ray tracing simulation revealed that the light extraction through the top face of the air-voids embedded LED was dramatically increased due to a strong light reflection and redirection by the air voids. [J1529]

"Approaches for achieving highly efficient exciplex-based organic light-emitting devices"

We studied the performance of exciplex-based organic light-emitting devices (OLEDs) made of different electron transporting materials (ETMs) with similar electron affinities to minimize the effect of the lowest unoccupied molecular orbital levels. A strong correlation was observed between the intensity of exciplex emission and the choice of ETMs. The intensity of exciplex emission relied on interfacial charge accumulation densities at organic/organic contacts, which in turn determined device color and efficiency. Contrary to common belief, highly efficient exciplex-based OLEDs can be achieved, provided that the involved organic materials have high carrier mobility, high photoluminescence quantum yield, and suitable electron energy levels. [J1530]

"Dichromatic color tuning with InGaN-based light-emitting diodes"

Color tuning GaN based light-emitting diodes (LEDs) both electrically and optically was investigated. Color mixing of two LED dies, one nonpolar ($\lambda_p=467\text{nm}$) and one semipolar ($\lambda_p=574\text{nm}$), produced white light. Electrically, the correct current was supplied to each die in order to change its correlated color temperature and Commission Internationale de l'Eclairage (CIE) chromaticity coordinates from 3287 K and (0.425, 0.413) to 7242 K and (0.303, 0.315). The optical polarization anisotropy inherent in nonpolar and semipolar wurtzite GaN allowed color tuning optically with the use of a polarizer. Several regions of the CIE diagram were explored using this method and are discussed. [J1531]

"On the efficiency droop in InGaN multiple quantum well blue light emitting diodes and its reduction with p -doped quantum well barriers"

Multiple quantum well (MQW) InGaN light emitting diodes with and without electron blocking layers, with relatively small and large barriers, with and without p-type doping in the MQW region emitting at 420nm were used to determine the genesis of efficiency droop observed at injection levels of approximately $\geq 50\text{A/cm}^2$. Pulsed electroluminescence measurements, to avoid heating effects, revealed that the efficiency peak occurs at 900A/cm² current density for the Mg-doped barrier, near 550A/cm² for the lightly doped n-GaN injection layer, meant to bring the electron injection level closer to that of holes, and below 220A/cm² for the undoped InGaN barrier cases. For samples with GaN barriers (larger band discontinuity) or without p-AlGaNelectron blocking layers the droop occurred at much lower current densities ($\leq 110\text{A/cm}^2$). In contrast, photoluminescence measurements revealed no efficiency droop for optical carrier generation rates corresponding to the maximum current density employed in pulsed injection measurements. All the data are consistent with heavy effective mass of holes, low hole injection efficiency (due to relatively lower p-doping) leading to severe electron leakage being responsible for efficiency droop. [J1532]

"Molecular beam epitaxial growth of InAsN:Sb for midinfrared Optoelectronics"

We report molecular beam epitaxial growth and characterization of dilute nitride InAsN:Sb. X-ray diffraction, energy dispersive x-ray spectrometry, and electron probe microanalysis revealed that nitrogen incorporation is significantly enhanced by introduction of Sb flux during growth, together with a dramatic improvement of the photoluminescence. These observations were attributed to the surfactant effect of Sb which suppresses the surface diffusion length of nitrogen and improves the homogeneity of the alloy. Sb incorporation is enhanced with the presence of nitrogen which was associated with the surface kinetic of growth. InAsN:Sb/InAsP-i-n light emitting diodes operating near 4.0μm were also realized. [J1533]

"Controlling bulk aggregation state in semiconducting conjugated polymer solution"

Dynamic light scattering measurements disclosed the ubiquity of large aggregate species (i.e., generally above 100 nm in hydrodynamic radius) in the precursor solutions customarily used to fabricate polymer-based light-emitting diodes (PLEDs). Transformation of these species into nanoscale thin films is expected to influentially interfere with the performance of the fabricated PLEDs. Controlling these large aggregate species was noticed to require strategies at variance with the convectional ones of controlling the more localized aggregation state. The present observations suggest that compromising the bulk and the local solution aggregation states is essential in producing tunable and high-performance PLEDs. [J1534]

"Transient reverse current phenomenon in a p-n heterojunction comprised of poly(3,4-ethylene-dioxythiophene):poly(styrene-sulfonate) and ZnO nanowall"

We report the characteristics of a p-n heterojunction diode comprised of a poly(3,4-ethylene-dioxythiophene):poly(styrene-sulfonate) (PEDOT:PSS) as the hole-conducting p-type polymer and n-type ZnO nanowall networks. ZnO nanowall networks were synthesized on a GaN/sapphire substrate without metal

catalyst using hot-wall type metal organic chemical vapor deposition. The p-nheterojunction diodes of PEDOT:PSS/ZnO nanowall exhibited a space charge limited current phenomena at forward bias and a transient reverse current recovery when a sudden reverse bias was applied from the forward bias condition. The minority carrier lifetime was estimated to be 2.5 ns. [J1535]

"Application of mixed interface in white-electrophosphorescent devices: An efficient approach to adjust the distributions of carriers"

The distributions of carriers in white organic light-emitting devices can be tuned effectively by incorporating a mixed interface layer, consisting of 4,7-diphenyl-1,10-phenanthroline doped in N,N'-dicarbazolyl-4-4'-biphenyl. By adjusting the thickness and the BPhen concentration of the mixed interface, the optimal devices exhibit maximum current and power efficiencies of 20.9 cd/A and 19.9 lm/W, respectively, and slightly modified Commission Internationale De L'Eclairage coordinates, from (0.3174 0.3276) to (0.3141 0.3218). This is attributed to the good distributions of carriers between two emissive layers by inserting the mixed interface, thereby improving both the exciton formation probability and the charge transport balance. [J1536]

"Enhancement in output power of blue gallium nitride-based light-emitting diodes with omnidirectional metal reflector under electrode pads"

In this study, we demonstrate a GaN-based light-emitting diode (LED) with nonalloyed metal contacts onto the n⁺-GaNsurface and transparent contact layer (indium tin oxide) to serve as the n-type electrode (cathode) and the p-type electrode pad (anode), respectively. Comparing with the conventional LEDs, which the electrode pads and/or Ohmic contacts form through conventional Cr/Au metal contacts, the nonalloyed metal contacts (Ag/Cr/Au or Al/Cr/Au) used in the present experimental blue LEDs also play the role of reflector to prevent the emitted light from absorption by the opaque electrode pads with low reflectivity (Cr/Au). With an injection current of 20 mA, the enhancement in the light output power has approximately a 14% magnitude compared to the GaN-based LEDs without Ag or Al reflectors under the Cr/Au electrode pads. [J1537]

"Directional emission control and increased light extraction in GaN photonic crystal light emitting diodes"

Limitations in extraction efficiency of gallium nitride (GaN) photonic crystal (PhC) light emitting diodes (LEDs) are addressed by implementing an LED design using both two-dimensional PhCs in-plane and index guiding layers (IGLs) in the vertical direction. The effects of PhCs on light extraction and emission directionality from GaN LEDs are studied experimentally. Angular-resolved electroluminescence clearly shows the combined effect of controlling the vertical mode profile with the IGLs and tailoring the emission profile with the periodicity of the PhC lattice. Increases in directional emission as high as 3.5 times are achieved by taking advantage of this directionality and guided mode control. [J1538]

"Thermal characterization of light-emitting diodes in the frequency domain"

We report on a method for the measurement of thermal relaxation time constants within light-emitting diodes (LEDs) in the frequency domain. The method is based on the phase shift of the forward voltage waveform with respect to that of the harmonically modulated forward current due to the sensitivity of the forward voltage to junction temperature. The phase shift was shown to exhibit dips at angular frequencies equal to inverse thermal time constants. Extraction of thermal time constants was demonstrated for common low-power and high-power LEDs. The measured thermal time constants (0.1-100 ms) were linked to heat flows between the LED components. [J1539]

"Highly efficient and color stable phosphorescent white light-emitting diodes by using a charge confining emitting layer structure"

Quantum efficiency of white phosphorescent organic light-emitting diodes was improved by using a device architecture to confine charges inside an emitting layer. The charge confinement was achieved by stacking two emitting layers with different charge transport properties. An emitting layer with electron transport type host was stacked on an emitting layer with hole transport type host. A maximum quantum efficiency of 18.3% and a current efficiency of 31.5 cd/A were achieved with a color coordinate of (0.38, 0.36). In addition, there was little change in the emission spectra from 200 to 10,000 cd/m². [J1540]

"Improved thermal management of GaN/sapphire light-emitting diodes embedded in reflective heat spreaders"

Using maskless lithography and electroforming techniques, we have demonstrated an enhanced performance of GaN/sapphire light-emitting diode (LED) embedded in a reflective copper heat spreader. The chip size and dominant wavelength of the blue emitter used in this research is 141mm² and 455 nm, respectively. The cup-shaped LED heat sink is electroformed on sapphire directly using the spin-coated photoresist coated with the Au/Cr/Ag mirror as a mold and dicing into the embedded LED with a Cu base dimension of 343mm², which effectively enhances the heat dissipation down to the metal frame and reaps the light flux generated from the side emission. With the aid of a reflective heat spreader, the encapsulated LED sample driven at 1 A yields the light output power of 700 mW and around 2.7-times increase in the wall-plug efficiency compared to that of the conventional GaN/sapphire LED. Infrared thermal images confirm the GaN/sapphire LED with more efficient heat extraction and better temperature uniformity. These results exhibit an alternative solution to thermal management of high power LED-on-sapphire samples besides the laser lift-off technique. [J1541]

"Improved electron injection in polymer light-emitting diodes using anionic conjugated polyelectrolyte"

We report improved performance in polymer light-emitting diodes incorporating conjugated polyelectrolytes as an electron injection layer (EIL). When we introduce water soluble conjugated polymers, poly[9,9'-bis(4-sulfonatobutyl)fluorene-co-alt-1,4-phenylene] (anionic PFP), between the aluminum (Al) cathode and emissive layer, the devices show an increased electroluminescence efficiency with a lowered turn-on voltage. We believe the mobile Na⁺ ions in the EIL layer directly influences the device efficiency by forming a low work function layer at the interface between the EIL and Al cathode, thereby facilitating the electron injection into the emissive layer. [J1542]

"Highly efficient, deep-blue phosphorescent organic light emitting diodes with a double-emitting layer structure"

We have demonstrated a highly efficient, deep-blue organic light-emitting diode (OLED) using a host material with a high triplet energy. The OLED device that we have prepared utilizes a phosphorescent guest material, iridium(III)bis(4',6'-difluorophenylpyridinato)tetrakis(1-pyrazolyl)borate, exhibits a peak quantum efficiency of about 15.7%. We employed a double-emitting layer (DEL) structure that distributes the carrier recombination region within the device. In this DEL structure, the emission mechanism is such that the energy transfers from the host material in one emitting layer, and the other emitting layer provides for direct charge trapping in the guest material. This DEL structure proved to be quite useful in achieving the reported device characteristics. [J1543]

"Low voltage and very high efficiency deep-blue phosphorescent organic light-emitting devices"

We report on very high efficiency deep-blue phosphorescent organic light-emitting devices (PHOLEDs) based on iridium(III) bis(4',6'-difluorophenylpyridinato)tetrakis(1-pyrazolyl)borate (Flr6). Dual emissive layers consisting of an N,N'-dicarbazolyl-3,5-benzene layer doped with 4wt% Flr6 and a p-bis(triphenylsilyl)benzene layer doped with 25wt% Flr6 were employed to maximize exciton generation on Flr6 molecules. Combined with the p-i-n device structure, we achieved a low turn-on voltage of 3.2V and very high power efficiencies of 25±2lm/W at 100cd/m² and 20±2lm/W at 1000cd/m² for such deep-blue PHOLEDs with peak emission at a wavelength of 458nm. [J1544]

"n-In Ga N /p-Ga N single heterostructure light emitting diode with p -side down"

The effects of negative polarization charge at the n-InGaN/p-GaN interface on the performance of hydride vapor phase-epitaxy deposited single heterostructure n-InGaN/p-GaN LEDs with p-side down are investigated. The strong peak emission wavelength blueshift and concomitant superlinear increase in light output as the injection current increases below 25A/cm² are characteristic of radiative tunneling. We show that the combination of two-dimensional hole gas formation on the n-InGaN side of the heterointerface and enhancement of the electron barrier to transport across this interface results in only 10% efficiency droop up to 500A/cm² without implementation of an AlGaIn electron-blocking layer or a second heterointerface. [J1545]

"Enhanced spontaneous emission in a photonic-crystal light-emitting diode"

We report direct evidence of enhanced spontaneous emission in a photonic-crystal (PhC) light-emitting diode. The device consists of p-i-n heterojunction embedded in a suspended membrane, comprising a layer of self-assembled quantum dots. Current is injected laterally from the periphery to the center of the PhC. A well-isolated emission peak at 1.3μm from the PhC cavity mode is observed, and the enhancement of the spontaneous emission rate is clearly evidenced by time-resolved electroluminescence measurements, showing that our diode

switches off in a time shorter than the bulk radiative and nonradiative lifetimes. [J1546]

"Publisher's Note: "Thermal characterization of light-emitting diodes in the frequency domain" [JAppl. Phys. Lett. 93, 103508 (2008)]"

First Page of the Article [J1547]

"Improvement in carrier transport and recombination of white phosphorescent organic light-emitting devices using a composite blue emitter"

We demonstrate high-efficiency white phosphorescent organic light-emitting devices (PHOLEDs) based on a yellow and composite blue emitters. The composite blue emitter is constructed from a wide-band-gap host, organometallic iridium dopant, and a carrier-transporting material. Under the same driving current density and emissive color, the current efficiency of the white PHOLEDs can be enhanced by a factor of 1.4 comparing to that of using typical blue emitter composed of host and dopant only. Attaching an outcoupling enhancement film onto glass substrate, the white PHOLEDs with a current efficiency of 47 cd/A, a power efficiency of 32 lm/W, and a CIE_{x,y}(CIE: Commission Internationale d'Eclairage) of (0.40,0.44) at a practical brightness of 1000cd/m² can be achieved. [J1548]

"A soluble nonionic surfactant as electron injection material for high-efficiency inverted bottom-emission organic light emitting diodes"

A soluble nonionic surfactant, polyethylenimine 80% ethoxylated (PEIE) solution, was used as the electron injection material in inverted bottom-emission organic light emitting diodes (OLEDs). The transparent PEIE film was formed on indium-tin-oxide cathode by simple spin-coating method and it was found that the electron injection was greatly enhanced. The devices with PEIE electron injection layer had achieved significant enhancement in luminance and efficiency. The maximum luminance reached 47 000cd/m², and the maximum luminance efficiency and power efficiency arrived at 19.7 cd/A and 10.6 lm/W, respectively. Our results indicate that PEIE is a promising electron injection material to realize high performance OLEDs. [J1549]

"Effects of triplet energies and transporting properties of carrier transporting materials on blue phosphorescent organic light emitting devices"

We have studied the effects of the hole transporting layers and electron transporting layers on the device efficiencies of iridium(III) bis[(4,6-di-fluorophenyl)-pyridinato-N,C2'] picolinate (FIrpic) doped 3,5'-N,N'-dicarbazole-benzene (mCP) host blue phosphorescent organic light emitting diodes. We found that the device efficiency is very sensitive to the hole transporting materials used and both the triplet energy and carrier transport properties affect the device efficiency. On the other hand, there is no apparent correlation between the device efficiency and the triplet energy of the electron transporting material used. Instead, the device efficiency is affected by the electron mobility of the electron transporting layer only. [J1550]

"Spin injection effects on exciton formation in organic semiconductors"

The effects of spin-polarized electron and hole injection from ferromagnetic contacts on the formation and distribution of singlet and triplet excitons in a conjugated organic semiconductor are modeled. Electron and hole transport in the semiconductor are described by spin-dependent device equations for a structure resembling an organic light emitting diode. The formation of electron-hole pairs at a given site is modeled as a Langevin process, and the subsequent local relaxation into the lowest energy exciton states is described by rate equations. Once formed, excitons may recombine in the semiconductor or diffuse through the material and recombine at the contact interfaces. The model calculations yield steady-state spatial profiles for singlet and triplet excitons. It is shown that spin-polarized injection increases the formation of singlet excitons, and that the diffusion of excitons has significant effects on the triplet exciton profile. [J1551]

"Suppression of the subband parasitic peak by 1 nm i-Al N interlayer in AlGaIn deep ultraviolet light-emitting diodes"

The origin and suppression of the subband parasitic peak in AlGaIn deep ultraviolet light-emitting diodes have been studied. The parasitic peak is clarified to come from a p-AlGaIn cladding layer and to be related to Mg dopants. By using 1nm-i-AlN as an interlayer between the active region and the p-AlGaIn cladding layer, this peak is suppressed efficiently. The devices with such an interlayer show improved output power by a factor of 4 at injection current density of 20A/cm², except that the series resistance and turn-on voltage are slightly increased. [J1552]

"Near-ultraviolet excitable orange-yellow Sr₃(Al₂O₅)Cl₂:Eu²⁺ phosphor for potential application in light-emitting diodes"

Sr₃(Al₂O₅)Cl₂phosphor doped with Eu²⁺ was prepared by a solid-state reaction. This phosphor emits a broad orange-yellow luminescence with a peak wavelength of 620 nm and a full width at half maximum of about 175 nm under near-ultraviolet (NUV) excitation at 400 nm. Yellow light-emitting diodes (LEDs) for general lighting were fabricated by combining Sr₃(Al₂O₅)Cl₂:Eu²⁺ phosphor with an NUV chip. The phosphor-converted LEDs had a color temperature of about 2300 K and their color rendering index was 74. [J1553]

"Efficient single layer solution-processed blue-emitting electrophosphorescent devices based on a small-molecule host"

We report highly efficient single layer solution-processed blue small-molecule electrophosphorescent organic light-emitting diodes with iridium (III) bis[2-(4,6-difluorophenyl)-pyridinato-N,C2']picolate (FIrpic) doped into a wide-gap 9,9-bis[4-(3,6-di-tert-butylcarbazol-9-yl)phenyl]fluorene (TBCPF) as the emission layer. An optimized device with 1,3-bis[(4-tert-butylphenyl)-1,3,4-oxadiazolyl]phenylene as the electron-transporting component doped into the emission layer, with a blue electrophosphorescence peaked at 474 nm from FIrpic, shows a maximum luminance efficiency of 12.7 cd/A at 190 A/m² and brightness of 19900 cd/m² at 20 V. We attribute the high performance to the excellent film forming ability and high triplet energy of TBCPF. [J1554]

"Broadband quantum dot micro-light-emitting diodes with parabolic sidewalls"

Arrays of long wavelength, self-organized InGaAs quantum dot micron sized light-emitting diodes (μ -LEDs) with parabolic sidewalls are introduced. The parabolic profiles of the μ -LEDs produced by resist reflow and controlled dry etching improve the extraction efficiency from the LEDs by redirection of the light into the escape cone by reflection from the sidewalls. A fourfold increase in the substrate emitted power density compared to a reference planar LED is measured. The reflected light is verified to be azimuthally polarized. The spectral width of the emission can be greater than 200 nm. [J1555]

"Achieving three-peak white organic light-emitting devices using wavelength-selective mirror electrodes"

We report an effective approach based on wavelength-selective mirrors for implementing three-peak white-emitting organic light-emitting devices (OLEDs). Such three-peak white OLEDs have electroluminescence spectra matching better with the transmission spectra of typical color filters and thus give much enhanced color gamut for full-color OLED display applications. The wavelength-selective mirror uses the metal/dielectric stack that is compatible with the OLED fabrication. [J1556]

"Bonding of GaN structures with Si(100) substrates using sequentially deposited NiAu metal layers"

A process has been developed to bond gallium nitride structures grown on sapphire with silicon substrates, using sequentially deposited nickel-gold thin metal layers. Temperature and pressure treatment results in alloying of NiAu with robust interface bond strength of 7.1 MPa between GaN and Si. Transmission electron microscopy showed bright and dark regions of varying nickel-gold composition with uniform layer thickness. Micro-Raman and x-ray photoelectron spectroscopy revealed compressive stress relaxation and Ga-Ni and Au-Si alloying phases, respectively. The transferred light emitting diodes exhibit a turn-on voltage of 2.5 V and could sustain beyond 300 mA, proving a way to have vertical structure light emitting diodes on Si substrates. [J1557]

"Influence of doping profile on the efficiency of blue phosphorescent organic light-emitting diodes"

We demonstrate that electroluminescent efficiency of blue phosphorescent organic light-emitting diodes could be improved by changing doping profile in the emissive layer (EML) of the device containing iridium(III)bis(4,6-difluorophenyl)-pyridinato-N,C2' picolate (FIrpic) and N,N'-dicarbazolyl-3,5-benzene (mCP). By examining the changes of recombination zone and current density with a partially doped EML, we found that most of the recombination occurred at the EML close to the electron transporting layer (ETL). Electron injection and transport were enhanced by increasing doping ratio at the EML close to the ETL and such a stepwise doping profile resulted in almost 40 % improved power efficiency compared to that of a conventional device. [J1558]

"Near-field scanning optical microscopy with monolithic silicon light emitting diode on probe tip"

We describe optical and topographic imaging using a light emitting diode monolithically integrated on a silicon probe tip for near-field scanning optical microscopy (NSOM). The light emission resulted from a silicon dioxide

layer buried between a phosphorus-doped N+silicon layer and a gallium-doped P+silicon region locally created at the tip by a focused ion beam. The tip was employed in a standard NSOM excitation setup. The probe successfully measured optical as well as topographic images of a chromium test pattern with imaging resolutions of 400 and 50nm, respectively. The directional resolution dependence of the acquired images directly corresponds to the shape, size, and polarity of the light source on the probe tip. To our knowledge, this report is the first successful near-field imaging result directly measured by such tip-embedded light sources. [J1559]

"Ultraviolet emission from Sb-doped p -type ZnO based heterojunction light-emitting diodes"

Heterojunction light emitting diodes (LEDs) were fabricated by making Au/Nitop Ohmic contacts on Sb-doped p-type ZnO film with low specific contact resistivity and Al/Tiback Ohmic contacts on n-type Si substrate. Near-band edge and deep-level emissions were observed from the LED devices at both low temperatures and room temperature, which is due to band-to-band and band-to-deep level radiative recombinations in ZnO, respectively. The electroluminescence emissions precisely match those of photoluminescence spectra from Sb-doped p-type ZnO, indicating that the ZnO layer acts as the active region for the radiative recombinations of electrons and holes in the diode operation. [J1560]

"Ni O /Zn O light emitting diodes by solution-based growth"

Heterojunction NiO/ZnOlight emitting diodes have been fabricated using low temperature solution-based growth methods. While negligible light emission has been obtained for the as-grown NiO film, devices with annealed NiO film exhibit room-temperature electroluminescence (EL), which was attributed to the detrimental effects of nickel oxide hydroxide in as-grown NiO layers. The device performance can be further modified by insertion of the organic layers between NiO and ZnO and the EL spectra exhibited dependence on the bias voltage. For higher bias voltages, strong UV-violet emission peak can be obtained in spite of the dominance of defect emission in the photoluminescence spectra. [J1561]

"Highly efficient bilayer green phosphorescent organic light emitting devices"

We present a highly efficient green phosphorescent device comprising only of two organic layers. A host material bis[2-(2-hydroxyphenyl)-pyridine]beryllium having a good electron transporting and energy transfer characteristics, and a wide band gap hole transport material N,N'-di(4-(N,N'-diphenyl-amino)phenyl)-N,N'-diphenylbenzidine lead to the fabrication of a simplified high efficiency device. The driving voltage value of 3.3Vto reach a luminance of 1000cd/m2is reported. The maximum current- and power-efficiency values of 38.30cd/Aand 46.60lm/Ware demonstrated in this device. Results reveal a practical way to fabricate highly efficient truly bilayer organic devices for trouble-free manufacturing processes. [J1562]

"Ga N /In Ga N light emitting diodes with embedded photonic crystal obtained by lateral epitaxial overgrowth"

We introduce GaN/InGaNlight emitting diodes with a dielectric photonic crystal embedded in the epitaxial layer by lateral epitaxial overgrowth on a patterned GaN template. Overgrowth, coalescence, and epitaxial growth of the pnjunction within a thickness of 500nmis obtained using metal-organic chemical vapor deposition. This design strongly modifies the distribution of guided modes, as confirmed by angle-resolved measurements. The regime of operation and potential efficiency of such structures are discussed. [J1563]

"Enhanced light output of GaN-based light-emitting diodes with ZnO nanorod arrays"

We report enhanced light output of GaN-based light-emitting diodes (LEDs) with vertically aligned ZnO nanorod arrays. The ZnO nanorod arrays were prepared on the top layer of GaN LEDs using catalyst-free metalorganic vapor phase epitaxy. Compared to conventional GaN LEDs, light output of GaN LEDs with the ZnO nanorod arrays increased up to 50% and 100% at applied currents of 20 and 50mA, respectively. The source of the enhanced light output is also discussed. [J1564]

"In As /Ga Sb cascaded active region superlattice light emitting diodes for operation at 3.8 mcm"

We report on the growth and characterization of InAs/GaSbsuperlattice light emitting diodes (LEDs) operating in the midwave infrared at 3.8mcmat 77K. Devices were grown by solid source molecular beam epitaxy on (100) GaSb substrates and were fabricated into 120 \times 120mcm2mesa devices using wet etching. By employing an eight-stage cascaded active region design, output powers in excess of 1.5mWwere achieved at 77Kwith 100mApeak drive current and a 50% duty cycle. Operating characteristics of the devices were examined from room temperature to 77Kunder quasi-dc excitation conditions. [J1565]

"Low roll-off power efficiency organic light-emitting diodes consisted of nondoped ultrathin phosphorescent layer"

Low roll-off power efficiency (η_p) organic light-emitting diodes at high current density were fabricated using a nondoped ultrathin bis[2-(4-tertbutylphenyl)benzothiazolato-N,C2'] iridium (acetylacetonate) phosphorescent layer and thin N,N'-di(naphthalene-2-yl)-N,N'-diphenyl-benzidine separate layer. A maximum η_p of 8.48 lm/W and luminance efficiency of 20.26 cd/A at 2014 cd/m² were obtained from the device. The η_p roll-off percentage of ultrathin phosphor layer device was reduced to 20% at a current density of 20 mA/cm², which is about 40% for conventional phosphorescent device. The low roll off of efficiency was attributed to the direct carrier trapping and confining emission zone function of the ultrathin phosphor layer. [J1566]

"Hybrid optoelectronics: A polymer laser pumped by a nitride light-emitting diode"

We demonstrate indirect electrically pumped lasing in a hybrid polymer laser. The lasers comprise a corrugated fluorene copolymer waveguide on an InGaN light-emitting diode and were driven under nanosecond pulsed operation. We observe the onset of distributed feedback lasing at 568 nm for peak drive currents above 144 A. Angle-resolved photoluminescence measurements identify the lasing mechanism as band edge feedback from a photonic stopband in the TE₀ waveguide mode. [J1567]

"Enhancing the quantum efficiency of InGaN green light-emitting diodes by trimethylindium treatment"

This work demonstrates the effectiveness of using trimethylindium (TMIn) treatment to improve the luminescence efficiency of InGaN/GaN quantum wells grown by metal-organic vapor-phase epitaxy. Photoluminescence, x-ray diffraction, atomic force microscopy, and high-resolution transmission electron microscopy indicate that the treatment leads to a smoother InGaN surface and InGaN/GaN interface with substantial decrease in V-shape defects density, compared to the samples without treatment. Green light-emitting diodes prepared by this method exhibit higher output power than the control device. These improvements are attributed to the surface smoothing process in TMIn ambient, resulting in an abrupt InGaN/GaN interface. [J1568]

"Role of barrier layers in electroluminescence from SiN-based multilayer light-emitting devices"

We report the effects of barrier layer on the electroluminescence properties of the SiN-based multilayer light-emitting devices (LEDs). It is found that the emission efficiency is significantly enhanced by more than one order of magnitude compared to that of LED without barrier layer. Meanwhile, the emission wavelength can also be tuned from 620 to 510 nm by controlling the Si/N ratio of the barrier layer. The improved performance of LEDs can be attributed to the variation in the band offset between the Si-rich SiN well layer and the N-rich SiN barrier layer. [J1569]

"Inkjet printed polymer light-emitting devices fabricated by thermal embedding of semiconducting polymer nanospheres in an inert matrix"

An aqueous dispersion of semiconducting polymer nanospheres was used to fabricate polymer light-emitting devices by inkjet printing in an easy-to-apply process with a minimum feature size of 20 μm. To form the devices, the electroluminescent material was printed on a nonemitting polystyrene matrix layer and embedded by thermal annealing. The process allows the printing of light-emitting thin-film devices without extensive optimization of film homogeneity and thickness of the active layer. Optical micrographs of printed device arrays, electroluminescence emission spectra, and I/V characteristics of printed ITO/PEDOT:PSS/PS/SPN/Al devices are presented. [J1570]

"Hybrid spacer for high-efficiency white organic light-emitting diodes"

High-efficient white organic light-emitting diodes (WOLEDs) were fabricated by using the following three different emitting materials: 4'-((2,2-diphenylvinyl)-1-[4-(N,N-diphenylamino)-styryl]-terphenyl for blue emission, fac-tris(2-phenylpyridine) iridium(III) for green emission, and bis(5-benzoyl-2-phenylpyridinato-C,N)iridium(III) (acetylacetonate) for red emission. For higher efficiency, a hybrid spacer (HS) was inserted between each emissive layer (blue-red, red-green, and green-blue emissive layers). It was found that the WOLEDs using HS showed maximum power efficiency of 28.69 lm/W, maximum external quantum efficiency of 13.1%, and Commission Internationale de l'Eclairage coordinates (CIE_{x,y}) of (x=0.37, y=0.37). [J1571]

"Silicon light emitting diodes emitting over the 1.2-1.4 μm wavelength region in the extended optical communication band"

Here, we demonstrate bulk silicon light emitting diodes operating over the 1.2-1.35 μm range. This is achieved by the implantation of the rare earth thulium, incorporated in the trivalent Tm^{3+} state, into silicon p-n junctions. Light emitting diodes operating under forward bias have been obtained by codoping of boron to reduce the thermal quenching. Seven sharp lines are observed, corresponding to known internal Tm^{3+} transitions in the manifold from the 3H_5 to the 3H_6 ground states. This center, together with the basic 1.15 μm silicon emitters and Si:Er devices operating at 1.54 μm , now enables significant coverage of the extended (1.1-1.8 μm) optical communications band in silicon. [J1572]

"A nearly ideal phosphor-converted white light-emitting diode"

A phosphor-converted light-emitting diode was obtained with nearly ideal blue-to-white conversion loss of only 1%. This is achieved using internal reflection to steer phosphor emission away from lossy surfaces, a reflector material with high reflectivity, and a remotely located organic phosphor having (1) unity quantum efficiency (η_q), (2) homogeneous refractive index to minimize scattering, and (3) refractive index-matched to the encapsulation to eliminate total internal reflection. An inorganic composite phosphor is also reported with a nearly homogeneous refractive index to minimize diffuse scattering of emitted light, thereby maximizing the effective phosphor η_q and light extraction. [J1573]

"Improvement of light extraction from GaN-based thin-film light-emitting diodes by patterning undoped GaN using modified laser lift-off"

To improve light extraction from GaN-based light-emitting diodes (LEDs), we demonstrated an approach of modified laser lift-off (M-LLO) technique for patterning undoped GaN (u-GaN). The M-LLO consists in sequentially forming a two-dimensional triangular lattice pattern with a 4 μm period on a polymer layer over a sapphire substrate backplane by UV imprint and delivering the pattern onto u-GaN accompanied with the removal of the sapphire substrate. The enhancement of light extraction from GaN-based M-LLO LED with a reflective Ag film on the 120 nm deep u-GaN pattern was about 31% and 100% compared to that of a LLO-LED with a reflective film and a conventional LED with a sapphire substrate, respectively. [J1574]

"Sb-doped p-ZnO /Ga-doped n-ZnO homojunction ultraviolet light emitting diodes"

ZnO p-n homojunction light emitting diodes were fabricated based on p-type Sb-doped ZnO/n-type Ga-doped ZnO thin films. Low resistivity Au/NiO and Au/Ti contacts were formed on top of p-type and n-type ZnO layers, respectively. Au/NiO contacts on p-type ZnO exhibited a low specific resistivity of $7.4 \times 10^{-4} \Omega \text{ cm}^2$. The light emitting diodes yielded strong near-band-edge emissions in temperature-dependent and injection current-dependent electroluminescence measurements. [J1575]

"Single zinc-doped indium oxide nanowire as driving transistor for organic light-emitting diode"

Zn-doped In_2O_3 nanowires (NWs) were prepared by simple chemical vapor deposition and were systematically characterized. Field-effect transistors (FETs) constructed from the Zn-doped In_2O_3 nanowires exhibit excellent performance characteristics such as high mobility, "high-on-state" current of 105 A and large on/off current ratio of 107. Single-NW-FETs can successfully drive an organic light-emitting diode, revealing the application potential of Zn-doped In_2O_3 NW-FETs in high-performance displays. [J1576]

"Excess carrier dynamics of InGaN/GaN multiple-quantum-well light-emitting diodes with various silicon barrier doping profiles"

This study investigates the carrier dynamics of InGaN/GaN light-emitting diodes with various doping profiles in the active region by using time-resolved photoluminescence experiments. Excess carrier lifetime strongly depends on excitation intensity when the quantum wells in the active region comprise doped and undoped barriers. The measured lifetime is shorter when the excitation intensity is lower. Competition between radiative recombination in quantum wells with undoped barriers and carrier tunneling from quantum wells with undoped barriers to wells with doped barriers is responsible for this phenomenon. Reducing the excitation intensity causes more carriers to undergo faster recombination in doped quantum wells. [J1577]

"Self-assembled monolayers of protonated poly(amidoamine) dendrimers on indium tin oxide"

We have investigated the change of work function of indium tin oxide (ITO) anodes induced by adsorption of positively charged poly(amidoamine) (PAMAM) dendrimers. Kelvin probe characterization of the functionalized ITO films and electroabsorption measurements on polymer light-emitting diodes incorporating poly(9,9-dioctylfluorene) active layers revealed an abrupt (0.55 eV) lowering of the effective work function upon addition of the adsorbed layer and a weak dependence on the PAMAM generation. We interpret our results with an

electrostatic model accounting for both positively charged amines and for possible contaminations providing compensating negative charges. [J1578]

"Cascade single-chip phosphor-free white light-emitting diodes"

In order to resolve the problems existing in the conventional phosphor-converted light-emitting-diodes (LEDs) and red-green-blue LEDs, the cascade single-chip phosphor-free white LED was proposed with GaAs/GaN heterojunction direct wafer bonding. Corresponding to the color-matching calculation, the white LED demonstrated the CIE chromaticity coordinates of about (0.3, 0.3) at 20mA, which was very close to the ideal white light position (1/3, 1/3) on the chromaticity diagram. The fabrication and the electrical and optical performances of such white LEDs were described. [J1579]

"High performance of GaN thin films grown on sapphire substrates coated with a silica-submicron-sphere monolayer film"

A high-performance, GaN-based light emitting diode (LED) was prepared using a metal organic chemical vapor deposition method on a silica-sphere, monolayer-coated sapphire substrate. Various surface coverage ratios of the silica submicron spheres with diameters ranging from 300 to 550 nm were deposited on the sapphire substrate using a spin-coating method. The LED output power was increased 2.5-fold compared with the LED constructed without silica spheres and uniform light distribution was achieved. In addition, LED output power was dependent on silica-sphere size and surface coverage of the substrates. [J1580]

"Polymeric tandem organic light-emitting diodes using a self-organized interfacial layer"

The authors have demonstrated efficient polymeric tandem organic light-emitting diodes (OLEDs) with a self-organized interfacial layer, which was formed by differences in chemical surface energy. Hydrophilic poly(styrene sulfonate)-doped poly(3,4-ethylene dioxythiophene) (PEDOT:PSS) was spin coated onto the hydrophobic poly(9,9-dioctylfluorene) (PFO) surface and a PEDOT:PSS bubble or dome was built as an interfacial layer. The barrier heights of PEDOT:PSS and PFO in the two-unit tandem OLED induced a charge accumulation at the interface in the heterojunction and thereby created exciton recombination at a much higher level than in the one-unit reference. This effect was confirmed in both the hole only and the electron only devices. [J1581]

"Control of quantum-confined Stark effect in InGaN /GaN multiple quantum well active region by p - type layer for III-nitride-based visible light emitting diodes"

We demonstrate the control of the quantum-confined Stark effect in InGaN/GaN quantum wells (QWs), grown along the [0001] direction as part of the active region of visible light emitting diodes (LEDs). The effect can be altered by modifying the strain applied to the active region by the hole injection and contact layers. The optical characteristics and electrostatic potentials of the active region of the visible LEDs with different p-type layers are compared. LEDs with p-InGaN on top of the active region show a reduced blueshift in the peak wavelength with increasing injection current and a lower potential difference across the QW than those with p-GaN layers. The electrostatic potentials across the QW have estimated average values of 0.8 and 1.3 MV/cm for the active region of LEDs of current study with p-InGaN and p-GaN layers, respectively. [J1582]

"Extraction enhancement in organic light emitting devices by using metallic nanowire arrays"

The extraction efficiency of organic light emitting devices is enhanced by depositing metallic nanowires on the glass surface and indium tin oxide (ITO) anode. For the aluminum tris-(8-hydroxyquinoline) (Alq3) based devices, a 100 nm-width and 450 nm-period gold nanowire array increases light extraction up to 46% from glass substrate and 80% from the organic layer. Such metallic nanowire arrays double the brightness with small absorption, only 10% lower than ITO glass. In addition, colors of the devices can be selected by the period of nanowire array. We demonstrated blue to red light emission by using single Alq3-based device. [J1583]

"Beams of the Future? [J Microwave Surfing]"

Which technology offers all of the following advantages? 1. full-duplex gigabit Ethernet throughput 2. no RF-spectrum licensing 3. immunity to EMI 4. low-cost installation in less than a day. The answer is free-space optics (FSO), a line-of-sight optical link. [J1584]

"Implantable insulin pump, the first OLED TV, measuring without a ruler..."

In this issue, editors Maria Ebling and Mark Corner cover an implantable medical device, a wrist phone, and a new OLED TV. They also cover new dynamic train information available in Japanese trains, a camera-phone-

based measurement tool, and a tool that will make creating Web site mashups easier. [J1585]

"Blue light emitting diodes grown on freestanding (11-20) a-plane GaN substrates"

Visible blue light emitting diodes have been produced on freestanding nonpolar GaN (11-20) a-plane substrates by metal-organic chemical vapor deposition. The growth conditions have been optimized for smooth growth morphology of GaN nonpolar homoepitaxial layers without surface features, leading to light emitting diode epitaxial structures that are free of crystalline defects such as threading dislocations and stacking faults. Electroluminescence of light emitting diodes exhibit peak wavelengths of 450nm and are independent of current level at low current densities before the heating effects are evidenced. [J1586]

"A multiaxial stretchable interconnect using liquid-alloy-filled elastomeric microchannels"

We report on the fabrication and characterizations of a multiaxial stretchable interconnect using room-temperature liquid-alloy-filled elastomeric microchannels. Polydimethylsiloxane (PDMS) microchannels coated at the bottom with a gold wetting layer were used as the reservoirs which were subsequently filled by room-temperature liquid alloy using microfluidic injection technique. Using a diamond-shaped geometry to provide biaxial performance, a maximum stretchability of 100% was achieved ($\Delta R = 0.24\Omega$). Less than 0.02 Ω resistance variation was measured for 180° bending. Active electronics, light emitting diode, was also integrated onto the PDMS substrate with stretchable interconnects to demonstrate stable electrical connection during stretching, bending, and twisting. [J1587]

"Optical anisotropy in ultraviolet InGaN/GaN quantum-well light-emitting diodes with a general crystal orientation"

The crystal orientation effect on optical anisotropy in ultraviolet InGaN/GaN quantum-well (QW) light-emitting diodes are investigated using the non-Markovian gain model with many-body effects. The spontaneous emission for the y-polarization largely increases with a crystal angle because of the reduction in the spontaneous and piezoelectric polarizations. On the other hand, that for the x-polarization is shown to reach a maximum near $\theta = 24^\circ$ and begin to decrease when the crystal angle further increases. The absolute value of the anisotropy rapidly increases with a crystal angle and begins to saturate to be about one when a crystal angle exceeds about 50° . This is because, in the case of QW structures with large crystal angles, the states constituting the topmost valence subband near the band edge become predominantly |Y'-like. [J1588]

"Surface plasmon coupled electroluminescent emission"

Besides directly emitting light, electroluminescence in organic light emitting diodes (OLEDs) can excite surface plasmons (SPs) on the metal electrodes of the device. By designing a microcavity OLED with thin film metal electrodes, we can directly probe a SP mode by leaky wave extraction with a high refractive index glass prism coupler. Additional angle and polarization resolved reflection measurements on the OLED multilayer structure together with transfer matrix calculations allow us to unequivocally characterize the electroluminescent-driven SP mode. [J1589]

"Dual-color emitting quantum-dot-quantum-well CdSe-ZnS heteronanocrystals hybridized on InGaN/GaN light emitting diodes for high-quality white light generation"

We report white light generation by hybridizing green-red emitting (CdSe)ZnS/CdSe(core)/shell quantum-dot-quantum-well heteronanocrystals on blue InGaN/GaN light emitting diodes with the photometric properties of tristimulus coordinates (x,y)=(0.36,0.30), luminous efficacy of optical radiation $LE = 278 \text{ lm/W}$, correlated color temperature $CCT = 3929 \text{ K}$, and color-rendering index $CRI = 75.1$. We present the photometric analysis and the quantum mechanical design of these dual-color emitting heteronanocrystals synthesized to achieve high-quality white light when hybridized on light emitting diodes. Using such multicolor emitting heteronanocrystals facilitates simple device implementation while providing good photometric properties. [J1590]

"Phosphorus doped ZnO light emitting diodes fabricated via pulsed laser deposition"

ZnO-based light emitting diodes were fabricated on c-plane sapphire using ZnO:P/Zn_{0.9}Mg_{0.1}O/ZnO/Zn_{0.9}Mg_{0.1}O/ZnO:Gap-i-n heterostructures. The p-i-n heterojunction diodes are rectifying and show light emission under forward bias. The electroluminescence spectra shows deep level emission at low bias, but near band edge ultraviolet emission at high voltage bias. A decrease in leakage currents in as-fabricated structures was achieved via low temperature oxygen annealing. [J1591]

"Excimer-based red/near-infrared organic light-emitting diodes with very high quantum efficiency"

Various light output measures of red/near-infrared (NIR) excimer-based organic light-emitting diodes (LEDs) are reported for different cathodes (Al, Al/LiF, Ca, and Ca/PbO₂). By using a selected phosphor (PtL₂Cl) from a series of terdentate cyclometallated efficient phosphorescent Pt(II) complexes, PtLnCl, as the neat film emitting layer and a Ca/Pb(IV)O₂ cathode, the authors achieve unusually high forward viewing external quantum efficiencies of up to 14.5% photons/electron and a power conversion efficiency of up to 6% at a high emission forward output of 25mW/cm². These are the highest efficiencies reported for a NIR organic LED. Electron tunneling through thin insulating layers of LiF and Pb(IV)O₂ and the difference in band bending at the organic electron transporting layer and the cathode between the samples are used to explain this performance achievement. [J1592]

"Efficient simple structure red phosphorescent organic light emitting devices with narrow band-gap fluorescent host"

Using a narrow band-gap fluorescent host material, bis(10-hydroxybenzo[h] quinolinato)beryllium complex, efficient red phosphorescent organic light emitting diodes (PHOLEDs) comprising two layers have been reported. Significantly low driving voltage of 4.5V to reach a luminance of 1000cd/m² is reported in this simple structure PHOLEDs. The current and power efficiencies of bilayered red PHOLED are 9.66cd/A and 6.90lm/W, respectively, promising for low power display and lighting applications. [J1593]

"Extremely low voltage and high bright p-i-n fluorescent white organic light-emitting diodes"

Extremely low voltage white organic light-emitting devices (WOLEDs) with fluorescent emitters are realized exploiting p-i-n structure. White light is obtained by two complementary colors system, in which the yellow and the blue emitting components are based on 5,6,11, 12-tetraphenylnaphthacene (rubrene) and 4,4-bis-2, 2-diphenylvinyl-1, 1-spirobiphenyl (Spiro-DPVBi), respectively. The effects on the device performances of various electron blocking layers and hosts for rubrene are discussed. The best device shows a luminance of 1000cd/m² at bias of as low as 2.9V, and 10000cd/m² at 4.7V with a maximum power efficiency of 8.7lm/W. The Commission Internationale de l'Eclairage chromaticity coordinates change from (0.36, 0.45) at 1000cd/m² to (0.33, 0.42) at 10000cd/m² showing high color stability. [J1594]

"Dielectric passivation effects on ZnO light emitting diodes"

Plasma-enhanced chemical vapor-deposited SiO₂ and SiNx were used to passivate ZnO heterojunction light emitting diodes (LEDs). Postdielectric deposition annealing was critical in obtaining good LED electrical and optical characteristics. No diode characteristics or light emission was observed unless the structures were annealed at 350°C after fabrication. Annealed diodes showed a band-edge electroluminescence (EL) (385nm) and a broad defect band with a peak at 930nm at room temperature. The SiO₂ and SiNx had very different passivation effects in terms of the electrical and EL characteristics of the LEDs. After annealing, the SiO₂ passivated ZnO LEDs showed diode I-V characteristics and emitted light. However, the annealed SiNx-passivated ZnO LEDs showed leaky diode characteristics and no light emission. We attribute these differences to the role of hydrogen on the LEDs. [J1595]

"Polyfluorene-based light-emitting diodes with an azide photocross-linked poly(3,4-ethylene dioxythiophene):(polystyrene sulfonic acid) hole-injecting layer"

We used a water-soluble bis(fluorinated phenyl azide) to cross-link a poly(ethylene dioxythiophene):poly(styrene sulphononic acid) (PEDOT:PSS), hole-injection layer, with a view to its future use with water-soluble emitters. To enable direct comparison with conventional PEDOT:PSS, we studied the cross-linked films in diodes incorporating the organic-solvent soluble polymer poly(9,9'-dioctylfluorene-alt-benzothiadiazole). Kelvin probe characterization of the PEDOT:PSS and electroabsorption measurements of the devices consistently show a 0.2eV increase of the PEDOT:PSS work function upon cross-linking. We also observe a 70-fold reduction in resistivity, an increase of the current above threshold and a decrease of the "leakage" current below threshold. [J1596]

"Mixed ligands 8-hydroxyquinoline aluminum complex with high electron mobility for organic light-emitting diodes"

A mixed ligands 8-hydroxyquinoline complex (Alq₂A) with improved electron mobility was designed for organic light-emitting diodes. The electron mobility in Alq₂A was determined via transient electroluminescence (EL) from bilayer devices with structure of indium tin oxide/4,4'-bis[N-(1-naphthyl)-N-Phenyl amino]biphenyl/Alq₂A/LiF/Al. It was found that the electron mobility in Alq₂A is between (2.7 and 4.4) × 10⁻⁶ cm²/Vs at electric fields ranging

between 1.424106 and 2.404106 V/cm, which is higher than that in Alq3. The Alq2 also shows a higher EL efficiency in steady-state EL studies, which is considered to be derived from (1) improved electron mobility, (2) high fluorescence efficiency, and (3) good film-forming. [J1597]

"A single-layer permeation barrier for organic light-emitting displays"

Films of a hybrid material with part-SiO₂ part-silicone character are deposited as environmental barriers on bottom-emitting and on transparent organic light-emitting diodes. Devices coated with this barrier have lifetimes of up to 7500 h when stored at 65°C and 85% relative humidity, by far exceeding the industrial requirement of 1000 h. The intensity of the Si-O-Si absorption at the wavenumber of 1075 cm⁻¹, the wetting angle by water, and the indentation hardness support the interpretation of a homogeneous material with the properties of a SiO₂-silicone hybrid. The films remain intact over 58600 cycles of bending to 0.2% tensile strain. [J1598]

"Epitaxially grown n-ZnO/MgO/TiN/n⁺-Si (111) heterostructured light-emitting diode"

Epitaxial n-ZnO/MgO/TiN/n⁺-Si heterostructured light-emitting diodes have been fabricated. The epitaxial growth of MgO/TiN on Si(111) was established by pulsed laser deposition, which was further employed as a buffer layer for epitaxial growth of ZnO layer by metal-organic chemical-vapor deposition. Good epitaxial quality was found using high-resolution x-ray diffraction and transmission electron microscopy. A strong wide electroluminescence band, ranging from 350 to 850 nm and centered at 530 nm, was observed from the diode when a positive voltage was applied on Si substrate. The diode exhibited a linear light-output-current characteristic with an injection current up to 192 mA. [J1599]

"Erratum: "High efficiency tandem organic light-emitting devices with Al/WO₃/Au" [JAppl. Phys. Lett. 91, 123504 (2007)]"

First Page of the Article [J1600]

"Strong orange/red electroluminescence from hydrogenated polymorphous silicon carbon light-emitting devices"

We report on electroluminescent P-I-N diodes containing silicon nanocrystals embedded in an amorphous silicon carbon matrix as emitting material. The as-deposited devices mostly contain amorphous Si nanoparticles and emit weakly in the IR. After a forming process consisting of the application of a high current density to the structure, the intensity of the electroluminescence increases by a factor of 30 and shifts to the red. The forming process is characterized by electroluminescence measurements and the induced crystallization of the nanoparticles is evidenced by Raman scattering spectroscopy measurements. These results are interpreted as a metal induced crystallization. [J1601]

"Green light emitting diodes on a -plane GaN bulk substrates"

We report the development of 520-540 nm green light emitting diodes (LEDs) grown along the nonpolar a-axis of GaN. GaInN/GaN-based quantum well structures were grown in homoepitaxy on both, a-plane bulk GaN and a-plane GaN on r-plane sapphire. LEDs on GaN show higher, virtually dislocation-free crystalline quality and three times higher light output power when compared to those on r-plane sapphire. Both structures show a much smaller wavelength blue shift for increasing current density (~ 10 nm for 0.1 to 12.7 A/cm²) than conventional LEDs grown along the polar c-axis. [J1602]

"Efficient GaN slab vertical light-emitting diode covered with a patterned high-index layer"

We demonstrate the enhancement of light extraction from a wide-area (500 \times 500 μ m²) GaN slab light-emitting diode (LED) that results from covering it with a TiO₂-patterned layer. To fabricate this device, a Cu supporter is electroplated onto the p-GaN face followed by detaching the sapphire substrate with a laser lift-off process. At the standard current of 60 mA, the wall-plug efficiency of the TiO₂-patterned LED is 14.8%, i.e., the efficiency is enhanced by a factor of 1.8 over that of nonpatterned LEDs. Our three-dimensional finite-difference time-domain computations confirm that this output increases with the index of the patterned layer. [J1603]

"Polarized light emission from photonic crystal light-emitting diodes"

We have experimentally studied polarization characteristics of the two-dimensional photonic crystal (PhC) light-emitting diodes (LEDs) using an annular structure with square lattice and observed a strong polarization dependence of the lattice constant and orientation of the PhC. The extracted light from the GaN PhC LEDs has P/S ratios of 5.5 ($\sim 85\%$ polarization light) for light propagating in the Γ direction and 2.1

(68%polarization light) for the Gamma Mdirection, respectively. Based on the couple mode theory, the dependence of polarization behaviors on different lattice constant and orientation was found to be in good agreement with theoretical discussion. [J1604]

"Analysis of V defects in GaN-based light emitting diodes by scanning transmission electron microscopy and electron beam induced current"

In the fabrication of InGaN/GaN multiple quantum well light emitting diodes so-called V defects are common, but little is known about their electrical activity. Scanning transmission electron microscopy is capable of directly observing these defects, while electron beam induced current (EBIC) techniques can be used to probe electronic behavior of semiconductor defects. These techniques were combined to obtain localized measurements and our results indicate that V defects suppress the EBIC signal near the core of the defect and produce a displacement in the p-n junction location. Furthermore, the EBIC profile suggests that minority carrier diffusion lengths are longer inside the defect. [J1605]

"Enhanced performance of organic light-emitting diodes with an air-stable n -type hole-injection layer"

An air-stable n-type organic semiconductor, N,N-bis(4-trifluoromethoxybenzyl)-1,4,5,8-naphthalene-tetracarboxylic di-imide (NTCDI-OCF₃), can function as an excellent hole-injection layer to improve the hole injection from an indium tin oxide (ITO) anode to a hole-transporting layer (HTL). Significantly improved hole injection was achieved by introducing an ultrathin layer of NTCDI-OCF₃ between ITO and HTL, leading to a lower operational voltage and relatively less power consumption. The results can be attributed to the reduced hole-injection energy barrier from ITO to HTL, as shown by x-ray photoelectron spectroscopy measurements, due to the surface dipole that is formed by the NTCDI-OCF₃. The thickness dependence of NTCDI-OCF₃ was also examined. [J1606]

"The Fabrication of Vertical Light-Emitting Diodes Using Chemical Lift-Off Process"

Vertical light-emitting diodes (LEDs) were successfully fabricated by a chemical lift-off process using a selectively etchable CrN buffer layer. The novel CrN metallic layer worked well as a buffer layer for growth of the GaN LED and was etched out clearly during selective chemical etching. The vertical LED by chemical lift-off showed very good current-voltage performance with low series resistance of 0.65 Ω and low operated voltage of 3.11 V at 350 mA. Also, this device could be operated at a much higher injection forward current (1118 mA at 3.70 V) by thermally conductive metal substrate which enabled the high current operation with excellent heat dissipation. [J1607]

"Luminance Enhancement of Flip-Chip Light-Emitting Diodes by Geometric Sapphire Shaping Structure"

The flip-chip light-emitting diodes (FC-LEDs) with geometric sapphire shaping structure were investigated. The sapphire shaping structure was formed on the bottom side of the sapphire substrate by a chemical wet etching technique for light extraction purpose. The crystallography-etched facets were (1010) M-plane, (1102) R-plane, and (1120) A-plane against the (0001) c-axis with the angles range between 29deg~60deg. These large slope oblique sidewalls are useful for light extraction efficiency enhancement. The light-output power of sapphire shaping FC-LEDs was increased 55% (at 350-mA current injection) compared to that of conventional FC-LEDs. [J1608]

"One-Shot Exposure for Patterning Two-Dimensional Photonic Crystals to Enhance Light Extraction of InGaN-Based Green LEDs"

To promote the feasibility of using photonic crystals to enhance light extraction of light-emitting diodes (LEDs) for industrial applications, the request for the high-yield and simple exposure process to pattern two-dimensional photonic crystals (2DPCs) becomes rather urgent. In this work, we developed a one-shot three-beam laser interference system to fabricate a 2DPC on an InGaN-based green LED to address its performance for backlight display applications. Using the current exposure system we develop here, a submicro-patterned area of 6 mm in diameter can be achieved. The experimental results show that the operating voltage of a 1 times 1 mm² in-area LED incorporated with the 2DPC is around 4 V, and the light extraction efficiency is enhanced by a factor of 2.1. [J1609]

"GaN Light-Emitting Diode with Deep-Angled Mesa Sidewalls for Enhanced Light Emission in the Surface-Normal Direction"

We have fabricated and characterized GaN LED devices whose mesa sidewalls are intentionally made deep and angled. The angled sidewalls efficiently deflect the photons guided laterally along the GaN epitaxial (epi) layer to a direction normal to the surface via total internal reflection. Regardless of the sidewall angle, the sidewall-deflector-integrated (SDI) LEDs exhibit significant enhancement in the light output from the device surface. The largest enhancement, which occurs when the mesa sidewall angle is about 30deg, is greater than 2times. Computer simulations based on ray optics correctly reproduce the sidewall angle dependence of the enhancement factor. Near-field emission patterns as well as space-resolved electroluminescence spectra also support that the enhancement in the light output is due to those additional photons that are guided laterally and deflected by the angled mesa sidewalls. [J1610]

"Automatic System for Measuring and Controlling the Length of a Moving Product in Industries"

This paper describes the design and development of a very simple low-cost online system for measuring the length of moving billets in the steel industry. Few photosensors, digital logic gates, and light-emitting diodes are used to track and display the wide variation in billet length. Not a single amplifier or comparator is used in photosensor circuit. The comparative study shows its superiority over other costly dimension-measuring systems, viz., shaft encoder, laser Doppler meter, and charge-coupled-device camera. Before, an operator had a risk of an accident while crossing the hot-cobble-prone area for measuring the billet length. However, today, the length of each billet is displayed in a pulpit, thereby increasing the safety. The measuring error in the billet length, ranging from +100 to -100 mm, is reduced to +50 mm. The fluctuation in linear velocity of an incoming billet to a flying shear causes wide variation in its cut lengths. To overcome this severe problem, the speed of the flying shear is adjusted during the tail end of each billet. The benefit of the system is in the tune of Rs 49.5 times 106 (approximately U.S. \$1.26 times 106) per annum, whereas the payback period is less than 15 days. Apart from the different steel products like the slab, bloom, and rail, the developed system is also useful in the dimensional measurement of the products in nonferrous industries. [J1611]

"Cool white III-nitride light emitting diodes based on phosphor-free indium-rich InGaN nanostructures"

Phosphor-free cool white emitting light emitting diodes (LEDs) have been fabricated using a dual stacked InGaN/GaN multiple quantum wells (MQWs) comprising of a lower set of MQWs emitting yellow and an upper set of MQWs emitting blue. The lower set of MQWs incorporates indium-rich InGaN connected-dot nanostructures with a height of 1.0 nm in the well. The well is first grown with an InGaN layer serving as the wetting layer, then treated with trimethylindium (TMIn) to initiate nanostructure growth of another InGaN layer to complete the well layer. This gives a broadened yellow emission peak. With the combination of emission from the upper blue emitting InGaN/GaN MQWs subsequently grown, cool white light emission is achieved. The In-rich nanostructures formed during TMIn treatment enhance indium incorporation in InGaN well and also act as effective radiative recombination sites for carriers at the lower set of MQWs. [J1612]

"Optical detection of deoxyribonucleic acid hybridization with In Ga N /Ga N multiple quantum wells"

Based on the high surface sensitivity of piezoelectric polarization of strained nitride semiconductors, surface functionalized nitride light emitting devices (LEDs) provide an excellent opportunity for the development of biological sensors. To demonstrate our working principle, a probe chip based on In_{0.22}Ga_{0.78}N/GaN multiple quantum wells has been constructed and exposed to target DNA solutions, matched and/or mismatched, with different concentrations. The pronounced changes of photoluminescence spectra as well as Raman scattering A₁(LO) spectra in matched target DNA clearly illustrate the feasibility of our proposed mechanism. The results shown here open up a new possibility for the application of nitride LEDs in biosensor engineering. [J1613]

"Enhanced characteristics of blue In Ga N /Ga N light-emitting diodes by using selective activation to modulate the lateral current spreading length"

We have studied the characteristics of blue InGaN/GaN multiple quantum-well light-emitting diodes (LEDs) after reducing the length of the lateral current path through the transparent layer through formation of a peripheral high-resistance current-blocking region in the Mg-doped GaN layer. To study the mechanism of selective activation in the Mg-doped GaN layer, we deposited titanium (Ti), gold (Au), Ti/Au, silver, and copper individually onto the Mg-doped GaN layer and investigated their effects on the hole concentration in the p-GaN layer. The Mg-doped GaN layer capped with Ti effectively depressed the hole concentration in the p-GaN layer by over one order of magnitude relative to that of the as-grown layer. This may suggest that high resistive regions are formed by diffusion of Ti and depth of high resistive region from the p-GaN surface depends on the capped Ti film thickness. Selective activation of the Mg-doped GaN layer could be used to modulate the length of the lateral

current path. Furthermore, the external quantum efficiency of the LEDs was improved significantly after reducing the lateral current spreading length. In our best result, the external quantum efficiency was 52.3% higher (at 100mA) than that of the as-grown blue LEDs. [J1614]

"Highly efficient green phosphorescent organic light-emitting diodes with simplified device geometry"

We report on the performance of green phosphorescent organic light-emitting diodes based on the well-known host 4,4'-di(carbazol-9-yl)-biphenyl and the green phosphor emitter fac tris(2-phenylpyridinato-N,C2') iridium. Using a spin-coated hole-injection/transport layer of poly(N-vinyl-carbazole) and a hole-blocking/electron-transport layer of 2,9-dimethyl-4,7-diphenyl-1,10-phenanthroline, devices with efficiencies of 21.2% and 72cd/Aat 100cd/m²were obtained in a simplified device geometry that requires the deposition of only two organic layers from the vapor phase. [J1615]

"Erratum: "Upconversion electroluminescence in InAs quantum dot light-emitting diodes" [JAppl. Phys. Lett. 92, 091121 (2008)]"

First Page of the Article [J1616]

"High efficiency electrophosphorescence device using a thin cleaving layer in an Ir-complex doped emitter layer"

The authors demonstrate a considerable increase in current efficiency of fac-tris(2-phenylpyridine) iridium doped phosphorescent organic green-light emitting diode in which a thin 4,7 diphenyl-1,10-phenanthroline (Bphen) layer acts as a cleaving layer. As 4nmBphen layer divides the emitting layer (EML) into two sub-EMLs, a maximum current efficiency of 53cd/A(corresponding to external efficiency quantum of 15%) is obtained, which is higher for 2.3 folds than that of the device without it, especially the current efficiency increases 64% over the reference device at a luminance of 40000cd/m². The increases are demonstrated to the high electron mobility and special energy level alignment of Bphen with 4,4'-N,N'-dicarbazole-biphenyl host. The efficiency improvement attributes to a higher exciton formation probability in the recombination zone and better balance of the carrier injection. The detail enhancement mechanism of the efficiency is also discussed. [J1617]

"Quantum efficiency improvement in anthracene-based organic light-emitting diodes codoped with a hole-trapping material"

We focus on organic light-emitting diodes having an N,N'-di(1-naphthyl)-N,N'-diphenylbenzidine (NPB) hole-transport layer, a doped light-emitting layer (LEL) based on a 9,10-diarylanthracene (DAA), and a tris(8-quinolinolato)aluminum (Alq) electron-transport layer. The addition of a hole-trapping codopant, e.g., NPB, to the LEL can triple the external quantum efficiency (EQE), which can reach 3%-6%. We discuss (a) the magnitude of the effect and the causes, (b) the effect on the drive voltage, emission spectrum, and operating lifetime, and (c) the approaches to higher EQEs of 5%-10%. We compare (a) various blue and green LEL dopants, (b) NPB codopant with aminated polycyclic aromatic hydrocarbons, which reduce the EQE, and (c) the DAA-based cells with their Alq-based counterparts. [J1618]

"Nanoepitaxy to improve the efficiency of InGaN light-emitting diodes"

InGaN/GaNblue light-emitting diode (LED) structures are grown on nanoepitaxial lateral overgrown (NELO) GaN template on sapphire substrates by metal organic chemical vapor deposition. Nanopore arrays in SiO₂film are fabricated on the underlying GaN using anodic alumina as etch masks, resulting in a nanoporous SiO₂mask layer with an average nanopore diameter and interpore distance of 60 and 110nm, respectively. The LED on NELO GaN demonstrates low defect density, which is revealed by cross-sectional transmission electron microscopy. More importantly, the LED on NELO GaN demonstrates a higher output power, one order of magnitude higher at 80mA, and an enhancement of the emission efficiency compared to that of the LED on planar GaN. This is mainly attributed to the improvement of light extraction efficiency by random scattering at the interface of the nanoporous SiO₂mask. The nanoporous SiO₂mask acts as both a threading dislocation reduction layer and a light scattering layer to enhance both internal quantum efficiency and external light extraction efficiency. The use of NELO method improves both internal quantum efficiency and external quantum efficiency for III-nitrides based optoelectronic devices. [J1619]

"Multilayer white polymer light-emitting diodes with deoxyribonucleic acid-cetyltrimethylammonium complex as a hole-transporting/ electron-blocking layer"

Using a thin film of deoxyribonucleic acid-cetyltrimethylammonium (DNA-CTMA) complex as a hole-transporting/electron-blocking layer, we have developed a sequential solution-processing approach for constructing multilayer (up to five layers) white polymer light-emitting diodes, incorporating the poly(9,9-dioctylfluorene-2,7-diyl)/poly[2-methoxy-5(2'-ethyl-hexyloxy)-1, 4-phenylene vinylene] emissive layer. These devices were demonstrated to show a low turn-on voltage (~ 5 V), high efficiency (10.0 cd/A), and high brightness (10500 cd/m²) with an improved white-color stability. [J1620]

"Effect of InGaN quantum dot size on the recombination process in light-emitting diodes"

The effect of InGaN quantum dot (QD) size on the performance of light-emitting diodes (LEDs) was investigated by varying the QD size from 1.32 to 2.81 nm. The electroluminescence peak of the LEDs containing small QDs (1.32 nm) was redshifted with increasing input current while that of large QDs (2.81 nm) was blueshifted up to 40 mÅ due to the screening effect of the piezoelectric field. The optical output power of LEDs fabricated with small QDs was much higher compared to those with large QDs. These results were attributed to a weaker piezoelectric field and enhanced quantum confinement in small QDs. [J1621]

"Enhanced emission efficiency of GaN/InGaN multiple quantum well light-emitting diode with an embedded photonic crystal"

A photonic crystal (PC) structure of periodic SiO₂ pillar cubic array is embedded in n-GaN layer of InGaN/GaN multiple quantum well (MQW) blue (480 nm) light-emitting diode (LED). The diameter, period, and depth of SiO₂ pillar are 124 ± 6, 230 ± 10, and 130 ± 10 nm, respectively. The increments of 70% for external quantum efficiency, 17% for internal quantum efficiency, and 45% for light extraction efficiency from photoluminescence measurement, and 33% for optical output power at 20 mA are observed for LEDs with an embedded PC layer. This improvement can be attributed to the increased extraction efficiency by PC effect as well as increased internal quantum efficiency due to the decrease of dislocation density in n-GaN layer because of an epitaxial lateral over-growth process. [J1622]

"Highly efficient red organic light-emitting devices based on a fluorene-triphenylamine host doped with an Os(II) phosphor"

We report highly efficient red-light-emitting devices based on a fluorene-triphenylamine tris[4-(9-phenylfluoren-9-yl)phenyl]amine (TFTPA) host doped with an osmium phosphor. The sterically hindered fluorene peripheries provided a compatible environment for the osmium dopant and alleviated concentration quenching of the phosphor at high doping levels. Increasing the doping concentration from 7 to 21 wt% dramatically decreased the driving voltage of the TFTPA-based devices, leading to improved power efficiency. The 21 wt% Os-doped device exhibited maximum luminous and powder efficiencies of 29.9 cd/A and 25.2 lm/W, combined with high efficiencies at high brightness. At 1000 cd/m² the efficiencies remained 29.2 cd/A and 22.2 lm/W. [J1623]

"High efficiency deep-blue organic light-emitting diode with a blue dye in low-polarity host"

A high efficiency deep-blue organic light-emitting diode was fabricated using a blue light-emitting dye, 2,7-bis[2[phenyl(m-tolyl)amino]-9,9-dimethyl-fluorene-7-yl]-9,9-dimethyl-fluorene, doped in a low-polarity host, 4,4'-bis(9-carbazolyl)-biphenyl. The resulting device showed a highly saturated blue light with Commission Internationale de l'Eclairage coordinates of (0.14, 0.08) and a record-high external quantum efficiency of 5.1% at 100 cd/m². The highly saturated blue emission may be attributed to effective solid-state solvation of the employed host, being able to effectively separate the blue dopants due to similar host-guest polarity. The high efficiency may result from efficient energy transfer from the host to dopant and a proper device architecture, leading excitons to favorably form on the host instead of on the dopant. [J1624]

"One-step preparation of Ca- α -SiAlON:Eu²⁺ fine powder phosphors for white light-emitting diodes"

A simple methodology for producing yellow-emitting Ca- α -SiAlON:Eu²⁺ phosphors for white light-emitting diodes has been developed, which consists of postsynthesis activation of fine α -SiAlON powders prepared by the gas-reduction-nitridation method. Phase-pure, fine Ca- α -SiAlON:Eu²⁺ phosphors possessing the particle size ranging 0.9–2.8 μ m and high quantum efficiencies of 44%–55% under near-UV to blue light excitation are obtained as the process developed. The chromaticity coordinate of the synthesized Ca- α -SiAlON:Eu²⁺ can be tailored by simply controlling the activator concentration, enabling the creation of a broad range of warm-white light with the correlated color temperatures of 3500–2600 K. [J1625]

"Indistinguishable photons from a diode"

We generate indistinguishable photons from a semiconductor diode containing an InGaAs/GaAs quantum dot. By using an all-electrical technique to populate and control a single-photon emitting state, we filter out dephasing by Stark shifting the emission energy on time scales below the dephasing time of the state. By mixing consecutive photons on a beam splitter, we observe two-photon interference with a visibility of 64%. [J1626]

"Effects of interlayers on phosphorescent blue organic light-emitting diodes"

We demonstrate that the electroluminescence efficiencies of blue organic light-emitting diodes can be significantly enhanced by the incorporation of interlayers at the hole transporting layer (HTL)/emitting layer (EML) and/or EML/electron transporting layer (ETL) interfaces. Blue light-emitting iridium(III)bis(4,6-difluorophenyl)pyridinato-N,C2') picolinate was doped in an m-bis-(triphenylsilyl)benzene (UGH3) host and hole transporting wide band gap materials were introduced between the HTL and the EML as interlayers in order to block triplet exciton quenching and reduce electron overflow. The effects of adding a second undoped UGH3 interlayer at the EML/ETL interface were also studied. When the appropriate interlayers were added, the device performances were found to be dramatically enhanced, with peak external quantum and power efficiencies of 20.1% and 29.2lm/W. [J1627]

"Crystal structure and photoluminescence of Mn²⁺-Mg²⁺ codoped gamma aluminum oxynitride (gamma -Al O N) : A promising green phosphor for white light-emitting diodes"

This letter reports on the crystal structure and luminescence of a green gamma aluminum oxynitride phosphor. This phosphor, codoped with Mn²⁺ and Mg²⁺, shows a single cubic spinel phase, with Mn²⁺ and Mg²⁺ substituting Al³⁺ in the tetrahedral sites. It shows a broad emission band centered at 520nm and a full width at half maximum of 44nm. The green phosphor exhibits a small thermal quenching and high internal quantum efficiency of 62% under the blue light irradiation, enabling it to be used in high color rendering white light-emitting diodes. [J1628]

"Effect of the barrier composition on the polarization fields in near UV InGaN light emitting diodes"

The electroluminescence from near ultraviolet (UV) light emitting diodes containing InGaN multiple quantum wells (MQWs) with GaN, AlGaN, and InAlGaN barriers was investigated. Based on band-structure calculations the observed wavelength shift in the peak emission with increasing injection current is attributed to the screening of the polarization fields and to band gap renormalization. InGaN MQWs with almost zero net polarization have been realized. No blueshift in the emission spectra of these devices was observed over the entire current range. [J1629]

"Organic light emitting diodes using a Ga:ZnO anode"

We report the application of gallium doped zinc oxide (GZO) films as anodes in organic light emitting diodes (OLEDs). Pulsed laser deposited GZO films of differing Ga composition are examined. Bilayer OLEDs using GZO and indium tin oxide (ITO) anodes are compared. Relative to ITO, the GZO anodes have a slightly better sheet resistance and transparency in the visible spectral region. Device data suggest that GZO effectively injects holes into an aromatic triamine hole transporting layer. Indium-free anodes such as GZO are expected to improve OLED stability while lowering the cost per unit area, which is crucial for OLED based lighting applications. [J1630]

"High efficiency and low efficiency roll off in white phosphorescent organic light-emitting diodes by managing host structures"

High efficiency phosphorescent white organic light-emitting diodes with little efficiency roll off were developed by managing the charge transport properties of the host materials. The emitting layers were stacked at a sequence of red/blue/green from the hole transport layer side and charge injection could be easily controlled by changing the host materials in the red and green emitting layers. A high quantum efficiency of 13% was obtained at a luminance of 1000cd/m². In addition, the quantum efficiency of the white device at low luminance was maintained up to 10000cd/m² without any decrease. [J1631]

"Influence of pulse width on electroluminescence and junction temperature of AlInGaN deep ultraviolet light-emitting diodes"

The behavior of electroluminescence (EL) and junction temperature of AlInGaN deep ultraviolet light-emitting diodes under pulse-width modulation is investigated. The redshift of both emissions from quantum-well (P1) and localized (P2) states in the EL spectra and the increase of intensity ratio of P1 to P2 are observed with the

increase of duty cycle. The photoluminescence of p-GaN contact layer is adopted to measure the junction temperature, which shows a linear relation with the duty cycle. Meanwhile, the duty cycle coefficient of junction temperature increases with the increase of injection current. The EL behaviors are explained by the thermal effect induced by pulse current at high duty cycle. [J1632]

"Green phosphorescent light-emitting diodes from polymer doped with iridium complex"

We demonstrate efficient organic light-emitting diodes by using a phosphorescent host/guest system consisting of a recently developed green electrophosphorescent molecule, bis[(4,6-difluorophenyl)-8-methylpyridinato-N,C2']iridium pyrazinate [(dfmppy)2Irprz], as the guest and a blend of poly(N-vinylcarbazole) (PVK) with 2-(4-biphenyl)-5-(4-tert-butylphenyl)-1,3,4-oxadiazole (PBD) as the host and different cathode structures such as a triple layer of BAlq/LiF/Al and a bilayer of CsF/Al. The electrophosphorescence emission was characteristic of (dfmppy)2Irprz, with its maximum at 563 nm with Commission International de L'Eclairage coordinates of (0.43, 0.53). The device with 0.5 wt% of (dfmppy)2Irprz in PVK/PBD (60:40 wt%) with a CsF (2 nm)/Al bilayer exhibited an external quantum efficiency of 6.2%, luminescence efficiency of 17.3 cd/A, luminous power efficiency of 24.2 lm/W, and maximum brightness of 10220 cd/m². [J1633]

"Enhancement of organic magnetoresistance by electrical conditioning"

We demonstrate that electrical conditioning can be used as an efficient method to enhance the organic magnetoresistance effect in organic light emitting diodes. Depending on duration and intensity of the conditioning process the absolute value of the magnetoresistance effect can be increased from 1% to values exceeding 15% at 40 mT in devices based on poly(paraphenylene vinylene). Qualitatively, the increase in magnetoresistance can be correlated with a decrease in luminance during the conditioning process. From this we conclude that device degradation mechanisms are responsible for the enhancement of organic magnetoresistance. [J1634]

"Threshold voltage shift and formation of charge traps induced by light irradiation during the fabrication of organic light-emitting diodes"

We examined the effects of ambient light on the device properties of an organic light-emitting diode, indium tin oxide/4,4'-bis[N-(1-naphthyl)-N-phenylamino]-biphenyl (α -NPD)/tris-(8-hydroxyquinolate) aluminum (Alq3)/Al, during fabrication using displacement current measurement. Light irradiation induces a shift in the threshold voltage for hole injection and results in the formation of charge traps in the Alq3 layer. The voltage shift implies a reduction in charge density at the α -NPD/Alq3 interface. The origin of the interfacial charge can be attributed to dipole moment ordering in the Alq3 layer. [J1635]

"Ultraviolet nanoimprinted polymer nanostructure for organic light emitting diode application"

Light extraction efficiency of a conventional organic light emitting diode (OLED) remains limited to approximately 20% as most of the emission is trapped in the waveguide and glass modes. An etchless simple method was developed to fabricate two-dimensional nanostructures on glass substrate directly by using ultraviolet (UV) curable polymer resin and UV nanoimprint lithography in order to improve output coupling efficiency of OLEDs. The enhancement of the light extraction was predicted by the three-dimensional finite difference time domain method. OLEDs integrated on nanoimprinted substrates enhanced electroluminescence intensity by up to 50% compared to the conventional device. [J1636]

"Highly flexible and transparent In Zn Sn O_x /Ag /In Zn Sn O_x multilayer electrode for flexible organic light emitting diodes"

By inserting a very thin layer of Ag between two layers of amorphous indium zinc tin oxide (IZTO), we fabricated a highly flexible, low resistance, and highly transparent IZTO-Ag-IZTO multilayer electrode on a polyethylene terephthalate (PET) substrate. Due to surface plasmon resonance (SPR) effects and the ductility of the Ag layer, the IZTO-Ag-IZTO electrode exhibited a low sheet resistance of 4.99 Ω /sq. and a high transparency of 86% as well as superior flexibility despite the very thin thickness of the IZTO layer (30 nm). It was found that the transition of the Ag layer from distinct islands to a continuous film occurred at a critical thickness (14 nm). Continuity of the Ag film is very important for SPR in IZTO-Ag-IZTO electrode. The current density-voltage-luminance characteristics of flexible organic light emitting diodes (OLEDs) fabricated on IZTO-Ag-IZTO/PET were better than those of flexible OLEDs fabricated on an ITO/PET substrate due to the low sheet resistance and high work function of the IZTO. [J1637]

"Power efficiency improvement in a tandem organic light-emitting diode"

When a tandem light-emitting diode (OLED) utilizes unoptimized electroluminescent (EL) units, it is fairly easy to

improve the power efficiency of such a device. However, when a tandem OLED utilizes optimized EL units, improved power efficiency can only be achieved if each intermediate connector has excellent carrier injection capabilities along with a negligible voltage drop across it. Four organic intermediate connectors were studied in this work, one of which consisting of a Li-doped 4,7-diphenyl-1,10-phenanthroline layer and a 1,4,5,8,9,11-hexaazatriphenylene hexacarbonitrile layer, exhibits the best power efficiency improvement for tandem OLEDs. [J1638]

"Spin injection from Co₂MnGa into an InGaAs quantum well"

We have demonstrated spin injection from a full Heusler alloy Co₂MnGa film into a (100) InGaAs quantum well in a semiconductor light-emitting diode structure at a temperature of 5K. The detection is performed in the oblique Hanle geometry, allowing quantification of the effective spin lifetime and spin detection efficiency (22±4%). This work builds on existing studies on off-stoichiometric Heusler injectors into similar light-emitting-diode structures. The role of injector stoichiometry can therefore be quantitatively assessed with the result that the spin injection efficiency increases by a factor of approximately 2 as compared with an off-stoichiometric Co_{2.4}Mn_{1.6}Ga injector. [J1639]

"Color-stable, efficient fluorescent pure-white organic light-emitting diodes with device architecture preventing excessive exciton formation on guest"

Color-stable, high-efficiency fluorescent pure-white organic light-emitting diodes were fabricated using an electroluminescence-efficient blue host 2-(N,N-diphenylamino)-6-[4-(N,N-diphenylamino)styryl]naphthalene and yellow 5,6,11,12-tetra-phenylnaphthacene in a single emissive layer. The resultant power efficiency, at 100cd/m², for example, was 9.5lm/W, and its emission changed from (0.321, 0.357) to (0.315, 0.344) for brightness increasing from 100 to 10000cd/m². The high color stability may be attributed to the device structure enabling the generation of excitons on host so that lesser excitons would form on guest, preventing exciton-quenching-caused blueshift. [J1640]

"Efficient deep-blue phosphorescent organic light-emitting device with improved electron and exciton confinement"

We report a significant improvement in the efficiency of deep-blue phosphorescent organic light-emitting devices based on the electrophosphorescent dye bis(4',6'-difluorophenylpyridinato)tetrakis(1-pyrazolyl) borate (Flr6). Using 1,1-bis[(di-4-tolylamino)phenyl]cyclohexane (TAPC) as the hole transport layer (HTL), we achieved a maximum external quantum efficiency of $\eta_{\text{EQE}} = (18 \pm 1)\%$, which is approximately 50% higher than $\eta_{\text{EQE}} = 12\%$ in a previously reported device with bis[N-(1-naphthyl)-N-phenyl-amino]biphenyl as the HTL. The maximum luminous power efficiency was also improved from $(14 \pm 1)\text{lm/W}$ to $(18 \pm 1)\text{lm/W}$. We attribute this efficiency improvement to the enhanced electron and exciton confinement provided by TAPC. [J1641]

"Temperature dependence of polarized electroluminescence side emission from (0001)-oriented blue and violet InGaN/GaN light-emitting diodes"

Temperature dependent polarized electroluminescence from (0001)-oriented blue and violet InGaN/GaN multiple-quantum-well (MQW) light-emitting diodes (LEDs) has been investigated. The viewing angle dependent light emission is found to be highly polarized perpendicular to the electrical field in the MQWs. The polarization ratio of 410nm LEDs exhibits monotonic decrease with increasing temperature from room temperature to 200°C. In contrast, the polarization ratio of 470nm LEDs initially increases with increasing temperature and then decreases at higher temperatures. This result suggests that carrier localization in quantum-dot-like structures could relax the polarization-related optical selection rule. Meanwhile, polarization ratios of side emission from both LEDs decrease at elevated injection current levels. [J1642]

"Surface recombination and facet heating in high-power diode lasers"

Surface recombination velocities and surface temperatures at front facets of standard broad-area lasers emitting at 808nm were investigated by time-resolved two-color photoluminescence and micro-Raman spectroscopy. Surface recombination velocities in the range between 105 and 106 cm/s are determined for devices with tailored surface properties. The results clearly show that increased surface recombination velocities are accompanied by increased facet temperatures. Reabsorption of light generated in the diode lasers leads to an additional enhancement of facet heating for surfaces of minor structural quality. The methodological approach presented here paves the way for improved analytical access to diode laser facet properties. [J1643]

"Optical properties of yellow light-emitting diodes grown on semipolar (112 $\bar{2}$) bulk GaN substrates"

We demonstrate high power yellow InGaN single-quantum-well light-emitting diodes (LEDs) with a peak emission wavelength of 562.7nm grown on low extended defect density semipolar (1122) bulk GaN substrates by metal organic chemical vapor deposition. The output power and external quantum efficiency at drive currents of 20 and 200mA under pulsed operation (10% duty cycle) were 5.9mW, 13.4% and 29.2mW, 6.4%, respectively. It was observed that the temperature dependence of the output power of InGaN LEDs was significantly smaller than that of AlInGaP LEDs. [J1644]

"High efficiency and stability in air of the encapsulation-free hybrid organic-inorganic light-emitting diode"

High efficiency and stability in an encapsulation-free hybrid organic-inorganic light-emitting diode (HOILED) have been achieved by controlling the hole carrier concentration by the use of a cesium compound layer acting as a hole-blocking unit. The low efficiency and brightness of the conventional HOILED are caused by insufficient blocking on the titanium dioxide (TiO₂) interface. Electroluminescence with high brightness (10000Cd/m^2 at 4V) and efficiency ($7.2\text{Cd/Aat } 3.6\text{V}$) was observed. Higher than required emission reaching 600Cd/m^2 at 6V can be observed after keeping the TiO₂-free improved HOILED in air for 172h. [J1645]

"Strong Efficiency Improvement of SOI-LEDs Through Carrier Confinement"

Contemporary silicon light-emitting diodes in silicon-on-insulator (SOI) technology suffer from poor efficiency compared to their bulk-silicon counterparts. In this letter, we present a new device structure where the carrier injection takes place through silicon slabs of only a few nanometer thick. Its external quantum efficiency of 1.4×10^{-4} at room temperature, with a spectrum peaking at 1130 nm, is almost two orders higher than reported thus far on SOI. The structure diminishes the dominant role of nonradiative recombination at the n⁺ and p⁺ contacts, by confining the injected carriers in an SOI peninsula. With this approach, a compact infrared light source can be fabricated using standard semiconductor processing steps [J1646]

"Unidirectional, Efficiency-Controlled Coupling from Microcavity Using Reflection Feedback"

We propose a microcavity-to-waveguide side coupling system with a reflector at one end of the waveguide for the feedback. Using this system, one can get a unidirectional output from a microcavity-based light emitter, where the output coupling efficiency and the cavity loss can be enhanced or suppressed through tuning optical phase of the feedback. Theoretical calculations are confirmed by finite-difference time domain (FDTD) simulation of the coupling between a photonic crystal cavity and a microfiber with a perfect mirror attached. Unidirectional coupling from the photonic crystal cavity to the fiber with efficiency of 90% is demonstrated in the simulation [J1647]

"100-lm/W InGaAlP Thin-Film Light-Emitting Diodes With Buried Microreflectors"

Thin-film light-emitting diodes (LEDs) belong to the most successful LED concepts for achieving high efficiencies. The incorporation of buried microreflectors with inclined facets prevents the light generation under the top contact and bondpad and offers an additional light extraction scheme. As a result, an external quantum efficiency of 50% could be demonstrated at a wavelength of 650 nm, and a luminous efficiency of more than 100 lm/W could be achieved in the wavelength range from 595 to 620 nm [J1648]

"Nitride-Based High-Power Flip-Chip LED With Double-Side Patterned Sapphire Substrate"

A nitride-based high-power flip-chip (FC) light-emitting diode (LED) with a double-side patterned sapphire substrate (PSS) was proposed and realized. Under 350-mA current injection, it was found that forward voltages were 3.24, 3.26, and 3.25 V for the conventional FC LED, FC LED prepared on PSS, and FC LED with double-side PSS, respectively. It was found that the 350-mA LED output powers were 79.3, 98.1, and 121.5 mW for the conventional FC LED, FC LED prepared on PSS, and FC LED with double-side PSS, respectively. In other words, we can enhance the electroluminescence intensity by 53% without increasing operation voltage of the fabricated LED [J1649]

"Parallel Addressing Scheme for Voltage-Programmed Active-Matrix OLED Displays"

This paper presents a novel parallel addressing scheme for voltage-programmed active-matrix organic light-emitting diode (OLED) displays which provides high precision recovery of the threshold voltage shift. As a result, the uniformity over the panel is significantly improved. In addition, a new pixel circuit is presented that is capable of providing a predictably higher current as the pixel ages, so as to compensate for the OLED luminance degradation [J1650]

"Interdigitated Multipixel Arrays for the Fabrication of High-Power Light-Emitting Diodes With Very Low Series Resistances, Reduced Current Crowding, and Improved Heat Sinking"

The paper reports on a novel mask design consisting of interdigitated multipixel arrays for the fabrication of high-power light-emitting diodes (LED) with very low series resistance, reduced current crowding, and improved heat sinking. The reduction in the series resistance was mainly achieved by reducing the bulk n-resistance and the n-contact resistance, and by increasing the effective perimeter of the mesa. The small dimension of the individual pixel improved the lateral current spreading. The distributed matrix of the micropixels also resulted in an improved thermal management, effectively rendering a high cw drive-current operation. Thermal simulations showed that the junction temperature for large area power chips dropped by more than 60% by adopting the new mask design. Significant improvement in electrical and optical performances was observed when the mask was applied to a 400 nm InGaN/GaN blue LED wafer, as compared to a standard square-shaped LED with an equal active area and fabricated from the same epitaxial wafer. Series resistance as low as 0.5 Ω was measured for 300 μm devices. On a Cu header, a peak output power of 115 mW was obtained at 3.15 A cw drive current. A 700 μm LED on a header had a peak output power of 200 mW at 3.15 A cw drive current [J1651]

"Flexible Full-Color AMOLED on Ultrathin Metal Foil"

Full-color active-matrix organic light-emitting diode panels, driven by poly-Si thin-film transistors (poly-Si TFTs), were successfully fabricated on thin metal foil substrates. The p-channel poly-Si TFTs on metal foil showed a field-effect mobility of 82.9 cm^2/Vs , subthreshold slope of 0.34 V/dec, threshold voltage of -1.67 V, and off-current of $6.6 \times 10^{-14} \text{ A}/\mu\text{m}$. The 5.6-in panel had 160 times RGB times 350 pixels, each of which had a pixel circuit of two TFTs and one capacitor [J1652]

"Improved Reliability and ESD Characteristics of Flip-Chip GaN-Based LEDs With Internal Inverse-Parallel Protection Diodes"

In this letter, a GaN/sapphire light-emitting diode (LED) structure was designed with improved electrostatic discharge (ESD) performance through the use of a shunt GaN ESD diode connected in inverse-parallel to the GaN LED. Thus, electrostatic charge can be discharged from the GaN LED through the shunt diode. We found that the ESD withstanding capability of GaN/sapphire LEDs incorporating this ESD-protection feature could be increased from several hundreds up to 3500 V in the human body model. Furthermore, flip-chip (FC) technology was also used to produce ESD-protected LEDs to further improve light output power and reliability. At a 20-mA current injection, the output power of the FC LEDs showed an improvement of around 60%. After a 1200-h aging test, the luminous intensities of the FC LEDs featuring an internal ESD-protection diode decreased by 4%. This decay percentage was far less than those of non-FC LEDs [J1653]

"High-Confinement Strained MQW for Highly Polarized High-Power Broadband Light Source"

This letter presents highly polarized edge light-emitting diodes with high-confinement, strained, multiple quantum-well active regions. We demonstrate +40 dB of polarization extinction along with 16 dBm of output power from an 800- μm -long centered quantum-well device. By characterizing the polarization extinction and gain of devices with different lengths and optical confinement, we show that the polarization extinction is dominated by the polarization sensitivity of the gain [J1654]

"Ultra-Fine Pitch Stencil Printing for a Low Cost and Low Temperature Flip-Chip Assembly Process"

This paper presents the results of a packaging process based on the stencil printing of isotropic conductive adhesives (ICAs) that form the interconnections of flip-chip bonded electronic packages. Ultra-fine pitch (sub-100- μm), low temperature (100degC), and low cost flip-chip assembly is demonstrated. The article details recent advances in electroformed stencil manufacturing that use microengineering techniques to enable stencil fabrication at apertures sizes down to 20 μm and pitches as small as 30 μm . The current state of the art for stencil printing of ICAs and solder paste is limited between 150- μm and 200- μm pitch. The ICAs-based interconnects considered in this article have been stencil printed successfully down to 50- μm pitch with consistent printing demonstrated at 90- μm pitch size. The structural integrity of the stencil after framing and printing is also investigated through experimentation and computational modeling. The assembly of a flip-chip package based on copper column bumped die and ICA deposits stencil printed at sub-100- μm pitch is described. Computational fluid dynamics modeling of the print performance provides an indicator on the optimum print parameters. Finally, an organic light emitting diode display chip is packaged using this assembly process [J1655]

"High-Performance GaN-Based Vertical-Injection Light-Emitting Diodes With TiO₂-SiO₂ Omnidirectional Reflector and n-GaN Roughness"

We have designed and fabricated a new type of GaN-based thin-film vertical-injection light-emitting diode (LED) with TiO₂-SiO₂ omnidirectional reflector (ODR) and n-GaN roughness. The associated ODR designed for LED operation wavelength at 455 nm was integrated with patterned conducting channels for the purpose of vertical current spreading. With the help of laser lift-off and photo-electrochemical etching technologies, at a driving current of 350 mA and with chip size of 1 mm times 1 mm, the light-output power and the external quantum efficiency of our thin-film LED with TiO₂-SiO₂ ODR reached 330 mW and 26.7%. The result demonstrated 18% power enhancement when compared with the results from the thin-film LED with Al reflector replace [J1656]

"GaN Surface-Emitting Laser With Monolithic Cavity-Folding Mirrors"

We report on the demonstration of a GaN-based surface-emitting laser (SEL) in a folded-cavity (FC) scheme. Two 45deg-angled sidewall deflectors were monolithically integrated at both the edges of an otherwise conventional InGaN multiple-quantum-well edge-emitting laser structure. Despite a low effective mirror reflectivity of $R(<1\%)$, the optically pumped broad-area laser structure produced laser oscillation in the vertical direction with a low threshold pump intensity of $\sim 350 \text{ kW/cm}^2$. Computer simulations on the FC, which was based on the finite-difference time-domain method, not only quantified the cavity quality of our FC-SEL device but also suggested methods to lower the laser threshold [J1657]

"Monolithically integrated III-Sb CW super-luminal light emitting diodes on non-miscut Si (100) substrates"

Reported is super-luminescent emission under room-temperature, continuous-wave conditions from GaSb quantum-well-based light emitting diodes (LED), monolithically integrated on Si (100) substrates. The LEDs are realised with substrate growth temperature under 500degC for the entire process and the Si (001) substrate is non-miscut. The lattice mismatch at the AlSb/Si interface is accommodated by interfacial misfit dislocation arrays (IMF) resulting in low defect-density III-Sb material without thick metamorphic buffers. The devices are grown in etched trenches on the Si substrate to reduce anti-phase domains in the III-Sb. The n-Si substrate is contacted directly and thus current flows through the III-Sb/Si IMF interface. The diodes have extremely low leakage current density ($J_{\text{leakage}} < 0.2 \text{ A/cm}^2$) in the reverse bias (-10 V) and show very good diode characteristics but exhibit a slightly elevated forward resistance ($R \sim 27 \text{ } \Omega$), likely to be because of the IMF. The super-luminal spectra peaks at 2.14 μm with maximum output power $\sim 0.125 \text{ mW}$ [J1658]

"Beyond Blue"

This paper presents the use of zinc oxide in UV emitting devices. It is a better material than gallium nitride for making these devices because it naturally emits at those wavelengths more efficiently. The main hurdle to making zinc oxide devices has been getting stable-reliable p-type material with an excess of holes, or electron deficiencies. Making an LED or laser diode requires a junction between p-type and n-type material. But when some of the zinc oxide is engineered to act as p-type material, it tends to revert to its natural n-type state after few months, which would cause a device to fail. This paper discusses some ways on how to make a p-type material [J1659]

"High-Efficiency 1-mm² AlGaInP LEDs Sandwiched by ITO Omni-Directional Reflector and Current-Spreading Layer"

A 1-mm² AlGaInP light-emitting diode (LED) sandwiched by an omni-directional reflector (ODR) and current-spreading layer is presented. The vertical-conducting bottom ODR consists of p-GaP, dispersive dot-contacts of Au-AuBe-Au acting as ohmic contacts, an intermediate low-refractive index layer of indium-tin-oxide, and a silver layer. A Si substrate, which acted as a heat sink, was bonded to the ODR-covered LED structure using a metal-to-metal bonding process. It was found that the maximum output power of the ODR-LED on Si reached 304 mW at 650 mA, and the output power did not saturate up to 650-mA injection current. The external quantum efficiency of 31.8% was obtained at 100 mA, and 19.4% achieved even at currents of up to 800 mA. Furthermore, under a forward current of 350 mA, the ODR-LEDs remained highly reliable after 1000-h testing at room temperature [J1660]

"A New Approach to Color Adjustment for Mobile Application Displays with a Skin Protection Algorithm on a CIE1931 Diagram"

Mobile displays use liquid crystal displays (LCDs). Such displays have various problems, such as narrow color

gamut and color saturation. We propose an algorithm to solve these problems by using data processing without panel replacement. In general, the subtle problems in color adjustment are skin color conversion and color saturation. The human skin tone is the color that is typically remembered; viewers feel awkward when skin colors are converted to unnatural colors. This paper proposes as a solution a skin protection algorithm that detects human skin colors and protects skin colors from changing. It also introduces adaptive quadratic curves that reproduce natural appearances more vividly without color saturation. In addition, the system does not use field-to-field processing but pixel-to-pixel processing in real time so that the incoming image can be displayed without field flickering [J1661]

"Nearly White-Light Emission From GaN-Based Light-Emitting Diodes Integrated With a Porous SiO₂ Layer"

In this letter, we develop a nearly white-light-emitting device by integrating blue/green emission from a GaN-based light-emitting diode with red emission from a porous SiO₂ layer. The porous SiO₂ layer was fabricated by a novel process procedure to create Si nanocrystals on top of the n-type GaN layer. Red light is generated from the metal-oxide-semiconductor (Ni-Au-SiO₂oxide-n-type GaN) structure due to the electron-hole recombination in the Si nanocrystals. The device shows a blue light emission at a low biased voltage and nearly white-light emission (green and red colors) at a bias voltage between 14 and 16 V. Our results show the potential of applying such an integrated structure to white-light illumination [J1662]

"Multibeam Optical System and Neural Processing for Turbidity Measurement"

This paper presents a turbidity measuring system based on a modulated four infrared (IR) light beam architecture with advanced data processing. The turbidity sensing component consists of a pair of IR light-emitting diodes (LEDs) connected to a current drive controlled through the pulsewidth modulated (PWM) outputs of a multifunction input/output board. The scattered and transmitted IR light in the media under test is detected by a two-channel IR photodiode module that includes a set of transimpedance and programmable gain amplifier. The voltages proportional to the detectors' output currents, are acquired using a 12-bit ADC included in a microcontroller and RS232 transmitted to a laptop personal computer (PC) that works as an advanced control and processing unit. Using optimal neural network processing architectures, an accurate extraction of the turbidity information is performed. A practical approach concerning the neural network architectures [multilayer perceptron single-input-single-output (SISO), multiple-input-single-output (MISO)] including neural network training and testing is discussed in the paper. The multi-input architectures prove to be a robust and general solution for the proposed application. Results from a turbidity measuring system that was designed for automated standalone remote operation with sensing channel autocalibration capabilities are presented [J1663]

"Nitride-Based Schottky Barrier Sensor Module With High Electrostatic Discharge Reliability"

In this study, we proposed and realized a nitride-based Schottky barrier sensor module with high electrostatic discharge (ESD) reliability. By including a Si-based ESD protection chip into the module, we can significantly enhance endurable ESD voltages under both forward and reverse human-body-mode (HBM) ESD stresses. It was found that the fabricated module can endure reverse HBM ESD stress of 7.5 KV and forward HBM ESD stress larger than 8 KV. It was also found that the inclusion of the Si-based ESD protection chip will not result in a decrease in detector responsivity [J1664]

"Lifetime Tests and Junction-Temperature Measurement of InGaN Light-Emitting Diodes Using Patterned Sapphire Substrates"

The authors demonstrate nitride-based blue light-emitting diodes with an InGaN/GaN (460 nm) multiple quantum-well structure on the patterned sapphire substrates (PSSs) compared with conventional sapphire substrates (CSSs) using metal-organic chemical vapor deposition. According to full-width at half-maximum of high-resolution X-ray diffraction and transmission electron microscopy micrographs, the dislocation density of GaN epilayers grown on the PSS was lower than those of the CSS. It was found that the output power of devices on PSS was 26% larger than that of CSS. The lifetime defined by 50% loss in output power was 590 and 305 h at 85 degC for the PSS and CSS, respectively. It was also found that the junction temperature and thermal resistance were smaller for the PSS. These improvements are attributed to the reduction in dislocation density using PSS structure [J1665]

"Asymmetric Electrical Properties of Corbino a-Si:H TFT and Concepts of Its Application to Flat Panel Displays"

Inverted stagger hydrogenated-amorphous-silicon (a-Si:H) Corbino thin-film transistors (TFTs) were fabricated

with a five-photomask process used in the processing of the active-matrix liquid-crystal displays (AM-LCD). The authors show that the a-Si:H Corbino TFT has the asymmetric electrical characteristics under different drain-bias conditions. To accommodate for these differences when the electrical device parameters are extracted, the authors developed asymmetric geometric factors. The ON-OFF current ratio can be significantly enhanced by choosing the outer electrode as the drain, while the field-effect mobility and threshold voltage are identical when different drain-bias conditions are used. Finally, the authors developed concepts of its possible application to AM-LCDs and active-matrix organic light-emitting displays [J1666]

"Efficient LED back-light power supply for liquid-crystal-display"

A highly efficient light-emitting-diode back-light power supply is proposed for liquid-crystal display. The proposed power supply consists of a bridgeless boost rectifier for power-factor correction and the asymmetrical half-bridge flyback converter with synchronous rectifier (SR) for DC-DC power conversion. In the proposed bridgeless boost rectifier, the diode reverse-recovery losses are reduced by achieving zero-current turn-off of the output diodes, as well as zero-current turn-on of the additional diodes. The reverse-recovery transients of the diodes are improved by a simple passive snubber circuit. For a DC-DC converter, the asymmetrical half-bridge flyback converter operates under zero-voltage switching for the power switches, and the SR switch operates under zero-current switching. The analysis of the proposed converter is presented and its design considerations are discussed in detail. Experimental results based on 28 V, 300 W back-light power are provided to demonstrate the performance of the proposed converter [J1667]

"Efficient White OLEDs Employing Phosphorescent Sensitization"

We have investigated white-emitting organic light-emitting devices (WOLEDs) making use of both blue-phosphor-sensitized orange-red fluorescence and the residual blue phosphorescence. By carefully adjusting the concentrations the phosphor and the fluorophore in the emitting layer and choosing the carrier-transport layers in the device structure, WOLEDs containing a single phosphor-sensitized emitting layer (type-I devices) can give colors close to the equal-energy white (0.33, 0.33), CRI up to 75, and efficiencies up to (10%, 23 cd/A, 13.4lm/W). Furthermore, by doping a green phosphor into the poorly emitting electron-transport layer (type-II devices) to recycle excitons formed there, the EL efficiencies can be further enhanced up to (12.1%, 35.3 cd/A, 23.9lm/W). In both types of devices, the phosphor sensitization reduces population of triplet excitons in the emitting region and substantially mitigates the efficiency roll-off with the driving current or brightness that is often observed in all-phosphor OLEDs. At the brightness of 1000 cd/m², both types of devices retain quantum and cadmium per ampere (cd/A) efficiencies similar to their peak values [J1668]

"Efficient and Rigorous Modeling of Light Emission in Planar Multilayer Organic Light-Emitting Diodes"

In this paper, we propose a technique to enable efficient and rigorous modeling of light emission in planar organic light-emitting diodes (OLEDs) composed of an arbitrary number of layers with different permittivity (including metals of a complex permittivity). The effects of the change of exciton radiative decay rate are explicitly included in the simulation. The numerical implementation of the technique is comprehensively discussed through an illustrative example. By using the proposed method, a bottom emitting OLED with a thick glass substrate is rigorously analyzed. The calculated results show a good agreement with the experimental results. The proposed method is efficient and well suited for optimizing OLEDs with complicated device structures. As a demonstration, we optimize the two-unit tandem top-emitting OLEDs with three types of charge generating layer. The results and design guidelines are given and discussed in detail [J1669]

"Optimization of Light-Diffracting Photonic-Crystals for High Extraction Efficiency LEDs"

Photonic-crystal (PhC)-assisted light extraction is a promising method for ultrahigh efficiency, planar light-emitting diodes (LEDs). However, modeling of such structures is challenging due to the variety of their parameters and the heavy computational burden they represent. We present a thorough theoretical discussion of the optimization of PhC LEDs, which relies both on approximate treatments and on rigorous 3-D calculations. Two material systems (GaAs and GaN) are investigated, leading to quite different optimal regimes. Notably, it appears that besides the properties of the 2-D PhC itself, design of the vertical structure plays a major role in optimization [J1670]

"Guest Editorial"

The 17 articles in this special issue focus on solid-state lighting technology. Topics covered include organic light emitting diodes, high brightness GaN-based LEDs, device physics and processing, inorganic phosphors, techniques for improved light extraction, and a description of the next generation lighting initiative of the U.S.

Department of Energy. This issue was jointly prepared with the IEEE Journal of Selected Topics in Quantum Electronics and co-distributed to subscribers of IEEE Journal of Selected Topics in Quantum Electronics. [J1671]

"ELiXIR-Solid-State Luminaire With Enhanced Light Extraction by Internal Reflection"

A phosphor-converted light-emitting diode (pcLED) luminaire featuring enhanced light extraction by internal reflection (ELiXIR) with efficacy of 60 lm/W producing 18 lumens of yellowish green light at 100 mA is presented. The luminaire consists of a commercial blue high power LED, a polymer hemispherical shell lens with interior phosphor coating, and planar aluminized reflector. High extraction efficiency of the phosphor-converted light is achieved by separating the phosphor from the LED and using internal reflection to steer the light away from lossy reflectors and the LED package and out of the device. At 10 and 500mA, the luminaire produces 2.1 and 66 lumens with efficacies of 80 and 37 lm/W, respectively. Technological improvements over existing commercial LEDs, such as more efficient pcLED packages or, alternatively, higher efficiency green or yellow for color mixing, will be essential to achieving 150-200 lm/W solid-state lighting. Advances in both areas are demonstrated [J1672]

"Next-Generation Lighting Initiative at the U.S. Department of Energy: Catalyzing Science Into the Marketplace"

Solid-state lighting (SSL) is a pivotal emerging technology that promises to fundamentally alter and improve lighting systems-and buildings-of the future, significantly lowering energy use and costs and enhancing the quality of our building environments. No other lighting technology offers our nation so much potential to conserve electricity, at a time when our nation needs bold solutions to achieve greater energy independence. Major research and market introduction challenges must be addressed before the full promise of SSL is realized. This paper discusses the role of the U.S. Department of Energy (DOE) as a catalyst in accelerating SSL technology advances, as it works in partnership with industry, research and academic organizations, and market transformation partners. Through a series of ongoing, interactive workshops, DOE and its partners have developed an extensive plan designed to ensure that DOE funds the appropriate research and development (R&D) topics and commercialization support strategies to help our nation's best and brightest lighting experts move SSL from the laboratory into the marketplace [J1673]

"Solution-Processed Organic Light-Emitting Diodes for Lighting"

In this paper, the vapor-deposited and solution-processed organic light-emitting diode (OLED) technology development paradigms are described and then compared with respect to their prospects for enabling general lighting applications. Two key development needs are improved device efficiency and lower cost fabrication methods. Progress in these areas for solution-processed OLEDs is illustrated by describing recent methods for attaining high efficiency blue emission and introducing novel low cost process methods for device fabrication which enable high performance devices without the need for any vacuum processing steps [J1674]

"High Brightness GaN-Based Light-Emitting Diodes"

This paper reviews our recent progress of GaN-based high brightness light-emitting diodes (LEDs). Firstly, by adopting chemical wet etching patterned sapphire substrates in GaN-based LEDs, not only could increase the extraction quantum efficiency, but also improve the internal quantum efficiency. Secondly, we present a high light-extraction 465-nm GaN-based vertical light-emitting diode structure with double diffuse surfaces. The external quantum efficiency was demonstrated to be about 40%. The high performance LED was achieved mainly due to the strong guided-light scattering efficiency while employing double diffuse surfaces [J1675]

"Nitride-Based Green Light-Emitting Diodes With Various p-Type Layers"

The performance characteristics of green light-emitting diodes (LEDs) grown by metal-organic chemical-vapor deposition were investigated to study the dependence of the device performance on the materials and the growth conditions of p-type layer grown after the InGaN multiple-quantum-well active region. The electrical and structural qualities of Mg-doped p-In_{0.04}Ga_{0.96}N and p-GaN layers grown under different growth conditions were studied to optimize the growth conditions of p-type hole injection layers of green LEDs. A free-hole concentration of $p = 1.6 \times 10^{18} \text{ cm}^{-3}$ with a resistivity of $0.33 \Omega \text{ cm}$ was achieved for p-GaN:Mg layers grown at 1040°C. Lower hole concentrations and mobilities and rough surfaces were obtained when the growth temperature was decreased to 930°C in H₂ ambient. In the case of p-In_{0.04}Ga_{0.96}N grown at 840°C in N₂, a significant improvement of the hole concentration was achieved due to the reduced ionization activation energy of Mg acceptors in InGaN. Also we observed that as-grown p-GaN layers grown in N₂ ambient showed p-type properties without Mg dopant activation. The electrical and optical properties of In_{0.25}Ga_{0.75}

N/GaN multiple-quantum-well green LEDs with such different p-layers were investigated. The electroluminescence intensity was improved for the LEDs with p-In_{0.04}Ga_{0.96}N layers grown at 840degC as compared to the LEDs with p-GaN layers grown at higher temperatures due to the reduced thermal damage to the active region, high hole injection, and low piezoelectric field induced in the active region. p-InGaN layers are very attractive candidates for the p-layer in green LED structures. The low temperature and N₂ ambient used during the growth of InGaN layers are beneficial to protect the InGaN active region containing high-indium composition quantum-well layers in addition to the advantage of providing a higher hole concentration. However, the LEDs with p-In_{0.04}Ga_{0.96}N layer showed a slightly higher turn on voltage which could originate from the potential barrier for hole transport at the interface of the p-InGaN layer and the last GaN quantum-well barrier. To reduce this problem, we designed and characterized an LED structure having a graded indium composition in the p-In_{0.04}Ga_{0.96}N layer in order to improve hole transport into the active region. Optimized LEDs with p-InGaN layers grown in a N₂ ambient showed much brighter electroluminescence due to low damage to the active region during p-InGaN layer growth [J1676]

"Solid-State Pressure-Tolerant Illumination for MBARI's Underwater Low-Light Imaging System"

A significant amount of energy is consumed by the typical illumination systems of underwater vehicles. Attempts to utilize more efficient LED illumination underwater have been unsuccessful because the light-emitting diodes (LEDs) were coupled to a standard imaging system and they were not able to generate enough light to adequately illuminate the scene. In cases where the LEDs were grouped together, to provide more scene illumination, the lighting assembly was inefficient in size. The recent availability of high intensity LEDs provides a way to produce efficient and adequate lighting from a compact assembly. This paper covers the development of a deep ocean assembly based on these high intensity LEDs [J1677]

"Performance of High Power Light Emitting Diodes in Display Illumination Applications"

The performance of liquid crystal displays and micro display projection systems is for a large part determined by the lamps and illumination optics they are using. Traditionally, gas discharge lamps are used, but light-emitting diode lamps are gradually taking over because of their attractive characteristics. We will discuss how the transfer to light-emitting diodes in the various display architectures changes the key performance parameters, remaining technical challenges, and prospects for future improvement [J1678]

"Status and Future of High-Power Light-Emitting Diodes for Solid-State Lighting"

Status and future outlook of III-V compound semiconductor visible-spectrum light-emitting diodes (LEDs) are presented. Light extraction techniques are reviewed and extraction efficiencies are quantified in the 60%+ (AlGaInP) and ~80% (InGaN) regimes for state-of-the-art devices. The phosphor-based white LED concept is reviewed and recent performance discussed, showing that high-power white LEDs now approach the 100-lm/W regime. Devices employing multiple phosphors for "warm" white color temperatures (~3000-4000 K) and high color rendering (CRI>80), which provide properties critical for many illumination applications, are discussed. Recent developments in chip design, packaging, and high current performance lead to very high luminance devices (~50 Mcd/m² white at 1 A forward current in 1mm² chip) that are suitable for application to automotive forward lighting. A prognosis for future LED performance levels is considered given further improvements in internal quantum efficiency, which to date lag achievements in light extraction efficiency for InGaN LEDs [J1679]

"Light Extraction From Solution-Based Processable Electrophosphorescent Organic Light-Emitting Diodes"

Molecular dye dispersed solution processable blue emitting organic light-emitting devices have been fabricated and the resulting devices exhibit efficiency as high as 25 cd/A. With down-conversion phosphors, white emitting devices have been demonstrated with peak efficiency of 38 cd/A and luminous efficiency of 25 lm/W. The high efficiencies have been a product of proper tuning of carrier transport, optimization of the location of the carrier recombination zone and, hence, microcavity effect, efficient down-conversion from blue to white light, and scattering/isotropic remission due to phosphor particles. An optical model has been developed to investigate all these effects. In contrast to the common misunderstanding that light out-coupling efficiency is about 22% and independent of device architecture, our device data and optical modeling results clearly demonstrated that the light out-coupling efficiency is strongly dependent on the exact location of the recombination zone. Estimating the device internal quantum efficiencies based on external quantum efficiencies without considering the device architecture could lead to erroneous conclusions [J1680]

"Books: Tales of Nakamura [Jreview of Brilliant! Shuji Nakamura and the Revolution in Lighting

Technology (Johnstone, B.; 2007)]"

This book not only provides a biography of Shuji Nakamura, developer of the bright blue light-emitting diode (LED), but it also offers an insightful first look at several key players in a solid-state lighting industry that is already grossing more than \$4 billion annually. [J1681]

"Resonant-Cavity-Enhanced Far-Infrared Upconversion Imaging Devices"

We have carried out a detailed investigation on the application of resonant cavities to the photon-frequency-upconversion-based far-infrared (FIR) semiconductor imaging devices. The employment of a bottom mirror (BM) enhances the FIR photon absorption efficiency and, therefore, increases the quantum efficiency of GaAs homojunction interfacial work-function internal photoemission (HIWIP) FIR detectors. Significant improvement of the extraction efficiency could be achieved in resonant cavity enhanced (RCE) GaAs-AlGaAs near-infrared (NIR) light-emitting diodes (LEDs) through redirecting as many NIR photons as possible into the escape cone. Under the optimal structural parameters, we have predicted that the upconversion quantum efficiency of the integrated HIWIP-BM-RCE-LED imaging device could be boosted to 5-6 times of the normal HIWIP-LED upconverter without any resonant cavities. As a consequence of few reincarnation cycles needed by NIR photons to escape in the photon recycling process, we can further expect sharp and high-resolution imaging in HIWIP-BM-RCE-LED [J1682]

"Knowledge Extraction From Neural Networks Using the All-Permutations Fuzzy Rule Base: The LED Display Recognition Problem"

A major drawback of artificial neural networks (ANNs) is their black-box character. Even when the trained network performs adequately, it is very difficult to understand its operation. In this letter, we use the mathematical equivalence between ANNs and a specific fuzzy rule base to extract the knowledge embedded in the network. We demonstrate this using a benchmark problem: the recognition of digits produced by a light emitting diode (LED) device. The method provides a symbolic and comprehensible description of the knowledge learned by the network during its training [J1683]

"Visible Light Emission by a Reverse-Biased Integrated Silicon Diode"

In this paper, the paper discussed the emission of visible light by a monolithically integrated silicon diode under reverse bias. The emission of light is achieved using a special defect-engineered buried layer. The light is emitted as punctiform sources by the defects located at the p-n junction of the reverse-biased diode. The influence of the defects on the electrical behavior is manifested as a current-dependent electroluminescence [J1684]

"Violet Electroluminescence of AlInGaN-InGaN Multiquantum-Well Light-Emitting Diodes: Quantum-Confined Stark Effect and Heating Effect"

Electroluminescence (EL) from AlInGaN-InGaN multiquantum-well violet light-emitting diodes is investigated as a function of forward bias. Two distinct regimes have been identified: 1) quantum-confined Stark effect at low and moderately high forward biases; 2) heating effect at high biases. In the different regimes, the low-temperature EL spectra exhibit different spectral features which are discussed in detail [J1685]

"Improvement of Reliability of GaN-Based Light-Emitting Diodes by Selective Wet Etching With p-GaN"

In an attempt to enhance the reliability of GaN-based light-emitting diodes (LEDs), the selective wet chemical etching of p-GaN surface in the GaN-based LEDs using KOH+NaOH in an ethylene glycol solution was investigated. The leakage currents of the etched LED under forward and reverse bias voltages were much lower, compared to those of a nonetched LED. The etched LED also showed improved light extraction efficiency and the degradation rate of light output power at a high injection current of 300 mA was slower than that for a nonetched LED. These results can be attributed to a decrease in the surface defects, an increase in hole concentration, and the increased surface roughness of the etched p-GaN [J1686]

"Sequential Color LED Backlight Driving System for LCD Panels"

In this paper, a sequential color light emitting diode (LED) backlight driving system for liquid crystal display (LCD) panels is proposed. Due to improvement on luminous efficacy, long life and wide color gamut, LED has gradually substituted for cold cathode fluorescent lamp as backlight. The proposed driving system adopts sequential color scanning scheme to improve light utilization efficiency by removing color filter. To meet display performance

requirement that chromaticity variation Δu_{uv} needs to be limited below 0.002, this paper also proposes a family of output current ripple free topologies to control the average driving current precisely, which in turn can reduce chromaticity variation. In addition, an LED bypass circuit is proposed to prevent LED arrays from open-circuit, and a driving voltage resetter is introduced to eliminate current spikes, improving backlight reliability and availability significantly. A forward-type output current ripple free converter has been built to sequentially drive color LED arrays, from which experimental measurements have verified the discussed performance and feasibility of the proposed system [J1687]

"InGaN–GaN MQW Metal–Semiconductor–Metal Photodiodes With Semi-Insulating Mg-Doped GaN Cap Layers"

InGaN-GaN multiple-quantum-well metal-semiconductor-metal photodiodes (PDs) with in situ grown 40-nm-thick unactivated semi-insulating Mg-doped GaN cap layer were successfully fabricated. The dark leakage current of this PD was comparably much smaller than that of conventional PD without the semi-insulating layer, because of a thicker and higher potential barrier of semi-insulating cap layer, and also a smaller number of surface states involved. For the PDs with the semi-insulating Mg-doped GaN cap layers, the responsivity at 380nm was 0.372A/W when biasing at 5 V. In short, incorporating a semi-insulating Mg-doped GaN cap layer into the PDs beneficially leads to the suppression of dark current and a corresponding improvement in the ultraviolet-to-visible rejection ratio [J1688]

"Broadband quantum dot superluminescent LED with angled facet formed by focused ion beam etching"

Broadband quantum dot superluminescent light emitting diodes (LEDs) are realised by focused ion beam etching an angled facet in an edge emitting dot-in-well laser diode structure. The device exhibits a large and flat emission spectral width up to 142 nm at 0.3 mW, maximum CW output power as high as 3 mW, and effective facet reflectivity $<1 \times 10^{-6}$ [J1689]

"GaN-based Indium-tin-oxide light emitting diodes with nanostructured silicon upper contacts"

GaN-based indium-tin-oxide (ITO) light emitting diodes (LEDs) with p-GaN, n+-short period superlattice (SPS) and nanostructured silicon contact layers were fabricated. It was found that surface of the ITO LED with nanostructured silicon layer was very rough. It was also found that 20 mA forward voltages measured from ITO LEDs with p-GaN, n+-SPS and nanostructured silicon contact layers were 6.01, 3.25 and 3.26 V, respectively. Compared with ITO LED with n+-SPS, it was found that output power of ITO LED with nanostructured silicon contact was 17% larger. Furthermore, it was found that ITO LED with nanostructured silicon contact was more reliable. [J1690]

"Foreword Special Issue on Lighting Applications"

The 25 papers in this special section focus on lighting applications. Some of the issues addressed include: lamp modeling; lamp-ballast interaction and stability issues; power factor correction for off-line electronic ballasts; lamp driving and power control; ballast auxiliary circuits; and new light sources and their applications. [J1691]

"Highly Visible Photocatalytic Activity of Fluorine and Nitrogen Co-doped Nanocrystalline Anatase Phase Titanium Oxide Converted From Ammonium Oxotrifluorotitanate"

The formation of high-quality fluorine and nitrogen co-doped nanocrystalline anatase phase titanium oxide converted from ammonium oxotrifluorotitanate discoid crystal by means of thermal treatment is reported in this study. The decomposition rate of methylene blue under 450 nm light-emitting diode illumination demonstrates an excellent visible photocatalytic activity. The highest visible photocatalytic activity is obtained at the thermal treatment temperature of 600 degC. We confirm the positive roles of fluorine and nitrogen in titanium oxide in the area of visible photocatalytic activity. There is one-to-one correspondence between the life of an electron and hole pair and photocatalytic activity [J1692]

"Light–Output Enhancement of Nano-Roughened GaN Laser Lift-Off Light-Emitting Diodes Formed by ICP Dry Etching"

In this paper, we report the fabrication and characteristics of nano-roughened GaN laser lift-off (LLO) light-emitting diodes (LEDs) with different scale surface roughness. The surface roughness of devices was controlled by inductively coupled plasma reactive ion etching. Using this fabrication method to form nano-scaled roughness, the electrical property was almost not degraded. Furthermore, the light-output power and wall-plug efficiency of

LLO LED could be both significantly enhanced about two times using this simple method [J1693]

"Realization of ultraviolet electroluminescence from ZnO homojunction with n-ZnO/p-ZnO:As/GaAs structure"

ZnO homojunction light-emitting diode with n-ZnO/p-ZnO:As/GaAs structure is produced by metal organic chemical vapor deposition. The p-type ZnO:As film is obtained out of thermal diffusion of arsenic from GaAs substrate with subsequent thermal annealing at 550°C. The n-type layer is composed of unintentionally doped ZnO film. Desirable rectifying behavior is observed from the current-voltage curve of the ZnO p-n homojunction. Furthermore, two distinct electroluminescence bands centered at 3.2 and 2.5 eV are obtained from the junction under forward bias at room temperature. [J1694]

"Red and near infrared polarized light emissions from polyfluorene copolymer based light emitting diodes"

The authors report polarized red, electroluminescence peak at 705 nm and near infrared, electroluminescence peak at 950 nm, light emission from light emitting diodes based on two polyfluorene copolymers. The copolymers are synthesized from a fluorene monomer combined with donor-acceptor-donor comonomers and designed to have a low band gap and form birefringent liquid crystalline phases. Emission occurs from aligned thin films of polymer layers. The emissive layers are aligned by spin coating on a layer of rubbed conducting polymer poly(3,4-ethylene dioxythiophene)-poly(styrene sulphonate) and thermally converted into glassy nematic liquid crystalline state. [J1695]

"Ultraviolet light-emitting diodes with self-assembled InGaN quantum dots"

A photoluminescence study showed that the self-assembled InGaN quantum dots (QDs) provide strongly localized recombination sites for carriers and that the piezoelectric field-induced quantum-confined Stark effect (QCSE) is small because the height of QDs is too small to separate the wave functions of electrons and holes. The InGaN QD light-emitting diode (LED) showed an emission peak at 400 nm, and the peak was redshifted with increasing injection current, indicating a small QCSE. The light output power of an InGaN QD LED increased linearly with increasing injection current due to the strongly localized recombination sites of the InGaN QDs. [J1696]

"High-efficiency deep blue host for organic light-emitting devices"

High-efficiency deep blue organic light-emitting devices have been fabricated using asymmetrically substituted 9-(alpha-naphthyl)-10-(beta-naphthyl)-anthracene as blue host material and diphenyl-[4-(2-[1,1';4',1'']terphenyl-4-yl-vinyl)-phenyl]amine as dopant emitter. With an optimized device structure and doping concentration, the deep blue electroluminescent (EL) device achieved an EL efficiency of 4.9 cd/A and an external quantum efficiency of 4.4% at a current density of 20 mA/cm² at saturated blue Commission Internationale de l'Eclairage coordinates of (0.15, 0.13). The deep blue device also has a current efficiency which is invariable with driving conditions ranging from 10 to 100 mA/cm². [J1697]

"Highly stable three-band white light from an InGaN-based blue light-emitting diode chip precoated with (oxy)nitride green/red phosphors"

A three-band white light-emitting diode (LED) was fabricated using an InGaN-based blue LED chip that emits 455 nm blue light, and green phosphor SrSi₂O₂N₂:Eu and red phosphor CaSiN₂:Ce that emit 538 nm green and 642 nm red emissions, respectively, when excited by the 455 nm blue light. The luminous efficacy of this white LED is about 30 lm/W at a dc of 20 mA. With increasing dc from 5.0 to 60 mA, both the coordinates x and y of the white LED tend to be the same, and consequently the T_c is the same and the R_a increases to 92.2. [J1698]

"Role of gross well-width fluctuations in bright, green-emitting single InGaN/GaN quantum well structures"

Gross well-width fluctuations have been observed by transmission electron microscopy (TEM) in single InGaN/GaN quantum wells (QWs) grown by metal-organic vapor phase epitaxy. Similar thickness variations are observed in commercial, green InGaN/GaN multi-QW light emitting diodes. Atomic force microscopy studies of equivalent epilayers suggest that these fluctuations arise from a network of interlinking InGaN strips, which are found (using TEM) to be indium rich at their centers. Plan-view TEM indicates that 90±8% of all threading dislocations (TDs) intersect the QW plane between the InGaN strips. Excitons may be localized at the strips' centers, preventing nonradiative recombination at TDs. [J1699]

"Role of the electron blocking layer in the low-temperature collapse of electroluminescence in nitride light-emitting diodes"

The low-temperature breakdown of the electroluminescence intensity (ELI) of blue/violet InGaN-based light-emitting diodes (LEDs) is shown to be independent of the structural details of the LED active region. Instead, the presence of an electron blocking layer (EBL) plays a decisive role. The authors attribute the ELI collapse to the low-temperature hole-blocking properties of the EBL. However, removing the EBL leads to a much reduced ELI because of a disproportional increase of electron overflow processes, which shows that the presence of an EBL in blue/violet InGaN-based LEDs is still essential. Optimization of the EBL by means of Mg doping is discussed.

[J1700]

"Impact of Joule heating on the brightness homogeneity of organic light emitting devices"

Joule heating and its impact on the brightness homogeneity are investigated since the luminance distribution is a key issue in large area organic light emitting diodes. In addition to previous reports, it is also important to consider the device temperature as a main factor for determining the luminance homogeneity. At a luminance of 1000cd/m² the active area reaches an average temperature of 40.6°C and a peak of 46.2°C. The increased device temperature is leading to higher local current densities resulting in a reduced brightness homogeneity. Modeling confirms these results and can be used for further device layout optimization. [J1701]

"Analysis of spatial coherence of organic light-emitting devices through investigation of interference effects observed in top-emitting devices"

Interference effects in top-emitting organic light-emitting diodes (OLEDs) containing an air gap of 15μm are studied over a range of angles in order to obtain information about the spatial coherence properties. The devices display effects similar to a Fabry-Perot étalon illuminated by a source with a broad spectral range, but the interference effects diminish rapidly with angle, which is inexplicable with simple thin film optics. The results suggest that this effect is due to the spatial coherence of the OLED. From an analysis of the interference pattern a number of device parameters can also be determined. [J1702]

"Organic light-emitting diodes with photonic crystals on glass substrate fabricated by nanoimprint lithography"

The authors have fabricated organic light-emitting diodes (OLEDs) having two-dimensional photonic crystals (PC) as light extraction elements by employing nanoimprint lithography technique. PCs were imprinted on the glass substrate and OLED layers were formed on the imprinted side of the glass substrate. The device having PC showed the improvement of luminance by a factor of 1.5 compared to normal devices. The authors conclude that the nanoimprint lithography is very useful for the fabrication of the OLEDs with PC. [J1703]

"Effect of transparent film desiccant on the lifetime of top-emitting active matrix organic light emitting diodes"

The effects of a transparent film desiccant on the lifetime of top-emitting active matrix organic light emitting diodes (AMOLEDs) were investigated. The transparent film desiccants were prepared by mixing solutions dispersed with calcium oxide powders and ultraviolet-curable resins. As the solid content in the solutions increased from 15 to 30 wt%, the average particle size increased from 107 to 240 nm, whereas the transmittance of the films decreased from 98% to 80% in the visible range. The devices encapsulated with the transparent film desiccants which contained 20 wt% CaO exhibited no dark spots and 97% of the initial luminance, even after being stored for over 500 h at 70°C and 90% relative humidity. Also, the operational lifetime of these devices was 1850 h, ten times longer than that of a device without desiccant. These results confirmed that the transparent film desiccants, which absorbed the moisture that penetrated into the devices, could be applied to the encapsulation of top-emitting AMOLEDs. [J1704]

"Electrophosphorescence from triplet excimers in poly-(N-vinylcarbazole)"

The authors have observed electrophosphorescence from triplet excimer in poly-(N-vinylcarbazole) (PVK) polymer at room temperature. The triplet excimer appears to be influenced by the PVK molecular conformation. This observation is very important to the understanding of the mechanism of triplet exciton formation in PVK. It is, therefore, an important consideration in selecting materials for phosphor-doped organic light-emitting diode applications. [J1705]

"Thermally stable luminescence of K Sr P O₄ :Eu²⁺ phosphor for white light UV light-emitting

diodes"

A novel blue phosphor based on phosphate host matrix, KSrPO_4 doped with Eu^{2+} , was prepared by solid state reaction. The phosphor invariably emits blue luminescence with a peak wavelength at 424 nm under ultraviolet excitation at 360 nm. Eu^{2+} -doped KSrPO_4 phosphors show higher thermally stable luminescence which was found to be better than commercially available $\text{Y}_3\text{Al}_5\text{O}_{12}:\text{Ce}^{3+}$ phosphor at temperature higher than 225°C.

[J1706]

"Nanovoid nature and compression effects in organic light emitting diode"

Compressing the organic layers in organic light emitting diode (OLED) is introduced as an effective process for improving the performance of organic electroluminescent devices. This process involves applying physical pressure to the organic layers of the device. The OLED fabricated by this method shows a notable increase in luminance intensity and current efficiency when compared with compression-free device, the current efficiency almost doubling. The organic layers have nanovoids and the compression results in a denser packing of organic molecules, leading to a better charge transport. [J1707]

"Enhanced electrophosphorescence of copper complex based devices by codoping an iridium complex"

Evidently enhanced electrophosphorescence of $[\text{Cu}(\text{bis}[2-(\text{diphenylphosphino})\text{phenyl}] \text{ ether})(6,7\text{-dicyanodipyrido}[2,2\text{-d':}2',3'\text{-f']\text{quinoxaline})] \text{ BF}_4$ (Cu complex) by codoping bis[(4,6-difluorophenyl)-pyridinato-N, C2](picolinato)Ir(III) (FIrpic) into the same host, 4,4'-N,N'-dicarbazole-biphenyl, was demonstrated. The device codoped with 8 wt% FIrpic and 2 wt% Cu complex shows a maximum current efficiency and power efficiency of 26.6 cd/A and 17.8 lm/W, respectively, which were increased by factors of 2.6 and 2.1 compared with the 2 wt% Cu complex monodoped device. The improvements of the devices were testified to the efficient energy transfer from FIrpic to the Cu complex. The detail of the energy transfer mechanism between the two phosphors was also proposed.

[J1708]

"Development of green, yellow, and amber light emitting diodes using InGaN multiple quantum well structures"

The authors present optical and electrical data for long wavelength (573-601 nm) InGaN/GaN multiple quantum well light emitting diodes (LEDs) grown by metal organic chemical vapor deposition. These results are achieved by optimizing the active layer growth temperature and the quantum well width. Also, the p-GaN is grown at low temperature to avoid the disintegration of the InGaN quantum wells with high InN content. A redshift is observed for both the green and yellow LEDs upon decreasing the injection current at low current regime. In the case of the yellow LED, this shift is enough to push emission into the amber (601 nm). [J1709]

"Top-emitting 230 dots /in. active-matrix polymer light-emitting diode displays on flexible metal foil substrates"

A top-emitting 230 dots/in. monochrome active-matrix polymer light-emitting diode (PLED) display having the VGA format and fabricated on a flexible steel foil utilizing the polycrystalline silicon thin-film transistor (TFT) technology is reported. The pixel circuitry architecture consists of the conventional two TFT circuitries made of two p-channel metal-oxide-semiconductor (PMOS) transistors and one storage capacitor. The average field-effect hole mobility and threshold voltage of the PMOS polysilicon TFTs fabricated on the metal foil are $37(\pm 4) \text{ cm}^2/\text{Vs}$ and $-1.9(\pm 0.6) \text{ V}$, respectively. The light turn-on voltage of the PLED is 4.0 V. [J1710]

"Phosphor-free white-light light-emitting diode of weakly carrier-density-dependent spectrum with prestrained growth of InGaN/GaN quantum wells"

The authors grew a white-light InGaN/GaN quantum-well (QW) light-emitting diode epitaxial structure with its electroluminescence spectrum close to the ideal condition in the Commission International de l'Eclairage chromaticity based on the prestrained metal-organic chemical vapor deposition technique. The prestrained growth leads to the efficient yellow emission from three InGaN/GaN QWs of increased indium incorporation. The color mixing for white light is implemented by adding a blue-emitting QW at the top of the yellow-emitting QWs. The blueshifts of the blue and yellow spectral peaks of the generated electroluminescence spectra are only 1.67 and 8 nm, respectively, when the injection current increases from 10 to 70 mA. Such small blueshifts imply that the piezoelectric fields in their QWs are significantly weaker than those previously reported. [J1711]

"Excitonic ultraviolet lasing in ZnO-based light emitting devices"

The authors have fabricated ultraviolet (UV) laser diodes based on ZnO/BeZnO films. The devices have p-n heterojunction structures with a multiple quantum well (MQW) active layer sandwiched between guide-confinement layers. The MQW active layer comprises undoped ZnO and BeZnO, while the two guide-confinement layers were As-doped p-type ZnO/BeZnO and Ga-doped n-type BeZnO/ZnO films, respectively. The exciton binding energy in the MQW region is exceptionally large (263 meV). Exciton-related lasing was observed by optically pumping the MQWs. ZnO/BeZnO-based diodes showed laser action by current injection at room temperature. The lasing mechanism is inelastic exciton-exciton collision. [J1712]

"Enhanced light output from aligned micropit InGaN-based light emitting diodes using wet-etch sapphire patterning"

The authors have demonstrated an effective method to obtain high light output power of GaN-based light-emitting diodes (LEDs) by simultaneous enhancement of internal quantum efficiency and light extraction efficiency. Micropit InGaN/GaN LEDs were fabricated on hexagonal-shaped GaN template through wet-etched substrate patterning. The result indicated that under optimized growth condition of high temperature GaN template, micropits could be formed and distributed in an aligned manner by growing on wet-etch patterned sapphire substrate. The LED structures showed superior optical output power, which directly resulted from not only effective elimination of threading dislocation of the epitaxial layers but also significant increase in light extraction efficiency via the inclined facets of aligned micropits. [J1713]

"Highly efficient and stable red phosphorescent organic light-emitting device using bis[2-(2-benzothiazoyl)phenolato]zinc(II) as host material"

The red-emitting phosphorescent organic light-emitting device employing Bis[2-(2-benzothiazoyl)phenolato]zinc(II) (Zn(BTP)₂) as a host material has been demonstrated. The device generates saturated red emission with Commission Internationale de l'Eclairage coordinates of (0.67, 0.33), characterized by a low driving voltage of 3.2 V and high external quantum efficiency of 10.3% at 10 mA/cm². Moreover, the efficiency and lifetime are improved by using 30% NPB-doped Zn(BTP)₂ host in the emitting layer, where NPB is 4,4'-bis(N-phenyl-1-naphthyl-amino)biphenyl. The maximum external quantum efficiency of the device reaches 12.6% at 1.7 mA/cm². The device has exhibited excellent stability. The half-luminance lifetime is 240 h at 80 mA/cm² (initial luminance of 6070 cd/m²). The relationship between the employed host material and device performance is discussed. [J1714]

"Nitride-based near-ultraviolet light emitting diodes with meshed p-GaN"

This investigation presents nitride-based near ultraviolet light emitting diodes (LEDs) with a meshed p-GaN layer. With 20 mA injection current, it was found that forward voltages were 3.33 and 3.39 V while output powers were 9.0 and 10.6 mW for the meshed indium-tin-oxide (ITO) LED and meshed p-GaN LED, respectively. The larger LED output power is attributed to increased light extraction efficiency. [J1715]

"Influence of hole transport units on the efficiency of polymer light emitting diodes"

Charge transport and electroluminescence efficiency in spirobifluorene polymers containing triarylamine as hole transport unit have been studied. The hole mobility as measured by the time-of-flight technique was found to be on the order of 10⁻⁴ cm²/V·s. The field and temperature dependences of the mobility are in accord with the Gaussian disorder model. Best device efficiencies of the blue emitting materials are in the range of 2.9 cd/A. The influence of the hole transport unit on charge transport and device efficiency is analyzed. The efficiency depends critically on the amount of the hole transport unit and decreases with increasing hole mobility. [J1716]

"High-efficiency low operation voltage organic light-emitting diodes"

The authors report a simple approach to reduce power consumption of organic light-emitting diodes. Introducing a 2,9-dimethyl-4,7-diphenyl-1,10-phenanthroline layer into the emissive layer can dramatically improve the carrier recombination efficiency. The presence of an interlayer of tris(8-quinolinolato)aluminum (Alq₃) within the hole-transport layer also gives rise to the similar phenomenon. Furthermore, they modified the anode with the ultrathin hexadecafluorocopper phthalocyanine layer in order to further enhance the electroluminescent properties. They obtained the high performance light-emitting diodes using Alq₃ as the emissive layer with a high current efficiency of 7.63 cd/A and a low turn-on voltage of 2.89 V. [J1717]

"Electrical Stress Degradation of Small-Grain Polysilicon Thin-Film Transistors"

This paper is focused on the stability of n-channel laser-crystallized polysilicon thin-film transistors (TFTs) submitted to a hydrogenation process during the fabrication and with small grains dimension. With the aid of

numerical simulations, we investigate the effects of static stress using two types of procedures: the on stress and the hot carrier stress. Results show that the variations of trap state density into the whole polysilicon layer and not only near the drain junction are responsible for the degradation of TFTs performances in both the two types of stress and that the interface trap states play a negligible role compared to the bulk trap states [J1718]

"High-Reflectance and Thermally Stable AgCu Alloy p-Type Reflectors for GaN-Based Light-Emitting Diodes"

We report on the formation of high-quality AgCu alloy p-type reflectors for GaN-based light-emitting diodes (LEDs). Compared with Ag contacts, the AgCu alloy reflectors produce lower specific contact resistance ($7.5 \times 10^{-5} \Omega \text{cm}^2$), higher light reflectance (89.5% at 400 nm), and better thermal stability (absence of interfacial voids), when annealed at 400 degC in $\text{N}_2 : \text{O}_2 (=1:1)$ ambient. LEDs fabricated with the AgCu reflectors show light output power better than that of LEDs with the Ag reflectors. The ohmic mechanism for the AgCu alloy reflectors is explained in terms of the formation of Ag-Ga solid solution and the presence of Cu-oxide nano-particles at the contact/GaN interface [J1719]

"Fabrication of Dicing-Free Vertical-Structured High-Power GaN-Based Light-Emitting Diodes With Selective Nickel Electroplating and Patterned Laser Liftoff Techniques"

Through the use of selective nickel (Ni) electroplating, patterned laser liftoff technique, and surface roughing of the top n-GaN epilayer, a novel process for the fabrication of vertical-structured metal-substrate GaN-based light-emitting diodes (VM-LEDs) to avoid difficulties in Ni substrate dicing and improve device yield was proposed and demonstrated. In conjunction with a sidewall passivation with SiO_2 and keeping the size of epilayer smaller than that of Ni island, a considerable improvement in yield and device performance were shown. As compared to conventional lateral-structured GaN-based LEDs, VM-LEDs show an increase in light output power about 174% at 350 mA with a significant decrease in forward voltage from 3.5 to 3.17 V [J1720]

"Polarity Balanced Driving Scheme to Suppress the Degradation of V_{th} in a-Si:H TFT Due to the Positive Gate Bias Stress for AMOLED"

In this paper, we propose a new amorphous silicon (a-Si:H) thin-film transistor (TFT) pixel circuit employing negative bias annealing for active-matrix organic light-emitting diode (AMOLED). This circuit consists of two driving TFTs, four switching TFTs, and two storage capacitors. The new driving scheme adopting negative bias annealing entitled polarity balanced driving (PBD) successfully suppresses the troublesome V_{th} shift in a-Si:H TFT. The proposed pixel circuit was verified by simulation and fabrication. When a severe electrical bias is applied more than 24 hours and a temperature is increased up to 60 degC rather than a room temperature, the current stability (I_{after_stress}/I_{max}) of the proposed PBD pixel is 0.97 while that of the conventional one is 0.72. Our experimental results show that the proposed PBD can improve a stability of a-Si:H TFT because the applied negative gate bias can successfully suppress V_{th} shift of the current-driving a-Si:H TFT [J1721]

"The Preparation of Nanocrystalline Silicon by Plasma-Enhanced Hydrogenation for the Fabrication of Light-Emitting Diodes"

The fabrication of nanocrystalline silicon light-emitting diodes is reported using a novel plasma-enhanced hydrogenation method. The fabrication process consisted of the deposition of amorphous silicon on a silicon substrate, a hydrogen plasma treatment, and subsequent annealing, and the deposition of TiO_2 , indium-tin oxide, and metal contact layers. The entire process was performed at temperatures below 400 degC and is compatible with standard silicon fabrication technologies. The current-voltage (I-V) characteristics of the device showed a rectifying diode behavior where electrons tunneled through the thin TiO_2 layer and recombined with the holes injected from the P-type silicon substrate leading to photon generation. The structure of the nanocrystalline silicon films was investigated by scanning electron and transmission electron microscopies, and the spectral distribution of the emitted light was measured by a cathodoluminescence [J1722]

"VT Compensation Circuit for AM OLED Displays Composed of Two TFTs and One Capacitor"

In this paper, we propose the threshold-voltage compensation pixel circuit that is composed of two thin-film transistors (TFTs) and one capacitor (2T1C). It not only compensates the deviation of the threshold voltage of the driver TFT but also actualizes the large aperture ratio for organic light-emitting diode (OLED) devices as well as the traditional 2T1C circuit. We show the result of SPICE simulation for the pixel circuit; it indicates that the circuit can allocate the relatively large aperture ratio for OLED devices [J1723]

"Nitride-based high power flip-chip near-UV leds with reflective submount"

Nitride-based high power flip-chip near-ultraviolet (UV) light emitting diodes (LEDs) with a reflective mirror are fabricated by depositing Al onto a Si submount. It is demonstrated that the Al layer coated onto a Si submount can effectively reflect downward emitting photons for flip-chip LEDs. Although the operation voltage of the proposed LEDs is slightly increased, it is found that the output power is at least 30% higher than that of conventional LEDs. It is also found that flip-chip near-UV LEDs are more reliable than conventional non-flip-chip LEDs [J1724]

"GaN-based light-emitting diodes prepared on vicinal sapphire substrates"

Thin InGaN epitaxial layers and GaN-based light-emitting diodes (LEDs) on conventional and vicinal cut sapphire substrates are prepared. It is found that indium atoms are distributed much more uniformly in the samples prepared on vicinal cut sapphire substrates. It is also found that stronger electroluminescence intensity can be achieved without the band-filling effect of localised states from the LEDs with vicinal cut sapphire substrate. With 20 mA current injection, it is found that 44% electroluminescence intensity enhancement can be achieved by using the 1deg tilted sapphire substrate [J1725]

"Phase fluorometric glucose biosensor using oxygen as transducer and enzyme-doped xerogels"

The development of a glucose biosensor based on co-immobilisation of oxygen (O₂) responsive luminophore and glucose oxidase (GOx) within nanoporous solgel-derived xerogels is described. The biosensor operates in the frequency domain and exploits the effect of glucose and O₂ consumption by GOx on the luminophore excited-state lifetime (i.e. phase angle). The biosensor consists of a modulated light emitting diode as the excitation source and a silicon photodiode as the detector. This sensing methodology establishes the viability for low-cost and accurate biosensors that operate at a low modulation frequency (tens of kHz). The biosensor is stable, reproducible, and provides an analytically reliable response from 0.5 to 15 mM glucose [J1726]

"Narrow Tunable Polysilane Optical Waveguide Bragg Grating Filters"

A new Bragg grating filter (BGF) in a polysilane waveguide has been fabricated by a two-beam interferometric photobleaching method using a He-Cd laser. A narrow reflected bandwidth of 0.4 nm was measured using a 1.55- μ m light-emitting diode. The temperature dependence of the BGF was measured as 0.096 nm/degC with temperature control over a range between 30 degC and 70 degC and exhibited a good coincidence with the theoretical values [J1727]

"Phosphor Thermometry in White Light-Emitting Diodes"

A method for the in situ measurement of phosphor temperature in high-power white light-emitting diodes (LEDs) was demonstrated. The method is based on the dependence of the fluorescence decay time in inorganic phosphors on temperature. The decay time was estimated using the frequency-domain technique, which relies on the measurement of the phase shift of the sinusoidal waveform of fluorescence relative to that of the photoexcitation, obtained by driving the LED at high-frequency current. LEDs containing a single phosphor ("cool-white") and a phosphor blend ("warm-white") were examined. By comparison of the phosphor temperature with that of the LED junction and metal mount, the character of the spatial profile of temperature within the LED packages was revealed [J1728]

"ZnSe based white light emitting diode on homoepitaxial ZnSe substrate"

ZnSe-based white light emitting diodes (LEDs) were homoepitaxially prepared on ZnSe substrates by molecular beam epitaxy. It was found to be possible to simultaneously observe the greenish-blue emission at 483 nm originating from the epitaxial layer and the weaker ZnSe substrate-related orange emission centred at around 595 nm. It was found that the emission wavelength of the LED and the measured chromaticity coordinate were almost independent of the injected current. It was also found that the turn-on voltage and the 20 mA operation voltage of the fabricated LED were 2.25 and 4 V, respectively [J1729]

"InGaN Light-Emitting Diode With Quasi-Quantum-Dot-Shaped Active Layer Using SiCN Interfacial Layer"

A quasi-quantum-dot (QQD)-shaped InGaN-GaN multiple-quantum-well light-emitting diode (LED) was achieved using a silicon carbon nitride (SiCN) interfacial layer. QQDs with ~100-nm diameter and ~4-nm height were uniformly formed inside the InGaN active layer due to strain and affinity difference between the InGaN and SiCN layer. The surface morphology and structural properties of QQD-LED were measured with atomic force microscopy, secondary ion mass spectrometry, and X-ray diffraction. Device performance of QQD-LEDs were evaluated and compared with normal LEDs. The QQD-LED showed ~15% higher photoluminescence intensity

and ~10% higher optical output power [J1730]

"Stability of nc-Si:H TFTs With Silicon Nitride Gate Dielectric"

We report the fabrication and characterization of bottom-gate and top-gate nanocrystalline silicon (nc-Si:H) thin-film transistors (TFTs) with amorphous-silicon nitride (a-SiN_x:H) as the gate dielectric. The devices were fabricated using standard 13.56-MHz plasma-enhanced chemical vapor deposition at 240 degC. Here, the same 80-nm nc-Si:H channel, 300-nm a-SiN_x:H gate dielectric, and 60-nm n+nc-Si:H ohmic contact layers were used in both TFT structures. We analyzed the effects of gate configuration on TFT performance and, in particular, the electrical stability. The stability tests were carried out at a gate bias stress in the range from 20 to 40 V. The nc-Si:H TFTs demonstrated much better threshold-voltage (V_T) stability compared with the amorphous-silicon (a-Si:H) counterparts, offering great promise for applications in active-matrix organic light-emitting diode (AMOLED) displays [J1731]

"Motion Characterizations of Lateral Micromachined Sensor Based on Stroboscopic Measurements"

In this paper, we illustrate the capabilities of the Planar Motion Analyzer (PMA) with a study of the dynamic behavior of a micromachined structure. Dynamic characterizations and measurement settings are also demonstrated. The optical measurement system uses the light-emitting diode (LED) based vibration measurement technique for imaging, and then measuring the lateral resonant frequency and sensor displacements, as well. The PMA analyzes in-plane vibrations of a MEMS device under a clear microscope. Its working principle is based on the stroboscopic principle. Based on this principle, characterization results in both time and frequency domains can be accurately generated and analyzed. Our device example for the measurement is a tunneling-based micro-resonator, which was fabricated using the Backside Released SOI process. The tunneling behavior of the sensor can be observed by controlling the motion of the tunneling tip towards the opposing electrode with a typical gap of 10 Å. This very small gap can be easily achieved by the Bode measurement of PMA for shifting the LED-strobe flashes at a small increment of phase angle over the whole motion of the sensor. In other words, smaller motions of the tip will be easily achieved, when the number of shots per period are larger. For our tunneling measurement, the phase angle shift is 0.5deg with 720 shots per period. The lateral moving proof mass is suspended by the folded springs, and its tip protrudes to an opposing electrode by means of electrostatic forces. The tunneling current has been observed to be exponentially increasing, when the tunneling gap is decreasing. However, the further large current is actually a contacting current, when the mechanical contact happens between the tunneling tip and the opposing electrode. The resonant frequency of the device is ~5 kHz obtained from the Bode measurement [J1732]

"High-quality thin-film passivation by catalyzer-enhanced chemical vapor deposition for organic light-emitting diodes"

The thin-film passivation of organic light-emitting diodes (OLEDs) by a SiN_x film grown by catalyzer-enhanced chemical vapor deposition was investigated. Using a tungsten catalyzer connected in series, a high-density SiN_x passivation layer was deposited on OLEDs and bare polycarbonate (PC) substrates at a substrate temperature of 50°C. Despite the low substrate temperature, the single SiN_x passivation layer, grown on the PC substrate, exhibited a low water vapor transmission rate of (2-6)×10⁻² g/m²/day and a high transmittance of 87%. In addition, current-voltage-luminescence results of an OLED passivated with a 150-nm-thick SiN_x film compared to nonpassivated sample were identical indicating that the performance of an OLED is not critically affected by radiation from tungsten catalyzer during the SiN_x deposition. Moreover, the lifetime to half initial luminance of an OLED passivated with the single 150-nm-thick SiN_x layer was 2.5 times longer than that of a nonpassivated sample. [J1733]

"Elucidation of the electron injection mechanism of evaporated cesium carbonate cathode interlayer for organic light-emitting diodes"

Vacuum evaporated Cs₂CO₃ has been proven to be an efficient electron injection material for organic light-emitting diodes. In our study, an improved quartz crystal microbalance method has been adopted to investigate the electron injection mechanism of evaporated Cs₂CO₃. It is concluded that Cs₂CO₃ decomposes to metallic cesium during thermal evaporation and the thin layer of metallic cesium that is deposited onto the organic layer is responsible for the enhanced electron injection. The metallic cesium mechanism reveals that the function of the Cs₂CO₃ interlayer is independent of the cathode metal, which has also been verified by our experiments. [J1734]

"Increase in midwave infrared light emitting diode light output due to substrate thinning and

texturing"

Midwave infrared (MWIR) light sources with high optical power are required for many applications. The authors report here the MWIR (3.8mcmpeak) light emission from an interband cascade light emitting diode (LED) structure with 18 cascaded active/injection regions grown on GaSb substrate. The light emission is observed from the substrate side of the device. An increase of six times of light output power is observed due to substrate thinning and another 50% increase is observed due to texturing the emission surface. The authors observed 400mW emission power for room temperature operation with 15mA LED injection current. Experiments were carried out with different grating patterns and etch depths. The device with a 2mcm square grating and a 1mcm etch depth has the highest optical emission power. [J1735]

"A Novel LTPS-TFT Pixel Circuit Compensating for TFT Threshold-Voltage Shift and OLED Degradation for AMOLED"

This letter presents a novel pixel circuit that uses low-temperature polycrystalline-silicon thin-film transistors (LTPS-TFTs) composed of one driving and four switching TFTs for active-matrix organic light-emitting diodes (AMOLEDs) with a voltage-source method. The proposed circuit effectively enables threshold-voltage-shift correction of the drive TFT and compensates for degradation of the OLED using a feedback structure [J1736]

"AMOLED Pixel Circuit With Electronic Compensation of Luminance Degradation"

A new voltage-programmed pixel circuit using hydrogenated amorphous silicon (a-Si:H) thin-film transistors (TFTs) for active-matrix organic light-emitting diodes (AMOLEDs) is presented. In addition to compensating for the shift in threshold voltage of TFTs, the circuit is capable of compensating for OLED luminance degradation by employing the shift in OLED voltage as a feedback of OLED degradation [J1737]

"Novel Color-Sequential Transflective Liquid Crystal Displays"

A novel transflective liquid crystal display architecture and its system driving schemes are proposed. In the reflective mode, the ambient light is used to readout the displayed images. While in the transmissive mode, a color-sequential light emitting diode backlight is used to eliminate the color filters. Under such device configuration, several advantages such as increased brightness and maximized color saturation for both transmissive and reflective modes can be achieved [J1738]

"High-Power 1.3- μ m Quantum-Dot Superluminescent Light-Emitting Diode Grown by Molecular Beam Epitaxy"

In this letter, we demonstrate the improved performance of 1.3- μ m seven-layered InAs-GaAs quantum-dot superluminescent light-emitting diodes by the engineering of the epitaxial growth conditions alone, namely the thickness of the low-temperature GaAs spacer layer between quantum-dot layers. For laser devices, a significant reduction in threshold current density and increase in external efficiency is observed, while for superluminescent diode structures, a ~ 4 fold increase in CW power at a given drive current is obtained [J1739]

"Not Ready to Wear"

The Philips Photonics Textiles research group has developed a piece of flexible material that allows people to upload reconfigurable flashing fashion statements and messages on garments, furniture, and accessories using mobile phones. Called Lumalive, the photonic textile is studded with 100 inorganic light-emitting diodes and some drive electronics. It functions as a removable display that is water-resistant but not washable. While Lumalive is a novel idea, it has a number of drawbacks that make it difficult to market. Aside from having a short battery life, Lumalive is vulnerable to hacking and has no practical use [J1740]

"CMOS-Based Phase Fluorometric Oxygen Sensor System"

The design and development of a phase fluorometric oxygen (O_2) sensor system using single-chip CMOS detection and processing integrated circuit (DPIC) and sol-gel derived xerogel thin-film sensor elements is described. The sensor system determines analyte concentrations using the excited state lifetime measurements of an O_2 -sensitive luminophore (tris(4,7-diphenyl-1,10-phenanthroline)ruthenium (II)) embedded in the xerogel matrix. A light emitting diode (LED) is used as the excitation source, and the fluorescence is detected by the DPIC using a 16times16 phototransistor array on-chip. The DPIC also consists of a current mirror, current-to-voltage converter, amplifier, bandpass filter, and phase detector. The DPIC output is a dc voltage that corresponds to the detected fluorescence phase shift. With a 14-kHz modulation frequency, the entire system including driving the LED consumes 80 mW of average power. The sensor system provides stable, reproducible,

analytically reliable, and fast response (~ 20 s) to changes in the gaseous oxygen concentrations and establishes the viability for low cost, low power and miniaturized biochemical sensor systems [J1741]

"Numerical Device Simulation of Double-Heterostructure Organic Laser Diodes Including Current-Induced Absorption Processes"

We investigate the impact of induced absorption caused by injected charge carriers and excited states on the threshold current density of an organic laser diode using numerical simulations. The electrical properties of the device are described by a self consistent drift-diffusion model. The optical properties are calculated using a transfer matrix method. Nonradiative annihilation processes are included employing typical rate constants. In our approach, a three-layer double-heterostructure (DH) with typical organic material properties is studied, which exhibits a threshold current density of 564 A/cm². For this virtual device, upper limits for the charge carrier and triplet-triplet absorption cross section $\sigma_{\text{carrier}} = 1.53 \times 10^{-3} \sigma_{\text{SE}}$ and $\sigma_{\text{T1TN}} = 4.34 \times 10^{-3} \sigma_{\text{SE}}$ have been calculated as a function of the stimulated emission cross section σ_{SE} . Additionally, the role of device geometry and material properties concerning induced absorptions is studied. It is shown that the impact of absorption processes is not strongly influenced by the device geometry. By increasing the charge carrier mobilities to $\mu = 2$ cm²/V in the transport layers and $\mu = 0.2$ cm²/V in the emission layer, the impact of polaron absorption can be greatly reduced. In this case, laser operation might still be possible if σ_{carrier} and σ_{SE} are within the same order of magnitude. Decreasing the triplet lifetime τ_{T1} is a promising way to reduce the impact of triplet-triplet absorption. For σ_{T1TN} and σ_{SE} being within the same order of magnitude, the triplet lifetime τ_{T1} has to be reduced to 1 ns for laser operation.

[J1742]

"The Engineering and Initial Results of a Transformable Low-cost High-Resolution PET Camera"

We have developed a high-resolution transformable positron emission tomography (PET) camera that can be configured into either a whole-body mode (83-cm detector ring diameter, 13-cm axial field-of-view (AFOV)) or a brain/breast/axilla (54-cm detector ring diameter, 21-cm AFOV) mode. The camera has 12 rectangular detector modules, and the detector gap between adjacent modules is very small and remains constant for each configuration. Each module has a large detection area (13 cm times 21 cm) and 38016 bismuth germanate (BGO) detector crystals of 2.7 times 2.7 times 18 mm³ with built-in front-end electronics. To improve spatial sampling, the gantry on which the camera is mounted can be rotated 30deg with a fine step size of 1deg, and the high-speed electronics and detector modules also rotate along with the gantry. This system uses only 924 photomultiplier tubes (PMT) by applying a low-cost high-resolution PMT-quadrant-sharing detector design. To compensate for the slower scintillation timing of BGO detectors, the camera is equipped with the "HYPER", high-yield pile-up event recovery front-end electronics. A fast light-emitting diode (LED) cross-reference PMT tuning method is used to maintain the PMT gain balance. The system has been constructed and tested for preliminary imaging characteristics. The system sensitivity is 4.2% for whole-body and 9.2% for brain/breast/axilla mode measured with Na-22 at center of field of view (FOV). For brain/breast/axilla modes, the transaxial image resolutions at 0 and 10 cm were found to be 2.7 and 4.0 mm, respectively, while for whole-body mode, the image resolutions were 3.3 and 3.9 mm. The slice thickness resolution ranged from 2.6 to 3.3 mm for middle 7 detector rings in brain/breast/axilla modes. High quality Hoffman brain phantom images were obtained in both brain and whole-body modes. [J1743]

"The Design of the Cooling System for the CMS Barrel Electromagnetic Calorimeter"

CMS is one of the four experiments being constructed for the LHC. The electromagnetic calorimeter (ECAL) is made of lead tungstate (PbWO₄) crystals. Scintillation light from the crystals in the barrel is detected by avalanche photo diodes (APD). The number of scintillation photons emitted by the crystals and the amplification of the APD are both temperature dependent. Keeping the constant term of the energy resolution (the contribution to the fractional energy resolution which is independent of energy) below a few tenths of percent requires the temperature of the the crystals and APDs to be stabilized to within 0.1 K while for example previously built L3 detector using another type of crystals had a temperature stability around 1 K which is the standard requirement for cooling systems at CERN. In this contribution, we describe the innovative solutions which have been developed and implemented to achieve this performance. [J1744]

"Image Quality Enhancement Driving Method of Flat Panel Displays for TV Applications"

The image quality enhancement driving method compensates the output channel non-uniformity by diffusing output voltage errors throughout adjacent channels with sharing several adjacent output driving circuits which have their own offset errors, resulting in increase in PSNR and reduction in the standard deviation. This paper presents a performance verification of the driving method by analyzing it mathematically and systematically. This

paper also shows the experimental results that the errors due to the channel-to-channel random offsets become hardly noticeable when the proposed driving method is applied to an AMOLED driver IC. To optimize the tradeoff among the performance, design complexity, and the number of sharing output channels, we derive that the optimized number of sharing channels is 3 at 60 Hz frame rate using the concept of critical flicker frequency.

[J1745]

"High-Detectivity Nitride-Based MSM Photodetectors on InGaN-GaN Multiquantum Well With the Unactivated Mg-Doped GaN Layer"

InGaN-GaN multiquantum-well (MQW) metal-semiconductor-metal (MSM) photodetectors (PDs) with the unactivated Mg-doped GaN cap layer were successfully fabricated. It was found that we could achieve a dark current by as much as six orders of magnitude smaller by inserting the unactivated Mg-doped GaN cap layer. For MSM photodetectors with the unactivated Mg-doped GaN cap layer, the responsivity at 380 nm was found to be 0.372 A/W when the device was biased at 5 V. The UV-to-visible rejection ratio was also estimated to be around 1.96 times 10^3 for the photodetectors with the unactivated Mg-doped GaN cap layer. With a 5-V applied bias, we found that minimum noise equivalent power and normalized detectivity of our PDs were 4.09 times 10^{-14} W and 1.18 times $10^{13} \text{ cm}^2 \text{ Hz}^0.5 \text{ W}^{-1}$, respectively. Briefly, incorporating the unactivated Mg-doped GaN layer into the PDs beneficially brings about the suppression of dark current and a corresponding improvement in the device characteristics. [J1746]

"Comparison of Usability of Oxide Apertures and Photonic Crystals Used to Create Radial Optical Confinements in 650-nm GaInP VCSELs"

Threshold characteristics of GaAs-based 650-nm gallium indium phosphide (GaInP) vertical-cavity surface-emitting diode lasers (VCSELs) with two different optical confinement structures are investigated with the aid of a self-consistent, fully-physical VCSEL model. Efficacy of the optical confinement introduced by the oxide aperture is compared with an alternative single-defect photonic-crystal design with holes etched throughout the whole VCSEL. Initially, photonic-crystal VCSEL reveals 10% lower threshold electrical power than that of the analogous oxide-confined VCSEL. Further optimization of the current injection allows for an additional 20% threshold reduction. The photonic-crystal confinement concept appears to be a very prospective solution for VCSEL configurations, for which oxidation is unfeasible, e.g., for possible nitride or phosphide VCSELs. [J1747]

"Spatial and Temporal Resolution of Conjugate Conduction-Convection Thermal Resistance"

A transient, 3-D solution to the heat conduction equation with a small square heat source on an adiabatic surface and Newtonian convection on the opposite side was obtained using Green's functions. The geometry conservatively models conduction spreading resistance encountered by small, concentrated heat sources such as light-emitting diodes and integrated circuits in general, mounted to larger substrates such as the base of a heat sink experiencing Newtonian convection. The solution is presented for a range of nondimensional parameters. Superposition techniques can also be used to extend the applicability of the current solution to the temperature prediction of arbitrary heat flux patterns in certain cases. This technique only holds for applications where the heat transfer coefficient is not a function of temperature, such as thermal management strategies designed to rely on forced convection with air. [J1748]

"Thermal Resistance Measurement of LED Package with Multichips"

Thermal transient measurements of high power GaN-based light-emitting diodes (LEDs) with multichip designs are presented and discussed in the paper. Once transient cooling curve was obtained, the structure function theory was applied to determine the thermal resistance of packages. The total thermal resistance from junction to ambient considering optical power is 19.87 K/W, 10.78 K/W, 6.77 K/W for the one-chip, two-chip and four-chip packages, respectively. The contribution of each component to the total thermal resistance of the package can be determined from the cumulative structure function and differential structure function. The total thermal resistance of multichip packages is found to decrease with the number of chips due to parallel heat dissipation. However, the effect of the number of chips on thermal resistance of package strongly depends on the ratio of partial thermal resistance of chip and that of slug. Therefore, an important thermal design rule for packaging of high power multichip LEDs has been analogized. [J1749]

"Human-Body-Model Electrostatic-Discharge and Electrical-Overstress Studies of Buried-Heterostructure Semiconductor Lasers"

Optoelectronic components such as laser diodes, light-emitting diodes, and photodiodes are susceptible to electrostatic discharge (ESD) and electrical overstress (EOS). Human-body model (HBM) is the most widely

adopted method for the characterization of the ESD performance. In this paper, we report a comprehensive study of the ESD and EOS characteristics of buried-heterostructure (BH) semiconductor lasers using the HBM. Threshold current, optical power, optical spectrum, and reverse-bias current are characterized during the ESD study. We show that the ESD-failure thresholds depend upon the polarity. The chip can sustain the highest ESD stress under forward bias and the lowest one under forward/reverse bias. We also show that the BH lasers exhibit two types of ESD-degradation behavior. The soft degradation is characterized by a gradual increase in the threshold current, whereas the hard degradation is identified by a sudden jump in the threshold current during the ESD voltage ramp. The ESD-degradation behavior seems to be influenced by the cavity length. The failure-analysis results show that about 27% of the ESD failure is related to facet damage. The damage regions occur at the upper laser mesa structure and form preferentially on the bond-pad side. The preferential formation of the facet damage is suggestive of current-crowding effect. We have also found that the ESD-degradation behavior is a function of the facet damage. The soft-degradation failure shows a stronger correlation with the facet damage than the hard-degradation one. Finally, we demonstrate that the ESD performance of the laser can be improved by adding a protection diode. [J1750]

"Quantum Dots in Imaging [JIn the Spotlight]"

Biotechnology reported the successful development of a self-illuminating type of quantum dot that can reveal its presence without the need for an external light source. In this article, we describe the major techniques for producing quantum dots and applications of the two classes of quantum dots (colloidal and epitaxial) in imaging. [J1751]

"A New Pixel Circuit Compensating for Brightness Variation in Large Size and High Resolution AMOLED Displays"

A new pixel design and driving method for active-matrix organic light-emitting diode (AMOLED) display using low-temperature polycrystalline silicon thin-film transistor (LTPS-TFT) is proposed. The new circuit consists of five TFTs and one capacitor to eliminate the variation in the threshold voltage of the TFTs, and the drop in the supply voltage in a single frame operation. The proposed pixel circuit has been verified to realize uniform output current by the simulation work using HSPICE software. The simulated error rate of the output current is also discussed in this paper. The novel pixel design has great potential for use in large size and high resolution AMOLED displays. [J1752]

"Highly Reliable High-Brightness GaN-Based Flip Chip LEDs"

The properties of indium-tin-oxide (ITO)/Ni films as transparent ohmic contacts of nitride-based flip chip (FC) light emitting diodes (LEDs) were studied. It was found that 300degC rapid thermal annealed (RTA) ITO(15 nm)/Ni(1 nm) could provide good electrical and optical properties for FC LED applications. It was also found that 20-mA operation voltage and output power of the 465-nm FC LEDs with ITO/Ni/Ag reflective mirror were 3.16 V and 21 mW, respectively. Furthermore, it was found that output intensity of the proposed LED only decayed by 5% after 1200 h under 30-mA current injection at room temperature. [J1753]

"Full-Vectorial Three-Dimensional Finite Element Optical Simulation of Vertical-Cavity Surface-Emitting Lasers"

The electromagnetic problem of modeling vertical-cavity surface-emitting lasers with their full 3D structure is analyzed. The vectorial Helmholtz equation is discretized on prism elements, and the resulting complex symmetric generalized eigen- problem is solved by an efficient numerical technique. The full-vectorial treatment enables one to determine the polarization characteristics of these lasers. The model is compared to 2D calculations and is demonstrated for advanced laser diodes incorporating surface reliefs and photonic crystal patterns. [J1754]

"Numerical Analysis of Multilayer Organic Light-Emitting Diodes"

We make a comparative analysis of two different multilayer organic light-emitting diodes (OLEDs), one of which has an emitting layer (EML), and the other has a carrier transport controlling layer (CTCL) embedded between a hole transport layer (HTL) and an electron transport layer (ETL). The key differences between them lie in the carrier mobilities (relatively low for EML but high for CTCL) and energy levels of the middle layer. An in-depth numerical analysis has been done to provide guidelines for the design of trilayer OLED structures, especially in the context of mobility and energy level offsets. Furthermore, we focus on the transient response and carrier charge and discharge dynamics of those devices. Other than the HTL/CTCL/ETL structure, the transient current balance of the HTL/EML/ETL structure is shown to be much affected by the energy level offsets at the

organic/organic interfaces due to the slow carrier dynamics in the EML. It is also demonstrated that the electroluminescence (EL) delay upon turn-on is mainly determined by the electron transport passing through the ETL and further EML, while the fast EL decay upon turn-off is by the rapid discharge of the abrupt accumulation of carriers at the organic/organic interfaces. [J1755]

"News Briefs"

A leading semiconductor design software-tool vendor has developed an approach that would increase chip performance by running wiring diagonally as well as horizontally and vertically, as is the case now-between transistors, on-chip memory, and other processor elements. This paper discusses the advantages of Candence's X Architecture approach that uses wiring which runs diagonally along with the connections that run horizontally or vertically in some layers. [J1756]

"Location-Aware IEEE 802.11 for Spatial Reuse Enhancement"

In this paper, we propose an enhancement to the IEEE 802.11 distributed coordination function (DCF). The enhancement improves the level of channel spatial reuse; thus, it improves overall network data throughput in dense deployments. Our modification, named the location-enhanced DCF (LED), incorporates location information in DCF frame exchange sequences so that stations sharing the communication channel are able to make better interference predictions and blocking assessments. Hence, more concurrent transmissions can be conducted in densely deployed wireless LANs. The potential performance enhancement of LED is studied both analytically and via ns-2 simulations. The results show that the LED method achieves significant throughput improvements over the original DCF. [J1757]

"GaN-Based Power LEDs With CMOS ESD Protection Circuits"

A power light-emitting diode (LED) module has been successfully designed and demonstrated by combining GaN-based power LEDs with CMOS electrostatic discharge (ESD) protection circuits through a flip-chip process. It was found that we could enhance the power LED output intensity by 20% by using the flip-chip technology. Lifetimes of flip-chip power LEDs were also found to be better. It was also found that the use of CMOS ESD protection circuits did not degrade the output intensity and lifetime of flip-chip power LEDs. Furthermore, it was found that we could not only significantly enhance the reverse ESD characteristics but could also enhance the positive ESD characteristics of nitride-based LEDs by using the CMOS ESD protection circuits. [J1758]

"Correction to "Enhancement of Flip-Chip Light-Emitting Diodes With Omni-Directional Reflector and Textured Micropillar Arrays""

First Page of the Article [J1759]

"A Simple and Effective Approach to Improve the Output Linearity of Switched-Current AMOLED Pixel Circuitry"

Switched-current (S-I)-type pixel circuits are widely studied for high-performance active-matrix organic light-emitting-diode displays but suffer significant sampling and hold (S/H) nonidealities. In this letter, a simple and effective capacitive compensation method is proposed to suppress the S/H nonidealities and, thus, to greatly improve the current-reproducing accuracy and the output linearity of the circuits. The analysis procedure clearly demonstrates the operation mechanism of the method, and the simulation results of simulation program with integrated circuit emphasis prove its excellent applicability for S-I pixel circuits. [J1760]

"GaN-Based High-Q Vertical-Cavity Light-Emitting Diodes"

We report a fabrication and demonstration of a GaN-based high-Q vertical-cavity light-emitting diode (VCLED). The GaN VCLED is composed of a 25-pair high-reflectivity (98%) GaN/AlN distributed Bragg reflector (DBR), an eight-pair SiO₂/Ta₂O₅ dielectric DBR (99%), and a three-lambda optical thickness InGaN/GaN active region. It shows a very narrow linewidth of 0.52 nm, corresponding to a cavity Q-value of 895 at a driving current of 10 mA and a dominant emission peak wavelength at 465.3 nm. In addition, this VCLED emission linewidth continues to decrease with an increasing injection current, suggesting a possible realization of GaN-based vertical-cavity surface emitting lasers. [J1761]

"Matrix-Addressable Micropixelated InGaN Light-Emitting Diodes With Uniform Emission and Increased Light Output"

Micropixelated InGaN light-emitting diodes (micro-LEDs) have a wide number of potential applications in areas

including microdisplays, fluorescence-based assays and microscopy, and cell micromanipulation. Here, we present fabrication and performance details of matrix-addressable micro-LED devices which show significant improvements over their earlier counterparts. Devices with 64 x 64 micropixel elements, each of them having a 16- μm -diameter emission aperture on a 50- μm pitch, have been fabricated at blue (470 nm), green (510 nm), and UV (370 nm) wavelengths, respectively. Importantly, we have adopted a scheme of running n-metal tracks adjacent to each n-GaN mesa, so that resistance variation between the devices is reduced to below 8%, in contrast to the earlier fivefold resistance variation encountered. We have also made improvements to the spreading-layer formation scheme, resulting in significant increases in output power per element, improved current handling, and reduced turn-on voltages. These devices have been combined with a computer-driven programmable driver interface operating in constant-current mode, and representative microdisplay outputs are presented. [J1762]

"Enhanced Light Output of GaN-Based Light-Emitting Diodes by Using Omnidirectional Sidewall Reflectors"

We report on the enhancement of light output in GaN-based light-emitting diodes (LEDs) by using omnidirectional sidewall reflectors. Optical ray-tracing simulation results show that the light extraction efficiency of LEDs can vary in the range of 15.0%-24.4%, depending on the mesa depth, reflectivity, and profile angle of mesa sidewalls. Based on these findings, LEDs are fabricated with SiO₂-Al omnidirectional sidewall reflectors (at a mesa depth of 1.6 μm and a sidewall profile-angle of 42deg). The LEDs show an enhancement of the light output by 18%, as compared with reference LEDs. [J1763]

"Absolute Distance Measurement With Improved Accuracy Using Laser Diode Self-Mixing Interferometry in a Closed Loop"

We present a new method for the measurement of the absolute distance of a remote target based on the laser diode self-mixing interferometry technique, which is assisted by an electronic feedback loop that is capable of improving the measurement accuracy. The feedback loop supplies a periodic change of the emitted wavelength that exactly corresponds to a single interferometric fringe. This allows the measurement of the target distance with higher accuracy, which, in principle, is limited only by the detection shot noise and not by the fringe quantization error that is typical for the conventional fringe-counting approaches. We developed a prototype that is capable of measuring the target distance with 0.3-mm accuracy in the 0.2- to 3-m range. [J1764]

"Thermal analysis of an 80 W light-emitting diode street lamp"

Light-emitting diode (LED) street lamps rely heavily on successful thermal management, which strongly affects the optical extraction and the reliability/durability of the LED lamp. A thermal analysis of an 80 W LED street lamp was done. Sixteen thermocouples were used to measure the temperatures at 16 different positions of the street lamp. The results demonstrated that the temperature of the frame and the heat sink of the 80 W LED street lamp remained stable at about 42degC after several hours of lighting at a room temperature of 11degC, and the bulk material resistance of the heat sink could be neglected. Numerical simulation was also used to analyse the temperature distribution of the lamp. The reliability of the numerical model was proven by a comparison of simulation results with the experimental data. Through simulations and the corresponding analyses it was found that the tested 80 W LED street lamp would have poor reliability at an environment temperature of 45degC. [J1765]

"DC Current-Induced Rollover of Illumination Efficiency of GaN-Based Power LEDs"

Pulse drive currents were utilized to investigate dc current-induced rollover of illumination efficiency of GaN-based power light-emitting diodes (LEDs). By using the pulse drive currents, we can separate the effects that junction temperature and current injection have on dc current-induced rollover of illumination efficiency of GaN-based power LEDs. Comparing the measurement results obtained from pulse and dc drive currents, we verified that junction temperature and current injection were the major causes of dc current-induced rollover of illumination efficiency of power LEDs. [J1766]

"Investigation of a Dynamic Corona to Normal Glow Transition in a Neon Gas Diode"

The development of the spatial distribution of the emitted lights from a gas diode during the positive corona to normal glow discharge transition is investigated. The diode consists of a rod anode and a cylinder cathode and is filled with neon at a pressure of 1.33 mbar. Investigations are performed both in the dynamic and stationary regimes. In the dynamic regime, the slowly increasing voltage is applied to the diode, and the time development of the emitted light from the different positions in the diode is measured. In the stationary regime, the slowly

increasing applied voltage is restituted with the stepping voltage, which allowed a series of stationary regimes with different values of current to be established (from 5 nA to 10 μ A). The intensity of the emitted light from the different positions in the diode along the diode axes is measured by a scanning technique, starting from the anode up to the space behind the cathode with a 0.1-mm precision. These distributions are compared with the corresponding photographic records of the emitted lights from the diode to confirm the spatial distributions of the emitted lights. The results of these investigations show that the light emission for the smallest detected current (from 5 to 100 nA) is ordinate near the anode surface and that this kind of discharge should be defined as the positive corona. With the increase in the current, the conduction channel to the cathode is made because of the discharge transfer from the corona to the normal glow for current values of about 1 μ A. The real-time measurement shows that, in the present condition, corona appears and vanishes in about 2 ms and that the transition to the stationary normal glow is about 10 ms. The increase in the emitted light that was detected corresponds to the second and third stages of the normal glow discharge formation in the gas diode when the initial breakdown channel appears, grows, and changes up to the final stationary discharge regime. [J1767]

"2007 Index Journal of Display Technology Vol. 3"

{no data available} [J1768]

"Thermally Stable Mirror Structures for Vertical-Conducting GaN/Mirror/Si Light-Emitting Diodes"

Vertical-conducting GaN/mirror/Si light-emitting diodes (LEDs) with thermally stable mirrors have been fabricated using a combination of wafer-bonding and laser liftoff techniques. The thermal stabilities of NiO-Ag, NiO-Ag-Ni, and NiO-Au-Ag mirrors and their effects on the performance of mirror-substrate LEDs were studied. It is found that the NiO-Ag-Ni mirror presents the best performance, where the specific contact resistance and the reflectivity can achieve $5.1 \times 10^{-3} \Omega \cdot \text{cm}^2$ and 92% at 470 nm after oxidation annealing at 500°C for 10 min. The top Ni layer could protect the Ag mirror from clustering during the thermal treatment process. The output powers of the GaN-sapphire and GaN/mirror/Si LEDs with NiO-Au-Ag and NiO-Ag-Ni mirrors show 4.5, 4.3, and 13 mW, respectively. [J1769]

"Nitride-Based Near-Ultraviolet Mesh MQW Light-Emitting Diodes"

We have demonstrated nitride-based near-ultraviolet mesh multiquantum-well (MQW) light-emitting diodes (LEDs) by etching through the MQW active region. With 20-mA injection current, it was found that forward voltages were 3.29, 3.31, and 3.38 V while output powers were 7.5, 9.0, and 11.3 mW for the planar indium-tin-oxide (ITO) LED, mesh ITO LED, and mesh MQW LED, respectively. The larger LED output power is attributed to the increased light extraction efficiency. [J1770]

"Electrical Compensation of OLED Luminance Degradation"

This letter presents a stable compensation scheme for active-matrix organic light-emitting-diode (AMOLED) displays based on the observed strong interdependence between the luminance degradation of organic light-emitting diodes (OLEDs) and its current drop under bias stress. This feedback-based compensation provides 30% improvement in luminance stability under 1600 h of accelerative stress. To employ this scheme in AMOLED displays, a new pixel circuit is presented that provides on-pixel electrical access to the OLED current without compromising the aperture ratio. [J1771]

"CDP Servo System Control using Fuzzy Logic Control"

Several servo mechanisms, such as focusing, spindling, tracking and sledding, are continuously balanced to make compact disc player (CDP) to play audio or video contents. However, due to the inconsistent uneven surface of the disc, the speed control of a spindle motor along the track radius, and unexpected random shock; the servo mechanism is very complicatedly driven in non-linear method. This paper will discuss on how to approach this method, how to develop and how to evaluate each algorithm based on the model of each servo mechanism using Fuzzy Logic Control1. [J1772]

"Toward a scalable modular robotic system"

In this article, we propose a simple docking method using an onboard camera module. It has two key ideas: one is image processing using a camera module and LEDs equipped on the modules, and the other is a special modular configuration designed for docking, which absorbs positional errors. We also designed a self-reconfiguration sequence to integrate a docked robot into a periodic structure. The effectiveness of the proposed method is examined by docking/integration experiments using 18 modules. [J1773]

"MEMS-based packaging of a UV-LED array"

A packaging solution that accurately positions a microlens array over a UV-LED array for the purpose of either collimating or focusing the light emitted by the LEDs is presented. The assembled device can be used for mask-free lithography or for postfluorescence lifetime imaging of biological samples. The microdevice proposed permits the simultaneous dynamic monitoring of the microlens array in the vertical direction through electrostatic actuation and in the horizontal direction through magnetic actuation. Displacements of more than 70 μm can be achieved for the vertical actuation with less than 1% deviation over 17 h. The device, manufactured through a modified UV-LIGA process, can either be postprocessed on top of the UV-LED array or be temporarily connected to the optoelectronic component depending on whether continuous monitoring of the microlens array is required. [J1774]

"LED Technologies for Optocouplers: Fundamental Issues and Hardness Assurance"

Radiation damage is examined for several different LED technologies used in optocouplers, including those with wavelengths near 700 nm that are used in radiation-tolerant devices, and have not been widely studied. Forward diode characteristics and reverse recovery time measurements are examined as potential parameters for hardness assurance. [J1775]

"A Word in Your Ear [JResources: Tools & Toys]"

{no data available} [J1776]

"Multichannel Reflective PPG Earpiece Sensor With Passive Motion Cancellation"

This paper addresses the design considerations of a novel earpiece photoplethmograph (PPG) sensor and its in-situevaluation results. The device is encapsulated with multiple LEDs and photodiodes based on a reflective PPG design. A compact and low power circuitry was developed for signal control and conditioning. PPG signals with an averaged ac/dc ratio of 0.001-0.01 and 10% relative strength (compared to finger-based approach) were recorded from the superior and posterior auricular skins. The integrity of PPG signal and accuracy of heart rate detection were evaluated and the results showed that with adequate optical shielding and the proposed passive motion cancellation, the device was able to reliably detect heart rate both during rest and moderate exercise. The proposed sensor design is low power, easy to wear compared to conventional earlobe PPG devices. [J1777]

"Visible InGaN/GaN Quantum-Dot Materials and Devices"

General properties of III-V nitride-based quantum dots (QDs) are presented, with a special emphasis on InGaN/GaN QDs for visible optoelectronic devices. Stranski-Krastanov GaN/AlN dots are first discussed as a prototypical system. It is shown that the optical transition energies are governed by a giant quantum-confined Stark effect, which is the consequence of the presence of a large built-in internal electric field of several MV/cm. Then we move to InGaN/GaN QDs, reviewing the different fabrication approaches and their main optical properties. In particular, we focus on InGaN dots that are formed spontaneously by In composition fluctuations in InGaN quantum wells. Finally, some advantages and limitations of nitride laser diodes with active regions based on InGaN QDs are discussed, pointing out the requirements on dot uniformity and density in order to be able to exploit the expected quantum confinement effects in future devices. [J1778]

"Ge/Si Self-Assembled Quantum Dots and Their Optoelectronic Device Applications"

In recent years, quantum dots have been successfully grown by self-assembling processes. For optoelectronic device applications, the quantum-dot structures have advantages such as reduced phonon scattering, longer carrier lifetime, and lower detector noise due to low-dimensional confinement effect. Comparing to traditional optoelectronic III-V and other materials, self-assembled Ge quantum dots grown on Si substrates have a potential to be monolithically integrated with advanced Si-based technology. In this paper, we describe the growth of self-assembled, guided Ge quantum dots, and Ge quantum-dot superlattices on Si. For dot growth, issues such as growth conditions and their effects on the dot morphology are reviewed. Then vertical correlation and dot morphology evolution are addressed in relation to the critical thickness of Ge quantum-dot superlattices. In addition, we also discuss the quantum-dot p-i-p photodetectors (QDIPs) and n-i-n photodetectors for mid-infrared applications, and the quantum-dot p-i-n photodetectors for 1.3-1.55 μm for communications applications. The wavelength of SiGe p-i-p QDIP can be tuned by the size as grown by various patterning methods. Photoresponse is demonstrated for an n-i-n structure in both the mid-infrared and far-infrared wavelength ranges. The p-i-n diodes exhibit low dark current and high quantum efficiency. The characteristics of fabricated light-emitting diode (LED) devices are also discussed, and room-temperature electroluminescence is observed for Ge quantum-dot LED. The results indicate that Ge dot materials are potentially applicable for mid-

infrared (8-12 μm) detectors as well as fiber-optic (1.3-1.55 μm) communications. [J1779]

"Mixed Color Sequential Technique for Reducing Color Breakup and Motion Blur Effects"

This paper proposes a mixed color sequential (MCS) algorithm with high contrast enhancement technique in RGB light-emitting diode (LED) backlight display. Owing to synchronous control of liquid crystal display (LCD) and LED panels, high quality image with suppressed color breakup (CBU) and motion blur effects is achieved by our novel color sequential technique. Importantly, MCS algorithm is useful for color filter-less optical compensated bend (OCB) panel display for alleviating CBU and motion blur effects. Furthermore, high contrast image is also presented on LCD panel because of mixed red-green-blue (RGB) and cyan-magenta-yellow (CMY) backlights with optimum power consumption. In other words, MCS algorithm with high contrast enhancement technique can have the better performance compared with other field sequential color techniques. Experimental results demonstrate by an actual RGB backlight module for 32-in 1366*768 LCD panel the improvement of CBU and motion blur effects. [J1780]

"Improvement of Light Extraction From Patterned Polymer Encapsulated GaN-Based Flip-Chip Light-Emitting Diodes by Imprinting"

To improve surface light extraction of GaN-based flip-chip light-emitting diodes (FC-LEDs), we employed an imprint approach of thermosetting polymer for patterning microscale surface grating on the polymer encapsulant. One-dimensional (1-D) and two-dimensional (2-D) taper-like polymer gratings with a period of 6 μm were successfully realized on encapsulant above the sapphire backplane of GaN LED. By adopting the 1-D and 2-D taper-like grating encapsulant, the improvement of light extraction from the 1 mm times 1 mm FC-blue LED with a reflective Ag film on the p-side was about 18.5% and 31.9% compared to the LED encapsulated by flat polymer, respectively. To evaluate the concept of a diffraction grating in enhancement of light extraction, we performed a simulation of diffraction based on 1-D rigorous coupled wave analysis with the supporting experiments. [J1781]

"High-performance light emitting diode backlight driving system for large-screen liquid crystal display"

A high-performance light emitting diode backlight driving system is proposed for large-screen liquid crystal display. The proposed system consists of a boost converter for power factor correction (PFC) and an active-clamp converter for dc-dc power conversion. With coupled inductors and simple passive components, the proposed PFC circuit minimises the switching losses by reducing the reverse-recovery current. The active-clamp converter operates under zero-voltage switching for the power switches and its output rectifier is composed of a current doubler and a synchronous rectifier for reducing conduction loss. The proposed backlight driving system is analysed and its design consideration is discussed in detail. Experimental results for a 300 W (3.3 V/90 A) prototype at a constant switching frequency of 100 kHz are presented to verify the analysis and the performance of the proposed system. [J1782]

"Systematic Study of the Effects of Modulation p-Doping on 1.3- μm Quantum-Dot Lasers"

The effects of modulation p-doping on 1.3- μm InGaAs-InAs quantum-dot (QD) lasers are systematically investigated using a series of wafers with doping levels from 0 to 18 acceptors per QD. Various characterization techniques for both laser diodes and surface-emitting light-emitting diode structures are employed. We report: 1) how the level of modulation p-doping alters the length dependant laser characteristics (in turn providing insight on various key parameters); 2) the effect of modulation p-doping on the temperature dependence of a number of factors and its role in obtaining an infinite T_0 ; 3) how increasing concentrations of modulation p-doping affects the saturated gain, differential gain, and gain profile of the lasers; and finally, 4) the effect modulation p-doping has on the small signal modulation properties of 1.3- μm QD lasers. In each of these areas, the role of modulation p-doping is established and critically discussed. [J1783]

"Capacitance-Voltage and Current-Voltage Measurements of Nitride Light-Emitting Diodes"

Capacitance-voltage (C-V) and current-voltage (I-V) characteristics of nitride light-emitting diodes were measured. The apparent carrier distributions obtained from the C-V curves yielded much information about the samples, including information about the presence of acceptor-like defects in the active layer and the problem of electron overflow. The inconsistency between the experimental and simulated I-V curves also supported the presence of the defects. After compensating the acceptor-like defects by Si dopants and adjusting the overlap between the depletion region and the light-emitting structure, device performance was improved. [J1784]

"A Novel Blocking Technology for Improving the Short-Channel Effects in Polycrystalline Silicon TFT Devices"

An original blocking technology is proposed for improving the short-channel characteristics of polycrystalline silicon thin-film transistors (poly-Si TFTs). In particular, two types of modified devices called poly-Si TFT with block oxide and poly-Si on partial insulator (POPI)-TFT are designed for the first time in this field to enhance device performance. The proposed TFT structures can significantly reduce short-channel effects when compared with a thick source/drain (S/D) poly-Si TFT (i.e., the fully depleted TFT). In addition, an ultrathin (UT) S/D structure (UT-TFT) is designed to verify that the block oxide TFT devices do achieve improved performance without needing the thin active layers and ultrashallow junction depth. Also, the POPI-TFT is found to reduce the thermal instability through its natural body-tied scheme. [J1785]

"Reversible Degradation of Ohmic Contacts on p-GaN for Application in High-Brightness LEDs"

This paper analyzes the high-temperature long-term stability of ohmic contacts on p-type gallium nitride (p-GaN). The contributions of the ohmic contacts and semiconductor material degradation are separated by adopting the transmission line method (TLM). Before stress, the current-voltage (I-V) curves measured at the pads of the TLMs showed a linear shape, indicating a good ohmic behavior of the contacts. Thermal treatment at 250degC was found to induce the worsening of the electrical characteristics of the contacts: identified degradation modes consist of a shift of the I-V curves toward higher voltages and strong nonlinearity of the characteristics around zero. This paper shows that the high-temperature instabilities of ohmic contacts on p-GaN are related to the interaction between the device surface and the plasma-enhanced chemical vapor deposition SiN passivation layer. Hydrogen contained in the passivation layer is supposed to play an important role in the degradation process: the interaction with the acceptor dopant at the metal/semiconductor interface induces the decrease of the effective acceptor concentration. As a consequence, both the ohmic contact characteristics and the semiconductor sheet resistance are worsened. [J1786]

"Enhanced Light Extraction From Triangular GaN-Based Light-Emitting Diodes"

This study investigated the characteristics of a triangular light-emitting diode (LED) and compared it to a standard quadrangular LED. The total radiant flux from the packaged triangular LED increased by 48% and 24% at input currents of 20 and 100 mA, respectively, compared to that of a quadrangular LED which was grown on patterned sapphire substrate. In light far-field beam distribution, the light extraction in the horizontal direction of the LED was much higher than that of the quadrangular LED due to the enhancement of light emission from the side walls of the triangular LED. [J1787]

"Gradient Doping of Mg in p-Type GaN for High Efficiency InGaN-GaN Ultraviolet Light-Emitting Diode"

The performance of a InGaN-GaN multiple quantum-well (MQW) ultraviolet (UV) light-emitting diode (LED) with an emission of 385 nm was enhanced by a gradient doping of Mg in the p-GaN layer. The optical output power was enhanced by 21% at an input current of 20 mA compared to that of a UV LED with a uniformly doped p-GaN layer. The improved performance of the UV LED could be attributed to the decrease in diffusion of Mg into MQW and the suppression of electron transport from the conduction band of the MQW to the acceptor level of the deep donor acceptor pair bands in the p-GaN layer by a gradient doping of Mg in p-GaN layer. [J1788]

"Current and Temperature Dependent Characteristics of Deep-Ultraviolet Light-Emitting Diodes"

The electrical and optical characteristics of the 340- and 280-nm AlGaIn-based deep-ultraviolet multiple-quantum-well light-emitting diodes (LEDs) at low temperatures (5-300 K) and various injection currents were studied. The negligible blue shift of the peak energy with increasing current density and monotonic blue shift with decreasing temperature suggest the absence of localized state emission. In the 340-nm LED, a band-tail state emission centered at 353 nm was dominated at low currents around 150 K, whereas the 280-nm LED exhibited minimal defect emission over the entire temperature range. The internal quantum efficiencies of both LEDs at room temperature were found to be less than 5%, indicating that there is significant room for improvement in structure design and material quality. [J1789]

"High-Temperature Stability of 650-nm Resonant-Cavity Light-Emitting Diodes Fabricated Using Wafer-Bonding Technique on Silicon Substrates"

AlGaInP-based visible 650-nm GaInP-AlGaInP resonant-cavity light-emitting diodes (RCLEDs) with high-temperature stability were fabricated by wafer-bonding techniques on Si substrates. In this study, the metal-bonding RCLEDs (MBRCLEDs) devices were designed with 84-μm apertures for light output. The MBRCLEDs

with a maximum wall-plug efficiency of 13.7% were demonstrated at an injection current of 2.5 mA. In addition, the improved heat sinking of MBRLEDs led to lower junction temperature, and resulted in a very low power decay of 0.31 dB from room temperature to 100degC at an injection current of 20 mA. [J1790]

"Implementation of Side Effects in Thermal Characterization of RGB Full-Color LEDs"

This letter presents a useful thermal-characterization method for RGB full-color light-emitting diodes (LEDs). The superposition method was employed to calculate thermal resistances of a high-power RGB full-color LED package to implement the side effect. Independent driving of a single chip in the RGB package clearly exhibited a side effect on the other two chips. It was shown that driving a red chip at 350 mA, current induced 4.8degC temperature rise for the green and blue chips, which is about 30% of the temperature rise in the red chip itself. A thermal-resistance-coupling matrix was structured and used for the calculation of the junction temperatures of the chips. It was demonstrated that the superposition method can be employed for an accurate prediction of the junction temperature rises for the RGB full-color LED package. [J1791]

"Transport Mechanism of SiGe Dot MOS Tunneling Diodes"

The blockage of hole transport due to excess holes in SiGe dots was observed in the MOS tunneling diodes for the first time. The five layers of self-assembled SiGe dots are separated by 74-nm Si spacers and capped with a 130-nm Si. The hole tunneling current from Pt gate electrode to p-type Si dominates the inversion current at positive gate bias and is seven orders of magnitude higher than the Al gate/oxide/p-Si device. The large work function of Pt is responsible for the hole transport current from Pt to p-Si. The incorporation of SiGe dots confines the excess holes in the valence band and forms a repulsive barrier to reduce the hole transport current from Pt to SiGe dots by 2-3 orders of magnitude in comparison with the Pt/oxide/p-Si device. This repulsive barrier also reduces the hole tunneling current from SiGe dots to Pt at negative gate bias. [J1792]

"Factors Affecting Hamamatsu H8500 Flat Panel PMT Calibration for Gamma Ray Imaging"

The Hamamatsu H8500 Flat Panel PMT is the latest technological advancement in gamma ray imaging. Its compact size makes it attractive for medical imaging applications. To study and compare image performance a Flat Panel PMT, representing the present production, was coupled to CsI(Tl) and NaI(Tl) scintillation arrays with 3 mm and 1.8 mm pixel size respectively and connected to a multi-anode electronic readout. Furthermore, a pulsed blue LED coupled to an optical fiber was utilized to scan the tube with different light distributions. This study investigated how PMT anode gain uniformity response, scintillation light distribution and intensity influence the spatial resolution, the position linearity and the image noise. Each crystal in the scintillation array produces a different charge distribution, which depends on the match between the anode size and the scintillation array lattice. The NaI(Tl) array demonstrated to fit both PMT characteristics and dynamic range of electronic read out, due to the charge distribution adequate to the anode size. For CsI(Tl) crystal, the pulse height calibration resulted more critical, due to the narrow light distribution. In conclusion, the use of Flat Panel tube with selected anode gain uniformity could represent the cheapest and easiest solution to obtain the best image quality, in particular for scintillator array with smaller pixel size. [J1793]

"A Dynamic 3-D Surface Profilometer With Nanoscale Measurement Resolution and MHz Bandwidth for MEMS Characterization"

Commercialization of microelectromechanical systems (MEMS) has made accurate dynamic characterization a major challenge in design and fabrication. In view of this need, a dynamic 3-D surface profilometer involving white light interferometric scanning principle with a stroboscopic LED light source was developed. The developed instrument was applied to a microcantilever beam used in atomic force microscopy (AFM) to analyze its full-field resonant vibratory behavior. The first five resonant vibration modes were fully characterized with vertical measurement accuracy of 3-5 nm and vertical measurement in the range of tens of micrometers. The experimental results were consistent with the outcomes of the theoretical simulation by ANSYS. Using stroboscopic illumination and white light vertical scanning techniques, the developed static and dynamic 3D nanoscale surface profilometry of MEMS devices can achieve measurement range of tens of micrometers and dynamic bandwidth of up to 1-MHz resonance frequency. [J1794]

"Spectrally Beam-Combined Fiber Lasers for High-Average-Power Applications"

Spectrally beam-combined (SBC) laser systems, wherein multiple laser outputs are spectrally multiplexed into a single high-quality beam, are rapidly advancing the power scaling frontier for high-average-power beam-combined fiber lasers with near-perfect beam quality. We describe two- and three-channel SBC fiber lasers featuring 93% power-combining efficiency, near-diffraction-limited beam quality, average output powers in excess of 500 W, and excellent prospects for additional power scaling. To our knowledge, this level of optical

performance represents the highest combination of beam quality and average power obtained so far for a beam-combined fiber laser system. [J1795]

"Let there be (a new kind of) light [JNEWS]"

Recent events on the business front and advances in the lab could soon transform the way about lighting our homes and buildings. Significant strides in developing organic light-emitting diodes (OLEDs) may allow architects in the next few years to integrate this power-efficient and tractable technology into basic building materials, enabling entire structures to be turned into luminous edifices. Konica Minolta Holdings, a Tokyo-based manufacturer of imaging products, and General Electric Co., one of the world's largest lightbulb makers, formed a strategic alliance to accelerate development of OLED lighting and vowed to ship products in the next three years. A major challenge all OLED manufacturers face is how to make their products cost-competitive with the ultracheap incandescent and fluorescent lighting products on the market. [J1796]

"Study of Phosphor Thermal-Isolated Packaging Technologies for High-Power White Light-Emitting Diodes"

A novel packaging configuration for high-power phosphor-converting white light-emitting diodes (LEDs) application is reported. In this packaging configuration, a thermal-isolated encapsulant layer was used to separate the phosphor coating layer from the LED chip and the submount. Experimental and finite-element method simulation results proved that this thermal management can prevent the heat of LED chip from transferring to the phosphor coating layer. The surface temperature of the phosphor coating layer is a 16.8degC lower than that of the conventional packaging at 500-mA driver current for 1-mm power GaN-based LED chip. Experimental results also show that this packaging configuration can improve the light-emitting power performance and color characteristics stability of the white LED, especially under high current operating condition. [J1797]

"Low-Light Auto-Focus Enhancement for Digital and Cell-Phone Camera Image Pipelines"

Images captured by a digital or cell-phone camera in low-light environments usually suffer from a lack of sharpness due to the failure of the camera's passive auto-focus (AF) system to locate the peak in-focus position of a sharpness function that is extracted from the image. In low-light, the sharpness function becomes flat, making it quite difficult to locate the peak. In this paper, a systematic approach is introduced to address the problem of low-light AF by performing computationally simple image enhancement preprocessing steps as part of the image pipeline. These enhancement steps elevate the sharpness function peak, leading to auto-focusing in low-light conditions. A sharpness junction quality measure along with experimental guidelines are presented for determining the most prominent enhancement steps for low-light AF. The implementation results on an actual digital camera platform are also shown to demonstrate the effectiveness of our solution. [J1798]

"Carrier Transport Mechanism in a Nanoparticle-Incorporated Organic Bistable Memory Device"

In this letter, the conduction mechanism in nanoparticle-contained polymer memory was investigated experimentally and theoretically. The current-voltage characteristics showed that the device switches from an initial low-conductivity state to a high-conductivity state upon application of an external electric field at room temperature. The current transition exhibited a very narrow voltage range that causes an abrupt increase of current. A trap-filled space-charge-limited current model was proposed and supported by the experimental data to explain the transport mechanism in organic memory. [J1799]

"Organic-Inorganic Hybrid Optical Upconverter"

We report a hybrid organic-inorganic optical upconverter that converts input 1.5- μm infrared light to output visible light. The device was made by direct tandem integration of an inorganic InGaAs/InP photodetector with an organic light-emitting diode (OLED). Incoming 1.5- μm light optical radiation is absorbed by the semiconductor p-i-n detector. The resultant photocurrent drives the OLED to emit visible light at ~ 520 nm in wavelength. The ratio of the photocurrent-induced versus dark-current-induced visible light emission was measured to be over 100 at a device bias of 14 V at room temperature. Devices with different configurations of the hole transport layer (HTL) were fabricated and tested. It was found that the devices with an HTL of C60/CuPc/NPB exhibited a lowest turn-on voltage (~ 3.8 V). The results show that the interfacial structure at the inorganic-organic interface plays a vital role in enabling the integration of the hybrid organic-inorganic devices. [J1800]

"Free engineering of buried oxide patterns in GaAs/AlAs epitaxial structures"

The formation of a buried aluminium oxide from the surface of a GaAs/AlAs epitaxial structure is presented and

validated through the localised electroluminescence in a light emitting diode device. This oxidation method relies on photolithography, plasma treatment and wet thermal oxidation. This enables localised buried oxide areas to be formed by a vertical oxidation process applied from the surface. Because of this new technology, the shape of the oxidised areas can be freely designed, unlike when using the standard lateral oxidation technology.

[J1801]

"Polymer Light-Emitting Electrochemical Cells for High-Efficiency Low-Voltage Electroluminescent Devices"

Organic light-emitting devices exhibiting high power conversion efficiency and long operating lifetime may potentially be achieved with the polymer light-emitting electrochemical cell (LEC) configuration. An LEC device typically uses a thin layer of conjugated polymer sandwiched between two contact electrodes. The polymer layer contains an ionically conductive species that are essential in the formation of a light-emitting p-i-n junction. LEC devices are characterized with balanced electron and hole injections, high current density at relatively low bias voltages (2-4 V), and high electroluminescent power efficiency. We will describe the working mechanism of the LECs and review the recent developments in LEC materials, device fabrication and performance. Among the important developments are planar (surface-typed) LECs, bilayer LECs that emit different colors at forward and reverse biases, frozen p-i-n junction LECs that functions like diodes, and phosphorescent LECs. Extensive efforts have been made to improve the LEC performance by controlling the blend morphology, including the use of bipolar surfactant additives and new electrolytes, the synthesis of conjugated polymers with ion-transporting main chain segments or side groups and polyelectrolyte. Degradation mechanisms that limit the lifetime of the LECs will also be discussed [J1802]

"A Novel Voltage Driving Method Using 3-TFT Pixel Circuit for AMOLED"

A novel voltage driving method using three thin-film transistors (TFTs) for active-matrix organic light-emitting diodes (OLEDs) is presented and verified by automatic integrated circuit modeling SPICE simulation. The proposed novel 3-TFT pixel circuit, which successfully compensates for the threshold voltage variations, uses few TFTs with simplified control signals, and the current nonuniformity of the proposed circuit is 0.19% to 1.99% throughout the entire data range. To compensate for variations in OLED current, the proposed circuit utilizes a novel driving scheme that uses a diode connection current source with a biased voltage. [J1803]

"Improving the Luminescence of InGaN–GaN Blue LEDs Through Selective Ring-Region Activation of the Mg-Doped GaN Layer"

In this study, we used the selective ring-region activation technique to restrain the surface leakage current and to monitor the luminescence characteristics of InGaN–GaN multiple quantum-well blue light-emitting diodes (LEDs). To access the current blocking region after forming a periphery high-resistance ring-region of the Mg-doped GaN layer and to reduce the degree of carrier trapping by the surface recombination centers, we deposited a titanium film onto the Mg-doped GaN epitaxial layer to form a high-resistance current blocking region. To characterize their luminescence performance, we prepared LEDs incorporating titanium films of various widths of the highly resistive current blocking layer. The hole concentration in the Mg-doped GaN epitaxial layer decreased from $3.45 \times 10^{17} \text{ cm}^{-3}$ to $3.31 \times 10^{16} \text{ cm}^{-3}$ after capping with a 250-nm-thick layer of titanium and annealing at 700 degC under a nitrogen atmosphere for 30 min. Furthermore, the luminescence characteristics could be improved by varying the width of the highly resistive region of the current blocking area; in our best result, the relative electroluminescence intensity was 30% (20 mA) and 50% (100 mA) higher than that of the as-grown blue LEDs [J1804]

"Organic Light-Emitting Diodes Fabricated by a Solution Process and Their Stress Tolerance"

Polymeric organic light-emitting diodes (PLEDs) were fabricated by solution process, and their stress tolerance were studied by continually pressing the PLEDs fabricated on polymeric substrates. Two types of host materials, poly(nvinylcarbazole) (PVCz) and starburst small-molecule 1,3,5-tris[4-(diphenylamino)phenyl] benzene (TDAPB) were employed as host for the PLEDs doped with phosphorescent materials. Two iridium complexes are employed as dopants, fac-tris(2-phenyl- pyridine) iridium [Ir(ppy) 3] and tris(1-phenylisoquinoline) iridium (III) [Ir(piq)3] for green-emitting and red-emitting phosphorescent materials, respectively. The external quantum efficiency and power efficiency were 8.2% and 17.3 lm/W, and 6.3% and 3.0 lm/W for a device with Ir(ppy)3doped TDAPB and Ir(piq)3doped PVCz-TDAPB mixture host, respectively. Pushing tolerance tests were performed for PLEDs fabricated on polymeric substrates. The device continued to emit light after a pushing test consisting of more than 20 000 steps. In this paper, we discuss the fabrication and characteristics of PLEDs prepared using starburst TDAPB and phosphorescent materials for green and red emissive materials by a solution process. We discuss the pushing tolerance for PLEDs fabricated on a polymeric substrate [J1805]

"Optimization of the Luminescence Efficiencies in Solution-Processed Phosphorescent Dendrimers"

We demonstrate that photoluminescence (PL) quantum yield and PL lifetime of fac-tris(2-phenylpyridyl) iridium(III) [Ir(ppy)₃]-cored dendrimers in neat film and dispersed into a 4,4'-bis(N-carbazolyl)biphenyl host can be significantly improved by a simple adjustment of the solution preparation. Quenching of the PL in these materials is due to an energy transfer of the triplet excitons to less-emissive sites and can be reduced by blending the phosphorescent molecules into a suitable wide energy gap host or by increasing the number of attached dendrons. We show here that the concentration of these quenchers can also be controlled by changing the time spent by the dendrimer solution under illumination prior to spin-coating. By optimizing the film preparation procedure, the external efficiency of devices made from neat dendrimer films was increased from 2% to 10% [J1806]

"Charge Transport and Injection to Phenylamine-Based Hole Transporters for OLEDs Applications"

We studied the hole injection and transporting properties of four phenylamine-based hole-transporters useful for organic light-emitting diodes. The hole-transporting properties were examined in details by time-of-flight technique whereas their hole-injecting properties by current-voltage measurements and dark-current space-charge-limited-current technique (DI-SCLC). All materials were found to exhibit essentially trap-free hole transports. We discovered that a conducting polymeric anode, PEDOT:PSS, can act effectively as an Ohmic contact for hole injection into the PA compounds for DI-SCLC experiments [J1807]

"LEDs Could Borrow From Beetles"

This paper discusses the on how to improve LED's whiteness and effectivity in industrial applications. The concept is based on a shell of the Cyphochilus beetle. To achieve is, they have made a synthetic version of the beetle shell. One factor is that the beetle's whiteness may have the important industrial implications: the relatively large amount of empty space within the cuticle structure. It's at the interface between the cuticle filaments and the air in the spaces that light scattering takes place [J1808]

"Fabrication of Microcavity Light-Emitting Diodes Using Highly Reflective AlN-GaN and Ta₂O₅-SiO₂ Distributed Bragg Mirrors"

We report the fabrication of microcavity light-emitting diodes (MCLEDs) with high reflectivity and crack-free AlN-GaN distributed Bragg reflector (DBR). The 5λ microcavity structure consists of an n-type GaN, ten pairs InGaN-GaN multiple quantum wells and p-type GaN sandwiched between the hybrid cavity mode of an AlN-GaN and a Ta₂O₅-SiO₂DBR. The AlN-GaN DBR has 29 periods with insertion of six AlN-GaN superlattice layers showing a crack-free surface morphology and a high peak reflectivity of 99.4% with a stopband of 21 nm. The output power of MCLED is about 11 W at an injection current of 7 mA. The electroluminescence has a polarization property with a degree of polarization of about 51%. [J1809]

"CMOS integrated luminescence oxygen multi-sensor system"

A miniaturised luminescence multi-sensor system is reported, which combines addressable micro-light emitting diodes (LEDs) for optical excitation, sol-gel derived xerogel recognition elements for encapsulation of luminophores, and a CMOS integrated circuit for photodetection and signal processing. As a prototype, three surface-mount type micro-LEDs coated with oxygen (O₂) sensitive xerogel thin films are presented. Each xerogel sensor operates satisfactorily over the entire range of O₂ concentrations but has a different sensitivity and response profile to O₂. The described integrated system establishes the viability for low-cost and low-power biochemical sensor systems with improved accuracy and certainty [J1810]

"High-Performance Chemical-Bath-Deposited Zinc Oxide Thin-Film Transistors"

Solution-processed transparent zinc oxide (ZnO) transistors are demonstrated using a chemical bath deposition process for ZnO deposition. The process is glass compatible and amenable to producing fully transparent electronics. Mobility as high as 3.5 cm²/V s with on-off ratios of ~10⁵ is realized. The transparency of ZnO allows for complete coverage of the pixel by the pixel drive transistors; analysis shows that the performance achieved herein is sufficient even to drive high-brightness organic light-emitting diode (OLED) displays by exploiting the high mobility and optical transparency of these devices. This makes this technology extremely attractive for use in active-matrix OLED display applications. [J1811]

"An 848 Pixel Array Pen-Input OLED Screen Based on Organic Magnetoresistance"

We present the design principles for a pen-input organic light-emitting diode (OLED) display based on the

recently discovered organic magnetoresistance effect (OMAR). In the prototypical OLED material Alq3, OMAR is as large as 10% for small magnetic fields, $B=10$ mT at room temperature. We construct a pen-input screen consisting of an 8 times 8 pixel OMAR array made from Alq3, together with a magnetic pen that emits an ac magnetic field. We describe a multiplexed detection scheme that uses a single filter/amplifier circuit to sequentially scan the individual pixels for the presence of the magnetic pen. For this scheme to work efficiently, it requires using frequencies on the order of 100 kHz. We demonstrate that our OMAR devices can indeed follow such high frequencies under certain operating conditions [J1812]

"Top-emitting OLED pixel employing cathode-contact structure with a-Si:H thin-film transistors"

An active-matrix organic light emitting diode (OLED) display employing a hydrogenated amorphous silicon thin-film transistor prefers a cathode-contact structure to an anode-contact structure. A new normal top-emitting OLED employing cathode-contact structure is proposed. To implement normal OLED structure, the cathode layer on top is separated as sub-pixels by a negative photoresist separator. The current of the cathode-contact structure is maintained 20% higher after 20 h than that of the anode-contact structure during the accelerated life test. [J1813]

"Single-Technology-Based Statistical Calibration for High-Performance Active-Matrix Organic LED Displays"

Active-matrix organic light-emitting-diode (AMOLED) displays based on amorphous hydrogenated silicon (a-Si:H) thin-film transistors (TFTs) are the state of the art in display technology, owing to the feasibility of low-cost fabrication and accessibility to well-established TFT-LCD fabrication. While the a-Si:H TFT offers excellent matching of device properties over large areas, it suffers from a gate-bias-dependent threshold voltage shift in time, leading to grayscale inaccuracies. In order to counter this problem, many compensation circuits have been designed. The purpose of the compensation circuit is to estimate the threshold voltage shift in driver TFTs and apply a correction so as to maintain a constant brightness. However, all of the compensation circuits designed to date suffer from low spatial and temporal resolution and reliability issues or high cost due to the use of custom-made CMOS technology. In this paper, we focus on building AMOLED display systems solely based on a-Si:H TFT technology along with the use of off-the-shelf CMOS components to lower costs. Furthermore, we achieve high spatial and temporal resolution and high yield with the use of a two-TFT voltage programmed pixel circuit along with a statistical based external calibration circuit. [J1814]

"Thermo Effects on Flexible Panel Substrate"

Cyclic olefin copolymer (COC) was used as flexible polymer substrate for the next-generation flat-panel displays (FPD). Surface roughness and optical properties of different thermally treated flexible polymer substrates were observed with an atomic force microscope (AFM) and a visible spectrometer, respectively. In addition, in this study, we found that the turn-on voltages, luminance, and driving current of the flexible organic light emitting devices (OLEDs) were strongly affected by the thermal history of the flexible substrate. [J1815]

"LED-Based Projection Systems"

A novel design methodology for LED-array-based projection displays has been developed. By combining etendue limitation, system intensity, and efficiency requirements, a novel parameter space is proposed. Using this parameter space, LED lens-array and compound parabolic concentrator (CPC)-array illumination systems have been designed. A 1000-lm LED light source is built. Based on these lens-array and CPC-array illuminators, several LED-based liquid crystal on silicon (LCOS) projection systems are suggested. Among them, a one-panel LCOS projection system is proposed and tested. The method discussed here should be useful in the design of LED-array illumination systems for projectors in general. [J1816]

"Pervasive Computing Helps Fans Get Into the Game"

Pervasive computing devices give fans more control over their experience and more information about the games they love, even when they're miles away. Mobile devices have put sports into the pocket of the fan. Mobile content and messaging deals let consumers access their sports when and where they want to. Prior to the use of the wireless caddie, the application provider, set up a Wi-Fi network around each course. With the new devices, the existing network offers more ubiquitous coverage with less set-up time. Extraction relies on an image-processing technique that can pull out information and decode the barcodes. According to IBM, when this system is in place, any mobile device can be used with a blacklight-LED-enabled camera as the reader. [J1817]

"Radiation Damage in Power MOSFET Optocouplers"

Radiation damage is investigated in optocouplers with power MOSFET output stages. They differ from conventional optocouplers, incorporating an intermediate photovoltaic chip to allow the MOSFET gate voltage to be controlled by the light-emitting diode. These optocouplers are sensitive to ionization as well as displacement damage, and can fail catastrophically from degradation in either the power MOSFET or the LED. Radiation testing must take both mechanisms into account. [J1818]

"Fast Switching Liquid Crystals for Color-Sequential LCDs"

High birefringence ($0.3 < \Delta n < 0.4$) and relatively low-viscosity liquid crystal mixtures containing isothiocyanato tolane and isothiocyanato terphenyl liquid crystals are developed. A twisted-nematic (TN) 1.6- μm thin cell for color-sequential liquid crystal display with $\sim 1\text{-ms}$ response time is demonstrated. [J1819]

"LED Backlight Driving System for Large-Scale LCD Panels"

This paper presents an LED backlight driving system for large-scale liquid crystal display panels. High efficiency, high power factor, circuit simplicity, and low cost can be achieved by using a single-stage charge-pump asymmetrical half-bridge converter. To regulate the LED current and brightness for the LED backlight system, some current sharing methods are presented and compared. The requirements for the current sharing and luminance balance among paralleled LED arrays can be satisfied while current ripple is eliminated significantly. Because of the addition of bypass diodes, an alternative current path can be offered when a single LED fails. The LED array will not be extinguished. Reliability of the LED backlight system can thus be improved effectively. A laboratory prototype has been built and tested. The simulation and experimental results are shown to verify the feasibility of the proposed method. [J1820]

"Electrical and Optical Gain Lever Effects in InGaAs Double Quantum-Well Diode Lasers"

In multisection laser diodes, the amplitude or frequency modulation (AM or FM) efficiency can be improved using the gain lever effect. To study gain lever, InGaAs double quantum-well (DQW) edge-emitting lasers have been fabricated with integrated passive waveguides and dual sections providing a range of split ratios from 1:1 to 9:1. Both the electrical and the optical gain lever have been examined. An electrical gain lever with greater than 7-dB enhancement of AM efficiency was achieved within the range of appropriate dc biasing currents, but this gain dropped rapidly outside this range. We observed a 4-dB gain in the optical AM efficiency under nonideal biasing conditions. This value agreed with the measured gain for the electrical AM efficiency under similar conditions. We also examined the gain lever effect under large signal modulation for digital logic switching applications. To get a useful gain lever for optical gain quenched logic, a long control section is needed to preserve the gain lever strength and a long interaction length between the input optical signal and the lasing field of the diode must be provided. The gain lever parameter space has been fully characterized and validated against numerical simulations of a semi-3-D hybrid beam propagation method (BPM) model for the coupled electron-photon rate equation. We find that the optical gain lever can be treated using the electrical injection model, once the absorption in the sample is known. [J1821]

"Current-Scaling a-Si:H TFT Pixel-Electrode Circuit for AM-OLEDs: Electrical Properties and Stability"

We fabricated and characterized the hydrogenated amorphous-silicon thin-film transistor (a-Si:H TFT) pixel-electrode circuit with the current-scaling function that can be used for active-matrix organic light-emitting displays (AM-OLEDs). As expected from previously reported simulation results, the fabricated pixel-electrode circuit showed an enhanced current-scaling performance for a high-resolution AM-OLED based on a-Si:H TFTs in comparison to other types of current-driven pixel circuits. It also showed a better electrical and thermal stability for different OLED current levels in comparison to the conventional current-driven pixel-electrode circuit. [J1822]

"Noncontact Material Identification and Distance Measurement Using Effective Capacitance With CdS Cells"

We propose a novel noncontact sensing method for material identification and for detection of the distance between the sensor and the surface of a material by using its electrical and optical properties. In the proposed method, capacitance between the terminals of a pair of CdS cells, called the effective capacitance, is measured, and several capacitance values are obtained by changing the emission strength of the light emitting diode, thus changing the resistance value of the CdS cells. From these values, it is possible to identify the materials and to detect the distance between the CdS cells and the material. In this paper, we compare four kinds of effective capacitance measurement methods using a pair of CdS cells and describe the proposed measurement method. In addition, this paper discusses the measurement accuracy of effective capacitance values in the proposed

method and demonstrates its ability to identify six material samples-clear, white, and black acrylic, clear vinyl chloride, brown bakelite, and aluminum-and to detect the distance between the CdS cells and the material.

[J1823]

"Linear Cascade Arrays of GaN-Based Green Light-Emitting Diodes for High-Speed and High-Power Performance"

In the following study, we demonstrated linear cascade GaN-based light-emitting-diode (LED) arrays at a wavelength of approximately 520 nm. Experimental LEDs were analyzed with the goal to improve the output power and differential efficiency of a single LED. The study shows that using arrays with up to four LEDs connected in series, we can achieve four times the improvement in output power (differential quantum efficiency) under the same bias current as compared to a single LED apparatus. We have also measured the modulation-speed performance of experimental LEDs, and both devices exhibit similar 3-dB bandwidth (90 MHz) under the same bias currents. Experimental results indicate that the cascade connection offers the advantages of significantly enhanced external differential efficiency and provision of a method to use a constant-voltage power supply. The current crowding problem and resistance-capacitance-limited bandwidth degradation issues in a large active area LED can also be minimized using the connection demonstrated in our experiment. [J1824]

"New Technologies for Rural Lighting in Developing Countries: White LEDs"

Most of the third-world rural areas, especially in sub-Saharan Africa, are still without electricity. The few existing off-grid and upcoming installations are remote and characterized by limited resources that call for drastic conservation measures. For the majority of these emerging consumers, lighting is the priority load. Rural electrical lighting load models are characterized by inaccuracies due to technical omissions, highlighted in this paper, and result in energy wastage. Solutions to the third-world problems need not follow similar paths to those of the developed world. In fact, cutting-edge technologies like the cell phone have already leapfrogged rural communications where expensive infrastructure had been perennially cited as the impediment. In this paper, another futuristic technology, the white light emitting diode (LED), for general lighting, is poised to create yet another revolution in African rural electrification. [J1825]

"Consideration of the Actual Current-Spreading Length of GaN-Based Light-Emitting Diodes for High-Efficiency Design"

Based on the proposed experimental method, the current spreading length of GaN-based light-emitting diodes (LEDs) was measured and analyzed for practical device design. In this study, Thompson's and Guo's models, which are categorized according to vertical series resistance (in particular, p-type contact resistance), were used to extract device parameters. It was shown that the measured current spreading length strongly depends on the injected current density. For LEDs fabricated with low-resistance p-type contacts, this behavior could be explained in terms of the accelerated current crowding with higher current densities occurring as a result of the reduced voltage drop across the junction, which is in good agreement with Thompson's relation. However, for LEDs fabricated with high-resistance p-contacts, unlike Guo's prediction, the measured current spreading length also showed a strong dependence on the injected current density. This was attributed to thermal heating at the p-contact, resulting in the reduction of the voltage drop across the p-contact and so junction voltage, which is also in agreement with Thompson's model. Based on the measured parameters and the design rule, efficient p-type reflectors, namely, hybrid reflectors were designed. Compared with conventional ones, LEDs fabricated with the hybrid reflectors exhibited better output power at a reasonable forward voltage, indicating that the proposed method is effective in understanding the actual current spreading and hence the practical design of high-efficiency LEDs. [J1826]

"Enhancement of Flip-Chip Light-Emitting Diodes With Omni-Directional Reflector and Textured Micropillar Arrays"

The flip-chip light-emitting diodes (FC-LEDs) with a conductive omni-directional reflector and textured micropillar arrays were investigated. The micropillar arrays structure was formed on the bottom side of sapphire substrate by dry etching process to increase the light-extraction efficiency. The light output power of the FC-LED was increased by 65% for a 3.2- μm textured micropillar on the bottom side of the sapphire substrate. Our work offers promising potential for enhancing output powers of commercial light-emitting devices. [J1827]

"Low-Noise and High-Detectivity GaN-Based UV Photodiode With a Semi-Insulating Mg-Doped GaN Cap Layer"

GaN-based ultraviolet photodiodes with a semi-insulating Mg-doped GaN cap layer were fabricated and

characterized. Dark leakage current of the aforementioned photodiodes was much smaller than that of the conventional ones without the Mg-doped GaN cap layer due to a thicker and higher potential barrier and less amounts of interface states after inserting the Mg-doped GaN cap layer. The ultraviolet to visible rejection ratio is 3.44×10^3 by inserting a semi-insulating Mg-doped GaN cap layer with a -IV applied bias. In this study, we also discuss the noise characteristics. It was found that minimum noise equivalent power and maximum detectivity of our photodiode were 1.2×10^{-12} W and 9.34×10^{11} cmHz^{0.5}W⁻¹, respectively. [J1828]

"A Reconfigurable, Low Power, Temperature Compensated IC for 8-segment Gamma Correction Curve in TFT, OLED and PDP Displays"

In the market sector of consumer products based on TFT, OLED, PDP, and other displays, there is a demand for the capability of driving different displays by means of different gamma curves with the same driver circuit. Therefore, the display driver must have a built-in reconfigurable gamma correction circuitry able to correct the gamma curve of different types of displays. The presented solution proposes a reconfigurable gamma correction circuitry having high accuracy in the generated voltage levels and high flexibility in producing gamma correction curves. The configuration circuitry is digitally temperature compensated and the whole IC has low power consumption with respect to the target product sector. [J1829]

"Light Output Improvement of InGaN-Based Light-Emitting Diodes by Microchannel Structure"

We propose a microchannel structure with deep holes to enhance the extraction efficiency of InGaN-based light-emitting diodes (LEDs). Two different depth microchannel LEDs are examined experimentally. One has air holes penetrated through the active layer and the other does not. It is found that the light extraction efficiency in the LED with the penetrated air holes is significant larger than that in the LED without penetrating holes. The reason can be attributed to the microchannel waveguide behaviors. In comparison to the conventional LEDs, the light output power of our fabricated LEDs with and without penetrating holes improved by 43.5% and 5.1%, respectively. [J1830]

"The Electroluminescent Decay Mechanism of Rare-Earth Ions in OLEDs Based on a Terbium Complex"

The organic light-emitting diodes (OLEDs) based on terbium (Tb) complexes show sharp green emission spectrum with excellent color purity. However, the brightness of Tb-OLEDs is generally weak. Here, the electroluminescent (EL) decay mechanism of Tb-OLEDs is studied by arbitrarily using tris-(1-phenyl-3-methyl-4-isobutyl-5-pyrazolone)-bis(triphenyl phosphine oxide) terbium as the emitting layer. The device shows high EL efficiency at low current density but rapid reduction of device efficiency at higher current density. The transient EL is investigated for understanding the decay process of excited Tb³⁺ ions. Together with theoretical studies, exciton quenching is proposed to explain the decay of the Tb-OLEDs which is important for optimizing and engineering the material and device structures. The EL from the mixed layer of the Tb and europium (Eu) complexes is also studied. We find that the EL performance and transient decay of the excited Tb ions are modified by energy transfer from Tb to Eu in the OLEDs. [J1831]

"Demonstration of high power blue-green light emitting diode on semipolar (1122) bulk GaN substrate"

Blue-green InGaN/GaN multiple-quantum-well light emitting diodes with peak emission wavelength of 480 nm were grown on low extended defect density semipolar (1122) bulk GaN substrates by conventional metal organic chemical vapour deposition. The calculated external quantum efficiency and output power at a drive current of 20 mA under pulsed operations (10% duty cycle) were 18% and 9 mW, respectively. The device exhibited small electroluminescence wavelength shift (4.5 nm) with drive currents ranging from 30 to 100 mA, indicating significant reduction of polarisation-related internal electric fields. [J1832]

"A Microjet Array Cooling System for Thermal Management of High-Brightness LEDs"

In this paper, a microjet-based cooling system is proposed for the thermal management of high-power light-emitting diodes (LEDs). Preliminary experimental investigation and numerical simulation on such an active cooling system are conducted. In the experiment investigation, thermocouples are packaged with LED chips to measure the temperature and evaluate the cooling performance of the proposed system. The experimental results demonstrate that the microjet-based cooling system works well. For a 2 times 2 LED chip array, when the input power is 5.6 W and the environment temperature is 28degC, without any active cooling techniques, the temperature of 2 times 2 LED chip array substrate reaches 72degC within 2 min and will continue to increase sharply. However, by using the proposed cooling system, when the flow rate of micropump is 9.7 mL/s, the

maximum LED substrate temperature measured by the thermocouples will remain stable at about 36.7degC. As for the numerical optimization, the comparison between the simulation and experimental results is presented to confirm the feasibility of the simulation model. By using the simulation model, the effects of microjet diameter, top cavity height, micropump flow rate, and jet device material on system performance are numerically studied. According to the preliminary test and numerical optimization, an optimized microjet cooling system is fabricated and applied in thermal management of a 220-W LED lamp. The temperature test demonstrates that the cooling system has good performance. [J1833]

"Direct Encapsulation of Organic Light-Emitting Devices (OLEDs) Using Photo-Curable co - Polyacrylate/Silica Nanocomposite Resin"

Direct encapsulation of organic light-emitting devices (OLEDs) was realized by using highly transparent, photo-curable co-polyacrylate/silica nanocomposite resin. Feasibility of such a resin for OLED encapsulation was evaluated by physical/electrical property analysis of resins and driving voltage/luminance/lifetime measurement of OLEDs. Electrical property analysis revealed a higher electrical insulation of photocured nanocomposite resin film at $3.20 \times 10^{12} \Omega$ in comparison with that of oligomer film at $1.18 \times 10^{12} \Omega$ at 6.15 V to drive the bare OLED. This resulted a lower leakage current and the device driving voltage was efficiently reduced so that the nanocomposite-encapsulated OLED could be driven at a lower driving voltage of 6.09 V rather than 6.77 V for the oligomer-encapsulated OLED at the current density of 20 mA/cm². Luminance measurement revealed a less than 1.0% luminance difference of OLEDs encapsulated by various types of resins, which indicates that the photo-polymerization takes very little effect on the light-emitting property of OLEDs. Lifetime measurement of OLEDs found that, the time span for the normalized luminance of device drops to 80%, for nanocomposite-encapsulated OLED is 350.17 h in contrast to 16.83 h for bare OLED and 178.17 h for the oligomer-encapsulated OLED. This demonstrates that nanocomposite resin with optimum properties is feasible to OLED packaging and a compact device structure could be achieved via the method of direct encapsulation. [J1834]

"Low-Noise and High-Detectivity GaN UV Photodiodes With a Low-Temperature AlN Cap Layer"

Here, we present the characteristics of a novel GaN- based ultraviolet (UV) photodiode (PD) with a low-temperature (LT) AlN cap layer. The dark leakage current for the PD with the LT-AlN cap layer was shown to be about four orders of magnitude smaller than that for the conventional PDs. It was found that we could achieve larger UV to visible rejection ratio by inserting an LT-AlN cap layer. It was also found that we could improve minimum noise equivalent power and maximum normalized detectivity of the PD by inserting an LT-AlN cap layer. [J1835]

"A Low-Cost Double-Fiber Model Distributed Optical Fiber Sensor"

This paper presents a novel low-cost, double-fiber model optical fiber sensor for distributed strain monitoring. The sensor is composed of two fibers: the active fiber and the passive fiber. Localized strain makes light couple from the active fiber to the passive fiber. The output of the active fiber is used for strain value sensing, whereas the double-ended outputs of the passive fiber are used for strain position sensing. Distributed sensing is realized based on the attenuation of the passive fiber, which has a greater attenuation coefficient than the active fiber. Since light emission and detection are performed by light-emitting diodes and photodiodes with a common preamp circuit, the entire system is realized with an extremely low cost, compared with other distributed optical fiber sensor systems. The theoretical model and limit parameter analysis, including the maximum length and the spatial resolution, are proposed with the experimental prototype model sensor that has been developed and tested. The performance of sensor is confirmed by a theoretical analysis and experimental results. [J1836]

"Influence of Dislocation Loops on the Near-Infrared Light Emission From Silicon Diodes"

The infrared light emission of forward-biased silicon diodes is studied. Through ion implantation and anneal, dislocation loops were created near the diode junction. These loops suppress the light emission at the band-to-band peak around 1.1 μm . The so-called D1 line at 1.5 μm is strongly enhanced by these dislocation loops. We report a full study of photoluminescence and electroluminescence of these diodes. The results lead to new insights for the manufacturing approach of practical infrared light sources in integrated circuits. [J1837]

"Double interfacial layers for highly efficient organic light-emitting devices"

The authors report on a highly efficient phosphorescent organic light-emitting device (PHOLED) achieved by introducing nanoscale double interfacial layers, made by ultrathin surfactant and low work-function metal layers. It is shown that double interfacial layers play multiple roles in the enhancement of device performance: increasing electron injection, hole blocking, and reducing surface roughness of electroluminescent layer. With double interfacial layers, a PHOLED has shown efficiency as high as 60cd/A with a current density of

1.6mA/cm² and a luminance of 1000cd/m² at 6.5V, which is higher than that of a control device with a single CsF interfacial layer. [J1838]

"Efficient white-light-emitting diodes based on polyfluorene doped with fluorescent chromophores"

Orange-red emitting small molecule chromophores, 4,7-di-2-thienyl-2,1,3-benzothiadiazole, 4,7-(2'-diselenophenyl)-2,1,3-benzothiadiazole, and 4,7-bis(N-methylpyrrol-2-yl)-2,1,3-benzothiadiazole were synthesized and used for fabrication of fluorescent white-emitting device with polyfluorene (PFO) as host by solution processing. By careful controlling of dopant concentration, balanced narrow band-gap (NGB) electroluminescence (EL) emission can be obtained by solution processing due to the incomplete energy transfer from PFO to narrow band gap molecules. EL spectra of the obtained devices were very stable at a wide range of operating voltage. The best white-emitting device reached luminous efficiency of 7.54cd/A with the CIE coordinates (0.33, 0.34) at luminance over 1000cd/m². [J1839]

"Enhancement of light extraction efficiency of InGaN quantum wells light emitting diodes using SiO₂/polystyrene microlens arrays"

Improvement of light extraction efficiency of InGaN quantum wells light emitting diodes (LEDs) using SiO₂/polystyrene microspheres was demonstrated experimentally. The utilization of SiO₂/polystyrene microlens arrays on InGaN quantum wells LEDs, deposited via rapid convective deposition, allows the increase of the effective photon escape cone and reduction in the Fresnel reflection. Improvement of output power by 219% for InGaN quantum wells LEDs emitting at peak wavelength of 480nm with SiO₂/polystyrene microspheres microlens arrays was demonstrated. [J1840]

"Gallium-nitride-based microcavity light-emitting diodes with air-gap distributed Bragg reflectors"

We report on the realization of highly efficient InGaN microcavity light-emitting diodes incorporating a high index contrast air-gap distributed Bragg reflector (DBR). Detailed analysis deduces an effective cavity length of 500nm and cavity mode orders of 5 and 6 for measured Fabry-Perot fringes. A value reflectivity of 70% was determined for the 4.5 period air/AI_{0.08}Ga_{0.92}N DBR through the analysis of cavity finesse based on the angle-resolved photoluminescence (PL) data. A fivefold improvement in light extraction efficiency was verified by electrical probing as well as angle-resolved PL measurements. [J1841]

"Current spreading of III-nitride light-emitting diodes using plasma treatment"

In this study, (CF₄+O₂) plasma is used to selectively treat the p-type GaN region underneath the bonding pad of the anode electrode of III-nitride light-emitting diodes (LEDs). A more uniform light emission distribution is observed in the far-field pattern of the plasma-treated devices and a 16% enhancement of the output intensity under the same biasing current is obtained. The maximum current that can be applied is also higher for the plasma-treated device. Not only does the plasma treatment of the p-GaN layer lead to a highly insulating region but also it does not degrade the device performance. Results from this study indicate that the plasma treatment is able to improve the current spreading of the III-nitride LEDs. [J1842]

"Effect of neutral beam etching of p-GaN on the GaN device characteristics"

GaN materials were etched using a CF₄-based neutral beam, and its etch damage characteristics were compared with those etched with a CF₄-based inductively coupled plasma (ICP). Photoluminescence data showed that the neutral beam etched GaN materials show fewer defects on the surface compared to the GaN materials etched by ICP. Also, the current-voltage characteristics of GaN light emitting diodes fabricated with p-GaN etched by the neutral beam showed less damage compared to those fabricated with p-GaN by the ICP. When a photonic crystal-like structure having 2-μm-diameter microlens array was formed using the neutral beam etching on the p-GaN of the GaN device, an increase of 20% in the optical emission intensity could be observed without significantly increasing the forward voltage (0.7V). [J1843]

"Planar photonic crystals infiltrated with nanoparticle/polymer composites"

Infiltration of planar two-dimensional silicon photonic crystals with nanocomposites using a simple yet effective melt processing technique is presented. The nanocomposites that were developed by evenly dispersing functionalized TiO₂ nanoparticles into a photoconducting polymer were completely filled into photonic crystals with hole sizes ranging from 90 to 500nm. The infiltrated devices show tuning of the photonic band gap that is controllable by the adjustment of the nanoparticle loading level. These results may be useful in the development of tunable photonic crystal based devices and hybrid light emitting diodes and solar cells. [J1844]

"Air stable hybrid organic-inorganic light emitting diodes using ZnO as the cathode"

An air stable hybrid organic-inorganic light emitting device is presented. This architecture makes use of metal oxides as charge injecting materials into the light emitting polymer, avoiding the use of air sensitive cathodes commonly employed in organic light emitting diode manufacturing. We report the application of zinc oxide as a cathode in an organic light emitting device. This electroluminescent device shows high brightness levels reaching 6500cd/m² at voltages as low as 8V. Compared to a conventional device using low workfunction metal cathodes, our device shows a lower turn-on voltage and it can operate in air. [J1845]

"Effects of interfacial stability between electron transporting layer and cathode on the degradation process of organic light-emitting diodes"

The authors have demonstrated that the increase of electron injection barrier height between tris(8-hydroxyquinoline)aluminum (Alq₃) and LiF/Alcathode is one of the most critical parameters to determine the reliability of organic light-emitting diode with the typical structure of indium tin oxide/N,N'-bis(naphthalen-1-yl)-N,N'-bis(phenyl) benzidine/Alq₃/LiF/Al. The electrical properties of several devices (hole only, electron only, and integrated double-layered devices) have been measured in the function of operating time to analyze the bulk and interface property changes. Bulk properties of trap energy and mobility in an organic layer have been estimated by using trap-charge-limited currents and transient electroluminescence measurements. [J1846]

"Epitaxial growth and structural analysis of AlN/GaN heterostructures"

Single crystal AlN thin films were epitaxially grown on GaN/sapphire (0001) substrates on a macroscopic scale by magnetron sputtering. The microscopic structure and orientation degree of the AlN epilayers were studied by high-resolution transmission electron microscopy, high-resolution x-ray diffraction, and reciprocal spacing mapping. It was revealed that the AlN epilayers have high in-plane and out-of-plane orientation degrees and low defect density. The electrical and optical properties of the AlN epilayers were also studied, and the results suggest that the AlN epilayers grown by sputtering may be employed in the fabrication of GaN-based light-emitting diode devices with increased efficiency. [J1847]

"Modifications of the exciton lifetime and internal quantum efficiency for organic light-emitting devices with a weak/strong microcavity"

A comprehensive analysis is given on the modifications of the exciton lifetime and internal quantum efficiency (η_{int}) for organic light-emitting devices (OLEDs). A linear relation is derived between the exciton lifetime and η_{int} , which is difficult to measure directly. The internal quantum efficiency can thus be estimated easily through the measurement of the exciton lifetime. The exciton lifetimes for OLEDs with weak or strong microcavity are studied experimentally and theoretically. The modification of the exciton lifetime is well explained through the microcavity effect and surface plasmon resonance. An excellent agreement between the experimental and theoretical results is achieved. [J1848]

"Quantum-well and localized state emissions in AlInGaN deep ultraviolet light-emitting diodes"

Injection current and temperature dependence of electroluminescence (EL) is investigated in AlInGaN deep ultraviolet light-emitting diodes. Two EL bands with different behaviors are observed. The high-energy band (P1) shows a monotonous redshift and an amazing increase of intensity with increasing current, however, a "U"-shaped shift and a saturation of intensity at high current are measured for the low-energy band (P2). Accordingly, P1 and P2 are attributed to emissions from quantum-well and localized states, respectively, with P1 dominant at high current and high temperature and P2 the main emission mechanism under low temperature and low current. Modeled data based on the theory of random population for localized states in quantum wells taking into account self-heating effect agree well with the experimental results. [J1849]

"Influences of submonolayer proteins on organic light-emitting diodes"

The authors sandwiched protein molecules into the layered structure of organic light-emitting diodes (OLEDs). Light emission from the OLEDs was suppressed on the area with the protein submonolayers of 4-7 nm thick. They found that this suppression depended on the density of the proteins and light emission efficiency reflected molecular properties. A bovine serum albumin layer decreased both the current and light emission, keeping the efficiency almost unchanged. In the case of cytochrome C, the emission was suppressed while current increased, resulting in low efficiency. [J1850]

"Size dependence of nonlinear optical absorption and refraction of Mn-doped ZnSe nanocrystals"

Nonlinear refractive index and nonlinear absorption coefficient of high-quality Mn:ZnSe nanocrystals are measured by z-scan technique at 800nm wavelength. The synthesized nanocrystals with nucleation doping have tunable wavelength (between 565-610nm), high quantum yield (50%), and high thermal as well as photochemical stabilities. The unique nanocrystal structure (with a MnSe core, Zn_{1-x}Mn_xSe diffusion region, and an outer ZnSe layer) shows size-dependent nonlinear effects, which can be qualitatively explained by a simple model using crystal field. Studies of nonlinear optical properties are very important and necessary for high-power optical applications (such as light-emitting diodes and lasers) of such Mn-doped ZnSe nanocrystals. [J1851]

"Design of high-efficiency GaN-based light emitting diodes with vertical injection geometry"

The authors report on the design and fabrication of high-efficiency GaN-based light emitting diodes (LEDs) with vertical-injection geometry. Based on the analyses of LED test patterns fabricated with various n-electrode dimensions, a design rule for vertical LEDs is proposed. It is found that the suppression of the vertical current under nelectrodes and the efficient injection of the spreading current across the nlayers are essential to fabricate high-efficiency LEDs. Introduction of the current blocking layer along with well-designed branched nelectrodes results in a large enhancement of power efficiency by a factor of 1.9, compared with that of reference LEDs. [J1852]

"The development of Thomson scattering system on HL-2A tokamak"

A new Thomson scattering diagnostic system is successfully developed to measure core plasma electron temperature (Te) and density (ne) of HL-2A tokamak (major radius R=165cm, minor radius a=40cm). In this system, a standard lamp-monochromator combination is utilized for the calibration of spectral responses. By sweeping in the range of 750-1200nm with a step of 2nm, the work can be done automatically for one-point calibration and then for other. Electronic gain calibration and gain monitoring are done by pulsed light emitting diode light. By utilizing an intense Nd:YAG laser of pulse energy up to 4J and employing good quality interference filters in the five-channel filter polychromator to suppress greatly the stray light, the TS system can be routinely used to make measurements with good quality data. After each HL-2A plasma discharge, the measured Te and ne data are transferred to HL-2A database for lookup and analyses. [J1853]

"White organic light-emitting devices with a bipolar transport layer between blue fluorescent and orange phosphorescent emitting layers"

White organic light-emitting devices based on an orange phosphorescent iridium complex, bis(2-(2-fluorophenyl)-1,3-benzothiazolato-N,C2') iridium (acetylacetonate) [(F-BT)2Ir(acac)] and blue fluorescent 4,4'-bis(2,2'-diphenylvinyl)-1,1'-biphenyl are reported. By introducing a bipolar transport 4,4'-N,N'-dicarbazole-biphenyl layer between the fluorescent and the phosphorescent emission layers, additional light emission from (F-BT)2Ir(acac) is observed. The authors attributed it to the elimination of the Dexter energy transfer between the two emitters. Pure white emission with Commission Internationale de l'Eclairage coordinates of (0.33, 0.34) and a maximum luminance of 40960 cd/m² were obtained. The maximum current efficiency and the color rendering index of the device are 13.4 cd/A and 71, respectively. [J1854]

"Optical upconversion devices based on photosensitizer-doped organic light-emitting diodes"

The optical upconversion of infrared light to visible light has been achieved in photosensitizer-doped organic light-emitting diodes, where poly(N-vinylcarbazole) doped with infrared photosensitizer of 2,4,7-trinitro-9-fluorenylidene malonitrile was used as hole-transporting layer, and tris(8-hydroxyquinoline) aluminum acted as both emitting and electron-transporting layers. Both electroluminescent intensity and current were enhanced under infrared illumination. The enhancement ratio was obtained as 2.45 times for electroluminescent emission and 1.45 times for current. This work brought forth a prototype design for novel flexible organic optical upconversion device used in near infrared field. [J1855]

"Semitransparent Cu electrode on a flexible substrate and its application in organic light emitting diodes"

A semitransparent nanomesh Cu electrode on a polyethylene terephthalate (PET) substrate using metal transfer from a polydimethylsiloxane (PDMS) stamp and nanoimprint lithography is reported. A nanoscale dense mesh pattern is replicated by using a high modulus PDMS stamp. It is found that a uniform pressure of 30 psi and a temperature of 100 °C are needed for the transfer of the Cu mesh structure from the PDMS stamp onto the PET substrate. A fabricated semitransparent Cu electrode exhibits high transmittance in the visible range and good electrical conductivity. The authors show that the transmittance is increased by reducing the linewidth of the mesh pattern and an average transmittance of 75% is achieved. An organic light emitting diode on a flexible

substrate is fabricated to demonstrate the potential use of a semitransparent Cu electrode as a transparent conducting electrode. [J1856]

"Fabrication of GaN-based metal-oxide-semiconductor light-emitting diodes operating in ultraviolet spectral region"

Integrated light-emitting diodes (LEDs) that operate in the UV spectral region were fabricated using GaN layers grown on sapphire substrates by metal-organic vapor phase epitaxy. Schottky-type LEDs and metal-oxide-semiconductor (MOS) LEDs were realized. The near-band-edge emission of GaN was observed in the electroluminescent spectra with reversed bias under pulsed-voltage conditions. The insertion of an aluminum oxide layer in the GaN-based LED leads to an increase in electroluminescent intensity. [J1857]

"Enhanced forward emission from ZnO via surface plasmons"

By using metal-insulator-metal (MIM) as the cap layer, we have enhanced the photoluminescent emission from ZnO in the forward direction via coupling of surface plasmons. The basic principle behind the enhancement involves two steps. First, the overall light emission efficiency of ZnO is increased significantly due to the coupling and scattering of nonradiative surface plasmons at the metal/ZnO interface. The forward emission is then increased by enhanced transmission due to the excitation of radiative surface plasmons in the MIM structure. As a result, the forward emission from MIM/ZnO is found to be 7 and 3.5 times stronger than that from uncapped ZnO and M/ZnO. We expect that the MIM structure could evolve as an effective means in fabricating high brightness light emitting diodes from semiconductors. [J1858]

"Sensitized electrophosphorescence of infrared emission diode based on copper phthalocyanine by an ytterbium complex"

By inserting a layer of (dibenzoylmethanato)3-(bathophenanthroline)-ytterbium (Yb-C) between copper phthalocyanine (CuPc) emitting layer and electron transport layer, intense and broadband electroluminescence (EL) were achieved at 930-1300nm spectral region in a phosphorescent EL device. The intensity and bandwidth are increased by about 50 and 4 times, respectively, compared with the EL device without Yb-C layer. The improvement in the EL intensity and band broadening were attributed to the energy transfer from Yb-C to CuPc and the overlapping of the Yb3+ near-infrared emission band with the CuPc emission band. [J1859]

"Highly efficient red electrophosphorescence from a solution-processed zwitterionic cyclometalated iridium(III) complex"

A mononuclear red-emitting zwitterionic iridium(III) complex, bis(1-(phenyl)isoquinolinato) iridium(III) (2,2'-bipyridine-3-ol-3'-olate), was synthesized and used as a triplet emitter doped in a polymeric host in solution-processed electrophosphorescent light-emitting diodes. We achieved a high luminous efficiency (LE) of 12.62 cd/A with fast response time in the device using the dopant unlike in the device using cationic iridium(III) phosphorescent materials. A hole transporting polymeric interlayer between the anode and the emitting layer improved the LE and decreased the exciton quenching at high electric fields. [J1860]

"Effect of threading defects on InGaN /GaN multiple quantum well light emitting diodes"

Photoelectrochemical etching was used to measure the threading defect (TD) density in InGaN multiple quantum well light-emitting diodes (LEDs) fabricated from commercial quality epitaxial wafers. The TD density was measured in the LED active region and then correlated with the previously measured characteristics of these LEDs. It was found that the reverse leakage current increased exponentially with TD density. The temperature dependence of this dislocation-related leakage current was consistent with a hopping mechanism at low reverse-bias voltage and Poole-Frenkel emission at higher reverse-bias voltage. The peak intensity and spectral width of the LED electroluminescence were found to be only weakly dependent on TD density for the measured TD range of 1.4×10^7 - $2.4 \times 10^8 \text{ cm}^{-2}$. [J1861]

"Realization of n-Zn_{1-x}Mg_xO / i-ZnO / SiO_x / n⁺-Si heterostructured n-i-n light-emitting diodes by low-cost ultrasonic spray pyrolysis"

n-Zn_{1-x}Mg_xO / i-ZnO / SiO_x / n⁺-Si heterostructured light-emitting diodes have been demonstrated by low-cost ultrasonic spray pyrolysis. The current-voltage measurement shows typical characteristics of a back-to-back diode due to the double Schottky barriers induced by the SiO_x layer. Blue electroluminescence peaking at 460 nm was observed at room temperature when a positive bias of 4 V was applied on the Si substrate. The electroluminescence is suggested to be dominated by the donor-acceptor pair recombination in the i-ZnO layer,

where the holes were injected from the valence band of Si into the acceptor level of i-ZnO. [J1862]

"Self-propagating high temperature synthesis of yellow-emitting Ba₂Si₅N₈:Eu²⁺ phosphors for white light-emitting diodes"

High-performance nitride phosphors, Ba₂Si₅N₈:Eu²⁺, were prepared by the self-propagating high temperature synthesis method. The broadband absorption in the range of 380-500nm indicated that the resultant phosphors were effectively excited by an InGaN blue light-emitting diode (400/470nm). The emission peak position of Ba₂-xEu_xSi₅N₈(x=0-0.3) varied from 572 to 650nm with increasing Eu²⁺ concentration, and the intensity was maximized at x=0.04. The optimized sample gave a strong yellow emission peak at 580nm. The redshifting behavior of the emission band was attributed to three factors: energy migration, crystal field strengthening, and reabsorption. [J1863]

"Interface electronic structure of the organic light-emitting devices: Photoemission and x-ray absorption studies of Al/KF/Alq₃ interface"

The chemistry of organic light-emitting diode interface composed of KF sandwiched between the Al and Alq₃ was investigated using near-edge x-ray absorption fine structure (NEXAFS) as well as x-ray and ultraviolet photoelectron spectroscopy techniques. At the earliest stages of KF deposition on Alq₃, changes in F K-edge NEXAFS spectra indicated a strong chemical reaction, which is responsible for the dipole layer formation seen in valence-band spectra. For Al deposition on KF/Alq₃, the reactions inferred from observed spectral changes are not consistent with the commonly believed KF dissociation and AlF₃ formation scenarios. [J1864]

"Microcavity top-emitting organic light-emitting devices integrated with microlens arrays: Simultaneous enhancement of quantum efficiency, cd/A efficiency, color performances, and image resolution"

A long bothering issue in microcavity organic light-emitting devices (OLEDs) is the difficulty to simultaneously achieve enhanced cd/A efficiency, enhanced external quantum efficiency, enhanced color saturation, and stable colors with viewing angles in the same device design. In this work, we show that microcavity top-emitting OLEDs integrated with microlenses may provide a universal approach for simultaneously achieving all these desired nice characteristics. Furthermore, the pixel blurring often occurring in employment of microlenses to conventional bottom-emitting OLEDs is significantly suppressed by combination of top-emitting microcavity OLEDs and microlenses. [J1865]

"Low resistance as-deposited Cr/Au contacts on p-type GaN"

The influence of several predeposition surface treatments and different contact metals to the electrical properties of metal/p-GaN contacts was studied. A low resistance as-deposited Cr/Au Ohmic contact was achieved, using boiling aqua regia as surface treatment. The Ohmic resistance of Cr/Au contacts with 50μm interspacing was found to be 50Ω, while the specific contact resistivity value was measured 2.64×10⁻³Ω cm². Direct comparison with the standard oxidized Ni/Au contacts confirmed the superior characteristics of the Cr/Au contact scheme. Violet emission was readily obtained when the as-deposited Cr/Au contacts were used as the p-electrode of a light emitting diode emitting at 385nm. [J1866]

"Effect of internal electrostatic fields in InGaN quantum wells on the properties of green light emitting diodes"

Variations in the strength of the piezoelectric field inside InGaN quantum wells have been observed along the growth direction in InGaN-based diodes emitting light in the green region. The internal electrostatic potential distribution across the active region consisting of five InGaN quantum wells has been determined by electron holography in a transmission electron microscope. The strength of the piezoelectric field decreases in the direction towards the p-n junction. Its effect on light emission has been evaluated by depth-profiling cathodoluminescence, where the emission from two peaks becomes increasingly distinct with increasing excitation voltage. The drop in piezoelectric field strength is proposed to be related to the neutralization of piezoelectric charges by hydrogen ions which are initially abundant in the p-region and diffuse into the quantum wells during thermal annealing. [J1867]

"Single-step fabrication of Fresnel microlens array on sapphire substrate of flip-chip gallium nitride light emitting diode by focused ion beam"

A simple one-step focused ion beam milling technique was used to fabricate a Fresnel microlens array on the

backside of sapphire substrate of a gallium nitride blue light emitting diode. The optical output power from the flip-chip gallium nitride blue light emitting diode is enhanced to about 1.68 times at the injection current of 20mA. The spatial light distribution from the backside of flip-chip gallium nitride blue light emitting diode with a Fresnel microlens array shows a uniform and stronger light emission. [J1868]

"Heteroepitaxy of AlGaIn on bulk AlN substrates for deep ultraviolet light emitting diodes"

The authors report the growth of AlGaIn epilayers and deep ultraviolet (UV) light emitting diodes (LEDs) on bulk AlN substrates. Heteroepitaxial nucleation and strain relaxation are studied through controlled growth interruptions. Due to a low density of preexisting dislocations in bulk AlN, the compressive strain during AlGaIn heteroepitaxy cannot be relieved effectively. The built-up of strain energy eventually induces either an elastic surface roughening or plastic deformation via generation and inclination of dislocations, depending on the stressor interlayers and growth parameters used. AlGaIn LEDs on bulk AlN exhibit noticeable improvements in performance over those on sapphire, pointing to a promising substrate platform for III-nitride UV optoelectronics. [J1869]

"Nanoimprinted circular grating distributed feedback dye laser"

The authors demonstrate an optically pumped surface emitting polymer dye laser fabricated by nanoimprint lithography. The laser is based on an organic dye hosted within a poly(methylmethacrylate) matrix coated on a transparent substrate, and the laser cavity consists of a second order circular grating distributed feedback structure. The authors achieved lasing at 618nm with 0.18nm linewidth and 1.31mW/mm² pump threshold. The nanoimprinted solid-state dye laser offers a low-cost coherent light source for laboratory-on-chip spectroscopy systems. The laser also has a low pump threshold and a geometry well matched to light-emitting diode pump sources, which provide an interesting alternative for constructing portable polymer laser devices. [J1870]

"Hole-transporting-layer-free high-efficiency fluorescent blue organic light-emitting diodes"

High-efficiency fluorescent blue organic light-emitting diodes were fabricated using hole-injection and carrier-confining effective device architecture without a hole-transporting layer. The diodes consist of 125nm indium tin oxide/300nm blue-emissive layer/400nm electron-transporting layer/10nm lithium fluoride/1500nm aluminum. A high efficiency of 6.0% (12.5lm/W) at 100cd/m² with a pan-blue emission of (0.19, 0.31) when trans-1,2-bis-(6-(N,N-dip-tolylamino)naphthalene-2-yl)ethene was used in the emissive layer, or 3.9% (6.7lm/W) with a blue emission of (0.15, 0.20) when 2-(N,N-diphenylamino)-6-[4-(N,N-diphenylamino)-styryl]naphthalene was used. Besides having a thinner device structure, the marked improvement in efficiency is attributable mainly to the relatively low hole-injection barrier. [J1871]

"Effect of acceptor on efficiencies of exciplex-type organic light emitting diodes"

The relationship between the electroluminescent (EL) efficiencies of interfacial exciplex emission and the lowest unoccupied molecular orbital (LUMO) of the acceptors systematically investigated. A nearly linear relationship was observed between LUMOs of acceptors and exciplex efficiency for a fixed donor of 4,4',4''-tris[3-methyl-phenyl(phenyl)amino]-triphenylamine in exciplex-type devices. This result indicates that the lower the LUMO of the acceptor is, the higher the EL efficiency of the exciplex is. The effect of acceptor on the efficiencies of exciplex-type devices is attributable to the interactions between the donor and acceptor molecules, which were closely related to the matched LUMOs and intermolecular conformations overlap between donor and acceptor molecules. [J1872]

"Broadband and time-resolved absorption spectroscopy with light emitting diodes: Application to etching plasma monitoring"

Broad band absorption spectroscopy is widely used to measure the concentration of radicals, which is important to understand the physical chemistry of many plasmas. It is possible to increase the sensitivity of this technique and to perform time-resolved measurement by using light emitting diodes (LEDs) as a light source. The method is applied to detect CF₂ radicals and Cl₂ molecules in high density plasmas. The detection limit over 10ms integration time is as low as 3mTorr of Cl₂. We conclude that the absorption spectroscopy with LEDs opens possibilities for precise process control and fundamental analysis of reactive media. [J1873]

"Multidimensional ZnO light-emitting diode structures grown by metal organic chemical vapor deposition on p-Si"

A multidimensional ZnO light-emitting diode (LED) structure comprising film/nanorods/substrate was fabricated on a p-type Si substrate using metal organic chemical vapor deposition at relatively low growth temperature. The

filmlike top layer used for the metal contact was continuously formed on the ZnO nanorods by varying the growth conditions and the resulting structure allowed us to utilize the nanorods with intense emission as an active layer. We investigated the performance of the resulting multidimensional LED. An extremely high breakdown voltage and low reverse leakage current as well as typical rectification behavior were observed in the I-V characteristics. [J1874]

"Effect of dislocation density on efficiency droop in GaInN/GaN light-emitting diodes"

Measurements of light-output power versus current are performed for GaInN/GaN light-emitting diodes grown on GaN-on-sapphire templates with different threading dislocation densities. Low-defect-density devices exhibit a pronounced efficiency peak followed by droop as current increases, whereas high-defect-density devices show low peak efficiencies and little droop. The experimental data are analyzed with a rate equation model to explain this effect. Analysis reveals that dislocations do not strongly impact high-current performance; instead they contribute to increased nonradiative recombination at lower currents and a suppression of peak efficiency. The characteristics of the dominant recombination mechanism at high currents are consistent with processes involving carrier leakage. [J1875]

"InGaN/GaN light emitting diodes on nanoscale silicon on insulator"

The authors report on the fabrication of InGaN/GaN-based light emitting diodes (LEDs) on nanoscale silicon-on-insulator (SOI) substrates. The LED structures are grown on (111)-oriented 45nm thick SOI overlayer by metal organic chemical vapor deposition. Square-shaped mesa patterns are created by standard LED processing steps including multiple-mask photolithography, inductive coupled plasma etching, and contact metallization. Due to the high reflective Si/SiO₂ beneath AlN buffer and high refractive contrasts at the interfaces, the authors observed multiple interference peaks from LEDs on SOI and such effect resulted in an increased integrated electroluminescence intensity when compared to LED structures fabricated on bulk Si(111). [J1876]

"ZnO-on-GaN heterojunction light-emitting diode grown by vapor cooling condensation technique"

The growth of ZnO-on-GaN heterostructures was implemented using the vapor cooling condensation system. The technique thus developed was employed to fabricate both the p-GaN/n-ZnO:In(p-n) and p-GaN/i-ZnO/n-ZnO:In(p-i-n) heterojunction light-emitting diodes (LEDs). A rectifying diodelike behavior was clearly observed from both the p-n and p-i-n heterojunction LEDs, with the forward turn-on voltage of 3V and the reverse breakdown voltage of -15V determined for the p-n heterojunction LEDs, compared to 7 and -23V, respectively, for the p-i-n heterojunction LEDs. Based on the results of photoluminescence and electroluminescence studies conducted on these LED structures, the ZnO layer responsible for the peak emission wavelength of 385nm were also verified experimentally. [J1877]

"A highly efficient wide-band-gap host material for blue electrophosphorescent light-emitting devices"

We report on an efficient wide-band-gap host material for blue electrophosphorescence devices, namely, 1,2-trans-di-9-carbazolylcyclobutane (DCz). Photophysical studies show that lower-energy excimer formation between the carbazole units can be efficiently suppressed in a DCz film, thus maintaining its high triplet-state energy and inducing an exothermic energy transfer from DCz to iridium(III)bis[(4,6-difluorophenyl)-pyridinato-N,C2']picolinate (FIrpic). Electrophosphorescent devices comprising a FIrpic:DCz emitting layer exhibit a superior performance with a maximum external quantum efficiency of 9.8%, a maximum luminance efficiency of 21.5cd/A, and a maximum power efficiency of 15.0lm/W at 0.01mA/cm². [J1878]

"Formation of Ohmic hole injection by inserting an ultrathin layer of molybdenum trioxide between indium tin oxide and organic hole-transporting layers"

Current density-voltage (J-V) characteristics of hole-only devices using indium tin oxide (ITO) anode and N,N'-diphenyl-N,N'-bis(1-naphthyl)-1,1'-biphenyl-4,4'-diamine (alpha-NPD) layers were measured with various thicknesses of a molybdenum trioxide (MoO₃) buffer layer inserted between ITO and alpha-NPD. The device with a 0.75-nm-thick MoO₃ layer forms Ohmic hole injection at the ITO/MoO₃/alpha-NPD interfaces and J-V characteristics of this device are controlled by a space-charge-limited current. Results of X-ray photoelectron and ultraviolet/visible/near-infrared absorption studies revealed that this Ohmic hole injection is attributable to an electron transfer from ITO and alpha-NPD to MoO₃. [J1879]

"Nonpolar m-plane thin film GaN and InGaN/GaN light-emitting diodes on LiAlO₂ (100) substrates"

The nonpolar m-plane (1100) thin film GaN and InGaN/GaN light-emitting diodes (LEDs) grown by metal-organic chemical vapor deposition on LiAlO₂(100) substrates are reported. The LEDs emit green light with output power of 80 mW under a direct current of 20 mA for a 400 μ m² device. The current versus voltage (I-V) characteristic of the diode shows soft rectifying properties caused by defects and impurities in the p-n junction. The electroluminescence peak wavelength dependence on injection current, for currents in excess of 20 mA, saturates at 515-516 nm. This proves the absence of polarization fields in the active region present in c-plane structures. The light output intensity versus current (L-I) characteristic of the diode exhibits a superlinear relation at low injection current caused by nonradiative centers providing a shunt path and a linear light emission zone at high current level when these centers are saturated. [J1880]

"A stable blue host material for organic light-emitting diodes"

We have developed a high performance fluorescent host material, 6-anthracene-9-yl-2,3-di-p-tolyl benzo[b]thiophene (ATB), for blue organic light-emitting diodes. ATB formed a stable amorphous solid state film with a high glass transition temperature ($T_g = 116^\circ\text{C}$). The multilayer devices fabricated using ATB as a blue host material showed higher power efficiency (6.4 lm/W at 1000 cd/m²) than the conventional device using 2-tert-butyl-9,10-di(2-naphthyl)anthracene (TBADN) (4.3 lm/W at 1000 cd/m²). The half lifetime of the ATB device (6480 h at 1000 cd/m²) was also enhanced compared to the TBADN device (5341 h at 1000 cd/m²). [J1881]

"Highly efficient p-i-n white organic light emitting devices with tandem structure"

Highly efficient tandem p-i-n white organic light emitting devices have been fabricated. Utilizing an optical transparent bilayer with doped organic p-n junction that consists of 4,7-diphenyl-1,10-phenanthroline: 2% cesium carbonate (Cs₂CO₃)/N,N'-bis(1-naphthyl)-N,N'-diphenyl-1,1'-biphenyl-4,4'-diamine: 50% v/v tungsten oxide (WO₃) as the connecting layer, the tandem p-i-n white device achieved an electroluminescence efficiency of 23.9 cd/A and a power efficiency of 7.8 lm/W at 20 mA/cm² with a Commission Internationale de l'Eclairage coordinates of (0.30, 0.43). The electroluminescent color of this tandem p-i-n white organic light-emitting diode device will not change significantly with respect to drive current variation and forward viewing angle. [J1882]

"Blue-emitting InGaN-GaN double-heterostructure light-emitting diodes reaching maximum quantum efficiency above 200 A /cm²"

Auger recombination is determined to be the limiting factor for quantum efficiency for InGaN-GaN (0001) light-emitting diodes (LEDs) at high current density. High-power double-heterostructure (DH) LEDs are grown by metal-organic chemical vapor deposition. By increasing the active layer thickness, DH LEDs can reach a maximum in quantum efficiency at current densities above 200 A/cm². Encapsulated thin-film flip-chip DH LEDs with peak wavelength of 432 nm have an external quantum efficiency of 40% and output power of 2.3 W at 2 A. [J1883]

"A new switched-capacitor frequency modulated driver for light emitting diodes"

A new type of drivers for light emitting diodes (LEDs) is introduced based on the switched-capacitor frequency modulation. In contrast to conventional constant dc current drivers, the current pulse is provided by this new switched-capacitor LED driver. In the present driver, the charging capacitor is charged and discharged through a LED and the current flow direction is controlled by a metal oxide semiconductor switch. The input current (and thus the LED brightness) is proportional to the switch clock frequency at relatively low frequencies and becomes saturated at relatively high frequencies. This new driver circuit is simple and robust and maintains high efficiency for a wide range of input powers. In addition, the dimming control is easily realized by modulating clock frequency. Finally, this LED driver consumes no dc current and thus provides inherent protection to LED in standby mode. [J1884]

"Efficient green organic light-Emitting devices with a nondoped dual-functional electroluminescent material"

An efficient nondoped green organic light-emitting device was demonstrated by using a dual-functional electroluminescent material, 4,4',4''-tris[8-(7,10-diphenylfluoranthenyl)] phenylamine (TDPFPA). TDPFPA was shown to be a good hole transporting [with a mobility of (1.1-1.2) $\times 10^{-4}$ cm²V⁻¹s⁻¹ at (1.8-5.6) $\times 10^5$ V/cm] and efficient fluorescent material with an exceptionally high glass transition temperature of 237°C. The device with a simple structure of indium tin oxide/TDPFPA/4,7-diphenyl-1,10-phenanthroline/LiF/Al showed green emission with Commission Internationale de l'Eclairage coordinates of (0.24, 0.54), a current efficiency of 9.9 cd/A, and power efficiency of 10.6 lm/W. [J1885]

"White light-emitting diodes based on a single InGaN emission layer"

White light-emitting InGaN/GaN diode with an InGaN underlying layer grown on the (0001) sapphire substrate was fabricated by low pressure metal-organic vapor phase epitaxy. The electroluminescence measurements show that the emitted white light is composed of blue and yellow lights, centered at around 440 and 570nm, respectively, for an injection current of 20mA. Cross-sectional transmission electron microscopy reveals that In-rich quantum dots were formed in InGaN wells due to phase separation of indium. It is suggested that the yellow and blue lights come from In-rich quantum dots and the low-indium regions, respectively, in InGaN quantum wells. [J1886]

"Structure-function relationships of conjugated polyelectrolyte electron injection layers in polymer light emitting diodes"

The characteristics of conjugated polymer light-emitting diodes containing poly(2-methoxy-5-(2'-ethylhexyloxy)-1,4-phenylene vinylene) as the emissive layer and cationic or anionic conjugated polyelectrolytes (CPEs) as the electron injection layer are reported. Structure variations involving backbone, type of counterion, and charge were used to establish structure-function relationships. More efficient electron injection from Al and better device performance are attained with CPEs bearing negative charges. For cationic CPEs having the same counterion but different conjugated structures, one observes better device efficiency using the material with higher electron mobility. Thus, both charge and backbone are important for optimizing device performance. [J1887]

"The origin of electron injection improvement in organic light-emitting devices with an organic oxide/rubrene electron injection layer"

The electronic structure of tris(8-hydroquinoline) aluminum (Alq3)/rubrene/poly(ethylene glycol) dimethyl ether (PEGDE)/Al interfaces was studied using in situ ultraviolet photoelectron spectroscopy (UPS) and x-ray photoelectron spectroscopy (XPS). The UPS and XPS spectra allowed us to evaluate the complete energy level diagrams and to analyze the chemical interactions at the interfaces. When a PEGDE/rubrene double layer was inserted between Al and Alq3, the electron injection barrier height was greatly reduced compared to the interface without PEGDE/rubrene or with a single insertion layer of either PEGDE or rubrene. [J1888]

"Nanolasers to enable data storage beyond 10 Tbit /in. 2"

A focused ion beam (FIB) fabricated nanolaser is demonstrated to be able to focus light with power of over 250nW into a 30nm spot. To fabricate a nanolaser, a 100nm thick aluminum film was deposited on the emitting edge of a diode laser. FIB was used to etch various apertures into the film. The power was measured by a scanning near-field optical microscope in the near-field regime with a 10nm separation between the probe and the air bearing surface of the nanolaser. Out of four different shapes under study, "C"-shape aperture was found to have the highest throughput. [J1889]

"Surface plasmon coupling effect in an In Ga N /Ga N single-quantum-well light-emitting diode"

The authors demonstrate the coupling effects between the quantum well (QW) and surface plasmon (SP) generated nearby on the p-type side in an InGaN/GaN single-QW light-emitting diode (LED). The QW-SP coupling leads to the enhancement of the electroluminescence (EL) intensity in the LED sample designed for QW-SP coupling and reduced SP energy leakage, when compared to a LED sample of weak QW-SP coupling or significant SP energy loss. In the LED samples of significant QW-SP coupling, the blueshifts of the photoluminescence and EL emission spectra are observed, indicating one of the important features of such a coupling process. The device performance can be improved by using the n-type side for SP generation such that the device resistance can be reduced and the QW-SP coupling effect can be enhanced (by further decreasing the distance between the QW and metal) because of the higher carrier concentration in the n-type layer. [J1890]

"Defect related issues in the "current roll-off" in InGaN based light emitting diodes"

Defect related contributions to the reduction of the internal quantum efficiency of InGaN-based multiple quantum well light emitting diodes under high forward bias conditions are discussed. Screening of localization potentials for electrons is an important process to reduce the localization at high injection. The possible role of threading dislocations in inducing a parasitic tunneling current in the device is discussed. Phonon-assisted transport of holes via tunneling at defect sites along dislocations is suggested to be involved, leading to a nonradiative parasitic process enhanced by a local temperature rise at high injection. [J1891]

"An ultrathin (100 mcm thick) flexible light plate fabricated using self-alignment and lift-off"

techniques"

An ultrathin (100 nm thick) flexible light plate was designed and fabricated on a parylene template using a combination of self-alignment and lift-off techniques. The solid-state InGaN light-emitting diodes (LEDs) ($\lambda = 465 \text{ nm}$) was used as the light source to overcome the problem of conventional organic light-emitting devices which require perfect encapsulation against the permeation of water and oxygen. After the sidewalls of LEDs were passivated by the photodefinable polymer, the LED chip array can be further sandwiched by the indium-tin oxide (ITO) and Al electrodes to form a thin-film package with all the processing temperatures below 250°C . The ITO-coated transparent parylene template can be peeled off from the glass carrier after forming the ultrathin LED light plate. The flexible light plates present no damage even after they were flexed 1000 times around a 3-cm-diameter cylinder. The present self-alignment or mask-less process is a very promising approach to flexible backlight applications. [J1892]

"Diffusion-controlled charge injection model for organic light-emitting diodes"

We present a compact model to describe the charge injection for organic light-emitting diodes. By identifying a critical distance where the concentration of carriers in the extended states equals that of the trapped carriers, we obtain a model for the injection current, which links the drift-diffusion and the multiple-trapping theories. This model yields the injection current as a function of electric field, temperature, and barrier height between metal and organic semiconductor. Good agreement with recent experimental data is observed. The effect of the field-dependent mobility on the injection current is also discussed. [J1893]

"Temperature dependence of polarized electroluminescence from nonpolar m-plane InGaN-based light emitting diodes"

An accurate method of estimating polarized light emission was presented for nonpolar m-plane InGaN-based blue light emitting diodes, where the unpolarized component caused by unintentional light scattering was eliminated as noise. The polarization ratios of electroluminescence (EL) at 300 and 100 K were 0.85 and 0.98, respectively. The energy difference between the highest and the second highest valence bands was estimated to be 129 meV from the temperature dependence of the spectrally integrated EL intensities under the assumption of Fermi statistics. This value agreed with the one (118 meV) obtained directly from the difference of the EL peak energies between two polarized components, the electric fields perpendicular and parallel to the c-axis. [J1894]

"Increase of light extraction from GaN based light emitting diodes incorporating patterned structure by colloidal lithography"

The light extraction efficiency of light emitting diodes (LEDs) was enhanced by incorporating nanoscale patterns inside the LED structure. A hole patterned p-GaN layer and a pillar patterned indium-tin-oxide (ITO) contact layer were fabricated by using colloidal lithography with size-tunable polystyrene spheres. It was found that the light output power (at 20 mA) of the LEDs with the hole patterned p-GaN layer and the pillar patterned ITO contact layer were enhanced by 21% and 10%, respectively, compared with the conventional LED due to the increase of the extraction probability of the internally reflected photons through the patterns. [J1895]

"Cryptand based solid-state electrolytes in polymer light-emitting devices"

In order to gain improved insight into the fundamental mode of operation of light-emitting electrochemical cells (LECs), LECs were prepared from a solid-state electrolyte, consisting of the cryptand (Kryptofix® 222, [2.2.2] cryptand) and lithium triflate, and a blue emitting low-Stokes-shift poly(para-phenylene). The devices reveal LEC-like characteristics, however, their evolution appears on a longer time scale, which is a consequence of reduced cation conductivity of the [2.2.2] cryptands compared to commonly used ion conductors and decelerated electrochemical doping near the cathode. It is possible to study the location and direction of the emission zone shift during device operation. [J1896]

"Auger recombination in InGaN measured by photoluminescence"

The Auger recombination coefficient in quasi-bulk $\text{In}_x\text{Ga}_{1-x}\text{N}$ ($x = 9\% - 15\%$) layers grown on GaN (0001) is measured by a photoluminescence technique. The samples vary in InN composition, thickness, and threading dislocation density. Throughout this sample set, the measured Auger coefficient ranges from 1.4×10^{-30} to $2.04 \times 10^{-30} \text{ cm}^6 \text{ s}^{-1}$. The authors argue that an Auger coefficient of this magnitude, combined with the high carrier densities reached in blue and green InGaN/GaN (0001) quantum well light-emitting diodes (LEDs), is the reason why the maximum external quantum efficiency in these devices is observed at very low current densities. Thus, Auger recombination is the primary nonradiative path for carriers at typical LED operating currents and is the reason behind the drop in efficiency with increasing current even under room-temperature (short-pulsed, low-

duty-factor) injection conditions. [J1897]

"Green light-emitting diodes with self-assembled In-rich InGaN quantum dots"

A green light-emitting diode (LED) was fabricated using self-assembled In-rich InGaN quantum dots (QDs). The photoluminescence studies showed that the QDs provide thermally stable deeply localized recombination sites for carriers with negligibly small piezoelectric field. The electroluminescence spectra of the LED showed a peak in the green spectral range and the dominant peak was blueshifted with increasing injection current due to the distribution of depth of the potential wells of QDs. The output power of the LED increased with increasing injection current, indicating that the potential wells are thermally stable and deeply localized in the QDs. [J1898]

"Improved color stability in white phosphorescent organic light-emitting diodes using charge confining structure without interlayer"

Color stability of white organic light-emitting diodes was improved by using a charge confining device structure, which can confine charges at the center of the emitting layer. A red phosphorescent emitting layer was sandwiched between blue phosphorescent emitting layers and there was little change of color coordinate from 100 to 10000 cd/m². [J1899]

"Low operating voltage bright organic light-emitting diode using iridium complex doped in 4,4'-bis[JN-1-naphthyl-N-phenyl-amino]biphenyl"

A low driving voltage organic light-emitting diode using a yellow phosphor bis[2-(4-tert-butylphenyl)benzothiazolato-N,C2'] iridium (acetylacetonate) as a dopant and 4,4'-bis[N-1-naphthyl-N-phenyl-amino]biphenyl as a host was fabricated. The device without p- or n-doped transporting layer shows a turn-on voltage as low as 2.45V, and a luminance of 1000 cd/m² at 4.3V. A maximum luminance of 23230 cd/m² at 10V was achieved. The decrease of the device turn-on voltage may result from direct charge carrier trapping in the dopant and hole only transporting characteristic of the host material. Both charge carrier trapping and energy transfer mechanisms were found in the electroluminescence process. [J1900]

"Electrically pumped photonic crystal distributed feedback quantum cascade lasers"

We demonstrate electrically pumped, room temperature, single mode operation of photonic crystal distributed feedback (PCDFB) quantum cascade lasers emitting at $\lambda = 4.75 \mu\text{m}$. Ridge waveguides of 100 μm width were fabricated with both PCDFB and Fabry-Perot feedback mechanisms. The Fabry-Perot device has a broad emitting spectrum and a double lobed far-field character. The PCDFB device, as expected, has primarily a single spectral mode and a diffraction limited far field characteristic with a full angular width at half maximum of 2.4°. This accomplishment represents the first step in power scaling of single mode, midinfrared laser diodes operating at room temperature. [J1901]

"Spectrally narrowed edge emission from organic light-emitting diodes"

A dramatic spectrally narrowed edge emission (SNEE) from small molecular organic light-emitting diodes at room temperature, with a full width at half maximum of 5-10 nm, is described. The results show that this emission is due to irregular waveguide modes that leak from the indium tin oxide anode to the glass substrate at a grazing angle. Measurements of variable stripe length devices exhibit an apparent weak optical gain, but there is no observable threshold bias associated with this SNEE. Hence this apparent "optical gain" is suspected to result from misalignment of the propagating leaky waveguide mode and the collecting optics. [J1902]

"Sensing electron transport in a blue-emitting copolymer by transient electroluminescence"

A variation of the transient electroluminescence technique is introduced which allows us to selectively study the electron transport in a thin polymer layer. It relies on the formation of an insoluble interlayer from a formerly solvable polymer and enables probing of unipolar electron transport despite of injection barriers. It opens up possibilities to gain insight into the operation of light-emitting diodes. Applicability to a blue-emitting spirobifluorene-based copolymer is shown by comparison to time-of-flight results for electron and hole transport and evidence supplied for an intermixing of electron and hole dynamics through blocking of electrons at the polymer/anode interface. [J1903]

"Boron-doped carbon nanotube coating for transparent, conducting, flexible photonic devices"

Conducting transparent polymer materials were made by applying boron-doped single-walled carbon nanotubes to the surfaces of glass and flexible polyethylene terephthalate film substrates. Optical transmission and sheet

resistance measurements showed that the boron-doped coated samples had sheet resistances of $7\text{k}\Omega/\square$ and flat optical transmission of 89% for visible light. Temperature and humidity tests showed that the materials remained conductive after nearly 150 h of testing. The materials are robust and even maintain their conducting properties after being folded. Fabrication of a simple light emitting device demonstrates usage of the material as a flexible transparent electrode. [J1904]

"Optical properties of air-stable semiconducting copolymer based on polythiophene"

Optical properties of thiophene based copolymer poly(2,5-bis(3-dodecylthiophen-2-yl)thieno[2,3-b]thiophene) (pBTCT) thin films have been investigated by means of optical absorption, photoluminescence (PL), PL quantum efficiency, time-resolved PL, and electroluminescence measurements. It is found that pBTCT exhibits relatively higher PL quantum efficiency ($\Phi_{\text{PL}} = 16\%$) in solid state than poly(3-hexylthiophene) (P3HT). Although the PL quantum efficiency is relatively higher, the transition dipole moment of the lowest excited state of pBTCT is not large, as found in P3HT. The electroluminescence from pBTCT light-emitting diodes is observed and its spectrum is essentially the same as the PL spectrum of pBTCT. [J1905]

"Charge carrier mobility of mixed-layer organic light-emitting diodes"

The authors report the investigation of the charge transport behaviors in mixed thin films of N,N'-diphenyl-N,N'-bis(1-naphthyl)-1,1'-biphenyl-4,4'-diamine and tris(8-hydroxyquinoline) aluminum. The extracted electron and hole drift mobility were found to be sensitive to the compositional fraction and interpreted by energy levels, charge mobilities of neat compounds, and microscopic networks within the mixed systems. The carrier conduction characteristics, therefore, were used to illustrate the electrical and optical properties of the organic light emitting devices with a mixed layer and present direct evidences on the role of the mixed layer in these devices. [J1906]

"Enhanced light extraction from GaN-based green light-emitting diode with photonic crystal"

This letter reports the properties of GaN-based green light-emitting diodes (LEDs) having a p-GaN photonic crystal layer with a photonic bandgap (PCWG) and without a photonic bandgap (PCOG). With decreasing the photoluminescence (PL) detection angle from 140° to 60° , the enhancement of PL intensity of LED with PCWG was largely increased from 9 to 25 times, compared to that of LEDs without a patterned structure, while the PL intensity of LED with PCOG was increased from 4.6 to 5.6 times. The electroluminescence output power of green LEDs with a PCWG was enhanced about two times compared to LEDs with a PCOG. These results suggest that the light extraction of green LEDs can be greatly increased by using PCWG instead of PCOG. [J1907]

"Novel optical method for background reduction in resonant photoacoustics"

We report a new way of reducing the background originated by window absorption in resonant photoacoustics. The technique employs a secondary light source that is absorbed by the window but not by the gas sample. This auxiliary source is modulated 180° apart from the one used to probe the gas. This way the window is heated almost uniformly during each cycle, thus lessening the associated background signal. We tested the scheme on a photoacoustic setup, conceived to measure NO_2 , which is excited by an array of blue light-emitting diodes. Another array of near-infrared, light-emitting diodes served as the secondary light source. With the addition of this canceling method, the detection limit was decreased to 4% of the previous reached without it. [J1908]

"Rotating sample holder at low temperature"

A low temperature rotary device (cryoturbine) for use in extended x-ray-absorption fine structure measurements in fluorescence mode has been designed and manufactured. The instrument works at a temperature close to liquid Nitrogen and can reach frequencies up to 100 Hz with good stability. The rotation speed is measured with a light-emitting diode driven in stroboscopic mode by a simple electronic circuit. [J1909]

"High-efficiency nondoped white organic light-emitting devices"

High-efficiency nondoped white organic light-emitting devices (WOLEDs) were demonstrated by using both the intrinsic and exciplex emissions from a single electroluminescent material, 4,4',4''-trispyrenylphenylamine (TPyPA). The simple device structure of indium tin oxide/N,N'-bis(1-naphthyl)-N,N'-diphenyl-1,1'-biphenyl-4,4'-diamine/TPyPA/4,7-diphenyl-1,10-phenanthroline/LiF/Al exhibited a luminance of 10000cd/m^2 at a low driving voltage of 4.5 V, and high current and power efficiencies of 9.4cd/A and 9.0lm/W , respectively. Such WOLED showed excellent color stability and purity with the Commission Internationale de L'Eclairage coordinates of (0.31, 0.35), which remained unchanged over a wide range of luminance from 100 to 20000cd/m^2 . [J1910]

"The influence of visible light on transparent zinc tin oxide thin film transistors"

The characteristics of transparent zinc tin oxide thin film transistors (TTFTs) upon illumination with visible light are reported. Generally, a reversible decrease of threshold voltage V_{th} , saturation field effect mobility μ_{sat} , and an increase of the off current are found. The time scale of the recovery in the dark is governed by the persistent photoconductivity in the semiconductor. Devices with tuned [Zn]:[Sn] ratio show a shift of V_{th} of less 2V upon illumination at 5mW/cm² (brightness 30000cd/m²) throughout the visible spectrum. These results demonstrate TTFTs which are candidates as pixel drivers in transparent active-matrix organic light emitting diode displays. [J1911]

"Near-infrared photoluminescence of erbium tris(8-hydroxyquinoline) spin-coated thin films induced by low coherence light sources"

The authors present the characterization of spin-coated erbium tris(8-hydroxyquinoline) (ErQ3) solution on glass substrates under high temperature conditions. Absorption and infrared photoluminescence, induced by laser and light emitting diode sources, were measured and compared to cast and evaporated ErQ3 samples. A broad absorption band and 1.52 μ m luminescence were observed, suggesting spin coating as a valid deposition technique for processing of organic infrared emitting diodes. [J1912]

"Combinatorial preparation and characterization of thin-film multilayer electro-optical devices"

In this article we present a setup for the combinatorial vapor deposition of thin-film multilayer devices as well as methods for the fast and efficient analytic screening of the libraries obtained. The preparation setup is based on a commercially available evaporation chamber equipped with various evaporation sources for both organic and metallic materials. The combinatorial approach is realized by the combination of a rotation stage for the substrate, a five-mask sampler, and an additional mask whose position can be deliberately varied along one axis during the evaporation process. The latter is used to evaporate linear as well as step gradients by continuous or stepwise movement of a shutter mask. The mask sampler allows to define the sectors of the library and to evaporate more complex structures, e.g., an electrode layout. Finally, the simultaneous evaporation of two or more materials enables us to produce layers of varying composition ratio in general and doped materials, in particular. For the control of the evaporation process we have developed an automation software, which is particularly helpful for complex library designs and which grants excellent repeatability of experiments. Efficient and fast characterization of the obtained libraries is realized by (i) a purely optical setup and (ii) an electro-optical setup. (i) The UV/vis reader FLASHScan® 530 permits to map out the UV/vis absorbance or fluorescence of the whole library. The UV/vis absorbance is primarily used to determine layer thicknesses and to confirm thickness uniformity across larger regions. The fluorescence measurements are used to determine the composition of layers containing fluorescent dyes. (ii) For a detailed short- and long-term electro-optical analysis we have developed an automated measurement system, which allows the characterization of 8480 optoelectronic devices and to study their degradation behavior. Both solar cells and organic light-emitting diodes can be tested. Finally, we have developed a data analysis software to extract characteristic values from the huge amount of data and with this facilitate the finding of systematic dependencies. [J1913]

"Noncontact simultaneous dual wavelength photoplethysmography: A further step toward noncontact pulse oximetry"

We present a camera-based device capable of capturing two photoplethysmographic (PPG) signals at two different wavelengths simultaneously, in a remote noncontact manner. The system comprises a complementary metal-oxide semiconductor camera and dual wavelength array of light emitting diodes (760 and 880nm). By alternately illuminating a region of tissue with each wavelength of light, and detecting the backscattered photons with the camera at a rate of 16 frames/wavelengths, two multiplexed PPG wave forms are simultaneously captured. This process is the basis of pulse oximetry, and we describe how, with the inclusion of a calibration procedure, this system could be used as a noncontact pulse oximeter to measure arterial oxygen saturation (SpO_2) remotely. Results from an experiment on ten subjects, exhibiting normal SpO_2 readings, that demonstrate the instrument's ability to capture signals from a range of subjects under realistic lighting and environmental conditions are presented. We compare the signals captured by the noncontact system to a conventional PPG signal captured concurrently from a finger, and show by means of a J. Bland and D. Altman [Lancet 327, 307 (1986); Statistician 32, 307 (1983)] test, the noncontact device to be comparable to a contact device as a monitor of heart rate. We highlight some considerations that should be made when using camera-based "integrative" sampling methods and demonstrate through simulation, the suitability of the captured PPG signals for application of existing pulse oximetry calibration procedures. [J1914]

"High speed single charge coupled device Cranz-Schardin camera"

This article describes an ultrahigh speed visualization system based on a miniaturization of the Cranz-Schardin principle. It uses a set of high power light emitting diodes (LEDs) (Golden Dragon) as the light source and a highly sensitive charge coupled device (CCD) camera for reception. Each LED is fired in sequence and images the refraction index variation between two relay lenses, on a partial region of a CCD image sensor. The originality of this system consists in achieving several images on a single CCD during a frame time. The number of images is 4. The time interval between successive firings determines the speed of the imaging system. This time lies from 100ns to 10 μ s. The light pulse duration lies from 100ns to 10 μ s. The principle and the optical and electronic parts of such a system are described. As an example, some images of acoustic waves propagating in water are presented. [J1915]

"Quantum random number generator based on photonic emission in semiconductors"

We report upon the realization of a novel fast nondeterministic random number generator whose randomness relies on the intrinsic randomness of the quantum physical processes of photonic emission in semiconductors and subsequent detection by the photoelectric effect. Timing information of detected photons is used to generate binary random digits-bits. The bit extraction method based on the restartable clock method theoretically eliminates both bias and autocorrelation while reaching efficiency of almost 0.5 bits per random event. A prototype has been built and statistically tested. [J1916]

"Evaluation of gas permeation barrier properties using electrical measurements of calcium degradation"

In this work, we developed a thin calcium degradation method introducing sensitive electrical resistance monitoring. We have demonstrated structural models of the inorganic/organic thin films to evaluate barrier properties against water and oxygen permeation. The time-dependent transmission curve of a multibarrier coated on both sides of the polyethersulfone substrate had a linear slope which was measured as 5.17 $\times 10^{-3}$ g/m² day at 20°C and 60% relative humidity. This system can measure an accurate permeation rate with a high sensitivity in the measurable range of 10⁻¹⁰–10⁻⁶ g/m² day. In addition, the test structure devised is applicable to various fabrication techniques for passivation layers with durability and ultralow permeability for flexible organic light emitting diodes. [J1917]

"Optical extinction monitor using cw cavity enhanced detection"

We present details of an apparatus capable of measuring optical extinction (i.e., scattering and/or absorption) with high precision and sensitivity. The apparatus employs one variant of cavity enhanced detection, specifically cavity attenuated phase shift spectroscopy, using a near-confocal arrangement of two high reflectivity ($R = 0.9999$) mirrors in tandem with an enclosed cell 26 cm in length, a light emitting diode (LED), and a vacuum photodiode detector. The square wave modulated light from the LED passes through the absorption cell and is detected as a distorted wave form which is characterized by a phase shift with respect to the initial modulation. The amount of that phase shift is a function of fixed instrument properties-cell length, mirror reflectivity, and modulation frequency-and of the presence of a scatterer or absorber (air, particles, trace gases, etc.) within the cell. The specific implementation reported here employs a blue LED; the wavelength and spectral bandpass of the measurement are defined by the use of an interference filter centered at 440 nm with a 20 nm wide bandpass. The monitor is enclosed within a standard 19 in. rack-mounted instrumentation box, weighs 10 kg, and uses 70 W of electrical power including a vacuum pump. Measurements of the phase shift induced by Rayleigh scattering from several gases (which range in extinction coefficient from 0.4–32 Mm⁻¹) exhibit a highly linear dependence ($r^2 = 0.99997$) when plotted as the cotangent of the phase shift versus the expected extinction. Using heterodyne demodulation techniques, we demonstrate a detection limit of 0.04 Mm⁻¹ (4×10^{-10} cm⁻¹) (2σ) in 10 s integration time and a base line drift of less than ± 0.1 Mm⁻¹ over a 24 h period. Detection limits decrease as the square root of integration time out to 150 s. [J1918]

"Quantum-confined Stark effects in the m-plane In_{0.15}Ga_{0.85}N/GaN multiple quantum well blue light-emitting diode fabricated on low defect density freestanding GaN substrate"

Quantum-confined Stark effects (QCSEs) in a polarization-free m-plane In_{0.15}Ga_{0.85}N/GaN multiple quantum well (MQW) blue light-emitting diode fabricated on the low defect density (DD) freestanding GaN substrate were investigated. The electroluminescence (EL) peak at 2.74 eV little shifted to the higher energy with the increase in current because of the absence of the polarization fields. The effective radiative lifetime increased and the nonradiative lifetime decreased with the increase in the junction field, and the results were quantitatively explained in terms of field-induced QCSE including tunneling escape of holes from the MQW. As a result of the use of the low DD substrate, the equivalent internal quantum efficiency, which was approximated as the

spectrally integrated EL intensity at 300K divided by that at 150K, of 43% was achieved. [J1919]

"Highly efficient white organic light-emitting diodes with single small molecular emitting material"

We demonstrate a highly efficient white organic light emitting device with fluorescent small molecule 4,4'-bis(9-(1-naphthyl)anthracene-10-yl)biphenyl (BUBH-3). With a simple device architecture of indium tin oxide/tris 4,4',4"-tris-N-naphthyl-N-phenylamino-triphenylamine (60nm)/N,N'-bis-(1-naphthyl)-N,N'-diphenyl-1,1'-biphenyl-4,4'-diamine (10nm)/BUBH-3 (45nm)/Alq3(15nm)/LiF(1nm)/Al(150nm), a white light with CIE_{x,y}color of (0.31,0.36) was generated. The device achieved one of the best single-emitting-material electroluminescence performance of white organic light-emitting devices with efficiencies of 7.0cd/A and 3.17lm/W at 6.9V. [J1920]

"On spectral and thermal behaviors of AlGaInP light-emitting diodes under pulse-width modulation"

Behavior of the emission spectrum, junction temperature, and charge carrier temperature of low-power AlGaInP light-emitting diodes (LEDs) with different colors under pulse-width-modulation (PWM) dimming is investigated. The blueshift of the peak wavelength and the bandwidth narrowing in the emission spectra of the studied LEDs with shortening pulse are found. A linear relation of the junction temperature and carrier temperature of the studied LEDs to their duty cycle is detected. Perceivable changes in color of AlGaInP LEDs under the PWM scheme are observed. [J1921]

"Efficiency droop behaviors of In Ga N /Ga N multiple-quantum-well light-emitting diodes with varying quantum well thickness"

InGaN/GaN multiple-quantum-well (MQW) light-emitting diodes with varied InGaN quantum well thicknesses are fabricated and characterized. The investigation of luminous efficiency versus current density reveals a variety of efficiency droop behaviors. It is found that the efficiency droop can be drastically reduced by increasing the quantum well thickness of the MQW structures. On the other hand, relative internal quantum efficiency (IQE) measurements indicate that a thinner well results to higher IQEs owing to the greater spatial overlap of electron and hole distribution functions. [J1922]

"Study of nonpolar m-plane In Ga N /Ga N multiquantum well light emitting diodes grown by homoepitaxial metal-organic chemical vapor deposition"

Nonpolar m-plane (1100)InGaN-based light emitting diodes (LEDs) grown on low-extended defect density bulk m-plane GaN substrates offer great potential for high performance devices due to the absence of polarization-related internal electric fields. To optimize the quantum well (QW) structure, systematic sets of near blue-ultraviolet LEDs using different well widths, barrier widths, and QW periods were packaged and tested. With increasing current, high power LEDs were realized with fairly flat external quantum efficiency and blueshift-free peak wavelength for QWs with thicknesses from 8 to 20 nm, barrier widths from 10 to 22 nm, and QW numbers from 4 to 10. [J1923]

"Origin of efficiency droop in GaN-based light-emitting diodes"

The efficiency droop in GaInN/GaN multiple-quantum well (MQW) light-emitting diodes is investigated. Measurements show that the efficiency droop, occurring under high injection conditions, is unrelated to junction temperature. Furthermore, the photoluminescence output as a function of excitation power shows no droop, indicating that the droop is not related to MQW efficiency but rather to the recombination of carriers outside the MQW region. Simulations show that polarization fields in the MQW and electron blocking layer enable the escape of electrons from the MQW region and thus are the physical origin of the droop. It is shown that through the use of proper quaternary AlGaInN compositions, polarization effects are reduced, thereby minimizing droop and improving efficiency. [J1924]

"Reproducible resistive switching in nonvolatile organic memories"

Resistive switching in nonvolatile, two terminal organic memories can be due to the presence of a native oxide layer at an aluminum electrode. Reproducible solid state memories can be realized by deliberately adding a thin sputtered Al₂O₃ layer to nominal electron-only, hole-only, and bipolar organic diodes. Before memory operation, the devices have to be formed at an electric field of 109 V/m, corresponding to soft breakdown of Al₂O₃. After forming, the structures show pronounced negative differential resistance and the local maximum in the current scales with the thickness of the oxide layer. The polymer acts as a current limiting series resistance. [J1925]

"Damage-free electrodes fabrication for top emitting organic light emitting diodes by transfer"

fabrication"

We report a simple procedure for the integration of the top emitting organic light emitting diode (TOLED), which permits minimum defects at the interface between a top metal electrode and an organic film. This method relies on the transfer of patterned metal electrodes to an organic substrate with a relatively high adhesive property. TOLED, integrated by the transfer fabrication, demonstrates better performance, a reduction of turn-on voltage and an increase of maximum current efficiency, in comparison with fabricated devices by conventional shadow mask method. [J1926]

"Formation and reduction of pyramidal hillocks on m-plane {11 00} GaN"

Surface morphology and hillock reduction were studied on m-plane {1100}n-type GaN films and light emitting diode structures grown by metal organic chemical vapor deposition on low defect-density m-plane GaN substrates. For nominally on-axis m-plane films, predominantly pyramidal hillocks were observed, which were composed of two faces symmetrically inclined by 0.1° - 0.25° to the $\pm[1120]$ direction and two faces inclined by 0.5° - 0.95° to the $[0001]$ c- and the $[0001]$ c+ directions, respectively. All faces of the pyramidal hillocks for the nominally on-axis GaN films had clearly defined step-terrace structures. Gradual changes in nominal miscut angles from 0° to 10° along the a and the c-directions succeeded in a continuous hillock reduction yielding atomically flat surfaces. [J1927]

"Very thin photoalignment films for liquid crystalline conjugated polymers: Application to polarized light-emitting diodes"

Photoaligned polyimide films with different film thicknesses were prepared on quartz substrates, and uniaxially aligned glassy poly(9,9-dioctylfluorenyl-2,7-diyl) (PFO) layers were formed on top. The photoluminescence polarization ratio of the PFO layer rapidly increased with increasing polyimide film thickness, and beyond a thickness of 1.6 nm, it was saturated at 11. This result shows that the 1.6-nm-thick photoaligned polyimide film works as a good alignment layer for PFO. We succeeded in fabricating a polarized light-emitting diode with a polarization ratio of 29 at 459 nm and a brightness of 700 cd/m² by using a 2.8-nm-thick polyimide photoalignment layer. [J1928]

"Low efficiency roll off at high current densities in Ir-complex based electrophosphorescence diode with exciton diffusing and fluorescence compensating layers"

We demonstrate a fac-tris(2-phenylpyridine) iridium-based electrophosphorescent organic green-light emitting diode with a considerably reduced current-efficiency roll off at high current density. Such a low roll off of efficiency was achieved by inserting nondoped 4,4'-N,N'-dicarbazole-biphenyl (CBP) layer and a tris-(8-hydroxy-quinoline) aluminum (Alq3) layer between the emitting and electron-transporting layers to diffuse excitons from the emitting layer. The Alq3 layer is found to contribute as a complementary green fluorescent emitter at high current density. Thus, only a small decrease from 20.7 to 16.7 cd/A was detected in current efficiency when the current density increases from 3.9 to 100 mA/cm². A high current efficiency of 12.6 cd/A was achieved even at 350 mA/cm², indicating that the efficiency roll off was drastically reduced when compared with the device without CBP and Alq3 layers. [J1929]

"Polarization of light emission by 460 nm Ga In N /Ga N light-emitting diodes grown on (0001) oriented sapphire substrates"

Measurements on the polarization of top- and side-emitted light as a function of direction are performed for 460 nm GaInN unpackaged and packaged light-emitting diode (LED) chips with a multiquantum well (MQW) GaInN/GaN active region grown on (0001) oriented sapphire substrates. Side emission is found to be highly polarized with the electric field in the plane of the MQW. Intensity ratios for in-plane to normal-to-plane polarization reach values as high as 7:1, while the total intensity for the in-plane polarization is more than twice as large compared to the normal-to-plane polarization. Despite these measured polarization characteristics, conventional packaged LEDs are found to be virtually unpolarized due to packaging. [J1930]

"A comprehensive study of the effect of reactive end groups on the charge carrier transport within polymerized and nonpolymerized liquid crystals"

Polymerizable liquid crystalline semiconductors, referred to as reactive mesogens (RMs), consist of π -conjugated cores with reactive end groups decoupled by an aliphatic spacer. These can be polymerized within the mesophase, maintaining the self-assembled morphology and charge transport characteristics. The polymerized films can then be used in organic electronic applications such as charge transport layers in organic light emitting diodes and field effect transistors. We present a systematic study of the effect of reactive end

groups on charge transport in calamitic liquid crystals (RMs) using the time-of-flight technique. Several different compounds were synthesized with a variation in both the liquid crystal (LC) mesogenic core group and the functional end groups. The reactive end groups in most cases affect the mesophase charge transport compared to the nonreactive LC mesophase transport. This manifests itself as a reduction in mobility, varying from a factor of 4 in the best case to as large as two orders of magnitude. In the best systems studied, however, the reactive end group effect on the transport, compared to the nonreactive mesophase transport, is negligible. Polymerized reactive mesogens do maintain long-range transport, with comparable mobilities to those of the phase in which they were polymerized over a broad temperature range, including room temperature. The hole and electron mobilities found in polymerized systems are explored using the Holstein small polaron model in the nonadiabatic limit, yielding the relevant polaron binding energies and bandwidths, and using the Bassler Gaussian disorder model, yielding the relevant energetic disorder parameters. [J1931]

"Anomalous excitation dependence of electroluminescence in In Ga N /Ga N light-emitting diodes"

We have systematically investigated the anomalous excitation dependence of the electroluminescence (EL) in InGaN/GaN multiple-quantum-well light-emitting diodes over a temperature range from 300 to 20 K. Initially, an increase in the emission intensity occurred upon decreasing the temperature, until a maximum was reached at the temperature T_m . A blueshift in the position of the EL peak was followed by a redshift that occurred at the crossover temperature T_c . Both of these characteristic temperatures correlate with the presence of statistic microbarriers arising from potential inhomogeneity. The higher the In content incorporated into the heterobarriers, named multiple quantum barriers, the lower the values of T_m and T_c obtained from the spectral observations; this phenomenon implies an augmentation in the microscopic nonradiative transport through the microbarriers. An increase in the injection current also led to decreases in both of these characteristic temperatures. In addition, a functional correlation exists between the values of T_c and T_m . All of these experimental results suggest that InGaN/GaN microstructures can be viewed as disordered collections of InGaN nanocrystallites. Further experimental verification will be necessary if this phenomenological model is to be used to account for the properties of any other disorderlike heteromaterials. [J1932]

"Kelvin probe force and surface photovoltage microscopy observation of minority holes leaked from active region of working In Ga As /Al Ga As /Ga As laser diode"

A method for direct observation of carrier leakage from active regions of working semiconductor light-emitting diodes and lasers is suggested. In this method, Kelvin probe force and surface photovoltage microscopies are used to measure local changes in the surface potential of the device mirror on which a high concentration of the leaked carriers is expected. The applicability of the method is demonstrated by studying in detail the leakage current on the mirrors of high-power InGaAs/AlGaAs/GaAs laser diodes in action. It is shown that minority holes arrive at the mirror surface from the active zone of the laser and spread over to regions of the emitter and substrate. This observation is confirmed by exposing the mirror to external light with photon energy exceeding the band gap of the laser structure and measuring the generated surface photovoltage. Owing to surface channels formed by the surface band bending, the holes can move tens of micrometers from the place of their generation. The leakage currents are evaluated on the basis of the surface potential distributions observed. It is found that as the injection current of the laser increases, the leakage current grows until onset of lasing. [J1933]

"Operational degradation of organic light-emitting diodes: Mechanism and identification of chemical products"

Despite the importance of the operational lifetime of organic light-emitting diodes (OLEDs) in practical applications, little is known about the nature of chemical reactions associated with efficiency losses during operation. To gain an insight into a chemical mechanism of operational degradation, we studied operation-induced changes in chemical compositions of fluorescent and phosphorescent OLEDs utilizing carbazole derivatives in emissive layers. We detected substantial losses of the emissive components, including the carbazole-derived host 4,4'-bis(N-carbazolyl)biphenyl (CBP) and, if present, phosphorescent dopant. Several different materials were found only in the degraded OLEDs, and some of them were isolated and identified by nuclear magnetic resonance and mass spectrometry. A similar set of products was found upon UV irradiation of CBP films. Structures of degradation products suggest that the key step in operational degradation of OLEDs is homolytic cleavage of weaker bonds, e.g., an exocyclic C-N bond in CBP, in the excited state, followed by radical addition reactions to yield stabilized pi radicals. Overall, OLED operation leads to the accumulation of the neutral radical species and their reduced or oxidized forms, acting as nonradiative recombination centers and luminescence quenchers. [J1934]

"Photoreflectance symmetry and amplitude study of quantum dots in microcavity light emitting"

diode structure: The cavity-ground state exciton resonance"

A quantum dot (QD) microcavity emitting around 1.3μm at room temperature is studied by photoreflectance (PR) and photoluminescence. The temperature dependence of the PR spectra line shape and amplitude allows determining the tuning condition of the quantum dot ground state transition with the cavity mode. Our study suggests a way to find the exciton energy when the distinct QD features are hidden by the broadening of the QD dielectric function in combination with the relatively narrow cavity-mode width. [J1935]

"Structural analysis of strained p -type Al Ga N /Ga N superlattice"

We investigated the nanostructure of AlGa_N/Ga_Nstrained-layer superlattice (SLS) cladding in the GaN-based violet laser diode (LD) and the AlInGa_N-based ultraviolet (UV) light emitting diode (LED) with a scanning transmission electron microscope (STEM). In the p-SLS cladding, comprising 34 pairs of p-Al_{0.1}Ga_{0.9}N/p-GaN:Mg layers in the GaN-based LD, the Al_{0.1}Ga_{0.9}N and GaN layers were distinguished as dark and bright bands 6nm wide in the high-angle annular dark-field (HAADF) STEM images. Threading dislocations (TDs) were observed. Among TDs that came from the underlying layer, some run outside through the SLS, and the others disappeared within the SLS, which discloses a role of the SLS in suppressing defect propagation. A HAADF-STEM image of the TD with a dark line along the center of a bright contour was found. The dark line, which was darker than the surrounding matrix, is striking. One of the probable explanations for the dark line that may be considered is local segregation of light atoms (Mg or Al) in Cottrell atmosphere around the dislocation core. In the HAADF-STEM image of the UV LED wafer, the AlInGa_N and AlInGa_N:Si layers in the MQW were definitely resolved, appearing as dark and bright bands. HAADF-STEM also distinguished between the AlGa_N and GaN layers in the p-SLS cladding in the UV LED wafer. [J1936]

"Ultraviolet semiconductor laser diodes on bulk AlN"

Current-injection ultraviolet lasers are demonstrated on low-dislocation-density bulk AlN substrates. The AlGaInN heterostructures were grown by metalorganic chemical vapor deposition. Requisite smooth surface morphologies were obtained by growing on near-c-plane AlN substrates, with a nominal off-axis orientation of less than 0.5°. Lasing was obtained from gain-guided laser diodes with uncoated facets and cavity lengths ranging from 200 to 1500 μm. Threshold current densities as low as 13 kA/cm² were achieved for laser emission wavelengths as short as 368 nm, under pulsed operation. The maximum light output power was near 300 mW with a differential quantum efficiency of 6.7%. This (first) demonstration of nitride laser diodes on bulk AlN substrates suggests the feasibility of using such substrates to realize nitride laser diodes emitting from the near to deep ultraviolet spectral regions. [J1937]

"Millisecond radiative recombination in poly(phenylene vinylene)-based light-emitting diodes from transient electroluminescence"

The current and electroluminescence transient responses of standard poly(phenylene vinylene)-based light-emitting devices have been investigated. The electroluminescence time response is longer (milliseconds scale) than the current switch-off time by more than one order of magnitude, in the case of small area devices (0.1 cm²). For large area devices (6 cm²) the electroluminescence decay time decreases from 1.45 ms to 100 μs with increasing bias voltage. The fast current decay limits the electroluminescence decay at higher voltages. Several approaches are discussed to interpret the observed slow decrease of electroluminescence after turning off the bias. One relies upon the Langevin-type bimolecular recombination kinetics which is governed by the minority carriers (electrons), and another focuses on the slow release of trapped electrons as possible explanations. Additionally, we show that the device current density is mainly determined by the transport of the fastest carriers (holes). [J1938]

"Photoluminescence decay time and electroluminescence of p-Si /β -FeSi₂ particles /n-Si and p-Si /β -FeSi₂ film /n-Si double-heterostructures light-emitting diodes grown by molecular-beam epitaxy"

We have epitaxially grown Si/β -FeSi₂/Si(SFS) structures with β -FeSi₂ particles on Si(001), and SFS structures with β -FeSi₂ continuous films on both Si(001) and Si(111) substrates by molecular-beam epitaxy. All the samples exhibited the same photoluminescence (PL) peak wavelength of approximately 1.54 μm at low temperatures. However, the PL decay times for the 1.54 μm emission were different, showing that the luminescence originated from different sources. The decay curves of the SFS structures with β -FeSi₂ continuous films were fitted assuming a two-component model, with a short decay time (τ₁ = 10 ns) and a long decay time (τ₂ = 100 ns), regardless of substrate surface orientation. The short decay time was comparable to that obtained in the SFS structure with β -FeSi₂ particles. The short decay time was due to carrier recombination in β -FeSi₂, whereas the long decay time was probably due to a defect-related D1 line in Si.

We obtained 1.6 mcd/electroluminescence (EL) at a low current density of 2 A/cm² up to around room temperature. The temperature dependence of the EL peak energy of the SFS diodes with β -FeSi₂ particles can be fitted well by the semiempirical Varshni's law. However, EL peak positions of the SFS diodes with the β -FeSi₂ films showed anomalous temperature dependence; they shifted to a higher energy with increasing temperature, and then decreased. These results indicate that the EL emission originated from several transitions. [J1939]

"Combination of a polyaniline anode and doped charge transport layers for high-efficiency organic light emitting diodes"

Up to now, most organic light emitting diodes (OLEDs) have utilized inorganic materials as transport anodes. In this study, we show that conductive polymers are suitable for this purpose as well. Polyaniline anodes, with a conductivity of 200 S/cm, are used to inject holes into the adjacent organic layers. Due to electrical doping of the electron and hole transport layer with an intrinsic emission layer sandwiched in between (pin-OLED), the devices reach high luminance at low voltage. The phosphorescent emitters Ir(MDQ)₂(acac) and Ir(ppy)₃, as well as the fluorescent emitter Spiro-DPVBi, are implemented within pin-OLEDs using a polyaniline anode. By the use of different host materials, a green double-emitting OLED is demonstrated and compared to the corresponding single emission layer device. Furthermore, a white OLED combining fluorescent and phosphorescent emitting layers is presented, reaching 8.9 lm/W at 1000 cd/m². The results demonstrate an efficient charge carrier injection from the polymer into the p-type doped hole transport layer, leading to good power efficiencies of the OLEDs. [J1940]

"Improved performance in organic light emitting diodes with a mixed electron donor-acceptor film involved in hole injection"

Organic light emitting diodes using a mixed layer of electron acceptor 3, 4, 9, 10 perylene-tetracarboxylic dianhydride and electron donor copper phthalocyanine (PTCDA:CuPc) on indium tin oxide (ITO) anodes were fabricated. The device properties were found to be strongly dependent on the thickness of the PTCDA:CuPc film: both the power efficiency and the driving voltage of the device were optimized with a thickness of PTCDA:CuPc ranging from 10 to 20 nm. As compared to the conventional ITO/CuPc hole injection structure, the ITO/PTCDA:CuPc hole injection structure could remarkably enhance both the luminance and the power efficiencies of devices. A mechanism of static-induced, very efficient hole-electron pairs generation in mixed PTCDA:CuPc films was proposed to explain the experimental phenomena. The structural and optical properties of PTCDA:CuPc film were examined as well. [J1941]

"Emission mechanism in organic light-emitting devices comprising a europium complex as emitter and an electron transporting material as host"

The emission mechanism in organic light-emitting devices, where the emission layer is composed of Eu(DBM)3pyzphen (DBM = Dibenzoylmethane, pyzphen = pyrazino-[2,3-f][1,10]-phenanthroline) doped into electron transporting/hole blocking material BPhen (4,7-diphenyl-1, 10-phenanthroline), is investigated. Energy transfer and carrier trapping simultaneously exist in the luminescence process, and carrier trapping is a main process. Direct carrier trapping by Eu(DBM)3pyzphen molecules is confirmed by the difference of electroluminescence and photoluminescence spectra as well as J-V characteristics. Efficient Foster and Dexter energy transfer from BPhen to Eu(DBM)3pyzphen molecules were speculated in terms of analysis of photoluminescence spectra of fixed solutions, triplet energies, and phosphorescent lifetimes. Based on these mechanisms, the overall performances of these devices were improved. High efficiencies were obtained under carrier trapping by Eu(DBM)3pyzphen molecules, and the emission of BPhen was eliminated by efficient energy transfer from the BPhen to Eu(DBM)3pyzphen molecules. [J1942]

"Photoelectron spectrum from a thin organic layer exposed to intense x rays"

When an organic layer on a conducting substrate is exposed to intense x rays, such as in scanning photoelectron microscopy (SPEM), the photoelectron spectrum for the exposed area shows a kinetic energy shift towards higher binding energy due to the accumulation of local charges. We present experimental evidence that in the thin organic layer of approximately 100 nm thickness in organic light-emitting devices, there exists an unshifted spectral component besides the local-charging-shifted spectral component. This finding enabled us to reliably investigate the chemical structures of organic layers using SPEM, which was shown to be advantageous in obtaining the space-resolved chemical structural information of a specimen. [J1943]

"The carrier-trapping effect of dye doped in Alq"

The electroluminescence (EL) of an organic light-emitting diode specially fabricated with a pure thin dye layer 4-

(dicyanomethylene)-2-t-butyl-6(1,1,7,7-tetramethyljulolidyl-9-enyl)-4H-pyran (DCJTB) of 1-nm thickness inserted at the interface between N,N'-bis-(1-naphthyl)-diphenyl-1,1'-biphenyl-4,4'-diamine and tris(8-quinolinolato) aluminum has been investigated. The EL behavior of this device changed dramatically at a driving voltage of about 12.25V, which has been ascribed to the breakage of the thin DCJTB layer. It is suggested that not only such thin layer of DCJTB can transport electrons and holes, but also trap them. A comparison of the EL performance with four other devices confirms this mechanism. Therefore, the high efficiency and long life of the dye doped Alq devices are attributed to the hole and electron trapping effect and the high photoluminescence efficiency of the dye. [J1944]

"A conceptual model of light coupling by pillar diffraction gratings"

Diffraction structures such as pillar gratings are a promising way of coupling light into or out of thin semiconductor devices, for applications in thin film solar cells and light-emitting diodes. In this paper we show that the diffuse transmittance behavior of pillar gratings can be understood using the concept of grating mode interference and that the optimum heights of the grating and an estimate of the optimum period can be predicted with the effective index method. Furthermore, the method also gives good results for structures outside the range for which it was derived, including circular pillars and quasiperiodic structures. We also show that pillar gratings offer substantially improved performance over groove gratings for thin film silicon solar cells. [J1945]

"Improving the stability of organic light-emitting devices by using a hole-injection-tunable-anode-buffer-layer"

Introducing a hole-injection-tunable-anode-buffer-layer (HITABL) at the indium tin oxide anode contact of an organic light-emitting device can finely tune hole injection to establish proper charge balance, thus remarkably improves its operational stability. The HITABL consists of two sublayers: (i) an 2.5nm thick metal (e.g., Ca, Mg, or Ag) sublayer and (ii) an 10nm thick tetrafluorotetracyanoquinodimethane (F4TCNQ)doped N'-di(naphthalene-1-yl)-N,N'-diphenyl-benzidine sublayer. Hole injection can be tuned by changing (i) the metal in the first sublayer and/or (ii) the concentration of the F4TCNQ dopant in the second sublayer. The choice of the metal used in the first sublayer and/or the concentration of F4TCNQ in the second sublayer affect the hole-injection efficiency. Therefore, by using the HITABL, one can make the necessary diminutive adjustments to the hole injection of a device and achieve proper charge balance, resulting in a significant improvement in operational stability. [J1946]

"Enhanced thermal stability in organic light-emitting diodes through nanocomposite buffer layers at the anode/organic interface"

The effect of doped buffer layers at the anode/organic interface in small molecule organic light-emitting diodes was investigated. Appropriate doping of N,N'-bis(1-naphthyl)-N,N'-diphenyl-1,1'-biphenyl-4,4'-diamine (NPB) and Cu-phthalocyanine (CuPc) layers using LiF or C60 molecules leads to improved interfacial morphology and thermal stability for both standard indium tin oxide or metals anodes, such as Au and Ag. Graded interfaces remain stable at temperatures well above the hole transport layer (i.e., NPB) glass transition temperature. [J1947]

"Improved performances of organic light-emitting diodes with metal oxide as anode buffer"

We demonstrate extremely stable and highly efficient organic light-emitting diodes (OLEDs) based on molybdenum oxide (MoO₃) as a buffer layer on indium tin oxide (ITO). The significant features of MoO₃ as a buffer layer are that the OLEDs show low operational voltage, high electroluminescence (EL) efficiency and good stability in a wide range of MoO₃ thickness. A green OLED with structure of ITO/MoO₃/N,N'-di(naphthalene-1-yl)-N,N'-diphenyl-benzidine (NPB)/NPB: tris(8-hydroxyquinoline) aluminum (Alq₃):10-(2-benzothiazolyl)-2,3,6,7-tetrahydro-1,1,7,7-tetramethyl-1H, 5H, 11H-(1)-benzopyrroprano(6,7-8-i,j)quinolizin-11-one (C545T)/Alq₃/LiF/Al shows a long lifetime of over 50000h at 100cd/m² initial luminance, and the power efficiency reaches 15lm/W. The turn-on voltage is 2.4V, and the operational voltage at 1000cd/m² luminance is only 6.9V. The significant enhancement of the EL performance is attributed to the improvement of hole injection and interface stability at anode. [J1948]

"Space charge layers in organic field-effect transistors with Gaussian or exponential semiconductor density of states"

Space charge layers (SCLs) in metal-insulator-semiconductor (MIS) structures are critical for the operation of field-effect transistors (FETs). For many organic semiconductors, transport takes place as hopping in Gaussian or exponentially distributed states. However, existing theoretical descriptions of a SCL and advanced device simulation programs suppose a density of states other than a Gaussian or an exponential, employing often the

nondegenerate limit for the concentrations. We present results of a simulation study for the MIS structure as the basic module of the FET and for a thin semiconducting layer on a metal substrate. The second system was extensively investigated by photoelectron spectroscopy to characterize the metal-organics interface occurring at the source/drain contact of FETs and as anode and cathode in organic light emitting diodes. For broader distributions, the densities deviate strongly from the nondegenerate limit which leads indeed in a MIS structure to a strong deviation of the dependence of the surface electric field (and, hence, the areal charge) on the surface potential. However, as one can control only the gate voltage directly, the dependency on this quantity determines device operation. For the variations of the layer thickness and gate insulator thickness, and doping in the wide range of interest, this dependency deviates only slightly from the nondegenerate approximation, essentially in the depletion region by a flatband voltage shift. In the accumulation region, which is determinative for FET operation, the remaining deviation can be removed almost perfectly by considering this flatband voltage shift. For the thin organic layer on a metal substrate, numerical simulations confirm the applicability of an analytical approximation for band bending and floating potential [G. Paasch et al, J. Appl. Phys. 93, 6084 (2003)] for the nondegenerate case and for the exponential distribution. Indeed, for small barriers at the interface, a band bending of up to the order of 100 meV can occur within the first 2 nm near the interface. In the interpretation of photoemission data such contribution will appear as part of the measured interface dipole. [J1949]

"Improvements of external quantum efficiency of InGaN-based blue light-emitting diodes at high current density using GaN substrates"

InGaN-based blue light-emitting diodes (LEDs) with different quantum well (QW) thicknesses were grown on freestanding GaN substrates with low threading dislocation densities (TDDs) and on c-plane sapphire substrates. In the case of thin QWs of 3nm thickness, the external quantum efficiencies (EQEs) of LEDs on GaN substrates, as well as those on sapphire substrates, decreased with increasing forward current, indicating that carrier localization is in play on both types of substrates. For thicker 5-nm-thick QWs, the EQEs of LEDs grown on GaN substrates improved at high current densities, while those on sapphire substrates decreased even at low current densities. The LED with 5-nm-thick QWs on the GaN substrate mounted p-side down and molded with epoxy showed EQE as high as 26% at 125A/cm². Cathodoluminescence observations of the active layers on GaN substrates revealed that the expansion of nonradiative areas related to TDDs, which are responsible for the deterioration of the EQE of the LED on the sapphire substrate, had been suppressed. [J1950]

"Enhancement in the efficiency of light emission from silicon by a thin Al₂O₃ surface-passivating layer grown by atomic layer deposition at low temperature"

Thin Al₂O₃ surface-passivating layers grown by atomic layer deposition at 100°C were demonstrated to be instrumental in producing efficient light emission from silicon. External quantum efficiency up to 1.34·10⁻⁴ was observed from silicon metal-insulator-semiconductor light-emitting diodes with a 5nm Al₂O₃ surface-passivating layer as the insulator, which is more than tenfold that from similar devices with a 5nm SiO₂ insulator layer thermally oxidized at 1000°C. Anomalous temperature dependences of the photoluminescence intensities and spectra at low temperatures indicate the presence of bound excitonic traps at the Al₂O₃/Si interface. The enhanced light emission may be attributed to the temporary capture of excitons by the interfacial bound excitonic traps, which effectively reduces nonradiative recombination. [J1951]

"Fabry-Perot effects in In Ga N /Ga N heterostructures on Si-substrate"

A strong intensity modulation is found in spatially and angular resolved photoluminescence spectra of InGaN/GaN heterostructures and quantum wells epitaxially grown on Si(111) substrates. This Fabry-Perot effect results from the high refractive index contrasts at the GaN/Si and the Air/InGaN interfaces. It can be used for a wavelength stabilization of the sample upon temperature change and, e.g., in the case of light emitting diodes, to additionally reduce the blueshift at increasing injection currents. A simple geometric approach has been chosen to calculate the influence of layer thickness, absorption and refractive indices, as well as detection angle. The cavity can be described quantitatively by a simple three layer Fabry-Perot model. An analytical expression is derived for the external luminescence line shape. Microphotoluminescence measurements at samples with the silicon substrate locally removed corroborate the model. [J1952]

"Electrical and optical simulation of organic light-emitting devices with fluorescent dopant in the emitting layer"

A complete model for the quantitative simulation of electrical and optical characteristics for organic light-emitting devices with fluorescent dopant in the host is presented. This simulation model consists of three parts: charged carrier transport model, exciton model, and emission and optical model. In the first part, we include not only charge carrier trapping but also direct carrier recombination phenomena on the fluorescent dopant. In the second

part, Forster [Discuss. Faraday Soc. 27, 7 (1959)] energy transfer from the host molecule to the dopant molecule is included in exciton model. In addition, the quenching phenomena related to dopant concentration and electrode are also considered in this study. In the optical model, the thin-film optics is applied to calculate the interference effect of the device. Results for several multilayer devices with different fluorescent dopant concentrations are presented. On the basis of the experimental data of a typical doped device, we have found good agreement between the simulation results and the experimental data. [J1953]

"Luminescence properties of blue $\text{La}_{1-x}\text{Ce}_x\text{Al}(\text{Si}_{6-z}\text{Al}_z)(\text{N}_{10-z}\text{O}_z)(z=1)$ oxynitride phosphors and their application in white light-emitting diode"

This letter reports blue oxynitride phosphors of $\text{La}_{1-x}\text{Ce}_x\text{Al}(\text{Si}_{6-z}\text{Al}_z)(\text{N}_{10-z}\text{O}_z)(z=1)$ (termed JEM crystal phase) and their application for the white light-emitting diodes (LEDs). The JEM phosphor can be excited by 405nm light efficiently, and its spectrum can be tuned widely by changing the Ce concentration. The emission spectrum of this phosphor is as wide as 110nm full width at half maximum, which is convenient to solid state lighting. The preparation of white LED was attempted by using a 405nm InGaN chip and oxynitride phosphors in this work. High color rendering index 95 was achieved in white LED with various correlated color temperatures, indicating the suitability of the JEM phosphor in solid-state lightings. [J1954]

"Vertical organic light emitting transistor"

The authors demonstrate a vertical organic light emitting transistor achieved by stacking a capacitor on top of an organic light emitting diode (OLED). This unique device has dual functions, emitting light as an OLED and switching current as a transistor. When the capacitor is under bias, the storage charges on the thin electrode shared by two cells modulate the charge injection of the OLED active cell, hence controlling the current flow and subsequently tuning the light emission. Due to the vertical integration, this device can be operated at low voltage, which provides a solution for OLED display applications. [J1955]

"Polarization engineering via staggered InGaN quantum wells for radiative efficiency enhancement of light emitting diodes"

Staggered InGaN quantum wells (QWs) grown by metal-organic chemical vapor deposition are demonstrated as improved active region for visible light emitters. Theoretical studies indicate that InGaN QW with step-function-like In content in the quantum well offers significantly improved radiative recombination rate and optical gain in comparison to the conventional type-I InGaN QW. Experimental results of light emitting diode (LED) structure utilizing staggered InGaN QW show good agreement with theory. Polarization band engineering via staggered InGaN quantum well allows enhancement of radiative recombination rate, leading to the improvement of photoluminescence intensity and LED output power. [J1956]

"Fabrication of two-dimensional photonic crystal patterns on GaN-based light-emitting diodes using thermally curable monomer-based nanoimprint lithography"

The fabrication process of photonic crystals in a p-GaN layer was established to improve the light extraction efficiency of light-emitting diodes (LEDs) by using nanoimprint lithography and inductively coupled plasma (ICP) etching process. Due to low etch selectivity of imprinted pattern, Cr mask patterns were lifted-off from the p-GaN surface and ICP etch process was followed using SiCl_4 -based plasma. As a result, two-dimensional pillar array patterns were uniformly fabricated on the p-GaN layer and the photoluminescence intensity of the photonic crystal patterned LED was increased by 2.6 fold compared to that of the same LED sample without photonic crystal patterns. [J1957]

"Temperature-insensitive photonic crystal fiber interferometer for absolute strain sensing"

The authors report a highly sensitive ($\sim 2.8\text{pm}/\mu\text{m}$ epsilon) wavelength-encoded strain sensor made from a piece of photonic crystal fiber (PCF) spliced to standard fibers. The authors intentionally collapse the PCF air holes over a short region to enlarge the propagating mode of the lead-in fiber which allows the coupling of only two modes in the PCF. The transmission spectrum of the interferometer is stable and sinusoidal over a broad wavelength range. The sensor exhibits linear response to strain over a large measurement range, its temperature sensitivity is very low, and for its interrogation a battery-operated light emitting diode and a miniature spectrometer are sufficient. [J1958]

"Improving carrier transport and light emission in a silicon-nanocrystal based MOS light-emitting diode on silicon nanopillar array"

A silicon-nanocrystal (nc-Si) based metal-oxide-semiconductor light-emitting diode (MOSLED) on Si nanopillar array with size, height, and density of 30nm, 350nm, and $2.84 \times 10^{10} \text{cm}^{-2}$, respectively, is characterized. The nanopillar roughened Si surface contributes to the improved turn-on characteristics by enhancing Fowler-Nordheim tunneling and reducing effective barrier height, providing the MOSLED a maximum optical power of $0.7 \mu\text{W}$ obtained at biased current of $375 \mu\text{A}$. The optical intensity, turn-on current, and power-current slope of nc-Si MOSLED on high-aspect-ratio Si nanopillar array are $140 \mu\text{W/cm}^2$, $5 \mu\text{A}$, $2 \pm 0.8 \text{mW/A}$, respectively. A maximum external quantum efficiency of 0.1% is reported. [J1959]

"Organic light-emitting diodes with structured cathode"

Organic light-emitting diode (OLED) devices were fabricated with a structured polymer-cathode interface. The devices have a layered structure indium tin oxide/poly(3,4-ethylenedioxythiophene):poly(styrene sulfonate)/poly(2-methoxy-5-[(2'-ethylhexyl)oxy]-p-phenylenevinylene)/Al. The light-emitting polymer layers were patterned via a stamp imprinting process, followed by vapor deposition of the cathode. Devices employing the structured cathode showed improved electron injection and increased brightness when compared to conventional flat cathode devices. Electrostatic modeling of the structured cathode geometry revealed localized increase in electric field leading to enhanced electron tunneling through the polymer-cathode interface. Thus, improved OLED performance was demonstrated from cathode microstructuring. [J1960]

"Transparent organic light-emitting diodes using resonant tunneling double barrier structures"

A semitransparent cathode of indium tin oxide (ITO)/Ag/ITO was developed as a resonant tunneling double barrier structure for transparent organic light-emitting diodes. A weak negative differential resistance was observed in devices using a 100nm thick ITO/Ag/ITO layer as a cathode in combination with a thin LiF/Al layer. The current injection of devices was dominated by resonant tunneling, which induced no luminance at low voltage. This was achieved by employing an e-beam evaporated ITO/Ag/ITO cathode due to the double quantum barriers of ITO and the quantum well of Ag. The authors also applied the multilayer cathode to small molecule devices, which showed the same resonant tunneling currents. [J1961]

"Small molecule based and solution processed highly efficient red electrophosphorescent organic light emitting devices"

The authors report the very high luminous efficiency in solution processed red electrophosphorescent organic light emitting devices using small molecular host and guest materials. The maximum luminous efficiency reached 12.7cd/A , corresponding to external quantum efficiency of 15.1%, with its emission peak wavelength of 620nm and the Commission Internationale de l'Eclairage coordinates of (0.65, 0.33). Along with these excellent performances of the solution processed device, which were comparable to those of the vacuum deposited counterpart device with similar structure and materials, the comparative study on both devices suggests the merits of the solution process adopting robust small molecular materials only. [J1962]

"High brightness stable white and yellow light-emitting diodes from ambipolar polyspirofluorenes with high charge carrier mobility"

We have used two polyspirofluorenes, spirodiethylhexyloxy polyfluorene (spiro-diEHPF) and triphenylamine-grafted spirodiethylhexyloxy polyfluorene (spiro-TPA50-diEHPF), which exhibit rather high charge mobilities in the order of 10^{-3} - $10^{-4} \text{cm}^2/\text{Vs}$. The light-emitting devices with rubrene-doped spiro-diEHPF show maximal luminances of $36\,000$ and $70\,000 \text{cd/m}^2$ with maximal efficiencies 3.5 and 9cd/A for the white and yellow emissions, respectively. For rubrene-doped triphenylamine-grafted polymer, spiro-TPA50-diEHPF, the maximal luminances and efficiencies are $56\,000 \text{cd/m}^2$ and 9cd/A for white-emitting devices and $72\,000 \text{cd/m}^2$ and 14cd/A for yellow emission. Furthermore, the electroluminescence profiles of the investigated devices show nearly independent of the applied voltages. [J1963]

"Current injection and transport in polyfluorene"

A comprehensive numerical model is established for the electrical processes in a sandwich organic semiconductor device with high carrier injection barrier. The charge injection at the anode interface with 0.8eV energy barrier is dominated by the hopping among the gap states of the semiconductor caused by disorders. The Ohmic behavior at low voltage is demonstrated to be not due to the background doping but the filaments formed by conductive clusters. In bipolar devices with low work function cathode it is shown that near the anode the electron traps significantly enhance hole injection through Fowler-Nordheim tunneling, resulting in rapid increases of the hole carrier and current in comparison with the hole-only devices. [J1964]

"Crystal growth and properties of LiAlO₂ and nonpolar GaN on LiAlO₂ substrate"

In this study, the growth and properties of LiAlO₂ material and a nonpolar GaN-based light-emitting-diode (LED) structure on LiAlO₂ have been investigated. The LiAlO₂ material is grown by the Czochralski pulling technique and is used as a substrate for nonpolar nitride growth. An improved surface roughness can be obtained by a four-step polishing process. With subsequent nitridation treatment, a pure M-plane (101₀)GaN can be obtained. An electron microscope shows an abundance of cracks that are oriented parallel to the (001) and (100) planes of the LiAlO₂ substrate on the rear surface of GaN. The absence of the polarization-induced electric field of a GaN-based LED structure on LiAlO₂ was shown by using photoluminescence measurements. Therefore, this approach is promising to further increase the luminescence performance of GaN-based LEDs. [J1965]

"Blue electroluminescent properties of poly(N-arylcarbazole-2,7-ylene) homopolymers"

To investigate electroluminescence behaviors of a series of poly(N-phenyl-2,7-carbazole)s having 2-ethylhexyloxy (PEHOC), triethylene oxide (PTEOC), or diphenylamino (PDPAC) group at the N-phenyl portion, single-layer devices of organic light-emitting diode using the as-prepared polymer as the emitting layer material were fabricated. All the devices showed brightness above 1000 cd/m² at 10 V with moderate luminous efficiencies. The PEHOC (m, p-disubstituted) and PTEOC (p-substituted) devices exhibited a trivial but undesirable redshift due to electro-oxidation and aggregation of the polymer under high driving voltages, while the PDPAC (m-substituted) device displayed a blue electroluminescence [$\lambda_{\text{max}}=450\text{ nm}$ and CIE (x,y)=0.159,0.173] which had no difference compared with the photoluminescence spectrum. [J1966]

"Recombination dynamics in ultraviolet light-emitting diodes with Si-doped Al_xGa_{1-x}N/Al_yGa_{1-y}N multiple quantum well active regions"

Ultraviolet (UV) light-emitting diodes with Al_xGa_{1-x}N/Al_yGa_{1-y}N multiple quantum well active regions, doped in the barriers with different Si doping levels, show a sharp near-band edge emission line (UV luminescence). Some samples have a broad subband gap emission band centered at about 500 nm (green luminescence) in addition to the near-band edge emission. The electroluminescence intensities of the UV and green emission line are studied as a function of the injection current. For the sample grown on the AlN substrate under optimized growth conditions, the UV luminescence intensity increases linearly with the injection current, following a power law with an exponent of 1.0, while the green luminescence intensity increases sublinearly with the injection current. On the contrary, the samples grown on the sapphire substrate show a superlinear (to the power of 2.0) and linear (to the power of 1.0) dependence on the injection current for the UV and green luminescence, respectively. A theoretical model is proposed to explain the relationship between the luminescence intensities and the injection current. The results obtained from the model are in excellent agreement with the experimental results. The model provides a method to evaluate the dominant recombination process by measuring the exponent of the power-law dependence. [J1967]

"Cathodoluminescence characterization of organic semiconductor materials for light emitting device applications"

We report the development of a cathodoluminescence-based characterization technique for the investigation of organic semiconductor materials for organic light emitting device (OLED) applications. While photoluminescence is known to predominantly address singlet exciton excitation and recombination processes, cathodoluminescence is able to simultaneously probe singlet and triplet exciton dynamics which is of importance for electroluminescence. Especially, in the case of the so-called triplet harvester materials, the generation of triplet excitons during cathodoluminescence opens the way for materials characterization without device fabrication. The paper (i) shows how cathodoluminescence can be applied for the characterization of organic semiconductor materials, (ii) points out the general measurement factors, (iii) discusses the special features of cathodoluminescence, electroluminescence as well as photoluminescence spectra, and (iv) outlines the potential of cathodoluminescence by presenting a brief study of a triplet harvester material systems. Main emphasis is put on the presentation of the characterization tool to partly replace the necessity of OLED fabrication. For that reason widely used conjugated polymers and small molecule semiconductor systems have been selected. [J1968]

"Comprehensive analysis and optimal design of top-emitting organic light-emitting devices"

We present an accurate analysis of light emission in top-emitting organic light-emitting devices (TOLEDs) by explicitly considering the Purcell effect. TOLEDs are optimized separately for maximum zero-degree luminance, maximum electroluminescence (EL) efficiency, and wide viewing angle with high EL efficiency. For fluorescent material with an internal quantum efficiency (η_{int0}) of 0.25, the maximum zero-degree luminance and EL efficiency can be achieved by locating the emitters around the first antinode of the microcavity while for

phosphorescent material with $\eta_{\text{int}}=1.0$, the maximum zero-degree luminance and EL efficiency are around the second antinode. Through relaxing the efficiency by 10%-20%, the angular intensity distribution can be even better than the Lambertian distribution; meanwhile, the color shows only a small variation over an angle range of 150°. Our results, which are in good agreement with experiments, show that the Purcell effect on TOLED performances is significant and should be carefully examined in studying TOLEDs. [J1969]

"Sr 3 B 2 O 6 :Ce 3+ ,Eu 2+ : A potential single-phased white-emitting borate phosphor for ultraviolet light-emitting diodes"

The Ce³⁺/Eu²⁺+coactivated Sr₃B₂O₆phosphors exhibit varied hues from blue through white and eventually to yellow-orange by resonance-type energy transfer from Ce³⁺to Eu²⁺and tuning the relative proportion of Ce³⁺/Eu²⁺properly. The authors have demonstrated that electric dipole-dipole interaction dominates the energy transfer mechanism in Sr₃B₂O₆:Ce³⁺,Eu²⁺phosphor, and the critical distance of energy transfer has been estimated to be about 30Eby both spectral overlap and concentration quenching methods. They have also shown that under the excitation of UV radiation, white light is generated by coupling 434 and 574nmemission bands attributed to Ce³⁺and Eu²⁺radiations, respectively. [J1970]

"Relationship between host energy levels and device performances of phosphorescent organic light-emitting diodes with triplet mixed host emitting structure"

Green phosphorescent organic light-emitting diodes (PHOLEDs) with a triplet mixed host emitting layer were developed and device performances were studied by changing host materials in light-emitting layer. Power efficiency of green PHOLEDs could be improved from 12.7to29.1lm/Wby using triplet mixed host emitting layer. Combination of hole-transport-type host with good hole injection properties and electron-transport-type host with good electron injection properties was effective to get high efficiency in triplet mixed host devices. [J1971]

"Luminescence properties of Tb 3+ -Sm 3+ codoped glasses for white light emitting diodes"

Photoluminescence properties of silicate and borosilicate glasses codoped with Tb³⁺and Sm³⁺ions have been characterized by excitation and emission spectroscopies. When excited by ultraviolet light the glasses emit a combination of green and orange-red wavelengths giving white light. The ratio of the intensities of orange-red to green emissions can be tuned by varying both the concentration of the Sm³⁺ion and an the composition of the glass matrix. The excitation and emission spectra show a self-quenching effect for the Sm³⁺ions and an energy transfer from Tb³⁺(⁵D₄)to Sm³⁺(⁴G_{5/2}). [J1972]

"Chemical structure of the bilayer Ag /Li 2 O cathode interface in organic light emitting diodes"

The chemical structure of the interface between Ag with Li₂Oand tri(8-hydroxyquinoline) aluminum (Alq) was investigated by using in situ characterization of x-ray photoelectron spectroscopy (XPS) and ultraviolet photoelectron spectroscopy (UPS). Li₂Oon Ag had lower barrier height than LiF on Ag. XPS and UPS results show the interaction between Li₂Oand Alq leads to gap state formation in highest occupied molecular orbital of Alq. Efficient bottom-emitting devices employing such a cathode scheme have been demonstrated. [J1973]

"Soft-x-ray spectroscopy experiment of liquids"

The authors show an experimental setup to carry out soft-x-ray fluorescence spectroscopy of liquids under an ultrahigh vacuum (UHV) condition. The flow liquid cell has a window to attain compatibility with UHV conditions of the fluorescence spectrometer and synchrotron radiation beamline. The soft-x-ray photons enter the liquid cell through a 100nmthick silicon nitride window, and the emitted soft x rays exit through the same window to be detected by photon diode and microchannel plate detectors. This setup allows liquids and, in particular, liquid-solid interfaces to be studied. Such a liquid cell has been used to study the electronic structure of a variety of systems ranging from water solutions of inorganic salts and nanomaterials under wet conditions. [J1974]

"Electrical properties of organic light-emitting diodes by indium tin oxide chemical-mechanical polishing process"

In this study, the optimum process parameters and the influences of their process parameters were investigated for indium tin oxide chemical-mechanical polishing (ITO-CMP) with a sufficient removal amount and good planarity. Next, the organic light-emitting display (OLED) device with the structure of glass/ITO/poly[2-methoxy-5-(2-ethylhexyloxy)-p-phenylenevinylene]/Al using a polished ITO surface as a bottom electrode (anode) was fabricated. The electrical characteristics, such as sheet resistance and current-voltage (I-V)relationship, are discussed in order to evaluate the possibility of the CMP application for an OLED device using an ITO film. The surface morphology and I-Vcharacteristics of ITO thin film were improved after the CMP process using optimized

process parameters compared to that of the as-deposited thin film before the CMP process. [J1975]

"Influence of low temperature thermal annealing on the performance of microcrystalline silicon thin-film transistors"

Top-gate staggered microcrystalline silicon thin-film transistors (μ c-Si:HTFTs) were prepared by plasma enhanced chemical vapor deposition at temperatures below 200°C. The μ c-Si:HTFTs exhibit high effective electron mobilities (device mobilities) of up to 35 cm²/Vs for long channel devices. Due to the high carrier mobility μ c-Si:HTFTs are promising devices for large area electronics such as organic light-emitting diode displays or radio frequency identification devices. The fabrication process of the μ c-Si:HTFTs is similar to the fabrication process of amorphous silicon thin-film transistors, which facilitates an easy transfer of the technology to industry. In this paper, the influence of postfabrication low temperature thermal annealing (150°C) on the device properties of top-gate staggered μ c-Si:HTFTs is investigated. Low temperature thermal annealing reduces the device threshold voltage and subthreshold slope. Furthermore, the annealing step results in an increase of the effective mobility for long channel transistors, whereas the effective mobility for short channel transistors is reduced. The influence of the postfabrication low temperature thermal annealing on the device performances will be discussed in detail. [J1976]

"Largely variable electroluminescence efficiency with current and temperature in a blue (In, Ga)N multiple-quantum-well diode"

Electroluminescence (EL) efficiency of a blue In_{0.3}Ga_{0.7}N multiple-quantum-well diode has been investigated as a function of current between 0.001 and 20 mA at various temperatures (20-300 K). The low-temperature EL quenching previously observed below 100 K at a driving current of 20 mA does not occur at 0.001 mA and is found to be strongly dependent on the current level. Largely variable temperature-dependent EL quantum efficiency with current suggests that the injected carrier capture efficiency by radiative recombination centers plays a decisive role for determination of the EL efficiency under the forward bias condition. [J1977]

"Effect of facet angle on effective facet reflectivity and operating characteristics of quantum dot edge emitting lasers and superluminescent light-emitting diodes"

The authors report the creation of low reflectivity angled facets by focused-ion-beam postfabrication etching. A method to directly measure the effective facet reflectivity of such facets, utilizing gain saturation effects in the quantum dots is described. The reflectivities of the angled facets are shown to decrease by increasing the facet angle from 0° to 15°. With a reflectivity of 1/40-6 obtained for a facet with a 15° angle, allowing quantum dot superluminescent light-emitting diodes to be fabricated. The use of different angled facets to control the emission wavelength of both quantum dot lasers and superluminescent light-emitting diodes is outlined. [J1978]

"CO₂ laser rapid-thermal-annealing SiO_x based metal-oxide-semiconductor light emitting diode"

Structural damage enhanced near-infrared electroluminescence (EL) of a metal-oxide-semiconductor light emitting diode (MOSLED) made on SiO_x film with buried nanocrystallite Si after CO₂ laser rapid thermal annealing (RTA) at an optimized intensity of 6 kW/cm² for 1 ms is demonstrated. CO₂ laser RTA induced oxygen-related defects are capable of improving Fowler-Nordheim tunneling mechanism of carriers at metal/SiO_x interface. The CO₂ laser RTA SiO_x film reduces Fowler-Nordheim tunneling threshold to 1.8 MV/cm, facilitating an enhanced EL power of an indium tin oxide/SiO_x/p-Si/AlMOSLED up to 50 nW at a current density of 2.3 mA/cm². [J1979]

"Use of ZnO thin films as sacrificial templates for metal organic vapor phase epitaxy and chemical lift-off of GaN"

Continued development of GaN-based light emitting diodes is being hampered by constraints imposed by current non-native substrates. ZnO is a promising alternative substrate but it decomposes under the conditions used in conventional GaN metal organic vapor phase epitaxy (MOVPE). In this work, GaN was grown on ZnO/c-Al₂O₃ using low temperature/pressure MOVPE with N₂ as a carrier and dimethylhydrazine as a N source. Characterization confirmed the epitaxial growth of GaN. The GaN was lifted-off the c-Al₂O₃ by chemically etching away the ZnO underlayer. This approach opens up the way for bonding of the GaN onto a support of choice. [J1980]

"231-261 nm AlGaIn deep-ultraviolet light-emitting diodes fabricated on AlN multilayer buffers grown by ammonia pulse-flow method on sapphire"

The authors demonstrated AlGaIn multiquantum-well (MQW) deep-ultraviolet light-emitting diodes (LEDs) with

wavelengths in the range of 231-261nm, fabricated on low threading dislocation density AlN buffers formed through an ammonia (NH₃) pulse-flow multilayer growth technique. The authors obtained a single-peaked operation of the AlGaIn-MQW LED with a wavelength of 231nm, which is the shortest wavelength of AlGaIn-based LED on sapphire. The maximum output power and external quantum efficiency of the 261 and 231nm LEDs were 1.65mW and 0.23% under room-temperature (RT) continuous-wave (cw) operation, and approximately 5mW and 0.001% under RT pulsed operation, respectively. [J1981]

"Deep saturation of junction voltage at large forward current of light-emitting diodes"

The dependences of series resistance, ideality factor, and junction voltage of light-emitting diodes (LEDs) on applied voltage or current were characterized accurately using alternating current (ac) behavior combined with I-V plot (acI-V method). The deep saturation of junction voltage and simultaneous decrease of ideality factor of LEDs at large forward current, which imply the pinning of quasi-Fermi levels, were observed. Comparing with our recent study of the similar phenomenon of laser diodes, in which the junction voltage jumps abruptly to a saturated value at lasing threshold, the changes of junction voltage of LEDs are gradual. In addition, the decrease of series resistance with the increasing current and the negative capacitance effect of LEDs were also investigated. [J1982]

"Growth condition dependence of spin-polarized electroluminescence in Fe/MgO/light-emitting diodes"

We compared the electroluminescence (EL) polarization of two Fe/MgO/light-emitting-diode (LED) structures grown at different substrate temperatures for MgO growth: room temperature and 400°C. Two spin-LED wafers were prepared on molecular beam epitaxy grown LEDs by e-beam evaporation: one was LED/MgO (RT)/Fe (RT)/Au cap (RT), and the other was LED/MgO (400°C)/Fe (150°C)/Au cap (90°C). Spin-polarized EL was clearly observed in the latter sample, while the EL polarization was hardly observed in the former sample. The reasons for the near absence of EL polarization in the former sample are considered to be the degradation of the tunneling junction resulting from the crystallinity and the As-rich surface of the LED. [J1983]

"Enhanced light emission from phosphorescent single-layered organic light-emitting devices doped with ionic salt by simultaneous thermal and electrical annealing"

We studied the effect of thermal and electrical annealing on the light emission of phosphorescent single-layered organic light-emitting devices (PHOLEDs) doped with ionic salt. From the annealed green PHOLEDs with only an Al cathode, we clearly observed homogeneous and enhanced electrophosphorescent emission over 50000cd/m². The efficiency of the device was also improved. The device operates at relatively low voltages and achieves a high peak current efficiency of over 30cd/A, even at 1000cd/m². These improved characteristics regarding luminescence and efficiency indicate clearly that simultaneous annealing can induce proper adsorption of charged salt ions at the electrode surfaces. This adsorption will lead to an increased and balanced injection of carriers. [J1984]

"Light output improvement of InGaIn ultraviolet light-emitting diodes by using wet-etched stripe-patterned sapphire substrates"

GaN-based epilayers are grown on wet-etched stripe-patterned sapphire substrates, with stripes along the sapphire and sapphire directions, for 400nm ultraviolet light-emitting diodes (LEDs). The effects of the etching depth and stripe orientation on the structural and optical properties of the GaN layer as well as on the LEDs are investigated. Much better material quality and light output power are obtained when the GaN and the LEDs are grown on a 0.9μm deep patterned sapphire substrate with stripes along the sapphire direction. Stripe-orientation dependent growth modes accounting for the observed experimental results are proposed. [J1985]

"Recent progress in solution processable organic light emitting devices"

Organic light emitting devices (OLEDs) have been the subject of intense research because of their potential for flat panel display and solid state lighting applications. While small molecule OLEDs with very high efficiencies have been demonstrated, solution processable devices are more desirable for large size flat panel display and solid state applications because they are compatible with low cost, large area roll-to-roll manufacturing process. In this review paper, we will present the recent progress made in solution processable OLEDs. The paper will be divided into three parts. In the first part of the paper, we will focus on the recent development of fluorescent polymer OLEDs based on conjugated polyfluorene copolymers. Specifically, we will present results of carrier transport and injection measurements, and discuss how the charge transport and injection properties affect the device performance. In the second part of the paper, we will focus on the recent progress on phosphorescent

dye-dispersed nonconjugated polymer OLEDs. Specifically, we will present our recent results on high efficiency green and blue emitting devices based on the dye-dispersed polymer approach. Similar to fluorescent conjugated polymer OLEDs, charge transport and injection properties in dye-dispersed polymer OLEDs also play an important role in the device performance. In the third part of this paper, we will present our results on white emitting phosphorescent OLEDs. Two approaches have been used to demonstrate white emitting OLEDs. First, white emitting OLEDs were made using blue emitting OLEDs with downconversion phosphors. Second, white emitting OLEDs were made by dispersing red, green, and blue phosphorescent dyes into the light emitting layer. High efficiency devices have been demonstrated with both approaches. [J1986]

"Polysilane based organic light emitting diodes: Simultaneous ultraviolet and visible emission"

While most organic light emitting diodes are designed to emit in the visible region, we report a series of polysilane based diodes for developing ultraviolet emitters at room temperature. These reported devices can also be controlled to simultaneously emit both ultraviolet and visible light, very close to the equienergy white point [Commission Internationale de l'Eclairage coordinate (0.33,0.33)]. Furthermore, the color coordinate of the visible emission is independent of the applied voltage. Therefore, the reported polysilane organic light emitting diodes can also be used as a white light source in which the ultraviolet emission from the same device provides an opportunity to modulate the color. While the origin of ultraviolet emission in electroluminescence is ascribed to an excitonic emission from the σ - σ^* transition, consistent with its presence in the photoluminescence spectrum, we assign visible emission to defects states, based on degradation studies of the electroluminescent device. [J1987]

"Fabrication of organic light-emitting diode pixels by laser-assisted forward transfer"

Fabrication of a polymer light-emitting device was achieved by a laser forward transfer technique using the decomposition of a thin triazene polymer film by a XeCl excimer laser. The dry deposition process allows transfer of a bilayer consisting of the electroluminescent polymer poly[2-methoxy-5-(2-ethylhexyloxy)-1,4-phenylenevinylene] covered with an aluminum electrode onto a receiver substrate. The soft transfer results in laterally well resolved pixels ($\approx 500\text{nm}$), whose fluorescence as well as electroluminescence spectra remain unaltered. The rectifying and smooth current-voltage characteristics add to the merits of this laser-based transfer method that opens up the possibility of direct-writing heat- and UV-sensitive materials. [J1988]

"Enhanced luminescence of SrSi_2O_7 :Eu²⁺ phosphors by codoping with Ce³⁺, Mn²⁺, and Dy³⁺ ions"

The authors report here the enhanced luminescence properties of SrSi_2O_7 doped with Eu and M (M=Ce, Dy, and Mn). The Eu and Eu, Mn-codoped powders were prepared by a solid state reaction at temperatures between 1400 and 1600°C under $\text{H}_2(25\%)-\text{N}_2(75\%)$ atmosphere. The Eu, M-codoped $\text{Sr}_{1-x}\text{ySi}_2\text{O}_7$ phosphors have the monoclinic structure with lattice parameters $a = 15.6\text{\AA}$, $b = 16.2\text{\AA}$, $c = 9.4\text{\AA}$, and $\beta = 91^\circ$. The phosphors can be efficiently excited in the UV to visible region, making them attractive as conversion phosphors for a light emitting diode application. A green-yellow emission was observed for Eu, M-codoped $\text{Sr}_{1-x}\text{ySi}_2\text{O}_7$. The addition of Mn in the Eu site in SrSi_2O_7 remarkably enhances the luminescent intensity by the factor of 144%, 148%, and 168% for Ce, Dy, and Mn, respectively. [J1989]

"Balanced charge injection in multilayer polymer light-emitting diode with water soluble nonconjugated polymer dispersed by ionic compounds"

The authors have fabricated highly efficient polymeric light-emitting diode (PLED) from ionic compound dispersed water soluble nonconjugated polymer, polyurethane (PU), which was used as an ultrathin hole blocking and electron injection layer (HB-EIL) on the top of commercially available blue-emitting polymer, polyfluorene. The device with HB-EIL showed a maximum quantum efficiency of 1.7%, while the one without HB-EIL showed an efficiency of 0.6%. They propose that the better performance in PLED with PU layer was due to a well balanced charge injection in emitting layer after the enhanced electron injection due to ionic compound in the insulating PU layer. [J1990]

"Reduced injection current induced blueshift in an InGaN/GaN quantum-well light-emitting diode of prestrained growth"

The authors demonstrate the smaller blueshift in increasing injection current level of an InGaN/GaN quantum-well (QW) light-emitting diode (LED) of a longer electroluminescence (EL) peak wavelength based on the prestrained growth technique when compared with the result of a LED of a shorter EL peak wavelength based on the conventional growth technique. The smaller blueshift can be attributed to more contribution to light emission from

the deeper QWs of higher indium contents when the injection current level is increased in the prestrain sample. It can also be attributed to the stronger carrier localization because of the stronger composition clustering in the prestrain sample of higher indium contents. Carrier localization can reduce the influences of the quantum-confined Stark effect and its screening process. [J1991]

"Interfacial electronic structure of N,N'-bis(1-naphthyl)-N,N'-diphenyl-1,1'-biphenyl-4,4'-diamine/copper phthalocyanine:C 60 composite/Au studied by ultraviolet photoemission spectroscopy"

The interfacial electronic structures of N,N'-bis(1-naphthyl)-N,N'-diphenyl-1,1'-biphenyl-4,4'-diamine (NPB)/copper phthalocyanine (CuPc)/Au, NPB/C60/Au, and NPB/CuPc:C60composite/Au were investigated by in situ ultraviolet photoelectron spectroscopy to understand the highly efficient hole injection in organic light-emitting diode. The hole-injection barrier of CuPc:C60/Au was 0.52 eV, while those of CuPc/Au and C60/Au were 0.96 and 1.62 eV, respectively. The lowered injection barrier is attributed to the smaller interface dipole of CuPc:C60 compared to that of pristine CuPc. This small interface dipole pulled up the highest occupied molecular orbital of CuPc in composite, which results in the decreased hole-injection barrier. [J1992]

"2.5λ microcavity InGaN light-emitting diodes fabricated by a selective dry-etch thinning process"

The authors report on InGaN microcavity light-emitting diodes with an effective thickness of 450 nm at the emission wavelength of 415 nm. The starting material for the flip-chip laser lift-off device is a structure with an active region embedding six InGaN/GaN quantum wells, 60-nm-thick AlGaIn, and a GaN template grown on a c-plane sapphire substrate. High-precision control of the final microcavity thickness was facilitated by SF₆-based selective inductively coupled plasma etching on the flipped material with an etch rate of ≥5:1 for GaN:Al_xGa_{1-x}N, where x ≥ 0.15. Pronounced microcavity effects were observed by angular measurements, in agreement with the theoretical cavity-mode dispersion characteristics. [J1993]

"High efficient and low color-temperature white light-emitting diodes with Tb₃Al₅O₁₂:Ce³⁺ phosphor"

High efficient Tb₃Al₅O₁₂:Ce³⁺ (TAG:Ce³⁺) phosphors were prepared in a solid-state reaction method with various fluxes. The results show that addition of proper flux can decrease the phase-forming temperature of the TAG crystals and improve the morphology as well as enhance the photoluminescence of the phosphors greatly. High efficient and low color-temperature white light-emitting diodes (WLEDs) were fabricated with the TAG:Ce³⁺ phosphor. Good performances of the WLEDs indicate that a mixture of H₃BO₃ and LiF is an excellent flux for synthesis of TAG:0.04Ce³⁺ phosphor and is beneficial to the fabrication of high efficient WLEDs. [J1994]

"Investigation of the transient symmetric H state in a pi cell"

The so-called symmetric H(H_s) state has been reported to have submillisecond response times, which results from the symmetric profile of the liquid crystal director; however, no direct evidence has been obtained to show the profile symmetry. The difficulty in proving this symmetric structure by direct observation results from the short lifetime of H_s state (typically around a few tens of milliseconds). In the work reported here, the authors utilize a burst driving method along with stroboscopic illumination from blue and red light emitting diodes to capture conoscopic images for the H_s director profile; these showed good agreement with their modeling. [J1995]

"Highly efficient p-i-n -type organic light emitting diodes on ZnO:Al substrates"

Aluminum doped zinc oxide (ZAO) is presented in this letter as an alternative transparent electrode: optimized ZAO films offer excellent parameters for organic light emitting diodes (OLEDs). The ZAO films are applied to various p-i-n-type OLEDs. By using green phosphorescent molecules in a double emitter structure, very high efficiencies were obtained, namely, 54.6 cd/A and 61.5 lm/W for 100 cd/m² at 2.78 V. Additionally, white OLEDs on ZAO demonstrated pure white emission independent of the luminance and high efficiencies of 12.6 cd/A and 14.5 lm/W for 100 cd/m² at 2.6 V, which is comparable to indium-tin-oxide based white OLEDs. [J1996]

"Surface plasmon leakage in its coupling with an InGaN/GaN quantum well through an Ohmic contact"

The authors demonstrate the leakage of surface plasmon (SP) through the Ohmic contact of either p-type or n-type GaN layer in the coupling process between SP and an InGaN/GaN quantum well (QW). It is shown that the photoluminescence (PL) intensity is significantly reduced when an Ohmic contact is formed, in contrast to the

case of significant PL enhancement when an insulating thin layer is applied between the doped semiconductor and metal. The observation implies that, in using the SP-QW coupling for enhancing emission in a light-emitting diode, the metals for Ohmic contact and SP generation must be isolated from each other. A thin dielectric interlayer in the region for SP-QW coupling is useful for avoiding the leakage of SP energy. [J1997]

"Improving polymer light-emitting diodes efficiency using interlayers based on cross-linkable polymers"

The efficiency of light-emitting diodes based on poly[(2-methoxy)-5-(2'-ethyl-hexyloxy)-1,4-phenylenevinylene] increases upon formation of interlayers, on top of poly(3,4-ethylenedioxythiophene) doped with polystyrene sulfonic acid (PEDOT:PSS), made of acid-initiated cross-linkable polyfluorenes. The use of this type of polymers allows for the formation of thicker interlayers leading to higher efficiencies when comparing with similar devices with interlayers formed by the parent non-cross-linkable polymers. This efficiency increase is attributed to a combination of electron and exciton confinement away from PEDOT:PSS. [J1998]

"The role of magnetic fields on the transport and efficiency of aluminum tris(8-hydroxyquinoline) based organic light emitting diodes"

Magnetoresistance and efficiency measurements of aluminum tris(8-hydroxyquinoline) (Alq3) based organic light emitting diode structures have been made as a function of magnetic field and Alq3 thickness. Both positive and negative magnetoresistances can be observed depending on the thickness of the Alq3 layer, the drive voltage, and the applied field. In all devices, large increases in device efficiency are observed. We suggest that the increase in device efficiency is due to conversion of triplet states into singlets through a hyperfine scale interaction. The changes in the magnetoresistance are a result of the reduction in the triplet concentration and operate either through the reduced role of free carrier trapping at triplet states or through the reduction in triplet dissociation at the cathode interface depending on the Alq3 thickness. [J1999]

"In-plane magnetic anisotropies of sputtered Co 0.7 Fe 0.3 films on AlGaAs(001) spin light emitting diode heterostructures"

The in-plane magnetic properties of Co_{0.7}Fe_{0.3} films sputtered onto Al_{0.1}Ga_{0.9}As and Al_{0.1}Ga_{0.9}As/GaAs epilayers are consistent with a strongly oriented bcc crystal structure with clean metal-semiconductor interfaces. However, the interface induced uniaxial magnetic anisotropy is oriented along one of the in-plane, rather than, as is the case in molecular beam epitaxy-grown films. Resonant x-ray measurements show interfacial magnetic disorder in films on Al_{0.1}Ga_{0.9}As, which accounts for the difference in magnetic anisotropy behavior between samples on Al_{0.1}Ga_{0.9}As and Al_{0.1}Ga_{0.9}As/GaAs epilayer substrates, and which may have significant consequences for the spin-injection efficiency across such interfaces. [J2000]

"Charge carriers at organic heterojunction interface: Exciplex emission or electroplex emission?"

We report the electroluminescence (EL) of organic heterojunction devices based on N,N'-diphenyl-N,N'-bis(3-methylphenyl)-(1,1'-biphenyl)-4,4'-diamine (TPD) and 2-(4'-biphenyl)-5-(4"-tert-butylphenyl)-1,3,4-oxadiazole (PBD). Besides monomolecular emissions from TPD, there are two additional EL peaks at around 460 and 480 nm from the bilayer device indium tin oxide (ITO)/TPD(100 nm)/PBD(45 nm)/Al. Our experimental data confirmed that the EL emission maximized at around 460 nm is from electroplex as the result of charge carriers cross recombination at the TPD/PBD interface and the EL emission maximized at around 480 nm originates from (TPD*PBD)-type exciplex. [J2001]

"A conceptual model of the diffuse transmittance of lamellar diffraction gratings on solar cells"

Diffraction gratings are effective ways of increasing the light absorption of solar cells and the light extraction of light-emitting diodes. In this paper, we show that simplified modal analysis can be used as a conceptual model for understanding the behavior of the diffuse transmittance of lamellar diffraction gratings on infinite substrates. We use simplified modal analysis to predict the optimum values of period and height for the gratings, and achieve excellent agreement with rigorous coupled wave analysis. Furthermore, we show that for thin film solar cells with front surface gratings and flat rear reflectors, modal analysis can be used to predict the optimum parameters for maximum light trapping. [J2002]

"Nonequilibrium transport of charge carriers and transient electroluminescence in organic light-emitting diodes"

An analytic theory of nonequilibrium hopping charge transport in disordered organic materials includes

quasiequilibrium (normal) and extremely nonequilibrium (dispersive) regimes as limiting cases at long and short times, respectively. In the intermediate interval of time quasiequilibrium value of mobility is nearly established while the coefficient of field-assisted diffusion continues to increase (quasidispersive regime). Therefore, normalized time dependencies of transient current in time-of-flight (TOF) conditions are practically independent of field strength and sample thickness, in good agreement both with data of TOF experiments for molecularly doped polymers and results of numerical simulations of Gaussian disorder model. An analytic model of transient electroluminescence (TEL) is developed on the base of the mentioned theory. Strong asymmetry of mobilities is presumed. In analogy with TOF transients, dispersion parameter of normalized TEL intensity is anomalously large and almost field independent in the quasidispersive regime of transport. The method for determination of mobility from TEL data is proposed. [J2003]

"Light emission from an ambipolar semiconducting polymer field effect transistor: Analysis of the device physics"

Light emitting field-effect transistors (LEFETs) were fabricated with a low work function metal (calcium) and a high work function metal (gold) as the source and drain electrodes. The gold electrode serves as the source for holes into the pi band and the drain for electrons from the pi *band; the calcium electrode serves as the source for electrons into the pi *band and the drain for holes from the pi band. For 65V V_G 103V, the LEFET operates in the ambipolar regime. The emission zone has been spatially resolved (as it is moved across the channel by sweeping the gate voltage) using confocal microscopy; the full width at half maximum is 2mcm. At the gate voltage extremes ($V_G=0$ or $V_G=150$ V), the electron (hole) density extends all the way across the 16mcm channel such that the electron (hole) accumulation layer functions as the cathode (anode) for a light-emitting diode, with opposite carrier injection by tunneling; i.e., the carrier densities are sufficiently high that the accumulation layer functions as a low resistance contact, implying near metallic transport. [J2004]

"Surface plasmon enhanced silicon solar cells"

Thin-film solar cells have the potential to significantly decrease the cost of photovoltaics. Light trapping is particularly critical in such thin-film crystalline silicon solar cells in order to increase light absorption and hence cell efficiency. In this article we investigate the suitability of localized surface plasmons on silver nanoparticles for enhancing the absorbance of silicon solar cells. We find that surface plasmons can increase the spectral response of thin-film cells over almost the entire solar spectrum. At wavelengths close to the band gap of Si we observe a significant enhancement of the absorption for both thin-film and wafer-based structures. We report a sevenfold enhancement for wafer-based cells at $\lambda = 1200$ nm and up to 16-fold enhancement at $\lambda = 1050$ nm for 1.25 mcm thin silicon-on-insulator (SOI) cells, and compare the results with a theoretical dipole-waveguide model. We also report a close to 12-fold enhancement in the electroluminescence from ultrathin SOI light-emitting diodes and investigate the effect of varying the particle size on that enhancement. [J2005]

"The influence of subgap features in the electromodulation and built-in voltage measurements of polyfluorene blue light-emitting diodes with anodic charge injection layers"

We report on electroabsorption (EA) and built-in voltage (VBI) measurements of polymer light-emitting diodes with the general structure ITO/PEDOT:PSS/emitting polymer/LiF/Ca/Al where ITO is indium tin oxide, PEDOT:PSS is poly(3,4-ethylene dioxythiophene) doped with poly(styrene sulfonate), and the emitting polymer is either poly(9,9-dioctylfluorene), poly(9,9-dioctyl-fluorene-alt-bis-N,N'-(4-butyl-phenyl)-bis-N,N'-phenyl-1,4-phenylenediamine), or poly(9,9-dioctylfluorene-alt-N-(4-butylphenyl)-diphenylamine). We find that the EA nulling voltage, i.e., the dc bias at which the EA signal vanishes, depends on the frequency of the ac voltage and on the incident photon wavelength. Such dependence poses a problem for accurate measurement of the built-in voltage (VBI), which is the voltage generated between the electrodes upon equilibration of the Fermi levels through the heterostructure. We find that the EA signal is mixed with a smaller intensity signal which can be ascribed to excited state absorption (ESA). We propose a method for separating the excited state absorption signal and producing accurate VBI measurements. We also demonstrate that in our devices the ESA contribution to the electromodulated ($\Delta T/T$) signal is negligible with respect to the accuracy with which VBI can be determined from the nulling voltage of $\Delta T/T$ and can thus be safely ignored. [J2006]

"Mode dynamics of high power (InAl)GaN based laser diodes grown on bulk GaN substrate"

Time resolved scanning near-field optical microscopy was employed to study spatial and temporal dynamics of III-nitride-system-based blue light emitting laser diodes with a ridge width of 20 mcm deposited on high pressure grown bulk GaN substrate. Devices were driven in a pulse regime with a current pulse length of 500 ns. Temperature effects and fluctuation in carrier concentration resulted in a complicated dynamic picture of the photon field evolution. The guided modes did not reach a stable form during a driving pulse. Due to a large

antiguinding factor which is characteristic for nitride compounds, filamentation processes were clearly observable leading to the formation of up to four filaments across the ridge, each about 3 mcm. Analysis of spatial and temporal evolution of the guided mode revealed strong light leakage into the highly absorptive substrate. Separation between the adjacent cavity modes equals to 0.57 nm which corresponds to the cavity length of 50 mcm being very close to the thickness of GaN substrate. Detection of near-field-to-far-field evolution evidenced a considerable beam steering as a result of temperature and carrier induced refractive index changes. [J2007]

"High-efficiency blue multilayer polymer light-emitting diode based on poly(9,9-dioctylfluorene)"

A highly efficient blue polymer light-emitting diode based exclusively on commercial poly(9,9-dioctylfluorene) and poly[(9,9-dioctylfluorenyl-2,7-diyl)-co-(4,4'-(N-(4-s-butylphenyl)) diphenylamine)] is demonstrated. High electroluminescent efficiency is achieved by enhancing electron currents and making devices in multilayered structures. CsF/Al is used as the efficient electron injection cathode, and the fabrication process is in the glove box to enhance electron mobility by reducing oxygen adsorption. The multilayer structure is prepared by the liquid buffer layer technique. The maximum efficiency is 2.5 cd/A at deep blue with the corresponding external quantum efficiency of 2%. [J2008]

"Triarylamine siloxane anode functionalization/hole injection layers in high efficiency/high luminance small-molecule green- and blue-emitting organic light-emitting diodes"

High efficiency/high luminance small-molecule organic light-emitting diodes (OLEDs) are fabricated by combining thin, covalently bound triarylamine hole injection/adhesion interlayers with hole- and exciton-blocking/electron transport interlayers in tris(8-hydroxyquinolato)aluminum(III) (Alq) and tetrakis(2-methyl-8-hydroxyquinolino)borate (BQ4-)-based OLEDs. Green-emitting OLEDs with maximum luminance 85 000 cd/m², power and forward external quantum efficiencies as high as 15.2 lm/W and 4.4±0.5%, respectively, and turn-on voltages 4.5 V are achieved in devices of the structure, ITO/N,N'-diphenyl-N,N'-bis(p-trichlorosilylpropylphenyl)(1,1'-biphenyl)-4,4'-diamine (TPD-Si2)/1,4-bis(1-naphthylphenylamino)biphenyl (NPB)/Alq doped with N,N'-di(3-heptyl)quinacridone (DIQA)/2,9-dimethyl-4,7-diphenyl-1,10-phenanthroline (BCP)/Li/AgMg. Also, bright and efficient blue-emitting OLEDs with turn-on voltages 5.0 V, maximum luminance 30 000 cd/m², and 5.0 lm/W and 1.6±0.2% power and external forward quantum efficiencies, respectively, are achieved in devices of the structure, ITO/TPD-Si2/NPB/BQ4-/BCP/Li/Al. TPD-Si2 interlayers are fabricated by spin casting N,N'-diphenyl-N,N'-bis(p-trichlorosilylpropylphenyl)(1,1'-biphenyl)-4,4'-diamine onto the ITO surface, while BCP interlayers are introduced by thermal evaporation. The excellent OLED performance is attributed to the differing functions of the above two interlayers: (1) The TPD-Si2 layer has a direct impact on hole injection by reducing the injection barrier and improving interfacial cohesion, and an indirect but strong effect on electron injection by altering internal electric fields. (2) The BCP layer, doped with lithium, directly reduces the electron injection barrier. Incorporation of both interlayers in OLED structures affords synergistically enhanced hole/electron injection and recombination efficiency. The results demonstrate a strategy to enhance OLED performance and an alternative strategy to increase electron density in electron-limited devices. [J2009]

"Strong optical emissions from two-dimensional metal photonic crystals with semiconductor multiple quantum wells"

We investigated two-dimensional (2D) metal photonic crystals (PhCs) with semiconductor multiple quantum wells as an active material. The 2D metal PhCs were fabricated using only a lift-off process. The lift-off process leads to a simpler fabrication process than the one for conventional PhCs and avoids any process damage induced by dry etching. The 2D metal PhCs exhibited clear photonic band effects: (1) photoluminescence (PL) peak positions changed depending on the lattice constant and (2) the PL intensity from 2D metal PhCs was higher than that without 2D metal PhCs. These effects are suitable for fabricating light-emitting diodes with a high external quantum efficiency. PL intensity depending on PL excitation power revealed slightly improved luminescence efficiency than the sample without 2D metal PhCs. [J2010]

"Forward current-voltage characteristics of an AlGaInP light-emitting diode"

This work discusses the temperature-dependent forward current-voltage characteristics of an AlGaInP light-emitting diode. From 300 to 470 K, all curves have the same ideality factor of $n=1.58$. The temperature-dependent saturation currents are in excellent agreement with the thermal activation behavior over ten decades of current and with an activation energy of $E_a=1.405$ eV. Based on the discussion of the barrier for forward current flow, nE_a corresponds to the band gap of the active layer. Various mechanisms of current flow for pn junctions and Schottky diodes were examined and verified. Therefore, the $nE_a=2.22$ eV of the sample corresponds to the band gap of the barriers in the active layer. This value is consistent with the band gap of $(\text{Al}_x\text{Ga}_{1-x})_0.5\text{In}_{0.5}\text{P}$ for $x=0.58$. [J2011]

"Effect of multiquantum barriers on performance of InGaN/GaN multiple-quantum-well light-emitting diodes"

In this paper we demonstrate that the improvement in the emission intensity afforded by the introduction of multiquantum barrier (MQB) structures in an InGaN/GaN multiple-quantum-well (MQW) light-emitting diode (LED) is attributable to increased excitation cross sections. Over the temperature range from 300 to 20 K, the excitation cross sections of the MQW emissions possessing MQB structures were between 9.6×10^{-12} and $5.3 \times 10^{-15} \text{ cm}^2$, while those possessing GaN barriers were between 8.1×10^{-12} and $4.5 \times 10^{-15} \text{ cm}^2$. We found, however, that the figure of merit for the LED light output was the capture fraction of the cross section; we observed that the dependence of the optical intensity on the temperature coincided with the evolution of the capture fraction. This analysis permitted us to assign the capture cross-section ratios at room temperature for the MQWs with MQBs and with GaN barriers as 0.46 and 0.35. Furthermore, the MQW system possessing well-designed MQB structures not only exhibited the thermally insensitive luminescence but also inhibited energetic carrier overflow. [J2012]

"Electroluminescence from lattice defects of photonic crystal slabs in blue-light-emitting diodes"

Lattice defect structures embedded into perfect photonic crystal slabs have been fabricated onto the GaN surfaces of InGaN/GaN multi-quantum-well light-emitting diodes. The photonic crystal slab with a triangular lattice constant of 230 nm showed suppressed light extraction for the electroluminescence at a peak of 464 nm, but the light radiated through lattice defects. The perfect photonic crystal slab shows the cooperative phenomenon of a light scattering similar to Wood's anomaly in a metallic grating, and lattice defects result in the leaky modes of light extractions by breaking the symmetry of cooperative light scattering. [J2013]

"Noise characterization of light-emitting devices based on conjugated copolymers of fluorene and thiophene moieties"

Degradation induced changes in the structural and optical properties of polyfluorene-based light-emitting diodes are examined by using electroluminescence and low frequency noise (LFN) spectroscopic techniques. The materials studied are poly[2,7-(9,9'-dihexylfluorene)-alt-bithiophene] (P1) and poly[2,7-(9,9'-dihexylfluorene)-alt-thieno[3,2-b]thiophene] (P2). Improved emission spectra for a light-emitting device based on polymer P2 in terms of current efficiency, spectra stability, and lifetime are observed. A polymer P2-based device also presents long lifetime predicted by the smaller slope in the initial LFN spectra. Correlation of device LFN spectra with polymer structure change and lifetime is established. The increase in noise level predicts the undergoing degradation in bulk material and the increase in the noise slope predicts the fluctuation of carrier number and change in polymer structure. The redshift in emission spectrum for P2 after long-time driving is also picked up by the LFN spectrum. [J2014]

"Metal-organic chemical vapor deposition growth of InGaN/GaN high power green light emitting diode: Effects of InGaN well protection and electron reservoir layer"

We investigated the effects of the well protection layer (WPL) and electron reservoir layer (ERL) on the emission properties of InGaN/GaN green multiple quantum wells (MQWs). In order to increase their emission wavelength by preventing the volatile InGaN well, a thin GaN WPL was coated subsequently on each well layer at the same temperature before ramping-up the temperature to grow the GaN barrier. It was found that the WPL directly influenced the indium content and optical properties of the MQW. The indium content was in fact increased, as was evident from the x-ray diffraction and photoluminescence experiments. Then, to explore the possibility of enhancing the quantum efficiency by increasing the electron capture rate, a superlattice ERL composed of ten pairs of InGaN/GaN was embedded between the MQW and n-GaN. The electroluminescence intensity of the green light emitting diode with the ERL was up to three times higher than that of the diode without the ERL. These results imply that the carrier capture by the MQW is significantly improved by the additional superlattice ERL, which consequently leads to the enhancement of the quantum efficiency. [J2015]

"Effects of doped dye on the charge carrier injection, transport, and electroluminescent performance in polymeric light-emitting diodes"

The effects of doped fluorescent dye 4-(dicyanomethylene)-2-i-propyl-6-(1,1,7,7-tetramethyljulolidyl-9-enyl)-4H-pyran (DCJTI) on the charge carrier injection, transport and electroluminescence (EL) performance in polyfluorene (PFO)-based polymer light-emitting diodes (PLEDs) were investigated by steady-state current-voltage (I-V) characteristics and transient EL measurements. A red EL from DCJTI was observed and the EL performance depended strongly on the DCJTI concentration. The analysis of the steady-state I-V characteristics at different DCJTI concentrations found that three regions was shown in the I-V characteristics, and each region

was controlled by different processes depending on the applied electric field. The effect of the dopant concentration on the potential-barrier height of the interface is estimated using the Fowler-Nordheim model. The dopant concentration dependence of the current-voltage relationship indicated clearly the carrier trapping by the DCJTl molecules. The mobility in DCJTl: PFO changed significantly with the DCJTl concentration, and showed a nontrivial dependence on the doping level. The behavior may be understood in terms of the formation of an additional energy disorder due to potential fluctuation caused by the Coulomb interaction of the randomly distributed doping molecules. [J2016]

"Efficient and extremely long-lived organic light-emitting diodes based on dinaphthylperylene"

We describe a synergistic effect of a lifetime-extending light-emitting-layer (LEL) additive and improved electron injection and transport in organic light-emitting diodes (OLEDs). Previously reported di(2-naphthyl)perylene (DNP) serves as the LEL additive capable of extending the operating lifetime of OLEDs by over two orders of magnitude. Using 2-phenyl-9,10-di(2-naphthyl)anthracene (PADN) as an electron-transport layer (ETL) and a separate layer of 4,7-diphenyl-1,10-phenanthroline (BPhen) as an electron-injection layer (EIL) significantly improves electron delivery into the charge recombination zone relative to traditional ETL made of tris(8-quinolinolate)aluminum (Alq). This ETL|EIL combination not only results in approximately seven times lower electric field in the ETL and, thus, lower drive voltage and higher efficiency devices, but can also increase device lifetime substantially. In a representative device containing a red-emitting LEL dopant [Commission Internationale de l'Eclairage 1931 2° color chromaticity coordinates (CIE_{x,y}) of 0.65, 0.35], the external quantum efficiency, electroluminescence yield, drive voltage, and operating half-life (t₅₀) can reach 5.8%, 6.5cd/A, 4.5V, and 1000000h, respectively, all at 20mA/cm² current density. [J2017]

"Electroluminescence analysis of high efficiency Cu (In ,Ga)Se 2 solar cells"

We compare the electroluminescence (EL) of polycrystalline ZnO/CdS/Cu(In,Ga)Se₂ heterojunction solar cells with similar band gaps but different open circuit voltages, indicating a difference in the electronic quality of the absorber. Temperature dependent EL measurements reveal that all cells feature transitions from donor-acceptor pair recombination at lower temperature to band to band recombination at higher temperatures. However, the less efficient cells show a longer transition range with donor-acceptor pair recombination still apparent at room temperature. We find further that the part of the room temperature spectrum that is due to band to band transitions in the respective cells is relatively broader than expected from a direct semiconductor with a homogeneous band gap. We analyze this spectral broadening by a model that accounts for band gap fluctuations of the absorber material. The experimental results show that the dominant part of this spectral broadening results from the intentional band gap grading and not from stochastic band gap fluctuations. We show further that the spectral EL emission is linked to the photovoltaic external quantum efficiency by electro-optical reciprocity. In a similar way, the external EL quantum efficiency is related to the open circuit voltage of the device. We verify experimentally that the difference between radiative and measured open circuit voltage determines the EL external quantum efficiency of the solar cell. The best Cu(In,Ga)Se₂ solar cell reaches an external light emitting diode quantum efficiency of around 0.1%. [J2018]

"Characterization of triplet-triplet annihilation in organic light-emitting diodes based on anthracene derivatives"

We report that the steady-state electroluminescence in organic light-emitting diodes (OLEDs) based on anthracene derivatives has a substantial contribution from annihilation of triplet states generated by recombining charge carriers. For the OLED devices of the following general structure: indium tin oxide/N,N'-diphenyl-N,N'-bis(1-naphthyl)-1,1'-biphenyl-4,4'-diamine/9,10-bis(2-naphthyl)-2-t-butylanthracene/Alq₃(tris(8-hydroxyquinolate)aluminum)/LiF/Al, triplet-triplet annihilation contributes as much as 3%-6% of the overall electroluminescence. The intensity of triplet-triplet annihilation-related emission strongly varies with the current density and pulse width, being quadratic and linear functions of current density at low (< 5mA/cm²) and high (> 10mA/cm²) current density regimes, respectively. We find that quenching by charge carriers is the dominant decay process for the triplet states under a wide range of operating conditions, yielding triplet-state lifetimes from tens to hundreds of microseconds. The decrease in charge-carrier concentrations through improved injection and transport may be expected not only to lower operational voltage but also to enhance triplet-triplet annihilation and, consequently, overall electroluminescence efficiency. [J2019]

"Competition between excitons and exciplexes: Experiments on multilayered organic light emitting diodes"

The electronic processes responsible for charge transport and electroluminescence in multilayered organic light emitting diodes (OLEDs) are very sensitive to the properties of the organic heterojunction. In particular, the

height of the energy barrier affects the way in which electrons and holes meet at the heterojunction, the way in which the barrier is crossed, and the probability for photon creation. We investigate these aspects experimentally using a family of OLED devices in which different hole transporting materials are used in otherwise identical device architectures to vary the interfacial hole barrier over a wide energy range. We find that the quantum efficiency of the device is maximum for low-energy barriers and drops for high barrier values where a redshifted electroluminescence spectrum is observed. This shift is attributed to exciplex generation at the heterojunction. The contributions of exciton and exciplex annihilation in radiative and nonradiative channels to the charge flow within the heterojunction region are separated and quantified. [J2020]

"Erratum: "Metal-organic chemical vapor deposition growth of InGaN/GaN high power green light emitting diode: Effects of InGaN well protection and electron reservoir layer" [JJ. Appl. Phys. 102, 053519 (2007)]"

First Page of the Article [J2021]

"Tuning hole injection and charge recombination with self-assembled monolayer on silver anode in top-emitting organic light-emitting diodes"

A series of n-alkanethiol, cyano-terminated n-alkanethiol, and fluorine-substituted benzyl mercaptans were used to modify the silver anode in the fabrication of top-emitting electroluminescent devices. The efficiency of charge injection and device performance were investigated. The study shows that the size/direction of the dipole associated with the monolayer-forming molecule serves to modulate the metal work function and the charge injection barrier, whereas the alkyl chain length allows a fine tuning of charge balance in the recombination zone. A high current efficiency of 10.2cd/A and a luminescence of 10800cd/m² at 200mA were achieved with the NC-C11-SH-modified devices. [J2022]

"Energy-recycling pixel for active-matrix organic light-emitting diode display"

The authors report a pixel structure for active-matrix organic light-emitting diode (OLED) displays that has a hydrogenated amorphous silicon solar cell inserted between the driving polycrystalline Si thin-film transistor and the pixel OLED. Such an active-matrix OLED pixel structure not only exhibits a reduced reflection (and thus improved contrast) compared to conventional OLEDs but also is capable of recycling both incident photon energies and internally generated OLED radiation. Such a feature of energy recycling may be of use for portable/mobile electronics, which are particularly power aware. [J2023]

"Improved hole-injection contact for top-emitting polymeric diodes"

In this letter, an efficient hole-injection contact was achieved for the top-emitting polymeric light-emitting diodes (PLEDs). The anode has a structure of metal/molybdenum oxide/poly(3,4-ethylenedioxythiophene) poly(styrenesulfonate) (PEDOT:PSS). It has been found that hole injection was significantly improved by inserting a thin layer of MoO₃ between aluminum and PEDOT:PSS. An ultraviolet photoelectron spectroscopy (UPS) was used to investigate the change of work function, and photovoltaic measurement confirmed that the improved hole injection is due to the reduction of barrier height, resulted from the addition of transition metal oxide. PEDOT:PSS layer was found necessary in anode structure to further enhance the hole injection and electroluminescence efficiency. A peak power efficiency of 11.42lm/W was achieved at current density of 1.2mA/cm² for the white emission top-emitting PLEDs. [J2024]

"Enhanced outcoupling from organic light-emitting diodes using aperiodic dielectric mirrors"

Aperiodic dielectric stacks between the substrate and transparent anode in organic light-emitting diodes are used to improve the optical outcoupling efficiency. The authors demonstrate that a nine-layer SiO₂/SiNx aperiodic dielectric stack improves the brightness by 80% within a 60° viewing cone for a red-emitting organic light-emitting diode, while maintaining a Lambertian emission pattern. As the refractive index contrast between the two materials used in a two-component multilayer dielectric stack is increased, a brightness improvement of 170% in a 60° viewing cone is achievable while maintaining a Lambertian emission profile. [J2025]

"Energy barriers from ferromagnetic contacts to semiconducting polymers"

The authors present built-in potential, current-voltage (I-V), and electroluminescence-voltage (EL-V) measurements of as deposited and plasma oxidized ferromagnetic metal/polymer/Ca light-emitting diode structures. They specifically considered Co, Fe, Ni, and a Ni:Fe alloy in contact with poly[2-methoxy,5-(2'-ethyl-hexyloxy)-1,4-phenylene vinylene] and poly(9,9-dioctylfluorene). Built-in potential measurements showed that the oxidized films had hole Schottky barriers corresponding closely to the pristine metal work function, whereas

the as deposited films had barriers 0.65-0.95eV larger. Plasma oxidation improved hole injection, consistent with the reduced energy barriers, as demonstrated by I-V and EL-V measurements. These results enable design of spin based organic electronic devices. [J2026]

"Light enhancement by the formation of an Al oxide honeycomb nanostructure on the n -GaN surface of thin-GaN light-emitting diodes"

By using a micron polystyrene ball array as a template, an Al oxide honeycomb structure was produced on the n-GaN surface of a thin-GaN light-emitting diode (LED). The Al oxide honeycomb structure consists of the networking hexagonal Al oxide nanowall. With the Al oxide honeycomb nanostructure, the total lighting output of thin-GaN LED was enhanced by 35%. The authors believe that the networking nanowall of the Al oxide honeycomb structure acted as a waveguide to extract the light emitted to the outer medium effectively. [J2027]

"Improved long-term thermal stability of In Ga N /Ga N multiple quantum well light-emitting diodes using Ti B 2-and Ir-based p -Ohmic contacts"

InGaN/GaN multiple quantum well light-emitting diodes (MQW-LEDs) were fabricated with either Ni/Au/TiB₂/Ti/Au or Ni/Au/Ir/Au p-Ohmic contacts and annealed at 200 and 350°C for 45 days. By comparison with companion devices with conventional Ni/Au Ohmic contacts fabricated on the same wafer, MQW-LEDs with TiB₂- and Ir-based Ohmic metallization schemes showed superior long-term thermal stability as judged by the change in turn-on voltage, leakage current, and output power, a promising result for applications where reliable operation at high temperature is required. [J2028]

"High power and high efficiency blue light emitting diode on freestanding semipolar (101 1) bulk GaN substrate"

Blue InGaN/GaN multiple-quantum-well light emitting diodes with a peak emission wavelength of 444 nm were grown on low extended defect density semipolar (1011) bulk GaN substrates by conventional metal-organic chemical vapor deposition. The calculated external quantum efficiency and output power at a drive current of 20 mA under pulsed operations (10% duty cycle) were 29% and 16.21 mW, respectively. The device exhibited virtually no peak electroluminescence wavelength shift with increasing drive currents, indicating a significant reduction of polarization-related internal electric fields. [J2029]

"Organic light-emitting devices integrated with solar cells: High contrast and energy recycling"

In this letter, the authors report that by integrating organic light-emitting devices (OLEDs) with solar cells, luminous ambient-light reflection as low as 1.4% (even superior to that achieved with polarizers) can be achieved without compromising the electroluminescence efficiency for high-contrast display applications. Furthermore, in such a configuration, the photon energies of the incident ambient light and the portion of OLED emission not getting outside of the device can be recycled into useful electrical power via the photovoltaic action, instead of being totally wasted as in other reported contrast-enhancement techniques. These features, the authors believe, shall make this technique attractive for high-contrast display applications and portable/mobile electronics that are highly power aware. [J2030]

"Highly transparent and low-resistant ZnNi/indium tin oxide Ohmic contact on p -type GaN"

The authors report the improvement of GaN light-emitting diodes (LEDs) by applying a ZnNi/indium tin oxide (ITO) (5 nm/380 nm) electrode with high transparency and low resistance to p-GaN. The Pt/ITO (5 nm/380 nm), Ni/Au/ITO (2.5 nm/5 nm/380 nm), and Ni/Au (2.5 nm/5 nm) electrodes were prepared and annealed at 400, 500, and 600°C for 1 min in air. The ZnNi/ITO contacts showed the lowest specific contact resistance of $1.27 \times 10^{-4} \Omega \text{ cm}^2$ and the highest transmittance of 90% at 460 nm. LEDs fabricated with ZnNi/ITO electrodes showed the best performance with a forward voltage of 3.28 V and a typical brightness of 11.7 mcd at 20 mA. [J2031]

"Heat flow in Al Ga In P /Ga As light-emitting diodes"

The differential equations of heat flow with boundary conditions suited to light-emitting diodes (LEDs) were analytically solved. An AlGaInP/GaAs LED is considered as an example. The agreement between the theoretical and experimental evolutions of the junction temperature demonstrates the accuracy of this analytical solution. Additionally, since the increase of the junction temperature depends on the thermal properties of the substrate, the measured junction temperature together with the analytical solution yield the thermal properties of the substrate. [J2032]

"Transient property of optically pumped organic film of different fluorescence lifetimes"

The authors have investigated the direct relationship between the fluorescence lifetime (FL) and the transient photoluminescence (PL) response of organic materials to examine the applicability of organic light-emitting diodes as light sources for optical communications. Transient PL responses of organic materials with different FLs were measured as a frequency dependence of PL intensity pumped by a modulated violet laser diode. The authors have revealed that the cutoff frequency of PL intensity is significantly related to FL of an organic film. The -3dB cutoff frequency of 1,4-bis[2-[4-[N,N-di(p-tolyl)amino]phenyl]vinyl]benzene (DSB) has reached about 160MHz, which is much higher than that of other organic materials. This is because the FL of DSB is shortest among all the organic materials used in this study. [J2033]

"Photoactivated and patternable charge transport materials and their use in organic light-emitting devices"

Organic light-emitting devices (OLEDs) usually employ at least one organic semiconductor layer that acts as a hole-injection material. The prototypical example is a conjugated polymer such as poly(3,4-ethylenedioxythiophene) heavily doped with polystyrene sulfonic acid. Here, the authors describe a chemical doping strategy for hole injection material formulation that enables spatial patterning of the material conductivity through optical activation. The strategy utilizes an organic photoacid generator (PAG) dispersed in a polymeric organic semiconductor host. Upon UV irradiation, the PAG decomposes and generates a strong protonic acid that subsequently dopes the host. The authors demonstrate an OLED made with such a light-activated hole-injection material and show that arbitrary emission patterning can be accomplished. This approach may provide a simple, low cost path toward specialty lighting and signage applications for OLED technology. [J2034]

"Enhancement of quantum efficiency of organic light emitting devices by doping magnetic nanoparticles"

Magnetic nanoparticles of CoFe are used as dopants to enhance the quantum efficiency of electroluminescence in a single layer organic light emitting device (OLED). The enhancement of quantum efficiency increases with both increasing density of CoFe nanoparticles and external magnetic field. For a given OLED with 0.1wt%doping, the enhancement of the quantum efficiency reaches 27% and 32% without and with a magnetic field, respectively. The origin of these improvements could be attributed to the simultaneous increases of the portion of excitons among total charge carriers and the fraction of singlets among the total excitons [J2035]

"Mid-infrared Al_xIn_{1-x}Sb light-emitting diodes"

The properties of Al_xIn_{1-x}Sb light-emitting diodes (LEDs) have been investigated as a function of aluminum concentrations between 0% and 8.8%. By varying the aluminum concentration it is possible to tailor the peak emission wavelength to match the characteristic absorption of CO₂, CO, CH₄, NO, and NO₂, making these diodes suitable for use in infrared gas sensing applications. The total emitted power and internal quantum efficiency were found to have maxima of 27mW/cm² and 4.2%, respectively, at a composition of 2.5%, where the peak emission was found to be 5.3μm, making LEDs of this composition particularly suited to the detection of NO. [J2036]

"Visual-infrared electroluminescence emission from ZnO/GaAs heterojunctions grown by metal-organic chemical vapor deposition"

The light-emitting diode of p-ZnO/n-GaAs heterojunction was grown by metal-organic chemical vapor deposition. The p-ZnO films have been formed by the doping As atoms which diffuse into ZnO film from GaAs substrate. The p-type behavior of As-doped ZnO films based on As-doped p-ZnO/n-GaAs, p-ZnO/p-GaAs heterojunction was studied by carrying out I-V measurements and x-ray photoelectron spectroscopy. The I-V characteristic of p-ZnO/n-GaAs heterojunction showed characteristic of rectifying diode and visual-infrared electroluminescence emission under forward current injection at room temperature. The I-V of the heterojunction had a threshold voltage of 2.5V. [J2037]

"Phosphorescent organic light-emitting device with an ambipolar oxadiazole host"

In this letter, the authors demonstrated a phosphorescent organic light-emitting device (OLED) with a lower driving voltage and a longer operation lifetime based on 2,2'-bis[5-phenyl-2-(1,3,4)oxadiazolyl]biphenyl, an oxadiazole (OXD) derivative, as the host of the emitting layer doped with a common green-emitting phosphorescent dopant, fac-tris(2-phenylpyridine) iridium [Ir(ppy)₃]. Rather than an electron transporting materials, the OXD exhibits an ambipolar transport characteristic with suitable Ir(ppy)₃ concentrations due to its low highest occupied molecular orbital value (5.9eV) and the hole-transporting characteristics of Ir(ppy)₃. It

results in a 2.4V voltage reduction and a 2.6 times lifetime elongation of the OXD-based device, as compared to the conventional phosphorescent OLED. [J2038]

"Dichromatic InGaN-based white light emitting diodes by using laser lift-off and wafer-bonding schemes"

An InGaN-based dual-wavelength blue/green (470nm/550nm) light emitting diode (LED) with three terminal operations has been designed and fabricated by using sapphire laser lift-off and wafer-bonding schemes. The device is equivalent to a parallel connection of blue and green LEDs; thus the effective electrical resistance of the device could be reduced. The luminous efficiency is 40lm/Wat 20mA, accompanied by a broad electroluminescence emission with a combination of blue and green colors. This monolithically integrated dichromatic lighting structure has great potential in the application of the solid-state lighting. [J2039]

"Effects of laser sources on the reverse-bias leakages of laser lift-off GaN-based light-emitting diodes"

The KrF pulsed excimer laser (248nm) and the frequency-tripled neodymium doped yttrium aluminum garnet laser (355nm) have been used to separate GaN thin films from sapphire substrates and transfer to bond other substrate. However, these processes would increase the dislocation density, resulting in an increase of the leakage current. In this study, the effects of these two laser sources on the reverse-bias leakages of InGaN-GaN light-emitting diodes were studied. [J2040]

"White light emitting diode by using alpha -Ca₂P₂O₇:Eu²⁺, Mn²⁺ phosphor"

The alpha -Ca₂P₂O₇:Eu²⁺, Mn²⁺ phosphors show two emission bands peaking at around 416 (blue) and 600nm (orange), originating from the allowed f-d transition of Eu²⁺ and the forbidden 4T₁-6A₁ transition of Mn²⁺, respectively, under near ultraviolet (UV) excitation at 400nm. Spectroscopy and fluorescence lifetime measurements demonstrate that energy transfer from Eu²⁺ to Mn²⁺ performs with transfer efficiency as high as 65% for Mn²⁺ concentration of 12mol%. The authors have fabricated a white light emitting diode (LED) through the integration of GaN near-UV chip and two phosphor blends (alpha -Ca₂P₂O₇:Eu²⁺, Mn²⁺ blue-orange phosphor and Ba₂SiO₄:Eu²⁺ green phosphor) into a single package. The white LED shows color rendering index of 78, luminescent efficiency of 9lm/W, and low color point variation against forward-bias currents. [J2041]

"Nonlithographic patterning through inkjet printing via holes"

The authors demonstrate a patterning technique, through creating via-hole structures on insulator-coated substrates via inkjet printing, the resolution of which meets the requirements for flat-panel display applications. The authors also fabricate polymer light-emitting diode arrays by subsequently inkjet printing light-emitting polymers onto the inkjet-patterned substrate. The resultant devices exhibit good performances. Hence, this nonlithographic patterning technique provides a way of patterning large-area substrates for applications such as flat-panel displays. [J2042]

"Probing electronic excitations in organic light-emitting diodes via Raman scattering"

The authors present Raman scattering studies from ethyl-hexyl substituted polyfluorene (PF)-based light-emitting diodes in the presence of injected and photogenerated charge carriers. The Raman background systematically increases with increased charge density and the Raman peaks exhibit asymmetric line shapes characteristic of a Breit-Wigner-Fano (BWF) resonance, indicating interference effects between the electronic continuum and phonons. A complete BWF line shape analysis of the intraring stretch mode at 1605cm⁻¹ is provided. These results are compared with p-doped PF; by increasing the doping concentration, it is seen that the center of the electronic continuum lies at 0.2eV. [J2043]

"Temperature-dependent electroluminescence spectra of organic light emitting diodes based on thermally evaporated bis-imido-phenylene vinylene derivative"

This letter reports on the effect of temperature on the electroluminescence spectrum of organic light-emitting diodes based on a low molecular weight compound. Bis-imido-phenylene vinylene derivative has been chosen as green-emitting molecule because of its similarity with poly-phenylene-vinylene derivatives. The electroluminescence spectra are found softly dependent on the degree of crystallinity of the layer and strongly dependent on the temperature. Electroluminescence spectra are fitted with multiple Gaussian peaks corresponding to phonon replica. With increasing temperature a blueshift of the zero-phonon line is observed. This phenomenon, commonly observed with poly-phenylene-vinylene derivatives, is usually explained as a reduction of the effective conjugation length. Such a model cannot be used with small molecules due to a finite

conjugation length. A model of thermally activated statistic occupation of excited states is used to fully describe the experimental data. The results definitely rule out any significant role of a reduction of the conjugation length by increasing the temperature. It is also found that increasing the degree of order of the molecular morphology induces a reduction of the width of density of excited states. [J2044]

"Time- and locally resolved photoluminescence of semipolar Ga In N /Ga N facet light emitting diodes"

The authors investigate the carrier lifetime and photoluminescence (PL) intensity of a semipolar GaInN/GaN sample which was realized by growing five GaInN/GaN quantum wells on the {1101} side facets of selectively grown n-GaN stripes that have a triangular shape running along the 20° direction. Time- and locally resolved PL measurements show drastically reduced lifetimes for the semipolar sample of only 650 ps at 4 K whereas lifetimes exceeding 50 ns were found for a polar reference sample. Furthermore, more than a doubling of the luminescence intensity and a significantly reduced blueshift of the PL peak wavelength with increasing excitation power density provide further evidence for the presence of reduced piezoelectric fields in the semipolar sample. [J2045]

"Ce³⁺/Eu²⁺ codoped Ba₂ZnS₃: A blue radiation-converting phosphor for white light-emitting diodes"

The Ce³⁺/Eu²⁺ codoped Ba₂ZnS₃ phosphor shows intense blue absorption and tunable green-to-red emission. The energy transfer from Ce³⁺ to Eu²⁺ in this phosphor has been demonstrated to be a resonant type via an electric dipole-dipole mechanism. The Ba₂ZnS₃:Ce³⁺,Eu²⁺ phosphor would be the great potential application as a blue radiation-converting phosphor for white light-emitting diodes. [J2046]

"High efficiency phosphorescent organic light emitting diodes using triplet quantum well structure"

Light emission in phosphorescent quantum well structure which can confine excitons within an emitting layer was investigated. A multilayer quantum well structure which has a narrow triplet band gap host material sandwiched between wide triplet band gap host materials was designed, and device performances were studied. The multilayer emitting structure gave high efficiency of 47 cd/A compared with 11 cd/A of standard green devices. [J2047]

"Enhancement of hole injection using ozone treated Ag nanodots dispersed on indium tin oxide anode for organic light emitting diodes"

The authors report the enhancement of hole injection using an indium tin oxide (ITO) anode covered with ultraviolet (UV) ozone-treated Ag nanodots for fac tris (2-phenylpyridine) iridium Ir(ppy)₃-doped phosphorescent organic light-emitting diodes (OLEDs). X-ray photoelectron spectroscopy and UV-visible spectrometer analysis exhibit that UV-ozone treatment of the Ag nanodots dispersed on the ITO anode leads to formation of Ag₂O nanodots with high work function and high transparency. Phosphorescent OLEDs fabricated on the Ag₂O nanodot-dispersed ITO anode showed a lower turn-on voltage and higher luminescence than those of OLEDs prepared with a commercial ITO anode. It was thought that, as Ag nanodots changed to Ag₂O nanodots by UV-ozone treatment, the decrease of the energy barrier height led to the enhancement of hole injection in the phosphorescent OLEDs. [J2048]

"Ambipolar organic light emitting field effect transistors with modified asymmetric electrodes"

The authors report on gate-controlled light emission from an organic field effect transistor composed of a vapor-deposited thin film of alpha,omega-bis(biphenyl-4-yl)-terthiophene (BP3T) with an electron injection layer of pentacene for the drain electrode. A n-triacontane thin film vapor deposited on a Si/SiO₂ wafer was used as a buffer layer for the gate dielectric. The location of emission zones within the channel where both injected carriers recombine was controlled by the gate voltage. The insertion of the pentacene and n-triacontane layers improved the threshold voltage and mobility for electrons, resulting in balanced ambipolar carrier injection and transport. [J2049]

"Single-dopant organic white electrophosphorescent diodes with very high efficiency and its reduced current density roll-off"

Very high-efficiency organic white light electrophosphorescent diodes (WLEDs) have been fabricated using an efficient N C N-coordinated platinum (II) complex phosphor dopant. Their white light emanation is underlain by the simultaneous emission of monomer in blue and excimer in red. By optimizing the phosphor concentration

and confining the electron-hole recombination zone to the emitter layer in the devices, the authors achieve their unusually high forward viewing external quantum efficiency (QE) up to $15.5 \pm 0.2\%$ and $13.0 \pm 0.2\%$ photons/electron at low and high drive current densities, corresponding to 40 and 1300 cd/m², respectively. The current density where QE drops by half of its peak value is greater than three times that of the highest efficiency single-dopant WLEDs reported hitherto. The performance parameters of the presented devices can be further improved by using efficient dopants with the emission spectrum shifted towards blue. [J2050]

"Formation process of high reflective Ni /Ag /Au Ohmic contact for GaN flip-chip light-emitting diodes"

The combinations of Ni, Ag, and Au which form both Ohmic and reflective multilayer contacts for flip-chip light-emitting diode applications are examined. A strong interdiffusion of Ohmic metals and GaN during the annealing process is found to result in poor reflectance (63% at the wavelength of 465nm). The authors propose a two step metallization method, the Ni/Ag double layer is first deposited/annealed followed by the deposition of Au, to improve the correspondent reflectivity (as high as 92%). This method is different from the conventional one step Ni/Ag/Au formation method in which these three metals are deposited together and then annealed. The secondary ion mass spectrometry depth profiles indicate that a wide interdiffusion region existed only in the conventional one step formation samples; thus the low reflectivity of Ni/Ag/Au-annealed contacts can be attributed to the strong interdiffusion of Ohmic metal into GaN. Their proposed two step metallization method avoids the strong interdiffusion and improves the reflectivity effectively. [J2051]

"Highly circularly polarized electroluminescence from organic light-emitting diodes with wide-band reflective polymeric cholesteric liquid crystal films"

The authors have observed highly circularly polarized electroluminescence from organic light-emitting diodes (OLEDs) using wide-band reflector consisting of three-layered left-handed polymeric cholesteric liquid crystal (PCLC) films. By simply attaching the wide-band reflective PCLC reflector to a conventional OLED, the authors obtained a high degree of circular polarization, i.e., the ratio of brightness between right- and left-handed circularly polarized electroluminescences is over 10 over the whole emission band. [J2052]

"Integrated ZnO nanotips on GaN light emitting diodes for enhanced emission efficiency"

Enhancement of light extraction from an integrated ZnO nanotips/GaN light emitting diode (LED) is demonstrated. The device is composed of a GaN LED with a Ga-doped ZnO (GZO) transparent conductive layer and ZnO nanotips grown on GZO for light extraction. The light output power of a ZnO nanotips/GZO/GaN LED exhibits 1.7 times enhancement, in comparison with a conventional Ni/Au-p-metal LED. The higher emission efficiency is attributed to the enhanced light transmission and scattering in the ZnO/GaN multilayer. [J2053]

"Efficient multilayer white polymer light-emitting diodes with aluminum cathodes"

Efficient multilayer white polymer light-emitting diodes (WPLEDs) with aluminum cathodes are fabricated. The multilayer structure is composed of a water soluble hole-injection layer, a toluene-soluble emissive layer, and an alcohol-soluble emissive layer. The polarity difference of the solvents used for spin coating these polymers allows for realization of the multilayer polymer structure. The recombination zone confined at the interface of the two emissive polymers avoids exciton quenching by electrodes, and white emission is realized by harvesting photons emitted from the two emissive polymers. A maximum luminous efficiency of 16.9 cd/A and a power efficiency of 11.1 lm/W are achieved for this WPLED. [J2054]

"Saturated and efficient blue phosphorescent organic light emitting devices with Lambertian angular emission"

The authors employ a microcavity to optimize the color of a phosphorescent organic light emitting device (OLED) based on the-sky blue phosphor Irpic. The output of the OLED is filtered by scattering media to correct the angular emission intensity profile and eliminate the angular dependence of the color. With a holographic diffuser as the scattering medium, the microcavity OLED achieves an external quantum efficiency of $(5.5 \pm 0.6)\%$, as compared to $(3.8 \pm 0.4)\%$ for a conventional structure. The color coordinates of the microcavity OLED with holographic diffuser are $(x,y)=(0.116 \pm 0.004, 0.136 \pm 0.010)$ with minimal angular color shift and a nearly ideal Lambertian angular emission profile. [J2055]

"Single-layer organic light-emitting diodes using naphthyl diamine"

N,N'-diphenyl-N,N'-bis(1-naphthyl)(1,1'-biphenyl)-4,4'-diamine (NPB), a common hole transporter, was employed to fabricate single-layer organic light-emitting diodes (OLEDs). With a quasi-Ohmic anode, NPB device exhibited

a bulk-limited hole current in the low-voltage region. Electron injection and light emission were clearly observed for applied voltages exceeding 4V. In order to confine the recombination zone, intentional doping was applied to the single-layer device. After doping with perylene, the luminance and current efficiency of NPB device increased dramatically. It is expected that more efficient single-layer OLEDs can be achieved by using the doping strategy. [J2056]

"Room temperature midinfrared electroluminescence from GaInAsSbP light emitting diodes"

Room temperature electroluminescence in the midinfrared near 4μm is reported from GaInAsSbP light emitting diodes grown on GaSb by liquid phase epitaxy. Comparison of the electro- and photoluminescence revealed that light is generated on the p-side of the diode. The energy shift (24 meV) is consistent with band gap narrowing and recombination via band tail states due to the Zn doping ($1.4 \times 10^{18} \text{ cm}^{-3}$) in the p-layer of the structure. The temperature dependent behavior of the luminescence and the improved emission intensity was attributed to recombination from localized states arising from electrostatic potential fluctuations due to compositional inhomogeneities in these alloys. [J2057]

"Polarization of edge emission from III-nitride light emitting diodes of emission wavelength from 395 to 455 nm"

Polarization-resolved edge-emitting electroluminescence of InGaN/GaN multiple quantum well (MQW) light emitting diodes (LEDs) from 395 to 455 nm was measured. Polarization ratio decreased from 3.2 of near-ultraviolet LEDs (395 nm) to 1.9 of blue LEDs (455 nm). Based on TE mode dominant emissions in InGaN/GaN MQWs, compressive strain in well region favors TE mode, indium induced quantum-dot-like behavior leads to an increased TM component. As wavelength increased, indium enhanced quantum-dot-like behavior became obvious and E// electroluminescence signal increased thus lower polarization ratio. Electroluminescence spectrum shifts confirmed that quantum dot-like behaviors rather than strain might be dominant in modifying luminescence mode of InGaN/GaN MQWs from near ultraviolet to blue. [J2058]

"Material design of hole transport materials capable of thick-film formation in organic light emitting diodes"

In this study, the authors show an empirical guideline for designing hole transport materials (HTMs) that suppress rises in driving voltage even with a few hundred nanometer thick film in the organic light emitting diodes (OLEDs). In a device structure of indium tin oxide (110 nm)/hole transport layer (HTL) (X nm)/4,4'-N,N'-bis[N-(1-naphthyl)-N-phenyl-amino]biphenyl (10 nm)/tris-(8-hydroxyquinoline)aluminum (Alq₃) (50 nm)/MgAg (100 nm)/Ag (10 nm), the authors compared electroluminescence characteristics of the OLEDs having a thin-film HTL (X=50 nm) and a thick-film HTL (X=300 nm) using 13 kinds of HTMs. They observed a closed correlation between suppression of the driving voltage and the HTMs' thermal characteristics. Highly thermally stable HTMs resulted in a small increase in the driving voltage. [J2059]

"Electron mobility in tris(8-hydroxyquinoline)aluminum (Alq₃) films by transient electroluminescence from single layer organic light emitting diodes"

Single layer devices of indium tin oxide/Alq₃/Al were constructed with varying the active areas from 1 to 8 mm² and the thicknesses from 30 to 50 nm. Average electric field across the Alq₃ layer during the transient state was estimated from the accumulated charges at the interfaces of the devices. The electron mobility could thus be calculated by assuming that the injected charge carriers moved under the average electric field rather than the instantaneous field. The resulting mobility could be determined uniquely in a device thickness. The electron drift mobility was shown to behave similarly to the time-of-flight results. [J2060]

"365 nm operation of n-nanowire/p-gallium nitride homojunction light emitting diodes"

The authors report gallium nitride (GaN) nanoscale light emitting diodes utilizing n-GaN nanowire/p-GaN substrate homojunctions. Utilizing electric field assisted alignment, n-type gallium nitride nanowires were placed on the surface of a p-doped GaN thin film. Electroluminescence with 365 nm peak wavelength and 25 nm full width half maximum was observed from these p-n junctions. These nanowire/epilayer p-n junction diodes were passivated with a thin layer of SiO₂ and did not exhibit any parasitic emission related to the bulk or surface defects. The present fabrication scheme, utilizing only batch fabrication techniques, yields reliable, electrically injected nanoscale ultraviolet light sources. [J2061]

"Al-based Ohmic reflectors with low leakage currents and high reflectance for p-GaN flip-chip processes"

The authors report the improvement of InGaN/GaN light-emitting diodes on Al reflectors, commonly used as n-type GaN contacts. A Cu-doped indium oxide (CIO) (5nm)/indium tin oxide (ITO) (380nm) interlayer was deposited and annealed at 500°C, after which an Al (400nm)/Ti-W(30nm) layer was sputtered on the ITO interlayer to reflect the light. The reflectance of CIO/ITO/Al/Ti-W was 92% at 460nm, higher than that of the popular Ni/Ag/Pt scheme, and the forward voltage was 3.2-3.3V, similar to that of the Ni/Ag/Pt contact. Furthermore, the mean leakage current of CIO/ITO/Al/Ti-W was 0.12 μ A, much lower than 0.54 μ A of Ni/Ag/Pt at -5V. [J2062]

"Highly efficient white organic light-emitting diodes using two emitting materials for three primary colors (red, green, and blue)"

The authors have demonstrated highly efficient white organic light-emitting diodes (WOLEDs) by using two emissive materials as a dopant, 1,4-bis[2-(7-N-diphenylamino-2-(9,9-diethyl-9H-fluoren-2-yl)) vinyl] benzene (DAF-ph) and iridium(III) bis(5-acetyl-2-phenylpyridinato-N,C2') acetylacetonate ((acppy)2Ir(acac)). It was found that the OLED fabricated in this study emitted a white color consisting of three primary colors (red, green, and blue). The luminance-voltage (L-V) characteristics of the WOLEDs showed the maximum luminance of 30500 cd/m² at 14V and the maximum luminous efficiency of 38.0 cd/A, respectively. The CIE coordinates of the WOLED also showed (x=0.33, y=0.40) at 10V. [J2063]

"Lifetime improvement of green phosphorescent organic light-emitting diodes by charge confining device structure"

Lifetime improvement of green phosphorescent organic light-emitting diodes by charge confinement inside an emitting layer was investigated. Excitons were confined within the emitting layer by using a charge confining structure with a high doping concentration at the center of the emitting layer. The lifetime of green devices could be improved by more than five times by confining the excitons at the center of the emitting layer. [J2064]

"Efficiency enhancement and voltage reduction in white organic light-emitting devices"

High-efficiency and low operating voltage fluorescent white organic light-emitting devices (WOLEDs) have been realized by doping either 4,7-diphenyl-1,10-phenanthroline (BPhen) or N,N'-bis(1-naphthyl)-N,N'-diphenyl-1,1'-biphenyl-4,4'-diamine (NPB) into the blue light-emissive layer. Devices doped with BPhen (or NPB) exhibited a maximum power efficiency of 8.7 lm/W (7.6 lm/W), about 74% higher than that of the reference device (5.0 lm/W). Such performance improvement is ascribed to the incorporation of a better electron-transporting layer and an improved carrier transport through the emissive layer by mixing with the higher drift mobility materials. It provides a simple and general means to improve the power efficiency of WOLED. [J2065]

"Efficient electrofluorescent organic light-emitting diodes by sequential doping"

The authors reported a highly efficient electrofluorescent organic light-emitting diode fabricated by sequential doping. An archetypal device utilizing 4-(dicyanomethylene)-2-methyl-6-(p-dimethyl aminostyryl)-4H-pyran as dopant in a matrix of tris-(8-hydroxyquinoline) aluminum was investigated. The emission layer consists of a few repeating cells, similar to a multiple quantum well structure, which are made of sequentially evaporated host and dopant. An external quantum efficiency as high as 3.38% photons/electron was obtained. By avoiding coevaporation, sequential doping should render better control on device performance and day-to-day repeatability. [J2066]

"Poly(9,9-dioctylfluorene)-based light-emitting diodes with pure beta -phase emission"

The authors report on poly(9,9-dioctylfluorene) (PFO)-based light-emitting diodes exhibiting an emission spectrum which was previously attributed to the so-called beta phase. These devices were prepared by drop cast from dilute toluene solutions. Photoluminescence and electroluminescence spectra, recorded at room temperature, show no evidence of the usual amorphous phase emission. Devices with pure beta -phase emission exhibit a higher color stability, upon increase of the driving voltage, than those based on amorphous PFO. [J2067]

"Efficient, single-layer molecular organic light-emitting diodes"

The authors demonstrate efficient molecular organic light-emitting diodes that use direct hole injection from poly(3,4-ethylene-dioxythio-phenylene):poly(styrene-sulfonate) into a single layer of tris(8-hydroxyquinoline) aluminum (III) for carrier transport and electroluminescence. Single-layer devices have a lower operating bias and higher luminous power efficiency than conventional bilayer devices with a 4,4-bis[N-1-naphthyl-N-phenyl-

amino]biphenyl hole transport layer. The current density-voltage characteristics of single-layer devices follow Schottky-Richardson behavior and are consistent with an Ohmic contact at the anode. [J2068]

"Highly efficient near-infrared organic excimer electrophosphorescent diodes"

The authors report the fabrication of very high efficiency near-infrared (NIR) organic light-emitting diodes (LEDs) based on a series of terdentate cyclometallated phosphorescent Pt(II) complexes PtLCas the emitting layer. The LEDs exhibit exclusive NIR excimeric phosphorescence peaking between 705 and 720nm for three different organic ligands (L). Due to the high excimer emission quantum yields of these Pt complexes and to confinement of the recombination zone within the emission layer, unusually high external quantum efficiencies from 9.8% to 10.7% photons/electron and a high forward light output exceeding 15mW/cm² were achieved. [J2069]

"Anodic nanoclusters of GaN"

The authors report an anodization of the deposited Al layer on a p-GaN surface of InGaN/GaN multi-quantum-well light-emitting-diode structures, which forms the anodic nanoclusters of GaN as well as the disordered alumina nanopore layer. The GaN nanoclusters show the shape of the radial hemisphere similar to an orange. The formation mechanism comes from the nanofluidic channel for supplying the electrolyte in electrochemical etching reaction. The nanorods with a diameter of about 100nm in nanocluster structures enhance the photoluminescence intensity by three times compared to the bare sample without anodization. [J2070]

"Photonic crystal effect on light emission from In Ga N /Ga N multi-quantum-well structures"

Triangular hole arrays with nanoscaled lattice constants of 230 and 460nm were fabricated on a p-type GaN epitaxial layer grown on an InGaN/GaN multi-quantum-well light emitting diode structure by metal-organic chemical vapor deposition. The hole geometries of dry-etched thin slabs for triangular lattice constants of 230 and 460nm possessed diameters of 223 and 218nm at the surface, and 108 and 76nm at the bottom, with depths of 31 and 27nm, respectively. The hole array with a lattice constant of 230nm enhances photoluminescence intensity at wavelengths of 364 and 406nm, but reduces light extraction at a wavelength of 450nm, which indicates destructive surface diffraction correlated with light scattering in the photonic crystal structure. [J2071]

"Effects of strained InGaN interlayer on contact resistance between p-Ga N and indium tin oxide"

Indium tin oxide (ITO), with its transparency and strong adhesion to GaN, has been used as a replacement for Ni/Au as a contact on p-GaN. However, ITO suffers from high contact resistance on p-GaN. In this work, low contact resistance between ITO and the p-GaN layer was consistently achieved using various strained InGaN layers as the interface layers between ITO and p-GaN layer. The doping of InGaN, whether n-type or p-type, has a relatively weak effect on the contact resistance as long as the thickness of the InGaN layer is adequately controlled. The secondary-ion-mass spectroscopy depth profile reveals that the n-type InGaN strained contact layer was also heavily doped with Mg. Results of this study demonstrate that the piezoelectric field between InGaN and p-GaN is important in reducing the barrier height of Ohmic contact. [J2072]

"Thin metal intracavity contact and lateral current-distribution scheme for GaN-based vertical-cavity lasers"

The authors report an effective lateral current-distribution scheme to achieve uniform hole injection in GaN-based vertical-cavity lasers. A thin (5nm) intracavity Pd/Au layer is used to simultaneously achieve a low-resistance Ohmic contact and effective lateral current distribution across a circular injection aperture. Precise placement of a thin metal layer in a vertical-cavity laser is shown to yield negligible single-pass optical loss. Light-emitting diodes utilizing this intracavity contact and lateral current-distribution scheme are demonstrated, with effective lateral current distribution observed for aperture diameters up to 36μm. Continuous-wave operation at current densities exceeding 10kA/cm² is demonstrated. [J2073]

"Electrically driven light emission from single colloidal quantum dots at room temperature"

Light emission from single colloidal CdSe/ZnS(core/shell) nanocrystals embedded in electrically driven organic light emitting devices is demonstrated at room temperature. Spectral diffusion and blinking from individual quantum dots were observed both in electro- and photoluminescence. The authors propose a model in which the nanocrystals act as seeds for the formation of current channels that lead to enhanced exciton recombination in the vicinity of the quantum dots. This work demonstrates that individual semiconductor nanocrystals can serve as emissive probes in organic light emitting devices and that they can be used to manipulate device structure and properties at the nanometer scale. [J2074]

"Low roll-off of efficiency at high current density in phosphorescent organic light emitting diodes"

The authors demonstrate that the reduction of quantum efficiency with increasing current density in phosphorescent light emitting diodes (PhOLEDs) is related to the formation of excitons in hole transporting layer based on the analysis of emission spectra and exciton formation zone. Low roll-off of efficiency in a PhOLED was achieved using dual emitting layers (D-EMLs) by confining the exciton formation near the interface between the emitting layers. The external quantum efficiency was maintained almost constant up to 22mA/cm²(10000cd/m²) by adopting the D-EMLs in Ir(ppy)₃ based PhOLEDs, resulting in high external quantum efficiency ($\eta_{\text{ext}}=13.1\%$) at high luminance. [J2075]

"High efficiency phosphorescent organic light-emitting diodes using carbazole-type triplet exciton blocking layer"

Device performances of green phosphorescent organic light-emitting diodes using (4,4'-N,N'-dicarbazole)biphenyl (CBP) and N,N'-dicarbazolyl-3,5-benzene (mCP) as an exciton blocking layer were investigated. CBP and mCP were introduced between hole transport layer and emitting layer to block triplet exciton quenching and efficient hole transport to emitting layer. The efficiency of green devices could be improved by more than three times by using mCP exciton blocking layer. [J2076]

"Photophysics of Pt-porphyrin electrophosphorescent devices emitting in the near infrared"

The triplet annihilation dynamics of near infrared organic light-emitting devices are studied with peak electrophosphorescence at a wavelength of 772nm using a platinum-porphyrin derivative Pt(II)-tetraphenyltetrabenzoporphyrin as dopant. Both the photoluminescent decay transients of the thin films and the quantum efficiency versus current density characteristics of devices using tris(8-hydroxyquinoline) aluminum or 4,4'-bis(N-carbazolyl)biphenyl (CBP) as hosts are fitted by a model based on triplet-triplet annihilation. When the phosphor is codoped with Ir(III) bis(2-phenyl quinolyl-N,C2') acetylacetonate in CBP, the quantum efficiency is enhanced, and the observed decrease of efficiency at high current densities is explained by field-induced charge pair dissociation. The external quantum efficiency has a maximum of $(8.5 \pm 0.3)\%$, decreasing to $(5.0 \pm 0.3)\%$ at 1mA/cm². [J2077]

"Erratum: "Spatial coherence properties of electroluminescence from Alq₃-based organic light emitting diodes" [JAppl. Phys. Lett. 89, 061124 (2006)]"

First Page of the Article [J2078]

"Dual electron donor/electron acceptor character of a conjugated polymer in efficient photovoltaic diodes"

The authors report efficient photovoltaic diodes which use poly((9,9-dioctylfluorene)-2,7-diyl-alt-[4,7-bis(3-hexylthien-5-yl)-2,1,3-benzothiadiazole]-2',2''-diyl) (F8TBT) both as electron acceptor, in blends with poly(3-hexylthiophene), and as hole acceptor, in blends with (6,6)-phenyl C61-butyric acid methyl ester. In both cases external quantum efficiencies of over 25% are achieved, with a power conversion efficiency of 1.8% under simulated sunlight for optimized F8TBT/poly(3-hexylthiophene) devices. The ambipolar nature of F8TBT is also demonstrated by the operation of light-emitting F8TBT transistors. The equivalent p- and n-type operation in this conjugated polymer represent an important extension of the range of useful n-type materials which may be developed. [J2079]

"2-phosphor-converted white light-emitting diodes using oxynitride/nitride phosphors"

Green α -sialon:Yb²⁺ and red Sr₂Si₅N₈:Eu²⁺ oxynitride/nitride phosphors have been demonstrated as potential downconversion luminescent materials for white light-emitting diodes (LEDs). In this letter, the authors attempt to fabricate white LEDs by combining α -sialon:Yb²⁺ and Sr₂Si₅N₈:Eu²⁺ with a blue LED die and report their optical properties. These two phosphors lend themselves for use in 2-phosphor-converted white LEDs with promising properties: a wide range of tunable correlated color temperature (2700-6700K), acceptable color rendering index (82-83), and luminous efficacy (17-23lm/W). These LEDs are acceptable for general lighting. [J2080]

"Change of interface dipole energy with interfacial layer thickness and O₂ plasma treatment in metal/organic interface"

The authors determined the interface dipole energies between interfacial layers with different thicknesses coated

on indium tin oxides (ITOs) and 4,4'-bis[N-(1-naphthyl)-N-phenyl-amino]biphenyl using ultraviolet and synchrotron radiation photoemission spectroscopy. The interface dipole energy increased as a function of interfacial layer thickness up to 4nm. After O₂plasma treatment on thick-metal (4nm)coated ITO, the work function and interface dipole energy increased. In thin-metal (2nm)coated ITO, no change in the interface dipole energy was found though the work function increased. Thus, the O₂plasma treated thin (2nm)interfacial layer reduced the hole injection barrier. [J2081]

"Fabrication of deeply undercut GaN-based microdisk structures on silicon platforms"

The authors demonstrate the use of a dry releasing technique to achieve deeply undercut GaN-based microdisk structures supported by silicon platforms. Varying dimensions of microdisk structures on silicon posts with large air gaps are fabricated by a XeF₂-based dry etching of the underlying silicon material. The residual stress variation in these microdisks is studied by high spectral resolution micro-Raman mapping. Such a fabrication technique may effectively improve the light extraction efficiency from GaN-based microdisk light emitting diodes on silicon substrates. [J2082]

"Influences of resonant wavelengths on performances of microcavity organic light-emitting devices"

In this letter, we investigate theoretically and experimentally the influences of resonant wavelengths on performances of microcavity organic light-emitting devices. Results show that by setting the normal-direction resonant wavelength around the peak wavelength of the intrinsic emission, one obtains the highest luminance enhancement along the normal direction and hardly detectable color shift with viewing angles, yet accompanied by highly directed emission. On the other hand, the highest enhancement (1.4times) in external quantum efficiencies and the most uniform brightness distribution are obtained by setting the normal-direction resonant wavelength of 20-40nm longer than the peak wavelength of the intrinsic emission, yet with noticeable color shift over viewing angles. Due to the trade-offs between different emission characteristics in choosing the resonant wavelength, the exact design of microcavity devices would depend on actual applications. [J2083]

"Enhanced electroluminescence efficiency of oxidized amorphous silicon nitride light-emitting devices by modulating Si /N ratio"

The authors had reported green-yellow electroluminescence (EL) from N-rich oxidized amorphous silicon nitride (a-SiN:O)light-emitting devices (LEDs) in a previous work. In this work, a significantly enhanced EL intensity was obtained in the LED by employing Si-rich a-SiN:O instead of N-rich a-SiN:O as luminescent active layer. Moreover, the Si-rich a-SiN:O devices also exhibit lower turn-on voltage and the external quantum efficiency is found to be three times higher than that of the N-rich a-SiN:O devices. The electrical characteristics analyses reveal that the injection barrier for Si-rich a-SiN:O devices is reduced by 30% compared to that of N-rich a-SiN:O devices, which results in a remarkably enhanced carrier-injection efficiency and gives rise to the notable improved performances of the LEDs. [J2084]

"Electric-field-assisted bipolar charge generation from internal charge separation zone composed of doped organic bilayer"

For studying the mechanism of electric-field-assisted bipolar charges spouting from an internal charge separation (ICS) zone, three different categories of organic thin-film devices, which contain p-nheterojunction bilayer of tetrafluorotetracyanoquinodimethane-doped N,N'-bis(3-methylphenyl)-1,1'-biphenyl-4,4'-diamine and Mg-doped tris(8-quinolinolato)aluminum(III) for the ICS zone, have been fabricated. The bipolar charge separation mechanism in p- and n-doped organic bilayer system was explained in terms of the charge generation-recombination mechanism used in traditional inorganic p-nhomojunction diodes. [J2085]

"Electrical spin injection into p -doped quantum dots through a tunnel barrier"

The authors have demonstrated by electroluminescence the injection of spin polarized electrons through Co/Al₂O₃/GaAs tunnel barrier into p-doped InAs/GaAs quantum dots embedded in a p-i-nGaAs light emitting diode. The spin relaxation processes in the p-doped quantum dots are characterized independently by optical measurements (time and polarization-resolved photoluminescence). The measured electroluminescence circular polarization is about 15% at low temperature in a 2T magnetic field, proving an efficient electrical spin injection yield in the quantum dots. Moreover, this electroluminescence circular polarization is stable up to 70K. [J2086]

"Color-tunable electroluminescence from white organic light-emitting devices through coupled surface plasmons"

The authors report color-tunable electroluminescence from white organic light-emitting devices (WOLEDs)

through coupling of surface plasmons in a metal/insulator/metal (MIM) structure. The MIM structure was fabricated by depositing Ag and 2, 9-dimethyl-4, 7-diphenyl-1, 10-phenanthroline (BCP) films on the Ag cathode of a WOLED. The transmission wavelength through the MIM structure depends on the thickness of the middle BCP layer and can be tuned in the visible range. Therefore, the broadband emission from WOLEDs is selectively transmitted, and color-tunable EL emission was obtained. Blue, green, and red light emissions were observed when the BCP layer thicknesses are 70, 100, and 130nm, respectively. [J2087]

"Via-hole-based vertical GaN light emitting diodes"

A vertical GaN-light emitting diode (LED) has been fabricated on a sapphire substrate with periodic via holes formed by a laser drilling technique. n-contact metal which was deposited on the backside of sapphire substrate was directly connected with an Ohmic metal of n-GaN layer through the via holes. The via-hole-based vertical GaN-LED demonstrated an optical power improvement of up to 12.5% with lower forward operating voltage compared with a conventional GaN-LED. In addition, this vertical LED showed just 0.8% and 1.5% variations of optical power and operation voltage at the 500h reliability test. [J2088]

"White p-i-n organic light-emitting devices with high power efficiency and stable color"

Highly efficient p-i-n two-component white organic light-emitting devices have been fabricated with a thin dual emission layer system comprised of one codeposited emitting layer with blue and yellow dyes and one blue emitting layer, which gives rise to a balance white emission. The p-i-n white device achieved an electroluminescence efficiency of 10 cd/A and a power efficiency of 9.3 lm/W at 1000 cd/m² and a low voltage of 3.4 V with a Commission Internationale de l'Eclairage coordinates of (0.32, 0.43). The electroluminescent color of this p-i-n white organic light-emitting diode device has been shown to be immune to drive current density variations. [J2089]

"Electrically driven telecommunication wavelength single-photon source"

An electrically driven 1.3 μ m single-photon source is demonstrated. The source contains InAs quantum dots within a planar cavity light-emitting diode. Electroluminescence (EL) spectra show clear emission lines and from time resolved EL we estimate a primary decay time of 1 ns. Time-varying Stark shifts are studied and proposed for truncating the emission in jitter-sensitive applications (optimization for 2 ns detector gate width demonstrated) and for relaxing excitation pulse-length requirements. A correlation measurement demonstrates suppression of multiphoton emission to below 28% of the Poissonian level before correction for detector dark counts, suggesting $g(2)(0) = 0.19$ for the source itself. [J2090]

"Measurements of current spreading length and design of GaN-based light emitting diodes"

The authors report on the experimental method to measure the current spreading length in GaN-based light emitting diodes (LEDs) based on a one-dimensional current-distribution model neglecting vertical series resistance of the LEDs. It is clearly shown that the measured current spreading length is in good agreement with the calculated results, exhibiting a strong dependence on the injected current density (or forward bias voltage). LEDs fabricated with hybrid p-type reflectors by using the proposed design rule and measured current spreading lengths show enhancement of the output power by 10% as compared to LEDs made with standard reflectors. [J2091]

"Enhanced efficiency of multilayer organic light-emitting diodes with a low-refractive index hole-transport layer: An effect of improved outcoupling?"

The authors report on an internal device modification for multilayer organic light-emitting diodes (OLEDs) with enhanced efficiency that promises high compatibility with conventional manufacturing processes. By copolymerization of a hole-conducting monomer with a compound possessing a lower refractive index, a hole-transport layer with reduced optical density but slightly reduced hole-transport properties is formed. Multilayer OLEDs based on this reduced-index layer show a 25% increased efficiency compared to reference devices. The results are compared to optical simulations of the dipole emission from thin organic films. It is found that the efficiency improvement is only to some extent due to enhanced outcoupling resulting directly from the reduced refractive index but primarily due to a change of the width of the emission zone. [J2092]

"ZnO light-emitting diodes fabricated on Si substrates with homobuffer layers"

ZnO homojunction light-emitting diodes (LEDs), comprised of N-Al codoped p-type ZnO and Al-doped n-type ZnO layers, were fabricated on Si substrates with homobuffer layers. The current-voltage measurements showed typical diode characteristic with a threshold voltage of about 3.3 V. The electroluminescence (EL) bands at

110K consisted of a near-band-edge emission at 3.18eV and a deep level emission at 2.58eV. The EL emissions were assigned as radiative recombinations, presumably of donor-acceptor pairs, in the p-type layer of the LED. The quenching of EL with temperature was attributed to the degradation of p-type conducting of the ZnO:(N,Al) layer. [J2093]

"Highly efficient simplified organic light emitting diodes"

The authors report on highly efficient organic light emitting diodes (OLEDs) consisting of only two organic layers. The key to the simplification is the direct injection of holes into the wide band gap hole transport material 4,4',4''-tris(N-carbazolyl)-triphenyl amine (highest occupied molecular orbital is 5.9eV) through an indium tin oxide/tungsten oxide (WO₃) anode. Kelvin probe analysis has revealed an extremely high work function of 6.4eV for WO₃. The efficiencies of the simplified OLEDs exceed 40lm/W and 45cd/A at a brightness of 100cd/m², unsurpassed by other comparably simple OLED devices. Therefore, our OLED architecture demonstrates highly efficient, yet easy to fabricate devices. [J2094]

"Effect of ionization potential change in poly(3,4-ethylenedioxythiophene):poly(styrenesulfonic acid) on the performance of polymer light emitting diodes due to its reaction with indium tin oxide"

Poly(3,4-ethylenedioxythiophene):poly(styrenesulfonic acid) (PEDOT:PSS) is usually used to facilitate hole injection in polymer light emitting diodes. The authors used ultraviolet photoelectron spectroscopy to investigate ionization potential (IP) changes of PEDOT:PSS spin coated on indium tin oxide (ITO), and found that increasing delay time to baking after spin coating decreases its IP and increases hole injection barrier to emitting polymer. The IP change is attributed to dedoping of PEDOT in PEDOT:PSS due to reaction of ITO with protons in PSS and those in doped PEDOT in the presence of water. To get good performance of bipolar device, PEDOT:PSS film should be baked right after spin coating. [J2095]

"Electromigration of the conducting polymer in organic semiconductor devices and its stabilization by cross-linking"

X-ray photoelectron spectroscopy (XPS) measurement of the ratio of poly(3,4-ethylenedioxythiophene) (PEDT) to polystyrenesulfonate (PSS) reveals accumulation of PEDT⁺ at the interface between the PEDT:PSSH hole-injection layer and the organic semiconductor during diode operation. This ionic drift of PEDT⁺ occurs even at low fields of 1Vcm⁻¹, which will have an impact on the operational stability of the characteristics of organic light-emitting diodes. XPS and Raman spectroscopy indicate that dedoping of PEDT⁺ does not occur significantly in hole-only devices. Cross-linking at the 1mol% level can stabilize the conducting polymer sufficiently against electromigration. [J2096]

"Efficient blue and white organic light-emitting devices based on a single bipolar emitter"

Excellent bipolar carrier transport properties of 2,7-dipyrenyl-9,9'-dimethyl-fluorene (DPF) have been elucidated by using different device structures. A nondoped device using DPF as host emitter showed highly-efficient blue emission with a maximum efficiency of 6.0cd/A and CIE coordinates of x=0.15 and y=0.19. Another device based on rubrene-doped DPF as emission layer gave pure high-efficiency white emission with good color stability, a maximum efficiency of 10.5cd/A, and CIE coordinates of x=0.28 and y=0.35. The excellent bipolar transport capability and high performance as both emitter and host suggest that DPF is an efficient and versatile material for various applications in organic light-emitting devices. [J2097]

"Nitride-based light emitting diodes with indium tin oxide electrode patterned by imprint lithography"

The authors propose a simple, low cost, and mass producible imprint lithography method to texture indium tin oxide (ITO) contact layer of nitride-based light emitting diodes (LEDs). Under 20mA current injection, it was found that forward voltages were 3.24, 3.25, and 3.24V while the LED output powers were 11.7, 12.6, and 13.3mW for the conventional ITO LED, ITO LED patterned with 1.75μm holes, and ITO LED patterned with 0.85μm holes, respectively. [J2098]

"Highly efficient solution-processed phosphorescent multilayer organic light-emitting diodes based on small-molecule hosts"

The authors report on highly efficient phosphorescent organic light-emitting diodes (OLEDs) based on a low-molecular weight electron-conducting, bis-spirobifluorene host doped with a soluble derivative of the green emitter fac-tris(2-phenylpyridine) iridium (III) [Ir(ppy)₃]. All organic layers were spin coated and a strong improvement of performance was achieved by introduction of a hole-transporting double layer based on cross-linkable low-molecular weight molecules. The devices combine the easy fabrication procedure known from

polymer-based OLEDs with the higher efficiency of small molecules. Maximum luminous and power efficiencies of 59cd/A and 58lm/W, respectively, are obtained, combined with a low driving voltage and high efficiencies even at high brightnesses. At 1000cd/m² the efficiencies are as high as 55cd/A and 49lm/W. [J2099]

"Efficient electron injection in organic light-emitting diodes using lithium quinolate/Ca/Al cathodes"

Device performances of green devices with cathode structure of lithium quinolate (Liq)/Ca/Al were investigated and electron injection mechanism was studied using ultraviolet photoelectron spectroscopy. Power efficiency could be improved by 70% by using Liq/Ca/Al cathode structure due to efficient electron injection, and interfacial energy barrier lowering by Liq/Ca/Al metal cathode was observed. [J2100]

"Transparent conducting C₆₀:LiF nanocomposite thin films for organic light-emitting diodes"

C₆₀:LiF nanocomposite thin films were synthesized by physical vapor coevaporation. It is found that the nanocomposite films are extremely conductive even at high LiF concentrations of up to 75wt% and that the films form Ohmic contacts with Al electrodes. IR measurements showed evidence of charge transfer from LiF to C₆₀. Scanning electron microscope studies showed that C₆₀:LiF (75wt%) nanocomposite forms uniform films. Compared with an archetypical tris(8-hydroxyquinolino)aluminum based device, OLEDs with the C₆₀:LiF composite electron transport materials have lower driving voltages and higher power efficiencies. [J2101]

"Negative capacitance in organic semiconductor devices: Bipolar injection and charge recombination mechanism"

The authors report negative capacitance at low frequencies in organic semiconductor based diodes and show that it appears only under bipolar injection conditions. They account quantitatively for this phenomenon by the recombination current due to electron-hole annihilation. Simple addition of the recombination current to the well established model of space charge limited current in the presence of traps yields excellent fits to the experimentally measured admittance data. The dependence of the extracted characteristic recombination time on the bias voltage is indicative of a recombination process which is mediated by localized traps. [J2102]

"Near-infrared to visible light optical upconversion by direct tandem integration of organic light-emitting diode and inorganic photodetector"

The authors report a hybrid organic/inorganic optical upconversion device that converts 1.5 μm infrared light to 520 nm visible light. The device was made by direct tandem integration of an inorganic InGaAs/InP photodetector with an organic light-emitting diode (OLED). Optical upconversion with an external efficiency of 0.7% W/W at room temperature has been achieved. Interfacial structure at the inorganic-organic interface was found to play a vital role in enabling the integration of the hybrid tandem upconverter. Both sulfur-terminated InP surface and nanocarbon fullerene interlayer were found crucial to form a good interface contact, permitting continuous flow of photocarriers from the inorganic detector into the OLED. [J2103]

"Enhanced light outcoupling in a thin film by texturing meshed surfaces"

The authors demonstrate a method of texturing a meshed surface on a poly(dimethyl siloxane) (PDMS) film for improving light extraction. This meshed surface is fabricated through a casting process by using a self-organized porous film as a template. Experimental results show that the light outcoupling efficiency increases on the meshed surface of a freestanding PDMS film with large incident angles. The external quantum efficiency of an organic light-emitting diode with the textured PDMS film was also demonstrated to have an enhancement of 46%. [J2104]

"Integration of In₂O₃ nanoparticle based ozone sensors with GaInN/GaN light emitting diodes"

There is a high demand for compact low-cost ozone sensors. It has been shown recently that In₂O₃ nanolayers can act as ozone sensitive films activated at room temperature by ultraviolet light. In the present work, the authors integrate ultrathin layers of In₂O₃ nanoparticles and a GaInN/GaN based blue light emitting diode (LED) on a single sensor chip. The integrated sensor was found to be sensitive to O₃ concentrations as low as 40 ppb. These results demonstrate that by integrating GaInN/GaN based blue LEDs and metal oxide sensing layers back to back on a single chip, compact and robust gas sensors can be realized. [J2105]

"Low driving voltage and high stability organic light-emitting diodes with rhenium oxide-doped hole transporting layer"

The authors report a promising metal oxide-doped hole transporting layer (HTL) of rhenium oxide (ReO₃)-doped

N,N'-diphenyl-N,N'-bis (1,1'-biphenyl)-4,4'-diamine (NPB). The tris(8-hydroxyquinoline) aluminum-based organic light-emitting diodes with ReO₃-doped NPB HTL exhibit driving voltage of 5.2-5.4V and power efficiency of 2.2-2.3lm/W at 20mA/cm², which is significantly improved compared to those (7.1V and 2.0lm/W, respectively) obtained from the devices with undoped NPB. Furthermore, the device with ReO₃-doped NPB layer reveals the prolonged lifetime than that with undoped NPB. Details of ReO₃ doping effects are described based on the UV-Vis absorption spectra and characteristics of hole-only devices. [J2106]

"Aggregation-induced emissions of tetraphenylethene derivatives and their utilities as chemical vapor sensors and in organic light-emitting diodes"

Nonemissive tetraphenylethene (TPE) 1 and its diphenylated derivative 2 were induced to emit intensely by aggregate formation. Crystalline aggregates of the dyes emitted bluer lights than their amorphous counterparts. The emissions of the TPE dyes could be switched off and on continuously and reversibly by wetting and dewetting with solvent vapors, respectively, manifesting their ability to optically sense volatile organic compounds. The light-emitting diodes fabricated from 1 and 2 were turned on at 2.9 and 5V and emitted blue lights with maximum luminance of 1800 and 11000cd/m², respectively. [J2107]

"Full-color electroluminescence from ZnO-based heterojunction diodes"

Red, green, and blue electroluminescence have been observed from ZnO-based heterojunction diodes consisting of n-ZnO/n-Mg_yZn_{1-y}O/Zn_{1-x}Cd_xO/p-Si layers. The heterostructures were grown by remote-plasma-enhanced metal-organic chemical vapor deposition. The rectifying I-V characteristics at room temperature reveal the red, green, and blue wavelengths near 720, 520, and 480nm, respectively, when the diodes are forward biased. It is observed that the emission color can be controlled by changing the cadmium content in the emission layer. [J2108]

"Anisotropy of light extraction from two-dimensional photonic crystal light-emitting diodes"

Anisotropic light extraction of photonic crystal (PhC) light-emitting diodes in the azimuthal direction has been investigated with an annular structure of triangular PhC lattice. The optical images of the photoluminescence light extraction are obtained with laser excitation. For increasing lattice constant, sixfold symmetric patterns with varying numbers of petals in multiples of six are observed and analyzed. A map of the anisotropy for various lattice constants and numerical apertures is constructed. Several features of light propagations associated with the PhC are observed including the focusing and collimating behaviors. [J2109]

"High efficiency tandem organic light-emitting devices with Al/WO₃/Au interconnecting layer"

An interconnecting layer of Al (2nm)/WO₃ (3nm)/Au (16nm) was studied for application in tandem organic light-emitting devices. It can be seen that the Al/WO₃/Au structure plays the role of an excellent interconnecting layer. The introduction of WO₃ in the connection unit significantly improves the device efficiency as compared to the case of Al/Au. Thus, the current efficiency of the two-unit tandem devices is enhanced by two factors with respect to the one-unit devices. The green two-unit tandem device of indium tin oxide/MoO₃/4,4'-N,N'-bis[N-(1-naphthyl)-N-phenyl-amino]biphenyl (NPB)/tris(8-hydroxyquinoline) aluminum (Alq₃):10-(2-benzothiazolyl)-1,1,7,7-tetramethyl-2,3,6,7-tetrahydro-1H,5H,11H-[1]benzopyrano[6,7,8-ij]quinolizin-11-one (C545T)/Alq₃/LiF/Al/WO₃/Au/MoO₃/NPB/Alq₃:C545T/Alq₃/LiF/Al showed a maximum current efficiency of 33.9cd/A and a power efficiency of 12.0lm/W. [J2110]

"Reduced efficiency roll-off in phosphorescent organic light emitting diodes by suppression of triplet-triplet annihilation"

The authors investigate phosphorescent organic light emitting diodes comprising mixed films of fac tris(2-phenylpyridine) iridium dispersed in 4,4',4'-tris(N-carbazolyl)-triphenylamine (TCTA) as emission layer (EML). Based on the results of photoluminescence experiments, they intermit the EML with thin neat layers of TCTA acting as an exciton blocking layer inside the EML which suppresses triplet-triplet annihilation. They show that this EML structure leads to an improved roll-off behavior: Starting at the initial external quantum efficiencies (IEQE) of 15.8% and 14.4% at low brightness for the reference and interlayer device, respectively, those structures yield critical current densities j_{cof} of 140mA/cm² and 270mA/cm² defining the current density of half-value IEQE. [J2111]

"Enhancement of the light output performance for GaN-based light-emitting diodes by bottom pillar structure"

A three-dimensional model with finite difference and time domain was established to investigate the

enhancement of the light output intensity of GaN light-emitting diodes (LEDs) with bottom pillar (BP) structure. Through comparing the normalized light extraction intensity of GaN LEDs with or without BP in different dimensions, the theoretical results show that the light output intensity in the LED with BP structure involved could be enhanced by about 30%. The influence of BP structure on the light output intensity of a LED could be explained by the physical model of light interaction. In addition, the experimental results also show the same trend to the theoretical calculations. [J2112]

"ZnO-based light-emitting metal-insulator-semiconductor diodes"

The ZnO-based metal-insulator-semiconductor (MIS) diode was fabricated by using an insulator ZnO layer and an n-ZnO layer grown by radio frequency magnetron sputtering. The current-voltage of the ZnO MIS diodes showed a good diode characteristic with a threshold voltage of 8.9V and a band-edge emission at 380nm at room temperature. The electroluminescence emission of ZnO MIS was attributed to the generation of holes in the insulating ZnO layer at the high threshold voltage of 8.9V via an impact ionization process. [J2113]

"Near ultraviolet light emitting diode composed of n-GaN /ZnO coaxial nanorod heterostructures on a p-GaN layer"

The authors report on the fabrication and characteristics of near ultraviolet nanorod light emitting diodes (LEDs) composed of n-GaN/ZnO nanorod heterostructures on p-GaN substrates. The nanorod LEDs consist of the vertically aligned n-GaN/ZnO coaxial nanorod arrays grown on a p-GaN substrate. The LEDs demonstrated strong near ultraviolet emission at room temperature. The nanorod LEDs were turned on at a forward-bias voltage of 5V, and exhibited a large light emitting area. From electroluminescent spectra, dominant emission peaks were observed at 2.96 and 3.24 eV for an applied current of 2mA. The origins of the strong and large area light emission are also discussed in terms of enhanced carrier injection from n-GaN nanostructures to p-GaN substrates. [J2114]

"Enhanced light extraction of GaN-based light-emitting diodes by using textured n -type GaN layers"

The authors report on the enhancement of the light extraction efficiency of GaN-based light-emitting diodes (LEDs) via the texturing of n-type layers. Compared with standard LEDs, LED fabricated with the textured n-type layers produced a significant improvement in the output power, depending on the reflectivity of the n-electrode, the etch-pit size, and the chip dimension. The textured LEDs were found to yield the output power enhancement as high as 54%. However, it was also found that the electrical property of the textured LEDs can be degraded when the size of the etch pits is too large, indicating that a well-controlled texturing process is required for the realization of high-efficiency LEDs. [J2115]

"The effect of silicon doping in the selected barrier on the electroluminescence of InGaN/GaN multiquantum well light emitting diode"

The effect of silicon doping in the selected barrier on the electroluminescence of InGaN/GaN multiquantum well light emitting diode (LED) was studied using dual wavelength LEDs. The result verified that the hole carrier transport is easily blocked by the silicon doped barrier, and the dominant electron and hole recombination occurs at the wells between p-GaN and the silicon doped barrier. The electroluminescence spectrum and the wavelength blueshift of the silicon doped LEDs were compared with undoped LEDs. The numerical simulation was done to clearly explain the hole blocking effect by the silicon doped barrier. [J2116]

"Enhanced efficiency of GaN-based light-emitting diodes with periodic textured Ga-doped ZnO transparent contact layer"

GaN-based light-emitting diodes (LEDs) with indium tin oxide (ITO)/Ga-doped ZnO (GZO) composite oxide films serving as a transparent contact layer (TCL) were demonstrated. In this study, the wall-plug efficiency of LEDs (LED-III) with textured ITO/GZO composite TCL can be markedly improved by 200% and 45% of magnitude as compared to conventional LEDs with Ni/Au TCL (LED-II) and planar ITO/GZO TCL (LED-I), respectively. Compared to LED-II, this enhancement is due to the enhanced light extraction efficiency of ITO/GZO composite TCL with high transparency. Compared to LED-I, ZnO-based TCL with a higher refractive index ($n \approx 2.0$) allows further enhancement of light extraction through the creation of a textured structure on transparent conductive oxide TCL deposited on the top surface of LEDs. In addition, the ITO/GZO composite TCL with a thickness of 550nm is far larger than that of Ni/Au TCL with a thickness of approximately 15nm. Therefore, in addition to the effect of high transparency, the thicker ITO/GZO TCL with low lateral resistance would also act as a current-spreading layer leading to an enhancement of light extraction. [J2117]

"Effect of periodic deflector embedded in In Ga N /Ga N light emitting diode"

This letter proposes a concept of InGaN/GaN light emitting diodes with periodic deflector embedded structure (PDE-LED). The PDE-LED was grown on a sapphire substrate with SiO₂ hexagonal patterned mask using selective metal-organic chemical deposition. More than 200 artificial inverted polygonal pyramids (AIPPs), which included six R planes and six N planes deflectors with inclined angles of 57° and 61°, respectively, were formed and periodically distributed on masked area. These AIPP deflectors revealed a superior capability of enhancing light extraction efficiency mainly because the AIPP deflector structure could provide multiple chances for photons to escape from the LED sidewall as opposed to a rectangular conventional LED. Thus, the light output power of the PDE-LED was 1.51 times higher than that of a conventional LED at an injection current of 20mA, while forward bias voltage and leakage current were compatible to those of conventional LEDs. [J2118]

"Spectral broadening in electroluminescence of white organic light-emitting diodes based on complementary colors"

The authors report the optical and electroluminescent (EL) properties of white organic light-emitting diodes (OLEDs) which have two emitters with similar structures: 1, 1, 4, 4-tetraphenyl-1, 3-butadiene and 2,9-dimethyl-4,7-diphenyl-1,10-phenanthroline have an emission peak of 400nm around the near ultraviolet, and tris-(8-hydroxyquinoline) aluminum doped with 4-(dicyanomethylene)-2-methyl-6-(p-dimethylaminostyryl)-4H-pyran has an emission peak of 580nm producing a yellow color. The EL spectra of the white OLED have shown a broadening through visual range from 400 to 780nm. This spectral broadening is related to an exciplex emission at the organic solid interface. [J2119]

"Hybrid inorganic/organic microstructured light-emitting diodes produced using photocurable polymer blends"

Light-emitting diodes (LEDs) in the form of a one-dimensional array of microstripes emitting at 370nm were fabricated from AlInGaN inorganic semiconductor. These micro light sources were then used to "directly write" microstructures in photocurable blends of organic light-emitting polymers (LEPs) spin coated onto the LED surface. In this way, thin microstripes of LEP as narrow as 50μm have been fabricated and integrated with the micro-LEDs. These "self-aligned" polymer microstripes serve as wavelength downconverters under further excitation by the UV micro-LEDs, producing hybrid inorganic/organic microstructured LEDs. [J2120]

"Gallium nitride based microcavity light emitting diodes with 2λ effective cavity thickness"

Gallium nitride based microcavity light emitting diodes less than 400nm thick emitting at a peak wavelength of 455nm have been fabricated. The epitaxial structure was grown by metal organic chemical vapor deposition, and the device was fabricated using a laser lift-off process. Cavity thinning was carried out using inductively coupled plasma etching until a cavity length of roughly 2λ (375nm, corresponding to a cavity order of 4 for λ = 455nm in GaN) was achieved. Devices are presented that show perfectly detuned angular emission and perfectly resonant emission between the cavity length and emission wavelength. [J2121]

"Highly efficient transparent organic light-emitting diodes by ion beam assisted deposition-prepared indium tin oxide cathode"

The authors have investigated the effects of indium tin oxide (ITO) deposited by ion beam assisted e-beam evaporation on the performance of polymer light-emitting diodes. ITO was evaporated as a cathode onto a thin Mg:Ag layer by an e-beam process, and its performance as a transparent cathode was subsequently compared to that of Mg:Ag and sputtering-prepared ITO. Polymer devices' luminance and efficiency were improved by more than ten times by ion beam assisted deposition (IBAD)-prepared ITO deposition, with little observable damage to the organic layer. Implementation of the IBAD process resulted in the reduction of the interfacial energy barrier which induced band bending. Furthermore, outcoupling with ITO resulted in enhanced luminance. [J2122]

"Erratum: "Fabrication of 5,6,11,12,-tetraphenyl-naphthacene doped 4-bis(2,2-diphenylvinyl)-1,1-biphenyl white organic light-emitting device" [JAppl. Phys. Lett. 89, 223514 (2006)]"

First Page of the Article [J2123]

"Low voltage and fast speed all-polymeric optocouplers"

An all-polymeric optocoupler has been demonstrated with a polymer light-emitting diode (PLED) as the light

source (input unit) and a polymer/fullerene photodiode (PD) as the detector (output unit). The electroluminescence (EL) peak of the PLED is 560nm, and the entire EL spectrum is within the response range of the PD. The optocoupler can work at low driving voltages, 5V on the PLED and 0V on the PD. The output photocurrent increases linearly with input current, and the current density transfer ratio reaches 1.5%. The frequency response of the optocoupler is at 500kHz. With comparable performance to their inorganic counterparts, the all-polymeric optocouplers demonstrated here will bring the technology of organic photonic devices one step closer to commercialization. [J2124]

"Comprehensive study of time-lapsed peak shift in InGaN quantum well structures: Discrimination of localization effect from internal field effect"

Time-lapsed emission peak shift behaviors in blue-light-emitting InGaN multiple quantum well (MQW) laser diodes with different well widths are systematically investigated by means of excitation power-dependent, time-resolved optical analysis. By investigating the main emission peak shift as a function of both time evolution and excitation power density, the amount of time-lapsed emission peak shift can be differentiated by two contributions: the excitation power dependent and independent ones. The authors conclude that the power-dependent (power-independent) time-lapsed peak shift can be attributed to the internal electric-field (carrier localization) effect present in vertical growth (lateral in-plane) direction of InGaN MQW laser diode structures. [J2125]

"Interface formation between poly(9,9-dioctylfluorene) and poly(3,4-ethylenedioxythiophene):poly(styrenesulfonic acid)"

By using ultraviolet photoelectron spectroscopy, the hole-injection barrier of poly-(9,9-dioctylfluorene) (PFO) cast on top of poly(3,4-ethylenedioxythiophene):poly(styrene sulfonic acid) (PEDOT:PSS) electrode is found to vary with thickness of both films, as confirmed by current profiles of hole-dominated and bipolar devices. The variation can be attributed to a migration of PSS chain as a dopant into PFO layer, as indicated by the broadening and shifting (towards higher binding energy) of highest occupied molecular orbital edge peak of PFO film. The barrier at the thinnest PEDOT:PSS film (15nm) is found to be the smallest due to the least extent of doping by PSS chains. [J2126]

"Three-color polymeric light-emitting devices using selective photo-oxidation of multilayered conjugated polymers"

The authors present a method for fabricating three-color polymer light-emitting devices by low-cost spin-coating and dry photopatterning processes. This method employed two emissive polymer layers in tandem, with each layer separately patterned by a photo-oxidation process. Different combinations of the two patterned layers give rise to the three primary colors, with the emission spectrum of each color essentially the same as that from individual constituent red-, green-, or blue-emitting polymers, and with luminous efficiencies comparable to that from the corresponding standard single-color devices. This method may provide a low-cost, high throughput procedure to manufacture polymeric flat-panel display devices. [J2127]

"Ultrawide band quantum dot light emitting device by postfabrication laser annealing"

An ultrawide band quantum dot (QD) light emitting device (LED) with bandwidth of 360nm covering 1284-1644nm spectral range has been demonstrated by postfabrication laser-irradiation technique. The integrated light output of the QD LED was found to increase by four times after laser annealing, attributed to the improved homogeneity of the QDs and enhanced lateral electrical and optical confinements at the active region after intermixing. Large wavelength blueshift of 315nm has been obtained at the laser annealed region and an overall increase in bandwidth of 22% has been obtained in the QD LED after postfabrication laser annealing. [J2128]

"Extrahigh color rendering white light-emitting diode lamps using oxynitride and nitride phosphors excited by blue light-emitting diode"

The blue-light-excitation-type white light-emitting diode (LED) lamps are considered to be very suitable for lighting for art objects, shop window displays, and medical applications because they do not give infrared ray and ultraviolet ray. But their color rendering indices are needed to be improved for such applications. In this letter, the authors have fabricated white LED lamps with a broad range of color temperatures, and realized extrahigh color rendering index Ra values of 95-98 in them, using four oxynitride/nitride phosphors and a blue LED die. It means UV LED die is not always necessary for high color rendering white LED lamps. The luminous efficacies of white LED lamps are 28-35lm/W, which are sufficiently high for extremely high color rendering white LED lamps. [J2129]

"Use of anisotropic laser etching to the top n-GaN layer to alleviate current-crowding effect in vertical-structured GaN-based light-emitting diodes"

To equalize the resistance of all possible current paths in regular vertical-conducting metal-substrate GaN-based light-emitting diodes (VM-LEDs), an anisotropic laser etching to the surface layer (n-GaN) of 40μm VM-LEDs for improving light emission uniformity and light output power is proposed and demonstrated. The feasibility of the proposed scheme was verified by current and light emission distribution as well as light extraction rate simulations. In conjunction with a nonuniform excimer laser beam irradiation through a mask and rotation of the epitaxy wafer, VM-LEDs with a concave-surface n-GaN layer were also fabricated. Typical improvement in light output power by 38%-26% at an injection current of 350mA as compared to the one without anisotropic etching has been obtained. [J2130]

"Fabrication and characterization of red-emitting electroluminescent devices based on thiol-stabilized semiconductor nanocrystals"

Thiol-capped CdTe nanocrystals were used to fabricate light-emitting diodes, consisting of an emissive nanocrystal multilayer deposited layer by layer, sandwiched between indium tin oxide and aluminum electrodes. The emissive and electrical properties of devices with different numbers of nanocrystal layers were studied. The improved structural homogeneity of the nanocrystal multilayer allowed for stable and repeatable current- and electroluminescence-voltage characteristics. These indicate that both current and electroluminescence are electric-field dependent. Devices were operated under ambient conditions and a clear red light was detected. The best performing device shows a peak external efficiency of 0.51% and was measured at 0.35mA/cm² and 3.3V. [J2131]

"Efficient current injection scheme for nitride vertical cavity surface emitting lasers"

The authors report the realization of InGaN/GaN light emitting diodes (LEDs) with an electrical injection design suitable for vertical cavity surface emitting lasers. Controlled oxidation of an AlInN interlayer lattice matched to GaN allows confining the injected current in a 3μm diameter aperture. Submicron-scale characterization of the current flow and optical properties is achieved by means of microelectroluminescence measurements. LEDs can be safely driven, in continuous mode operation, up to current densities higher than 20kA/cm². [J2132]

"Blue light emitting diodes based on fluorescent CdSe/ZnS nanocrystals"

The authors report on the blue electroluminescence from CdSe/ZnS core/shell nanocrystals prepared from ultrasmall, magic size CdSe clusters that have a diameter of less than 2nm. The light emitting device consists of an active layer of nanocrystals blended with 4,4',N,N'-diphenylcarbazole and an evaporated electron transporting/hole blocking layer made of 2,9-dimethyl-4,7-diphenyl-1,10-phenanthroline. A blue, stable electroluminescence at 485nm from the hybrid device was observed, in good agreement with the photoluminescence spectra of a solid film of the same nanocrystals used for the device. [J2133]

"Room temperature p-n ZnO blue-violet light-emitting diodes"

ZnO p-n junction light-emitting diodes (LEDs) were fabricated on c-plane Al₂O₃ substrates by plasma-assisted molecular beam epitaxy. Gas mixture of N₂ and O₂ was used as the p-type dopant, by which the double-donor doping of N₂(O) can be avoided significantly. The fabricated p-type ZnO layers have a higher hole density and carrier mobility. The LEDs showed a very good rectification characteristic with a low threshold voltage of 4.0V even at a temperature above 300K. The LEDs can even emit intensive electroluminescence in the blue-violet region at the temperature of 350K. The blue-violet emission was attributed to the donor-acceptor pair recombination at the p-type layer of the LED. [J2134]

"Yellow-emitting Sr₃SiO₅:Ce³⁺,Li⁺ + phosphor for white-light-emitting diodes and yellow-light-emitting diodes"

In this letter, a yellow-emitting Sr₃SiO₅:Ce³⁺,Li⁺ + phosphor is reported. Through transitions of 5d→4f (2F_{7/2} and 2F_{5/2}) in Ce³⁺, the phosphor showed a very broad and strong yellow emission under near ultraviolet (UV) or blue light excitation. The energy levels of Ce³⁺ in Sr₃SiO₅ were suggested from its absorption and excitation spectra. White light could be obtained by combining this phosphor with 460 or 405nm light-emitting diodes (LEDs) [(x,y)=(0.3086,0.3167) or (0.3173, 0.3103)]. Additionally, a yellow LED was fabricated using a near-UV LED (380nm chip) with Sr₃SiO₅:Ce³⁺,Li⁺. [J2135]

"Active-matrix OLED on bendable metal foil"

This brief reports a flexible active-matrix organic light-emitting diode display based on a poly-Si thin-film transistor (TFT) backplane. The p-channel poly-Si TFTs on metal foil exhibited a maximum field-effect mobility of 86.1 cm²/Vs, threshold voltage of 3.5 V, gate voltage swing of 0.8 V/dec, and the minimum off current of 10-12 A/μm at V_{ds}=-0.1 V. A 4.1-in active-matrix backplane was fabricated with the poly-Si TFT with a conventional pixel circuit consisting of 2 TFTs and one capacitor. The scan driver circuits with PMOS were integrated on the flexible metal foil. The top emission, organic light emitting display having a brightness of 100 cd/m². [J2136]

"The use of transparent conducting indium-zinc oxide film as a current spreading layer for vertical-structured high-power GaN-based light-emitting diodes"

In this study, the performance of vertical-structured high-power GaN-based light-emitting diodes (VM-LEDs) with a transparent and low-resistant indium-zinc oxide (IZO) film as a current spreading layer (CSL) was investigated. Nickel electroplating and patterned laser liftoff techniques were employed for the transfer of sapphire substrate to nickel substrate. The novel IZO CSL atop n-side-up VM-LEDs offering benefits of superior current spreading ability, larger extraction efficiency, and lower forward voltage drop was demonstrated. As compared to the regular LED without IZO CSL, the use of an IZO CSL with an optimum thickness of around 300 nm leads to an increase in light output power by 97.1 (67.8)% and a decrease in forward voltage drop by 4.9 (15.5)% under an injection current of 350 (800) mA [J2137]

"Temperature-dependent electroluminescence of AlGaIn-based UV LEDs"

The electrical and optical characteristics of AlGaIn-based ultraviolet (UV) light-emitting diodes (LEDs) (265-365 nm) at elevated temperatures (25°C-175°C) were investigated, and compared to those of InGaIn-based visible LEDs (400-465 nm). Strong carrier localization and localized-state emission were retained in the InGaIn LEDs up to 175°C, leading to temperature-independent emission intensity at low-energy tails. The deep-UV LEDs, however, showed dominant band-edge emission, much smaller alloy broadening, and weaker localization effects. The optical power of the UV LEDs decreased much more rapidly with increasing temperature. The characteristic temperature was in the range of 31-73 K, and decreased with increasing Al content in the active region. These findings implicate the lack of localization effects in AlGaIn alloys as one of the causal factors in the poor thermal performance of the UV LEDs and suggest that increasing carrier-confining potentials will provide a critical means to improve their radiative efficiencies. [J2138]

"Depletion-mode TFT made of low-temperature poly-Si"

This brief reports the fabrication and characterization of a depletion-mode p-channel low-temperature polycrystalline silicon (poly-Si) thin-film transistor (TFT). The poly-Si channel was significantly doped by B ions to make a hole-accumulation layer at zero gate voltage. The depletion-mode poly-Si TFT is normally ON-state, so that the current can flow from the source to the drain at zero gate voltage. The TFT exhibited a field-effect mobility of 60 cm²/V·s, a threshold voltage of 18 V, an on/of current ratio of 10⁶, and a gate voltage swing of 1.1 V/dec. [J2139]

"A new framework for characterization of halftone textures"

Characterization of halftone texture is important for quantitative assessment of halftone quality. In this paper, we develop a new framework based on directional local sequency analysis and a filter bank structure. We decompose a halftone image into subband images, from which we can easily reconstruct the original halftone. Based on these subband images, we define the directional sequency spectrum which is analogous to the two-dimensional Fourier spectrum, and formulate several texture measures. Two test image sets are used to justify these measures. [J2140]

"Far-field radiation pattern of red emitting thin-film resonant cavity LEDs"

AlGaInP thin-film resonant cavity light-emitting diodes (RCLEDs) show an improved performance compared to standard red emitting RCLEDs. External quantum efficiencies at 650 nm of 23% and 18% with and without encapsulation, respectively, have been obtained for devices showing a maximum emission in the normal direction. Thanks to the high angle-averaged reflectivity of the bottom hybrid mirror, a strong photon recycling effect occurs in these structures. The decrease of the absorption with increasing injection level reduces photon recycling and increases extraction of lateral guided modes. The redirection of part of the emission from the vertical to the lateral direction with increasing current density is reflected in the evolution of the far-field radiation pattern. [J2141]

"Performance of the optically-coupled current-mirror with its input stage cooled to cryogenic"

temperature"

The Optically-Coupled Current-Mirror (OCCM) is a novel feedback circuit architecture that allows linear transmission of analog signals via optical fibers. Its most distinctive feature is that the input stage is galvanically isolated and passive, as it consists just on the back-to-back connection of a LED and a photodiode. Only those components are required to be in close contact with the detector, and no power supply is required to be brought to the input stage. All active components are located at a safe distance, therefore saving them from being exposed to radiation, as it is common in most experiments at particle accelerators. We have investigated the properties of the OCCM when its passive input stage is cooled to cryogenic temperatures. Results have been extremely interesting as, for instance, the sharp increase in open-loop gain observed when cooling to 77 K, due to an enhanced LED efficiency. This translates into a higher dynamic range and still better linearity, opening new opportunities for the transmission of current signals generated in cryogenic detectors. [J2142]

"Radiation simulations of top-emitting organic light-emitting devices with two- and three-microcavity structures"

We demonstrate the simulation results of the radiation properties from top-emitting organic light-emitting devices (top-emitting OLEDs) with two- and three-microcavity structures based on the general electromagnetic theory. The parameters of the layer thickness and complex refractive index of each layer, the locations and density of the oscillating dipoles, and the emission photoluminescence spectrum are varied to optimize the device performance. In evaluating the device performances, the output spectrum, the intensity distribution, and the viewing-angle characteristics of a top-emitting OLED are concerned. The simulation results are consistent with the Fabry-Perot cavity equation, which can be used as a guideline for designing a two-cavity top-emitting OLED. In such a design process, the dipole position is chosen first. Then the thicknesses of the whole organic layer, the semitransparent cathode, and the dielectric layer are adjusted for optimizing the device performance. In a three-cavity top-emitting OLED, not only the emission intensity and the viewing angle can be optimized at the same time, but also the emission wavelength can be independently tuned. Besides, the use of a three-cavity structure helps to narrow the spectral width and increase the color purity [J2143]

"Improving the performance of organic light-emitting diodes containing BCP/LiF/Al by thermal annealing"

In this paper, we examined the effect of post-packaging annealing on the performance of organic light-emitting diodes containing tris-(8-hydroxyquinoline) aluminum (Alq₃) or 2,9-Dimethyl-4,7-diphenyl-1,10-phenanthroline (BCP) in direct contact with a LiF-Al bilayer cathode. The detailed electroluminescent (EL) characteristics were compared before and after annealing at 70 degC for 5 hrs. It was found that better luminous efficiency as well as greater power efficiency could be achieved for devices with BCP/LiF/Al structure. However, other devices consisting of Alq₃/LiF/Al were less affected. It is believed that the thermal treatment helps to enhance the electron injection for the former, and less helpful for the latter [J2144]

"Maximizing Alq₃/ OLED internal and external efficiencies: charge balanced device structure and color conversion outcoupling lenses"

In this paper, we report bright, efficient Alq₃-based [tris-(8-hydroxyquinoline) aluminum] organic light-emitting diode (OLED) structures that incorporate hemispherical lenses for increased output power efficiency. The 6-layer hybrid (polymer/small molecule) OLED structure contains two spin-coated polymer layers and four thermally evaporated small molecule layers. This structure results in balanced charge injection, thus leading to a more efficient device. The use of index-matched transparent lenses resulted in luminous and external quantum efficiency of 7.5 lm/W and 8%, respectively. The size and shape of the lens was used to control the angular power distribution. Lenses incorporating color conversion media were used to achieve high OLED efficiency in various colors. Saturated yellow, orange, and red devices with external quantum efficiencies as high ~4% were obtained from this approach [J2145]

"High-performance metal-induced lateral-crystallization polysilicon thin-film transistors with multiple nanowire channels and multiple gates"

In this study, pattern-dependent nickel (Ni) metal-induced lateral-crystallization (Ni-MILC) polysilicon thin-film transistors (poly-Si TFTs) with ten nanowire channels and multigate structure were fabricated and characterized. Experimental results reveal that applying ten nanowire channels improves the performance of an Ni-MILC poly-Si TFT, which thus has a higher ON current, a lower leakage current, and a lower threshold voltage (V_{th}) than single-channel TFTs. Furthermore, the experimental results reveal that combining the multigate structure and ten nanowire channels further enhances the entire performance of Ni-MILC TFTs, which thus have a low leakage current, a high ON/OFF ratio, a low V_{th}, a steep subthreshold swing, and kink-free output characteristics. The

multigate structure with ten-nanowire-channel Ni-MILC TFTs has a few poly-Si grain boundary defects, a low lateral electrical field, and a gate-channel shortening effect, all of which are associated with such high-performance characteristics. [J2146]

"Memory effect in the current-voltage characteristic of 8-hydroquinoline aluminum salt films"

This letter investigated the reproducible bistable resistance switching characteristics of a single-layer organic device based on 8-hydroquinoline aluminum (Alq3) fabricated by spin coating. By controlling the ON-state current through the Alq3 films, it has been possible to achieve various resistance states of the films. In addition, the resistance of the ON-state Alq3 films also affects the threshold current and voltage to switch off the device. The independence of the current-injected direction to erase the ON state implies that the filament theory could elucidate the observed phenomenon. The ratio between low- and high-resistance states can reach five orders of magnitude, which will be a potential material for nonvolatile memory application. [J2147]

"Monte-Carlo based simulation of surface light emission profiles from AlGaInP light emitting diodes"

Light emission profiles from AlGaInP LEDs are compared with those obtained via Monte-Carlo simulation and a lossy transmission line model. Results show good agreement for devices with thin current spreading layers. However, for thicker layers, geometric effects dominate the output profile, resulting in discrepancies between experimental data and the transmission line model. The simulation of emission profiles confirms this discrepancy, caused by light escaping from below the p-contact. [J2148]

"Enhancing the output power of GaN-based LEDs grown on wet-etched patterned sapphire substrates"

GaN-based light-emitting diodes (LEDs) with emitting wavelength of 450 nm were grown on patterned sapphire substrates (PSSs) fabricated by chemical wet etching. The crystallography-etched facet was {1-102} R-plane with a 57deg against {0001} C-axis and had superior capability for enhancing light extraction efficiency. The light output power of the PSS LED was 1.15 times higher than that of the conventional LED at an injection current of 20 mA. The output power and external quantum efficiency were estimated to be 9 mW and 16.4%, respectively. The improvement was attributed not only to geometrical shapes of {1-102} crystallography-etched facets that efficiently scatter the guided light to find escape cones, but also to dislocation density reduction by adopting the PSS growth scheme [J2149]

"Carrier Transport and Optical Properties of InGaN SQW With Embedded AlGaIn -Layer"

We investigate the carrier transport and optical properties of a thick InGaIn single quantum well (SQW) where an AlGaIn delta-layer is embedded. By way of simulation, it is found that the carrier density distribution in the active region is more uniform in such a QW structure, compared to a double QW (DQW) configuration showing a discontinuity in the hole quasi-Fermi level due to the large effective mass of the holes along with the strong piezoelectric field. Through the photoluminescence (PL) measurements, we have shown that the PL peak energy varies depending sensitively on the delta-layer thickness, providing an extra degree of freedom in the wavelength-tuning control. In particular, such a QW structure is highly desired for long-wavelength emission as the wavelength tuning can be achieved with lower indium composition. The embedded delta-layer also increases the wave function overlap between holes and electrons, thereby shortening the PL lifetime. The results of PL measurements are shown to be consistent with the self-consistent numerical results. A possible application of the proposed QW structure is to the design of long-wavelength light-emitting diodes and laser diodes [J2150]

"Target Localization Utilizing the Success Rate in Infrared Pattern Recognition"

The architecture of an indoor target localization system employing a small number of infrared-emitting diodes and sensors is presented in this paper. The properties of infrared light and magnetic fields have already been exploited for position localization in distances of several centimeters. Ultrasonic waves and laser light can be used for longer distance estimation if the system is capable of accurately measuring the time of flight of the reflected signals. The proposed approach intends to cover a distance of several meters without requiring high accuracy measurements and sensors of increased precision. The digital infrared patterns that are transmitted from a constant position are recognized by a pair of sensors mounted on the moving target, with varying success rate depending on the distance and the angular displacement from the transmitter. Processing the success rate instead of the analogue signal intensity requires low-cost digital microcontroller systems of moderate precision and computational power. Moreover, longer distances can be covered since attenuated, noisy, or scrambled patterns are also important for the position estimation in the proposed approach. A proper modeling of the pattern recognition success rate is presented in order to estimate distances of several meters with an adjustable

estimation error. The use of multiple infrared pattern transmitting devices results in extension of the area covered and a reduction of the estimation error due to additional crosschecks that may be accomplished. The area covered can be increased by a factor between 20% and 100% depending on the allowed range overlapping of the transmitting devices. The potential topology of these devices is also discussed and analyzed. The presented system can be used in several virtual reality and robotics applications [J2151]

"Study of Laser-Debonded GaN LEDs"

Detailed investigations of laser-debonded GaN-based light-emitting diodes (LEDs) grown by metal-organic chemical vapor deposition (MOCVD) on sapphire substrates were reported. The debonded surface was roughened by photoelectrochemical (PEC) etching in a mixture of potassium hydroxide (KOH) and peroxydisulfate ($K_2S_2O_8$) solution. The power for the laser-assisted debonding process has been systematically optimized. The data show that as long as the laser power does not exceed the optimal value, there is no degradation in the current-voltage (I-V) characteristics, the brightness, as well as the low-frequency noise properties of the devices. The roughness of the debonded surface is systematically varied using different etching times. Experimental results demonstrate strong dependencies of the luminous intensity of the device on the roughness of the debonded surface. A 60% improvement in the luminous intensity of the debonded and roughened LED compared to the original on-sapphire device was observed. This increase in the extraction efficiency is attributed to the reduction in the total internal reflection at the roughened GaN/air interface [J2152]

"Characterization of an Integrated Fluorescence-Detection Hybrid Device With Photodiode and Organic Light-Emitting Diode"

A new integrated fluorescence-detection hybrid device with a photodiode and an organic light-emitting diode (OLED), and its characteristics are presented. To detect the fluorescent signal using OLED as a light source, a finger-type photodiode with low parasitic resistance was designed, which utilizes the side depletion region in the p+n junction. In addition, OLED was designed to have the peak intensity at an excitation wavelength from rhodamine 6G. The integrated fluorescence-detection hybrid device fabricated had a background signal of 153 nA and a limit of detection of 1 μ M, and was applied in the competitive assay [J2153]

"Equivalent Circuit Description of Threshold Voltage Shift in a-Si:H TFTs From a Probabilistic Analysis of Carrier Population Dynamics"

Amorphous hydrogenated silicon thin-film transistors (TFTs) are critical components in large area display and sensor systems, and the need for TFT circuits has been increasing. However, the intrinsic metastability associated with the TFT leads to a threshold voltage shift (VTshift) with time, under prolonged gate bias. For design of reliable TFT circuits, it is imperative to accurately predict this instability for time-varying analog gate bias. In this paper, the author model the threshold voltage variation using a probabilistic analysis of the electron population dynamics as prescribed by the defect pool and charge trapping mechanisms. The model is then extended for prediction of the effect of variable gate bias, and in particular the device history, on the VTshift. Based on this model, a passive equivalent circuit is synthesized to accurately predict the VTshift in TFTs for applications in active matrix organic light emitting diode displays and sensors [J2154]

"LED array integrated with Si driving circuits for LED printer printhead"

A 600 dots per inch LED array chip integrated with Si drivers using a three-dimensional epitaxial thin-film bonding has been developed. Performance tests showed high emitted light power (47 μ W at an LED current of 1 mA) with smaller variations ($\pm 7\%$), and long lifetime. Test results provide good enough characteristics to use the LED array chip in a high-printing-speed LED printer printhead. [J2155]

"Enhancement of Brightness Uniformity by a New Voltage-Modulated Pixel Design for AMOLED Displays"

This letter presents a new pixel design and driving method for active-matrix organic light-emitting diode (AMOLED) displays using low-temperature polycrystalline silicon thin-film transistors (TFTs). The proposed pixel circuit consists of five TFTs and one capacitor to eliminate the variation in the threshold voltage of the TFTs, and the drop in the supply voltage in a single frame operation by the source-follower-type connection and the bootstrap. The proposed pixel circuit has been verified to realize uniform output current by the simulation work using the HSPICE software. The novel pixel design has great potential for use in large-size and high-resolution AMOLED displays [J2156]

"Leakage and charge injection optimization in a-Si AMOLED displays"

In this paper, we examine the effect of switch thin-film transistor (TFT) leakage and charge injection on the operation and driving of amorphous silicon (a-Si) active matrix organic light-emitting diode (AMOLED) displays. Charge injection causes an undesirable and immediate drop in the data voltage stored on the storage capacitor CS when the switch TFT is turned off, and the leakage of the switch TFT causes the charge on CS to gradually leak out over the frame time. While making the row line negative helps reduce the leakage, it increases the voltage swing on the row line and causes more charge injection. We have demonstrated that for a given VDD, there is an optimal negative gate drive voltage on the switch TFT that minimizes the overall drop in data voltage on CS over the frame time. In addition, we have also shown that even though this optimal driving point changes with aging of the display since both leakage and V_T increase over time, it is possible to keep the voltage drop on CS constant irrespective of aging. The analysis provides the designer with a means to improve the long term grey-scale performance of the AMOLED display [J2157]

"Self-Assembled Nanotiles of Heteroepitaxial SiC on Si"

Using an organometallic ion-beam deposition technique, self-assembled silicon carbide (SiC) nanotiles were fabricated on Si wafers. Nanosized semiconducting tiles are important in electronics and photonics technologies and will be applicable for single-electron and microlight-emitting devices. The SiC is a wide bandgap semiconductor used for UV light emitters and power devices. While many fabrication trials have been performed for silicon and germanium nanodots, to the authors' knowledge, no prior reports of a heteroepitaxial growth of SiC nanodots or nanotiles have been made [J2158]

"Army-Backed Flexible Display Effort: A Symbol of Public-Private Partnership"

The primary driver behind the Army's interest in promoting flexible displays is that the technology's physical properties offer vastly superior, if unquantifiable, advantages in safety for its frontline troops. The Army envisions an initial application of the flexible displays as a credit-card-sized device on a foil substrate. The author looks briefly at the features and applications, technological challenges, and dual use principles, promise, and perils [J2159]

"A driving scheme for active-matrix organic light-emitting diode displays based on feedback"

A scheme of driving active matrix organic light emitting diode (AMOLED) displays with hydrogenated amorphous silicon (a-Si) thin-film transistors (TFTs) is presented. By sending a feedback voltage from each pixel to a column driver during the programming cycle, the driving scheme can compensate for the instability of the TFTs, in particular, the shift in the threshold voltage. Measurement results show no change in the OLED current in the presence of a 1.3-V shift in the threshold voltage. Based on circuit analysis, a simple lead compensator and an accelerating pulse were employed to achieve fast pixel programming for a wide range of OLED currents. Simulation results show a programming time of less than 70 μ s for OLED currents as low as 50 nA [J2160]

"Full-Color OLEDs Integrated by Dry Dye Printing"

Dry dye printing and solvent-enhanced dye diffusion were used to locally dope a previously spin-coated poly(9-vinylcarbazole) (PVK) polymer film with different dyes to fabricate side-by-side red, green, and blue (RGB) organic light-emitting device pixels. The fabrication details and the resolution and stability of this patterning technique are discussed. The technique was then used to make combined polymer/small-molecule devices, in which the printability of polymer for color integration was combined with the superior transport properties and thin-layer capabilities of small molecules for high efficiency and low leakage current. To reduce reverse leakage current and raise efficiency, a blanket tris-8-hydroxyquinoline aluminum (Alq3) electron transport layer was deposited on top of the polymer layer after the dye diffusion step, along with a 2,9-dimethyl-4,7-diphenyl-1,10-phenanthroline hole/exciton blocking layer between the Alq3 and the PVK to ensure that all light emission occurred from the doped polymer and not from the Alq3. Devices with this hybrid doped polymer/small molecule structure have an extremely low reverse leakage current (with a rectification ratio of 10^6 at plusmn 10 V). The electroluminescence efficiency of the devices was optimized by varying the dye concentration of the printing plate. A three-color passive-matrix test array with 300 μ m times 1 mm RGB subpixels was demonstrated with this structure [J2161]

"Photonic crystal structure effect on the enhancement in the external quantum efficiency of a red LED"

The enhancement in external quantum efficiency of a red light-emitting diode (LED) from photonic crystal (PhC) hole patterns was investigated. A red LED was chosen because its epitaxial layers are relatively free from defects as compared to GaN-based LEDs. The peak emission wavelength was 642 nm, and a triangular-lattice

PhC was designed with a hole diameter to lattice distance ratio of 0.5. The lattice distance to wavelength ratio (a/λ) was varied from 0.2 to 4.6 in order to evaluate the enhancement in the external quantum efficiency. An improvement in efficiency greater than 75% was obtained for a/λ between 0.6 and 2.0. This improvement of the optical characteristics occurred with unchanged electrical properties [J2162]

"High-brightness white-light source based on up-conversion phosphors"

We report the implementation of a new, high brightness, high efficiency white-light source based on up-conversion phosphors. Up-conversion materials absorb near infrared light and re-emit in red, green, and blue. It is possible to combine these colors to create a white-light source. Such a source has the same appealing characteristics as those reported for up-conversion displays: very high brightness operation without damage to the emitters, long lifetimes, and efficiencies comparable to those of existing technologies. In addition, they offer simplicity of fabrication and a variety of operating modes. Here we demonstrate a 7-lm/W D65 white light emitter yielding 2 kcd/m² on a simple diffuser [J2163]

"Effect of resonant cavity in wafer-bonded Green InGaN LED with dielectric and silver mirrors"

The green InGaN-based resonant cavity light-emitting diodes (RCLEDs) on Si substrates were fabricated using laser liftoff and wafer bonding techniques. Five-pair TiO₂--SiO₂ distributed Bragg reflectors (reflectivity: 85%) and an Ag metal layer (reflectivity: 99%) were employed as the top and bottom mirrors, respectively. The light output power of the RCLED at room temperature is 1.5 times the magnitude of a similar structure without a resonant cavity at an injecting current density of 600 A/cm². The mode spectrum exhibits a line width of approximately 5.5 nm at the dominant peak wavelength of 525 nm, which indicates a quality factor of 100. Under various injection current densities, a low thermally induced red shift in the 525-nm emission peak was observed. This indicates that the resonant microcavity effect contributes to the stability of electroluminescence emission wavelength [J2164]

"Lateral mode discrimination and self-stabilization in ridge waveguide laser diodes"

Lateral mode discrimination and output stability is experimentally investigated in ridge waveguide laser diodes, having various residual guide thicknesses outside the ridge region. It is found that a critical residual thickness exists below which the lasers emit in a single mode, with a low threshold current. Above this critical value, the threshold current rises rapidly with the residual guide thickness, and the lasers oscillate simultaneously in the two lowest order lateral modes. Increasing the injected current intensity, in this regime, results in nonlinear light output-current curves, but also improves mode discrimination in favor of the fundamental mode, until single-mode operation is re-established. A simple mechanism is suggested to explain this phenomenon [J2165]

"Precompensation for anticipated erasures in LTI interpolation systems"

This paper considers compensation of anticipated erasures in a discrete-time (DT) signal such that the desired interpolation can still be accomplished, with minimum error, through a linear time-invariant (LTI) filter. The algorithms presented may potentially be useful in the compensation of a fault in a digital-to-analog converter where samples are dropped at known locations prior to reconstruction. Four algorithms are developed. The first is a general solution that, in the presence of erasures, minimizes the squared error for arbitrary LTI interpolation filters. In certain cases, e.g., oversampling and a sinc-interpolating filter, this solution is specialized so it perfectly compensates for erasures. The second solution is an approximation to the general solution that computes the optimal, finite-length compensation for arbitrary LTI interpolation filters. The third is a finite-length windowed version of the oversampled, sinc-interpolating solution using discrete prolate spheroidal sequences. The last is an iterative algorithm in the class of projection onto convex sets. Analysis and results from numerical simulations are presented. [J2166]

"Electroluminescence of InAs-GaSb heterodiodes"

The electroluminescence of a Type II InAs-GaSb superlattice heterodiode has been studied as a function of injection current and temperature in the spectral range between 3 and 13 μ m. The heterodiode comprises a Be-doped midwavelength infrared (MWIR) superlattice with an effective bandgap around 270 meV and an undoped long wavelength infrared (LWIR) superlattice with an effective bandgap of 115 meV. At high injection currents and elevated temperatures the band to band transitions of both superlattices can be observed. By increasing the temperature the intensity of the MWIR emission component shows a well defined thermally activated increase. The activation energy of the Beryllium doping was evaluated to be 28 meV. [J2167]

"The effect of dislocation loops on the light emission of silicon LEDs"

Remarkably strong infrared light emission was recently observed from silicon p+-n diodes. In several publications a causal relation is proposed between the larger-than-expected light intensity and the existence of lattice damage around the junction. In this letter, we present direct experimental evidence that lattice damage is in fact detrimental to the efficiency of light emission of silicon LEDs. The experiments call for a revision of the explanation for strong light emission in this type of devices. [J2168]

"Optical in situ characterization of isotactic polypropylene crystallization using an LED array in avalanche-photoreceiver mode"

An experiment that is useful in investigating crystallinity evolution during fast cooling, comparable with cooling rates attained in industrial processes, is extremely attractive. In this paper, a setup able to quench thin polymer films while recording the sample thermal history and light intensity of a laser beam transmitted by the sample is described. A particular feature of the optical-measurement setup is the use of the light-emitting diode (LED) array as a receiver, enabling the monitoring of changes in the polarization properties as changes in light scattering of the polymer during crystallization. Furthermore, it could be demonstrated that the LED array can be used as a linear optical detector with photocurrent gain values exceeding ten when polarized slightly below reverse-bias breakdown. [J2169]

"A new configuration of nematic liquid crystal thermography with applications to GaN-based devices"

In this paper, a new configuration of nematic liquid crystal thermography (NLCT) that uses laser illumination to improve the contrast of thermal images on device chips is reported. The wavelength is selected so that the laser light is not absorbed by the device under measurement. The most important application of this new configuration is to measure the junction temperature of light-emitting devices (LEDs). Traditional NLCT cannot be used on LEDs, because the light emitted by the device overwhelms the light reflected from the nematic liquid crystal (NLC) layer coated on the device surface. Thus, the temperature information carried by the reflected light is lost. Using laser illumination and a color filter, this difficult measurement has been made a reality. This new configuration is extended to studying the thermal performance of heterojunction field effect transistors (HFETs) built on AlGaIn/GaN structure grown on sapphire and SiC substrates, respectively. This technique is nondestructive and can be performed in real time during device operation. It has a submicrometer spatial resolution and a $\pm 1^\circ\text{C}$ temperature accuracy. The thermal resistance of HFETs and LEDs has been measured with this method. The new measurement configuration is a valuable tool for studying the thermal performance of GaN-based as well as other semiconductor devices. It provides the device engineers and physicists additional information to improve device structures and performance. [J2170]

"Stability of amorphous-silicon TFTs deposited on clear plastic substrates at 250°C to 280° C"

Amorphous-silicon (a-Si) thin-film transistors (TFTs) were fabricated on a free-standing new clear plastic substrate with high glass transition temperature (T_g) of $>315^\circ\text{C}$ and low coefficient of thermal expansion of [J2171]

"Enhanced reliability by diamond-like carbon in single-layer organic light emitting diodes"

Diamond-like carbon (DLC) layers with thickness of 1.5 nm were incorporated, by pulsed laser deposition technique, in organic light emitting diodes (OLEDs), which consisted of a single light-emitting layer of polystyrene (PS) as the host material, but co-doped with N,N'-diphenyl-N,N'-bis(3-methylphenyl)-1,1'-biphenyl-4,4'-diamine (TPD) and Tris-(8-hydroxyquinoline)-Aluminium (Alq3). For unstable ITO/doped-PS/Al OLEDs, which easily failed with poor light emission when the doped-PS layer used was too thin, the insertion of DLC in the ITO/doped-PS/DLC/Al structure restored the device operation to maximum operating voltage and hence full brightness. [J2172]

"InGaIn-CdSe-ZnSe quantum dots white LEDs"

White light-emitting diodes (WLEDs) were fabricated by combining blue InGaIn chips with luminescent colloidal core-shell CdSe-ZnSe quantum dots (QDs). The core-shell CdSe-ZnSe QDs synthesized by thermal deposition approach exhibited high photoluminescence efficiency with a quantum yield more than 40%, and size-tunable emission wavelengths from 510 to 620 nm. Three-band red-green-blue WLED was successfully assembled by blue InGaIn chips and green-emitting and red-emitting CdSe-ZnSe QDs. Based on QDs with flexibly selected color, the WLEDs exhibited white light with a CIE-1931 coordinate of (0.33, 0.33) and color rendering index Ra of 91. [J2173]

"Enhanced light output of GaN-based power LEDs with transparent Al-doped ZnO current spreading layer"

In this study, Al-doped ZnO (AZO) Ni-AZO and NiOx--AZO films were deposited on p-type GaN films. The depositions were followed by thermal annealing to form Ohmic contacts. The p-GaN-AZO contacts exhibited a non-Ohmic electrical characteristic. However, electrical characteristic could be greatly improved by insertion of Ni or NiOx between AZO film and p-GaN layer. In case of 141 nm ultraviolet light-emitting diodes (LEDs) with Ni-AZO contacts, the light output approached saturation point when the injection current was about 400 mA. However, the saturation point was as high as 500 mA for the LEDs with NiOx--AZO contacts. The lower saturation point could be due to the fact that the resistivity of Ni-AZO films was higher than that of NiOx--AZO films, thus leading to a severe current crowding effect. The increased resistivity of the Ni-AZO films could be attributed to the interdiffusion between Ni and AZO films. When compared to the LEDs with Ni-Au Ohmic contacts, the light output of the LEDs with Ni-AZO and NiOx--AZO contacts was higher by 38.2% and 60.6% at 350 mA, respectively. [J2174]

"630-nm n-type Modulation-doped AlGaInP-AlInP multiquantum-well light-emitting diode"

AlGaInP-AlInP multiple quantum-well (MQW) light-emitting diodes (LEDs) with n-type modulation-doped (MD) structure were grown by metal-organic vapor-phase epitaxy. Their characteristics were then evaluated using current-voltage (I-V), electroluminescence and output power measurements. Experimental results indicated that the LEDs exhibited a higher output power, a lower dynamic resistance, and a smaller wavelength variation than conventional LEDs. The n-type MD-MQW LEDs exhibited a higher external quantum efficiency (7.19%) and a larger maximum output power (14.84 mW) under the dc operation as compared to those of 6.73% and 12.55 mW for the conventional LEDs, respectively. This could be tentatively attributed to the better junction heating effect resulting from the n-type MD-MQW structure in which the electron thermal velocity is suppressed, especially at a high-level injection. These positive results could also be explained by the MD-MQW LED supplying a higher electron concentration than in the conventional structure. [J2175]

"Broad-band superluminescent light-emitting diodes incorporating quantum dots in compositionally modulated quantum wells"

We propose and demonstrate a technique for tailoring the emission bandwidth of 1.3 μm quantum dot superluminescent light-emitting diodes. A broadening of the emission is achieved by incorporating the InAs quantum dot layers in InGaAs quantum wells of different indium compositions. These structures exhibit a broader and flatter emission compared to a simple dot-in well structure comprised of wells of identical indium composition. [J2176]

"Nitride-based photodiode at 510-nm wavelength for plastic optical fiber communication"

We demonstrate a GaN-based waveguide photodiode at a wavelength of around 510 nm for plastic optical fiber communication. Compared with the performance of an Si-based photodiode in the same wavelength regime, our device can achieve better external efficiency. It also enjoys the unique advantage of monolithic integration with the GaN-based green-amber light-emitting-diode (LED). Our demonstrated photodiode exhibits high external efficiency (73%) and a 600-MHz electrical bandwidth. Under forward bias, this device can also serve as a transmitter (LED), and the measured optical center wavelength is around 515 nm with a 70-MHz electrical bandwidth. [J2177]

"High mobility nanocrystalline silicon transistors on clear plastic substrates"

We demonstrate nanocrystalline silicon (nc-Si) top-gate thin-film transistors (TFTs) on optically clear, flexible plastic foil substrates. The silicon layers were deposited by plasma-enhanced chemical vapor deposition at a substrate temperature of 150°C. The n-channel nc-Si TFTs have saturation electron mobilities of 18 cm²V⁻¹s⁻¹ and transconductances of 0.22 $\mu\text{S}/\mu\text{m}$. With a channel width to length ratio of 2, these TFTs deliver up to 0.1 mA to bottom emitting electrophosphorescent organic light-emitting devices (OLEDs) which were fabricated on a separate glass substrate. These results suggest that high-current, small-area OLED driver TFTs can be made by a low-temperature process, compatible with flexible clear plastic substrates. [J2178]

"Rapid thermal annealed InGaN/GaN flip-chip LEDs"

Nitride-based flip-chip (FC) light-emitting diodes (LEDs) emitting at 465 nm with Ni transparent ohmic contact layers and Ag reflective mirrors were fabricated. With an incident light wavelength of 465 nm, it was found that transmittance of normalized 300°C rapid thermal annealed (RTA) Ni(2.5 nm) was 93% while normalized reflectance of 300°C RTA Ni(2.5 nm)/Ag(200 nm) was 92%. It was also found that 300°C RTA Ni(2.5 nm) formed

good ohmic contact on n+short-period-superlattice structure with specific contact resistance of $7.84 \times 10^{-4} \Omega \cdot \text{cm}^2$. With 20-mA current injection, it was found that forward voltage and output power were 3.15 V and 16.2 mW for FC LED with 300°C RTA Ni(2.5 nm)/Ag(200 nm). Furthermore, it was found that reliabilities of FC LEDs were good. [J2179]

"Low-resistance Ohmic contacts to digital alloys of n-AlGaIn/AlN"

Low contact resistance to digital alloys of n-type AlGaIn/AlN with high average Al concentration is described. Low-energy electron diffraction was used to evaluate surface precleaning with HCl and buffered HF. The contact metallization consisting of a stack of Ti/Al/Ti/Au, 20/100/45/60 nm in thickness, was e-beam deposited and etch-patterned. The lowest specific contact resistance of $5.64 \times 10^{-5} \Omega \cdot \text{cm}^2$ was obtained after annealing in N₂ ambient at 700°C. [J2180]

"A new analog buffer using P-type poly-Si TFTs for active matrix displays"

A new simple analog buffer employing p-type low-temperature poly-Si thin-film transistors (TFTs) are proposed and fabricated for the integrated data driving circuits of AMLCD and AMOLED. The new analog buffer does not use any capacitors to store the threshold voltage of a poly-Si TFT, so that it could reduce the output offset by the subthreshold current of poly-Si TFT. The simulation and experimental result exhibit that the buffer output successfully charges the buffer load (≈ 20 pF) to the input value quickly by the boot-strapping. The measured output offset voltages are less than ± 70 mV when the input varies from 1 to 10 V. [J2181]

"Analysis of rail potential and stray current for Taipei Metro"

Taipei Metro adopted the diode-grounded scheme for stray current collection in construction of its cross rail network. During operation of the network, a high rail-to-earth potential (V_{rail}) has been observed at the east end of the Blue Line (i.e., stations BL13-BL16). To find effective countermeasures, a series of field tests in a step-by-step development nature was conducted from 1999-2000, which led to the decision of disconnecting the impedance bond at G11 of the tie line so that the negative return current of the Blue Line cannot flow to the rails of the Red-Green Line, and vice versa (detailed in Sections III-A and V-C). This decision was implemented through contract-out work in 2003. Since then, the V_{rail} has been lowered by almost half before disconnection. To gain the insight characteristic before the contract-out, numerical simulations were also conducted by simulating the multi-train and multisection features of the cross transportation network. The simulation results (for V_{rail} and stray current, or I_{stray}) were consistent with the field-test results. This paper presents the design of these field tests and their test results in comparison with the simulation results, based on which the countermeasures for reducing V_{rail} and the present status after V_{rail} reduction at Taipei Metro are presented. [J2182]

"Designing low-cost modified cladding sensors: a structured approach"

In this paper, a novel solution for signal conditioning, fiber illumination, and measurement is proposed for an optical fiber sensor based on a modified cladding sensing element. The presented technique has properties of compactness and low cost, due to the use of very common optoelectronic components, and flexibility, since it could be employed for different kinds of optical fiber sensors. In particular, a prototype has been realized and characterized for the measurement of liquid temperature. [J2183]

"Alternate half-field stimulation technique for SSVEP-based brain-computer interfaces"

A technique of half-field alternate visual stimulation, combined with differential EEG signal measurement, is applied to acquire steady-state brain-evoked signals. Taking the difference of two signals, measured with properly placed electrodes, enhances the visual-evoked potential (VEP) and suppresses the noise components. An array of different-flash-frequency light-emitting-diode (LED) pairs forms a multiple-choice table. By fixating at different LED pairs, the user communicates (by the VEP of corresponding frequency) his/her decision about the selection of the table entry. [J2184]

"Green emission from InP-GaP quantum-dot light-emitting diodes"

The green electroluminescent emission from light-emitting diodes (LEDs) based on the InP-GaP quantum-dot (QD) system is investigated and discussed. The active region of the diode consists of stacked self-assembled Stranski-Krastanov indium phosphide QDs accompanied by thin quantum-well wetting layers (WLs) and embedded in a gallium phosphide matrix. LEDs based on this QD system exhibit both red and green emission. The red electroluminescence at about 720 nm originates from direct-band-gap recombination within the QDs themselves and dominates for low current. The green emission at about 550 nm appears to originate from the

WL and dominates for higher current density. The marked difference in current-dependence of the green (WL) and red (QD) emission peaks enables the control of the color of the emitted light through the drive current and, thus, allows a realization of color-tunable LEDs. [J2185]

"Self-pulsation dynamics in narrow stripe semiconductor lasers"

In this paper, we address the physical origin of self-pulsation in narrow stripe edge emitting semiconductor lasers. We present both experimental time-averaged polarization-resolved near-field measurements performed with a charged-coupled device camera and picosecond time resolved near-field measurements performed with a streak camera. These results demonstrate dynamic spatial-hole burning during pulse formation and evolution. We conclude from these experimental results that the dominant process which drives the self-pulsation in this type of laser diode is carrier induced effective refractive index change induced by the spatial-hole burning. [J2186]

"Flexible AM OLED panel driven by bottom-contact OTFTs"

Active matrix organic-light-emitting-diode (AM OLED) panels, driven by organic thin-film transistors (OTFT), have been successfully fabricated on a flexible plastic substrate. The pixel circuit consists of two bottom-contact pentacene OTFTs working as switching and driving transistors. The panel has 16 × 16 pixels, each of which have an OLED using a phosphorescent material with an emission efficiency of 30 cd/A. A tantalum oxide (Ta₂O₅) film with a dielectric constant of 24, prepared by the anodization of Tantalum (Ta), was used as the gate insulator of the OTFTs. The passivation layer on the OTFTs was formed by a layer of silicon dioxide (SiO₂) and two layers of polyvinyl alcohol. Using OTFTs with a Ta₂O₅ gate insulator, the authors have realized a flexible active matrix OLED panel driven with a low voltage of -12 V. [J2187]

"Experimental characterization of integrated optical wireless components"

Line of sight optical links can provide extremely high bandwidth communications between terminals, but in order to maintain alignment between transmitter and receiver, tracking is required. In this letter, we report results from a "solid-state" tracking transmitter and receiver. The transmitter consists of a custom complementary metal-oxide-semiconductor (CMOS) integrated circuit that is flip-chip bonded to a seven-element resonant cavity light-emitting diode. The receiver uses a custom seven-element InGaAs detector array that is flip-chip bonded to a CMOS integrated circuit. Results from an initial link demonstration show overall system operation at 100 Mb/s/channel, for Manchester coded data. [J2188]

"Contributions of sidewall illumination and current spreading to the light emission of InGaN-GaN light-emitting diode arrays"

We investigate the contribution of sidewall illumination in InGaN-GaN quantum-well-based light-emitting diode (LED) arrays with various cell radii. The intensity contribution from the array sidewall decreases with the increase of radius as the perimeter/area ratio is reduced. We then compare the effects of current spreading in the LED arrays of different sizes and conclude that the effect of current spreading needs to be given full consideration when the cell size in a microarray becomes larger. This letter provides a novel approach to calculate the intensity contributions of sidewall illumination and current spreading to GaN-based LED arrays. [J2189]

"Electroluminescence from the Ge quantum dot MOS tunneling diodes"

A Ge quantum dot (QD) light-emitting diode (LED) is demonstrated using a MOS tunneling structure for the first time. The oxide film was grown by liquid phase deposition at 50°C to reduce the thermal budget. The infrared emission of 1.5 μm was observed from Ge QD MOS LEDs, similar to the p-type-intrinsic-n-type structure reported previously. At the negative gate bias, the electrons in the Al gate electrode tunnel to the Ge QD through the ultrathin oxide and recombine radiatively with holes to emit the 1.5 μm infrared. The electrons also recombine with holes in the Si cap, and the band edge emission from Si is also observed. [J2190]

"Influence of transistor parameters on the noise margin of organic digital circuits"

The concept of noise margin is crucial in the design and operation of digital logic circuits. Analytical expressions for the transfer curves of an inverter based on two depletion-mode p-type organic thin-film transistors (OTFTs) were calculated. Based on these expressions, the values for the noise margin of organic-based inverters were calculated. In this paper, the influence of the OTFT parameters on the noise margin is presented. Knowing that statistical variations of the transistor parameters are inherent to OTFT technology, these statistical variations are also taken into account. Finally, a circuit yield analysis is presented. [J2191]

"Low-frequency wireless communications System-infrared laboratory experiments"

A communications systems course laboratory component using an infrared (IR) communication system has been developed as part of the wireless education initiative at the Rose-Hulman Institute of Technology (RHIT), Terre Haute, IN. Students build the system up over several laboratory periods from distinct subsystems, each of which illustrates specific communications concepts. The multiweek laboratory project has the features of being easy to implement on breadboards owing to the low modulation frequency and of being highly motivational to students because of their interest in building a "working system" with a familiar application. The course, the curricular context, and the laboratory experiments are described, along with student survey data on the perceived effectiveness of the laboratories. The students and instructors have found this laboratory project to be very effective in reinforcing classroom concepts, motivating students, and enhancing debugging skills. [J2192]

"Device and circuit level optimization for high performance a-Si:H TFT-based AMOLED displays"

Active matrix organic light-emitting diode (AMOLED) displays with amorphous hydrogenated silicon (a-Si:H) thin-film transistor (TFT) backplanes are becoming the state of art in display technology. Though a-Si:H TFTs suffer from an intrinsic device instability, which in turn leads to an instability in pixel brightness, there have been many pixel driving methods that have been introduced to counter this. However, there are issues with these circuits which limit their applicability in terms of speed and resolution. This paper highlights these issues and provides detailed design considerations for the choice of pixel driver circuits in general. In particular, we discuss the circuit and device level optimization of the pixel driver circuit in a-Si:H TFT AMOLED displays for high gray scale accuracy, subject to constraints of power consumption, and temporal and spatial resolution. [J2193]

"Butterfly effect [Light emitting diodes]"

A UK team of optical physicists has discovered that the structure of the groundbreaking light emitting diode (LED) developed by Alexei Erchak at the Massachusetts Institute of Technology in Cambridge in 2001 can also be found in the fluorescent wings of the male African swallowtail butterflies of the *Priniceps nireus* species. In addition, the team found that the structure of these wings is subtly different from the MIT design in a way that may offer clues for improving LEDs further. [J2194]

"Performance of InGaN-GaN LEDs fabricated using glue bonding on 50-mm Si substrate"

Vertical InGaN-GaN light-emitting diodes (LEDs) epitaxial films were successfully fabricated on a 50-mm Si substrate using glue bonding and laser liftoff technology. A high-temperature stable organic film, rather than a solder metal, was used as the bonding agent. It was found that the light output of the vertical InGaN LED chip exceeded that of the conventional sapphire-substrate LEDs by about 20% at an injection current of 20 mA. The vertical InGaN LEDs operated at a much higher injection forward current (280 mA) than sapphire-substrate LEDs (180 mA). The radiation pattern of the vertical InGaN LEDs is more symmetrical than that of the sapphire-substrate LEDs. Furthermore, the vertical InGaN LEDs remain highly reliable after 1000 h of testing [J2195]

"Review of the properties of up-conversion phosphors for new emissive displays"

In this paper, we review the properties of up-conversion (UC) materials and assess their potential for a new display technology. UC materials absorb near infrared light and re-emit in the visible. Some of their most appealing characteristics for displays are: a wide color gamut with very saturated colors, very high brightness operation without damage to the emitters, long lifetimes and efficiencies comparable to those of existing technologies. Other advantages include simplicity of fabrication, versatility of operation modes, and the potential for greatly reduced display weight and depth. [J2196]

"White LED based on polyfluorene Co-polymers blend on plastic substrate"

We report on high-performance, white light emission from polyfluorene co-polymers blend and study of the optoelectrical properties of polymer blend light-emitting devices (PLEDs) fabricated on plastic substrate. Our results show that efficient white light emission via energy transfer, producing higher device efficiencies and luminance in comparison with the conventional single PLEDs, can be realized by blending carrier donor (host) and acceptor (guest) organic polyfluorene co-polymers. A maximum luminance of 7400 cd/m² was achieved at 13 V with Internationale de L'Eclairage coordinates of (0.33, 0.33). Maximum emission efficiency of 2.0 cd/A and power efficiency of 1.1 lm/W are obtained for white light PLEDs on plastic substrate. [J2197]

"Electrically bistable memory device based on spin-coated molecular complex thin film"

We present an organic electrically bistable memory device based on the molecular complex film composed of

tetracyanoquinodimethane and a soluble methanofullerene derivative [6,6]-phenyl C61-butyric acid methyl ester. The device has an Al/molecules/Al sandwich-like structure. The molecular layer was formed by spin-coating technique instead of expensive vacuum deposition method. The current-voltage characteristics show that the device switches from the initial "low" conduction state to "high" conduction state upon application of external electric field at room temperature. The on/off ratio is up to 106. Either state has been found to remain stable for more than five months, even after the external electric field is removed. The device presented is of potential use for low-cost write-once-read-many-times memory applications. [J2198]

"Control of the color contrast of a polychromatic light-emitting device with CdSe-ZnS nano-crystals on an InGaN-GaN quantum-well structure"

Blue-red polychromatic light-emitting devices are fabricated by attaching red-emitting CdSe-ZnS nano-crystals on a blue-emitting InGaN-GaN multiple-quantum-well (MQW) structure. To improve the red/blue intensity contrast, holes of different diameters are fabricated for increasing the direct contact area between the MQW active regions and CdSe-ZnS nano-crystals. By comparing the devices of 10-, 50-, 60-, and 70- μm hole diameters, and a reference device of no hole, it is found that the hole diameter of 60 μm represents an optimized condition from the viewpoint of maintaining high quantum efficiency. However, the device of 10- μm holes has the highest red/blue intensity ratio, which corresponds to a 36% increase. This result is attributed to its largest side-wall area in the holes among various samples [J2199]

"GaN-based LEDs with Al-deposited V-shaped sapphire facet mirror"

A GaN-based light-emitting diodes (LEDs) with V-shaped sapphire facet reflector was fabricated using the double transferred scheme and sapphire chemical wet etching. The {1-102} R-plane V-shaped facet reflector with a 57° against {0001} C-axis has the superior capability for enhancing the light extraction efficiency. The light output power of the V-shaped sapphire facet reflector LED was 1.4 times higher than that of a flat reflector LED at an injection current of 20 mA. The significant improvement is attributable to the geometrical shape of sapphire facet reflector that efficiently redirects the guided light inside the chip toward to the top escape-cone of the LED surface. [J2200]

"White Light Emission of Monolithic Carbon-Implanted InGaN-GaN Light-Emitting Diodes"

We presented white emission of carbon-implanted InGaN-GaN light-emitting diodes. By using the blue light emitting from the InGaN-GaN multiple quantum well to excite the carbon-implanted Mg-doped GaN layer, the yellow-green light emission was obtained. To mix the blue light and the generated yellow-green light, white emission can be obtained in the monolithic InGaN-GaN light-emitting diodes [J2201]

"Electromagnetic modeling of organic light-emitting devices"

Based on the rigorous electromagnetic wave theory, a numerical model for simulating the radiation characteristics of organic light-emitting devices (OLEDs) is developed. In particular, a novel method for overcoming the numerical difficulty in taking the thick glass substrate into account is proposed. The numerical results confirm the importance of the effects of the thick glass substrate. The algorithms based on the numerical model are then used for evaluating the dependencies of OLED radiation characteristics on various parameters, including the thickness of different device layers and the cathode metal variety. In the study of the effect of emission layer (EML) thickness, it is found that the radiation spectral peak red shifts with increasing EML thickness. This trend is consistent with the experimental result. [J2202]

"Improvement in the characteristics of GaN-based light-emitting diodes by inserting AlGaIn-GaN short-period superlattices in GaN underlayers"

We report the influence of short-period superlattice (SPSL)-inserted structures in the underlying undoped GaN on the characteristics of GaN-based light-emitting diodes (LEDs). The measurements of current-voltage (I-V) curves indicate that GaN-based LEDs having pseudomorphic $\text{Al}_{0.3}\text{Ga}_{0.7}\text{N}(2\text{ nm})$ -GaN(2 nm) SPSL-inserted structures exhibit improvements in device characteristics with the best LED being inserted with two sets of five-pair $\text{Al}_{0.3}\text{Ga}_{0.7}\text{N}(2\text{ nm})$ -GaN(2 nm) SPSL structure. Based upon the results of etch pit counts, double-crystal X-ray diffraction measurements and transmission electron microscopic observations of the GaN-based LEDs, it was found that the $\text{Al}_{0.3}\text{Ga}_{0.7}\text{N}(2\text{ nm})$ -GaN(2 nm) SPSL-inserted structures tended to serve as threading dislocation filters in the LEDs so that the improved I-V characteristics were achieved. [J2203]

"White light generation with CdSe-ZnS nanocrystals coated on an InGaN-GaN quantum-well blue/Green two-wavelength light-emitting diode"

We grew and processed a blue/green two-wavelength light-emitting diode (LED) based on the mixture of two kinds of quantum wells (QW) in epitaxial growth. The X-ray diffraction and photoluminescence measurements indicated that the crystalline structure and the basic optical property of individual kinds of QW are not significantly changed in the mixed growth. The relative electroluminescence (EL) intensity of the two colors depends on the injection current level, which controls the hole concentration distribution among the QWs. At low injection levels, the top green-emitting QW dominates in EL. As the injection current increases, the blue-emitting QWs beneath become dominating. We also coated CdSe-ZnS nanocrystals on the top of the two-wavelength LED for converting blue photons into red light. With the coating of such nanocrystals, the device emits blue, green, and red lights for white light generation [J2204]

"Programmable reconfigurable self-assembly: parallel heterogeneous integration of chip-scale components on planar and nonplanar surfaces"

This paper reports on a programmable reconfigurable self-assembly (PRS) process to enable heterogeneous integration of components on nonplanar substrates. The proposed process makes use of solder-based receptors that can be activated electrically. Metal contacts on segmented semiconductor devices bind to liquid-solder-based-receptors on a substrate during the fluidic self-assembly. Programmability is implemented using solder-based receptors that can be switched "ON" and "OFF" using integrated heaters. We have evaluated the feasibility of the proposed PRS concept through computer simulations using ANSYS to estimate: i) the necessary power to heat selected receptors to above the melting point of the solder and ii) the minimal spacing between receptors for preventing thermal crosstalk. A prototype platform has been fabricated to experimentally test the PRS process. The programmable sequential assembly of multiple types of components onto target positions has been demonstrated, including 300- μm -sized light-emitting diodes (LEDs) and silicon dies. Three types of defects were identified and eliminated using improved component designs, transient heating, and adequate heat sinks. A prototype color LED display segment that contains a total of 36 red, green, and yellow LED segments and 72 interconnects has been used to test the concept. The outlined process provides a new concept to the parallel integration of microdevices and systems that require electrical interconnects between components. [J2205]

"Improvement of light extraction efficiency of flip-chip light-emitting diode by texturing the bottom side surface of sapphire substrate"

A high light-extraction efficiency was demonstrated in the flip-chip light-emitting diode (FCLED) with a textured sapphire substrate. The bottom side of a sapphire substrate was patterned using a dry etching process to increase the light-extraction efficiency. Light output power measurements indicated that the scattering of photons emitted in the active layer was considerably enhanced at the textured sapphire substrate resulting in an increase in the probability of escaping from the FCLED. The light-output power of the FCLED was increased by 40.2% for a 0.4- μm deep FCLED with a periodic distance of 13- μm mesh-type texture on the bottom side of the sapphire substrate [J2206]

"Selective wet etching of p-GaN for efficient GaN-based light-emitting diodes"

The selective wet etching of a p-GaN layer by using a solution of KOH in ethylene glycol (KE) was studied to enhance the optical and electrical performance of the GaN-based light-emitting diodes (LEDs). The surface of the p-GaN, which was selectively etched in the KE solution, showed hexagonal-shaped etch pits. The light-output power of etched LEDs was improved by 29.4% compared to that of the nonetched LED. This improvement was attributed to the increase in the probability of photons to escape due to the increased surface area of textured surface and the reduction in contact resistance of the ohmic layer resulting from the increased contact area and hole concentration on the textured p-GaN. The reverse leakage current of the LED was also greatly decreased due to the surface passivation and the removal of defective regions from the p-GaN. [J2207]

"Highly coherent electronically tunable waveguide extended cavity diode laser"

A frequency agile extended cavity diode laser using an integrated Bragg reflector in a Ti: Fe: LiNbO₃ waveguide is developed and characterized. The laser emits up to 7 mW in the 1.5- μm telecommunication window. The emission spectrum exhibits a 18-kHz linewidth, >40-dB sidemode suppression ratio, and a wavelength stability of ± 1 pm over hours. Very fast mode hop-free frequency tuning is achieved through the electrooptic effect, with a tuning slope of 55.5 MHz/V. [J2208]

"Low turn-on voltage and series resistance of polarization-induced InGaN-GaN LEDs by using p-InGaN/p-GaN superlattice"

We have demonstrated high-performance InGaN-GaN multiple quantum-wells light-emitting diodes (LEDs) using polarization-induced (PI) p-InGaN-GaN superlattice. Electrical measurements show that PI LEDs produce much lower series resistance and turn-on voltage (at 20 mA) as compared to those of normal LEDs without the superlattice. It is also shown that the output power and photon wavelength of the PI LEDs remain electrically stable up to a high stress region of 200 mA. However, those of normal LEDs become electrically and optically degraded in excess of 120 mA. These results show that the use of the PI effect is very effective to the improvement of the electrical properties of LEDs. [J2209]

"The 75 mm diameter photonic XP43D2 photomultiplier with the screening grid at the anode for timing experiments"

Requirements given by large scale physics experiments and applications in border security monitoring prompted to upgrade existing large 75 mm and 130 mm diameter PMTs towards better timing properties. First, the existing dynode structure of XP4312 was improved by inserting a screening grid in front of the anode, following that applied to the XP20D0. The performance of the new XP43D2 photomultiplier was studied in comparison to XP4312 PMT. The time jitter of the new PMT was measured using a fast light pulser based on an XP22 light emitting diode. The timing properties in coincidence experiments were measured with large NaI(Tl) and plastic scintillators for ⁶⁰Co and ²²Na gamma rays and discussed in terms of the measured photoelectron numbers. [J2210]

"Low-frequency noise measurement and analysis in organic light-emitting diodes"

Low-frequency noise characteristics of organic light-emitting diodes are investigated. Two noise components were found in experimental low-frequency noise records, namely: 1) 1/f Gaussian noise from device bulk materials and 2) an excessive frequency-related part of noise related to device interfaces or defects and traps. 1/f noise is said to be related to carrier mobility. Degradation, especially photo-oxidation of the electroluminescence polymer, is a possible reason that affects carrier mobility. The excessive part of noise is believed to be related to the carrier numbers and could come from the interface deterioration, defects and traps generation and furnish. The excessive part of noise increases much faster during device stress. This shows that the degradation related interface defects and traps is much faster. [J2211]

"Enhanced brightness and efficiency of organic light-emitting diodes with an LiF in the Alq3"

Highly efficient and bright organic light-emitting diodes have been realized by inserting a thin insulating lithium fluoride (LiF) layer in the tris-(8-hydroxyquinoline) aluminum (Alq3) with conventional organic layers. By comparing the performances of newly devised devices as a function of the position of the LiF in the Alq3 layer, the authors propose the optimal position of the LiF in the Alq3 layer. Experimental results show that the efficiency and brightness of the newly devised device with LiF in the Alq3 layer were seven times higher than that without LiF in the Alq3 layer. [J2212]

"Indium-tin-oxide-free organic light-emitting device"

Sapphire substrates coated with a gold (Au) layer in place of indium-tin-oxide (ITO) on glass substrates are used as hole-injecting anodes in organic light-emitting devices (OLEDs). Due to the unique quality of the sapphire/Au interface and the match of the Au work function with the highest occupied molecular orbital level of the adjacent hole transport layer (HTL) and the smoothness of the interface, the ITO-free OLED, with the structure sapphire/Au/HTL/poly(p-phenylenevinylene)/Ca/Ag, achieved an increase in current efficiency by more than a factor of three. In addition, the flawless sapphire substrate and anode/polymer interface make dark nonemissive areas decrease in number and area. The diodes show substantially slower degradation, and the lifetime in air increases by a factor of two or more. [J2213]

"Silicon Nanocrystal Field-Effect Light-Emitting Devices"

We describe the operation of a light-emitting device in which silicon nanocrystals are electrically pumped via the field-effect electroluminescence (EL) mechanism. In contrast to the simultaneous bipolar carrier injection used in conventional p-n junction light-emitting diodes, this device employs sequential unipolar programming of both electrons and holes across a tunneling barrier from the same semiconductor channel. Light emission is strongly correlated with the injection of second carriers into nanocrystals that have been previously programmed with charges of the opposite sign. The properties of this device are well described by the model of a charge injection through Coulomb field modified tunneling processes. We additionally consider limiting performance bounds for potential future devices fabricated from nanocrystals with different radiative emission rates [J2214]

"Nitride-Based Light Emitting Diodes With Textured Sidewalls and Pillar Waveguides"

Nitride-based light emitting diodes (LEDs) with sidewall texture and pillar waveguides (STPW) were fabricated using conventional lithography method. With 20-mA injection current, it was found that forward voltages were 3.16 and 3.15 V for the conventional LED and the LED with STPW, respectively. It was also found that 20-mA LED output powers were 8.4 and 10.1 mW for conventional LED and the LED with STPW, respectively. The enhancement is attributed to the out-coupling of lateral waveguide mode in the near horizontal directions [J2215]

"Effect of Space Charge Region Width on Er-Related Luminescence in Reverse Biased Si:Er-Based Light Emitting Diodes"

In this paper, an effect of space charge region (SCR) width on Er-related electroluminescence (EL) in reverse biased Si:Er-based light-emitting diodes (LEDs) is under investigation. It is concluded that a trivial widening of the SCR in the examined LEDs with triangular and trapezoidal electric field profiles through SCR does not result in a desirable increase in the Er-related EL intensity. The tunnel transit-time diode structure with a complicated electric field profile through SCR is offered to increase the Er-related EL intensity. The difficulties hampering this process in erbium EL from reverse biased LEDs are under discussion [J2216]

"Physics and Device Structures of Highly Efficient Silicon Quantum Dots Based Silicon Nitride Light-Emitting Diodes"

An electrically driven light emitter from silicon is a long-standing problem in silicon photonics. Recently, significant progress has been made using silicon quantum dots (Si QDs) embedded in the silicon nitride thin films, transparent doping layers and electrodes, and surface-modified structures. This paper provides an overview of the progress in the device physics and fabrications of the Si QD light-emitting diodes (LEDs) including new device structures to improve the light extraction efficiency as well as highlights in the growth of the Si QDs and their quantum confinement effects (QCEs) [J2217]

"Efficiency Improvement of GaN-Based LEDs with ITO Texturing Window Layers Using Natural Lithography"

In conventional GaN light-emitting diodes (LEDs), a significant gap exists between the internal and external efficiencies owing to the narrow escape cone for light in high refractive index semiconductors. In this paper, p-side-up GaN/sapphire LEDs with surface-textured indium-tin-oxide (ITO) window layers were investigated using natural lithography with polystyrene spheres as the etching mask. Under optimum etching conditions, the surface roughness of the ITO film can reach 140 nm, while the polystyrene sphere on the textured ITO surface is maintained at about 250-300 nm in diameter. The LEDs fabricated using the surface-textured ITO provided an output power that exceeded that of the planar-surface LED by about 30% and 40% at 20 and 400 mA current injection, respectively. After calculating, the extraction quantum efficiency of ITO/GaN LEDs with and without textured surface is 22.6% and 17.4%, respectively. There is about 5.3% improvement in the extraction quantum efficiency [J2218]

"Cryogenic Behavior of Optoelectronic Devices for the Transmission of Analog Signals Via Fiber Optics"

The transmission of analog signals via fiber optics is a subject of interest for applications with detectors operating at cryogenic temperature, at ground or on space borne instruments. For those detectors, both thermal and galvanic decoupling shall be required. For a better understanding of the cryogenic performance of cooled optoelectronic devices, we have investigated an infrared AlGaAs LEDs, a Si p-i-n photodiode, a Si photodiode, and an avalanche photodiode (APD). Results of a study related to the photodiode's dark currents at low temperature is presented. In fact, we have clearly measured a strong reduction of the dark current when these devices are cooled down [J2219]

"Enhanced carrier confinement in AlInGaN-InGaN quantum wells in near ultraviolet light-emitting diodes"

To increase carrier confinement, the GaN barrier layer was substituted with an AlInGaN quaternary barrier layer which was lattice-matched to GaN in the GaN-InGaN multiple quantum wells (MQWs). Photoluminescence (PL) and high-resolution X-ray diffraction measurements showed that the AlInGaN barrier layer has a higher bandgap energy than the originally used GaN barrier layer. The PL intensity of the five periods of AlInGaN-InGaN MQWs was increased by three times compared to that of InGaN-GaN MQWs. The electroluminescence (EL) emission peak of AlInGaN-InGaN MQWs ultraviolet light-emitting diode (UV LED) was blue-shifted, compared to a GaN-InGaN MQWs UV LED and the integrated EL intensity of the AlInGaN-InGaN MQWs UV LED increased linearly

up to 100 mA. These results indicated that the AlInGaN-InGaN MQWs UV LED has a stronger carrier confinement than a GaN-InGaN MQWs UV LED due to the larger barrier height of the AlInGaN barrier layer compared to a GaN barrier layer [J2220]

"Pulse-width modulation for microcontroller servo control"

First Page of the Article [J2221]

"High efficiency and improved ESD characteristics of GaN-based LEDs with naturally textured surface grown by MOCVD"

The following paper presents a study on GaN-based light-emitting diodes (LEDs) with naturally textured surface grown by metal-organic chemical vapor deposition. The study utilizes a well-known approach of increasing light extraction efficiency. The approach is based on naturally formed V-shaped pits on surface that originate from low-temperature-growth (LTG) conditions of topmost p-GaN contact layer. In our experiment, the high-temperature-grown (HTG) p-GaN layer was inserted between the p-AlGaIn electron-blocking layer and the LTG p-GaN contact layer, in order to suppress pit-related threading dislocations (TDs). These TDs may intersect the underlying active layer. The results of the experiment show that GaN-based LEDs with the HTG p-GaN insertion layer can effectively endure negative electrostatic discharge voltage of up to 7000 V. We also noted that application of 20-mA current injection yields output power of about 16 mW for the LEDs emitting around 465 nm. The output power results correspond to an external quantum efficiency of around 30% [J2222]

"Equalization of Gaussian-Like Spectra via Optical Lattice Filters With Symmetric-Feedback Structure"

This paper presents a scheme for equalizing Gaussian-like spectra by using all-fiber lattice filters with a symmetric feedback structure. With the proposed design strategy and feedback structure, the output power of Gaussian-like spectra is maximized, and the designed equalization filter can flatten the Gaussian-like spectra in the maximally flat sense while satisfying specified spectrum performance. The design scheme is able to efficiently and systematically determine the optimal coefficients of the lattice filter through a recursion algorithm. As an illustrative example, the proposed scheme is applied to the design of an all-fiber equalization filter to flatten the output spectrum of a superluminescence light-emitting diode. Simulation and experimental results are carried out to verify the theoretical analysis [J2223]

"Comprehensive above-threshold analysis of antiresonant reflecting optical waveguide edge-emitting diode laser"

A three-dimensional (3-D) above-threshold analysis has been performed for laterally antiguided laser structures of the antiresonant-reflecting-optical-waveguide type, of relatively large core width ($\sim 10 \mu\text{m}$), for high-power, single-spatial-mode operation. A 3-D numerical code has been developed, which takes into account carrier diffusion in the quantum well as well as edge radiation losses. The laser characteristics are calculated as functions of the above-threshold drive level. Within the simulation, 3-5 higher order optical modes on a "frozen background" are computed by the Arnoldi algorithm. Because of the nonuniform gain saturation of the lasing mode, the modal gains for higher order modes increase with the drive current due to increasing overlap of their fields with the two-dimensional gain distribution. The onset of threshold for higher order modes puts an upper limit on the range for stable single-mode operation. The above-threshold analysis is done for various values of the width of the reflector region, below and above the lateral-antiresonance condition. It is found that the maximum intermodal discrimination, which in turn provides the maximum single-mode power, is obtained when the reflector-region width is $\sim 25\%$ larger than its value at antiresonance. Then, for $10\text{-}\mu\text{m}$ -core devices, stable, single-mode operation is found to occur to drive levels as high as $41 \times$ threshold, with single-mode output powers as high as 1.45 W. [J2224]

"Design and fabrication of temperature-insensitive InGaP-InGaAlP resonant-cavity light-emitting diodes"

Visible InGaP-InGaAlP resonant-cavity light-emitting diodes with low-temperature sensitivity output characteristics were demonstrated. By means of widening the resonant cavity to a thickness of three wavelength (3λ), the degree of power variation between 25°C and 95°C for the devices biased at 20 mA was apparently reduced from -2.1 dB for the standard structure design (1λ cavity) to -0.6 dB. An output power of 2.4 mW was achieved at 70 mA. The external quantum efficiency achieved a maximum of 3% at 13 mA and dropped slowly with increased current for the device. The external quantum efficiency at 20mA dropped only 14% with elevated temperature from 25°C to 95°C . The current dependent far-field patterns also showed

that the emission always took place perfectly in the normal direction, which was suitable for plastic fiber data transmission [J2225]

"Nitride-based flip-chip LEDs with transparent Ohmic contacts and reflective mirrors"

Nitride-based flip-chip light-emitting diodes (LEDs) with various transparent ohmic contacts and reflective mirrors were fabricated. At 470 nm, it was found that Ni could provide 92% transmittance while Ag could provide 92.4% reflectively. It was also found that the 20-mA forward voltages measured from LEDs with Ni+Ag, Ni+Al, and Ni+Pt were 3.15, 3.29, and 3.18 V while the output powers were 16, 13.3, and 11.6 mW, respectively. Furthermore, it was found that lifetimes of the fabricated flip-chip LEDs were good [J2226]

"The Improvement of Polycrystalline Silicon TFTs Fabricated by Employing Periodic Metal Pads"

Polysilicon films with regular-sized and large grains were fabricated by employing periodic metal (Cr-Al) pads as the heat sinks and with underlying silicon oxynitride (SiON) as the heat absorption layer. The poly-Si could grow to regular hexagonal grains after excimer laser annealing (ELA). The thin-film transistors (TFTs) fabricated by this method show uniform characteristics that are suitable for large-area applications. The TFT achieves a field-effect mobility of 270 cm²/V·s and an on-off current ratio exceeding 10⁸. It is found that the TFT with the smaller channel width and length results in a better subthreshold swing because it contains fewer grain boundaries and, thus, fewer defects. After comparing the performance of TFTs using either double-metal Cr-Al or single-metal Al photonic-crystal pads, it is found that the Cr could efficiently impede the diffusion of Al into Si during ELA [J2227]

"Microstripe-array InGaN light-emitting diodes with individually addressable elements"

High-performance InGaN light-emitting diodes consisting of 120 side-by-side and individually addressable microstripe elements have been successfully fabricated. Each stripe in these devices is 24 μm in width and 3600 μm long, with a center-to-center spacing between adjacent stripes of 34 μm. The emission wavelengths demonstrated range from ultraviolet (UV) (370 nm) to blue (470 nm) and green (520 nm). The devices show good uniformity and performance due to finger-pattern n-electrodes running between adjacent stripes. In the case of the UV devices for example, turn-on voltages are around 3.5 V and continuous-wave output powers per stripe ~80 μW at 20 mA. A major feature of these devices is their ability to generate pattern-programmable emission, which offers applications in areas including structured illumination wide-field sectioning optical microscopy [J2228]

"Active-Matrix Amorphous-Silicon TFTs Arrays at 180 on Clear Plastic and Glass Substrates for Organic Light-Emitting Displays"

An amorphous-silicon thin-film transistor (TFT) process with a 180 degC maximum temperature using plasma-enhanced chemical vapor deposition has been developed on both novel clear polymer and glass substrates. The gate leakage current, threshold voltage, mobility, and on/off ratio of the TFTs are comparable with those of standard TFTs on glass with deposition temperature of 300 degC-350 degC. Active-matrix pixel circuits for organic light-emitting displays (LEDs) on both glass and clear plastic substrates were fabricated with these TFTs. Leakage current in the switching TFT is low enough to allow data storage for video graphics array timings. The pixels provide suitable drive current for bright displays at a modest drive voltage. Test active matrices with integrated polymer LEDs on glass showed good pixel uniformity, behaved electrically as expected for the TFT characteristics, and were as bright as 1500 cd/m² [J2229]

"Nitride-based flip-chip p-i-n photodiodes"

Nitride-based flip-chip p-i-n photodiodes were fabricated and characterized. It was found that we could achieve a small dark current of 5 times 10⁻¹⁰ A at -5 V and a large rejection ratio larger than three orders of magnitude. It was also found that the photodiodes only detect optical signals with wavelengths between 365 and 378 nm. Furthermore, it was found that peak responsivity occurs at around 370 nm with a value of 0.21 A/W at zero bias which corresponds to 70% external quantum efficiency [J2230]

"Si nanocluster sensitization of Er-doped silica for optical amplifier using top-pumping visible LEDs"

A review is presented of Si nanocluster sensitization of Er-doped silica for planar optical amplifiers using top-pumping 470-nm light-emitting diodes (LEDs). The motivation and basic physical principles underlying the nanocluster sensitization are first reviewed. The material structures necessary for optimum performances are presented, with emphasis on the need for nanoscale engineering of the composition and structure. Evidence of optical gain using commercial GaN-visible LEDs are presented, and the simulation results of possible device

performances described. Finally, some possible future directions for research are discussed [J2231]

"Fluidic heterogeneous microsystems assembly and packaging"

The nonrobotic fabrication of packaged microsystems that contain nonidentical parts has been accomplished by a directed self-assembly process. The self-assembly process uses geometrical shape recognition to identify different components and subsequent bond formation between liquid solder and metal-coated areas to form mechanical and electrical connections. We applied this concept of shape recognition and subsequent formation of contacts to assemble and package microsystems that contained nonidentical subunits. The self-assembly of three-component assemblies is demonstrated by sequentially adding device segments to the assembly solution including 200- μm -sized light-emitting diodes. Six hundred AlGaInP-GaAs light-emitting diode segments self-assembled onto device carriers in 2min without defects. Encapsulation units self-assembled onto the LED-carrier assemblies to form a three-dimensional (3-D) circuit path to operate the final device. The reported procedure provides a new route to the creation of autonomous heterogeneous microsystems including the realization of autonomous wireless sensor system that requires nonidentical units: CMOS circuitry, Non-CMOS sensor unit for sensing, III-V components for communication, and encapsulation units to form 3-D electrical interconnects. The creation of such systems is being discussed and a proof of concept experiment is being demonstrated [J2232]

"Where's My Holodeck? The New Frontier of Media Display"

The author discusses unconventional displays of the future, such as handheld projectors the size of a matchbox, organic LEDs (OLEDs), electrophoretic ink, Guricon bichromal beads, roll-up electronic newspapers, and rewritable displays in supermarkets. [J2233]

"The effect of different bonding temperatures on the mechanical and electrical performance of NCF-bonded flip-chip-on-flex packages"

Liquid crystal displays (LCDs) and organic light emitting diodes (OLEDs) are the technology involved in electronic displays in order to get a better viewing angle and high-density resolution products. Fine-pitch, flip-chip interconnection is one method which is able to enhance the display performance with high color resolution. Nonconducting film (NCF) is a novel material developed for fine-pitch applications. This study investigates the temperature effect on the electrical contact performance of an NCF-bonded chip-on-flexible (COF) substrate package. The changes in contact resistance after reflow at a peak temperature of 260degC for three times were measured with a four-point probe method. The bonding temperature has a significant effect on the peel strength of the NCF-bonded COF. A high peel strength for the NCF COF bonded at a high temperature indicated that the NCF obtained sufficient mechanical strength to hold the interconnection joints. A low bonding temperature is preferable to obtain good electrical contact, but sufficient high temperature is needed to ensure a good mechanical and reliable joint. An excessively high bonding temperature is to be avoided because it gives instant curing at the contact point which restricts good electrical conduction. An NCF with a curing degree of ~86% was needed to ensure sufficient and reliable electrical joints in the COF [J2234]

"Silicon-based packaging platform for light-emitting diode"

A novel concept of silicon-based packaging platform with microreflector and embedded electrode-guided interconnections was development for a package component of a light-emitting diode (LED). TracePro and ANSYS software were respectively used to understand the optical and thermal characteristics of the package component. Simulation results show the microreflector at several certain specific dimensions can be used to achieve high brightness, and the carrier made of silicon wafer compared with that of aluminum stage can minimize the thermal stresses caused by mismatch of thermal expansion coefficient. The novel packaging platform was fabricated by silicon bulk micromachining and solder reflow techniques. Various solutions in fabricating embedded solder interconnections were explored to accomplish the electrode-guided interconnections. Experimental results show the method using solder paste reflow can achieve better yield and performance. The electrical resistances of such solder interconnections with the height of 100 μm were measured to be less than 5 Ω . As such, this technique can be applied broadly in packaging for conventional optoelectronic semiconductor devices such as laser diodes and image sensors [J2235]

"Detection of high-speed voltage waveforms in GaN devices using electric-field-induced second-harmonic generation"

We use electric-field-induced second-harmonic generation (EFISHG) to measure high-speed voltage waveforms in commercial GaN light-emitting diodes (LEDs). The output of an ultrafast passively mode-locked Ti: sapphire laser is reflected from the surface of a GaN UV LED. Copropagating with the specularly reflected Ti: sapphire

fundamental is second-harmonic light that is proportional to and synchronous with a high-speed voltage pulse that reverse biases the LED. The measured amplitude of the detected pulse was found to vary with dc bias across the p-n junction of the LED indicating that the detected voltage waveform was localized to the p-n junction. Because of synchronous detection, the detection bandwidth (<10 THz) is limited only by the pulsewidth of the probe laser pulse (<100 fs) [J2236]

"Low-cost and low-loss multimode waveguides of photodefinable epoxy"

To satisfy the urgent need for low-cost multimode planar waveguides, we developed photodefined, multimode-fiber compatible waveguides with low-cost commercially available epoxies showing low losses from 550 to 1100 nm and around 1300nm [J2237]

"Optimization of the active-Layer structure for the deep-UV AlGaIn light-emitting diodes"

The dependence of the active-layer structure on the performance of the deep-UV AlGaIn light-emitting diodes (LEDs) was theoretically investigated with an APSYS simulation program. Several structure parameters such as well width, well number, barrier height, barrier width, and doping type were employed to study how these parameters change the band structures as well as the carrier distributions. The band offset and bowing parameter used in the theoretical analysis were extracted from the experimental results. Theoretical analysis shows that the nonuniform carrier distributions as well as the low hole concentrations, which caused by polarization-induced tilted band structures, play important roles in improving the performance of the AlGaIn LEDs. Compensating this asymmetric band structure and increasing the hole density are the important keys to improve the AlGaIn LED performance. Numerical simulation results suggest that the higher output power can be obtained when the active layer consists of only one quantum well with a width of 1-3 nm and two thicker n-doped barriers with a small Al composition [J2238]

"Analysis of temperature-dependent optical gain in GaN-InGaIn quantum-well structures"

The temperature dependent spectral gain in InGaIn-GaN multiple quantum-well structures with 10% In content is investigated. Mode gain is measured in a temperature range between 239 K and 312 K using the Hakki-Paoli technique and compared to simulations. The simulation accounts for temperature-dependent polarization dephasing, and hence homogeneous broadening, in a rigorous fashion, without any fit parameter. It is found that the evolution of the gain spectrum with temperature at different drive currents can be modeled using a temperature-independent single value for inhomogeneous broadening. The resulting compositional fluctuations are compared to structural measurements [J2239]

"GaN-based light-emitting diode structure with monolithically integrated sidewall deflectors for enhanced surface emission"

To improve the overall surface emission efficiency, the structure of a standard GaN light-emitting diode (LED) was modified; the mesa sidewalls were etched at an angle, and deep enough to reach the sapphire substrate. Photoexcitation experiments, including photoluminescence and near- and far-field emission patterns, were performed on LED-like test devices, and results indicated that the angled sidewalls efficiently deflect photons that are initially guided laterally within the GaN epilayer in the off-surface direction. For a sidewall angle of 30deg, the total surface emission strength was improved by a factor exceeding three. Computer simulations produced results consistent with the experimental observations [J2240]

"Heart of a new machine [Jrobot that can express different moods]"

Graduate students at Carnegie Mellon's Entertainment Technology Center has designed a robot that features five different "moods." Called Quasi, the 76-centimeter tall robot is a captivating character that goes beyond the standard animatronic amusement park figures. Quasi can express happiness, sadness, anger, confusion, and embarrassment. These moods are conveyed most obviously by the color of its light-emitting-diode eyes and antennae. The moods are controlled by a finite state machine, a software-based behavioral model that triggers certain actions when specific conditions are met. [J2241]

"Design of a low-cost optical instrument for pH fluorescence measurements"

This paper describes the electronic design and the performance of a low-cost fiber-optic instrument for pH fluorescent measurements. The chemical sensing phase consists of an organic pH indicator (mercurochrome) immobilized in a sol-gel matrix placed at the end of a fiber optic by means of a steel grid. The active phase was excited by means of a high-intensity blue light-emitting diode. The light signal was modulated to avoid external interference. Fluorescence emission is detected by a low-cost photodiode. To avoid drifts in excitation light

emission intensity, a ratiometric measurement was proposed. To perform such measurements, two fiber-optic measurement channels were used. One of them was employed to measure only the pH indicator fluorescent emission intensity. The second channel was employed to measure only the intensity of the excitation light reflected by the sensing phase. The ratio between both signals is only proportional to pH and proved to be independent of excitation light intensity. The sensor is useful over the pH range of 4-8, providing highly reliable results [J2242]

"The improvement in modulation speed of GaN-based Green light-emitting diode (LED) by use of n-type barrier doping for plastic optical fiber (POF) communication"

We demonstrate a high-speed GaN-based light-emitting diode at a wavelength of around 500 nm for the application to plastic optical fiber communication. By use of the n-type doping in the GaN barrier layers of the In_xGa_{1-x}N-GaN-based multiple-quantum-well (MQW), superior performance of modulation-speed (120 versus 40 MHz) and output power to the undoped control under the same bias current has been observed. According to the measured electrical-to-optical bandwidths and extracted RC-limited bandwidths of both devices, the superior speed performance can be attributed to higher electron/hole radiative recombination rate in the n-doped MQW than that of undoped MQW [J2243]

"Using the Taguchi method to improve the brightness of AlGaInP MQW LED by wet oxidation"

To increase the external quantum efficiency of a light-emitting diode (LED) while limiting its forward voltage (V_f), we prepared both (Al_xGa_{1-x})_{0.5}In_{0.5}P LED and buried oxides through selective wet oxidation of the AlAs layers of AlAs-GaAs distributed Bragg reflectors. The wet oxidation process forms a stable Al₂O₃ material that acts as an insulation layer and affects both the carrier and optical confinements. To determine the tradeoff conditions for LED oxidation, we used the Taguchi method which is a robust technique that is often used to analyze significant trends that occur under a set of oxidation conditions. In this study, we used an L₉orthogonal array to measure the effects that a series of factors have upon the maximum brightness performance of the LED in an effort to limit the values of V_f. Relative to the as-grown LED, the oxidized LED that had been treated under the tradeoff wet-oxidation conditions displayed a sharply enhanced brightness (62.4% increase) in conjunction with only a slightly increased value of V_f(only a 24.5% increase) [J2244]

"Flip-Chip p(GaN)-i(GaN)-n(AlGaIn) Narrowband UV-A Photosensors"

Flip-chip p(GaN)-i(GaN)-n(AlGaIn) photosensors with extremely low dark currents were fabricated and characterized. It was found that the sensor with a 0.5-μm-thick Si-doped n⁺-Al_{0.15}Ga_{0.85}N layer could only detect optical signals with wavelength in between 325 and 360 nm. With an incident wavelength of 355 nm, the authors achieved a peak responsivity of 0.16 A/W at zero bias, which corresponds to an external quantum efficiency of 56% [J2245]

"Introducing Lance Griffiths, Associate Editor for GOLD [JThe GOLD Report]"

{no data available} [J2246]

"Low-Cost Surface-Mount LED Gas Sensor"

A low-cost chemical sensor comprising surface-mount light-emitting diodes (LEDs) has been developed for colorimetric gas detection. The device consists of a pair of LEDs connected to a simple PIC microcontroller circuit and in the most basic form, requires the use of only two input-output (I/O) pins on the chip. The key features of this sensor are the use of a LED rather than a photodiode for light detection and an all-digital light detection protocol that leads to a reduction in cost and power consumption by avoiding the need for an analog-to-digital converter. The surface-mount diodes employed are more compact than standard LEDs and are more amenable to coating by solid-state sensor films. Results from sensors employing a chemochromic ammonia sensitive film are presented, and the detection of this target is demonstrated in the parts-per-million range. The configuration is applicable to a wide range of colorimetric gas sensing materials [J2247]

"Piezoelectric actuators employing PVDF coated with flexible PEDOT-PSS polymer electrodes"

Piezoelectric polymer sheets usually have metallic electrodes that considerably stiffen the sheet and correspondingly decrease its piezoelectric response in actuator and sensor applications. We have developed both airbrush and inkjet printing methods for applying electrodes of the conducting polymer poly(ethylene dioxythiophene) (PEDOT-PSS) to sheets of poly(vinylidene fluoride) (PVDF). PEDOT-PSS electrodes of reasonable thickness have considerably higher resistance than metal electrodes. We calculated the voltage and current response as a function of position on the electrodes of a single "electroded" PVDF sheet. We did this

both for a rectangular sheet with an ac voltage applied at one end, and for a semicircular sheet with ac voltage applied to a small semicircular metal tab. By finding the response as a function of frequency, we can determine the necessary electrode thickness for various applications. Next we calculated the extension-mode piezoelectric response of a rectangular sheet to an ac voltage applied at one end. We made and tested bimorphs of two such electroded sheets that are glued together to give a bending response. We have also constructed actuators made of two bimorphs attached together at both ends. Better response is achieved than for similar actuators constructed from sheets with metal electrodes. Finally, we compare results for these high-displacement, low-force actuators with those for low-displacement, high-force actuators of direct extension designs, and propose a cylindrical actuator design with intermediate displacement and force [J2248]

"UV-LED controlled GaN-based SAW phase shifter"

The UV-LED controlled phase shifter of an RF signal based on a GaN-sapphire surface-acoustic-wave (SAW) filter has been implemented. At the optical wavelength 298 nm and SAW frequency 307 MHz, the UV-induced relative change in SAW velocity per unit optical power density is $2 \times 10^{-6} (\mu\text{W}/\text{mm}^2)^{-1}$ corresponding to 3.7deg phase shift. The phase modulation of an RF signal by rectangular UV pulses has been demonstrated. The efficiency of the phase shifter can be considerably improved by proper selection of sheet-resistivity of the GaN layer [J2249]

"Space charges and traps in polymer electronics"

A review is undertaken of the role of space charges and traps in polymer electronic devices. The origin of the space charges considered include electrode injection leading to space-charge-limited currents in organic light emitting diodes (OLEDs), ionized impurities leading to rectification at Schottky junctions and mobile ion effects. Also considered are the effects of traps on the performance of organic metal-insulator-semiconductor field-effect transistors (MISFETs) [J2250]

"Polarization Insensitive Asymmetric Ridge Waveguide Design for Semiconductor Optical Amplifiers and Super Luminescent Light-Emitting Diodes"

A polarization-insensitive waveguide design featuring a novel asymmetric ridge structure is proposed. This design relaxes former stringent constraints imposed on material compositions (i.e., refractive indices) and geometrical dimensions in an attempt to reach low polarization sensitivity over a broad wavelength operating range. In conjunction with a bulk active region with an isotropic gain, such a design is highly desirable for its potential to eliminate the polarization dependence of the optical gain in semiconductor optical amplifiers or output power in super luminescent light-emitting diodes [J2251]

"Piezoelectrets from thermo-formed bubble structures of fluoropolymer-electret films"

Cellular and porous polymers with internal bipolar space charge can exhibit large piezoelectric thickness coefficients and have therefore led to significant advances in the understanding and the application of piezoelectricity in polymer electrets. As possible alternatives to these cellular ferroelectrets, other potentially useful configurations of space-charge electrets, such as bi-layer or multi-layer stacks of at least one "soft" porous and one "hard" non-porous electret film have been suggested and investigated. Extending the concept of cellular or porous polymer electrets with microscopic voids, we propose and describe novel piezoelectret structures with regular arrays of millimeter-sized bubbles that are formed between fluoro-ethylene-propylene (Teflonreg-FEP) films via a vacuum-assisted thermal process. After internal charging by means of high impulse voltages, the bubble structures exhibit rather large piezoelectric activities in their thickness direction, with phenomenological quasi-static d_{33} coefficients of up to 500 pC/N (or pm/V) which quite strongly decrease with the amplitude of the applied force. The electromechanical behavior of the new piezoelectrets has been modeled in analogy to the operation of electret microphones [J2252]

"Orange–Red Light-Emitting Diodes Based on a Prestrained InGaN–GaN Quantum-Well Epitaxy Structure"

The implementations of an orange and a red light-emitting diode (LED), which are fabricated with a prestrained InGaN-GaN quantum-well (QW) epitaxy structure, are demonstrated. The prestrain condition is created by growing a low-indium QW before the growth of five high-indium QWs. Without the prestrain condition, the five high-indium QWs of the same growth condition lead to green electroluminescence emission. With the prestrained growth, indium incorporation in the QWs grown after the low-indium one becomes higher and hence the orange-red LEDs can be fabricated for elongating the emission wavelength by more than 100 nm. Although the crystal quality and electrical properties of the orange-red LEDs may need to be improved, our results have shown the

important effect of prestrained growth for elongating the LED wavelength [J2253]

"Polymeric MOEMS Variable Optical Attenuator"

In this letter, we take advantage of the high coefficient of thermal expansion (CTE) of a chemically amplified, epoxy-based negative polymer (SU-8) to define a low-power consumption polymeric variable optical attenuator that combines the working principles of microoptoelectromechanical systems and photonic lightwave circuits. The SU-8 symmetric structure comprises a seismic mass and four mechanical beams. Three multimode waveguides are defined on this structure: two of them are located on the frame and the third one in the middle of the seismic mass. Aluminum is used as a heater electrode extending over two of the mechanical beams and part of the seismic mass. When a dc voltage is applied, the mechanical beams bend, resulting in a misalignment between the waveguides. Experimental results have shown a power consumption of 12 mW at 20 dB with a working wavelength of 633nm emitted from a light-emitting diode [J2254]

"High Light-Extraction GaN-Based Vertical LEDs With Double Diffuse Surfaces"

High light-extraction (external quantum efficiency ~40%) 465-nm GaN-based vertical light-emitting diodes (LEDs) employing double diffuse surfaces were fabricated. This novel LED structure includes one top transmitted diffuse surface and another diffuse omnidirectional reflector (ODR) on the bottom of a LED chip. The diffusive ODR consists of a roughened p-type GaN layer, an indium-tin-oxide (ITO) low refractive index layer, and an Al layer. The surface of the p-type GaN-layer was naturally roughened while decreasing the growth temperature to 800 degC. After flip-bonding onto a Si substrate by AuSn eutectic metal and laser lift-off processes to remove the sapphire substrate, an anisotropic etching by dilute potassium hydroxide (KOH) was employed on the N-face n-GaN layer to obtain transmitted diffuse surfaces with hexagonal-cone morphology. The double diffused surfaces LEDs show an enhancement of 56% and 236% in light output power compared to single side diffused surface and conventional LEDs, respectively. The devices also show a low leakage current in the order of magnitude of 10⁻⁸A at -5 V and a calculated external quantum efficiency of about 40%. The high scattering efficiency of double diffused surfaces could be responsible for the enhancement in the device light output power [J2255]

"Enhanced Light Extraction in GaInN Light-Emitting Diode With Pyramid Reflector"

GaInN light-emitting diodes (LEDs) that employ a reflector consisting of an array of three-dimensional (3-D) SiO₂pyramids and a Ag layer are demonstrated to have enhanced light extraction compared with GaInN LEDs with planar Ag reflector. Ray tracing simulations reveal that the pyramid reflector provides 14.1% enhancement in extraction efficiency. Consistent with the simulation, it is experimentally demonstrated that GaInN LEDs with the pyramid reflector show 13.9% higher light output than LEDs with a planar Ag reflector. The enhancement is attributed to the appearance of an additional escape cone for light extraction enabled by the 3-D pyramid reflector [J2256]

"Highly Reliable Nitride-Based LEDs With Internal ESD Protection Diodes"

Nitride-based light-emitting diodes (LEDs) with internal electrostatic-discharge (ESD) protection diodes emitting at 460 nm were proposed and realized. By building an internal GaN p-n junction diode, a negative ESD-induced pulse current is expected to flow through the protection diode without damaging the major LED. The ESD characteristic of the fabricated LEDs was obviously improved with this design. Furthermore, the dimension of the internal p-n diode would influence the capacity for tolerating the ESD stress. It was found that a negative ESD threshold could be significantly increased from 300-400 to 2000 V. On the other hand, the authors managed to bring down the 20-mA operation voltage to 3.29 V using the n-metal finger, which entails a good current spreading under operation as the result of a reduced current-crowding effect. Since a good current spreading beneficially alleviates the thermal effect under long-term operation, an effective pattern layout design clearly would also prolong the lifetime of the proposed LEDs [J2257]

"Alternating-Current White Thin-Film Light-Emitting Diodes Based on Hydrogenated Amorphous Carbon Layer"

Alternating-current white thin-film light-emitting diodes (ACW-TFLEDs) have been fabricated and demonstrated with composition-graded hydrogenated intrinsic amorphous silicon carbide (i-a-SiC: H) layers. It was found that H₂-plasma treatment of luminescent i-a-C: H layer played an important role in decreasing the ACW-TFLED electroluminescence (EL) threshold voltage, increasing the brightness, and broadening the EL spectrum. The EL spectra of the ACW-TFLED under either dc forward or reverse bias, or the sinusoidal alternating-current voltage were qualitatively very similar, with a peak wavelength at about 505 nm and a broad full-width at half maximum (FWHM) about 240 nm. This device revealed a brightness about 800(500)cd/m² under dc forward (reverse) bias at an injection current density of 600 mA/cm² [J2258]

"Ubiquitous Experience Media"

We exploit recorded activities as a good source of human-human and human-robot communication for sharing experience, memory, and knowledge. In particular, we're interested in audiovisual, ubiquitous, and wearable-experience-capturing technology as interaction-grounded lifelong tools. We've developed several devices-such as a wearable interaction tracker-that facilitate an indexed recording of human experiences [J2259]

"A New Poly-Si TFT Current-Mirror Pixel for Active Matrix Organic Light Emitting Diode"

A new poly-Si thin-film-transistor (TFT) current-mirror-active-matrix-organic-light-emitting-diode (AMOLED) pixel, which successfully compensates for the variation of the threshold voltage as well as mobility in the excimer laser annealed poly-Si TFT pixel, is designed and fabricated. The OLED current (IOLED) of the proposed pixel does not depend on the operating temperature. When the temperature of pixel is increased from 27 degC to 60 degC, the IOLED of the new pixel circuit composed of four TFTs and one capacitor increases only about 1.5%, while that of a conventional pixel composed of two TFTs and one capacitor increases about 37%. At room temperature, nonuniformity of the IOLED in the proposed circuit was also considerably suppressed at around 9%. We have successfully fabricated a 1.2-in AMOLED panel (96times96timesred green blue) to evaluate the performance of the proposed pixel. A troublesome residual image caused by the hysteresis phenomenon of the poly-Si TFT was almost eliminated in the proposed AMOLED panel as a result of current programming [J2260]

"Stable Organic LED Displays Using RMS Estimation of Threshold Voltage Dispersion"

Active matrix organic light-emitting-diode (OLED) displays using the amorphous silicon (a-Si:H) thin-film transistor (TFT) as the active element offer a promising avenue for high-performance displays. However, the TFT is prone to a gate-bias-dependent threshold voltage shift (VTshift) which leads to current instability, thus affecting the pixel brightness. This brief discusses an rms error estimation technique with an HVCMOS-TFT implementation to stabilize the OLED current [J2261]

"Enhancement of Performance of Si Nanocrystal Light-Emitting Diodes by Using Ag Nanodots"

Effects of Ag nanodots on silicon nanocrystal (nc-Si) light-emitting diodes (LEDs) are investigated. The electrical property of the nc-Si LED with Ag nanodots was enhanced compared to that of the nc-Si LED without ones. This was attributed to the increase in the electric field due to the formation of Ag nanodots at the contact interface, indicating that the current could flow more efficiently from the indium tin oxide layer to n-SiC film. The formation of Ag nanodots with a size of 3~6 nm was confirmed by using a high-resolution transmission electron microscope analysis. Moreover, light output power of the nc-Si LED with Ag nanodots was enhanced [J2262]

"Enhancement of InGaN–GaN Indium–Tin–Oxide Flip-Chip Light-Emitting Diodes With TiO₂–SiO₂ Multilayer Stack Omnidirectional Reflector"

Enhancement of light extraction of GaN-based flip-chip indium-tin-oxide light-emitting diodes (FC ITO LEDs) with an omnidirectional reflector (ODR) is presented. The ODR consisting of alternating layers of TiO₂ and SiO₂ is designed to possess a complete photonic bandgap within the blue region of interest, and it is fabricated by E-beam deposition. At a driving current of 300mA and a chip size of 1 mm×1 mm, the light output power of the FC ITO LEDs with the ODR reaches 156 mW. This is an enhancement of 31% when compared with the same device with an Al mirror instead. Furthermore, by examining the radiation patterns, the FC ITO LED with the ODR shows stronger enhancement around the vertical direction. Our work offers promising potential for enhancing output powers of commercial light-emitting devices [J2263]

"InP-Based Transverse Junction Light-Emitting Diodes for White-Light Generation at Infrared Wavelengths"

We demonstrate a novel white-light light-emitting-diode (LED) structure that operates at infrared wavelengths for broadening optical bandwidth performance. The nonuniform carrier distribution problem that occurs in the multiple quantum wells (MQWs) of traditional vertical p-n junction LEDs can be totally eliminated by incorporating a transverse p-n junction with MQWs which have different center wavelengths. The wide optical 3-dB bandwidth achieved (~550 nm) is very stable and varies only negligibly with the bias current. For a bias current of 60 mA, a tremendously wide 3-dB optical bandwidth (580 nm, 1042 ~ 1622nm) has been demonstrated [J2264]

"High-reflectivity Al-Pt nanostructured Ohmic contact to p-GaN"

The effect of nanoscale Pt islands on the electrical characteristics of contacts to p-type gallium nitride (GaN) has

been investigated to explore the feasibility for the flip-chip configuration light-emitting diodes (LEDs) using an Al-based reflector. An as-deposited Al contact to p-GaN with a net hole concentration of $3 \times 10^{17} \text{ cm}^{-3}$ was rectifying. However, an Al contact with nanoscale Pt islands at the interface exhibited ohmic behavior. A specific contact resistivity of $2.1 \times 10^{-3} \Omega \text{ m}^2$ and a reflectance of 84% at 460 nm were measured for the Al contact with nanoscale Pt islands. Current-voltage temperature measurements revealed a Schottky barrier height reduction from 0.80 eV for the Al contact to 0.58 eV for the Al contact with nanoscale Pt islands. The barrier height reduction may be attributed to electric field enhancement and the enhanced tunneling due to the presence of the nanoscale Pt islands. This will offer an additional silver-free option for the p-type ohmic contact in flip-chip configuration LEDs. Theory suggests that the ohmic contact characteristics may be improved further with smaller Pt islands that will enhance tunneling across the interface with the GaN and in the vicinity of the Pt-Al interface [J2265]

"Directional Control of Light-Emitting-Diode Emission Via a Subwavelength-Apertured Metal Surface"

A thin Au film with a hexagonal array of subwavelength apertures has been integrated onto a semiconductor light-emitting diode. This produces a highly directional far-field pattern with a strong polarization dependence and alters the spectral shape of the light emission from the semiconductor. A two-dimensional k-space analysis of the experimental data shows good agreement with a simple model of surface plasmon to photon coupling via the periodic structure of the metal film [J2266]

"High-sensitivity detection of narrowband light in a more intense broadband background using coherence interferogram phase"

This paper describes an optical interferometric detection technique, known as the interferogram phase step shift, which detects narrowband, coherent, and partially coherent light in more intense broadband incoherent background light using changes in the phase gradient with the optical path difference of the coherence interferogram to distinguish the bandwidth or coherence of the signal from that of the background. The detection sensitivity is assessed experimentally by measuring the smallest signal-to-background ratio or signal-to-clutter ratio (SCR), which causes a detectable change in the self-coherence interferogram phase. This minimum detectable SCR (MDSCR) is measured for the multimode He-Ne laser, resonant-cavity light-emitting diode (LED), narrowband-filtered white light, and LED signal sources in a more intense tungsten-halogen-lamp white-light background. The highest MDSCRs to date, to the authors' knowledge, are -46.42 dB for coherent light and -31.96 dB for partially coherent light, which exceed those of existing automatic single-domain techniques by 18.97 and 4.51 dB with system input dynamic ranges of 19.24 and 11.39 dB, respectively. The sensitivity dependence on the signal-to-system bandwidth ratio and on the relative offset of their central wavelengths is also assessed, and optimum values are identified [J2267]

"Poly(dimethylsiloxane)-Based Packaging Technique for Microchip Fluorescence Detection System Applications"

A simplified integration process including packaging is presented, which enables the realization of the portable fluorescence detection system. A fluorescence detection microchip system consisting of an integrated p-i-n photodiode, an organic light-emitting diode as the light source, an interference filter, and a microchannel was developed. The on-chip fluorescence detector fabricated by poly(dimethylsiloxane) (PDMS)-based packaging had a thin-film structure. A silicon-based integrated p-i-n photodiode combined with an optical filter removed the background noise, which was produced by an excitation source, on the same substrate. The active area of the finger-type p-i-n photodiode was extended to obtain a higher detection sensitivity of fluorescence. The sensitivity and the limit of detection (LOD; $S/N=3$) of the system were 0.198 nA/ μM and 10 μM , respectively [J2268]

"IGBT-Based Cost-Effective Energy-Recovery Circuit for Plasma Display Panel"

A new insulated-gate-bipolar-transistor (IGBT)-based cost-effective energy-recovery circuit (ERC) for a plasma display panel (PDP) is proposed. Since it is composed of two small resonant inductors and four power diodes instead of the conventional large auxiliary circuit, it features a simpler structure, less mass, fewer power devices, higher efficiency, and lower cost. Since all its power switches are turned off under the zero-current switching operation, IGBTs can be employed as power switches. Moreover, the very stable and uniform light emitted from a PDP proves the high quality of screen. Therefore, it is well suitable for the consumer-affordable hang-on-the-wall TVs which have the desirable features such as thinness, lightness, high efficiency, low price, etc. To confirm the validity of the proposed ERC, a comparative analysis and experimental results based on a whole ac PDP driver equipped with the proposed circuit for the 42-in PDP are presented [J2269]

"Localised joule heating in AlGaInP light emitting diodes"

First Page of the Article [J2270]

"Physics and Device Structures of Highly Efficient Silicon Quantum Dots Based Silicon Nitride Light-Emitting Diodes"

An electrically driven light emitter from silicon is a long-standing problem in silicon photonics. Recently, significant progress has been made using silicon quantum dots (Si QDs) embedded in the silicon nitride thin films, transparent doping layers and electrodes, and surface-modified structures. This paper provides an overview of the progress in the device physics and fabrications of the Si QD light-emitting diodes (LEDs) including new device structures to improve the light extraction efficiency as well as highlights in the growth of the Si QDs and their quantum confinement effects (QCEs). [J2271]

"Efficiency Improvement of GaN-Based LEDs with ITO Texturing Window Layers Using Natural Lithography"

In conventional GaN light-emitting diodes (LEDs), a significant gap exists between the internal and external efficiencies owing to the narrow escape cone for light in high refractive index semiconductors. In this paper, p-side-up GaN/sapphire LEDs with surface-textured indium-tin-oxide (ITO) window layers were investigated using natural lithography with polystyrene spheres as the etching mask. Under optimum etching conditions, the surface roughness of the ITO film can reach 140 nm, while the polystyrene sphere on the textured ITO surface is maintained at about 250–300 nm in diameter. The LEDs fabricated using the surface-textured ITO provided an output power that exceeded that of the planar-surface LED by about 30% and 40% at 20 and 400 mA current injection, respectively. After calculating, the extraction quantum efficiency of ITO/GaN LEDs with and without textured surface is 22.6% and 17.4%, respectively. There is about 5.3% improvement in the extraction quantum efficiency. [J2272]

"Introduction to the Issue on Silicon Photonics"

{no data available} [J2273]

"High-Temperature Degradation of GaN LEDs Related to Passivation"

This paper describes the thermally activated failure mechanisms of GaN light-emitting diode (LED)-test structures related with the presence of a hydrogen-rich SiN passivation layer. It is shown that the properties of the passivation layer can remarkably affect devices' stability during high-temperature stress: Degradation mechanisms identified consist of radiative efficiency loss, emission crowding, and forward-current decrease. The radiative efficiency degradation was found to be thermally activated, with activation energy equal to 1.3 eV. This failure mechanism of LEDs is attributed to the thermally activated indiffusion of hydrogen from the passivation layer to p-type region of the diodes, with subsequent p-doping compensation and/or worsening of the transport properties of the p-side ohmic contact and p-type semiconductor [J2274]

"Sixty Thousand Hour Light Output Reliability of AlGaInP Light Emitting Diodes"

Both fixed current density and variable current density stress conditions are used to study light output degradation of $(\text{Al}_x\text{Ga}_{1-x})_0.5\text{In}_{0.5}\text{P}$ light-emitting diodes (LEDs) as functions of LED stress current and LED stress time. Quantification of the resulting data indicates that $(\text{Al}_x\text{Ga}_{1-x})_0.5\text{In}_{0.5}\text{P}$ LED degradation, D , is a linear function of current density, J , and a logarithmic function of stress time, t , for stress times as long as 60 000 hours in duration. For stress times long enough and current densities high enough to saturate any short-term effects $(\text{Al}_x\text{Ga}_{1-x})_0.5\text{In}_{0.5}\text{P}$ LED degradation is therefore quantified by the empirical equation $D=D_1+D_2J+(D_3+D_4J)\ln(t)$, where D_1 , D_2 , D_3 , and D_4 are independent of LED stress current and LED stress time. Within the limits of the data presented here, this equation is shown to accurately describe light output degradation of individual LED lamps, the average degradation behavior of individual LED wafers, and the average degradation behavior of a distribution of multiple LED wafers. The resulting expression may thus provide helpful guidance in quantifying the tradeoff between LED flux and LED degradation, both of which depend linearly on current density [J2275]

"Effect of Space Charge Region Width on Er-Related Luminescence in Reverse Biased Si:Er-Based Light Emitting Diodes"

In this paper, an effect of space charge region (SCR) width on Er-related electroluminescence (EL) in reverse biased Si:Er-based light-emitting diodes (LEDs) is under investigation. It is concluded that a trivial widening of

the SCR in the examined LEDs with triangular and trapezoidal electric field profiles through SCR does not result in a desirable increase in the Er-related EL intensity. The tunnel transit-time diode structure with a complicated electric field profile through SCR is offered to increase the Er-related EL intensity. The difficulties hampering this process in erbium EL from reverse biased LEDs are under discussion. [J2276]

"Improved Light Extraction of Nitride-Based Flip-Chip Light-Emitting Diodes Via Sapphire Shaping and Texturing"

A novel flip-chip structure of GaN-sapphire light-emitting diodes (LEDs) was developed to improve the external quantum efficiency, where the sapphire substrate was textured and shaped with beveled sidewalls using a wet etching technique. The forward voltage of the conventional flip-chip and shaped flip-chip GaN LEDs were 2.84 and 2.85 V at 20 mA, respectively. This indicates that the GaN LED was not destroyed during the sapphire wet etching process. It was found that the output power increased from 9.3 to 14.2 mW, corresponding to about 52% increases in the external quantum efficiency. The results agree well with the simulation data that the shaped flip-chip GaN LED can provide better light extraction efficiency than that of the conventional flip-chip sample [J2277]

"Introduction to the Issue on Silicon Photonics"

{no data available} [J2278]

"Electrically Injected Quantum-Dot Photonic Crystal Microcavity Light-Emitting Arrays With Air-Bridge Contacts"

We demonstrate direct electrical carrier injection into membrane photonic crystal (PC) microcavities with quantum-dot radiating elements via metallic air-bridges. The bridges are 300 nm tall, 200-400 nm wide, 3-13 μm long, and have surface contact width \sim 200-300 nm. We demonstrate arrays of electrically injected membrane PC microcavities interconnected by nano-bridges. The technology demonstrated here represents an attractive route to fabricate densely packed electrically injected PC light sources [J2279]

"Silicon Nanocrystal Field-Effect Light-Emitting Devices"

We describe the operation of a light-emitting device in which silicon nanocrystals are electrically pumped via the field-effect electroluminescence (EL) mechanism. In contrast to the simultaneous bipolar carrier injection used in conventional p-n junction light-emitting diodes, this device employs sequential unipolar programming of both electrons and holes across a tunneling barrier from the same semiconductor channel. Light emission is strongly correlated with the injection of second carriers into nanocrystals that have been previously programmed with charges of the opposite sign. The properties of this device are well described by the model of a charge injection through Coulomb field modified tunneling processes. We additionally consider limiting performance bounds for potential future devices fabricated from nanocrystals with different radiative emission rates. [J2280]

"Junction Temperature-Controlled Spectrum in a Two-Color InGaN–GaN Quantum-Well Light-Emitting Diode"

We demonstrate the dependence of the output spectrum on the Ohmic-contact thickness in a blue/green two-color InGaN–GaN quantum-well (QW) light-emitting diode. By decreasing the metal thickness of the p-type Ohmic contact on the device, the contact resistance is increased and hence the junction temperature is raised. With the junction temperature raised, the probability for the hole to escape from the first QW (green emitting) and be captured by the next QWs is increased for more effective emission of blue light such that the blue/green intensity ratio can be adjusted. The conclusion of higher junction temperature in a sample of a thinner p-type metal layer is consistent with the measurement results of output power versus injection current and current versus applied voltage. The measurement based on the transmission-line method also shows the increasing trend of contact resistance in decreasing the p-type metal thickness [J2281]

"Process and Characteristics of Fully Silicided Source/Drain (FSD) Thin-Film Transistors"

In this paper, high-performance fully silicided source/drain (FSD) thin-film transistors (TFTs) with FSD and ultrashort source/drain extension (SDE) fabricated by the implant-to-silicide (ITS) technique are studied thoroughly. Using the ITS technique, not only the implantation damage but also the silicide spiking is avoided so that the thermal budget can be decreased obviously. The offstate current (I_{off}) of the FSD TFTs is equal to (n-channel) or smaller than (p-channel) that of the conventional TFTs. At onstate, due to the FSD and the SDE structure, the parasitic resistance of the S/D region and the carrier-injection resistance between silicide and channel are reduced. Therefore, superior onstate/offstate current ratio can be obtained. The influences of annealing temperature and time are also examined in this paper. A 600degC/30-s rapid thermal annealing is sufficient to

diffuse and activate dopants and, then, fabricate high-performance FSD TFTs. Excellent short-channel behavior of the FSD TFT is also confirmed. To conclude, the high-performance FSD TFT with low parasitic resistance fabricated by low-thermal-budget process is very promising for active-matrix liquid-crystal display, active-matrix organic light-emitting-diode display, and system-on-panel applications [J2282]

"A Current-Mode Display Driver IC Using Sample-and-Hold Scheme for QVGA Full-Color AMOLED Displays"

A display driver IC based on a current-sink driving scheme has been developed for QVGA (240times320), low-temperature poly-silicon (LTPS) active matrix organic light-emitting diodes (AMOLEDs) displays. The current-mode driver IC consists of a source driver block and a controller block. It uses a sample-and-hold scheme in the source driver block. The source driver block has 720 channel outputs, an 8-bit segmented DAC, a pre-charge generation block, and a 64-level gray scale (64 selections out of 256 gray levels for Gamma correction) per channel. The source driver output current ranges from 10 nA to 10 μ m. The controller block generates control signals for the source driver and LTPS drivers (emission and scan driver), which are integrated on the panel glass. The current-mode driver IC was fabricated in a 0.18- μ m CMOS technology (two poly and four metals) with 5.3-V high-voltage transistor devices [J2283]

"A Stable Voltage-Programmed Pixel Circuit for a-Si:H AMOLED Displays"

Hydrogenated amorphous silicon (a-Si:H) active matrix organic light-emitting diode (AMOLED) displays are attractive given the potentially low manufacturing cost and ultimately low-temperature fabrication enabling using flexible substrates. Although the conventional two thin-film transistor (2-TFT) AMOLED voltage-programmed pixel circuit (VPPC) can provide high resolution and high yield, the 2-TFT VPPC is prone to image retention over time due to shift in the threshold voltage (VT-shift) of a-Si:H TFTs. This paper presents a new driving scheme that not only preserves the simplicity of the 2-TFT VPPC, but also demonstrates high uniformity. Experimental results indicate that the current drop in the new driving scheme is less than 11% after 15 days of operation whereas it is over 50% for the conventional driving scheme. Moreover, the new driving scheme is less sensitive to temperature variations due to an internal feedback mechanism. After a 70% change in the temperature, the current in the conventional driving scheme increases by as much as 300%. However, the current in the driving scheme presented here is approximately constant [J2284]

"Enhanced Light Output in Roughened GaN-Based Light-Emitting Diodes Using Electrodeless Photoelectrochemical Etching"

We have demonstrated enhanced output power from roughened GaN-based light-emitting diodes (LEDs) by using electrodeless photoelectrochemical etching with a chopped source (ELPEC-CS etching). It was found that the 20-mA output power of the ELPEC-CS treated LED (with roughened surfaces on the top p-type and bottom n-type GaN surface as well as the mesa sidewall) was 1.41 and 2.57 times as high as those LEDs with a roughened p-type GaN surface and a conventional surface, respectively. The light output pattern of the ELPEC-CS treated LED was five times greater than the conventional LED at 0deg which was caused by the roughened GaN surface that improved the light extraction efficiency of the LED [J2285]

"Blood Test"

This paper describes how vascular patterns can provide a new means of identification and authentication. The new type of biometric identification device takes advantage of the fact that the network of vessels in each person's hand forms a pattern that can be distinguished from anyone else's. Unlike fingerprint scanners, vascular recognition systems do not require users to touch the sensors and remain unaffected by a user's blood pressure. With a strong combination of usability and accuracy, vascular recognition systems have the potential to be used in a wide range of applications [J2286]

"Laser on Silicon"

Silicon is not a natural for producing and manipulating light. Nevertheless, Intel and Luxtera each have been able to produce silicon versions of optoelectronic components by binding a light emitter made from indium phosphide to a silicon laser cavity. The key was in making a kind of glass glue, a thin layer of oxidized material, on both the indium-phosphide light emitter and the silicon laser and then bonding them together. Applying a voltage to the indium phosphide device produces light that passes through the glass into the silicon [J2287]

"An Output Channel Nonuniformity Compensation Driving Method in Flat Panel Display Driving Circuits"

Modern flat panel displays, including thin-film transistor liquid crystal displays (TFT-LCDs) and organic light-emitting diodes (OLEDs), pursue more and more natural color expression. This requires the data driving system should produce very fine and accurate signal voltages or currents. Especially, the uniformity among channels of a driving system is critically important because the color or luminance differences among columns are easily noticeable. We propose a simple and efficient driving method for solving the artifacts caused by the existing nonuniformity among channels of a driving system, and confirms its impact by simulations using C-programming. The nonuniformity among channels mostly stem from the random offset of the output circuits of a driving system, which in turn is caused by the process variations. The proposed driving method shares N-output circuits between N-output channels such that the existing offsets of the channels are averaged out. Thus, the output signal error due to the offsets spreads out among the channels, improving the uniformity between the channels [J2288]

"Amorphous Silicon Display Backplanes on Plastic Substrates"

Amorphous silicon (a-Si) thin-film transistor (TFT) backplanes are very promising for active-matrix organic light-emitting diode displays (AMOLEDs) on plastic. The technology benefits from a large manufacturing base, simple fabrication process, and low production cost. The concern lies in the instability of the TFTs threshold voltage (VT) and its low device mobility. Although VT-instability can be compensated by means of advanced multi-transistor pixel circuits, the lifetime of the display is still dependent on the TFT process quality and bias conditions. A-Si TFTs with field-effect mobility of 1.1 cm²/V·s and pixel driver circuits have been fabricated on plastic substrates at 150 degC. The circuits are characterized in terms of current drive capability and long-term stability of operation. The results demonstrate sufficient and stable current delivery and the ability of the backplane on plastic to meet AMOLED requirements [J2289]

"Phosphor-Free GaN-Based Transverse Junction Light Emitting Diodes for the Generation of White Light"

We demonstrate a GaN-based phosphor-free near-white-light light-emitting-diode (LED) structure that operates in the visible wavelengths and offers broadening and flattening optical bandwidth performance. The incorporation of GaN-based dual wavelengths (blue and green) multiple-quantum-wells with a transverse p-n junction produces a device which can directly generate stable and near visible white-light emissions. The shape of the optical spectra (440-560 nm) are invariable from low to very high levels of bias currents. The problems of nonuniform carrier distribution and bias dependent electroluminescence spectra that occur in traditional phosphor-free white-light or near-white-light LEDs (with vertical p-n junctions) are eliminated by the demonstrated structure [J2290]

"Temperature-Dependent Dynamic Behaviors of Organic Light-Emitting Diode"

A systematic investigation of temperature-dependent dynamic behaviors of NPD-Alq₃organic light-emitting diodes (OLEDs) is carried out. Through an in-depth numerical analysis, it has been found that the luminance decreases and consequently the turn-on voltage increases with decreasing temperature due to a reduction of thermally activated hopping speed, which retards the rise of electroluminescence (EL) upon turn-on as well as the discharge upon turn-off of OLEDs. Most importantly, however, the device efficiency is literally raised as the temperature decreases, a direct consequence of enhanced charge-balance factor. It is also demonstrated that the EL delay upon turn-on is mostly determined by the electron transport through the electron transport layer (ETL), while the fast EL decay (short-lived EL tail) upon turn-off is mainly by the rapid discharge of the steep pileup of carriers at the NPD/Alq₃interface. The long-lived EL tail is shown to be more pronounced under lower temperatures. In response to a train of voltage pulses, the delay of EL occurring for the first voltage pulse has vanished for the subsequent pulses regardless of temperature due to space charges remaining inside the device after turn-off (in the "off-state"). However, it appears that the pulse-to-pulse interference by the space charge effects is more significant under lower temperatures [J2291]

"Quantitative Comparison of Color Performances Between IPS and MVA LCDs"

Color gamut and color shifts of the film-compensated multi-domain in-plane-switching (IPS) and multi-domain vertical alignment (MVA) liquid crystal displays (LCDs) are calculated quantitatively using light-emitting diodes (LEDs) and cold-cathode fluorescent lamp (CCFL) backlight. Simulation results indicate that the LED backlight exhibits better angular color uniformity and smaller color shifts than CCFL. In addition, the color gamut can be further widened and the color shift reduced when using color-sequential RGB-LED backlight without color filters. In general, both IPS and MVA LCDs show relatively small color shift under different backlights, but MVA has a lower color shift using the optimized uniaxial compensation films [J2292]

"Measurement of Electron Mobility in Alq3 From Optical Modulation Measurements in Multilayer Organic Light-Emitting Diodes"

The dynamic characteristics of multilayer organic light-emitting diodes (OLEDs) determine the refresh rate in display applications, and are of great importance for practical organic displays. They also serve as an important tool in studying the transport mechanisms in organic conductors. Here, the modulation characteristics of several conventional small-molecule OLED structures [consisting of ITO/PEDOT:PSS(50 nm)/TPD(50 nm)/Alq3(various)/LiF(1 nm)/Al(90 nm)] are measured and analyzed in terms of mobility in and thickness of the Alq3 layer. Their optical response was shown to be limited by electron transport across the Alq3. Extracted electron mobilities were about $2\text{--}4 \times 10^{-6} \text{ cm}^2/\text{Vs}$ (consistent with that reported in the literature) and near-identical values for mobility were obtained from devices of different thicknesses, suggesting that this method measures mobility independent of interface trap charging. This novel technique is a complement to large signal time of flight or delay time measurements (which can include interface and trap charging during the measurement) and can serve as a flexible method to study transport in actual devices [J2293]

"Ultrastable and efficient red organic light emitting diodes with doped transport layers"

We demonstrate extremely stable and highly efficient red p-i-n-type organic light emitting diodes (OLEDs) based on an iridium-based electrophosphorescent dye in suitable host materials. The OLEDs reach lifetimes well above 14107 h at 100 cd/m^2 initial luminance and reach at the same time a performance of 12.4% external quantum efficiency. This high lifetime is attributed to a combination of the low current density needed to reach a certain luminance and to the high stability of the materials against both charge carriers and excitons. [J2294]

"Spatial coherence properties of electroluminescence from Alq3-based organic light emitting diodes"

We report the measurement of spatial coherence properties of light emitted by organic electroluminescent devices based on tris-(8-hydroxyquinoline) aluminum. Coherence measurements were performed using Young's double slit experiment. Fourier-transform technique was used for the measurement of visibility of the interference fringes from which the modulus of the degree of spatial coherence was determined. Experimental results were compared with the theoretical values and it is shown that the coherence properties of the light emitted by a simple organic light emitting device match with those of practical Lambertian sources. [J2295]

"Stable inverted bottom-emitting organic electroluminescent devices with molecular doping and morphology improvement"

Stable inverted bottom-emitting organic light-emitting diodes (IBOLEDs) have been investigated by inserting n-type Cs2O dopant between indium-tin oxide bottom cathode and Alq3, the combination of which not only improved the morphology of organic layer but enhanced the lifetime of the IBOLED. This n-type doped IBOLED achieved efficiencies of 5.2 cd/A and 2.0 lm/W at 20 mA/cm^2 . The 20% decay lifetime (t_{80}) of Cs2O doped IBOLED is 270 h which is about 1.7 times more stable than that of the conventional OLED (160 h) and 2.5 times of Li doped IBOLED (104 h). [J2296]

"Highly efficient and stable inverted bottom-emission organic light emitting devices"

The authors report the development of highly efficient and stable C545T doped green fluorescent Alq3 inverted bottom-emission organic light emitting device (OLED), with a device configuration of ITO/Mg/Cs2O:Bphen/Alq3/C545T:Alq3/NPB/VO3/Al, that achieved a maximum current efficiency of 23.7 cd/A and a power efficiency of 12.4 lm/W which are two times better than those of the conventional OLED. At a brightness level of 100 cd/m^2 , the device required driving current density only as low as 0.5 mA/cm^2 at a driving voltage of only 5.0 V and its half-lifetime $T_{1/2}$ in excess of 104000 h . [J2297]

"Organic oxide/Al composite cathode in small molecular organic light-emitting diodes"

This study addresses the feasibility of using an organic oxide/Al composite cathode to fabricate the small molecular organic light-emitting diodes (OLEDs). A supplementary organic buffer film is placed at the interface between the tris(8-hydroxyquinoline) aluminum (Alq3) and the organic oxide/Al complex layers. Incorporating the rubrene/poly(ethylene glycol) dimethyl ether (PEGDE) buffer layers into the composite cathode structure markedly improves the performance of devices. The luminous efficiencies of Alq3-based OLEDs biased at 100 mA/cm^2 are 4.8 and 5.1 cd/A for rubrene (5E)/PEGDE (15E)/Al and rubrene (5E)/PEGDE (15E)/LiF(5E)/Al cathode devices, and 1.3 and 3.8 cd/A for devices with Al and LiF (5E)/Al cathodes, respectively. [J2298]

"Ni /Au contact to silicon quantum dot light-emitting diodes for the enhancement of carrier injection and light extraction efficiency"

The effect of Ni/Au metal contact on the carrier injection and the electroluminescence of silicon quantum dot light-emitting diodes (LEDs) was investigated. An LED with an annealed Ni/Au contact at 400°C in air showed a lower threshold voltage compared to that of an as-deposited Ni/Au contact by forming a nickel silicide, which has a lower work function than Ni at the interface between metal layers and silicon nitride. The optical output power of the LED with the annealed Ni/Au contact was also increased due to a highly transparent NiO layer and a lowly resistant Au layer. [J2299]

"Excitation of fluorescence decay using a 265 nm pulsed light-emitting diode: Evidence for aqueous phenylalanine rotamers"

The authors describe the characteristics and application of a 265 nm AlGaIn light-emitting diode (LED) operated at 1 MHz repetition rate, 1.2 ns pulse duration, 1.32 mW average power, 2.3 mW peak power, and 12 nm bandwidth. The LED enables the fluorescence decay of weakly emitting phenylalanine to be measured routinely, even in dilute solution. For pH of 6-9.2, the authors find evidence for a biexponential rather than monoexponential decay, providing direct evidence for the presence of phenylalanine rotamers with a photophysics closer to the other two fluorescent amino acids tryrosine and tryptophan than has previously been reported. [J2300]

"Green fluorescent organic light-emitting device with external quantum efficiency of nearly 10%"

Green fluorescent organic light-emitting device (OLED) exhibiting a high external quantum efficiency of nearly 10% has been developed. The OLED consists of simple three organic layers, using NPB, 0.8% C545T doped TPBA, and DBzA as a hole-transporting layer, an emitting layer, and an electron-transporting layer, respectively, [fluorocarbon coated indium tin oxide/NPB (60 nm)/0.8% C545T doped TPBA (40 nm)/DBzA (20 nm)/LiF (1 nm)/Al], where NPB is 4,4'-bis (N-phenyl-1-naphthylamino)biphenyl, C545T is 10-(2-benzothiazolyl)-1,1,7,7-tetramethyl-2,3,6,7-tetrahydro-1H,5H,11H-benzo[*l*]pyrano[6,7-*h*]quinolizin-11-one, TPBA is 9,9',10,10'-tetraphenyl-2,2'-bianthracene, and DBzA is 9,10-bis[4-(6-methylbenzothiazol-2-yl)phenyl]anthracene. The high external quantum efficiency is maintained in the wide range of current density of 2-100 mA/cm². The current efficiency and power efficiency of the OLED are also very high, 29.8 cd/A and 26.2 lm/W, respectively, at a current density of 20 mA/cm². The OLED is promising for practical use with high color purity with Commission Internationale de L'Eclairage coordinates of (0.24, 0.62) and long half-lifetime of 71 h at a current density of 80 mA/cm² (initial luminance of 23900 cd/m²). [J2301]

"Integration of polymer light-emitting diode and polymer waveguide on Si substrate"

We integrate a polymer light-emitting diode (PLED) and a polymer waveguide on a Si substrate. The light emitted from the PLED is coupled to the waveguide by a diffuser and a reflection layer with coupling efficiency about 1%. There is no delay nor distortion between PLED emission and the light propagation in the waveguide. Good direct modulation characteristics of the waveguide output are demonstrated up to 200 kHz. The device structure and processes are based on easy spin coating and are compatible to Si technology. [J2302]

"Degradation mechanism of organic light-emitting device investigated by scanning photoelectron microscopy coupled with peel-off technique"

The authors present space-resolved spectroscopic data on organic layers of a degraded organic light-emitting device. The data were obtained using a scanning photoelectron microscope (SPEM) coupled with peel-off technique to directly probe the uncontaminated organic layers, which were covered with cathode layer. The SPEM images of the degraded device show different and small size distributions of tris-8-hydroxy quinoline aluminum (Alq₃) and hole-transport layers compared to that of as-prepared device. The analysis indicates that bonding strength between Alq₃ and cathode layers and between the Alq₃ and hole transport layers becomes weak as the device degrades, presumably due to structural deformation of the organic layers. [J2303]

"Room temperature defect related electroluminescence from ZnO homojunctions grown by ultrasonic spray pyrolysis"

ZnO homojunction light-emitting diode was grown on single-crystal GaAs (100) substrate by ultrasonic spray pyrolysis. This diode was comprised of N-In codoped p-type ZnO and unintentionally doped n-type ZnO film. Ohmic contact on n-type ZnO layer and GaAs substrate was formed by Zn/Au and Au/Ge/Ni alloyed metal electrodes, respectively. An electroluminescence emission associated with defects was observed from the ZnO homojunction under forward current injection at room temperature. The I-V characteristics of the homojunction

showed a threshold voltage of 4V under forward bias. [J2304]

"Role of hole playing in improving performance of organic light-emitting devices with an Al₂O₃ layer inserted at the cathode-organic interface"

The role of hole playing in improving electron injection in the presence of an Al₂O₃ layer at the organic-cathode interface is discussed. It is deduced that, according to the model of tunneling barrier reduction and the carrier transporting mechanism in organic light-emitting devices, electron injection will be enhanced only if holes are injected and accumulated at the organic-buffer interface. The validity of this analysis is well confirmed by experimental results. The observed abnormal characteristic of operating voltage varying with the Al₂O₃ layer thickness and the efficiency improvement are also well explained by the model. [J2305]

"White organic light-emitting devices with a phosphorescent multiple emissive layer"

A phosphorescent multiple emissive layer, in which a blue emissive layer is sandwiched between red and green ones, is employed in a white organic light-emitting device (OLED). This OLED has a maximum luminance of 48000 cd/m² at 17V, a maximum power efficiency of 9.9 lm/W at 4V, and a color rendering index of 82. In addition, the emission color of this device is fairly stable at high luminances: its Commission Internationale de l'Eclairage coordinate slightly changes from (0.431, 0.436) to (0.400, 0.430) when the luminance ranges from 2000 to 40000 cd/m². [J2306]

"Temperature dependence of the electrical activity of localized defects in InGaN-based light emitting diodes"

Traps govern the temperature dependence of current in III-nitride quantum heterostructures, but frequently electrical measurements result unable to identify how many and what kind of defects take part in the conduction. The present work shows how a combined electrical and optical characterization in temperature can detect localized defects involved in injection mechanisms in InGaN/AlGaIn/GaN blue light emitting diodes. At least two different traps assisting the carrier injection by tunneling and playing an active role below and above 175K, respectively, are identified in or nearby the active layers. [J2307]

"Trapped whispering-gallery optical modes in white light-emitting diode lamps with remote phosphor"

Three-dimensional ray tracing simulations show that a significant fraction of the phosphorescence emitted in high-power white light-emitting diode lamps with a remote phosphor is trapped as whispering-gallery modes propagating along the circumference of the encapsulant. The whispering-gallery modes, which are a significant optical loss mechanism and occur for multiple shapes of the encapsulation dome, are shown to be sensitively dependent on the diffusivity of the reflector cup employed in the lamp. By employing a diffuse reflector cup, up to 86% of the trapped modes is extracted out from the encapsulant. In addition, it is experimentally demonstrated that the phosphorescence efficiency is improved by up to 12.2% as the diffusivity of the reflector increases. The experimental results are consistent with theoretical ray tracing simulations. [J2308]

"Singlet excimer electroluminescence within N,N'-di-1-naphthalenyl-N,N'-diphenyl-[1,1'-biphenyl]-4,4'-diamine based diodes"

The authors report the fabrication of organic light-emitting diodes based on N,N'-di-1-naphthalenyl-N,N'-diphenyl-[1,1'-biphenyl]-4,4'-diamine (NPB) that emit via singlet excimer states. When the film deposition rate of NPB is reduced from 17 to 1 nm/min, they observe a reduction in intensity of the photoluminescence peak at 437 nm and the evolution of a new, broader peak at 503 nm. From optical absorption and time resolved photoluminescence data the authors attribute this new peak to singlet excimer emission. The authors demonstrate green electroluminescence from organic diodes that utilize this effect. The possible morphological variations resulting in the monomer to excimer transition are discussed. [J2309]

"Highly transparent and conductive double-layer oxide thin films as anodes for organic light-emitting diodes"

Double-layer transparent conducting oxide thin film structures containing In-doped CdO (CIO) and Sn-doped In₂O₃ (ITO) layers were grown on glass by metal-organic chemical vapor deposition and ion-assisted deposition (IAD), respectively, and used as anodes for polymer light-emitting diodes (PLEDs). These films have a very low overall In content of 16 at.%. For 180-nm-thick CIO/ITO films, the sheet resistance is 5.6 Ω/□, and the average optical transmittance is 87.1% in the 400-700 nm region. The overall figure of merit ($\Phi = T_{10}/R_{\text{sheet}}$) of

the double-layer CIO/ITO films is significantly greater than that of single-layer CIO, IAD-ITO, and commercial ITO films. CIO/ITO-based PLEDs exhibit comparable or superior device performance versus ITO-based control devices. CIO/ITO materials have a much lower sheet resistance than ITO, rendering them promising low In content electrode materials for large-area optoelectronic devices. [J2310]

"Prestrained effect on the emission properties of In Ga N /Ga N quantum-well structures"

The authors demonstrate the spectral redshift of the quantum wells (QWs) designated for green emission into the orange range in a light-emitting diode by adding a violet-emitting QW at the bottom in metal-organic chemical vapor deposition. An electroluminescence redshift of 53nm was obtained. The cathodoluminescence spectra indicated that the long-wavelength QWs close to the violet one were strongly influenced by this added QW and mainly emitted the orange photons. Those near the top were less affected. This influence is supposed to originate from the prestrained effect in the barrier layer right above the violet QW. Such a prestrained effect is expected to be more effective when the underlying QW is well shaped and the heterojunction strain is strong, like the case of the violet QW. This effect is weak between the high-indium QWs, in which the formation of indium-rich clusters releases the strain. [J2311]

"High-brightness top-emissive polymer light-emitting diodes utilizing organic oxide/Al /Ag composite cathode"

This work presents the fabrication of high-brightness (over 30000cd/m²) top-emissive polymer light-emitting diodes (PLEDs) using a hybrid semitransparent cathode capable of efficient injection of electrons. The composite cathode is comprised of the organic oxide/Al complex as the injection buffer layer covered by a thin Ag overlayer. The anode is made of Ag:Ag₂O coated on the glass substrate. The electroluminescence (EL) efficiency of 8.9cd/A for phenyl-substituted poly(para-phenylene vinylene) copolymer based top-emissive PLED markedly exceeds that of 4.3cd/A for the control device with the bottom-emissive configuration. The high performance is attributed to the balanced injection of charge carriers and the effective extraction of EL emission from the top cathode. The optical microcavity effect significantly promotes the EL emission in the direction along the surface normal. [J2312]

"Improved light outcoupling for top-emitting organic light-emitting devices"

Light outcoupling for the top-emitting organic light-emitting device (TEOLED) with the structure of Si/SiO₂/Ag/Ag₂O/4,4', 4''-tris(3-methylphenylphenylamino)triphenylamine/4, 4'-bis[N-(1-naphthyl-1-)-N-phenyl-amino]-biphenyl/tris-(8-hydroxyquinoline) aluminum (Alq₃)/LiF/Al/Ag is improved by optimizing the semitransparent Al/Ag cathode and employing a ZnS top-capping layer. To both provide a fine electron injection and reduce Al absorption in the visible area, Al thickness is adjusted to 0.3nm. With another 32-nm-thick ZnS film as a refractive index-matching layer onto the optimized Al (0.3nm)/Ag(18nm) electrode, the maximum luminance and efficiency for the TEOLED based on Alq₃ emission reach 145474cd/m²(13V) and 12.2cd/A(5V), respectively. [J2313]

"Optical properties of neodymium-containing polymethylmethacrylate films for the organic light emitting diode color filter"

In order to improve the primary color purity of the organic light emitting diode (OLED), neodymium(Nd)-containing polymethylmethacrylate (PMMA) films have been fabricated by a solvent casting method, and their optical properties have been investigated as functions of Nd content in films. The study has revealed that absorption in Nd-containing PMMA films is due to intratransition within the 4f shell of the Nd³⁺ ion, and that it becomes larger with an increase in the Nd concentration in films. In OLED devices with color filters, luminance from unnecessary emissive light is sufficiently reduced, resulting in a wider color gamut and higher color purity. [J2314]

"Increase of blue electroluminescence from Ce-doped Si O 2 layers through sensitization by Gd 3+ ions"

Efficient blue electroluminescence peak at around 440nm with a maximum output power density of 34mW/cm² was obtained from Ce and Gd coimplanted metal-oxide-semiconductor light emitting devices. Energy transfer from Gd³⁺ to Ce³⁺ ions was observed during the excitation process, leading to a more than threefold increase of the external quantum efficiency of the blue Ce³⁺ luminescence up to 1.8%. This is evidenced by the increase of the excitation cross section of Ce³⁺ ions from 4.84·10⁻¹³ to 3.54·10⁻¹² cm² and the simultaneous reduction of the decay time and the impact cross section of Gd³⁺ ions. [J2315]

"Mesa-size-dependent color contrast in flip-chip blue/green two-color InGaN/GaN multi-quantum-well micro-light-emitting diodes"

The authors fabricate blue/green two-wavelength, InGaN/GaN quantum-well (QW), flip-chip micro-light-emitting diodes (μ -LEDs) of different mesa sizes by stacking QWs of different indium contents. It is found that the blue/green contrast ratio of such a μ -LED increases with the mesa size. The relatively stronger blue intensity in a device of a larger mesa area is due to its higher operation junction temperature such that hole migration can be enhanced through thermally exciting holes to escape from the QW (green emitting) closest to the p-type layer and to be captured by the neighboring QWs (blue emitting). The higher junction temperature in such a μ -LED of a larger mesa area is due to its smaller ratio of the sidewall surface area over the active volume, leading to the less effective sidewall heat radiation and light extraction. [J2316]

"Prospective emission efficiency and in-plane light polarization of nonpolar m-plane In_xGa_{1-x}N/GaN blue light emitting diodes fabricated on freestanding GaN substrates"

Prospective equivalent internal quantum efficiency (η_{int}) of approximately 34% at 300K was demonstrated for the blue emission peak of nonpolar m-plane (1100)In_xGa_{1-x}N/GaN multiple quantum well light emitting diodes (LEDs) fabricated on freestanding m-plane GaN substrates. Although the η_{int} value is yet lower than that of conventional c-plane blue LEDs (~70%), the results encourage one to realize high performance green, amber, and red LEDs by reducing the concentration of nonradiative defects, according to the absence of the quantum-confined Stark effects due to the polarization fields parallel to the quantum well normal. The electric field component of the blue surface emission was polarized perpendicular to the c-axis with the in-plane polarization ratio of 0.58 at 300K. [J2317]

"Mid-infrared electroluminescence at room temperature from InAsSb multi-quantum-well light-emitting diodes"

Room-temperature electroluminescence is reported from InAsSb multiple-quantum-well light-emitting diodes. The diodes exhibited emission in the mid-infrared peaking near 4 μ m. The spectral dependence on injection current at 4K was investigated and two transitions were identified, centered at 4.05 and 3.50 μ m, which are associated with the eigenstates of the confined holes inside the quantum well. The use of an Sb predeposition and As flux surface exposure during epitaxial growth was observed to have a major effect on the electroluminescence output. [J2318]

"Theoretical demonstration of enhancement of light extraction of flip-chip GaN light-emitting diodes with photonic crystals"

The authors demonstrate, using finite-difference time-domain modeling, an enhancement in the extraction efficiency of flip-chip GaN light-emitting diodes (LEDs) using photonic crystals. The authors compare the extraction efficiencies of four configurations of a flip-chip GaN LED: with and without photonic crystal (PhC) layers, with a perfect reflecting mirror, and a bottom PhC reflector on GaN in combination with a top PhC extractor on sapphire. The authors show that, by using a photonic crystal layer as a bottom reflector, they can enhance the extraction efficiency similar to that of a mirror, yet the PhC reflector has the advantage that the metallic mirror loss can be avoided. [J2319]

"New possibilities for the measurement of wavelength-resolved photoconductivity"

We report a new setup for the measurement of photoconductivity that is based on discrete quasimonochromatic light-emitting diodes. This setup allows new possibilities combining preexposure and measurement at different wavelengths as well as the possibility of rapidly switching from one wavelength to any other at will and also varying the irradiance over a comparatively wide range. It is also easy to use an equalized photonic flux over the entire operating wavelength range. We show the interest of using a normalized photoconductivity coefficient that takes into account the distribution of light in the sample's volume and characterizes the specific properties of the material. We report typical results obtained in different conditions for the same undoped Bi₁₂TiO₂₀ photorefractive crystal. [J2320]

"Simple hybrid current-voltage source for the characterization of organic light-emitting devices"

Some organic light-emitting devices (OLEDs) behave better and longer when driven with alternating bias. It is believed that the reverse bias helps to remove the trapped charges and prevents permanent drift of ionic dopants or ion migration from electrodes. OLEDs behave much like diodes. When driven with a voltage source, the highly asymmetrical exponential I-V curve of diodes makes the accurate control of the forward current

difficult. Using a voltage-controlled current source, the voltage can constantly adjust to maintain the desired current through the device. The reverse resistance of a diode is large. Using a current source to reverse bias can produce a large reverse voltage that would destroy the junction. In this article we present an electronic device used to drive and characterize organic light-emitting devices. It consists of a high voltage ($\pm 225\text{V}$) hybrid source, which alternatively generates direct voltage-controlled current pulses, up to 200 mA, and reverse voltage-controlled voltage pulses. Furthermore, it allows simultaneous measurement of both, direct and reverse, current and voltage. This hybrid source, driven by an arbitrary wave form generator, makes possible the dynamical characterization of OLED when submitted to a wide variety of current and voltage signals. [J2321]

"System for measuring the junction temperature of a light emitting diode immersed in liquid nitrogen"

A versatile system has been developed for the measurement under LABVIEW™ control of junction temperatures in a light emitting diode (LED). Measurements are reported on a commercially available high-intensity InGaAlP LED immersed in liquid nitrogen and driven by currents in the range of 18.5-204mA. The measured junction temperature has an expanded uncertainty of $\pm 2\text{K}$ at the 95% level of confidence for temperatures from 70 to 298K. Using the measured junction temperatures, the junction-to-case thermal resistance of the LED was established as 440K/W for devices with intact encapsulation and 307K/W for partial encapsulation. [J2322]

"Precision of gray level response time measurements of medical liquid crystal display"

We characterized the instrumentation needed for accurate measurements of temporal response of liquid crystal displays for medical imaging applications. We investigated the effect of display and detector noise on the minimum measurable gray level (or luminance) difference. For a typical display, a gray level difference of 5 at high gray levels and 20 at low gray levels is needed to obtain an accurate measurement. A less noisy light emitting diode light source is employed to study the smallest measurable luminance difference at different luminance levels. We found that luminance differences of the order of 0.5cd/m² can be measured with an uncertainty of 10%. [J2323]

"Simple ac circuit for breast cancer detection and object detection"

The detection of subsurface objects by near infrared (NIR) spectroscopy and imaging has usually been done with a large number of source positions and a corresponding large number of detector positions. Significant signals have been obtained with a multitude of sources and detectors, to be exact, 4 multiwavelength light emitting diodes (LEDs) and 16 nearby detectors photodiode silicon diode detectors. A great simplification is made by a dedicated device in which two out of phase sources and a single detector, used in a differential circuit, enable sensitive detection of the appearance of a functionally induced inhomogeneity, for example, a breast cancer or a brain functional signal. By using two LED NIR sources in antiphase at a wavelength appropriate to blood volume increment for the in detection of breast cancer angiogenesis, it is possible to design and construct a very efficient handheld scanner which will indicate the presence of a subsurface angiogenesis by creating imbalance of the optical patterns of the two 800nm LED sources. Localization and an estimate of the size of the subsurface object may be obtained by scanning the device serially across the breast, as shown in a dynamic 1cm³ model tumor to be valid to a depth of 5cm. [J2324]

"Highly efficient white organic light emitting diodes comprising an interlayer to separate fluorescent and phosphorescent regions"

White organic light emitting diodes combining the phosphorescent green and orange-red emitting systems fac tris(2-phenylpyridine) iridium doped 4,4',4''-tris(N-carbazolyl)-triphenylamine (TCTA) and iridium(III)bis(2-methyldibenzo-[f,h]quinoxaline)(acetylacetonate) doped N,N'-di(naphthalen-1-yl)-N,N'-diphenyl-benzidine with the blue fluorescent dye 2,2',7,7'-tetrakis(2,2-diphenylvinyl)spiro-9,9'-bifluorene (Spiro-DPVBi) are presented. By introducing a thin layer of coevaporated TCTA and 2,2',2''(1,3,5-benzenetriyl) tris-[1-phenyl-1H-benzimidazole] between the phosphorescent and the fluorescent region, both singlet and triplet excitons are confined efficiently, whereas charge carriers still pass easily this interlayer. Furthermore, the interlayer suppresses Dexter transfer of the phosphorescent excitons to the nonradiative triplet state of Spiro-DPVBi. Best devices reach a current efficiency of 16.3cd/A at 100cd/m² and a color rendering index of 85 at warm white CIE chromaticity coordinates of (0.47, 0.42). Due to the use of electrically doped charge transport layers, 100cd/m² are obtained at 2.95V with a power efficiency of 17.4lm/W. [J2325]

"Highly efficient organic light-emitting diodes based on donor-acceptor small molecules"

The authors have fabricated highly efficient organic light-emitting diodes from donor-acceptor small molecules, 2-

(4-methyl-quinolin-2-yl)-10-phenyl-phenothiazine (MQPTZ) and 2-(4-phenyl-quinolin-2-yl)-10-phenyl-phenothiazine (PQPTZ). Their devices turned on at 4.0V and emitted strong green light near 510nm. The maximum luminance of 60 000 and 55000cd/m² at 10.4V and the maximum power efficiencies of 5.75 and 2.5lm/W at 5V were obtained from the MQPTZ and the PQPTZ, respectively. The overall performance of their devices in terms of current-voltage, luminance, and external quantum efficiency were discussed and compared with those from the device with tris-(8-hydroxyquinolineolato) aluminum. [J2326]

"Efficient ultraviolet-blue polymer light-emitting diodes based on a fluorene-based non-conjugated polymer"

Efficient UV-blue polymer light-emitting diodes based on a fluorene-based nonconjugated polymer, poly[2,7-(9,9-dihexylfluorene)-alt-4,4'-phenylether] (PFPE), are fabricated. The device with PFPE as emitting layer shows a very narrow ultraviolet-blue electroluminescence emission with a peak at 397nm and a maximal external quantum efficiency of 1.07%. By blending PFPE into poly(N-vinylcarbazole) (PVK), the device performance can be further improved. A maximum external quantum efficiency of 1.81%, with a maximum irradiance power density of 1223mW/cm², was reached by using a blend of PVK and PFPE in the weight ratio of 95:5 as emitting layer. [J2327]

"Remanent electrical spin injection from Fe into Al Ga As /Ga As light emitting diodes"

We compare surface and edge emission electroluminescence of spin-polarized light emitting diodes with Fe contacts. The edge emission geometry permits transduction of the spin state variable between the electron spin and optical polarization utilizing the in-plane remanent magnetization and low coercive fields of the metal contacts. The spin injection efficiencies are similar for electron spins oriented normal to the surface plane and in plane. The lower circular polarization consistently observed in edge emission at low magnetic fields is attributed to a partial out-of-plane orientation of the heavy hole angular momentum which persists even in wide quantum wells. [J2328]

"High performance thin-film flip-chip InGaN-GaN light-emitting diodes"

Data are presented on the operation of thin-film flip-chip InGaN/GaN multiple-quantum-well light-emitting diodes (LEDs). The combination of thin-film LED concept with flip-chip technology is shown to provide surface brightness and flux output advantages over conventional flip-chip and vertical-injection thin-film LEDs. Performance characteristics of blue, white, and green thin-film flip-chip 141mm² LEDs are described. Blue (441nm) thin-film flip-chip LEDs are demonstrated with radiance of 191mW/mm²sr at 1A drive, more than two times brighter than conventional flip-chip LEDs. An encapsulated thin-film flip-chip blue LED lamp is shown to have external quantum efficiency of 38% at forward current of 350mA. A white lamp based on a YAG:Ce phosphor coated device exhibits luminous efficacy of 60lm/W at 350mA with peak efficiency of 96lm/W at 20mA and luminance of 38Mcd/m² at 1A drive current. Green (517nm) devices exhibit luminance of 37Mcd/m² at 1A. [J2329]

"Red-light-emitting diodes fabricated by near-ultraviolet InGaN chips with molybdate phosphors"

Phosphors Na₅La(MoO₄)₄:xEu³⁺ and NaEu(MoO₄)₂ were prepared with a solid-state reaction technique. Their photoluminescent properties were investigated at room temperature. Bright red-light-emitting diodes were fabricated by coating the phosphors onto near-ultraviolet/violet-emitting InGaN chips, respectively. The diodes prepared with phosphor Na₅Eu(MoO₄)₄ show appropriate CIE chromaticity coordinates (x=0.65, y=0.34) and exhibit more intensive red emission than that prepared with NaEu(MoO₄)₂, indicating that Na₅Eu(MoO₄)₄ may be applied as an excellent red component for near-ultraviolet InGaN-based white diodes. [J2330]

"Organic light-emitting diodes having exclusive near-infrared electrophosphorescence"

Near-infrared (NIR) emission is demonstrated from phosphorescent organic light-emitting diodes containing blends of polymeric host and heavy metal complex, iridium(III) bis(1-pyrenyl-isoquinolinato-N,C') acetylacetonate. The devices exhibit exclusive NIR emission with a peak value at 720nm. Forward light output exceeds 100mW/cm², and the external quantum efficiency is nearly 0.1%. These values are shown to increase upon using a hole blocking layer in the device architecture. [J2331]

"Enhancement of electron injection in polymer light-emitting diodes with a supramolecular insulating nanolayer on the bottom cathode"

With the aim of enhancing the electron injection of a polymer light-emitting diode (PLED), a supramolecular insulating nanolayer that reacts with the cathode (Ag) was inserted between the bottom cathode and the emitting

material. The PLED threshold voltage (for 1cd/m²) was found to decrease from 5.6to4.2V as a result of the introduction of the nanolayer. Synchrotron radiation photoelectron spectroscopy results show that inserting the supramolecular insulating nanolayer results in a decrease in the work function of about 0.7eV. This reduction lowers the electron injection barrier and produces an increase in the luminance. [J2332]

"Enhanced output of GaN-based light-emitting diodes with stripe-contact electrodes"

High brightness GaN-based light-emitting diodes(LEDs) with stripe-contact electrodes have been developed. The p-type Ohmic contact layer is composed of oxidized Ni/Austripes and NiO stripes. A Ag (3000E)omnidirectional reflector covers the p-type contact. The n-type contact is a Ti/Alplanar film with a Ti/Alstripe. All Ni/Au, NiO, and Ti/Alstripes surround the center of the LED mesa. At 20mAcurrent operation, the light output power of GaN-based LEDs with the stripe-contact electrodes is 16.26%-35.37% higher than that of the conventional LEDs. [J2333]

"Monolithic microspectrometer using tunable ferroelectric liquid crystals"

A vertically aligned deformed helix ferroelectric liquid crystal is used to fabricate a thermally controllable monolithic microspectrometer using a single liquid crystal cell and a photodiode. The device has an active range over the entire visible spectrum from 400-720nmachieving an optimal resolution of 12nm in short wavelength regime to 20-25nm in the long wavelength regime. Operation is demonstrated through spectral reconstruction of the mercury emission spectra and a broadband white light emitting diode using a commercial spectrometer and the liquid crystal based spectrometer. [J2334]

"Greatly improved performance of 340 nm light emitting diodes using a very thin GaN interlayer on a high temperature AlN buffer layer"

This letter reports a simple approach to significantly improve the performance of 340nmultraviolet light emitting diodes (UV-LEDs) on an AlN buffer layer. Greatly improved optical and electrical properties of the 340nmUV-LED have been achieved by using a very thin GaN interlayer (10-20nm), deposited on AlN as a buffer layer directly on sapphire prior to growth of the UV-LED structure. Compared with the UV-LED without the thin GaN interlayer, the output power of the LED with it is increased by a factor of 2.2, and the applied bias voltage at 20mAdrops from 6.5to 5V. High resolution transmission electron observation indicates that the thin GaN interlayer can effectively stop the penetration of the dislocations in the AlN buffer layer into the overlying AlGaIn layer, while most of the dislocations in the AlN buffer layer in the UV-LED without the thin GaN interlayer can propagate into the overlying AlGaIn layer. Therefore, the enhanced performance of the 340nmUV-LEDs results from a massive reduction in dislocation density in the overlying device structure due to the very thin GaN interlayer. Since it is extremely difficult to reduce the dislocation density in an AlN layer on sapphire, the simple and reliable approach reported in this letter provides a good alternative option to prevent the propagation of dislocations from an AlN buffer into an overlying device structure. [J2335]

"Tunable full-color-emitting La_{0.827}Al_{11.9}O_{19.09}:Eu²⁺, Mn²⁺ phosphor for application to warm white-light-emitting diodes"

La_{0.827}Al_{11.9}O_{19.09}:Eu²⁺, Mn²⁺ showed three emission bands when excited by ultraviolet light. A blue emission originates from Eu²⁺, whereas both green and red emissions originate from Mn²⁺. The luminescent mechanism is explained invoking the energy transfer of Eu²⁺→Mn²⁺ and Mn²⁺(tetrahedralsite)→Mn²⁺(octahedralsite). This energy transfer was confirmed by faster decay times of the blue and green emissions as energy donors. The emitted color of La_{0.827}Al_{11.9}O_{19.09}:Eu²⁺, Mn²⁺ can be easily tailored from blue to red through variations of the Mn²⁺ content. The white-light-emitting diode fabricated via a combination of an ultraviolet light-emitting diode (λ_{peak}=385nm) with La_{0.827}Al_{11.9}O_{19.09}:Eu²⁺, Mn²⁺ showed a warm white light (T_c=3559K). [J2336]

"Efficient blue electroluminescence from neutral alcohol-soluble polyfluorenes with aluminum cathode"

Efficient blue polymer light-emitting diodes (PLEDs) have been fabricated with a neutral alcohol-soluble polyfluorene, i.e., poly(9,9-bis(6'-diethoxyphosphorylhexyl)fluorene) (PF-EP), as the emitting layer, high work-function Al as the cathode, and poly(vinyl carbazole) as the hole-transporting layer. The PLEDs display a maximum luminous efficiency of 4.0cd/A and the luminous efficiency 2.4cd/A in a wide range of current densities. It is found that the promising performance of the devices is attributed to the fact that the PF-EP is not only an efficient blue light-emitting polymer, but it also can facilitate efficient electron injection at the Al/PF-EP interface. [J2337]

"Carrier dynamics and electrostatic potential variation in InGaN quantum wells grown on {112 2} GaN pyramidal planes"

InGaN quantum wells grown in the conventional [0001] direction are known to exhibit long carrier lifetimes that are attributed to strong internal electric fields due to spontaneous and piezoelectric polarization. These fields are expected to be considerably reduced in other crystal geometries. In this work, the authors have investigated the carrier dynamics of InGaN single quantum wells grown parallel to {1122} planes. The carrier lifetimes, measured by time-resolved cathodoluminescence, are considerably smaller than for quantum wells grown in the conventional c-plane geometry. In addition, the lifetime does not change significantly with varying indium composition or increasing well width. Electron holography measurements of the electrostatic potential across these quantum wells confirm that the internal fields in this geometry are negligible. These results are of interest for the development of higher-efficiency light-emitting diodes using alternative substrate orientations. [J2338]

"Improved electroluminescent performances of europium-complex based devices by doping into electron-transporting/hole-blocking host"

High-efficiency, pure red organic light-emitting devices were fabricated by doping a europium-complex Eu(DBM)3pyzphen (DBM=dibenzoylmethane, pyzphen=pyrazino[2,3-f][1,10]phenanthroline) into 4,7-diphenyl-1,10-phenanthroline as emission layer. A maximum current efficiency of 5.1 cd/A at the current density of 1.2 mA/cm² and a maximum luminance of 1400 cd/m² were obtained from a 25 wt% Eu(DBM)3pyzphen doped device. High efficiencies were maintained at high current densities and high luminance. For example, at the current density of 10 mA/cm², the efficiency reached 3.8 cd/A. It means that the efficiency roll-off, a major obstacle to the development of Eu-complex organic light-emitting devices, was greatly alleviated. The mechanisms behind the improvement are discussed. [J2339]

"Modeling white light-emitting diodes with phosphor layers"

With a blue light-emitting diode and a phosphor layer to downconvert blue light to a second light, such as yellow, white light can be produced. The authors developed a one-dimensional model to describe the light propagating in the phosphor layer in terms of light absorption, conversion, and reflection. The parameters required for the model were determined from the data obtained by using multiple-layer phosphor films. The model predicts that, with a reflector between the diode and the phosphor layer that is blue-light transparent but reflects other visible light, the normalized white light intensity is above 0.9, higher than that of conventional packages (0.6-0.8). [J2340]

"Vertical injection thin-film Al Ga N /Al Ga N multiple-quantum-well deep ultraviolet light-emitting diodes"

Vertically injected thin-film ultraviolet light-emitting diodes operating at 325 and 280 nm are demonstrated. Low-temperature AlN interlayers allow crack-free growth of Al_xGa_{1-x}N with compositions up to x=0.53 on GaN-on-sapphire templates. The GaN layer allows laser-induced separation of the highly strained epi stack from the sapphire substrate with high yield. Cathode contacts are formed on nitrogen-face Al_xGa_{1-x}N (up to x=0.53) and allow vertical injection of current into the active region. Controlled roughening of the nitrogen-face Al_xGa_{1-x}N is also demonstrated through photoelectrochemical etching and results in 2.54 light extraction gain for 325 and 280 nm devices. [J2341]

"Highly efficient GaN-based light emitting diodes with micropits"

Light emitting diodes (LEDs) on GaN templates with high-density V-shaped micropits have been grown and characterized by transmission electron microscopy, scanning electron microscopy, and photoluminescence. Higher emission efficiency has been obtained for the fabricated LEDs compared with those without V-shaped pits. The high efficiency of the LEDs is mainly attributed to the increase in light extraction efficiency due to the light extraction from the sidewalls of the V-shaped pits. The improved internal quantum efficiency of the device resulting from the reduction of the dislocation density in the light emitting area also contributes to the high efficiency of the LEDs. [J2342]

"Wavelength-tunable and thermally stable Li -alpha -sialon :Eu 2+ oxynitride phosphors for white light-emitting diodes"

Eu²⁺-activated Li-alpha -sialon is a promising yellow phosphor for white light-emitting diodes (LEDs). This letter reports that the emission of Eu²⁺ in Li-alpha -sialon can be tuned widely (563-586 nm) by tailoring the composition or controlling the Eu²⁺ concentration. The thermal stability of Li-alpha -sialon:Eu²⁺, relying a little on the

composition and the Eu²⁺ concentration, remains high in a wide temperature range (25-200°C). Moreover, the chromaticity of Li-alpha-sialon:Eu²⁺ does not shift with changes in temperature. Using a single Li-alpha-sialon:Eu²⁺ phosphor, highly efficient white LEDs (46-55lm/W) with different color temperatures (3000-5200K) can be fabricated. [J2343]

"Broad wavelength modulating and design of organic white diode based on lighting by using exciplex emission from mixed acceptors"

Modulating electroluminescent (EL) spectra from interfacial exciplex emissions were observed by varying the ratios of two acceptors of exciplex-type devices in which the emissive wavelengths were tuned from 530 to 656 nm. In the devices 4,4',4''-tris[3-methyl-phenyl(phenyl)amino]triphenylamine and (bathocuproine:scdolinium-(dibenzoyl-methane)3bathophenyl-phenanthroline) mixtures were used as donor and acceptor materials, respectively. In terms of the exciplex broad band emission a white organic light emitting diode was demonstrated by skillfully designing the structure when blue subband was subjoined in the white spectrum. The white device behaves the Commission Internationale de l'Eclairage coordinates of (0.32, 0.35) with higher color stability at various biases, a color rendering index of 90.4, and a maximum luminance of 425 cd/m², respectively, although the EL efficiency needs to be further improved. The emission mechanism of the broad exciplex band formed by two mixed acceptors was also discussed. [J2344]

"Self-assembled monolayer-modified Ag anode for top-emitting polymer light-emitting diodes"

A self-assembled monolayer (SAM), 4-fluorothiophenol (4-FTP), is employed to modify the Ag anode of a top-emitting polymer light-emitting diode (T-PLED) to enhance the hole injection and the performance of a T-PLED device. The results show that the reflectivity of the Ag anode does not decrease due to the formation of a SAM. A brightness of 68981 cd/m² and a luminous efficiency of 10.3 cd/A have been achieved for the 4-FTP-modified device. The improved performance is attributed to the work function increase of the Ag/4-FTP anode due to the presence of fluorine atoms at the outer surface of the modified anode. [J2345]

"Color-variable organic light-emitting device by external light irradiation"

The authors demonstrate a color-variable organic light-emitting device by external light irradiation, where an organic photoelectric conversion layer out of titanyl phthalocyanine is inserted between blue- and green-emitting layers. By near-infrared (780 nm) laser irradiation, the emission color is varied from blue to green. The color coordinate in Commission Internationale de l'Eclairage chromaticity is varied from (0.201, 0.193) to (0.302, 0.445). The color change mechanism can be interpreted by the change in carrier balance caused by the photocarrier generation in the device, resulting in the change in charge recombination site. [J2346]

"Electrical and photoconductive properties of vertical ZnO nanowires in high density arrays"

High density vertical zinc oxide nanowire arrays were fabricated using highly ordered channels in anodic alumina membranes via chemical vapor deposition assisted by electrochemical deposition methods. Using conductive atomic force microscopy, the electrical transport and photoconduction of individual vertical nanowires were investigated. A negative photoconductivity was observed as a result of electron trapping in the alumina membrane. In contrast, positive photoconductivity was observed using a thermally annealed anodic alumina membrane as the nanowire growth template. These studies provide a pathway for constructing highly integrated nanoscale electronic and optoelectronic circuits, such as logic circuits, light emitting diodes, solar cells, and ultrahigh resolution imaging sensors. [J2347]

"White polymeric light-emitting diodes with high color rendering index"

The efficient white polymeric light-emitting diodes based on a white emissive polymer doped with a red phosphorescent dopant were fabricated by spin-coating method. The emission spectrum of the device is broadened to cover the full visible region by doping the red phosphorescent dye and thereby realizes white emission with high color-rendering index (CRI). By controlling the contents of the doped electron-transporting 2-(4-biphenyl)-5-(4-tert-butylphenyl)-1,3,4-oxadiazole and the red phosphorescent dopant, a luminous efficiency as high as 5.3 cd/A and a power efficiency of 3 lm/W were obtained with a CRI of 92. [J2348]

"Optical characteristics and microstructure of ZnO quantum dots-SiO₂ nanocomposite films prepared by sputtering methods"

ZnO quantum dots (QDs)-SiO₂ nanocomposite films were prepared using the target-attached radio-frequency sputtering. The transmission electron microscopy revealed the uniform dispersion of ZnO QDs with diameters about 2-7 nm in amorphous SiO₂ matrix. The photoluminescence showed that small ZnO QDs are able to emit

white light with luminescence spectra similar to those of the present GaN-based light emitting diode (LED). The calculated chromaticity coordinates of emitting light evidenced the feasibility of ZnO QDs-SiO₂nanocomposite films as the fluorescence material in optoelectronic devices. [J2349]

"Cascaded active regions in 2.4 mcm GaInAsSb light-emitting diodes for improved current efficiency"

By cascading multiple GaInAsSb active regions, the authors have fabricated 2.4mcm light-emitting diodes that, for a given light output, operate at reduced current and higher voltage, which can be advantageous for battery-powered sensor applications. Tunnel heterojunctions separating emission regions add no measurable series resistance. Devices are demonstrated at room temperature with continuous wave output. [J2350]

"GaSb quantum-well-based "buffer-free" vertical light emitting diode monolithically embedded within a GaAs cavity incorporating interfacial misfit arrays"

The authors demonstrate a monolithic, electrically injected, vertically emitting GaSb/AlGaSb light emitting diode (LED) emitting at 1.6mcm comprised of a hybrid GaAs/GaSb-based structure. The LED is comprised of a GaSb/AlGaSb quantum well/barrier active region embedded within high index contrast GaAs/AlGaAs distributed Bragg reflectors (DBRs) using two interfacial misfit (IMF) arrays to relieve the strain induced from the high 8% lattice mismatch between the material systems. The first IMF is formed under compressive strain conditions to enable strain-free, defect-free deposition of GaSb active region directly on the lower GaAs/AlAs DBRs without need for thick buffer. The second IMF is formed under tensile conditions to enable the upper GaAs/AlAs DBRs on the GaSb active region. The device demonstrates a maximum output power of 3.5mW. Initial diode optical and electrical characteristics along with IMF band structure are discussed. [J2351]

"Fabrication of 5,6,11,12 -tetraphenyl-naphthacene doped 4-bis(2,2-diphenylvinyl)-1,1-biphenyl white organic light-emitting device"

Using a blue emitting material, 4-bis(2,2-diphenylvinyl)-1,1-biphenyl and orange dopant 5,6,11,12-tetraphenyl-naphthacene, white organic light-emitting devices have been fabricated. An insignificant variation in Commission Internationale de l'Eclairage color index with the applied voltage is reported. Transient electroluminescence measurements show a delay time in the microsecond range ($\sim 26\mu s$). The authors propose a device configuration for the white light emission, having a color stability and low delay time. [J2352]

"In situ determination of interface dipole energy in organic light emitting diodes with iridium interfacial layer using synchrotron radiation photoemission spectroscopy"

The interface dipole energies between 4,4'-bis[N-(1-naphtyl)-N-phenyl-amino]biphenyl and Ir interfacial layers with different thicknesses (2 and 20nm) coated on indium tin oxides (ITO) were measured in situ using synchrotron radiation photoemission spectroscopy. In 20nm Ir coated ITO, the work function increment of 0.15eV due to O₂ plasma treatment was accompanied by an increase of interface dipole energy. In 2nm Ir coated ITO, no change in the interface dipole energy was found. Thus, the work function increase (0.45eV) in the 2nm Ir by O₂ plasma treatment reduced the hole injection barrier by about 0.45eV. [J2353]

"Molecular monolayer modification of the cathode in organic light-emitting diodes"

The effects of alkanethiol self-assembled monolayers (SAMs) attached to the gold cathode of organic light-emitting diodes made by soft contact lamination are investigated. In spite of reported work function lowering by alkanethiol SAMs, the results from this work showed that their primary effect in carrier transport is to act as a thin insulating layer, causing current reduction. At the same time, the luminescence efficiency was enhanced because the SAMs reduce exciton quenching by the metal cathode. A two-order-of-magnitude enhancement at light emission onset was observed for a hexadecanethiol modified device. [J2354]

"Highly efficient green phosphorescent single-layered organic light-emitting devices"

The authors studied the highly efficient green electrophosphorescent light-emission from single-layered organic light-emitting devices made by a simple wet process with a composite solution. The solution was prepared by predissolving organic charge transport, host compounds with green phosphorescent guest iridium complex, and a copolymer of oxadiazole units. The fabricated devices show excellent performances, i.e., operation at relatively low voltages, resulting in a high peak current efficiency (η_c) of 48cd/A and power efficiency (η_p) of 45lm/W at a current density of 0.02mA/cm². Even at 1000cd/m² (2mA/cm²), high η_c of 50cd/A and η_p of 22lm/W were obtained. [J2355]

"Directional edge-emitting UV random laser diodes"

The authors have achieved directional coherent random lasing from p-GaN/i-ZnO-SiO₂nanocomposite/n-ZnO heterojunction diodes. This is due to the use of relatively low refractive indexed carrier injection layers (i.e., cladding layers) and relatively high refractive indexed intrinsic layer with stripes of ZnO clusters (i.e., core layer) that allows the transverse confinement of in-plane closed-loop random cavities. Hence, directional lasing emission can be observed from the edge of the diodes. However, the choice of highly concentrated ZnO clusters, which is supposed to enhance the transverse confinement and optical gain, is not preferred for the fabrication of intrinsic layer. This is because the influence of corrugation effect (i.e., strong surface scattering) supersedes the transverse optical confinement of the diodes. [J2356]

"Nonresonant carrier tunneling in arrays of silicon nanocrystals"

Silicon nanocrystals are of interest in the nascent field of silicon microphotonics, with potential applications as waveguide amplifiers, light-emitting diodes, and silicon-based lasers. Comparing computational simulations and experiment, it is shown that nonresonant carrier tunneling in ensembles of silicon nanocrystals is a controlling factor in the luminescence. In thin film silicon nanocrystal composites, only the larger particles can be luminescent as a result of rapid carrier tunneling, suggesting that these applications may only be achieved for well-isolated nanocrystals or for arrays with a narrow distribution of sizes. [J2357]

"Quantum efficiency enhancement in top-emitting organic light-emitting diodes as a result of enhanced intrinsic quantum yield"

The authors compare red, green, and blue top- and conventional bottom-emitting organic light-emitting diodes (OLEDs) based on iridium complexes. Surprisingly, red top-emitting OLEDs are much more efficient than their bottom-emitting counterpart, while for green and blue devices, top and bottom emitters are comparable. The authors explain these results by an improved internal quantum efficiency only in the red top-emitting OLED: Due to strong microcavity effect, spontaneous emission of emitters in all top-emitting devices is enhanced. However, only the internal quantum yield of the red emitters is then improved due to its comparable radiative and nonradiative decay rates. They also show that the efficiency roll-off at higher current densities is reduced in top-emitting OLEDs. [J2358]

"Electron transport in naphthylamine-based organic compounds"

Two naphthylamine-based hole transporters, namely, N,N'-diphenyl-N,N'-bis(1-naphthyl)(1,1'-biphenyl)-4,4'-diamine (NPB) and 4,4',4''-tris(n-(2-naphthyl)-n-phenyl-amino)-triphenylamine (2TNATA), were found to possess electron transporting (ET) abilities. From time-of-flight measurements, values of electron mobilities for NPB and 2TNATA are (6-9)·10⁻⁴ and (1-3)·10⁻⁴ cm²/Vs, respectively, under an applied electric field range of 0.04-0.8 MV/cm at 290K. An organic light-emitting diode that employed NPB as the ET material was demonstrated. The electron conducting mechanism of NPB and 2TNATA in relation to the Marcus theory [Rev. Mod. Phys. 65, 599 (1993)] from quantum chemistry will be discussed. [J2359]

"Vertical AlGaIn deep ultraviolet light emitting diode emitting at 322 nm fabricated by the laser lift-off technique"

A vertical AlGaIn deep ultraviolet (DUV) light emitting diode (LED) emitting at 322 nm was fabricated by the laser lift-off technique. The emission area extended to the entire electrode uniformly, and the current crowding was suppressed effectively in the devices. As a result, the differential conductance of the vertical LED was improved by a factor of 5 and the operation voltage was reduced to half, compared to that of the lateral LED. The self-heating effect was effectively suppressed even at high-current-density operation. The vertical structure in the high resistive AlGaIn LED has potential application in high-power AlGaIn DUV devices. [J2360]

"Infrared emission from Ge metal-insulator-semiconductor tunneling diodes"

The Ge light-emitting diode with 1.8 μm strong infrared emission is demonstrated using a metal-insulator-semiconductor tunneling structure. The intensity of a Ge device is one order of magnitude stronger than a similar Si device. At the positive gate bias, the holes in the Al gate electrode tunnel to the n-type Ge through the ultrathin oxide and recombine radiatively with electrons. An electron-hole-plasma model can be used to fit all the emission spectra from room temperature down to 65K. From the measurement temperature range, the extracted band gap is 40 meV lower than the reported band gap data, and the linewidth drops from 70 to 25 meV. The longitudinal acoustic phonon (28 meV) and/or the band gap renormalization at high carrier density are proposed to be responsible for the reduction of photon energy. The band gap reduction on the mechanically strained n-

type Ge and Si is also investigated experimentally and theoretically. [J2361]

"Improved luminance intensity of InGaN-GaN light-emitting diode by roughening both the p-GaN surface and the undoped-GaN surface"

The InGaN-GaN epitaxial films were grown by low-pressure metal-organic chemical vapor deposition on a sapphire substrate, and then the light-emitting diode (LED) with double roughened (p-GaN and undoped-GaN) surfaces was fabricated by surface-roughening, wafer-bonding, and laser lift-off technologies. It was found that the front side luminance intensity of double roughened LED was 2.77 times higher than that of the conventional LED at an injection current of 20mA. The backside luminance intensity was 2.37 times higher than that of the conventional LED. This is because the double roughened surfaces can provide photons multiple chances to escape from the LED surface, and redirect photons, which were originally emitted out of the escape cone, back into the escape cone. [J2362]

"Bright semipolar GaInN/GaN blue light emitting diode on side facets of selectively grown GaN stripes"

The authors demonstrate the fabrication and evaluation of bright semipolar GaInN/GaN blue light emitting diodes (LEDs). The structures are realized by growing five GaInN/GaN quantum wells on the {1101} side facets of selectively grown n-GaN stripes with triangular shape running along the $\langle 20\bar{1}0 \rangle$ direction covered with a Mg-doped GaN top layer. The growth was done by metal organic vapor phase epitaxy using a conventional [0001] sapphire substrate. The devices have circular mesa structures with diameters between 70 and 140 μm . Continuous wave on-wafer optical output powers as high as 700 μW and 3 mW could be achieved under dc conditions for 20 and 110 mA, respectively. The current dependent blueshift of the peak emission wavelength caused by screening effects of the piezoelectric field was only 1.5 nm for currents between 1 and 50 mA. This is less than half the value measured on c-plane LEDs and confirms the reduced piezoelectric field in our LED structures. [J2363]

"Effective modification of indium tin oxide for improved hole injection in organic light-emitting devices"

We demonstrate modification of the indium tin oxide (ITO) surface with an ultrathin layer of hexadecafluorocopper phthalocyanine (F16CuPc) can significantly enhance hole injection as a result of the formation of an interfacial dipole layer. The dipole layer produces a surface potential shift, which reduces the hole injection energy barriers and thus improves the hole injection efficiency. The devices with anode modification exhibit significantly enhanced luminance efficiencies and dramatically decreased operation voltages, compared to devices with the bare ITO anode. The minimum turn-on voltage of 2.6 V and the maximum efficiency of 5.1 cd/A are achieved. [J2364]

"Dissociation of iridium(III) phosphorescent emitters upon adsorption on Cu(110) revealed by scanning tunneling microscopy"

The phosphorescent emitters used in organic light emitting diodes (OLEDs) play a crucial role for tuning the color and the luminescence intensity. The authors have investigated by scanning tunneling microscopy the adsorption of iridium(III) phosphorescent emitter molecules used in OLEDs on a partly oxidized Cu(110) surface. Surprisingly they find that 50% of the emitters have dissociated upon adsorption at the substrate. The findings suggest that the decrease in the lifetime of OLEDs, which are manufactured by vacuum vaporization technique, is due to the dissociation of emitter molecules present in the device. [J2365]

"Ca test of Al₂O₃ gas diffusion barriers grown by atomic layer deposition on polymers"

Quantitative Ca tests were used to determine the water vapor transmission rate (WVTR) through 25 nm thick Al₂O₃ gas diffusion barriers grown on plastic by atomic layer deposition (ALD). The measured WVTRs were 1.7 $\times 10^{-5}$ g/m² day at 38 °C and 6.5 $\times 10^{-5}$ g/m² day at 60 °C. Based on the apparent activation energy, the WVTR at 23 °C is estimated to be only 6 $\times 10^{-6}$ g/m² day. The WVTR values for the Al₂O₃ ALD film are very similar to the WVTR value for the glass control. These Ca tests indicate that Al₂O₃ ALD gas diffusion barriers should enable display and lighting applications of highly moisture sensitive organic light-emitting diodes on plastic. [J2366]

"Dry formation of polymer hole injection layer for top emitting organic light emitting diodes"

Dry formation of polymer hole injection layer is introduced as an effective method for improving the performance of top emitting organic light emitting diodes (TOLEDs). This method involves transferring a metal/polymer bilayer to the surface of organic layers of the device by pressing. An added advantage of this method is the ability to

pattern the anode in the transfer process. Fabrication of the inverted TOLED by this method results in a drastic reduction of the turn-on voltage, from 14.5 to 6.5 V, when compared with a reference. [J2367]

"Color tunable organic light-emitting diodes by using europium organometallic complex"

Using the rare-earth special feature of a sharp emission spectrum, voltage-controlled continuous color tuning of organic light-emitting diodes is achieved. Europium(dibenzoylmethanato)3(bathophenanthroline) is used as the strategic starting point close to the red corner of the Commission International de l'Eclairage chromaticity diagram for a wide color tuning. The end point and path of the color tuning can be engineered by doping the hole-transport emitting layer with dyes. The mechanisms of color tuning have been investigated and explained by the efficiency reduction of the europium complex and the extension of carrier recombination zone with driving voltage. The effect of exciplex on the color tuning is also studied. [J2368]

"MoO_x modified Ag anode for top-emitting organic light-emitting devices"

Efficient top-emitting organic light-emitting devices (TOLEDs) using a thin MoO_x layer modified Ag as the effective hole-injection anode are demonstrated. With tris-(8-hydroxy quinoline)aluminum as emitting layer and trilayer LiF/Al/Ag as semitransparent cathode, the Ag/MoO_x based TOLED shows a turn-on voltage of 2.67 V and a maximum current efficiency of 7.27 cd/A, which are much better than those (3.92 V, 6.12 cd/A) obtained from Ag/Ag₂O based TOLED and those (5.25 V, 3.5 cd/A) obtained from the corresponding bottom-emitting organic light-emitting devices. Contact potential difference measurement shows that the work function of Ag/MoO_x is higher than those of Ag/Ag₂O and ozone-treated indium tin oxide, leading to a stronger hole injection. The good performance of Ag/MoO_x based TOLED is attributed to the efficient hole injection from the Ag/MoO_x anode as well as a microcavity effect. [J2369]

"InGaN-light emitting diode with high density truncated hexagonal pyramid shaped p-GaN hillocks on the emission surface"

To increase the light extraction efficiency, high density truncated hexagonal pyramid shaped submicron p-GaN hillocks were formed on the emission surface of an InGaN/GaN multiple quantum well light emitting diode (LED) using an in situ silicon carbon nitride self-masking layer. The self-assembled hillock density was raised up to a low 10⁹ cm⁻² using several nanometers of a Si_{0.4}C_{0.6}N₁ self-masking layer. The self-assembled hillock LED resulted in the optical power improvement up to 80% with similar electrical properties as a normal LED. This device showed a higher electrostatic discharge pass yield at over 1000 V reverse stress voltage. [J2370]

"Triphenylamine-functionalized rhenium (I) complex as a highly efficient yellow-green emitter in electrophosphorescent devices"

A complex (3-ethyl-2-(4'-triphenylamino)imidazo[4,5-f] 1,10-phenanthroline) Re(CO)₃Br functionalized by a hole-transport group triphenylamine was used to fabricate organic light-emitting devices (OLEDs). A current efficiency up to 17.6 cd/A corresponding to a power efficiency of 9.2 mW/A and a peak brightness as high as 6500 cd/m² were obtained. These results represent the best values reported for OLEDs based on rhenium complexes. Enhanced carrier injection capability of Re complex and efficient charge-trapping formation followed by triplet exciton confinement in the emissive layer make for the outstanding electrophosphorescent performances. [J2371]

"Long-lifetime, high-efficiency white organic light-emitting diodes with mixed host composing double emission layers"

A long-lifetime, high-efficiency white organic light-emitting diode was fabricated with a mixed host in one of double emission layers. The first layer comprised yellow rubrene doped in a mixed host consisting of 50% N,N'-diphenyl-N,N'-bis-(1-naphthyl)-1,1'-biphenyl-4,4'-diamine (NPB) and 50% 2-(t-butyl)-9,10-bis(2'-naphthyl)anthracene (TBADN). The second layer comprised blue 4,4'-bis[2-{4-(N,N-diphenylamino)phenyl}vinyl]biphenyl doped in TBADN. This device exhibited the longest lifetime, five times that of its pure NPB counterpart. The resulting efficiency was 6.0 lm/W (10.9 cd/A) at 10 mA/cm², 33% better than that of the NPB counterpart. These improvements were attributable to the mixed-host structure, which effectively dispersed carriers and gave a good charge balance. [J2372]

"Extremely low voltage organic light-emitting diodes with p-doped alpha-sexithiophene hole transport and n-doped phenyldipyrenylphosphine oxide electron transport layers"

Organic light-emitting diodes with p-doped alpha-sexithiophene and n-doped phenyldipyrenylphosphine oxide carrier transport layers are fabricated. In the doped diodes, the authors demonstrate an extremely low driving

voltage of 2.9V at a current density of 100mA/cm² and very high luminance at a low driving voltage: 1000cd/m² at 2.4V, 10000cd/m² at 2.8V, and 92000cd/m² at 4.5V. Such lowered driving voltages and enhanced luminance characteristics are attributed to the generation of free charge carriers by charge transfer from matrix to dopant molecules, resulting in an increase in electrical conductivities and formation of Ohmic contacts at metal/organic interfaces. [J2373]

"Red electrophosphorescent top emission organic light-emitting device with Ca /Ag semitransparent cathode"

Using a Ca (10nm)/Ag(10nm) semitransparent cathode and efficient electron transport and/or buffer layer, red electrophosphorescent top emission organic light-emitting device has been fabricated. A low turn-on voltage of 4.6V and clean electrophosphorescence peaks at 616 and 674nm are reported. X-ray photoelectron spectroscopy depth profiling measurements reveal the presence of Ca(OH)₂ in Ca/Ag bilayer cathode and the skin depth over 15nm in the visible region is determined in this structure. Results show that the compositional modification of the Ca/Ag cathode enhances its optical transparency and final performance of the electrophosphorescent top emission device. [J2374]

"Highly power efficient organic light-emitting diodes with a p -doping layer"

In this letter, the authors demonstrate p-i-n organic light-emitting diodes (OLEDs) incorporating a p-doped transport layer which comprises tungsten oxide (WO₃) and 4,4',4''-tris(N-(2-naphthyl)-N-phenyl-amino)triphenylamine (2-TNATA) to replace the volatile tetrafluoro-tetracyanoquinodimethane. The authors propose the 2-TNATA:WO₃ composition functions as a p-doping layer which significantly improves hole injection and conductivity of the device that leads to the fabrication of tris(8-quinolinolato)aluminum based p-i-n OLEDs with long lifetime, low driving voltage (3.1V), and high power efficiency (3.5lm/W) at 100cd/m². [J2375]

"Highly efficient deep blue organic electroluminescent device based on 1-methyl-9,10-di(1-naphthyl)anthracene"

The authors have developed 2-methyl-9,10-di(1-naphthyl)anthracene (alpha ,alpha -MADN) as an effective wide band gap host material for Förster energy transfer to the unsymmetrical mono(styryl)amine deep blue fluorescent dopant (BD-1). This guest/host emitting system, at the optimal doping concentration of 3%, can also increase the probability of carrier recombination near the hole-transport/emitting layer interface for the blue organic light emitting device which produces electroluminescence efficiencies of 3.3cd/A and 1.3lm/W and a deep blue CIE_{x,y} color coordinates of (0.15, 0.13) that are 50% better than those of the traditional beta ,beta -isomeric host (MADN) with the same dopant. [J2376]

"Relationship between indium tin oxide surface treatment and hole injection in C60 modified devices"

The effect of indium tin oxide (ITO) surface treatment on hole injection in organic light-emitting diode with C60 as a buffer layer on ITO was studied. Double surface dipole layer was induced on oxygen plasma treated ITO surface, while no dipole formation was observed on ITO without surface treatment. Interfacial energy barrier between ITO and hole transport layer was reduced by 0.4eV by C60 modification on oxygen plasma treated ITO surface, while there was no change of interfacial energy barrier by C60 on ITO without surface treatment. [J2377]

"Green polyfluorene-conducting polymer interfaces: Energy level alignment and device performance"

Photoemission studies on interfaces between an electroluminescent green polyfluorene (GPF) and two conducting polymers comprising ethylenedioxythiophene and sulfonate moieties are reported. Despite the chemical similarity of both conducting polymers, the hole injection barriers to GPF were found to differ by 0.35eV and the interface dipoles by up to -0.4eV. Polymer light emitting devices fabricated with the two conducting polymers exhibit nearly identical current-voltage characteristics, but the luminance-voltage characteristic is enhanced by a factor of 20 by the presence of near-surface poly(styrenesulfonate). We attribute the enhancement to the electron- blocking behavior of the sulfonate moieties at the GPF interface and the concomitant modification of the device built-in voltage. [J2378]

"Effect of exciplex formation on organic light emitting diodes based on rare-earth complex"

An exciplex can be formed due to the charge transfer between the lowest unoccupied molecular orbital (LUMO) of the acceptor and the highest occupied molecular orbital (HOMO) of the donor. By introducing a mixing layer

composed of [N,N'-diphenyl-N,N'-bis (3-methylphenyl)-1,1'-diphenyl-4,4'-diamine] (TPD) and europium(dibenzoylmethanato)3(bathophenanthroline)[Eu(DBM)3bath] and a graded interface, elimination of light emission from the exciplex and significant luminescence enhancement of trivalent europium ions (Eu^{3+}) in organic light emitting devices have been achieved. The elimination mechanism of exciplex emission based on the concept that an exciplex can be formed between LUMO of the acceptor (Eu complex) and HOMO of donor (TPD) was investigated. To comprehensively understand the mechanism, devices consisting of a Eu(DBM)3bath as the emitting material and the devices using other rare-earth (RE) complex [RE(DBM)3bath] as the emitting material were fabricated with the same device configuration. As a reference, four spin-coated films with the blend composed of TPD and the gadolinium complex [Gd(DBM)3bath] were also fabricated. The electroluminescence (EL) spectra from the devices and photoluminescence spectra from the spin-coating films were fully investigated. The results show that the exciplex was formed by the charge transfer from the donor TPD to the acceptor RE complex, the exciplex state that acted as a transient excited state can be controlled by altering the molecular ratio in the mixing films. The relation of the exciplex formation based on EL devices with the RE complex versus the variety of the RE ions is also discussed by manipulating the energy level of the excited state. [J2379]

"Single crystalline aluminum nitride films fabricated by nitriding $\alpha\text{-Al}_2\text{O}_3$ "

Single crystalline aluminum nitride (AlN) is a key material for deep-ultraviolet light emitting devices. In the present study, high-quality single crystalline AlN films have been fabricated by nitriding $\alpha\text{-Al}_2\text{O}_3$ with a precise control of driving force of nitridation reaction. This process provides the α -axis oriented AlN film as large as 50.8 mm in diameter formed on (0001) and (1120) planes of $\alpha\text{-Al}_2\text{O}_3$ substrates. The crystalline qualities of the films have the values of full width at half maximum of rocking curves using (0002) and (1010) planes of AlN for tilt and twist components as follows; Tilt = 165 arcsec and twist = 540 arcsec in the case of nitriding (0001) plane of $\alpha\text{-Al}_2\text{O}_3$ and tilt = 127 arcsec and twist = 237 arcsec in the case of nitriding (1120) plane of $\alpha\text{-Al}_2\text{O}_3$. [J2380]

"Multilayer green polymer light emitting diodes with improved efficiency and lifetime"

We report on green polymer light emitting diodes with improved efficiency and lifetime using a cross-linked hole transporting layer in this study. The poly[(9,9-dioctylfluorene)-alt-(triphenylamine)], which was used as a hole transporting material, was cross-linked by UV irradiation. The emitting layer of a green copolymer, poly[(9,9-dioctylfluorene)-co-(benzodiathiazole)], was spin coated from its solution on the top of the cross-linked hole transporting layer to prepare a multilayer device. By introducing the cross-linked hole transporting layer, the maximum luminance, efficiency, external quantum efficiency, and, especially, the lifetime of the multilayer green device were greatly increased compared with those of a single layer device. These were supposed to be caused by an improvement of carrier injection balance in the emitting layer, a decrease in the reduction-oxidation degradation of the emitting material, and fewer impurities entering the emitting layer due to the function of the cross-linked hole transporting layer. [J2381]

"Current and optical noise of GaN/AlGaN light emitting diodes"

Low frequency noise of current and light intensity of ultraviolet light emitting diodes (LED) with wavelength from 265 to 340 nm are the superposition of the 1/f and generation-recombination noise. The dependence of generation-recombination noise on the LED current has a maximum caused by a relatively shallow trap level in the quantum well. The upper bound of this trap level concentration is estimated to be $N_t = 7.4 \times 10^{15} \text{ cm}^{-3}$. The relative spectral noise density of the light intensity fluctuations decreased with an increase of the LED forward current. At high currents, the difference in the noise level for LEDs with different wavelength is small and is of the same order of magnitude or even smaller than for visible LEDs. [J2382]

"Inhomogeneous luminance in organic light emitting diodes related to electrode resistivity"

In organic light emitting diodes (OLEDs) with transparent electrodes, the luminance usually becomes inhomogeneous if the size of the pixel increases above 10 μm . A theoretical model for inhomogeneous voltage and luminance in OLEDs is provided together with an approximate analytical solution for the problem in case of cylindrical symmetry. Experimental observations of inhomogeneous luminance are compared with numerical simulations based on the theoretical model, proving the applicability of the approximations made in the theoretical model. [J2383]

"A method of accurately determining the positions of the edges of depletion regions in semiconductor junctions"

The technique of electron beam induced current (EBIC) in the scanning electron microscopy can be used to extract the depletion width in a variety of materials and devices. This article reviews current methods available for identifying the positions of the edges of the depletion layer and proposes an alternative methodology that

uses the first derivative of the logarithmic EBIC profile. It was found that the precision of this method is only dependent upon the accuracy in which one can determine the lateral dimension of the beam-sample interaction. The proposed method is then applied to a gallium nitride light emitting diode device to verify the practicality of the technique. [J2384]

"Influence of carrier conductivity and injection on efficiency and chromaticity in small-molecule white organic light-emitting diodes based on 4,4'-bis(2,2'-diphenylvinyl)-1,1'-spirobiphenyl and rubrene"

Organic light-emitting devices (OLEDs) employing yellow-emitting 5,6,11,12-tetraphenylanthracene (rubrene) and blue-emitting 4,4'-bis(2,2'-diphenylvinyl)-1,1'-spirobiphenyl are optimized using a vacuum thermal evaporator. The influence of various hole injection/hole transport stacks and electron transport materials on the device performance and the electroluminescence spectra are discussed. Device characteristics are explained by the charge carrier distribution among the organic layers. OLEDs with warm-white emission with color coordinates of $x=0.43$ and $y=0.42$ were produced with power and current efficiencies of 5 lm/W and 10.9 cd/A, respectively, at a luminance of 1000 cd/m². The maximum external quantum efficiency at a current density of 20 mA/cm² was 4.6%. [J2385]

"Exciton migration in organic thin films"

Limitations of the analytical method for calculating the exciton distribution in organic thin films, attributed to the improper boundary conditions when the organic film approaches the exciton diffusion length, were analyzed by comparison with an exciton random walk simulation. The random walk simulation results are in better agreement with in situ photoluminescence measurements than predictions based on the one-dimensional (1D) diffusion equation, especially for thin films (~ 15 nm). The three-dimensional exciton diffusion length in tris(8-hydroxyquinoline) aluminum is determined to be 26 nm, equivalent to 15 nm upon projection to 1D. The result is not sensitive to the molecular size, a parameter arbitrarily set in the simulation. In addition, the exciton distribution in operating organic light emitting devices was also simulated. [J2386]

"Temperature dependence of electroluminescence from silicon p-i-n light-emitting diodes"

The temperature dependence of electroluminescence from silicon p-i-n light-emitting diodes with a layer of β -FeSi₂ particles inserted in intrinsic silicon was investigated. Anomalous blueshift of the peak energy and enhanced electroluminescence intensity of the silicon band-edge emission were observed at temperatures from 50 to 200 K. The electroluminescence intensity was enhanced due to longer diffusion paths of the injected electrons at elevated temperature, as well as thermal escape of the electrons from the β -FeSi₂ particles. The low peak energy compared to that from bulk silicon at low temperature is due to the bound electron-hole pairs induced by the strain potential at the interface between silicon and β -FeSi₂ particles. The blueshift of the peak is ascribed to the transition of bound electron-hole pairs into free excitons at elevated temperature. Room temperature electroluminescence from such a silicon light-emitting diode can be obtained at a low current density of 0.3 A/cm². [J2387]

"Field dependent negative capacitance in small-molecule organic light-emitting diodes"

Frequency dependent charge transport in organic light-emitting diodes, including marked negative capacitance (NC), is reproduced through an equivalent circuit model. The robustness of the model is tested through impedance spectroscopy characterization as a function of bias changes and layer thickness modifications. Correlations with current-voltage measurements reveal that the NC occurs once trap assisted space charge limited transport is reached. Through variation of the organic layer thicknesses, the magnitude of the NC response can be precisely tuned. In particular, increasing the thickness of the electron transport layer increases the NC magnitude, whereas hole transport layer thickness modifications have little effect on the magnitude of NC. Subsequent modeling indicates that alterations in the distribution of the electric field across the individual organic layers account for the observed variations in NC. In addition, it is found that the time constants for the inductive elements of the model increase with applied bias, unlike their capacitive counterparts, suggesting that an accumulation of charge at the organic/organic interface is responsible for both the increasing NC and redistribution of the applied field. [J2388]

"Performance improvement of top-emitting organic light-emitting diodes by an organic capping layer: An experimental study"

The optical outcoupling of top-emitting organic light-emitting diodes (OLEDs) can be improved by a thin dielectric capping layer on top of the transparent cathode. We investigate the emission properties of a set of top-emitting

OLEDs with the same device structure, but different organic capping layer thicknesses to understand the capping layer effect. We demonstrate that the distribution pattern of the emitted light from top-emitting OLEDs depends strongly on the capping layer thickness, showing not only a maximum current efficiency enhancement by a factor of 1.38 (up to 78cd/A in forward direction at 1000cd/m²), but also a quantum efficiency improvement by 35%. This leads to a device efficiency of up to 17.8% and 69lm/W at a brightness of 1000cd/m². We show that this efficiency enhancement is not due to the redistribution of emitted light, but mainly due to the improvement of outcoupling efficiency by changing the optical structure of the devices with the organic capping layer. The maximum outcoupling efficiency is achieved at a capping layer thickness where the top contact stack (cathode+capping layer) shows low absorption and high reflection. [J2389]

"Effect of magnesium oxide buffer layer on performance of inverted top-emitting organic light-emitting diodes"

The effect of magnesium oxide (MgO) buffer layer between cathode and emitting materials on performance of inverted top-emitting organic light-emitting diodes (ITOLEDs) was investigated. The operation voltage at the current density of 100mA/cm² decreased from 14.9 to 9.7V for ITOLEDs with 1nm thick MgO buffer layers. The maximum luminance value increased about 78% in ITOLEDs using MgO buffer layer, which is 1000cd/m² at the current density of 191mA/cm². Synchrotron radiation photoelectron spectroscopy results revealed that the atomic concentration of Al-O bond increased after deposition of MgO on Al, indicating the oxidation of Al surface. Secondary electron emission spectra showed that the work function increased about 0.8eV by inserting the insulating MgO buffer layer. Therefore, the enhancement of device performance results from the decrease of the energy barrier for electron injection based on the tunneling model. [J2390]

"Doping effect of blue light-emitting electron transport molecule in blue organic light-emitting devices"

Here we report the doping effect of blue light-emitting electron transport molecules on the performance of blue organic light-emitting devices (OLEDs). 4,4'-N,N'-dicarbazole-biphenyl (CBP) was chosen as a blue emission material (layer) for two main reasons: its wide band gap makes it suitable for blue emission; and its shifted energy band structure allows for easy electron injection. However, the main drawback of CBP is the low electron mobility and the large hole injection barrier. In order to overcome these weak points, the CBP nanolayer (50nm thick) in blue OLEDs has been doped with 2-(2-hydroxyphenyl)benzoxazole lithium (LiPBO), which is known to be a blue light-emitting electron transport material. The result showed that the device performance (charge injection voltage, turn-on voltage, and current efficiency) was improved by doping the LiPBO molecule, an improvement that can be attributed to the enhanced electron mobility and the reduced hole injection barrier of the LiPBO-doped CBP nanolayer. However, the blue color purity of OLEDs marginally deteriorated as a result of the LiPBO doping. The worst Commission Internationale de l'Eclairage (CIE) color coordinate of OLEDs was x=0.16 and y=0.18 at 16V, while the standard coordinates are x=0.14 and y=0.08, which is possibly due to the formation of exciplexes in a nanoscale. [J2391]

"Polymer light emitting diodes and poly(di-n-octylfluorene) thin films as fabricated with a microfluidics applicator"

A microfluidics applicator is used in the fabrication of a polyfluorene based polymer light emitting diode (PLED). This procedure results in a single contiguous polymer trace and, as a consequence of the high deposition speed, shows unusual characteristics in both the film morphology and polymer microstructure. These aspects are studied using fluorescence microscopy, profilometry, and optical absorption and emission spectroscopies. Room temperature analysis of the poly(di-n-octylfluorene) indicates that the combination of high-speed deposition and rapid drying process traps the polymer into a metastable conformational state. Optical spectroscopy at reduced temperature identifies emission from at least two distinct conformational chromophores. At elevated temperature there is an abrupt, irreversible transition to a more conventional structural form. Electroluminescence data from PLED test devices are shown and this demonstrates some of the unique opportunities afforded by this method of polymer film formation and device fabrication. Device operation is not optimized. [J2392]

"Organic light emitting devices with enhanced outcoupling via microlenses fabricated by imprint lithography"

High efficiency white organic light emitting devices (WOLEDs) with optical outcoupling enhanced by hexagonal polymethylmethacrylate microlens arrays fabricated by imprint lithography on a glass substrate are demonstrated. Monte Carlo and finite difference time domain simulations of the emitted light are used to optimize the microlens design. The measured enhancement of light outcoupling and the angular dependence of the extracted light intensity are in agreement with the simulation. Using microlens arrays, we demonstrate a

fluorescent/phosphorescent WOLED with a maximum external quantum efficiency of $(14.3 \pm 0.3)\%$ at 900 cd/m^2 and power efficiency of $21.6 \pm 0.5 \text{ lm/W}$ at 220 cd/m^2 . The electroluminescent spectra at viewing angles from normal to the substrate plane, to 60° off normal, remain almost unchanged, giving a color rendering index of 87. [J2393]

"Organic light-emitting devices using polyacene derivatives as a hole-transporting layer"

Three polyacene derivatives, 2-tert-butyl-9,10-di(2-naphthyl)anthracene (TBADN), 9,9',10,10'-tetraphenyl-2,2'-bianthracene, and 5,6,11,12-tetraphenylnaphthacene (rubrene), are found to successfully function as hole-transporting layers (HTLs) in red organic light-emitting devices (OLEDs) using tetraphenyldibenzoperiflanthene as an emitter. Compared with an OLED with the most widely used HTL material, the arylamine derivative, 4,4'-bis(N-phenyl-1-naphthylamino)biphenyl (NPB), the OLEDs with the polyacene derivatives exhibit advantageous performance such as lower driving voltage, higher electroluminescence efficiency, or longer luminance lifetime, depending on the employed HTL material. Current efficiency of the red OLED with a TBADN HTL is 5.5 cd/A with Commission Internationale de L'Eclairage chromaticity coordinates of $(x=0.66, y=0.34)$, which is much higher than the value of 2.1 cd/A with the same chromaticity for the OLED with a NPB HTL. The driving voltage and luminance lifetime of the red OLED with rubrene HTL are improved compared with the OLED with a NPB HTL. The hole injection properties of the proposed HTL materials are discussed. The results indicate that the polyacene derivatives are promising for use in OLEDs as a class of HTLs, expanding the variety of HTL materials available for optimizing the performance of OLEDs. [J2394]

"Absorption enhancement due to scattering by dipoles into silicon waveguides"

We develop an optical model for absorption enhancement and diffuse reflectance by metal nanoparticles on a silicon waveguide. A point dipole treatment is used, including the effects of the waveguide on both the angular emission spectrum and scattering cross section of the dipoles. The model agrees very well with our experimental results of greatly enhanced electroluminescence and photocurrent from silicon-on-insulator light-emitting diodes and also gives very good agreement with previously reported diffuse reflectance measurements. The results suggest that the main mechanism in the enhancement of diffuse reflectance in this system is a dramatic enhancement in the scattering cross section of waveguided light, rather than a waveguide-mediated dipole-dipole interaction. We also put lower bounds on the radiative efficiency of scattering by the nanoparticles. [J2395]

"Far-infrared upconversion imaging devices: Imaging characteristics and quantum efficiency"

We have carried out an investigation of imaging characteristics and quantum efficiency of far-infrared (FIR) semiconductor imaging devices. The realization of the FIR imaging employs the concept of photon frequency upconversion in GaAs homojunction interfacial work-function internal photoemission (HIWIP) FIR detectors integrated with GaAs/AlGaAs near-infrared light-emitting diodes (LEDs). Satisfying images have been expected through the analysis of modulation transfer function of the system, where the FIR detector parameters play key roles in the low spatial frequency image contrast, while those of LEDs dominate in the high spatial frequency range. We have examined in detail the dependence of the quantum efficiency on the emitter layer number, thickness, doping concentration, and applied bias of the FIR detectors, as well as the active layer thickness and internal quantum efficiency of the LEDs. The present study has also yielded an optimal structure for the integrated HIWIP-LED FIR imaging devices. [J2396]

"General method to evaluate substrate surface modification techniques for light extraction enhancement of organic light emitting diodes"

The external light output of organic light emitting diodes (OLEDs) can be increased by modifying the light emitting surface. The apparent light extraction enhancement is given by the ratio between the efficiency of the unmodified device and the efficiency of the modified device. This apparent light extraction enhancement is dependent on the OLED architecture itself and is not the correct value to judge the effectiveness of a technique to enhance light outcoupling due to substrate surface modification. We propose a general method to evaluate substrate surface modification techniques for light extraction enhancement of OLEDs independent from the device architecture. This method is experimentally demonstrated using green electrophosphorescent OLEDs with different device architectures. The substrate surface of these OLEDs was modified by applying a prismatic film to increase light outcoupling from the device stack. It was demonstrated that the conventionally measured apparent light extraction enhancement by means of the prismatic film does not reflect the actual performance of the light outcoupling technique. Rather, by comparing the light extracted out of the prismatic film to that generated in the OLED layers and coupled into the substrate (before the substrate/air interface), a more accurate evaluation of light outcoupling enhancement can be achieved. Furthermore we show that substrate surface modification can change the output spectrum of a broad band emitting OLED. [J2397]

"Nonlithographic nanopatterning through anodic aluminum oxide template and selective growth of highly ordered GaN nanostructures"

Ordered GaN nanostructures, i.e., nanopore and nanodot arrays, have been demonstrated by combining a nonlithographic nanopatterning technique and nanoscale selective epitaxial growth. Hexagonal-close-packed nanopore arrays were fabricated in GaN surfaces and SiO₂ surfaces on GaN films by inductively coupled plasma etching using anodic aluminum oxide templates as etching masks. Selective area growth through nanopores in SiO₂ by metal organic chemical vapor deposition results in ordered GaN nanodot arrays with an average dot diameter and height of 60 and 100 nm, respectively. The diameter and density of the GaN nanopore arrays and nanodot arrays are controlled by that of the anodic aluminum oxide template, which can be tuned in a wide range by controlling the anodization conditions. Applying anodic aluminum oxide as an etching mask provides an effective nonlithographic and free of foreign catalysts method to fabricate ordered and dense nitride nanostructures for either bottom-up or top-down technique in the application of high efficiency nitride light emitting diodes. [J2398]

"Improvement of electrical and optical properties of p-GaN Ohmic metals under ultraviolet light irradiation annealing processes"

We report the improvement of electrical and optical properties of p-GaN Ohmic metals, ZnNi(10 nm)/Au(10 nm), by ultraviolet (UV) light irradiation. After UV light irradiation, the specific contact resistance of p-GaN decreased slightly from 2.99×10^{-4} to $2.54 \times 10^{-4} \Omega \text{ cm}^2$, while the transmittance of the contact layer increased from 75% to 85% at a wavelength of 460 nm. In addition, the forward voltage of InGaN/GaN light-emitting diode chip at 20 mA decreased from 3.55 to 3.45 V, and the output power increased from 18 to 25 mW by UV light irradiation. The low resistance and high transmittance of the p-GaN Ohmic metals are attributed to the reduced Schottky barrier by the formation of gallium oxide and the increased oxidation of p-Ohmic metals, respectively, due to ozone generated from oxygen during UV light irradiation. [J2399]

"Voltage-controlled multicolor emitting devices"

Voltage-controlled multicolor emitting devices were fabricated by combining an organic light-emitting diode and a solid-state electrochemiluminescent device. Though the device has a simple stacking structure with Ru(II) complex, tris(8-hydroxyquinolino) aluminum, 4,4'-bis(2,2'-diphenylvinyl)-1,1'-biphenyl, and N,N'-bis(naphthalen-1-yl)-N,N'-bis(phenyl)-benzidine as basic materials, it is able to stably emit different colors, from pure green to pure red or from pure blue to pure red, under different driving biases. Its luminance can reach up to 1836 cd/m² with current efficiency reaching 1.84 cd/A. The Ru(II) complex is considered to play a dominant role in this kind of device due to its unique reversible redox property. [J2400]

"Hole mobility and electroluminescence properties of a dithiophene indenofluorene"

The development of organic laser diodes requires the availability of organic thin films that can attain high mobility without luminescence quenching. A dithiophene-substituted indenofluorene compound was designed as a compromise between luminous efficiency and mobility and has been studied in organic light-emitting diode and organic field-effect transistor devices. A relatively high luminous efficiency of 1 cd/A at a luminance of 1400 cd/m² and a hole field-effect mobility of $1.2 \times 10^{-2} \text{ cm}^2/\text{Vs}$ are reported in those two respective devices. [J2401]

"In GaN/GaN blue light emitting diodes with modulation-doped AlGaIn/GaN heterostructure layers"

The modulation-doped AlGaIn/GaN heterostructure layers were used to improve the output power and efficiency of nitride-based blue light emitting diodes (LEDs). It was found that the output power of LEDs with the modulation-doped AlGaIn/GaN layers measured at 20 mA injection current was increased from 4.8 to 6 mW. It was also found that the modulation-doped AlGaIn/GaN layers can effectively spread pulse current. Nitride-based blue LEDs with the modulation-doped AlGaIn/GaN layer can even endure a 3000 V reverse electrostatic discharge pulse voltage. [J2402]

"Stable a-Si:H circuits based on short-term stress stability of amorphous silicon thin film transistors"

Hydrogenated amorphous silicon (a-Si:H) technology is interesting for large-area active matrix structure due to its good uniformity over large-area, low-temperature, and low-cost fabrication, and its industrial accessibility. However, the circuits implemented in this technology suffer from the instability of the material under prolonged

bias stress. To improve the circuit stability, we present a circuit design technique based on the stability of a-Si:H thin film transistors (TFTs) under short-term bias stress. Here, an a-Si:H local current source (LCS) is used to adjust the circuit current bias. Since the LCS circuit is under stress for a small fraction of operation time, its current remains stable. The measurement and analysis of the LCS circuit indicate that the a-Si:HTFT is stable under short-term bias stress for over 50000h. Also, we present a pixel circuit based on this technique for active matrix organic light emitting diode displays. [J2403]

"Electrical spin injection in forward biased Schottky diodes based on InGaAs-GaAs quantum well heterostructures"

The authors demonstrate efficient hole spin injection from a ferromagnetic metal (Ni) contact in a forward biased light emitting Schottky diode (LESD) fabricated on a GaAs based heterostructure with a quantum well (QW). The spin polarization of the injected holes was detected by measuring the circular polarization of the electroluminescence (EL) from the near surface InGaAs/GaAsQW. An intermediate gold layer has been used in order to improve the spin injection efficiency. Over 40% degree of circular polarization of the EL has been observed at T=2K for the LESD structure with Au-Ni-Au Schottky contact. [J2404]

"Thermal properties and degradation behavior of red-emitting high-power diode lasers"

The thermal properties and the degradation behavior of high-power broad-area diode lasers emitting at 650nm are analyzed. Imaging thermography is applied to assess the bulk temperature while the facet temperature is measured by micro-Raman spectroscopy. Although no visible facet alteration is observed, power degradation is found to be accompanied by increased temperatures at the facets. The immediate vicinity of them also turns out to be the starting point for the creation of defect networks within the quantum well seen in cathodoluminescence images. The observed behavior is compared to that known for near-infrared emitting devices. [J2405]

"Encapsulation-free hybrid organic-inorganic light-emitting diodes"

The authors have fabricated encapsulation-free hybrid organic inorganic light-emitting diodes (HOLEDs), with improved air stability performance by incorporating two different metal oxide layers. One metal oxide layer is a titanium dioxide layer that provides the electron-injection layer, and the other is a molybdenum oxide that injects holes. While our HOLED device exhibits a lower threshold voltage and a higher air stability than conventional devices using a Ca/Alcathode, a similar luminance output was observed. [J2406]

"Fabrication of highly efficient and stable doped red organic light-emitting device using 2-methyl-9,10-di(2-naphthyl)anthracene and tris(8-hydroxyquinolino)aluminum as cohost materials"

The authors fabricated red organic light-emitting devices using DCJTB as red dopant, and blue-emitting MADN and green-emitting Alq3 as cohost materials for emission layers. The luminance efficiency of 2% DCJTB-doped Alq3(20%)/MADN(80%) device was 5.42cd/A at 20mA/cm², while that of equivalently doped Alq3 single-host device was 1.79cd/A, and remained over 5.2cd/A up to 200mA/cm². At the benchmark luminance of 7680cd/m², the power efficiency of DCJTB-doped Alq3/MADN device was 4.1 times better than that of Alq3 single-host device. Moreover, the half-decay lifetime of DCJTB-doped Alq3/MADN device measured at an initial luminance of 1000cd/m² was 14000h. [J2407]

"White organic light-emitting diodes with fine chromaticity tuning via ultrathin layer position shifting"

Nondoped white organic light-emitting diodes using an ultrathin yellow-emitting layer of rubrene (5,6,11,12-tetraphenyl naphthalene) inserted on either side of the interface between a hole-transporting 4,4'-bis[N-(1-naphthyl)-N-phenylamino]biphenyl (alpha-NPB) layer and a blue-emitting 4,4'-bis(2,2'-diphenylvinyl)-1,1'-biphenyl (DPVBi) layer are described. Both the thickness and the position of the rubrene layer allow fine chromaticity tuning from deep blue to pure yellow via bright white with CIE coordinates (x=0.33, y=0.32), an eta ext of 1.9%, and a color rendering index of 70. Such a structure also provides an accurate sensing tool to measure the exciton diffusion length in both DPVBi and NPB (8.7 and 4.9nm, respectively). [J2408]

"Observations of electrical and luminescence anomalies in InGaN/GaN blue light-emitting diodes"

Unique correlations between the electrical and optical characteristics of InGaN/(In)GaN multiple quantum-well light-emitting diodes (LEDs) were investigated over a broad range of temperatures. The dependence of nonunity ideality factors extracted from the current-voltage analysis on temperature determines the carrier-transport mechanisms in the heterodevices. The pseudotemperatures T₀ for the LEDs with multiquantum barriers and with

GaN barriers were found to be 945 and 1385K, respectively, at temperatures of 180-300K while having values of 1195 and 2720K below about 180K. Correspondingly, the temperature-dependent electroluminescence observations suggest that the Toanomaly caused the spectral intensity to deteriorate. [J2409]

"Highly transparent cathodes comprised of rare earth and Au stacked layers for top-emission organic light emitting diodes"

We report the transparent cathodes comprised of a low work function rare earth element (RE) and a Au capping layer for top-emission organic light emitting diodes (TOLEDs). The Sm/Au, Yb/Au, Gd/Au, and Dy/Au cathodes possess a transmittance up to 60% when the RE/Au thickness is 5/10nm. The light extraction efficiencies for the TOLEDs with a silicon anode and a RE/Au cathode are computed to be 9%-13%, markedly higher than that for a similar device but with an Al/Au cathode. The surface plasmon polaritons at the Yb(orSm)/Au cathode are found to be much weaker than those at the Al/Au cathode. [J2410]

"Electroluminescence efficiency of blue In Ga N /Ga N quantum-well diodes with and without an n-In Ga N electron reservoir layer"

The temperature dependence of the electroluminescence (EL) spectral intensity has been investigated in detail between $T=20$ and 300K at various injection current levels for a set of two blue InGa_{0.18}N/GaN multiple-quantum-well (MQW) light-emitting diodes (LEDs) with and without an additional n-doped In_{0.18}Ga_{0.82}N electron reservoir layer (ERL). The radiative recombination efficiency of the main blue emission band ($\lambda = 480$ nm) is found to be significantly improved at all temperature regions and current levels when the additional ERL is introduced. For high injection currents I_f , i.e., large forward bias voltages V_f , a quenching of the EL intensity is observed for $T > 100$ K for both LED structures, accompanying appearance of short-wavelength satellite emissions around 380-430nm. Furthermore, the low-temperature intensity reduction of the main EL band is stronger for the LED without the ERL than with the ERL. For low I_f , i.e., small V_f , however, no quenching of the EL intensity is observed for both LEDs even below 100K and the short-wavelength satellite emissions are significantly reduced. These results of the main blue emission and the short-wavelength satellite bands imply that the unusual evolution of the EL intensity with temperature and current is caused by variations of the actual potential field distribution due to both internal and external fields. They significantly influence the carrier capture efficiency- by radiative recombination centers within the active MQW layer and the carrier escape out of the active regions into high-energy recombination centers responsible for the short-wavelength satellite emissions. [J2411]

"Light-polarization characteristics of electroluminescence from In Ga N /Ga N light-emitting diodes prepared on (112 2) -plane GaN"

Light polarization and emission spectra from InGa_{0.18}N/GaN quantum-well light-emitting diodes (LEDs) were investigated. The LEDs were prepared on the (1122) plane of wurtzite GaN. Polarization and spectrum measurement was performed at different observation angles with respect to the LED surface. Partially polarized electroluminescence was confirmed at any angle of observation, where the emission intensity tended to be greater when a polarizer was aligned along the c-axis of the InGa_{0.18}N/GaN LED structure. The results clearly indicated the inclination of the c-axis relative to the LED surface. As a result, two light polarizations were identified and they were assigned to two different electronic transitions in relation to emission peak energies. Possible alteration of the valence-band structure was suggested due to the induced strain. [J2412]

"Modeling organic light-emitting diodes incorporating nanocrystal quantum dots"

Based on a rate equation model, we have investigated theoretically the performance of a model organic light-emitting diode (OLED), which is activated by a single emissive layer of nanocrystals (NCs) embedded between electron- and hole-transporting organic films. Our model combines a unified description of diffusion-controlled charge transport in the organic semiconductors, exciton formation and kinetics at the organic-organic interface, and Forster injection of the excitons into the nanocrystals. We have used the resultant rate equation model to study the light intensity and quantum efficiency of the NC-OLED as a function of the concentration of the nanocrystals, assuming the latter are arranged on a regular two-dimensional lattice in the emissive layer. We have identified an optimal nanocrystal density and shown that the NC-OLED performance is affected mainly by the efficiency of the Forster injection of excitons into the nanocrystals, whereas it is much less sensitive to the exciton kinetics at the organic-organic interface. [J2413]

"Long persistent light emitting diode"

Light emitting diodes (LEDs) coated with Sr₂MgSi₂O₇:Eu²⁺,Nd³⁺(blue), SrAl₂O₄:Eu²⁺,Dy³⁺(green), SrS:Eu²⁺,Y³⁺,Ce³⁺(orange), and CaS:Eu²⁺,Tm³⁺,Ce³⁺(red) long persistent phosphors were prepared. LEDs

which have a 450nm blue emission were used as an excitation source for the coated phosphors. Blue (475nm), green (520nm), orange (606nm), and red (650nm) emissions of the phosphors were found for each coated LED. Long persistent afterglow emissions from the phosphors excited by using LEDs were obtained. The persistence time of the phosphors' afterglow emissions coated on LEDs is found in the same order of magnitude as the phosphorescence persistence time of the long persistent phosphors. [J2414]

"Improving operating lifetime of organic light-emitting diodes with polycyclic aromatic hydrocarbons as aggregating light-emitting-layer additives"

It is common in organic light-emitting diode technology to construct a light-emitting-layer (LEL) host with materials that resist luminescence-reducing aggregation, which is one of the common reasons behind a phenomenon widely referred to as concentration quenching. However, if a host material in its aggregated state has a substantial quantum yield of fluorescence (e.g., at least several percents), it may yet be useful. We describe a group of aggregating flat and rigid polycyclic aromatic hydrocarbons (PAHs) as LEL additives. These molecules readily form emissive aggregates when added to the LEL. In the resulting devices, the aggregates show low-to-moderate external quantum efficiencies (EQE) of 0.2%-1.3%. Significantly, the addition of these PAHs increases device half-life (t_{50}) 4-200 times, depending on the additive, up to 100000 hours on operation at 40mA/cm². The lifetime increase occurs with many diverse classes of PAHs. The EQE can be improved to 3.7% by further adding a proper dopant while maintaining the increased lifetime. A possible link between the ability to aggregate and the lifetime increase is illustrated by comparing aggregation-prone perylene and aggregation-resistant 2,5,8,11-tetra-*t*-butylperylene (TBP). Despite the similarity between the two additives with respect to their initial device performance, perylene's stronger ability to aggregate correlates with the eight times longer half-life versus that for TBP. [J2415]

"Quantitative assessment of diffusivity and specularity of surface-textured reflectors for light extraction in light-emitting diodes"

Surface-textured reflectors fabricated by natural lithography and ion beam etching have a specular and a diffusive component of the reflectivity. The diffusely and specularly reflected powers of surface-textured reflectors are measured and analyzed quantitatively in terms of a theoretical model. The diffusive-power-to-total-power ratio is determined and shown to strongly depend on the surface texture. The light extraction efficiency from a waveguide clad by a partially diffuse reflector is analyzed and shown to be enhanced. [J2416]

"Design, growth, fabrication, and characterization of In As /Ga As 1.3 μm quantum dot broadband superluminescent light emitting diode"

In this paper we discuss a technique for broadening the emission and gain spectra of 1.3μm quantum dot superluminescent light emitting diodes (SLEDs). By incorporating different amounts of indium in different wells of a multi-dot-in-well stack we are able to tailor the emission and gain spectra of the devices. This technique allows us to overlap the ground state of one dot-in-well (DWELL) with the excited state of another to achieve broader and flatter emission spectra compared to a SLED design comprising DWELL layers of constant indium composition. Due to the low internal loss of these structures, this broadening is achieved without a significant reduction in the output power of the devices. [J2417]

"High power ultraviolet light emitting diodes based on Ga N /Al Ga N quantum wells produced by molecular beam epitaxy"

In this paper, we report on the growth by molecular beam epitaxy and fabrication of high power nitride-based ultraviolet light emitting diodes emitting in the spectral range between 340 and 350nm. The devices were grown on (0001) sapphire substrates via plasma-assisted molecular beam epitaxy. The growth of the light emitting diode (LED) structures was preceded by detailed materials studies of the bottom n-AlGaIn contact layer, as well as the GaN/AlGaIn multiple quantum well (MQW) active region. Specifically, kinetic conditions were identified for the growth of the thick n-AlGaIn films to be both smooth and to have fewer defects at the surface. Transmission-electron microscopy studies on identical GaN/AlGaIn MQWs showed good quality and well-defined interfaces between wells and barriers. Large area mesa devices (800×800μm²) were fabricated and were designed for backside light extraction. The LEDs were flip-chip bonded onto a Si submount for better heat sinking. For devices emitting at 340nm, the measured differential on-series resistance is 3Ω with electroluminescence spectrum full width at half maximum of 18nm. The output power under dc bias saturates at 0.5mW, while under pulsed operation it saturates at approximately 700mW to a value of 3mW, suggesting that thermal heating limits the efficiency of these devices. The output power of the investigated devices was found to be equivalent with those produced by the metal-organic chemical vapor deposition and hydride vapor-phase epitaxy methods. The devices emitting at 350nm were investigated under dc operation and the output power saturates at 4.5mW under

200mA drive current. [J2418]

"Direct observation of the evolution of occupied and unoccupied energy levels of two silole derivatives at their interfaces with magnesium"

The electronic structures of 2,5-bis(6'-(2',2''-bipyridyl))-1,1-dimethyl-3,4-diphenyl silacyclopentadiene (PyPySPyPy) and 2,5-di-(3-biphenyl)-1,1-dimethyl-3,4-diphenyl silacyclopentadiene (PPSPP) at their interfaces with Mg were investigated using ultraviolet, inverse, and x-ray photoemission spectroscopies. PyPySPyPy and PPSPP have been used as both electron injection/transport layers and emitters in high-efficiency organic light-emitting diodes (OLEDs). Deposition of either PyPySPyPy or PPSPP onto Mg results in the appearance of two energy levels within the energy gap of the organic. Upon deposition of Mg onto PyPySPyPy there is a shift of the occupied energy level structure to higher binding energy, away from the Fermi level, and appearance of two energy levels within the energy gap of PyPySPyPy. The lowest unoccupied molecular orbital is also shifted to higher binding energy. Upon deposition of Mg onto PPSPP there is also a rigid shift of the occupied energy level structure to higher binding energy, away from the Fermi level, but there are no apparent energy levels created within the energy gap of PPSPP. The different chemical reactivity of the two silole derivatives with magnesium is shown to have pronounced effects on the formation of cathode contacts in OLED structures. [J2419]

"Direct 120 V, 60 Hz operation of an organic light emitting device"

We report on lighting panels based on ruthenium(II) tris-bipyridine complexes that can be sourced directly from a standard US outlet. With the aid of the ionic liquid 1-butyl-3-methylimidazolium, the conductivity of the light emitting layer was enhanced to achieve device operation at a 60Hz frequency. Lighting panels were prepared using a cascaded architecture of several electroluminescent devices. This architecture sustains high input voltages, provides fault tolerance, and facilitates the fabrication of large area solid-state lighting panels. Scalability of the drive voltage, radiant flux, and external quantum efficiency is demonstrated for panels with up to N=36 devices. Direct outlet operation is achieved for panels with N=16, 24, and 36 devices. [J2420]

"Spin injection light-emitting diode with vertically magnetized ferromagnetic metal contacts"

We analyze the electrical injection of spin-polarized electrons into a (GaIn)As/GaAs light-emitting diode. Using an Fe/Tb multilayer structure with perpendicular magnetic anisotropy and a reverse-biased Schottky contact, we demonstrate spin injection even in remanence between 90 and 260K. The maximum degree of circular polarization of the emitted light is 0.75% at 90K. [J2421]

"Injection and transport processes in organic light emitting diodes based on a silole derivative"

This paper reports on charge injection and transport in electroluminescent devices based on a silole derivative 1,1-dimethyl-2,5-bis(p-2,2'-dipyridylaminophenyl)-3,4-diphenylsilole (DMPPS). The devices are composed of tin doped indium oxide (In₂O₃:Sn or ITO)/poly(3,4-ethylene dioxithiophene doped with poly(styrene sulfonate))/DMPPS/metal. Current-voltage and luminance-voltage characteristics are first performed as a function of the electron injection barrier height and of the organic layer thickness. The voltage dependence of current and luminance varies with the metal cathode, i.e., Ca, Al, Cu, and Au. The effect of the DMPPS thickness in a double carrier device shows that electrons predominate and are bulk limited. An accurate investigation is carried out as a function of temperature for hole-only and bipolar devices, i.e., with gold and calcium cathodes. Hole-only devices (with Au cathode) exhibit an Ohmic behavior for low voltages. A hopping mechanism (thermally assisted tunnel transfer between localized states) agrees with experimental data, since activation energy is found close to 50meV. The electron transfer limitation is located at the DMPPS/cathode interface and the Fowler-Nordheim mechanism is qualitatively consistent with experimental data at high voltages. With a Ca cathode, electron conduction is preponderant and is bulk limited. A power dependence $J \propto V_m^{1/2}$ with $m = 2$ is consistent with the model of trap charge limited conduction. The total electron trap density was estimated to be $2.4 \times 10^{18} \text{ cm}^{-3}$. [J2422]

"Extremely high quantum efficiency of donor-acceptor-pair emission in N-and-B-doped 6H-SiC"

High-efficiency visible light emission in N-and-B-doped 6H-SiC epilayers was observed in photoluminescence measurements at room temperature. The orange-yellow light emission due to the recombination of donor-acceptor pairs (DAPs) has a broad spectrum with a peak wavelength of 576nm and a full width at half maximum of 110nm at 250K. The high B concentration of more than 10^{18} cm^{-3} improves the emission efficiency of the DAP recombination at a high temperature. Compared with the photoluminescence spectrum of GaN at 10K, a high quantum efficiency of 95% was estimated for the highly B-doped sample. From time-resolved photoluminescence measurements, a DAP recombination time of 5.0ms was obtained, which is in good agreement with the calculated value by the rate equation with the assumption of a 95% internal quantum

efficiency. This is quite promising as a light-emitting medium by optical pumping, as well as monolithic light sources combined with nitride-based light-emitting diodes grown on the DA-doped SiC epilayer. [J2423]

"Design of the tunnel contacts and the transport region of all-electrical spin-injection-detection devices"

The design of an all-electrical spin-injection-detection device is discussed. It is shown that the use and the design of tunnel barriers cannot simply be copied from the spin light-emitting diodes, where they have already been demonstrated. Using one-dimensional and two-dimensional self-consistent simulations, the doping levels of the tunnel contacts and the spin-transport region are engineered to obtain an optimal tunnel barrier resistance and an optimal current distribution in the spin-transport region. [J2424]

"Improving the light extraction efficiency of red-emitting conjugated polymer light emitting diodes"

We demonstrate a significant improvement in the external electroluminescence efficiency of red-emitting polymer light emitting diodes (LEDs) by modifying the optical structure of the device. By using a cathode composed of a thin (5nm) film of calcium backed with an optically thick film of silver, we measured improvements in the external efficiency of polymer LEDs by a factor of 1.6 times compared to a device using a cathode composed of calcium backed with lower reflectivity aluminum. By incorporating the LED into a microcavity structure (to form a resonant cavity LED) it is possible to obtain additional (but rather smaller) improvements in external efficiency of the order of 1.15 times, compared to a standard LED utilizing the same cathode. By combining high reflectivity cathode/mirror materials with a low finesse cavity structure, we show that the external efficiency of a LED can be improved by as much as 1.8 times compared to a standard (noncavity) LED. Our results are in good agreement with those of theoretical calculations and demonstrate the real improvements in device external efficiency that can be achieved by reducing optical losses within the LED structure. [J2425]

"Influence of short-term low current dc aging on the electrical and optical properties of InGaN blue light-emitting diodes"

This work describes an experiment on degradation mechanisms of InGaN light-emitting diode (LED) test structures which do not fulfill the requirements of longlife products. We present a combined capacitance-voltage (C-V), deep level transient spectroscopy (DLTS), electroluminescence (EL), and cathodoluminescence (CL) study of short-term instabilities of InGaN/GaN LEDs submitted to low current aging tests at room temperature. In the early stages of the aging tests, the EL and CL characterizations showed an optical power decrease, more prominent at low current levels. The C-V profiles indicated that the stress induced an apparent charge increase, well related to the deep level changes detected by DLTS and to the optical power decrease. It is supposed that the main cause of the degradation is the generation of nonradiative paths, due to the generation/propagation of defects activated by carrier transport. [J2426]

"Correlation between electroluminescence efficiency and stability in organic light-emitting devices under pulsed driving conditions"

We investigated the effect of using pulsed current (pc) versus direct current (dc) driving mode on the electroluminescence (EL) efficiency and operational stability of tris(8-hydroxy-quinoline)aluminum (AlQ3)-based organic light-emitting devices. The results show that the dependence of device stability on the driving mode correlates with the relative EL efficiency under the pc and dc driving modes, where the mode that gives higher EL efficiency at any given current density also gives higher operational stability regardless of the duty cycle. [J2427]

"Modeling the influence of charge traps on single-layer organic light-emitting diode efficiency"

We investigate theoretically the role of carrier trapping on the efficiency of single-layer organic light-emitting diodes (OLEDs) by incorporating traps into the OLED device model of Davids et al [J. Appl. Phys. 82, 6319 (1997)]. Carrier trapping directly affects the density and mobility balance between electrons and holes through its effects on injection and mobility. In addition, trap-mediated changes in density alter recombination rates and spatial profiles of recombination that become important when excited state quenching at metallic contacts is considered. We illustrate these various influences of traps on device efficiency through computations on a series of model devices. Good agreement is obtained with previous experiments by Menon et al [Chem. Mater. 14, 3668 (2002)], where energetic disorder from transport traps was shown to reduce device efficiency. Our model, however, predicts circumstances where traps will improve device efficiency as well and can assist with selection of contacts to realistic organic materials. [J2428]

"Organic light-emitting diode driven by organic thin film transistor on plastic substrates"

A method for fabricating an organic light-emitting diode (OLED) connected to an organic thin film transistor (OTFT) on plastic substrates without heating is proposed. A three-dimensional pixel structure consisting of an OLED and an OTFT is prepared by the proposed method, and the characteristics of the device are tuned by refinement of structural parameters. By room-temperature fabrication, the OTFT with passivation film can be formed on a poly(ethylene naphthalate) plastic substrate, and the transparent anode of the OLED can be fabricated on the passivation film directly. OLED emission is thus generated directly by the current flowing through the OTFT, and the emission intensity is fully controllable by the gate voltage. [J2429]

"Optical characterization of ZnMnO-based dilute magnetic semiconductor structures"

n-type ZnMnO spin injection layers were grown by pulsed laser deposition on top of n-ZnMgO/ZnO/p-AlGaIn/p-GaIn hybrid spin light-emitting diode (LED) structures synthesized by molecular-beam epitaxy. Both the ZnMnO/ZnMgO/ZnO/AlGaIn/GaIn structures and control ZnMnO samples show no or very low (up to 10% at the lowest temperatures) optical (spin) polarization at zero field or 5T, respectively. This indicates difficulties in generating spin polarization by optical spin orientation or possible efficient spin losses. The results are similar to those found earlier for GaMnN/InGaIn/AlGaIn spin-LED structures and indicate that these wide-band-gap dilute magnetic semiconductors with weak spin-orbit interaction and hexagonal symmetry are not attractive for spin-LED applications. [J2430]

"1.32 μm InAs /GaAs quantum-dot resonant-cavity light-emitting diodes grown by metalorganic chemical vapor deposition"

The first demonstration of InAs/GaAs quantum-dot (QD) resonant-cavity light-emitting diode (RCLED) operating at 1.32 μm at room temperature is reported. A single-layer InAs QDs inserted in GaAs matrix as the active medium was grown by metalorganic chemical vapor deposition. The bottom and top mirrors of QD RCLEDs were fabricated by employing epitaxial AlGaAs/GaAs pairs and one dielectric SiO₂/Si₃N₄ pair as distributed Bragg reflectors (DBRs), respectively. As compared to the nonresonant QD LEDs, the RCLEDs exhibit a forward voltage of 1.13 V at 20 mA, a peak wavelength of 1.318 μm , a narrower full width at half maximum in the electroluminescent spectrum of 14 meV at 20 mA, a high Q factor of 73.9, a low redshift rate with injection current of 0.033 nm/mA, and a higher light-output power of 28 μW at 100 mA. [J2431]

"Fabrication and photoluminescence of InGaIn-based nanorods fabricated by plasma etching with nanoscale nickel metal islands"

InGaIn-based nanorods with a rod density of $3.04 \times 10^{10} \text{ cm}^{-2}$ were fabricated from a light-emitting diode structure by an inductively coupled plasma dry-etching with nanoscale nickel metal islands. The nanoscale nickel metal islands were formed from a Ni film by a rapid thermal annealing at 850°C for 1 min. The influence of thicknesses of Ni metal film on the diameter and density of nanorods was also investigated. Structural and optical properties of the InGaIn-based nanorods were studied with field-emission scanning electron microscopy, transmission electron microscopy, and photoluminescence. The diameters and heights of nanorods were estimated to be 60–100 nm and more than 0.28 μm , respectively. The emission-peak wavelength of nanorods showed a blueshift of 5.1 nm from that of the bulk structure. An enhancement by a factor of five times in photoluminescence intensity of nanorods compared to that of the bulk structure was also observed in this work. The blueshift is attributed to the strain relaxation in the well, quantum-confinement effect, or a combination of the two, which result in the enhancement in emission intensity. [J2432]

"Amber GaNP -based light-emitting diodes directly grown on GaP (100) substrates"

Growth and fabrication of GaNP-based amber light-emitting diodes (LEDs) are reported. A simple p-i-n heterojunction LED structure, emitting at 612 nm, was grown directly on a transparent GaP(100) substrate. Current-voltage (I-V) characteristics of 380 $\mu\text{m} \times 380 \mu\text{m}$ LED chips are comparable to those of conventional AlInGaP-based LEDs, but GaNP-based LEDs exhibit a much higher breakdown voltage. The significant simplicity of a one-step growth process of GaNP-based LEDs is an advantage over etch removing of a GaAs absorbing substrate and wafer bonding to a GaP transparent substrate for conventional AlInGaP-based LEDs. [J2433]

"Blue light-emitting diode-based, enhanced resonant excitation of longitudinal acoustic modes in a closed pipe with application to N O₂"

We present a new, very compact resonant photoacoustic system based on a simple closed pipe, transversally

illuminated by an array of blue light-emitting diodes uniformly distributed along the tube to produce an acoustic signal from NO₂-N₂ samples. The illumination is modulated in a particular way as to produce amplification of the acoustic resonance corresponding to the second longitudinal mode. The linearity of the system for NO₂ trace detection is studied. This arrangement provides a simple, compact, and cheap setup, useful for both measuring emissions from diesel engines and teaching photoacoustic spectroscopy in gases. [J2434]

"Portable digital microscope apparatus"

This article successfully presented the concept of digital camera changing digital microscope using additional adapter with one lens, light emitting diodes, single AAA battery cell, and simple construction without interfering digital camera function. It will be very friendly using general instrument to record miniature target image data in scientific and engineering fields in the future. [J2435]

"Honeycomb GaN micro-light-emitting diodes"

An optimized design for a micro-light-emitting diode array is presented. Based on a honeycomb hexagonal closed-packed structure, the packing density of individual elements can be increased to over 80% to minimize wastage of junction area. The extended sidewall area provides additional light extraction pathways. The honeycomb light-emitting diode (LED) emits twice as much light compared to a conventional broad area LED with equal junction area, and 50% more light than a microdisk array LED. The significant improvement in efficiency makes the additional processing step worthwhile. [J2436]

"Simulation of vertical and lateral ZnO light-emitting diodes"

All-ZnO light-emitting diodes (LEDs) offer the promise of a low-cost, brighter alternative to existing GaN-based light emitters for solid-state lighting applications, in part due to the higher exciton binding energy of ZnO. We have used ISE TCAD™ simulations to examine the effect of active, n- and p-layer dopings and thicknesses on the optical output intensity and current-voltage characteristics of both vertical and lateral geometry ZnO LEDs. The latter geometry is attractive for ultralow structures with the ZnO deposited on glass substrates. The current density distribution is more uniform in the vertical structures but there is little difference in optical output power as a function of doping or layer thickness between the two geometries. [J2437]

"Amorphous selenium based photodetector driven by field emission current from N-doped diamond cold cathode"

Operation of prototype photodetector using a-Se based target and diamond cold cathode is investigated. In our previous study, successful operation of the prototype photodetector as a unit pixel in future imaging device was reported. Clear photoresponse was obtained even at 10⁻⁵ Torr, several orders of magnitude higher than the pressure used for conventional imaging tube devices. Electron emission characteristics of diamond are widely reported, but the precise fabrication process of a-Se based target film is covered with patents. In this study, we have fabricated following three types of target films: (A) a-Se film without incorporation, (B) a-Se film with incorporation of arsenic (As), and (C) a-Se film with incorporation of As and tellurium (Te). Successful operation of the photodetector driven by diamond cathode with target C was observed. The detector showed clear response to red, green, and blue light-emitting diodes in addition to white halogen light. [J2438]

"Molecular beam epitaxy growth of midinfrared "W" light emitting diodes on InAs"

We have studied how midwave infrared (MWIR) photo- and electroluminescence of type-II "W" InAs/InGaSb/InAs/AlGaAsSb quantum well structures depend on molecular beam epitaxy growth conditions and substrate material. All samples were grown with Sb₄, in contrast to most recent reports that use Sb₂. Resulting devices represent the highest reported external differential efficiency for molecular beam epitaxy grown light emitting diodes emitting in the 4.3-4.6 μm wavelength range in the continuous wave mode at the room temperature. Another important aspect of the work is the finding that MWIR emitters on InAs substrates are superior to those on conventionally used GaSb substrates. [J2439]

"Fabrication of organic light-emitting devices on flexible substrates using a combined roller imprinting and photolithography-patterning technique"

A patterning method has been developed to fabricate patterned organic light-emitting devices (OLEDs) (60×80 mm²) with a pixel size of 500×300 μm² on flexible polyethylene terephthalate substrates. The patterns of the pixel array were defined in crossed-strip style with indium tin oxide anode and patterned using a combination of roller-type imprinting lithography and photolithography (CRIP) followed by wet etching. Compared with conventional imprint lithography or photolithography, the CRIP technique has the advantages of better uniformity,

less force, consuming less time, lower cost, and higher aspect ratio. The performance of the CRIP OLEDs was the following: the turn-on voltage at 1cd/m² was 7.5V and the maximum luminance was 13530cd/m² at 17.5V. The highest luminous efficiency reached 1.27lm/W (3.23cd/A) at a luminance of 4.8cd/m² and kept the values stable from 5 to 15V. The performance was comparable to that of devices patterned by conventional photolithography.

[J2440]

"Wavelength-resolved low-frequency noise of GaInN/GaN green light emitting diodes"

Light intensity low-frequency noise was studied in green GaInN/GaN quantum well light emitting diodes. The light intensity noise was measured as a function of wavelength within the light emitting diode spectral emission line. The spectral noise density is found to increase with decreasing wavelength. Comparing the wavelength-resolved noise with the total light noise, we found that the emission intensity fluctuates synchronously across the entire linewidth. The source of this noise can be ascribed to nonradiative recombination centers.

[J2441]

"Impedance of space-charge-limited currents in organic light-emitting diodes with double injection and strong recombination"

The impedance model for a one-carrier space-charge-limited (SCL) current has been applied to explain some experimental features of double carrier organic light-emitting diodes. We report the analytical model of impedance of bipolar drift transport in SCL regime in the limit of infinite recombination. In this limit the ac impedance function is identical to that of a single carrier device, with a transit time modified by the sum of mobilities for electrons and holes, $\mu_n + \mu_p$. The static capacitance $C(\omega \rightarrow 0)$ is a factor of 34 lower than the geometric capacitance, as observed for single carrier devices, but it is shifted to higher frequencies. It follows that impedance measurements in the dual-carrier organic diodes with strong recombination provide the combination of $\mu_n + \mu_p$. For the mobilities of the different carriers to be determined separately, additional information is required.

[J2442]

"Operating longevity of organic light-emitting diodes with perylene derivatives as aggregating light-emitting-layer additives: Expansion of the emission zone"

We describe aggregating perylene derivatives as light-emitting-layer (LEL) additives in organic light-emitting diodes (OLEDs). These molecules readily form emissive aggregates when added to the LEL. In the resulting devices, the aggregates show moderate external quantum efficiencies of 0.9%-1.7%, which can be improved to 2.7%-4.0% by further adding a proper dopant. Importantly, addition of these polycyclic aromatic hydrocarbons increases the half-life (t_{50}) of undoped and doped OLEDs by 30-150 times. Thus, 11cd/A green and 5.2cd/A red devices are produced that have pure color, Commission Internationale de l'Eclairage 1931 2° color chromaticity coordinates (CIEx,y) 0.32, 0.63 and 0.64, 0.36, respectively, and t_{50} of 30 000 and 200 000h, respectively, upon operation at 40mA/cm². A possible link between the thickness of the emission zone and the lifetime increase is illustrated by comparing aluminum 8-hydroxyquinoline chelate (Alq₃) as an LEL host versus an Alq₃+dibenzo[b,k]perylene mixed host using C545T as an emissive probe. The comparison suggests that the emission zone and probably the electron-hole recombination zone are expanded for the mixed host.

[J2443]

"Top-emitting polymer light-emitting diodes with environmentally stable cathodes"

We report the demonstration of polymer-based top-emitting diodes that employed environmentally stable cathode materials. The device employed an emissive polymer blend that we reported previously [Deng et al Appl. Phys. Lett. 84, 3522 (2004)]. By constructing a semitransparent cathode using the stable metals Al and Ag, bright light emission through the top cathode was achieved. An index-matching overlayer deposited by spin coating was shown to enhance the transmission efficiency through the top electrode. Microcavity effects were observed for the device by replacing the indium tin oxide anode with Au, resulting in wavelength tunability of the device.

[J2444]

"High-efficiency white organic light-emitting devices using a blue iridium complex to sensitize a red fluorescent dye"

We report the fabrication of high-efficiency white organic light-emitting devices (WOLEDs) by using a blue phosphorescent dye iridium (III) tris(5-(2,4-difluoro-phenyl)-10,10-dimethyl-4-aza-tricycloundeca-2,4,6-triene) (Ir(F2-mppy)₃) to sensitize the red dye [2-methyl-6- [2-(2,3,6,7-tetrahydro-1H-c5H-benzo[ij]quinolizin-9-yl)ethenyl]-4H-pyran-4-ylidene]propane-din-itrile (DCM2). Ir(F2-mppy)₃ and DCM2 were codoped into the 4,4'-N,N'-dicarbazole-biphenyl (CBP) host. The WOLEDs with 8wt% Ir(F2-mppy)₃ and 0.5wt% DCM2 showed white emission with a color rendering index of 70. The maximum luminance and maximum current efficiency of the device are, respectively, 16220cd/m² and 9.28cd/A.

[J2445]

"Highly efficient organic light-emitting diodes with metal/fullerene anode"

Metal/fullerene bilayers have been studied as hole injection electrodes for use in organic light-emitting diodes (OLEDs). In the case of a simple emission zone structure, it is found that OLEDs with the Au/C₆₀ anodes have much lower (~ 10 V) driving voltages and much higher current efficiencies (five times higher) than OLEDs with a simple Au anode. This anode structure was found to be applicable for all types of light-emitting structures including fluorescent and phosphorescent dye-doped systems. The formation of a primary bond at the Au/C₆₀ interface is explained as the major cause for efficient hole injection from Au to C₆₀. The hole transfer barrier between C₆₀ and the adjacent hole transport layer is also found critical in selecting suitable matching materials to achieve highly efficient OLEDs. [J2446]

"Tunable, narrow, and enhanced electroluminescent emission from porous-silicon-reflector-based organic microcavities"

Microcavity organic light-emitting diodes (MC-OLEDs) based on porous silicon distributed Bragg reflectors (PS-DBRs) have been realized, and improved structural, optical, and electrical properties have been observed. In the device, a multilayer OLED functions as the central active element, sandwiched between a top silver film and a bottom PS-DBR formed by electrochemical etching of a p⁺⁺-Si substrate. Field-emission scanning-electron-microscopy cross-sectional images show that there exist nanoscale layered structures and flat interfaces inside the cavity. Widths of green and red electroluminescent (EL) peaks emitted from the MC-OLEDs are 8 and 12 nm, respectively, greatly reduced in comparison with 85 and 70 nm measured from noncavity structures. The narrowed EL emission from the MC-OLEDs is directional and in single mode, with off-resonant optical modes highly suppressed, which is mainly due to the good optical properties of PS-DBR with high reflectivity in a wide smooth stop band. Further increases in the green and red EL intensities by factors of about 6 and 4, respectively, are achievable. The improvement is physically attributable to the spatial redistribution of the photon density of states in the cavities. In addition, current-brightness-voltage properties and lifetime-related parameters of the devices are discussed. Such device structure and emission patterns of the MC-OLEDs should be useful in silicon compatible optical interconnects and light-emitting diode array printing. [J2447]

"Theoretical and experimental analysis of current spreading in AlGaInP light emitting diodes"

The profile of light emission from aluminum gallium indium phosphide (AlGaInP) light emitting diodes has been studied and compared with the theoretical modeling of current spreading using a lossy transmission line model of current injected into the active region. Discrepancies between the experimentally determined emission profile and the theoretically predicted current injected into the active region have been analyzed and explained using a Monte Carlo ray tracing simulation which considers the trajectories of the photons after leaving the active region and the particular geometry of the device current, die size, and current spreading layer resistance upon the emitted emission profile. The combination of the current spreading and ray tracing models give very good agreement with the experimental emission profiles for both thin and thick current spreading layers. [J2448]

"Lifetime study of polymer light-emitting electrochemical cells"

The lifetime and degradation characteristics of frozen-junction polymer light-emitting electrochemical cells have been studied. Two seemingly minor factors, the end group of the same luminescent polymer and the type of substrate on which the device is constructed, have shown profound effects on the stress behaviors of these devices operated at a nominal operating temperature of 200 K. In devices made on glass substrates, an anomalous large increase in light intensity and driving voltage has been observed under constant current stress measurement. This has been attributed to the relaxation of the electrochemical doping, which leads to reduced photoluminescence quenching and increased resistance in the polymer film. The doping relaxation is accelerated by the poor thermal conductivity of glass substrate, which causes significant temperature rise in the device due to self-heating. Evidence also suggests that doping relaxation can even occur at below the glass transition temperature of the polymer electrolyte. All devices are shown to be short lived when operated at or above 250 K due to fast doping relaxation. However, devices made on sapphire substrates based on 3,5-dimethyl phenyl-terminated poly[5-(2'-ethylhexyloxy)-2-methoxy-1,4-phenylene vinylene] are remarkably stable when operated at 200 K, with an estimated half-life of 700 h even when stressed at a very high current density of 1 A/cm². [J2449]

"Stable and highly bright white organic light-emitting diode based on 4,4',4''-tris(N-3-methylphenyl-N-phenyl-amino)-triphenylamine"

A stable and very bright white organic light-emitting diode (WOLED) was fabricated with the structure ITO/m-MTDATA (30 nm)/NPB(30 nm)/DPVBi (11 nm)/Alq₃:DCJTb(50 nm)/LiF(1 nm)/Al(250 nm). White light emission was

achieved by combining blue and orange emissions emitted from DPVBi and Alq3:DCJTB layers, respectively. Inserting an m-MTDATA layer between ITO and NPB improved the charge balance in the recombination zone, improving the stability of the emission color of WOLED. The maximum luminance was 20590cd/m² at 13V with CIE coordinates of x=0.30, y=0.31. The maximum power and current efficiencies were 6.01lm/W at 5V and 6.2cd/A at 5V, respectively. Conversely, the WOLED without an m-MTDATA buffer layer exhibited unstable emission characteristic. [J2450]

"Flat panel displays for ubiquitous product applications and related impurity doping technologies"

Various kinds of flat panel displays such as liquid crystal displays (LCDs), plasma display panels and organic light emitting diode (OLED) displays are briefly evaluated from the perspective of applicability to ubiquitous products. It is clarified that the LCDs and OLED displays are suitable for realizing mobile electronic products with a high quality display, since these displays can use active devices on the backplanes to form active matrix displays and can integrate peripheral circuits of the displays and functional circuits of mobile electronics for a ubiquitous era. It is clarified further that the low temperature polycrystalline silicon (LTPS) thin film transistor (TFT) is the most promising active device for the backplane of such active matrix displays because the LTPS TFT has the possibility to enhance its performance without raising the cost. The low temperature poly-Si TFT fabrication process is introduced, and its key technologies such as crystallization, gate oxide formation, and impurity doping are surveyed. As the property of polycrystalline silicon (poly-Si) influences not only the TFT performance itself but also the efficiency of impurity doping and the integrity of the gate oxide, the crystallinity of the poly-Si is reviewed. After that, the history of the development and the state of the art in impurity doping technology and its issues are addressed in detail. Finally, foreseeing the application of LTPS TFT, the realization of OLED displays, and the progress of LTPS TFT for integrating higher functional circuits for ubiquitous applications, the requirements for impurity doping in such progress are addressed. In particular, the single grain silicon technology and the scaling down of the TFT size, which are thought to be highly effective to enhance the performance of TFTs, and issues of impurity doping technology relating to them are discussed. [J2451]

"Poly(N -vinylcarbazole) doped with a pyrazoloquinoline dye: A deep blue light-emitting composite for light-emitting diode applications"

We investigated the spectral properties of light-emitting diodes based on a deep blue-emitting pyrazoloquinoline dye doped into a poly(N-vinylcarbazole)-based matrix. Even though the electroluminescence (EL) of the host is redshifted and broadened with respect to the emission of the dye, the EL spectrum becomes fully dominated by the dye emission at concentrations of ca. 2wt%. This is attributed to a competition of exciplex formation on the matrix and exciton formation on the dye. [J2452]

"Distribution of optical emission between guided modes and free space in a semiconductor nanowire"

We study the distribution of the emitted power between the free-space modes and guided modes in a semiconductor nanowire. We analyze all possible dipole orientations and nanowire radii in the range from very small to comparable to the wavelength. Our theoretical approach is based on the Fourier transform technique and equivalent to the construction of Green's function for a dipole at an arbitrary location inside the nanowire. We show that the total emitted power can exhibit rather pronounced oscillations as a function of the frequency and radius. The far-field pattern is also very sensitive to the frequency and radius, especially in the regime when leaky (or whispering gallery) modes with finite axial wave numbers are excited. We discuss the enhancement of emission into guided modes due to formation of Fabry-Perot cavity in a finite length nanowire. Our results yield directly the extraction efficiencies and angular distribution of radiation of light-emitting diodes made of nanowires. [J2453]

"The influence of acceptor anneal temperature on the performance of InGaN/GaN quantum well light-emitting diodes"

Temperature-dependent measurements of the pulsed light-current characteristics of InGaN light-emitting diodes that were thermally annealed at different temperatures have been investigated. A distinct light output, at a fixed current density, with operating temperature arises where the light output increases as the operating temperature is reduced from 300 K, reaches a maximum, and then decreases with subsequent reductions of the operating temperature. We observe that light-emitting diodes thermally annealed at higher temperatures, which is believed to increase the number of electrically activated acceptors in the layers, have a lower light output below 300 K and the maximum light output shifts to higher operating temperatures. Measured absorption and emission spectra show that the thermal anneal process has not affected the structure of the quantum wells within these samples. The light output, for a fixed current density, has been simulated as a function of operating temperature,

and we find that by changing the concentration of acceptor atoms, compensating donor atoms, and the hole mobility in the layers, the trends observed experimentally can be reproduced. On the basis of the simulations we find that the distinct behavior of the light output with operating temperature is due to the combination of Shockley-Reed-Hall recombination, at operating temperatures around 300 K, and electron drift leakage, at operating temperature below 300 K, and the increase of the acceptor concentration results in an increased electron drift leakage due to the change of the concomitant hole mobility. The simulations support the view that the experimental observations can be explained through changes of the acceptor concentration in the layers when the thermal anneal temperature is increased. [J2454]

"Bipolar carrier transport in a conjugated polymer by complex admittance spectroscopy"

We report the bipolar transport properties of the LUMATION™ (Sumitomo Chemical) 1300 Series green-emitting polymer investigated by means of admittance spectroscopy. Analysis of the inductive response in single-carrier polymer diodes yields electron and hole mobilities which are in excellent agreement with the results of independent measurements. Admittance measurements in dual injection diodes, in combination with the analysis of current-voltage characteristics, provide evidence that the dual injection diodes operate in space-charge-limited regime, indicative of strong recombination within the material. Our results provide strong evidence that the space-charge-related admittance response of dual-carrier diodes is dominated by combined electron-hole response, which corresponds to the sum of electron and hole mobilities. This implies that electron and hole mobilities cannot be obtained separately from admittance measurements in space-charge-limited dual-carrier devices. [J2455]

"Voltammetric study of Bphen electron-transport layer in contact with Li F /Al cathode in organic light-emitting diodes"

We report that the similarities of I-V characteristics of organic light-emitting diodes (OLEDs) incorporating Bphen (4,7-diphenyl-1,10-phenanthroline) electron-transport layer, with or without lithium doping, do not stem from the analogous compositions of the respective electron-transport layers. Voltammetric studies of OLED devices of the following general structure: anode | NPB (N,N'-diphenyl-N,N'-bis(1-naphthyl)-1,1'-biphenyl-4,4'-diamine) | TBADN (9,10-bis(2-naphthyl)-2-t-butylanthracene) | Bphen | LiF | Al, indicate that the bulk of the Bphen electron-transport layer has insulating rather than semiconducting properties. A previously unknown feature is also detected by voltammetry: the presence of a macroscopic dipole comprised of a negative interfacial charge at the NPB | TBADN interface and a positive charge in the Bphen layer and/or at the TBADN | Bphen interface, which could result from the diffusion of lithium ions. We also find that, in contrast to the bulk of the Bphen layer, its thin sublayer has, in fact, semiconducting properties, which also could be reasonably explained by the diffusion of lithium ions along with the migration of a countercharge, e.g., electron hopping between Bphen molecules. [J2456]

"A room-temperature continuous-wave operating midinfrared light emitting device"

An optimized light source for the 4-5 μm wavelength region with a continuous-wave output power of 2 mW at ambient temperature is introduced. The device is based on a narrow-gap lead salt semiconductor chip, which is optically pumped by a standard high-power diode laser array. Surface patterning is employed and leads to an up to sixfold increase in out-coupling efficiency compared to untreated chip surfaces. A model is presented that explains this enhancement of the light extraction. Output efficiencies of 44-104% are achieved. [J2457]

"Influence of carrier injection on the electromodulation response of trap-rich polymer light-emitting diodes"

We investigate the influence of carrier injection on the electric field distribution in polyfluorene-based polymer light-emitting diodes containing poly(3,4-ethylenedioxythiophene)-poly(styrene sulfonate) (PEDOT:PSS). The devices show strong charge-induced electromodulation spectra due to the accumulation of trapped electrons close to the PEDOT:PSS/polyfluorene interface. The trapped electrons cause the potential to drop preferentially at the interface, enhancing hole injection and substantially reducing the magnitude of the electric field in the bulk semiconductor. The detailed operating mechanisms of such "trap-rich" devices are poorly understood, and in this paper we perform a series of temperature-dependent current-voltage sweeps and electromodulation measurements to clarify the role of the injected charge. We find that the devices show strong field redistribution only at room temperature and that devices operating at lower temperatures (< 100 K) resemble trap-free light-emitting diodes with a uniform electric field that extends through the bulk. We consider also the effects of pixel aging and show that field redistribution effects are reduced after extended device operation. [J2458]

"Influence of residual oxygen impurity in quaternary InAlGaN multiple-quantum-well active layers"

on emission efficiency of ultraviolet light-emitting diodes on GaN substrates"

The influence of residual impurities in quaternary InAlGaN active layers on the emission efficiency of 350nm band ultraviolet light-emitting diodes on GaN substrates has been investigated. Secondary ion mass spectrometry and capacitance-voltage measurements have revealed that a large amount of oxygen is incorporated into the InAlGaN active layers owing to relatively low growth temperatures for Al-content epitaxial films. The increase of the InAlGaN growth temperature from 780 to 830 °C results in both the residual oxygen level decrease from 1.4×10^{18} to 4.4×10^{17} cm⁻³ and the output power improvement from 0.6 to 2.6 mW at 100 mA. It is also found that devices containing lower oxygen concentration in the InAlGaN active layers demonstrate a higher electroluminescence intensity ratio of the band-edge emission from the well layers to the donor-acceptor-pair emission from the p-type layers at low temperatures. These experimental results, in conjunction with numerical calculations, suggest that the reduction in the oxygen impurity level in the InAlGaN active layers has an effect on suppressing the electron leakage current into the p-type layers, and thus improving the internal quantum efficiency of InAlGaN-based ultraviolet light-emitting diodes. [J2459]

"Optical properties of AlGaIn /GaN multiple quantum well structure by using a high-temperature AlN buffer on sapphire substrate"

We demonstrated highly improved optical properties of the AlGaIn/GaN multiple quantum well (MQW) structure grown on a GaN layer with significant reduction of dislocations achieved using an AlN buffer directly grown on a sapphire substrate at high temperature, in comparison with the MQW grown using a conventional two-step technique. An enhancement of room-temperature photoluminescence intensity by up to one order of magnitude has been observed, compared with the conventional MQW. Transmission electron microscopy measurements indicated that the dislocation density of the GaN grown using the AlN buffer technique was dramatically reduced. Furthermore, the significantly improved optical properties of this MQW using this AlN buffer technique were also demonstrated by increasing the thickness of the GaN layer underneath, whose crystal quality can be improved by increasing thickness, confirmed by detailed x-ray measurements. Since the technique can significantly improve the optical efficiency in the ultraviolet (UV) spectral region without involvement of any ex situ patterning process, it should be highlighted in the development of high performance UV light-emitting diodes, currently a highly regarded research area. [J2460]

"Effects of metal-doped indium-tin-oxide buffer layers in organic light-emitting devices"

Organic light-emitting devices were fabricated by using different metal (V, Zr, Hf)-doped indium-tin-oxide (ITO) buffer layers on an ITO anode. The metal-doped ITO buffer layers were 15 nm thick with different metal concentrations. Both resistivity and work function of the ITO buffer layer were manipulated by these metal dopants. Different effects on the devices, such as reduced turn-on voltage, improved luminance, and enhanced current efficiency, were investigated. A low turn-on voltage was observed for devices with small work function and resistivity. The lowest turn-on voltage (3 V) was found on a device with a V-doped ITO buffer layer. The devices usually have a similar current density (J)-voltage (V) characteristics, but not the luminance-J or the current efficiency-J characteristics when the ITO buffer layers have the same work function. The devices with the Hf-doped ITO buffer layers show the best luminance performance among those considered. At 100 mA/cm², a luminance of 15,000 cd/m², and a current efficiency of 15 cd/A have been achieved. The balance between the carrier concentration and the energy barrier for the hole injection is possibly responsible for such performance. [J2461]

"Electroluminescence from ZnO nanowires in n-ZnO film/ZnO nanowire array/p-GaN film heterojunction light-emitting diodes"

ZnO nanowire-array-embedded n-ZnO/p-GaN heterojunction light-emitting diodes were fabricated by growing Mg-doped p-GaN films, ZnO nanowire arrays, and polycrystalline n-ZnO films consecutively. Electroluminescence emission having the wavelength of 386 nm was observed under forward bias in the heterojunction diodes and the UV-violet light was emerged from the ZnO nanowires. The heterojunction diode was thermal treated in hydrogen ambient to increase the electron injection rate from the n-ZnO films into the ZnO nanowires. High concentration of electrons supplied from the n-ZnO films activated the radiative recombination in the ZnO nanowires, i.e., increased the light-emitting efficiency of the heterojunction diode. [J2462]

"Highly efficient organic electroluminescent device with modified cathode"

One of the key parameters for high efficiency organic electrophosphorescent light emitting diodes is charge injection into the phosphorescence compound. By introducing a hybrid device architecture, and incorporating electron and hole interfacial layers with lowest unoccupied molecular orbital and highest occupied molecular orbital levels similar to that of the phosphorescence compound, on the cathode and the anode side of the

device, respectively, charge injection properties were improved. A green electrophosphorescence device with luminous efficacy of 50lm/Wat luminance efficiency reaching 55cd/Awas demonstrated. [J2463]

"1.54 mcm Si:Er light emitting diode with memory function"

We report a memory effect in electroluminescence of Er-doped silicon light emitting diodes: applying a voltage pulse in reverse-bias direction below breakdown we observe 1.54mcmemission only, if a forward pulse was issued before. This effect occurs for temperatures $T \leq 120\text{K}$ in sublimation molecular-beam epitaxy grown structures. This finding opens perspectives for the development of a fully complementary metal-oxide-semiconductor compatible electro-optical converter with a memory function, operating in the 1.5mcmtelecommunication band. Such an element could find numerous applications in telecommunication and silicon photonics and optoelectronics circuitry. [J2464]

"Blue polymer electrophosphorescent devices with different electron-transporting oxadiazoles"

We report that the performances of blue polymer electrophosphorescent devices are crucially depending on the choice of the electron transporting material incorporated into the emissive layer. Devices with 1,3-bis[(4-tert-butylphenyl)-1,3,4-oxadiazolyl]phenylene (OXD-7) doped at 40wt%into a poly(vinylcarbazole) matrix exhibited significantly higher efficiencies than those with 2-(4-biphenyl)-5-(4-tert-butylphenyl)-1,3,4-oxadiazole (PBD), yielding maximum luminous and power efficiency values of 18.2 Cd/A and 8.8 lm/W, respectively. Time resolved photoluminescence measurements revealed a long lifetime phosphorescence component in layers with PBD, which we assign to significant triplet harvesting by this electron-transporting component. [J2465]

"Oblique Hanle measurements of InAs /GaAs quantum dot spin-light emitting diodes"

We report on studies of electrical spin injection from ferromagnetic Fe contacts into semiconductor light emitting diodes containing single layers of InAs/GaAsself-assembled quantum dots (QDs). An oblique magnetic field is used to manipulate the spin of the injected electrons in the semiconductor. This approach allows us to measure the injected steady-state spin polarization in the QDs, Pspinas well as estimate the spin losses in the QD spin detector. After subtraction of magneto-optical effects not related to spin injection, we measured a Pspinof 7.5% at 15 K and estimated an injected spin polarization before QD recombination of around 20%. [J2466]

"Control of carrier transport in organic semiconductors by aluminum doping"

Control of carrier transport in organic semiconductors by aluminum doping is realized in organic light-emitting devices (OLEDs) for which electroluminescence can sensitively reflect the status of carrier transport. It is found that an Al-doped layer with proper thickness (1-10nm)may block hole transport completely and enhance electron transport to some extent regardless of its location in the organic carrier transport layers. Improvement in the efficiency of OLEDs with an aluminum cathode is achieved upon the introduction of a very thin (3nm)Al-doped region near the light-emitting area. The current efficiency obtained with such Al-doped devices is about 30% higher than that with undoped devices. [J2467]

"Fluorocarbon film as cathode protective coating in organic light-emitting devices"

The present work demonstrates the use of fluorocarbon (CFx)film as a cathode protective layer to enhance the stability of organic light-emitting devices (OLEDs). Devices with the CFxcathode protective layer showed a threefold increase in operational lifetime, about 10000h, comparing to those without the CFxlayer. Growth of dark spots was significantly suppressed. The superior moisture-resistant capability of the CFxis attributed to its hydrophobic nature and low moisture permeation. As most OLED production lines are already equipped with CFxdeposition facilities, the present cathode protective coating can be easily adopted for further stability enhancement without additional capital investment. [J2468]

"White-electrophosphorescent devices based on copper complexes using 2-(4-biphenyl)-5-(4-tert-butyl-phenyl)-1,3,4-oxadiazole as chromaticity-tuning layer"

Efficient white organic light-emitting diodes based on copper complex, [Cu(bis[2-(diphenylphosphino)phenyl]ether)(6,7-dicyanodipyrido[2,2-d:2',3'-f]quinoxaline)]BF₄[Cu(I) complex], in which the white emission composed of yellow emission from Cu(I) complex doped 4,4'-N,N'-dicarbazole-biphenyl (CBP) layer and blue emission from N,N'-diphenyl-N,N'-bis(1-naphthyl)-(1,1'-benzidine)-4,4'-diamine layer, were fabricated. A thin 2-(4-biphenyl)-5-(4-tert-butyl-phenyl)-1,3,4-oxadiazole (Bu-PBD) layer sandwiched between the two emission layers acts as a chromaticity-tuning layer. The white device with 10nm, 2wt%Cu(I) complex doped CBP layer and 2nmBu-PBD layer shows CIE coordinates of (0.33,0.36) at applied bias of 10V, a maximum luminance of 2466cd/m², and a maximum current efficiency of 6.76cd/A, corresponding to the power

efficiency of 3.85lm/W. The efficient white emission is attributed to the simultaneous exciton formation in both emission layer. The working mechanism of the thin Bu-PBD layer for achieving white emission was also discussed. [J2469]

"Influence of metallic nanoparticles on the performance of organic electrophosphorescence devices"

We investigate the influence of metallic nanoparticles on the performance of phosphorescence organic light emitting diodes. The metallic nanoparticles display appropriate surface plasmon resonances in the visible region of the spectrum close to the emission band of the triplet emitter to accelerate the spontaneous emission rate of the phosphorescence compound. We have incorporated gold nanoparticles in the interface between alternative buffer layers and a phosphorescence based light emitting layer. In the case of Al4083 poly(3,4-ethylenedioxy thiophene):poly(styrene sulfonate) buffer layer, the interface modification with gold nanoparticles results in a 33% improvement in the luminance efficiency of tris(2-(4-tolyl)phenylpyridine) iridium based phosphorescence organic light emitting diodes. [J2470]

"1.1 mcm near-infrared electrophosphorescence from organic light-emitting diodes based on copper phthalocyanine"

We demonstrated near-infrared organic light-emitting devices employing copper phthalocyanine (CuPc) doped into 4,4'-N,N'-dicarbazole-biphenyl (CBP). Room-temperature electrophosphorescence was observed at about 1.1mcm due to transitions from the first excited triplet state to the singlet ground state (T1-S0) of CuPc. There existed very weak emission of CBP from undoped devices, and at lower doping concentrations ($\leq 12\text{wt}\%$) the driving voltages of doped devices were higher than that of undoped devices. The results indicated that Forster [Ann. Physik. (Leipzig) 2, 55 (1948)] and Dexter [J. Chem. Phys. 21, 836 (1953)] energy transfers play a minor role in these devices, and direct charge trapping appears to be the dominant mechanism. [J2471]

"Efficient, color-stable fluorescent white organic light-emitting diodes with single emission layer by vapor deposition from solvent premixed deposition source"

Efficient, color-stable fluorescent white organic light-emitting diodes (OLEDs) with single emission layer were fabricated by vapor deposition from solvent premixed mixtures of 1,4-bis(2,2-diphenylvinyl)biphenyl doped with 4-(dicyanomethylene)-2-methyl-6-(julolidin-4-yl-vinyl)-4H-pyran and/or 10-(2-benzothiazolyl)-2,3,6,7-tetrahydro-1,1,7,7-tetramethyl-1H,5H,11H-(1)benzopyrano(6,7,8-l, j)quinolizine-11-one. The power efficiencies at 100 cd/m² were 4.6 lm/W for the two-spectrum pure white OLEDs and 7.2 lm/W m² for the three-spectrum ones with white emission. By using a different host of 10,10'-bis(biphenyl-4-yl)-9,9'-bianthryl and a greenish-blue dye of di(triphenylamine)-1,4-divinylnaphthalene, the three-spectrum OLEDs with a power efficiency of 6.8 lm/W at 100 cd/m² were obtained. [J2472]

"Interdigitated multipixel arrays for the fabrication of high-power light-emitting diodes with very low series resistances"

We report on the fabrication of high-power light-emitting diodes (LEDs) with very low series resistance by employing a mask design consisting of interdigitated multipixel arrays. The reduction in the series resistance was mainly achieved by reducing the bulk resistance and the n-contact resistance by increasing the effective perimeter of the mesa. The small separation of the p and n contacts of the individual pixel improved lateral current spreading. The distributed array of pixels also resulted in improved thermal management, effectively rendering high continuous-wave (cw) drive current operation. Significant improvement in electrical and optical performances was observed when the mask was applied to a 400nm InGaN/GaN violet LED wafer, compared to a standard square-shaped LED with equal active area and fabricated from the same epitaxial wafer. Series resistance of less than 1Ω was measured for 300mcm devices. A peak output power of 115mW was obtained at 3.15A cw drive current for the unpackaged device. [J2473]

"Observation of minority-carrier traps in In Ga N /Ga N multiple-quantum-well light-emitting diodes during deep-level transient spectroscopy measurements"

An unusual appearance of a peak in the deep-level transient spectroscopy (DLTS) data for minority-carrier traps from an InGaN/GaN multiple-quantum-well (MQW) light-emitting diode, under a bias condition provided by a square pulse of varying height superimposed over the reverse-bias voltage, is newly observed and analyzed. The peak is attributed to hole traps, having the estimated activation energy of 0.7eV, in the last one (toward the p-side) among the GaN barrier layers in the MQW structure. We have found that the Delta C/Cr-versus temperature pattern from the DLTS measurement agrees well with the pattern predicted from the model of hole

traps, i.e., the minority-carrier traps, in the MQW barrier layer, whose occupation probability is governed by the local hole quasi-Fermi level. [J2474]

"Enhanced performance of an InGa_N-Ga_N light-emitting diode by roughening the undoped-GaN surface and applying a mirror coating to the sapphire substrate"

An InGa_N-Ga_N light-emitting diode (LED) with a roughened undoped-GaN surface and a silver mirror on the sapphire substrate was fabricated through a double transfer method. It was found that, at an injection current of 20mA, its luminance intensity was 100% larger than conventional LEDs. Its output power was 49% larger than conventional LEDs. [J2475]

"Retraction: "Effect of aluminum cathodes prepared by ion-beam-assisted deposition in organic light-emitting devices" [JAppl. Phys. Lett. 85, 1051 (2004)]"

First Page of the Article [J2476]

"Fabrication and efficiency improvement of micropillar In Ga N /Cu light-emitting diodes with vertical electrodes"

We present a micropillar surface structure based on the enhancement of the light extraction efficiency of the near-ultraviolet (409nm)vertical-conducting InGa_N light-emitting diode (LED) with an electroplated Cu substrate. The micropillar InGa_N/CuLED (chip size: 141mm²) was fabricated using a combination of patterned sapphire substrate (PSS), laser lift-off, and copper electroplating processes. The PSS and Cu substrate can offer the advantages of dislocation reduction and thermal heat sink, respectively. It was found that the light output power (at 350mA) of the micropillar InGa_N/CuLED sample can be improved by 39% as compared with that of the conventional InGa_N/CuLED one. This significant enhancement in output power could be attributed to the increase of the extraction efficiency which is a result of the increase in photon escaping probability caused by scattering the emission light at the micropillar surface. The light extraction efficiency can be further optimized by tuning the micropillar spacing, as evidenced by the ray-tracing simulation result. [J2477]

"Temperature-dependent built-in potential in organic semiconductor devices"

The temperature dependence of the built-in voltage of organic semiconductor devices is studied. The results are interpreted using a simple analytical model for the band bending at the electrodes. It is based on the notion that, even at zero current, diffusion may cause a significant charge density in the entire device, and hence a temperature dependent band bending. Both magnitude and temperature dependence of the built-in potential of various devices are consistently described by the model, as the effects of a thin LiF layer between cathode and active layer. [J2478]

"Organic light-emitting device luminaire for illumination applications"

The total light output of an organic light-emitting device (OLED) with a truncated square-pyramid luminaire is shown to be 1.8-2.1 times greater than the forward emission of an OLED without a luminaire. Luminaires increase the amount of outcoupled light by reducing waveguiding in the glass substrate, and they are made from 1.2-cm-thick acrylic and attached to the OLED glass substrate using index matching fluid. Based on experimental results and ray tracing models, the ratio of the OLED total emission to the OLED forward emission is found to be independent of luminaire taper angles between 30° and 80°. [J2479]

"Nitride light-emitting diodes grown on Si (111) using a TiN template"

Nitride light-emitting diodes (LEDs) are grown on a Si (111) substrate with a TiN template. Transmission electron microscopy and x-ray diffraction indicate that the epitaxial relation follows Si(1,1,1)||TiN(1,1,1)||AlN(0,0,1), Si[1,1,0]||TiN[1,1,0], and Si[0,0,1]||TiN[0,0,1]. The reflectance measurement and simulation results indicate that the TiN can be adopted as a reflector to mitigate the substrate absorption problem, thus increasing the extraction efficiency of nitride LEDs grown on Si. [J2480]

"Carbon nanotube sheets as electrodes in organic light-emitting diodes"

High performance organic light-emitting diodes (OLEDs) were implemented on transparent and conductive single-wall carbon nanotube sheets. At the maximum achieved brightness of 2800cdm⁻²the luminance efficiency of our carbon nanotube-based OLED is 1.4cdA⁻¹which is comparable to the 1.9cdA⁻¹measured for an optimized indium tin oxide anode device made under the same experimental conditions. A thin parylene buffer layer between the carbon nanotube anode and the hole transport layer is required in order to readily achieve the

measured performance. [J2481]

"Ultraviolet electroluminescence and blue-green phosphorescence using an organic diphosphine oxide charge transporting layer"

We report electroluminescence at 338nm from a simple bilayer organic light-emitting device (OLED) made using 4,4'-bis(diphenylphosphine oxide) biphenyl (PO1). In an OLED geometry, the material is preferentially electron transporting. Doping the PO1 layer with iridium(III)bis(4,6-(di-fluorophenyl)-pyridinato-N,C2')picolate (FIrpic) gives rise to electrophosphorescence with a peak external quantum efficiency of 7.8% at 0.09mA/cm² and 5.9% at 13mA/cm². The latter current density is obtained at 6.3V applied forward bias. [J2482]

"Thermally stable and highly reflective AgAl alloy for enhancing light extraction efficiency in GaN light-emitting diodes"

The properties of a AgAl alloy reflector layer deposited on a p-GaN layer for use in high-efficiency GaN flip-chip light-emitting diodes (FCLEDs) were investigated. The AgAl layer showed good adhesion properties compared to a layer of Ag on p-GaN. In addition, no agglomeration was found, indicating that the AgAl layer is thermally stable due to the formation of oxidized Al on the surface and at the interface of the AgAl layer. The InGaN/GaN multiquantum well light-emitting diode with the annealed AgAl layer showed good I-V characteristic and an enhanced optical output power compared to that with an annealed Ag layer due to the high reflectivity (86.7% at 465 nm), smooth surface after annealing, and good Ohmic property of AgAl. These results clearly indicate that a AgAl layer on p-GaN constitutes a promising reflector and Ohmic scheme for achieving high-brightness FCLEDs. [J2483]

"Embodiment of the warm white-light-emitting diodes by using a Ba 2+ codoped Sr 3 Si O 5 :Eu phosphor"

The shifts of the emission band to longer wavelength (yellow-orange) of the Sr₃SiO₅:Eu yellow phosphor under the 450-470 nm excitation range have been achieved by adding the codoping element (Ba²⁺) in the host. In order to apply to white-light-emitting diodes (LEDs) with warm white and high color rendering index, we have fabricated white LEDs through the integration of the InGaN blue LED chip and the two phosphor blends (Sr₂SiO₄:Eu yellow phosphor + Ba²⁺-co-doped Sr₃SiO₅:Eu yellow-orange phosphor) into a single package. By employing two phosphors, covering a red region, the white LEDs show a warm white in the range of 2500-5000 K correlated color temperature and a good color rendering of over 85. [J2484]

"Band gap renormalization and carrier localization effects in InGaN /GaN quantum-wells light emitting diodes with Si doped barriers"

The optical properties of two kinds of InGaN/GaN quantum-wells light emitting diodes, one of which was doped with Si in barriers while the other was not, are comparatively investigated using time-integrated photoluminescence and time-resolved photoluminescence techniques. The results clearly demonstrate the coexistence of the band gap renormalization and phase-space filling effect in the structures with Si doped barriers. It is surprisingly found that photogenerated carriers in the intentionally undoped structures decay nonexponentially, whereas carriers in the Si doped ones exhibit a well exponential time evolution. A new model developed by O. Rubel, S. D. Baranovskii, K. Hantke, J. D. Heber, J. Koch, P. Thomas, J. M. Marshall, W. Stolz, and W. H. Ruhle [J. Optoelectron. Adv. Mater. 7, 115 (2005)] was used to simulate the decay curves of the photogenerated carriers in both structures, which enables us to determine the localization length of the photogenerated carriers in the structures. It is found that the Si doping in the barriers not only leads to remarkable many-body effects but also significantly affects the carrier recombination dynamics in InGaN/GaN layered heterostructures. [J2485]

"Efficiency improvement of phosphorescent organic light-emitting diodes using semitransparent Ag as anode"

The emission efficiency in an organic light-emitting diode (OLED) based on fac tris(phenyl pyridine)iridium [Ir(ppy)₃] is greatly improved using a semitransparent Ag anode. With surface modification of the Ag anode, excellent light coupling and hole injection properties can be realized. The Ag-based OLED exhibits a maximum current efficiency of 81 cd/A and a power efficiency of 79 lm/W, compared with 46 cd/A and 39 lm/W for an indium-tin oxide anode device, respectively. [J2486]

"High-efficiency polymer light-emitting diodes based on poly[J2-methoxy-5-(2-ethylhexyloxy)-1,4-

phenylene vinylene] with plasma-polymerized CHF₃-modified indium tin oxide as an anode"

We demonstrate that introducing a thin CF_x film formed by plasma polymerization of CHF₃ on an indium tin oxide (ITO) anode surface for a polymer light-emitting diode with the structure, ITO/CF_x/poly[2-methoxy-5-(2-ethylhexyloxy)-1,4-phenylene vinylene](MEH-PPV)/Ca/Al, can lead to a high device performance (5.1 cd/A and 24000 cd/m²). The high device performance can be attributed to a better balance between hole and electron fluxes, resulting from a formation of interfacial dipole at the CF_x/MEH-PPV interface to provide a hole blocking effect and an enhancement of electron/hole recombination. [J2487]

"Ba₅SiO₄Cl₆:Eu²⁺: An intense blue emission phosphor under vacuum ultraviolet and near-ultraviolet excitation"

An intense blue emission of Eu²⁺-doped Ba₅SiO₄Cl₆ under vacuum ultraviolet and near-ultraviolet excitation was observed. The material exhibits an emission peak at 440 nm with relative intensity 50% under 147 nm, 90% under 254 nm, 120% under 366 nm, and 220% under 405 nm excitation as compared with the commercial blue phosphor BaMgAl₁₀O₁₇:Eu²⁺. It is a very promising candidate as a blue-emitting phosphor for potential applications in display and light-emitting diode devices. [J2488]

"Photonic-crystal GaN light-emitting diodes with tailored guided modes distribution"

We relate the currently limited efficiency of photonic crystal (PhC)-assisted gallium nitride light-emitting diodes (LEDs) to the existence of unextracted guided modes. To remedy this, we introduce epitaxial structures which modify the distribution of guided modes. LEDs are fabricated according to this concept, and the tailored band structure is determined experimentally. We investigate theoretically the consequences of this improvement, which significantly enhances the potential for efficient light extraction by PhCs. [J2489]

"High-efficiency blue light-emitting electrophosphorescent device with conjugated polymers as the host"

Highly efficient blue polymer phosphorescent organic light-emitting diode (PPHOLET)-containing iridium(III) bis(2,4-difluorophenyl-2-pyridine) (2-(4H-1, 2, 4-triazol-3-yl)pyridine) [Ir(PPF)₂(PZ)] complex embedded into wide-gap poly(9,9'-alkyl-3, 6-silafluorene) (PSiFC₆C₆) has been fabricated. Despite the significant quenching of photophosphorescence emission of the iridium complexes by a PSiFC₆C₆ host polymer, organic light-emitting diodes containing Ir(PPF)₂(PZ) doped into the polymer host PSiFC₆C₆ emit high-efficiency blue light peaked at 462 nm. The maximal external quantum and luminance efficiencies were, respectively, 4.8% photons/electrons and 7.2 cd/A at 644 cd/m² and with Commission Internationale de l'Eclairage coordinates of (0.15, 0.26). [J2490]

"InSb /AlInSb quantum-well light-emitting diodes"

We have investigated the room-temperature electroluminescent properties of InSb/AlIn_{1-x}Sb quantum-well light-emitting diodes. The maximum emission from diodes containing quantum wells occurred at significantly higher energies than the band gap of InSb. Close agreement between experimental and theoretical data confirms that recombination occurs within the quantum well. [J2491]

"Organic photocouplers consisting of organic light-emitting diodes and organic photoresistors"

We have fabricated one kind of organic photocoupler with organic light-emitting diode as the input unit and pentacene photoresistor as the output unit. The wavelength of the emitting light was 522 nm. The output current of the photocoupler linearly increased with its input current and the ratio of the transfer current density reached 3. When the output voltages were 60 V, the ratio of the maximum output current to the minimum output current was 150. The breakdown voltage between the input unit and the output unit was more than 10 kV and the response time of the device was about 6.5 s. We believe this kind of device is promising in the full organic optoelectronic integrated circuits. [J2492]

"Plastic deformation of a continuous organic light emitting surface"

A continuous organic light emitting diode (OLED) surface was shaped by plastic deformation from flat to dome. The OLED dome, now under an average tensile strain of 2.2%, remained operational. This shapeability is achieved by combining a substrate and a device structure that keep functioning in the plastic deformation regime. The technique of conformally shaping a continuous macroelectronic surface could become useful for the manufacture of arbitrarily shaped solid state light sources and mechanical transducers. [J2493]

"Charge injection in polymer light-emitting diodes based on poly[J(9,9-dioctylfluorenyl-2,7-diyl)-co-

(1,4-phenylene)]"

In this letter, the electrical properties of polymer light-emitting diodes based on polyfluorene derivative, named poly[(9,9-dioctylfluorenyl-2,7-diyl)-co-(1,4-phenylene)] (F8P), were studied. Indium tin oxide (ITO)/polymer/metal [magnesium (Mg) and calcium (Ca)] structures were used to study the effect of the barrier height on the charge injection at the polymer/metal (anode) interfaces. For ITO/F8P/Mg devices, strong temperature influence on the dc conductivity was observed in the forward direction, and afterwards, in the reverse direction, the conductivity was totally temperature independent. On the other hand, ITO/F8P/Ca devices presented temperature-dependent conductivities for both polarities. [J2494]

"Organic light-emitting devices with a mixture emitting layer of tris-(8-hydroxyquinoline) aluminum and 4,4'-bis(carbazol-9-yl)-biphenyl"

Organic light-emitting devices with a mixture of tris-(8-hydroxyquinoline) aluminum (Alq3) and 4,4'-bis(carbazol-9-yl)-biphenyl (CBP) as the emitting layer have been fabricated. The devices were fabricated in the same run with a standard device without CBP for comparison, with an identical structure of indium tin oxide (ITO)/m-MTDATA (80nm)/NPB(20nm)/CBP:Alq3(40nm)/BCP(10nm)/Alq3(60nm)/Mg:Ag(200nm), where m-MTDATA is 4,4',4''-tris(N-3-methylphenyl-N-phenyl-amino) triphenylamine, which is used to improve hole injection; NPB is N,N'-di(naphth-2-yl)-N,N'-diphenyl-benzidine; and BCP is 2,9-Dimethyl-4,7-diphenyl-1,110-phenanthroline. The ratio of CBP to Alq3 in mixture was varied from 0 to 2. For device with a ratio of 0.5, the current efficiency and power efficiency were significantly improved by 35% and 32%, respectively, compared to the standard device with Alq3 only as emitting layer. By increasing the ratio to 2, the current efficiency and power efficiency were dropped by 20% and 11%, respectively. The electroluminescence spectra showed a slight blueshift with the increase of CBP to Alq3 ratio. [J2495]

"Next generation of oxide photonic devices: ZnO-based ultraviolet light emitting diodes"

Results are presented for ZnO-based ultraviolet light emitting diodes (LEDs) that employ a BeZnO/ZnO active layer comprised of seven quantum wells. Arsenic and gallium are used for p-type and n-type layers. The ZnO-based LEDs show two dominant electroluminescence peaks located in the ultraviolet spectral region between 360 and 390nm, as well as a broad peak at 550nm. [J2496]

"Efficient blue organic light-emitting devices based on oligo(phenylenevinylene)"

Highly bright and efficient blue organic light-emitting devices based on two oligo(phenylenevinylene) derivatives, 1,4-di(4'-N,N-diphenylaminostyryl)benzene (DPA-DSB) and 2,5,2',5'-tetrastyryl-biphenyl (TSB), are fabricated. Using poly(3,4-ethylenedioxythiophene):poly(styrene sulfonic acid) combined with 4,4',4''-tri(N-carbazolyl) triphenylamine as the hole-transporting layer and DPA-DSB doped TSB as the blue emitter, a maximum luminous efficiency of 12.2 cd/A (corresponding to an external quantum efficiency of 6.2%) and a maximum power efficiency of 6.39lm/W are obtained. The maximum brightness of 17350cd/m² is attained. These fairly high brightness and efficiencies are due to the efficient energy transfer from TSB to DPA-DSB and depression of concentration quenching by doping. [J2497]

"High performance organic light-emitting diodes fabricated via a vacuum-free lamination process"

We demonstrate high performance organic light-emitting diodes (OLEDs) fabricated via a vacuum-free, direct lamination process. The OLEDs were made by laminating an anode component to a separately engineered cathode component using a roll laminator. We further present a solution-based chemical n-doping strategy to enable efficient electron injection from an inert cathode into polymeric organic semiconductors. The n-doping strategy is demonstrated by chemically reducing a conjugated light-emitting polymer with an alkali metal in an organic solvent. The metal reduced conjugated polymer, when employed as an electron injection layer, yields laminated OLEDs with efficiency comparable to conventionally fabricated devices utilizing a vacuum-deposited, reactive metal cathode. These designs and techniques should enable applications such as lighting where extremely low cost device fabrication is required. [J2498]

"Combinatorial study of exciplex formation at the interface between two wide band gap organic semiconductors"

Combinatorial screening of exciplex formation in blends of 4,4',4''-tris[2-naphthyl (phenyl)-amino] triphenylamine (2-TNATA), and 2,2',7,7'-tetrakis(2,2'-diphenylvinyl) spiro-9,9'-bifluorene (spiro-DPVB) is described. The blended layer was incorporated in ITO/[2-TNATA]/[1:1 2-TNATA:spiro-DPVB]/[N,N'-diphenyl-N,N'-bis(1-naphthylphenyl)-1,1'-bi-phenyl-4,4'-diamine (NPB)]/[spiro-DPVB]/[tris(8-hydroxyquinoline) Al]/CsF/Al organic light-emitting devices; the thickness of the blend and NPB layers were varied systematically. The

electroluminescence quantum yield decreased as the blended layer thickness increased. The NPB spacer layer reduced the exciplex formation; an 8-nm-thick layer completely suppressed it. [J2499]

"ZnO p-n junction light-emitting diodes fabricated on sapphire substrates"

A ZnO p-n junction light-emitting diode (LED) was fabricated on a-plane Al₂O₃ substrate by plasma-assisted molecular-beam epitaxy. NO plasma activated by a radio frequency atomic source was used to grow the p-type ZnO layer of the LED. The current-voltage measurements at low temperatures showed a typical diode characteristic with a threshold voltage of about 4.0 V under forward bias. With increasing temperature, the rectification characteristic was degraded gradually, and faded away at room temperature. Electroluminescence band of the ZnO p-n junction LED was located at the blue-violet region and was weakened significantly with increase of temperature. This thermal quenching of the electroluminescence was attributed to the degradation of the diode characteristic with temperature. [J2500]

"Efficient white-light-emitting diodes based on poly(N-vinylcarbazole) doped with blue fluorescent and orange phosphorescent materials"

We have fabricated polymer white-light-emitting devices possessing a single emitting layer containing a hole-transporting host polymer, poly(N-vinylcarbazole), and an electron-transporting auxiliary, 2-(4-biphenyl)-5-(4-tert-butylphenyl)-1,3,4-oxadiazole, doped with a blue-light-emitting amino-substituted distyrylarylene fluorescent dye and an orange-light-emitting osmium phosphor. The doubly doped device exhibited an intense white emission having Commission Internationale de l'Eclairage coordinates of (0.33, 0.34), a high external quantum efficiency of 6.12% (13.2 cd/A), and a maximum brightness of 11306 cd/m². The color coordinates remained unchanged over a range of operating voltages, even at luminance as high as 14104 cd/m². [J2501]

"Efficient organic light-emitting devices using an iridium complex as a phosphorescent host and a platinum complex as a red phosphorescent guest"

We demonstrated efficient organic light-emitting devices (OLEDs) using a phosphorescent host/guest system consisting of bis(2-phenylpyridinato-N,C2')iridium(acetylacetonate) [(ppy)₂Ir(acac)] as a host and a platinum complex (Pt-SA-1) as a guest. The OLED using (ppy)₂Ir(acac) film doped with Pt-SA-1 (1 wt%) showed an ideal red emission via efficient energy transfer from the host to the guest. The external quantum efficiency of the device was as high as 8.3%. The driving voltage was significantly reduced compared with a device using a conventional host of 4,4'-di(carbazole-9-yl)biphenyl, which resulted from the enhancement of the hole injection from the hole-transport layer to the host. [J2502]

"Highly efficient solution processed blue organic electrophosphorescence with 14 lm /W luminous efficacy"

We report highly efficient solution processed blue electrophosphorescent organic light emitting diodes (PHOLEDs) utilizing a phosphorescent dye and a nonconjugated polymer host, molecularly doped with electron transporting molecules. Based on a bilayer device architecture blue PHOLEDs with luminous efficacy of 14 lm/W at luminous efficiency reaching 22 cd/A are demonstrated. Analysis of device performance indicates that this high efficiency is achieved by a combination of improved charge balance and light outcoupling efficiency. Our results demonstrate that simple solution processed devices can have efficiencies similar to those published to date for small molecule multilayer PHOLEDs based on the same emitter. [J2503]

"Highly efficient top emitting organic light-emitting diodes with organic outcoupling enhancement layers"

We demonstrate high-efficiency top emitting organic light-emitting diodes employing silver (Ag) for both anode and cathode. Following the p-i-n doping and double emission layer concepts, the devices show a very high efficiency of 50 cd/A at 1000 cd/m² with a driving voltage of only 2.85 V. The efficiency can be further improved to 78 cd/A by tuning the optical structure with an organic capping layer. A simple explanation based on the transmittance of the top contact cannot explain this efficiency enhancement. Instead, we theoretically show that this capping effect is dependent on the overall optical structure of the device. [J2504]

"Optical power degradation mechanisms in AlGaIn-based 280 nm deep ultraviolet light-emitting diodes on sapphire"

We present a study of reliability of AlGaIn-based 280 nm deep ultraviolet light-emitting diodes on sapphire substrate grown by migration-enhanced metal-organic chemical vapor deposition. Two modes of optical power

degradation were observed: catastrophic and gradual. The catastrophic degradation is believed to be due to metal alloying at macroscopic defects in the top layers of the light-emitting diode structure. For the gradual power degradation, two time constants were determined, which were temperature and bias dependent. For the temperature-dependent part, the values of the activation energies and room-temperature degradation rates at dc currents of 10 and 20mA were determined to be 0.23 and 0.27eV and 1.31×10^{-3} and $5.93 \times 10^{-3} \text{ h}^{-1}$, respectively. [J2505]

"Organic light-emitting diodes based on a cohost electron transporting composite"

The efficiency of green organic electroluminescent devices have been improved by cohosting the electron dominant complex, 4,7-diphenyl-1,10-phenanthroline into the traditional electron transporting layer of tris (8-hydroxyquinoline) aluminum. In this cohost strategy, we demonstrate that the luminous efficiency is enhanced by 20% while the driving voltage can be reduced by 30% in a uniformly mixed composition as compared to the traditional device configuration. The corresponding device lifetime under atmospheric condition is extended by a factor of 1.8, attributed to the reduction of the accumulated positive charges near the electron-hole recombination regime. Results indicate that the knowledge of bulk conductivity engineering of organic n-type transporters is essential in enhancing organic light-emitting devices. [J2506]

"InGaN light-emitting diodes with naturally formed truncated micropylramids on top surface"

GaN-based light-emitting diodes (LEDs) with truncated micropylramids surfaces performed by metalorganic chemical vapor deposition were demonstrated. In this study, a growth-interruption step and an Mg-treatment process were simultaneously performed to create multiple truncated micropylramids on LED surface. Experimental results indicated that GaN-based LEDs with the truncated micropylramids on the top surface demonstrate improved external efficiency of around 60% at 20mA. It is worth noting that the typical 20mA driven forward voltage is only 0.15V higher than that of conventional LEDs (LEDs with specular surface). [J2507]

"Highly efficient white organic light-emitting diode"

We present a highly efficient white electroluminescence device by the combination of a solution processed blue organic phosphorescence light-emitting diode with appropriate down-conversion phosphor system. The use of this down-conversion system produced an extraordinary enhancement on device performance, resulting in a white electroluminescence device with luminance efficacy of 25lm/W at luminance efficiency reaching 39cd/A. The extraordinary enhancement on device performance is attributed to isotropic radiation pattern of the excited phosphor particles, leading to high light extraction properties. [J2508]

"Low specific contact resistance Ti /Au contacts on ZnO"

Ti/Au Ohmic contacts on heavily Al-doped ($n = 10^{19} \text{ cm}^{-3}$) n-ZnO produce low specific contact resistivity of $2.4 \times 10^{-7} \Omega \text{ cm}^2$ in the as-deposited condition and extremely low minimum values of $6 \times 10^{-8} \Omega \text{ cm}^2$ after annealing at 300°C. The contact resistance is independent of measurement temperature after low temperature anneals, suggesting that tunneling is the dominant transport mechanism in the contacts. The contact morphology roughens after annealing at 150°C and Auger electron spectroscopy depth profiling shows Zn outdiffusion through the metal and intermixing of Au and Ti. However, the morphology does not significantly worsen after anneals at 450°C. This metallization scheme looks very attractive for the n-electrode of ZnO-based light-emitting diode structures. [J2509]

"Control of magnetic-field effect on electroluminescence in Alq₃-based organic light emitting diodes"

The magnetic-field effect on electroluminescence (EL) has been investigated for the tris-(8-hydroxyquinolino) aluminum (Alq₃)-based organic light emitting diode. The EL intensity sharply increases up to 8% with increasing magnetic field to 500 Oe at room temperature. The magnetic field effect on EL depends on the interface structure between a hole transporting and a light emitting layers, indicating the importance of the spin-state dynamics of the electron-hole pairs at the interface. [J2510]

"Fabrication of genuine single-quantum-dot light-emitting diodes"

We present a simple approach for the fabrication of genuine single quantum-dot light-emitting diodes. A submicron wide bottom contact stripe is formed by focused ion beam implantation doping into a GaAs buffer layer. Successive overgrowth with a thin intrinsic layer incorporating self-assembled InAs quantum dots, followed by a top contact layer of complementary doping type and standard photolithographic processing, allows for electrical cross sections in the sub- μm^2 range. In devices with sufficiently low dot densities, only one single dot

is expected to be electrically addressed. Both the observed current versus voltage characteristics and the evolution of the electroluminescence spectra as a function of applied voltage clearly demonstrate that this goal has been achieved. [J2511]

"Broadband 6 μ m λ 8 μ m superluminescent quantum cascade light-emitting diodes"

Midinfrared emission from intersubband superluminescent light-emitting diodes is reported. We have obtained broadband emission spectra at around 7 μ m with a full width at half maximum of 2 μ m, using quantum-cascade-laser active regions designed to emit at 11 different wavelengths simultaneously. By introducing additional mirror loss in the Fabry-Perot resonator using just a single cleaved facet, with the other mirror formed by wet etching, the laser threshold current is significantly increased and superlinear light-current characteristics are observed. Optical peak powers of several tens of μ W are measured at low temperatures. [J2512]

"Metalorganic vapor phase epitaxy grown In Ga N /Ga N light-emitting diodes on Si(001) substrate"

We present GaN-based light emitting diode structures on a Si(001) substrate. The 2.3 μ m thick, crack-free layers were grown by metalorganic vapor phase epitaxy using a high-temperature AlN seed layer and 4° off-oriented substrates. This allows us to grow a flat, fully coalesced, and single crystalline GaN layer on Si(001). For preventing crack formation, four AlN interlayers were inserted in the buffer structure. The optically active layers consist of five-fold InGaN/GaN multiple quantum wells showing a bright electroluminescence at 490 nm at room temperature. The crystallographic structure was analyzed by x-ray diffraction measurements and the optical properties were determined by photo- and electroluminescence. [J2513]

"Highly efficient room-temperature tunnel spin injector using CoFe/MgO(001)"

Semiconductor spintronics is a promising technology in which the spin states of electrons are utilized as an additional degree of freedom for device operation. One of its prerequisites is the ability to inject spin-polarized electrons into semiconductors. An overview is presented of recent progress in spin injection using an injector based on a crystalline CoFe/MgO(001) tunnel structure. The spin polarization of the electrons that were injected into a GaAs quantum-well light-emitting diode was inferred from electroluminescence polarization from the quantum well. Spin polarizations of 57% at 100 K and 47% at room temperature were obtained. The spin polarization was found to exhibit a strong dependence on bias and temperature, which can be explained on the basis of spin relaxation within the GaAs. [J2514]

"Influence of dehydrated nanotubed titanic acid on polymer light-emitting diodes with phosphorescent dye"

In this letter, we demonstrate that hole injection and transport in polymer light-emitting diodes with phosphorescent dye Ir(ppy)₃ can be significantly enhanced by doping p-type conductive dehydrated nanotubed titanic acid into poly(vinylcarbazole) (PVK) films at 2 wt.%. At the same time, both energy transfer and exciton recombination efficiency are improved because of the open and straight conformation of the PVK molecule in the nanocomposite. The performance of these devices was greatly improved, showing higher luminance, enhanced efficiency, and a lower turn-on voltage. [J2515]

"Highly efficient white-light-emitting diodes fabricated with short-wavelength yellow oxynitride phosphors"

We have already reported orangish yellow Ca- α -SiAlON:Eu²⁺+phosphors, and applied them to fabricate warm white light-emitting diodes (LEDs). In this letter, we report on greenish yellow Li- α -SiAlON:Eu²⁺+phosphors, and use them to create daylight when coupled to an InGaN blue LED chip (460 nm). The newly discovered Li- α -SiAlON:Eu²⁺+phosphors emit at shorter wavelengths of 573-577 nm under the 460 nm excitation, and exhibit a smaller Stokes shift than Ca- α -SiAlON:Eu²⁺+phosphors. By using this short-wavelength yellow oxynitride phosphor, bright daylight emissions from white LEDs can be generated. Thus, highly efficient white LEDs with tunable white light can be fabricated with α -SiAlON:Eu²⁺+phosphors, enabling them for a wider range of applications. [J2516]

"Evolution of luminance by voltage in organic light-emitting diodes"

We study degradation behaviors of luminance and voltage in organic light-emitting diodes. We find that normalized luminance and inverse normalized voltage with time, $L(t)$ and $V(t)^{-1}$, follow the stretched exponential decay. On this basis, we derive a general relation of luminance and voltage with time as $L(t) = V(t)^{-\Delta(t)}$, where $\Delta(t)$ indicates a decay exponent, which is attributed to time-dependent space-charge limitation. Here the observation of higher $\Delta(t)$ at higher initial luminance explains why luminance decay is faster at higher

initial luminance. [J2517]

"Transparent indium zinc oxide top cathode prepared by plasma damage-free sputtering for top-emitting organic light-emitting diodes"

We report on plasma damage-free sputtering of an indium zinc oxide (IZO) top cathode layer for top-emitting organic light-emitting diodes (TOLEDs) by using a box cathode sputtering (BCS) technique. A sheet resistance of 42.6Ω/cm and average transmittance above 88% in visible range were obtained even in IZO layers deposited by BCS at room temperature. The TOLED with the IZO top cathode layer shows electrical characteristics and lifetime comparable to a TOLED with only thermally evaporated Mg-Ag cathode. In particular, it is shown that the TOLED with the IZO top cathode film shows very low leakage current density of 1×10^{-5} mA/cm² at reverse bias of -6V. This suggests that there is no plasma damage caused by the bombardment of energetic particles during IZO sputtering using the BCS system. [J2518]

"GaInN light-emitting diode with conductive omnidirectional reflector having a low-refractive-index indium-tin oxide layer"

Enhancement of light extraction in a GaInN light-emitting diode (LED) employing a conductive omnidirectional reflector (ODR) consisting of GaN, an indium-tin oxide (ITO) nanorod low-refractive-index layer, and an Ag layer is presented. An array of ITO nanorods is deposited on p-type GaN by oblique-angle electron-beam deposition. The refractive index of the nanorod ITO layer is 1.34 at 461nm, significantly lower than that of dense ITO layer, which is $n=2.06$. The GaInN LEDs with GaN/low-nITO/Ag ODR show a lower forward voltage and a 31.6% higher light-extraction efficiency than LEDs with Ag reflector. This is attributed to enhanced reflectivity of the ODR that employs the low-nITO layer. [J2519]

"Enhancement of optical properties in organic light emitting diodes using the Mg-Al alloy cathode and IrOx-coated indium tin oxide anode"

We report the enhancement of quantum efficiency using the Mg-Al alloy cathode and IrOx-coated indium tin oxide (ITO) anode in organic light emitting diodes (OLEDs). The external quantum efficiency at the current density of 64 mA/cm² increased from 0.04% to 1.89% as the Al cathode and ITO anode changed to the Mg-Al cathode and IrOx-coated ITO anode, respectively. Synchrotron radiation photoelectron spectroscopy results show that the work function of IrOx-coated ITO is higher by 0.5 eV than that of the ITO and the work function of the Mg-Al alloy is lower by 0.2 eV than that of Al. Thus, both the hole and electron injection energy barriers were simultaneously lowered, reducing the turn-on voltage and increasing the quantum efficiency of OLEDs. [J2520]

"Organic oxide/Al composite cathode in efficient polymer light-emitting diodes"

This work presents the fabrication of efficient polymer light-emitting diodes (PLEDs) by thermally evaporating a salt-free neutral organic-oxide buffer layer onto the surface of the electroluminescent film in a vacuum before the device cathode, made of Al-rather than the low work function metals, such as Ca or Ba-is deposited. The electroluminescence (EL) efficiency of phenyl-substituted poly(para-phenylene vinylene) copolymer-based PLEDs with an organic oxide/Al composite cathode, reaches 8.86 cd/A, which is markedly higher than those, 5.26 cd/A and 0.11 cd/A, of devices with Ca/Al and Al cathodes, respectively. The device performance is improved by the formation of a specific organic oxide/Al complex at the cathode interface during the deposition of Al, facilitating the injection of electrons and eliminating the metal-induced quenching sites of luminescence in the EL layer near the recombination region. [J2521]

"Multilayer organic electrophosphorescent white light-emitting diodes without exciton-blocking layer"

We demonstrate high-efficiency white organic light-emitting diodes with two emissive layers, in which different hosts are employed. With the energy gap of the two hosts, there was no exciton-blocking layer between the emissive layers to confine the diffusion of excitons. The phosphorescent dye, bis[(4,6-difluorophenyl)-pyridinato-N, C2'] (picolinato) Ir(III) and bis (1-phenyl-isoquinoline) (acetylacetonate) iridium (III) [Ir(pic)2acac] were employed as guests, while N,N'-dicarbazolyl-1, 4-dimethene-benzene and 4, 4'-N, N'-dicarbazole-biphenyl were employed as hosts, respectively. The device exhibited white emission by controlling the thickness of the emissive layers and the maximum current efficiency and luminance were 10.5 cd/A and 22000 cd/m², respectively. [J2522]

"White-light generation and energy transfer in Sr Zn₂ (P O₄)₂ :Eu, Mn phosphor for ultraviolet light-emitting diodes"

The $\text{SrZn}_2(\text{PO}_4)_2:\text{Eu}^{2+},\text{Mn}^{2+}$ phosphor shows two emission bands under ultraviolet radiation; the one observed at 416nm is attributed to Eu^{2+} occupying the Sr^{2+} sites and the other asymmetric band deconvoluted into two peaks was found to center at 538 and 613nm, which originate from Mn^{2+} occupying two different Zn^{2+} sites. The energy transfer from Eu^{2+} to Mn^{2+} has been demonstrated to be a resonant type via a dipole-quadrupole mechanism. By utilizing the principle of energy transfer and appropriate tuning of activator contents, we have demonstrated that $\text{SrZn}_2(\text{PO}_4)_2:\text{Eu}^{2+},\text{Mn}^{2+}$ is potentially useful as an ultraviolet-convertible phosphor for white-light emitting diodes. [J2523]

"Enhancement of the light output of GaN-based ultraviolet light-emitting diodes by a one-dimensional nanopatterning process"

We have demonstrated the enhancement of the output power of ultraviolet GaN-based light-emitting diodes (LEDs) by using one-dimensionally nanopatterned Cu-doped indium oxide (CIO)/indium tin oxide (ITO) p-type contact layers. The one-dimensional (1D) nanopatterns (250nm in width and 100nm in depth) are defined using a TiO_2 1D nanomask fabricated by means of a surface relief grating technique. When fabricated with the nanopatterned p-contact layers, the output power of LEDs is improved by 40 and 63% at 20mA as compared to those fabricated with the unpatterned CIO/ITO and conventional Ni/Au contacts, respectively. [J2524]

"General method to solution-process multilayer polymer light-emitting diodes"

An intermediate liquid buffer layer is introduced to overcome the dissolution problem of solution-processed multilayer conjugated polymer light-emitting diodes. This method can be applied to arbitrary combinations of polymers with no restriction on solvents. As an example, a hole-blocking layer is successfully spin coated on the common p-type emissive polymer layers. One green- and two blue-emitting polymers are chosen as the emissive layers. The electron-hole balance and efficiency are significantly improved by the addition of hole-blocking layer. The electroluminescence efficiency can be increased up to nine times, while the luminance up to seven times. In particular, 1.5cd/A is obtained for deep blue emission from poly(9,9-dioctyl-fluorene) with 1,3,5-tris(N-phenylbenzimidazol-2-yl)benzene spin coated as the hole-blocking material. [J2525]

"Polymer bilayer structure via inkjet printing"

We report the formation of a polymer bilayer structure by inkjet printing poly(9,9'-dioctylfluorene-co-benzothiadiazole) (F8BT) from p-xylene solution onto a poly(9,9'-dioctylfluorene-co-N-(4-butylphenyl)diphenylamine (TFB) thin film. Despite the compatibility of both polymers with the same organic solvent, a TFB layer under the later-deposited F8BT was directly observed through fluorescence microscopy. Micro-Raman spectroscopy reveals that this bottom layer is 10nm thick for a film made by inkjet printing F8BT onto a TFB film of 20nm thickness. The bilayer structure leads to enhanced efficiency for light-emitting diodes in comparison with devices made from spin-coated TFB:F8BT blend films. [J2526]

"Characterization and luminescence properties of $\text{Sr}_2\text{Si}_5\text{N}_8:\text{Eu}^{2+}$ phosphor for white light-emitting-diode illumination"

Eu^{2+} -doped ternary nitride phosphor, $\text{Sr}_2\text{Si}_5\text{N}_8:\text{Eu}^{2+}$, was prepared by the carbothermal reduction and nitridation method. The Rietveld refinement analysis showed that the single phase products were obtained. Two main absorption bands were observed on the diffuse reflection spectra peaking at about 330 and 420nm, so that the resultant phosphor can be effectively excited by InGaN light-emitting diodes. The emission peak position of $(\text{Sr}_{1-x}\text{Eu}_x)_2\text{Si}_5\text{N}_8:\text{Eu}^{2+}$ series varied from 618 to 690nm with increasing Eu^{2+} ion concentration. The redshift behavior of the emission band was discussed on the basis of the configuration coordination model. [J2527]

"Enhanced emission from Si-based light-emitting diodes using surface plasmons"

Excitation of surface plasmons on metallic nanoparticles has potential for increasing the absorption and emission from thin Si devices. We report an eight-fold enhancement in electroluminescence from silicon-on-insulator light-emitting diodes at 900nm via excitation of surface plasmon resonance in silver nanoparticles, along with a redshift in the electroluminescence by 70nm by overcoating the nanoparticles with ZnS. The enhancement is due to coupling between the electromagnetic excitations of the silver nanoparticles and the waveguide modes. [J2528]

"Surface plasmon-polariton mediated emission from phosphorescent dendrimer light-emitting diodes"

We present experimental results showing electroluminescence from a dendrimer based organic light-emitting diode (OLED) mediated via surface plasmon polariton (SPP) modes. A combination of angle dependent

electroluminescence, photoluminescence, and reflectance measurements is used to identify emission originating from the guided modes of the device. It is found that the SPP modes, which are usually nonradiative, are coupled to light by a wavelength scale periodic microstructure. It is demonstrated that the necessary microstructure can be readily fabricated by solvent-assisted micromoulding. Our results indicate that such an approach may offer a means to increase the efficiency of dendrimer based OLEDs. [J2529]

"Growth of III-nitride photonic structures on large area silicon substrates"

We report on the growth of high quality aluminum nitride (AlN) and gallium nitride (GaN) epilayers on large area (6in.diameter) silicon (111) substrates by metal organic chemical vapor deposition. We have demonstrated the feasibility of growing crack-free high quality III-nitride photonic structures and devices on 6inchSi substrates through the fabrication of blue light emitting diodes based upon nitride multiple quantum wells with high performance. The demonstration further enhances the prospects for achieving photonic integrated circuits based upon nitride-on-Si material system. [J2530]

"ZnO light-emitting diode grown by plasma-assisted metal organic chemical vapor deposition"

We report a breakthrough in fabricating ZnO homojunction light-emitting diode by metal organic chemical vapor deposition. Using NO plasma, we are able to grow p-type ZnO thin films on n-type bulk ZnO substrates. The as-grown films on glass substrates show hole concentration of 10^{16} - 10^{17} cm⁻³ and mobility of 1-10cm²V⁻¹s⁻¹. Room-temperature photoluminescence spectra reveal nitrogen-related emissions. A typical ZnO homojunction shows rectifying behavior with a turn-on voltage of about 2.3V. Electroluminescence at room temperature has been demonstrated with band-to-band emission at I=40mA and defect-related emissions in the blue-yellow spectrum range. [J2531]

"Enhanced emission efficiency in organic light-emitting diodes using deoxyribonucleic acid complex as an electron blocking layer"

Enhanced electroluminescent efficiency using a deoxyribonucleic acid (DNA) complex as an electron blocking (EB) material has been demonstrated in both green- and blue-emitting organic light-emitting diodes (OLEDs). The resulting so-called BioLEDs showed a maximum luminous efficiency of 8.2 and 0.8cd/A, respectively. The DNA-based BioLEDs were as much as 10% more efficient and 30% brighter than their OLED counterparts. [J2532]

"White light from polymer light-emitting diodes: Utilization of fluorenone defects and exciplex"

A white light polymer light-emitting diode was demonstrated with a double layer configuration: poly[N,N'-bis(4-butylphenyl)-N,N'-bis(phenyl)benzidine] (poly-TPD) blended with poly(N-vinylcarbazole) as both hole-transporting layer and electron-blocking layer, blue-emissive poly(9,9-dihexylfluorene-alt-co-2,5-dioctyloxy-para-phenylene) (PDHFDOP) blended with green-emissive poly[6,6'-(9,9'-dihexylfluorene)-co-(9,9'-dihexylfluorene-3-thiophene-5'-yl)] as an emissive layer. By annealing the emissive layer at a relatively high temperature, fluorenone defects were generated into PDHFDOP, which formed an exciplex with poly-TPD, as a red emitter. The devices exhibit a maximum brightness of 4800cd/m² and a maximum luminous efficiency of 3cd/A. Moreover, the Commission Internationale de L'Eclairage coordinates of the emitted light is close to that of pure white light and is insensitive to the applied voltages. [J2533]

"Effects of symmetry of GaN-based two-dimensional photonic crystal with quasicrystal lattices on enhancement of surface light extraction"

We demonstrate enhancement of surface light extraction from two-dimensional photonic crystals (2D-PCs) on the electrical injected GaN-based light emitters. The effects of symmetry of PCs on light extraction were studied. 2.5 times enhancement of surface emission was obtained from the PCs with an octagonal symmetric quasicrystal lattice (8PQC) compared to that from a nonpatterned region. Additionally the surface emission from PCs with dodecagonal symmetric quasicrystal lattice (12PQC) exhibited about 1.7 and 1.4 times higher emission than regular PCs with triangular lattice and 8PQC, respectively. Consequently, the 12PQC provides a favorable consideration of 2D-PC in light extraction from light emitting diode. [J2534]

"Improved light outcoupling for phosphorescent top-emitting organic light-emitting devices"

Light outcoupling for top-emitting organic light-emitting devices is improved by using a semitransparent multilayer cathode structure of Al(2.5nm)/Ag(0.5nm)/Al(1nm)/Ag(0.5nm)/Al(0.5nm)/Ag(11nm). In addition, an excellent transparency of 70% is achieved with a 78-nm-thick tris-(8-hydroxyquinoline) aluminum (Alq3) film as a top-capping layer, which is overlaid onto the cathode. The electroluminescence intensity with this Alq3-covered cathode is increased by a factor of 1.9-3.1 (applied voltage from 7 to 21V) compared with the conventional

cathode Al(4nm)/Ag(12nm). This enhancement can be attributed to a gradual change of index refraction and extinction coefficient in the multilayer cathode (actually, not multilayer Al/Ag, but an Al:Ag alloylike configuration) and to the reduction of top Ag reflection by overlaying an Alq₃-capping layer onto the cathode. Besides, photoluminescence of the top-capping Alq₃ layer is helpful to improve device luminance. [J2535]

"Observation of deep level defects within the waveguide of red-emitting high-power diode lasers"

The waveguides of 650nm emitting high-power laser diodes are analyzed regarding the presence of deep level defects by photoelectrical techniques, namely, photocurrent spectroscopy, laser beam induced current, and near-field optical beam induced current (NOBIC). Deep level configurations in pristine devices and the kinetics of defect creation during device operation are monitored and discussed. The localization of the defects within the epitaxial layer sequence is done by NOBIC. We show that light, which is confined within the laser waveguide, interacts with the deep level defects detected. This demonstrates that the presence of deep level defects directly affects the device properties. [J2536]

"Photonic crystal laser lift-off GaN light-emitting diodes"

We report on the fabrication and study of laser lift-off GaN-based light-emitting diodes, thinned down to the microcavity regime, incorporating two-dimensional photonic crystal diffraction gratings. Angle-resolved measurements reveal the photonic behavior of the devices, which strongly depends on the GaN thickness. Data point out the detrimental role of metal absorption. We explore theoretically the possibility to limit this loss channel. [J2537]

"Thermally stimulated current studies on neutron irradiation induced defects in GaN"

The evaluation of the neutron irradiation induced defects in GaN is studied using a thermally stimulated current (TSC) method with excitation above (below) the energy band gap using ultraviolet (blue, green, red, and infrared) emitting diodes. Annealing at 1000°C, a broad TSC spectrum for excitation by the ultraviolet light is resolved by five traps, P1 (ionization energy is 200meV), P2(270meV), P3(380meV), P4(490meV), and P5(595meV). Infrared illumination shows a remarkable reduction in TSC for the P2 and P3 traps, indicating the photoquenching behavior. The possible origins of the observed five traps are discussed. [J2538]

"Efficient single-active-layer organic light-emitting diodes with fluoropolymer buffer layers"

In the present Letter, efficient organic light-emitting diodes (OLEDs) with tris(8-hydroxyquinolino) aluminum (Alq₃) as a single-active layer have been prepared by using a series of fluoropolymer buffer layers. The OLEDs with a 10-nm-thick poly(tetrafluoroethylene-perfluoroalkylvinylethers) (PFA) buffer layer had a current efficiency of 4.46cd/A at a current density of 2000A/m², whereas conventional double-layer OLEDs with N,N'-bis-(1-naphthyl)-N,N'-diphenyl-1,1'-biphenyl-4,4'-diamine (NPB) and Alq₃ showed a current efficiency of only 3.81cd/A at the same condition in our experiment. The effect of the insulating fluoropolymer buffer layers could be interpreted to enhance hole injection and improve carrier balance. [J2539]

"Effects of Ag/indium tin oxide contact to a SiC doping layer on performance of Si nanocrystal light-emitting diodes"

We report on the effects of a very thin Ag (2.5nm) interlayer between the indium tin oxide (ITO) current spreading layer and a SiC doping layer on silicon nanocrystals (nc-Si) embedded in silicon nitride film on the electrical and optical performance of the light-emitting diodes (LEDs). The forward voltage at a current of 20mA of the nc-Si LED with a Ag interlayer was decreased by 2.5V compared to that of the nc-Si LED without one due to the decrease in the contact resistance. In addition, the light output power of the nc-Si LED with a Ag interlayer was also enhanced by 40%. This result strongly indicates that the Ag/ITO contact scheme can serve as a highly promising contact scheme to a SiC film for the realization of the nc-Si LEDs with a high efficiency. [J2540]

"Work function and implications of doped poly(3,4-ethylenedioxythiophene)-co-poly(ethylene glycol)"

We report work function and conductivity measurements of the block copolymer poly(3,4-ethylenedioxythiophene)-co-poly(ethylene glycol) (PEDOT-PEG) doped with perchlorate or para-toluenesulfonate anions. The electronic and chemical properties of doped PEDOT-PEG are discussed in the context of the hole injection for organic light emitting diodes. We show that different dopants can result in significant differences in conductivity with only small alterations to the work function. [J2541]

"Efficient light extraction and beam shaping from flexible, optically integrated organic light-emitting diodes"

Efficient out-coupling light extraction and optical beam shaping have been combined to form an integrated, flexible illuminator that is based on organic light-emitting diodes (OLEDs). Spherical refractive microlenses were replicated by a cost-effective UV-casting technique onto a plastic foil to achieve the customized Gaussian distribution of the electroluminescence of an OLED pixel (50µm) matrix. The fabricated optical device, namely a ceiling light illuminator, shows an improvement of 70% in the out-coupled emission measured in the far field. The result corresponds to the theoretical prediction for isotropic emitting sources. [J2542]

"Room temperature ultraviolet emission at 357 nm from polysilane based organic light emitting diode"

We have fabricated an organic light emitting diode using poly(n-butylphenylsilane) which has an emission in deep ultraviolet at 357nm at room temperature. The device structure used is glass/indium tin oxide/poly(3,4-ethylenedioxythiophene) poly(styrenesulfonate)/polysilane (emitting material)/calcium/aluminum. These devices emit ultraviolet light with a turn-on voltage of 8V. The electroluminescence spectrum of the device in the ultraviolet range is identical to the photoluminescence spectrum of the polysilane thin film. From these devices, we also observe an additional emission in the visible region, which is not present in the photoluminescence spectrum of the material. The visible emission has a color coordinate of (0.36,0.35), which can be modulated to a required white light coordinate by down converting the ultraviolet emission. [J2543]

"Efficient pure-white organic light-emitting diodes with a solution-processed, binary-host employing single emission layer"

Efficient white light-emitting diodes were fabricated with a solution-processed single emission layer composing a molecular and polymeric materials mixed binary host. The main host used was a molecule of 4,4'-bis-(carbazol-9-yl) biphenyl and the assisting host used was a blue light-emitting polyfluorene-derived copolymer of poly[(9,9-dioctylfluorenyl-2,7-diyl)-alt-co-(9-hexyl-3,6-carbazole)]. The hosts were doped via solution-mixing a green dye of tris(2-phenylpyridine) iridium (III) and a red dye of bis[2-(2'-benzo-thienyl)-pyridyl]-nato-N,C3,(acetylacetonate) iridium (III). One resultant device having a pure white emission of Commission Internationale de l'Eclairage (0.33, 0.33) has a maximum power efficiency of 4.2lm/W at 802cd/m² and a maximum brightness of 11800cd/m². The better efficiency performance may be attributed to the addition of the assisting host, which halves the energy barrier for holes to inject into the light-emitting zone. [J2544]

"Electroluminescence at 375 nm from a ZnO /Ga N :Mg /c-Al₂O₃ heterojunction light emitting diode"

n-ZnO/p-GaN:Mg heterojunction light emitting diode (LED) mesas were fabricated on c-Al₂O₃ substrates using pulsed laser deposition for the ZnO and metal organic chemical vapor deposition for the GaN:Mg. High crystal quality and good surface morphology were confirmed by x-ray diffraction and scanning electron microscopy. Room temperature (RT) photoluminescence (PL) showed an intense main peak at 375nm and a negligibly low green emission indicative of a near band edge excitonic emission from a ZnO layer with low dislocation/defect density. The LEDs showed I-V characteristics confirming a rectifying diode behavior and a RT electroluminescence (EL) peaked at about 375nm. A good correlation between the wavelength maxima for the EL and PL suggests that recombination occurs in the ZnO layer and that it may be excitonic in origin. This also indicates that there is significant hole injection from the GaN:Mg into the ZnO. [J2545]

"Electrical spin injection from ZnMnSe into InGaAs quantum wells and quantum dots"

We report on efficient injection of electron spins into InGaAs-based nanostructures. The spin light-emitting diodes incorporate an InGaAs quantum well or quantum dots, respectively, as well as a semimagnetic ZnMnSe spin-aligner layer. We show a circular polarization degree of up to 35% for the electroluminescence from InGaAs quantum wells and up to 21% for InGaAs quantum dots. We can clearly attribute the polarization of the emitted photons to the spin alignment in the semimagnetic layer by comparison to results from reference devices (where the ZnMnSe is replaced by ZnSe) and from all-optical measurements. [J2546]

"Electroluminescence mapping of CuGaSe₂ solar cells by atomic force microscopy"

The authors report on the observation of electroluminescence (EL) in CuGaSe₂ solar cells using tapping-mode atomic force microscopy based on tuning-fork sensors. Individually injected current pulses are seen during intermittent contact driven by an external bias applied to the conducting tip. It follows that EL can be stimulated when the solar cell is forward biased during the contact cycle. Local I-V characteristics show evidence for EL,

with a threshold voltage of 3.0-3.7V. Mapping of the photon emission suggests that grain boundaries effectively isolate grain interiors, which behave as individual light-emitting diodes. [J2547]

"White organic light-emitting device based on a compound fluorescent-phosphor-sensitized-fluorescent emission layer"

The authors demonstrate a combination fluorescent and phosphor-sensitized-fluorescent white organic light-emitting device (WOLED), employing the conductive host material, 4,4'-bis(9-ethyl-3-carbazovinylen)-1,1'-biphenyl, doped with the phosphorescent green, and the fluorescent red and blue emitters, fac-tris(2-phenylpyridinato-N,C2') iridium (III), 4-(dicyanomethylene)-2-t-butyl-6-(1,1,7,7-tetramethyljulolidyl-9-enyl)-4H-pyran, and 4,4'-bis(9-ethyl-3-carbazovinylen)-1-1'-biphenyl, respectively. Although two fluorescent dopants are employed along with only a single phosphor, this simple structure can, in principle, achieve 100% internal quantum efficiency. In the prototype, the phosphor-sensitized WOLED exhibits total external quantum and power efficiencies of $\eta_{\text{ext,tot}}=13.1\pm0.5\%$ and $\eta_{\text{p,tot}}=20.2\pm0.7\text{lm/W}$, respectively, at a luminance of 800cd/m² with Commission Internationale de L'Eclairage chromaticity coordinates of (x=0.38, y=0.42) and a color rendering index of 79. [J2548]

"Enhanced light-extraction in GaInN near-ultraviolet light-emitting diode with Al-based omnidirectional reflector having Ni Zn /Ag microcontacts"

Enhancement of light extraction in a GaInN near-ultraviolet light-emitting diode (LED) employing an Al-based omnidirectional reflector (ODR) consisting of GaN, a SiO₂ low-refractive-index layer perforated by an array of NiZn/Ag microcontacts, and an Al layer is presented. A theoretical calculation reveals that a SiO₂/AlODR has much higher reflectivity than both a SiO₂/AgODR and a Ag reflector at a wavelength of 400nm. It is experimentally shown that GaInN near-ultraviolet LEDs with GaN/SiO₂/AlODR have 16% and 38% higher light output than LEDs with SiO₂/AgODR and Ag reflector, respectively. The higher light output is attributed to enhanced reflectivity of the Al-based ODR in the near-ultraviolet wavelength range. [J2549]

"Improving the power efficiency of white light-emitting diode by doping electron transport material"

Highly efficient white light emission was realized via the partial energy transfer from blue host polyfluorene (PF) to orange light emission dopant rubrene. A more balanced charge transport was achieved by adding an electron transport material, 2-(4-biphenyl)-5-(4-tert-butylphenyl)-1,3,4-oxadiazole (PBD), into the PF-rubrene system to enhance the electron transportation. Efficiency improvement by as much as a factor of 2 has been observed through the addition of PBD. These devices can easily reach high luminance at low driving voltages, thus achieving high power efficiency at high luminance (14.8, 13.5, and 12.0lm/W at the luminances of 1000, 2000, and 4000cd/m², respectively). Therefore, this performance is an important approach toward solid-state lighting application. The enhancement is mainly attributed to three factors: increased electron transport property of the host material, increased photoluminescence quantum efficiency, and the shifting of emission zone away from cathode contact. The reported efficiency is among the highest values reported in the white emission polymer light-emitting diodes. [J2550]

"Effective organic-based connection unit for stacked organic light-emitting devices"

A bilayer connection unit of Mg-doped Alq₃ and F4-TCNQ-doped m-MTDATA was investigated for application in stacked organic light-emitting device. This connection unit led to a stacked OLED with a luminous efficiency twice that of a single-unit OLED. Electronic structures, including relevant electron energy levels, of the various interfaces in the stacked OLED were studied by using ultraviolet photoemission spectroscopy and used to discuss the working mechanisms of the stacked OLED. The p-type dopant F4-TCNQ was shown to induce a large band bending of 1.36eV and facilitates efficient carrier injection from the connection units into the carrier-transporting layers. [J2551]

"Enhanced performance of white polymer light-emitting diodes using polymer blends as hole-transporting layers"

White polymer light-emitting diodes (WPLEDs) with the Commission Internationale de l'Enclaire coordinates of (0.32, 0.34) are demonstrated with poly(9,9-dioctylfluorene-2,7-diyl) as host and poly(5-methoxy-2-(2'-ethyl-hexylthio)-p-phenylenevinylene) as guest. Blends of poly[N,N'-bis(4-butylphenyl)-N,N'-bis(phenyl)benzidine] (poly-TPD) and poly(N-vinyl-carbazole) (PVK) are introduced into bilayer devices as hole-transporting layers (HTLs). Because the blends combined the hole-injection and hole-transporting capabilities of poly-TPD with electron-blocking capability of PVK, WPLEDs with the blends as HTLs exhibit enhanced performance in comparison with single-layer device and bilayer devices with pure poly-TPD or pure PVK as HTL. With a 1:1

weight ratio of poly-TPD to PVK in the blend, the WPLED achieves a maximum brightness of 5000cd/m² with a maximum electroluminescent efficiency of 3.15cd/A. [J2552]

"Effect of doping profile on the lifetime of green phosphorescent organic light-emitting diodes"

The lifetime of green phosphorescent light-emitting diodes was improved by using a graded doping structure in light-emitting layer. A green device with high doping concentration at the hole transport layer and light-emitting layer interface showed longer lifetime than a conventional device with uniform doping concentration for the whole light-emitting layer by more than 60%. [J2553]

"Effects of compressive strain on optical properties of In_xGa_{1-x}N/GaN quantum wells"

In_{0.2}Ga_{0.8}N/GaN multiple quantum well (MQW) blue light emitting diode (LED) structure was grown on a specially designed sapphire substrate (with increasing thickness from the edge to the center within a single wafer). X-ray diffraction revealed that the GaN lattice constant *c* decreases continuously from the edge to the center, indicating a continuous variation in the compressive strain. The spectral peak positions of the electroluminescence (EL) spectra exhibited a blueshift when probed at the edge as compared to the center, which is a direct consequence of the continuous variation in the compressive strain across the wafer. Based on the experimental results, a ratio of elastic stiffness constants (*C*₃₃/*C*₁₃) for GaN was deduced to be 5.0±1.0, which was in agreement with the calculated value of 4.0. A linear relation of the EL emission peak position of LEDs with the biaxial strain was observed, and a linear coefficient of 19meV/GPa characterizing the relationship between the band gap energy and biaxial stress of In_{0.2}Ga_{0.8}N/GaN MQWs was also obtained. [J2554]

"Use of cross-linkable polyfluorene in the fabrication of multilayer polyfluorene-based light-emitting diodes with improved efficiency"

The authors report the use of a cross-linkable polyfluorene to fabricate multilayer light-emitting diodes (LEDs), thereby avoiding the restriction to combine polymeric solutions in different solvents. In particular, we find that for LEDs fabricated with a hole-injection layer of poly(3,4-ethylenedioxythiophene) doped with polystyrene sulfonic acid (PEDOT), with magnesium cathodes and with poly(9,9-dioctylfluorene-*alt*-benzothiadiazole) (F8BT), as emissive layer, its electroluminescence efficiency increases from 2 to 5.5cd/A upon insertion of the cross-linked polyfluorene between PEDOT and F8BT. This efficiency increase is attributed to an improvement of charge carrier balance within the F8BT emissive layer and a reduction of exciton quenching at PEDOT interface. [J2555]

"Utilization of water/alcohol-soluble polyelectrolyte as an electron injection layer for fabrication of high-efficiency multilayer saturated red-phosphorescence polymer light-emitting diodes by solution processing"

Highly efficient multilayer red polymer light-emitting diodes were fabricated by solution processing from iridium complex, bis(1-(3-(9,9-dimethyl-fluorene-2-yl)phenyl)isoquinoline-C₂,N') iridium(III)acetylacetonate, doped into polyfluorene as a host and with a water/alcohol-soluble polymer, poly[(9,9-bis(3'-((N,N-dimethyl)-N-ethylammonium)propyl)-2,7-fluorene)-2,7-(9,9-dioctylfluorene)-4,7-(2,1,3-benzoselenadiazole)]dibromide (PFN) as electron injection layer. The device with the structure ITO/PEDOT-PSS(50nm)/PVK(40nm)/PFO:PBD:Ir(DMFPQ)2acac(2%,75nm)/PFN(20nm)/Ba(4.5nm)/Al(150nm) showed an external quantum efficiency of 18.0% and luminance efficiency of 9.8Cd/A at a current density of 1.1mA/cm², a peak emission at λ_{max} =636nm, and Commission International de l'Eclairage coordinates of (0.665, 0.319). The efficiency remained as high as QE=11.1%, and LE=6.0cd/A, at a current density of 100mA/cm², and a luminance of 6140cd/m². [J2556]

"Origin of forward leakage current in GaN-based light-emitting devices"

The authors fabricated GaN-based light-emitting diodes (LEDs) on two different GaN templates with the same LED structure. One on thin GaN template ($\sim 2\mu\text{m}$) with high dislocation density [low (10⁹cm⁻²)] grown by metal-organic vapor-phase epitaxy (sample A) and the other on thick GaN template ($\sim 20\mu\text{m}$) with comparatively low dislocation density [high (10⁸cm⁻²)] by hydride vapor-phase epitaxy (sample B). In order to understand the mechanism of leakage current in LEDs, the correlation between current-voltage characteristics and etch pit density of LEDs was studied. [J2557]

"White emission from liquid-crystalline copolymers containing oxadiazole moieties in the side chain"

A liquid-crystalline polymer in the side chain was synthesized through copolymerization of a bipolar carrier-transporting monomer with a liquid-crystalline monomer containing oxadiazole moieties substituted with trifluoromethyl groups. A single-layer light-emitting diode of indium tin oxide (ITO)/copolymer/MgAg emitted white

light with a maximum luminous efficiency of 0.1cd/A. The origin of the white emission in the copolymer is the electroplex between bipolar carrier-transporting moieties and strong electron-withdrawing moieties. Furthermore, a simple multilayer device with configuration of ITO/poly(3,4-ethylenedioxythiophene)/poly(styrenesulfonic acid)/copolymer/MgAg device showed white emission with CIE 1931 chromaticity coordinates (x,y): (0.30, 0.33).

[J2558]

"Green top-emitting organic light emitting device with transparent Ba /Ag bilayer cathode"

Using a vacuum thermal technique, semitransparent Ba/Agbilayer cathode has been fabricated for the top-emitting organic light emitting devices. In this work, optical transparency over 60% in the visible region and low sheet resistance of about 15 Ω /sqin the Ba (10nm)/Ag(8nm)structure are reported. The surface and compositional morphologies of the cathode play a crucial role in determining the optical properties. Top-emitting organic light emitting device using this cathode has been fabricated and studied. [J2559]

"Surface plasmon mediated emission in resonant-cavity light-emitting diodes"

In this letter the authors describe a particular method to outcouple in air, via surface plasmons (SPs), optical radiation trapped in leaky waveguide modes of a resonant-cavity light-emitting diode. The deposition of a thin metal layer on the device surface creates SP modes at both the metal-dielectric interfaces. The successive overcoating of the metal layer with a thin polymer film and the roughening of its surface produce outcoupling of radiation trapped in leaky modes via SP modes. Experimental results for polarization resolved reflectivity and emission spectra are in excellent agreement with theoretical predictions. [J2560]

"Spin injection from perpendicular magnetized ferromagnetic delta -Mn Ga into (Al,Ga)As heterostructures"

Electrical spin injection from ferromagnetic delta -MnGa into an (Al,Ga)As p-i-nlight-emitting diode (LED) is demonstrated. The delta -MnGalayers show strong perpendicular magnetocrystalline anisotropy, enabling detection of spin injection at remanence, without an applied magnetic field. The bias and temperature dependence of the spin injection are found to be qualitatively similar to Fe-based spin LED devices. A Hanle effect is observed and demonstrates complete depolarization of spins in the semiconductor in a transverse magnetic field. [J2561]

"Comparative study of single and multiemissive layers in inverted white organic light-emitting devices"

The authors have fabricated and compared highly efficient inverted white organic light-emitting devices (WOLEDs) with a single emission layer (SEL) and with a multiemission layer (MEL). The efficiency levels of the WOLEDs with a SEL and a MEL achieved 13.0cd/A, 10.6lm/Wand 11.3cd/A, 7.3lm/W, respectively. The projected half lifetime of a SEL device under an initial luminance of 400cd/m²is expected to be over 34000h, which is five times better than that of a MEL device of 6350h. The Commission International de l'Eclairage coordinates of a SEL device are not affected by aging. [J2562]

"Dark spot formation mechanism in organic light emitting diodes"

The authors report electroluminescence degradation in organic light emitting diode operated at a high current density of 500mA/cm²under nitrogen ambient. The turn-on voltage increased from 6to10V, and a number of dark spots were produced when the device was operated for 420min. Microscope image showed that dark spots are related to many protrusions and hollows formed on Al electrode. X-ray diffraction and scanning photoemission microscope spectra indicate that the Joule heat from high electric field induced the crystallization of 4'-bis[N-(1-naphthyl)-N-phenyl-amino]biphenyl, forming dark spots via peeling off of the Al cathode. [J2563]

"Ohmic contacts to plasma etched n-Al 0.58 Ga 0.42 N"

Plasma etching is required to expose n-Al_xGa_{1-x}Nlayers for bottom-emitting ultraviolet light emitting diodes grown on sapphire. However, etching can increase the difficulty of forming Ohmic contacts. X-ray photoelectron spectroscopy and cathodoluminescence reveal how the semiconductor changes with etching and help explain why it becomes more difficult to form an Ohmic contact. A V/Al/V/Aumetallization has been investigated for Ohmic contacts to n-Al_{0.58}Ga_{0.42}Netched with a BC13/Cl₂/Archemistry. Increased V thickness and higher annealing temperatures were required to obtain a specific contact resistance of 4.7 $\times 10^{-4}\Omega$ cm²for etched n-Al_{0.58}Ga_{0.42}Ncompared to optimized contacts on unetched films. [J2564]

"In Sb /Al x In 1-x Sb quantum-well light-emitting diodes with high internal quantum efficiencies"

The properties of InSb/Al_xIn_{1-x}Sb quantum-well light-emitting diodes have been investigated as a function of temperature from 300 to 15 K. Over the whole range, the peak emission occurred at significantly higher energies than the band gap of InSb but below the band gap of the Al_xIn_{1-x}Sb barriers, confirming that emission is from the quantum wells. Maximum internal quantum efficiencies of 65% and 85% were measured at 15 K for diodes containing 40 and 20 nm quantum wells, respectively. [J2565]

"Efficient nondoped white organic light-emitting diodes based on electromers"

The authors report excellent white organic light-emitting diodes (WOLEDs) made of 9,9-bis[4-(di-p-tolyl)aminophenyl]-2,7-bis(diphenylamino)fluorene (TADPF) or 9,9-bis[4-(di-p-tolyl)aminophenyl]-2,7-bis(9-carbazolyl)fluorene (TAKF). The superposition of a yellow emission coming from the TADPF or TAKF electromer and a blue emission originating from bis(2-(2-hydroxyphenyl)benzothiazolate)zinc gives rise to a pure white-light emission. The multilayer device using TADPF shows a maximum luminance of 5123 cd/m², a current efficiency of 2.8 cd/A, and Commission Internationale d'Eclairage chromaticity coordinates of (0.33, 0.33). This result is the optimal for WOLEDs based on electromers so far reported. [J2566]

"Hole-transporting interlayers for improving the device lifetime in the polymer light-emitting diodes"

The authors report the effect of thermal treatment of hole-transporting interlayers between a polymeric hole injection layer and an emitting layer (EML) on the luminous efficiency and the lifetime performance in blue polymer light-emitting diodes. As the thermal annealing temperature of the interlayer increased, the hole mobility of the interlayer tended to decrease, which results in reducing the hole current injected into the EML in the devices. Hence, the device luminous efficiency decreased due to lower electron-hole balance. Nevertheless, the device lifetime increased, which can be attributed to the formation of the thicker interlayer and the better defined interlayer/EML interface. [J2567]

"Efficient 1.54 mcm light emitting diode with nanometer thick polycrystalline Si anode and organic sandwich structure"

This letter reports that the 1.54 mcm electroluminescence efficiency of the organic light emitting diode (OLED) with a structure of nanometer thick polycrystalline silicon (NTPS)/NPB/ErQ/AIQ/Al is two orders of magnitude higher than that of the OLED with a structure of thick crystalline silicon/NPB/ErQ/Al, which is similar to the OLED reported in literature [Curry et al, Appl. Phys. Lett. 77, 2271 (2000)]. Such an improvement is mainly attributed to the fact that hole injection is controlled by NTPS anode and holes are blocked by AIQ to match electron injection, and a higher light out coupling as well. [J2568]

"Stacked white organic light-emitting devices based on a combination of fluorescent and phosphorescent emitters"

We demonstrate a white stacked organic light-emitting device (WSOLED) employing the blue fluorescent emitter, 4,4'-bis(9-ethyl-3-carbazovylene)-1,1'-biphenyl, and the green and red phosphorescent emitters, fac-tris(2-phenylpyridinato-N,C2') iridium (III) and iridium (III) bis(2-phenyl quinolyl-N,C2') acetylacetonate, respectively. The charge generation region consists of a Li-doped electron transport layer and a highly transparent MoO_x thin film. For a two-element white SOLED (2-WSOLED), the combination of red and green phosphors with a blue fluorophore yields maximum external quantum and power efficiencies of $\eta_{\text{ext}} = 23\% \pm 2\%$ at a current density of $J = 1 \text{ mA/cm}^2$ and $\eta_{\text{p}} = 14 \pm 1 \text{ lm/W}$ at $J = 0.17 \text{ mA/cm}^2$, respectively. Due to the low optical and electrical losses of the charge generation layer, the efficiencies scale approximately linearly with the number of independent emissive elements in the WSOLED. Hence, for a 3-WSOLED, the total external and power efficiencies estimated for operation of the device in a light fixture are $\eta_{\text{ext,tot}} = 57\% \pm 6\%$ and $\eta_{\text{p,tot}} = 22 \pm 2 \text{ lm/W}$, respectively, at a luminance of 1000 cd/m², with Commission Internationale de L'Eclairage chromaticity coordinates of (x=0.38, y=0.4--4), and a color rendering index of 82. The high-efficiency, high brightness, stacked white OLED is potentially useful for solid state lighting applications. [J2569]

"On the use of Monte Carlo modeling in the mathematical analysis of scanning electron microscopy-electron beam induced current data"

Electron beam induced current (EBIC) is often used to evaluate minority carrier properties in semiconductors. Various mathematical models have been proposed; the most advanced is that of Bonard and Ganiere [J. Appl. Phys. 79, 6987 (1996)]. However, in order to apply this model to EBIC experiments, the lateral and depth distributions of the electron-hole-pair generation in the sample must be known. This letter presents a straightforward method based on Monte Carlo simulation of the electron beam interaction with the sample to

evaluate these distribution parameters. A quantitative experimental example from a GaN-based light emitting diode is presented to test the proposed method. [J2570]

"Enhancement of light extraction from a silicon quantum dot light-emitting diode containing a rugged surface pattern"

The enhancement in light extraction efficiency from a periodic micron-scale rugged surface pattern on Si quantum dot light-emitting-diode (Si-QD LED) structures was investigated, both numerically and experimentally. Micron-scale rugged surface patterns were fabricated on the top layer of the Si-QD LED to increase the extraction of light from the active layer. The optimum light extraction condition for a Si-QD LED corresponded to a pattern size/period ratio of 0.7. In experiments, the luminescent powers of a Si-QD LED with/without micron-scale surface patterns increase linearly with current density, and the efficiency of light extraction was enhanced by a factor of 2.8. [J2571]

"Investigation of Cr- and Al-based metals for the reflector and Ohmic contact on n-GaN in GaN flip-chip light-emitting diodes"

This letter investigates three composite metals used as a reflector and Ohmic contact on n-GaN to simplify the process in a flip-chip light-emitting diode (FCLED). The investigated composite metals were Ti/Al/Ti/Au, Cr/Al/Cr/Au, and Cr/Ti/Au. The specific contact resistivities of the Ti/Al/Ti/Au, Cr/Al/Cr/Au, and Cr/Ti/Au Ohmic contacts on n-GaN were changed from 1.4×10^{-4} , 1.7×10^{-4} , and $1.9 \times 10^{-4} \Omega \text{ cm}^2$ to 1.3×10^{-4} , 1.1×10^{-4} , and $3.3 \times 10^{-5} \Omega \text{ cm}^2$, respectively, after 500 h of thermal stress. The corresponding operating voltages of FCLEDs with different composite metals were changed by less than 1%. After 96 h of thermal stress, the luminous intensities of the three structures decreased by 6.2%, 11.1%, and 1.4%, respectively. The GaN FCLED that was fabricated with Cr/Ti/Au as a reflector and an Ohmic contact on n-GaN exhibits good thermal stability and luminous intensity. [J2572]

"Synthesis of high quality n-type CdS nanobelts and their applications in nanodevices"

High quality n-type CdS nanobelts (NBs) were synthesized via an in situ indium doping chemical vapor deposition method and fabricated into field effect transistors (FETs). The electron concentrations and mobilities of these CdS NBs are around $(1.0 \times 10^{16} - 3.0 \times 10^{17})/\text{cm}^3$ and $100 - 350 \text{ cm}^2/\text{Vs}$, respectively. An on-off ratio greater than 10^8 and a subthreshold swing as small as 65 mV/decade are obtained at room temperature, which give the best performance of CdS nanowire/nanobelt FETs reported so far. n-type CdS NB/p⁺-Si heterojunction light emitting diodes were fabricated. Their electroluminescence spectra are dominated by an intense sharp band-edge emission and free from deep-level defect emissions. [J2573]

"Metal electrode effects on spin-orbital coupling and magnetoresistance in organic semiconductor devices"

This letter reports the modifications of spin-orbital coupling and magnetoresistance of conjugated polymer upon deposition of metal electrode based on organic light-emitting diodes of poly[2-methoxy-5-(2'-ethylhexyloxy)-1,4-phenylenevinylene]. We find that the reverse bias yields a largely increased magnetoresistance when the electron-hole capture zone is away from the metal electrode as compared to the forward bias with the electron-hole capture zone close to the metal electrode. The electroluminescence suggests that the deposited metal atoms enhance the spin-orbital coupling at the polymer/metal interface and consequently lead to electron-hole capture zone dependent magnetic field effects in organic semiconductor devices. [J2574]

"Highly efficient top-emitting organic light-emitting diodes with self-assembled monolayer-modified Ag as anodes"

A series of p-substituted benzylmercaptans was used to form self-assembled monolayers (SAMs) on silver surface to serve as the anode in the fabrication of top-emitting organic light-emitting diodes. SAMs with electron-withdrawing substituents such as cyano and trifluoromethyl groups led to enhanced hole injection and electroluminescent performance, whereas the opposite is true for electron-donating groups. Direct quantitative correlation between the molecular dipole moment/work function or work function/hole injection does not exist. A high current efficiency of 12 cd/A was obtained, which is two and half times that of the conventional bottom-emitting device of the same layer structure. [J2575]

"Improvement of near-ultraviolet nitride-based light emitting diodes with mesh indium tin oxide contact layers"

The authors have demonstrated nitride-based near-ultraviolet (NUV) light emitting diodes (LEDs) with mesh indium tin oxide (ITO) contact layer. With 20mA injection current, it was found that forward voltages were 3.94 and 4.05V while the output powers were 7.54 and 9.02mW for the planar ITO LED and mesh ITO LED, respectively. The larger LED output power should be attributed partially to the reduced absorption of ITO in the NUV region and partially to the better current spreading. [J2576]

"Room-temperature In As Sb P /In As light emitting diodes by liquid phase epitaxy for midinfrared (3-5 μm) dynamic scene projection"

The InAsSbP/InAs light emitting diodes (LEDs) grown by liquid phase epitaxy and tuned at several wavelengths inside the 3-5 μm band were tested. Light pattern, radiation apparent temperature (T_a), thermal resistance, and self-heating details were characterized at $T=300\text{K}$ in microscale by calibrated infrared cameras operating in the 3-5 and 8-12 μm bands. The authors show that LEDs dynamically simulate very hot ($T_a \geq 750\text{K}$) targets as well as cold objects and low observable. They resume that low cost LEDs enable a platform for photonic scene projection devices able to compete with thermal microemitter technology. Proposals on how to further increase LEDs performance are given. [J2577]

"Nitride-based light-emitting diodes with p-Al In Ga N surface layers prepared at various temperatures"

The authors have prepared bulk p-AlInGa layers and light-emitting diodes (LEDs) with p-AlInGa surface layers by metal organic chemical vapor deposition. They found that the surfaces of the LEDs with p-AlInGa layers are rough with high density of hexagonal pits. They also found that the pit width and the pit density depend on the growth temperature of the p-AlInGa layer. Furthermore, it is found that a 62% enhancement in output intensity can be achieved from the LED with an 820°C p-AlInGa cap layer without increasing the LED operation voltage. [J2578]

"Erratum: "Green fluorescent organic light-emitting device with external quantum efficiency of nearly 10%" [JAppl. Phys. Lett. 89, 063504 (2006)]"

First Page of the Article [J2579]

"Hexagonal pyramid shaped light-emitting diodes based on ZnO and GaN direct wafer bonding"

The authors report on hexagonal pyramid shaped light-emitting diode (LED) based on ZnO and GaN wafer bonding. After direct wafer bonding of an n-type ZnO substrate to a III-nitride LED wafer, O-plane ZnO was selectively etched to form an electrode having a truncated hexagonal pyramid shape. This wafer bonded LED chip was evaluated with optical output power as a function of forward current and was 2.2 times higher than a conventional-type LED chip having thin Ni (5nm)/Au(10nm) p-type electrode at forward current condition of 20mA. [J2580]

"Recombination zone in mixed-host organic light-emitting devices"

In this letter, the authors had quantitatively investigated the recombination zone in the mixed-host (MH) emitting layer (EML) of an organic light-emitting device with different mixed ratios experimentally and theoretically. The MH-EML consisted of a hole-transport layer (HTL) and an electron-transport layer fabricated by coevaporation. When the mixed ratio of the HTL in the EML increases, the driving voltage increases then decreases; this can be well demonstrated by an electrical model with different carrier mobilities. A blueshift was also observed due to the solid state solvation effect combined with the exciton shift from the anode to the cathode side. [J2581]

"Defect reduction and efficiency improvement of near-ultraviolet emitters via laterally overgrown GaN on a GaN/patterned sapphire template"

An approach to improve the defect density and internal quantum efficiency of near-ultraviolet emitters was proposed using a combination of epitaxial lateral overgrowth (ELOG) and patterned sapphire substrate (PSS) techniques. Especially, a complementary dot array pattern corresponding to the underlying PSS was used for the ELOG-SiO₂ mask design. Based on the transmission-electron-microscopy and etch-pit-density results, the ELOG/SiO₂/GaN/PSS structure can reduce the defect density to a level of 10⁵cm⁻². The internal quantum efficiency of the InGaN-based ELOG-PSS light-emitting diode (LED) sample showed three times in magnitude as compared with that of the conventional GaN/sapphire one. Under a 20mA injection current, the output powers of ELOG-PSS, PSS, and conventional LED samples were measured to be 3.3, 2.9, and 2.5mW, respectively. The enhanced output power could be due to a combination of the reduction in dislocation density (by ELOG)

and improved light extraction efficiency (by PSS). Unlike the previous double ELOG approaches, the presented ELOG-PSS structure needs only one regrowth process and will have high potential in future high-quality ultraviolet emitters, even blue/green laser diode applications. [J2582]

"Silicon light-emitting transistor for on-chip optical interconnection"

The authors propose a light-emitting field-effect transistor with the active layer made of the ultrathin single crystal silicon with the (100) surface orientation. The ambipolar carrier injections from the highly impurity doped regions to the ultrathin silicon are achieved in complementary-metal-oxide-semiconductor compatible planar structures and the optical intensities are controlled by the gate voltage. By using the device, they have demonstrated that a simple electrical signal can be transferred by light and detected on the same silicon chip as photocurrents controlled by the gate bias. [J2583]

"Efficient blue organic light-emitting device based on N, N'-di(naphth-2-yl)-N, N'-diphenyl-benzidine with an exciton-confining structure"

A blue organic light-emitting device with improved efficiency and excellent color purity is reported (Commission Internationale de l'Eclairage coordinates of $x=0.1659$ and $y=0.0772$ at 5V), where N, N'-di(naphth-2-yl)-N, N'-diphenyl-benzidine (NPB), a traditional hole-transporting layer, was used as the emission layer. A significant increase in efficiency was achieved by confining the excitons within the NPB layer by two wide-band-gap hole-blocking layers sandwiching the NPB layer. This structure also increases the direct exciton formation at the NPB layer by promoting electrons to cross the NPB layer, responsible for further efficiency improvement. Optimized structure showed an external quantum efficiency of 1.38%, which accounts for a 25% increase compared to a standard device. [J2584]

"Growth and fabrication of InGaNP-based yellow-red light emitting diodes"

The authors describe the growth and fabrication of InGaNP quantum well (QW)-based yellow-red light emitting diodes (LEDs) grown directly on transparent GaP (100) wafers. The dependence of $\ln y_{\text{Ga1-yN0.005P0.995}}/\text{GaP}$ conduction and valence band offsets on the In composition was calculated, and the dependence of $\text{Al}_{0.14}\text{Ga}_{0.86}\text{P}$ band offsets on the Al concentration was also calculated. Using $\text{Al}_{0.14}\text{Ga}_{0.86}\text{P}$ cladding layers increases the light output from a LED chip by 15%. InGaNP/GaP multiple QW LED structures show an increase of light output and saturation current. [J2585]

"Planarized SiNx/spin-on-glass photonic crystal organic light-emitting diodes"

The light extraction characteristics of low-index spin-on-glass (SOG)-assisted, planarized photonic crystal organic light-emitting diodes (PC OLEDs) are reported. The light extraction efficiencies of planarized two-dimensional (2D) SiNx/SOGPC OLEDs (type II) and 2D SiNx/SOGPC OLEDs with an additional high-index SiNx layer (type III) are significantly better under typical operating conditions than those of the first generation of 2D $\text{SiO}_2/\text{SiNxPC}$ OLEDs (type I). The enhancements in the extraction efficiencies of type-II and type-III PC OLEDs are about 63% and 85%, respectively, with respect to those of conventional OLEDs with indium tin oxide layers of identical thicknesses. These improvements in extraction efficiencies are attributed not only to the liberation of the photons trapped in the high-index guiding layer but also to a reduction in the surface plasmon contribution. [J2586]

"Characteristics of an organic light-emitting diode utilizing a phosphorescent, shallow hole trap"

The authors demonstrate the effects of incorporating a phosphorescent, shallow hole trap in an organic light-emitting diode. They present device properties as a function of trap concentration including electron only, hole only, and bipolar current-voltage (I-V) characteristics, electroluminescence (EL) and photoluminescence spectra, and diode quantum efficiency. They specifically considered poly(9,9-dioctylfluorene) doped with an Ir phosphor. Built-in potential and I-V measurements were used to determine that the phosphor is a shallow trap. The EL spectrum is dominated by phosphor emission for concentrations above 0.1wt%. The effects of incorporating the phosphor are shown to be consistent with quasiequilibrium statistics. [J2587]

"Enhanced luminescence of $\text{Y}_3\text{Al}_5\text{O}_{12}:\text{Ce}^{3+}$ nanophosphor for white light-emitting diodes"

Results pertaining to the development of highly dispersible stand-alone particles of Ce^{3+} -doped $\text{Y}_3\text{Al}_5\text{O}_{12}$ nanophosphor and their luminescence are presented. The yellow light-emitting nanophosphor was produced as a result of a single-step auto-combustion process, which requires no auxiliary annealing treatments prior to any practical application. The structure, photoluminescence, and chromaticity of the powder nanophosphor samples with the compositions $\text{Y}(\text{3-x})\text{Al}_5\text{O}_{12}:\text{xCe}^{3+}$ ($x=0.01-1$) are featured in the letter. The

nanophosphor absorbs light efficiently in the visible region of 400-500nm, and shows single broadband emission peaking at 560nm. The luminescence yield is almost analogous to the samples made from other conventional methods. Hence, it could be an apt candidate for generating white light when coupled to a blue light-emitting diode ($\lambda_{em}=450nm$). [J2588]

"Contrast improvement of organic light-emitting devices with Sm:Ag cathode"

Sm:Ag, easily fabricated via simple thermal evaporation, was investigated as a single-layer light-absorbing cathode to increase the contrast ratio of organic light-emitting devices (OLEDs). The performance of OLEDs with Sm:Ag cathode was found to be comparable to that of the traditional OLEDs with Mg:Ag cathode in terms of brightness, electroluminescence (EL) efficiency, and turn-on voltage. The maximum EL efficiency of the device with Sm:Ag black cathode is 2.72cd/A at 15V, while the contrast ratio reaches 390:1 at 10V under 140 lx of ambient light, which is 8 times better than that of the traditional device. The lower EL efficiency and enhanced contrast are due to the reduced optical reflectance of Sm:Ag black cathode, which was calculated to be about 0.15. [J2589]

"Improved efficiency for white organic light-emitting devices based on phosphor sensitized fluorescence"

Efficiency of white organic light-emitting devices (WOLEDs) based on phosphor sensitized fluorescence is improved by using an unusual device structure, in which an undoped blue emissive layer is sandwiched between two phosphorescent doped ones. This blue emissive layer blocks a triplet-triplet energy transfer between the two phosphorescent emissive layers, leading to balanced emissions of blue, green, yellow, and red. Thus, an efficient WOLED with a maximum luminous efficiency of 13.8cd/A, a maximum power efficiency of 8.0lm/W, a color rendering index of 79, and Commission Internationale de L'Eclairage coordinates of (0.33, 0.35) is achieved. [J2590]

"Blue light-emitting polymer with polyfluorene as the host and highly fluorescent 4-dimethylamino-1,8-naphthalimide as the dopant in the sidechain"

The dopant/host concept, which is an efficient approach to enhance the electroluminescence (EL) efficiency and stability for organic light-emitting diodes (OLEDs) devices, has been applied to design efficient and stable blue light-emitting polymers. By covalently attaching 0.2mol% highly fluorescent 4-dimethylamino-1,8-naphthalimide (DMAN) unit (photoluminescence quantum efficiency: $\Phi_{PL}=0.84$) to the pendant chain of polyfluorene, an efficient and colorfast blue light-emitting polymer with a dopant/host system and a molecular dispersion feature was developed. The single-layer device (indium tin oxide/PEDOT/polymer/Ca/Al) exhibited the maximum luminance efficiency of 6.85cd/A and maximum power efficiency of 5.38lm/W with the CIE coordinates of (0.15, 0.19). Moreover, no undesired long-wavelength green emission was observed in the EL spectra when the device was thermal annealed in air at 180°C for 1h before cathode deposition. These significant improvements in both efficiency and color stability are due to the charge trapping and energy transfer from polyfluorene host to highly fluorescent DMAN dopant in the molecular level. [J2591]

"High-efficiency InGaN -based light-emitting diodes with nanoporous GaN:Mg structure"

In this research nanoporous structures on p-type GaN:Mg and n-type GaN:Si surfaces were fabricated through a photoelectrochemical (PEC) oxidation and an oxide-removing process. The photoluminescence (PL) intensities of GaN and InGaN/GaN multi-quantum-well (MQW) structures were enhanced by forming this nanoporous structure to increase light extraction efficiency. The PL emission peaks of an MQW active layer have a blueshift phenomenon from 465.5nm (standard) to 456.0nm (nanoporous) measured at 300K, which was caused by partially releasing the compressive strain from the top GaN:Mg layers. The internal quantum efficiency could be increased by a partial strain release that induces a lower piezoelectric field in the active layer. The thermal activation energy of a nanoporous structure (85meV) is higher than the standard one (33meV) from a temperature dependent PL measurement. The internal quantum efficiency and light extraction efficiency of an InGaN/GaN MQW active layer are significantly enhanced by this nanoporous GaN:Mg surface, and this PEC treated nanoporous structure is suitable for high-power lighting applications. [J2592]

"All-organic active matrix flexible display"

We have fabricated pentacene organic thin-film transistor (OTFT) driven active matrix organic light-emitting diode (OLED) displays on flexible polyethylene terephthalate substrates. These displays have 484x480 bottom-emission OLED pixels with two pentacene OTFTs used per pixel. Parylene is used to isolate the OTFTs and OLEDs with good OTFT yield and uniformity. [J2593]

"Co-planar spin-polarized light-emitting diodes"

Studies of spin manipulation in semiconductors have benefited from the possibility of growing these materials of high quality on top of optically active III-V systems. The induced electroluminescence in these layered semiconductor heterostructures has been used for a reliable spin detection. In semiconductors with strong spin-orbit (SO) interaction, the sensitivity of vertical devices may be insufficient, however, because of the separation of the spin aligner part and the spin detection region by one or more heterointerfaces and because of the short spin coherence length. Here we demonstrate that highly sensitive spin detection can be achieved using a lateral arrangement of the spin polarized and optically active regions. Using our co-planar spin-polarized light-emitting diodes we detect electrical field induced spin generation in a semiconductor heterojunction two-dimensional hole gas. The polarization results from spin asymmetric recombination of injected electrons with strongly SO coupled two-dimensional holes. The possibility of detecting spin polarization of a two-dimensional electron gas (2DEG) induced by the local strayfield of a magnetized Co microstructure deposited on top of the 2DEG close to the co-planar diode junction is also demonstrated. [J2594]

"Tuning emission color of electroluminescence from two organic interfacial exciplexes by modulating the thickness of middle gadolinium complex layer"

Electroluminescent colors of organic light-emitting diodes (OLEDs) can be tuned by modulating the thickness of gadolinium (Gd) complex layer sandwiched between an electron-transporting layer (ETL) and a hole-transporting layer (HTL). The emission colors, which originate from the two interfacial exciplexes simultaneously, can be tuned from green to orange by increasing the thickness of the Gd-complex layer. The atom force microscope images have proved that there are many gaps in the thinner Gd-complex layers. Therefore, besides the exciplex formation between Gd complex and HTL, the exciplex between ETL and HTL is also formed. The results demonstrate that a simple way of color tuning can be realized by inserting a thin layer of color tuning material between HTL with lower ionization potentials and ETL with higher electron affinities. Moreover, photovoltaic device and white OLED based on the two exciplexes are also discussed. [J2595]

"Erratum: "Improved electroluminescent efficiency of organic light emitting devices by co-doping N, N' -Dimethyl-quinacridone and Coumarin6 into tris-(8-hydroxyquinoline) aluminum" [JAppl. Phys. Lett. 87, 213501 (2005)]"

First Page of the Article [J2596]

"Direct Al cathode layer sputtering on LiF /Alq 3 using facing target sputtering with a mixture of Ar and Kr"

Using facing target sputtering (FTS) with a mixture of Ar and Kr, direct Al cathode sputtering on LiF/Alq3 layers was accomplished without the need for a protective layer against plasma damage. Organic light emitting diodes (OLEDs) with a directly sputtered Al cathode in a mixture of Ar and Kr showed a much lower leakage current density ($1.4 \times 10^{-5} \text{ mA/cm}^2$ at -6V) than those ($1.4 \times 10^{-1} \text{ mA/cm}^2$ at -6V) of OLEDs with an Al cathode prepared by FTS or dc sputtering in a pure Ar ambient. This indicates that the bombardment of energetic particles is effectively restricted by mixing a heavy noble gas. Based on the current-voltage curve for the OLED, a possible mechanism is proposed to explain the effect of a heavy noble gas mixture on electrical properties of OLEDs for direct Al cathode sputtering by FTS. [J2597]

"Selective light emission from flexible organic light-emitting devices using a dot-nickel embedded indium tin oxide anode"

This work demonstrates selective light emission from organic light-emitting diodes (OLEDs) with an Al/tris(8-hydroxyquinoline) aluminum N,N'-bis-(1-naphthyl)-N,N'-diphenyl-1, 1'-biphenyl-4, 4'-diamine/nickel-embedded indium tin oxide (ITO)/ polyethylene terephthalate film structure. Embedding Ni in the surfaces of ITO anodes can reduce the OLED turn-on voltage by 2.3V, allowing the OLED to be selectively emitted. This approach based on Ni-embedded ITO approach can prevent crosstalks in passive OLED addressing because the lateral electric current is negligible outside the Ni-embedded area. It also reduces the roughness of the ITO surface by polishing. Therefore, this method can simultaneously improve the optoelectrical characteristics and increase the lifetime of an OLED device. [J2598]

"Enhancing light outcoupling of organic light-emitting devices by locating emitters around the second antinode of the reflective metal electrode"

Due to generally low conductivity and low carrier mobilities of organic materials, organic light-emitting devices

(OLEDs) are typically optimized for light outcoupling by locating emitters around the first antinode of the metal electrode. In this letter, by utilizing device structures containing conductive doping, we investigate theoretically and experimentally the influences of the location of emitters relative to the metal electrode on OLED emission, and show that substantial enhancement in light outcoupling (1.2 times) or forward luminance (1.6 times) could be obtained by placing emitters around the second antinode instead of the first antinode. Depending on the detailed condition, the second-antinode device may also give more directed emission as often observed in strong-microcavity devices yet without suffering a color shift with viewing angles. [J2599]

"Enhanced efficiency in polymer light-emitting diodes due to the improvement of charge-injection balance"

The authors report the enhancement of efficiency of polymer light-emitting diodes (PLEDs) in the study. According to the experimental results, we find that PLEDs, fabricated on irradiated indium-tin-oxide surfaces by KrFexcimer laser, with an organic layer between the cathode and the emitting layer may lead to the improvement of charge-injection balance and prevention of cathode metal quenching, resulting in a remarkable increase in external quantum efficiency. [J2600]

"Near-infrared electroluminescence based on perylenediimide-doped tris(8-quinolinolato) aluminum"

For the purpose of exploring near-infrared emission, the photoluminescence (PL) and electro-luminescence (EL) of N,N'-bis(neopentyl)-3,4:9,10-perylenebis(dicarboximide) (BNPTCD): tris(8-quinolinolato)aluminum (Alq3)mixed films were investigated. It was found that BNPTCD:Alq3mixed films exhibit PL in the near-infrared wavelength region and that organic light-emitting diodes using Alq3highly doped with BNPTCD as an emitting layer exhibit near-infrared EL with a peak at 805 nm originating from BNPTCD aggregates. [J2601]

"Optimization scheme for the quantum efficiency of GaInN-based green-light-emitting diodes"

We have optimized the internal quantum efficiency (IQE) of GaInN/GaNquantum-well (QW) structures. For an emission wavelength of 460nm, a high IQE of 73% was achieved. For a longer emission wavelength, calculations predict higher oscillator strength for thinner QWs but higher In content. We observe an improvement in IQE of almost 50% when reducing the QW width from 2.7nmto1.8nm, and increasing the In content for the whole blue to green spectral region with IQE=40%at 525nm. The typical saturation of the output power with increasing current that occurs, particularly for green-light-emitting diodes, is extremely weak in our structures. [J2602]

"Thermal stability improvement by using Pd /NiO /Al /Ti /Au reflective ohmic contacts to p -GaN for flip-chip ultraviolet light-emitting diodes"

The thermal stability, optical reflectivity, and contact resistivity of Pd/NiO/Al/Ti/Auohmic contacts to p-type GaN were investigated. In contrast to Pd/Ni/Al/Ti/Au counterparts, the ohmic contacts Pd/NiO/Al/Ti/Auretained their specific contact resistivity ($3.34 \times 10^{-2} \Omega \text{ cm}^2$) and high reflectivity ($75\% @ 370 \text{ nm}$) after a long thermal aging at 200 °C for 100 h in nitrogen ambient. According to the results of the secondary ion mass spectroscopy in-depth profiles study, it is found that the NiO layer is more transparent and a better diffusion barrier than Ni to prevent the penetration of upper metals into p-type GaN during thermal treatment. [J2603]

"Phosphorescence of red Os (fptz)₂ (P Ph 2 Me)₂ doped organic light-emitting devices with n and p hosts"

We have applied a sterically hindered red phosphorescent dopant Os(fptz)₂(PPh₂Me)₂[fptz=3-trifluoromethyl-5-(2-pyridyl)-1,2,4-triazole, PPh₂Me=phosphineligand] in p-type 4,4'-N,N'-dicarbazole-biphenyl or n-type bis(2-methyl-8-quinolinolato)(p-phenylphenolato) aluminum host and found that the latter produced higher luminance efficiency at lower doping concentration. We present a model to rationalize this phenomenon in which the n-type host impedes hole transport, which leads to narrower recombination zone near the hole transport layer/emission layer interface than the p-type host, hence, more effective recombination. [J2604]

"Efficient hole injection in organic light-emitting diodes using C60 as a buffer layer for Al reflective anodes"

The hole injection of the organic light-emitting diodes with Al as a reflective anode for top-emitting devices was improved by using C60 as a thin buffer layer between Al and a hole transport layer. The driving voltage of the devices with C60 buffer layer was 5.5Vcompared with 11Vfor the devices without C60 buffer layer. The

decrease of interfacial energy barrier by interface dipole formation between Al and C60 contributed to the low driving voltage of the devices. [J2605]

"High-efficiency microcavity top-emitting organic light-emitting diodes using silver anode"

Top-emitting organic light-emitting diodes (TOLEDs) employing highly reflective Ag as anode and semitransparent LiF/Al/Agas cathode were fabricated. The hole injection efficiency of Ag anode can be significantly improved with surface modification using a CF₄ plasma. With C545T-doped Alq₃ emitter, the top-emitting device shows a low turn-on voltage of 2.65V. The optimized microcavity TOLED shows a current efficiency enhancement of 65% and a total outcoupling efficiency enhancement of 35%, compared with a conventional OLED. No color variation was observed in the forward 140° forward viewing cone. Strong dependence of efficiency on Ag cathode thickness was observed, in good agreement with numerical simulations. [J2606]

"GaN light-emitting diodes with Archimedean lattice photonic crystals"

We study GaN-based light emitting diodes incorporating an omnidirectional photonic crystal with Archimedean lattice. Photonic bands are observed over several Brillouin zones, revealing reciprocal space symmetries and evidencing the omnidirectionality of the photonic crystal. Intensities of the diffracted bands are found to agree with the Fourier transform of the crystal lattice, and confirm its Archimedean nature. [J2607]

"Anomalous temperature characteristics of single wide quantum well InGaN laser diode"

By using an atypically wide quantum well (95E) in the active layer of InGaN violet light emitting laser diode, we managed to fabricate a device characterized by very high thermal stability of the threshold current. The characteristic T₀ temperature was measured to be 302K, which is the highest reported value up to date. After thermal cycling of the device, T₀ drops down to the lower value of 220K. The very high value of T₀ in our devices is accompanied by anomalous temperature behavior of the device slope efficiency. The slope efficiency improves with increasing temperature, reaches a maximum and then gradually decreases. This behavior we interpret as the competition between a regular increase of the thermal carrier escape and an improvement of carrier capture efficiency with an opposite temperature dependence. The latter mechanism we tentatively attribute to the temperature quenching of the ballistic transport related carrier leakage from the active region of the laser diode. [J2608]

"Optical upconverter with integrated heterojunction phototransistor and light-emitting diode"

We report an optical upconversion device that converts input 1.5mcm light to output 0.87mcm light with a built-in gain mechanism. The device consists of an InGaAs/InP heterojunction phototransistor (HPT) integrated with a GaAs/AlGaAs light-emitting diode (LED) by wafer fusion process. Incoming 1.5mcm optical radiation is absorbed by the HPT, generating an amplified photocurrent. The resultant photocurrent drives the LED that emits at 0.87mcm, which could be detected by a conventional silicon charge-coupled device. Upconversion is demonstrated at room temperature with a gain of 20 from the HPT and an overall external upconversion efficiency of 0.07W/W. [J2609]

"Study of hole concentration of 1,4-bis[N-(1-naphthyl)-N'-phenylamino]-4,4' diamine doped with tungsten oxide by admittance spectroscopy"

The effect of tungsten oxide (WO₃) incorporation into 1,4-bis[N-(1-naphthyl)-N'-phenylamino]-4,4'diamine (NPB) layer is investigated in NPB-tris(8-hydroxyquinoline)aluminum heterojunction organic light-emitting diodes. The admittance spectroscopy studies show that increasing the WO₃ volume percentage from 0% to 16% can increase the hole concentration of the NPB layer from 1.9741014 to 1.9041017 cm⁻³ and decrease the activation energy of the resistance of the NPB layer from 0.354 to 0.176 eV. Thus, this incorporation reduces the Ohmic loss and increases the band bending in the NPB layer near the interface, resulting in an improved hole injection via tunneling through a narrow depletion region. [J2610]

"Analysis and control of the active area scaling effect on white organic light emitting diodes towards lighting applications"

The authors investigate the scaling of the performances on white organic light emitting diode in devices having active regions ranging from 0.25 to 9 cm². They observe a drop in the luminance and in the current density with increasing active area of the devices. A model where both these effects are ascribed to the spread of the current leakage on the indium tin oxide surface is proposed. To limit the consequences of these effects on the device performances, they insert a pattern of metal stripes onto the anode contact. This results in a device with a

maximum luminance of 1800cd/m² on a surface of 9cm². [J2611]

"Enhanced light emission from one-layered organic light-emitting devices doped with organic salt by simultaneous thermal and electrical annealing"

The authors studied the effect of thermal and electrical annealing on light emission of fluorescent one-layered organic light-emitting devices (OLEDs) doped with organic salts. From the annealed OLEDs, we clearly observed homogeneous and enhanced electroluminescent (EL) emission over the whole active area with fast responses. Moreover, improved efficiency was also observed from annealed phosphorescent OLEDs. These improved EL characteristics indicate that simultaneous annealing can induce proper adsorption of charged salt ions at the electrode surfaces, leading to enhanced electroluminescence of one-layered OLEDs due to increased and balanced injection of carriers. [J2612]

"Lithium manganese oxide as an effective buffer layer between organic and metal layers in organic light-emitting devices"

Tris(8-hydroxyquinolato)aluminum (Alq₃)-based organic light-emitting devices using a thermally deposited lithium manganese oxide layer between aluminum (Al) cathode and Alq₃ have been fabricated. The highest luminance efficiency obtained with a 1-nm-thick LiMnO₂ layer is very similar to that of the device with 1-nm-thick LiF. However, the device with an 18nmLiMnO₂ layer obtained a longer operational stability although the luminance efficiency is lower. The improvements are attributed to lithium extractions of the lithium manganese oxide layer and the interfacial properties between Alq₃ and Al are discussed. [J2613]

"Electric-field-induced fluorescence quenching in dye-doped tris(8-hydroxyquinoline) aluminum layers"

The authors measured electric-field-induced fluorescence quenching (EFIFQ) in both undoped and fluorescent dye-doped tris(8-hydroxyquinoline)aluminum (Alq₃) layers of organic light-emitting devices. Results show that doped Alq₃ layers demonstrate smaller EFIFQ than undoped ones. The phenomenon is attributed to the narrower energy band gap of the guest molecule relative to that of the host material, which makes it less prone to electric-field-induced dissociation of the excited state. Results also show that increasing the concentration of the guest material or decreasing its band gap leads to a decrease in EFIFQ. [J2614]

"Organic light-emitting device on a scanning probe cantilever"

Organic light-emitting devices (OLEDs) were fabricated on scanning probe cantilevers using a combination of thermally evaporated molecular organic compounds and metallic electrodes. Ion beam milling was used to define the emissive region in the shape of a ring having a diameter of less than 5μm and a narrow width. Stable light emission was observed from the device at forward bias, with a current-voltage response similar to that of archetypal OLEDs. Based on this device, a novel electrically pumped scanning optical microscopy tool is suggested. [J2615]

"Lateral light emitting n-i-p diodes in In Sb /Al x In 1-x Sb quantum wells"

Lateral light emitting diodes have been fabricated in InSb/Al_xIn_{1-x}Sb quantum wells using a simple bevel etching technique. The peak in emission was found to be in the range of 4-5μm, confirming that the emission was from the quantum well. [J2616]

"Fairly pure ultraviolet electroluminescence from ZnO-based light-emitting devices"

Fairly pure ultraviolet (UV) electroluminescence (EL) was realized on a ZnO-based metal-insulator (SiO_x, x ≤ 2)-semiconductor structure on a silicon substrate, which was easily fabricated by the reactive direct current sputtering and electron beam evaporation. The UV EL originated from the near-band-edge (NBE) emission of ZnO was achieved at room temperature when the device was under sufficient forward bias with the negative voltage applied on the silicon substrate. Moreover, the intermediate SiO_x layer should be thick enough to confine the electrons in the conduction band of ZnO beneath the ZnO/SiO_x interface, which is critical for generation of NBE emission from ZnO. [J2617]

"Improving the stability of organic light-emitting devices by using a thin Mg anode buffer layer"

Introducing a thin Mg layer at the hole injection contact of organic light-emitting devices remarkably improves their operational stability. Devices in which a 2.5nm thick Mg layer is inserted between the indium tin oxide anode and a tetrafluoro-tetracyanoquinodimethane-doped hole transport material layer exhibit a significantly

longer lifetime compared to similar devices without the Mg layer. After 600h of operation at a current density of 62.5 mA/cm² with a 50% duty cycle, the luminance of devices containing the Mg layer decreases by only 10% of the initial value. The stability enhancement resulting from using the Mg layer is attributed to improved balance in charge injection at the anode and cathode contacts. [J2618]

"Voltage drop in an (Al_xGa_{1-x})_{0.5}In_{0.5}P light-emitting diode probed by Kelvin probe force microscopy"

The authors report on quantitative investigations of the voltage drop across the heterostructure layer sequence of an operating AlGaInP light-emitting diode via Kelvin probe force microscopy for different external biases between -2.0 and +1.86 V. In the low voltage regime, most of the voltage drops in the active layer. For bias voltages above +1.5 V, however, they found an additional voltage drop on the p-side of the device, which reduces the power efficiency of the light-emitting diode. [J2619]

"Determination of junction temperature in AlGaInP/GaAs light emitting diodes by self-excited photoluminescence signal"

The photoluminescence (PL) of the GaAs substrate excited by the electroluminescence of the active layer is adopted to determine the junction temperature in AlGaInP/GaAs light emitting diodes. Based on the Varshni equation for GaAs, the temperature measured by this approach is consistent with that obtained by the emission peak energy shift approach. As the PL signal is generated within the substrate, no calibration dependent on the device structure is necessary to determine the junction temperature of the device. [J2620]

"Thermally crosslinked hole-transporting layers for cascade hole-injection and effective electron-blocking/exciton-confinement in phosphorescent polymer light-emitting diodes"

A bilayer hole-injection/transport structure was prepared by thermally crosslinking two separate hole-transport layers (HTL). The resulting films possess excellent optical quality and solvent resistance. Cascade hole-injection and effective electron-blocking/exciton confinement can be achieved for light-emitting diodes (LEDs) using blue phosphorescent emitters, such as bis(4',6'-difluorophenyl)pyridinato)tetrakis(1-pyrazolyl)borate. The first HTL was based on tetraphenyldiamine (TPD) has its highest occupied molecular orbit (HOMO) level lies at -5.3 eV, and the second HTL with 4,4',4''-tri(N-carbazolyl)triphenylamine has its HOMO level lies at -5.7 eV. The preliminary results from blue LEDs using these cascade HTLs showed much improved device performance than those only use a single layer hole-transporting polymer. [J2621]

"Highly efficient 7,8,10-triphenylfluoranthene-doped blue organic light-emitting diodes for display application"

We have demonstrated an organic light-emitting diode based on blue-fluorescent dopant 7,8,10-triphenylfluoranthene in a host of dipyrrenylfluorene derivatives. The device shows pure blue emission with a peak wavelength of 456 nm and Commission International de L'Eclairage coordinate at (0.164, 0.188). An electroluminescence efficiency as high as 3.33 cd/A and external quantum efficiency of 2.48% can be achieved. Comparison of the photoluminescence and electroluminescence spectra reveals a nearly identical exciton relaxation and efficient energy transfer from the host to the dopant. [J2622]

"Blue-yellow ZnO homostructural light-emitting diode realized by metalorganic chemical vapor deposition technique"

We report on the realization of ZnO homojunction light-emitting diodes (LEDs) fabricated by metalorganic chemical vapor deposition on (0001) ZnO bulk substrate. The p-type ZnO epilayer was formed by nitrogen incorporation using N₂O gas as oxidizing and doping sources. Distinct electroluminescence (EL) emissions in the blue and yellow regions were observed at room temperature by the naked eye under forward bias. The EL peak energy coincided with the photoluminescence peak energy of the ZnO epilayer, suggesting that the EL emissions emerge from the ZnO epilayer. In addition, the current-voltage and light output-voltage characteristics of ZnO homojunction LEDs have also been studied. [J2623]

"Fullerene-organic nanocomposite: A flexible material platform for organic light-emitting diodes"

CuPc:C60 organic-nanocarbon composite coated metals (Au, Ag, and ITO) are found to form efficient hole injection anode structures for organic light-emitting diodes (OLEDs). A significant increase (two times) in current efficiency has been observed in OLEDs when the nanocomposite anode structures are used to replace the conventional CuPc/indium tin oxide hole injection structure. Moreover, the composite anode structures

enable the use of simple metal electrodes for efficient and stable OLEDs. The composite provides, through a controlled variation in the C60 concentration, a flexible material platform in regulating the hole injection and transport through the various layers in an OLED. [J2624]

"Comment on "Singlet-singlet and singlet-heat annihilations in fluorescence-based organic light-emitting diodes under steady-state high current density" [JAppl. Phys. Lett. 86, 213506 (2005)]"

First Page of the Article [J2625]

"High efficiency red organic light-emitting devices using tetraphenyldibenzoperiflanthene-doped rubrene as an emitting layer"

Red organic light-emitting devices (OLEDs) have been developed employing a novel fluorescent emitting layer, tetraphenyldibenzoperiflanthene-doped rubrene. The devices are characterized by low driving voltage below 4V at a current density of 20 mA/cm² and high color purity with Commission Internationale de l'Eclairage coordinates of (0.66, 0.34). The OLED using the novel emitting layer in combination with the electron-transporting layer consisting of 9,10-bis[4-(6-methylbenzothiazol-2-yl)phenyl]anthracene exhibits a high power efficiency of 5.3 lm/W at a current density of 20 mA/cm². The half-luminance lifetime of the red OLED is 223 h at a current density of 80 mA/cm² (initial luminance of 3570 cd/m²). Both the driving voltage and current efficiency of the device are significantly improved compared to a device using tris(8-quinolinolato)aluminum as an electron-transporting layer. The studies on charge transport for the host materials indicate that the high efficiency is attributed to the improved charge injection and balance in the device. [J2626]

"InGaN quantum wells with small potential fluctuation grown on InGaN underlying layers"

A series of InGaN quantum wells (QWs) emitting blue-green, blue, violet, or ultraviolet light was grown on InGaN underlying layers (ULs). The potential fluctuation in these InGaN QWs was carefully measured using time-resolved photoluminescence, taking several steps to reduce the quantum confinement Stark effect. The potential fluctuation of InGaN QWs on InGaN ULs was smaller than that on conventional GaN ULs with the identical emission wavelength. A violet-light-emitting diode using an InGaN UL had the electroluminescence intensity approximately five times higher than the one using a conventional GaN UL under the low injection-current conditions, indicating that an InGaN UL effectively eliminates the nonradiative recombination centers in the InGaN QWs. [J2627]

"Bias voltage dependence of the electron spin injection studied in a three-terminal device based on a (Ga,Mn)As/n⁺-GaAs Esaki diode"

We investigated injection of spin polarized electrons in a (Ga,Mn)As/n⁺-GaAs Esaki diode (ED) by using a three-terminal device integrating a (Ga,Mn)As ED and a light emitting diode (LED). Electroluminescence polarization (PEL) from the LED was measured under the Faraday configuration as a function of bias voltages applied independently to the Esaki diode and to the LED. The maximum PEL of 32.4% was observed when the valence electrons near the Fermi energy of (Ga,Mn)As are ballistically injected into the LED. [J2628]

"First direct observation of self-imaging effect in active multimode-interference semiconductor laser diodes"

We report the first direct observation of the self-imaging effect in active multimode-interference semiconductor laser diodes (MMI-SLDs). Interference patterns inside laser diode waveguides were obtained by using the electroluminescence (EL) method. To the best of our knowledge, this result is the first direct observation of the self-imaging effect in self-photon-emitting active waveguides such as laser diodes. The observed EL pattern confirms the adequateness of the design of the higher light output-aimed MMI-SLDs. [J2629]

"Secure Device Pairing Based on a Visual Channel: Design and Usability Study"

"Pairing" is the establishment of authenticated key agreement between two devices over a wireless channel. Such devices are ad hoc in nature as they lack any common preshared secrets or trusted authority. Fortunately, these devices can be connected via auxiliary physical (audio, visual, tactile) channels which can be authenticated by human users. They can, therefore, be used to form the basis of a pairing operation. Recently proposed pairing protocols and methods are based upon bidirectional physical channels. However, various pairing scenarios are asymmetric in nature, i.e., only a unidirectional physical channel exists between two devices (such as between a cell phone and an access point). In this paper, we show how strong mutual authentication can be achieved even with a unidirectional visual channel, where prior methods could provide only a weaker property

termed as presence. This could help reduce the execution time and improve usability of prior pairing methods. In addition, by adopting recently proposed improved pairing protocols, we propose how visual channel authentication can be used even on devices that have very limited displaying capabilities, all the way down to a device whose display consists of a cheap single light-source, such as a light-emitting diode. We present the results of a preliminary usability study evaluating our proposed method. [J2630]

СПИСОК ЛИТЕРАТУРЫ

- J1106.** Fang H. Luminescent properties in the strain adjusted phosphor-free GaN based white light-emitting diode. / Fang H., Sang L. W., Zhao L. B., Qi S. L., Zhang Y. Z., Yang X. L., Yang Z. J., Zhang G. Y. // Applied Physics Letters. - 2008. - Vol. 93, No. 26. - P. 261117-261117-3. ↑
- J1107.** Wu Zhaoxin. Comment on "Surface plasmon coupled electroluminescent emission" [Appl. Phys. Lett. 92, 103304 (2008)]. / Wu Zhaoxin, Liang Shixiong, Jiao Bo, Zhao Xuanke, Hou Xun. // Applied Physics Letters. - 2008. - Vol. 93, No. 26. - P. 266101-266101-2. ↑
- J1108.** Koller D. M. Response to "Comment on 'Surface plasmon coupled electroluminescent emission'" [Appl. Phys. Lett. 93, 266101 (2008)]. / Koller D. M., Hohenau A., Dittlbacher H., Galler N., Aussenegg F. R., Leitner A., Krenn J. R., Eder S., Sax S., List E. J. W. // Applied Physics Letters. - 2008. - Vol. 93, No. 26. - P. 266102-266102-2. ↑
- J1109.** Huang Fei. Lithium salt doped conjugated polymers as electron transporting materials for highly efficient blue polymer light-emitting diodes. / Huang Fei, Shih Ping-I, Liu Michelle S., Shu Ching-Fong, Jen Alex K.-Y. // Applied Physics Letters. - 2008. - Vol. 93, No. 24. - P. 243302-243302-3. ↑
- J1110.** Fattal D. Design of an efficient light-emitting diode with 10 GHz modulation bandwidth. / Fattal D., Fiorentino M., Tan M., Houg D., Wang S. Y., Beausoleil Raymond G. // Applied Physics Letters. - 2008. - Vol. 93, No. 24. - P. 243501-243501-3. ↑
- J1111.** Yang Y. A p-n homojunction ZnO nanorod light-emitting diode formed by As ion implantation. / Yang Y., Sun X. W., Tay B. K., You G. F., Tan S. T., Teo K. L. // Applied Physics Letters. - 2008. - Vol. 93, No. 25. - P. 253107-253107-3. ↑
- J1112.** Hekmatshoar Bahman. Highly stable amorphous-silicon thin-film transistors on clear plastic. / Hekmatshoar Bahman, Cherenack Kunigunde H., Kattamis Alex Z., Long Ke, Wagner Sigurd, Sturm James C. // Applied Physics Letters. - 2008. - Vol. 93, No. 3. - P. 032103-032103-3. ↑
- J1113.** Yu X. A pure 1.5 mcm electroluminescence from metal-oxide-silicon tunneling diode using dislocation network. / Yu X., Seifert W., Vyvenko O. F., Kittler M., Wilhelm T., Reiche M. // Applied Physics Letters. - 2008. - Vol. 93, No. 4. - P. 041108-041108-3. ↑
- J1114.** Ha Mi-Young. Low voltage organic light-emitting devices with triphenylphosphine oxide layer. / Ha Mi-Young, Moon Dae-Gyu. // Applied Physics Letters. - 2008. - Vol. 93, No. 4. - P. 043306-043306-3. ↑
- J1115.** Meerheim Rico. High-efficiency monochrome organic light emitting diodes employing enhanced microcavities. / Meerheim Rico, Nitsche Robert, Leo Karl. // Applied Physics Letters. - 2008. - Vol. 93, No. 4. - P. 043310-043310-3. ↑
- J1116.** Dahal R. Current-injected 1.54 mcm light emitting diodes based on erbium-doped GaN. / Dahal R., Ugolini C., Lin J. Y., Jiang H. X., Zavada J. M. // Applied Physics Letters. - 2008. - Vol. 93, No. 3. - P. 033502-033502-3. ↑
- J1117.** Schubert Martin F. Polarization-matched Ga In N /Al Ga In N multi-quantum-well light-emitting diodes with reduced efficiency droop. / Schubert Martin F., Xu Jiuru, Kim Jong Kyu, Schubert E. Fred, Kim Min Ho, Yoon Sukho, Lee Soo Min, Sone Cheolsoo, Sakong Tan, Park Yongjo. // Applied Physics Letters. - 2008. - Vol. 93, No. 4. - P. 041102-041102-3. ↑
- J1118.** Bergenek K. Enhanced light extraction efficiency from AlGaInP thin-film light-emitting diodes with

photonic crystals. / Bergenek K., Wiesmann Ch., Wirth R., OFaolain L., Linder N., Streubel K., Krauss T. F. // Applied Physics Letters. - 2008. - Vol. 93, No. 4. - P. 041105-041105-3. ↑

J1119. Ishida Kunio. A revised Kubelka-Munk theory for spectral simulation of phosphor-based white light-emitting diodes. / Ishida Kunio, Mitsuishi Iwao, Hattori Yasushi, Nunoue Shinya. // Applied Physics Letters. - 2008. - Vol. 93, No. 24. - P. 241910-241910-3. ↑

J1120. Kingsley James W. Optical nanolithography using a scanning near-field probe with an integrated light source. / Kingsley James W., Ray Sumon K., Adawi Ali M., Leggett Graham J., Lidzey David G. // Applied Physics Letters. - 2008. - Vol. 93, No. 21. - P. 213103-213103-3. ↑

J1121. Takagi Rie. Metal patterning using maskless vacuum evaporation process based on selective deposition of photochromic diarylethene. / Takagi Rie, Masui Kyoko, Nakamura Shinichiro, Tsujioka Tsuyoshi. // Applied Physics Letters. - 2008. - Vol. 93, No. 21. - P. 213304-213304-3. ↑

J1122. Kim Jong Kyu. Elimination of total internal reflection in GaInN light-emitting diodes by graded-refractive-index micropillars. / Kim Jong Kyu, Noemaun Ahmed N., Mont Frank W., Meyaard David, Schubert E. Fred, Poxson David J., Kim Hyunsoo, Sone Cheolsoo, Park Yongjo. // Applied Physics Letters. - 2008. - Vol. 93, No. 22. - P. 221111-221111-3. ↑

J1123. Mandlik Prashant. Diffusion of atmospheric gases into barrier-layer sealed organic light emitting diodes. / Mandlik Prashant, Han Lin, Wagner Sigurd, Silvernail Jeff A., Ma Rui-Qing, Hack Michael, Brown Julie J. // Applied Physics Letters. - 2008. - Vol. 93, No. 20. - P. 203306-203306-3. ↑

J1124. Kita Takashi. Narrow-band deep-ultraviolet light emitting device using Al 1-x Gd x N. / Kita Takashi, Kitayama Shinya, Kawamura Masashi, Wada Osamu, Chigi Yoshitaka, Kasai Yoshihiro, Nishimoto Tetsuro, Tanaka Hiroyuki, Kobayashi Mikihiro. // Applied Physics Letters. - 2008. - Vol. 93, No. 21. - P. 211901-211901-3. ↑

J1125. Liang Chih-Hao. Synthesis and photoluminescence characteristics of color-tunable BaY 2 ZnO 5 :Eu 3+ phosphors. / Liang Chih-Hao, Chang Yee-Cheng, Chang Yee-Shin. // Applied Physics Letters. - 2008. - Vol. 93, No. 21. - P. 211902-211902-3. ↑

J1126. Meng Jian Xin. Efficient energy transfer for Ce to Nd in Nd /Ce codoped yttrium aluminum garnet. / Meng Jian Xin, Li Jin Qing, Shi Zhao Pu, Cheah Kok Wai. // Applied Physics Letters. - 2008. - Vol. 93, No. 22. - P. 221908-221908-3. ↑

J1127. Bergenek K. Directional light extraction from thin-film resonant cavity light-emitting diodes with a photonic crystal. / Bergenek K., Wiesmann Ch., Zull H., Wirth R., Sundgren P., Linder N., Streubel K., Krauss T. F. // Applied Physics Letters. - 2008. - Vol. 93, No. 23. - P. 231109-231109-3. ↑

J1128. Shen Kun-Ching. Enhanced and partially polarized output of a light-emitting diode with its InGaN/GaN quantum well coupled with surface plasmons on a metal grating. / Shen Kun-Ching, Chen Cheng-Yen, Chen Hung-Lu, Huang Chi-Feng, Kiang Yean-Woei, Yang C. C., Yang Ying-Jay. // Applied Physics Letters. - 2008. - Vol. 93, No. 23. - P. 231111-231111-3. ↑

J1129. Cho Chu-Young. In Ga N /Ga N multiple quantum wells grown on microfacets for white-light generation. / Cho Chu-Young, Park Il-Kyu, Kwon Min-Ki, Kim Ja-Yeon, Park Seong-Ju, Jung Dong-Ryul, Kwon Kwang-Woo. // Applied Physics Letters. - 2008. - Vol. 93, No. 24. - P. 241109-241109-3. ↑

J1130. Chen Chun-Yu. Light-emitting polymer space-charge-limited transistor. / Chen Chun-Yu, Chao Yu-Chiang, Meng Hsin-Fei, Horng Sheng-Fu. // Applied Physics Letters. - 2008. - Vol. 93, No. 22. - P. 223301-223301-3. ↑

J1131. Lee J. Erratum: "Degradation studies on high-voltage-driven organic light-emitting device using in situ on-operation method with scanning photoelectron microscopy" [Appl. Phys. Lett. 93, 133310 (2008)]. / Lee J., Sohn S., Yun H. J., Shin H. J. // Applied Physics Letters. - 2008. - Vol. 93, No. 22. - P. 229901-229901-1. ↑

J1132. Xie Guohua. Erratum: "Very low turn-on voltage and high brightness tris-(8-hydroxyquinoline)aluminum-based organic light-emitting diodes with a MoO x p -doping layer" [Appl. Phys. Lett. 92, 093305 (2008)]. / Xie Guohua, Meng Yanlong, Wu Fengmin, Tao Chen, Zhang Dandan, Liu Mingjun, Xue Qin, Chen Wen, Zhao Yi. // Applied Physics Letters. - 2008. - Vol. 93, No. 22. - P. 229902-229902-1. ↑

- J1133.** Feng Jing. Enhancement of surface plasmon-mediated radiative energy transfer through a corrugated metal cathode in organic light-emitting devices. / Feng Jing, Okamoto Takayuki, Naraoka Ryo, Kawata Satoshi. // Applied Physics Letters. - 2008. - Vol. 93, No. 5. - P. 051106-051106-3. ↑
- J1134.** Li Jianfeng. Indium tin oxide modified transparent nanotube thin films as effective anodes for flexible organic light-emitting diodes. / Li Jianfeng, Hu Liangbing, Liu Jun, Wang Lian, Marks Tobin J., Gruner George. // Applied Physics Letters. - 2008. - Vol. 93, No. 8. - P. 083306-083306-3. ↑
- J1135.** Murdoch G. B. A comparison of CuO and Cu₂O hole-injection layers for low voltage organic devices. / Murdoch G. B., Greiner M., Helander M. G., Wang Z. B., Lu Z. H. // Applied Physics Letters. - 2008. - Vol. 93, No. 8. - P. 083309-083309-3. ↑
- J1136.** Stathopoulos N. A. A combined experimental and simulation study on thickness dependence of the emission characteristics in multicolor single layer organic light-emitting diodes. / Stathopoulos N. A., Vasilopoulou M., Palilis L. C., Georgiadou D. G., Argitis P. // Applied Physics Letters. - 2008. - Vol. 93, No. 8. - P. 083310-083310-3. ↑
- J1137.** Wang Q. Influence of annealing temperature on optical properties of InGaN quantum dot based light emitting diodes. / Wang Q., Wang T., Bai J., Cullis A. G., Parbrook P. J., Ranalli F. // Applied Physics Letters. - 2008. - Vol. 93, No. 8. - P. 081915-081915-3. ↑
- J1138.** Fehse Karsten. Lifetime of organic light emitting diodes on polymer anodes. / Fehse Karsten, Meerheim Rico, Walzer Karsten, Leo Karl, Lovenich Wilfried, Elschner Andreas. // Applied Physics Letters. - 2008. - Vol. 93, No. 8. - P. 083303-083303-3. ↑
- J1139.** Gao X. D. Mechanism of charge generation in p-type doped layer in the connection unit of tandem-type organic light-emitting devices. / Gao X. D., Zhou J., Xie Z. T., Ding B. F., Qian Y. C., Ding X. M., Hou X. Y. // Applied Physics Letters. - 2008. - Vol. 93, No. 8. - P. 083304-083304-3. ↑
- J1140.** Helander M. G. Contact formation at the C₆₀/alkali-metal fluoride/Al interface. / Helander M. G., Wang Z. B., Lu Z. H. // Applied Physics Letters. - 2008. - Vol. 93, No. 8. - P. 083311-083311-3. ↑
- J1141.** Mezyk J. Exciton dissociation in tris(2-phenylpyridine) iridium (III) probed by electric field-assisted time-resolved photoluminescence. / Mezyk J., Meinardi F., Tubino R., Cocchi M. // Applied Physics Letters. - 2008. - Vol. 93, No. 9. - P. 093301-093301-3. ↑
- J1142.** Park Byoungchoo. Solution processable ionic p-i-n phosphorescent organic light-emitting diodes. / Park Byoungchoo, Han Mi Young, Oh Seung Seok. // Applied Physics Letters. - 2008. - Vol. 93, No. 9. - P. 093302-093302-3. ↑
- J1143.** Wang Hui. Current efficiency in organic light-emitting diodes with a hole-injection layer. / Wang Hui, Klubek Kevin P., Tang C. W. // Applied Physics Letters. - 2008. - Vol. 93, No. 9. - P. 093306-093306-3. ↑
- J1144.** Ho Meng-Huan. Electrical characterization of organic light-emitting diodes using dipotassium phthalate as n-type dopant. / Ho Meng-Huan, Hsieh Ming-Ta, Chen Teng-Ming, Chen Jenn-Fang, Hwang Shiao-Wen, Chen Chin H. // Applied Physics Letters. - 2008. - Vol. 93, No. 8. - P. 083505-083505-3. ↑
- J1145.** Carrington P. J. Room temperature midinfrared electroluminescence from InSb/InAs quantum dot light emitting diodes. / Carrington P. J., Solov'ev V. A., Zhuang Q., Krier A., Ivanov S. V. // Applied Physics Letters. - 2008. - Vol. 93, No. 9. - P. 091101-091101-3. ↑
- J1146.** Im Won Bin. A yellow-emitting Ce³⁺ phosphor, La_{1-x}Ce_xSr₂AlO₅, for white light-emitting diodes. / Im Won Bin, Kim Young-II, Fellows Natalie N., Masui Hisashi, Hirata G. A., DenBaars Steven P., Seshadri Ram. // Applied Physics Letters. - 2008. - Vol. 93, No. 9. - P. 091905-091905-3. ↑
- J1147.** Jang Ja-Soon. High output power GaN-based light-emitting diodes using an electrically reverse-connected p-Schottky diode and p-InGaN-GaN superlattice. Applied Physics Letters. - 2008. - Vol. 93, No. 8. - P. 081118-081118-3. ↑
- J1148.** Walker Bright. Solution-processed small molecule-based blue light-emitting diodes using conjugated polyelectrolytes as electron injection layers. / Walker Bright, Tamayo Arnold, Yang Jihua, Brzezinski Jacek Z., Nguyen Thuc-Quyen. // Applied Physics Letters. - 2008. - Vol. 93, No. 6. - P. 063302-063302-3. ↑

- J1149.** Chen En-Chen. Polymer infrared proximity sensor. / Chen En-Chen, Tseng Shin-Rong, Ju Jia-Hong, Yang Chia-Ming, Meng Hsin-Fei, Horng Sheng-Fu, Shu Ching-Fong. // Applied Physics Letters. - 2008. - Vol. 93, No. 6. - P. 063304-063304-3. ↑
- J1150.** Jeon Soon-Ok. 100% internal quantum efficiency and stable efficiency roll-off in phosphorescent light-emitting diodes using a high triplet energy hole transport material. / Jeon Soon-Ok, Yook Kyoung Soo, Joo Chul Woong, Lee Jun Yeob, Ko Kwang-Youn, Park Jong-Yek, Baek Yong Gu. // Applied Physics Letters. - 2008. - Vol. 93, No. 6. - P. 063306-063306-3. ↑
- J1151.** Jain R. Migration enhanced lateral epitaxial overgrowth of AlN and AlGaIn for high reliability deep ultraviolet light emitting diodes. / Jain R., Sun W., Yang J., Shatalov M., Hu X., Sattu A., Lunev A., Deng J., Shturm I., Bilenko Y., Gaska R., Shur M. S. // Applied Physics Letters. - 2008. - Vol. 93, No. 5. - P. 051113-051113-3. ↑
- J1152.** Zukauskas A. Spectral optimization of phosphor-conversion light-emitting diodes for ultimate color rendering. / Zukauskas A., Vaicekauskas R., Ivanauskas F., Vaitkevicius H., Shur M. S. // Applied Physics Letters. - 2008. - Vol. 93, No. 5. - P. 051115-051115-3. ↑
- J1153.** Kim Sung Hyun. Organic light emitting bistable memory device with high on/off ratio and low driving voltage. / Kim Sung Hyun, Yook Kyoung Soo, Lee Jun Yeob, Jang Jyongsik. // Applied Physics Letters. - 2008. - Vol. 93, No. 5. - P. 053306-053306-3. ↑
- J1154.** Yook Kyoung Soo. High efficiency, color stability, and stable efficiency roll off in three color hybrid white organic light emitting diodes. / Yook Kyoung Soo, Jeon Soon Ok, Joo Chul Woong, Lee Jun Yeob. // Applied Physics Letters. - 2008. - Vol. 93, No. 7. - P. 073302-073302-3. ↑
- J1155.** Chiu C. H. Nanoscale epitaxial lateral overgrowth of GaN-based light-emitting diodes on a SiO₂ nanorod-array patterned sapphire template. / Chiu C. H., Yen H. H., Chao C. L., Li Z. Y., Yu Peichen, Kuo H. C., Lu T. C., Wang S. C., Lau K. M., Cheng S. J. // Applied Physics Letters. - 2008. - Vol. 93, No. 8. - P. 081108-081108-3. ↑
- J1156.** Bayram C. A hybrid green light-emitting diode comprised of n-ZnO/(InGaIn/GaN) multi-quantum-wells/p-GaN. / Bayram C., Teherani F. Hosseini, Rogers D. J., Razeghi M. // Applied Physics Letters. - 2008. - Vol. 93, No. 8. - P. 081111-081111-3. ↑
- J1157.** Stier A. V. Electrical spin injection and optical detection in InAs based light emitting diodes. / Stier A. V., Meining C. J., McCombe B. D., Chado I., Grabs P., Schmidt G., Molenkamp L. W. // Applied Physics Letters. - 2008. - Vol. 93, No. 8. - P. 081112-081112-3. ↑
- J1158.** Schwartz Gregor. Balanced ambipolar charge carrier mobility in mixed layers for application in hybrid white organic light-emitting diodes. / Schwartz Gregor, Ke Tung-Huei, Wu Chung-Chih, Walzer Karsten, Leo Karl. // Applied Physics Letters. - 2008. - Vol. 93, No. 7. - P. 073304-073304-3. ↑
- J1159.** Meyer J. Indium-free transparent organic light emitting diodes with Al doped ZnO electrodes grown by atomic layer and pulsed laser deposition. / Meyer J., Gorn P., Hamwi S., Johannes H.-H., Riedl T., Kowalsky W. // Applied Physics Letters. - 2008. - Vol. 93, No. 7. - P. 073308-073308-3. ↑
- J1160.** Suchalkin Sergey. GaSb based light emitting diodes with strained InGaAsSb type I quantum well active regions. / Suchalkin Sergey, Jung Seungyong, Kipshidze Gela, Shterengas Leon, Hosoda Takashi, Westerfeld David, Snyder Donald, Belenky Gregory. // Applied Physics Letters. - 2008. - Vol. 93, No. 8. - P. 081107-081107-3. ↑
- J1161.** Shakya P. The magnetic field effect on the transport and efficiency of group III tris(8-hydroxyquinoline) organic light emitting diodes. / Shakya P., Desai P., Somerton M., Gannaway G., Kreouzis T., Gillin W. P. // Journal of Applied Physics. - 2008. - Vol. 103, No. 10. - P. 103715-103715-5. ↑
- J1162.** Jeong Soon Moon. Polarization-tunable electroluminescence using phase retardation based on photonic bandgap liquid crystal. / Jeong Soon Moon, Ha Na Young, Takezoe Hideo, Nishimura Suzushi, Suzuki Goro. // Journal of Applied Physics. - 2008. - Vol. 103, No. 11. - P. 113101-113101-4. ↑
- J1163.** Parshin Mikhail A. Hole transport in blue and white emitting polymers. / Parshin Mikhail A., Ollevier Jeroen, Van der Auweraer Mark, de Kok Margreet M., Nicolai Herman T., Hof Andre J., Blom Paul W. M. //

Journal of Applied Physics. - 2008. - Vol. 103, No. 11. - P. 113711-113711-7. ↑

J1164. Ohnishi Tsuyoshi. Defects and transport in complex oxide thin films. / Ohnishi Tsuyoshi, Shibuya Keisuke, Yamamoto Takahisa, Lippmaa Mikk. // Journal of Applied Physics. - 2008. - Vol. 103, No. 10. - P. 103703-103703-6. ↑

J1165. Cheng T.-H. Digital communication using Ge metal-insulator-semiconductor light-emitting diodes and photodetectors. / Cheng T.-H., Liao M. H., Yeh Lingyen, Lee T.-L., Liang M.-S., Liu C. W. // Journal of Applied Physics. - 2008. - Vol. 103, No. 1. - P. 016103-016103-3. ↑

J1166. Chen Jun. Enhanced efficiency in near-infrared inorganic/organic hybrid optical upconverter with an embedded mirror. / Chen Jun, Ban Dayan, Feng Xiaodong, Lu Zhenghong, Fatholoulumi Saeed, SpringThorpe Anthony J., Liu H. C. // Journal of Applied Physics. - 2008. - Vol. 103, No. 10. - P. 103112-103112-5. ↑

J1167. Arslan Engin. The persistent photoconductivity effect in AlGaIn/GaN heterostructures grown on sapphire and SiC substrates. / Arslan Engin, Butun Serkan, Lisesivdin S. Bora, Kasap Mehmet, Ozcelik Suleyman, Ozbay Ekmel. // Journal of Applied Physics. - 2008. - Vol. 103, No. 10. - P. 103701-103701-7. ↑

J1168. Zhao L. X. Degradation of GaN-based quantum well light-emitting diodes. / Zhao L. X., Thrush E. J., Humphreys C. J., Phillips W. A. // Journal of Applied Physics. - 2008. - Vol. 103, No. 2. - P. 024501-024501-6. ↑

J1169. Pavesi M. Implications of changes in the injection mechanisms on the low temperature electroluminescence in In Ga N /Ga N light emitting diodes. / Pavesi M., Manfredi M., Rossi F., Meneghini M., Meneghesso G., Zanoni E., Zehnder U. // Journal of Applied Physics. - 2008. - Vol. 103, No. 2. - P. 024503-024503-5. ↑

J1170. Matsushima Toshinori. Enhanced hole injection and transport in molybdenum-dioxide-doped organic hole-transporting layers. / Matsushima Toshinori, Adachi Chihaya. // Journal of Applied Physics. - 2008. - Vol. 103, No. 3. - P. 034501-034501-8. ↑

J1171. Baek Heume-II. Simple white organic light emitting diodes with improved color stability and efficiency using phosphorescent and fluorescent emitters. / Baek Heume-II, Lee Changhee. // Journal of Applied Physics. - 2008. - Vol. 103, No. 12. - P. 124504-124504-5. ↑

J1172. Jo Sung Jin. Increase in indium diffusion by tetrafluoromethane plasma treatment and its effects on the device performance of polymer light-emitting diodes. / Jo Sung Jin, Kim Chang Su, Kim Jong Bok, Ryu Seung Yoon, Noh Joo Hyon, Baik Hong Koo, Kim Youn Sang, Lee Se-Jong. // Journal of Applied Physics. - 2008. - Vol. 103, No. 11. - P. 114502-114502-4. ↑

J1173. Shin Dong-Youn. Theoretical investigation of the influence of nozzle diameter variation on the fabrication of thin film transistor liquid crystal display color filters. / Shin Dong-Youn, Smith Patrick J. // Journal of Applied Physics. - 2008. - Vol. 103, No. 11. - P. 114905-114905-11. ↑

J1174. Yokoyama Daisuke. Spectrally narrow emissions at cutoff wavelength from edges of optically and electrically pumped anisotropic organic films. / Yokoyama Daisuke, Moriwake Masato, Adachi Chihaya. // Journal of Applied Physics. - 2008. - Vol. 103, No. 12. - P. 123104-123104-13. ↑

J1175. Croxall A. F. Patterned backgating using single-sided mask aligners: Application to density-matched electron-hole bilayers. / Croxall A. F., Das Gupta K., Nicoll C. A., Thangaraj M., Farrer I., Ritchie D. A., Pepper M. // Journal of Applied Physics. - 2008. - Vol. 104, No. 11. - P. 113715-113715-5. ↑

J1176. Hiramatsu Hidenori. Characterization of copper selenide thin film hole-injection layers deposited at room temperature for use with p -type organic semiconductors. / Hiramatsu Hidenori, Koizumi Ikue, Kim Ki-Beom, Yanagi Hiroshi, Kamiya Toshio, Hirano Masahiro, Matsunami Noriaki, Hosono Hideo. // Journal of Applied Physics. - 2008. - Vol. 104, No. 11. - P. 113723-113723-8. ↑

J1177. Chen Sy-Hann. Nanoscale surface electrical properties of aluminum zinc oxide thin films investigated by scanning probe microscopy. / Chen Sy-Hann, Yu Chang-Feng, Lin Yung-Shao, Xie Wen-Jia, Hsu Ting-Wei, Tsai Din Ping. // Journal of Applied Physics. - 2008. - Vol. 104, No. 11. - P. 114314-114314-6. ↑

J1178. Chen Mei-Hsin. The roles of thermally evaporated cesium carbonate to enhance the electron injection in organic light emitting devices. / Chen Mei-Hsin, Wu Chih-I. // Journal of Applied Physics. - 2008. - Vol. 104,

No. 11. - P. 113713-113713-4. ↑

J1179. Park Seoung-Hwan. Electronic and optical properties of 530 nm strain-compensated hybrid InGaN/InGaN/ZnO quantum well light-emitting diodes. / Park Seoung-Hwan, Lee Yong-Tak, Park Jongwoon. // Journal of Applied Physics. - 2008. - Vol. 104, No. 3. - P. 036106-036106-3. ↑

J1180. Hoex B. On the c-Si surface passivation mechanism by the negative-charge-dielectric Al₂O₃. / Hoex B., Gielis J. J. H., van de Sanden M. C. M., Kessels W. M. M. // Journal of Applied Physics. - 2008. - Vol. 104, No. 11. - P. 113703-113703-7. ↑

J1181. Renaud Cedric. Study of trap states in polyspirobifluorene based devices: Influence of chromophore addition. / Renaud Cedric, Nguyen Thien-Phap. // Journal of Applied Physics. - 2008. - Vol. 104, No. 11. - P. 113705-113705-8. ↑

J1182. Gao Haiyong. Enhancement of the light output power of InGaN/GaN light-emitting diodes grown on pyramidal patterned sapphire substrates in the micro- and nanoscale. / Gao Haiyong, Yan Fawang, Zhang Yang, Li Jinmin, Zeng Yiping, Wang Guohong. // Journal of Applied Physics. - 2008. - Vol. 103, No. 1. - P. 014314-014314-5. ↑

J1183. Khan M. A. Electron mobility of 4,7-diphenyl-1,10-phenanthroline estimated by using space-charge-limited currents. / Khan M. A., Xu Wei, Khizar-ul-Haq, Bai Yu, Jiang X. Y., Zhang Z. L., Zhu W. Q. // Journal of Applied Physics. - 2008. - Vol. 103, No. 1. - P. 014509-014509-4. ↑

J1184. Fang H. Analysis of mass transport mechanism in InGaN epitaxy on ridge shaped selective area growth GaN by metal organic chemical vapor deposition. / Fang H., Yang Z. J., Wang Y., Dai T., Sang L. W., Zhao L. B., Yu T. J., Zhang G. Y. // Journal of Applied Physics. - 2008. - Vol. 103, No. 1. - P. 014908-014908-4. ↑

J1185. Dussaigne A. High doping level in Mg-doped GaN layers grown at low temperature. / Dussaigne A., Damilano B., Brault J., Massies J., Feltin E., Grandjean N. // Journal of Applied Physics. - 2008. - Vol. 103, No. 1. - P. 013110-013110-6. ↑

J1186. Nikiforov A. Yu. Effects of bias on cathodoluminescence in ZnCdSe quantum well light emitting diodes. / Nikiforov A. Yu., Cargill G. S., Guo S. P., Tamargo M. C. // Journal of Applied Physics. - 2008. - Vol. 104, No. 11. - P. 114506-114506-24. ↑

J1187. Lim J. T. Top-emitting organic light-emitting diodes with Ba /Ag /indium tin oxide cathode and built-in potential analyses in these devices. / Lim J. T., Lee J. H., Yeom G. Y., Lee E. H., Kim T. W. // and Films Journal of Vacuum Science & Technology A: Vacuum, Surfaces. - 2008. - Vol. 26, No. 4. - P. 961-965. ↑

J1188. Liao M. H. 2.0 mcm electroluminescence from Si /Si 0.2 Ge 0.8 type II heterojunctions. / Liao M. H., Cheng T.-H., Liu C. W., Yeh Lingyen, Lee T.-L., Liang M.-S. // Journal of Applied Physics. - 2008. - Vol. 103, No. 1. - P. 013105-013105-4. ↑

J1189. Xing Rubo. Undercut structure fabricated by complementary-structure micropatterning technique for the passive-matrix display of organic light-emitting diodes. / Xing Rubo, Xuan Yu, Ma Dongge, Han Yanchun. // Journal of Vacuum Science & Technology B: Microelectronics and Nanometer Structures. - 2008. - Vol. 26, No. 1. - P. 1-5. ↑

J1190. Clarysse Trudo. Insights in junction photovoltage based sheet resistance measurements for advanced complementary metal-oxide semiconductor. / Clarysse Trudo, Moussa Alain, Zangerle Thomas, Schaus Frederic, Vandervorst Wilfried, Faifer Vladimir, Current Michael. // Journal of Vacuum Science & Technology B: Microelectronics and Nanometer Structures. - 2008. - Vol. 26, No. 1. - P. 420-424. ↑

J1191. Zhang Yu. Fully sealed carbon nanotube flat-panel light source and its application as thin film transistor-liquid-crystal display backlight. / Zhang Yu, Deng S. Z., Xu N. S., Chen Jun. // Journal of Vacuum Science & Technology B: Microelectronics and Nanometer Structures. - 2008. - Vol. 26, No. 3. - P. 1033-1037. ↑

J1192. Satoh Toshikazu. Interfacial reactions between indium tin oxide and triphenylamine tetramer layers induced by photoirradiation. / Satoh Toshikazu, Fujikawa Hisayoshi, Yamamoto Ichiro, Murasaki Takanori, Kato Yoshifumi. // Journal of Applied Physics. - 2008. - Vol. 103, No. 9. - P. 093543-093543-4. ↑

J1193. Vaitonis Z. Measurement of the junction temperature in high-power light-emitting diodes from the high-energy wing of the electroluminescence band. / Vaitonis Z., Vitta P., Zukauskas A. // Journal of Applied Physics. - 2008. - Vol. 103, No. 9. - P. 093110-093110-7. ↑

J1194. Neyts Kristiaan. Conductor grid optimization for luminance loss reduction in organic light emitting diodes. / Neyts Kristiaan, Real Alfonso, Marescaux Matthias, Mladenovski Saso, Beeckman Jeroen. // Journal of Applied Physics. - 2008. - Vol. 103, No. 9. - P. 093113-093113-5. ↑

J1195. Rossi F. Field dependence of the carrier injection mechanisms in InGaN Quantum wells: Its effect on the luminescence properties of blue light emitting diodes. / Rossi F., Salviati G., Pavesi M., Manfredi M., Meneghini M., Zanoni E., Zehnder U. // Journal of Applied Physics. - 2008. - Vol. 103, No. 9. - P. 093504-093504-7. ↑

J1196. Feng Weifeng. A switched supply tunable red-green-blue light emitting diode driver. / Feng Weifeng, Shi Frank G., He Yongzhi, Zhao Bin. // Review of Scientific Instruments. - 2008. - Vol. 79, No. 4. - P. 044701-044701-5. ↑

J1197. Wang Pin. A whole-field polariscope using a liquid crystal polarization rotator. / Wang Pin, Asundi Anand. // Review of Scientific Instruments. - 2008. - Vol. 79, No. 6. - P. 063105-063105-5. ↑

J1198. Torbrugge S. Improvement of a dynamic scanning force microscope for highest resolution imaging in ultrahigh vacuum. / Torbrugge S., Lubbe J., Troger L., Cranney M., Eguchi T., Hasegawa Y., Reichling M. // Review of Scientific Instruments. - 2008. - Vol. 79, No. 8. - P. 083701-083701-7. ↑

J1199. Shimomura T. Development of a compact optical system for microarray scanning using a DVD pickup head. / Shimomura T., Izawa C., Matsui T. // Review of Scientific Instruments. - 2008. - Vol. 79, No. 3. - P. 035101-035101-6. ↑

J1200. Hui Lin. Flexible organic light-emitting diodes with improved performance by insertion of an UV-sensitive layer. / Hui Lin, Junsheng Yu, Nana Wang, Chunhua Huang, Yadong Jiang. // Journal of Vacuum Science & Technology B: Microelectronics and Nanometer Structures. - 2008. - Vol. 26, No. 4. - P. 1379-1381. ↑

J1201. Palma A. J. Portable light-emitting diode-based photometer with one-shot optochemical sensors for measurement in the field. / Palma A. J., Ortigosa J. M., Lapresta-Fernandez A., Fernandez-Ramos M. D., Carvajal M. A., Capitan-Vallvey L. F. // Review of Scientific Instruments. - 2008. - Vol. 79, No. 10. - P. 103105-103105-8. ↑

J1202. Yoo S. J. Hyperthermal neutral beam sources for material processing (invited). / Yoo S. J., Kim D. C., Joung M., Kim J. S., Lee B. J., Oh K. S., Kim K. U., Kim Y. H., Kim Y. W., Choi S. W., Son H. J., Park Y. C., Jang J.-N., Hong M. P. // Review of Scientific Instruments. - 2008. - Vol. 79, No. 2. - P. 02C301-02C301-5. ↑

J1203. Wu L. K. Enhanced light absorption in Ga N /Al Ga N midinfrared detectors and application for pixel-less upconversion imaging. / Wu L. K., Hao H. L., Shen W. Z. // Journal of Applied Physics. - 2008. - Vol. 103, No. 4. - P. 044507-044507-7. ↑

J1204. Kim Moojin. Effects of high pressure annealing on the characteristics of solid phase crystallization poly-Si thin-film transistors. / Kim Moojin, Kim Kyoung-Bo, Lee Ki-Yong, Yu CheolHo, Kim Hye-Dong, Chung Ho-Kyoon. // Journal of Applied Physics. - 2008. - Vol. 103, No. 4. - P. 044508-044508-5. ↑

J1205. Giebink N. C. Intrinsic luminance loss in phosphorescent small-molecule organic light emitting devices due to bimolecular annihilation reactions. / Giebink N. C., DAndrade B. W., Weaver M. S., Mackenzie P. B., Brown J. J., Thompson M. E., Forrest S. R. // Journal of Applied Physics. - 2008. - Vol. 103, No. 4. - P. 044509-044509-9. ↑

J1206. Huh Jin Woo. Characteristics of organic light-emitting diodes with conducting polymer anodes on plastic substrates. / Huh Jin Woo, Kim Young Min, Park Young Wook, Choi Jin Hwan, Lee Jin Woo, Lee Jong Woo, Yang Jae Woong, Ju Sung Hoo, Paek Kyeong Kap, Ju Byeong Kwon. // Journal of Applied Physics. - 2008. - Vol. 103, No. 4. - P. 044502-044502-6. ↑

J1207. Li Fenghong. Blue organic light-emitting diodes based on Mes 2 B [p-4,4' -biphenyl-NPh(1-naphthyl)]. / Li Fenghong, Jia Wenli, Wang Suning, Zhao Yiqun, Lu Zheng-Hong. // Journal of Applied Physics. - 2008. - Vol. ↑

103, No. 3. - P. 034509-034509-6. ↑

J1208. Rosenow Thomas Conrad. Near-infrared organic light emitting diodes based on heavy metal phthalocyanines. / Rosenow Thomas Conrad, Walzer Karsten, Leo Karl. // Journal of Applied Physics. - 2008. - Vol. 103, No. 4. - P. 043105-043105-4. ↑

J1209. Shakya P. Magnetoresistance in triphenyl-diamine derivative blue organic light emitting devices. / Shakya P., Desai P., Kreouzis T., Gillin W. P. // Journal of Applied Physics. - 2008. - Vol. 103, No. 4. - P. 043706-043706-5. ↑

J1210. Mont Frank W. High-refractive-index TiO₂-nanoparticle-loaded encapsulants for light-emitting diodes. / Mont Frank W., Kim Jong Kyu, Schubert Martin F., Schubert E. Fred, Siegel Richard W. // Journal of Applied Physics. - 2008. - Vol. 103, No. 8. - P. 083120-083120-6. ↑

J1211. Bernardo Gabriel. Spin cast thin polymer interlayers in polymer light-emitting diodes: Thickness control through use of cross-linkable polymers. / Bernardo Gabriel, Charas Ana, Alcacer Luis, Morgado Jorge. // Journal of Applied Physics. - 2008. - Vol. 103, No. 8. - P. 084510-084510-7. ↑

J1212. Reynolds C. L. Tunneling entity in different injection regimes of InGaN light emitting diodes. / Reynolds C. L., Patel A. // Journal of Applied Physics. - 2008. - Vol. 103, No. 8. - P. 086102-086102-2. ↑

J1213. Zaumseil Jana. Quantum efficiency of ambipolar light-emitting polymer field-effect transistors. / Zaumseil Jana, McNeill Christopher R., Bird Matt, Smith Darryl L., Paul Ruden P., Roberts Matthew, McKiernan Mary J., Friend Richard H., Sirringhaus Henning. // Journal of Applied Physics. - 2008. - Vol. 103, No. 6. - P. 064517-064517-10. ↑

J1214. Kim Sung Hyun. Triplet host engineering for triplet exciton management in phosphorescent organic light-emitting diodes. / Kim Sung Hyun, Jang Jyongsik, Yook Kyoung Soo, Lee Jun Yeob, Gong Myoung-Seon, Ryu Sangouk, Chang Gee-keun, Chang Ho Jung. // Journal of Applied Physics. - 2008. - Vol. 103, No. 5. - P. 054502-054502-4. ↑

J1215. Baek Heume-II. Electroluminescence characteristics of n-type matrix materials doped with iridium-based green and red phosphorescent emitters. / Baek Heume-II, Lee Changhee. // Journal of Applied Physics. - 2008. - Vol. 103, No. 5. - P. 054510-054510-6. ↑

J1216. Meneghini M. A model for the thermal degradation of metal/(p-GaN) interface in GaN-based light emitting diodes. / Meneghini M., Rigutti L., Trevisanello L. R., Cavallini A., Meneghesso G., Zanoni E. // Journal of Applied Physics. - 2008. - Vol. 103, No. 6. - P. 063703-063703-7. ↑

J1217. Karim A. Influence of exposure to 980 nm laser radiation on the luminescence of Si:Er/O light-emitting diodes. / Karim A., Du C.-X., Hansson G. V. // Journal of Applied Physics. - 2008. - Vol. 104, No. 12. - P. 123110-123110-6. ↑

J1218. Yu Young-Jun. p-type doping in organic light emitting diodes based on fluorinated C60. / Yu Young-Jun, Solomeshch Olga, Chechik Helena, Goryunkov A. A., Tuktarov R. F., Choi Dong Hoon, Jin Jung-II, Eichen Yoav, Tessler Nir. // Journal of Applied Physics. - 2008. - Vol. 104, No. 12. - P. 124505-124505-3. ↑

J1219. Aggarwal Ravi. Fabrication of Ag-tetracyanoquinodimethane nanostructures using ink-jet printing/vapor-solid chemical reaction process. / Aggarwal Ravi, Narayan Roger J., Xiao Kai, Geohegan David B. // Journal of Vacuum Science & Technology B: Microelectronics and Nanometer Structures. - 2008. - Vol. 26, No. 6. - P. L48-L52. ↑

J1220. Nowy Stefan. Light extraction and optical loss mechanisms in organic light-emitting diodes: Influence of the emitter quantum efficiency. / Nowy Stefan, Krummacher Benjamin C., Frischeisen Jorg, Reinke Nils A., Brutting Wolfgang. // Journal of Applied Physics. - 2008. - Vol. 104, No. 12. - P. 123109-123109-9. ↑

J1221. Zang F. X. Reduced efficiency roll-off in phosphorescent organic light emitting diodes at ultrahigh current densities by suppression of triplet-polaron quenching. / Zang F. X., Sum T. C., Huan A. C. H., Li T. L., Li W. L., Zhu Furong. // Applied Physics Letters. - 2008. - Vol. 93, No. 2. - P. 023309-023309-3. ↑

J1222. Langridge Justin M. A broadband absorption spectrometer using light emitting diodes for ultrasensitive, in situ trace gas detection. / Langridge Justin M., Ball Stephen M., Shillings Alexander J. L., Jones Roderic L. // ↑

Review of Scientific Instruments. - 2008. - Vol. 79, No. 12. - P. 123110-123110-14.

J1223. Huang Chi-Feng. Enhanced efficiency and reduced spectral shift of green light-emitting-diode epitaxial structure with prestrained growth. / Huang Chi-Feng, Liu Tzu-Chi, Lu Yen-Cheng, Shiao Wen-Yu, Chen Yung-Sheng, Wang Jyun-Kai, Lu Chih-Feng, Yang C. C. // Journal of Applied Physics. - 2008. - Vol. 104, No. 12. - P. 123106-123106-7. ↑

J1224. Kim Hyunsoo. Light extraction enhancement of GaN-based light emitting diodes using MgF₂/Al omnidirectional reflectors. / Kim Hyunsoo, Lee Sung-Nam, Park Youngjo, Kim Kyoung-Kook, Kwak Joon Seop, Seong Tae-Yeon. // Journal of Applied Physics. - 2008. - Vol. 104, No. 5. - P. 053111-053111-4. ↑

J1225. Tsai Chia-Hung. Surface modification of ZnO film by hydrogen peroxide solution. / Tsai Chia-Hung, Wang Wei-Chin, Jenq Feng-Lin, Liu Chien-Chih, Hung Chen-I, Houg Mau-Phon. // Journal of Applied Physics. - 2008. - Vol. 104, No. 5. - P. 053521-053521-4. ↑

J1226. Katkova Marina A. Electroluminescent characteristics of scandium and yttrium 8-quinolinolates. / Katkova Marina A., Ilichev Vasilii A., Konev Alexey N., Bochkarev Mikhail N., Vitukhnovsky Alexey G., Parshin Mikhail A., Pandey Lesley, Van der Auweraer Mark. // Journal of Applied Physics. - 2008. - Vol. 104, No. 5. - P. 053706-053706-3. ↑

J1227. Tripathy S. GaN-based microdisk light emitting diodes on (111)-oriented nanosilicon-on-insulator templates. / Tripathy S., Sale T. E., Dadgar A., Lin V. K. X., Zang K. Y., Teo S. L., Chua S. J., Blasing J., Krost A. // Journal of Applied Physics. - 2008. - Vol. 104, No. 5. - P. 053106-053106-7. ↑

J1228. Cardozo B. L. Patterning of polyfluorene based polymer light emitting diodes by reversal imprint lithography. / Cardozo B. L., Pang S. W. // Journal of Vacuum Science & Technology B: Microelectronics and Nanometer Structures. - 2008. - Vol. 26, No. 6. - P. 2385-2389. ↑

J1229. Lu Chih-Feng. Dependence of spectral behavior in an InGaN/GaN quantum-well light-emitting diode on the prestrained barrier thickness. / Lu Chih-Feng, Huang Chi-Feng, Chen Yung-Sheng, Yang C. C. // Journal of Applied Physics. - 2008. - Vol. 104, No. 4. - P. 043108-043108-5. ↑

J1230. Liao L. S. Moisture exposure to different layers in organic light-emitting diodes and the effect on electroluminescence characteristics. / Liao L. S., Tang C. W. // Journal of Applied Physics. - 2008. - Vol. 104, No. 4. - P. 044501-044501-8. ↑

J1231. Liu Hong-Mei. High-efficiency endothermic energy transfer in polymeric light-emitting devices based on cyclometalated Ir complexes. / Liu Hong-Mei, Wang Peng-Fei, He Jian, Zheng Caijun, Zhang Xiao-Hong, Chew Siew-Ling, Lee Chun-Sing, Chang Jack, Lee Shuit-Tong. // Applied Physics Letters. - 2008. - Vol. 92, No. 2. - P. 023301-023301-3. ↑

J1232. Ryu Seung Yoon. Transparent organic light-emitting diodes consisting of a metal oxide multilayer cathode. / Ryu Seung Yoon, Noh Joo Hyon, Hwang Byoung Har, Kim Chang Su, Jo Sung Jin, Kim Jong Tae, Hwang Hyeon Seok, Baik Hong Koo, Jeong Hee Seong, Lee Chang Ho, Song Seung Yong, Choi Seung Ho, Park Si Young. // Applied Physics Letters. - 2008. - Vol. 92, No. 2. - P. 023306-023306-3. ↑

J1233. Kim Sung Hyun. Stable efficiency roll-off in phosphorescent organic light-emitting diodes. / Kim Sung Hyun, Jang Jyongsik, Yook Kyoung Soo, Lee Jun Yeob. // Applied Physics Letters. - 2008. - Vol. 92, No. 2. - P. 023513-023513-3. ↑

J1234. Zhu T. Mist fabrication of light emitting diodes with colloidal nanocrystal quantum dots. / Zhu T., Shanmugasundaram K., Price S. C., Ruzyllo J., Zhang F., Xu J., Mohny S. E., Zhang Q., Wang A. Y. // Applied Physics Letters. - 2008. - Vol. 92, No. 2. - P. 023111-023111-3. ↑

J1235. Chamings J. Physical properties and efficiency of GaNP light emitting diodes. / Chamings J., Ahmed S., Sweeney S. J., Odnoblyudov V. A., Tu C. W. // Applied Physics Letters. - 2008. - Vol. 92, No. 2. - P. 021101-021101-3. ↑

J1236. Kuo Hon-Yi. A Sn-based metal substrate technology for the fabrication of vertical-structured GaN-based light-emitting diodes. / Kuo Hon-Yi, Wang Shui-Jinn, Wang Pei-Ren, Uang Kai-Ming, Chen Tron-Min, Kuan Hon. // Applied Physics Letters. - 2008. - Vol. 92, No. 2. - P. 021105-021105-3. ↑

- J1237.** Xu Yun. Phosphor-conversion white light using InGaN ultraviolet laser diode. / Xu Yun, Chen Lianghui, Li Yuzhang, Song Guofeng, Wang Yuping, Zhuang Weidong, Long Zhen. // Applied Physics Letters. - 2008. - Vol. 92, No. 2. - P. 021129-021129-3. ↑
- J1238.** Horng Ray-Hua. Light extraction enhancement of InGaN light-emitting diode by roughening both undoped micropillar-structure GaN and p-GaN as well as employing an omnidirectional reflector. / Horng Ray-Hua, Zheng Xinhe, Hsieh Chuang-Yu, Wu Dong-Sing. // Applied Physics Letters. - 2008. - Vol. 93, No. 2. - P. 021125-021125-3. ↑
- J1239.** Funato M. Emission color tunable light-emitting diodes composed of InGaN multifacet quantum wells. / Funato M., Hayashi K., Ueda M., Kawakami Y., Narukawa Y., Mukai T. // Applied Physics Letters. - 2008. - Vol. 93, No. 2. - P. 021126-021126-3. ↑
- J1240.** Misaki Masahiro. Highly efficient polarized polymer light-emitting diodes utilizing oriented films of beta-phase poly(9,9-dioctylfluorene). / Misaki Masahiro, Chikamatsu Masayuki, Yoshida Yuji, Azumi Reiko, Tanigaki Nobutaka, Yase Kiyoshi, Nagamatsu Shuichi, Ueda Yasukiyo. // Applied Physics Letters. - 2008. - Vol. 93, No. 2. - P. 023304-023304-3. ↑
- J1241.** Kim Ja-Yeon. Enhanced light extraction efficiency in flip-chip GaN light-emitting diodes with diffuse Ag reflector on nanotextured indium-tin oxide. / Kim Ja-Yeon, Kwon Min-Ki, Park Il-Kyu, Cho Chu-Young, Park Seong-Ju, Jeon Dong-Min, Kim Je Won, Kim Yong Chun. // Applied Physics Letters. - 2008. - Vol. 93, No. 2. - P. 021121-021121-3. ↑
- J1242.** Liu J. P. Barrier effect on hole transport and carrier distribution in InGaN/GaN multiple quantum well visible light-emitting diodes. / Liu J. P., Ryou J.-H., Dupuis R. D., Han J., Shen G. D., Wang H. B. // Applied Physics Letters. - 2008. - Vol. 93, No. 2. - P. 021102-021102-3. ↑
- J1243.** Zukauskas A. Rendering a color palette by light-emitting diodes. / Zukauskas A., Vaicekauskas R., Ivanauskas F., Vaitkevicius H., Shur M. S. // Applied Physics Letters. - 2008. - Vol. 93, No. 2. - P. 021109-021109-3. ↑
- J1244.** Hovel S. Room temperature electrical spin injection in remanence. / Hovel S., Gerhardt N. C., Hofmann M. R., Lo F.-Y., Ludwig A., Reuter D., Wieck A. D., Schuster E., Wende H., Keune W., Petravic O., Westerholt K. // Applied Physics Letters. - 2008. - Vol. 93, No. 2. - P. 021117-021117-3. ↑
- J1245.** Chin Patrick T. K. Energy transfer in hybrid quantum dot light-emitting diodes. / Chin Patrick T. K., Hikmet Rifat A. M., Janssen Rene A. J. // Journal of Applied Physics. - 2008. - Vol. 104, No. 1. - P. 013108-013108-6. ↑
- J1246.** Wong F. L. Long-lifetime thin-film encapsulated organic light-emitting diodes. / Wong F. L., Fung M. K., Tao S. L., Lai S. L., Tsang W. M., Kong K. H., Choy W. M., Lee C. S., Lee S. T. // Journal of Applied Physics. - 2008. - Vol. 104, No. 1. - P. 014509-014509-4. ↑
- J1247.** Meerheim Rico. Influence of charge balance and exciton distribution on efficiency and lifetime of phosphorescent organic light-emitting devices. / Meerheim Rico, Scholz Sebastian, Olthof Selina, Schwartz Gregor, Reineke Sebastian, Walzer Karsten, Leo Karl. // Journal of Applied Physics. - 2008. - Vol. 104, No. 1. - P. 014510-014510-8. ↑
- J1248.** Helander M. G. Comparison of Alq₃/alkali-metal fluoride/Al cathodes for organic electroluminescent devices. / Helander M. G., Wang Z. B., Mordoukhovski L., Lu Z. H. // Journal of Applied Physics. - 2008. - Vol. 104, No. 9. - P. 094510-094510-6. ↑
- J1249.** Chen Zhifeng. Luminescence quenching in low doped polymer light-emitting diodes. / Chen Zhifeng, Wang Hui, Li Aizhen, Shen Yong, Wang Yaxue, Zhang Wei, Yu Hancheng, Huang Jinwang, Lai Tianshu, Ji Liangnian. // Journal of Applied Physics. - 2008. - Vol. 104, No. 9. - P. 093513-093513-5. ↑
- J1250.** Kondakova Marina E. High-efficiency, low-voltage phosphorescent organic light-emitting diode devices with mixed host. / Kondakova Marina E., Pawlik Thomas D., Young Ralph H., Giesen David J., Kondakov Denis Y., Brown Christopher T., Deaton Joseph C., Lenhard Jerome R., Klubek Kevin P. // Journal of Applied Physics. - 2008. - Vol. 104, No. 9. - P. 094501-094501-17. ↑
- J1251.** Grzanka S. Carrier recombination mechanisms in nitride single quantum well light-emitting diodes

revealed by photo- and electroluminescence. / Grzanka S., Franssen G., Targowski G., Czernecki R., Khachapuridze A., Makarowa I., Wisniewska R., Mensz P., Perlin P., Suski T. // Journal of Applied Physics. - 2008. - Vol. 104, No. 9. - P. 094504-094504-4. ↑

J1252. Zinovchuk A. V. The effect of current crowding on the heat and light pattern in high-power AlGaAs light emitting diodes. / Zinovchuk A. V., Malyutenko O. Yu., Malyutenko V. K., Podoltsev A. D., Vilisov A. A. // Journal of Applied Physics. - 2008. - Vol. 104, No. 3. - P. 033115-033115-5. ↑

J1253. Matsushima Toshinori. Enhancing power conversion efficiencies and operational stability of organic light-emitting diodes by increasing carrier injection efficiencies at anode/organic and organic/organic heterojunction interfaces. / Matsushima Toshinori, Murata Hideyuki. // Journal of Applied Physics. - 2008. - Vol. 104, No. 3. - P. 034507-034507-4. ↑

J1254. Fung M. K. Charge generation layer in stacked organic light-emitting devices. / Fung M. K., Lau K. M., Lai S. L., Law C. W., Chan M. Y., Lee C. S., Lee S. T. // Journal of Applied Physics. - 2008. - Vol. 104, No. 3. - P. 034509-034509-5. ↑

J1255. Kang Nam Su. Correlation of photoluminescent quantum efficiency and device characteristics for the soluble electrophosphorescent light emitter with interfacial layers. / Kang Nam Su, Ju Byeong-Kwon, Kim Ji Whan, Kim Jang-Joo, Yu Jae-Woong, Chin Byung Doo. // Journal of Applied Physics. - 2008. - Vol. 104, No. 2. - P. 024511-024511-8. ↑

J1256. Herng T. S. Ferromagnetic Cu doped ZnO as an electron injector in heterojunction light emitting diodes. / Herng T. S., Lau S. P., Yu S. F., Tsang S. H., Teng K. S., Chen J. S. // Journal of Applied Physics. - 2008. - Vol. 104, No. 10. - P. 103104-103104-6. ↑

J1257. Scholz Sebastian. Self-doping and partial oxidation of metal-on-organic interfaces for organic semiconductor devices studied by chemical analysis techniques. / Scholz Sebastian, Huang Qiang, Thomschke Michael, Olthof Selina, Sebastian Philipp, Walzer Karsten, Leo Karl, Oswald Steffen, Corten Cathrin, Kuckling Dirk. // Journal of Applied Physics. - 2008. - Vol. 104, No. 10. - P. 104502-104502-10. ↑

J1258. Bange Sebastian. The role of poly(3,4-ethylenedioxythiophene):poly(styrenesulphonate) as a hole injection layer in a blue-emitting polymer light-emitting diode. / Bange Sebastian, Kuksov Andriy, Neher Dieter, Vollmer Antje, Koch Norbert, Ludemann Aurelie, Heun Susanne. // Journal of Applied Physics. - 2008. - Vol. 104, No. 10. - P. 104506-104506-7. ↑

J1259. Xiong Tao. The modification of self-assembled monolayer on indium tin oxide as cathode in inverted bottom-emitting organic light-emitting diodes. / Xiong Tao, Ma Dongge. // Journal of Applied Physics. - 2008. - Vol. 104, No. 6. - P. 064506-064506-3. ↑

J1260. Kuna Ladislav. Improvement of light extraction from high-power flip-chip light-emitting diodes by femtosecond laser direct structuring of the sapphire backside surface. / Kuna Ladislav, Haase Anja, Sommer Christian, Zinterl Ernst, Krenn Joachim R., Wenzl Franz P., Pachler Peter, Hartmann Paul, Tasch Stefan, Leising Gunther. // Journal of Applied Physics. - 2008. - Vol. 104, No. 7. - P. 074507-074507-7. ↑

J1261. Jarikov Viktor V. Operating lifetime recovery in organic light-emitting diodes having an azaaromatic hole-blocking/electron-transporting layer. / Jarikov Viktor V., Klubek Kevin P., Liao Liang-Sheng, Brown Christopher T. // Journal of Applied Physics. - 2008. - Vol. 104, No. 7. - P. 074914-074914-5. ↑

J1262. Seidel S. High efficient two color white phosphorescent organic light emitting diode. / Seidel S., Krause R., Hunze A., Schmid G., Kozlowski F., Dobbartin T., Winnacker A. // Journal of Applied Physics. - 2008. - Vol. 104, No. 6. - P. 064505-064505-4. ↑

J1263. Matsushima Toshinori. Marked improvement in electroluminescence characteristics of organic light-emitting diodes using an ultrathin hole-injection layer of molybdenum oxide. / Matsushima Toshinori, Jin Guang-He, Murata Hideyuki. // Journal of Applied Physics. - 2008. - Vol. 104, No. 5. - P. 054501-054501-6. ↑

J1264. Wang Tong-Wen. Effects of the GaN and AlN nucleation layers on the crack-free AlGaIn templates. / Wang Tong-Wen, Chen Nie-Chuan, Lien Wei-Chieh, Wu Meng-Chyi, Shih Chuan-Feng. // Journal of Applied Physics. - 2008. - Vol. 104, No. 6. - P. 063104-063104-5. ↑

J1265. Mirza B. I. Recombination processes in midinfrared Al x In 1-x Sb light-emitting diodes. / Mirza B. I.,

Nash G. R., Smith S. J., Buckle L., Coomber S. D., Emeny M. T., Ashley T. // Journal of Applied Physics. - 2008. - Vol. 104, No. 6. - P. 063113-063113-7. ↑

J1266. Mares J. W. Hybrid CdZnO/GaN quantum-well light emitting diodes. / Mares J. W., Falanga M., Thompson A. V., Osinsky A., Xie J. Q., Hertog B., Dabiran A., Chow P. P., Karpov S., Schoenfeld W. V. // Journal of Applied Physics. - 2008. - Vol. 104, No. 9. - P. 093107-093107-5. ↑

J1267. Cao X. A. On the origin of efficiency roll-off in InGaN-based light-emitting diodes. / Cao X. A., Yang Y., Guo H. // Journal of Applied Physics. - 2008. - Vol. 104, No. 9. - P. 093108-093108-4. ↑

J1268. Geyer Ulf. Large-scale patterning of indium tin oxide electrodes for guided mode extraction from organic light-emitting diodes. / Geyer Ulf, Hauss Julian, Riedel Boris, Gleiss Sebastian, Lemmer Uli, Gerken Martina. // Journal of Applied Physics. - 2008. - Vol. 104, No. 9. - P. 093111-093111-5. ↑

J1269. Keppens A. High power light-emitting diode junction temperature determination from current-voltage characteristics. / Keppens A., Ryckaert W. R., Deconinck G., Hanselaer P. // Journal of Applied Physics. - 2008. - Vol. 104, No. 9. - P. 093104-093104-8. ↑

J1270. Ishikawa Yukari. Color control of white photoluminescence from carbon-incorporated silicon oxide. / Ishikawa Yukari, Vasin A. V., Salonen J., Muto S., Lysenko V. S., Nazarov A. N., Shibata N., Lehto V.-P. // Journal of Applied Physics. - 2008. - Vol. 104, No. 8. - P. 083522-083522-6. ↑

J1271. Rolfe N. Separating the roles of electrons and holes in the organic magnetoresistance of aluminum tris(8-hydroxyquinoline) organic light emitting diodes. / Rolfe N., Desai P., Shakya P., Kreouzis T., Gillin W. P. // Journal of Applied Physics. - 2008. - Vol. 104, No. 8. - P. 083703-083703-4. ↑

J1272. Kondakov Denis Y. Role of chemical reactions of arylamine hole transport materials in operational degradation of organic light-emitting diodes. Journal of Applied Physics. - 2008. - Vol. 104, No. 8. - P. 084520-084520-9. ↑

J1273. Chia-Shou Chang. Microchip Self-Assembly on a Substrate Using Plasma Treatment. / Chia-Shou Chang, Ruoh-Huey Uang, Enboa Wu. // IEEE Transactions on Advanced Packaging. - 2008. - Vol. 31, No. 2. - P. 404-409. ↑

J1274. Hyunsoo Kim. High-Efficiency GaN-Based Light-Emitting Diodes Fabricated With Metallic Hybrid Reflectors. / Hyunsoo Kim, Sung-Nam Lee, Yongjo Park, Tae-Yeon Seong. // IEEE Electron Device Letters. - 2008. - Vol. 29, No. 6. - P. 582-584. ↑

J1275. Sommer C. Tailoring of the Color Conversion Elements in Phosphor-Converted High-Power LEDs by Optical Simulations. / Sommer C., Wenzl F.P., Hartmann P., Pachler P., Schweighart M., Leising G. // IEEE Photonics Technology Letters. - 2008. - Vol. 20, No. 9. - P. 739-741. ↑

J1276. Chaji G.R. A Current-Mode Comparator for Digital Calibration of Amorphous Silicon AMOLED Displays. / Chaji G.R., Nathan A. // IEEE Transactions on Circuits and Systems II: Express Briefs. - 2008. - Vol. 55, No. 7. - P. 614-618. ↑

J1277. Zhengyuan Xu. Ultraviolet Communications: Potential and State-Of-The-Art. / Zhengyuan Xu, Sadler B.M. // IEEE Communications Magazine. - 2008. - Vol. 46, No. 5. - P. 67-73. ↑

J1278. {no data available}. Gamesman problems. IEEE Potentials. - 2008. - Vol. 27, No. 3. - P. 48. ↑

J1279. Kuo H.-Y. Corrections to "Use of Elastic Conductive Adhesive as the Bonding Agent for the Fabrication of Vertical Structure GaN-Based LEDs on Flexible Metal Substrate" [1 Apr 08 523-525]. / Kuo H.-Y., Wang S.-J., Wang P.-R., Uang K.-M., Chen T.-M., Chen S.-L., Lee W.-C., Hsu H.-K., Chou J.-C., Wu C.-H. // IEEE Photonics Technology Letters. - 2008. - Vol. 20, No. 12. - P. 1072. ↑

J1280. Ying-Chih Chen. The Hybridization of CdSe/ZnS Quantum Dot on InGaN Light-Emitting Diodes for Color Conversion. / Ying-Chih Chen, Chun-Yuan Huang, Yan-Kuin Su, Wen-Liang Li, Chia-Hsien Yeh, Yu-Cheng Lin. // IEEE Transactions on Nanotechnology. - 2008. - Vol. 7, No. 4. - P. 503-507. ↑

J1281. Yan-Kuin Su. White Light Emission From DBPPV and CdSe/ZnS Quantum Dots Dually Hybridized on InGaN Light-Emitting Diodes. / Yan-Kuin Su, Ping-Chieh Tsai, Chun-Yuan Huang, Ying-Chih Chen. // IEEE

Electron Device Letters. - 2008. - Vol. 29, No. 6. - P. 575-577. ↑

J1282. Yan Zhou. One-Component, Low-Temperature, and Fast Cure Epoxy Encapsulant With High Refractive Index for LED Applications. / Yan Zhou, Nguyen Tran, Yuan Chang Lin, Yongzhi He, Shi F.G. // IEEE Transactions on Advanced Packaging. - 2008. - Vol. 31, No. 3. - P. 484-489. ↑

J1283. An-Ting Cheng. Improved Light Output of Nitride-Based Light-Emitting Diodes by Lattice-Matched AlInN Cladding Structure. / An-Ting Cheng, Yan-Kuin Su, Wei-Chi Lai. // IEEE Photonics Technology Letters. - 2008. - Vol. 20, No. 12. - P. 970-972. ↑

J1284. {no data available}. News brief: I See You. IEEE Spectrum. - 2008. - Vol. 45, No. 5. - P. 13. ↑

J1285. Kyu Hyeon Jeong. Optical Injection-Induced Polarization Switching Dynamics in 1.5- μ m Wavelength Single-Mode Vertical-Cavity Surface-Emitting Lasers. / Kyu Hyeon Jeong, Kyong Hon Kim, Seoung Hun Lee, Min Hee Lee, Byeung-Soo Yoo, Shore K.A. // IEEE Photonics Technology Letters. - 2008. - Vol. 20, No. 10. - P. 779-781. ↑

J1286. Zhang Z.Y. High-Power Quantum-Dot Superluminescent LED With Broadband Drive Current Insensitive Emission Spectra Using a Tapered Active Region. / Zhang Z.Y., Hogg R.A., Jin P., Choi T.L., Xu B., Wang Z.G. // IEEE Photonics Technology Letters. - 2008. - Vol. 20, No. 10. - P. 782-784. ↑

J1287. Yu J. Using Integrated Optical Feedback to Counter Pixel Aging and Stabilize Light Output of Organic LED Display Technology. / Yu J., Tischler J.R., Sodini C.G., Bulovic V. // Journal of Display Technology. - 2008. - Vol. 4, No. 3. - P. 308-313. ↑

J1288. Sungmin Hwang. A Method for Current Spreading Analysis and Electrode Pattern Design in Light-Emitting Diodes. / Sungmin Hwang, Jongin Shim. // IEEE Transactions on Electron Devices. - 2008. - Vol. 55, No. 5. - P. 1123-1128. ↑

J1289. Punke M. Optical Data Link Employing Organic Light-Emitting Diodes and Organic Photodiodes as Optoelectronic Components. / Punke M., Valouch S., Kettlitz S.W., Gerken M., Lemmer U. // Journal of Lightwave Technology. - 2008. - Vol. 26, No. 7. - P. 816-823. ↑

J1290. Huang S.Y. Thermal Stability Improvement of Vertical Conducting Green Resonant-Cavity Light-Emitting Diodes on Copper Substrates. / Huang S.Y., Horng R.H., Liu P.L., Wu J.Y., Wu H.W., Wu D.S. // IEEE Photonics Technology Letters. - 2008. - Vol. 20, No. 10. - P. 797-799. ↑

J1291. Jassi M. Degradation Study of Organic Semiconductor Devices Under Electrical and Optical Stresses. / Jassi M., Gurunath R., Sundar Kumar Iyer S. // IEEE Electron Device Letters. - 2008. - Vol. 29, No. 5. - P. 442-444. ↑

J1292. Hwang S. Improved ESD voltage by inserting floating metal ring in GaN-based light emitting diodes. / Hwang S., Shim J. // Electronics Letters. - 2008. - Vol. 44, No. 9. - P. 590. ↑

J1293. Lin C.H. Enhanced Vertical Extraction Efficiency From a Thin-Film InGaN-GaN Light-Emitting Diode Using a 2-D Photonic Crystal and an Omnidirectional Reflector. / Lin C.H., Yen H.H., Lai C.F., Huang H.W., Chao C.H., Kuo H.C., Lu T.C., Wang S.C., Leung K.M. // IEEE Photonics Technology Letters. - 2008. - Vol. 20, No. 10. - P. 836-838. ↑

J1294. Chia-En Lee. Further Enhancement of Nitride-Based Near-Ultraviolet Vertical-Injection Light-Emitting Diodes by Adopting a Roughened Mesh-Surface. / Chia-En Lee, Yea-Chen Lee, Hao-Chung Kuo, Tien-Chang Lu, Shing-Chung Wang. // IEEE Photonics Technology Letters. - 2008. - Vol. 20, No. 10. - P. 803-805. ↑

J1295. Po Han Chen. Diamond Heat Spreader Layer for High-Power Thin-GaN Light-Emitting Diodes. / Po Han Chen, Ching Liang Lin, Liu Y.K., Te Yuan Chung, Cheng-Yi Liu. // IEEE Photonics Technology Letters. - 2008. - Vol. 20, No. 10. - P. 845-847. ↑

J1296. Chen J.J. Enhanced Output Power of GaN-Based LEDs With Nano-Patterned Sapphire Substrates. / Chen J.J., Su Y.K., Lin C.L., Chen S.M., Li W.L., Kao C.C. // IEEE Photonics Technology Letters. - 2008. - Vol. 20, No. 13. - P. 1193-1195. ↑

J1297. Jaehee Cho. Improved Emission Efficiency in InGaN Light-Emitting Diodes Using Reverse Bias in

Pulsed Voltage Operation. / Jaehee Cho, Euijoon Yoon, Hyunsoo Kim, Yongjo Park, Joon Seop Kwak. // IEEE Photonics Technology Letters. - 2008. - Vol. 20, No. 13. - P. 1190-1192. ↑

J1298. Ya-Ju Lee. Study of GaN-Based Light-Emitting Diodes Grown on Chemical Wet-Etching-Patterned Sapphire Substrate With V-Shaped Pits Roughening Surfaces. / Ya-Ju Lee, Hao-Chung Kuo, Tien-Chang Lu, Shing-Chung Wang, Kar Wai Ng, Kei May Lau, Zu-Po Yang, Chang A.S.-P., Shawn-Yu Lin. // Journal of Lightwave Technology. - 2008. - Vol. 26, No. 11. - P. 1455-1463. ↑

J1299. Ching-Hua Chiu. Nano-Processing Techniques Applied in GaN-Based Light-Emitting Devices With Self-Assembly Ni Nano-Masks. / Ching-Hua Chiu, Ming-Hua Lo, Tien-Chang Lu, Peichen Yu, Huang H.W., Hao-Chung Kuo, Shing-Chung Wang. // Journal of Lightwave Technology. - 2008. - Vol. 26, No. 11. - P. 1445-1454. ↑

J1300. Gong-Ru Lin. Microwatt MOSLED Using With Buried Si Nanocrystals on Si Nano-Pillar Array. / Gong-Ru Lin, Yi-Hao Pai, Cheng-Tao Lin. // Journal of Lightwave Technology. - 2008. - Vol. 26, No. 11. - P. 1486-1491. ↑

J1301. Musienko Y. SSPM Readout of LSO, (Lu-Y)AP:Ce and PWO-II Pixels for PET Detector Modules. / Musienko Y., Auffray E., Fedorov A., Korzhik M., Lecoq P., Reucroft S., Swain J. // IEEE Transactions on Nuclear Science. - 2008. - Vol. 55, No. 3. - P. 1352-1356. ↑

J1302. Li G.F. Organic light-emitting device with surface-modified tungsten-doped indium oxide anode. / Li G.F., Zhang Q., Yu F., Liu C., Wu H.R. // Electronics Letters. - 2008. - Vol. 44, No. 13. - P. 818-819. ↑

J1303. Nicholes S.C. Highly Polarized Single-Chip ELED Sources Using Oppositely Strained MQW Emitters and Absorbers. / Nicholes S.C., Raring J.W., Norberg E.J., Wang C.S., Dummer M.M., DenBaars S.P., Coldren L.A. // IEEE Photonics Technology Letters. - 2008. - Vol. 20, No. 14. - P. 1267-1269. ↑

J1304. Pflumm C. A Numerical Scheme to Model Current and Voltage Excitation of Organic Light-Emitting Diodes. / Pflumm C., Gartner C., Lemmer U. // IEEE Journal of Quantum Electronics. - 2008. - Vol. 44, No. 8. - P. 790-798. ↑

J1305. Hoa Le Minh. High-Speed Visible Light Communications Using Multiple-Resonant Equalization. / Hoa Le Minh, O'Brien D., Faulkner G., Lubin Zeng, Kyungwoo Lee, Daekwang Jung, YunJe Oh. // IEEE Photonics Technology Letters. - 2008. - Vol. 20, No. 14. - P. 1243-1245. ↑

J1306. Benisty H. Investigation of Extracting Photonic Crystal Lattices for Guided Modes of GaAs-Based Heterostructures. / Benisty H., Danglot J., Talneau A., Enoch S., Pottage J.M., David A. // IEEE Journal of Quantum Electronics. - 2008. - Vol. 44, No. 8. - P. 777-789. ↑

J1307. Gnauck A.H. High-Capacity Optical Transmission Systems. / Gnauck A.H., Tkach R.W., Chraplyvy A.R., Li T. // Journal of Lightwave Technology. - 2008. - Vol. 26, No. 9. - P. 1032-1045. ↑

J1308. Chung-Hsun Jang. Effect of Thickness of the p-AlGaIn Electron Blocking Layer on the Improvement of ESD Characteristics in GaN-Based LEDs. / Chung-Hsun Jang, Sheu J.K., Tsai C.M., Shei S.C., Lai W.C., Chang S.J. // IEEE Photonics Technology Letters. - 2008. - Vol. 20, No. 13. - P. 1142-1144. ↑

J1309. Fleming B. Automotive Safety and Convenience Electronics [Automotive Electronics]. IEEE Vehicular Technology Magazine. - 2008. - Vol. 3, No. 1. - P. 10-40. ↑

J1310. Ray-Hua Horng. Phosphor-Free White Light From InGaIn Blue and Green Light-Emitting Diode Chips Covered With Semiconductor-Conversion AlGaInP Epilayer. / Ray-Hua Horng, Pin Han, Dong-Sing Wu. // IEEE Photonics Technology Letters. - 2008. - Vol. 20, No. 13. - P. 1139-1141. ↑

J1311. Keller J.C. Creating a chemical. IEEE Women in Engineering Magazine. - 2008. - Vol. 2, No. 1. - P. 38-40. ↑

J1312. Yi Yang. Investigation of the Nonthermal Mechanism of Efficiency Rolloff in InGaIn Light-Emitting Diodes. / Yi Yang, Xian An Cao, Chunhui Yan. // IEEE Transactions on Electron Devices. - 2008. - Vol. 55, No. 7. - P. 1771-1775. ↑

J1313. Brusso B.C. From crystallography to visible light [History]. IEEE Industry Applications Magazine. - 2008.

- Vol. 14, No. 4. - P. 8-10. ↑

J1314. Zhang H.M. Real-Time Color-Tunable Electroluminescence From Stacked Organic LEDs Using Independently Addressable Middle Electrode. / Zhang H.M., Choy W.C.H. // IEEE Photonics Technology Letters. - 2008. - Vol. 20, No. 13. - P. 1154-1156. ↑

J1315. Dupuis R.D. History, Development, and Applications of High-Brightness Visible Light-Emitting Diodes. / Dupuis R.D., Krames M.R. // Journal of Lightwave Technology. - 2008. - Vol. 26, No. 9. - P. 1154-1171. ↑

J1316. Meneghini M. A Review on the Reliability of GaN-Based LEDs. / Meneghini M., Trevisanello L.-R., Meneghesso G., Zanoni E. // IEEE Transactions on Device and Materials Reliability. - 2008. - Vol. 8, No. 2. - P. 323-331. ↑

J1317. Destrueel P. A look on the bright side. / Destrueel P., Jolinat P., Seguy I., Ablart G., Farenc J. // IEEE Industry Applications Magazine. - 2008. - Vol. 14, No. 4. - P. 12-17. ↑

J1318. Sugiura H. Qualify with flying colors. / Sugiura H., Kaneko H., Kagawa S., Someya J., Tanizoe H. // IEEE Industry Applications Magazine. - 2008. - Vol. 14, No. 4. - P. 26-30. ↑

J1319. Kening Zhou. Quasi-Active Power Factor Correction Circuit for HB LED Driver. / Kening Zhou, Jian Guo Zhang, Yuvarajan S., Da Feng Weng. // IEEE Transactions on Power Electronics. - 2008. - Vol. 23, No. 3. - P. 1410-1415. ↑

J1320. Kumagai J. Ash Nehro-Everything is Illuminated [dream jobs 2008]. IEEE Spectrum. - 2008. - Vol. 45, No. 2. - P. 40-42. ↑

J1321. Guhne T. Demonstration of semipolar (11-22) InGaN/ GaN blue-green light emitting diode. / Guhne T., DeMierry P., Nemoz M., Beraudo E., Chenot S., Nataf G. // Electronics Letters. - 2008. - Vol. 44, No. 3. - P. 231-232. ↑

J1322. {no data available}. Ney Robinson Salvi dos Reis-Into the Wild [dream jobs 2008]. IEEE Spectrum. - 2008. - Vol. 45, No. 2. - P. 39-40. ↑

J1323. Xueqiang Liu. A Testing Method on Poly-Si Thin-Film Transistor Array for Active-Matrix Organic Emitting Display. / Xueqiang Liu, Tong Zhang, Lijie Wang, Zhiqiang Xia, Mingyou Li, Shiyong Liu. // Journal of Display Technology. - 2008. - Vol. 4, No. 2. - P. 229-232. ↑

J1324. {no data available}. Karaoke-bot [tools & toys]. IEEE Spectrum. - 2008. - Vol. 45, No. 2. - P. 25. ↑

J1325. Frechette M.F. Nanostructured polymer microcomposites: A distinct class of insulating materials. / Frechette M.F., Larocque R.Y., Trudeau M., Veillette R., Rioux R., Pelissou S., Besner S., Javan M., Cole K., That M.-T.T., Desgagnes D., Castellon J., Agnel S., Toureille A., Platbrood G. // IEEE Transactions on Dielectrics and Electrical Insulation. - 2008. - Vol. 15, No. 1. - P. 90-105. ↑

J1326. Boucherif A. InAsSb based mid-infrared optical upconversion devices operable at thermoelectric temperatures. / Boucherif A., Ban D., Luo H., Dupont E., Wasilewski Z.R., Liu H.C., Paltiel Y., Raizman A., Sher A. // Electronics Letters. - 2008. - Vol. 44, No. 4. - P. 312-313. ↑

J1327. Lee C.M.G. Flat-panel autostereoscopic 3D display. / Lee C.M.G., Travis A.R.L., Lin R. // IET Optoelectronics. - 2008. - Vol. 2, No. 1. - P. 24-28. ↑

J1328. Heng Xu. Combining Multicore Imaging Fiber With Matrix Addressable Blue/Green LED Arrays for Spatiotemporal Photonic Excitation at Cellular Level. / Heng Xu, Davitt K.M., Wei Dong, Yoon-Kyu Song, Patterson W.R., Aizenman C.D., Nurmikko A.V. // IEEE Journal of Selected Topics in Quantum Electronics. - 2008. - Vol. 14, No. 1. - P. 167-170. ↑

J1329. Jae-Hoon Lee. Enhancement of InGaN-Based Vertical LED With Concavely Patterned Surface Using Patterned Sapphire Substrate. / Jae-Hoon Lee, Jeong-Tak Oh, Seok-Boem Choi, Yong-Chun Kim, Hyun-Ick Cho, Jung-Hee Lee. // IEEE Photonics Technology Letters. - 2008. - Vol. 20, No. 5. - P. 345-347. ↑

J1330. Yea-Chen Lee. Enhancing the Light Extraction of $(\text{Al}_x\text{Ga}_{1-x})_{0.5}\text{In}_{0.5}\text{P}$ -Based Light-Emitting Diode Fabricated via Geometric Sapphire Shaping. / Yea-Chen Lee, Chia-En Lee, Hao-Chung Kuo, Tien-Chang

Lu, Shing-Chung Wang. // IEEE Photonics Technology Letters. - 2008. - Vol. 20, No. 5. - P. 369-371. ↑

J1331. Joonmo Park. Improved Light Output of Photonic Crystal Light-Emitting Diode Fabricated by Anodized Aluminum Oxide Nano-Patterns. / Joonmo Park, Jin-Kyoung Oh, Kwang-Woo Kwon, Young-Ho Kim, Sung-Soo Jo, Jun Key Lee, Sang-Wan Ryu. // IEEE Photonics Technology Letters. - 2008. - Vol. 20, No. 4. - P. 321-323. ↑

J1332. Yi-Cheng Hsu. Failure Mechanisms Associated With Lens Shape of High-Power LED Modules in Aging Test. / Yi-Cheng Hsu, Yu-Kuan Lin, Ming-Hung Chen, Chun-Chin Tsai, Jao-Hwa Kuang, Sheng-Bang Huang, Hung-Lieh Hu, Yeh-I Su, Wood-Hi Cheng. // IEEE Transactions on Electron Devices. - 2008. - Vol. 55, No. 2. - P. 689-694. ↑

J1333. Zaus E.S. Design of Highly Transparent Organic Photodiodes. / Zaus E.S., Tedde S., Rauch T., Furst J., Dohler G.H. // IEEE Transactions on Electron Devices. - 2008. - Vol. 55, No. 2. - P. 681-684. ↑

J1334. Alvarez A.L. Analytical Evaluation of the Ratio Between Injection and Space-Charge Limited Currents in Single Carrier Organic Diodes. / Alvarez A.L., Arredondo B., Romero B., Quintana X., Gutierrez-Llorente A., Mallavia R., Oton J.M. // IEEE Transactions on Electron Devices. - 2008. - Vol. 55, No. 2. - P. 674-680. ↑

J1335. Ming-Kwei Lee. Light Extraction Efficiency Enhancement of GaN Blue LED by Liquid-Phase-Deposited ZnO Rods. / Ming-Kwei Lee, Chen-Lin Ho, Po-Chun Chen. // IEEE Photonics Technology Letters. - 2008. - Vol. 20, No. 4. - P. 252-254. ↑

J1336. Shi J.-W. High-Speed GaN-Based Green Light-Emitting Diodes With Partially n-Doped Active Layers and Current-Confined Apertures. / Shi J.-W., Sheu J.-K., Chen C.-H., Lin G.-R., Lai W.-C. // IEEE Electron Device Letters. - 2008. - Vol. 29, No. 2. - P. 158-160. ↑

J1337. Vaidya V. Comparison of Pentacene and Amorphous Silicon AMOLED Display Driver Circuits. / Vaidya V., Soggs S., Jungbae Kim, Haldi A., Haddock J.N., Kippelen B., Wilson D.M. // IEEE Transactions on Circuits and Systems I: Regular Papers. - 2008. - Vol. 55, No. 5. - P. 1177-1184. ↑

J1338. Chun-Yuan Huang. Single-Layered Hybrid DBPPV-CdSe-ZnS Quantum-Dot Light-Emitting Diodes. / Chun-Yuan Huang, Yan-Kuin Su, Ten-Chin Wen, Tzung-Fang Guo, Ming-Lung Tu. // IEEE Photonics Technology Letters. - 2008. - Vol. 20, No. 4. - P. 282-284. ↑

J1339. Lin J.C. Improved External Quantum Efficiency of GaN p-i-n Photodiodes With a TiO₂ Roughened Surface. / Lin J.C., Su Y.K., Chang S.J., Lan W.H., Huang K.C., Cheng Y.C., Lin W.J. // IEEE Photonics Technology Letters. - 2008. - Vol. 20, No. 4. - P. 285-287. ↑

J1340. Buso S. Performance Degradation of High-Brightness Light Emitting Diodes Under DC and Pulsed Bias. / Buso S., Spiazzi G., Meneghini M., Meneghesso G. // IEEE Transactions on Device and Materials Reliability. - 2008. - Vol. 8, No. 2. - P. 312-322. ↑

J1341. Sekiguchi H. GaN/AlGaIn nanocolumn ultraviolet light-emitting diodes grown on n-(111) Si by RF-plasma-assisted molecular beam epitaxy. / Sekiguchi H., Kishino K., Kikuchi A. // Electronics Letters. - 2008. - Vol. 44, No. 2. - P. 151-152. ↑

J1342. Buttgen B. Robust Optical Time-of-Flight Range Imaging Based on Smart Pixel Structures. / Buttgen B., Seitz P. // IEEE Transactions on Circuits and Systems I: Regular Papers. - 2008. - Vol. 55, No. 6. - P. 1512-1525. ↑

J1343. Chang-Yu Wu. Multistring LED Backlight Driving System for LCD Panels With Color Sequential Display and Area Control. / Chang-Yu Wu, Tsai-Fu Wu, Jiun-Ren Tsai, Yaow-Ming Chen, Chien-Chih Chen. // IEEE Transactions on Industrial Electronics. - 2008. - Vol. 55, No. 10. - P. 3791-3800. ↑

J1344. Chung-Hao Tien. Tandem Light-Guides With Micro-Line-Prism Arrays for Field-Sequential-Color Scanning Backlight Module. / Chung-Hao Tien, Yen-Hsing Lu, Yuan-Jung Yao. // Journal of Display Technology. - 2008. - Vol. 4, No. 2. - P. 147-152. ↑

J1345. Hwang J.M. Efficiency Enhancement of Light Extraction in LED With a Nano-Porous GaP Surface. / Hwang J.M., Hung W.H., Hwang H.L. // IEEE Photonics Technology Letters. - 2008. - Vol. 20, No. 8. - P. 608-610. ↑

- J1346.** Trevisanello L. Accelerated Life Test of High Brightness Light Emitting Diodes. / Trevisanello L., Meneghini M., Mura G., Vanzi M., Pavesi M., Meneghesso G., Zanoni E. // IEEE Transactions on Device and Materials Reliability. - 2008. - Vol. 8, No. 2. - P. 304-311. ↑
- J1347.** Miao C. InGaN/GaN multi-quantum-well planar metal-semiconductor-metal light-emitting diodes. / Miao C., Lu H., Du X.Z., Li Y., Zhang R., Zheng Y.D. // Electronics Letters. - 2008. - Vol. 44, No. 6. - P. 441-442. ↑
- J1348.** Chia-En Lee. High-Brightness InGaN-GaN Flip-Chip Light-Emitting Diodes With Triple-Light Scattering Layers. / Chia-En Lee, Yea-Chen Lee, Hao-Chung Kuo, Tien-Chang Lu, Shing-Chung Wang. // IEEE Photonics Technology Letters. - 2008. - Vol. 20, No. 8. - P. 659-661. ↑
- J1349.** Loeser M. Multidimensional Electro-Opto-Thermal Modeling of Broad-Band Optical Devices. / Loeser M., Witzigmann B. // IEEE Journal of Quantum Electronics. - 2008. - Vol. 44, No. 6. - P. 505-514. ↑
- J1350.** Tong-Miin Liou. Effects of Impact Inertia and Surface Characteristics on Deposited Polymer Droplets in Microcavities. / Tong-Miin Liou, Chia-Yen Chan, Chien-Chung Fu, Kuan-Cheng Shih. // Journal of Microelectromechanical Systems. - 2008. - Vol. 17, No. 2. - P. 278-287. ↑
- J1351.** Arif R.A. Spontaneous Emission and Characteristics of Staggered InGaN Quantum-Well Light-Emitting Diodes. / Arif R.A., Hongping Zhao, Yik-Khoon Ee, Tansu N. // IEEE Journal of Quantum Electronics. - 2008. - Vol. 44, No. 6. - P. 573-580. ↑
- J1352.** Zhu Y.H. Improved performance of 264 nm emission AlGaIn-based deep ultraviolet light-emitting diodes. / Zhu Y.H., Sumiya S., Zhang J.C., Miyoshi M., Shibata T., Kosaka K., Tanaka M., Egawa T. // Electronics Letters. - 2008. - Vol. 44, No. 7. - P. 493-495. ↑
- J1353.** Chen T.M. Current Spreading and Blocking Designs for Improving Light Output Power from the Vertical-Structured GaN-Based Light-Emitting Diodes. / Chen T.M., Uang K.M., Wang S.J., Kuo H.Y., Tsai C.C., Lee W.C., Kuan H. // IEEE Photonics Technology Letters. - 2008. - Vol. 20, No. 9. - P. 703-705. ↑
- J1354.** Jianzheng Hu. Thermal and Mechanical Analysis of High-Power LEDs With Ceramic Packages. / Jianzheng Hu, Lianqiao Yang, Moo Whan Shin. // IEEE Transactions on Device and Materials Reliability. - 2008. - Vol. 8, No. 2. - P. 297-303. ↑
- J1355.** {no data available}. News Brief [EYE-PODS]. IEEE Spectrum. - 2008. - Vol. 45, No. 3. - P. 15. ↑
- J1356.** Gerginov V. Laser Noise Cancellation in Single-Cell CPT Clocks. / Gerginov V., Knappe S., Shah V., Hollberg L., Kitching J. // IEEE Transactions on Instrumentation and Measurement. - 2008. - Vol. 57, No. 7. - P. 1357-1361. ↑
- J1357.** Jones W.D. Silicon Slivers for Flexible Circuits. IEEE Spectrum. - 2008. - Vol. 45, No. 3. - P. 15. ↑
- J1358.** Chien-Chun Wang. Improved Extraction Efficiency of Light-Emitting Diodes by Modifying Surface Roughness With Anodic Aluminum Oxide Film. / Chien-Chun Wang, Hung-Chi Lu, Chien-Chih Liu, Fenq-Lin Jenq, Yeong-Her Wang, Mau-Phon Houng. // IEEE Photonics Technology Letters. - 2008. - Vol. 20, No. 6. - P. 428-430. ↑
- J1359.** Shi J.-W. Phosphor-Free GaN-Based Transverse Junction White-Light Light-Emitting Diodes With Regrown n-Type Regions. / Shi J.-W., Chen C.-C., Wang C.-K., Lin C.-S., Sheu J.-K., Lai W.-C., Kuo C.-H., Tun C.-J., Yang T.-H., Tsao F.-C., Chyi J.-I. // IEEE Photonics Technology Letters. - 2008. - Vol. 20, No. 6. - P. 449-451. ↑
- J1360.** Rong-Hwei Yeh. Optoelectronic Characteristics of Direct-Current and Alternating-Current White Thin-Film Light-Emitting Diodes Based on Hydrogenated Amorphous Silicon Nitride Film. / Rong-Hwei Yeh, Tai-Rong Yu, Te-Cheng Chung, Shih-Yung Lo, Jyh-Wong Hong. // IEEE Transactions on Electron Devices. - 2008. - Vol. 55, No. 4. - P. 978-985. ↑
- J1361.** Sumpf B. 5.6-W Broad-Area Lasers With a Vertical Far-Field Angle of 31 Emitting at 670 nm. / Sumpf B., Zorn M., Maiwald M., Staske R., Fricke J., Ressel P., Erbert G., Weyers M., Trankle G. // IEEE Photonics Technology Letters. - 2008. - Vol. 20, No. 8. - P. 575-577. ↑
- J1362.** Meneghini M. Reliability of Deep-UV Light-Emitting Diodes. / Meneghini M., Pavesi M., Trivellin N.,

Gaska R., Zanoni E., Meneghesso G. // IEEE Transactions on Device and Materials Reliability. - 2008. - Vol. 8, No. 2. - P. 248-254. ↑

J1363. Hon-Yi Kuo. Use of Elastic Conductive Adhesive as the Bonding Agent for the Fabrication of Vertical Structure GaN-Based LEDs on Flexible Metal Substrate. / Hon-Yi Kuo, Shui-Jinn Wang, Pei-Ren Wang, Kai-Ming Uang, Tron-Min Chen, Shiue-Lung Chen, Wei-Chi Lee, Hong-Kuei Hsu, Jui-Chiang Chou, Chung-Han Wu. // IEEE Photonics Technology Letters. - 2008. - Vol. 20, No. 7. - P. 523-525. ↑

J1364. Chaji G.R. Low-Power Low-Cost Voltage-Programmed a-Si:H AMOLED Display for Portable Devices. / Chaji G.R., Nathan A. // Journal of Display Technology. - 2008. - Vol. 4, No. 2. - P. 233-237. ↑

J1365. Min-Yann Hsieh. InGaN-GaN Nanorod Light Emitting Arrays Fabricated by Silica Nanomasks. / Min-Yann Hsieh, Cheng-Yin Wang, Liang-Yi Chen, Min-Yung Ke, JianJang Huang. // IEEE Journal of Quantum Electronics. - 2008. - Vol. 44, No. 5. - P. 468-472. ↑

J1366. Chun-Yuan Huang. Hybrid CdSe-ZnS Quantum Dot-InGaN-GaN Quantum Well Red Light-Emitting Diodes. / Chun-Yuan Huang, Yan-Kuin Su, Ying-Chih Chen, Ping-Chieh Tsai, Cheng-Tien Wan, Wen-Liang Li. // IEEE Electron Device Letters. - 2008. - Vol. 29, No. 7. - P. 711-713. ↑

J1367. Bingfeng Fan. Thermal Study of High-Power Nitride-Based Flip-Chip Light-Emitting Diodes. / Bingfeng Fan, Hao Wu, Yu Zhao, Yulun Xian, Baijun Zhang, Gang Wang. // IEEE Transactions on Electron Devices. - 2008. - Vol. 55, No. 12. - P. 3375-3382. ↑

J1368. Ray-Hua Horng. Enhanced Luminance Efficiency of Wafer-Bonded InGaN-GaN LEDs With Double-Side Textured Surfaces and Omnidirectional Reflectors. / Ray-Hua Horng, Shao-Hua Huang, Chuang-Yu Hsieh, Xinhe Zheng, Dong-Sing Wu. // IEEE Journal of Quantum Electronics. - 2008. - Vol. 44, No. 11. - P. 1116-1123. ↑

J1369. Sun-Rong Jan. Blue Electroluminescence From Metal/Oxide/6H-SiC Tunneling Diodes. / Sun-Rong Jan, Tzu-Huan Cheng, Tzer-An Hung, Ping-Sheng Kuo, Ming Han Liao, Yu Deng, Chee Wee Liu. // IEEE Transactions on Electron Devices. - 2008. - Vol. 55, No. 12. - P. 3590-3593. ↑

J1370. Wong A.K.Y. A Low-Power CMOS Front-End for Photoplethysmographic Signal Acquisition With Robust DC Photocurrent Rejection. / Wong A.K.Y., Kong-Pang Pun, Yuan-Ting Zhang, Ka Nang Leung. // IEEE Transactions on Biomedical Circuits and Systems. - 2008. - Vol. 2, No. 4. - P. 280-288. ↑

J1371. Jang Yeon Kwon. Bottom-Gate Gallium Indium Zinc Oxide Thin-Film Transistor Array for High-Resolution AMOLED Display. / Jang Yeon Kwon, Kyoung Seok Son, Ji Sim Jung, Tae Sang Kim, Myung Kwan Ryu, Kyung Bae Park, Byung Wook Yoo, Jung Woo Kim, Young Gu Lee, Kee Chan Park, Sang Yoon Lee, Jong Min Kim. // IEEE Electron Device Letters. - 2008. - Vol. 29, No. 12. - P. 1309-1311. ↑

J1372. Koerperick E.J. Active Region Cascading for Improved Performance in InAs-GaSb Superlattice LEDs. / Koerperick E.J., Olesberg J.T., Hicks J.L., Prineas J.P., Boggess T.F. // IEEE Journal of Quantum Electronics. - 2008. - Vol. 44, No. 12. - P. 1242-1247. ↑

J1373. Caballero A. 5 GHz 200 Mbit/s radio over polymer fibre link with envelope detection at 650 nm wavelength. / Caballero A., Jensen J.B., Yu X., Monroy I.T. // Electronics Letters. - 2008. - Vol. 44, No. 25. - P. 1479-1480. ↑

J1374. Neshataeva E. Electrically driven ZnO nanoparticle light emitting device. / Neshataeva E., Kummell T., Ebberts A., Bacher G. // Electronics Letters. - 2008. - Vol. 44, No. 25. - P. 1485-1487. ↑

J1375. Yu-Zung Chiou. The Effect of Electrode Layout on Nitride-Based Light-Emitting Diodes. IEEE Transactions on Device and Materials Reliability. - 2008. - Vol. 8, No. 4. - P. 647-651. ↑

J1376. Jinn-Kong Sheu. Ga-Doped ZnO Transparent Conductive Oxide Films Applied to GaN-Based Light-Emitting Diodes for Improving Light Extraction Efficiency. / Jinn-Kong Sheu, Ming-Lun Lee, Lu Y.S., Shu K.W. // IEEE Journal of Quantum Electronics. - 2008. - Vol. 44, No. 12. - P. 1211-1218. ↑

J1377. Fleming B. Solid State Headlights [Automotive Electronics]. IEEE Vehicular Technology Magazine. - 2008. - Vol. 3, No. 3. - P. 12-15. ↑

- J1378.** Li F.M. Zinc Oxide Nanostructures and High Electron Mobility Nanocomposite Thin Film Transistors. / Li F.M., Hsieh G.-W., Dalal S., Newton M.C., Stott J.E., Hiralal P., Nathan A., Warburton P.A., Unalan H.E., Beecher P., Flewitt A.J., Robinson I., Amaratunga G., Milne W.I. // IEEE Transactions on Electron Devices. - 2008. - Vol. 55, No. 11. - P. 3001-3011. ↑
- J1379.** Chih-Hung Yen. A New AlGaInP Multiple-Quantum-Well Light-Emitting Diode With a Thin Carbon-Doped GaP Contact Layer Structure. / Chih-Hung Yen, Yi-Jung Liu, Nan-Yi Huang, Kuo-Hui Yu, Tzu-Pin Chen, Li-Yang Chen, Tsung-Han Tsai, Chong-Yi Lee, Wen-Chau Liu. // IEEE Photonics Technology Letters. - 2008. - Vol. 20, No. 23. - P. 1923-1925. ↑
- J1380.** Tak Jeong. Enhanced Light Output Power of GaN-Based Vertical Light-Emitting Diodes by Using Highly Reflective ITO-Ag-Pt Reflectors. / Tak Jeong, Kang Ho Kim, Hyun Haeng Lee, Seung Jae Lee, Sang Hern Lee, Jong Hyeob Baek, June Key Lee. // IEEE Photonics Technology Letters. - 2008. - Vol. 20, No. 23. - P. 1932-1934. ↑
- J1381.** Shouu-Jinn Chang. GaN-Based MSM Photodetectors Prepared on Patterned Sapphire Substrates. / Shouu-Jinn Chang, Jhou Y.D., Lin Y.C., Wu S.L., Chen C.H., Wen T.C., Wu L.W. // IEEE Photonics Technology Letters. - 2008. - Vol. 20, No. 22. - P. 1866-1868. ↑
- J1382.** Conti J.P. Displays 2.0 [COMMS display technology]. Engineering & Technology. - 2008. - Vol. 3, No. 13. - P. 72-75. ↑
- J1383.** Takeda K. Polarization-Insensitive All-Optical Flip-Flop Using Tensile-Strained Multiple Quantum Wells. / Takeda K., Kanema Y., Takenaka M., Tanemura T., Nakano Y. // IEEE Photonics Technology Letters. - 2008. - Vol. 20, No. 22. - P. 1851-1853. ↑
- J1384.** Yea-Chen Lee. High-Performance (Al Ga) In P-Based Flip-Chip Light-Emitting Diode With a Geometric Sapphire Shaping Structure. / Yea-Chen Lee, Hao-Chung Kuo, Chia-En Lee, Tien-Chang Lu, Shing-Chung Wang. // IEEE Photonics Technology Letters. - 2008. - Vol. 20, No. 23. - P. 1950-1952. ↑
- J1385.** Hyun Kyong Cho. Laser Ltoff GaN Thin-Film Photonic Crystal GaN-Based Light-Emitting Diodes. / Hyun Kyong Cho, Sun-Kyung Kim, Duk Kyu Bae, Bong-Cheol Kang, Jeong Soo Lee, Yong-Hee Lee. // IEEE Photonics Technology Letters. - 2008. - Vol. 20, No. 24. - P. 2096-2098. ↑
- J1386.** Maiorano V. Very Long Operational Lifetime at High Initial Luminance of Deep Red Phosphorescent Organic Light-Emitting Diodes With Double Emission Layers. / Maiorano V., Mazzeo M., Mariano F., Ben Khalifa M., Carallo S., Dussert-Vidalet B., Cingolani R., Gigli G. // IEEE Photonics Technology Letters. - 2008. - Vol. 20, No. 24. - P. 2105-2107. ↑
- J1387.** Zhanao Tan. Stable Binary Complementary White Light-Emitting Diodes Based on Quantum-Dot/Polymer-Bilayer Structures. / Zhanao Tan, Hedrick B., Fan Zhang, Ting Zhu, Jian Xu, Henderson R.H., Ruzyllo J., Wang A.Y. // IEEE Photonics Technology Letters. - 2008. - Vol. 20, No. 23. - P. 1998-2000. ↑
- J1388.** Tao Dai. Light Extraction Improvement From GaN-Based Light-Emitting Diodes With Nano-Patterned Surface Using Anodic Aluminum Oxide Template. / Tao Dai, Bei Zhang, Xiang Ning Kang, Kui Bao, Wen Zhu Zhao, Dong Sheng Xu, Guo Yi Zhang, Zi Zhao Gan. // IEEE Photonics Technology Letters. - 2008. - Vol. 20, No. 23. - P. 1974-1976. ↑
- J1389.** Zongyuan Liu. Optical Analysis of Color Distribution in White LEDs With Various Packaging Methods. / Zongyuan Liu, Sheng Liu, Kai Wang, Xiaobing Luo. // IEEE Photonics Technology Letters. - 2008. - Vol. 20, No. 24. - P. 2027-2029. ↑
- J1390.** Fournier F. Design Methodology for High Brightness Projectors. / Fournier F., Rolland J. // Journal of Display Technology. - 2008. - Vol. 4, No. 1. - P. 86-91. ↑
- J1391.** Danner A.J. Fabrication of Efficient Light-Emitting Diodes With a Self-Assembled Photonic Crystal Array of Polystyrene Nanoparticles. / Danner A.J., Benzong Wang, Soo-Jin Chua, Jeong-Ki Hwang. // IEEE Photonics Technology Letters. - 2008. - Vol. 20, No. 1. - P. 48-50. ↑
- J1392.** Jongwoon Park. Dual Partial Dye Doping for Chromaticity Tuning and Performance Enhancement of White OLEDs. / Jongwoon Park, Suganuma N., Kawakami Y. // Journal of Display Technology. - 2008. - Vol. 4, No. 1. - P. 61-69. ↑

- J1393.** Hekmatshoar B. Reliability of Active-Matrix Organic Light-Emitting-Diode Arrays With Amorphous Silicon Thin-Film Transistor Backplanes on Clear Plastic. / Hekmatshoar B., Kattamis A.Z., Cherenack K.H., Ke Long, Jian-Zhang Chen, Wagner S., Sturm J.C., Rajan K., Hack M. // IEEE Electron Device Letters. - 2008. - Vol. 29, No. 1. - P. 63-66. ↑
- J1394.** Hoshino K. Direct Fabrication of Nanoscale Light Emitting Diode on Silicon Probe Tip for Scanning Microscopy. / Hoshino K., Rozanski L.J., Vanden Bout D.A., Xiaojing Zhang. // Journal of Microelectromechanical Systems. - 2008. - Vol. 17, No. 1. - P. 4-10. ↑
- J1395.** Chen-Shane Chu. A Plastic Optical Fiber Sensor for the Dual Sensing of Temperature and Oxygen. / Chen-Shane Chu, Yu-Lung Lo. // IEEE Photonics Technology Letters. - 2008. - Vol. 20, No. 1. - P. 63-65. ↑
- J1396.** Chih-Lung Lin. A Novel Voltage-Feedback Pixel Circuit for AMOLED Displays. / Chih-Lung Lin, Tsung-Ting Tsai, Yung-Chih Chen. // Journal of Display Technology. - 2008. - Vol. 4, No. 1. - P. 54-60. ↑
- J1397.** Min-Hao Michael Lu. Power Consumption and Temperature Increase in Large Area Active-Matrix OLED Displays. / Min-Hao Michael Lu, Hack M., Hewitt R., Weaver M.S., Brown J.J. // Journal of Display Technology. - 2008. - Vol. 4, No. 1. - P. 47-53. ↑
- J1398.** Miettinen I. Effects of Saccade Length and Target Luminance on the Refresh Frequency Threshold for the Visibility of Color Break-Up. / Miettinen I., Nasanen R., Hakkinen J. // Journal of Display Technology. - 2008. - Vol. 4, No. 1. - P. 81-85. ↑
- J1399.** Reichelt S. Development of an Implantable Pulse Oximeter. / Reichelt S., Fiala J., Werber A., Forster K., Heilmann C., Klemm R., Zappe H. // IEEE Transactions on Biomedical Engineering. - 2008. - Vol. 55, No. 2. - P. 581-588. ↑
- J1400.** Senfar Wen. Representations of Relative Display Gamut Size. Journal of Display Technology. - 2008. - Vol. 4, No. 1. - P. 18-23. ↑
- J1401.** Lin Ke. Correlation of Current Noise Behavior and Dark Spot Formation in Organic Light-Emitting Diodes. / Lin Ke, Kumar R.S., Vijila C., Soo Jin Chua, Sun X.W. // IEEE Electron Device Letters. - 2008. - Vol. 29, No. 1. - P. 67-69. ↑
- J1402.** Tringe J.W. Radiation Effects on InGaN Quantum Wells and GaN Simultaneously Probed by Ion Beam-Induced Luminescence. / Tringe J.W., Conway A.M., Felter T.E., Chan W.J.M., Casteliz J., Lordi V., Xia Y., Stevens C.G., Wetzel C. // IEEE Transactions on Nuclear Science. - 2008. - Vol. 55, No. 6. - P. 3633-3637. ↑
- J1403.** Chang S.J. Nitride-Based LEDs With a Hybrid Al Mirror DBR Backside Reflector. / Chang S.J., Shen C.F., Hsieh M.H., Kuo C.T., Ko T.K., Chen W.S., Shei S.C. // Journal of Lightwave Technology. - 2008. - Vol. 26, No. 17. - P. 3131-3136. ↑
- J1404.** Xu Y.B. Hybrid Spintronic Structures With Magnetic Oxides and Heusler Alloys. / Xu Y.B., Hassan S., Wong P., Wu J., Claydon J.S., Lu Y.X., Damsgaard C.D., Hansen J.B., Jacobsen C.S., Zhai Y., van der Laan G., Feidenhans R., Holmes S.N. // IEEE Transactions on Magnetics. - 2008. - Vol. 44, No. 11. - P. 2959-2965. ↑
- J1405.** Ikkawi R. Design, Fabrication, and Characterization of Near-Field Apertures for 1 Tbit/in Areal Density. / Ikkawi R., Amos N., Hijazi Y., Litvinov D., Khizroev S. // IEEE Transactions on Magnetics. - 2008. - Vol. 44, No. 11. - P. 3364-3367. ↑
- J1406.** Mansell R. Observation of Phonon Replica Emission in an In-Situ Fe/GaAs Spin LED. / Mansell R., Laloe J.-B., Holmes S.N., Khan I., Yasar M., Petrou A., Farrer I., Jones G., Ritchie D.A., Bland J. // IEEE Transactions on Magnetics. - 2008. - Vol. 44, No. 11. - P. 2666-2669. ↑
- J1407.** Tran N.T. Studies of Phosphor Concentration and Thickness for Phosphor-Based White Light-Emitting-Diodes. / Tran N.T., Shi F.G. // Journal of Lightwave Technology. - 2008. - Vol. 26, No. 21. - P. 3556-3559. ↑
- J1408.** Kim K.M. Aluminium-based packaging platform for led using selectively anodising method. / Kim K.M., Shin S.H., Lee Y.K., Choi S.M., Kwon Y.S. // Electronics Letters. - 2008. - Vol. 44, No. 1. - P. 24-25. ↑
- J1409.** Khanna R. Aging and Stability of GaN High Electron Mobility Transistors and Light-Emitting Diodes With-and Ir-Based Contacts. / Khanna R., Stafford L., Voss L.F., Pearton S.J., Wang H.T., Anderson T., Sheng-

Chun Hung, Ren F. // IEEE Transactions on Device and Materials Reliability. - 2008. - Vol. 8, No. 2. - P. 272-276. ↑

J1410. Hao Wang. Active Packaging Method for Light-Emitting Diode Lamps With Photosensitive Epoxy Resins. / Hao Wang, Kyu-Seung Lee, Jae-Hyoung Ryu, Chang-Hee Hong, Yong-Hoon Cho. // IEEE Photonics Technology Letters. - 2008. - Vol. 20, No. 2. - P. 87-89. ↑

J1411. Grubor J. Broadband Information Broadcasting Using LED-Based Interior Lighting. / Grubor J., Randel S., Langer K.-D., Walewski J.W. // Journal of Lightwave Technology. - 2008. - Vol. 26, No. 24. - P. 3883-3892. ↑

J1412. Witzigmann B. Analysis of Gain and Luminescence in Violet and Blue GaInN-GaN Quantum Wells. / Witzigmann B., Tomamichel M., Steiger S., Veprek R.G., Kojima K., Schwarz U.T. // IEEE Journal of Quantum Electronics. - 2008. - Vol. 44, No. 2. - P. 144-149. ↑

J1413. Lianqiao Yang. Thermal Analysis of GaN-Based Light Emitting Diodes With Different Chip Sizes. / Lianqiao Yang, Jianzheng Hu, Lan Kim, Moo Whan Shin. // IEEE Transactions on Device and Materials Reliability. - 2008. - Vol. 8, No. 3. - P. 571-575. ↑

J1414. Yu-Lin Wang. Materials and Process Development for ZnMgO/ZnO Light-Emitting Diodes. / Yu-Lin Wang, Fan Ren, Kim H.S., Norton D.P., Pearton S.J. // IEEE Journal of Selected Topics in Quantum Electronics. - 2008. - Vol. 14, No. 4. - P. 1048-1052. ↑

J1415. Wern-Yarng Shieh. Design of the Radiation Pattern of Infrared Short-Range Communication Systems for Electronic-Toll-Collection Applications. / Wern-Yarng Shieh, Ti-Ho Wang, Yen-Hsih Chou, Chi-Chang Huang. // IEEE Transactions on Intelligent Transportation Systems. - 2008. - Vol. 9, No. 3. - P. 548-558. ↑

J1416. Sargent E.H. Solution-Processed Infrared Optoelectronics: Photovoltaics, Sensors, and Sources. IEEE Journal of Selected Topics in Quantum Electronics. - 2008. - Vol. 14, No. 4. - P. 1223-1229. ↑

J1417. Fujita M. Light Emission From Silicon in Photonic Crystal Nanocavity. / Fujita M., Tanaka Y., Noda S. // IEEE Journal of Selected Topics in Quantum Electronics. - 2008. - Vol. 14, No. 4. - P. 1090-1097. ↑

J1418. Pate R. Tabletop Resonant Infrared Matrix-Assisted Pulsed Laser Evaporation of Light-Emitting Organic Thin Films. / Pate R., Lantz K.R., Stiff-Roberts A.D. // IEEE Journal of Selected Topics in Quantum Electronics. - 2008. - Vol. 14, No. 4. - P. 1022-1030. ↑

J1419. Zhang H.M. Indium Tin Oxide Modified by Au and Vanadium Pentoxide as an Efficient Anode for Organic Light-Emitting Devices. / Zhang H.M., Choy W.C.H. // IEEE Transactions on Electron Devices. - 2008. - Vol. 55, No. 9. - P. 2517-2520. ↑

J1420. Lee H.-S. Corrections to "Low-Forward-Voltage-Drop 4H-SiC BJTs Without Base Contact Implantation". / Lee H.-S., Domeij M., Zetterling C.-M., Ostling M. // IEEE Transactions on Electron Devices. - 2008. - Vol. 55, No. 9. - P. 2531. ↑

J1421. Hojin Lee. Dynamic Response of Normal and Corbino a-Si:H TFTs for AM-OLEDs. / Hojin Lee, Chiang C.-S., Kanicki J. // IEEE Transactions on Electron Devices. - 2008. - Vol. 55, No. 9. - P. 2338-2347. ↑

J1422. Jae-Hoon Lee. Stress Reduction and Enhanced Extraction Efficiency of GaN-Based LED Grown on Cone-Shape-Patterned Sapphire. / Jae-Hoon Lee, Oh J.T., Kim Y.C., Jung-Hee Lee. // IEEE Photonics Technology Letters. - 2008. - Vol. 20, No. 18. - P. 1563-1565. ↑

J1423. Keunjoo Kim. Lattice Constant Effect of Photonic Crystals on the Light Output of Blue Light-Emitting Diodes. / Keunjoo Kim, Jaeho Choi, Jong Bae Park, Sang Cheol Jeon, Jin Soo Kim, Hee Mok Lee. // IEEE Photonics Technology Letters. - 2008. - Vol. 20, No. 17. - P. 1455-1457. ↑

J1424. McDowell J. Design of a color sensing system to aid the color blind. IEEE Potentials. - 2008. - Vol. 27, No. 4. - P. 34-39. ↑

J1425. Ducanhez A. Fabrication and Characterization of GaSb-Based Monolithic Resonant-Cavity Light-Emitting Diodes Emitting Around 2.3 μm and Including a Tunnel Junction. / Ducanhez A., Cerutti L., Gassenq A., Grech P., Genty F. // IEEE Journal of Selected Topics in Quantum Electronics. - 2008. - Vol. 14, No. 4. - P. 1014-1021. ↑

- J1426.** Villanueva A. A Novel Gaze Estimation System With One Calibration Point. / Villanueva A., Cabeza R. // IEEE Transactions on Systems, Man, and Cybernetics, Part B: Cybernetics. - 2008. - Vol. 38, No. 4. - P. 1123-1138. ↑
- J1427.** Tae-Wook Kim. Reliable Organic Nonvolatile Memory Device Using a Polyfluorene-Derivative Single-Layer Film. / Tae-Wook Kim, Seung-Hwan Oh, Hyejung Choi, Gunuk Wang, Hyunsang Hwang, Dong-Yu Kim, Takhee Lee. // IEEE Electron Device Letters. - 2008. - Vol. 29, No. 8. - P. 852-855. ↑
- J1428.** Ming-Kwei Lee. Enhancement of Light Extraction Efficiency of Gallium Nitride Flip-Chip Light-Emitting Diode With Silicon Oxide Hemispherical Microlens on its Back. / Ming-Kwei Lee, Chen-Lin Ho, Cho-Han Fan. // IEEE Photonics Technology Letters. - 2008. - Vol. 20, No. 15. - P. 1293-1295. ↑
- J1429.** Min Yann Hsieh. Improvement of External Extraction Efficiency in GaN-Based LEDs by Nanosphere Lithography. / Min Yann Hsieh, Cheng Yin Wang, Liang Yi Chen, Tzu Pu Lin, Min Yung Ke, Yun Wei Cheng, Yi Cheng Yu, Cheng Pin Chen, Dong Ming Yeh, Chih Feng Lu, Chi Feng Huang, Yang C.C., Jian Jang Huang. // IEEE Electron Device Letters. - 2008. - Vol. 29, No. 7. - P. 658-660. ↑
- J1430.** Kim H.G. Improved GaN-Based LED Light Extraction Efficiencies via Selective MOCVD Using Peripheral Microhole Arrays. / Kim H.G., Cuong T.V., Na M.G., Kim H.K., Kim H.Y., Ryu J.H., Hong C.-H. // IEEE Photonics Technology Letters. - 2008. - Vol. 20, No. 15. - P. 1284-1286. ↑
- J1431.** Lianqiao Yang. Dynamic Thermal Analysis of High-Power LEDs at Pulse Conditions. / Lianqiao Yang, Jianzheng Hu, Moo Whan Shin. // IEEE Electron Device Letters. - 2008. - Vol. 29, No. 8. - P. 863-866. ↑
- J1432.** Wen-Hung Chuang. Numerical Study on Quantum Efficiency Enhancement of a Light-Emitting Diode Based on Surface Plasmon Coupling With a Quantum Well. / Wen-Hung Chuang, Jyh-Yang Wang, Yang C.C., Yean-Woei Kiang. // IEEE Photonics Technology Letters. - 2008. - Vol. 20, No. 16. - P. 1339-1341. ↑
- J1433.** Jongwoon Park. Energy Loss Mechanism in Organic and Inorganic Light-Emitting Diodes. / Jongwoon Park, Taewon Kim, Jongho Lee, Dongchan Shin. // IEEE Photonics Technology Letters. - 2008. - Vol. 20, No. 16. - P. 1408-1410. ↑
- J1434.** Sambandan S. Software Prediction of Threshold Voltage Shift for Amorphous Silicon TFT-Based Displays. / Sambandan S., Ng T., Endicott F. // Journal of Display Technology. - 2008. - Vol. 4, No. 3. - P. 304-307. ↑
- J1435.** Sung-Nam Lee. Behaviors of Emission Wavelength Shift in AlInGaIn-Based Green Laser Diodes. / Sung-Nam Lee, Ryu H.Y., Paek H.S., Son J.K., Sung Y.J., Kim K.S., Kim H.K., Kim H., Jang T., Ha K.H., Nam O.H., Park Y. // IEEE Electron Device Letters. - 2008. - Vol. 29, No. 8. - P. 870-872. ↑
- J1436.** Jaechul Park. Source/Drain Series-Resistance Effects in Amorphous Gallium-Indium Zinc-Oxide Thin Film Transistors. / Jaechul Park, Changjung Kim, Sunil Kim, Ihun Song, Sangwook Kim, Donghun Kang, Hyuck Lim, Huaxiang Yin, Ranju Jung, Eunha Lee, Jaecheol Lee, Kee-Won Kwon, Youngsoo Park. // IEEE Electron Device Letters. - 2008. - Vol. 29, No. 8. - P. 879-881. ↑
- J1437.** Jeung-Mo Kang. Fabrication and Thermal Analysis of Wafer-Level Light-Emitting Diode Packages. / Jeung-Mo Kang, Jeong-Hyeon Choi, Du-Hyun Kim, Jae-Wook Kim, Yong-Seon Song, Geun-Ho Kim, Sang-Kook Han. // IEEE Electron Device Letters. - 2008. - Vol. 29, No. 10. - P. 1118-1120. ↑
- J1438.** Su Y.K. GaN Metal-Semiconductor-Metal Photodetectors With SiN/GaN Nucleation Layer. / Su Y.K., Chang S.J., Jhou Y.D., Wu S.L., Liu C.H. // IEEE Sensors Journal. - 2008. - Vol. 8, No. 10. - P. 1693-1697. ↑
- J1439.** Locci S. Modeling of Short-Channel Effects in Organic Thin-Film Transistors. / Locci S., Morana M., Orgiu E., Bonfiglio A., Lugli P. // IEEE Transactions on Electron Devices. - 2008. - Vol. 55, No. 10. - P. 2561-2567. ↑
- J1440.** Kabra D. Model for Studies of Lateral Photovoltaic Effect in Polymeric Semiconductors. / Kabra D., Verma J., Vidhyadhiraja N. S., Narayan K. S. // IEEE Sensors Journal. - 2008. - Vol. 8, No. 10. - P. 1663-1671. ↑
- J1441.** Ruchi Agrawal. Mechanism of Resistive Switching in 3, 4, 9, 10 Perylenetetracarboxylic Dianhydride (PTCDA) Sandwiched Between Metal Electrodes. / Ruchi Agrawal, Kumar P., Ghosh S. // IEEE Transactions on

Electron Devices. - 2008. - Vol. 55, No. 10. - P. 2795-2799. ↑

J1442. Orita K. Integration of Photonic Crystals on GaN-Based Blue LEDs Using Silicon Mold Substrates. / Orita K., Takase Y., Fukushima Y., Usuda M., Ueda T., Takigawa S., Tanaka T., Ueda D., Egawa T. // IEEE Journal of Quantum Electronics. - 2008. - Vol. 44, No. 10. - P. 984-989. ↑

J1443. Shibata S. Organic-Inorganic Hybrid Materials for Photonic Applications. / Shibata S., Yano T., Segawa H. // IEEE Journal of Selected Topics in Quantum Electronics. - 2008. - Vol. 14, No. 5. - P. 1361-1369. ↑

J1444. Sunho Jang. Thermal Analysis of LED Arrays for Automotive Headlamp With a Novel Cooling System. / Sunho Jang, Moo Whan Shin. // IEEE Transactions on Device and Materials Reliability. - 2008. - Vol. 8, No. 3. - P. 561-564. ↑

J1445. Fujita S. Luminescence Characteristics of YAG Glass-Ceramic Phosphor for White LED. / Fujita S., Sakamoto A., Tanabe S. // IEEE Journal of Selected Topics in Quantum Electronics. - 2008. - Vol. 14, No. 5. - P. 1387-1391. ↑

J1446. Chang S.J. GaN-Based Schottky Barrier Photodetectors With a 12-Pair Mg N -GaN Buffer Layer. / Chang S.J., Lee K.H., Chang P.C., Wang Y.C., Yu C.L., Kuo C.H., Wu S.L. // IEEE Journal of Quantum Electronics. - 2008. - Vol. 44, No. 10. - P. 916-921. ↑

J1447. Liang-Jyi Yan. Improved Light Extraction Efficiency in AlGaInP Light-Emitting Diodes by Applying a Periodic Texture on the Surface. / Liang-Jyi Yan, Sheu J.K., Wei-Chih Wen, Tien-Fu Liao, Ming-Jong Tsai, Chih-Sung Chang. // IEEE Photonics Technology Letters. - 2008. - Vol. 20, No. 20. - P. 1724-1726. ↑

J1448. Maiwald M. Wavelength-Stabilized Compact Diode Laser System on a Microoptical Bench With 1.5-W Optical Output Power at 671 nm. / Maiwald M., Ginolas A., Muller A., Sahm A., Sumpf B., Erbert G., Trankle G. // IEEE Photonics Technology Letters. - 2008. - Vol. 20, No. 19. - P. 1627-1629. ↑

J1449. Wu M.K. Ultraviolet Electroluminescence From n-ZnO-SiO₂-ZnO Nanocomposite/p-GaN Heterojunction Light-Emitting Diodes at Forward and Reverse Bias. / Wu M.K., Shih Y.T., Li W.C., Chen H.C., Chen M.J., Kuan H., Yang J.R., Shiojiri M. // IEEE Photonics Technology Letters. - 2008. - Vol. 20, No. 21. - P. 1772-1774. ↑

J1450. Soo Young Kim. Flexible Organic Light-Emitting Diodes Using a Metal Peel-Off Method. / Soo Young Kim, Kisoo Kim, Kihyon Hong, Jong-Lam Lee. // IEEE Photonics Technology Letters. - 2008. - Vol. 20, No. 22. - P. 1836-1838. ↑

J1451. Jae-Hyun Ryou. Effect of Silicon Doping in the Quantum-Well Barriers on the Electrical and Optical Properties of Visible Green Light-Emitting Diodes. / Jae-Hyun Ryou, Jae Limb, Wonseok Lee, Jianping Liu, Lochner Z., Dongwon Yoo, Dupuis R.D. // IEEE Photonics Technology Letters. - 2008. - Vol. 20, No. 21. - P. 1769-1771. ↑

J1452. Linping Mu. A Color Stable Blue Light-Emitting Device Using a Pyrazolo[3,4-b]Quinoline Derivative as an Emitter. / Linping Mu, Zhiquan He, Jing Wang, Guanbao Hui, Yongsheng Wang, Xiping Jing, Danel A., Kulig E. // IEEE Photonics Technology Letters. - 2008. - Vol. 20, No. 21. - P. 1781-1783. ↑

J1453. Huang J.J. Effect of the Phase Shift in a Periodic Anode on the Emission Spectra of Top-Emitting Organic Light-Emitting Diodes. / Huang J.J., Su Y.K., Juang F.S., Liu Y.H., Chang S.J. // IEEE Photonics Technology Letters. - 2008. - Vol. 20, No. 21. - P. 1784-1786. ↑

J1454. Sang-Mook Kim. Optical and Structural Properties of InGaN-AlGaIn Ultraviolet Light-Emitting Diodes. / Sang-Mook Kim, Jae Bum Kim, Junggeun Jhin, Jong Hyeob Baek, In Hwan Lee, Gun Young Jung. // IEEE Photonics Technology Letters. - 2008. - Vol. 20, No. 23. - P. 1911-1913. ↑

J1455. Jin-Wei Shi. Linear Cascade GaN-Based Green Light-Emitting Diodes With Invariant High-Speed/Power Performance Under High-Temperature Operation. / Jin-Wei Shi, Chen P.-Y., Chen C.-C., Jinn-Kong Sheu, Wei-Chi Lai, Yun-Chih Lee, Po-Shen Lee, Shih-Pu Yang, Mount-Learn Wu. // IEEE Photonics Technology Letters. - 2008. - Vol. 20, No. 23. - P. 1896-1898. ↑

J1456. Hung-Cheng Lin. Light Output Enhancement of InGaIn Light-Emitting Diodes Grown on Masklessly Etched Sapphire Substrates. / Hung-Cheng Lin, Ruo-Syuan Lin, Jen-Inn Chyi, Chia-Ming Lee. // IEEE Photonics Technology Letters. - 2008. - Vol. 20, No. 19. - P. 1621-1623. ↑

- J1457.** Jun-Rong Chen. Fabrication and Characterization of Temperature Insensitive 660-nm Resonant-Cavity LEDs. / Jun-Rong Chen, Tsung-Shine Ko, Tien-Chang Lu, Yi-An Chang, Hao-Chung Kuo, Yen-Kuang Kuo, Jui-Yen Tsai, Li-Wen Lai, Shing-Chung Wang. // Journal of Lightwave Technology. - 2008. - Vol. 26, No. 13. - P. 1891-1900. ↑
- J1458.** Hyun Min Cho. Metal-Core Printed Circuit Board With Alumina Layer by Aerosol Deposition Process. / Hyun Min Cho, Hyeong Joon Kim. // IEEE Electron Device Letters. - 2008. - Vol. 29, No. 9. - P. 991-993. ↑
- J1459.** Nayaki M.P. Real-time corrosion mapping of steel surfaces using an optoelectronic instrument based on lightwave scattering. / Nayaki M.P., Kabilan A.P. // IET Science, Measurement & Technology. - 2008. - Vol. 2, No. 5. - P. 269-274. ↑
- J1460.** Masui Hisashi. Optical polarization characteristics of In Ga N /Ga N light-emitting diodes fabricated on GaN substrates oriented between (101 0) and (101 1) planes. / Masui Hisashi, Yamada Hisashi, Iso Kenji, Nakamura Shuji, DenBaars Steven P. // Applied Physics Letters. - 2008. - Vol. 92, No. 9. - P. 091105-091105-3. ↑
- J1461.** Cai Xiuyu. Electron and hole transport in a wide bandgap organic phosphine oxide for blue electrophosphorescence. / Cai Xiuyu, Padmaperuma Asanga B., Sapochak Linda S., Vecchi Paul A., Burrows Paul E. // Applied Physics Letters. - 2008. - Vol. 92, No. 8. - P. 083308-083308-3. ↑
- J1462.** Park Il-Kyu. Phosphor-free white light-emitting diode with laterally distributed multiple quantum wells. / Park Il-Kyu, Kim Ja-Yeon, Kwon Min-Ki, Cho Chu-Young, Lim Jae-Hong, Park Seong-Ju. // Applied Physics Letters. - 2008. - Vol. 92, No. 9. - P. 091110-091110-3. ↑
- J1463.** Baumgartner A. Upconversion electroluminescence in InAs quantum dot light-emitting diodes. / Baumgartner A., Chaggar A., Patane A., Eaves L., Henini M. // Applied Physics Letters. - 2008. - Vol. 92, No. 9. - P. 091121-091121-3. ↑
- J1464.** Yeh Dong-Ming. White-light light-emitting device based on surface plasmon-enhanced Cd Se /Zn S nanocrystal wavelength conversion on a blue/green two-color light-emitting diode. / Yeh Dong-Ming, Huang Chi-Feng, Lu Yen-Cheng, Yang C. C. // Applied Physics Letters. - 2008. - Vol. 92, No. 9. - P. 091112-091112-3. ↑
- J1465.** Jeong Soon Moon. Enhancement of normally directed light outcoupling from organic light-emitting diodes using nanoimprinted low-refractive-index layer. / Jeong Soon Moon, Araoka Fumito, Machida Yoshimi, Ishikawa Ken, Takezoe Hideo, Nishimura Suzushi, Suzuki Goro. // Applied Physics Letters. - 2008. - Vol. 92, No. 8. - P. 083307-083307-3. ↑
- J1466.** Setlur A. A. Eu 2+ -Mn 2+ phosphor saturation in 5 mm light emitting diode lamps. / Setlur A. A., Shiang J. J., Happek U. // Applied Physics Letters. - 2008. - Vol. 92, No. 8. - P. 081104-081104-3. ↑
- J1467.** Xiang Hai-Feng. Star-configured carbazole as an efficient near-ultraviolet emitter and hole-transporting material for organic light-emitting devices. / Xiang Hai-Feng, Xu Zong-Xiang, Roy V. A. L., Che Chi-Ming, Lai P. T., Zeng Peng-Ju, Niu Fang-Fang, Liu Ya-Wei, Tang Wei-Qun, He Cai-Jie, Niu Han-Ben. // Applied Physics Letters. - 2008. - Vol. 92, No. 7. - P. 073305-073305-3. ↑
- J1468.** Lee Sung-Nam. Monolithic InGaN-based white light-emitting diodes with blue, green, and amber emissions. / Lee Sung-Nam, Paek H. S., Kim H., Jang T., Park Y. // Applied Physics Letters. - 2008. - Vol. 92, No. 8. - P. 081107-081107-3. ↑
- J1469.** Li Xiao. Very high-efficiency organic light-emitting diodes based on cyclometallated rhenium (I) complex. / Li Xiao, Zhang Dongyu, Li Wenlian, Chu Bei, Han Liangliang, Zhu Jianzhuo, Su Zisheng, Bi Defeng, Wang Dan, Yang Dongfang, Chen Yiren. // Applied Physics Letters. - 2008. - Vol. 92, No. 8. - P. 083302-083302-3. ↑
- J1470.** Ho Cheuk-Lam. High-efficiency and color-stable white organic light-emitting devices based on sky blue electrofluorescence and orange electrophosphorescence. / Ho Cheuk-Lam, Lin Mei-Fang, Wong Wai-Yeung, Wong Wai-Kwok, Chen Chin H. // Applied Physics Letters. - 2008. - Vol. 92, No. 8. - P. 083301-083301-3. ↑
- J1471.** Kim Hyunsoo. Leakage current origins and passivation effect of GaN-based light emitting diodes fabricated with Ag p -contacts. / Kim Hyunsoo, Cho Jaehee, Park Yongjo, Seong Tae-Yeon. // Applied Physics Letters. - 2008. - Vol. 92, No. 9. - P. 092115-092115-3. ↑

- J1472.** Damilano B. Monolithic white light emitting diodes using a (Ga,In)N/GaN multiple quantum well light converter. / Damilano B., Dussaigne A., Brault J., Huault T., Natali F., Demolon P., De Mierry P., Chenot S., Massies J. // Applied Physics Letters. - 2008. - Vol. 93, No. 10. - P. 101117-101117-3. ↑
- J1473.** Park Eun-Hyun. The effect of the last quantum barrier on the internal quantum efficiency of InGaN-light emitting diode. / Park Eun-Hyun, Jang Jin, Gupta Shalini, Ferguson Ian, Jeon Soo-Kun, Lim Jae-Gu, Lee Jun-Serk, Kim Cheol-Hoi, Park Joong-Seo. // Applied Physics Letters. - 2008. - Vol. 93, No. 10. - P. 101112-101112-3. ↑
- J1474.** Ma Ping. Enhanced electroluminescence intensity of In Ga N /Ga N multi-quantum-wells based on Mg-doped GaN annealed in O₂. / Ma Ping, Gai Yanqin, Wang Junxi, Yang Fuhua, Zeng Yiping, Li Jinmin, Li Jingbo. // Applied Physics Letters. - 2008. - Vol. 93, No. 10. - P. 102112-102112-3. ↑
- J1475.** Vaynzof Yana. Enhancement of electron injection into a light-emitting polymer from an aluminum oxide cathode modified by a self-assembled monolayer. / Vaynzof Yana, Dennes T. Joseph, Schwartz Jeffrey, Kahn Antoine. // Applied Physics Letters. - 2008. - Vol. 93, No. 10. - P. 103305-103305-3. ↑
- J1476.** Leem Dong-Seok. Highly efficient tandem p-i-n organic light-emitting diodes adopting a low temperature evaporated rhenium oxide interconnecting layer. / Leem Dong-Seok, Lee Jae-Hyun, Kim Jang-Joo, Kang Jae-Wook. // Applied Physics Letters. - 2008. - Vol. 93, No. 10. - P. 103304-103304-3. ↑
- J1477.** Dou X. M. Single-photon-emitting diode at liquid nitrogen temperature. / Dou X. M., Chang X. Y., Sun B. Q., Xiong Y. H., Niu Z. C., Huang S. S., Ni H. Q., Du Y., Xia J. B. // Applied Physics Letters. - 2008. - Vol. 93, No. 10. - P. 101107-101107-3. ↑
- J1478.** Kim Kyung-Ho. Solution-based formation of multilayers of small molecules for organic light emitting diodes. / Kim Kyung-Ho, Huh Sung-Yoon, Seo Soon-min, Lee Hong H. // Applied Physics Letters. - 2008. - Vol. 92, No. 9. - P. 093307-093307-3. ↑
- J1479.** Xie Guohua. Very low turn-on voltage and high brightness tris-(8-hydroxyquinoline) aluminum-based organic light-emitting diodes with a Mo O x p -doping layer. / Xie Guohua, Meng Yanlong, Wu Fengmin, Tao Chen, Zhang Dandan, Liu Mingjun, Xue Qin, Chen Wen, Zhao Yi. // Applied Physics Letters. - 2008. - Vol. 92, No. 9. - P. 093305-093305-3. ↑
- J1480.** Chao Yu-Chiang. Polymer hot-carrier transistor with low bandgap emitter. / Chao Yu-Chiang, Xie Ming-Hong, Dai Ming-Zhi, Meng Hsin-Fei, Horng Sheng-Fu, Hsu Chain-Shu. // Applied Physics Letters. - 2008. - Vol. 92, No. 9. - P. 093310-093310-3. ↑
- J1481.** Tan S. T. Ultraviolet and visible electroluminescence from n-Zn O /Si O x /(n,p)-Si heterostructured light-emitting diodes. / Tan S. T., Sun X. W., Zhao J. L., Iwan S., Cen Z. H., Chen T. P., Ye J. D., Lo G. Q., Kwong D. L., Teo K. L. // Applied Physics Letters. - 2008. - Vol. 93, No. 1. - P. 013506-013506-3. ↑
- J1482.** Yook Kyoung Soo. Transparent organic light emitting diodes using a multilayer oxide as a low resistance transparent cathode. / Yook Kyoung Soo, Jeon Soon Ok, Joo Chul Woong, Lee Jun Yeob. // Applied Physics Letters. - 2008. - Vol. 93, No. 1. - P. 013301-013301-3. ↑
- J1483.** Zaumseil Jana. Electroluminescence imaging and microstructure of organic light-emitting field-effect transistors. / Zaumseil Jana, Kline R. Joseph, Sirringhaus Henning. // Applied Physics Letters. - 2008. - Vol. 92, No. 7. - P. 073304-073304-3. ↑
- J1484.** Lee Tae-Woo. High-efficiency stacked white organic light-emitting diodes. / Lee Tae-Woo, Noh Taeyong, Choi Byoung-Ki, Kim Myeong-Suk, Shin Dong Woo, Kido Junji. // Applied Physics Letters. - 2008. - Vol. 92, No. 4. - P. 043301-043301-3. ↑
- J1485.** Wang R. S. Studies of oxide/ZnO near-interfacial defects by photoluminescence and deep level transient spectroscopy. / Wang R. S., Gu Q. L., Ling C. C., Ong H. C. // Applied Physics Letters. - 2008. - Vol. 92, No. 4. - P. 042105-042105-3. ↑
- J1486.** Campbell I. H. Efficient, visible organic light-emitting diodes utilizing a single polymer layer doped with quantum dots. / Campbell I. H., Crone B. K. // Applied Physics Letters. - 2008. - Vol. 92, No. 4. - P. 043303-043303-3. ↑

- J1487.** Qian Lei. Effects of ultraviolet light irradiation on poly(vinylcarbazole). / Qian Lei, Bera Debasis, Holloway Paul H. // Applied Physics Letters. - 2008. - Vol. 92, No. 5. - P. 053303-053303-3. ↑
- J1488.** Arnold Michael S. Direct vapor jet printing of three color segment organic light emitting devices for white light illumination. / Arnold Michael S., McGraw Gregory J., Forrest Stephen R., Lunt Richard R. // Applied Physics Letters. - 2008. - Vol. 92, No. 5. - P. 053301-053301-3. ↑
- J1489.** Galtrey M. J. Compositional inhomogeneity of a high-efficiency In x Ga 1-x N based multiple quantum well ultraviolet emitter studied by three dimensional atom probe. / Galtrey M. J., Oliver R. A., Kappers M. J., McAleese C., Zhu D., Humphreys C. J., Clifton P. H., Larson D., Cerezo A. // Applied Physics Letters. - 2008. - Vol. 92, No. 4. - P. 041904-041904-3. ↑
- J1490.** Nizamoglu Sedat. Color-converting combinations of nanocrystal emitters for warm-white light generation with high color rendering index. / Nizamoglu Sedat, Zengin Gulis, Demir Hilmi Volkan. // Applied Physics Letters. - 2008. - Vol. 92, No. 3. - P. 031102-031102-3. ↑
- J1491.** Xiong Tao. Cesium hydroxide doped tris-(8-hydroxyquinoline) aluminum as an effective electron injection layer in inverted bottom-emission organic light emitting diodes. / Xiong Tao, Wang Fengxia, Qiao Xianfeng, Ma Dongge. // Applied Physics Letters. - 2008. - Vol. 92, No. 26. - P. 263305-263305-3. ↑
- J1492.** Kraker Elke. Integrated organic electronic based optochemical sensors using polarization filters. / Kraker Elke, Haase Anja, Lamprecht Bernhard, Jakopic Georg, Konrad Christian, Kostler Stefan. // Applied Physics Letters. - 2008. - Vol. 92, No. 3. - P. 033302-033302-3. ↑
- J1493.** Kohnen Anne. Simultaneous color and luminance control of organic light-emitting diodes for mood-lighting applications. / Kohnen Anne, Meerholz Klaus, Hagemann Malte, Brinkmann Matthias, Sinzinger Stefan. // Applied Physics Letters. - 2008. - Vol. 92, No. 3. - P. 033305-033305-3. ↑
- J1494.** Lee Jaewon. Cavity effects on light extraction in organic light emitting devices. / Lee Jaewon, Chopra Neetu, So Franky. // Applied Physics Letters. - 2008. - Vol. 92, No. 3. - P. 033303-033303-3. ↑
- J1495.** Wang Dan. Highly efficient green organic light-emitting diodes from single exciplex emission. / Wang Dan, Li Wenlian, Chu Bei, Su Zisheng, Bi Defeng, Zhang Dongyu, Zhu Jianzhuo, Yan Fei, Chen Yiren, Tsuboi Taiju. // Applied Physics Letters. - 2008. - Vol. 92, No. 5. - P. 053304-053304-3. ↑
- J1496.** Liu Hongyu. Laminated active matrix organic light-emitting devices. / Liu Hongyu, Sun Runguang. // Applied Physics Letters. - 2008. - Vol. 92, No. 6. - P. 063304-063304-3. ↑
- J1497.** Zhang Yong. High-efficiency and solution processible multilayer white polymer light-emitting diodes using neutral conjugated surfactant as an electron injection layer. / Zhang Yong, Huang Fei, Jen Alex K.-Y., Chi Yun. // Applied Physics Letters. - 2008. - Vol. 92, No. 6. - P. 063303-063303-3. ↑
- J1498.** Matsushima Toshinori. Suppression of exciton annihilation at high current densities in organic light-emitting diode resulting from energy-level alignments of carrier transport layers. / Matsushima Toshinori, Adachi Chihaya. // Applied Physics Letters. - 2008. - Vol. 92, No. 6. - P. 063306-063306-3. ↑
- J1499.** Zhao W. Q. Passivated p -type silicon: Hole injection tunable anode material for organic light emission. / Zhao W. Q., Ran G. Z., Xu W. J., Qin G. G. // Applied Physics Letters. - 2008. - Vol. 92, No. 7. - P. 073303-073303-3. ↑
- J1500.** Zhang Deqiang. Lithium cobalt oxide as electron injection material for high performance organic light-emitting diodes. / Zhang Deqiang, Li Yang, Zhang Guohui, Gao Yudi, Duan Lian, Wang Liduo, Qiu Yong. // Applied Physics Letters. - 2008. - Vol. 92, No. 7. - P. 073301-073301-3. ↑
- J1501.** Lewis L. Electroless nickel/gold Ohmic contacts to p -type GaN. / Lewis L., Casey D. P., Jeyaseelan A. V., Rohan J. F., Maaskant P. P. // Applied Physics Letters. - 2008. - Vol. 92, No. 6. - P. 062113-062113-3. ↑
- J1502.** David Aurelien. Carrier distribution in (0001)In Ga N /Ga N multiple quantum well light-emitting diodes. / David Aurelien, Grundmann Michael J., Kaeding John F., Gardner Nathan F., Mihopoulos Theodoros G., Krames Michael R. // Applied Physics Letters. - 2008. - Vol. 92, No. 5. - P. 053502-053502-3. ↑
- J1503.** Schwartz Gregor. Reduced efficiency roll-off in high-efficiency hybrid white organic light-emitting

diodes. / Schwartz Gregor, Reineke Sebastian, Walzer Karsten, Leo Karl. // Applied Physics Letters. - 2008. - Vol. 92, No. 5. - P. 053311-053311-3. ↑

J1504. Lee M. K. High light extraction efficiency of gallium nitride light emitting diode with silicon oxide hemispherical microlens. / Lee M. K., Ho C. L., Fan C. H. // Applied Physics Letters. - 2008. - Vol. 92, No. 6. - P. 061103-061103-3. ↑

J1505. Amo A. Optically induced ultrafast quenching of the semiconductor quantum well luminescence. / Amo A., Ballarini D., Sanvitto D., Kozhemyakina E., Vina L., Lemaître A., Bajoni D., Bloch J. // Applied Physics Letters. - 2008. - Vol. 92, No. 6. - P. 061912-061912-3. ↑

J1506. Kim Hyung Gu. Spatial distribution of crown shaped light emission from a periodic inverted polygonal deflector embedded in an In Ga N /Ga N light emitting diode. / Kim Hyung Gu, Cuong Tran Viet, Jeong Hyun, Woo Seung Hee, Cha Ok Hwan, Suh Eun-Kyung, Hong Chang-Hee, Cho Hyung Koun, Kong Bo Hyun, Jeong Mun Seok. // Applied Physics Letters. - 2008. - Vol. 92, No. 6. - P. 061118-061118-3. ↑

J1507. Zhu D. X. Highly polarized white-light emission from a single copolymer based on fluorene. / Zhu D. X., Zhen H. Y., Ye H., Liu X. // Applied Physics Letters. - 2008. - Vol. 93, No. 16. - P. 163309-163309-3. ↑

J1508. Sharma Asha. Stabilization of the work function of indium tin oxide using organic surface modifiers in organic light-emitting diodes. / Sharma Asha, Kippelen Bernard, Hotchkiss Peter J., Marder Seth R. // Applied Physics Letters. - 2008. - Vol. 93, No. 16. - P. 163308-163308-3. ↑

J1509. Ni Xianfeng. Reduction of efficiency droop in InGaN light emitting diodes by coupled quantum wells. / Ni Xianfeng, Fan Qian, Shimada Ryoko, Ozgur Umit, Morkoc Hadis. // Applied Physics Letters. - 2008. - Vol. 93, No. 17. - P. 171113-171113-3. ↑

J1510. Choi Sang Hun. The effect of electrode heat sink in organic-electronic devices. / Choi Sang Hun, Lee Tae Il, Baik Hong Koo, Roh Hee Hwan, Kwon Ohmyoung, Suh Dong hak. // Applied Physics Letters. - 2008. - Vol. 93, No. 18. - P. 183301-183301-3. ↑

J1511. Arians R. Electrically driven single quantum dot emitter operating at room temperature. / Arians R., Gust A., Kummell T., Kruse C., Zaitsev S., Bacher G., Hommel D. // Applied Physics Letters. - 2008. - Vol. 93, No. 17. - P. 173506-173506-3. ↑

J1512. Anzenbacher Pavel. High-purity white light from a simple single dopant host-guest white organic light-emitting diode architecture. / Anzenbacher Pavel, Montes Victor A., Takizawa Shin-ya. // Applied Physics Letters. - 2008. - Vol. 93, No. 16. - P. 163302-163302-3. ↑

J1513. Ko Seung H. Nanomaterial enabled laser transfer for organic light emitting material direct writing. / Ko Seung H., Pan Heng, Ryu Sang G., Misra Nipun, Grigoropoulos Costas. P., Park Hee K. // Applied Physics Letters. - 2008. - Vol. 93, No. 15. - P. 151110-151110-3. ↑

J1514. Ma Liang. Investigation of Eu-Mn energy transfer in $A_3MgSi_2O_8:Eu^{2+}, Mn^{2+}$ ($A=Ca, Sr, Ba$) for light-emitting diodes for plant cultivation. / Ma Liang, Wang Da-jian, Mao Zhi-yong, Lu Qi-fei, Yuan Zhi-hao. // Applied Physics Letters. - 2008. - Vol. 93, No. 14. - P. 144101-144101-3. ↑

J1515. Lu Y. MgO thickness dependence of spin injection efficiency in spin-light emitting diodes. / Lu Y., Truong V. G., Renucci P., Tran M., Jaffres H., Deranlot C., George J.-M., Lemaître A., Zheng Y., Demaille D., Binh P.-H., Amand T., Marie X. // Applied Physics Letters. - 2008. - Vol. 93, No. 15. - P. 152102-152102-3. ↑

J1516. Chen Ping. Color-stable and efficient stacked white organic light-emitting devices comprising blue fluorescent and orange phosphorescent emissive units. / Chen Ping, Xue Qin, Xie Wenfa, Duan Yu, Xie Guohua, Zhao Yi, Hou Jingying, Liu Shiyong, Zhang Liying, Li Bin. // Applied Physics Letters. - 2008. - Vol. 93, No. 15. - P. 153508-153508-3. ↑

J1517. Tseng Shin-Rong. Multilayer polymer light-emitting diodes by blade coating method. / Tseng Shin-Rong, Meng Hsin-Fei, Lee Kuan-Chen, Horng Sheng-Fu. // Applied Physics Letters. - 2008. - Vol. 93, No. 15. - P. 153308-153308-3. ↑

J1518. Xie Kai. Organic cesium salt as an efficient electron injection material for organic light-emitting diodes. / Xie Kai, Qiao Juan, Duan Lian, Li Yang, Zhang Deqiang, Dong Guifang, Wang Liduo, Qiu Yong. // Applied

Physics Letters. - 2008. - Vol. 93, No. 18. - P. 183302-183302-3. ↑

J1519. Yang Xiaohui. Highly efficient excimer-based white phosphorescent devices with improved power efficiency and color rendering index. / Yang Xiaohui, Wang Zixing, Madakuni Sijesh, Li Jian, Jabbour Ghassan E. // Applied Physics Letters. - 2008. - Vol. 93, No. 19. - P. 193305-193305-3. ↑

J1520. Granstrom J. Encapsulation of organic light-emitting devices using a perfluorinated polymer. / Granstrom J., Swensen J. S., Moon J. S., Rowell G., Yuen J., Heeger A. J. // Applied Physics Letters. - 2008. - Vol. 93, No. 19. - P. 193304-193304-3. ↑

J1521. Qi Xiangfei. Stacked white organic light emitting devices consisting of separate red, green, and blue elements. / Qi Xiangfei, Slocumsky Michael, Forrest Stephen. // Applied Physics Letters. - 2008. - Vol. 93, No. 19. - P. 193306-193306-3. ↑

J1522. Yang Chung Chieh. Improving light output power of InGaN-based light emitting diodes with pattern-nanoporous p-type GaN:Mg surfaces. / Yang Chung Chieh, Lin Chia Feng, Lin Chun Min, Chang Cheng Chien, Chen Kuei Ting, Chien Jui Fen, Chang Chung Ying. // Applied Physics Letters. - 2008. - Vol. 93, No. 20. - P. 203103-203103-3. ↑

J1523. Saha D. A monolithically integrated magneto-optoelectronic circuit. / Saha D., Basu D., Bhattacharya P. // Applied Physics Letters. - 2008. - Vol. 93, No. 19. - P. 194104-194104-3. ↑

J1524. Yoon Ji-hwan. Analysis of efficiency characteristics of green phosphorescent organic light-emitting devices. / Yoon Ji-hwan, Park Il-soo. // Applied Physics Letters. - 2008. - Vol. 93, No. 19. - P. 193303-193303-3. ↑

J1525. Ding B. F. Electroluminescence and magnetoresistance of the organic light-emitting diode with a La 0.7 Sr 0.3 Mn O 3 anode. / Ding B. F., Zhan Y. Q., Sun Z. Y., Ding X. M., Hou X. Y., Wu Y. Z., Bergenti I., Dediu V. // Applied Physics Letters. - 2008. - Vol. 93, No. 18. - P. 183307-183307-3. ↑

J1526. Peng Juan. Simultaneous light emissions from two different types of fluorophores in diblock copolymer micellar films. / Peng Juan, Chen Minjie, Qiu Feng, Yang Yuliang, Sohn Byeong-Hyeok, Kim Dong Ha. // Applied Physics Letters. - 2008. - Vol. 93, No. 18. - P. 183303-183303-3. ↑

J1527. Williams Christopher D. Multiwalled carbon nanotube sheets as transparent electrodes in high brightness organic light-emitting diodes. / Williams Christopher D., Robles Raquel Ovalle, Zhang Mei, Li Sergey, Baughman Ray H., Zakhidov Anvar A. // Applied Physics Letters. - 2008. - Vol. 93, No. 18. - P. 183506-183506-3. ↑

J1528. Kang Seung-Hee. Quantum-dot light-emitting diodes utilizing Cd Se /Zn S nanocrystals embedded in Ti O 2 thin film. / Kang Seung-Hee, Kumar Ch. Kiran, Lee Zonghoon, Kim Kyung-Hyun, Huh Chul, Kim Eui-Tae. // Applied Physics Letters. - 2008. - Vol. 93, No. 19. - P. 191116-191116-3. ↑

J1529. Park Eun-Hyun. Air-voids embedded high efficiency InGaN-light emitting diode. / Park Eun-Hyun, Jang Jin, Gupta Shalini, Ferguson Ian, Kim Cheol-Hoi, Jeon Soo-Kun, Park Joong-Seo. // Applied Physics Letters. - 2008. - Vol. 93, No. 19. - P. 191103-191103-3. ↑

J1530. Lai S. L. Approaches for achieving highly efficient exciplex-based organic light-emitting devices. / Lai S. L., Chan M. Y., Tong Q. X., Fung M. K., Wang P. F., Lee C. S., Lee S. T. // Applied Physics Letters. - 2008. - Vol. 93, No. 14. - P. 143301-143301-3. ↑

J1531. Fellows Natalie N. Dichromatic color tuning with InGaN-based light-emitting diodes. / Fellows Natalie N., Sato Hitoshi, Lin You-da, Chung Roy B., DenBaars Steven P., Nakamura Shuji. // Applied Physics Letters. - 2008. - Vol. 93, No. 12. - P. 121112-121112-3. ↑

J1532. Xie Jinqiao. On the efficiency droop in InGaN multiple quantum well blue light emitting diodes and its reduction with p-doped quantum well barriers. / Xie Jinqiao, Ni Xianfeng, Fan Qian, Shimada Ryoko, Ozgur Umit, Morkoc Hadis. // Applied Physics Letters. - 2008. - Vol. 93, No. 12. - P. 121107-121107-3. ↑

J1533. Zhuang Q. Molecular beam epitaxial growth of InAsN:Sb for midinfrared Optoelectronics. / Zhuang Q., Godenir A., Krier A., Tsai G., Lin H. H. // Applied Physics Letters. - 2008. - Vol. 93, No. 12. - P. 121903-121903-3. ↑

- J1534.** Hua Chi-Chung. Controlling bulk aggregation state in semiconducting conjugated polymer solution. / Hua Chi-Chung, Kuo Chih-Yuan, Chen Show-An. // Applied Physics Letters. - 2008. - Vol. 93, No. 12. - P. 123303-123303-3. ↑
- J1535.** Maeng Jongsun. Transient reverse current phenomenon in a p-n heterojunction comprised of poly(3,4-ethylene-dioxythiophene):poly(styrene-sulfonate) and ZnO nanowall. / Maeng Jongsun, Jo Minseok, Kang Seok-Ju, Kwon Min-Ki, Jo Gunho, Kim Tae-Wook, Seo Jaeduck, Hwang Hyunsang, Kim Dong-Yu, Park Seong-Ju, Lee Takhee. // Applied Physics Letters. - 2008. - Vol. 93, No. 12. - P. 123109-123109-3. ↑
- J1536.** Wang Yu. Application of mixed interface in white-electrophosphorescent devices: An efficient approach to adjust the distributions of carriers. / Wang Yu, Hua Yulin, Wu Xiaoming, Zhang Lijuan, Hou Qingchuan, Zhang Nan, Ma Liang, Cheng Xiaoman, Yin Shougen. // Applied Physics Letters. - 2008. - Vol. 93, No. 11. - P. 113302-113302-3. ↑
- J1537.** Sheu J. K. Enhancement in output power of blue gallium nitride-based light-emitting diodes with omnidirectional metal reflector under electrode pads. / Sheu J. K., Hung I-Hsiu, Lai W. C., Shei S. C., Lee M. L. // Applied Physics Letters. - 2008. - Vol. 93, No. 10. - P. 103507-103507-3. ↑
- J1538.** McGroddy K. Directional emission control and increased light extraction in GaN photonic crystal light emitting diodes. / McGroddy K., David A., Matorioli E., Iza M., Nakamura S., DenBaars S., Speck J. S., Weisbuch C., Hu E. L. // Applied Physics Letters. - 2008. - Vol. 93, No. 10. - P. 103502-103502-3. ↑
- J1539.** Vitta P. Thermal characterization of light-emitting diodes in the frequency domain. / Vitta P., Zukauskas A. // Applied Physics Letters. - 2008. - Vol. 93, No. 10. - P. 103508-103508-3. ↑
- J1540.** Yook Kyoung Soo. Highly efficient and color stable phosphorescent white light-emitting diodes by using a charge confining emitting layer structure. / Yook Kyoung Soo, Jeon Soon Ok, Joo Chul Woong, Lee Jun Yeob. // Applied Physics Letters. - 2008. - Vol. 93, No. 11. - P. 113301-113301-3. ↑
- J1541.** Horng R. H. Improved thermal management of GaN/sapphire light-emitting diodes embedded in reflective heat spreaders. / Horng R. H., Chiang C. C., Hsiao H. Y., Zheng X., Wu D. S., Lin H. I. // Applied Physics Letters. - 2008. - Vol. 93, No. 11. - P. 111907-111907-3. ↑
- J1542.** Jin Youngeup. Improved electron injection in polymer light-emitting diodes using anionic conjugated polyelectrolyte. / Jin Youngeup, Bazan Guillermo C., Heeger Alan J., Kim Jin Young, Lee Kwanghee. // Applied Physics Letters. - 2008. - Vol. 93, No. 12. - P. 123304-123304-3. ↑
- J1543.** Fukagawa H. Highly efficient, deep-blue phosphorescent organic light emitting diodes with a double-emitting layer structure. / Fukagawa H., Watanabe K., Tsuzuki T., Tokito S. // Applied Physics Letters. - 2008. - Vol. 93, No. 13. - P. 133312-133312-3. ↑
- J1544.** Eom Sang-Hyun. Low voltage and very high efficiency deep-blue phosphorescent organic light-emitting devices. / Eom Sang-Hyun, Zheng Ying, Chopra Neetu, Lee Jaewon, So Franky, Xue Jiangeng. // Applied Physics Letters. - 2008. - Vol. 93, No. 13. - P. 133309-133309-3. ↑
- J1545.** Reed M. L. n-In Ga N /p-Ga N single heterostructure light emitting diode with p -side down. / Reed M. L., Readinger E. D., Shen H., Wraback M., Syrkin A., Usikov A., Kovalenkov O. V., Dmitriev V. A. // Applied Physics Letters. - 2008. - Vol. 93, No. 13. - P. 133505-133505-3. ↑
- J1546.** Francardi M. Enhanced spontaneous emission in a photonic-crystal light-emitting diode. / Francardi M., Balet L., Gerardino A., Chauvin N., Bitauld D., Li L. H., Alloing B., Fiore A. // Applied Physics Letters. - 2008. - Vol. 93, No. 14. - P. 143102-143102-3. ↑
- J1547.** Vitta P. Publisher's Note: "Thermal characterization of light-emitting diodes in the frequency domain" [Appl. Phys. Lett. 93, 103508 (2008)]. / Vitta P., Zukauskas A. // Applied Physics Letters. - 2008. - Vol. 93, No. 13. - P. 139901-139901-1. ↑
- J1548.** Lee Meng-Ting. Improvement in carrier transport and recombination of white phosphorescent organic light-emitting devices using a composite blue emitter. / Lee Meng-Ting, Lin Jin-Sheng, Chu Miao-Tsai, Tseng Mei-Rung. // Applied Physics Letters. - 2008. - Vol. 93, No. 13. - P. 133306-133306-3. ↑
- J1549.** Xiong Tao. A soluble nonionic surfactant as electron injection material for high-efficiency inverted

bottom-emission organic light emitting diodes. / Xiong Tao, Wang Fengxia, Qiao Xianfeng, Ma Dongge. // Applied Physics Letters. - 2008. - Vol. 93, No. 12. - P. 123310-123310-3. ↑

J1550. Lee Jaewon. Effects of triplet energies and transporting properties of carrier transporting materials on blue phosphorescent organic light emitting devices. / Lee Jaewon, Chopra Neetu, Eom Sang-Hyun, Zheng Ying, Xue Jiangeng, So Franky, Shi Jianmin. // Applied Physics Letters. - 2008. - Vol. 93, No. 12. - P. 123306-123306-3. ↑

J1551. Yunus M. Spin injection effects on exciton formation in organic semiconductors. / Yunus M., Ruden P. P., Smith D. L. // Applied Physics Letters. - 2008. - Vol. 93, No. 12. - P. 123312-123312-3. ↑

J1552. Zhang J. C. Suppression of the subband parasitic peak by 1 nm i-Al N interlayer in AlGaIn deep ultraviolet light-emitting diodes. / Zhang J. C., Zhu Y. H., Egawa T., Sumiya S., Miyoshi M., Tanaka M. // Applied Physics Letters. - 2008. - Vol. 93, No. 13. - P. 131117-131117-3. ↑

J1553. Tang Yu-Sheng. Near-ultraviolet excitable orange-yellow $\text{Sr}_3(\text{Al}_2\text{O}_5)_2\text{Cl}_2:\text{Eu}^{2+}$ phosphor for potential application in light-emitting diodes. / Tang Yu-Sheng, Hu Shu-Fen, Ke Wei-Chih, Lin Chun Che, Bagkar Nitin C., Liu Ru-Shi. // Applied Physics Letters. - 2008. - Vol. 93, No. 13. - P. 131114-131114-3. ↑

J1554. Hou Liudong. Efficient single layer solution-processed blue-emitting electrophosphorescent devices based on a small-molecule host. / Hou Liudong, Duan Lian, Qiao Juan, Li Wei, Zhang Deqiang, Qiu Yong. // Applied Physics Letters. - 2008. - Vol. 92, No. 26. - P. 263301-263301-3. ↑

J1555. Tanriseven Selim. Broadband quantum dot micro-light-emitting diodes with parabolic sidewalls. / Tanriseven Selim, Maaskant Pleun, Corbett Brian. // Applied Physics Letters. - 2008. - Vol. 92, No. 12. - P. 123501-123501-3. ↑

J1556. Lu Yin-Jui. Achieving three-peak white organic light-emitting devices using wavelength-selective mirror electrodes. / Lu Yin-Jui, Chang Chih-Hao, Lin Chun-Liang, Wu Chung-Chih, Hsu Hsiang-Lun, Chen Liang-Jyi, Lin Yu-Ting, Nishikawa Ryuji. // Applied Physics Letters. - 2008. - Vol. 92, No. 12. - P. 123303-123303-3. ↑

J1557. Arokiaraj J. Bonding of GaN structures with Si(100) substrates using sequentially deposited NiAu metal layers. / Arokiaraj J., Leong Cheong Kee, Lixian Vivian, Yong Anna Marie, Xincal Wang. // Applied Physics Letters. - 2008. - Vol. 92, No. 12. - P. 124105-124105-3. ↑

J1558. Lee Jonghee. Influence of doping profile on the efficiency of blue phosphorescent organic light-emitting diodes. / Lee Jonghee, Lee Jeong-Ik, Song Ki-Im, Lee Su Jin, Chu Hye Yong. // Applied Physics Letters. - 2008. - Vol. 92, No. 13. - P. 133304-133304-3. ↑

J1559. Hoshino Kazunori. Near-field scanning optical microscopy with monolithic silicon light emitting diode on probe tip. / Hoshino Kazunori, Rozanski Lynn J., Vanden Bout David A., Zhang Xiaojing. // Applied Physics Letters. - 2008. - Vol. 92, No. 13. - P. 131106-131106-3. ↑

J1560. Mandalapu L. J. Ultraviolet emission from Sb-doped p-type ZnO based heterojunction light-emitting diodes. / Mandalapu L. J., Yang Z., Chu S., Liu J. L. // Applied Physics Letters. - 2008. - Vol. 92, No. 12. - P. 122101-122101-3. ↑

J1561. Xi Y. Y. Ni O / Zn O light emitting diodes by solution-based growth. / Xi Y. Y., Hsu Y. F., Djuricic A. B., Ng A. M. C., Chan W. K., Tam H. L., Cheah K. W. // Applied Physics Letters. - 2008. - Vol. 92, No. 11. - P. 113505-113505-3. ↑

J1562. Jeon Woo Sik. Highly efficient bilayer green phosphorescent organic light emitting devices. / Jeon Woo Sik, Park Tae Jin, Park Jung Joo, Kim Sun Young, Jang Jin, Kwon Jang Hyuk, Pote Ramchandra. // Applied Physics Letters. - 2008. - Vol. 92, No. 11. - P. 113311-113311-3. ↑

J1563. David Aurelien. Ga N / In Ga N light emitting diodes with embedded photonic crystal obtained by lateral epitaxial overgrowth. / David Aurelien, Moran Brendan, McGroddy Kelly, Matioli Elison, Hu Evelyn L., DenBaars Steven P., Nakamura Shuji, Weisbuch Claude. // Applied Physics Letters. - 2008. - Vol. 92, No. 11. - P. 113514-113514-3. ↑

J1564. An Sung Jin. Enhanced light output of GaN-based light-emitting diodes with ZnO nanorod arrays. / An Sung Jin, Chae Jee Hae, Yi Gyu-Chul, Park Gil H. // Applied Physics Letters. - 2008. - Vol. 92, No. 12. - P.

121108-121108-3. ↑

J1565. Koerperick E. J. In As /Ga Sb cascaded active region superlattice light emitting diodes for operation at 3.8 mcm. / Koerperick E. J., Olesberg J. T., Boggess T. F., Hicks J. L., Wassink L. S., Murray L. M., Prineas J. P. // Applied Physics Letters. - 2008. - Vol. 92, No. 12. - P. 121106-121106-3. ↑

J1566. Wang Jun. Low roll-off power efficiency organic light-emitting diodes consisted of nondoped ultrathin phosphorescent layer. / Wang Jun, Yu Junsheng, Li Lu, Wang Tao, Yuan Kai, Jiang Yadong. // Applied Physics Letters. - 2008. - Vol. 92, No. 13. - P. 133308-133308-3. ↑

J1567. Yang Y. Hybrid optoelectronics: A polymer laser pumped by a nitride light-emitting diode. / Yang Y., Turnbull G. A., Samuel I. D. W. // Applied Physics Letters. - 2008. - Vol. 92, No. 16. - P. 163306-163306-3. ↑

J1568. Lin Hung-Cheng. Enhancing the quantum efficiency of InGaN green light-emitting diodes by trimethylindium treatment. / Lin Hung-Cheng, Lin Ruo-Syuan, Chyi Jen-Inn. // Applied Physics Letters. - 2008. - Vol. 92, No. 16. - P. 161113-161113-3. ↑

J1569. Huang Rui. Role of barrier layers in electroluminescence from SiN-based multilayer light-emitting devices. / Huang Rui, Dong Hengping, Wang Danqing, Chen Kunji, Ding Honglin, Wang Xiang, Li Wei, Xu Jun, Ma Zhongyuan. // Applied Physics Letters. - 2008. - Vol. 92, No. 18. - P. 181106-181106-3. ↑

J1570. Fisslthaler Evelin. Inkjet printed polymer light-emitting devices fabricated by thermal embedding of semiconducting polymer nanospheres in an inert matrix. / Fisslthaler Evelin, Sax Stefan, Scherf Ullrich, Mauthner Gernot, Moderegger Erik, Landfester Katharina, List Emil J. W. // Applied Physics Letters. - 2008. - Vol. 92, No. 18. - P. 183305-183305-3. ↑

J1571. Seo Ji Hoon. Hybrid spacer for high-efficiency white organic light-emitting diodes. / Seo Ji Hoon, Park Il Hoon, Kim Gu Young, Lee Kum Hee, Kim Min Kyu, Yoon Seung Soo, Kim Young Kwan. // Applied Physics Letters. - 2008. - Vol. 92, No. 18. - P. 183303-183303-3. ↑

J1572. Lourenco M. A. Silicon light emitting diodes emitting over the 1.2-1.4 mcm wavelength region in the extended optical communication band. / Lourenco M. A., Gwilliam R. M., Homewood K. P. // Applied Physics Letters. - 2008. - Vol. 92, No. 16. - P. 161108-161108-3. ↑

J1573. Allen Steven C. A nearly ideal phosphor-converted white light-emitting diode. / Allen Steven C., Steckl Andrew J. // Applied Physics Letters. - 2008. - Vol. 92, No. 14. - P. 143309-143309-3. ↑

J1574. Bao Kui. Improvement of light extraction from GaN-based thin-film light-emitting diodes by patterning undoped GaN using modified laser lift-off. / Bao Kui, Kang Xiang Ning, Zhang Bei, Dai Tao, Sun Yong Jian, Fu Qiang, Lian Gui Jun, Xiong Guang Cheng, Zhang Guo Yi, Chen Yong. // Applied Physics Letters. - 2008. - Vol. 92, No. 14. - P. 141104-141104-3. ↑

J1575. Chu S. Sb-doped p-Zn O /Ga -doped n-Zn O homojunction ultraviolet light emitting diodes. / Chu S., Lim J. H., Mandalapu L. J., Yang Z., Li L., Liu J. L. // Applied Physics Letters. - 2008. - Vol. 92, No. 15. - P. 152103-152103-3. ↑

J1576. Zhang Wenfeng. Single zinc-doped indium oxide nanowire as driving transistor for organic light-emitting diode. / Zhang Wenfeng, Jie Jiansheng, He Zhubing, Tao Silu, Fan Xia, Zhou Yechun, Yuan Guodong, Luo Linbao, Zhang Wenjun, Lee Chun-Sing, Lee Shuit-Tong. // Applied Physics Letters. - 2008. - Vol. 92, No. 15. - P. 153312-153312-3. ↑

J1577. Li Yun-Li. Excess carrier dynamics of In Ga N /Ga N multiple-quantum-well light-emitting diodes with various silicon barrier doping profiles. / Li Yun-Li, Lai Wei-Chih, Chang Yun-Chorng. // Applied Physics Letters. - 2008. - Vol. 92, No. 15. - P. 152109-152109-3. ↑

J1578. Latini Gianluca. Self-assembled monolayers of protonated poly(amidoamine) dendrimers on indium tin oxide. / Latini Gianluca, Wykes Michael, Schlapak Robert, Howorka Stefan, Cacialli Franco. // Applied Physics Letters. - 2008. - Vol. 92, No. 1. - P. 013511-013511-3. ↑

J1579. Guo X. Cascade single-chip phosphor-free white light-emitting diodes. / Guo X., Shen G. D., Guan B. L., Gu X. L., Wu D., Li Y. B. // Applied Physics Letters. - 2008. - Vol. 92, No. 1. - P. 013507-013507-3. ↑

- J1580.** Ueda Kazumasa. High performance of GaN thin films grown on sapphire substrates coated with a silica-submicron-sphere monolayer film. / Ueda Kazumasa, Tsuchida Yoshihiko, Hagura Nobuhiro, Iskandar Ferry, Okuyama Kikuo, Endo Yoshiyuki. // Applied Physics Letters. - 2008. - Vol. 92, No. 10. - P. 101101-101101-3. ↑
- J1581.** Ryu Seung Yoon. Polymeric tandem organic light-emitting diodes using a self-organized interfacial layer. / Ryu Seung Yoon, Kim Jong Tae, Noh Joo Hyon, Hwang Byoung Har, Kim Chang Su, Jo Sung Jin, Hwang Hyeon Seok, Kang Seok Ju, Baik Hong Koo, Lee Chang Ho, Song Seung Yong, Lee Se Jong. // Applied Physics Letters. - 2008. - Vol. 92, No. 10. - P. 103301-103301-3. ↑
- J1582.** Ryou J.-H. Control of quantum-confined Stark effect in InGaN /GaN multiple quantum well active region by p -type layer for III-nitride-based visible light emitting diodes. / Ryou J.-H., Lee W., Limb J., Yoo D., Liu J. P., Dupuis R. D., Wu Z. H., Fischer A. M., Ponce F. A. // Applied Physics Letters. - 2008. - Vol. 92, No. 10. - P. 101113-101113-3. ↑
- J1583.** Hsu Shen-Yu. Extraction enhancement in organic light emitting devices by using metallic nanowire arrays. / Hsu Shen-Yu, Lee Ming-Chang, Lee Kuang-Li, Wei Pei-Kuen. // Applied Physics Letters. - 2008. - Vol. 92, No. 1. - P. 013303-013303-3. ↑
- J1584.** Bansal R. Beams of the Future? [Microwave Surfing]. IEEE Microwave Magazine. - 2008. - Vol. 9, No. 1. - P. 30-36. ↑
- J1585.** Ebling Maria. Implantable insulin pump, the first OLED TV, measuring without a ruler.... / Ebling Maria, Corner Mark. // IEEE Pervasive Computing. - 2008. - Vol. 7, No. 1. - P. 8-9. ↑
- J1586.** Liu J. P. Blue light emitting diodes grown on freestanding (11-20) a -plane GaN substrates. / Liu J. P., Limb J. B., Ryou J.-H., Yoo D., Horne C. A., Dupuis R. D., Wu Z. H., Fischer A. M., Ponce F. A., Hanser A. D., Liu L., Preble E. A., Evans K. R. // Applied Physics Letters. - 2008. - Vol. 92, No. 1. - P. 011123-011123-3. ↑
- J1587.** Kim Hyun-Joong. A multiaxial stretchable interconnect using liquid-alloy-filled elastomeric microchannels. / Kim Hyun-Joong, Son Chulwoo, Ziaie Babak. // Applied Physics Letters. - 2008. - Vol. 92, No. 1. - P. 011904-011904-3. ↑
- J1588.** Park Seoung-Hwan. Optical anisotropy in ultraviolet In Ga N /Ga N quantum-well light-emitting diodes with a general crystal orientation. / Park Seoung-Hwan, Ahn Doyeol, Oh Jae-Eung. // Applied Physics Letters. - 2008. - Vol. 92, No. 1. - P. 011130-011130-3. ↑
- J1589.** Koller D. M. Surface plasmon coupled electroluminescent emission. / Koller D. M., Hohenau A., Dittlbacher H., Galler N., Aussenegg F. R., Leitner A., Krenn J. R., Eder S., Sax S., List E. J. W. // Applied Physics Letters. - 2008. - Vol. 92, No. 10. - P. 103304-103304-3. ↑
- J1590.** Nizamoglu Sedat. Dual-color emitting quantum-dot-quantum-well CdSe-ZnS heteronanocrystals hybridized on In Ga N /Ga N light emitting diodes for high-quality white light generation. / Nizamoglu Sedat, Mutlugun Evren, Ozel Tuncay, Demir Hilmi Volkan, Sapra Sameer, Gaponik Nikolai, Eychmuller Alexander. // Applied Physics Letters. - 2008. - Vol. 92, No. 11. - P. 113110-113110-3. ↑
- J1591.** Kim H. S. Phosphorus doped ZnO light emitting diodes fabricated via pulsed laser deposition. / Kim H. S., Lugo F., Pearton S. J., Norton D. P., Wang Yu-Lin, Ren F. // Applied Physics Letters. - 2008. - Vol. 92, No. 11. - P. 112108-112108-3. ↑
- J1592.** Cocchi M. Excimer-based red/near-infrared organic light-emitting diodes with very high quantum efficiency. / Cocchi M., Kalinowski J., Virgili D., Williams J. A. G. // Applied Physics Letters. - 2008. - Vol. 92, No. 11. - P. 113302-113302-3. ↑
- J1593.** Park Tae Jin. Efficient simple structure red phosphorescent organic light emitting devices with narrow band-gap fluorescent host. / Park Tae Jin, Jeon Woo Sik, Park Jung Joo, Kim Sun Young, Lee Yong Kyun, Jang Jin, Kwon Jang Hyuk, Pote Ramchandra. // Applied Physics Letters. - 2008. - Vol. 92, No. 11. - P. 113308-113308-3. ↑
- J1594.** Duan Y. Extremely low voltage and high bright p-i-n fluorescent white organic light-emitting diodes. / Duan Y., Mazzeo M., Maiorano V., Mariano F., Qin D., Cingolani R., Gigli G. // Applied Physics Letters. - 2008. - Vol. 92, No. 11. - P. 113304-113304-3. ↑

- J1595.** Wang Yu-Lin. Dielectric passivation effects on ZnO light emitting diodes. / Wang Yu-Lin, Kim H. S., Norton D. P., Pearton S. J., Ren F. // Applied Physics Letters. - 2008. - Vol. 92, No. 11. - P. 112101-112101-3. ↑
- J1596.** Winroth Gustaf. Polyfluorene-based light-emitting diodes with an azide photocross-linked poly(3,4-ethylene dioxythiophene):(polystyrene sulfonic acid) hole-injecting layer. / Winroth Gustaf, Latini Gianluca, Credgington Dan, Wong Loke-Yuen, Chua Lay-Lay, Ho Peter K.-H., Cacialli Franco. // Applied Physics Letters. - 2008. - Vol. 92, No. 10. - P. 103308-103308-3. ↑
- J1597.** Xu Bingshe. Mixed ligands 8-hydroxyquinoline aluminum complex with high electron mobility for organic light-emitting diodes. / Xu Bingshe, Chen Liuqing, Liu Xuguang, Zhou Hefeng, Xu Huixia, Fang Xiaohong, Wang Yanli. // Applied Physics Letters. - 2008. - Vol. 92, No. 10. - P. 103305-103305-3. ↑
- J1598.** Mandlik Prashant. A single-layer permeation barrier for organic light-emitting displays. / Mandlik Prashant, Gartside Jonathan, Han Lin, Cheng I-Chun, Wagner Sigurd, Silvernail Jeff A., Ma Rui-Qing, Hack Michael, Brown Julie J. // Applied Physics Letters. - 2008. - Vol. 92, No. 10. - P. 103309-103309-3. ↑
- J1599.** Sun X. W. Epitaxially grown n-Zn O /Mg O /Ti N /n+ -Si (111) heterostructured light-emitting diode. / Sun X. W., Zhao J. L., Tan S. T., Tan L. H., Tung C. H., Lo G. Q., Kwong D. L., Zhang Y. W., Li X. M., Teo K. L. // Applied Physics Letters. - 2008. - Vol. 92, No. 11. - P. 111113-111113-3. ↑
- J1600.** Zhang Hongmei. Erratum: "High efficiency tandem organic light-emitting devices with Al /WO 3 /Au " [Appl. Phys. Lett. 91, 123504 (2007)]. / Zhang Hongmei, Dai Yanfeng, Ma Dongge, Choy Wallace C. H. // Applied Physics Letters. - 2008. - Vol. 92, No. 10. - P. 109907-109907-1. ↑
- J1601.** Stenger I. Strong orange/red electroluminescence from hydrogenated polymorphous silicon carbon light-emitting devices. / Stenger I., Abramov A., Barthou C., Nguyen-Tran Th., Frigout A., Roca i Cabarrocas P. // Applied Physics Letters. - 2008. - Vol. 92, No. 24. - P. 241114-241114-3. ↑
- J1602.** Detchprohm Theeradetch. Green light emitting diodes on a -plane GaN bulk substrates. / Detchprohm Theeradetch, Zhu Mingwei, Li Yufeng, Xia Yong, Wetzel Christian, Preble Edward A., Liu Lianghong, Paskova Tanya, Hanser Drew. // Applied Physics Letters. - 2008. - Vol. 92, No. 24. - P. 241109-241109-3. ↑
- J1603.** Kim Sun-Kyung. Efficient GaN slab vertical light-emitting diode covered with a patterned high-index layer. / Kim Sun-Kyung, Cho Hyun Kyong, Bae Duk Kyu, Lee Jeong Soo, Park Hong-Gyu, Lee Yong-Hee. // Applied Physics Letters. - 2008. - Vol. 92, No. 24. - P. 241118-241118-3. ↑
- J1604.** Lai Chun-Feng. Polarized light emission from photonic crystal light-emitting diodes. / Lai Chun-Feng, Chi Jim-Yong, Yen Hsi-Hsuan, Kuo Hao-Chung, Chao Chia-Hsin, Hsueh Han-Tsung, Wang Jih-Fu Trevor, Huang Chen-Yang, Yeh Wen-Yung. // Applied Physics Letters. - 2008. - Vol. 92, No. 24. - P. 243118-243118-3. ↑
- J1605.** Progl C. L. Analysis of V defects in GaN-based light emitting diodes by scanning transmission electron microscopy and electron beam induced current. / Progl C. L., Parish C. M., Vitarelli J. P., Russell P. E. // Applied Physics Letters. - 2008. - Vol. 92, No. 24. - P. 242103-242103-3. ↑
- J1606.** Chu Ta-Ya. Enhanced performance of organic light-emitting diodes with an air-stable n -type hole-injection layer. / Chu Ta-Ya, Kwong C. Y., Song Ok-Keun. // Applied Physics Letters. - 2008. - Vol. 92, No. 23. - P. 233307-233307-3. ↑
- J1607.** Jun-Seok Ha. The Fabrication of Vertical Light-Emitting Diodes Using Chemical Lift-Off Process. / Jun-Seok Ha, Lee S.W., Hyun-Jae Lee, Lee Hyo-Jong, Lee S.H., Goto H., Kato T., Fujii K., Cho M.W., Yao T. // IEEE Photonics Technology Letters. - 2008. - Vol. 20, No. 3. - P. 175-177. ↑
- J1608.** Lee C.E. Luminance Enhancement of Flip-Chip Light-Emitting Diodes by Geometric Sapphire Shaping Structure. / Lee C.E., Kuo H.C., Lee Y.C., Tsai M.R., Lu T.C., Wang S.C., Kuo C.T. // IEEE Photonics Technology Letters. - 2008. - Vol. 20, No. 3. - P. 184-186. ↑
- J1609.** Mei-Li Hsieh. One-Shot Exposure for Patterning Two-Dimensional Photonic Crystals to Enhance Light Extraction of InGaN-Based Green LEDs. / Mei-Li Hsieh, Kuo-Chang Lo, Yi-Sheng Lan, Yang S.Y., Lin C.H., Liu H.M., Kuo H.C. // IEEE Photonics Technology Letters. - 2008. - Vol. 20, No. 2. - P. 141-143. ↑
- J1610.** Jae-Soong Lee. GaN Light-Emitting Diode with Deep-Angled Mesa Sidewalls for Enhanced Light

Emission in the Surface-Normal Direction. / Jae-Soong Lee, Joonhee Lee, Sunghwan Kim, Heonsu Jeon. // IEEE Transactions on Electron Devices. - 2008. - Vol. 55, No. 2. - P. 523-526. ↑

J1611. Khare M.R. Automatic System for Measuring and Controlling the Length of a Moving Product in Industries. IEEE Transactions on Instrumentation and Measurement. - 2008. - Vol. 57, No. 4. - P. 781-790. ↑

J1612. Soh C. B. Cool white III-nitride light emitting diodes based on phosphor-free indium-rich InGaN nanostructures. / Soh C. B., Liu W., Teng J. H., Chow S. Y., Ang S. S., Chua S. J. // Applied Physics Letters. - 2008. - Vol. 92, No. 26. - P. 261909-261909-3. ↑

J1613. Shih H. Y. Optical detection of deoxyribonucleic acid hybridization with In Ga N /Ga N multiple quantum wells. / Shih H. Y., Chen T. T., Wang C. H., Chen K. Y., Chen Y. F. // Applied Physics Letters. - 2008. - Vol. 92, No. 26. - P. 261910-261910-3. ↑

J1614. Lin Ray-Ming. Enhanced characteristics of blue In Ga N /Ga N light-emitting diodes by using selective activation to modulate the lateral current spreading length. / Lin Ray-Ming, Lu Yuan-Chieh, Chou Yi-Lun, Chen Guo-Hsing, Lin Yung-Hsiang, Wu Meng-Chyi. // Applied Physics Letters. - 2008. - Vol. 92, No. 26. - P. 261105-261105-3. ↑

J1615. Haldi A. Highly efficient green phosphorescent organic light-emitting diodes with simplified device geometry. / Haldi A., Domercq B., Kippelen B., Hreha R. D., Cho J.-Y., Marder S. R. // Applied Physics Letters. - 2008. - Vol. 92, No. 25. - P. 253502-253502-3. ↑

J1616. Baumgartner A. Erratum: "Upconversion electroluminescence in InAs quantum dot light-emitting diodes" [Appl. Phys. Lett. 92, 091121 (2008)]. / Baumgartner A., Chaggar A., Patane A., Eaves L., Henini M. // Applied Physics Letters. - 2008. - Vol. 92, No. 25. - P. 259903-259903-1. ↑

J1617. Yang Dongfang. High efficiency electrophosphorescence device using a thin cleaving layer in an Ir-complex doped emitter layer. / Yang Dongfang, Li Wenlian, Chu Bei, Zhang Dongyu, Zhu Jianzhao, Su Zisheng, Su Wenming, Han Liangliang, Bi Defeng, Chen Yiren, Yan Fei, Liu Huihui, Wang Dan. // Applied Physics Letters. - 2008. - Vol. 92, No. 25. - P. 253309-253309-3. ↑

J1618. Jarikov Viktor V. Quantum efficiency improvement in anthracene-based organic light-emitting diodes codoped with a hole-trapping material. Applied Physics Letters. - 2008. - Vol. 92, No. 24. - P. 244103-244103-3. ↑

J1619. Zang K. Y. Nanoepitaxy to improve the efficiency of InGaN light-emitting diodes. / Zang K. Y., Chua S. J., Teng J. H., Ang N. S. S., Yong A. M., Chow S. Y. // Applied Physics Letters. - 2008. - Vol. 92, No. 24. - P. 243126-243126-3. ↑

J1620. Sun Qingjiang. Multilayer white polymer light-emitting diodes with deoxyribonucleic acid-cetyltrimethylammonium complex as a hole-transporting/ electron-blocking layer. / Sun Qingjiang, Chang Dong Wook, Dai Liming, Grote James, Naik Rajesh. // Applied Physics Letters. - 2008. - Vol. 92, No. 25. - P. 251108-251108-3. ↑

J1621. Park Il-Kyu. Effect of InGaN quantum dot size on the recombination process in light-emitting diodes. / Park Il-Kyu, Kwon Min-Ki, Cho Chu-Young, Kim Ja-Yeon, Cho Chang-Hee, Park Seong-Ju. // Applied Physics Letters. - 2008. - Vol. 92, No. 25. - P. 253105-253105-3. ↑

J1622. Kwon Min-Ki. Enhanced emission efficiency of Ga N /In Ga N multiple quantum well light-emitting diode with an embedded photonic crystal. / Kwon Min-Ki, Kim Ja-Yeon, Park Il-Kyu, Kim Ki Seok, Jung Gun-Young, Park Seong-Ju, Kim Je Won, Kim Yong Chun. // Applied Physics Letters. - 2008. - Vol. 92, No. 25. - P. 251110-251110-3. ↑

J1623. Wu Chen-Hao. Highly efficient red organic light-emitting devices based on a fluorene-triphenylamine host doped with an Os(II) phosphor. / Wu Chen-Hao, Shih Ping-I, Shu Ching-Fong, Chi Yun. // Applied Physics Letters. - 2008. - Vol. 92, No. 23. - P. 233303-233303-3. ↑

J1624. Jou Jwo-Huei. High efficiency deep-blue organic light-emitting diode with a blue dye in low-polarity host. / Jou Jwo-Huei, Lin Yu-Pu, Hsu Mao-Fung, Wu Ming-Hsuan, Lu Ping. // Applied Physics Letters. - 2008. - Vol. 92, No. 19. - P. 193314-193314-3. ↑

J1625. Suehiro Takayuki. One-step preparation of Ca -alpha -Si Al O N :Eu 2+ fine powder phosphors for

white light-emitting diodes. / Suehiro Takayuki, Hirosaki Naoto, Xie Rong-Jun, Sakuma Ken, Mitomo Mamoru, Ibukiyama Masahiro, Yamada Suzuya. // Applied Physics Letters. - 2008. - Vol. 92, No. 19. - P. 191904-191904-3. ↑

J1626. Bennett A. J. Indistinguishable photons from a diode. / Bennett A. J., Patel R. B., Shields A. J., Cooper K., Atkinson P., Nicoll C. A., Ritchie D. A. // Applied Physics Letters. - 2008. - Vol. 92, No. 19. - P. 193503-193503-3. ↑

J1627. Lee Jonghee. Effects of interlayers on phosphorescent blue organic light-emitting diodes. / Lee Jonghee, Lee Jeong-Ik, Song Ki-Im, Lee Su Jin, Chu Hye Yong. // Applied Physics Letters. - 2008. - Vol. 92, No. 20. - P. 203305-203305-3. ↑

J1628. Xie Rong-Jun. Crystal structure and photoluminescence of Mn 2+ -Mg 2+ codoped gamma aluminum oxynitride (gamma -Al O N) : A promising green phosphor for white light-emitting diodes. / Xie Rong-Jun, Hirosaki Naoto, Liu Xue-Jian, Takeda Takashi, Li Hui-Li. // Applied Physics Letters. - 2008. - Vol. 92, No. 20. - P. 201905-201905-3. ↑

J1629. Knauer A. Effect of the barrier composition on the polarization fields in near UV InGaN light emitting diodes. / Knauer A., Wenzel H., Kolbe T., Einfeldt S., Weyers M., Kneissl M., Trankle G. // Applied Physics Letters. - 2008. - Vol. 92, No. 19. - P. 191912-191912-3. ↑

J1630. Berry J. J. Organic light emitting diodes using a Ga:ZnO anode. / Berry J. J., Ginley D. S., Burrows P. E. // Applied Physics Letters. - 2008. - Vol. 92, No. 19. - P. 193304-193304-3. ↑

J1631. Yook Kyoung Soo. High efficiency and low efficiency roll off in white phosphorescent organic light-emitting diodes by managing host structures. / Yook Kyoung Soo, Lee Jun Yeob. // Applied Physics Letters. - 2008. - Vol. 92, No. 19. - P. 193308-193308-3. ↑

J1632. Zhang J. C. Influence of pulse width on electroluminescence and junction temperature of AlInGaN deep ultraviolet light-emitting diodes. / Zhang J. C., Zhu Y. H., Egawa T., Sumiya S., Miyoshi M., Tanaka M. // Applied Physics Letters. - 2008. - Vol. 92, No. 19. - P. 191917-191917-3. ↑

J1633. Lee Seung-Joon. Green phosphorescent light-emitting diodes from polymer doped with iridium complex. / Lee Seung-Joon, Park Jin Su, Song Myungkwan, Yoon Kyung-Jin, Kim Young Inn, Jin Sung-Ho, Seo Hoe-Joo. // Applied Physics Letters. - 2008. - Vol. 92, No. 19. - P. 193312-193312-3. ↑

J1634. Niedermeier U. Enhancement of organic magnetoresistance by electrical conditioning. / Niedermeier U., Vieth M., Patzold R., Sarfert W., von Seggern H. // Applied Physics Letters. - 2008. - Vol. 92, No. 19. - P. 193309-193309-3. ↑

J1635. Noguchi Yutaka. Threshold voltage shift and formation of charge traps induced by light irradiation during the fabrication of organic light-emitting diodes. / Noguchi Yutaka, Sato Naoki, Tanaka Yuya, Nakayama Yasuo, Ishii Hisao. // Applied Physics Letters. - 2008. - Vol. 92, No. 20. - P. 203306-203306-3. ↑

J1636. Jeon Sohee. Ultraviolet nanoimprinted polymer nanostructure for organic light emitting diode application. / Jeon Sohee, Kang Jae-Wook, Park Hyung-Dol, Kim Jang-Joo, Youn Jae R., Shim Jongyoup, Jeong Jun-ho, Choi Dae-Geun, Kim Ki-Don, Altun Ali Ozhan, Kim Se-Heon, Lee Yong-Hee. // Applied Physics Letters. - 2008. - Vol. 92, No. 22. - P. 223307-223307-3. ↑

J1637. Choi Kwang-Hyuk. Highly flexible and transparent In Zn Sn O x /Ag /In Zn Sn O x multilayer electrode for flexible organic light emitting diodes. / Choi Kwang-Hyuk, Nam Ho-Jun, Jeong Jin-A, Cho Sung-Woo, Kim Han-Ki, Kang Jae-Wook, Kim Do-Geun, Cho Woon-Jo. // Applied Physics Letters. - 2008. - Vol. 92, No. 22. - P. 223302-223302-3. ↑

J1638. Liao L. S. Power efficiency improvement in a tandem organic light-emitting diode. / Liao L. S., Klubek K. P. // Applied Physics Letters. - 2008. - Vol. 92, No. 22. - P. 223311-223311-3. ↑

J1639. Hickey M. C. Spin injection from Co 2 Mn Ga into an InGaAs quantum well. / Hickey M. C., Damsgaard C. D., Holmes S. N., Farrer I., Jones G. A. C., Ritchie D. A., Jacobsen C. S., Hansen J. B., Pepper M. // Applied Physics Letters. - 2008. - Vol. 92, No. 23. - P. 232101-232101-3. ↑

J1640. Jou Jwo-Huei. Color-stable, efficient fluorescent pure-white organic light-emitting diodes with device

architecture preventing excessive exciton formation on guest. / Jou Jwo-Huei, Wang Chun-Jan, Lin Yu-Pu, Chung Yu-Chiao, Chiang Po-Hsuan, Wu Ming-Hsuan, Wang Chung-Pei, Lai Chun-Liang, Chang Champion. // Applied Physics Letters. - 2008. - Vol. 92, No. 22. - P. 223504-223504-3. ↑

J1641. Zheng Ying. Efficient deep-blue phosphorescent organic light-emitting device with improved electron and exciton confinement. / Zheng Ying, Eom Sang-Hyun, Chopra Neetu, Lee Jaewon, So Franky, Xue Jiangeng. // Applied Physics Letters. - 2008. - Vol. 92, No. 22. - P. 223301-223301-3. ↑

J1642. Du Xiaozhang. Temperature dependence of polarized electroluminescence side emission from (0001)-oriented blue and violet In Ga N /Ga N light-emitting diodes. / Du Xiaozhang, Lu Hai, Han Ping, Zhang Rong, Zheng Youdou. // Applied Physics Letters. - 2008. - Vol. 92, No. 20. - P. 203504-203504-3. ↑

J1643. Ziegler Mathias. Surface recombination and facet heating in high-power diode lasers. / Ziegler Mathias, Talalaev Vadim, Tamm Jens W., Elsaesser Thomas, Ressel Peter, Sumpf Bernd, Erbert Gotz. // Applied Physics Letters. - 2008. - Vol. 92, No. 20. - P. 203506-203506-3. ↑

J1644. Sato Hitoshi. Optical properties of yellow light-emitting diodes grown on semipolar (112 2) bulk GaN substrates. / Sato Hitoshi, Chung Roy B., Hirasawa Hirohiko, Fellows Natalie, Masui Hisashi, Wu Feng, Saito Makoto, Fujito Kenji, Speck James S., DenBaars Steven P., Nakamura Shuji. // Applied Physics Letters. - 2008. - Vol. 92, No. 22. - P. 221110-221110-3. ↑

J1645. Morii Katsuyuki. High efficiency and stability in air of the encapsulation-free hybrid organic-inorganic light-emitting diode. / Morii Katsuyuki, Kawase Takeo, Inoue Satoshi. // Applied Physics Letters. - 2008. - Vol. 92, No. 21. - P. 213304-213304-3. ↑

J1646. Tu Hoang. Strong Efficiency Improvement of SOI-LEDs Through Carrier Confinement. / Tu Hoang, Phuong LeMinh, Holleman J., Schmitz J. // IEEE Electron Device Letters. - 2007. - Vol. 28, No. 5. - P. 383-385. ↑

J1647. In-Kag Hwang. Unidirectional, Efficiency-Controlled Coupling from Microcavity Using Reflection Feedback. / In-Kag Hwang, Yong-Hee Lee. // IEEE Journal of Selected Topics in Quantum Electronics. - 2007. - Vol. 13, No. 2. - P. 209-213. ↑

J1648. Windisch R. 100-lm/W InGaAlP Thin-Film Light-Emitting Diodes With Buried Microreflectors. / Windisch R., Butendeich R., Illek S., Kugler S., Wirth R., Zull H., Streubel K. // IEEE Photonics Technology Letters. - 2007. - Vol. 19, No. 10. - P. 774-776. ↑

J1649. Shen C.F. Nitride-Based High-Power Flip-Chip LED With Double-Side Patterned Sapphire Substrate. / Shen C.F., Chang S.J., Chen W.S., Ko T.K., Kuo C.T., Shei S.C. // IEEE Photonics Technology Letters. - 2007. - Vol. 19, No. 10. - P. 780-782. ↑

J1650. Chaji G.R. Parallel Addressing Scheme for Voltage-Programmed Active-Matrix OLED Displays. / Chaji G.R., Nathan A. // IEEE Transactions on Electron Devices. - 2007. - Vol. 54, No. 5. - P. 1095-1100. ↑

J1651. Chakraborty A. Interdigitated Multipixel Arrays for the Fabrication of High-Power Light-Emitting Diodes With Very Low Series Resistances, Reduced Current Crowding, and Improved Heat Sinking. / Chakraborty A., Shen L., Mishra U.K. // IEEE Transactions on Electron Devices. - 2007. - Vol. 54, No. 5. - P. 1083-1090. ↑


J1652. Jae Kyeong Jeong. Flexible Full-Color AMOLED on Ultrathin Metal Foil. / Jae Kyeong Jeong, Dong Un Jin, Hyun Soo Shin, Hun Jung Lee, Minkyu Kim, Tae Kyung Ahn, Jaeseob Lee, Yeon Gon Mo, Ho Kyun Chung. // IEEE Electron Device Letters. - 2007. - Vol. 28, No. 5. - P. 389-391. ↑


J1653. Shih-Chang Shei. Improved Reliability and ESD Characteristics of Flip-Chip GaN-Based LEDs With Internal Inverse-Parallel Protection Diodes. / Shih-Chang Shei, Jinn-Kong Sheu, Chien-Fu Shen. // IEEE Electron Device Letters. - 2007. - Vol. 28, No. 5. - P. 346-349. ↑


J1654. Nicholes S.C. High-Confinement Strained MQW for Highly Polarized High-Power Broadband Light Source. / Nicholes S.C., Raring J.W., Dummer M., Tauke-Pedretti A., Coldren L.A. // IEEE Photonics Technology Letters. - 2007. - Vol. 19, No. 10. - P. 771-773. ↑


J1655. Kay R.W. Ultra-Fine Pitch Stencil Printing for a Low Cost and Low Temperature Flip-Chip Assembly Process. / Kay R.W., Stoyanov S., Glinski G.P., Bailey C., Desmulliez M.P.Y. // IEEE Transactions on




Components and Packaging Technologies. - 2007. - Vol. 30, No. 1. - P. 129-136. 


J1656. Huang H.W. High-Performance GaN-Based Vertical-Injection Light-Emitting Diodes With TiO₂ –SiO₂ Omnidirectional Reflector and n-GaN Roughness. / Huang H.W., Kuo H.C., Lai C.F., Lee C.E., Chiu C.W., Lu T.C., Wang S.C., Lin C.H., Leung K.M. // IEEE Photonics Technology Letters. - 2007. - Vol. 19, No. 8. - P. 565-567. 


J1657. Jae-Soong Lee. GaN Surface-Emitting Laser With Monolithic Cavity-Folding Mirrors. / Jae-Soong Lee, Joonhee Lee, Heonsu Jeon. // IEEE Photonics Technology Letters. - 2007. - Vol. 19, No. 8. - P. 577-579. 


J1658. Balakrishnan G. Monolithically integrated III-Sb CW super-luminal light emitting diodes on non-miscut Si (100) substrates. / Balakrishnan G., Mehta M., Kutty M.N., Patel P., Albrecht A.R., Rotella P., Krishna S., Dawson L.R., Huffaker D.L. // Electronics Letters. - 2007. - Vol. 43, No. 4. - P. 244-245. 


J1659. Predd P.P. Beyond Blue. IEEE Spectrum. - 2007. - Vol. 44, No. 3. - P. 14. 


J1660. Shun-Cheng Hsu. High-Efficiency 1-mm 2 AlGaInP LEDs Sandwiched by ITO Omni-Directional Reflector and Current-Spreading Layer. / Shun-Cheng Hsu, Dong-Sing Wu, Chong-Yi Lee, Juh-Yuh Su, Horng R.-H. // IEEE Photonics Technology Letters. - 2007. - Vol. 19, No. 7. - P. 492-494. 


J1661. Jooyoung Ha. A New Approach to Color Adjustment for Mobile Application Displays with a Skin Protection Algorithm on a CIE1931 Diagram. / Jooyoung Ha, Sungmok Lee, Tae-eung Kim, Wontae Choi, Bongsoo Kang. // IEEE Transactions on Consumer Electronics. - 2007. - Vol. 53, No. 1. - P. 191-196. 


J1662. Hsieh C.-H. Nearly White-Light Emission From GaN-Based Light-Emitting Diodes Integrated With a Porous SiO₂ Layer. / Hsieh C.-H., Ke M.-Y., Shih G.-A., Chiu T.-Y., Huang J. J. // IEEE Photonics Technology Letters. - 2007. - Vol. 19, No. 9. - P. 662-664. 


J1663. Postolache O.A. Multibeam Optical System and Neural Processing for Turbidity Measurement. / Postolache O.A., Girao P.M.B.S., Pereira J.M.D., Ramos H.M.G. // IEEE Sensors Journal. - 2007. - Vol. 7, No. 5. - P. 677-684. 


J1664. Horng J.J. Nitride-Based Schottky Barrier Sensor Module With High Electrostatic Discharge Reliability. / Horng J.J., Su Y.K., Chang S.J., Ko T.K., Shei S.C. // IEEE Photonics Technology Letters. - 2007. - Vol. 19, No. 10. - P. 717-719. 


J1665. Tsai P.C. Lifetime Tests and Junction-Temperature Measurement of InGaN Light-Emitting Diodes Using Patterned Sapphire Substrates. / Tsai P.C., Chuang R.W., Su Y.K. // Journal of Lightwave Technology. - 2007. - Vol. 25, No. 2. - P. 591-596. 


J1666. Hojin Lee. Asymmetric Electrical Properties of Corbino a-Si:H TFT and Concepts of Its Application to Flat Panel Displays. / Hojin Lee, Juhn-Suk Yoo, Chang-Dong Kim, In-Jae Chung, Kanicki J. // IEEE Transactions on Electron Devices. - 2007. - Vol. 54, No. 4. - P. 654-662. 


J1667. Choi W.Y. Efficient LED back-light power supply for liquid-crystal-display. / Choi W.Y., Kwon J.M., Kwon B.H. // IET Electric Power Applications. - 2007. - Vol. 1, No. 2. - P. 133-142. 

J1668. Chih-Hao Chang. Efficient White OLEDs Employing Phosphorescent Sensitization. / Chih-Hao Chang, Yin-Jui Lu, Chih-Che Liu, Yung-Hui Yeh, Chung-Chih Wu. // Journal of Display Technology. - 2007. - Vol. 3, No. 2. - P. 193-199. 

J1669. Xue-Wen Chen. Efficient and Rigorous Modeling of Light Emission in Planar Multilayer Organic Light-Emitting Diodes. / Xue-Wen Chen, Choy W.C.H., Sailing He. // Journal of Display Technology. - 2007. - Vol. 3, No. 2. - P. 110-117. 

J1670. David A. Optimization of Light-Diffracting Photonic-Crystals for High Extraction Efficiency LEDs. / David A., Benisty H., Weisbuch C. // Journal of Display Technology. - 2007. - Vol. 3, No. 2. - P. 133-148. 

J1671. So F. Guest Editorial. / So F., Steckl A. J. // Journal of Display Technology. - 2007. - Vol. 3, No. 2. - P. 90. 

J1672. Allen S.C. ELiXIR-Solid-State Luminaire With Enhanced Light Extraction by Internal Reflection. / Allen 

S.C., Steckl A.J. // Journal of Display Technology. - 2007. - Vol. 3, No. 2. - P. 155-159.

J1673. Brodrick J. Next-Generation Lighting Initiative at the U.S. Department of Energy: Catalyzing Science Into the Marketplace. Journal of Display Technology. - 2007. - Vol. 3, No. 2. - P. 91-97. ↑

J1674. Duggal A.R. Solution-Processed Organic Light-Emitting Diodes for Lighting. / Duggal A.R., Heller C.M., Shiang J.J., Jie Liu, Lewis L.N. // Journal of Display Technology. - 2007. - Vol. 3, No. 2. - P. 184-192. ↑

J1675. Ya-Ju Lee. High Brightness GaN-Based Light-Emitting Diodes. / Ya-Ju Lee, Tien-Chang Lu, Hao-Chung Kuo, Shing-Chung Wang. // Journal of Display Technology. - 2007. - Vol. 3, No. 2. - P. 118-125. ↑

J1676. Wonseok Lee. Nitride-Based Green Light-Emitting Diodes With Various p-Type Layers. / Wonseok Lee, Jae Limb, Jae-Hyun Ryou, Dongwon Yoo, Ewing M.A., Korenblit Y., Dupuis R.D. // Journal of Display Technology. - 2007. - Vol. 3, No. 2. - P. 126-132. ↑

J1677. McBride L.R. Solid-State Pressure-Tolerant Illumination for MBARI's Underwater Low-Light Imaging System. / McBride L.R., Scholfield J.T. // Journal of Display Technology. - 2007. - Vol. 3, No. 2. - P. 149-154. ↑

J1678. Harbers G. Performance of High Power Light Emitting Diodes in Display Illumination Applications. / Harbers G., Bierhuizen S.J., Krames M.R. // Journal of Display Technology. - 2007. - Vol. 3, No. 2. - P. 98-109. ↑

J1679. Krames M.R. Status and Future of High-Power Light-Emitting Diodes for Solid-State Lighting. / Krames M.R., Shchekin O.B., Mueller-Mach R., Mueller G.O., Ling Zhou, Harbers G., Craford M.G. // Journal of Display Technology. - 2007. - Vol. 3, No. 2. - P. 160-175. ↑

J1680. Krummacher B.C. Light Extraction From Solution-Based Processable Electrophosphorescent Organic Light-Emitting Diodes. / Krummacher B.C., Mathai M., So F., Choulis S., Vi-En Choong. // Journal of Display Technology. - 2007. - Vol. 3, No. 2. - P. 200-210. ↑

J1681. Riordan M. Books: Tales of Nakamura [review of Brilliant! Shuji Nakamura and the Revolution in Lighting Technology (Johnstone, B.; 2007)]. IEEE Spectrum. - 2007. - Vol. 44, No. 5. - P. 56-58. ↑

J1682. Wu L.K. Resonant-Cavity-Enhanced Far-Infrared Upconversion Imaging Devices. / Wu L.K., Shen W.Z. // IEEE Journal of Quantum Electronics. - 2007. - Vol. 43, No. 5. - P. 411-418. ↑

J1683. Kolman E. Knowledge Extraction From Neural Networks Using the All-Permutations Fuzzy Rule Base: The LED Display Recognition Problem. / Kolman E., Margaliot M. // IEEE Transactions on Neural Networks. - 2007. - Vol. 18, No. 3. - P. 925-931. ↑

J1684. Morschbach M. Visible Light Emission by a Reverse-Biased Integrated Silicon Diode. / Morschbach M., Oehme M., Kasper E. // IEEE Transactions on Electron Devices. - 2007. - Vol. 54, No. 5. - P. 1091-1094. ↑

J1685. Jun Li. Violet Electroluminescence of AlInGaN-InGaN Multiquantum-Well Light-Emitting Diodes: Quantum-Confined Stark Effect and Heating Effect. / Jun Li, Shi S.L., Wang Y.J., Xu S.J., Zhao D.G., Zhu J.J., Yang H., Lu F. // IEEE Photonics Technology Letters. - 2007. - Vol. 19, No. 10. - P. 789-791. ↑

J1686. Ha G.-Y. Improvement of Reliability of GaN-Based Light-Emitting Diodes by Selective Wet Etching With p-GaN. / Ha G.-Y., Park T.-Y., Kim J.-Y., Kim D.-J., Min K.-I., Park S.-J. // IEEE Photonics Technology Letters. - 2007. - Vol. 19, No. 11. - P. 813-815. ↑

J1687. Chien-Chih Chen. Sequential Color LED Backlight Driving System for LCD Panels. / Chien-Chih Chen, Chang-Yu Wu, Yaow-Ming Chen, Tsai-Fu Wu. // IEEE Transactions on Power Electronics. - 2007. - Vol. 22, No. 3. - P. 919-925. ↑

J1688. Yu C. L. InGaN-GaN MQW Metal-Semiconductor-Metal Photodiodes With Semi-Insulating Mg-Doped GaN Cap Layers. / Yu C. L., Chuang R. W., Chang S. J., Chang P. C., Lee K. H., Lin J. C. // IEEE Photonics Technology Letters. - 2007. - Vol. 19, No. 11. - P. 846-848. ↑

J1689. Zhang Z.Y. Broadband quantum dot superluminescent LED with angled facet formed by focused ion beam etching. / Zhang Z.Y., Luxmoore I.J., Jiang Q., Liu H.Y., Groom K.M., Childs D.T., Hopkinson M., Cullis A.G., Hogg R.A. // Electronics Letters. - 2007. - Vol. 43, No. 10. - P. 587-588. ↑

- J1690.** Kuo C.H. GaN-based Indium-tin-oxide light emitting diodes with nanostructured silicon upper contacts. / Kuo C.H., Chang S.J., Kuan H. // IET Optoelectronics. - 2007. - Vol. 1, No. 3. - P. 110-112. ↑
- J1691.** Alonso J. M. Foreword Special Issue on Lighting Applications. IEEE Transactions on Power Electronics. - 2007. - Vol. 22, No. 3. - P. 717-718. ↑
- J1692.** Ming-Kwei Lee. Highly Visible Photocatalytic Activity of Fluorine and Nitrogen Co-doped Nanocrystalline Anatase Phase Titanium Oxide Converted From Ammonium Oxotrifluorotitanate. / Ming-Kwei Lee, Tsung-Hsiang Shih, Chung-Min Shih. // IEEE Transactions on Nanotechnology. - 2007. - Vol. 6, No. 3. - P. 316-319. ↑
- J1693.** Kao C.-C. Light-Output Enhancement of Nano-Roughened GaN Laser Lift-Off Light-Emitting Diodes Formed by ICP Dry Etching. / Kao C.-C., Kuo H. C., Yeh K. F., Chu J. T., Peng W. L., Huang H. W., Lu T. C., Wang S. C. // IEEE Photonics Technology Letters. - 2007. - Vol. 19, No. 11. - P. 849-851. ↑
- J1694.** Sun J. C. Realization of ultraviolet electroluminescence from ZnO homojunction with n-Zn O /p-Zn O :As /Ga As structure. / Sun J. C., Zhao J. Z., Liang H. W., Bian J. M., Hu L. Z., Zhang H. Q., Liang X. P., Liu W. F., Du G. T. // Applied Physics Letters. - 2007. - Vol. 90, No. 12. - P. 121128-121128-3. ↑
- J1695.** Gadisa Abay. Red and near infrared polarized light emissions from polyfluorene copolymer based light emitting diodes. / Gadisa Abay, Perzon Erik, Andersson Mats R., Inganas Olle. // Applied Physics Letters. - 2007. - Vol. 90, No. 11. - P. 113510-113510-3. ↑
- J1696.** Park Il-Kyu. Ultraviolet light-emitting diodes with self-assembled InGaN quantum dots. / Park Il-Kyu, Kwon Min-Ki, Seo Seong-Bum, Kim Ja-Yeon, Lim Jae-Hong, Park Seong-Ju. // Applied Physics Letters. - 2007. - Vol. 90, No. 11. - P. 111116-111116-3. ↑
- J1697.** Gao Zhi Qiang. High-efficiency deep blue host for organic light-emitting devices. / Gao Zhi Qiang, Mi Bao Xiu, Chen Chin H., Cheah Kow Wai, Cheng Yuen Kit, Wen Wen-Shih. // Applied Physics Letters. - 2007. - Vol. 90, No. 12. - P. 123506-123506-3. ↑
- J1698.** Yang Chih-Chieh. Highly stable three-band white light from an InGaN-based blue light-emitting diode chip precoated with (oxy)nitride green/red phosphors. / Yang Chih-Chieh, Lin Chih-Min, Chen Yi-Jung, Wu Yi-Tsuo, Chuang Shih-Ren, Liu Ru-Shi, Hu Shu-Fen. // Applied Physics Letters. - 2007. - Vol. 90, No. 12. - P. 123503-123503-3. ↑
- J1699.** van der Laak Nicole K. Role of gross well-width fluctuations in bright, green-emitting single In Ga N /Ga N quantum well structures. / van der Laak Nicole K., Oliver Rachel A., Kappers Menno J., Humphreys Colin J. // Applied Physics Letters. - 2007. - Vol. 90, No. 12. - P. 121911-121911-3. ↑
- J1700.** Grzanka S. Role of the electron blocking layer in the low-temperature collapse of electroluminescence in nitride light-emitting diodes. / Grzanka S., Franssen G., Targowski G., Krowicki K., Suski T., Czernecki R., Perlin P., Leszczynski M. // Applied Physics Letters. - 2007. - Vol. 90, No. 10. - P. 103507-103507-3. ↑
- J1701.** Garditz C. Impact of Joule heating on the brightness homogeneity of organic light emitting devices. / Garditz C., Winnacker A., Schindler F., Paetzold R. // Applied Physics Letters. - 2007. - Vol. 90, No. 10. - P. 103506-103506-3. ↑
- J1702.** Hill Duncan. Analysis of spatial coherence of organic light-emitting devices through investigation of interference effects observed in top-emitting devices. / Hill Duncan, Leo Karl, He Gufeng, Huang Qiang. // Applied Physics Letters. - 2007. - Vol. 90, No. 10. - P. 101111-101111-3. ↑
- J1703.** Ishihara Kuniaki. Organic light-emitting diodes with photonic crystals on glass substrate fabricated by nanoimprint lithography. / Ishihara Kuniaki, Fujita Masayuki, Matsubara Ippei, Asano Takashi, Noda Susumu, Ohata Hiroshi, Hirasawa Akira, Nakada Hiroshi, Shimoji Noriyuki. // Applied Physics Letters. - 2007. - Vol. 90, No. 11. - P. 111114-111114-3. ↑
- J1704.** Lee Byoung Duk. Effect of transparent film desiccant on the lifetime of top-emitting active matrix organic light emitting diodes. / Lee Byoung Duk, Cho Yoon-Hyung, Kim Won-Jong, Oh Min Ho, Lee Jong Hyuk, Zang Dong Sik. // Applied Physics Letters. - 2007. - Vol. 90, No. 10. - P. 103518-103518-3. ↑
- J1705.** Qian Lei. Electrophosphorescence from triplet excimers in poly-(N -vinylcarbazole). / Qian Lei, Bera

Debasis, Holloway Paul H. // Applied Physics Letters. - 2007. - Vol. 90, No. 10. - P. 103511-103511-3. ↑

J1706. Tang Yu-Sheng. Thermally stable luminescence of K Sr P O 4 :Eu 2+ phosphor for white light UV light-emitting diodes. / Tang Yu-Sheng, Hu Shu-Fen, Lin Chun Che, Bagkar Nitin C., Liu Ru-Shi. // Applied Physics Letters. - 2007. - Vol. 90, No. 15. - P. 151108-151108-3. ↑

J1707. Kim Jong H. Nanovoid nature and compression effects in organic light emitting diode. / Kim Jong H., Seo Soon-min, Lee Hong H. // Applied Physics Letters. - 2007. - Vol. 90, No. 14. - P. 143521-143521-3. ↑

J1708. Su Zisheng. Enhanced electrophosphorescence of copper complex based devices by codoping an iridium complex. / Su Zisheng, Li Wenlian, Che Guangbo, Xu Maoliang, Kong Zhiguo, Wang Dan, Xin Qi, Han Liangliang, Chu Bei, Bi Defeng. // Applied Physics Letters. - 2007. - Vol. 90, No. 14. - P. 143505-143505-3. ↑

J1709. Barletta Philip T. Development of green, yellow, and amber light emitting diodes using InGaN multiple quantum well structures. / Barletta Philip T., Acar Berkman E., Moody Baxter F., El-Masry Nadia A., Emara Ahmed M., Reed Mason J., Bedair S. M. // Applied Physics Letters. - 2007. - Vol. 90, No. 15. - P. 151109-151109-3. ↑

J1710. Chuang Ta-Ko. Top-emitting 230 dots /in. active-matrix polymer light-emitting diode displays on flexible metal foil substrates. / Chuang Ta-Ko, Troccoli Matias, Kuo Po-Chin, Jamshidi-Roudbari Abbas, Hatalis Miltiadis K., Biaggio Ivan, Voutsas Apostolos T. // Applied Physics Letters. - 2007. - Vol. 90, No. 15. - P. 151114-151114-3. ↑

J1711. Huang Chi-Feng. Phosphor-free white-light light-emitting diode of weakly carrier-density-dependent spectrum with prestrained growth of In Ga N /Ga N quantum wells. / Huang Chi-Feng, Lu Chih-Feng, Tang Tsung-Yi, Huang Jeng-Jie, Yang C. C. // Applied Physics Letters. - 2007. - Vol. 90, No. 15. - P. 151122-151122-3. ↑

J1712. Ryu Y. R. Excitonic ultraviolet lasing in ZnO-based light emitting devices. / Ryu Y. R., Lubguban J. A., Lee T. S., White H. W., Jeong T. S., Youn C. J., Kim B. J. // Applied Physics Letters. - 2007. - Vol. 90, No. 13. - P. 131115-131115-3. ↑

J1713. Cuong T. V. Enhanced light output from aligned micropit InGaN-based light emitting diodes using wet-etch sapphire patterning. / Cuong T. V., Cheong H. S., Kim H. G., Kim H. Y., Hong C.-H., Suh E. K., Cho H. K., Kong B. H. // Applied Physics Letters. - 2007. - Vol. 90, No. 13. - P. 131107-131107-3. ↑

J1714. Kanno Hiroshi. Highly efficient and stable red phosphorescent organic light-emitting device using bis[2-(2-benzothiazoyl)phenolato]zinc(II) as host material. / Kanno Hiroshi, Ishikawa Kaori, Nishio Yoshitaka, Endo Ayataka, Adachi Chihaya, Shibata Kenichi. // Applied Physics Letters. - 2007. - Vol. 90, No. 12. - P. 123509-123509-3. ↑

J1715. Kuo C. H. Nitride-based near-ultraviolet light emitting diodes with meshed p-Ga N. / Kuo C. H., Feng H. C., Kuo C. W., Chen C. M., Wu L. W., Chi G. C. // Applied Physics Letters. - 2007. - Vol. 90, No. 14. - P. 142115-142115-3. ↑

J1716. Laquai Frederic. Influence of hole transport units on the efficiency of polymer light emitting diodes. / Laquai Frederic, Hertel Dirk. // Applied Physics Letters. - 2007. - Vol. 90, No. 14. - P. 142109-142109-3. ↑

J1717. Di Chong-an. High-efficiency low operation voltage organic light-emitting diodes. / Di Chong-an, Yu Gui, Liu Yunqi, Xu Xinjun, Song Yabin, Zhu Daoben. // Applied Physics Letters. - 2007. - Vol. 90, No. 13. - P. 133508-133508-3. ↑

J1718. Domenico Palumbo. Electrical Stress Degradation of Small-Grain Polysilicon Thin-Film Transistors. / Domenico Palumbo, Silvia Masala, Paolo Tassini, Alfredo Rubino, Dario della Sala. // IEEE Transactions on Electron Devices. - 2007. - Vol. 54, No. 3. - P. 476-482. ↑

J1719. Hyunsoo Kim. High-Reflectance and Thermally Stable AgCu Alloy p-Type Reflectors for GaN-Based Light-Emitting Diodes. / Hyunsoo Kim, Kwang Hyeon Baik, Jaehee Cho, Jeong Wook Lee, Sukho Yoon, Hyungkun Kim, Sung-Nam Lee, Cheolsoo Sone, Yongjo Park, Tae-Yeon Seong. // IEEE Photonics Technology Letters. - 2007. - Vol. 19, No. 5. - P. 336-338. ↑

J1720. Shiue-Lung Chen. Fabrication of Dicing-Free Vertical-Structured High-Power GaN-Based Light-Emitting

Diodes With Selective Nickel Electroplating and Patterned Laser Liftoff Techniques. / Shiue-Lung Chen, Shui-Jinn Wang, Kai-Ming Uang, Tron-Min Chen, Wei-Chi Lee, Bor-Wen Liou. // IEEE Photonics Technology Letters. - 2007. - Vol. 19, No. 6. - P. 351-353. ↑

J1721. Bong-Hyun You. Polarity Balanced Driving Scheme to Suppress the Degradation of V_{th} in a-Si:H TFT Due to the Positive Gate Bias Stress for AMOLED. / Bong-Hyun You, Jae-Hoon Lee, Min-Koo Han. // Journal of Display Technology. - 2007. - Vol. 3, No. 1. - P. 40-44. ↑

J1722. Jamei M. The Preparation of Nanocrystalline Silicon by Plasma-Enhanced Hydrogenation for the Fabrication of Light-Emitting Diodes. / Jamei M., Karbassian F., Mohajerzadeh S., Abdi Y., Robertson M.D., Yuill S. // IEEE Electron Device Letters. - 2007. - Vol. 28, No. 3. - P. 207-210. ↑

J1723. Shinya Ono. VT Compensation Circuit for AM OLED Displays Composed of Two TFTs and One Capacitor. / Shinya Ono, Koichi Miwa, Yuichi Maekawa, Takatoshi Tsujimura. // IEEE Transactions on Electron Devices. - 2007. - Vol. 54, No. 3. - P. 462-467. ↑

J1724. Shen C.F. Nitride-based high power flip-chip near-UV leds with reflective submount. / Shen C.F., Chang S.J., Ko T.K., Shei S.C., Lai W.C., Chang C.S., Chen W.S., Huang S.P., Ku Y.W., Horng R.H. // IET Optoelectronics. - 2007. - Vol. 1, No. 1. - P. 27-30. ↑

J1725. Lin J.C. GaN-based light-emitting diodes prepared on vicinal sapphire substrates. / Lin J.C., Su Y.K., Chang S.J., Lan W.H., Huang K.C., Chen W.R., Cheng Y.C., Lin W.J. // IET Optoelectronics. - 2007. - Vol. 1, No. 1. - P. 23-26. ↑

J1726. Bukowski R.M. Phase fluorometric glucose biosensor using oxygen as transducer and enzyme-doped xerogels. / Bukowski R.M., Chodavarapu V.P., Titus A.H., Cartwright A.N., Bright F.V. // Electronics Letters. - 2007. - Vol. 43, No. 4. - P. 202-204. ↑

J1727. Soichi Kobayashi. Narrow Tunable Polysilane Optical Waveguide Bragg Grating Filters. / Soichi Kobayashi, Masayuki Sawada, Toshihiro Suda, K. Ogura, H. Tsushima. // IEEE Photonics Technology Letters. - 2007. - Vol. 19, No. 6. - P. 363-365. ↑

J1728. Pranciskus Vitta. Phosphor Thermometry in White Light-Emitting Diodes. / Pranciskus Vitta, Paulius Pobedinskas, Artras Zukauskas. // IEEE Photonics Technology Letters. - 2007. - Vol. 19, No. 6. - P. 399-401. ↑

J1729. Chang S.J. ZnSe based white light emitting diode on homoepitaxial ZnSe substrate. / Chang S.J., Lin T.K., Chiou Y.Z., Huang B.R., Chang S.P., Chang C.M., Lin Y.C., Wong C.C. // IET Optoelectronics. - 2007. - Vol. 1, No. 1. - P. 39-41. ↑

J1730. Park E.-H. InGaN Light-Emitting Diode With Quasi-Quantum-Dot-Shaped Active Layer Using SiCN Interfacial Layer. / Park E.-H., Jeon S.-K., Kim C.-T., Kim D.-H., Park J.-S., Ferguson I. T., Yoo T.-K. // IEEE Photonics Technology Letters. - 2007. - Vol. 19, No. 1. - P. 24-26. ↑

J1731. Lee C.-H. Stability of nc-Si:H TFTs With Silicon Nitride Gate Dielectric. / Lee C.-H., Striakhilev D., Nathan A. // IEEE Transactions on Electron Devices. - 2007. - Vol. 54, No. 1. - P. 45-51. ↑

J1732. Ong A. O. Motion Characterizations of Lateral Micromachined Sensor Based on Stroboscopic Measurements. / Ong A. O., Tay F. E. H. // IEEE Sensors Journal. - 2007. - Vol. 7, No. 2. - P. 163-171. ↑

J1733. Kim Han-Ki. High-quality thin-film passivation by catalyzer-enhanced chemical vapor deposition for organic light-emitting diodes. / Kim Han-Ki, Kim Myung Soo, Kang Jae-Wook, Kim Jang-Joo, Yi Min-Su. // Applied Physics Letters. - 2007. - Vol. 90, No. 1. - P. 013502-013502-3. ↑

J1734. Li Yang. Elucidation of the electron injection mechanism of evaporated cesium carbonate cathode interlayer for organic light-emitting diodes. / Li Yang, Zhang De-Qiang, Duan Lian, Zhang Rui, Wang Li-Duo, Qiu Yong. // Applied Physics Letters. - 2007. - Vol. 90, No. 1. - P. 012119-012119-3. ↑

J1735. Das N. C. Increase in midwave infrared light emitting diode light output due to substrate thinning and texturing. Applied Physics Letters. - 2007. - Vol. 90, No. 1. - P. 011111-011111-3. ↑

J1736. Lin C.-L. A Novel LTPS-TFT Pixel Circuit Compensating for TFT Threshold-Voltage Shift and OLED Degradation for AMOLED. / Lin C.-L., Chen Y.-C. // IEEE Electron Device Letters. - 2007. - Vol. 28, No. 2. - P. 155-157. ↑

129-131. ↑

J1737. Shahin J. Ashtiani. AMOLED Pixel Circuit With Electronic Compensation of Luminance Degradation. / Shahin J. Ashtiani, G. Reza Chaji, Arokia Nathan. // Journal of Display Technology. - 2007. - Vol. 3, No. 1. - P. 36-39. ↑

J1738. Ju-Hyun Lee. Novel Color-Sequential Transflective Liquid Crystal Displays. / Ju-Hyun Lee, Xinyu Zhu, Shin-Tson Wu. // Journal of Display Technology. - 2007. - Vol. 3, No. 1. - P. 2-8. ↑

J1739. Ray S. K. High-Power 1.3- μ m Quantum-Dot Superluminescent Light-Emitting Diode Grown by Molecular Beam Epitaxy. / Ray S. K., Choi T. L., Groom K. M., Liu H. Y., Hopkinson M., Hogg R. A. // IEEE Photonics Technology Letters. - 2007. - Vol. 19, No. 2. - P. 109-111. ↑

J1740. Goldstein H. Not Ready to Wear. IEEE Spectrum. - 2007. - Vol. 44, No. 1. - P. 38-39. ↑

J1741. Vamsy P. Chodavarapu. CMOS-Based Phase Fluorometric Oxygen Sensor System. / Vamsy P. Chodavarapu, Daniil O. Shubin, Rachel M. Bukowski, Albert H. Titus, Alexander N. Cartwright, Frank V. Bright. // IEEE Transactions on Circuits and Systems I: Regular Papers. - 2007. - Vol. 54, No. 1. - P. 111-118. ↑

J1742. Gartner C. Numerical Device Simulation of Double-Heterostructure Organic Laser Diodes Including Current-Induced Absorption Processes. / Gartner C., Karnutsch C., Pflumm C., Lemmer U. // IEEE Journal of Quantum Electronics. - 2007. - Vol. 43, No. 11. - P. 1006-1017. ↑

J1743. Hongdi Li. The Engineering and Initial Results of a Transformable Low-cost High-Resolution PET Camera. / Hongdi Li, Wai-Hoi Wong, Baghaei H., Uribe J., Yu Wang, Yuxuan Zhang, Soonseok Kim, Ramirez R., Jiguo Liu, Shitao Liu. // IEEE Transactions on Nuclear Science. - 2007. - Vol. 54, No. 5. - P. 1583-1588. ↑

J1744. Teller O. The Design of the Cooling System for the CMS Barrel Electromagnetic Calorimeter. IEEE Transactions on Nuclear Science. - 2007. - Vol. 54, No. 5. - P. 1748-1752. ↑

J1745. Jin-Ho Kim. Image Quality Enhancement Driving Method of Flat Panel Displays for TV Applications. / Jin-Ho Kim, Soon-Sung Ahn, Oh-Kyong Kwon. // IEEE Transactions on Consumer Electronics. - 2007. - Vol. 53, No. 3. - P. 1147-1152. ↑

J1746. Ping-Chuan Chang. High-Detectivity Nitride-Based MSM Photodetectors on InGaN-GaN Multiquantum Well With the Unactivated Mg-Doped GaN Layer. / Ping-Chuan Chang, Yu C.L., Chang S.J., Lee K.H., Liu C.H., Wu S.L. // IEEE Journal of Quantum Electronics. - 2007. - Vol. 43, No. 11. - P. 1060-1064. ↑

J1747. Czyszanowski T. Comparison of Usability of Oxide Apertures and Photonic Crystals Used to Create Radial Optical Confinements in 650-nm GaInP VCSELs. / Czyszanowski T., Sarzala R.P., Piskorski L., Dems M., Wasiak M., Nakwaski W., Panajotov K. // IEEE Journal of Quantum Electronics. - 2007. - Vol. 43, No. 11. - P. 1041-1047. ↑

J1748. Rhee J. Spatial and Temporal Resolution of Conjugate Conduction-Convection Thermal Resistance. / Rhee J., Bhatt A.D. // IEEE Transactions on Components and Packaging Technologies. - 2007. - Vol. 30, No. 4. - P. 673-682. ↑

J1749. Lan Kim. Thermal Resistance Measurement of LED Package with Multichips. / Lan Kim, Moo Whan Shin. // IEEE Transactions on Components and Packaging Technologies. - 2007. - Vol. 30, No. 4. - P. 632-636. ↑

J1750. Jia-Sheng Huang. Human-Body-Model Electrostatic-Discharge and Electrical-Overstress Studies of Buried-Heterostructure Semiconductor Lasers. / Jia-Sheng Huang, Olson T., Isip E. // IEEE Transactions on Device and Materials Reliability. - 2007. - Vol. 7, No. 3. - P. 453-461. ↑

J1751. Towe E. Quantum Dots in Imaging [In the Spotlight]. IEEE Signal Processing Magazine. - 2007. - Vol. 24, No. 5. - P. 160-158. ↑

J1752. Hau-Yan Lu. A New Pixel Circuit Compensating for Brightness Variation in Large Size and High Resolution AMOLED Displays. / Hau-Yan Lu, Ting-Chang Chang, Ya-Hsiang Tai, Po-Tsun Liu, Sien Chi. // Journal of Display Technology. - 2007. - Vol. 3, No. 4. - P. 398-403. ↑

J1753. Chang S.J. Highly Reliable High-Brightness GaN-Based Flip Chip LEDs. / Chang S.J., Chen W.S.,

Shei S.C., Ko T.K., Shen C.F., Hsu Y.P., Chang C.S., Tsai J.M., Lai W.C., Lin A.J. // IEEE Transactions on Advanced Packaging. - 2007. - Vol. 30, No. 4. - P. 752-757. ↑

J1754. Nyakas P. Full-Vectorial Three-Dimensional Finite Element Optical Simulation of Vertical-Cavity Surface-Emitting Lasers. Journal of Lightwave Technology. - 2007. - Vol. 25, No. 9. - P. 2427-2434. ↑

J1755. Jongwoon Park. Numerical Analysis of Multilayer Organic Light-Emitting Diodes. / Jongwoon Park, Kawakami Y., Seoung-Hwan Park. // Journal of Lightwave Technology. - 2007. - Vol. 25, No. 9. - P. 2828-2836. ↑

J1756. Paulson Linda Dailey. News Briefs. Computer. - 2007. - Vol. 40, No. 9. - P. 20-22. ↑

J1757. Nadeem T. Location-Aware IEEE 802.11 for Spatial Reuse Enhancement. / Nadeem T., Lusheng Ji. // IEEE Transactions on Mobile Computing. - 2007. - Vol. 6, No. 10. - P. 1171-1184. ↑

J1758. Horng J.J. GaN-Based Power LEDs With CMOS ESD Protection Circuits. / Horng J.J., Su Y.K., Chang S.J., Chen W.S., Shei S.C. // IEEE Transactions on Device and Materials Reliability. - 2007. - Vol. 7, No. 2. - P. 340-346. ↑

J1759. Lee C.-E. Correction to "Enhancement of Flip-Chip Light-Emitting Diodes With Omni-Directional Reflector and Textured Micropillar Arrays". / Lee C.-E., Lee Y.-C., Kuo H.-C., Tsai M.-R., Cheng B. S., Lu T.-C., Wang S.-C., Kuo C.-T. // IEEE Photonics Technology Letters. - 2007. - Vol. 19, No. 18. - P. 1404. ↑

J1760. Xiaojun Guo. A Simple and Effective Approach to Improve the Output Linearity of Switched-Current AMOLED Pixel Circuitry. / Xiaojun Guo, Silva S.R.P. // IEEE Electron Device Letters. - 2007. - Vol. 28, No. 10. - P. 887-889. ↑

J1761. Tien-Chang Lu. GaN-Based High-Q Vertical-Cavity Light-Emitting Diodes. / Tien-Chang Lu, Tsung-Ting Kao, Chih-Chiang Kao, Jung-Tang Chu, Kang-Fan Yeh, Li-Fan Lin, Yu-Chun Peng, Hung-Wen Huang, Hao-Chung Kuo, Shing-Chung Wang. // IEEE Electron Device Letters. - 2007. - Vol. 28, No. 10. - P. 884-886. ↑

J1762. Gong Z. Matrix-Addressable Micropixelated InGaN Light-Emitting Diodes With Uniform Emission and Increased Light Output. / Gong Z., Zhang H.X., Gu E., Griffin C., Dawson M.D., Poher V., Kennedy G., French P.M.W., Neil M.A.A. // IEEE Transactions on Electron Devices. - 2007. - Vol. 54, No. 10. - P. 2650-2658. ↑

J1763. Kim Hyunsoo. Enhanced Light Output of GaN-Based Light-Emitting Diodes by Using Omnidirectional Sidewall Reflectors. / Kim Hyunsoo, Baik Kwang Hyeon, Cho Jaehee, Kim Kyoung-Kook, Lee Sung-Nam, Sone C., Park Y., Seong Tae-Yeon. // IEEE Photonics Technology Letters. - 2007. - Vol. 19, No. 19. - P. 1562-1564. ↑

J1764. Norgia M. Absolute Distance Measurement With Improved Accuracy Using Laser Diode Self-Mixing Interferometry in a Closed Loop. / Norgia M., Giuliani G., Donati S. // IEEE Transactions on Instrumentation and Measurement. - 2007. - Vol. 56, No. 5. - P. 1894-1900. ↑

J1765. Luo X. Thermal analysis of an 80 W light-emitting diode street lamp. / Luo X., Cheng T., Xiong W., Gan Z., Liu S. // IET Optoelectronics. - 2007. - Vol. 1, No. 5. - P. 191-196. ↑

J1766. Liao M.P. DC Current-Induced Rollover of Illumination Efficiency of GaN-Based Power LEDs. IEEE Photonics Technology Letters. - 2007. - Vol. 19, No. 24. - P. 2000-2002. ↑

J1767. Radovic M.K. Investigation of a Dynamic Corona to Normal Glow Transition in a Neon Gas Diode. / Radovic M.K., Maluckov C.A., Rancev S.A. // IEEE Transactions on Plasma Science. - 2007. - Vol. 35, No. 6. - P. 1738-1742. ↑

J1768. {no data available}. 2007 Index Journal of Display Technology Vol. 3. Journal of Display Technology. - 2007. - Vol. 3, No. 4. - P. 435-444. ↑

J1769. Shao-Hua Huang. Thermally Stable Mirror Structures for Vertical-Conducting GaN/Mirror/Si Light-Emitting Diodes. / Shao-Hua Huang, Ray-Hua Horng, Szu-Lung Li, Kuo-Wei Yen, Dong-Sing Wu, Chao-Kun Lin, Heng Liu. // IEEE Photonics Technology Letters. - 2007. - Vol. 19, No. 23. - P. 1913-1915. ↑

J1770. Kuo C.H. Nitride-Based Near-Ultraviolet Mesh MQW Light-Emitting Diodes. / Kuo C.H., Feng H.C. // IEEE Photonics Technology Letters. - 2007. - Vol. 19, No. 23. - P. 1901-1903. ↑

- J1771.** Chaji G.R. Electrical Compensation of OLED Luminance Degradation. / Chaji G.R., Ng C., Nathan A., Werner A., Birnstock J., Schneider O., Blochwitz-Nimoth J. // IEEE Electron Device Letters. - 2007. - Vol. 28, No. 12. - P. 1108-1110. ↑
- J1772.** Choi Y.C. CDP Servo System Control using Fuzzy Logic Control. / Choi Y.C., Chang-Hun Kim. // IEEE Transactions on Consumer Electronics. - 2007. - Vol. 53, No. 4. - P. 1314-1321. ↑
- J1773.** Murata S. Toward a scalable modular robotic system. / Murata S., Kakomura K., Kurokawa H. // IEEE Robotics & Automation Magazine. - 2007. - Vol. 14, No. 4. - P. 56-63. ↑
- J1774.** Luetzelschwab M. MEMS-based packaging of a UV-LED array. / Luetzelschwab M., Weiland D., Abraham E., Desmulliez M.P.Y. // IET Micro & Nano Letters. - 2007. - Vol. 2, No. 4. - P. 99-102. ↑
- J1775.** Johnston A.H. LED Technologies for Optocouplers: Fundamental Issues and Hardness Assurance. / Johnston A.H., Miyahira T.F. // IEEE Transactions on Nuclear Science. - 2007. - Vol. 54, No. 6. - P. 2450-2456. ↑
- J1776.** Cherry S. A Word in Your Ear [Resources: Tools & Toys]. IEEE Spectrum. - 2007. - Vol. 44, No. 12. - P. 65-66. ↑
- J1777.** Lei Wang. Multichannel Reflective PPG Earpiece Sensor With Passive Motion Cancellation. / Lei Wang, Lo B.P.L., Guang-Zhong Yang. // IEEE Transactions on Biomedical Circuits and Systems. - 2007. - Vol. 1, No. 4. - P. 235-241. ↑
- J1778.** Grandjean N. Visible InGaN/GaN Quantum-Dot Materials and Devices. / Grandjean N., Ilegems M. // Proceedings of the IEEE. - 2007. - Vol. 95, No. 9. - P. 1853-1865. ↑
- J1779.** Wang K.L. Ge/Si Self-Assembled Quantum Dots and Their Optoelectronic Device Applications. / Wang K.L., Dongho Cha, Jianlin Liu, Chen C. // Proceedings of the IEEE. - 2007. - Vol. 95, No. 9. - P. 1866-1883. ↑
- J1780.** Yi-Fu Chen. Mixed Color Sequential Technique for Reducing Color Breakup and Motion Blur Effects. / Yi-Fu Chen, Che-Chin Chen, Ke-Horng Chen. // Journal of Display Technology. - 2007. - Vol. 3, No. 4. - P. 377-385. ↑
- J1781.** Kui Bao. Improvement of Light Extraction From Patterned Polymer Encapsulated GaN-Based Flip-Chip Light-Emitting Diodes by Imprinting. / Kui Bao, Xiang Ning Kang, Bei Zhang, Tao Dai, Chang Xiong, Hang Ji, Guo Yi Zhang, Yong Chen. // IEEE Photonics Technology Letters. - 2007. - Vol. 19, No. 22. - P. 1840-1842. ↑
- J1782.** Lee J.-J. High-performance light emitting diode backlight driving system for large-screen liquid crystal display. / Lee J.-J., Kwon B.-H. // IET Electric Power Applications. - 2007. - Vol. 1, No. 6. - P. 946-955. ↑
- J1783.** Alexander R.R. Systematic Study of the Effects of Modulation p-Doping on 1.3- μm Quantum-Dot Lasers. / Alexander R.R., Childs D.T.D., Agarwal H., Groom K.M., Hui-Yun Liu, Hopkinson M., Hogg R.A., Ishida M., Yamamoto T., Sugawara M., Arakawa Y., Badcock T.J., Royce R.J., Mowbray D.J. // IEEE Journal of Quantum Electronics. - 2007. - Vol. 43, No. 12. - P. 1129-1139. ↑
- J1784.** Chen N.C. Capacitance-Voltage and Current-Voltage Measurements of Nitride Light-Emitting Diodes. / Chen N.C., Lien W.C., Wang Y.S., Liu H.H. // IEEE Transactions on Electron Devices. - 2007. - Vol. 54, No. 12. - P. 3223-3228. ↑
- J1785.** Jyi-Tsong Lin. A Novel Blocking Technology for Improving the Short-Channel Effects in Polycrystalline Silicon TFT Devices. / Jyi-Tsong Lin, Yi-Chuen Eng. // IEEE Transactions on Electron Devices. - 2007. - Vol. 54, No. 12. - P. 3238-3244. ↑
- J1786.** Meneghini M. Reversible Degradation of Ohmic Contacts on p-GaN for Application in High-Brightness LEDs. / Meneghini M., Trevisanello L.-R., Zehnder U., Meneghesso G., Zanoni E. // IEEE Transactions on Electron Devices. - 2007. - Vol. 54, No. 12. - P. 3245-3251. ↑
- J1787.** Ja-Yeon Kim. Enhanced Light Extraction From Triangular GaN-Based Light-Emitting Diodes. / Ja-Yeon Kim, Min-Ki Kwon, Jae-Pil Kim, Seong-Ju Park. // IEEE Photonics Technology Letters. - 2007. - Vol. 19, No. 23. - P. 1865-1867. ↑

- J1788.** Min-Ki Kwon. Gradient Doping of Mg in p-Type GaN for High Efficiency InGaN-GaN Ultraviolet Light-Emitting Diode. / Min-Ki Kwon, Il-Kyu Park, Ja-Yeon Kim, Jeom-Oh Kim, Bongjin Kim, Seong-Ju Park. // IEEE Photonics Technology Letters. - 2007. - Vol. 19, No. 23. - P. 1880-1882. ↑
- J1789.** Cao X.A. Current and Temperature Dependent Characteristics of Deep-Ultraviolet Light-Emitting Diodes. / Cao X.A., LeBoeuf S.F. // IEEE Transactions on Electron Devices. - 2007. - Vol. 54, No. 12. - P. 3414-3417. ↑
- J1790.** Lee Y.C. High-Temperature Stability of 650-nm Resonant-Cavity Light-Emitting Diodes Fabricated Using Wafer-Bonding Technique on Silicon Substrates. / Lee Y.C., Kuo H.C., Lee C.E., Lu T.C., Wang S.C., Chiou S.W. // IEEE Photonics Technology Letters. - 2007. - Vol. 19, No. 14. - P. 1060-1062. ↑
- J1791.** Lan Kim. Implementation of Side Effects in Thermal Characterization of RGB Full-Color LEDs. / Lan Kim, Moo Whan Shin. // IEEE Electron Device Letters. - 2007. - Vol. 28, No. 7. - P. 578-580. ↑
- J1792.** Kuo P.-S. Transport Mechanism of SiGe Dot MOS Tunneling Diodes. / Kuo P.-S., Lin C.-H., Peng C.-Y., Fu Y.-C., Liu C.W. // IEEE Electron Device Letters. - 2007. - Vol. 28, No. 7. - P. 596-598. ↑
- J1793.** Pani R. Factors Affecting Hamamatsu H8500 Flat Panel PMT Calibration for Gamma Ray Imaging. / Pani R., Pellegrini R., Cinti M.N., Trotta C., Trotta G., Scafe R., D'Addio L., Iurlaro G., Montani L., Bennati P., Ridolfi S., Cusanno F., Garibaldi F. // IEEE Transactions on Nuclear Science. - 2007. - Vol. 54, No. 3. - P. 438-443. ↑
- J1794.** Liang-Chia Chen. A Dynamic 3-D Surface Profilometer With Nanoscale Measurement Resolution and MHz Bandwidth for MEMS Characterization. / Liang-Chia Chen, Yao-Ting Huang, Kuang-Chao Fan. // IEEE/ASME Transactions on Mechatronics. - 2007. - Vol. 12, No. 3. - P. 299-307. ↑
- J1795.** Loftus T.H. Spectrally Beam-Combined Fiber Lasers for High-Average-Power Applications. / Loftus T.H., Thomas A.M., Hoffman P.R., Norsen M., Royse R., Anping Liu, Honea E.C. // IEEE Journal of Selected Topics in Quantum Electronics. - 2007. - Vol. 13, No. 3. - P. 487-497. ↑
- J1796.** Boyd J. Let there be (a new kind of) light [NEWS]. IEEE Spectrum. - 2007. - Vol. 44, No. 7. - P. 12-14. ↑
- J1797.** Bingfeng Fan. Study of Phosphor Thermal-Isolated Packaging Technologies for High-Power White Light-Emitting Diodes. / Bingfeng Fan, Hao Wu, Yu Zhao, Yulun Xian, Gang Wang. // IEEE Photonics Technology Letters. - 2007. - Vol. 19, No. 15. - P. 1121-1123. ↑
- J1798.** Gamadia M. Low-Light Auto-Focus Enhancement for Digital and Cell-Phone Camera Image Pipelines. / Gamadia M., Kehtarnavaz N., Roberts-Hoffman K. // IEEE Transactions on Consumer Electronics. - 2007. - Vol. 53, No. 2. - P. 249-257. ↑
- J1799.** Heng-Tien Lin. Carrier Transport Mechanism in a Nanoparticle-Incorporated Organic Bistable Memory Device. / Heng-Tien Lin, Zingway Pei, Yi-Jen Chan. // IEEE Electron Device Letters. - 2007. - Vol. 28, No. 7. - P. 569-571. ↑
- J1800.** Dayan Ban. Organic-Inorganic Hybrid Optical Upconverter. / Dayan Ban, Han S., Lu Z.H., Oogarah T., SpringThorpe A.J., Liu H.C. // IEEE Transactions on Electron Devices. - 2007. - Vol. 54, No. 7. - P. 1645-1650. ↑
- J1801.** Amat C. Free engineering of buried oxide patterns in GaAs/AlAs epitaxial structures. / Amat C., Almuneau G., Gallo P., Jalabert L., Moumdji S., Dubreuil P., Camps T., Doucet J.B., Havard E., Bardinal V., Fontaine C., Munoz-Yague A. // Electronics Letters. - 2007. - Vol. 43, No. 13. - P. 730-732. ↑
- J1802.** Qingjiang Sun. Polymer Light-Emitting Electrochemical Cells for High-Efficiency Low-Voltage Electroluminescent Devices. / Qingjiang Sun, Yongfang Li, Qibing Pei. // Journal of Display Technology. - 2007. - Vol. 3, No. 2. - P. 211-224. ↑
- J1803.** Chih-Lung Lin. A Novel Voltage Driving Method Using 3-TFT Pixel Circuit for AMOLED. / Chih-Lung Lin, Tsung-Ting Tsai. // IEEE Electron Device Letters. - 2007. - Vol. 28, No. 6. - P. 489-491. ↑
- J1804.** Lin R.-M. Improving the Luminescence of InGaN-GaN Blue LEDs Through Selective Ring-Region Activation of the Mg-Doped GaN Layer. / Lin R.-M., Jen-Chih Li, Yi-Lun Chou, Kuo-Hsing Chen, Yung-Hsiang

Lin, Yuan-Chieh Lu, Meng-Chyi Wu, Hung H., Wei-Chi Lai. // IEEE Photonics Technology Letters. - 2007. - Vol. 19, No. 12. - P. 928-930. ↑

J1805. Ohmori Y. Organic Light-Emitting Diodes Fabricated by a Solution Process and Their Stress Tolerance. / Ohmori Y., Kajii H., Hino Y. // Journal of Display Technology. - 2007. - Vol. 3, No. 2. - P. 238-244. ↑

J1806. Ribierre J.-C. Optimization of the Luminescence Efficiencies in Solution-Processed Phosphorescent Dendrimers. / Ribierre J.-C., Stevenson S.G., Samuel I.D.W., Staton S.V., Burn P.L. // Journal of Display Technology. - 2007. - Vol. 3, No. 2. - P. 233-237. ↑

J1807. So S.K. Charge Transport and Injection to Phenylamine-Based Hole Transporters for OLEDs Applications. / So S.K., Tse S.C., Tong K.L. // Journal of Display Technology. - 2007. - Vol. 3, No. 2. - P. 225-232. ↑

J1808. Mullins J. LEDs Could Borrow From Beetles. IEEE Spectrum. - 2007. - Vol. 44, No. 6. - P. 18-20. ↑

J1809. Huang G.S. Fabrication of Microcavity Light-Emitting Diodes Using Highly Reflective AlN-GaN and Ta₂O₅-SiO₂ Distributed Bragg Mirrors. / Huang G.S., Lu T.C., Kuo H.C., Wang S.C., Hou-Guang Chen. // IEEE Photonics Technology Letters. - 2007. - Vol. 19, No. 13. - P. 999-1001. ↑

J1810. Chodavarapu V.P. CMOS integrated luminescence oxygen multi-sensor system. / Chodavarapu V.P., Bukowski R.M., Titus A.H., Cartwright A.N., Bright F.V. // Electronics Letters. - 2007. - Vol. 43, No. 12. - P. 688-689. ↑

J1811. Redinger D. High-Performance Chemical-Bath-Deposited Zinc Oxide Thin-Film Transistors. / Redinger D., Subramanian V. // IEEE Transactions on Electron Devices. - 2007. - Vol. 54, No. 6. - P. 1301-1307. ↑

J1812. Veeraraghavan G. An 8 4 8 Pixel Array Pen-Input OLED Screen Based on Organic Magnetoresistance. / Veeraraghavan G., Nguyen T.D., Yugang Sheng, Mermer O., Wohlgenannt M. // IEEE Transactions on Electron Devices. - 2007. - Vol. 54, No. 6. - P. 1571-1577. ↑

J1813. Han C.-W. Top-emitting OLED pixel employing cathode-contact structure with a-Si:H thin-film transistors. / Han C.-W., Han M.-K., Kim M.S., Nam W.-J., Bae S.-J., Kim K.-Y., Chung I.-J. // Electronics Letters. - 2007. - Vol. 43, No. 11. - P. 623-624. ↑

J1814. Sambandan S. Single-Technology-Based Statistical Calibration for High-Performance Active-Matrix Organic LED Displays. / Sambandan S., Nathan A. // Journal of Display Technology. - 2007. - Vol. 3, No. 3. - P. 284-294. ↑

J1815. Shug-June Hwang. Thermo Effects on Flexible Panel Substrate. / Shug-June Hwang, Ming Chun Tseng, Kuo-Cheng Hwang, Hsin Her Yu. // Journal of Display Technology. - 2007. - Vol. 3, No. 3. - P. 253-258. ↑

J1816. Xing-Jie Yu. LED-Based Projection Systems. / Xing-Jie Yu, Ho Y.L., Tan L., Ho-Chi Huang, Hoi-Sing Kwok. // Journal of Display Technology. - 2007. - Vol. 3, No. 3. - P. 295-303. ↑

J1817. Dollarhide Maya. Pervasive Computing Helps Fans Get Into the Game. IEEE Pervasive Computing. - 2007. - Vol. 6, No. 3. - P. 7-10. ↑

J1818. Johnston A.H. Radiation Damage in Power MOSFET Optocouplers. / Johnston A.H., Miyahira T.F. // IEEE Transactions on Nuclear Science. - 2007. - Vol. 54, No. 4. - P. 1104-1109. ↑

J1819. Gauza S. Fast Switching Liquid Crystals for Color-Sequential LCDs. / Gauza S., Xinyu Zhu, Piecek W., Dabrowski R., Shin-Tson Wu. // Journal of Display Technology. - 2007. - Vol. 3, No. 3. - P. 250-252. ↑

J1820. Huang-Jen Chiu. LED Backlight Driving System for Large-Scale LCD Panels. / Huang-Jen Chiu, Shih-Jen Cheng. // IEEE Transactions on Industrial Electronics. - 2007. - Vol. 54, No. 5. - P. 2751-2760. ↑

J1821. Pocha M.D. Electrical and Optical Gain Lever Effects in InGaAs Double Quantum-Well Diode Lasers. / Pocha M.D., Goddard L.L., Bond T.C., Nikolic R.J., Vernon S.P., Kallman J.S., Behymer E.M. // IEEE Journal of Quantum Electronics. - 2007. - Vol. 43, No. 10. - P. 860-868. ↑

J1822. Hojin Lee. Current-Scaling a-Si:H TFT Pixel-Electrode Circuit for AM-OLEDs: Electrical Properties and

Stability. / Hojin Lee, Yen-Chung Lin, Shieh H.-P.D., Kanicki J. // IEEE Transactions on Electron Devices. - 2007. - Vol. 54, No. 9. - P. 2403-2410. ↑

J1823. Kimoto A. Noncontact Material Identification and Distance Measurement Using Effective Capacitance With CdS Cells. / Kimoto A., Tsuji S., Shida K. // IEEE Sensors Journal. - 2007. - Vol. 7, No. 10. - P. 1440-1446. ↑

J1824. Shi J.-W. Linear Cascade Arrays of GaN-Based Green Light-Emitting Diodes for High-Speed and High-Power Performance. / Shi J.-W., Sheu J.-K., Wang C.-K., Chen C.-C., Hsieh C.-H., Chyi J.-I., Lai W.-C. // IEEE Photonics Technology Letters. - 2007. - Vol. 19, No. 18. - P. 1368-1370. ↑

J1825. Sebitosi A.B. New Technologies for Rural Lighting in Developing Countries: White LEDs. / Sebitosi A.B., Pillay P. // IEEE Transactions on Energy Conversion. - 2007. - Vol. 22, No. 3. - P. 674-679. ↑

J1826. Hyunsoo Kim. Consideration of the Actual Current-Spreading Length of GaN-Based Light-Emitting Diodes for High-Efficiency Design. / Hyunsoo Kim, Jaehee Cho, Jeong Wook Lee, Sukho Yoon, Hyungkun Kim, Cheolsoo Sone, Yongjo Park, Tae-Yeon Seong. // IEEE Journal of Quantum Electronics. - 2007. - Vol. 43, No. 8. - P. 625-632. ↑

J1827. Chia-En Lee. Enhancement of Flip-Chip Light-Emitting Diodes With Omni-Directional Reflector and Textured Micropillar Arrays. / Chia-En Lee, Yi-Jiun Lee, Hao-Chung Kuo, Meng-Ru Tsai, Cheng B.S., Tien-Chang Lu, Shing-Chung Wang, Chia-Tai Kuo. // IEEE Photonics Technology Letters. - 2007. - Vol. 19, No. 16. - P. 1200-1202. ↑

J1828. Chang P.C. Low-Noise and High-Detectivity GaN-Based UV Photodiode With a Semi-Insulating Mg-Doped GaN Cap Layer. / Chang P.C., Yu C.L., Chang S.J., Lin Y.C., Liu C.H., Wu S.L. // IEEE Sensors Journal. - 2007. - Vol. 7, No. 9. - P. 1270-1273. ↑

J1829. Olivieri M. A Reconfigurable, Low Power, Temperature Compensated IC for 8-segment Gamma Correction Curve in TFT, OLED and PDP Displays. / Olivieri M., Mancuso R., Riedel F. // IEEE Transactions on Consumer Electronics. - 2007. - Vol. 53, No. 2. - P. 720-724. ↑

J1830. Liann-Be Chang. Light Output Improvement of InGaN-Based Light-Emitting Diodes by Microchannel Structure. / Liann-Be Chang, Yuan-Hsiao Chang, Ming-Jer Jeng. // IEEE Photonics Technology Letters. - 2007. - Vol. 19, No. 15. - P. 1175-1177. ↑

J1831. Liang C.J. The Electroluminescent Decay Mechanism of Rare-Earth Ions in OLEDs Based on a Terbium Complex. / Liang C.J., Choy C.H., Chunhui Huang. // IEEE Photonics Technology Letters. - 2007. - Vol. 19, No. 15. - P. 1178-1180. ↑

J1832. Zhong H. Demonstration of high power blue-green light emitting diode on semipolar (1122) bulk GaN substrate. / Zhong H., Tyagi A., Fellows N.N., Chung R.B., Saito M., Fujito K., Speck J.S., DenBaars S.P., Nakamura S. // Electronics Letters. - 2007. - Vol. 43, No. 15. - P. 825-826. ↑

J1833. Xiaobing Luo. A Microjet Array Cooling System for Thermal Management of High-Brightness LEDs. / Xiaobing Luo, Sheng Liu. // IEEE Transactions on Advanced Packaging. - 2007. - Vol. 30, No. 3. - P. 475-484. ↑

J1834. Wang Y.-Y. Direct Encapsulation of Organic Light-Emitting Devices (OLEDs) Using Photo-Curable co - Polyacrylate/Silica Nanocomposite Resin. / Wang Y.-Y., Hsieh T.-E., Chen I.-C., Chen C.-H. // IEEE Transactions on Advanced Packaging. - 2007. - Vol. 30, No. 3. - P. 421-427. ↑

J1835. Chang P.C. Low-Noise and High-Detectivity GaN UV Photodiodes With a Low-Temperature AlN Cap Layer. / Chang P.C., Yu C.L., Chang S.J., Lin Y.C., Wu S.L. // IEEE Sensors Journal. - 2007. - Vol. 7, No. 9. - P. 1289-1292. ↑

J1836. Chuantong Wang. A Low-Cost Double-Fiber Model Distributed Optical Fiber Sensor. / Chuantong Wang, Shida K. // IEEE Transactions on Instrumentation and Measurement. - 2007. - Vol. 56, No. 4. - P. 1481-1487. ↑

J1837. Tu Hoang. Influence of Dislocation Loops on the Near-Infrared Light Emission From Silicon Diodes. / Tu Hoang, Holleman J., Phuong LeMinh, Schmitz J., Mchedlidze T., Arguirov T., Kittler M. // IEEE Transactions on Electron Devices. - 2007. - Vol. 54, No. 8. - P. 1860-1866. ↑

- J1838.** Park Jin Ho. Double interfacial layers for highly efficient organic light-emitting devices. / Park Jin Ho, Oh Seung Seok, Kim Sun Woong, Choi Eun Ha, Hong Byoung Hee, Seo Yoon Ho, Cho Guang Sup, Park Byoungchoo, Lim Jongsun, Yoon Sung Cheol, Lee Changjin. // Applied Physics Letters. - 2007. - Vol. 90, No. 15. - P. 153508-153508-3. ↑
- J1839.** Fan Suqin. Efficient white-light-emitting diodes based on polyfluorene doped with fluorescent chromophores. / Fan Suqin, Sun Mingliang, Wang Jian, Yang Wei, Cao Yong. // Applied Physics Letters. - 2007. - Vol. 91, No. 21. - P. 213502-213502-3. ↑
- J1840.** Ee Yik-Khoon. Enhancement of light extraction efficiency of InGaN quantum wells light emitting diodes using Si O₂/polystyrene microlens arrays. / Ee Yik-Khoon, Arif Ronald A., Tansu Nelson, Kumnorkaew Pisist, Gilchrist James F. // Applied Physics Letters. - 2007. - Vol. 91, No. 22. - P. 221107-221107-3. ↑
- J1841.** Sharma Rajat. Gallium-nitride-based microcavity light-emitting diodes with air-gap distributed Bragg reflectors. / Sharma Rajat, Choi Yong-Seok, Wang Chiou-Fu, David Aurelien, Weisbuch Claude, Nakamura Shuji, Hu Evelyn L. // Applied Physics Letters. - 2007. - Vol. 91, No. 21. - P. 211108-211108-3. ↑
- J1842.** Lee Hsin-Ying. Current spreading of III-nitride light-emitting diodes using plasma treatment. / Lee Hsin-Ying, Pan Ke-Hao, Lin Chih-Chien, Chang Yun-Chorng, Kao Fu-Jen, Lee Ching-Ting. // Journal of Vacuum Science & Technology B: Microelectronics and Nanometer Structures. - 2007. - Vol. 25, No. 4. - P. 1280-1283. ↑
- J1843.** Park B. J. Effect of neutral beam etching of p-Ga N on the GaN device characteristics. / Park B. J., Min K. S., Lee H. C., Bae J. W., Kim D. W., Yeom G. Y. // Journal of Vacuum Science & Technology B: Microelectronics and Nanometer Structures. - 2007. - Vol. 25, No. 2. - P. 295-298. ↑
- J1844.** Tay Savas. Planar photonic crystals infiltrated with nanoparticle/polymer composites. / Tay Savas, Thomas Jayan, Momeni Babak, Askari Murtaza, Adibi Ali, Hotchkiss Peter J., Jones Simon C., Marder Seth R., Norwood Robert A., Peyghambarian N. // Applied Physics Letters. - 2007. - Vol. 91, No. 22. - P. 221109-221109-3. ↑
- J1845.** Bolink Henk J. Air stable hybrid organic-inorganic light emitting diodes using ZnO as the cathode. / Bolink Henk J., Coronado Eugenio, Repetto Diego, Sessolo Michele. // Applied Physics Letters. - 2007. - Vol. 91, No. 22. - P. 223501-223501-3. ↑
- J1846.** Chu Ta-Ya. Effects of interfacial stability between electron transporting layer and cathode on the degradation process of organic light-emitting diodes. / Chu Ta-Ya, Lee Yong-Han, Song Ok-Keun. // Applied Physics Letters. - 2007. - Vol. 91, No. 22. - P. 223509-223509-3. ↑
- J1847.** Yao Z. Q. Epitaxial growth and structural analysis of Al N /Ga N heterostructures. / Yao Z. Q., Zou Y. S., Yang Y., Zhang W. J., Lee S. T., Zhang Y. Z., Ye Z. Z. // Applied Physics Letters. - 2007. - Vol. 91, No. 22. - P. 221912-221912-3. ↑
- J1848.** Chen Xue-Wen. Modifications of the exciton lifetime and internal quantum efficiency for organic light-emitting devices with a weak/strong microcavity. / Chen Xue-Wen, Choy Wallace C. H., Liang C. J., Wai P. K. A., He Sailing. // Applied Physics Letters. - 2007. - Vol. 91, No. 22. - P. 221112-221112-3. ↑
- J1849.** Zhang J. C. Quantum-well and localized state emissions in AlInGaN deep ultraviolet light-emitting diodes. / Zhang J. C., Zhu Y. H., Egawa T., Sumiya S., Miyoshi M., Tanaka M. // Applied Physics Letters. - 2007. - Vol. 91, No. 22. - P. 221906-221906-3. ↑
- J1850.** Mizutani Wataru. Influences of submonolayer proteins on organic light-emitting diodes. / Mizutani Wataru, Tsukagoshi Kiyomi, Sakaguchi Koichi, Chikamatsu Masayuki, Yoshida Yuji. // Applied Physics Letters. - 2007. - Vol. 91, No. 2. - P. 024101-024101-3. ↑
- J1851.** Gan Chenli. Size dependence of nonlinear optical absorption and refraction of Mn-doped ZnSe nanocrystals. / Gan Chenli, Xiao Min, Battaglia David, Pradhan Narayan, Peng Xiaogang. // Applied Physics Letters. - 2007. - Vol. 91, No. 20. - P. 201103-201103-3. ↑
- J1852.** Kim Hyunsoo. Design of high-efficiency GaN-based light emitting diodes with vertical injection geometry. / Kim Hyunsoo, Kim Kyoung-Kook, Choi Kwang-Ki, Kim Hyungkun, Song June-O, Cho Jaehee, Baik Kwang Hyeon, Sone Cheolsoo, Park Yongjo, Seong Tae-Yeon. // Applied Physics Letters. - 2007. - Vol. 91, No.

2. - P. 023510-023510-3. ↑

J1853. Huang Y. The development of Thomson scattering system on HL-2A tokamak. / Huang Y., Zhang P., Feng Z., Liu C. H., Shi P. L., Ding X. T., Liu Yong. // Review of Scientific Instruments. - 2007. - Vol. 78, No. 11. - P. 113501-113501-5. ↑

J1854. Chen Ping. White organic light-emitting devices with a bipolar transport layer between blue fluorescent and orange phosphorescent emitting layers. / Chen Ping, Xie Wenfa, Li Jiang, Guan Tao, Duan Yu, Zhao Yi, Liu Shiyong, Ma Chunsheng, Zhang Liying, Li Bin. // Applied Physics Letters. - 2007. - Vol. 91, No. 2. - P. 023505-023505-3. ↑

J1855. Lu Jiashu. Optical upconversion devices based on photosensitizer-doped organic light-emitting diodes. / Lu Jiashu, Zheng Yuan, Chen Zhijian, Xiao Lixin, Gong Qihuang. // Applied Physics Letters. - 2007. - Vol. 91, No. 20. - P. 201107-201107-3. ↑

J1856. Kang Myung-Gyu. Semitransparent Cu electrode on a flexible substrate and its application in organic light emitting diodes. / Kang Myung-Gyu, Guo L. Jay. // Journal of Vacuum Science & Technology B: Microelectronics and Nanometer Structures. - 2007. - Vol. 25, No. 6. - P. 2637-2641. ↑

J1857. Honda T. Fabrication of GaN-based metal-oxide-semiconductor light-emitting diodes operating in ultraviolet spectral region. / Honda T., Kobayashi T., Komiyama S., Mashiyama Y. // Journal of Vacuum Science & Technology B: Microelectronics and Nanometer Structures. - 2007. - Vol. 25, No. 4. - P. 1529-1532. ↑

J1858. Lei D. Y. Enhanced forward emission from ZnO via surface plasmons. / Lei D. Y., Ong H. C. // Applied Physics Letters. - 2007. - Vol. 91, No. 21. - P. 211107-211107-3. ↑

J1859. Yan Fei. Sensitized electrophosphorescence of infrared emission diode based on copper phthalocyanine by an ytterbium complex. / Yan Fei, Li Wen Lian, Chu Bei, Li Tian Le, Su Wen Ming, Su Zi Sheng, Zhu Jian Zhuo, Yang Dong Fang, Zhang Guang, Bi De Feng, Han Liang Liang, Cheng Chuan Hui, Fan Zhao Qi, Yu Shu Kun, Du Guo Tong, Tsuboi Taiju. // Applied Physics Letters. - 2007. - Vol. 91, No. 20. - P. 203512-203512-3. ↑

J1860. Byun Younghun. Highly efficient red electrophosphorescence from a solution-processed zwitterionic cyclometalated iridium(III) complex. / Byun Younghun, Lyu Yi-Yeol, Das Rupasree Ragini, Kwon Ohyun, Lee Tae-Woo, Park Young Ja. // Applied Physics Letters. - 2007. - Vol. 91, No. 21. - P. 211106-211106-3. ↑

J1861. Ferdous M. S. Effect of threading defects on InGaN /GaN multiple quantum well light emitting diodes. / Ferdous M. S., Wang X., Fairchild M. N., Hersee S. D. // Applied Physics Letters. - 2007. - Vol. 91, No. 23. - P. 231107-231107-3. ↑

J1862. Zhao J. L. Realization of n-Zn $1-x$ Mg x O /i-Zn O /Si O x /n+ -Si heterostructured n-i-n light-emitting diodes by low-cost ultrasonic spray pyrolysis. / Zhao J. L., Sun X. W., Tan S. T., Lo G. Q., Kwong D. L., Cen Z. H. // Applied Physics Letters. - 2007. - Vol. 91, No. 26. - P. 263501-263501-3. ↑

J1863. Piao Xianqing. Self-propagating high temperature synthesis of yellow-emitting Ba 2 Si 5 N 8 :Eu $2+$ phosphors for white light-emitting diodes. / Piao Xianqing, Machida Ken-ichi, Horikawa Takashi, Hanzawa Hiromasa. // Applied Physics Letters. - 2007. - Vol. 91, No. 4. - P. 041908-041908-3. ↑

J1864. Lee J. Interface electronic structure of the organic light-emitting devices: Photoemission and x-ray absorption studies of Al /K F /Al q 3 interface. / Lee J., Lim J. S., Shin H. J., Park Y. // Applied Physics Letters. - 2007. - Vol. 91, No. 26. - P. 261902-261902-3. ↑

J1865. Yang Chih-Jen. Microcavity top-emitting organic light-emitting devices integrated with microlens arrays: Simultaneous enhancement of quantum efficiency, cd/A efficiency, color performances, and image resolution. / Yang Chih-Jen, Liu Su-Hao, Hsieh Hsing-Hung, Liu Chih-Che, Cho Ting-Yi, Wu Chung-Chih. // Applied Physics Letters. - 2007. - Vol. 91, No. 25. - P. 253508-253508-3. ↑

J1866. Kalaitzakis F. G. Low resistance as-deposited Cr /Au contacts on p -type GaN. / Kalaitzakis F. G., Pelekanos N. T., Prystawko P., Leszczynski M., Konstantinidis G. // Applied Physics Letters. - 2007. - Vol. 91, No. 26. - P. 261103-261103-3. ↑

J1867. Wu Z. H. Effect of internal electrostatic fields in InGaN quantum wells on the properties of green light

- emitting diodes. / Wu Z. H., Fischer A. M., Ponce F. A., Lee W., Ryou J. H., Limb J., Yoo D., Dupuis R. D. // Applied Physics Letters. - 2007. - Vol. 91, No. 4. - P. 041915-041915-3. ↑
- J1868.** Lee Ming-Kwei. Single-step fabrication of Fresnel microlens array on sapphire substrate of flip-chip gallium nitride light emitting diode by focused ion beam. / Lee Ming-Kwei, Kuo Kwei-Kuan. // Applied Physics Letters. - 2007. - Vol. 91, No. 5. - P. 051111-051111-3. ↑
- J1869.** Ren Z. Heteroepitaxy of AlGaIn on bulk AlN substrates for deep ultraviolet light emitting diodes. / Ren Z., Sun Q., Kwon S.-Y., Han J., Davitt K., Song Y. K., Nurmikko A. V., Cho H.-K., Liu W., Smart J. A., Schowalter L. J. // Applied Physics Letters. - 2007. - Vol. 91, No. 5. - P. 051116-051116-3. ↑
- J1870.** Chen Yan. Nanoimprinted circular grating distributed feedback dye laser. / Chen Yan, Li Zhenyu, Zhang Zhaoyu, Psaltis Demetri, Scherer Axel. // Applied Physics Letters. - 2007. - Vol. 91, No. 5. - P. 051109-051109-3. ↑
- J1871.** Jou Jwo-Huei. Hole-transporting-layer-free high-efficiency fluorescent blue organic light-emitting diodes. / Jou Jwo-Huei, Chiang Po-Hsuan, Lin Yu-Pu, Chang Chin-Yeh, Lai Chun-Liang. // Applied Physics Letters. - 2007. - Vol. 91, No. 4. - P. 043504-043504-3. ↑
- J1872.** Su W. M. Effect of acceptor on efficiencies of exciplex-type organic light emitting diodes. / Su W. M., Li W. L., Xin Q., Su Z. S., Chu B., Bi D. F., He H., Niu J. H. // Applied Physics Letters. - 2007. - Vol. 91, No. 4. - P. 043508-043508-3. ↑
- J1873.** Cunge G. Broadband and time-resolved absorption spectroscopy with light emitting diodes: Application to etching plasma monitoring. / Cunge G., Vempaire D., Touzeau M., Sadeghi N. // Applied Physics Letters. - 2007. - Vol. 91, No. 23. - P. 231503-231503-3. ↑
- J1874.** Kim Dong Chan. Multidimensional ZnO light-emitting diode structures grown by metal organic chemical vapor deposition on p-Si. / Kim Dong Chan, Han Won Suk, Cho Hyung Koun, Kong Bo Hyun, Kim Hyoung Sub. // Applied Physics Letters. - 2007. - Vol. 91, No. 23. - P. 231901-231901-3. ↑
- J1875.** Schubert Martin F. Effect of dislocation density on efficiency droop in Ga In N /Ga N light-emitting diodes. / Schubert Martin F., Chhajed Sameer, Kim Jong Kyu, Schubert E. Fred, Koleske Daniel D., Crawford Mary H., Lee Stephen R., Fischer Arthur J., Thaler Gerald, Banas Michael A. // Applied Physics Letters. - 2007. - Vol. 91, No. 23. - P. 231114-231114-3. ↑
- J1876.** Tripathy S. In Ga N /Ga N light emitting diodes on nanoscale silicon on insulator. / Tripathy S., Lin V. K. X., Teo S. L., Dadgar A., Diez A., Blasing J., Krost A. // Applied Physics Letters. - 2007. - Vol. 91, No. 23. - P. 231109-231109-3. ↑
- J1877.** Chuang Ricky W. ZnO-on-GaN heterojunction light-emitting diode grown by vapor cooling condensation technique. / Chuang Ricky W., Wu Rong-Xun, Lai Li-Wen, Lee Ching-Ting. // Applied Physics Letters. - 2007. - Vol. 91, No. 23. - P. 231113-231113-3. ↑
- J1878.** Whang Dong Ryeol. A highly efficient wide-band-gap host material for blue electrophosphorescent light-emitting devices. / Whang Dong Ryeol, You Youngmin, Kim Se Hun, Jeong Won-Ik, Park Young-Seo, Kim Jang-Joo, Park Soo Young. // Applied Physics Letters. - 2007. - Vol. 91, No. 23. - P. 233501-233501-3. ↑
- J1879.** Matsushima Toshinori. Formation of Ohmic hole injection by inserting an ultrathin layer of molybdenum trioxide between indium tin oxide and organic hole-transporting layers. / Matsushima Toshinori, Kinoshita Yoshiki, Murata Hideyuki. // Applied Physics Letters. - 2007. - Vol. 91, No. 25. - P. 253504-253504-3. ↑
- J1880.** Liu B. Nonpolar m-plane thin film GaN and In Ga N /Ga N light-emitting diodes on Li Al O₂ (100) substrates. / Liu B., Zhang R., Xie Z. L., Liu C. X., Kong J. Y., Yao J., Liu Q. J., Zhang Z., Fu D. Y., Xiu X. Q., Lu H., Chen P., Han P., Gu S. L., Shi Y., Zheng Y. D., Zhou J., Zhou S. M. // Applied Physics Letters. - 2007. - Vol. 91, No. 25. - P. 253506-253506-3. ↑
- J1881.** Kim Myeong-Suk. A stable blue host material for organic light-emitting diodes. / Kim Myeong-Suk, Choi Byoung-Ki, Lee Tae-Woo, Shin Dongwoo, Kang Sung Kee, Kim Jong Min, Tamura Shinichiro, Noh Taeyong. // Applied Physics Letters. - 2007. - Vol. 91, No. 25. - P. 251111-251111-3. ↑
- J1882.** Ho Meng-Huan. Highly efficient p-i-n white organic light emitting devices with tandem structure. / Ho

Meng-Huan, Chen Teng-Ming, Yeh Pu-Cheng, Hwang Shiao-Wen, Chen Chin H. // Applied Physics Letters. - 2007. - Vol. 91, No. 23. - P. 233507-233507-3. ↑

J1883. Gardner N. F. Blue-emitting InGa_N-Ga_N double-heterostructure light-emitting diodes reaching maximum quantum efficiency above 200 A/cm². / Gardner N. F., Muller G. O., Shen Y. C., Chen G., Watanabe S., Gotz W., Krames M. R. // Applied Physics Letters. - 2007. - Vol. 91, No. 24. - P. 243506-243506-3. ↑

J1884. Feng Weifeng. A new switched-capacitor frequency modulated driver for light emitting diodes. / Feng Weifeng, Shi Frank G. // Review of Scientific Instruments. - 2007. - Vol. 78, No. 11. - P. 114701-114701-4. ↑

J1885. Tong Qing-Xiao. Efficient green organic light-Emitting devices with a nondoped dual-functional electroluminescent material. / Tong Qing-Xiao, Lai Shiu-Lun, Chan Mei-Yee, Lai Ka-Ho, Tang Jian-Xin, Kwong Hoi-Lun, Lee Chun-Sing, Lee Shuit-Tong. // Applied Physics Letters. - 2007. - Vol. 91, No. 15. - P. 153504-153504-3. ↑

J1886. Wang X. H. White light-emitting diodes based on a single InGa_N emission layer. / Wang X. H., Jia H. Q., Guo L. W., Xing Z. G., Wang Y., Pei X. J., Zhou J. M., Chen H. // Applied Physics Letters. - 2007. - Vol. 91, No. 16. - P. 161912-161912-3. ↑

J1887. Garcia Andres. Structure-function relationships of conjugated polyelectrolyte electron injection layers in polymer light emitting diodes. / Garcia Andres, Yang Renqiang, Jin Youngeup, Walker Bright, Nguyen Thuc-Quyen. // Applied Physics Letters. - 2007. - Vol. 91, No. 15. - P. 153502-153502-3. ↑

J1888. Cho Kwanghee. The origin of electron injection improvement in organic light-emitting devices with an organic oxide/rubrene electron injection layer. / Cho Kwanghee, Cho Sang Wan, Whang Chung-Nam, Jeong Kwangho, Kang Seong Jun, Yi Yeonjin. // Applied Physics Letters. - 2007. - Vol. 91, No. 15. - P. 152107-152107-3. ↑

J1889. Ikkawi Rabee. Nanolasers to enable data storage beyond 10 Tbit/in.². / Ikkawi Rabee, Amos Nissim, Krichevsky Alexander, Chomko Roman, Litvinov Dmitri, Khizroev Sakhrat. // Applied Physics Letters. - 2007. - Vol. 91, No. 15. - P. 153115-153115-2. ↑

J1890. Yeh Dong-Ming. Surface plasmon coupling effect in an InGa_N/Ga_N single-quantum-well light-emitting diode. / Yeh Dong-Ming, Huang Chi-Feng, Chen Cheng-Yen, Lu Yen-Cheng, Yang C. C. // Applied Physics Letters. - 2007. - Vol. 91, No. 17. - P. 171103-171103-3. ↑

J1891. Monemar B. Defect related issues in the "current roll-off" in InGa_N based light emitting diodes. / Monemar B., Sernelius B. E. // Applied Physics Letters. - 2007. - Vol. 91, No. 18. - P. 181103-181103-3. ↑

J1892. Chiang Cheng-Chung. An ultrathin (100 nm thick) flexible light plate fabricated using self-alignment and lift-off techniques. / Chiang Cheng-Chung, Wu Dong-Sing, Horng Ray-Hua. // Applied Physics Letters. - 2007. - Vol. 91, No. 18. - P. 181108-181108-3. ↑

J1893. Li Ling. Diffusion-controlled charge injection model for organic light-emitting diodes. / Li Ling, Meller Gregor, Kosina Hans. // Applied Physics Letters. - 2007. - Vol. 91, No. 17. - P. 172111-172111-3. ↑

J1894. Nakagawa Satoshi. Temperature dependence of polarized electroluminescence from nonpolar m-plane InGa_N-based light emitting diodes. / Nakagawa Satoshi, Tsujimura Hiroki, Okamoto Kuniyoshi, Kubota Masashi, Ohta Hiroaki. // Applied Physics Letters. - 2007. - Vol. 91, No. 17. - P. 171110-171110-3. ↑

J1895. Kim Tae Sun. Increase of light extraction from Ga_N based light emitting diodes incorporating patterned structure by colloidal lithography. / Kim Tae Sun, Kim Sang-Mook, Jang Yun Hee, Jung Gun Young. // Applied Physics Letters. - 2007. - Vol. 91, No. 17. - P. 171114-171114-3. ↑

J1896. Mauthner Gernot. Cryptand based solid-state electrolytes in polymer light-emitting devices. / Mauthner Gernot, Scherf Ullrich, List Emil J. W. // Applied Physics Letters. - 2007. - Vol. 91, No. 13. - P. 133501-133501-3. ↑

J1897. Shen Y. C. Auger recombination in InGa_N measured by photoluminescence. / Shen Y. C., Mueller G. O., Watanabe S., Gardner N. F., Munkholm A., Krames M. R. // Applied Physics Letters. - 2007. - Vol. 91, No. 14. - P. 141101-141101-3. ↑

- J1898.** Park Il-Kyu. Green light-emitting diodes with self-assembled In-rich InGaN quantum dots. / Park Il-Kyu, Kwon Min-Ki, Kim Jeom-Oh, Seo Seong-Bum, Kim Ja-Yeon, Lim Jae-Hong, Park Seong-Ju, Kim Yoon-Seok. // Applied Physics Letters. - 2007. - Vol. 91, No. 13. - P. 133105-133105-3. ↑
- J1899.** Kim Sung Hyun. Improved color stability in white phosphorescent organic light-emitting diodes using charge confining structure without interlayer. / Kim Sung Hyun, Jang Jyongsik, Lee Jun Yeob. // Applied Physics Letters. - 2007. - Vol. 91, No. 12. - P. 123509-123509-3. ↑
- J1900.** Wang J. Low operating voltage bright organic light-emitting diode using iridium complex doped in 4,4'-bis[N-1-naphthyl-N-phenyl-amino]biphenyl. / Wang J., Jiang Y. D., Yu J. S., Lou S. L., Lin H. // Applied Physics Letters. - 2007. - Vol. 91, No. 13. - P. 131105-131105-3. ↑
- J1901.** Bai Y. Electrically pumped photonic crystal distributed feedback quantum cascade lasers. / Bai Y., Darvish S. R., Slivken S., Sung P., Nguyen J., Evans A., Zhang W., Razeghi M. // Applied Physics Letters. - 2007. - Vol. 91, No. 14. - P. 141123-141123-3. ↑
- J1902.** Tian Yun. Spectrally narrowed edge emission from organic light-emitting diodes. / Tian Yun, Gan Zhengqing, Zhou Zhaoqun, Lynch David W., Shinar Joseph, Kang Ji-hun, Park Q-Han. // Applied Physics Letters. - 2007. - Vol. 91, No. 14. - P. 143504-143504-3. ↑
- J1903.** Bange Sebastian. Sensing electron transport in a blue-emitting copolymer by transient electroluminescence. / Bange Sebastian, Kuksov Andriy, Neher Dieter. // Applied Physics Letters. - 2007. - Vol. 91, No. 14. - P. 143516-143516-3. ↑
- J1904.** Williams Quinton L. Boron-doped carbon nanotube coating for transparent, conducting, flexible photonic devices. / Williams Quinton L., Liu Xi, Walters Wilbur, Zhou Jian-Ge, Edwards Tylvia Y., Smith Franchesca L., Williams Gregory E., Mosley Brenitra L. // Applied Physics Letters. - 2007. - Vol. 91, No. 14. - P. 143116-143116-3. ↑
- J1905.** Shimizu Yusuke. Optical properties of air-stable semiconducting copolymer based on polythiophene. / Shimizu Yusuke, Kobayashi Takashi, Nagase Takashi, Naito Hiroyoshi. // Applied Physics Letters. - 2007. - Vol. 91, No. 14. - P. 141909-141909-3. ↑
- J1906.** Liu Shun-Wei. Charge carrier mobility of mixed-layer organic light-emitting diodes. / Liu Shun-Wei, Lee Jiun-Haw, Lee Chih-Chien, Chen Chin-Ti, Wang Juen-Kai. // Applied Physics Letters. - 2007. - Vol. 91, No. 14. - P. 142106-142106-3. ↑
- J1907.** Kim Ja-Yeon. Enhanced light extraction from GaN-based green light-emitting diode with photonic crystal. / Kim Ja-Yeon, Kwon Min-Ki, Lee Ki-Sung, Park Seong-Ju, Kim Sang Hoon, Lee Ki-Dong. // Applied Physics Letters. - 2007. - Vol. 91, No. 18. - P. 181109-181109-3. ↑
- J1908.** Gonzalez Martin. Novel optical method for background reduction in resonant photoacoustics. / Gonzalez Martin, Santiago Guillermo, Slezak Veronica, Peuriot Alejandro. // Review of Scientific Instruments. - 2007. - Vol. 78, No. 8. - P. 084903-084903-4. ↑
- J1909.** Pasternak Sebastien. Rotating sample holder at low temperature. / Pasternak Sebastien, Perrin Florian, Ciatto Gianluca, Palancher Herve, Steinmann Ricardo. // Review of Scientific Instruments. - 2007. - Vol. 78, No. 7. - P. 075110-075110-4. ↑
- J1910.** Tong Qing-Xiao. High-efficiency nondoped white organic light-emitting devices. / Tong Qing-Xiao, Lai Shiu-Lun, Chan Mei-Yee, Tang Jian-Xin, Kwong Hoi-Lun, Lee Chun-Sing, Lee Shuit-Tong. // Applied Physics Letters. - 2007. - Vol. 91, No. 2. - P. 023503-023503-3. ↑
- J1911.** Gorn P. The influence of visible light on transparent zinc tin oxide thin film transistors. / Gorn P., Lehnhardt M., Riedl T., Kowalsky W. // Applied Physics Letters. - 2007. - Vol. 91, No. 19. - P. 193504-193504-3. ↑
- J1912.** Penna S. Near-infrared photoluminescence of erbium tris(8-hydroxyquinoline) spin-coated thin films induced by low coherence light sources. / Penna S., Reale A., Pizzoferrato R., Tosi Beleffi G. M., Musella D., Gillin W. P. // Applied Physics Letters. - 2007. - Vol. 91, No. 2. - P. 021106-021106-3. ↑
- J1913.** Neuber Christian. Combinatorial preparation and characterization of thin-film multilayer electro-optical devices. / Neuber Christian, Bate Markus, Thelakkat Mukundan, Schmidt Hans-Werner, Hansel Helmut, Zettl

Heiko, Krausch Georg. // Review of Scientific Instruments. - 2007. - Vol. 78, No. 7. - P. 072216-072216-11. ↑

J1914. Humphreys Kenneth. Noncontact simultaneous dual wavelength photoplethysmography: A further step toward noncontact pulse oximetry. / Humphreys Kenneth, Ward Tomas, Markham Charles. // Review of Scientific Instruments. - 2007. - Vol. 78, No. 4. - P. 044304-044304-6. ↑

J1915. Deblock Y. High speed single charge coupled device Cranz-Schardin camera. / Deblock Y., Ducloux O., Derbesse L., Merlen A., Pernod P. // Review of Scientific Instruments. - 2007. - Vol. 78, No. 3. - P. 035111-035111-4. ↑

J1916. Stipcevic M. Quantum random number generator based on photonic emission in semiconductors. / Stipcevic M., Rogina B. Medved. // Review of Scientific Instruments. - 2007. - Vol. 78, No. 4. - P. 045104-045104-7. ↑

J1917. Choi Jin Hwan. Evaluation of gas permeation barrier properties using electrical measurements of calcium degradation. / Choi Jin Hwan, Kim Young Min, Park Young Wook, Huh Jin Woo, Ju Byeong Kwon, Kim In Sun, Hwang Hee Nam. // Review of Scientific Instruments. - 2007. - Vol. 78, No. 6. - P. 064701-064701-5. ↑

J1918. Kebabian Paul L. Optical extinction monitor using cw cavity enhanced detection. / Kebabian Paul L., Robinson Wade A., Freedman Andrew. // Review of Scientific Instruments. - 2007. - Vol. 78, No. 6. - P. 063102-063102-9. ↑

J1919. Onuma T. Quantum-confined Stark effects in the m-plane In 0.15 Ga 0.85 N /Ga N multiple quantum well blue light-emitting diode fabricated on low defect density freestanding GaN substrate. / Onuma T., Amaike H., Kubota M., Okamoto K., Ohta H., Ichihara J., Takasu H., Chichibu S. F. // Applied Physics Letters. - 2007. - Vol. 91, No. 18. - P. 181903-181903-3. ↑

J1920. Wang Lei. Highly efficient white organic light-emitting diodes with single small molecular emitting material. / Wang Lei, Lin Mei-Fang, Wong Wai-Kwok, Cheah Kok-Wai, Tam Hoi-Lam, Gao Zhi-Qiang, Chen Chin H. // Applied Physics Letters. - 2007. - Vol. 91, No. 18. - P. 183504-183504-3. ↑

J1921. Manninen Pasi. On spectral and thermal behaviors of AlGaInP light-emitting diodes under pulse-width modulation. / Manninen Pasi, Orrevelainen Pasi. // Applied Physics Letters. - 2007. - Vol. 91, No. 18. - P. 181121-181121-3. ↑

J1922. Li Y.-L. Efficiency droop behaviors of In Ga N /Ga N multiple-quantum-well light-emitting diodes with varying quantum well thickness. / Li Y.-L., Huang Y.-R., Lai Y.-H. // Applied Physics Letters. - 2007. - Vol. 91, No. 18. - P. 181113-181113-3. ↑

J1923. Kim Kwang-Choong. Study of nonpolar m-plane In Ga N /Ga N multiquantum well light emitting diodes grown by homoepitaxial metal-organic chemical vapor deposition. / Kim Kwang-Choong, Schmidt Mathew C., Sato Hitoshi, Wu Feng, Fellows Natalie, Jia Zhongyuan, Saito Makoto, Nakamura Shuji, DenBaars Steven P., Speck James S., Fujito Kenji. // Applied Physics Letters. - 2007. - Vol. 91, No. 18. - P. 181120-181120-3. ↑

J1924. Kim Min-Ho. Origin of efficiency droop in GaN-based light-emitting diodes. / Kim Min-Ho, Schubert Martin F., Dai Qi, Kim Jong Kyu, Schubert E. Fred, Piprek Joachim, Park Yongjo. // Applied Physics Letters. - 2007. - Vol. 91, No. 18. - P. 183507-183507-3. ↑

J1925. Verbakel Frank. Reproducible resistive switching in nonvolatile organic memories. / Verbakel Frank, Meskers Stefan C. J., Janssen Rene A. J., Gomes Henrique L., Colle Michael, Buchel Michael, de Leeuw Dago M. // Applied Physics Letters. - 2007. - Vol. 91, No. 19. - P. 192103-192103-3. ↑

J1926. Seo Soon-Min. Damage-free electrodes fabrication for top emitting organic light emitting diodes by transfer fabrication. / Seo Soon-Min, Jang Chang-Hyun. // Applied Physics Letters. - 2007. - Vol. 91, No. 19. - P. 192505-192505-3. ↑

J1927. Hirai A. Formation and reduction of pyramidal hillocks on m-plane {11 00} GaN. / Hirai A., Jia Z., Schmidt M. C., Farrell R. M., DenBaars S. P., Nakamura S., Speck J. S., Fujito K. // Applied Physics Letters. - 2007. - Vol. 91, No. 19. - P. 191906-191906-3. ↑

J1928. Sakamoto Kenji. Very thin photoalignment films for liquid crystalline conjugated polymers: Application to polarized light-emitting diodes. / Sakamoto Kenji, Miki Kazushi, Misaki Masahiro, Sakaguchi Koichi, Chikamatsu

Masayuki, Azumi Reiko. // Applied Physics Letters. - 2007. - Vol. 91, No. 18. - P. 183509-183509-3. ↑

J1929. Zhang Dongyu. Low efficiency roll off at high current densities in Ir-complex based electrophosphorescence diode with exciton diffusing and fluorescence compensating layers. / Zhang Dongyu, Li Wenlian, Chu Bei, Zhu Jianzhuo, Li Tianle, Han Lianglaing, Bi Defeng, Li Xiao, Yang Dongfang, Yan Fei, Liu Huihui, Wang Dan, Tsuboi Taiju. // Applied Physics Letters. - 2007. - Vol. 91, No. 18. - P. 183516-183516-3. ↑

J1930. Schubert Martin F. Polarization of light emission by 460 nm Ga In N /Ga N light-emitting diodes grown on (0001) oriented sapphire substrates. / Schubert Martin F., Chhajed Sameer, Kim Jong Kyu, Fred Schubert E., Cho Jaehee. // Applied Physics Letters. - 2007. - Vol. 91, No. 5. - P. 051117-051117-3. ↑

J1931. Baldwin R. J. A comprehensive study of the effect of reactive end groups on the charge carrier transport within polymerized and nonpolymerized liquid crystals. / Baldwin R. J., Kreouzis T., Shkunov M., Heeney M., Zhang W., McCulloch I. // Journal of Applied Physics. - 2007. - Vol. 101, No. 2. - P. 023713-023713-10. ↑

J1932. Nee Tzer-En. Anomalous excitation dependence of electroluminescence in In Ga N /Ga N light-emitting diodes. / Nee Tzer-En, Shen Hui-Tang, Wang Jen-Cheng, Wu Ya-Fen. // Journal of Applied Physics. - 2007. - Vol. 101, No. 2. - P. 023703-023703-6. ↑

J1933. Ankudinov A. V. Kelvin probe force and surface photovoltage microscopy observation of minority holes leaked from active region of working In Ga As /Al Ga As /Ga As laser diode. / Ankudinov A. V., Evtikhiev V. P., Ladutenko K. S., Rastegaeva M. G., Titkov A. N., Laiho R. // Journal of Applied Physics. - 2007. - Vol. 101, No. 2. - P. 024504-024504-8. ↑

J1934. Kondakov D. Y. Operational degradation of organic light-emitting diodes: Mechanism and identification of chemical products. / Kondakov D. Y., Lenhart W. C., Nichols W. F. // Journal of Applied Physics. - 2007. - Vol. 101, No. 2. - P. 024512-024512-7. ↑

J1935. Raino G. Photoreflectance symmetry and amplitude study of quantum dots in microcavity light emitting diode structure: The cavity-ground state exciton resonance. / Raino G., De Giorgi M., Todaro M. T., De Vittorio M., Tasco V., Passaseo A., Cingolani R. // Journal of Applied Physics. - 2007. - Vol. 101, No. 2. - P. 024511-024511-4. ↑

J1936. Tsai H. L. Structural analysis of strained p -type Al Ga N /Ga N superlattice. / Tsai H. L., Wang T. Y., Yang J. R., Chuo C. C., Hsu J. T., Ceh M., Shiojiri M. // Journal of Applied Physics. - 2007. - Vol. 101, No. 2. - P. 023521-023521-6. ↑

J1937. Kneissl Michael. Ultraviolet semiconductor laser diodes on bulk AlN. / Kneissl Michael, Yang Zhihong, Teepe Mark, Knollenberg Cliff, Schmidt Oliver, Kiesel Peter, Johnson Noble M., Schujman Sandra, Schowalter Leo J. // Journal of Applied Physics. - 2007. - Vol. 101, No. 12. - P. 123103-123103-5. ↑

J1938. Garcia-Belmonte Germa. Millisecond radiative recombination in poly(phenylene vinylene)-based light-emitting diodes from transient electroluminescence. / Garcia-Belmonte Germa, Montero Jose M., Barea Eva M., Bisquert Juan, Bolink Henk J. // Journal of Applied Physics. - 2007. - Vol. 101, No. 11. - P. 114506-114506-7. ↑

J1939. Suemasu T. Photoluminescence decay time and electroluminescence of p-Si /beta -FeSi 2 particles /n-Si and p-Si /beta -FeSi 2 film /n-Si double-heterostructures light-emitting diodes grown by molecular-beam epitaxy. / Suemasu T., Ugajin Y., Murase S., Sunohara T., Suzuno M. // Journal of Applied Physics. - 2007. - Vol. 101, No. 12. - P. 124506-124506-6. ↑

J1940. Fehse Karsten. Combination of a polyaniline anode and doped charge transport layers for high-efficiency organic light emitting diodes. / Fehse Karsten, Schwartz Gregor, Walzer Karsten, Leo Karl. // Journal of Applied Physics. - 2007. - Vol. 101, No. 12. - P. 124509-124509-4. ↑

J1941. Cao Guohua. Improved performance in organic light emitting diodes with a mixed electron donor-acceptor film involved in hole injection. / Cao Guohua, Qin Dashan, Cao Junsong, Guan Min, Zeng Yiping, Li Jinmin. // Journal of Applied Physics. - 2007. - Vol. 101, No. 12. - P. 124507-124507-4. ↑

J1942. Xin Q. Emission mechanism in organic light-emitting devices comprising a europium complex as emitter and an electron transporting material as host. / Xin Q., Li W. L., Su W. M., Li T. L., Su Z. S., Chu B., Li B. // Journal of Applied Physics. - 2007. - Vol. 101, No. 4. - P. 044512-044512-6. ↑

- J1943.** Jung M. C. Photoelectron spectrum from a thin organic layer exposed to intense x rays. / Jung M. C., Shin H. J., Chung J. // Journal of Applied Physics. - 2007. - Vol. 101, No. 3. - P. 034907-034907-4. ↑
- J1944.** Zhong G. Y. The carrier-trapping effect of dye doped in Alq. / Zhong G. Y., Kim D. E., Kwon O. K., Jang Y. K., Kwon Y. S. // Journal of Applied Physics. - 2007. - Vol. 101, No. 5. - P. 054507-054507-4. ↑
- J1945.** Catchpole K. R. A conceptual model of light coupling by pillar diffraction gratings. / Catchpole K. R., Green M. A. // Journal of Applied Physics. - 2007. - Vol. 101, No. 6. - P. 063105-063105-8. ↑
- J1946.** Luo Yichun. Improving the stability of organic light-emitting devices by using a hole-injection-tunable-anode-buffer-layer. / Luo Yichun, Aziz Hany, Xu Gu, Popovic Zoran D. // Journal of Applied Physics. - 2007. - Vol. 101, No. 5. - P. 054512-054512-4. ↑
- J1947.** Grozea D. Enhanced thermal stability in organic light-emitting diodes through nanocomposite buffer layers at the anode/organic interface. / Grozea D., Turak A., Yuan Y., Han S., Lu Z. H., Kim W. Y. // Journal of Applied Physics. - 2007. - Vol. 101, No. 3. - P. 033522-033522-6. ↑
- J1948.** You Han. Improved performances of organic light-emitting diodes with metal oxide as anode buffer. / You Han, Dai Yanfeng, Zhang Zhiqiang, Ma Dongge. // Journal of Applied Physics. - 2007. - Vol. 101, No. 2. - P. 026105-026105-3. ↑
- J1949.** Paasch G. Space charge layers in organic field-effect transistors with Gaussian or exponential semiconductor density of states. / Paasch G., Scheinert S. // Journal of Applied Physics. - 2007. - Vol. 101, No. 2. - P. 024514-024514-13. ↑
- J1950.** Akita Katsushi. Improvements of external quantum efficiency of InGaN-based blue light-emitting diodes at high current density using GaN substrates. / Akita Katsushi, Kyono Takashi, Yoshizumi Yusuke, Kitabayashi Hiroyuki, Katayama Koji. // Journal of Applied Physics. - 2007. - Vol. 101, No. 3. - P. 033104-033104-5. ↑
- J1951.** Chen M. J. Enhancement in the efficiency of light emission from silicon by a thin Al₂O₃ surface-passivating layer grown by atomic layer deposition at low temperature. / Chen M. J., Shih Y. T., Wu M. K., Tsai F. Y. // Journal of Applied Physics. - 2007. - Vol. 101, No. 3. - P. 033130-033130-4. ↑
- J1952.** Hums C. Fabry-Perot effects in InGaN/GaN heterostructures on Si-substrate. / Hums C., Finger T., Hempel T., Christen J., Dadgar A., Hoffmann A., Krost A. // Journal of Applied Physics. - 2007. - Vol. 101, No. 3. - P. 033113-033113-4. ↑
- J1953.** Lee Chih-Chien. Electrical and optical simulation of organic light-emitting devices with fluorescent dopant in the emitting layer. / Lee Chih-Chien, Chang Mei-Ying, Huang Ping-Tsung, Chen Yen Chun, Chang Yih, Liu Shun-Wei. // Journal of Applied Physics. - 2007. - Vol. 101, No. 11. - P. 114501-114501-11. ↑
- J1954.** Takahashi Kohsei. Luminescence properties of blue La_{1-x}Ce_xAl(Si_{6-z}Al_z)(N_{10-z}O_z)(z = 1) oxynitride phosphors and their application in white light-emitting diode. / Takahashi Kohsei, Hirosaki Naoto, Xie Rong-Jun, Harada Masamichi, Yoshimura Ken-ichi, Tomomura Yoshitaka. // Applied Physics Letters. - 2007. - Vol. 91, No. 9. - P. 091923-091923-3. ↑
- J1955.** Xu Zheng. Vertical organic light emitting transistor. / Xu Zheng, Li Sheng-Han, Ma Liping, Li Gang, Yang Yang. // Applied Physics Letters. - 2007. - Vol. 91, No. 9. - P. 092911-092911-3. ↑
- J1956.** Arif Ronald A. Polarization engineering via staggered InGaN quantum wells for radiative efficiency enhancement of light emitting diodes. / Arif Ronald A., Ee Yik-Khoon, Tansu Nelson. // Applied Physics Letters. - 2007. - Vol. 91, No. 9. - P. 091110-091110-3. ↑
- J1957.** Byeon Kyeong-Jae. Fabrication of two-dimensional photonic crystal patterns on GaN-based light-emitting diodes using thermally curable monomer-based nanoimprint lithography. / Byeon Kyeong-Jae, Hwang Seon-Yong, Lee Heon. // Applied Physics Letters. - 2007. - Vol. 91, No. 9. - P. 091106-091106-3. ↑
- J1958.** Villatoro Joel. Temperature-insensitive photonic crystal fiber interferometer for absolute strain sensing. / Villatoro Joel, Finazzi Vittoria, Minkovich Vladimir P., Pruneri Valerio, Badenes Goncal. // Applied Physics Letters. - 2007. - Vol. 91, No. 9. - P. 091109-091109-3. ↑
- J1959.** Lin Gong-Ru. Improving carrier transport and light emission in a silicon-nanocrystal based MOS light-

emitting diode on silicon nanopillar array. / Lin Gong-Ru, Lin Chun-Jung, Kuo Hao-Chung. // Applied Physics Letters. - 2007. - Vol. 91, No. 9. - P. 093122-093122-3. ↑

J1960. Liu Deang. Organic light-emitting diodes with structured cathode. / Liu Deang, Fina Michael, Chen Zhaoyang, Chen Xiaobo, Liu Gao, Johnson Steven, Mao Samuel S. // Applied Physics Letters. - 2007. - Vol. 91, No. 9. - P. 093514-093514-3. ↑

J1961. Ryu Seung Yoon. Transparent organic light-emitting diodes using resonant tunneling double barrier structures. / Ryu Seung Yoon, Jo Sung Jin, Kim Chang Su, Choi Sang Hun, Noh Joo Hyon, Baik Hong Koo, Jeong Hee Seong, Han Dong Won, Song Seung Yong, Lee Kyu Sung. // Applied Physics Letters. - 2007. - Vol. 91, No. 9. - P. 093515-093515-3. ↑

J1962. Kim Heekyung. Small molecule based and solution processed highly efficient red electrophosphorescent organic light emitting devices. / Kim Heekyung, Byun Younghun, Das Rupasree Ragini, Choi Byoung-Ki, Ahn Pil-Soo. // Applied Physics Letters. - 2007. - Vol. 91, No. 9. - P. 093512-093512-3. ↑

J1963. Peng Kang-Yung. High brightness stable white and yellow light-emitting diodes from ambipolar polyspirofluorenes with high charge carrier mobility. / Peng Kang-Yung, Huang Chih-Wei, Liu Ching-Yang, Chen Show-An. // Applied Physics Letters. - 2007. - Vol. 91, No. 9. - P. 093502-093502-3. ↑

J1964. Yang Chieh-Kai. Current injection and transport in polyfluorene. / Yang Chieh-Kai, Yang Chia-Ming, Liao Hua-Hsien, Horng Sheng-Fu, Meng Hsin-Fei. // Applied Physics Letters. - 2007. - Vol. 91, No. 9. - P. 093504-093504-3. ↑

J1965. Chou Mitch M. C. Crystal growth and properties of LiAlO₂ and nonpolar GaN on LiAlO₂ substrate. / Chou Mitch M. C., Hang D. R., Kalisch H., Jansen R. H., Dikme Y., Heuken Michael, Yablonskii G. P. // Journal of Applied Physics. - 2007. - Vol. 101, No. 10. - P. 103106-103106-5. ↑

J1966. Kobayashi Norifumi. Blue electroluminescent properties of poly(N-arylcarbazole-2,7-ylene) homopolymers. / Kobayashi Norifumi, Kijima Masashi. // Applied Physics Letters. - 2007. - Vol. 91, No. 8. - P. 081113-081113-3. ↑

J1967. Chen K. X. Recombination dynamics in ultraviolet light-emitting diodes with Si-doped Al_xGa_{1-x}N/Al_yGa_{1-y}N multiple quantum well active regions. / Chen K. X., Xi Y. A., Mont F. W., Kim J. K., Schubert E. F., Liu W., Li X., Smart J. A. // Journal of Applied Physics. - 2007. - Vol. 101, No. 11. - P. 113102-113102-5. ↑

J1968. Wellmann Peter J. Cathodoluminescence characterization of organic semiconductor materials for light emitting device applications. / Wellmann Peter J., Karl Ulrich, Kleber Sebastian, Schmitt Holger. // Journal of Applied Physics. - 2007. - Vol. 101, No. 11. - P. 113704-113704-6. ↑

J1969. Chen Xue-Wen. Comprehensive analysis and optimal design of top-emitting organic light-emitting devices. / Chen Xue-Wen, Choy Wallace C. H., He Sailing, Chui P. C. // Journal of Applied Physics. - 2007. - Vol. 101, No. 11. - P. 113107-113107-6. ↑

J1970. Chang Chun-Kuei. Sr₃B₂O₆:Ce³⁺,Eu²⁺: A potential single-phased white-emitting borate phosphor for ultraviolet light-emitting diodes. / Chang Chun-Kuei, Chen Teng-Ming. // Applied Physics Letters. - 2007. - Vol. 91, No. 8. - P. 081902-081902-3. ↑

J1971. Kim Sung Hyun. Relationship between host energy levels and device performances of phosphorescent organic light-emitting diodes with triplet mixed host emitting structure. / Kim Sung Hyun, Jang Jyongsik, Lee Jun Yeob. // Applied Physics Letters. - 2007. - Vol. 91, No. 8. - P. 083511-083511-3. ↑

J1972. Liang Xiaoluan. Luminescence properties of Tb³⁺-Sm³⁺ codoped glasses for white light emitting diodes. / Liang Xiaoluan, Yang Yunxia, Zhu Chaofeng, Yuan Shuanglong, Chen Guorong, Pring Allan, Xia Fang. // Applied Physics Letters. - 2007. - Vol. 91, No. 9. - P. 091104-091104-3. ↑

J1973. Joo Min Ho. Chemical structure of the bilayer Ag/Li₂O cathode interface in organic light emitting diodes. / Joo Min Ho, Baik Min Kyung, Choi Jong Kwon, Park Kyu Ho, Lee Jay Man, Sung Chang Je, Kim Myeong Seop, Yang Joong-Hwan, Kim Sung Tae. // and Films Journal of Vacuum Science & Technology A: Vacuum, Surfaces. - 2007. - Vol. 25, No. 4. - P. 996-998. ↑

J1974. Guo Jinghua. Soft-x-ray spectroscopy experiment of liquids. / Guo Jinghua, Tong Tyler, Svec Lukas,

Go John, Dong Chungli, Chiou Jau-Wern. // and Films Journal of Vacuum Science & Technology A: Vacuum, Surfaces. - 2007. - Vol. 25, No. 4. - P. 1231-1233. ↑

J1975. Choi Gwon-Woo. Electrical properties of organic light-emitting diodes by indium tin oxide chemical-mechanical polishing process. / Choi Gwon-Woo, Seo Yong-Jin, Lee Kang-Yeon, Lee Woo-Sun. // and Films Journal of Vacuum Science & Technology A: Vacuum, Surfaces. - 2007. - Vol. 25, No. 4. - P. 999-1002. ↑

J1976. Chan Kah-Yoong. Influence of low temperature thermal annealing on the performance of microcrystalline silicon thin-film transistors. / Chan Kah-Yoong, Bunte Eerke, Stiebig Helmut, Knipp Dietmar. // Journal of Applied Physics. - 2007. - Vol. 101, No. 7. - P. 074503-074503-6. ↑

J1977. Yamane Y. Largely variable electroluminescence efficiency with current and temperature in a blue (In, Ga)N multiple-quantum-well diode. / Yamane Y., Fujiwara K., Sheu J. K. // Applied Physics Letters. - 2007. - Vol. 91, No. 7. - P. 073501-073501-3. ↑

J1978. Zhang Z. Y. Effect of facet angle on effective facet reflectivity and operating characteristics of quantum dot edge emitting lasers and superluminescent light-emitting diodes. / Zhang Z. Y., Luxmoore I. J., Jin C. Y., Liu H. Y., Jiang Q., Groom K. M., Childs D. T., Hopkinson M., Cullis A. G., Hogg R. A. // Applied Physics Letters. - 2007. - Vol. 91, No. 8. - P. 081112-081112-3. ↑

J1979. Lin Gong-Ru. C O 2 laser rapid-thermal-annealing Si O x based metal-oxide-semiconductor light emitting diode. / Lin Gong-Ru, Lin Chun-Jung. // Applied Physics Letters. - 2007. - Vol. 91, No. 7. - P. 072103-072103-3. ↑

J1980. Rogers D. J. Use of ZnO thin films as sacrificial templates for metal organic vapor phase epitaxy and chemical lift-off of GaN. / Rogers D. J., Hosseini Teherani F., Ougazzaden A., Gautier S., Divay L., Lusson A., Durand O., Wyczisk F., Garry G., Monteiro T., Correia M. R., Peres M., Neves A., McGrouther D., Chapman J. N., Razeghi M. // Applied Physics Letters. - 2007. - Vol. 91, No. 7. - P. 071120-071120-3. ↑

J1981. Hirayama Hideki. 231-261 nm AlGaIn deep-ultraviolet light-emitting diodes fabricated on AlN multilayer buffers grown by ammonia pulse-flow method on sapphire. / Hirayama Hideki, Yatabe Tohru, Noguchi Norimichi, Ohashi Tomoaki, Kamata Norihiko. // Applied Physics Letters. - 2007. - Vol. 91, No. 7. - P. 071901-071901-3. ↑

J1982. Feng L. F. Deep saturation of junction voltage at large forward current of light-emitting diodes. / Feng L. F., Li D., Zhu C. Y., Wang C. D., Cong H. X., Zhang G. Y., Du W. M. // Journal of Applied Physics. - 2007. - Vol. 102, No. 9. - P. 094511-094511-4. ↑

J1983. Manago Takashi. Growth condition dependence of spin-polarized electroluminescence in Fe /Mg O /light-emitting diodes. / Manago Takashi, Sinsarp Asawin, Akinaga Hiro. // Journal of Applied Physics. - 2007. - Vol. 102, No. 8. - P. 083914-083914-4. ↑

J1984. Oh Seung Seok. Enhanced light emission from phosphorescent single-layered organic light-emitting devices doped with ionic salt by simultaneous thermal and electrical annealing. / Oh Seung Seok, Park Jin Ho, Kim Sun Woong, Park Byoungchoo. // Journal of Applied Physics. - 2007. - Vol. 102, No. 7. - P. 074503-074503-5. ↑


J1985. Pan Chang-Chi. Light output improvement of InGaIn ultraviolet light-emitting diodes by using wet-etched stripe-patterned sapphire substrates. / Pan Chang-Chi, Hsieh Chi-Hsun, Lin Chih-Wei, Chyi Jen-Inn. // Journal of Applied Physics. - 2007. - Vol. 102, No. 8. - P. 084503-084503-5. ↑


J1986. So Franky. Recent progress in solution processable organic light emitting devices. / So Franky, Krummacher Benjamin, Mathai Mathew K., Poplavskyy Dmitry, Choulis Stelios A., Choong Vi-En. // Journal of Applied Physics. - 2007. - Vol. 102, No. 9. - P. 091101-091101-21. ↑


J1987. Sharma Asha. Polysilane based organic light emitting diodes: Simultaneous ultraviolet and visible emission. / Sharma Asha, Katiyar Monica, Deepak, Seki Shu. // Journal of Applied Physics. - 2007. - Vol. 102, No. 8. - P. 084506-084506-7. ↑


J1988. Fardel Romain. Fabrication of organic light-emitting diode pixels by laser-assisted forward transfer. / Fardel Romain, Nagel Matthias, Nuesch Frank, Lippert Thomas, Wokaun Alexander. // Applied Physics Letters. - 2007. - Vol. 91, No. 6. - P. 061103-061103-3. ↑


- J1989.** Liu Ru-Shi. Enhanced luminescence of $\text{Sr Si}_2\text{O}_7:\text{Eu}^{2+}$ phosphors by codoping with Ce^{3+} , Mn^{2+} , and Dy^{3+} ions. / Liu Ru-Shi, Liu Yu-Huan, Bagkar Nitin C., Hu Shu-Fen. // Applied Physics Letters. - 2007. - Vol. 91, No. 6. - P. 061119-061119-3. ↑
- J1990.** Park Dong-Kyu. Balanced charge injection in multilayer polymer light-emitting diode with water soluble nonconjugated polymer dispersed by ionic compounds. / Park Dong-Kyu, Chun A-Rum, Kim Soo-Hong, Kim Min-Sook, Kim Choong-Gi, Kwon Tae-Woo, Cho Seong-Jin, Woo Hyung-Suk, Lee Jae-Gyoung, Lee Suck-Hyun, Guo Zhi-Xin. // Applied Physics Letters. - 2007. - Vol. 91, No. 5. - P. 052904-052904-3. ↑
- J1991.** Huang Chi-Feng. Reduced injection current induced blueshift in an InGaN/GaN quantum-well light-emitting diode of prestrained growth. / Huang Chi-Feng, Chen Cheng-Yen, Lu Chih-Feng, Yang C. C. // Applied Physics Letters. - 2007. - Vol. 91, No. 5. - P. 051121-051121-3. ↑
- J1992.** Cho Sang Wan. Interfacial electronic structure of N,N' -bis(1-naphthyl)- N,N' -diphenyl-1,1'-biphenyl-4,4'-diamine/copper phthalocyanine: C_{60} composite/Au studied by ultraviolet photoemission spectroscopy. / Cho Sang Wan, Yoo Kyung-Hwa, Jeong Kwangho, Whang Chung-Nam, Yi Yeonjin, Noh Myungkeun. // Applied Physics Letters. - 2007. - Vol. 91, No. 5. - P. 052102-052102-3. ↑
- J1993.** Choi Yong-Seok. 2.5λ microcavity InGaN light-emitting diodes fabricated by a selective dry-etch thinning process. / Choi Yong-Seok, Iza Michael, Matioli Elison, Koblmuller Gregor, Speck James S., Weisbuch Claude, Hu Evelyn L. // Applied Physics Letters. - 2007. - Vol. 91, No. 6. - P. 061120-061120-3. ↑
- J1994.** Chen Yibo. High efficient and low color-temperature white light-emitting diodes with $\text{Tb}_3\text{Al}_5\text{O}_{12}:\text{Ce}^{3+}$ phosphor. / Chen Yibo, Gong Menglian, Wang Gang, Su Qiang. // Applied Physics Letters. - 2007. - Vol. 91, No. 7. - P. 071117-071117-3. ↑
- J1995.** Yang Bo-Ru. Investigation of the transient symmetric H state in a pi cell. / Yang Bo-Ru, Elston Steve J., Raynes Peter, Shieh Han-Ping D. // Applied Physics Letters. - 2007. - Vol. 91, No. 7. - P. 071119-071119-3. ↑
- J1996.** Tomita Yuto. Highly efficient p-i-n -type organic light emitting diodes on ZnO:Al substrates. / Tomita Yuto, May Christian, Toerker Michael, Amelung Joerg, Eritt Michael, Loeffler Frank, Lubner Claus, Leo Karl, Walzer Karsten, Fehse Karsten, Huang Qiang. // Applied Physics Letters. - 2007. - Vol. 91, No. 6. - P. 063510-063510-3. ↑
- J1997.** Yeh Dong-Ming. Surface plasmon leakage in its coupling with an InGaN/GaN quantum well through an Ohmic contact. / Yeh Dong-Ming, Huang Chi-Feng, Lu Yen-Cheng, Chen Cheng-Yen, Tang Tsung-Yi, Huang Jeng-Jie, Shen Kun-Ching, Yang Ying-Jay, Yang C. C. // Applied Physics Letters. - 2007. - Vol. 91, No. 6. - P. 063121-063121-3. ↑
- J1998.** Bernardo G. Improving polymer light-emitting diodes efficiency using interlayers based on cross-linkable polymers. / Bernardo G., Charas A., Alcacer L., Morgado J. // Applied Physics Letters. - 2007. - Vol. 91, No. 6. - P. 063509-063509-3. ↑
- J1999.** Desai P. The role of magnetic fields on the transport and efficiency of aluminum tris(8-hydroxyquinoline) based organic light emitting diodes. / Desai P., Shakya P., Kreouzis T., Gillin W. P. // Journal of Applied Physics. - 2007. - Vol. 102, No. 7. - P. 073710-073710-5. ↑
- J2000.** Hindmarch A. T. In-plane magnetic anisotropies of sputtered $\text{Co}_{0.7}\text{Fe}_{0.3}$ films on $\text{AlGaAs}(001)$ spin light emitting diode heterostructures. / Hindmarch A. T., Kinane C. J., Marrows C. H., Hickey B. J., Henini M., Taylor D., Arena D. A., Dvorak J. // Journal of Applied Physics. - 2007. - Vol. 101, No. 9. - P. 09D106-09D106-3. ↑
- J2001.** Yang Shengyi. Charge carriers at organic heterojunction interface: Exciplex emission or electroplex emission?. / Yang Shengyi, Zhang Xiulong, Hou Yanbing, Deng Zhenbo, Xu Xurong. // Journal of Applied Physics. - 2007. - Vol. 101, No. 9. - P. 096101-096101-3. ↑
- J2002.** Catchpole K. R. A conceptual model of the diffuse transmittance of lamellar diffraction gratings on solar cells. Journal of Applied Physics. - 2007. - Vol. 102, No. 1. - P. 013102-013102-8. ↑
- J2003.** Nikitenko V. R. Nonequilibrium transport of charge carriers and transient electroluminescence in organic light-emitting diodes. / Nikitenko V. R., von Seggern H. // Journal of Applied Physics. - 2007. - Vol. 102, No. 10. ↑


- P. 103708-103708-9. 


J2004. Swensen James S. Light emission from an ambipolar semiconducting polymer field effect transistor: Analysis of the device physics. / Swensen James S., Yuen Jonathan, Gargas Dan, Buratto Steven K., Heeger Alan J. // Journal of Applied Physics. - 2007. - Vol. 102, No. 1. - P. 013103-013103-5. 


J2005. Pillai S. Surface plasmon enhanced silicon solar cells. / Pillai S., Catchpole K. R., Trupke T., Green M. A. // Journal of Applied Physics. - 2007. - Vol. 101, No. 9. - P. 093105-093105-8. 


J2006. Bodrozic Vladimir. The influence of subgap features in the electromodulation and built-in voltage measurements of polyfluorene blue light-emitting diodes with anodic charge injection layers. / Bodrozic Vladimir, Roberts M., Phillips N., Burroughes J. H., Mian Shabbir, Cacialli Franco. // Journal of Applied Physics. - 2007. - Vol. 101, No. 8. - P. 084507-084507-9. 


J2007. Swietlik T. Mode dynamics of high power (InAl)Ga_N based laser diodes grown on bulk GaN substrate. / Swietlik T., Franssen G., Czernecki R., Leszczynski M., Skierbiszewski C., Grzegory I., Suski T., Perlin P., Lauterbach C., Schwarz U. T. // Journal of Applied Physics. - 2007. - Vol. 101, No. 8. - P. 083109-083109-6. 


J2008. Tseng Shin-Rong. High-efficiency blue multilayer polymer light-emitting diode based on poly(9,9-dioctylfluorene). / Tseng Shin-Rong, Li Shiuan-Yi, Meng Hsin-Fei, Yu Yi-Hsiang, Yang Chia-Ming, Liao Hua-Hsien, Horng Sheng-Fu, Hsu Chian-Shu. // Journal of Applied Physics. - 2007. - Vol. 101, No. 8. - P. 084510-084510-4. 


J2009. Huang Qinglan. Triarylamine siloxane anode functionalization/hole injection layers in high efficiency/high luminance small-molecule green- and blue-emitting organic light-emitting diodes. / Huang Qinglan, Li Jianfeng, Marks Tobin J., Evmenenko Guennadi A., Dutta Pulak. // Journal of Applied Physics. - 2007. - Vol. 101, No. 9. - P. 093101-093101-13. 


J2010. Gozu Shin-ichiro. Strong optical emissions from two-dimensional metal photonic crystals with semiconductor multiple quantum wells. / Gozu Shin-ichiro, Ueta Akio, Akahane Kouichi, Yamamoto Naokatsu, Tsuchiya Masahiro, Ohtani Naoki. // Journal of Applied Physics. - 2007. - Vol. 101, No. 8. - P. 086107-086107-3. 


J2011. Chen N. C. Forward current-voltage characteristics of an AlGaInP light-emitting diode. / Chen N. C., Yang Y. K., Lien W. C., Tseng C. Y. // Journal of Applied Physics. - 2007. - Vol. 102, No. 4. - P. 043706-043706-4. 


J2012. Nee Tzer-En. Effect of multiquantum barriers on performance of In Ga N /Ga N multiple-quantum-well light-emitting diodes. / Nee Tzer-En, Wang Jen-Cheng, Shen Hui-Tang, Wu Ya-Fen. // Journal of Applied Physics. - 2007. - Vol. 102, No. 3. - P. 033101-033101-7. 

J2013. Kim Keunjoo. Electroluminescence from lattice defects of photonic crystal slabs in blue-light-emitting diodes. / Kim Keunjoo, Choi Jaeho, Park Jong Bae, Jeon Sang Cheol, Kim Jin Soo, Lee Hee Mok. // Journal of Applied Physics. - 2007. - Vol. 102, No. 4. - P. 046105-046105-3. 

J2014. Ke Lin. Noise characterization of light-emitting devices based on conjugated copolymers of fluorene and thiophene moieties. / Ke Lin, Tang Weihua, Song Yang, Chen Zhi Kuan, Chua Soo Jin. // Journal of Applied Physics. - 2007. - Vol. 102, No. 6. - P. 063103-063103-4. 

J2015. Ju Jin-Woo. Metal-organic chemical vapor deposition growth of InGa_N/Ga_N high power green light emitting diode: Effects of InGa_N well protection and electron reservoir layer. / Ju Jin-Woo, Kang Eun-Sil, Kim Hwa-Soo, Jang Lee-Woon, Ahn Haeng-Keun, Jeon Ju-Won, Lee In-Hwan, Baek Jong Hyeob. // Journal of Applied Physics. - 2007. - Vol. 102, No. 5. - P. 053519-053519-4. 

J2016. Chen Zhenyu. Effects of doped dye on the charge carrier injection, transport, and electroluminescent performance in polymeric light-emitting diodes. / Chen Zhenyu, Ma Dongge. // Journal of Applied Physics. - 2007. - Vol. 102, No. 2. - P. 024510-024510-6. 

J2017. Jarikov Viktor V. Efficient and extremely long-lived organic light-emitting diodes based on dinaphthylperylene. / Jarikov Viktor V., Kondakov Denis Y., Brown Christopher T. // Journal of Applied Physics. - 2007. - Vol. 102, No. 10. - P. 104908-104908-6. 



- J2018.** Kirchartz Thomas. Electroluminescence analysis of high efficiency Cu (In ,Ga)Se 2 solar cells. / Kirchartz Thomas, Rau Uwe. // Journal of Applied Physics. - 2007. - Vol. 102, No. 10. - P. 104510-104510-8. ↑
- J2019.** Kondakov D. Y. Characterization of triplet-triplet annihilation in organic light-emitting diodes based on anthracene derivatives. Journal of Applied Physics. - 2007. - Vol. 102, No. 11. - P. 114504-114504-5. ↑
- J2020.** Castellani M. Competition between excitons and exciplexes: Experiments on multilayered organic light emitting diodes. / Castellani M., Berner D. // Journal of Applied Physics. - 2007. - Vol. 102, No. 2. - P. 024509-024509-8. ↑
- J2021.** Ju Jin-Woo. Erratum: "Metal-organic chemical vapor deposition growth of InGaN/GaN high power green light emitting diode: Effects of InGaN well protection and electron reservoir layer" [J. Appl. Phys. 102, 053519 (2007)]. / Ju Jin-Woo, Kang Eun-Sil, Kim Hwa-Soo, Jang Lee-Woon, Ahn Haeng-Keun, Jeon Ju-Won, Lee In-Hwan, Baek Jong Hyeob. // Journal of Applied Physics. - 2007. - Vol. 102, No. 11. - P. 119901-119901-1. ↑
- J2022.** Wu Kun-Yang. Tuning hole injection and charge recombination with self-assembled monolayer on silver anode in top-emitting organic light-emitting diodes. / Wu Kun-Yang, Tao Yu-Tai, Huang Hung-Wei. // Applied Physics Letters. - 2007. - Vol. 90, No. 24. - P. 241104-241104-3. ↑
- J2023.** Yang Che-Yu. Energy-recycling pixel for active-matrix organic light-emitting diode display. / Yang Che-Yu, Cho Ting-Yi, Chen Yen-Yu, Yang Chih-Jen, Meng Chao-Yu, Yang Chieh-Hung, Yang Po-Chuan, Chang Hsu-Yu, Hsueh Chun-Yuan, Wu Chung-Chih, Lee Si-Chen. // Applied Physics Letters. - 2007. - Vol. 90, No. 23. - P. 233512-233512-3. ↑
- J2024.** Li Juo-Hao. Improved hole-injection contact for top-emitting polymeric diodes. / Li Juo-Hao, Huang Jinsong, Yang Yang. // Applied Physics Letters. - 2007. - Vol. 90, No. 17. - P. 173505-173505-3. ↑
- J2025.** Agrawal Mukul. Enhanced outcoupling from organic light-emitting diodes using aperiodic dielectric mirrors. / Agrawal Mukul, Sun Yiru, Forrest Stephen R., Peumans Peter. // Applied Physics Letters. - 2007. - Vol. 90, No. 24. - P. 241112-241112-3. ↑
- J2026.** Campbell I. H. Energy barriers from ferromagnetic contacts to semiconducting polymers. / Campbell I. H., Crone B. K. // Applied Physics Letters. - 2007. - Vol. 90, No. 24. - P. 242107-242107-3. ↑
- J2027.** Lin C. L. Light enhancement by the formation of an Al oxide honeycomb nanostructure on the n -GaN surface of thin-GaN light-emitting diodes. / Lin C. L., Chen P. H., Chan Chia-Hua, Lee C. C., Chen Chii-Chang, Chang Jeng-Yang, Liu C. Y. // Applied Physics Letters. - 2007. - Vol. 90, No. 24. - P. 242106-242106-3. ↑
- J2028.** Stafford L. Improved long-term thermal stability of In Ga N /Ga N multiple quantum well light-emitting diodes using Ti B 2-and Ir-based p -Ohmic contacts. / Stafford L., Voss L. F., Pearton S. J., Wang H. T., Ren F. // Applied Physics Letters. - 2007. - Vol. 90, No. 24. - P. 242103-242103-3. ↑
- J2029.** Zhong Hong. High power and high efficiency blue light emitting diode on freestanding semipolar (101 1) bulk GaN substrate. / Zhong Hong, Tyagi Anurag, Fellows Natalie N., Wu Feng, Chung Roy B., Saito Makoto, Fujito Kenji, Speck James S., DenBaars Steven P., Nakamura Shuji. // Applied Physics Letters. - 2007. - Vol. 90, No. 23. - P. 233504-233504-3. ↑
- J2030.** Yang Chih-Jen. Organic light-emitting devices integrated with solar cells: High contrast and energy recycling. / Yang Chih-Jen, Cho Ting-Yi, Lin Chun-Liang, Wu Chung-Chih. // Applied Physics Letters. - 2007. - Vol. 90, No. 17. - P. 173507-173507-3. ↑
- J2031.** Chae S. W. Highly transparent and low-resistant ZnNi/indium tin oxide Ohmic contact on p -type GaN. / Chae S. W., Kim K. C., Kim D. H., Kim T. G., Yoon S. K., Oh B. W., Kim D. S., Kim H. K., Sung Y. M. // Applied Physics Letters. - 2007. - Vol. 90, No. 18. - P. 181101-181101-3. ↑
- J2032.** Chen N. C. Heat flow in Al Ga In P /Ga As light-emitting diodes. / Chen N. C., Yang Y. K., Wang Y. N., Huang Y. C. // Applied Physics Letters. - 2007. - Vol. 90, No. 18. - P. 181104-181104-3. ↑
- J2033.** Fukuda Takeshi. Transient property of optically pumped organic film of different fluorescence lifetimes. / Fukuda Takeshi, Okada Tomoko, Wei Bin, Ichikawa Musubu, Taniguchi Yoshio. // Applied Physics Letters. - 2007. - Vol. 90, No. 23. - P. 231105-231105-3. ↑

- J2034.** Liu Jie. Photoactivated and patternable charge transport materials and their use in organic light-emitting devices. / Liu Jie, Lewis Larry N., Duggal Anil R. // Applied Physics Letters. - 2007. - Vol. 90, No. 23. - P. 233503-233503-3. ↑
- J2035.** Sun Cheng-Jun. Enhancement of quantum efficiency of organic light emitting devices by doping magnetic nanoparticles. / Sun Cheng-Jun, Wu Yue, Xu Zhihua, Hu Bin, Bai Jianmin, Wang Jian-Ping, Shen Jian. // Applied Physics Letters. - 2007. - Vol. 90, No. 23. - P. 232110-232110-3. ↑
- J2036.** Haigh M. K. Mid-infrared Al x In 1-x Sb light-emitting diodes. / Haigh M. K., Nash G. R., Smith S. J., Buckle L., Emeny M. T., Ashley T. // Applied Physics Letters. - 2007. - Vol. 90, No. 23. - P. 231116-231116-3. ↑
- J2037.** Du Guotong. Visual-infrared electroluminescence emission from Zn O /Ga As heterojunctions grown by metal-organic chemical vapor deposition. / Du Guotong, Cui Yongguo, Xiaochuan Xia, Li Xiangping, Zhu Huichao, Zhang Baolin, Zhang Yuantao, Ma Yan. // Applied Physics Letters. - 2007. - Vol. 90, No. 24. - P. 243504-243504-3. ↑
- J2038.** Lee Jiun-Haw. Phosphorescent organic light-emitting device with an ambipolar oxadiazole host. / Lee Jiun-Haw, Tsai Hsin-Hung, Leung Man-Kit, Yang Chih-Chiang, Chao Chun-Chieh. // Applied Physics Letters. - 2007. - Vol. 90, No. 24. - P. 243501-243501-3. ↑
- J2039.** Lee Y. J. Dichromatic InGaN-based white light emitting diodes by using laser lift-off and wafer-bonding schemes. / Lee Y. J., Lin P. C., Lu T. C., Kuo H. C., Wang S. C. // Applied Physics Letters. - 2007. - Vol. 90, No. 16. - P. 161115-161115-3. ↑
- J2040.** Wu Yewchung Sermon. Effects of laser sources on the reverse-bias leakages of laser lift-off GaN-based light-emitting diodes. / Wu Yewchung Sermon, Cheng Ji-Hao, Peng Wei Chih, Ouyang Hao. // Applied Physics Letters. - 2007. - Vol. 90, No. 25. - P. 251110-251110-3. ↑
- J2041.** Hao Zhendong. White light emitting diode by using alpha -Ca 2 P 2 O 7 :Eu 2+, Mn 2+ phosphor. / Hao Zhendong, Zhang Jiahua, Zhang Xia, Sun Xiaoyuan, Luo Yongshi, Lu Shaozhe, Wang Xiao-jun. // Applied Physics Letters. - 2007. - Vol. 90, No. 26. - P. 261113-261113-3. ↑
- J2042.** Xia Yajun. Nonlithographic patterning through inkjet printing via holes. / Xia Yajun, Friend Richard H. // Applied Physics Letters. - 2007. - Vol. 90, No. 25. - P. 253513-253513-3. ↑
- J2043.** Arif M. Probing electronic excitations in organic light-emitting diodes via Raman scattering. / Arif M., Guha S., Tsami A., Scherf U. // Applied Physics Letters. - 2007. - Vol. 90, No. 25. - P. 252105-252105-3. ↑
- J2044.** Wantz G. Temperature-dependent electroluminescence spectra of organic light emitting diodes based on thermally evaporated bis-imido-phenylene vinylene derivative. / Wantz G., Hirsch L., Dautel O. J. // Applied Physics Letters. - 2007. - Vol. 90, No. 16. - P. 162104-162104-3. ↑
- J2045.** Wunderer Thomas. Time- and locally resolved photoluminescence of semipolar Ga In N /Ga N facet light emitting diodes. / Wunderer Thomas, Bruckner Peter, Hertkorn Joachim, Scholz Ferdinand, Beirne Gareth J., Jetter Michael, Michler Peter, Feneberg Martin, Thonke Klaus. // Applied Physics Letters. - 2007. - Vol. 90, No. 17. - P. 171123-171123-3. ↑
- J2046.** Yang Woan-Jen. Ce 3+ /Eu 2+ codoped Ba 2 Zn S 3 : A blue radiation-converting phosphor for white light-emitting diodes. / Yang Woan-Jen, Chen Teng-Ming. // Applied Physics Letters. - 2007. - Vol. 90, No. 17. - P. 171908-171908-3. ↑
- J2047.** Kim Sung Hyun. High efficiency phosphorescent organic light emitting diodes using triplet quantum well structure. / Kim Sung Hyun, Jang Jyongsik, Hong Jae-Min, Lee Jun Yeob. // Applied Physics Letters. - 2007. - Vol. 90, No. 17. - P. 173501-173501-3. ↑
- J2048.** Moon Jong-Min. Enhancement of hole injection using ozone treated Ag nanodots dispersed on indium tin oxide anode for organic light emitting diodes. / Moon Jong-Min, Bae Jung-Hyeok, Jeong Jin-A, Jeong Soon-Wook, Park No-Jin, Kim Han-Ki, Kang Jae-Wook, Kim Jang-Joo, Yi Min-Su. // Applied Physics Letters. - 2007. - Vol. 90, No. 16. - P. 163516-163516-3. ↑
- J2049.** Yamane Kazuhiko. Ambipolar organic light emitting field effect transistors with modified asymmetric

electrodes. / Yamane Kazuhiko, Yanagi Hisao, Sawamoto Atsushi, Hotta Shu. // Applied Physics Letters. - 2007. - Vol. 90, No. 16. - P. 162108-162108-3. ↑

J2050. Cocchi M. Single-dopant organic white electrophosphorescent diodes with very high efficiency and its reduced current density roll-off. / Cocchi M., Kalinowski J., Virgili D., Fattori V., Develay S., Williams J. A. G. // Applied Physics Letters. - 2007. - Vol. 90, No. 16. - P. 163508-163508-3. ↑

J2051. Chang Liann-Be. Formation process of high reflective Ni /Ag /Au Ohmic contact for GaN flip-chip light-emitting diodes. / Chang Liann-Be, Shiue Ching-Chuan, Jeng Ming-Jer. // Applied Physics Letters. - 2007. - Vol. 90, No. 16. - P. 163515-163515-3. ↑

J2052. Jeong Soon Moon. Highly circularly polarized electroluminescence from organic light-emitting diodes with wide-band reflective polymeric cholesteric liquid crystal films. / Jeong Soon Moon, Ohtsuka Youko, Ha Na Young, Takanishi Yoichi, Ishikawa Ken, Takezoe Hideo, Nishimura Suzushi, Suzuki Goroh. // Applied Physics Letters. - 2007. - Vol. 90, No. 21. - P. 211106-211106-3. ↑

J2053. Zhong J. Integrated ZnO nanotips on GaN light emitting diodes for enhanced emission efficiency. / Zhong J., Chen H., Saraf G., Lu Y., Choi C. K., Song J. J., Mackie D. M., Shen H. // Applied Physics Letters. - 2007. - Vol. 90, No. 20. - P. 203515-203515-3. ↑

J2054. Niu Xiaodi. Efficient multilayer white polymer light-emitting diodes with aluminum cathodes. / Niu Xiaodi, Qin Chuanjiang, Zhang Baohua, Yang Junwei, Xie Zhiyuan, Cheng Yanxiang, Wang Lixiang. // Applied Physics Letters. - 2007. - Vol. 90, No. 20. - P. 203513-203513-3. ↑

J2055. Mulder C. L. Saturated and efficient blue phosphorescent organic light emitting devices with Lambertian angular emission. / Mulder C. L., Celebi K., Milaninia K. M., Baldo M. A. // Applied Physics Letters. - 2007. - Vol. 90, No. 21. - P. 211109-211109-3. ↑

J2056. Tse S. C. Single-layer organic light-emitting diodes using naphthyl diamine. / Tse S. C., Tsung K. K., So S. K. // Applied Physics Letters. - 2007. - Vol. 90, No. 21. - P. 213502-213502-3. ↑

J2057. Krier A. Room temperature midinfrared electroluminescence from GaInAsSbP light emitting diodes. / Krier A., Smirnov V. M., Batty P. J., Vasilev V. I., Gaggis G. S., Kuchinskii V. I. // Applied Physics Letters. - 2007. - Vol. 90, No. 21. - P. 211115-211115-3. ↑

J2058. Jia Chuanyu. Polarization of edge emission from III-nitride light emitting diodes of emission wavelength from 395 to 455 nm. / Jia Chuanyu, Yu Tongjun, Mu Sen, Pan Yaobo, Yang Zhijian, Chen Zhizhong, Qin Zhixin, Zhang Guoyi. // Applied Physics Letters. - 2007. - Vol. 90, No. 21. - P. 211112-211112-3. ↑

J2059. Aonuma Masaki. Material design of hole transport materials capable of thick-film formation in organic light emitting diodes. / Aonuma Masaki, Oyamada Takahito, Sasabe Hiroyuki, Miki Tetsuzou, Adachi Chihaya. // Applied Physics Letters. - 2007. - Vol. 90, No. 18. - P. 183503-183503-3. ↑

J2060. Park Hoon. Electron mobility in tris(8-hydroxyquinoline)aluminum (Alq₃) films by transient electroluminescence from single layer organic light emitting diodes. / Park Hoon, Shin Dong-Sub, Yu Hee-Sung, Chae Hee-Baik. // Applied Physics Letters. - 2007. - Vol. 90, No. 20. - P. 202103-202103-3. ↑

J2061. Motayed Abhishek. 365 nm operation of n -nanowire/p -gallium nitride homojunction light emitting diodes. / Motayed Abhishek, Davydov Albert V., He Maoqi, Mohammad S. N., Melngailis John. // Applied Physics Letters. - 2007. - Vol. 90, No. 18. - P. 183120-183120-3. ↑

J2062. Chae S. W. Al-based Ohmic reflectors with low leakage currents and high reflectance for p-Ga N flip-chip processes. / Chae S. W., Kim D. H., Kim T. G., Ko K. Y., Sung Y. M. // Applied Physics Letters. - 2007. - Vol. 90, No. 20. - P. 201113-201113-3. ↑

J2063. Seo Ji Hoon. Highly efficient white organic light-emitting diodes using two emitting materials for three primary colors (red, green, and blue). / Seo Ji Hoon, Seo Ji Hyun, Park Jung Hyun, Kim Young Kwan, Kim Jun Ho, Hyung Gun Woo, Lee Kum Hee, Yoon Seung Soo. // Applied Physics Letters. - 2007. - Vol. 90, No. 20. - P. 203507-203507-3. ↑

J2064. Kim Sung Hyun. Lifetime improvement of green phosphorescent organic light-emitting diodes by charge confining device structure. / Kim Sung Hyun, Jang Jyongsik, Lee Jun Yeob. // Applied Physics Letters. - 2007. -

Vol. 90, No. 20. - P. 203511-203511-3. ↑

J2065. Lai S. L. Efficiency enhancement and voltage reduction in white organic light-emitting devices. / Lai S. L., Chan M. Y., Fung M. K., Lee C. S., Lee S. T. // Applied Physics Letters. - 2007. - Vol. 90, No. 20. - P. 203510-203510-3. ↑

J2066. Divayana Y. Efficient electrofluorescent organic light-emitting diodes by sequential doping. / Divayana Y., Sun X. W. // Applied Physics Letters. - 2007. - Vol. 90, No. 20. - P. 203509-203509-3. ↑

J2067. Morgado J. Poly(9,9-dioctylfluorene)-based light-emitting diodes with pure beta -phase emission. / Morgado J., Alcacer L., Charas A. // Applied Physics Letters. - 2007. - Vol. 90, No. 20. - P. 201110-201110-3. ↑

J2068. Lane Paul A. Efficient, single-layer molecular organic light-emitting diodes. / Lane Paul A., Kushto Gary P., Kafafi Zakya H. // Applied Physics Letters. - 2007. - Vol. 90, No. 2. - P. 023511-023511-3. ↑

J2069. Cocchi M. Highly efficient near-infrared organic excimer electrophosphorescent diodes. / Cocchi M., Virgili D., Fattori V., Williams J. A. G., Kalinowski J. // Applied Physics Letters. - 2007. - Vol. 90, No. 2. - P. 023506-023506-3. ↑

J2070. Kim Keunjoo. Anodic nanoclusters of GaN. / Kim Keunjoo, Choi Jaeho, Bae Tae Sung. // Applied Physics Letters. - 2007. - Vol. 90, No. 18. - P. 181912-181912-3. ↑

J2071. Kim Keunjoo. Photonic crystal effect on light emission from In Ga N /Ga N multi-quantum-well structures. / Kim Keunjoo, Choi Jaeho, Jeon Sang Cheol, Kim Jin Soo, Lee Hee Mok. // Applied Physics Letters. - 2007. - Vol. 90, No. 18. - P. 181115-181115-3. ↑

J2072. Lee Chi-Ling. Effects of strained InGaN interlayer on contact resistance between p-Ga N and indium tin oxide. / Lee Chi-Ling, Lee Wei-I. // Applied Physics Letters. - 2007. - Vol. 90, No. 18. - P. 181125-181125-3. ↑

J2073. Feezell D. F. Thin metal intracavity contact and lateral current-distribution scheme for GaN-based vertical-cavity lasers. / Feezell D. F., Farrell R. M., Schmidt M. C., Yamada H., Ishida M., DenBaars S. P., Cohen D. A., Nakamura S. // Applied Physics Letters. - 2007. - Vol. 90, No. 18. - P. 181128-181128-3. ↑

J2074. Huang Hao. Electrically driven light emission from single colloidal quantum dots at room temperature. / Huang Hao, Dorn August, Bulovic Vladimir, Bawendi Mounji G. // Applied Physics Letters. - 2007. - Vol. 90, No. 2. - P. 023110-023110-3. ↑

J2075. Kang Jae-Wook. Low roll-off of efficiency at high current density in phosphorescent organic light emitting diodes. / Kang Jae-Wook, Lee Se-Hyung, Park Hyung-Dol, Jeong Won-Ik, Yoo Kyung-Mo, Park Young-Seo, Kim Jang-Joo. // Applied Physics Letters. - 2007. - Vol. 90, No. 22. - P. 223508-223508-3. ↑

J2076. Kim Sung Hyun. High efficiency phosphorescent organic light-emitting diodes using carbazole-type triplet exciton blocking layer. / Kim Sung Hyun, Jang Jyongsik, Lee Jun Yeob. // Applied Physics Letters. - 2007. - Vol. 90, No. 22. - P. 223505-223505-3. ↑


J2077. Sun Yiru. Photophysics of Pt-porphyrin electrophosphorescent devices emitting in the near infrared. / Sun Yiru, Borek Carsten, Hanson Kenneth, Djurovich Peter I., Thompson Mark E., Brooks Jason, Brown Julie J., Forrest Stephen R. // Applied Physics Letters. - 2007. - Vol. 90, No. 21. - P. 213503-213503-3. ↑


J2078. Saxena Kanchan. Erratum: "Spatial coherence properties of electroluminescence from Al q 3 -based organic light emitting diodes" [Appl. Phys. Lett. 89, 061124 (2006)]. / Saxena Kanchan, Mehta Dalip Singh, Srivastava Ritu, Kamalasanan M. N. // Applied Physics Letters. - 2007. - Vol. 90, No. 22. - P. 229901-229901-1. ↑


J2079. McNeill Christopher R. Dual electron donor/electron acceptor character of a conjugated polymer in efficient photovoltaic diodes. / McNeill Christopher R., Abrusci Agnese, Zaumseil Jana, Wilson Richard, McKiernan Mary J., Burroughes Jeremy H., Halls Jonathan J. M., Greenham Neil C., Friend Richard H. // Applied Physics Letters. - 2007. - Vol. 90, No. 19. - P. 193506-193506-3. ↑


J2080. Xie Rong-Jun. 2-phosphor-converted white light-emitting diodes using oxynitride/nitride phosphors. / Xie Rong-Jun, Hirotsuki Naoto, Kimura Naoki, Sakuma Ken, Mitomo Mamoru. // Applied Physics Letters. - 2007. - Vol. 90, No. 19. - P. 191101-191101-3. ↑


- J2081.** Kim Soo Young. Change of interface dipole energy with interfacial layer thickness and O₂ plasma treatment in metal/organic interface. / Kim Soo Young, Hong Kihyon, Lee Jong-Lam. // Applied Physics Letters. - 2007. - Vol. 90, No. 18. - P. 183508-183508-3. ↑
- J2082.** Vicknesh S. Fabrication of deeply undercut GaN-based microdisk structures on silicon platforms. / Vicknesh S., Tripathy S., Lin Vivian K. X., Wang L. S., Chua S. J. // Applied Physics Letters. - 2007. - Vol. 90, No. 7. - P. 071906-071906-3. ↑
- J2083.** Lin Chun-Liang. Influences of resonant wavelengths on performances of microcavity organic light-emitting devices. / Lin Chun-Liang, Chang Han-Chieh, Tien Kun-Cheng, Wu Chung-Chih. // Applied Physics Letters. - 2007. - Vol. 90, No. 7. - P. 071111-071111-3. ↑
- J2084.** Huang Rui. Enhanced electroluminescence efficiency of oxidized amorphous silicon nitride light-emitting devices by modulating Si/N ratio. / Huang Rui, Chen Kunji, Dong Hengping, Wang Danqing, Ding Honglin, Li Wei, Xu Jun, Ma Zhongyuan, Xu Ling. // Applied Physics Letters. - 2007. - Vol. 91, No. 11. - P. 111104-111104-3. ↑
- J2085.** Terai Masaya. Electric-field-assisted bipolar charge generation from internal charge separation zone composed of doped organic bilayer. / Terai Masaya, Tsutsui Tetsuo. // Applied Physics Letters. - 2007. - Vol. 90, No. 8. - P. 083502-083502-3. ↑
- J2086.** Lombez L. Electrical spin injection into p-doped quantum dots through a tunnel barrier. / Lombez L., Renucci P., Braun P. F., Carrere H., Marie X., Amand T., Urbaszek B., Gauffier J. L., Gallo P., Camps T., Arnoult A., Fontaine C., Deranlot C., Mattana R., Jaffres H., George J.-M., Binh P. H. // Applied Physics Letters. - 2007. - Vol. 90, No. 8. - P. 081111-081111-3. ↑
- J2087.** Feng Jing. Color-tunable electroluminescence from white organic light-emitting devices through coupled surface plasmons. / Feng Jing, Okamoto Takayuki, Simonen Janne, Kawata Satoshi. // Applied Physics Letters. - 2007. - Vol. 90, No. 8. - P. 081106-081106-3. ↑
- J2088.** Jung Hyun-Min. Via-hole-based vertical GaN light emitting diodes. / Jung Hyun-Min, Nam Gi-Yeon, Choi Byung-Kyun, Lee Tae-Hee, Kim Hyun-Suk, Jeon Soo-Kun, Park Eun-Hyun, Kim Chang-Tae. // Applied Physics Letters. - 2007. - Vol. 91, No. 11. - P. 111106-111106-3. ↑
- J2089.** Ho Meng-Huan. White p-i-n organic light-emitting devices with high power efficiency and stable color. / Ho Meng-Huan, Hsu Shih-Feng, Ma Jia-Wei, Hwang Shiao-Wen, Yeh Pu-Cheng, Chen Chin H. // Applied Physics Letters. - 2007. - Vol. 91, No. 11. - P. 113518-113518-3. ↑
- J2090.** Ward M. B. Electrically driven telecommunication wavelength single-photon source. / Ward M. B., Farrow T., See P., Yuan Z. L., Karimov O. Z., Bennett A. J., Shields A. J., Atkinson P., Cooper K., Ritchie D. A. // Applied Physics Letters. - 2007. - Vol. 90, No. 6. - P. 063512-063512-3. ↑
- J2091.** Kim Hyunsoo. Measurements of current spreading length and design of GaN-based light emitting diodes. / Kim Hyunsoo, Cho Jaehee, Lee Jeong Wook, Yoon Sukho, Kim Hyungkun, Sone Cheolsoo, Park Yongjo, Seong Tae-Yeon. // Applied Physics Letters. - 2007. - Vol. 90, No. 6. - P. 063510-063510-3. ↑
- J2092.** Kohnen Anne. Enhanced efficiency of multilayer organic light-emitting diodes with a low-refractive index hole-transport layer: An effect of improved outcoupling?. / Kohnen Anne, Gather Malte C., Riegel Nina, Zacharias Philipp, Meerholz Klaus. // Applied Physics Letters. - 2007. - Vol. 91, No. 11. - P. 113501-113501-3. ↑
- J2093.** Ye Z. Z. ZnO light-emitting diodes fabricated on Si substrates with homobuffer layers. / Ye Z. Z., Lu J. G., Zhang Y. Z., Zeng Y. J., Chen L. L., Zhuge F., Yuan G. D., He H. P., Zhu L. P., Huang J. Y., Zhao B. H. // Applied Physics Letters. - 2007. - Vol. 91, No. 11. - P. 113503-113503-3. ↑
- J2094.** Meyer J. Highly efficient simplified organic light emitting diodes. / Meyer J., Hamwi S., Bulow T., Johannes H.-H., Riedl T., Kowalsky W. // Applied Physics Letters. - 2007. - Vol. 91, No. 11. - P. 113506-113506-3. ↑
- J2095.** Chang Chih-Hao. Effect of ionization potential change in poly(3,4-ethylenedioxythiophene):poly(styrenesulfonic acid) on the performance of polymer light emitting diodes due to its reaction with indium tin oxide. / Chang Chih-Hao, Chen Show-An. // Applied Physics Letters. - 2007. - Vol. 91, No. 11. - P. 113506-113506-3. ↑


No. 10. - P. 103514-103514-3. 


J2096. Png Rui-Qi. Electromigration of the conducting polymer in organic semiconductor devices and its stabilization by cross-linking. / Png Rui-Qi, Chia Perq-Jon, Sivaramakrishnan Sankaran, Wong Loke-Yuen, Zhou Mi, Chua Lay-Lay, Ho Peter K-H. // Applied Physics Letters. - 2007. - Vol. 91, No. 1. - P. 013511-013511-3. 


J2097. Tao Silu. Efficient blue and white organic light-emitting devices based on a single bipolar emitter. / Tao Silu, Lee Chun Sing, Lee Shuit-Tong, Zhang Xiaohong. // Applied Physics Letters. - 2007. - Vol. 91, No. 1. - P. 013507-013507-3. 


J2098. Chang S. J. Nitride-based light emitting diodes with indium tin oxide electrode patterned by imprint lithography. / Chang S. J., Shen C. F., Chen W. S., Kuo C. T., Ko T. K., Shei S. C., Sheu J. K. // Applied Physics Letters. - 2007. - Vol. 91, No. 1. - P. 013504-013504-3. 


J2099. Rehmann Nina. Highly efficient solution-processed phosphorescent multilayer organic light-emitting diodes based on small-molecule hosts. / Rehmann Nina, Hertel Dirk, Meerholz Klaus, Becker Heinrich, Heun Susanne. // Applied Physics Letters. - 2007. - Vol. 91, No. 10. - P. 103507-103507-3. 


J2100. Kim Sung Hyun. Efficient electron injection in organic light-emitting diodes using lithium quinolate/Ca /Al cathodes. / Kim Sung Hyun, Jang Jyongsik, Lee Jun Yeob. // Applied Physics Letters. - 2007. - Vol. 91, No. 10. - P. 103501-103501-3. 


J2101. Zhao Y. Q. Transparent conducting C 60 :Li F nanocomposite thin films for organic light-emitting diodes. / Zhao Y. Q., Huang C. J., Ogundimu T., Lu Z. H. // Applied Physics Letters. - 2007. - Vol. 91, No. 10. - P. 103109-103109-3. 


J2102. Ehrenfreund E. Negative capacitance in organic semiconductor devices: Bipolar injection and charge recombination mechanism. / Ehrenfreund E., Lungenschmied C., Dennler G., Neugebauer H., Sariciftci N. S. // Applied Physics Letters. - 2007. - Vol. 91, No. 1. - P. 012112-012112-3. 


J2103. Ban D. Near-infrared to visible light optical upconversion by direct tandem integration of organic light-emitting diode and inorganic photodetector. / Ban D., Han S., Lu Z. H., Oogarah T., SpringThorpe A. J., Liu H. C. // Applied Physics Letters. - 2007. - Vol. 90, No. 9. - P. 093108-093108-3. 


J2104. Cheng Yu-Hung. Enhanced light outcoupling in a thin film by texturing meshed surfaces. / Cheng Yu-Hung, Wu Jia-Lin, Cheng Chien-Hong, Syao Kao-Chih, Lee Ming-Chang M. // Applied Physics Letters. - 2007. - Vol. 90, No. 9. - P. 091102-091102-3. 


J2105. Wang Ch. Y. Integration of In 2 O 3 nanoparticle based ozone sensors with Ga In N /Ga N light emitting diodes. / Wang Ch. Y., Cimalla V., Kups Th., Rohlig C.-C., Stauden Th., Ambacher O., Kunzer M., Passow T., Schirmacher W., Pletschen W., Kohler K., Wagner J. // Applied Physics Letters. - 2007. - Vol. 91, No. 10. - P. 103509-103509-3. 

J2106. Leem Dong-Seok. Low driving voltage and high stability organic light-emitting diodes with rhenium oxide-doped hole transporting layer. / Leem Dong-Seok, Park Hyung-Dol, Kang Jae-Wook, Lee Jae-Hyun, Kim Ji Whan, Kim Jang-Joo. // Applied Physics Letters. - 2007. - Vol. 91, No. 1. - P. 011113-011113-3. 

J2107. Dong Yongqiang. Aggregation-induced emissions of tetraphenylethene derivatives and their utilities as chemical vapor sensors and in organic light-emitting diodes. / Dong Yongqiang, Lam Jacky W. Y., Qin Anjun, Liu Jianzhao, Li Zhen, Tang Ben Zhong, Sun Jiaxin, Kwok Hoi Sing. // Applied Physics Letters. - 2007. - Vol. 91, No. 1. - P. 011111-011111-3. 

J2108. Nakamura A. Full-color electroluminescence from ZnO-based heterojunction diodes. / Nakamura A., Ohashi T., Yamamoto K., Ishihara J., Aoki T., Temmyo J., Gotoh H. // Applied Physics Letters. - 2007. - Vol. 90, No. 9. - P. 093512-093512-3. 

J2109. Lai Chun-Feng. Anisotropy of light extraction from two-dimensional photonic crystal light-emitting diodes. / Lai Chun-Feng, Kuo H. C., Chao C. H., Hsueh H. T., Wang J.-F. T., Yeh W. Y., Chi J. Y. // Applied Physics Letters. - 2007. - Vol. 91, No. 12. - P. 123117-123117-3. 

J2110. Zhang Hongmei. High efficiency tandem organic light-emitting devices with Al /W O 3 /Au interconnecting layer. / Zhang Hongmei, Dai Yanfeng, Ma Dongge. // Applied Physics Letters. - 2007. - Vol. 91, No. 1. - P. 013501-013501-3. 

No. 12. - P. 123504-123504-3.

J2111. Reineke Sebastian. Reduced efficiency roll-off in phosphorescent organic light emitting diodes by suppression of triplet-triplet annihilation. / Reineke Sebastian, Schwartz Gregor, Walzer Karsten, Leo Karl. // Applied Physics Letters. - 2007. - Vol. 91, No. 12. - P. 123508-123508-3. ↑

J2112. Wang Chien-Chun. Enhancement of the light output performance for GaN-based light-emitting diodes by bottom pillar structure. / Wang Chien-Chun, Ku Han, Liu Chien-Chih, Chong Kwok-Keung, Hung Chen-I, Wang Yeong-Her, Hwang Mau-Phon. // Applied Physics Letters. - 2007. - Vol. 91, No. 12. - P. 121109-121109-3. ↑

J2113. Hwang Dae-Kue. ZnO-based light-emitting metal-insulator-semiconductor diodes. / Hwang Dae-Kue, Oh Min-Suk, Lim Jae-Hong, Choi Yong-Seok, Park Seong-Ju. // Applied Physics Letters. - 2007. - Vol. 91, No. 12. - P. 121113-121113-3. ↑

J2114. An Sung Jin. Near ultraviolet light emitting diode composed of n-GaN /ZnO coaxial nanorod heterostructures on a p-GaN layer. / An Sung Jin, Yi Gyu-Chul. // Applied Physics Letters. - 2007. - Vol. 91, No. 12. - P. 123109-123109-3. ↑

J2115. Kim Hyunsoo. Enhanced light extraction of GaN-based light-emitting diodes by using textured n-type GaN layers. / Kim Hyunsoo, Cho Jaehee, Lee Jeong Wook, Yoon Sukho, Kim Hyungkun, Sone Cheolsoo, Park Yongjo, Seong Tae-Yeon. // Applied Physics Letters. - 2007. - Vol. 90, No. 16. - P. 161110-161110-3. ↑

J2116. Park Eun-Hyun. The effect of silicon doping in the selected barrier on the electroluminescence of In Ga N /Ga N multiquantum well light emitting diode. / Park Eun-Hyun, Kang David Nicol Hun, Ferguson Ian T., Park Soo-Kun Jeon Joong-Seo, Yoo Tae-Kyung. // Applied Physics Letters. - 2007. - Vol. 90, No. 3. - P. 031102-031102-3. ↑

J2117. Sheu Jinn-Kong. Enhanced efficiency of GaN-based light-emitting diodes with periodic textured Ga-doped ZnO transparent contact layer. / Sheu Jinn-Kong, Lu Y. S., Lee Min-Lum, Lai W. C., Kuo C. H., Tun Chun-Ju. // Applied Physics Letters. - 2007. - Vol. 90, No. 26. - P. 263511-263511-3. ↑

J2118. Kim Hyung Gu. Effect of periodic deflector embedded in In Ga N /Ga N light emitting diode. / Kim Hyung Gu, Na Min Gyu, Kim Hyun Kyu, Kim Hee Yun, Ryu Jae Hyoung, Cuong Tran Viet, Hong Chang-Hee. // Applied Physics Letters. - 2007. - Vol. 90, No. 26. - P. 261117-261117-3. ↑

J2119. Kim Young Min. Spectral broadening in electroluminescence of white organic light-emitting diodes based on complementary colors. / Kim Young Min, Park Young Wook, Choi Jin Hwan, Ju Byeong Kwon, Jung Jae Hoon, Kim Jai Kyeong. // Applied Physics Letters. - 2007. - Vol. 90, No. 3. - P. 033506-033506-3. ↑

J2120. Gu E. Hybrid inorganic/organic microstructured light-emitting diodes produced using photocurable polymer blends. / Gu E., Zhang H. X., Sun H. D., Dawson M. D., Mackintosh A. R., Kuehne A. J. C., Pethrick R. A., Belton C., Bradley D. D. C. // Applied Physics Letters. - 2007. - Vol. 90, No. 3. - P. 031116-031116-3. ↑

J2121. Pattison P. Morgan. Gallium nitride based microcavity light emitting diodes with 2λ effective cavity thickness. / Pattison P. Morgan, David Aurelien, Sharma Rajat, Weisbuch Claude, DenBaars Steven, Nakamura Shuji. // Applied Physics Letters. - 2007. - Vol. 90, No. 3. - P. 031111-031111-3. ↑

J2122. Ryu Seung Yoon. Highly efficient transparent organic light-emitting diodes by ion beam assisted deposition-prepared indium tin oxide cathode. / Ryu Seung Yoon, Choi Sang Hun, Kim Jong Tae, Kim Chang Su, Baik Hong Koo, Jeong Hee Seong. // Applied Physics Letters. - 2007. - Vol. 90, No. 3. - P. 033513-033513-3. ↑

J2123. Pode R. B. Erratum: "Fabrication of 5,6,11,12-tetraphenyl-naphthacene doped 4-bis(2,2-diphenylvinyl)-1,1-biphenyl white organic light-emitting device" [Appl. Phys. Lett. 89, 223514 (2006)]. / Pode R. B., Lee C. J., Han J. I., Moon D. G. // Applied Physics Letters. - 2007. - Vol. 90, No. 5. - P. 059901-059901-1. ↑

J2124. Yao Yan. Low voltage and fast speed all-polymeric optocouplers. / Yao Yan, Chen Hsiang-Yu, Huang Jinsong, Yang Yang. // Applied Physics Letters. - 2007. - Vol. 90, No. 5. - P. 053509-053509-3. ↑

J2125. Son J. K. Comprehensive study of time-lapsed peak shift in InGaN quantum well structures: Discrimination of localization effect from internal field effect. / Son J. K., Sakong T., Lee S. N., Paek H. S., Ryu

H., Ha K. H., Nam O., Park Y., Hwang J. S., Cho Y. H. // Applied Physics Letters. - 2007. - Vol. 90, No. 5. - P. 051918-051918-3. ↑

J2126. Chang Chih-Hao. Interface formation between poly(9,9-dioctylfluorene) and poly(3,4-ethylenedioxythiophene):poly(styrenesulfonic acid). / Chang Chih-Hao, Liao Jin-Long, Hung Ming-Chin, Chen Show-An. // Applied Physics Letters. - 2007. - Vol. 90, No. 6. - P. 063506-063506-3. ↑

J2127. Deng X. Y. Three-color polymeric light-emitting devices using selective photo-oxidation of multilayered conjugated polymers. / Deng X. Y., Wong K. Y., Mo Y. Q. // Applied Physics Letters. - 2007. - Vol. 90, No. 6. - P. 063505-063505-3. ↑

J2128. Chia C. K. Ultrawide band quantum dot light emitting device by postfabrication laser annealing. / Chia C. K., Chua S. J., Dong J. R., Teo S. L. // Applied Physics Letters. - 2007. - Vol. 90, No. 6. - P. 061101-061101-3. ↑

J2129. Kimura Naoki. Extrahigh color rendering white light-emitting diode lamps using oxynitride and nitride phosphors excited by blue light-emitting diode. / Kimura Naoki, Sakuma Ken, Hirafune Syunichiro, Asano Kenichiro, Hirosaki Naoto, Xie Rong-Jun. // Applied Physics Letters. - 2007. - Vol. 90, No. 5. - P. 051109-051109-3. ↑

J2130. Chen Tron-Min. Use of anisotropic laser etching to the top n-Ga N layer to alleviate current-crowding effect in vertical-structured GaN-based light-emitting diodes. / Chen Tron-Min, Wang Shui-Jinn, Uang Kai-Ming, Chen Shiue-Lung, Tsai Wei-Chih, Lee Wei-Chi, Tsai Ching-Chung. // Applied Physics Letters. - 2007. - Vol. 90, No. 4. - P. 041115-041115-3. ↑

J2131. Bertoni Cristina. Fabrication and characterization of red-emitting electroluminescent devices based on thiol-stabilized semiconductor nanocrystals. / Bertoni Cristina, Gallardo Diego, Dunn Steve, Gaponik Nikolai, Eychmuller Alexander. // Applied Physics Letters. - 2007. - Vol. 90, No. 3. - P. 034107-034107-3. ↑

J2132. Castiglia A. Efficient current injection scheme for nitride vertical cavity surface emitting lasers. / Castiglia A., Simeonov D., Buehlmann H. J., Carlin J.-F., Feltn E., Dorsaz J., Butte R., Grandjean N. // Applied Physics Letters. - 2007. - Vol. 90, No. 3. - P. 033514-033514-3. ↑

J2133. Rizzo Aurora. Blue light emitting diodes based on fluorescent Cd Se /Zn S nanocrystals. / Rizzo Aurora, Li Yanqin, Kudera Stefan, Della Sala Fabio, Zanella Marco, Parak Wolfgang J., Cingolani Roberto, Manna Liberato, Gigli Giuseppe. // Applied Physics Letters. - 2007. - Vol. 90, No. 5. - P. 051106-051106-3. ↑

J2134. Wei Z. P. Room temperature p-n ZnO blue-violet light-emitting diodes. / Wei Z. P., Lu Y. M., Shen D. Z., Zhang Z. Z., Yao B., Li B. H., Zhang J. Y., Zhao D. X., Fan X. W., Tang Z. K. // Applied Physics Letters. - 2007. - Vol. 90, No. 4. - P. 042113-042113-3. ↑

J2135. Jang Ho Seong. Yellow-emitting Sr 3 Si O 5 :Ce 3+ ,Li + phosphor for white-light-emitting diodes and yellow-light-emitting diodes. / Jang Ho Seong, Jeon Duk Young. // Applied Physics Letters. - 2007. - Vol. 90, No. 4. - P. 041906-041906-3. ↑

J2136. Jun Hyuk Cheon. Active-matrix OLED on bendable metal foil. / Jun Hyuk Cheon, Jong Hyun Choi, Ji Ho Hur, Jang J., Hyun Soo Shin, Jae Kyeong Jeong, Yeon Gon Mo, Ho Kyoong Chung. // IEEE Transactions on Electron Devices. - 2006. - Vol. 53, No. 5. - P. 1273-1276. ↑

J2137. Shui-Jinn Wang. The use of transparent conducting indium-zinc oxide film as a current spreading layer for vertical-structured high-power GaN-based light-emitting diodes. / Shui-Jinn Wang, Shiue-Lung Chen, Kai-Ming Uang, Wei-Chi Lee, Tron-Min Chen, Chao-Hsuing Chen, Bor-wen Liou. // IEEE Photonics Technology Letters. - 2006. - Vol. 18, No. 10. - P. 1146-1148. ↑

J2138. Cao X.A. Temperature-dependent electroluminescence of AlGaIn-based UV LEDs. / Cao X.A., LeBoeuf S.F., Stecher T.E. // IEEE Electron Device Letters. - 2006. - Vol. 27, No. 5. - P. 329-331. ↑

J2139. Son Y.D. Depletion-mode TFT made of low-temperature poly-Si. / Son Y.D., Kyung Dong Yang, Byung Seong Bae, Jang J., Munpyo Hong, Sung Jin Kim. // IEEE Transactions on Electron Devices. - 2006. - Vol. 53, No. 5. - P. 1260-1262. ↑

J2140. Ti-chiun Chang. A new framework for characterization of halftone textures. / Ti-chiun Chang, Allebach

J.P. // IEEE Transactions on Image Processing. - 2006. - Vol. 15, No. 5. - P. 1285-1299. ↑

J2141. R. Joray. Far-field radiation pattern of red emitting thin-film resonant cavity LEDs. / R. Joray, M. Illegems, R.P. Stanley, W. Schmid, R. Butendeich, R. Wirth, A. Jaeger, K. Streubel. // IEEE Photonics Technology Letters. - 2006. - Vol. 18, No. 9. - P. 1052-1054. ↑

J2142. Camin D.V. Performance of the optically-coupled current-mirror with its input stage cooled to cryogenic temperature. / Camin D.V., Grassi V. // IEEE Transactions on Nuclear Science. - 2006. - Vol. 53, No. 2. - P. 440-443. ↑

J2143. Jiun-Haw Lee. Radiation simulations of top-emitting organic light-emitting devices with two- and three-microcavity structures. / Jiun-Haw Lee, Kuan-Yu Chen, Chia-Chiang Hsiao, Hung-Chi Chen, Chih-Hsiang Chang, Yean-Woei Kiang, Yang C.C. // Journal of Display Technology. - 2006. - Vol. 2, No. 2. - P. 130-137. ↑

J2144. Sun J.X. Improving the performance of organic light-emitting diodes containing BCP/LiF/Al by thermal annealing. / Sun J.X., Zhu X.L., Yu M., Peng H.J., Wong M., Kwok H.S. // Journal of Display Technology. - 2006. - Vol. 2, No. 2. - P. 138-142. ↑

J2145. Weixin Li. Maximizing Alq/sub 3/ OLED internal and external efficiencies: charge balanced device structure and color conversion outcoupling lenses. / Weixin Li, Jones R.A., Allen S.C., Heikenfeld J.C., Steckl A.J. // Journal of Display Technology. - 2006. - Vol. 2, No. 2. - P. 143-152. ↑

J2146. Yung-Chun Wu. High-performance metal-induced lateral-crystallization polysilicon thin-film transistors with multiple nanowire channels and multiple gates. / Yung-Chun Wu, Ting-Chang Chang, Po-Tsun Liu, Cheng-Wei Chou, Yuan-Chun Wu, Chun-Hao Tu, Chun-Yen Chang. // IEEE Transactions on Nanotechnology. - 2006. - Vol. 5, No. 3. - P. 157-162. ↑

J2147. Chia-Hsun Tu. Memory effect in the current-voltage characteristic of 8-hydroquinoline aluminum salt films. / Chia-Hsun Tu, Yi-Sheng Lai, Dim-Lee Kwong. // IEEE Electron Device Letters. - 2006. - Vol. 27, No. 5. - P. 354-356. ↑

J2148. Kettle J. Monte-Carlo based simulation of surface light emission profiles from AlGaInP light emitting diodes. / Kettle J., Perks R.M. // Electronics Letters. - 2006. - Vol. 42, No. 9. - P. 553-555. ↑

J2149. Lee Y.J. Enhancing the output power of GaN-based LEDs grown on wet-etched patterned sapphire substrates. / Lee Y.J., Hwang J.M., Hsu T.C., Hsieh M.H., Jou M.J., Lee B.J., Lu T.C., Kuo H.C., Wang S.C. // IEEE Photonics Technology Letters. - 2006. - Vol. 18, No. 10. - P. 1152-1154. ↑

J2150. Jongwoon Park. Carrier Transport and Optical Properties of InGaN SQW With Embedded AlGaIn - Layer. / Jongwoon Park, Kaneta A., Funato M., Kawakami Y. // IEEE Journal of Quantum Electronics. - 2006. - Vol. 42, No. 10. - P. 1023-1030. ↑

J2151. Petrellis N. Target Localization Utilizing the Success Rate in Infrared Pattern Recognition. / Petrellis N., Konofaos N., Alexiou G.Ph. // IEEE Sensors Journal. - 2006. - Vol. 6, No. 5. - P. 1355-1364. ↑

J2152. Chung-Pui Chan. Study of Laser-Debonded GaN LEDs. / Chung-Pui Chan, Jie Gao, Tai-Man Yue, Surya C., Ng A.M.-C., Djuric A.B., Liu P.C.-K., Ming Li. // IEEE Transactions on Electron Devices. - 2006. - Vol. 53, No. 9. - P. 2266-2272. ↑

J2153. Kyeong-Sik Shin. Characterization of an Integrated Fluorescence-Detection Hybrid Device With Photodiode and Organic Light-Emitting Diode. / Kyeong-Sik Shin, Young-Hwan Kim, Kyeong-Kap Paek, Jung-Ho Park, Eun-Gyeong Yang, Tae-Song Kim, Ji-Yoon Kang, Byeong-Kwon Ju. // IEEE Electron Device Letters. - 2006. - Vol. 27, No. 9. - P. 746-748. ↑

J2154. Sambandan S. Equivalent Circuit Description of Threshold Voltage Shift in a-Si:H TFTs From a Probabilistic Analysis of Carrier Population Dynamics. / Sambandan S., Nathan A. // IEEE Transactions on Electron Devices. - 2006. - Vol. 53, No. 9. - P. 2306-2311. ↑

J2155. Ogihara M. LED array integrated with Si driving circuits for LED printer printhead. / Ogihara M., Fujiwara H., Mutoh M., Suzuki T., Igari T., Sagimori T., Kurokawa H., Kaneto T., Furuta H., Abiko I., Sakuta M. // Electronics Letters. - 2006. - Vol. 42, No. 15. - P. 881-883. ↑

- J2156.** Hau-Yan Lu. Enhancement of Brightness Uniformity by a New Voltage-Modulated Pixel Design for AMOLED Displays. / Hau-Yan Lu, Po-Tsun Liu, Ting-Chang Chang, Sien Chi. // IEEE Electron Device Letters. - 2006. - Vol. 27, No. 9. - P. 743-745. ↑
- J2157.** Sakariya K. Leakage and charge injection optimization in a-Si AMOLED displays. / Sakariya K., Nathan A. // Journal of Display Technology. - 2006. - Vol. 2, No. 3. - P. 254-257. ↑
- J2158.** Matsumoto T. Self-Assembled Nanotiles of Heteroepitaxial SiC on Si. / Matsumoto T., Kiuchi M., Sugimoto S., Goto S. // IEEE Transactions on Plasma Science. - 2006. - Vol. 34, No. 4. - P. 1109-1111. ↑
- J2159.** Goth G. Army-Backed Flexible Display Effort: A Symbol of Public-Private Partnership. IEEE Pervasive Computing. - 2006. - Vol. 5, No. 3. - P. 4-6. ↑
- J2160.** Ashtiani S.J. A driving scheme for active-matrix organic light-emitting diode displays based on feedback. / Ashtiani S.J., Nathan A. // Journal of Display Technology. - 2006. - Vol. 2, No. 3. - P. 258-264. ↑
- J2161.** Long K. Full-Color OLEDs Integrated by Dry Dye Printing. / Long K., Pschenitzka F., Lu M.-H., Sturm J.C. // IEEE Transactions on Electron Devices. - 2006. - Vol. 53, No. 9. - P. 2250-2258. ↑
- J2162.** Taesung Kim. Photonic crystal structure effect on the enhancement in the external quantum efficiency of a red LED. / Taesung Kim, Leisher P.O., Danner A.J., Wirth R., Streubel K., Choquette K.D. // IEEE Photonics Technology Letters. - 2006. - Vol. 18, No. 17. - P. 1876-1878. ↑
- J2163.** Milliez J. High-brightness white-light source based on up-conversion phosphors. / Milliez J., Rapaport A., Bass M., Cassanho A., Jenssen H.P. // Journal of Display Technology. - 2006. - Vol. 2, No. 3. - P. 307-311. ↑
- J2164.** Horng R.-H. Effect of resonant cavity in wafer-bonded Green InGaN LED with dielectric and silver mirrors. / Horng R.-H., Wei-Kai Wang, Shin-Yung Huang, Dong-Sing Wu. // IEEE Photonics Technology Letters. - 2006. - Vol. 18, No. 3. - P. 457-459. ↑
- J2165.** Achtenhagen M. Lateral mode discrimination and self-stabilization in ridge waveguide laser diodes. / Achtenhagen M., Hardy A., Harder C.S. // IEEE Photonics Technology Letters. - 2006. - Vol. 18, No. 3. - P. 526-528. ↑
- J2166.** Dey S.R. Precompensation for anticipated erasures in LTI interpolation systems. / Dey S.R., Russell A.I., Oppenheim A.V. // IEEE Transactions on Signal Processing. - 2006. - Vol. 54, No. 1. - P. 325-335. ↑
- J2167.** Hoffman D. Electroluminescence of InAs-GaSb heterodiodes. / Hoffman D., Hood A., Michel E., Fuchs F., Razeghi M. // IEEE Journal of Quantum Electronics. - 2006. - Vol. 42, No. 2. - P. 126-130. ↑
- J2168.** Tu Hoang. The effect of dislocation loops on the light emission of silicon LEDs. / Tu Hoang, Phuong LeMinh, Holleman J., Schmitz J. // IEEE Electron Device Letters. - 2006. - Vol. 27, No. 2. - P. 105-107. ↑
- J2169.** De Santis F. Optical in situ characterization of isotactic polypropylene crystallization using an LED array in avalanche-photoreceiver mode. / De Santis F., Ferrara M., Neitzert H.-C. // IEEE Transactions on Instrumentation and Measurement. - 2006. - Vol. 55, No. 1. - P. 123-127. ↑
- J2170.** Park J.H. A new configuration of nematic liquid crystal thermography with applications to GaN-based devices. / Park J.H., Lee C.C. // IEEE Transactions on Instrumentation and Measurement. - 2006. - Vol. 55, No. 1. - P. 273-279. ↑
- J2171.** Long K. Stability of amorphous-silicon TFTs deposited on clear plastic substrates at 250°C to 280° C. / Long K., Kattamis A.Z., Cheng I.-C., Gleskova H., Wagner S., Sturm J.C. // IEEE Electron Device Letters. - 2006. - Vol. 27, No. 2. - P. 111-113. ↑
- J2172.** Yap S.-S. Enhanced reliability by diamond-like carbon in single-layer organic light emitting diodes. / Yap S.-S., Yang R.-B., Yow H.-K., Tou T.-Y. // Electronics Letters. - 2006. - Vol. 42, No. 2. - P. 114-115. ↑
- J2173.** Hsueh-Shih Chen. InGaN-CdSe-ZnSe quantum dots white LEDs. / Hsueh-Shih Chen, Cheng-Kuo Hsu, Hsin-Yen Hong. // IEEE Photonics Technology Letters. - 2006. - Vol. 18, No. 1. - P. 193-195. ↑
- J2174.** Chun-Ju Tun. Enhanced light output of GaN-based power LEDs with transparent Al-doped ZnO current

spreading layer. / Chun-Ju Tun, Jinn-Kong Sheu, Bao-Jen Pong, Min-Lum Lee, Ming-Yu Lee, Cheng-Kang Hsieh, Ching-Chung Hu, Gou-Chung Chi. // IEEE Photonics Technology Letters. - 2006. - Vol. 18, No. 1. - P. 274-276. ↑

J2175. Chong-Yi Lee. 630-nm n-type Modulation-doped AlGaInP-AlInP multiquantum-well light-emitting diode. / Chong-Yi Lee, Juh-Yuh Su, Chi-Min Kuo. // IEEE Photonics Technology Letters. - 2006. - Vol. 18, No. 1. - P. 25-27. ↑

J2176. S.K. Ray. Broad-band superluminescent light-emitting diodes incorporating quantum dots in compositionally modulated quantum wells. / S.K. Ray, K.M. Groom, M.D. Beattie, H.Y. Liu, M. Hopkinson, R.A. Hogg. // IEEE Photonics Technology Letters. - 2006. - Vol. 18, No. 1. - P. 58-60. ↑

J2177. J.-W. Shi. Nitride-based photodiode at 510-nm wavelength for plastic optical fiber communication. / J.-W. Shi, H.-Y. Huang, J.-K. Sheu, S.-H. Hsieh, Y.-S. Wu, Ja-Yu Lu, F.-H. Huang, W.-C. Lai. // IEEE Photonics Technology Letters. - 2006. - Vol. 18, No. 1. - P. 283-285. ↑

J2178. Kattamis A.Z. High mobility nanocrystalline silicon transistors on clear plastic substrates. / Kattamis A.Z., Holmes R.J., I-Chun Cheng, Long K., Sturm J.C., Forrest S.R., Wagner S. // IEEE Electron Device Letters. - 2006. - Vol. 27, No. 1. - P. 49-51. ↑

J2179. Chen W.S. Rapid thermal annealed InGaN/GaN flip-chip LEDs. / Chen W.S., Shei S.C., Chang S.J., Su Y.K., Lai W.C., Kuo C.H., Lin Y.C., Chang C.S., Ko T.K., Hsu Y.P., Shen C.F. // IEEE Transactions on Electron Devices. - 2006. - Vol. 53, No. 1. - P. 32-37. ↑

J2180. Yun J. Low-resistance Ohmic contacts to digital alloys of n-AlGaIn/AlN. / Yun J., Choi K., Mathur K., Kuryatkov V., Borisov B., Kipshidze G., Nikishin S., Temkin H. // IEEE Electron Device Letters. - 2006. - Vol. 27, No. 1. - P. 22-24. ↑

J2181. Sang-Hoon Jung. A new analog buffer using P-type poly-Si TFTs for active matrix displays. / Sang-Hoon Jung, Woo-Jin Nam, Jae-Hoon Lee, Min-Koo Han. // IEEE Electron Device Letters. - 2006. - Vol. 27, No. 1. - P. 40-42. ↑

J2182. Shi-Lin Chen. Analysis of rail potential and stray current for Taipei Metro. / Shi-Lin Chen, Hsu S.-C., Chin-Tien Tseng, Kun-Hong Yan, Huang-Yu Chou, Tong-Ming Too. // IEEE Transactions on Vehicular Technology. - 2006. - Vol. 55, No. 1. - P. 67-75. ↑

J2183. Chiadini F. Designing low-cost modified cladding sensors: a structured approach. / Chiadini F., Paciello V., Paolillo A. // IEEE Transactions on Instrumentation and Measurement. - 2006. - Vol. 55, No. 2. - P. 477-482. ↑

J2184. Materka A. Alternate half-field stimulation technique for SSVEP-based brain-computer interfaces. / Materka A., Byczuk M. // Electronics Letters. - 2006. - Vol. 42, No. 6. - P. 321-322. ↑

J2185. F. Hatami. Green emission from InP-GaP quantum-dot light-emitting diodes. / F. Hatami, W.T. Masselink, V. Lordi, J.S. Harris Jr. // IEEE Photonics Technology Letters. - 2006. - Vol. 18, No. 7. - P. 895-897. ↑

J2186. Landais P. Self-pulsation dynamics in narrow stripe semiconductor lasers. / Landais P., Lynch S.A., O'Gorman J., Fischer I., Elsasser W. // IEEE Journal of Quantum Electronics. - 2006. - Vol. 42, No. 4. - P. 381-388. ↑

J2187. Mizukami M. Flexible AM OLED panel driven by bottom-contact OTFTs. / Mizukami M., Hirohata N., Iseki T., Ohtawara K., Tada T., Yagyu S., Abe T., Suzuki T., Fujisaki Y., Inoue Y., Tokito S., Kurita T. // IEEE Electron Device Letters. - 2006. - Vol. 27, No. 4. - P. 249-251. ↑

J2188. D.C. O'Brien. Experimental characterization of integrated optical wireless components. / D.C. O'Brien, G.E. Faulkner, K. Jim, D.J. Edwards, E.B. Zyambo, P. Stavrinou, G. Parry, J. Bellon, M.J. Sibley, R.J. Samsudin, D.M. Holburn, V.A. Lalithambika, V.M. Joyner, R.J. Mears. // IEEE Photonics Technology Letters. - 2006. - Vol. 18, No. 8. - P. 977-979. ↑

J2189. Yi-Chen Yu. Contributions of sidewall illumination and current spreading to the light emission of InGaN-GaN light-emitting diode arrays. / Yi-Chen Yu, Chih-Hao Hsieh, Ghien-An Shih, Tzu-Yang Chiu, Dong-Ming Yeh, Chih-Feng Lu, JianJang Huang, C.C. Yang. // IEEE Photonics Technology Letters. - 2006. - Vol. 18, No. 8. - P. 977-979. ↑

983-985. ↑

J2190. Liao M.H. Electroluminescence from the Ge quantum dot MOS tunneling diodes. / Liao M.H., Yu C.-Y., Guo T.-H., Lin C.-H., Liu C.W. // IEEE Electron Device Letters. - 2006. - Vol. 27, No. 4. - P. 252-254. ↑

J2191. De Vusser S. Influence of transistor parameters on the noise margin of organic digital circuits. / De Vusser S., Genoe J., Heremans P. // IEEE Transactions on Electron Devices. - 2006. - Vol. 53, No. 4. - P. 601-610. ↑

J2192. Padgett W.T. Low-frequency wireless communications System-infrared laboratory experiments. / Padgett W.T., Black B.A., Ferguson B.A. // IEEE Transactions on Education. - 2006. - Vol. 49, No. 1. - P. 49-57. ↑

J2193. Sambandan S. Device and circuit level optimization for high performance a-Si:H TFT-based AMOLED displays. / Sambandan S., Striakhilev D., Nathan A. // Journal of Display Technology. - 2006. - Vol. 2, No. 1. - P. 52-59. ↑

J2194. Mullins J. Butterfly effect [light emitting diodes]. IEEE Spectrum. - 2006. - Vol. 43, No. 2. - P. 14. ↑

J2195. Wei Chih Peng. Performance of InGaN-GaN LEDs fabricated using glue bonding on 50-mm Si substrate. / Wei Chih Peng, YewChung Sermon Wu. // IEEE Photonics Technology Letters. - 2006. - Vol. 18, No. 4. - P. 613-615. ↑

J2196. Rapaport A. Review of the properties of up-conversion phosphors for new emissive displays. / Rapaport A., Milliez J., Bass M., Cassanho A., Jenssen H. // Journal of Display Technology. - 2006. - Vol. 2, No. 1. - P. 68-78. ↑

J2197. Hojin Lee. White LED based on polyfluorene Co-polymers blend on plastic substrate. / Hojin Lee, Johnson A.R., Kanicki J. // IEEE Transactions on Electron Devices. - 2006. - Vol. 53, No. 3. - P. 427-434. ↑

J2198. Zhengchun Liu. Electrically bistable memory device based on spin-coated molecular complex thin film. / Zhengchun Liu, Fengliang Xue, Yi Su, Varahramyan K. // IEEE Electron Device Letters. - 2006. - Vol. 27, No. 3. - P. 151-153. ↑

J2199. Dong-Ming Yeh. Control of the color contrast of a polychromatic light-emitting device with CdSe-ZnS nano-crystals on an InGaN-GaN quantum-well structure. / Dong-Ming Yeh, Chi-Feng Huang, Horng-Shyang Chen, Tsung-Yi Tang, Chih-Feng Lu, Yen-Cheng Lu, Huang J.-J., Yang C.C., I-Shuo Liu, Wei-Fang Su. // IEEE Photonics Technology Letters. - 2006. - Vol. 18, No. 5. - P. 712-714. ↑

J2200. Y.J. Lee. GaN-based LEDs with Al-deposited V-shaped sapphire facet mirror. / Y.J. Lee, J.M. Hwang, T.C. Hsu, M.H. Hsieh, M.J. Jou, B.J. Lee, T.C. Lu, H.C. Kuo, S.C. Wang. // IEEE Photonics Technology Letters. - 2006. - Vol. 18, No. 5. - P. 724-726. ↑

J2201. Ching-Ting Lee. White Light Emission of Monolithic Carbon-Implanted InGaN-GaN Light-Emitting Diodes. / Ching-Ting Lee, Ue-Zhi Yang, Chi-Sen Lee, Pou-Sung Chen. // IEEE Photonics Technology Letters. - 2006. - Vol. 18, No. 19. - P. 2029-2031. ↑

J2202. Hung-Chi Chen. Electromagnetic modeling of organic light-emitting devices. / Hung-Chi Chen, Jiun-Haw Lee, Chia-Chiang Shiau, Chih-Chung Yang, Yean-Woei Kiang. // Journal of Lightwave Technology. - 2006. - Vol. 24, No. 6. - P. 2450-2457. ↑

J2203. Cheng-Liang Wang. Improvement in the characteristics of GaN-based light-emitting diodes by inserting AlGaIn-GaN short-period superlattices in GaN underlayers. / Cheng-Liang Wang, Jyh-Rong Gong, Ming-Fa Yeh, Bor-Jen Wu, Wei-Tsai Liao, Tai-Yuan Lin, Chung-Kwei Lin. // IEEE Photonics Technology Letters. - 2006. - Vol. 18, No. 14. - P. 1497-1499. ↑

J2204. Horng-Shyang Chen. White light generation with CdSe-ZnS nanocrystals coated on an InGaIn-GaN quantum-well blue/Green two-wavelength light-emitting diode. / Horng-Shyang Chen, Dong-Ming Yeh, Chih-Feng Lu, Chi-Feng Huang, Wen-Yu Shiao, Huang J.-J., Yang C.C., Liu I.-S., Wei-Fang Su. // IEEE Photonics Technology Letters. - 2006. - Vol. 18, No. 13. - P. 1430-1432. ↑

J2205. Jaehoon Chung. Programmable reconfigurable self-assembly: parallel heterogeneous integration of chip-scale components on planar and nonplanar surfaces. / Jaehoon Chung, Wei Zheng, Hatch T.J., Jacobs

H.O. // Journal of Microelectromechanical Systems. - 2006. - Vol. 15, No. 3. - P. 457-464. ↑

J2206. Dae-Seob Han. Improvement of light extraction efficiency of flip-chip light-emitting diode by texturing the bottom side surface of sapphire substrate. / Dae-Seob Han, Ja-Yeon Kim, Seok-In Na, Sang-Hoon Kim, Ki-Dong Lee, Bongjin Kim, Seong-Ju Park. // IEEE Photonics Technology Letters. - 2006. - Vol. 18, No. 13. - P. 1406-1408. ↑

J2207. Seok-In Na. Selective wet etching of p-GaN for efficient GaN-based light-emitting diodes. / Seok-In Na, Ga-Young Ha, Dae-Seob Han, Seok-Soon Kim, Ja-Yeon Kim, Jae-Hong Lim, Dong-Joon Kim, Kyeong-Ik Min, Seong-Ju Park. // IEEE Photonics Technology Letters. - 2006. - Vol. 18, No. 14. - P. 1512-1514. ↑

J2208. Crozatier V. Highly coherent electronically tunable waveguide extended cavity diode laser. / Crozatier V., Das B.K., Baili G., Gorju G., Bretenaker F., Le Gouet J.-L., Lorgere I., Sohler W. // IEEE Photonics Technology Letters. - 2006. - Vol. 18, No. 14. - P. 1527-1529. ↑

J2209. Jang J.-S. Low turn-on voltage and series resistance of polarization-induced InGaN-GaN LEDs by using p-InGaN/p-GaN superlattice. / Jang J.-S., Donghwan Kim, Tae-Yeon Seong. // IEEE Photonics Technology Letters. - 2006. - Vol. 18, No. 14. - P. 1536-1538. ↑

J2210. Szczesniak T. The 75 mm diameter photonic XP43D2 photomultiplier with the screening grid at the anode for timing experiments. / Szczesniak T., Gierlik M., Kapusta M., Moszynski M., Wolski D., Lavoute P., Rossignol E. // IEEE Transactions on Nuclear Science. - 2006. - Vol. 53, No. 3. - P. 1540-1546. ↑

J2211. Lin Ke. Low-frequency noise measurement and analysis in organic light-emitting diodes. / Lin Ke, Xin Yue Zhao, Kumar R.S., Soo Jin Chua. // IEEE Electron Device Letters. - 2006. - Vol. 27, No. 7. - P. 555-557. ↑

J2212. Young Min Kim. Enhanced brightness and efficiency of organic light-emitting diodes with an LiF in the Alq3. / Young Min Kim, Joo Won Lee, Jae Hoon Jung, Kyeong-Kap Paek, Man Young Sung, Jai Kyeong Kim, Byeong Kwon Ju. // IEEE Electron Device Letters. - 2006. - Vol. 27, No. 7. - P. 558-560. ↑

J2213. Lin Ke. Indium-tin-oxide-free organic light-emitting device. / Lin Ke, Peng Chen, Kumar R.S., Burden A.P., Soo-Jin Chua. // IEEE Transactions on Electron Devices. - 2006. - Vol. 53, No. 6. - P. 1483-1486. ↑

J2214. Walters R.J. Silicon Nanocrystal Field-Effect Light-Emitting Devices. / Walters R.J., Carreras J., Tao Feng, Bell L.D., Atwater H.A. // IEEE Journal of Selected Topics in Quantum Electronics. - 2006. - Vol. 12, No. 6. - P. 1647-1656. ↑

J2215. Shen C.F. Nitride-Based Light Emitting Diodes With Textured Sidewalls and Pillar Waveguides. / Shen C.F., Chang S.J., Ko T.K., Kuo C.T., Shei S.C., Chen W.S., Lee C.T., Chang C.S., Chiou Y.Z. // IEEE Photonics Technology Letters. - 2006. - Vol. 18, No. 23. - P. 2517-2519. ↑

J2216. Shmagin V.B. Effect of Space Charge Region Width on Er-Related Luminescence in Reverse Biased Si:Er-Based Light Emitting Diodes. / Shmagin V.B., Obolensky S.V., Remizov D.Yu., Kuznetsov V.P., Krasilnik Z.F. // IEEE Journal of Selected Topics in Quantum Electronics. - 2006. - Vol. 12, No. 6. - P. 1556-1560. ↑

J2217. Gun Yong Sung. Physics and Device Structures of Highly Efficient Silicon Quantum Dots Based Silicon Nitride Light-Emitting Diodes. / Gun Yong Sung, Nae-Man Park, Jae-Heon Shin, Kyung-Hyun Kim, Tae-Youb Kim, Kwan Sik Cho, Huh C. // IEEE Journal of Selected Topics in Quantum Electronics. - 2006. - Vol. 12, No. 6. - P. 1545-1555. ↑

J2218. Horng R.-H. Efficiency Improvement of GaN-Based LEDs with ITO Texturing Window Layers Using Natural Lithography. / Horng R.-H., Shao-Hua Huang, Chiao-Chih Yang, Dong-Sing Wu. // IEEE Journal of Selected Topics in Quantum Electronics. - 2006. - Vol. 12, No. 6. - P. 1196-1201. ↑

J2219. Camin D. V. Cryogenic Behavior of Optoelectronic Devices for the Transmission of Analog Signals Via Fiber Optics. / Camin D. V., Grassi V. // IEEE Transactions on Nuclear Science. - 2006. - Vol. 53, No. 6. - P. 3929-3933. ↑

J2220. Sung-Ho Baek. Enhanced carrier confinement in AlInGaIn-GaN quantum wells in near ultraviolet light-emitting diodes. / Sung-Ho Baek, Jeom-Oh Kim, Min-Ki Kwon, Il-Kyu Park, Seok-In Na, Ja-Yeon Kim, Bongjin Kim, Seong-Ju Park. // IEEE Photonics Technology Letters. - 2006. - Vol. 18, No. 11. - P. 1276-1278. ↑

- J2221.** Pinckney N. Pulse-width modulation for microcontroller servo control. IEEE Potentials. - 2006. - Vol. 25, No. 1. - P. 27-29. ↑
- J2222.** Tsai C.M. High efficiency and improved ESD characteristics of GaN-based LEDs with naturally textured surface grown by MOCVD. / Tsai C.M., Sheu J.K., Wang P.T., Lai W.C., Shei S.C., Chang S.J., Kuo C.H., Kuo C.W., Su Y.K. // IEEE Photonics Technology Letters. - 2006. - Vol. 18, No. 11. - P. 1213-1215. ↑
- J2223.** Wang Q. J. Equalization of Gaussian-Like Spectra via Optical Lattice Filters With Symmetric-Feedback Structure. / Wang Q. J., Dong Z. G., Zhang Y., Soh Y. C. // Journal of Lightwave Technology. - 2006. - Vol. 24, No. 12. - P. 5103-5110. ↑
- J2224.** Napartovich A.P. Comprehensive above-threshold analysis of antiresonant reflecting optical waveguide edge-emitting diode laser. / Napartovich A.P., Elkin N.N., Sukharev A.G., Troshchieva V.N., Vysotsky D.V., Nesnidal M., Stiers E., Mawst J., Botez D. // IEEE Journal of Quantum Electronics. - 2006. - Vol. 42, No. 6. - P. 589-599. ↑
- J2225.** Yi-An Chang. Design and fabrication of temperature-insensitive InGaP-InGaAlP resonant-cavity light-emitting diodes. / Yi-An Chang, Chun-Lung Yu, I-Tsung Wu, Hao-Chung Kuo, Tien-Chang Lu, Fang-I Lai, Li-Wen Lai, Li-Horng Lai, Shing-Chung Wang. // IEEE Photonics Technology Letters. - 2006. - Vol. 18, No. 16. - P. 1690-1692. ↑
- J2226.** Chang S.J. Nitride-based flip-chip LEDs with transparent Ohmic contacts and reflective mirrors. / Chang S.J., Chen W.S., Lin Y.C., Chang C.S., Ko T.K., Hsu Y.P., Shen C.F., Tsai J.M., Shei S.C. // IEEE Transactions on Advanced Packaging. - 2006. - Vol. 29, No. 3. - P. 403-408. ↑
- J2227.** Hsu-Yu Chang. The Improvement of Polycrystalline Silicon TFTs Fabricated by Employing Periodic Metal Pads. / Hsu-Yu Chang, Chao-Yu Meng, Ming-Wei Tsai, Bo-Chuan Yang, Tzu-Hung Chuang, Si-Chen Lee. // IEEE Transactions on Electron Devices. - 2006. - Vol. 53, No. 8. - P. 1939-1943. ↑
- J2228.** Zhang H.X. Microstripe-array InGaN light-emitting diodes with individually addressable elements. / Zhang H.X., Gu E., Jeon C.W., Gong Z., Dawson M.D., Neil M.A.A., French P.M.W. // IEEE Photonics Technology Letters. - 2006. - Vol. 18, No. 15. - P. 1681-1683. ↑
- J2229.** Long K. Active-Matrix Amorphous-Silicon TFTs Arrays at 180 on Clear Plastic and Glass Substrates for Organic Light-Emitting Displays. / Long K., Kattamis A.Z., Cheng I.-C., Gleskova H., Wagner S., Sturm J.C., Stevenson M., Yu G., O'Regan M. // IEEE Transactions on Electron Devices. - 2006. - Vol. 53, No. 8. - P. 1789-1796. ↑
- J2230.** Ko T.K. Nitride-based flip-chip p-i-n photodiodes. / Ko T.K., Chang S.J., Su Y.K., Chiou Y.Z., Chang C.S., Shei S.C., Sheu J.K., Lai W.C., Lin Y.C., Chen W.S., Shen C.F. // IEEE Transactions on Advanced Packaging. - 2006. - Vol. 29, No. 3. - P. 483-487. ↑
- J2231.** Shin J.H. Si nanocluster sensitization of Er-doped silica for optical amplification using top-pumping visible LEDs. / Shin J.H., Jinku Lee, Hak-seung Han, Ji-Hong Jhe, Jee Soo Chang, Se-Young Seo, Hansuek Lee, Namkyoo Park. // IEEE Journal of Selected Topics in Quantum Electronics. - 2006. - Vol. 12, No. 4. - P. 783-796. ↑
- J2232.** Wei Zheng. Fluidic heterogeneous microsystems assembly and packaging. / Wei Zheng, Jaehoon Chung, Jacobs H.O. // Journal of Microelectromechanical Systems. - 2006. - Vol. 15, No. 4. - P. 864-870. ↑
- J2233.** Foote J. Where's My Holodeck? The New Frontier of Media Display. IEEE Multimedia. - 2006. - Vol. 13, No. 3. - P. 104. ↑
- J2234.** Tan S.C. The effect of different bonding temperatures on the mechanical and electrical performance of NCF-bonded flip-chip-on-flex packages. / Tan S.C., Chan Y.C., Lui N.S.M. // IEEE Transactions on Advanced Packaging. - 2006. - Vol. 29, No. 3. - P. 570-575. ↑
- J2235.** Chingfu Tsou. Silicon-based packaging platform for light-emitting diode. / Chingfu Tsou, Yu-Sheng Huang. // IEEE Transactions on Advanced Packaging. - 2006. - Vol. 29, No. 3. - P. 607-614. ↑
- J2236.** Kane D.J. Detection of high-speed voltage waveforms in GaN devices using electric-field-induced second-harmonic generation. / Kane D.J., Wood W. // IEEE Photonics Technology Letters. - 2006. - Vol. 18, No. 1. - P. 1-3. ↑

15. - P. 1669-1671. ↑

J2237. Diemeer M. Low-cost and low-loss multimode waveguides of photodefinable epoxy. / Diemeer M., Hilderink L., Dekker R., Driessen A. // IEEE Photonics Technology Letters. - 2006. - Vol. 18, No. 15. - P. 1624-1626. ↑

J2238. Man-Fang Huang. Optimization of the active-Layer structure for the deep-UV AlGaIn light-emitting diodes. / Man-Fang Huang, Tsung-Hung Lu. // IEEE Journal of Quantum Electronics. - 2006. - Vol. 42, No. 8. - P. 820-826. ↑

J2239. Witzigmann B. Analysis of temperature-dependent optical gain in GaN-InGaIn quantum-well structures. / Witzigmann B., Laino V., Luisier M., Schwarz U.T., Fischer H., Feicht G., Wegscheider W., Rumbolz C., Lell A., Harle V. // IEEE Photonics Technology Letters. - 2006. - Vol. 18, No. 15. - P. 1600-1602. ↑

J2240. Jae-Soong Lee. GaN-based light-emitting diode structure with monolithically integrated sidewall deflectors for enhanced surface emission. / Jae-Soong Lee, Joonhee Lee, Sunghwan Kim, Heonsu Jeon. // IEEE Photonics Technology Letters. - 2006. - Vol. 18, No. 15. - P. 1588-1590. ↑

J2241. Krieger K. Heart of a new machine [robot that can express different moods]. IEEE Spectrum. - 2006. - Vol. 43, No. 7. - P. 48-51. ↑

J2242. Martin F.J.F. Design of a low-cost optical instrument for pH fluorescence measurements. / Martin F.J.F., Rodriguez J.C.C., Anton J.C.A., Perez J.C.V., Sanchez-Barragan I., Costa-Fernandez J.M., Sanz-Medel A. // IEEE Transactions on Instrumentation and Measurement. - 2006. - Vol. 55, No. 4. - P. 1215-1221. ↑

J2243. Shi J.-W. The improvement in modulation speed of GaN-based Green light-emitting diode (LED) by use of n-type barrier doping for plastic optical fiber (POF) communication. / Shi J.-W., Huang H.-Y., Sheu J.-K., Chen C.-H., Wu Y.-S., Lai W.-C. // IEEE Photonics Technology Letters. - 2006. - Vol. 18, No. 15. - P. 1636-1638. ↑

J2244. Lin R.-M. Using the Taguchi method to improve the brightness of AlGaInP MQW LED by wet oxidation. / Lin R.-M., Jen-Chih Li, Yi-Lun Chou, Meng-Chyi Wu. // IEEE Photonics Technology Letters. - 2006. - Vol. 18, No. 15. - P. 1642-1644. ↑

J2245. Ko T.K. Flip-Chip p(GaN)-i(GaN)-n(AlGaIn) Narrowband UV-A Photosensors. / Ko T.K., Shei S.C., Chang S.J., Su Y.K., Chiou Y.Z., Lin Y.C., Chang C.S., Chen W.S., Wang C.K., Sheu J.K., Lai W.C. // IEEE Sensors Journal. - 2006. - Vol. 6, No. 4. - P. 964-969. ↑

J2246. Griffiths L.A. Introducing Lance Griffiths, Associate Editor for GOLD [The GOLD Report]. IEEE Antennas and Propagation Magazine. - 2006. - Vol. 48, No. 6. - P. 237. ↑

J2247. Shepherd R.L. Low-Cost Surface-Mount LED Gas Sensor. / Shepherd R.L., Yerazunis W.S., King Tong Lau, Diamond D. // IEEE Sensors Journal. - 2006. - Vol. 6, No. 4. - P. 861-866. ↑

J2248. Schmidt V.H. Piezoelectric actuators employing PVDF coated with flexible PEDOT-PSS polymer electrodes. / Schmidt V.H., Lediaev L., Polasik J., Hallenberg J. // IEEE Transactions on Dielectrics and Electrical Insulation. - 2006. - Vol. 13, No. 5. - P. 1140-1148. ↑

J2249. Ciplys D. UV-LED controlled GaN-based SAW phase shifter. / Ciplys D., Shur M.S., Rimeika R., Sinus J., Gaska R., Bilenko Yu., Fareed Q. // Electronics Letters. - 2006. - Vol. 42, No. 21. - P. 1254-1255. ↑

J2250. Taylor D.M. Space charges and traps in polymer electronics. IEEE Transactions on Dielectrics and Electrical Insulation. - 2006. - Vol. 13, No. 5. - P. 1063-1073. ↑

J2251. Labukhin D. Polarization Insensitive Asymmetric Ridge Waveguide Design for Semiconductor Optical Amplifiers and Super Luminescent Light-Emitting Diodes. / Labukhin D., Xun Li. // IEEE Journal of Quantum Electronics. - 2006. - Vol. 42, No. 11. - P. 1137-1143. ↑

J2252. Altafim R.A.C. Piezoelectrets from thermo-formed bubble structures of fluoropolymer-electret films. / Altafim R.A.C., Basso H.C., Altafim R.A.P., Lima L., de Aquino C.V., Neto L.G., Gerhard-Multhaupt R. // IEEE Transactions on Dielectrics and Electrical Insulation. - 2006. - Vol. 13, No. 5. - P. 979-985. ↑

- J2253.** Horng-Shyang Chen. Orange-Red Light-Emitting Diodes Based on a Prestrained InGaN-GaN Quantum-Well Epitaxy Structure. / Horng-Shyang Chen, Chih-Feng Lu, Dong-Ming Yeh, Chi-Feng Huang, Jian-Jang Huang, Chih-Chung Yang. // IEEE Photonics Technology Letters. - 2006. - Vol. 18, No. 21. - P. 2269-2271. ↑
- J2254.** Llobera A. Polymeric MOEMS Variable Optical Attenuator. / Llobera A., Villanueva G., Cadarso V.J., Battgenbach S., Plaza J.A. // IEEE Photonics Technology Letters. - 2006. - Vol. 18, No. 22. - P. 2425-2427. ↑
- J2255.** Ya-Ju Lee. High Light-Extraction GaN-Based Vertical LEDs With Double Diffuse Surfaces. / Ya-Ju Lee, Hao-Chung Kuo, Tien-Chang Lu, Shing-Chung Wang. // IEEE Journal of Quantum Electronics. - 2006. - Vol. 42, No. 12. - P. 1196-1201. ↑
- J2256.** Xi J.-Q. Enhanced Light Extraction in GaInN Light-Emitting Diode With Pyramid Reflector. / Xi J.-Q., Hong Luo, Pasquale A.J., Jong Kyu Kim, Schubert E.F. // IEEE Photonics Technology Letters. - 2006. - Vol. 18, No. 22. - P. 2347-2349. ↑
- J2257.** Chang S.J. Highly Reliable Nitride-Based LEDs With Internal ESD Protection Diodes. / Chang S.J., Shen C.F., Shei S.C., Chuang R.W., Chang C.S., Chen W.S., Ko T.K., Sheu J.K. // IEEE Transactions on Device and Materials Reliability. - 2006. - Vol. 6, No. 3. - P. 442-447. ↑
- J2258.** Rong-Hwei Yeh. Alternating-Current White Thin-Film Light-Emitting Diodes Based on Hydrogenated Amorphous Carbon Layer. / Rong-Hwei Yeh, Tai-Rong Yu, Shih-Yung Lo, Jyh-Wong Hong. // IEEE Photonics Technology Letters. - 2006. - Vol. 18, No. 22. - P. 2341-2343. ↑
- J2259.** Mase K. Ubiquitous Experience Media. / Mase K., Sumi Y., Toriyama T., Tsuchikawa M., Ito S., Iwasawa S., Kogure K., Hagita N. // IEEE Multimedia. - 2006. - Vol. 13, No. 4. - P. 20-29. ↑
- J2260.** Jae-Hoon Lee. A New Poly-Si TFT Current-Mirror Pixel for Active Matrix Organic Light Emitting Diode. / Jae-Hoon Lee, Woo-Jin Nam, Byeong-Koo Kim, Hong-Seok Choi, Yong-Min Ha, Min-Koo Han. // IEEE Electron Device Letters. - 2006. - Vol. 27, No. 10. - P. 830-833. ↑
- J2261.** Sambandan S. Stable Organic LED Displays Using RMS Estimation of Threshold Voltage Dispersion. / Sambandan S., Nathan A. // IEEE Transactions on Circuits and Systems II: Express Briefs. - 2006. - Vol. 53, No. 9. - P. 941-945. ↑
- J2262.** Huh C. Enhancement of Performance of Si Nanocrystal Light-Emitting Diodes by Using Ag Nanodots. / Huh C., Jae-Heon Shin, Kyung-Hyun Kim, Chel-Jong Choi, Kwan Sik Cho, Hong J., Gun Yong Sung. // IEEE Photonics Technology Letters. - 2006. - Vol. 18, No. 19. - P. 2068-2070. ↑
- J2263.** Lin C.H. Enhancement of InGaN-GaN Indium-Tin-Oxide Flip-Chip Light-Emitting Diodes With TiO – SiO Multilayer Stack Omnidirectional Reflector. / Lin C.H., Lai C.F., Ko T.S., Huang H.W., Kuo H.C., Hung Y.Y., Leung K.M., Yu C.C., Tsai R.J., Lee C.K., Lu T.C., Wang S.C. // IEEE Photonics Technology Letters. - 2006. - Vol. 18, No. 19. - P. 2050-2052. ↑
- J2264.** Shi J.-W. InP-Based Transverse Junction Light-Emitting Diodes for White-Light Generation at Infrared Wavelengths. / Shi J.-W., Hung T.-J., Chen Y.-Y., Wu Y.-S., Wei Lin, Ying-Jay Yang. // IEEE Photonics Technology Letters. - 2006. - Vol. 18, No. 19. - P. 2053-2055. ↑
- J2265.** Ho Gyoung Kim. High-reflectivity Al-Pt nanostructured Ohmic contact to p-GaN. / Ho Gyoung Kim, Deb P., Sands T. // IEEE Transactions on Electron Devices. - 2006. - Vol. 53, No. 10. - P. 2448-2453. ↑
- J2266.** Harries M.D. Directional Control of Light-Emitting-Diode Emission Via a Subwavelength-Apertured Metal Surface. / Harries M.D., Summers H.D. // IEEE Photonics Technology Letters. - 2006. - Vol. 18, No. 21. - P. 2197-2199. ↑
- J2267.** Coutinho R.C. High-sensitivity detection of narrowband light in a more intense broadband background using coherence interferogram phase. / Coutinho R.C., Selviah D.R., Griffiths H.D. // Journal of Lightwave Technology. - 2006. - Vol. 24, No. 10. - P. 3654-3662. ↑
- J2268.** Young-Hwan Kim. Poly(dimethylsiloxane)-Based Packaging Technique for Microchip Fluorescence Detection System Applications. / Young-Hwan Kim, Kyeong-Sik Shin, Ji-Yoon Kang, Eun-Gyeong Yang, Kyeong-Kap Paek, Dae-Shik Seo, Byeong-Kwon Ju. // Journal of Microelectromechanical Systems. - 2006. -

Vol. 15, No. 5. - P. 1152-1158. ↑

J2269. Sang-Kyoo Han. IGBT-Based Cost-Effective Energy-Recovery Circuit for Plasma Display Panel. / Sang-Kyoo Han, Jun-Young Lee, Gun-Woo Moon, Myung-Joong Youn. // IEEE Transactions on Industrial Electronics. - 2006. - Vol. 53, No. 5. - P. 1546-1554. ↑

J2270. Kettle J. Localised joule heating in AlGaInP light emitting diodes. / Kettle J., Perks R.M., Dunstan P. // Electronics Letters. - 2006. - Vol. 42, No. 19. - P. 1122-1123. ↑

J2271. Sung G. Y. Physics and Device Structures of Highly Efficient Silicon Quantum Dots Based Silicon Nitride Light-Emitting Diodes. / Sung G. Y., Park N.-M., Shin J.-H., Kim K.-H., Kim T.-Y., Cho K. S., Huh C. // IEEE Journal of Selected Topics in Quantum Electronics. - 2006. - Vol. 12, No. 6. - P. 1545-1555. ↑

J2272. Horng R.-H. Efficiency Improvement of GaN-Based LEDs with ITO Texturing Window Layers Using Natural Lithography. / Horng R.-H., Huang S. H., Yang C.-C., Wu D.-S. // IEEE Journal of Selected Topics in Quantum Electronics. - 2006. - Vol. 12, No. 6. - P. 1196-1201. ↑

J2273. {no data available}. Introduction to the Issue on Silicon Photonics. IEEE Journal of Selected Topics in Quantum Electronics. - 2006. - Vol. 12, No. 6. - P. 1327-1328. ↑

J2274. Matteo Meneghini. High-Temperature Degradation of GaN LEDs Related to Passivation. / Matteo Meneghini, Lorenzo-Roberto Trevisanello, Ulrich Zehnder, Thomas Zahner, Uwe Strauss, Gaudenzio Meneghesso, Enrico Zanoni. // IEEE Transactions on Electron Devices. - 2006. - Vol. 53, No. 12. - P. 2981-2987. ↑

J2275. Grillot P.N. Sixty Thousand Hour Light Output Reliability of AlGaInP Light Emitting Diodes. / Grillot P.N., Krames M.R., Hanmin Zhao, Seng Hup Teoh. // IEEE Transactions on Device and Materials Reliability. - 2006. - Vol. 6, No. 4. - P. 564-574. ↑

J2276. Shmagin V. B. Effect of Space Charge Region Width on Er-Related Luminescence in Reverse Biased Si:Er-Based Light Emitting Diodes. / Shmagin V. B., Obolensky S. V., Remizov D. Y., Kuznetsov V. P., Krasilnik Z. F. // IEEE Journal of Selected Topics in Quantum Electronics. - 2006. - Vol. 12, No. 6. - P. 1556-1560. ↑

J2277. Shao-Hua Huang. Improved Light Extraction of Nitride-Based Flip-Chip Light-Emitting Diodes Via Sapphire Shaping and Texturing. / Shao-Hua Huang, Horng R.-H., Kuo-Sheng Wen, Yi-Feng Lin, Kuo-Wei Yen, Dong-Sing Wu. // IEEE Photonics Technology Letters. - 2006. - Vol. 18, No. 24. - P. 2623-2625. ↑

J2278. Fauchet P.M. Introduction to the Issue on Silicon Photonics. / Fauchet P.M., Shin J.H. // IEEE Journal of Selected Topics in Quantum Electronics. - 2006. - Vol. 12, No. 6. - P. 1327-1328. ↑

J2279. Chakravarty S. Electrically Injected Quantum-Dot Photonic Crystal Microcavity Light-Emitting Arrays With Air-Bridge Contacts. / Chakravarty S., Bhattacharya P., Mi Z. // IEEE Photonics Technology Letters. - 2006. - Vol. 18, No. 24. - P. 2665-2667. ↑

J2280. Walters R. J. Silicon Nanocrystal Field-Effect Light-Emitting Devices. / Walters R. J., J. C., Feng T., Bell L. D., Atwater H. A. // IEEE Journal of Selected Topics in Quantum Electronics. - 2006. - Vol. 12, No. 6. - P. 1647-1656. ↑

J2281. Lu C.-F. Junction Temperature-Controlled Spectrum in a Two-Color InGaN-GaN Quantum-Well Light-Emitting Diode. / Lu C.-F., Yeh D.-M., Chen H.-S., Huang C.-F., Huang J.-J., Yang C. C. // IEEE Photonics Technology Letters. - 2006. - Vol. 18, No. 24. - P. 2671-2673. ↑

J2282. Chia-Pin Lin. Process and Characteristics of Fully Silicided Source/Drain (FSD) Thin-Film Transistors. / Chia-Pin Lin, Yi-Hsuan Hsiao, Bing-Yue Tsui. // IEEE Transactions on Electron Devices. - 2006. - Vol. 53, No. 12. - P. 3086-3094. ↑

J2283. Jong Hak Baek. A Current-Mode Display Driver IC Using Sample-and-Hold Scheme for QVGA Full-Color AMOLED Displays. / Jong Hak Baek, Myunghee Lee, Jae Hoon Lee, Han Su Pae, Chang Ju Lee, Jin Tae Kim, Chang Sik Choi, Hong Kwon Kim, Tae Jin Kim, Ho Kyoong Chung. // IEEE Journal of Solid-State Circuits. - 2006. - Vol. 41, No. 12. - P. 2974-2982. ↑

J2284. Chaji G. R. A Stable Voltage-Programmed Pixel Circuit for a-Si:H AMOLED Displays. / Chaji G. R.,

Nathan A. // Journal of Display Technology. - 2006. - Vol. 2, No. 4. - P. 347-358. ↑

J2285. Shun-Cheng Hsu. Enhanced Light Output in Roughened GaN-Based Light-Emitting Diodes Using Electrodeless Photoelectrochemical Etching. / Shun-Cheng Hsu, Chong-Yi Lee, Jung-Min Hwang, Juh-Yuh Su, Dong-Sing Wu, Horng R.-H. // IEEE Photonics Technology Letters. - 2006. - Vol. 18, No. 23. - P. 2472-2474. ↑

J2286. Jones W.D. Blood Test. IEEE Spectrum. - 2006. - Vol. 43, No. 11. - P. 16-18. ↑

J2287. Moore S.K. Laser on Silicon. IEEE Spectrum. - 2006. - Vol. 43, No. 11. - P. 18. ↑

J2288. Kim J.-H. An Output Channel Nonuniformity Compensation Driving Method in Flat Panel Display Driving Circuits. / Kim J.-H., Ahn S.-S., Kwon C. H., Kim S.-Y., Lee J.-S., Choi B.-D. // Journal of Display Technology. - 2006. - Vol. 2, No. 4. - P. 386-392. ↑

J2289. Striakhilev D. Amorphous Silicon Display Backplanes on Plastic Substrates. / Striakhilev D., Nathan A., Vygranenko Y., Servati P., Lee C.-H., Sazonov A. // Journal of Display Technology. - 2006. - Vol. 2, No. 4. - P. 364-371. ↑

J2290. Shi J.-W. Phosphor-Free GaN-Based Transverse Junction Light Emitting Diodes for the Generation of White Light. / Shi J.-W., Huang H.-Y., Wang C.-K., Sheu J.-K., Lai W.-C., Wu Y.-S., Chen C.-H., Chu J.-T., Kuo H.-C., Wei-Ping Lin, Tsung-Hsun Yang, Chyi J.-I. // IEEE Photonics Technology Letters. - 2006. - Vol. 18, No. 24. - P. 2593-2595. ↑

J2291. Park J. Temperature-Dependent Dynamic Behaviors of Organic Light-Emitting Diode. / Park J., Kawakami Y. // Journal of Display Technology. - 2006. - Vol. 2, No. 4. - P. 333-340. ↑

J2292. Lu R. Quantitative Comparison of Color Performances Between IPS and MVA LCDs. / Lu R., Hong Q., Wu S.-T., Peng K.-H., Hsieh H.-S. // Journal of Display Technology. - 2006. - Vol. 2, No. 4. - P. 319-326. ↑

J2293. Mu H. Measurement of Electron Mobility in Alq3 From Optical Modulation Measurements in Multilayer Organic Light-Emitting Diodes. / Mu H., Klotzkin D. // Journal of Display Technology. - 2006. - Vol. 2, No. 4. - P. 341-346. ↑

J2294. Meerheim Rico. Ultrastable and efficient red organic light emitting diodes with doped transport layers. / Meerheim Rico, Walzer Karsten, Pfeiffer Martin, Leo Karl. // Applied Physics Letters. - 2006. - Vol. 89, No. 6. - P. 061111-061111-3. ↑

J2295. Saxena Kanchan. Spatial coherence properties of electroluminescence from Al q 3 -based organic light emitting diodes. / Saxena Kanchan, Mehta Dalip Singh, Srivastava Ritu, Kamalasanan M. N. // Applied Physics Letters. - 2006. - Vol. 89, No. 6. - P. 061124-061124-3. ↑

J2296. Chen Szu-Yi. Stable inverted bottom-emitting organic electroluminescent devices with molecular doping and morphology improvement. / Chen Szu-Yi, Chu Ta-Ya, Chen Jenn-Fang, Su Chien-Ying, Chen Chin H. // Applied Physics Letters. - 2006. - Vol. 89, No. 5. - P. 053518-053518-3. ↑

J2297. Chu Ta-Ya. Highly efficient and stable inverted bottom-emission organic light emitting devices. / Chu Ta-Ya, Chen Jenn-Fang, Chen Szu-Yi, Chen Chao-Jung, Chen Chin H. // Applied Physics Letters. - 2006. - Vol. 89, No. 5. - P. 053503-053503-3. ↑

J2298. Guo Tzung-Fang. Organic oxide/Al composite cathode in small molecular organic light-emitting diodes. / Guo Tzung-Fang, Yang Fuh-Shun, Tsai Zen-Jay, Wen Ten-Chin, Wu Ching-In, Chung Chia-Tin. // Applied Physics Letters. - 2006. - Vol. 89, No. 5. - P. 053507-053507-3. ↑

J2299. Kim Baek-Hyun. Ni /Au contact to silicon quantum dot light-emitting diodes for the enhancement of carrier injection and light extraction efficiency. / Kim Baek-Hyun, Cho Chang-Hee, Park Seong-Ju, Park Nae-Man, Sung Gun Yong. // Applied Physics Letters. - 2006. - Vol. 89, No. 6. - P. 063509-063509-3. ↑

J2300. McGuinness Colin D. Excitation of fluorescence decay using a 265 nm pulsed light-emitting diode: Evidence for aqueous phenylalanine rotamers. / McGuinness Colin D., Macmillan Alexander M., Sagoo Kulwinder, McLoskey David, Birch David J. S. // Applied Physics Letters. - 2006. - Vol. 89, No. 6. - P. 063901-063901-3. ↑

- J2301.** Okumoto Kenji. Green fluorescent organic light-emitting device with external quantum efficiency of nearly 10%. / Okumoto Kenji, Kanno Hiroshi, Hamaa Yuji, Takahashi Hisakazu, Shibata Kenichi. // Applied Physics Letters. - 2006. - Vol. 89, No. 6. - P. 063504-063504-3. ↑
- J2302.** Lin Yuan-Yu. Integration of polymer light-emitting diode and polymer waveguide on Si substrate. / Lin Yuan-Yu, Cheng Chung, Liao Hua-Hsien, Horng Sheng-Fu, Meng Hsin-Fei, Hsu Chain-Shu. // Applied Physics Letters. - 2006. - Vol. 89, No. 6. - P. 063501-063501-3. ↑
- J2303.** Shin H. J. Degradation mechanism of organic light-emitting device investigated by scanning photoelectron microscopy coupled with peel-off technique. / Shin H. J., Jung M. C., Chung J., Kim K., Lee J. C., Lee S. P. // Applied Physics Letters. - 2006. - Vol. 89, No. 6. - P. 063503-063503-3. ↑
- J2304.** Du G. T. Room temperature defect related electroluminescence from ZnO homojunctions grown by ultrasonic spray pyrolysis. / Du G. T., Liu W. F., Bian J. M., Hu L. Z., Liang H. W., Wang X. S., Liu A. M., Yang T. P. // Applied Physics Letters. - 2006. - Vol. 89, No. 5. - P. 052113-052113-3. ↑
- J2305.** Zhang S. T. Role of hole playing in improving performance of organic light-emitting devices with an Al₂O₃ layer inserted at the cathode-organic interface. / Zhang S. T., Zhou Y. C., Zhao J. M., Zhan Y. Q., Wang Z. J., Wu Y., Ding X. M., Hou X. Y. // Applied Physics Letters. - 2006. - Vol. 89, No. 4. - P. 043502-043502-3. ↑
- J2306.** Cheng Gang. White organic light-emitting devices with a phosphorescent multiple emissive layer. / Cheng Gang, Zhang Yingfang, Zhao Yi, Lin Yuanyuan, Ruan Chunyan, Liu Shiyong, Fei Teng, Ma Yuguang, Cheng Yanxiang. // Applied Physics Letters. - 2006. - Vol. 89, No. 4. - P. 043504-043504-3. ↑
- J2307.** Pavesi M. Temperature dependence of the electrical activity of localized defects in InGaN-based light emitting diodes. / Pavesi M., Manfredi M., Rossi F., Meneghini M., Zanoni E., Zehnder U., Strauss U. // Applied Physics Letters. - 2006. - Vol. 89, No. 4. - P. 041917-041917-3. ↑
- J2308.** Luo Hong. Trapped whispering-gallery optical modes in white light-emitting diode lamps with remote phosphor. / Luo Hong, Kim Jong Kyu, Xi Yangang Andrew, Schubert E. Fred, Cho Jaehee, Sone Cheolsoo, Park Yongjo. // Applied Physics Letters. - 2006. - Vol. 89, No. 4. - P. 041125-041125-3. ↑
- J2309.** Losio Paolo A. Singlet excimer electroluminescence within N,N'-di-1-naphthalenyl-N,N'-diphenyl-[1,1'-biphenyl]-4,4'-diamine based diodes. / Losio Paolo A., Khan Rizwan U. A., Gunter Peter, Yap Boon Kar, Wilson Jo S., Bradley Donal D. C. // Applied Physics Letters. - 2006. - Vol. 89, No. 4. - P. 041914-041914-3. ↑
- J2310.** Yang Yu. Highly transparent and conductive double-layer oxide thin films as anodes for organic light-emitting diodes. / Yang Yu, Wang Lian, Yan He, Jin Shu, Marks Tobin J., Li Shuyou. // Applied Physics Letters. - 2006. - Vol. 89, No. 5. - P. 051116-051116-3. ↑
- J2311.** Huang Chi-Feng. Prestrained effect on the emission properties of In Ga N /Ga N quantum-well structures. / Huang Chi-Feng, Tang Tsung-Yi, Huang Jeng-Jie, Shiao Wen-Yu, Yang C. C., Hsu Chih-Wei, Chen L. C. // Applied Physics Letters. - 2006. - Vol. 89, No. 5. - P. 051913-051913-3. ↑
- J2312.** Guo Tzung-Fang. High-brightness top-emissive polymer light-emitting diodes utilizing organic oxide/Al/Ag composite cathode. / Guo Tzung-Fang, Yang Fuh-Shun, Tsai Zen-Jay, Feng Guan-Weng, Wen Ten-Chin, Hsieh Sung-Nien, Chung Chia-Tin, Wu Ching-In. // Applied Physics Letters. - 2006. - Vol. 89, No. 5. - P. 051103-051103-3. ↑
- J2313.** Chen Shufen. Improved light outcoupling for top-emitting organic light-emitting devices. / Chen Shufen, Jie Zhonghai, Zhao Zhenyuan, Cheng Gang, Wu Zhijun, Zhao Yi, Quan Baofu, Liu Shiyong, Li Xue, Xie Wenfa. // Applied Physics Letters. - 2006. - Vol. 89, No. 4. - P. 043505-043505-3. ↑
- J2314.** Cho Y. Optical properties of neodymium-containing polymethylmethacrylate films for the organic light emitting diode color filter. / Cho Y., Choi Y. K., Sohn S. H. // Applied Physics Letters. - 2006. - Vol. 89, No. 5. - P. 051102-051102-3. ↑
- J2315.** Sun J. M. Increase of blue electroluminescence from Ce-doped Si O₂ layers through sensitization by Gd³⁺ ions. / Sun J. M., Prucnal S., Skorupa W., Helm M., Rebohle L., Gebel T. // Applied Physics Letters. - 2006. - Vol. 89, No. 9. - P. 091908-091908-3. ↑
- J2316.** Chen Horng-Shyang. Mesa-size-dependent color contrast in flip-chip blue/green two-color In Ga N /Ga

N multi-quantum-well micro-light-emitting diodes. / Chen Horng-Shyang, Yeh Dong-Ming, Lu Chih-Feng, Huang Chi-Feng, Lu Yen-Cheng, Chen Cheng-Yen, Huang Jian-Jang, Yang C. C. // Applied Physics Letters. - 2006. - Vol. 89, No. 9. - P. 093501-093501-3. ↑

J2317. Koyama T. Prospective emission efficiency and in-plane light polarization of nonpolar m-plane In_xGa_{1-x}N/GaN blue light emitting diodes fabricated on freestanding GaN substrates. / Koyama T., Onuma T., Masui H., Chakraborty A., Haskell B. A., Keller S., Mishra U. K., Speck J. S., Nakamura S., DenBaars S. P., Sota T., Chichibu S. F. // Applied Physics Letters. - 2006. - Vol. 89, No. 9. - P. 091906-091906-3. ↑

J2318. Krier A. Mid-infrared electroluminescence at room temperature from InAsSb multi-quantum-well light-emitting diodes. / Krier A., Stone M., Zhuang Q. D., Liu Po-Wei, Tsai G., Lin H. H. // Applied Physics Letters. - 2006. - Vol. 89, No. 9. - P. 091110-091110-3. ↑

J2319. Chao Chia-Hsin. Theoretical demonstration of enhancement of light extraction of flip-chip GaN light-emitting diodes with photonic crystals. / Chao Chia-Hsin, Chuang S. L., Wu Tzong-Lin. // Applied Physics Letters. - 2006. - Vol. 89, No. 9. - P. 091116-091116-3. ↑

J2320. Montenegro Renata. New possibilities for the measurement of wavelength-resolved photoconductivity. / Montenegro Renata, Inocente-Junior Nilson R., Frejlich Jaime. // Review of Scientific Instruments. - 2006. - Vol. 77, No. 4. - P. 043905-043905-6. ↑

J2321. Beaudoin Normand. Simple hybrid current-voltage source for the characterization of organic light-emitting devices. / Beaudoin Normand, Essiambre Sophie, Gauvin Serge. // Review of Scientific Instruments. - 2006. - Vol. 77, No. 2. - P. 026102-026102-3. ↑

J2322. Kirkup L. System for measuring the junction temperature of a light emitting diode immersed in liquid nitrogen. / Kirkup L., Kalceff W., McCredie G. // Review of Scientific Instruments. - 2006. - Vol. 77, No. 4. - P. 046107-046107-3. ↑

J2323. Liang Hongye. Precision of gray level response time measurements of medical liquid crystal display. / Liang Hongye, Badano Aldo. // Review of Scientific Instruments. - 2006. - Vol. 77, No. 6. - P. 065104-065104-5. ↑

J2324. Chance B. Simple ac circuit for breast cancer detection and object detection. / Chance B., Zhao Z., Wen S., Chen Y. // Review of Scientific Instruments. - 2006. - Vol. 77, No. 6. - P. 064301-064301-10. ↑

J2325. Schwartz Gregor. Highly efficient white organic light emitting diodes comprising an interlayer to separate fluorescent and phosphorescent regions. / Schwartz Gregor, Fehse Karsten, Pfeiffer Martin, Walzer Karsten, Leo Karl. // Applied Physics Letters. - 2006. - Vol. 89, No. 8. - P. 083509-083509-3. ↑

J2326. Oh Jae-Jin. Highly efficient organic light-emitting diodes based on donor-acceptor small molecules. / Oh Jae-Jin, Kim Ki-Won, Kim Min-Sook, Kwon Tae-Woo, Park Dong-Kyu, Cho Seong-Jin, Woo Hyung-Suk. // Applied Physics Letters. - 2006. - Vol. 89, No. 7. - P. 073504-073504-3. ↑

J2327. Huang Fei. Efficient ultraviolet-blue polymer light-emitting diodes based on a fluorene-based non-conjugated polymer. / Huang Fei, Niu Yu-Hua, Liu Michelle S., Zhou Xing-Hua, Tian Yan-Qing, Jen Alex K.-Y. // Applied Physics Letters. - 2006. - Vol. 89, No. 8. - P. 081104-081104-3. ↑

J2328. van t Erve O. M. J. Remanent electrical spin injection from Fe into AlGaAs/GaAs light emitting diodes. / van t Erve O. M. J., Kioseoglou G., Hanbicki A. T., Li C. H., Jonker B. T. // Applied Physics Letters. - 2006. - Vol. 89, No. 7. - P. 072505-072505-3. ↑

J2329. Shchekin O. B. High performance thin-film flip-chip InGaN-GaN light-emitting diodes. / Shchekin O. B., Epler J. E., Trottier T. A., Margalith T., Steigerwald D. A., Holcomb M. O., Martin P. S., Krames M. R. // Applied Physics Letters. - 2006. - Vol. 89, No. 7. - P. 071109-071109-3. ↑

J2330. Wang Zhengliang. Red-light-emitting diodes fabricated by near-ultraviolet InGaN chips with molybdate phosphors. / Wang Zhengliang, Liang Hongbin, Wang Jing, Gong Menglian, Su Qiang. // Applied Physics Letters. - 2006. - Vol. 89, No. 7. - P. 071921-071921-3. ↑

J2331. Williams Evan L. Organic light-emitting diodes having exclusive near-infrared electrophosphorescence. / Williams Evan L., Li Jian, Jabbour Ghassan E. // Applied Physics Letters. - 2006. - Vol. 89, No. 8. - P. 083506- ↑

083506-3.

J2332. Cho Jeong Ho. Enhancement of electron injection in polymer light-emitting diodes with a supramolecular insulating nanolayer on the bottom cathode. / Cho Jeong Ho, Lee Hwa Sung, Jang Yunseok, Lee Yongkyun, Kwon Soon Kab, Jang Jin, Cho Kilwon. // Applied Physics Letters. - 2006. - Vol. 89, No. 8. - P. 083508-083508-3. ↑

J2333. Zhu Yanxu. Enhanced output of GaN-based light-emitting diodes with stripe-contact electrodes. / Zhu Yanxu, Xu Chen, Liang Ting, Da Xiaoli, Zhang Jianming, Chen Libing, Shen Guangdi. // Applied Physics Letters. - 2006. - Vol. 89, No. 8. - P. 081127-081127-3. ↑

J2334. McMurdy John W. Monolithic microspectrometer using tunable ferroelectric liquid crystals. / McMurdy John W., Crawford Gregory P., Jay Gregory D. // Applied Physics Letters. - 2006. - Vol. 89, No. 8. - P. 081105-081105-3. ↑

J2335. Wang T. Greatly improved performance of 340 nm light emitting diodes using a very thin GaN interlayer on a high temperature AlN buffer layer. / Wang T., Lee K. B., Bai J., Parbrook P. J., Airey R. J., Wang Q., Hill G., Ranalli F., Cullis A. G. // Applied Physics Letters. - 2006. - Vol. 89, No. 8. - P. 081126-081126-3. ↑

J2336. Won Yu-Ho. Tunable full-color-emitting La 0.827 Al 11.9 O 19.09 :Eu 2+ ,Mn 2+ phosphor for application to warm white-light-emitting diodes. / Won Yu-Ho, Jang Ho Seong, Im Won Bin, Jeon Duk Young, Lee Jeong Soo. // Applied Physics Letters. - 2006. - Vol. 89, No. 23. - P. 231909-231909-3. ↑

J2337. Zhou Gang. Efficient blue electroluminescence from neutral alcohol-soluble polyfluorenes with aluminum cathode. / Zhou Gang, Geng Yanhou, Cheng Yanxiang, Xie Zhiyuan, Wang Lixiang, Jing Xiabin, Wang Fosong. // Applied Physics Letters. - 2006. - Vol. 89, No. 23. - P. 233501-233501-3. ↑

J2338. Srinivasan S. Carrier dynamics and electrostatic potential variation in InGaIn quantum wells grown on {112 2} GaN pyramidal planes. / Srinivasan S., Stevens M., Ponce F. A., Omiya H., Mukai T. // Applied Physics Letters. - 2006. - Vol. 89, No. 23. - P. 231908-231908-3. ↑

J2339. Xin Q. Improved electroluminescent performances of europium-complex based devices by doping into electron-transporting/hole-blocking host. / Xin Q., Li W. L., Che G. B., Su W. M., Sun X. Y., Chu B., Li B. // Applied Physics Letters. - 2006. - Vol. 89, No. 22. - P. 223524-223524-3. ↑

J2340. Kang Dun-Yen. Modeling white light-emitting diodes with phosphor layers. / Kang Dun-Yen, Wu Enboa, Wang Da-Ming. // Applied Physics Letters. - 2006. - Vol. 89, No. 23. - P. 231102-231102-3. ↑

J2341. Zhou L. Vertical injection thin-film Al Ga N /Al Ga N multiple-quantum-well deep ultraviolet light-emitting diodes. / Zhou L., Epler J. E., Krames M. R., Goetz W., Gherasimova M., Ren Z., Han J., Kneissl M., Johnson N. M. // Applied Physics Letters. - 2006. - Vol. 89, No. 24. - P. 241113-241113-3. ↑

J2342. Hao M. Highly efficient GaN-based light emitting diodes with micropits. / Hao M., Egawa T., Ishikawa H. // Applied Physics Letters. - 2006. - Vol. 89, No. 24. - P. 241907-241907-3. ↑

J2343. Xie Rong-Jun. Wavelength-tunable and thermally stable Li -alpha -sialon :Eu 2+ oxynitride phosphors for white light-emitting diodes. / Xie Rong-Jun, Hiroaki Naoto, Mitomo Mamoru, Sakuma Ken, Kimura Naoki. // Applied Physics Letters. - 2006. - Vol. 89, No. 24. - P. 241103-241103-3. ↑

J2344. Wang D. Broad wavelength modulating and design of organic white diode based on lighting by using exciplex emission from mixed acceptors. / Wang D., Li W. L., Su Z. S., Li T. L., Chu B., Bi D. F., Chen L. L., Su W. M., He H. // Applied Physics Letters. - 2006. - Vol. 89, No. 23. - P. 233511-233511-3. ↑

J2345. Chong Lai-Wan. Self-assembled monolayer-modified Ag anode for top-emitting polymer light-emitting diodes. / Chong Lai-Wan, Lee Yuh-Lang, Wen Ten-Chin, Guo Tzung-Fang. // Applied Physics Letters. - 2006. - Vol. 89, No. 23. - P. 233513-233513-3. ↑

J2346. Sakaguchi Koichi. Color-variable organic light-emitting device by external light irradiation. / Sakaguchi Koichi, Oosawa Takeru, Chikamatsu Masayuki, Yoshida Yuji, Azumi Reiko, Yase Kiyoshi. // Applied Physics Letters. - 2006. - Vol. 89, No. 22. - P. 223520-223520-3. ↑

J2347. Fan Zhiyong. Electrical and photoconductive properties of vertical ZnO nanowires in high density arrays. / Fan Zhiyong, Dutta Deepanshu, Chien Chung-Jen, Chen Hsiang-Yu, Brown Evan C., Chang Pai-Chun,

Lu Jia G. // Applied Physics Letters. - 2006. - Vol. 89, No. 21. - P. 213110-213110-3. ↑

J2348. Niu Xiaodi. White polymeric light-emitting diodes with high color rendering index. / Niu Xiaodi, Ma Liang, Yao Bing, Ding Junqiao, Tu Guoli, Xie Zhiyuan, Wang Lixiang. // Applied Physics Letters. - 2006. - Vol. 89, No. 21. - P. 213508-213508-3. ↑

J2349. Peng Yu-Yun. Optical characteristics and microstructure of ZnO quantum dots-SiO₂ nanocomposite films prepared by sputtering methods. / Peng Yu-Yun, Hsieh Tsung-Eong, Hsu Chia-Hung. // Applied Physics Letters. - 2006. - Vol. 89, No. 21. - P. 211909-211909-3. ↑

J2350. Prineas J. P. Cascaded active regions in 2.4 μm GaInAsSb light-emitting diodes for improved current efficiency. / Prineas J. P., Olesberg J. T., Yager J. R., Cao C., Coretsopoulos C., Reddy M. H. M. // Applied Physics Letters. - 2006. - Vol. 89, No. 21. - P. 211108-211108-3. ↑

J2351. Mehta M. GaSb quantum-well-based "buffer-free" vertical light emitting diode monolithically embedded within a GaAs cavity incorporating interfacial misfit arrays. / Mehta M., Balakrishnan G., Huang S., Khoshakhlagh A., Jallipalli A., Patel P., Kutty M. N., Dawson L. R., Huffaker D. L. // Applied Physics Letters. - 2006. - Vol. 89, No. 21. - P. 211110-211110-3. ↑

J2352. Pode R. B. Fabrication of 5,6,11,12 -tetraphenyl-naphthacene doped 4-bis(2,2-diphenylvinyl)-1,1-biphenyl white organic light-emitting device. / Pode R. B., Lee C. J., Han J. I., Moon D. G. // Applied Physics Letters. - 2006. - Vol. 89, No. 22. - P. 223514-223514-3. ↑

J2353. Kim Soo Young. In situ determination of interface dipole energy in organic light emitting diodes with iridium interfacial layer using synchrotron radiation photoemission spectroscopy. / Kim Soo Young, Lee Jong-Lam. // Applied Physics Letters. - 2006. - Vol. 89, No. 22. - P. 223515-223515-3. ↑

J2354. Lee Tae-Woo. Molecular monolayer modification of the cathode in organic light-emitting diodes. / Lee Tae-Woo, Hsu Julia W. P. // Applied Physics Letters. - 2006. - Vol. 89, No. 22. - P. 223511-223511-3. ↑

J2355. Kim Sun Woong. Highly efficient green phosphorescent single-layered organic light-emitting devices. / Kim Sun Woong, Park Jin Ho, Oh Seung Seok, Kim Doo Youp, Choi Eun Ha, Cho Guang Sup, Seo Yoon Ho, Kang Seung Oun, Park Byoungchoo, Saito Yuki, Watanabe Nobuhiro, Takezoe Hideo, Watanabe Junji. // Applied Physics Letters. - 2006. - Vol. 89, No. 21. - P. 213511-213511-3. ↑

J2356. Leong Eunice S. P. Directional edge-emitting UV random laser diodes. / Leong Eunice S. P., Yu S. F., Lau S. P. // Applied Physics Letters. - 2006. - Vol. 89, No. 22. - P. 221109-221109-3. ↑

J2357. Lockwood R. Nonresonant carrier tunneling in arrays of silicon nanocrystals. / Lockwood R., Hryciw A., Meldrum A. // Applied Physics Letters. - 2006. - Vol. 89, No. 26. - P. 263112-263112-3. ↑

J2358. Huang Qiang. Quantum efficiency enhancement in top-emitting organic light-emitting diodes as a result of enhanced intrinsic quantum yield. / Huang Qiang, Reineke Sebastian, Walzer Karsten, Pfeiffer Martin, Leo Karl. // Applied Physics Letters. - 2006. - Vol. 89, No. 26. - P. 263512-263512-3. ↑

J2359. Tse S. C. Electron transport in naphthylamine-based organic compounds. / Tse S. C., Kwok K. C., So S. K. // Applied Physics Letters. - 2006. - Vol. 89, No. 26. - P. 262102-262102-3. ↑

J2360. Kawasaki Koji. Vertical AlGaIn deep ultraviolet light emitting diode emitting at 322 nm fabricated by the laser lift-off technique. / Kawasaki Koji, Koike Choshio, Aoyagi Yoshinobu, Takeuchi Misaichi. // Applied Physics Letters. - 2006. - Vol. 89, No. 26. - P. 261114-261114-3. ↑

J2361. Liao M. H. Infrared emission from Ge metal-insulator-semiconductor tunneling diodes. / Liao M. H., Cheng T.-H., Liu C. W. // Applied Physics Letters. - 2006. - Vol. 89, No. 26. - P. 261913-261913-3. ↑

J2362. Peng Wei Chih. Improved luminance intensity of InGaIn-GaN light-emitting diode by roughening both the p-GaN surface and the undoped-GaN surface. / Peng Wei Chih, Wu Yew Chung Sermon. // Applied Physics Letters. - 2006. - Vol. 89, No. 4. - P. 041116-041116-3. ↑

J2363. Wunderer Thomas. Bright semipolar GaInN/GaN blue light emitting diode on side facets of selectively grown GaN stripes. / Wunderer Thomas, Bruckner Peter, Neubert Barbara, Scholz Ferdinand, Feneberg Martin, Lipski Frank, Schirra Martin, Thonke Klaus. // Applied Physics Letters. - 2006. - Vol. 89, No. 4.

- P. 041121-041121-3. ↑

J2364. Di Chong-an. Effective modification of indium tin oxide for improved hole injection in organic light-emitting devices. / Di Chong-an, Yu Gui, Liu Yunqi, Xu Xinjun, Song Yabin, Zhu Daoben. // Applied Physics Letters. - 2006. - Vol. 89, No. 3. - P. 033502-033502-3. ↑

J2365. Gersen H. Dissociation of iridium(III) phosphorescent emitters upon adsorption on Cu(110) revealed by scanning tunneling microscopy. / Gersen H., Schaub R., Xu W., Stensgaard I., Laegsgaard E., Linderorth T. R., Besenbacher F., Nazeeruddin Md. K., Graetzel M. // Applied Physics Letters. - 2006. - Vol. 89, No. 26. - P. 264102-264102-3. ↑

J2366. Carcia P. F. Ca test of Al₂O₃ gas diffusion barriers grown by atomic layer deposition on polymers. / Carcia P. F., McLean R. S., Reilly M. H., Groner M. D., George S. M. // Applied Physics Letters. - 2006. - Vol. 89, No. 3. - P. 031915-031915-3. ↑

J2367. Seo Soon-min. Dry formation of polymer hole injection layer for top emitting organic light emitting diodes. / Seo Soon-min, Kim Jong H., Lee Hong H. // Applied Physics Letters. - 2006. - Vol. 89, No. 25. - P. 253515-253515-3. ↑

J2368. Liang C. J. Color tunable organic light-emitting diodes by using europium organometallic complex. / Liang C. J., Choy Wallace C. H. // Applied Physics Letters. - 2006. - Vol. 89, No. 25. - P. 251108-251108-3. ↑

J2369. Cao Jin. MoO_x modified Ag anode for top-emitting organic light-emitting devices. / Cao Jin, Jiang XueYin, Zhang ZhiLin. // Applied Physics Letters. - 2006. - Vol. 89, No. 25. - P. 252108-252108-3. ↑

J2370. Park Eun-Hyun. InGaN-light emitting diode with high density truncated hexagonal pyramid shaped p-GaN hillocks on the emission surface. / Park Eun-Hyun, Ferguson Ian T., Jeon Soo-Kun, Park Joong-Seo, Yoo Tae-Kyung. // Applied Physics Letters. - 2006. - Vol. 89, No. 25. - P. 251106-251106-3. ↑

J2371. Liu Chunbo. Triphenylamine-functionalized rhenium (I) complex as a highly efficient yellow-green emitter in electrophosphorescent devices. / Liu Chunbo, Li Jiang, Li Bin, Hong Ziruo, Zhao Feifei, Liu Shiyong, Li Wenlian. // Applied Physics Letters. - 2006. - Vol. 89, No. 24. - P. 243511-243511-3. ↑

J2372. Tsai Yung-Cheng. Long-lifetime, high-efficiency white organic light-emitting diodes with mixed host composing double emission layers. / Tsai Yung-Cheng, Jou Jwo-Huei. // Applied Physics Letters. - 2006. - Vol. 89, No. 24. - P. 243521-243521-3. ↑

J2373. Matsushima Toshinori. Extremely low voltage organic light-emitting diodes with p-doped alpha-sexithiophene hole transport and n-doped phenyldipyrrenylphosphine oxide electron transport layers. / Matsushima Toshinori, Adachi Chihaya. // Applied Physics Letters. - 2006. - Vol. 89, No. 25. - P. 253506-253506-3. ↑

J2374. Lee C. J. Red electrophosphorescent top emission organic light-emitting device with Ca/Ag semitransparent cathode. / Lee C. J., Pode R. B., Han J. I., Moon D. G. // Applied Physics Letters. - 2006. - Vol. 89, No. 25. - P. 253508-253508-3. ↑

J2375. Chang Chan-Ching. Highly power efficient organic light-emitting diodes with a p-doping layer. / Chang Chan-Ching, Hsieh Ming-Ta, Chen Jenn-Fang, Hwang Shiao-Wen, Chen Chin H. // Applied Physics Letters. - 2006. - Vol. 89, No. 25. - P. 253504-253504-3. ↑

J2376. Ho Meng-Huan. Highly efficient deep blue organic electroluminescent device based on 1-methyl-9,10-di(1-naphthyl)anthracene. / Ho Meng-Huan, Wu Yao-Shan, Wen Shih-Wen, Lee Meng-Ting, Chen Teng-Ming, Chen Chin H., Kwok Kwong-Chau, So Shu-Kong, Yeung Kai-Tai, Cheng Yuen-Kit, Gao Zhi-Qiang. // Applied Physics Letters. - 2006. - Vol. 89, No. 25. - P. 252903-252903-3. ↑

J2377. Kim Sung Hyun. Relationship between indium tin oxide surface treatment and hole injection in C60 modified devices. / Kim Sung Hyun, Jang Jyongsik, Lee Jun Yeob. // Applied Physics Letters. - 2006. - Vol. 89, No. 25. - P. 253501-253501-3. ↑

J2378. Koch Norbert. Green polyfluorene-conducting polymer interfaces: Energy level alignment and device performance. / Koch Norbert, Elschner Andreas, Johnson Robert L. // Journal of Applied Physics. - 2006. - Vol. 100, No. 2. - P. 024512-024512-5. ↑

- J2379.** Wang D. Y. Effect of exciplex formation on organic light emitting diodes based on rare-earth complex. / Wang D. Y., Li W. L., Chu B., Liang C. J., Hong Z. R., Li M. T., Wei H. Z., Xin Q., Niu J. H., Xu J. B. // Journal of Applied Physics. - 2006. - Vol. 100, No. 2. - P. 024506-024506-6. ↑
- J2380.** Fukuyama Hiroyuki. Single crystalline aluminum nitride films fabricated by nitriding alpha -Al₂O₃. / Fukuyama Hiroyuki, Kusunoki Shin-ya, Hakomori Akira, Hiraga Kenji. // Journal of Applied Physics. - 2006. - Vol. 100, No. 2. - P. 024905-024905-7. ↑
- J2381.** Li J. Multilayer green polymer light emitting diodes with improved efficiency and lifetime. / Li J., Sano T., Hirayama Y., Tomita T., Fujii H., Wakisaka K. // Journal of Applied Physics. - 2006. - Vol. 100, No. 3. - P. 034506-034506-5. ↑
- J2382.** Sawyer S. Current and optical noise of GaN /AlGaIn light emitting diodes. / Sawyer S., Rumyantsev S. L., Shur M. S., Pala N., Bilenko Yu., Zhang J. P., Hu X., Lunev A., Deng J., Gaska R. // Journal of Applied Physics. - 2006. - Vol. 100, No. 3. - P. 034504-034504-5. ↑
- J2383.** Neyts Kristiaan. Inhomogeneous luminance in organic light emitting diodes related to electrode resistivity. / Neyts Kristiaan, Marescaux Matthias, Nieto Angel Ullan, Elschner Andreas, Lovenich Wilfried, Fehse Karsten, Huang Qiang, Walzer Karsten, Leo Karl. // Journal of Applied Physics. - 2006. - Vol. 100, No. 11. - P. 114513-114513-4. ↑
- J2384.** Ong Vincent K. S. A method of accurately determining the positions of the edges of depletion regions in semiconductor junctions. / Ong Vincent K. S., Kurniawan Oka, Moldovan Grigore, Humphreys Colin J. // Journal of Applied Physics. - 2006. - Vol. 100, No. 11. - P. 114501-114501-4. ↑
- J2385.** van Gemmern Philipp. Influence of carrier conductivity and injection on efficiency and chromaticity in small-molecule white organic light-emitting diodes based on 4,4' -bis (2,2' -diphenylvinyl)-1,1' -spirobiphenyl and rubrene. / van Gemmern Philipp, van Elsbergen Volker, Grabowski Stefan Peter, Boerner Herbert, Lobl Hans-Peter, Becker Heinrich, Kalisch Holger, Heuken Michael, Jansen Rolf H. // Journal of Applied Physics. - 2006. - Vol. 100, No. 12. - P. 123707-123707-6. ↑
- J2386.** Zhou Y. C. Exciton migration in organic thin films. / Zhou Y. C., Wu Y., Ma L. L., Zhou J., Ding X. M., Hou X. Y. // Journal of Applied Physics. - 2006. - Vol. 100, No. 2. - P. 023712-023712-5. ↑
- J2387.** Li Cheng. Temperature dependence of electroluminescence from silicon p-i-n light-emitting diodes. / Li Cheng, Lai Hongkai, Chen Songyan, Suemasu T., Hasegawa F. // Journal of Applied Physics. - 2006. - Vol. 100, No. 2. - P. 023506-023506-4. ↑
- J2388.** Pingree L. S. C. Field dependent negative capacitance in small-molecule organic light-emitting diodes. / Pingree L. S. C., Russell M. T., Marks T. J., Hersam M. C. // Journal of Applied Physics. - 2006. - Vol. 100, No. 4. - P. 044502-044502-10. ↑
- J2389.** Huang Qiang. Performance improvement of top-emitting organic light-emitting diodes by an organic capping layer: An experimental study. / Huang Qiang, Walzer Karsten, Pfeiffer Martin, Leo Karl, Hofmann Michael, Stubinger Thomas. // Journal of Applied Physics. - 2006. - Vol. 100, No. 6. - P. 064507-064507-5. ↑
- J2390.** Choi Ho Won. Effect of magnesium oxide buffer layer on performance of inverted top-emitting organic light-emitting diodes. / Choi Ho Won, Kim Soo Young, Kim Woong-Kwon, Hong Kihyon, Lee Jong-Lam. // Journal of Applied Physics. - 2006. - Vol. 100, No. 6. - P. 064106-064106-6. ↑
- J2391.** Kim Youngkyoo. Doping effect of blue light-emitting electron transport molecule in blue organic light-emitting devices. / Kim Youngkyoo, Moon Byoungseok, Ha Chang-Sik. // Journal of Applied Physics. - 2006. - Vol. 100, No. 6. - P. 064511-064511-6. ↑
- J2392.** Cheun H. Polymer light emitting diodes and poly(di-n -octylfluorene) thin films as fabricated with a microfluidics applicator. / Cheun H., Rugheimer P. P., Larson B. J., Gopalan P., Lagally M. G., Winokur M. J. // Journal of Applied Physics. - 2006. - Vol. 100, No. 7. - P. 073510-073510-7. ↑
- J2393.** Sun Yiru. Organic light emitting devices with enhanced outcoupling via microlenses fabricated by imprint lithography. / Sun Yiru, Forrest Stephen R. // Journal of Applied Physics. - 2006. - Vol. 100, No. 7. - P. 073106-073106-6. ↑

- J2394.** Okumoto Kenji. Organic light-emitting devices using polyacene derivatives as a hole-transporting layer. / Okumoto Kenji, Kanno Hiroshi, Hamada Yuji, Takahashi Hisakazu, Shibata Kenichi. // Journal of Applied Physics. - 2006. - Vol. 100, No. 4. - P. 044507-044507-5. ↑
- J2395.** Catchpole K. R. Absorption enhancement due to scattering by dipoles into silicon waveguides. / Catchpole K. R., Pillai S. // Journal of Applied Physics. - 2006. - Vol. 100, No. 4. - P. 044504-044504-8. ↑
- J2396.** Wu L. K. Far-infrared upconversion imaging devices: Imaging characteristics and quantum efficiency. / Wu L. K., Shen W. Z. // Journal of Applied Physics. - 2006. - Vol. 100, No. 4. - P. 044508-044508-6. ↑
- J2397.** Krummacher B. C. General method to evaluate substrate surface modification techniques for light extraction enhancement of organic light emitting diodes. / Krummacher B. C., Mathai M. K., Choong V., Choulis S. A., So F., Winnacker A. // Journal of Applied Physics. - 2006. - Vol. 100, No. 5. - P. 054702-054702-6. ↑
- J2398.** Wang Y. D. Nonlithographic nanopatterning through anodic aluminum oxide template and selective growth of highly ordered GaN nanostructures. / Wang Y. D., Zang K. Y., Chua S. J. // Journal of Applied Physics. - 2006. - Vol. 100, No. 5. - P. 054306-054306-4. ↑
- J2399.** Chae S. W. Improvement of electrical and optical properties of p-Ga N Ohmic metals under ultraviolet light irradiation annealing processes. / Chae S. W., Yoon S. K., Kwak J. S., Park Y. H., Kim T. G. // and Films Journal of Vacuum Science & Technology A: Vacuum, Surfaces. - 2006. - Vol. 24, No. 3. - P. 634-636. ↑
- J2400.** Wang Fuzhi. Voltage-controlled multicolor emitting devices. / Wang Fuzhi, Wang Ping, Fan Xing, Dang Xiangnan, Zhen Changgua, Zou Dechun, Kim Eun Hwa, Lee Do Nam, Kim Byeong Hyo. // Applied Physics Letters. - 2006. - Vol. 89, No. 18. - P. 183519-183519-3. ↑
- J2401.** Py C. Hole mobility and electroluminescence properties of a dithiophene indenofluorene. / Py C., Gorjanc T. C., Hadizad T., Zhang J., Wang Z. Y. // and Films Journal of Vacuum Science & Technology A: Vacuum, Surfaces. - 2006. - Vol. 24, No. 3. - P. 654-656. ↑
- J2402.** Chen Chin-Hsiang. In Ga N /Ga N blue light emitting diodes with modulation-doped Al Ga N /Ga N heterostructure layers. and Films Journal of Vacuum Science & Technology A: Vacuum, Surfaces. - 2006. - Vol. 24, No. 4. - P. 1001-1004. ↑
- J2403.** Chaji G. Reza. Stable a-Si :H circuits based on short-term stress stability of amorphous silicon thin film transistors. / Chaji G. Reza, Safavian Nader, Nathan Arokia. // and Films Journal of Vacuum Science & Technology A: Vacuum, Surfaces. - 2006. - Vol. 24, No. 3. - P. 875-878. ↑
- J2404.** Baidus N. V. Electrical spin injection in forward biased Schottky diodes based on InGaAs-GaAs quantum well heterostructures. / Baidus N. V., Vasilevskiy M. I., Gomes M. J. M., Dorokhin M. V., Demina P. B., Uskova E. A., Zvonkov B. N., Kulakovskii V. D., Brichkin A. S., Chernenko A. V., Zaitsev S. V. // Applied Physics Letters. - 2006. - Vol. 89, No. 18. - P. 181118-181118-3. ↑
- J2405.** Tien Tran Quoc. Thermal properties and degradation behavior of red-emitting high-power diode lasers. / Tien Tran Quoc, Weik Fritz, Tonn Jens W., Sumpf Bernd, Zorn Martin, Zeimer Ute, Erbert Gotz. // Applied Physics Letters. - 2006. - Vol. 89, No. 18. - P. 181112-181112-3. ↑
- J2406.** Morii Katsuyuki. Encapsulation-free hybrid organic-inorganic light-emitting diodes. / Morii Katsuyuki, Ishida Masaya, Takashima Takeshi, Shimoda Tatsuya, Wang Qing, Nazeeruddin Md. Khaja, Gratzel Michael. // Applied Physics Letters. - 2006. - Vol. 89, No. 18. - P. 183510-183510-3. ↑
- J2407.** Lee Young Gu. Fabrication of highly efficient and stable doped red organic light-emitting device using 2-methyl-9,10-di(2-naphthyl)anthracene and tris(8-hydroxyquinolinato)aluminum as cohost materials. / Lee Young Gu, Lee Ho-Nyeon, Kang Sung Kee, Oh Tae Sik, Lee Soonil, Koh Ken Ha. // Applied Physics Letters. - 2006. - Vol. 89, No. 18. - P. 183515-183515-3. ↑
- J2408.** Choukri Hakim. White organic light-emitting diodes with fine chromaticity tuning via ultrathin layer position shifting. / Choukri Hakim, Fischer Alexis, Forget Sebastien, Chenais Sebastien, Castex Marie-Claude, Ades Dominique, Siove Alain, Geffroy Bernard. // Applied Physics Letters. - 2006. - Vol. 89, No. 18. - P. 183513-183513-3. ↑
- J2409.** Nee Tzer-En. Observations of electrical and luminescence anomalies in In Ga N /Ga N blue light-

emitting diodes. / Nee Tzer-En, Wang Jen-Cheng, Shen Hui-Tang, Lin Chung-Han, Wu Ya-Fen. // and Films Journal of Vacuum Science & Technology A: Vacuum, Surfaces. - 2006. - Vol. 24, No. 4. - P. 1016-1019. ↑

J2410. Ran G. Z. Highly transparent cathodes comprised of rare earth and Au stacked layers for top-emission organic light emitting diodes. / Ran G. Z., Zhao W. Q., Dai L., Qin G. G. // Journal of Applied Physics. - 2006. - Vol. 100, No. 11. - P. 113107-113107-4. ↑

J2411. Otsuji N. Electroluminescence efficiency of blue In Ga N /Ga N quantum-well diodes with and without an n-In Ga N electron reservoir layer. / Otsuji N., Fujiwara K., Sheu J. K. // Journal of Applied Physics. - 2006. - Vol. 100, No. 11. - P. 113105-113105-7. ↑

J2412. Masui Hisashi. Light-polarization characteristics of electroluminescence from In Ga N /Ga N light-emitting diodes prepared on (112 2) -plane GaN. / Masui Hisashi, Baker Troy J., Iza Michael, Zhong Hong, Nakamura Shuji, DenBaars Steven P. // Journal of Applied Physics. - 2006. - Vol. 100, No. 11. - P. 113109-113109-5. ↑

J2413. Kohary K. Modeling organic light-emitting diodes incorporating nanocrystal quantum dots. / Kohary K., Burlakov V. M., Pettifor D. G. // Journal of Applied Physics. - 2006. - Vol. 100, No. 11. - P. 114315-114315-7. ↑

J2414. Jia D. Long persistent light emitting diode. / Jia D., Hunter D. N. // Journal of Applied Physics. - 2006. - Vol. 100, No. 11. - P. 113125-113125-6. ↑

J2415. Jarikov Viktor V. Improving operating lifetime of organic light-emitting diodes with polycyclic aromatic hydrocarbons as aggregating light-emitting-layer additives. Journal of Applied Physics. - 2006. - Vol. 100, No. 1. - P. 014901-014901-7. ↑

J2416. Xi Y. Quantitative assessment of diffusivity and specularity of surface-textured reflectors for light extraction in light-emitting diodes. / Xi Y., Li X., Kim J. K., Mont F., Gessmann Th., Luo H., Schubert E. F. // and Films Journal of Vacuum Science & Technology A: Vacuum, Surfaces. - 2006. - Vol. 24, No. 4. - P. 1627-1630. ↑

J2417. Ray S. K. Design, growth, fabrication, and characterization of In As /Ga As 1.3 mcm quantum dot broadband superluminescent light emitting diode. / Ray S. K., Groom K. M., Alexander R., Kennedy K., Liu H. Y., Hopkinson M., Hogg R. A. // Journal of Applied Physics. - 2006. - Vol. 100, No. 10. - P. 103105-103105-6. ↑

J2418. Cabalu J. S. High power ultraviolet light emitting diodes based on Ga N /Al Ga N quantum wells produced by molecular beam epitaxy. / Cabalu J. S., Bhattacharyya A., Thomidis C., Friel I., Moustakas T. D., Collins C. J., Komninou Ph. // Journal of Applied Physics. - 2006. - Vol. 100, No. 10. - P. 104506-104506-5. ↑

J2419. Watkins N. J. Direct observation of the evolution of occupied and unoccupied energy levels of two silole derivatives at their interfaces with magnesium. / Watkins N. J., Makinen A. J., Gao Y., Uchida M., Kafafi Z. H. // Journal of Applied Physics. - 2006. - Vol. 100, No. 10. - P. 103706-103706-6. ↑

J2420. Slinker Jason D. Direct 120 V, 60 Hz operation of an organic light emitting device. / Slinker Jason D., Rivnay Jonathan, DeFranco John A., Bernards Daniel A., Gorodetsky Alon A., Parker Sara T., Cox Marshall P., Rohl Richard, Malliaras George G., Flores-Torres Samuel, Abruna Hector D. // Journal of Applied Physics. - 2006. - Vol. 99, No. 7. - P. 074502-074502-5. ↑

J2421. Gerhardt N. C. Spin injection light-emitting diode with vertically magnetized ferromagnetic metal contacts. / Gerhardt N. C., Hovel S., Brenner C., Hofmann M. R., Lo F.-Y., Reuter D., Wieck A. D., Schuster E., Keune W., Halm S., Bacher G., Westerholt K. // Journal of Applied Physics. - 2006. - Vol. 99, No. 7. - P. 073907-073907-6. ↑

J2422. Huby N. Injection and transport processes in organic light emitting diodes based on a silole derivative. / Huby N., Hirsch L., Wantz G., Vignau L., Barriere A. S., Parneix J. P., Aubouy L., Gerbier P. // Journal of Applied Physics. - 2006. - Vol. 99, No. 8. - P. 084907-084907-6. ↑

J2423. Kamiyama S. Extremely high quantum efficiency of donor-acceptor-pair emission in N-and-B-doped 6H-Si C. / Kamiyama S., Maeda T., Nakamura Y., Iwaya M., Amano H., Akasaki I., Kinoshita H., Furusho T., Yoshimoto M., Kimoto T., Suda J., Henry A., Ivanov I. G., Bergman J. P., Monemar B., Onuma T., Chichibu S. F. // Journal of Applied Physics. - 2006. - Vol. 99, No. 9. - P. 093108-093108-4. ↑

J2424. Van Dorpe P. Design of the tunnel contacts and the transport region of all-electrical spin-injection-

detection devices. / Van Dorpe P., Vanheertum R., Boukari H., Van Roy W., Borghs G. // Journal of Applied Physics. - 2006. - Vol. 99, No. 8. - P. 08S702-08S702-3. ↑

J2425. Adawi Ali M. Improving the light extraction efficiency of red-emitting conjugated polymer light emitting diodes. / Adawi Ali M., Connolly Liam G., Whittaker David M., Lidzey David G., Smith Euan, Roberts Matthew, Qureshi Faisal, Foden Clare, Athanassopoulou Nicky. // Journal of Applied Physics. - 2006. - Vol. 99, No. 5. - P. 054505-054505-8. ↑

J2426. Rossi Francesca. Influence of short-term low current dc aging on the electrical and optical properties of InGaN blue light-emitting diodes. / Rossi Francesca, Pavesi Maura, Meneghini Matteo, Salviati Giancarlo, Manfredi Manfredo, Meneghesso Gaudenzio, Castaldini Antonio, Cavallini Anna, Rigutti Lorenzo, Strass Uwe, Zehnder Ulrich, Zanoni Enrico. // Journal of Applied Physics. - 2006. - Vol. 99, No. 5. - P. 053104-053104-7. ↑

J2427. Luo Yichun. Correlation between electroluminescence efficiency and stability in organic light-emitting devices under pulsed driving conditions. / Luo Yichun, Aziz Hany, Popovic Zoran D., Xu Gu. // Journal of Applied Physics. - 2006. - Vol. 99, No. 5. - P. 054508-054508-4. ↑

J2428. Konezny S. J. Modeling the influence of charge traps on single-layer organic light-emitting diode efficiency. / Konezny S. J., Smith D. L., Galvin M. E., Rothberg L. J. // Journal of Applied Physics. - 2006. - Vol. 99, No. 6. - P. 064509-064509-12. ↑

J2429. Tsukagoshi Kazuhito. Organic light-emitting diode driven by organic thin film transistor on plastic substrates. / Tsukagoshi Kazuhito, Tanabe Jun, Yagi Iwao, Shigeto Kunji, Yanagisawa Keiichi, Aoyagi Yoshinobu. // Journal of Applied Physics. - 2006. - Vol. 99, No. 6. - P. 064506-064506-5. ↑

J2430. Buyanova I. A. Optical characterization of ZnMnO-based dilute magnetic semiconductor structures. / Buyanova I. A., Chen W. M., Ivill M. P., Pate R., Norton D. P., Pearton S. J., Dong J. W., Osinsky A., Hertog B., Dabiran A. M., Chow P. P. // Journal of Vacuum Science & Technology B: Microelectronics and Nanometer Structures. - 2006. - Vol. 24, No. 1. - P. 259-262. ↑

J2431. Huang Kun-Fu. 1.32 μm InAs /GaAs quantum-dot resonant-cavity light-emitting diodes grown by metalorganic chemical vapor deposition. / Huang Kun-Fu, Lee Feng-Ming, Hu Chih-Wei, Peng Te-Chin, Wu Meng-Chyi, Lin Chia-Chien, Hsieh Tung-Po, Chyi Jen-Inn. // Journal of Vacuum Science & Technology B: Microelectronics and Nanometer Structures. - 2006. - Vol. 24, No. 4. - P. 1922-1924. ↑

J2432. Huang H. W. Fabrication and photoluminescence of InGaN-based nanorods fabricated by plasma etching with nanoscale nickel metal islands. / Huang H. W., Chu J. T., Hsueh T. H., Ou-Yang M. C., Kuo H. C., Wang S. C. // Journal of Vacuum Science & Technology B: Microelectronics and Nanometer Structures. - 2006. - Vol. 24, No. 4. - P. 1909-1912. ↑

J2433. Odnoblyudov V. A. Amber GaNP -based light-emitting diodes directly grown on GaP (100) substrates. / Odnoblyudov V. A., Tu C. W. // Journal of Vacuum Science & Technology B: Microelectronics and Nanometer Structures. - 2006. - Vol. 24, No. 5. - P. 2202-2204. ↑

J2434. Santiago Guillermo D. Blue light-emitting diode-based, enhanced resonant excitation of longitudinal acoustic modes in a closed pipe with application to N O 2. / Santiago Guillermo D., Gonzalez Martin G., Peuriot Alejandro L., Gonzalez Francisco, Slezak Veronica B. // Review of Scientific Instruments. - 2006. - Vol. 77, No. 2. - P. 023108-023108-3. ↑

J2435. Hsu Feng-Chang. Portable digital microscope apparatus. / Hsu Feng-Chang, Lee Chien-Shing, Huang Kuo-Cheng, Chen Po-Jui, Chen Fong-Zhi, Liao Tai-Shan. // Review of Scientific Instruments. - 2006. - Vol. 77, No. 11. - P. 116106-116106-2. ↑

J2436. Choi H. W. Honeycomb GaN micro-light-emitting diodes. / Choi H. W., Chua S. J. // Journal of Vacuum Science & Technology B: Microelectronics and Nanometer Structures. - 2006. - Vol. 24, No. 2. - P. 800-802. ↑

J2437. Jang Soohwan. Simulation of vertical and lateral ZnO light-emitting diodes. / Jang Soohwan, Chen J. J., Ren F., Yang Hyuck-Soo, Han Sang-Youn, Norton D. P., Pearton S. J. // Journal of Vacuum Science & Technology B: Microelectronics and Nanometer Structures. - 2006. - Vol. 24, No. 2. - P. 690-694. ↑

J2438. Kato Nanako. Amorphous selenium based photodetector driven by field emission current from N-doped diamond cold cathode. / Kato Nanako, Saito Ichitaro, Yamaguchi Hisato, Okamura Hideki, Okano Ken, Yamada

Takatoshi, Butler Tim, Rupesinghe Nalin L., Amaratunga Gehan A. J. // Journal of Vacuum Science & Technology B: Microelectronics and Nanometer Structures. - 2006. - Vol. 24, No. 2. - P. 1035-1039. ↑

J2439. Kuznetsov Vladimir V. Molecular beam epitaxy growth of midinfrared "W" light emitting diodes on InAs. / Kuznetsov Vladimir V., Wicks G. W. // Journal of Vacuum Science & Technology B: Microelectronics and Nanometer Structures. - 2006. - Vol. 24, No. 3. - P. 1548-1552. ↑

J2440. Kao Po-Ching. Fabrication of organic light-emitting devices on flexible substrates using a combined roller imprinting and photolithography-patterning technique. / Kao Po-Ching, Chu Sheng-Yuan, Zhan Chuan-Yi, Hsu Lien-Chung, Liao Wen-Chang. // Journal of Vacuum Science & Technology B: Microelectronics and Nanometer Structures. - 2006. - Vol. 24, No. 3. - P. 1278-1282. ↑

J2441. Rumyantsev S. L. Wavelength-resolved low-frequency noise of Ga In N /Ga N green light emitting diodes. / Rumyantsev S. L., Wetzel C., Shur M. S. // Journal of Applied Physics. - 2006. - Vol. 100, No. 8. - P. 084506-084506-4. ↑

J2442. Pitarch Angeles. Impedance of space-charge-limited currents in organic light-emitting diodes with double injection and strong recombination. / Pitarch Angeles, Garcia-Belmonte Germa, Bisquert Juan, Bolink Henk J. // Journal of Applied Physics. - 2006. - Vol. 100, No. 8. - P. 084502-084502-5. ↑

J2443. Jarikov Viktor V. Operating longevity of organic light-emitting diodes with perylene derivatives as aggregating light-emitting-layer additives: Expansion of the emission zone. / Jarikov Viktor V., Young Ralph H., Vargas J. Ramon, Brown Christopher T., Klubek Kevin P., Liao Liang-Sheng. // Journal of Applied Physics. - 2006. - Vol. 100, No. 9. - P. 094907-094907-7. ↑

J2444. Deng X. Y. Top-emitting polymer light-emitting diodes with environmentally stable cathodes. / Deng X. Y., Ho M. K., Wong K. Y. // Journal of Applied Physics. - 2006. - Vol. 99, No. 1. - P. 016103-016103-3. ↑

J2445. Xie W. F. High-efficiency white organic light-emitting devices using a blue iridium complex to sensitize a red fluorescent dye. / Xie W. F., Chew S. L., Lee C. S., Lee S. T., Wang P. F., Kwong H. L. // Journal of Applied Physics. - 2006. - Vol. 100, No. 9. - P. 096114-096114-3. ↑

J2446. Han Sijin. Highly efficient organic light-emitting diodes with metal/fullerene anode. / Han Sijin, Yuan Yanyan, Lu Zheng-Hong. // Journal of Applied Physics. - 2006. - Vol. 100, No. 7. - P. 074504-074504-6. ↑

J2447. Qiu X. J. Tunable, narrow, and enhanced electroluminescent emission from porous-silicon-reflector-based organic microcavities. / Qiu X. J., Tan X. W., Wang Z., Liu G. Y., Xiong Z. H. // Journal of Applied Physics. - 2006. - Vol. 100, No. 7. - P. 074503-074503-6. ↑

J2448. Perks R. M. Theoretical and experimental analysis of current spreading in AlGaInP light emitting diodes. / Perks R. M., Porch A., Morgan D. V., Kettle J. // Journal of Applied Physics. - 2006. - Vol. 100, No. 8. - P. 083109-083109-7. ↑

J2449. Zhang Yanguang. Lifetime study of polymer light-emitting electrochemical cells. / Zhang Yanguang, Gao Jun. // Journal of Applied Physics. - 2006. - Vol. 100, No. 8. - P. 084501-084501-8. ↑

J2450. Yang Su-Hua. Stable and highly bright white organic light-emitting diode based on 4,4',4"-tris(N-3-methylphenyl-N-phenyl-amino)-triphenylamine. / Yang Su-Hua, Liu Mine-Huang, Su Yan-Kuin. // Journal of Applied Physics. - 2006. - Vol. 100, No. 8. - P. 083111-083111-4. ↑

J2451. Suzuki Toshiharu. Flat panel displays for ubiquitous product applications and related impurity doping technologies. Journal of Applied Physics. - 2006. - Vol. 99, No. 11. - P. 111101-111101-15. ↑

J2452. Luszczyńska Beata. Poly(N -vinylcarbazole) doped with a pyrazoloquinoline dye: A deep blue light-emitting composite for light-emitting diode applications. / Luszczyńska Beata, Dobruchowska Ewa, Glowacki Ireneusz, Ulanski Jacek, Jaiser Frank, Yang Xiaohui, Neher Dieter, Danel Andrzej. // Journal of Applied Physics. - 2006. - Vol. 99, No. 2. - P. 024505-024505-4. ↑

J2453. Maslov A. V. Distribution of optical emission between guided modes and free space in a semiconductor nanowire. / Maslov A. V., Bakunov M. I., Ning C. Z. // Journal of Applied Physics. - 2006. - Vol. 99, No. 2. - P. 024314-024314-10. ↑

- J2454.** Thomson J. D. The influence of acceptor anneal temperature on the performance of InGaN/GaN quantum well light-emitting diodes. / Thomson J. D., Pope I. A., Smowton P. M., Blood P., Lynch R. J., Hill G., Wang T., Parbrook P. // Journal of Applied Physics. - 2006. - Vol. 99, No. 2. - P. 024507-024507-7. ↑
- J2455.** Poplavskyy Dmitry. Bipolar carrier transport in a conjugated polymer by complex admittance spectroscopy. / Poplavskyy Dmitry, So Franky. // Journal of Applied Physics. - 2006. - Vol. 99, No. 3. - P. 033707-033707-9. ↑
- J2456.** Kondakov D. Y. Voltammetric study of Bphen electron-transport layer in contact with Li F /Al cathode in organic light-emitting diodes. Journal of Applied Physics. - 2006. - Vol. 99, No. 2. - P. 024901-024901-4. ↑
- J2457.** Weik Fritz. A room-temperature continuous-wave operating midinfrared light emitting device. / Weik Fritz, Steinmeyer Gunter, Tomm Jens W., Glatthaar Regine, Vetter Uwe, Nurnus Joachim, Lambrecht Armin. // Journal of Applied Physics. - 2006. - Vol. 99, No. 11. - P. 114506-114506-4. ↑
- J2458.** Brewer P. J. Influence of carrier injection on the electromodulation response of trap-rich polymer light-emitting diodes. / Brewer P. J., deMello A. J., deMello J. C., Lane P. A., Bradley D. D. C., Fletcher R., O'Brien J. // Journal of Applied Physics. - 2006. - Vol. 99, No. 11. - P. 114502-114502-5. ↑
- J2459.** Kyono Takashi. Influence of residual oxygen impurity in quaternary InAlGaN multiple-quantum-well active layers on emission efficiency of ultraviolet light-emitting diodes on GaN substrates. / Kyono Takashi, Hirayama Hideki, Akita Katsushi, Nakamura Takao, Adachi Masahiro, Ando Koshi. // Journal of Applied Physics. - 2006. - Vol. 99, No. 11. - P. 114509-114509-7. ↑
- J2460.** Bai J. Optical properties of AlGaIn /GaN multiple quantum well structure by using a high-temperature AlN buffer on sapphire substrate. / Bai J., Wang T., Comming P., Parbrook P. J., David J. P. R., Cullis A. G. // Journal of Applied Physics. - 2006. - Vol. 99, No. 2. - P. 023513-023513-4. ↑
- J2461.** Chen T.-H. Effects of metal-doped indium-tin-oxide buffer layers in organic light-emitting devices. / Chen T.-H., Wu T. J., Chen J. Y., Liou Y. // Journal of Applied Physics. - 2006. - Vol. 99, No. 11. - P. 114515-114515-6. ↑
- J2462.** Jeong Min-Chang. Electroluminescence from ZnO nanowires in n-Zn O film/ZnO nanowire array/p-GaN film heterojunction light-emitting diodes. / Jeong Min-Chang, Oh Byeong-Yun, Ham Moon-Ho, Myoung Jae-Min. // Applied Physics Letters. - 2006. - Vol. 88, No. 20. - P. 202105-202105-3. ↑
- J2463.** Choulis Stelios A. Highly efficient organic electroluminescent device with modified cathode. / Choulis Stelios A., Mathai Mathew K., Choong Vi-En, So Franky. // Applied Physics Letters. - 2006. - Vol. 88, No. 20. - P. 203502-203502-3. ↑
- J2464.** Andreev B. A. 1.54 mcm Si:Er light emitting diode with memory function. / Andreev B. A., Krasilnik Z. F., Kryzhkov D. I., Kuznetsov V. P., Gregorkiewicz T., Jantsch W. // Applied Physics Letters. - 2006. - Vol. 88, No. 20. - P. 201101-201101-3. ↑
- J2465.** Yang X. H. Blue polymer electrophosphorescent devices with different electron-transporting oxadiazoles. / Yang X. H., Jaiser F., Klinger S., Neher D. // Applied Physics Letters. - 2006. - Vol. 88, No. 2. - P. 021107-021107-3. ↑
- J2466.** Itskos G. Oblique Hanle measurements of InAs /GaAs quantum dot spin-light emitting diodes. / Itskos G., Harbord E., Clowes S. K., Clarke E., Cohen L. F., Murray R., Van Dorpe P., Van Roy W. // Applied Physics Letters. - 2006. - Vol. 88, No. 2. - P. 022113-022113-3. ↑
- J2467.** Wang Z. J. Control of carrier transport in organic semiconductors by aluminum doping. / Wang Z. J., Wu Y., Zhou Y. C., Zhou J., Zhang S. T., Ding X. M., Hou X. Y., Zhu Z. Q. // Applied Physics Letters. - 2006. - Vol. 88, No. 22. - P. 222112-222112-3. ↑
- J2468.** Sun H. Y. Fluorocarbon film as cathode protective coating in organic light-emitting devices. / Sun H. Y., Lau K. M., Lau K. C., Chan M. Y., Fung M. K., Lee C. S., Lee S. T. // Applied Physics Letters. - 2006. - Vol. 88, No. 22. - P. 223503-223503-3. ↑
- J2469.** Su Zisheng. White-electrophosphorescent devices based on copper complexes using 2-(4-biphenyl)-5-(4-tert-butyl-phenyl)-1,3,4-oxadiazole as chromaticity-tuning layer. / Su Zisheng, Che Guangbo, Li Wenlian, Su

Wenming, Li Mingtao, Chu Bei, Li Bin, Zhang Zhiqiang, Hu Zhizhi. // Applied Physics Letters. - 2006. - Vol. 88, No. 21. - P. 213508-213508-3. ↑

J2470. Choulis Stelios A. Influence of metallic nanoparticles on the performance of organic electrophosphorescence devices. / Choulis Stelios A., Mathai Mathew K., Choong Vi-En. // Applied Physics Letters. - 2006. - Vol. 88, No. 21. - P. 213503-213503-3. ↑

J2471. Cheng Chuan-Hui. 1.1 mcm near-infrared electrophosphorescence from organic light-emitting diodes based on copper phthalocyanine. / Cheng Chuan-Hui, Fan Zhao-Qi, Yu Shu-Kun, Jiang Wen-Hai, Wang Xu, Du Guo-Tong, Chang Yu-Chun, Ma Chun-Yu. // Applied Physics Letters. - 2006. - Vol. 88, No. 21. - P. 213505-213505-3. ↑

J2472. Jou Jwo-Huei. Efficient, color-stable fluorescent white organic light-emitting diodes with single emission layer by vapor deposition from solvent premixed deposition source. / Jou Jwo-Huei, Chiu Yung-Sheng, Wang Chung-Pei, Wang Ren-Yang, Hu Huei-Ching. // Applied Physics Letters. - 2006. - Vol. 88, No. 19. - P. 193501-193501-3. ↑

J2473. Chakraborty Arpan. Interdigitated multipixel arrays for the fabrication of high-power light-emitting diodes with very low series resistances. / Chakraborty Arpan, Shen L., Masui H., DenBaars S. P., Mishra U. K. // Applied Physics Letters. - 2006. - Vol. 88, No. 18. - P. 181120-181120-3. ↑

J2474. Kim Jae Wook. Observation of minority-carrier traps in In Ga N /Ga N multiple-quantum-well light-emitting diodes during deep-level transient spectroscopy measurements. / Kim Jae Wook, Song G. Hugh, Lee Jhang W. // Applied Physics Letters. - 2006. - Vol. 88, No. 18. - P. 182103-182103-3. ↑

J2475. Peng Wei Chih. Enhanced performance of an InGa_N-Ga_N light-emitting diode by roughening the undoped-GaN surface and applying a mirror coating to the sapphire substrate. / Peng Wei Chih, Wu YewChung Sermon. // Applied Physics Letters. - 2006. - Vol. 88, No. 18. - P. 181117-181117-3. ↑

J2476. Jeong Soon Moon. Retraction: "Effect of aluminum cathodes prepared by ion-beam-assisted deposition in organic light-emitting devices" [Appl. Phys. Lett. 85, 1051 (2004)]. / Jeong Soon Moon, Koo Won Hoi, Choi Sang Hun, Jo Sung Jin, Baik Hong Koo, Lee Se-Jong, Song Kie Moon. // Applied Physics Letters. - 2006. - Vol. 88, No. 17. - P. 179901-179901-1. ↑

J2477. Wang W. K. Fabrication and efficiency improvement of micropillar In Ga N /Cu light-emitting diodes with vertical electrodes. / Wang W. K., Huang S. Y., Huang S. H., Wen K. S., Wu D. S., Horng R. H. // Applied Physics Letters. - 2006. - Vol. 88, No. 18. - P. 181113-181113-3. ↑

J2478. Kemerink M. Temperature-dependent built-in potential in organic semiconductor devices. / Kemerink M., Kramer J. M., Gommans H. H. P., Janssen R. A. J. // Applied Physics Letters. - 2006. - Vol. 88, No. 19. - P. 192108-192108-3. ↑

J2479. DAndrade Brian W. Organic light-emitting device luminaire for illumination applications. / DAndrade Brian W., Brown Julie J. // Applied Physics Letters. - 2006. - Vol. 88, No. 19. - P. 192908-192908-3. ↑

J2480. Chen N. C. Nitride light-emitting diodes grown on Si (111) using a TiN template. / Chen N. C., Lien W. C., Shih C. F., Chang P. H., Wang T. W., Wu M. C. // Applied Physics Letters. - 2006. - Vol. 88, No. 19. - P. 191110-191110-3. ↑

J2481. Aguirre C. M. Carbon nanotube sheets as electrodes in organic light-emitting diodes. / Aguirre C. M., Auvray S., Pigeon S., Izquierdo R., Desjardins P., Martel R. // Applied Physics Letters. - 2006. - Vol. 88, No. 18. - P. 183104-183104-3. ↑

J2482. Burrows P. E. Ultraviolet electroluminescence and blue-green phosphorescence using an organic diphosphine oxide charge transporting layer. / Burrows P. E., Padmaperuma A. B., Sapochak L. S., Djurovich P., Thompson M. E. // Applied Physics Letters. - 2006. - Vol. 88, No. 18. - P. 183503-183503-3. ↑

J2483. Kim Ja-Yeon. Thermally stable and highly reflective AgAl alloy for enhancing light extraction efficiency in GaN light-emitting diodes. / Kim Ja-Yeon, Na Seok-In, Ha Ga-Young, Kwon Min-Ki, Park Il-Kyu, Lim Jae-Hong, Park Seong-Ju, Kim Min-Ho, Choi Dongyoul, Min Kyeongik. // Applied Physics Letters. - 2006. - Vol. 88, No. 4. - P. 043507-043507-3. ↑

- J2484.** Park Joung Kyu. Embodiment of the warm white-light-emitting diodes by using a Ba 2+ codoped Sr 3 Si O 5 :Eu phosphor. / Park Joung Kyu, Choi Kyoung Jae, Yeon Jeong Ho, Lee Seung Jae, Kim Chang Hae. // Applied Physics Letters. - 2006. - Vol. 88, No. 4. - P. 043511-043511-3. ↑
- J2485.** Wang Y. J. Band gap renormalization and carrier localization effects in InGaN /GaN quantum-wells light emitting diodes with Si doped barriers. / Wang Y. J., Xu S. J., Li Q., Zhao D. G., Yang H. // Applied Physics Letters. - 2006. - Vol. 88, No. 4. - P. 041903-041903-3. ↑
- J2486.** Peng H. J. Efficiency improvement of phosphorescent organic light-emitting diodes using semitransparent Ag as anode. / Peng H. J., Zhu X. L., Sun J. X., Yu X. M., Wong M., Kwok H. S. // Applied Physics Letters. - 2006. - Vol. 88, No. 3. - P. 033509-033509-3. ↑
- J2487.** Hsiao Chung-Chin. High-efficiency polymer light-emitting diodes based on poly[2-methoxy-5-(2-ethylhexyloxy)-1,4-phenylene vinylene] with plasma-polymerized CHF 3 -modified indium tin oxide as an anode. / Hsiao Chung-Chin, Chang Chih-Hao, Jen Tzu-Hao, Hung Ming-Chin, Chen Show-An. // Applied Physics Letters. - 2006. - Vol. 88, No. 3. - P. 033512-033512-3. ↑
- J2488.** Zeng Qinghua. Ba 5 SiO 4 Cl 6 :Eu 2+ : An intense blue emission phosphor under vacuum ultraviolet and near-ultraviolet excitation. / Zeng Qinghua, Tanno Hiroaki, Egoshi Kiichirou, Tanamachi Nobutsugu, Zhang Shuxiu. // Applied Physics Letters. - 2006. - Vol. 88, No. 5. - P. 051906-051906-3. ↑
- J2489.** David Aurelien. Photonic-crystal GaN light-emitting diodes with tailored guided modes distribution. / David Aurelien, Fujii Tetsuo, Sharma Rajat, McGroddy Kelly, Nakamura Shuji, DenBaars Steven P., Hu Evelyn L., Weisbuch Claude, Benisty Henri. // Applied Physics Letters. - 2006. - Vol. 88, No. 6. - P. 061124-061124-3. ↑
- J2490.** Zhang Xiuju. High-efficiency blue light-emitting electrophosphorescent device with conjugated polymers as the host. / Zhang Xiuju, Jiang Changyun, Mo Yueqi, Xu Yunhua, Shi Huahong, Cao Yong. // Applied Physics Letters. - 2006. - Vol. 88, No. 5. - P. 051116-051116-3. ↑
- J2491.** Nash G. R. InSb /AlInSb quantum-well light-emitting diodes. / Nash G. R., Haigh M. K., Hardaway H. R., Buckle L., Andreev A. D., Gordon N. T., Smith S. J., Emeny M. T., Ashley T. // Applied Physics Letters. - 2006. - Vol. 88, No. 5. - P. 051107-051107-3. ↑
- J2492.** Dong Guifang. Organic photocouplers consisting of organic light-emitting diodes and organic photoresistors. / Dong Guifang, Hu Yan, Jiang Chongyun, Wang Liduo, Qiu Yong. // Applied Physics Letters. - 2006. - Vol. 88, No. 5. - P. 051110-051110-3. ↑
- J2493.** Bhattacharya R. Plastic deformation of a continuous organic light emitting surface. / Bhattacharya R., Wagner S., Tung Y.-J., Esler J., Hack M. // Applied Physics Letters. - 2006. - Vol. 88, No. 3. - P. 033507-033507-3. ↑
- J2494.** Yusoff A. Charge injection in polymer light-emitting diodes based on poly[(9,9-dioctylfluorenyl-2,7-diyl)-co-(1,4-phenylene)]. / Yusoff A., Hassan Z., Abu Hassan H. // Applied Physics Letters. - 2006. - Vol. 88, No. 24. - P. 242109-242109-3. ↑
- J2495.** Chen B. J. Organic light-emitting devices with a mixture emitting layer of tris-(8-hydroxyquinoline) aluminum and 4,4'-bis(carbazol-9-yl)-biphenyl. / Chen B. J., Sun X. W., Sarma K. R. // Applied Physics Letters. - 2006. - Vol. 88, No. 24. - P. 243505-243505-3. ↑
- J2496.** Ryu Yungryel. Next generation of oxide photonic devices: ZnO-based ultraviolet light emitting diodes. / Ryu Yungryel, Lee Tae-Seok, Lubguban Jorge A., White Henry W., Kim Bong-Jin, Park Yoon-Soo, Youn Chang-Joo. // Applied Physics Letters. - 2006. - Vol. 88, No. 24. - P. 241108-241108-3. ↑
- J2497.** Zhang Yingfang. Efficient blue organic light-emitting devices based on oligo(phenylenevinylene). / Zhang Yingfang, Cheng Gang, Chen Shufen, Li Yan, Zhao Yi, Liu Shiyong, He Feng, Tian Leilei, Ma Yuguang. // Applied Physics Letters. - 2006. - Vol. 88, No. 22. - P. 223508-223508-3. ↑
- J2498.** Liu Jie. High performance organic light-emitting diodes fabricated via a vacuum-free lamination process. / Liu Jie, Lewis Larry N., Faircloth Tami J., Duggal Anil R. // Applied Physics Letters. - 2006. - Vol. 88, No. 22. - P. 223509-223509-3. ↑
- J2499.** Li G. Combinatorial study of exciplex formation at the interface between two wide band gap organic

semiconductors. / Li G., Kim C. H., Zhou Z., Shinar J., Okumoto K., Shirota Y. // Applied Physics Letters. - 2006. - Vol. 88, No. 25. - P. 253505-253505-3. ↑

J2500. Jiao S. J. ZnO p-n junction light-emitting diodes fabricated on sapphire substrates. / Jiao S. J., Zhang Z. Z., Lu Y. M., Shen D. Z., Yao B., Zhang J. Y., Li B. H., Zhao D. X., Fan X. W., Tang Z. K. // Applied Physics Letters. - 2006. - Vol. 88, No. 3. - P. 031911-031911-3. ↑

J2501. Shih Ping-I. Efficient white-light-emitting diodes based on poly(N -vinylcarbazole) doped with blue fluorescent and orange phosphorescent materials. / Shih Ping-I, Shu Ching-Fong, Tung Yung-Liang, Chi Yun. // Applied Physics Letters. - 2006. - Vol. 88, No. 25. - P. 251110-251110-3. ↑

J2502. Tsuzuki Toshimitsu. Efficient organic light-emitting devices using an iridium complex as a phosphorescent host and a platinum complex as a red phosphorescent guest. / Tsuzuki Toshimitsu, Nakayama Yuji, Nakamura Junji, Iwata Takeshi, Tokito Shizuo. // Applied Physics Letters. - 2006. - Vol. 88, No. 24. - P. 243511-243511-3. ↑

J2503. Mathai Mathew K. Highly efficient solution processed blue organic electrophosphorescence with 14 lm /W luminous efficacy. / Mathai Mathew K., Choong Vi-En, Choulis Stelios A., Krummacher Benjamin, So Franky. // Applied Physics Letters. - 2006. - Vol. 88, No. 24. - P. 243512-243512-3. ↑

J2504. Huang Qiang. Highly efficient top emitting organic light-emitting diodes with organic outcoupling enhancement layers. / Huang Qiang, Walzer Karsten, Pfeiffer Martin, Lyssenko Vadim, He Gufeng, Leo Karl. // Applied Physics Letters. - 2006. - Vol. 88, No. 11. - P. 113515-113515-3. ↑

J2505. Gong Z. Optical power degradation mechanisms in AlGaIn-based 280 nm deep ultraviolet light-emitting diodes on sapphire. / Gong Z., Gaevski M., Adivarahan V., Sun W., Shatalov M., Asif Khan M. // Applied Physics Letters. - 2006. - Vol. 88, No. 12. - P. 121106-121106-3. ↑

J2506. Fong H. H. Organic light-emitting diodes based on a cohost electron transporting composite. / Fong H. H., Choy Wallace C. H., Hui K. N., Liang Y. J. // Applied Physics Letters. - 2006. - Vol. 88, No. 11. - P. 113510-113510-3. ↑

J2507. Sheu J. K. InGaIn light-emitting diodes with naturally formed truncated micropylramids on top surface. / Sheu J. K., Tsai C. M., Lee M. L., Shei S. C., Lai W. C. // Applied Physics Letters. - 2006. - Vol. 88, No. 11. - P. 113505-113505-3. ↑

J2508. Krummacher Benjamin C. Highly efficient white organic light-emitting diode. / Krummacher Benjamin C., Choong Vi-En, Mathai Mathew K., Choulis Stelios A., So Franky, Jermann Frank, Fiedler Tim, Zachau M. // Applied Physics Letters. - 2006. - Vol. 88, No. 11. - P. 113506-113506-3. ↑

J2509. Chen J.-J. Low specific contact resistance Ti /Au contacts on ZnO. / Chen J.-J., Jang Soohwan, Anderson T. J., Ren F., Li Yuanjie, Kim Hyun-Sik, Gila B. P., Norton D. P., Pearton S. J. // Applied Physics Letters. - 2006. - Vol. 88, No. 12. - P. 122107-122107-3. ↑

J2510. Odaka Hidefumi. Control of magnetic-field effect on electroluminescence in Al q 3 -based organic light emitting diodes. / Odaka Hidefumi, Okimoto Yoichi, Yamada Toshikazu, Okamoto Hiroshi, Kawasaki Masashi, Tokura Yoshinori. // Applied Physics Letters. - 2006. - Vol. 88, No. 12. - P. 123501-123501-3. ↑

J2511. Schmidt R. Fabrication of genuine single-quantum-dot light-emitting diodes. / Schmidt R., Scholz U., Vitzethum M., Fix R., Metzner C., Kailuweit P., Reuter D., Wieck A., Hubner M. C., Stuffer S., Zrenner A., Malzer S., Dohler G. H. // Applied Physics Letters. - 2006. - Vol. 88, No. 12. - P. 121115-121115-3. ↑

J2512. Zibik E. A. Broadband 6 μ m λ 8 μ m superluminescent quantum cascade light-emitting diodes. / Zibik E. A., Ng W. H., Revin D. G., Wilson L. R., Cockburn J. W., Groom K. M., Hopkinson M. // Applied Physics Letters. - 2006. - Vol. 88, No. 12. - P. 121109-121109-3. ↑

J2513. Schulze F. Metalorganic vapor phase epitaxy grown In Ga N /Ga N light-emitting diodes on Si(001) substrate. / Schulze F., Dadgar A., Blasing J., Diez A., Krost A. // Applied Physics Letters. - 2006. - Vol. 88, No. 12. - P. 121114-121114-3. ↑

J2514. Jiang X. Highly efficient room-temperature tunnel spin injector using CoFe/MgO(001). / Jiang X., Wang R., Shelby R. M., Parkin S. S. P. // IBM Journal of Research and Development. - 2006. - Vol. 50, No. 1. - P. 1-10.

111-120. ↑

J2515. Qian L. Influence of dehydrated nanotubed titanic acid on polymer light-emitting diodes with phosphorescent dye. / Qian L., Zhang T., Wang Y. S., Xu X. R., Jin Z. S., Du Z. L. // Applied Physics Letters. - 2006. - Vol. 88, No. 1. - P. 013510-013510-3. ↑

J2516. Xie Rong-Jun. Highly efficient white-light-emitting diodes fabricated with short-wavelength yellow oxynitride phosphors. / Xie Rong-Jun, Hiroaki Naoto, Mitomo Mamoru, Takahashi Kosei, Sakuma Ken. // Applied Physics Letters. - 2006. - Vol. 88, No. 10. - P. 101104-101104-3. ↑

J2517. Weon Byung Mook. Evolution of luminance by voltage in organic light-emitting diodes. / Weon Byung Mook, Kim Soo Young, Lee Jong-Lam, Je Jung Ho. // Applied Physics Letters. - 2006. - Vol. 88, No. 1. - P. 013503-013503-3. ↑

J2518. Kim Han-Ki. Transparent indium zinc oxide top cathode prepared by plasma damage-free sputtering for top-emitting organic light-emitting diodes. / Kim Han-Ki, Lee Kyu-Sung, Kwon J. H. // Applied Physics Letters. - 2006. - Vol. 88, No. 1. - P. 012103-012103-3. ↑

J2519. Kim Jong Kyu. GaInN light-emitting diode with conductive omnidirectional reflector having a low-refractive-index indium-tin oxide layer. / Kim Jong Kyu, Gessmann Thomas, Schubert E. Fred, Xi J.-Q., Luo Hong, Cho Jaehee, Sone Cheolsoo, Park Yongjo. // Applied Physics Letters. - 2006. - Vol. 88, No. 1. - P. 013501-013501-3. ↑

J2520. Kim Soo Young. Enhancement of optical properties in organic light emitting diodes using the Mg-Al alloy cathode and Ir O x-coated indium tin oxide anode. / Kim Soo Young, Lee Jong-Lam. // Applied Physics Letters. - 2006. - Vol. 88, No. 11. - P. 112106-112106-3. ↑

J2521. Guo Tzung-Fang. Organic oxide/Al composite cathode in efficient polymer light-emitting diodes. / Guo Tzung-Fang, Yang Fuh-Shun, Tsai Zen-Jay, Wen Ten-Chin, Hsieh Sung-Nien, Fu Yaw-Shyan, Chung Chia-Tin. // Applied Physics Letters. - 2006. - Vol. 88, No. 11. - P. 113501-113501-3. ↑

J2522. Lei Gangtie. Multilayer organic electrophosphorescent white light-emitting diodes without exciton-blocking layer. / Lei Gangtie, Wang Liduo, Qiu Yong. // Applied Physics Letters. - 2006. - Vol. 88, No. 10. - P. 103508-103508-3. ↑

J2523. Yang Woan-Jen. White-light generation and energy transfer in Sr Zn 2 (P O 4)2 :Eu ,Mn phosphor for ultraviolet light-emitting diodes. / Yang Woan-Jen, Chen Teng-Ming. // Applied Physics Letters. - 2006. - Vol. 88, No. 10. - P. 101903-101903-3. ↑

J2524. Hong Hyun-Gi. Enhancement of the light output of GaN-based ultraviolet light-emitting diodes by a one-dimensional nanopatterning process. / Hong Hyun-Gi, Kim Seok-Soon, Kim Dong-Yu, Lee Takhee, Song June-O., Cho J. H., Sone C., Park Y., Seong Tae-Yeon. // Applied Physics Letters. - 2006. - Vol. 88, No. 10. - P. 103505-103505-3. ↑

J2525. Tseng Shin-Rong. General method to solution-process multilayer polymer light-emitting diodes. / Tseng Shin-Rong, Lin Shi-Chang, Meng Hsin-Fei, Liao Hua-Hsien, Yeh Chi-Hung, Lai Huan-Chung, Horng Sheng-Fu, Hsu Chain-Shu. // Applied Physics Letters. - 2006. - Vol. 88, No. 16. - P. 163501-163501-3. ↑

J2526. Xia Yajun. Polymer bilayer structure via inkjet printing. / Xia Yajun, Friend Richard H. // Applied Physics Letters. - 2006. - Vol. 88, No. 16. - P. 163508-163508-3. ↑

J2527. Piao Xianqing. Characterization and luminescence properties of Sr 2 Si 5 N 8 :Eu 2+ phosphor for white light-emitting-diode illumination. / Piao Xianqing, Horikawa Takashi, Hanzawa Hiromasa, Machida Ken-ichi. // Applied Physics Letters. - 2006. - Vol. 88, No. 16. - P. 161908-161908-3. ↑

J2528. Pillai S. Enhanced emission from Si-based light-emitting diodes using surface plasmons. / Pillai S., Catchpole K. R., Ttrupke T., Zhang G., Zhao J., Green M. A. // Applied Physics Letters. - 2006. - Vol. 88, No. 16. - P. 161102-161102-3. ↑

J2529. Yates C. J. Surface plasmon-polariton mediated emission from phosphorescent dendrimer light-emitting diodes. / Yates C. J., Samuel I. D. W., Burn P. L., Wedge S., Barnes W. L. // Applied Physics Letters. - 2006. - Vol. 88, No. 16. - P. 161105-161105-3. ↑

- J2530.** Li J. Growth of III-nitride photonic structures on large area silicon substrates. / Li J., Lin J. Y., Jiang H. X. // Applied Physics Letters. - 2006. - Vol. 88, No. 17. - P. 171909-171909-3. ↑
- J2531.** Xu W. Z. ZnO light-emitting diode grown by plasma-assisted metal organic chemical vapor deposition. / Xu W. Z., Ye Z. Z., Zeng Y. J., Zhu L. P., Zhao B. H., Jiang L., Lu J. G., He H. P., Zhang S. B. // Applied Physics Letters. - 2006. - Vol. 88, No. 17. - P. 173506-173506-3. ↑
- J2532.** Hagen J. A. Enhanced emission efficiency in organic light-emitting diodes using deoxyribonucleic acid complex as an electron blocking layer. / Hagen J. A., Li W., Steckl A. J., Grote J. G. // Applied Physics Letters. - 2006. - Vol. 88, No. 17. - P. 171109-171109-3. ↑
- J2533.** Sun Q. J. White light from polymer light-emitting diodes: Utilization of fluorenone defects and exciplex. / Sun Q. J., Fan B. H., Tan Z. A., Yang C. H., Li Y. F., Yang Y. // Applied Physics Letters. - 2006. - Vol. 88, No. 16. - P. 163510-163510-3. ↑
- J2534.** Zhang Z. S. Effects of symmetry of GaN-based two-dimensional photonic crystal with quasicrystal lattices on enhancement of surface light extraction. / Zhang Z. S., Zhang B., Xu J., Xu K., Yang Z. J., Qin Z. X., Yu T. J., Yu D. P. // Applied Physics Letters. - 2006. - Vol. 88, No. 17. - P. 171103-171103-3. ↑
- J2535.** Chen Shufen. Improved light outcoupling for phosphorescent top-emitting organic light-emitting devices. / Chen Shufen, Zhao Yi, Cheng Gang, Li Jiang, Liu Chunli, Zhao Zhenyuan, Jie Zhonghai, Liu Shiyong. // Applied Physics Letters. - 2006. - Vol. 88, No. 15. - P. 153517-153517-3. ↑
- J2536.** Ropers Claus. Observation of deep level defects within the waveguide of red-emitting high-power diode lasers. / Ropers Claus, Tien Tran Quoc, Lienau Christoph, Tamm Jens W., Brick Peter, Linder Norbert, Mayer Bernd, Muller Martin, Tautz Sonke, Schmid Wolfgang. // Applied Physics Letters. - 2006. - Vol. 88, No. 13. - P. 133513-133513-3. ↑
- J2537.** David Aurelien. Photonic crystal laser lift-off GaN light-emitting diodes. / David Aurelien, Fujii Tetsuo, Moran Brendan, Nakamura Shuji, DenBaars Steven P., Weisbuch Claude, Benisty Henri. // Applied Physics Letters. - 2006. - Vol. 88, No. 13. - P. 133514-133514-3. ↑
- J2538.** Kuriyama K. Thermally stimulated current studies on neutron irradiation induced defects in GaN. / Kuriyama K., Ooi M., Onoue A., Kushida K., Okada M., Xu Q. // Applied Physics Letters. - 2006. - Vol. 88, No. 13. - P. 132109-132109-3. ↑
- J2539.** Wang H. F. Efficient single-active-layer organic light-emitting diodes with fluoropolymer buffer layers. / Wang H. F., Wang L. D., Wu Z. X., Zhang D. Q., Qiao J., Qiu Y., Wang X. G. // Applied Physics Letters. - 2006. - Vol. 88, No. 13. - P. 131113-131113-3. ↑
- J2540.** Huh Chul. Effects of Ag/indium tin oxide contact to a SiC doping layer on performance of Si nanocrystal light-emitting diodes. / Huh Chul, Park Nae-Man, Shin Jae-Heon, Kim Kyung-Hyun, Kim Tae-Youb, Cho Kwan Sik, Sung Gun Yong. // Applied Physics Letters. - 2006. - Vol. 88, No. 13. - P. 131913-131913-3. ↑
- J2541.** Sapp Shawn. Work function and implications of doped poly(3,4-ethylenedioxythiophene)-co-poly(ethylene glycol). / Sapp Shawn, Luebben Silvia, Losovyj Ya. B., Jeppson P., Schulz D. L., Caruso A. N. // Applied Physics Letters. - 2006. - Vol. 88, No. 15. - P. 152107-152107-3. ↑
- J2542.** Melpignano P. Efficient light extraction and beam shaping from flexible, optically integrated organic light-emitting diodes. / Melpignano P., Biondo V., Sinesi S., Gale Michael T., Westenhofer Susanne, Murgia M., Caria S., Zamboni R. // Applied Physics Letters. - 2006. - Vol. 88, No. 15. - P. 153514-153514-3. ↑
- J2543.** Sharma Asha. Room temperature ultraviolet emission at 357 nm from polysilane based organic light emitting diode. / Sharma Asha, Katiyar Monica, Deepak, Seki Shu, Tagawa Seiichi. // Applied Physics Letters. - 2006. - Vol. 88, No. 14. - P. 143511-143511-3. ↑
- J2544.** Jou Jwo-Huei. Efficient pure-white organic light-emitting diodes with a solution-processed, binary-host employing single emission layer. / Jou Jwo-Huei, Sun Ming-Chen, Chou Hung-Hsing, Li Chien-Hung. // Applied Physics Letters. - 2006. - Vol. 88, No. 14. - P. 141101-141101-3. ↑
- J2545.** Rogers D. J. Electroluminescence at 375 nm from a Zn O /Ga N :Mg /c-Al 2 O 3 heterojunction light emitting diode. / Rogers D. J., Hosseini Teherani F., Yasan A., Minder K., Kung P., Razeghi M. // Applied

Physics Letters. - 2006. - Vol. 88, No. 14. - P. 141918-141918-3. ↑

J2546. Loffler W. Electrical spin injection from ZnMnSe into InGaAs quantum wells and quantum dots. / Loffler W., Trondle D., Fallert J., Kalt H., Litvinov D., Gerthsen D., Lupaca-Schomber J., Passow T., Daniel B., Kvietkova J., Grun M., Klingshirn C., Hetterich M. // Applied Physics Letters. - 2006. - Vol. 88, No. 6. - P. 062105-062105-3. ↑

J2547. Romero Manuel J. Electroluminescence mapping of Cu Ga Se 2 solar cells by atomic force microscopy. / Romero Manuel J., Jiang C.-S., Abushama J., Moutinho H. R., Al-Jassim M. M., Noufi R. // Applied Physics Letters. - 2006. - Vol. 89, No. 14. - P. 143120-143120-3. ↑

J2548. Kanno Hiroshi. White organic light-emitting device based on a compound fluorescent-phosphor-sensitized-fluorescent emission layer. / Kanno Hiroshi, Sun Yiru, Forrest Stephen R. // Applied Physics Letters. - 2006. - Vol. 89, No. 14. - P. 143516-143516-3. ↑

J2549. Kim Jong Kyu. Enhanced light-extraction in GaInN near-ultraviolet light-emitting diode with Al-based omnidirectional reflector having Ni Zn /Ag microcontacts. / Kim Jong Kyu, Xi J.-Q., Luo Hong, Fred Schubert E., Cho Jaehee, Sone Cheolsoo, Park Yongjo. // Applied Physics Letters. - 2006. - Vol. 89, No. 14. - P. 141123-141123-3. ↑

J2550. Huang Jinsong. Improving the power efficiency of white light-emitting diode by doping electron transport material. / Huang Jinsong, Hou Wei-Jen, Li Jue-Hao, Li Gang, Yang Yang. // Applied Physics Letters. - 2006. - Vol. 89, No. 13. - P. 133509-133509-3. ↑

J2551. Law C. W. Effective organic-based connection unit for stacked organic light-emitting devices. / Law C. W., Lau K. M., Fung M. K., Chan M. Y., Wong F. L., Lee C. S., Lee S. T. // Applied Physics Letters. - 2006. - Vol. 89, No. 13. - P. 133511-133511-3. ↑

J2552. Sun Q. J. Enhanced performance of white polymer light-emitting diodes using polymer blends as hole-transporting layers. / Sun Q. J., Hou J. H., Yang C. H., Li Y. F., Yang Y. // Applied Physics Letters. - 2006. - Vol. 89, No. 15. - P. 153501-153501-3. ↑

J2553. Lee Jun Yeob. Effect of doping profile on the lifetime of green phosphorescent organic light-emitting diodes. Applied Physics Letters. - 2006. - Vol. 89, No. 15. - P. 153503-153503-3. ↑

J2554. Khan N. Effects of compressive strain on optical properties of In x Ga 1-x N /Ga N quantum wells. / Khan N., Li J. // Applied Physics Letters. - 2006. - Vol. 89, No. 15. - P. 151916-151916-3. ↑

J2555. Charas A. Use of cross-linkable polyfluorene in the fabrication of multilayer polyfluorene-based light-emitting diodes with improved efficiency. / Charas A., Alves H., Alcacer L., Morgado J. // Applied Physics Letters. - 2006. - Vol. 89, No. 14. - P. 143519-143519-3. ↑

J2556. Wang Lei. Utilization of water/alcohol-soluble polyelectrolyte as an electron injection layer for fabrication of high-efficiency multilayer saturated red-phosphorescence polymer light-emitting diodes by solution processing. / Wang Lei, Liang Bo, Huang Fei, Peng Junbiao, Cao Yong. // Applied Physics Letters. - 2006. - Vol. 89, No. 15. - P. 151115-151115-3. ↑

J2557. Lee S. W. Origin of forward leakage current in GaN-based light-emitting devices. / Lee S. W., Oh D. C., Goto H., Ha J. S., Lee H. J., Hanada T., Cho M. W., Yao T., Hong S. K., Lee H. Y., Cho S. R., Choi J. W., Choi J. H., Jang J. H., Shin J. E., Lee J. S. // Applied Physics Letters. - 2006. - Vol. 89, No. 13. - P. 132117-132117-3. ↑

J2558. Kawamoto Masuki. White emission from liquid-crystalline copolymers containing oxadiazole moieties in the side chain. / Kawamoto Masuki, Tsukamoto Takuji, Kinoshita Motoi, Ikeda Tomiki. // Applied Physics Letters. - 2006. - Vol. 89, No. 12. - P. 121920-121920-3. ↑

J2559. Lee C. J. Green top-emitting organic light emitting device with transparent Ba /Ag bilayer cathode. / Lee C. J., Pode R. B., Han J. I., Moon D. G. // Applied Physics Letters. - 2006. - Vol. 89, No. 12. - P. 123501-123501-3. ↑

J2560. Porta P. A. Surface plasmon mediated emission in resonant-cavity light-emitting diodes. / Porta P. A., Harries M., Summers H. D. // Applied Physics Letters. - 2006. - Vol. 89, No. 12. - P. 121120-121120-3. ↑

- J2561.** Adelman C. Spin injection from perpendicular magnetized ferromagnetic delta -Mn Ga into (Al,Ga)As heterostructures. / Adelman C., Hilton J. L., Schultz B. D., McKernan S., Palmström C. J., Lou X., Chiang H.-S., Crowell P. A. // Applied Physics Letters. - 2006. - Vol. 89, No. 11. - P. 112511-112511-3. ↑
- J2562.** Chu Ta-Ya. Comparative study of single and multiemissive layers in inverted white organic light-emitting devices. / Chu Ta-Ya, Chen Jenn-Fang, Chen Szu-Yi, Chen Chin H. // Applied Physics Letters. - 2006. - Vol. 89, No. 11. - P. 113502-113502-3. ↑
- J2563.** Kim Soo Young. Dark spot formation mechanism in organic light emitting diodes. / Kim Soo Young, Kim Kwang Young, Tak Yoon-Heung, Lee Jong-Lam. // Applied Physics Letters. - 2006. - Vol. 89, No. 13. - P. 132108-132108-3. ↑
- J2564.** Miller M. A. Ohmic contacts to plasma etched n-Al 0.58 Ga 0.42 N. / Miller M. A., Mohny S. E., Nikiforov A., Cargill G. S., Bogart K. H. A. // Applied Physics Letters. - 2006. - Vol. 89, No. 13. - P. 132114-132114-3. ↑
- J2565.** Mirza B. I. In Sb /Al x In 1-x Sb quantum-well light-emitting diodes with high internal quantum efficiencies. / Mirza B. I., Nash G. R., Smith S. J., Haigh M. K., Buckle L., Emeny M. T., Ashley T. // Applied Physics Letters. - 2006. - Vol. 89, No. 13. - P. 131110-131110-3. ↑
- J2566.** Xu Xinjun. Efficient nondoped white organic light-emitting diodes based on electroluminescence. / Xu Xinjun, Yu Gui, Di Chongan, Liu Yunqi, Shao Kefeng, Yang Lianming, Lu Ping. // Applied Physics Letters. - 2006. - Vol. 89, No. 12. - P. 123503-123503-3. ↑
- J2567.** Lee Tae-Woo. Hole-transporting interlayers for improving the device lifetime in the polymer light-emitting diodes. / Lee Tae-Woo, Kim Mu-Gyeom, Kim Sang Yeol, Park Sang Hun, Kwon Ohyun, Noh Taeyong, Oh Tae-Sik. // Applied Physics Letters. - 2006. - Vol. 89, No. 12. - P. 123505-123505-3. ↑
- J2568.** Zhao W. Q. Efficient 1.54 μm light emitting diode with nanometer thick polycrystalline Si anode and organic sandwich structure. / Zhao W. Q., Ran G. Z., Ma G. L., Xu W. J., Dai L., Liu W. M., Wang P. F., Qin G. G. // Applied Physics Letters. - 2006. - Vol. 89, No. 2. - P. 022109-022109-3. ↑
- J2569.** Kanno Hiroshi. Stacked white organic light-emitting devices based on a combination of fluorescent and phosphorescent emitters. / Kanno Hiroshi, Giebink Noel C., Sun Yiru, Forrest Stephen R. // Applied Physics Letters. - 2006. - Vol. 89, No. 2. - P. 023503-023503-3. ↑
- J2570.** Parish C. M. On the use of Monte Carlo modeling in the mathematical analysis of scanning electron microscopy-electron beam induced current data. / Parish C. M., Russell P. E. // Applied Physics Letters. - 2006. - Vol. 89, No. 19. - P. 192108-192108-3. ↑
- J2571.** Kim Kyung-Hyun. Enhancement of light extraction from a silicon quantum dot light-emitting diode containing a rugged surface pattern. / Kim Kyung-Hyun, Shin Jae-Heon, Park Nae-Man, Huh Chul, Kim Tae-Youb, Cho Kwan-Sik, Hong Jong Cheol, Sung Gun Yong. // Applied Physics Letters. - 2006. - Vol. 89, No. 19. - P. 191120-191120-3. ↑
- J2572.** Hsueh Kuang-Po. Investigation of Cr- and Al-based metals for the reflector and Ohmic contact on n-GaN in GaN flip-chip light-emitting diodes. / Hsueh Kuang-Po, Chiang Kuo-Chun, Hsin Yue-Ming, Wang Charles J. // Applied Physics Letters. - 2006. - Vol. 89, No. 19. - P. 191122-191122-3. ↑
- J2573.** Ma R. M. Synthesis of high quality n-type CdS nanobelts and their applications in nanodevices. / Ma R. M., Dai L., Huo H. B., Yang W. Q., Qin G. G., Tan P. H., Huang C. H., Zheng J. // Applied Physics Letters. - 2006. - Vol. 89, No. 20. - P. 203120-203120-3. ↑
- J2574.** Wu Yue. Metal electrode effects on spin-orbital coupling and magnetoresistance in organic semiconductor devices. / Wu Yue, Hu Bin. // Applied Physics Letters. - 2006. - Vol. 89, No. 20. - P. 203510-203510-3. ↑
- J2575.** Hung Ming-Chin. Highly efficient top-emitting organic light-emitting diodes with self-assembled monolayer-modified Ag as anodes. / Hung Ming-Chin, Wu Kun-Yang, Tao Yu-Tai, Huang Hung-Wei. // Applied Physics Letters. - 2006. - Vol. 89, No. 20. - P. 203106-203106-3. ↑
- J2576.** Kuo C. H. Improvement of near-ultraviolet nitride-based light emitting diodes with mesh indium tin oxide

contact layers. / Kuo C. H., Chen C. M., Kuo C. W., Tun C. J., Pan C. J., Pong B. J., Chi G. C. // Applied Physics Letters. - 2006. - Vol. 89, No. 20. - P. 201104-201104-3. ↑

J2577. Malyutenko V. K. Room-temperature In As Sb P /In As light emitting diodes by liquid phase epitaxy for midinfrared (3-5 mcm) dynamic scene projection. / Malyutenko V. K., Malyutenko O. Yu., Zinovchuk A. V. // Applied Physics Letters. - 2006. - Vol. 89, No. 20. - P. 201114-201114-3. ↑

J2578. Kuo C. H. Nitride-based light-emitting diodes with p-Al In Ga N surface layers prepared at various temperatures. / Kuo C. H., Kuo C. W., Chen C. M., Pong B. J., Chi G. C. // Applied Physics Letters. - 2006. - Vol. 89, No. 19. - P. 191112-191112-3. ↑

J2579. Okumoto Kenji. Erratum: "Green fluorescent organic light-emitting device with external quantum efficiency of nearly 10%" [Appl. Phys. Lett. 89, 063504 (2006)]. / Okumoto Kenji, Kanno Hiroshi, Hamada Yuji, Takahashi Hisakazu, Shibata Kenichi. // Applied Physics Letters. - 2006. - Vol. 89, No. 16. - P. 169901-169901-1. ↑

J2580. Murai Akihiko. Hexagonal pyramid shaped light-emitting diodes based on ZnO and GaN direct wafer bonding. / Murai Akihiko, Thompson Daniel B., Masui Hisashi, Fellows Natalie, Mishra Umesh K., Nakamura Shuji, DenBaars Steven P. // Applied Physics Letters. - 2006. - Vol. 89, No. 17. - P. 171116-171116-3. ↑

J2581. Hsiao Chih-Hung. Recombination zone in mixed-host organic light-emitting devices. / Hsiao Chih-Hung, Chen Yan-Hau, Lin Tien-Chun, Hsiao Chia-Chiang, Lee Jiun-Haw. // Applied Physics Letters. - 2006. - Vol. 89, No. 16. - P. 163511-163511-3. ↑

J2582. Wu D. S. Defect reduction and efficiency improvement of near-ultraviolet emitters via laterally overgrown GaN on a GaN/patterned sapphire template. / Wu D. S., Wang W. K., Wen K. S., Huang S. C., Lin S. H., Huang S. Y., Lin C. F., Horng R. H. // Applied Physics Letters. - 2006. - Vol. 89, No. 16. - P. 161105-161105-3. ↑

J2583. Saito Shin-ichi. Silicon light-emitting transistor for on-chip optical interconnection. / Saito Shin-ichi, Hisamoto Digh, Shimizu Haruka, Hamamura Hirotaka, Tsuchiya Ryuta, Matsui Yuichi, Mine Toshiyuki, Arai Tadashi, Sugii Nobuyuki, Torii Kazuyoshi, Kimura Shinichiro, Onai Takahiro. // Applied Physics Letters. - 2006. - Vol. 89, No. 16. - P. 163504-163504-3. ↑

J2584. Divayana Y. Efficient blue organic light-emitting device based on N, N' -di(naphth-2-yl)-N, N' -diphenylbenzidine with an exciton-confining structure. / Divayana Y., Sun X. W., Chen B. J., Lo G. Q., Jiang C. Y., Sarma K. R. // Applied Physics Letters. - 2006. - Vol. 89, No. 17. - P. 173511-173511-3. ↑

J2585. Odnoblyudov V. A. Growth and fabrication of InGaNp-based yellow-red light emitting diodes. / Odnoblyudov V. A., Tu C. W. // Applied Physics Letters. - 2006. - Vol. 89, No. 19. - P. 191107-191107-3. ↑

J2586. Kim Yoon-Chang. Planarized Si N x /spin-on-glass photonic crystal organic light-emitting diodes. / Kim Yoon-Chang, Cho Sang-Hwan, Song Young-Woo, Lee Yong-Jae, Lee Yong-Hee, Do Young Rag. // Applied Physics Letters. - 2006. - Vol. 89, No. 17. - P. 173502-173502-3. ↑

J2587. Campbell I. H. Characteristics of an organic light-emitting diode utilizing a phosphorescent, shallow hole trap. / Campbell I. H., Crone B. K. // Applied Physics Letters. - 2006. - Vol. 89, No. 17. - P. 172108-172108-3. ↑

J2588. Haranath D. Enhanced luminescence of Y 3 Al 5 O 12 :Ce 3+ nanophosphor for white light-emitting diodes. / Haranath D., Chander Harish, Sharma Pooja, Singh Sukhvir. // Applied Physics Letters. - 2006. - Vol. 89, No. 17. - P. 173118-173118-3. ↑

J2589. Lau K. C. Contrast improvement of organic light-emitting devices with Sm:Ag cathode. / Lau K. C., Xie W. F., Sun H. Y., Lee C. S., Lee S. T. // Applied Physics Letters. - 2006. - Vol. 88, No. 8. - P. 083507-083507-3. ↑

J2590. Cheng Gang. Improved efficiency for white organic light-emitting devices based on phosphor sensitized fluorescence. / Cheng Gang, Zhang Yingfang, Zhao Yi, Liu Shiyong, Ma Yuguang. // Applied Physics Letters. - 2006. - Vol. 88, No. 8. - P. 083512-083512-3. ↑

J2591. Liu Jun. Blue light-emitting polymer with polyfluorene as the host and highly fluorescent 4-dimethylamino-1,8-naphthalimide as the dopant in the sidechain. / Liu Jun, Min Changchun, Zhou Quanguo,

Cheng Yanxiang, Wang Lixiang, Ma Dongge, Jing Xiabin, Wang Fosong. // Applied Physics Letters. - 2006. - Vol. 88, No. 8. - P. 083505-083505-3. ↑

J2592. Lin Chia-Feng. High-efficiency InGaN -based light-emitting diodes with nanoporous GaN :Mg structure. / Lin Chia-Feng, Zheng Jing-Hui, Yang Zhong-Jie, Dai Jing-Jie, Lin Der-Yuh, Chang Chung-Ying, Lai Zhao-Xu, Hong C. S. // Applied Physics Letters. - 2006. - Vol. 88, No. 8. - P. 083121-083121-3. ↑

J2593. Zhou Lisong. All-organic active matrix flexible display. / Zhou Lisong, Wanga Alfred, Wu Sheng-Chu, Sun Jie, Park Sungkyu, Jackson Thomas N. // Applied Physics Letters. - 2006. - Vol. 88, No. 8. - P. 083502-083502-3. ↑

J2594. Kaestner B. Co-planar spin-polarized light-emitting diodes. / Kaestner B., Wunderlich J., Sinova J., Jungwirth T. // Applied Physics Letters. - 2006. - Vol. 88, No. 9. - P. 091106-091106-3. ↑

J2595. Li Mingtao. Tuning emission color of electroluminescence from two organic interfacial exciplexes by modulating the thickness of middle gadolinium complex layer. / Li Mingtao, Li Wenlian, Chen Lili, Kong Zhiguo, Chu Bei, Li Bin, Hu Zhizhi, Zhang Zhiqiang. // Applied Physics Letters. - 2006. - Vol. 88, No. 9. - P. 091108-091108-3. ↑

J2596. Su W. M. Erratum: "Improved electroluminescent efficiency of organic light emitting devices by co-doping N, N' -Dimethyl-quinacridone and Coumarin6 into tris-(8-hydroxyquinoline) aluminum" [Appl. Phys. Lett. 87, 213501 (2005)]. / Su W. M., Li W. L., Hong Z. R., Li M. T., Yu T. Z., Chu B., Li B., Zhang Z. Q., Hu Z. Z. // Applied Physics Letters. - 2006. - Vol. 88, No. 8. - P. 089901-089901-1. ↑

J2597. Kim Han-Ki. Direct Al cathode layer sputtering on LiF /Alq 3 using facing target sputtering with a mixture of Ar and Kr. / Kim Han-Ki, Kim Sang-Woo, Lee Kyu-Sung, Kim K. H. // Applied Physics Letters. - 2006. - Vol. 88, No. 8. - P. 083513-083513-3. ↑

J2598. Hsu Ching-Ming. Selective light emission from flexible organic light-emitting devices using a dot-nickel embedded indium tin oxide anode. / Hsu Ching-Ming, Tsai Chung-Lin, Wu Wen-Tuan. // Applied Physics Letters. - 2006. - Vol. 88, No. 8. - P. 083515-083515-3. ↑

J2599. Lin Chun-Liang. Enhancing light outcoupling of organic light-emitting devices by locating emitters around the second antinode of the reflective metal electrode. / Lin Chun-Liang, Cho Ting-Yi, Chang Chih-Hao, Wu Chung-Chih. // Applied Physics Letters. - 2006. - Vol. 88, No. 8. - P. 081114-081114-3. ↑

J2600. Lin Yow-Jon. Enhanced efficiency in polymer light-emitting diodes due to the improvement of charge-injection balance. / Lin Yow-Jon, Chou Wei-Yang, Lin Shih-Ting. // Applied Physics Letters. - 2006. - Vol. 88, No. 7. - P. 071108-071108-3. ↑

J2601. Del Cano Teodosio. Near-infrared electroluminescence based on perylenediimide-doped tris(8-quinolinolato) aluminum. / Del Cano Teodosio, Hashimoto Keisuke, Kageyama Hiroshi, De Saja Jose Antonio, Aroca Ricardo, Ohmori Yutaka, Shirota Yasuhiko. // Applied Physics Letters. - 2006. - Vol. 88, No. 7. - P. 071117-071117-3. ↑

J2602. Fuhrmann D. Optimization scheme for the quantum efficiency of GaInN-based green-light-emitting diodes. / Fuhrmann D., Netzel C., Rossow U., Hangleiter A., Ade G., Hinze P. // Applied Physics Letters. - 2006. - Vol. 88, No. 7. - P. 071105-071105-3. ↑

J2603. Pan Chang-Chi. Thermal stability improvement by using Pd /NiO /Al /Ti /Au reflective ohmic contacts to p -GaN for flip-chip ultraviolet light-emitting diodes. / Pan Chang-Chi, Chen Guan-Ting, Hsu Wen-Jay, Lin Chih-Wei, Chyi Jen-Inn. // Applied Physics Letters. - 2006. - Vol. 88, No. 6. - P. 062113-062113-3. ↑

J2604. Liu Tswen-Hsin. Phosphorescence of red Os (fptz)2 (P Ph 2 Me)2 doped organic light-emitting devices with n and p hosts. / Liu Tswen-Hsin, Hsu Shih-Feng, Ho Meng-Hung, Liao Chi-Hung, Wu Yao-Shan, Chen Chin H., Tung Yung-Liang, Wu Pei-Chi, Chi Yun. // Applied Physics Letters. - 2006. - Vol. 88, No. 6. - P. 063508-063508-3. ↑

J2605. Lee Jun Yeob. Efficient hole injection in organic light-emitting diodes using C60 as a buffer layer for Al reflective anodes. Applied Physics Letters. - 2006. - Vol. 88, No. 7. - P. 073512-073512-3. ↑

J2606. Peng Huajun. High-efficiency microcavity top-emitting organic light-emitting diodes using silver anode. /

Peng Huajun, Sun Jiabin, Zhu Xiuling, Yu Xiaoming, Wong Man, Kwok Hoi-Sing. // Applied Physics Letters. - 2006. - Vol. 88, No. 7. - P. 073517-073517-3. ↑

J2607. David Aurelien. GaN light-emitting diodes with Archimedean lattice photonic crystals. / David Aurelien, Fujii Tetsuo, Matioli Elison, Sharma Rajat, Nakamura Shuji, DenBaars Steven P., Weisbuch Claude, Benisty Henri. // Applied Physics Letters. - 2006. - Vol. 88, No. 7. - P. 073510-073510-3. ↑

J2608. Swietlik T. Anomalous temperature characteristics of single wide quantum well InGaP laser diode. / Swietlik T., Franssen G., Wisniewski P., Krukowski S., Łepkowski S. P., Marona L., Leszczynski M., Prystawko P., Grzegory I., Suski T., Porowski S., Perlin P., Czernecki R., Bering-Staniszevska A., Eliseev P. G. // Applied Physics Letters. - 2006. - Vol. 88, No. 7. - P. 071121-071121-3. ↑

J2609. Luo H. Optical upconverter with integrated heterojunction phototransistor and light-emitting diode. / Luo H., Ban D., Liu H. C., Wasilewski Z. R., Buchanan M. // Applied Physics Letters. - 2006. - Vol. 88, No. 7. - P. 073501-073501-3. ↑

J2610. Hsieh Ming-Ta. Study of hole concentration of 1,4-bis[N-(1-naphthyl)-N'-phenylamino]-4,4' diamine doped with tungsten oxide by admittance spectroscopy. / Hsieh Ming-Ta, Chang Chan-Ching, Chen Jenn-Fang, Chen Chin H. // Applied Physics Letters. - 2006. - Vol. 89, No. 10. - P. 103510-103510-3. ↑

J2611. Piliago C. Analysis and control of the active area scaling effect on white organic light emitting diodes towards lighting applications. / Piliago C., Mazzeo M., Salerno M., Cingolani R., Gigli G., Moro A. // Applied Physics Letters. - 2006. - Vol. 89, No. 10. - P. 103514-103514-3. ↑

J2612. Yim Youn Chan. Enhanced light emission from one-layered organic light-emitting devices doped with organic salt by simultaneous thermal and electrical annealing. / Yim Youn Chan, Park Jin Ho, Kim Sun Woong, Choi Eun Ha, Cho Guang Sup, Seo Yoon Ho, Kang Seung Oun, Park Byoungchoo, Cho Sang Hee, Kim In Tae, Han S. H., Lim Jongsun, Takezoe Hideo. // Applied Physics Letters. - 2006. - Vol. 89, No. 10. - P. 103507-103507-3. ↑

J2613. Liu Tswen-Hsin. Lithium manganese oxide as an effective buffer layer between organic and metal layers in organic light-emitting devices. Applied Physics Letters. - 2006. - Vol. 89, No. 10. - P. 102101-102101-3. ↑

J2614. Luo Yichun. Electric-field-induced fluorescence quenching in dye-doped tris(8-hydroxyquinoline) aluminum layers. / Luo Yichun, Aziz Hany, Popovic Zoran D., Xu Gu. // Applied Physics Letters. - 2006. - Vol. 89, No. 10. - P. 103505-103505-3. ↑

J2615. An Kwang H. Organic light-emitting device on a scanning probe cantilever. / An Kwang H., O'Connor Brendan, Pipe Kevin P., Zhao Yiyang, Shtein Max. // Applied Physics Letters. - 2006. - Vol. 89, No. 11. - P. 111117-111117-3. ↑

J2616. Smith S. J. Lateral light emitting n-i-p diodes in In Sb /Al x In 1-x Sb quantum wells. / Smith S. J., Nash G. R., Bartlett C. J., Buckle L., Emeny M. T., Ashley T. // Applied Physics Letters. - 2006. - Vol. 89, No. 11. - P. 111118-111118-3. ↑

J2617. Chen Peiliang. Fairly pure ultraviolet electroluminescence from ZnO-based light-emitting devices. / Chen Peiliang, Ma Xiangyang, Yang Deren. // Applied Physics Letters. - 2006. - Vol. 89, No. 11. - P. 111112-111112-3. ↑

J2618. Aziz Hany. Improving the stability of organic light-emitting devices by using a thin Mg anode buffer layer. / Aziz Hany, Luo Yichun, Xu Gu, Popovic Zoran D. // Applied Physics Letters. - 2006. - Vol. 89, No. 10. - P. 103515-103515-3. ↑

J2619. Katzer Kl.-D. Voltage drop in an (Al x Ga 1-x)0.5 In 0.5 P light-emitting diode probed by Kelvin probe force microscopy. / Katzer Kl.-D., Martin W., Bacher G., Jaeger A., Streubel K. // Applied Physics Letters. - 2006. - Vol. 89, No. 10. - P. 103522-103522-3. ↑

J2620. Chen N. C. Determination of junction temperature in Al Ga In P /Ga As light emitting diodes by self-excited photoluminescence signal. / Chen N. C., Wang Y. N., Tseng C. Y., Yang Y. K. // Applied Physics Letters. - 2006. - Vol. 89, No. 10. - P. 101114-101114-3. ↑

- J2621.** Niu Yu-Hua. Thermally crosslinked hole-transporting layers for cascade hole-injection and effective electron-blocking/exciton-confinement in phosphorescent polymer light-emitting diodes. / Niu Yu-Hua, Liu Michelle S., Ka Jae-Won, Jen Alex K.-Y. // Applied Physics Letters. - 2006. - Vol. 88, No. 9. - P. 093505-093505-3. ↑
- J2622.** Tseng Ricky J. Highly efficient 7,8,10-triphenylfluoranthene-doped blue organic light-emitting diodes for display application. / Tseng Ricky J., Chiechi Ryan C., Wudl Fred, Yang Yang. // Applied Physics Letters. - 2006. - Vol. 88, No. 9. - P. 093512-093512-3. ↑
- J2623.** Liu W. Blue-yellow ZnO homostructural light-emitting diode realized by metalorganic chemical vapor deposition technique. / Liu W., Gu S. L., Ye J. D., Zhu S. M., Liu S. M., Zhou X., Zhang R., Shi Y., Zheng Y. D., Hang Y., Zhang C. L. // Applied Physics Letters. - 2006. - Vol. 88, No. 9. - P. 092101-092101-3. ↑
- J2624.** Yuan Y. Y. Fullerene-organic nanocomposite: A flexible material platform for organic light-emitting diodes. / Yuan Y. Y., Han S., Grozea D., Lu Z. H. // Applied Physics Letters. - 2006. - Vol. 88, No. 9. - P. 093503-093503-3. ↑
- J2625.** Divayana Y. Comment on "Singlet-singlet and singlet-triplet annihilations in fluorescence-based organic light-emitting diodes under steady-state high current density" [Appl. Phys. Lett. 86, 213506 (2005)]. / Divayana Y., Chen B. J., Sun X. W. // Applied Physics Letters. - 2006. - Vol. 88, No. 9. - P. 096101-096101-2. ↑
- J2626.** Okumoto Kenji. High efficiency red organic light-emitting devices using tetraphenyl-dibenzoperiflanthene-doped rubrene as an emitting layer. / Okumoto Kenji, Kanno Hiroshi, Hamada Yuji, Takahashi Hisakazu, Shibata Kenichi. // Applied Physics Letters. - 2006. - Vol. 89, No. 1. - P. 013502-013502-3. ↑
- J2627.** Akasaka Tetsuya. InGaN quantum wells with small potential fluctuation grown on InGaN underlying layers. / Akasaka Tetsuya, Gotoh Hideki, Kobayashi Yasuyuki, Nakano Hidetoshi, Makimoto Toshiki. // Applied Physics Letters. - 2006. - Vol. 89, No. 10. - P. 101110-101110-3. ↑
- J2628.** Kohda M. Bias voltage dependence of the electron spin injection studied in a three-terminal device based on a (Ga,Mn)As/n+-GaAs Esaki diode. / Kohda M., Kita T., Ohno Y., Matsukura F., Ohno H. // Applied Physics Letters. - 2006. - Vol. 89, No. 1. - P. 012103-012103-3. ↑
- J2629.** Shimizu Syogo. First direct observation of self-imaging effect in active multimode-interference semiconductor laser diodes. / Shimizu Syogo, Razali Mohd Danni Bin, Kasahara Kenichi, Hamamoto Kiichi, Ohya Masaki, Naniwae Koichi, De Merlier Jan, Shiba Kazuhiro, Sudo Shinya, Sasaki Tatsuya. // Applied Physics Letters. - 2006. - Vol. 89, No. 1. - P. 011106-011106-3. ↑
- J2630.** Saxena N. Secure Device Pairing Based on a Visual Channel: Design and Usability Study. / Saxena N., Ekberg J.-E., Kostianen K., Asokan N. // IEEE Transactions on Information Forensics and Security. - 2011. - Vol. 6, No. 1. - P. 28-38. ↑